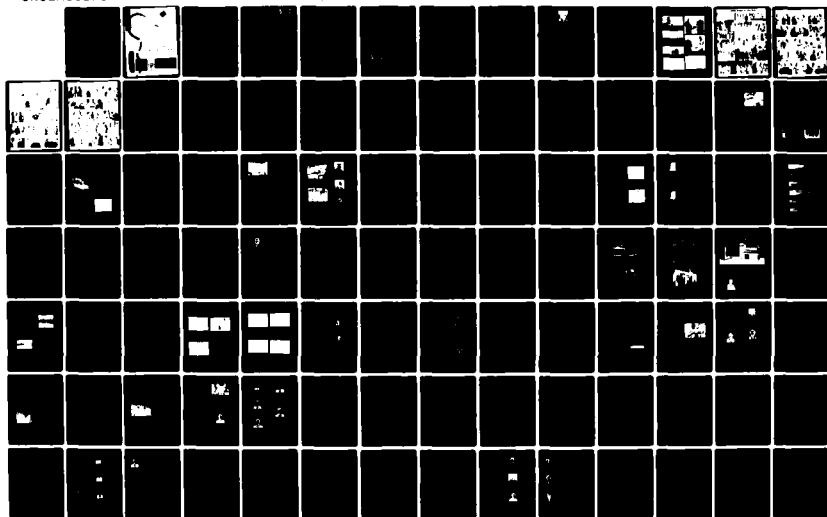


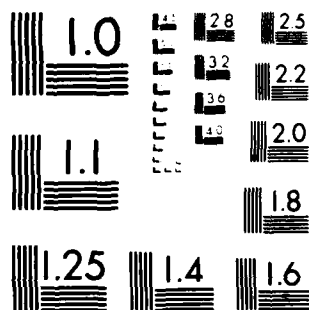
UNCLASSIFIED

NOV 82

F/G 20/6

NL





MICROCOPY RESOLUTION TEST CHART
NATIONAL BUREAU OF STANDARDS-1963-A

Fiber Optics
and Copper Wire:

Partners or Competitors?

Proceedings of the 31st
**International
Wire And Cable
Symposium**

November 16-18, 1982

DTIC FILE COPY



Sponsored by
U.S. Army Communications-Electronics Command,
Fort Monmouth, New Jersey

REPORT DOCUMENTATION PAGE		READ INSTRUCTIONS BEFORE COMPLETING FORM
1. REPORT NUMBER N/A	2. GOVT ACCESSION NO. AD-A125 062	3. RECIPIENT'S CATALOG NUMBER
4. TITLE (and Subtitle) Proceedings of 31st International Wire & Cable Symposium-1982		5. TYPE OF REPORT & PERIOD COVERED Final - November
7. AUTHOR(s) Various Director: E.F. GODWIN		6. PERFORMING ORG. REPORT NUMBER N/A
9. PERFORMING ORGANIZATION NAME AND ADDRESS System Analysis Team (DRSEL-COM-RM-3) MTD, CENCOMS, CECOM Ft Monmouth, NJ 07703		8. CONTRACT OR GRANT NUMBER(s) None
11. CONTROLLING OFFICE NAME AND ADDRESS Same as 9.		10. PROGRAM ELEMENT, PROJECT, TASK AREA & WORK UNIT NUMBERS Proj No 1L1 62701 AH92 AMC Code 612701.H92.MA.11.00
14. MONITORING AGENCY NAME & ADDRESS (if different from Controlling Office) Same as 9.		12. REPORT DATE Nov. 1982
		13. NUMBER OF PAGES 485
		15. SECURITY CLASS. (of this report) UNCLASSIFIED
		15a. DECLASSIFICATION/DOWNGRADING SCHEDULE
16. DISTRIBUTION STATEMENT (of this Report) Approved for Public Release: Distribution Unlimited.		
17. DISTRIBUTION STATEMENT (of the abstract entered in Block 20, if different from Report)		
18. SUPPLEMENTARY NOTES Proceedings of technical papers presented at 31st International Wire and Cable Symposium sponsored annually by US Army Communications/Electronics Command.		
19. KEY WORDS (Continue on reverse side if necessary and identify by block number) Aerospace electronics, cable design, cable evaluation, cable manufacture, cable materials, cable performance, cable testing, electronic wiring, fiber optics, fiber optic cables, fiber optic connectors, interconnections, military electronics, telephone communications, wire insulation, wire materials, wire testing.		
20. ABSTRACT (Continue on reverse side if necessary and identify by block number) The International Wire and Cable Symposium is the only symposium of its kind in the world. The proceedings include papers in the field of electrical and electronic wire and cable, materials, testing, evaluation, connections, splicing, installation, applications, fire retardancy, fiber optics, manufacturing processing, wire/cable design and manufacturing.		

DISTRIBUTION STATEMENT A

**Approved for public release;
Distribution Unlimited**

**DTIC
ELECTE
S MAR 21 1983 D**

COMPONENT PART NOTICE

B

THIS PAPER IS A COMPONENT PART OF THE FOLLOWING COMPILATION REPORT:

(TITLE): Proceedings of the International Wire and Cable Symposium (31st) Held at
Cherry Hill, New Jersey, November 16, 17 and 18, 1982.

(SOURCE): Army Communications-Electronics Command, Fort Monmouth, NJ.

TO ORDER THE COMPLETE COMPILATION REPORT USE AD-A125 662 .

**THE COMPONENT PART IS PROVIDED HERE TO ALLOW USERS ACCESS TO INDIVIDUALLY
AUTHORED SECTIONS OF PROCEEDINGS, ANNALS, SYMPOSIA, ETC. HOWEVER, THE
COMPONENT SHOULD BE CONSIDERED WITHIN THE CONTEXT OF THE OVERALL COMPILATION
REPORT AND NOT AS A STAND-ALONE TECHNICAL REPORT.**

THE FOLLOWING COMPONENT PART NUMBERS COMPRISE THE COMPILATION REPORT:

AD#:	P000 538	TITLE: Dynamic Detecting, Measuring, and Classifying Defects in Telephone Wire Insulation.
	AD-P000 539	Image Analysis, Microscopic, and Spectrochemical Study of the PVC Dry Blending Process.
	AD-P000 540	The Computer Is In: Now Your Troubles Begin.
	AD-P000 541	Automated Electrical Harness Manufacturing.
	AD-P000 542	Metal Forming and Inspection Control for Cable Sheathing.
	AD-P000 543	Computerization of the Pulp Wire Insulating Process.
	AD-P000 544	Development and Application of Optical Fiber Composite Overhead Ground Wire (OPT/GW).
	AD-P000 545	Gamma Irradiation Characteristics of Optical Fibers.
	AD-P000 546	Application of VAD Fiber Cable to Commercial Fiber Optic Transmission System (FOTS).
	AD-P000 547	Toll Message Lightguide Transmission Network in Manitoba.
	AD-P000 548	Optical Fiber Cable Fastened to Overhead Ground Wire with Lashing Rod.
	AD-P000 549	Easy and Practical Evaluation of Optical Fiber's Splices, Graded Index-Multimode, To Be Set Up in Plant.
	AD-P000 550	Pair Lay Distribution with Regard to Far-End Crosstalk in Symmetric Telecommunication Cable.
	AD-P000 551	Crosstalk, Insertion Loss, Sweep Frequency Analysis and Fixturing for Telephone Cables.
	AD-P000 552	Comparative Study of Analog and Digital Crosstalk Measurements Methods on Telephone Cables.
	AD-P000 553	Field Testers for Assessing 1.5 and 2.0 Mbit/s -- Digital Performance of Metallic-Pair Cables.
	AD-P000 554	Open-Circuit Admittance of a Telephone Cable Pair.
	AD-P000 555	Telecommunication Cables and Power Frequency Induction.
	AD-P000 556	Fiber Optic Connection System.
	AD-P000 557	On New Cable Accessories for Optical Fiber Cable System.
	AD-P000 558	Optical and Mechanical Characteristics of Microflame Fusion Splicing of Optical Fiber.
	AD-P000 559	Arc-Fusion Splice of Optical Fiber and Its Reliability in Field.

COMPONENT PART NOTICE (CON'T)

AD#: P000 560	TITLE: Flat Mass Splicing Process for Cylindrical V-Grooved Cables.
AD-P000 561	Test Results of Multichannel Hermaphroditic Optical Connectors Developed for the US Army.
AD-P000 562	Shielding Effectiveness of Composite Metals at Voice and Carrier Frequencies.
AD-P000 563	Structure and Characteristics of Cables for Robots.
AD-P000 564	A Crosstalk Model for Cross-Stranded Cables.
AD-P000 565	Impedance Irregularities in Telephone Networks.
AD-P000 566	Power Sum Crosstalk of PIC Cables as a Function of Cable Design.
AD-P000 567	Instantaneous Cable Sealing Technique: Theory and Typical Applications.
AD-P000 568	Pressure Blocking of Filled Cable.
AD-P000 569	Shield Bonding Terminal for Buried Service Wire.
AD-P000 570	Outdoor Connector with Advanced Weather Resistance.
AD-P000 571	A New Clamp-On Tap for Coaxial Data Networks.
AD-P000 572	Dropwire Leakage Due to a Faulty Connector: A General Model Based on Radiation from a Circumferential Slot.
AD-P000 573	Thermodynamic Interactions, Mechanical Properties and Property Retention in Polymeric Wire Coatings.
AD-P000 574	Investigation of Premature Depletion of Stabilizers from Solid Polyethylene Insulation.
AD-P000 575	Blending of a Block Copolymer Thermoplastic Rubber for Specific Wire and Cable Applications.
AD-P000 576	Behaviour of Zinc-Coatings on Steel Tapes in Armoured Cables.
AD-P000 577	Test Procedures for Determination of the Radiation Resistance of Cable Materials.
AD-P000 578	Suspension Light Absorption Measurement of Weatherable PVC Compounds.
AD-P000 579	Viscoelastic Analysis of Shrinkback.
AD-P000 580	Characterization of Ruggedized Fiber Optic Dual Wavelength Cables.
AD-P000 581	A Refined Tight Design Duct Cable for Low Loss Monomode Fibre.
AD-P000 582	Design Consideration for Jacketing Fiber Optic Cable.
AD-P000 583	Development of Nonmetallic, Loose-Groove Spacer-Type Optical Fiber Cable.
AD-P000 584	Self-Supporting Metal Free Optical Fibre Cable for Large Span Length.
AD-P000 585	Design and Performance of a Filled, High-Fiber-Count, Multimode Optical Cable.
AD-P000 586	Flame Retardant Halogenfree Thermoplastic Telecom Indoor Wiring.
AD-P000 587	Large Scale Fire Tests of Building Riser Cables.
AD-P000 588	A New Flame Resistant, High Temperature, Cross-Linked Polypropylene Compound Insulated Wire.
AD-P000 589	A Comprehensive Small Scale Smoke Test.
AD-P000 590	A New Construction of Halogen-Free Flame Retardant Insulated Wire with Double Layers.
AD-P000 591	Bandwidth Characterization of Fiber Waveguide Systems with Fusion-Spliced Multimode Graded-Index Fibers.

AD-P000 592	TITLE: Pure-Silica Core Optical Fiber and Fiber Cable for Radiation Fields.
AD-P000 593	Radiation Effects of Optical Silica Fiber and Radiation Hard Optical Transmission.
AD-P000 594	Design and Test Results of an Optical-Fiber Submarine Cable.
AD-P000 595	Computer Controlled Optical Time Domain Reflectometer Monitoring of Lightguide Cable Installations.
AD-P000 596	Practical Instrumentation for Fiber Optic Evaluation.

S **DTIC**
ELECTE **D**
 MAR 21 1983
B

Accession For	
NTIS GRA&I	<input checked="checked" type="checkbox"/>
DTIC TAB	<input type="checkbox"/>
Unannounced	<input type="checkbox"/>
Justification	
By _____	
Distribution _____	
Availability Codes	
Dist	Avail. and/or Special
A	

12

PROCEEDINGS OF 31ST INTERNATIONAL WIRE AND CABLE SYMPOSIUM

Sponsored by
US Army Communications-Electronics Command
(CECOM) Fort Monmouth, NJ

Cherry Hill, New Jersey
November 16, 17 and 18, 1982

APPROVED FOR PUBLIC RELEASE: DISTRIBUTION UNLIMITED

Author	
Title	
Availability	
Dist	A



31WC

A

30TH INTERNATIONAL WIRE AND CABLE SYMPOSIUM SYMPOSIUM COMMITTEE

Elmer F. Godwin, Director, GEF Associates-(201)741-8864
Winnie Conti, Assistant, US Army CECOM-(201)544-2770
John Brazee, Continental Telephone Service Corporation
Leo M. Chattler, DCM Industries Inc.
William Chervenak, Corning Glass Works
Robert Depp, Defense Electronics Supply Center
Paul Dobson, Valtec Corporation
Andrew Dunin, DuPont Canada Inc.
William Korcz, Shell Development Company
Joseph McCann, US Army CECOM
Eugene Riley, Anaconda-Ericsson, Inc.
John Santos, Phelps Dodge Communications Company
James Tyler, Essex Group
George Webster, Bell Laboratories
Austin Wetherell, Underwriters Laboratories

ADVISORY

Michael A. DeLucia, David W. Taylor Naval Ship R&D Center
Marta Farago, Northern Telecom Canada Ltd.
Irving Kolodny, General Cable Company
Joe Neigh, AMP, Inc.
Frank Short, Belden Corporation

TECHNICAL SESSIONS

Tuesday, 16 November 1982

9:30 a.m.	Session I	Panel Discussion-Fiber Optics and Metallic Cables Partners or Competitors
2:00 p.m.	Session II	Process and Manufacturing
2:00 p.m.	Session III	Fiber Optic Applications and Performance

Wednesday, 17 November 1982

9:00 a.m.	Session IV	Testing & Applications
9:00 a.m.	Session V	Fiber Optic Terminations/Connectors
2:00 p.m.	Session VI	Cable Design
2:00 p.m.	Session VII	Terminations/Connectors

Thursday, 18 November 1982

9:00 a.m.	Session VIII	Materials
9:00 a.m.	Session IX	Fiber Optic Cable Designs
2:00 p.m.	Session X	Fire, Smoke, and Toxicity Considerations
2:00 p.m.	Session XI	Fiber Optic Measurements

PAPERS

Responsibility for the contents rests upon the authors and not the symposium committee or its members. After the symposium, all the publication rights of each paper are reserved by their authors, and requests for republication of a paper should be addressed to the appropriate author. Abstracting is permitted, and it would be appreciated if the symposium is credited when abstracts or papers are republished. Requests for individual copies of papers should be addressed to the authors.



MESSAGE FROM THE DIRECTOR

On behalf of the U.S. Army Communications-Electronics Command (CECOM) and the symposium committee, welcome to the 31st Annual International Wire and Cable Symposium (IWCS). The symposium continues to command the attention of a world-wide audience of manufacturers, consultants, scientists, material suppliers and end product users. Last year's attendance of 1574 included representatives from 429 U.S. companies, 10 U.S. government agencies and 38 foreign countries. Of the 234 foreign attendees, 31 presented papers.

The response to the "Call For Papers" was excellent this year as demonstrated by the large number (59) of papers included in the technical program. The program will begin with a tutorial session "Fiber Optics and Metallic Cables-Partners or Competitors" followed by ten (10) other sessions addressing a wide spectrum of technical topics related to wire/cable and interconnections.

The objective of the IWCS committee is for the symposium to remain a reflection of the needs and interest of its attendees and supporters. Towards this objective, the committee's concern is for the technical program to include topics of pertinent interest to wire, cable, materials and connector manufacturers/users including fiber optics. For a particular year, any topical area may dictate by abstracts submitted, that a large part of the technical program address a specific topic. Over the years it is hoped that the program agenda will present a balance of the technical interest desired by its attendees and supporters. At all times the program will be a reflection of the current interests as indicated by the response to the "Call For Papers," which presently shows a high interest in fiber optics.

Over the years, the Director and committee members received many requests or suggestions from various attendees to relocate the symposium. After many years of considering the pros and cons of moving to another location, the committee has decided to hold the 33rd symposium (1984) in Reno, Nevada. It should be noted that for the present, the move is on a trial basis for one year. The 32nd symposium (1983) will remain in Cherry Hill, New Jersey. Symposium attendees will be informed well in advance of any future changes in location.

Committee members, Leo Chatter of the DCM International Corporation, and William Korcz of the Shell Development Company, are retiring from the committee. Leo and Bill, by their efforts and specialized knowledge, contributed significantly to the success of the symposium. On behalf of the committee, I thank them for their valuable contribution and wish them success in their future activities.

The committee continues to explore new ideas for improving the activities of the symposium, therefore, the committee solicits the continued support of all members of the wire and cable industry. Your comments and suggestions for improving the symposium are welcomed.


ELMER F. GODWIN
Director, IWCS

PROCEEDINGS

INTERNATIONAL WIRE & CABLE SYMPOSIUM

BOUND—AVAILABLE AT FORT MONMOUTH

23rd International Wire & Cable Symposium Proceedings—1974—7.00
 24th International Wire & Cable Symposium Proceedings—1975—7.00
 25th International Wire & Cable Symposium Proceedings—Not Available
 26th International Wire & Cable Symposium Proceedings—Not Available
 27th International Wire & Cable Symposium Proceedings—1978—8.00
 28th International Wire & Cable Symposium Proceedings—1979—8.00
 29th International Wire & Cable Symposium Proceedings—Not Available
 30th International Wire & Cable Symposium Proceedings—1981—10.00
 *31st International Wire & Cable Symposium Proceedings—1982—15.00
 *Extra copies: 1-3 \$15.00, next 4-10 \$10.00; next 11 and above \$8.00 each.

Make check or bank draft Payable in US dollars to the INTERNATIONAL WIRE & CABLE SYMPOSIUM and forward request to:

International Wire & Cable Symposium
 US Army Communications - Electronics Command
 ATTN: DRSEL-COM-RM-3 (W. Conti)
 Fort Monmouth, NJ 07703
 USA

PHOTOCOPIES—AVAILABLE AT DEPARTMENT OF COMMERCE

Photocopies are available for complete sets of papers for 1964 and 1966 thru 1981 Information on prices and shipping charges should be requested from the:

US Department of Commerce
 National Technical Information Service
 Springfield, Virginia 22151
 USA

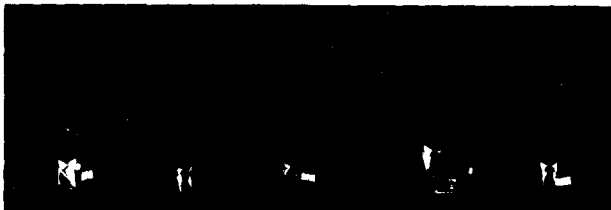
Include Title, Year and "AD" Number	
13th Annual Wire & Cable Symposium (1964)	—AD 787164
15th Annual Wire & Cable Symposium (1966)	—AD A006601
16th International Wire & Cable Symposium (1967)	—AD 787165
17th International Wire & Cable Symposium (1968)	—AD 787166
18th International Wire & Cable Symposium (1969)	—AD 787167
19th International Wire & Cable Symposium Proceedings 1970	—AD 714985
20th International Wire & Cable Symposium Proceedings 1971	—AD 733399
21st International Wire & Cable Symposium Proceedings 1972	—AD 752908
22nd International Wire & Cable Symposium Proceedings 1973	—AD 772914
23rd International Wire & Cable Symposium Proceedings 1974	—AD A003251
24th International Wire & Cable Symposium Proceedings 1975	—AD A017787
25th International Wire & Cable Symposium Proceedings 1976	—AD A032801
26th International Wire & Cable Symposium Proceedings 1977	—AD A047609
27th International Wire & Cable Symposium Proceedings 1978	—AD A062322
28th International Wire & Cable Symposium Proceedings 1979	—AD A081428
29th International Wire & Cable Symposium Proceedings 1980	—AD A096308
30th International Wire & Cable Symposium Proceedings 1981	—AD A110859

Kwic Index of Technical Papers, International Wire & Cable Symposium (1952-1975) —AD A027558

**Highlights of the 30th
International Wire and Cable Symposium
November 17, 18 & 19, 1981
Hyatt Cherry Hill, Cherry Hill, NJ**



Greetings by Dr. James Soos,
Director of CENCOMS, U.S.
Army Communications-Electronics
Command (CECOM), Fort Monmouth,
New Jersey



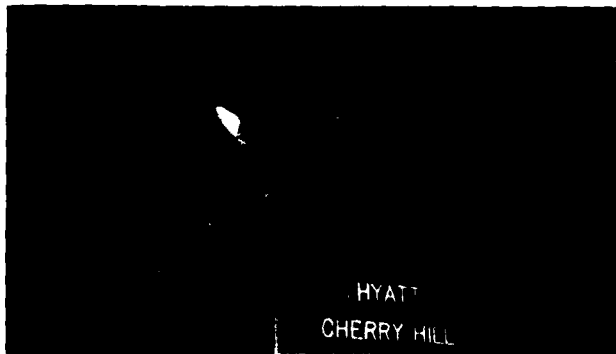
Panel Members - Tutorial Session
(left to right) Dr. D. Duke, V. P., Telecommunications Division,
Corning Glass Works; Dr. R. Y. Hung, Manager, Optical
Technologies Research Division, Thomas J. Watson Research
Center; Dr. I. Jacobs, Director, Wideband Transmission
Facilities Laboratory, Bell Laboratories; Mr. J. Kanely, Presi-
dent, Valtec Corporation;
Dr. L. Dworkin, Chief, Multichannel Transmission Division,
CENCOMS Fort Monmouth



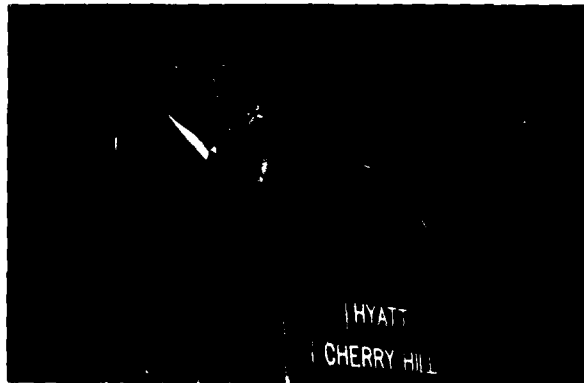
Mr. M. DeLucia, David W. Taylor Naval Ship R&D Center,
presenting the award for Outstanding Technical Paper to Mr.
Paul Kish, Northern Telecom Canada Ltd., and (bottom) for
Best Presentation to Mr. James Refi, Bell Laboratories



Dr. James Soos, Director, CENCOMS, Fort Monmouth, presen-
ting Retirement Certificate to Committee Member, Michael A.
DeLucia



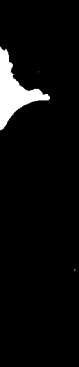
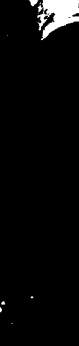
Banquet Guest Speaker - Major General E. J. DeLaune Jr.,
Director, Army Budget, Office of the Comptroller of Army



Brigadier General R. B. Morgan, Deputy Commanding General
for Research and Development, CECOM, Fort Monmouth offer-
ing greetings at the banquet

CANDID SCENES AT 30TH IWCS









AWARDS

<i>Outstanding Technical Paper</i>		<i>Best Presentation</i>
H. Lubars and J. A. Olszewski, General Cable Corp.—"Analysis of Structural Return Loss in CATV Coaxial Cable"	1968	N. Dean, B.I.C.C.—"The Development of Fully Filled Cables for the Distribution Network"
J.P. McCann, R. Sabia and B. Wargotz, Bell Laboratories—"Characterization of Filler and Insulation in Waterproof Cable"	1969	J.D. Kirk, Alberta Government Telephones—"Progress and Pitfalls of Rural Buried Cable"
D.E. Setzer and A.S. Windeler, Bell Laboratories—"A Low Capacitance Cable for the T2 Digital Transmission Line"	1970	Dr. O. Leuchs, Kable and Metalwerke—"A New Self-Extinguishing Hydrogen Chloride Binding PVC Jacketing Compound for Cables"
R. Lyenger, R. McClean and T. McManus, Bell Northern Research—"An Advanced Multi-Unit Coaxial Cable for Toll PCM Systems"	1971	S. Nordblad, Telefonaktiebolaget L.M. Ericsson—"Multi-Paired Cable of Nonlayer Design for Low Capacitance Unbalance Telecommunication Network"
J.B. Howard, Bell Laboratories—"Stabilization Problems with Low Density Polyethylene Insulations"	1972	N. Kojima, Nippon Telegraph and Telephone—"New Type Paired Cable for High Speed PCM Transmission"
Dr. H. Martin, Kabelmetal—"High Power Radio Frequency Coaxial Cables, Their Design and Rating"	1973	S. Kaufman, Bell Laboratories—"Reclamation of Water-Logged Buried PIC Telephone Cable"
D. Doty, AMP Inc.—"Mass Wire Insulation Displacing Termination of Flat Cable"	1974	R.J. Oakley, Northern Electric Co., Ltd.—"A Study into Paired Cable Crosstalk"
T.S. Choo, Dow Chemical U.S.A.—"Corrosion Studies on Shielding Materials for Underground Telephone Cables"	1975	G.H. Webster, Bell Laboratories—"Material Savings by Design in Exchange and Trunk Telephone Cable"
N.J. Cogelia, Bell Telephone Laboratories and G.K. Lavoie and J.F. Glahn, US Department of Interior—"Rodent Biting Pressure and Chemical Action and Their Effects on Wire and Cable Sheath"	1976	J.E. Wimsey, United States Air Force—"The Bare Base Electrical Systems"
Thomas K. McManus, Northern Telecom Canada Ltd. and R. Beveridge, Saskatchewan Telecommunications, Canada—"A New Generation of Filled Core Cable"	1977	Michael DeLucia, Naval Ship Research and Development Center—"Highly Fire-Retardant Navy Shipboard Cable"
Fumio Suzuki, Shizuyoshi Sato, Akinori Mori and Yoichi Suzuki, Sumitomo Electric Industries, Ltd., Japan—"Microcoaxial Cables Insulated with Highly Expanded Polyethylene By Chemical Blowing Method"	1978	William L. Schmacher, AMP Inc.—"Design Considerations for Single Fiber Connector"
S. Masaki, Y. Yamazaki and T. Ideguchi, Nippon Telegraph and Telephone Public Corporation, Japan—"New Aluminum Sheath Cable Used For Electromagnetic Shielding"	1979	Richard C. Mondello, Bell Labs.—"Design and Manufacture of An Experimental Lightguide Cable For Undersea Transmission Systems"
P. Kish and Y. LeBorgne, Northern Telecom Canada Limited, Montreal, Canada—"General Crosstalk Model For Paired Communication Cables"	1980	I. Wadehra, IBM Corporation—"Performance of Polyvinyl Chloride Communication Cables in Modified Steiner Tunnel Test"
C.J. Arroyo, N.J. Cogelia, Bell Laboratories, and R.J. Darsey, Western Electric—"Thermal Behavior of Experimental Plenum Cable Sheaths Determined in a Radiant Heat Chamber"	1981	J.J. Refi, Bell Laboratories—"Mean Power Sum Far-Field Crosstalk of PIC Cables as a Function of Average Twist Helix Angle"
		G.S. Anderson, Belden Corporation—"Installation of Fiber Optic Cable on 457 Meter Tower"

CONTRIBUTORS

A-C Polyethylene Allied Fibers and Plastics Company
Morristown, NJ

AEG Telefunken
Frankfurt, Germany

A.E. Petsche Co., Inc.
Arlington, TX

Albany International Corporation
Chatham, NY

Alcan Aluminio Do Brasil S.A.
Sao Paulo, Brasil

ALCAVE-Alambres Y Cables Venezolanos CA
Caracas, Venezuela

Alcoa Conductor Products Co.
Pittsburgh, PA

Allied Fibers & Plastics
Morristown, NJ

Alpha Wire Corporation
Elizabeth, NJ

Amercable Corporation
El Dorado, AR

American Hoechst Corporation
Leominster, MA

AMP, Inc.
Harrisburg, PA

Anaconda Aluminum Co.
Louisville, KY

Arnold Filled Associates/AFA Industries
Hackensack, NJ

Arvey Corporation
Cedar Grove, NJ

Associated Lead Inc.
Philadelphia, PA

ATC (PTY) Ltd.
Brits, Transvaal, South Africa

Austral Standard Cables Pty. Ltd.
Clayton, Victoria, Australia

Australian Telecommunications Commission
Melbourne, Australia

Beacon Reel Company
Beacon Falls, CT

Belden Corporation
Geneva, IL

Bell Canada
Toronto, Ontario, Canada

Berkshire Electric Cable Co.
Leeds, MA

Berk-Tek, Inc.
Reading, PA

BICC Telecommunications Cables Ltd.
Prescot, Merseyside, England

Boston Insulated Wire & Cable Co.
Hamilton, Ontario, Canada

Breen Color Concentrates, Inc.
Lambertville, NJ

The Bridge Mfg. Co.
Enfield, CT

Buchanan Crimp Tool Products
Union, NJ

Burgess Pigment Co.
Sandersville, GA

Cablerie d'Eupen S.A.
Eupen, Belgium

Cables de Comunicaciones, S.A.
Zaragoza, Spain

Camden Wire Co., Inc.
Camden, NY

Canada Wire and Cable Ltd.
Winnipeg, Manitoba, Canada

Carlew Chemicals Ltd.
Montreal, Quebec, Canada

Cary Chemicals
Edison, NJ

CasChem, Inc.
Bayonne, NJ

Centro de Investigacion de Standard Electrica
Madrid, Spain

Chase & Sons, Inc.
Randolph, MA

C-I-L, Inc.
Brampton, Ontario, Canada

Comm/Scope Company
Catawba, NC

Commonwealth Telephone Company
Dallas, PA

Copperweld Bimetallics Group
Pittsburgh, PA

Corning Glass Works
Corning, NY

Dainichi-Nippon Cables, Ltd.
Tokyo, Japan

David W. Riley, Consultant, Extrusion Engineers
Plainfield, NJ

DCM Industries, Inc.
San Leandro, CA

Delco Wire & Cable Inc.
Bristol, PA

Delphi Wire & Cable
Folcroft, PA

Dow Chemical USA
Midland, MI

Dow Corning Corporation
Midland, MI

Duncan M. Gillies Co., Inc.
West Boylston, MA

Dussek Campbell Ltd.
Belleville, Ontario, Canada

Dussek Campbell Ltd.
Crayford, Kent, England

Eastman Chemical Products, Inc.
Kingsport, TN

E.I. DuPont de Nemours
Wilmington, DE

The Electric Wire & Cable Co. of Israel
Haifa, Israel

Electrical Conductors
No. Chicago, IL

Electroconductores C.A.
 Caracas, Venezuela
Ensign-Bickford Industries, Inc.
 Simsbury, CT
Essex Group
 Decatur, IL
Excelsior Wire Corp.
 Los Angeles, CA
Facile Technologies Inc.
 Paterson, NJ
F&G Telecommunications Cables & Systems
 Koln, West Germany
Filotex
 Draveil, France
Formulabs Industrial Inks, Inc.
 Escondido, CA
Fujikura Cable Works Ltd.
 Tokyo, Japan
The Furukawa Electric Co., Ltd.
 Tokyo, Japan
Garlock Plastomer Products
 Newtown, PA
Gary Chemical Corporation
 Leominster, MA
Gavitt Wire & Cable Co., Inc.
 Brookfield, MA
Gem Gravure Company, Inc.
 West Hanover, MA
General Cable Company
 Edison, NJ
General Cable Company
 Greenwich, CT
General Electric Silicones
 Waterford, NY
General Engineering U.S.A. Ltd.
 So. Windsor, CT
Georgia Pacific Corporation
 Atlanta, GA
GTE Service Corporation
 Stamford, CT
Guill Tool & Engineering
 West Warwick, RI
Habia Cable Inc.
 Ronkonkoma, NY
Harbour Industries, Inc.
 Shelburne, VT
HiTemp Wires Co.
 Hauppauge, NY
Hong Kong Telephone Co. Ltd.
 Hong Kong, ROC
Hudson Wire Company
 Ossining, NY
Independent Cable, Inc.
 Hudson, MA
International Wire Products Company
 Wyckoff, NJ
ITT Electro-Optical Products Division
 Roanoke, VA
ITT Surprenant Division
 Clinton, MA
John Royle and Sons
 Pompton Lakes, NJ
Judd Wire Division, HVE
 Turners Falls, MA
Kable Tapes Ltd.
 Winnipeg, Manitoba, Canada
Kenrich Petrochemicals Inc.
 Bayonne, NJ
K. Miller Tool & Mfg. Co., Inc.
 West Springfield, MA
LaBarge Inc.
 Irving, CA
Lamart Corp.
 Clifton, NJ
Lowe Associates, J.J. Inc.
 Bedford Hills, NY
LTT-Lignes Telegraphiques et Telephoniques
 Conflans-St-Honorine, France
Maillefer Company
 South Hadley, MA
Major Wire Co., Inc.
 Chicopee, MA
Mark Mor Tool & Die Inc.
 Allenwood, NJ
Micro-Tek Corp.
 Cinnaminson, NJ
Monson Chemicals, Inc.
 Leominster, MA
The Montgomery Company
 Windsor Locks, CT
Montrose Products Co.
 Auburn, MA
Mossberg Hubbard
 Cumberland, RI
NEPTCO
 Pawtucket, RI
Nesor Alloy Corporation
 W. Caldwell, NJ
The New Brunswick Telephone Co., Ltd.
 Saint John, New Brunswick
Nippon Telegraph and Telephone Public Corp.
 Tokyo, Japan
NKF P.S. Weltevreden
 Waddinxveen, The Netherlands
Nokia Inc./Cable Machinery Division
 Atlanta, GA
Nonotuck Manufacturing Co.
 South Hadley, MA
Northeast Wire Co., Inc.
 Holyoke, MA
Northern Telecom Canada Ltd.
 Montreal, Quebec, Canada
Occidental Chemical Corporation
 Pottstown, PA
The Okonite Company
 Ramsey, NJ
OMYA, Inc.
 Proctor, VT
Pennwalt Corporation - Plastics Dept.
 Philadelphia, PA

Penreco
Butler, PA

Phalo Corporation
Shrewsbury, MA

Phillips Cables Ltd.
Vancouver, BC, Canada

Phillips Chemical Co.
Pasadena, TX

Pirelli Ericsson Cables Ltd.
Minto, NSW, Australia

Plastoid Corporation
New York, NY

Plymouth Rubber Company
Canton, MA

Polysar Rubber Services
East Brunswick, NJ

Prestolite Wire Division
Port Huron, MI

Radiation Dynamics, Inc.
Melville, NY

Radix Wire Company
Euclid, OH

Raychem Corporation
Cherry Hill, NJ

Raychem Corporation
Menlo Park, CA

Raychem - Telecommunications Div.
Menlo Park, CA

R.E. Carroll, Inc.
Trenton, NJ

Reichhold Chemicals, Inc.
Hackettstown, NJ

Reliance Comm/Tec
Chicago, IL

The Rochester Corporation
Culpeper, VA

The Rockbestos Company
Wallingford, CT

Santech, Inc.
Toronto, Ontario, Canada

Sartomer Company
West Chester, PA

SAT-Societe Anonyme de Telecommunications
Paris, France

Saytech, Inc.
Sayreville, NJ

SCAL
Paris, France

Shell Chemical Co.
Houston, TX

Showa Electric Wire & Cable Co., Ltd.
Kanagawa, Japan

Siecor Corporation
Hickory, NC

Siemens AG/NKE
Munich, West Germany

Southwest Plastics
Houston, TX

Sterling Davis Electric
Wallingford, CT

Sumitomo Electric Industries Ltd.
Yokohama, Japan

Sun Refining and Marketing Co.
Philadelphia, PA

The Swiss Insulating Works, Ltd.
Breitenbach, Switzerland

Syncro Machine Company
Perth Amboy, NJ

Taconic Plastics, Ltd.
Petersburg, NY

Tamaqua Cable Products Corp.
Schuylkill Haven, PA

Tatung Wire & Cable Co., Ltd.
Taipei, Taiwan, R.O.C.

Technical Coatings Company
Nutley, NJ

Teledyne Farris Engineering
Palisades Park, NJ

Teledyne Thermadics
Elm City, NC

Tenneco Chemicals, Inc.
Piscataway, NJ

Tensolite Company, Div. Carlisle Corp.
Buchanan, NY

Thermax Wire Corp.
Flushing, NY

Thomas & Betts Corporation
Raritan, NJ

3M Company
St. Paul, MN

Times Fiber Communications, Inc.
Wallingford, CT

Torpedo Wire & Strip Inc.
Pittsfield, PA

Trans-Met Engineering, Inc.
LaHabra, CA

Trea Industries Inc.
N. Kingstown, RI

Ugine Kuhlmann of America, Inc.
Paramus, NJ

Union Carbide Corporation
Tarrytown, NY

Union Carbide Corporation - Polyolefins Div.
Danbury, CT

USS Chemicals
Pittsburgh, PA

Valtec
West Boylston, MA

Videx Equipment Corp.
Paterson, NJ

Weber & Scher Mfg. Co. Inc.
Newark, NJ

Western Electric Co.
Springfield, NJ

Whitmor Wire & Cable Corp.
No. Hollywood, CA

Wilson-Fiberfil International
Neshanic Station, NJ

Wireonics Products Company
Winnetka, IL

Witco Chemical Corporation
New York, NY
W.L. Gore & Assoc. Inc.
Newark, DE

Wyre Wynd Inc.
Jewett City, CT
Wyrough and Loser, Inc.
Trenton, NJ
Zumbach Electronics Corp.
Elmsford, NY

TABLE OF CONTENTS

TUESDAY, NOVEMBER 16, 1982—9:30 AM—12:00 PM

Hunterdon and Cumberland Rooms

Greeting: Mr. Theodore Pfeiffer, Technical Director, US Army Communications-Electronics Command, Fort Monmouth, N.J.

SESSION I: FIBER OPTICS AND METALLIC CABLES—PARTNERS OR COMPETITORS

Chairperson: Dr. William Chervenak, Corning Glass Works

Panel Members:

Mr. David McMahon, Director of Marketing, Essex Group Telecommunications Products Division, Decatur, Illinois

Dr. A. G. Vedejs, Lightguide Technology Department, Bell Laboratories, Norcross, Georgia

Dr. M. Biskeborn, Director, Research and Development, Phelps Dodge, Elmsford, New York

Mr. Robert Sweiter, Vice President and Director, Corporation Planning & Development, Siecor, Hickory, North Carolina

Mr. Noel Dean, Director and Chief Engineer of Telecommunications, B.I.C.C., Prescott, Merseyside, England

TUESDAY, NOVEMBER 16, 1982—2:00—5:00 PM

Hunterdon Room

SESSION II: PROCESS AND MANUFACTURING

Chairperson: James Tyler, Essex Group

Dynamic Detecting, Measuring, and Classifying Defects in Telephone Wire Insulation—*T. P. Leahy, P. G. Koehler and T. P. Lichliter*, Western Electric, Omaha, Nebraska. 1

Image Analysis, Microscopic, and Spectrochemical Study of the PVC Dry Blending Process—*R. A. Burley and D. G. Hayashi*, Northern Telecom Canada Ltd., Lachine, Quebec, Canada. 10

The Computer Is In . . . Now Your Troubles Begin—*E. W. Crews*, Western Electric, Phoenix, Arizona. 16

Automated Electrical Harness Manufacturing—*J. W. Tarbox*, Tarbox Developments, San Diego, California. 23

Metal Forming and Inspection Control for Cable Sheathing—*W. D. Bohannon, Jr., and D. E. West*, Western Electric, Norcross, Georgia. 31

Computerization of the Pulp Wire Insulating Process—*V. L. LeNir, W. A. Cascarano*, Northern Telecom Canada Ltd., Lachine, Quebec, Canada, and *M. A. Shannon*, Northern Telecom Canada Ltd., Kingston, Ontario, Canada. 38

TUESDAY, NOVEMBER 16, 1982—2:00—5:00 PM

Gloucester Room

SESSION III: FIBER OPTIC APPLICATIONS AND PERFORMANCE

Chairperson: Paul Dobson, Valtec Corporation

Development and Application of Optical Fiber Composite Overhead Ground Wire (OPT/GW)—*T. Kobayashi, O. Watanabe, K. Inada, A. Okazato*, Fujikura Ltd., Chiba-ken, Japan, *H. Nabeshima, K. Tsujimoto*, The Kansai Electric Power Co., Inc., Osaka, Japan. . . 45

Gamma Irradiation Characteristics of Optical Fibers—*K. Shibuya, K. Yagi, N. Sugiyama, T. Kojima*, Showa Electric Wire and Cable Co., Ltd., Kanagawa, Japan, and *A. Yoshinaga*, Toshiba Corporation, Kawasaki, Japan. 51

Application of VAD Fiber Cable to Commercial Fiber Optic Transmission System (FOTS)—*M. Nishimura, H. Horima, O. Nishi, H. Yokota, S. Suzuki*, Sumitomo Electric Industries, Ltd., Yokohama, Japan, and *M. Iwazaki*, Nippon Telegraph and Telephone Public Corp., Tokyo, Japan. 63

Toll Message Lightguide Transmission Network in Manitoba—*H. K. Eastwood, E. Byzio, K. K. Hau*, Canstar Communications, Scarborough and Winnipeg, Canada, and *J. Petrin*, Manitoba Telephone System, Winnipeg, Canada. 70

Optical Fiber Cable Fastened to Overhead Ground Wire with Lashing Rod—*Y. Shirasaka, K. Fuse, S. Kume, M. Kurokawa, Y. Obara, L. Kimata*, and *M. Yoshizawa*, The Furukawa Electric Co., Ltd., Tokyo, Japan. . . 77

Easy and Practical Evaluation of Optical Fiber's Splices, Graded Index-Multimode, To Be Set Up in Plant—*J. Atn Balbas and J. Daz Cortijo*, Compania Telefonica Nacional de Espana, Madrid, Spain. 89

**WEDNESDAY, NOVEMBER 17, 1982—
9:00 AM-12:00 PM**

Hunterdon Room

SESSION IV: TESTING & APPLICATIONS

Chairperson: Leo Chatter, DCM International Corporation

- Pair Lay Distribution with Regard to Far-End Crosstalk in Symmetric Telecommunication Cable—*C. Tencer* and *A. T. Nogueira*, Pirelli S/A, Santo André, Brazil 98
- Crosstalk, Insertion Loss, Sweep Frequency Analysis and Fixturing for Telephone Cables—*J. S. Golt, Jr.*, Western Electric, Baltimore, Maryland 104
- Comparative Study of Analog and Digital Crosstalk Measurements Methods on Telephone Cables—*J. L. Marinosa*, and *V. Abada*, Cables de Comunicaciones, S. A., Zaragoza, Spain 109
- Field Testers for Assessing 1.5 and 2.0 Mbit/s—Digital Performance of Metallic-Pair Cables—*I. G. Dufour*, British Telecom, London, UK 122
- Open-Circuit Admittance of a Telephone Cable Pair—*R. J. Gerdes*, Continental Telephone Laboratories, Norcross, Georgia, and *J. A. Olszewski*, General Cable International, Inc., Edison, New Jersey 131
- Telecommunication Cables and Power Frequency Induction—*A. Ernbo*, Sieverts Kabelverk, Sundbyberg, Sweden, *G. A. Petersson*, Retired from Swedish Administration of Telecommunications 137

**WEDNESDAY, NOVEMBER 17, 1982
9:00 AM-12:00 PM**

Gloucester Room

SESSION V: FIBER OPTIC TERMINATIONS/CONNECTORS

Chairperson: George Webster, Bell Laboratories

- Fiber Optic Connection System—*B. D. Campbell*, *P. M. Simon*, *J. T. Triplett*, and *R. E. Tylor*, Raychem Corp., Menlo Park, California 149
- On New Cable Accessories for Optical Fiber Cable System—*T. Seike*, *M. Haraguchi*, *Y. Asano*, and *Y. Tokumaru*, Sumitomo Electric Industries, Ltd., Yokohama, Japan 153
- Optical and Mechanical Characteristics of

Microflame Fusion Splicing of Optical Fiber—*B. F. Rondan* and *A. A. Morales*, Centro de Investigación de Standard Eléctrica, S. A., Madrid, Spain 163

Arc-Fusion Splice of Optical Fiber and Its Reliability in Field—*M. Mivauchi*, Research & Development Bureau, N. T. T. Musashino, Tokyo, Japan, *M. Matsumoto* and *T. Haibara*, Ibaraki Electrical Communication Lab. N. T. T. Tokai, Ibaraki, Japan 169

Flat Mass Splicing Process for Cylindrical V-Grooved Cables—*R. Delebecque*, SAT, Paris, France, *E. Chazelas*, SILEC Montereau, France, and *D. Boscher*, CNET-LANNION, Lannion, France 178

Test Results of Multichannel Hermaphroditic Optical Connectors Developed for the US Army—*V. E. Kalomiris*, U.S. Army CECOM, Fort Monmouth, New Jersey 185

**WEDNESDAY, NOVEMBER 17, 1982—
2:00-5:00 PM**

Hunterdon Room

SESSION VI: CABLE DESIGN

Chairperson: Eugene Riley, Anaconda Ericsson, Inc.

Shielding Effectiveness of Composite Metals at Voice and Carrier Frequencies—*L. E. McBride*, *Y. Trenkler*, and *R. G. Delagi*, Texas Instruments, Inc., Attleboro, Massachusetts 193

Structure and Characteristics of Cables for Robots—*A. Yoshizawa*, *T. Maezawa*, and *E. Iwakabe*, The Furukawa Electric Co., Ltd., Tokyo, Japan 198

A Crosstalk Model for Cross-Stranded Cables—*N. Holte*, Electronics Research Laboratory (ELAB), Trondheim, Norway 207

Impedance Irregularities in Telephone Networks—*L. M. Chatter*, DCM International Corp., San Leandro, California 221

Power Sum Crosstalk of PIC Cables as a Function of Cable Design—*J. J. Refi*, Bell Laboratories, Norcross, Georgia 237

**WEDNESDAY, NOVEMBER 17, 1982—
2:00-5:00 PM**

Gloucester Room

SESSION VII: TERMINATIONS/CONNECTORS

Chairperson: John Santos, Phelps Dodge

Instantaneous Cable Sealing Technique:

Theory and Typical Applications— <i>R. H. Keith</i> , 3M Company, St. Paul, Minnesota. . . .	245
Pressure Blocking of Filled Cable— <i>R. J. Pokorny</i> and <i>G. W. Frost</i> , 3M Company, St. Paul, Minnesota.	256
Shield Bonding Terminal for Buried Service Wire— <i>B. Young</i> and <i>D. Lane</i> , AMP Inc., Winston-Salem, North Carolina.	265
Outdoor Connector with Advanced Weather Resistance— <i>M. Meyerstein</i> , Bell Northern Research, Ottawa, Canada.	265
A New Clamp-On Tap for Coaxial Data Networks— <i>J. Fetterolf</i> , AMP Inc., Harrisburg, Pennsylvania.	277
Dropwire Leakage Due to a Faulty Connector: A General Model Based on Radiation from a Circumferential Slot— <i>T. N. Lovern II</i> , Comm/Scope Co., Catawba, North Carolina, and <i>C. M. Butler</i> , University of Mississippi, University, Mississippi.	283

**THURSDAY, NOVEMBER 18, 1982—
9:00 AM-12:00 PM**

Hunterdon Room

SESSION VIII: MATERIALS

Chairperson: William Korcz,
Shell Development Company

Thermodynamic Interactions, Mechanical Properties and Property Retention in Polymeric Wire Coatings— <i>H. P. Schreiber</i> , Ecole Polytechnique, Montreal, Quebec, Canada, and <i>J. Checklund</i> , Northern Telecom Inc., Lachine, Quebec, Canada.	293
Investigation of Premature Depletion of Stabilizers from Solid Polyethylene Insulation— <i>B. L. Board</i> and <i>H. J. Ruddell</i> , Telecom Australia, Melbourne, Australia.	300
Blending of a Block Copolymer Thermoplastic Rubber for Specific Wire and Cable Applications— <i>A. C. Levy</i> and <i>R. Sabia</i> , Bell Laboratories, Norcross, Georgia.	313
Behaviour of Zinc-Coatings on Steel Tapes in Armoured Cables— <i>A. M. J. M. Claassens</i> , <i>A. T. M. Grooten</i> , and <i>J. Rozendaal</i> , NKF Kabel B.V., Waddinxveen, The Netherlands.	320
Test Procedures for Determination of the Radiation Resistance of Cable Materials— <i>E. L. Ney</i> , Siemens AG, Telecommunications Cables, Munich, West Germany, <i>H. Rost</i> and <i>R. H. Knoch</i> , Siemens AG, Telecommunications Cables, Neustadt/Cob., West Germany.	337
Suspension Light Absorption Measurement of Weatherable PVC Compounds— <i>P. C. War-</i>	

<i>ren</i> , Bell Laboratories, Murray Hill, New Jersey.	345
Viscoelastic Analysis of Shrinkback— <i>C. R. Taylor</i> , <i>H. M. Dillow</i> , and <i>C. J. Aloisio</i> , Bell Laboratories, Norcross, Georgia.	350

**THURSDAY, NOVEMBER 18, 1982—
9:00 AM-12:00 PM**

Gloucester Room

SESSION IX: FIBER OPTIC CABLE DESIGNS

Chairperson: Robert Depp, Defense Electronic Supply Center (DESC)

Characterization of Ruggedized Fiber Optic Dual Wavelength Cables— <i>P. S. Venkatesan</i> and <i>K. Korbelak</i> , General Cable Co., Edison, New Jersey.	358
A Refined Tight Design Duct Cable for Low Loss Monomode Fibre— <i>P. G. Hale</i> , <i>M. M. Ramsay</i> , <i>J. G. Titchmarsh</i> , Standard Telecommunication Laboratories Ltd., Essex, England, and <i>D. D. Jones</i> , <i>J. N. Russell</i> , <i>R. C. Townsend</i> , Standard Telephones & Cables, London, England.	371
Design Consideration for Jacketing Fiber Optic Cable— <i>M. M. Rahman</i> and <i>G. M. Davidson</i> , Pirelli Cables Inc., Surrey, British Columbia, Canada.	377
Development of Nonmetallic, Loose-Groove Spacer-Type Optical Fiber Cable— <i>O. Ichikawa</i> , <i>K. Sakamoto</i> , and <i>Y. Saitoh</i> —Sumitomo Electric Industries, Ltd., Yokohama, Japan.	381
Self-Supporting Metal Free Optical Fibre Cable for Large Span Length— <i>W. Schmidt</i> , <i>K. Kimmich</i> , and <i>S. Metz</i> , Standard Elektrik Lorenz AG, Stuttgart, Germany.	390
Design and Performance of a Filled, High-Fiber-Count, Multimode Optical Cable— <i>M. R. Santana</i> , <i>B. R. Fichenbaum</i> , <i>L. D. Tate</i> , and <i>R. Sabia</i> , Bell Laboratories, Norcross, Georgia.	396

**THURSDAY, NOVEMBER 18, 1982—
2:00-5:00 PM**

Hunterdon Room

**SESSION X: FIRE, SMOKE, AND TOXICITY
CONSIDERATIONS**

Chairperson: Austin Wetherell
Underwriters Laboratories

Flame Retardant Halogenfree Thermoplastic Telecom Indoor Wiring— <i>H. G. Dageforde</i> , <i>W.</i>	
---	--

Berchem, and *H. A. Mayer*, AEG-Telefunken Kabelwerke AG, Möchengladbach, West Germany..... 401

Large Scale Fire Tests of Building Riser Cables—*S. Kaufman* and *J. L. Williams*, Bell Laboratories, Norcross, Georgia, *E. E. Smith*, Bell Laboratories, Norcross, Georgia, and Ohio State University, Columbus, Ohio, and *L. J. Przybyla*, Underwriters Laboratories, Northbrook, Illinois..... 411

A New Flame Resistant, High Temperature, Cross-Linked Polypropylene Compound Insulated Wire—*H. Suzuki*, *T. Katahira*, *N. Sato*, and *K. Ishi*, Fujikura Ltd., Chiba-ken, Japan... 417

A Comprehensive Small Scale Smoke Test—*R. H. Whiteley*, Raychem Ltd., Swindon, England..... 427

A New Construction of Halogen-Free Flame Retardant Insulated Wire with Double Layers—*S. Yamamoto*, *M. Nishimura*, *A. Satou*, *H. Nakae* and *S. Fujimura*, The Furukawa Electric Co., Ltd., Tokyo, Japan... 437

THURSDAY, NOVEMBER 18, 1982—
2:00-5:00 PM

Gloucester Room

SESSION XI: FIBER OPTIC MEASUREMENTS

Chairperson: William Červenak
Corning Glass Works

Bandwidth Characterization of Fiber Waveguide Systems with Fusion-Spliced Multimode Graded-Index Fibers—*E. W. Riley*, Anaconda-Ericsson, Inc., Overland Park, Kansas..... 444

Pure-Silica Core Optical Fiber and Fiber Cable for Radiation Fields—*H. Tanaka*, *T. Hirashima*, and *T. Shintani*, Dainichi-Nippon Cables, Ltd., Tokyo, Japan..... 452

Radiation Effects of Optical Silica Fiber and Radiation Hard Optical Transmission—*H. Yoshida*, *T. Suematsu*, and *K. Sanada*, Fujikura Ltd., Tokyo, Japan..... 459

Design and Test Results of an Optical-Fiber Submarine Cable—*Y. Ejiri*, *M. Nunokawa*, *K. Furusawa*, and *Y. Niino*, KDD Research and Development Laboratories, Tokyo, Japan... 466

Computer Controlled Optical Time Domain Reflectometer Monitoring of Lightguide Cable Installations—*A. F. Judy*, *R. E. Fangmann*, *M. J. Swiderski*, Bell Laboratories, Norcross, Georgia..... 473

Practical Instrumentation for Fiber Optic Evaluation—*P. Wendland*, Photodyne Inc., Newbury Park, California..... 476

DYNAMIC DETECTING, MEASURING, AND CLASSIFYING DEFECTS
IN TELEPHONE WIRE INSULATION

T. P. LEAHY, P. G. KOEHLER AND T. P. LICHLITER

Western Electric Company
Omaha, Nebraska 68137

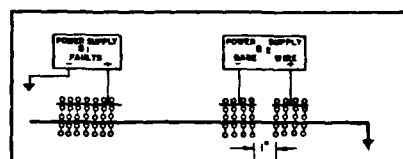
This paper covers a study of insulation defects and a system that will dynamically measure them. The system uses a planar probe which is electronically adjusted to be two dimensional, normal to the path of the wire. The system consists of two sets of user-set programmable comparators which allows the defects to be classified into three categories: pinholes, faults and bare wire.

The system counts and displays the number of each category of defect that appears on a reel of product. Also displayed is the length of the last defect encountered, the length of the product produced, the velocity of the production operation and the voltage applied to the probe.

All information displayed is available in binary coded decimal format to allow for data acquisition. This system may be used on any insulated conductor or group of conductors. Verification methods and accuracy results are included.

to detect and classify defects in insulated wire by the manufacturer. The state of the art on wire test systems remained static for many years primarily due to the excellent quality of the test systems produced by the test set manufacturers.

The basic test system used to assure the insulation quality of telephone wire consisted of a set of two power supplies and three distinct beaded chain electrodes.



A DEFECT IN THE INSULATION PASSING THE BEADED CHAIN ELECTRODE OF VOLTAGES SOURCE #1 WILL GROUND THROUGH THE WIRE AND GIVE THE INDICATION OF A FAULT. IF THE DEFECT IS ONE INCH OR MORE AS IT PASSES THROUGH THE BEADED CHAIN PROBES OF VOLTAGE SOURCE #2 IT WILL COMPLETE THE CIRCUIT AND GIVE THE INDICATION OF A BARE WIRE.

BACKGROUND

Since antiquity, the requirement that the insulation be continuous on telephone wire has remained unchanged. This has been further clarified to state that if the insulation or lack of insulation will pass a current from a relatively high voltage to the conductor, an insulation defect exists. These electrical insulation defects were classified into two categories:

1. Bare Wire - A defect that renders the wire unusable and defined as an insulation defect one inch or greater in length.
2. Fault - A serious defect that by itself does not render the wire unusable and defined as an insulation defect less than one inch in length.

It is virtually impossible to make perfect wire in extremely large quantities over a continuous period. The requirement would allow no bare wire; but, depending on the use of the wire, a small number of faults would be acceptable over a given length. This definition and these requirements were based upon a trade off of the needs for quality by the telephone companies and the ability

Figure 1

The use of free swinging beaded chains dictated a minimum separation of 1" between the electrode parts of the bare wire detector probe. This eliminated the possibility of beaded chains from one-half the probe coming in contact with the other half, thereby giving a false indication of bare wire.

During the period of the late 1970's, it was noted that there was a large number of field complaints due to wire shorting to the bays in which it was installed. A study of these defects revealed that the vast majority of them were under one inch but over 1/4 inch. At this time, it seemed apparent that the requirements were not sufficient to meet the quality desired by the telephone companies.

The following plan was initiated to improve the quality of the loose wire and to meet the actual requirements of the users:

1. Determine the actual defects that are produced in the wire by the production process.

2. Develop a test set more sensitive to the size of the defect.
3. Develop requirements that meet the needs of the telephone companies.

STUDY OF ACTUAL DEFECTS

The study of actual defects was necessary to determine the existing process capability and to allow a cost estimate of tighter requirements. The amount of process conformance scrap generated by these requirements would have to be added to the cost of the product produced.

The frequency of defects per thousand conductor feet of wire, separated into defects under one inch (faults) and defects one inch or over (bare wire) was a known factor. Records on these defects are maintained for each production operation. This information, although valuable, does not give the complete picture required for this investigation. The exact size of the defects, as well as their placement on the reel, was also desired.

To determine both these factors, a physical measurement of all defects and their position in the reel would be necessary. To gather all the data deemed necessary, the following ground rules were used:

1. The study would be restricted to loose irradiated wire which was the primary product of interest.
2. The study would be done subsequent to irradiation but prior to coiling. The plastic undergoes a physical change to final form at irradiation. The wire would be on reels at this point which would facilitate handling. At coiling, the wire would be in loose coils.
3. Approximately five million feet of product, apportioned by gage and type of wire would be examined. This would equate to one reel per pallet produced during the period of the study.
4. One repair rewinder would be modified and dedicated for the period of the study.
5. The equipment used would include:
 - a. One wire rewinder.
 - b. One test set with beaded chain electrodes.
 - c. A modification to the above equipment that would stop the rewinder at any defect that was encountered.
 - d. A 100 volt, direct current, source connected to a hand-held wand for pinpointing the defect.



Equipment Used for Study

Figure 2

6. Each defect, when pinpointed, would be measured to the closest 1/16 of an inch or classified as a pinhole, if not visible to the unaided eye. These measurements would be recorded along with its length from the outside end of the reel. In addition, the product type, gage, total length of product on the reel, and formation of product; i.e., single, pair, or triple wire would be recorded.

This study was done by the statistical quality control organization and was restricted to first shift operation to allow for engineering audit.

The results are summarized in Figure 3. Since a majority of the defects are too small to be measured, they were placed in a separate category entitled "Pinholes."

PRODUCT	GAGE	NUMBER OF REELS	TOTAL FOOTAGE	PINHOLES	DEFECTS FAULTS	BARE WIRE
DP-2	22	37	806,400	458	54	0
DP-2	24	28	736,000	61	0	0
DP-2	26	31	493,500	25	0	2
DT	20	17	241,000	55	2	2
DT	22	51	2,084,200	256	10	9
DM	24	30	1,297,200	174	34	2
DW	26	8	794,000	45	5	1
TOTALS		202	6,452,300	1,074	105	16

Figure 3

From Figure 3, it can be seen that the defect per thousand conductor feet was at a rate of 0.1852 or approximately one defect per 5000 feet of wire produced. A percentage of the total number of defects falling into each classification is shown in Figure 4.

Type of Defect	Percentage of Total
Pinhole	89.87
Fault	8.79
Bare Wire	1.34

Figure 4

A breakdown of the defects by actual size can be seen in the following bar chart. (Figure 5)

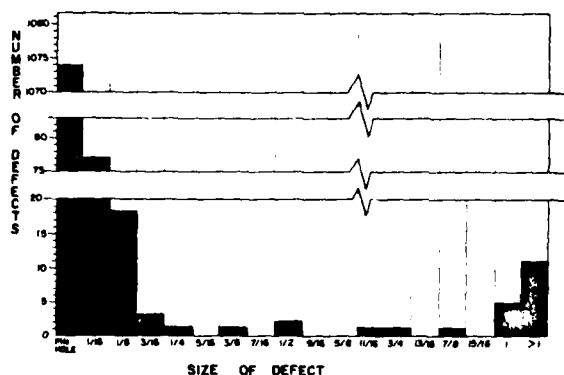


Figure 5

Figure 5 shows a vast majority of the defects are extremely small. There would be virtually no noticeable increase in product conformance cost by reducing the definition of a bare wire to "an electrical defect where copper conductor is visible to the unaided eye and one quarter of an inch or greater in length." This would change the percentage of defects falling into each classification as shown in Figure 6.

Type of Defect	Percentage of Total	Increase
Pinhole	89.87	0
Fault	8.28	(0.51)
Bare Wire	1.85	0.51

Figure 6

Over 30% of the defects appear in either the first or last 100 feet of the reel. This wire will normally be removed from the reels as remnants prior to the final coiling operation and will further reduce the effect of the tighter requirements.

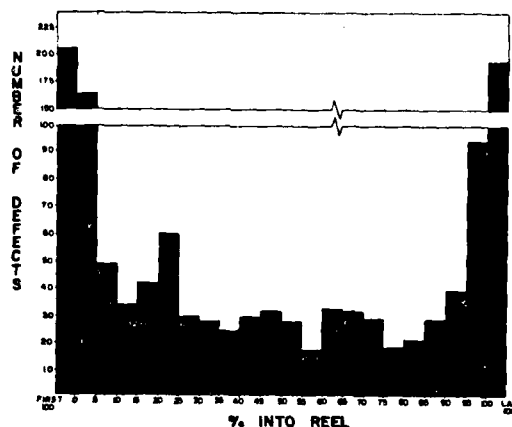


Figure 7

The results of this study will allow the tightening of requirements on loose wire. The new requirements will reduce the problems encountered by the users due to distributing frame wire shorts. In addition, if the new requirements recognize the pinhole as distinct from the fault, a substantial savings could be realized which would help offset the ever-increasing cost of manufacturing this product. This savings would flow through to the customer by holding future increases in prices.

Contact was made with the Product Engineering Control Center (PECC) to coordinate a set of new requirements for loose irradiated wire. The updated requirements would have to meet the needs of the telephone companies and the users within Western Electric as well as receive the approval of the Bell Telephone Laboratories (BTL). Studies by both PECC and BTL confirmed what had been gleaned from the field installers. Over 95% of the problems encountered in loose wire by the users were the result of defects in the insulation in excess of 1/4 inch. No known problems were associated with pinholes.

BTL and the users of this wire were in accord with Western Electric manufacturing in changing the definition of a fault from a defect in the insulation with a length under one inch to a defect in the insulation with a length under 1/4 inch. The definition of a pinhole was added at the product engineer's insistence to allow a closer shop control on the extrusion process. The definitions agreed upon were:

- Pinhole - A defect in the insulation where the conductor is not visible to the unaided eye.
- Fault - A defect in the insulation where conductor is visible to the unaided eye but less than 1/4 inch in length.
- Bare Wire - A defect in the insulation where conductor is visible to the unaided eye equal to or greater than 1/4 inch in length.

To facilitate the implementation of the new requirement on bare wire, BTL and PECC offered Western Electric a more liberal amount of smaller defects allowed per unit length of wire. This would help offset the cost of implementing these new requirements. The new requirements would not go into effect until such time as Western Electric could develop the test equipment necessary to assure PECC that these new requirements would be followed.

The proposed definitions stated above were a first approximation compromise between what the user wanted and what was believed possible for a production operation. A decision was made that the point of separation between a pinhole and a fault, as well as a fault and a bare wire, should be programmable in the test set. Thus, the test system could remain a viable unit as the extrusion process improved and the requirements changed over the foreseeable future.

METHODS OF MEETING NEW REQUIREMENTS

Normal methods of detecting the defects would be used in this system. In brief, a voltage would be applied to the product and when a defect was present a current would flow from the probe through the wire to ground. A current-controlled device, a switching transistor, would detect the current to show the defect.

The initial design specifications primarily were to measure defects to within one-tenth of an inch. This measurement would allow separation of the defects into one of the three categories. Using the measurement portion of the system, the length of the product produced is known and integration of this length over time yields the velocity of the wire. The voltage applied to the product is variable to allow for different gages and insulation types.

Length would be measured by contact means, that is, a very accurately constructed wheel with known circumference. The wire or wires would pass around the wheel and each rotation or portion of rotation could be detected.

The current flow between the probe and the wire exists whenever the defect is within the probe. This limits the accuracy of the system to the thickness of the probe normal to the wire. The width of the probe must approach a two-dimensional plane.

THE PLANAR PROBE

To develop a probe which approached a plane, there were constrictions from two sides. On one hand, the probe had to be extremely thin so as to reduce as much of the design error as possible. On the other hand, it had to be thick enough to provide physical strength to withstand everyday use including current burn when large defects passed through it, as well as the constant friction of the wire.

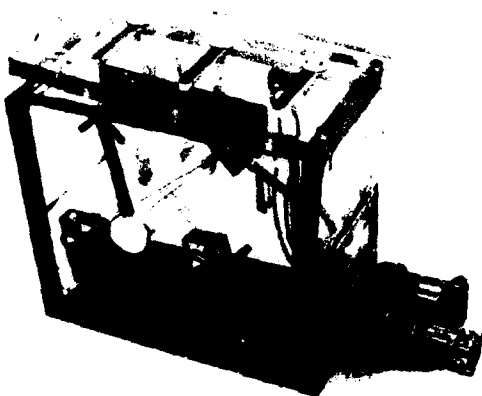
This unit would have to be fairly flexible. The probe must encircle the product at the closest proximity from single 26 gage wire up to four twisted 19 gage wires. In addition, the unit must be shop usable; that is, easy to string up for the operator and easily maintained.

Among the methods studied, the one chosen consisted of four select fingers taken from a number four crossbar small switch. These spring fingers are constructed of .022" diameter stainless spring wire and are approximately 2 inches long with a coiled spring section approximately 3/8" long on one end. A dampening spring is used to maintain better contact with the wire being tested. The fingers are set 90° apart to provide an encirclement of the wire by placing one finger on each quadrant of the wire.

Each spring finger is set to be overcompensated so that it will contact even the smallest gage wire to be tested. This overcompensation will also accommodate a slight misalignment as well as wire vibration. The spring action will allow a knot, when one reel of wire is tied to the next, to pass through the probe without damaging it.

To facilitate string-up, one-half of the probe is fixed and the other half is attached to the probe box door. When the probe is opened, the top half is moved away from the path of the wire. A slot in both sides of the probe box allows the wire to be easily seated in the probe.

The probe box is constructed of polycarbonate plastic to provide a more than adequate dielectric strength to protect the operator from the high voltage. The polycarbonate which is transparent will allow a visual examination of the status of the probe with respect to the product.



Planar Probe
Figure 8

LENGTH AND VELOCITY MEASUREMENTS

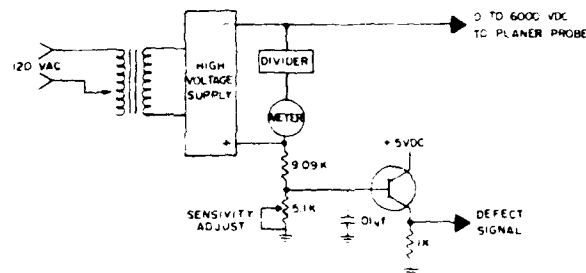
The measurement of length is made by running the wire around a wheel with a two-foot circumference adjusted for a 22 gage wire. The wheel is connected to an electro-optical transducer by means of two timing belt pulleys and a timing belt. The electro-optical transducer produces 1000 pulses per revolution and the pulleys provide a ratio of 5:12 which results in an output of 1200 pulses per foot or 100 pulses per inch. This signal is provided to a gated circuit which is controlled by a current flow signal from the probe. When a defect is detected by the probe, the pulse train from the transducer is released and counted. The count is the length of the defect in hundredths of an inch.

The transducer signal is also supplied to a divider circuit. One function of this circuit is to divide the pulse train by 1200. The resulting signal is the length of product produced in feet. The other function of the divider circuit is to divide the incoming pulse train by 12, thereby producing 100 pulses per foot to the velocity circuit. The velocity circuit consists of a one megahertz crystal oscillator and a divide by 600,000 subcircuit to produce an accurate one hundredth of a minute signal. The 100 pulses per foot input are counted, latched and displayed by

the one hundredth of a minute signal giving the velocity display in feet per minute.

DEFECT DETECTION

The voltage supplied to the probe is variable from 0 to 6000 volts to allow for all sizes of wire and insulation. This is accomplished by a variable transformer on the input side to the high voltage power supply.



Detection Circuit
Figure 9

The current flow signal is taken from the positive or ground side of the high voltage power supply. This side of the high voltage power supply is held above ground by a variable resistor which is used to control the sensitivity of the detector. This defect signal is supplied to the base of a switching transistor.

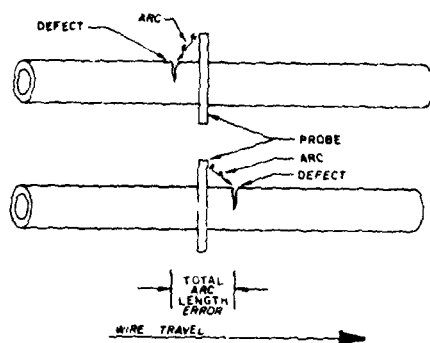
When current flows in the circuit, the transistor is turned on hard. The transistor output signal is very noisy and not acceptable as a digital signal. The signal, therefore, is treated by succeeding Schmidt triggers.



Raw Signal Conditioning
Figure 10

SIGNAL CORRECTION

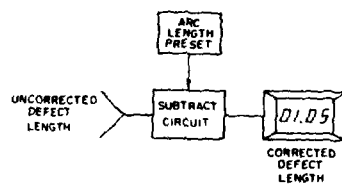
In the initial test stage of the prototype prove-in, a large constant error in defect length was noted. Defects being measured by the unit were approximately 1/4 inch larger than actual size. Close observation of the probe as the defects passed it revealed that the arc reaches out to the defect prior to the defect reaching the probe and the arc persists until the defect is past the probe.



Arc Length Error

Figure 11

The measurement of the defect is the length of the arc. The arc is in error by the length of the pre-firing of the arc, the width of the probe and the persistence of the arc after the probe. The above error remained constant within ± 0.03 inches for fixed hardware. Therefore, a circuit was designed to allow for a subtracting of this error. The corrected defect length is then supplied to the defect length display.



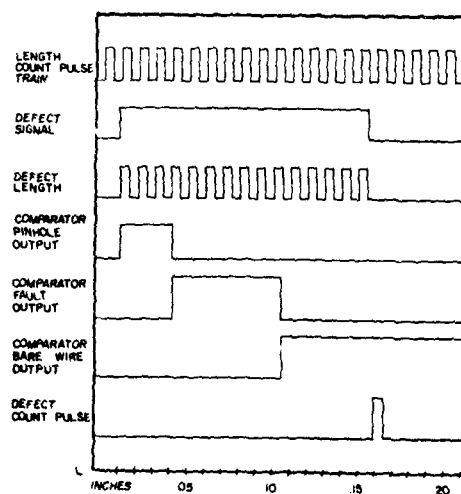
Arc Length Correction Circuit

Figure 12

It must be noted that the total arc length error will vary if either the probe or the high voltage supply is changed.

VARIABLE DEFECT SEPARATION

The corrected defect length is supplied from the display to a defect length comparator. The comparator also receives data from two sets of pre-sets: (1) separation point between pinhole and fault and (2) separation point between fault and bare wire. Since the defect length is being displayed while it is being measured, the displayed length will be increasing from zero to the final measurement. During the period that the defect is smaller than the separation point between a pinhole and fault, the comparator will indicate a pinhole and when the display is within the area of a fault, a fault will be indicated. Therefore, when the defect is a bare wire, a pinhole will first be indicated; then the pinhole indication will be removed when the length is in the fault area and a fault will be indicated. When the separation point between a fault and a bare wire is passed, the fault indication will be removed and a bare wire indication will result. The unit is completely asynchronous to allow for high speed flow-through of defect indications. If the defects were counted from the comparator one pinhole, one fault and one bare wire would be indicated for each bare wire. A pinhole and a fault would be indicated also for each fault measured. To eliminate the above, a retriggerable multivibrator was used. The negative edge of the positive defect signal produces a delayed pulse which counts the final state of the comparator circuit.



THE ABOVE TIMING DIAGRAM SHOWS (A) THE LENGTH COUNT PULSE TRAIN EACH PULSE 0.01 INCH (B) DEFECT SIGNAL (C) DEFECT LENGTH - 1.5 INCHES (D) COMPARATOR OUTPUT SIGNALS WITH PINHOLE MAXIMUM 0.3 INCHES, FAULT MAXIMUM 10 INCHES (E) DEFECT COUNT PULSE FIRED ON TRAILING EDGE OF DEFECT SIGNAL THIS WILL RESULT IN THE BARE WIRE COUNT BEING ADVANCED BY ONE

Figure 13

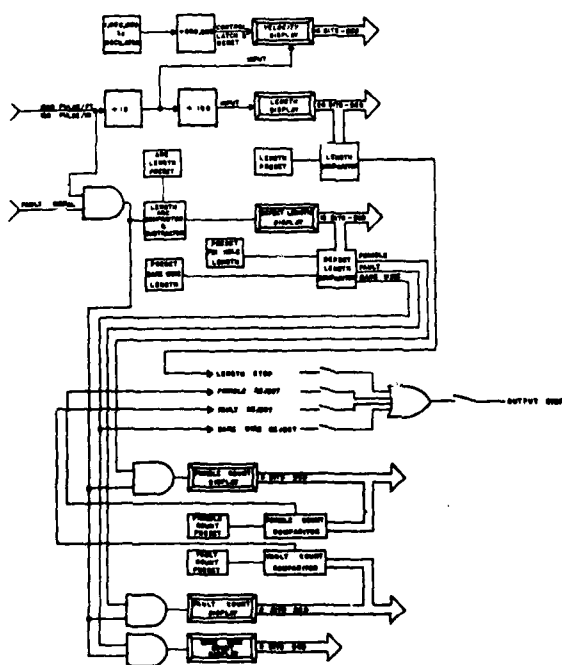
DEFECT COUNTING

A separate count of each type of defect must be maintained to determine the acceptability and quality of each reel of wire. Output information must be available not only whenever a bare wire is detected but also for a predetermined number of faults or a predetermined number of pinholes. The pinhole and fault count data is supplied to separate comparators which are also supplied with adjustable presets of the number of pinholes and faults that are acceptable within a reel. This provides a reject signal of 110 V AC whenever a bare wire or an unacceptable number of either pinholes or faults exist on a reel. This signal can be used to either stop the process or alert the operator to the status of the reel of product.

A "length stop" signal is also available for use to stop or automatically change the take-up reel and can be used for an automatic reset of the stored data. Any combination of the (1) length stop, (2) bare wire reject, (3) fault reject or (4) pinhole reject can be selected by switches to activate the 110 V AC output signal. In addition, the pinhole and fault reject can be user set from 0 to 99.

TEST SYSTEM OUTPUTS

All information gathered by this system is available in binary coded decimal format on a real time basis on one data plug. Also available on a real time basis are signals for either a pinhole, fault, or a bare wire to allow for a data acquisition unit to record type of defect and footage on the reel to simplify repair.

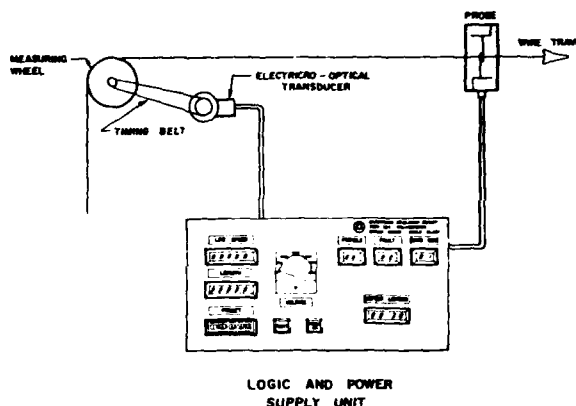


Block Diagram
Figure 14

RESULTS

Final Packaged Unit

The final unit consists of three parts: (1) the wire measuring apparatus, (2) the high voltage planar probe and (3) the logic and power supply unit.



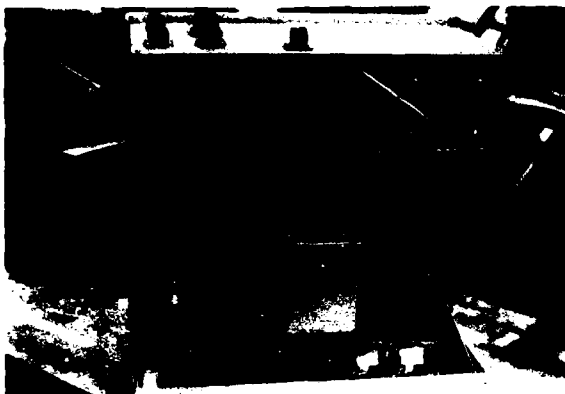
Electrical Insulation Defect Test Set
Figure 15

The wire measuring apparatus as described under "Length and Velocity Measurements" consists of a two-foot circumference measuring wheel, gear and timing belts, and an electrical optical transducer which converts the measured length to a digital signal for use by the logic power supply unit.

The planar probe is 6" x 6" x 4" in size and supplied with high voltage from the logic and high voltage supply unit. A high voltage interlock system is included to remove the voltage from the probe if the unit is opened.

The logic and power supply unit is approximately 18" x 18" x 8" in size. This unit contains all the controls and presets of the system. The only controls readily available to the operator are the footage preset, power "on" button and the reset button.

The internal controls are: pinhole to fault separation, fault to bare wire separation, arc length preset, pinholes allowable, faults allowable, sensitivity, local/remote reset, length stop on/off, pinhole reject on/off, fault on/off, bare wire reject on/off, output stop on/off, and voltage setting.



Top View of Logic and Power Supply Unit
Figure 16

ARC LENGTH ADJUSTMENT

The arc length error is dependent upon:

1. The high voltage supply
2. The current limiting components
3. The probe architecture
4. The interconnecting circuitry

Rather than attempting to measure the effect of each portion separately, it was easier to determine the total error. Several reels of 20 Gage steel wire with copper coating were prepared with hand produced defects of known lengths at known intervals. The arc correction was set at zero and these sample reels were tested on the system. The actual lengths of the defects were compared to the system measured length and from this a correction was obtained. This error was then applied at the arc correction. The sample reels were again run and the errors plotted. The actual defects ran the range from 0 to 2.00 inches in 0.1 inch increments. Approximately thirty of each size defect were used. The worst case error was 0.11 inches with the average being 0.06 inches. The error increased proportionately to the length of the defect. This was expected since the longer the arc was held the greater the heat produced by the current flow.

VERIFICATION

On-line verification and prove-in of individual units does not require the above procedure. In most instances, the area of primary consideration is the point of separation between the fault and bare wire. This is the point at which maximum accuracy is desired. With the system installed and the arc correction set to 0.00 a measured defect is placed on the product. This defect is then run through the system. The defect measurement displayed in the defect length window is then compared to the actual length to produce the arc correction. In actuality, this should be accomplished approximately ten times and an average used. In addition, the standard deviation should be calculated to provide the accuracy of the

installed system.

At the Omaha Works, the arc correction is determined around the area of 0.25". The arc corrections vary on these units from 0.09" to 0.23" with the average at 0.17". All systems are verified to an accuracy of approximately 0.06".

All test systems at Omaha are being verified once a month. Results recorded proved that this was not necessary and that once a quarter would be more than sufficient. It should be noted that scheduled verification of the units will not suffice if components are changed. Any change in components requires a reverification of the unit prior to the systems being used for production.

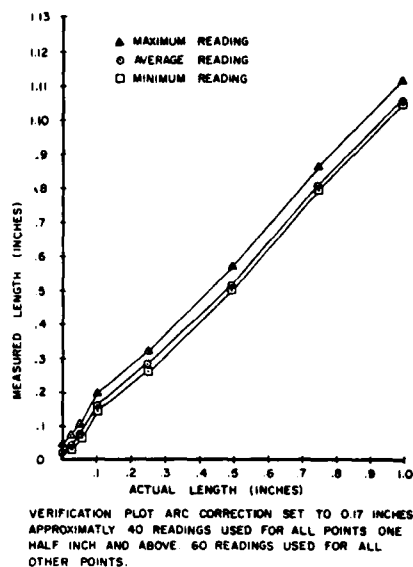


Figure 17

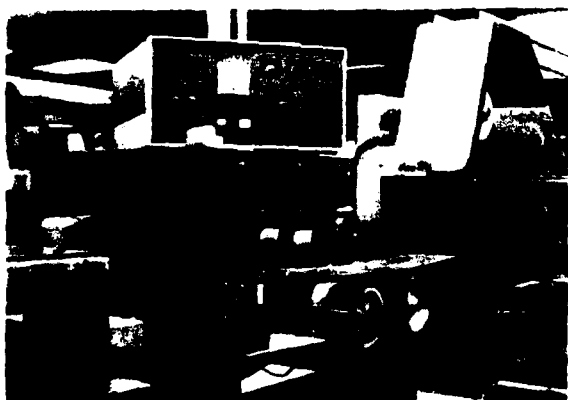
USES

The system is designed to measure and detect defects accurately over a range of speeds from zero to ten thousand feet per minute. At the higher range of this speed, defects not separated by approximately 1/4 inch will be counted as a single defect.

In addition, this system can be used with any type of wire regardless of insulation. Presently, the unit is used only on irradiated polyvinyl chloride insulated wire at Omaha. Although as more units are constructed, dual insulated polyethylene wire will be included. The use on IPVC wire has proved extremely successful on not only single wires but also on up to four wires twisted together.



Unit installed on IPVC Rewinder
Figure 18



Unit installed on Coiler
Figure 19



THOMAS P. LEAHY

Mr. Leahy received his BSEE from the University of Wyoming in 1969 and joined Western Electric at the Omaha Works. In 1975 he received his MSEE from the University of Nebraska and is presently assigned as a senior engineer in test set design for the Omaha cable plant.



PAUL G. KOEHLER

Mr. Koehler received a Bachelor of Science degree in mechanical engineering from North Dakota State University in 1969. A member of Tau Beta Pi and Pi Tau Sigma, his previous primary assignments included stranding and cabling, screened cable and twisting. He is currently a product engineer in plastic insulating.



T. P. LICHLITER

Mr. Lichliter received his Associate of Science degree in electronics from Central Technical Institute, Kansas City, and joined Western Electric in 1967. As an engineering associate his primary assignments have been with product test facilities.

AD P000539

IMAGE ANALYSIS, MICROSCOPIC, AND SPECTROCHEMICAL STUDY OF THE PVC DRY BLENDING PROCESS

R.A. Burley
D.G. Hayashi

NORTHERN TELECOM CANADA LIMITED
Lachine, Quebec Canada

ABSTRACT

The dry blending process used in the production of electrical grade pvc formulations has been studied using a combination of image analysis, microscopic, and spectrochemical techniques. The effects of raw materials, mixing time and temperature, and order of addition were evaluated with respect to the quality of the dry blend and the final product.

Changes in particle size distribution at various stages of the dry blending process were followed by image analysis techniques. Optical and scanning electron microscopy were used to assess morphological differences. Spectrochemical techniques were used to indicate chemical changes.

The properties and quality of dry blends were found to depend strongly on mixing time, mixing temperature, and order of addition.

INTRODUCTION

The dry blending process is the first step in the manufacture of many electrical grade PVC formulations. Although the process has been in use for some time and is widely used, operating parameters have been developed on an empirical basis, and there appears to be very little published information on the physical and chemical changes which occur during the process.

The objective of the present investigation was to apply the comparatively new technique of image analysis to study changes in the particle size distribution (PSD) of PVC granules during the dry blending process and to attempt to relate these findings to the quality of the dry blend and of the PVC formulations used as wire and cable insulations and jackets. Optical and scanning electron microscopy (SEM) were also used to study physical and morphological changes; spectrochemical techniques were used for analytical purposes and to detect chemical changes.

DESCRIPTION OF EQUIPMENT

Dry blending trials were performed with a laboratory scale Henschel mixer (Prodex Corp. Model 2-JSS, 22.9 cm diameter, 22.9 cm deep; volume 9,430 cm³). The mixer had no provision for temperature control. Heating of the charge was governed by mixing time and intensity.

The image analysis system was supplied by Cambridge Instrument Co. and consisted of a Quantimet 720/33 image analyzer equipped with a Vidicon scanner, a Digital PDP 11/03 data processor and LA 36 DEC writer II printer. The optical microscope used with this system was a Carl Zeiss Universal model with a stabilized power supply for the illumination sources.

The spectrometric equipment used included a Philips Electronics X-ray spectrometer and X-ray diffraction apparatus, and a Perkin-Elmer Model 225 infrared spectrophotometer.

The scanning electron microscope (SEM) was a JEOL Model No. JSM35C.

APPLICATION OF EQUIPMENT

Experimental dry blends were prepared in the Henschel mixer using charges of PVC powder ranging from about 1,000 to 2,000 g. Motor speeds up to 3,600 rpm were used. As the temperature increased with mixing, the motor was stopped at various temperatures up to 115°C to sample the dry blend with a long-handled spoon. The samples were immediately shaken with an approximately equal volume of powdered dry ice to prevent caking, then air dried and stored for subsequent examination.

Image analysis measurements on the dry blends were performed with the microscope operated in the reflection mode. The sample was sprinkled onto a front surfaced plane mirror to provide good optical contrast between the white particles and the bright background. The PSD was measured over the range of 50 to 450 μm in increments of 20 μm , which covers the range representing the bulk of the PVC. The lower limit of 50 μm was selected in order to eliminate the measurement of individual particles of fillers, stabilizers, etc. which usually have a chord size of less than 5 μm ; it also reduces the level of the "noise" component of the measurement. The PSD was displayed on the printer as a histogram along with the numerical data.

XRD and XRF measurements were made on specimens cut from 1.8 mm thick slabs after milling and molding the dry blends. Infrared transmission spectra were obtained from hot pressed thin films (about 0.05 mm thick) prepared from the slabs.

SEM examination was performed on fracture surfaces of the slabs. Backscattered electron images were used for the photomicrographs.

RESULTS AND DISCUSSION

1. PVC Resin Raw Material

Some salient data from PSD measurements on three raw material PVC resins from two different suppliers are summarized in Table 1. Information from the supplier of resins A and B stated that typical average particle sizes for these resins were 138 μm and 136 μm respectively. These values are in good agreement with the mode values (peak of PSD curve) shown.

Note also that the mean chord value for resin B is slightly less than that of A, in agreement with the supplier's indication of slightly smaller particle sizes for resin B. These results, along with reasonable agreements between actual sieve analyses and analyses calculated from image analysis measurements, inspired confidence in the validity of the new technique.

2. PVC Resin and DOP Plasticizer Dry Blend

Table 2 shows some of the salient data from PSD measurements made on dry blends containing only PVC resin and DOP plasticizer (75% PVC/25% DOP). Data for the raw material resin is included for comparison, as well as data for the resin after Henschel mixing (to 75°) but before the addition of plasticizer.

The results indicate only a minimal breakdown of the PVC resin alone by mixing to 75°C. The amount of material in the lowest size range increased very slightly and the "tail" of the distribution curve at the large size end moved to a slightly lower range. The mean chord and mode were unaffected.

As might be expected, the addition of plasticizer between 75 and 80°C resulted in a sudden general increase in particle size due to swelling of the granules by absorption of the plasticizer. This is shown by the significantly higher values for mean chord and mode, as well as by the decreased numbers of the smallest particles and the movement of the "tail" back into the 245 - 265 μm range.

With further mixing and increasing temperature there was a gradual general decrease in particle size and the PSD stabilized in the 100 - 115°C range to give a PSD very similar to that of the original raw material resin. The results suggest that, under the conditions of this experiment, there was an equilibrium established between the growth of granules by agglomeration and breaking of the granules by attrition of the mixing action.

3. Dry Blend of PVC Resin, Stabilizer, Filler, and Plasticizer

A dry blend having the composition shown in Table 3 was prepared by mixing all of the ingredients except the plasticizer until the temperature reached 75°C. A sample was removed at this point, and then mixing was continued with the addition of the plasticizer. Additional samples were taken when the temperature reached 80°, 90°, and 100°C.

Figure 1 shows the mean chord size of the dry blend plotted vs. the mixing temperature (or time). Results for the PVC-DOP dry blend (unfilled) described in section 2 above are also included. Comparison of the two sets of results indicates the following:

a. The mean chord size of the resin particles in the filled formulation shows a distinct decrease during the mixing period before the addition of plasticizer. The unfilled formulation does not show this effect. This result indicates that the inorganic filler and stabilizer have an abrasive action on the PVC granules during this period. The proportion of smaller particles (in the 50 to 70 μm range) also increased dramatically (from 2.2 to 19.5%) at this period of mixing, indicating the formation of debris from the larger granules.

b. The addition of plasticizer causes a larger increase in mean chord size in the filled formulation. There are two possible explanations for this effect:

- (i) The granules may be enlarged because of the incorporation of filler and stabilizer as well as plasticizer.
- (ii) Swelling of the granules may be greater because of the higher plasticizer/resin ratio in the filled formulation (about 1:2 instead of 1:3 as in the unfilled material).

c. Both formulations show the gradual decrease in mean chord size with continued mixing after the absorption of plasticizer. Unfortunately, the experiment with the filled formulation was not carried on long enough to determine whether or not it would show the stabilization of mean chord size observed in the unfilled formulation.

4. Order of Addition of Stabilizer

The simple formulation shown in Table 4 was used to study the effects of changing the order of addition of the stabilizer. In one case the resin and stabilizer were mixed together to 75°C before the addition of plasticizer ("front loading"); in the other case the stabilizer was added after the absorption of plasticizer by the resin ("back loading"). Some difficulty was experienced with caking of the "front loaded" dry blend in the Henschel mixer after addition of the plasticizer.

Salient features from the PSD measurements on the dry blends are summarized in Table 5, with the raw material resin included for comparison. The data indicate a slightly larger particle size in the front loaded blend.

When the dry blends were milled and molded into slabs, it was noted that the "front loaded" material was pale beige in colour, indicating the possibility of some resin decomposition. The "back loaded" material had a normal "off-white" colour.

Since trouble with caking had been experienced with the beige material, it was suspected that some of the stabilizer may have been lost, resulting in decomposition of the resin. Quantitative comparison of the lead contents of the two slabs by X-ray fluorescence analysis showed that this was not the case; their lead contents were practically identical.

A comparison of the infrared spectra of the "front" and "back loaded" materials showed that bands due to water of hydration and to the ionized carboxyl group of the dibasic lead phthalate stabilizer were significantly weaker in the "front loaded" material. Quantitative comparison indicated that about 25% of the stabilizer had been decomposed. This degree of decomposition was considerably greater than that resulting from heat aging the same specimens at 100°C for 7 days (ASTM Method D-1870).

A comparison of the X-ray diffraction (XRD) patterns of the "front" and "back loaded" materials also indicated significant decomposition or breakdown of crystal structure of the stabilizer. The intensity of the strongest XRD peak of the stabilizer (at about $7^\circ 2\theta$ using Cu K α radiation) in the "front loaded" material was only about 25% of that of the "back loaded" material. The indications of severe reduction in crystallite size were confirmed by microscopic examination (see below).

Examination of hot pressed thin films with the optical microscope showed that the "front loaded" material appeared to contain fewer and smaller needle-like crystals of the stabilizer than the "back loaded" sample. The differences in microscopic appearance were shown more vividly by SEM examination (see Figs. 2 a and 2 b). The SEM results show that the crystals of stabilizer were broken down much more severely in the "front loading" procedure and that many of the particles were smaller than the limit of resolution of the optical microscope (about 0.5 μm).

CONCLUSIONS

1. The results of this preliminary study show that the technique of image analysis can provide useful information concerning the particle size distributions of PVC resins and the changes which occur during the dry blending process. Present results were confined to the particle size range characteristic of the PVC granules, but the results indicate that future studies using electron microscopy may be of value in determining the size distribution changes which take place in the fillers and stabilizers during dry blending.

2. PVC granules undergo the following changes during a normal dry blending operation:

a. Slight attrition before addition of plasticizer. This effect is promoted by the presence of inorganic components.

b. Sharp increase in size due to plasticizer absorption.

c. Gradual reduction in size due to attrition by mixing.

d. Stabilization of particle size due to equilibrium between attrition and fusion. The final particle size distribution may be close to that of the original resin.

3. Changes in the order of addition may have profound influences on the quality of dry blends. Mixing of resin and stabilizer before the addition of plasticizer may cause more decomposition of these components in the dry blend than is encountered in normal heat aging tests on the finished product.

ACKNOWLEDGEMENT

The authors would like to thank Northern Telecom Canada Limited for permission to publish this paper. It is a pleasure to acknowledge the assistance of Mrs. Aranka Szaplanczay of Bell Northern Central Research Laboratories, Ottawa, Ontario who performed the SEM examinations, and of Mr. Claude Talbot of our laboratory who prepared some of the dry blends.

TABLE 1

SUMMARY OF PSD DATA FOR THREE RAW MATERIAL PVC RESINS

RESIN	A	B	C
Mean Chord (μm)	154	149	139
Mode (μm)	138	138	118
% in 50 - 70 μm range	2.2	1.7	0.3
Largest range with over 1% (μm)	245 - 265	245 - 265	225 - 245

TABLE 2

SUMMARY OF PSD DATA FOR DRY BLEND OF PVC RESIN AND DOP PLASTICIZER

DESCRIPTION	MEAN CHORD (μm)	MODE (μm)	% IN 50-70 μm RANGE	LARGEST RANGE WITH OVER 1% (μm)
Raw Material Resin	154	138	2.2	245 - 265
Resin Only Henschel Mixed to 75°C	154	138	2.4	225 - 245
PVC + DOP Mixed to 80°C	171	158	0.0	245 - 265
PVC + DOP Mixed to 90°C	164	158	1.9	245 - 265
PVC + DOP Mixed to 100°C	152	138	1.1	245 - 265
PVC + DOP Mixed to 110°C	155	138	2.4	225 - 245
PVC + DOP Mixed to 115°C	153	138	2.4	245 - 265

TABLE 3

COMPOSITION OF EXPERIMENTAL FILLED PVC DRY BLEND

COMPONENT	WEIGHT (g)	PHR	%
PVC Resin	1,043	100.00	45.96
DOP Plasticizer	537	51.49	23.66
Tribasic lead sulfate monohydrate stabilizer	63.5	6.09	2.80
Calcium carbonate filler	626	60.02	27.58
Total	2,269.5	217.60	100.00

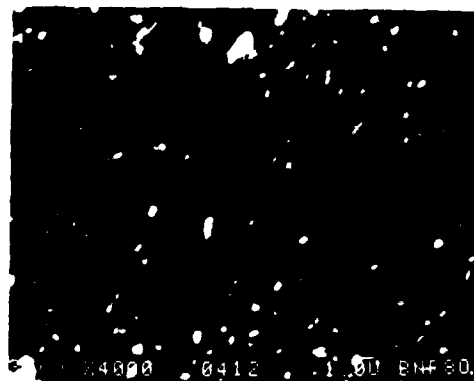
TABLE 4
COMPOSITION OF EXPERIMENTAL PVC DRY BLEND
FOR COMPARISON OF ORDER OF ADDITION OF STABILIZER

COMPONENT	PHR	%
PVC Resin	100.00	69.35
DOP Plasticizer	37.20	25.80
Dibasic lead phthalate	7.00	4.85
Total	144.20	100.00

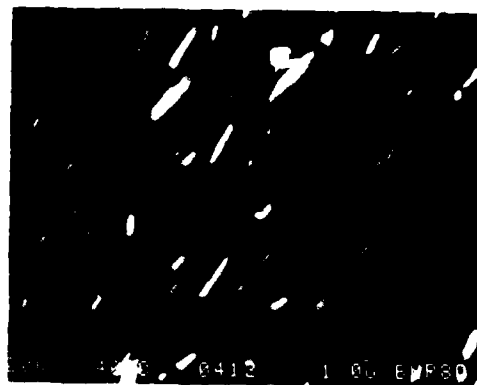
TABLE 5
SUMMARY OF PSD DATA FOR COMPARISON
OF ORDER OF ADDITION OF STABILIZER

MATERIAL	RAW MATERIAL RESIN	FRONT LOADED DRY BLEND	BACK LOADED DRY BLEND
Mean chord (um)	149	196	192
Mode (um)	138	216	197
% in 50-70 um range	1.7	1.9	3.4
Largest range with over 1% (um)	245 - 265	304 - 324	265 - 285

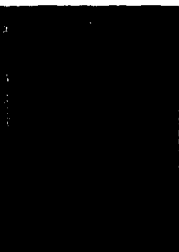
**FIGURE 2 - SEM PHOTOMICROGRAPHS OF FRACTURE
SURFACES OF SLABS MADE FROM
FRONT AND BACK LOADED DRY BLENDS.
MAGNIFICATION 4,000X**



**Fig. 2(a) - Front loaded lead stabilizer;
particles of stabilizer
represented by light areas.**



**Fig. 2(b) - Back loaded lead stabilizer;
particles of stabilizer
represented by light areas.**



R.A. Burley

The author has been employed at the Cable Division of Northern Telecom Canada Ltd. for 23 years. Most of his career has been spent in the application of spectrochemical techniques to the study of materials used in the cable industry. The ASTM Method for the "Analysis of Components in Poly (vinyl chloride) Compounds Using Infrared Spectrophotometry" (D-2124) was based on procedures developed in his laboratory. He is the author of about a dozen papers; the most recent was on "Spectrochemical Studies on the Heat Aging of Electrical Grade Poly(vinyl chloride) Formulations" presented at the annual conference of the Chemical Institute of Canada in 1979.



D.G. Hayashi

Dennis Hayashi is a graduate of Ryerson Polytechnical Institute (Toronto) in Polymer Technology. He joined Northern Telecom Canada Ltd. in 1970 and has been active in the research and development of materials for application in wire and cable.

THE COMPUTER IS IN...NOW YOUR TROUBLES BEGIN

E. W. Crews

Western Electric Co., Inc.
Phoenix, ArizonaABSTRACT

Microprocessors and other digital devices are finding their way into almost all wire and cable manufacturing processes. The primary advantage of selecting computer-controlled or digitally-controlled equipment is improved productivity. However, productivity can be adversely affected if this new equipment cannot be maintained or cannot be repaired quickly. Maintenance personnel require new skills and knowledge to repair and maintain computer-controlled or digitally-controlled equipment. A training program, properly structured to include education, documentation, and motivation, must be implemented for those responsible for the maintenance and repair of this highly sophisticated equipment. The training program to be discussed has evolved as a result of our experiences with various computer-controlled and digitally-controlled equipment.

INTRODUCTION

The training program to be discussed was initiated as a result of our experiences with the installation and maintenance of a microprocessor-controlled, wire-insulating takeup (the subject of a paper presented at the 30th International Wire and Cable Symposium) as well as several other projects involving microprocessors and digital electronics. We discovered that some of our maintenance personnel lacked the necessary skills to effectively maintain and repair this new and sophisticated equipment. Many suppliers expound the virtues of their new equipment, while in some cases they totally neglect to mention the skills required to maintain and repair it. Our first problem was to determine the required skills, and then to initiate a program to upgrade those maintenance people with deficiencies.

We decided to provide a well structured training program for our personnel consisting of two training phases: fundamentals and systems. We recognized that the limit to the complexity of the equipment we could

benefit from was dependent upon the skill level that our maintenance people could attain. To obtain the maximum benefit from the new high-tech equipment, it was necessary to provide a very thorough training program.

The training program was structured to our particular situation. We considered: (1) our personnel, (2) our equipment, and (3) the types of training courses available. The training program outlined here is not the only solution to the problem of upgrading of maintenance skills, but it is a practical approach to the problem.

PERSONNEL

The limit to the complexity of the equipment that can be maintained is dependent upon the skills of the maintenance organization. To properly structure a training program, it is necessary to evaluate the needs and potential of each maintenance man individually. The structure of the maintenance organization is important in determining the level of training required for each skilled trades group. The maintenance coverage requirements of the manufacturing operations will determine the number of maintenance personnel that must be trained.

Shown in Figure 1 is a composite look at the two skilled trades groups involved in the maintenance and repair of our computer-controlled equipment. Our typical electrician is 47 years old, has a high school education, and learned his trade in the military. Our typical technician is 43 years old, has two years of college, and learned his trade while in college. Many of our maintenance people had obtained their technical training long before digital electronics and microprocessors were taught in school and, in some cases, even before transistor theory was taught. Because of this, we decided to begin with a fundamentals course. Most of our skilled tradesmen had been away from an organized classroom atmosphere for many years. Because they were unaccustomed to the classroom, we structured the fundamentals phase as a self-study program.

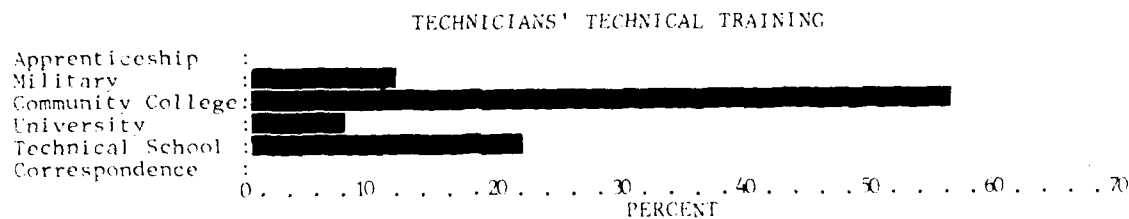
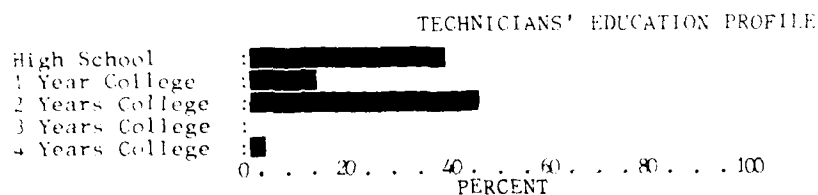
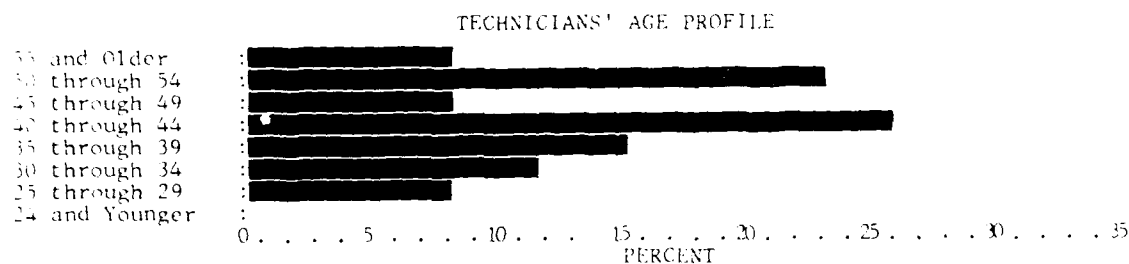
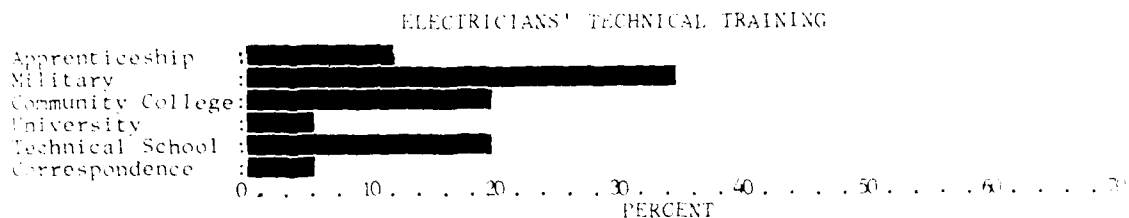
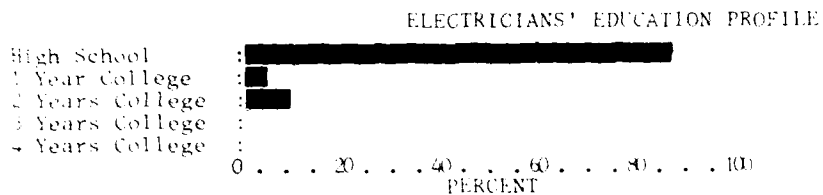
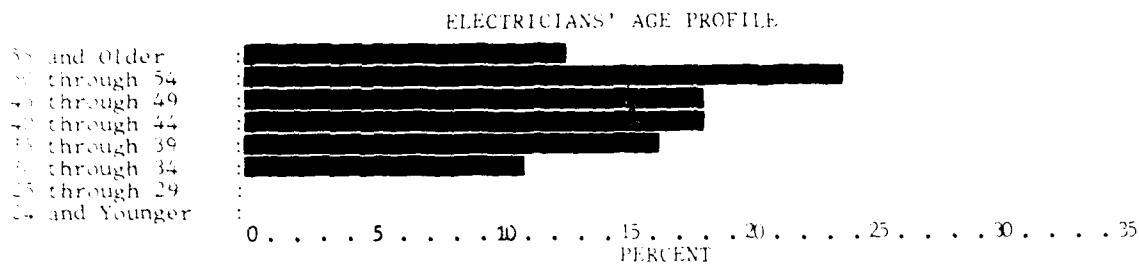


Figure 1 Personnel Evaluation

In the past, our electricians have had the responsibility of repairing and maintaining all electrical control equipment, while our technicians were responsible for the maintenance and repair of all digital equipment and all printed circuit boards. This historic division of work (loosely defined as high voltage versus low voltage) had, in itself, produced a problem. The new computer-controlled equipment fell into both the responsibilities of the electricians and the technicians. This difficulty has been solved by refining the work responsibilities of the two skilled trades groups. The electricians are still responsible for all control equipment, but that responsibility includes both the electrical and electronic components. The technicians are responsible for all testing, measuring, and data collection systems. The training program has been structured so that each skilled trades group can obtain the required skills without turning the electricians into technicians and the technicians into electricians.

The work schedule of our maintenance personnel had to be considered in the structure of the training program. Our manufacturing facility operates seven days a week on a three-shift per day basis. The maintenance organization provides electrical coverage on all three shifts. However, there are fewer maintenance people on the two night shifts than there are on the day shift. The extra day people are required for bench work and work that requires interfacing with the engineering organizations. The number of electricians and technicians that had to be trained on each shift was quite different. Also considered was the fact that our people had a rotating schedule of days off due to our seven-day coverage operations. Once again, the self-study approach to the fundamentals phase was the best option for our particular situation.

The supervisory requirements for the training program were undertaken by the maintenance organization. We were fortunate to have a supervisor within the maintenance organization with experience in the training area. His responsibilities included coordinating the program as directed by middle management. The training coordinator had to be able to communicate with both management and maintenance personnel. It was very important to have the right person in control of the day-to-day operations of the training program. The amount of time required to coordinate a training program is, of course, dependent upon the size of the program and decreases as the training progresses.

EQUIPMENT

There are two basic types of micro-

processor-controlled equipment. The first type can be described as supplier-designed equipment, and the second type can be described as user-designed equipment. As mentioned earlier, the limit to the complexity of the equipment to be maintained is dependent upon the skills required to maintain and repair the equipment. The importance of the relationship between the equipment and the training program becomes more evident when discussing documentation.

There are three subclasses of equipment categorized as supplier designed. They are: (1) specific use, (2) custom use, and (3) custom designed. The specific use equipment is designed by the supplier for a very specific application. Extruder heat controllers, electronic footage counters, and specialized testing equipment would be examples of this category. The custom use equipment would be less specialized and could be customized for a specific application through software prepared by the user or the supplier. Examples of this type of equipment would be programmable controllers and single board computers. The third subclass of equipment, custom designed, is sometimes described as an engineered system. A good example of this type of equipment would be a computer-controlled insulating or jacketing line.

For those wire and cable manufacturers with the technical staff, design of custom computer systems is possible. Western Electric and many other wire and cable manufacturers find it profitable to design and build their own custom microprocessor systems. Engineers can readily obtain the components for such systems from many equipment suppliers and integrate them into their production processes. Quite often, custom circuit boards are used in conjunction with purchased single board computers to provide the interfacing to unique manufacturing equipment. An example of this type of equipment would be the microprocessor-controlled wire insulating takeup previously mentioned.

THE MISSING LINK - TRAINING

Once the personnel had been evaluated and the equipment categorized, the educational program was structured. We assembled the training program to fit the unique situation of our manufacturing operations. The training program format included three major components: (1) education, (2) documentation, and (3) motivation.

EDUCATION

There are several educational formats available. Some of these include: (1) the classical classroom approach, (2) Cor-

respondence courses, (3) individual self-study, and (4) a coordinated self-study. Many commercial technical schools will contract with manufacturers to provide in-house training programs. These programs usually require a large number of maintenance personnel to attend class at the same time. With our seven-day, three-shift operation, this could not be easily coordinated and is quite expensive. Correspondence would have been used, but we felt that our people required a more structured and well-supervised program. Since a program conducted on company time would assure the required participation, it was concluded that a self-study program including laboratory exercises would be the best approach. Self-study programs can be structured for individuals or groups. If structured for individuals, each person must be provided with his own laboratory equipment. In a group-structured program, the laboratory equipment can be shared, thus reducing the cost of the program. Combining the group-structured program with direct supervision results in a coordinated self-study program. We selected this approach because it best fit our particular situation and offered the most benefits. Our program is offered seven days a week and on all three shifts. Our required classroom space is kept to a minimum since the room is used on a continuous basis with smaller groups of students.

The fundamentals training program is divided into eight areas of study. They are: (1) DC theory, (2) AC theory, (3) semiconductor theory, (4) electrical circuits, (5) operational amplifiers, (6) digital techniques, (7) test equipment, and (8) microprocessors. A schedule of recommended study times has been provided by the educational material supplier. They range from 20 hours for DC theory to 80 hours for microprocessors, with a recommended total of 300 hours for the entire fundamentals program. Although there is no limit on the time the student has to complete any phase of the program, he is encouraged to keep pace with the recommended time schedule. The student is assigned to three one-hour sessions in the training room each week during his normal work hours. The training material is given to the student to keep and as a result, we have some students that will study at home on their own time. We also encourage the student to use any idle time on the job to study.

The fundamentals course work is required of all electricians and technicians that participate in the program. The program is voluntary, but participation is obviously encouraged. The total program, if completed on company time only, requires

approximately two years to complete. After completing the fundamentals phase, the student may request some optional fundamentals courses. Six optional courses are available. These include such topics as: (1) OPTO electronics, (2) phase locked loops, (3) IC timers, (4) active filters, (5) assembly computer language, and (6) basic computer language.

After completing the electronic fundamentals phase of training, specialized training courses offered by the equipment supplier can be purchased. Courses for supplier designed equipment usually require more conventional classroom instruction and are more intensive in structure, with most courses being completed in one or two weeks of full-time study. By conducting these courses in-house, the living and travel expenses of the student can be avoided. Usually the costs of such courses are on a per-student basis with additional cost for the instructor's living and travel expenses while teaching. Unfortunately, scheduling of personnel becomes more difficult with these in-house courses, but fewer people are generally involved.

The training for user designed equipment is perhaps the most difficult to provide since it normally requires the preparation of training materials by the local engineering staff. Many hours and special talents are needed to prepare this type of training material. A classroom structure, similar to the courses offered for supplier designed equipment, is usually followed, although some videotaping has been tried. Costs for such specialized training material is divided among a relatively small number of students. The costs are probably higher than for courses offered by equipment suppliers. By videotaping the presentation of the training material per student cost can be reduced, and the tape provides a convenient resource for the maintenance organization.

DOCUMENTATION

The importance of proper documentation becomes more obvious as the specific systems courses begin. The documentation provided for the electrician or technician to maintain these systems usually comprises the training material for the courses. When we contract with an equipment supplier to provide training courses, we require that a complete set of documents be provided for each student. This allows the students to make notes on the drawings and instructions they will be using later to repair and maintain that specific equipment. Although this adds considerably to the cost of some courses, it is worthwhile. Listed below are the characteristics of

the documentation for each equipment category.

Supplier Designed - Specific Use Equipment: The documentation for this equipment is generally quite complete since the equipment has been designed for a specific application. Usually included are schematics, theory of operation, installation and calibration procedures, and troubleshooting guide. Since the equipment is for a specific application, the theory of operation usually covers the actual application in great detail. This simplifies the instruction process since the documentation provided becomes the training manual for the course.

Supplier Designed - Custom Use Equipment: Included in this category of equipment are programmable controllers. The documentation for this equipment is very specialized and does not normally include specific application information. The documentation would usually include such items as operating instructions, interfacing instructions, programming instructions, and maintenance and troubleshooting procedures. While these are sufficient for maintaining and repairing the programmable controller, it should be supplemented with documentation detailing the specific application and interfacing including schematics. Most equipment suppliers cannot furnish this supplemental material and as a result, the engineering staff usually has to prepare this documentation and assist in the training course. This obviously complicates the instruction process.

Supplier Designed - Custom Designed Equipment: This category of equipment, often called Engineered Systems, normally includes very detailed schematics and software (program) listings, but usually excludes information on the manufacturing process, overall theory of operation, and troubleshooting procedures. A good fundamentals training background is very important in understanding the documentation provided in this type of training. Because specific use and custom use equipment are normally included in engineered systems, some elements of the training program are well documented. However, to thoroughly understand the engineered system, the trainee must have a good understanding of the manufacturing process. This normally requires either extensive experience maintaining similar processing equipment or the involvement of the product engineering staff in the training process. As a result, this type of training course is not normally as well documented as it should be.

User Designed Equipment: The documentation for this category of equipment is the most difficult to obtain and is usually the poorest in structure and content. All documentation, with few exceptions, must be prepared by the design engineer. Because of other job responsibilities, engineers usually cannot devote the large amount of time required to prepare training documentation. As a result, instruction and training on user-designed equipment must be presented as a lecture series by the design engineer with whatever documentation he may be able to provide. This is less than satisfactory in most cases. The amount of information retained by the trainee in this type of course is much less than for a properly documented course. The quality of education for such a program is totally dependent on the ability of the design engineer to organize and present his lectures. Most engineers have little training as educators, and this presents a problem when organizing lecture material. Our experience in this area has not been good. Several courses have been organized by various engineers with varying amounts of documentation. The courses were well received by the trainees, but the retention of the material presented has been poor. A great deal of effort is being addressed to this problem, and better results are anticipated in the future as a result of the fundamentals training now in progress. Our hopes are that with a better background in electronic theory, the material presented by the engineer will be better understood.

MOTIVATION

The most difficult aspect of training is motivation. No matter how well structured the education program--or how thoroughly prepared the documentation--without the proper motivation, the training program is doomed to failure. The challenge is to motivate the maintenance man to participate and to keep pace. There is always some pressure from those that prefer not to participate on those that do. We attempt to keep the interest in the program high and to provide some sense of accomplishment in those that choose to participate. In the area of participation, we have had mixed results. Shown below are the levels of participation by our maintenance personnel:

Work Shift	Percent Participation Electicians	Technicians
Day	63	100
Evening	79	100
Midnight	85	100
Total	72	100

The response from our technicians has been very good. The electricians on the day shift, generally the most senior and the oldest, have the poorest level of participation in the fundamentals training program. The highest level of participation by our electricians is on the mid-night shift. Generally, the older the electrician, the less likely he is to get involved in the program.

The reason for the total participation by our technicians may relate to the fact that they as a group have a higher level of formal education and are probably less intimidated by classroom instruction. In addition to their excellent participation level, the technicians as a total group are approximately 8 percent ahead of schedule in their fundamentals training. The same cannot be said of our electricians. Shown below are percentages relating their progress in comparison to the recommended pace:

Work Shift	Electrician Status vs. Recommended (Percentage)
Day	-10.7
Evening	-15.7
Midnight	- 2.7
Total	-10.0

The midnight shift electricians have maintained a good pace and a good level of participation. The other two shifts require more attention to bring them up to a reasonable pace.

A recognition program has been initiated to encourage the trainees to continue with the program and to keep pace. Upon successful completion of the fundamentals training a special ceremony is arranged with members of management to present certificates of completion to the successful trainee. Since the maintenance personnel are hourly employees, and under Union contract, it is difficult to reward the extra efforts of the trainees that complete the entire training course. However, other awards are being considered.

SPECIAL ROLE OF THE ENGINEER

The engineer that has the responsibility to improve productivity through new state-of-the-art equipment has the added responsibility of understanding the maintenance man's point of view. Having to repair and maintain this high technology equipment without the necessary skills is upsetting. One goal of the training program is to make the maintenance man feel comfortable with the new equipment. The knowledgeable worker will accept technological change, while the worker with limited skills will always fight change. The engineer must

work with the maintenance organization to assist them in obtaining the necessary skills, and to be patient with the maintenance man as he learns these new skills.

An additional responsibility of the engineer is to provide an interface between management and the maintenance worker. Most engineers are in a position to understand the needs of management and the needs of the maintenance worker. It is his task, when selecting or designing new equipment, to integrate the needs of management to have a profitable piece of processing equipment with the needs of the maintenance man to have a machine that he can maintain.

CONCLUSIONS

The computer is here, and designers are going to find ways to use this new tool in every type of wire and cable manufacturing process. To compete in today's international market, productivity must increase, and the computer is the most popular technological change in equipment design to provide that needed increase in productivity. However, the productivity increases cannot be attained if the equipment cannot be maintained. Better educated and more highly skilled workers are required to maintain this new equipment. If these high-skilled workers are not already available, or if they cannot be hired off the street, then the current work force will have to be trained to do the job. This will require a full-time program of technical training. It cannot be a one-time operation, but it must be continuous and constantly upgraded as technology changes. Some of the current work force will not be interested in upgrading their skills. These workers will become obsolete if they do not change their attitudes. The tide of technology is growing. The maintenance man must learn to swim with the tide, or he will surely be swept away.

Our training program is approaching the end of the second year of operation. Most of our people have continued to support the program. The fundamentals phase of the training program is now almost complete. The benefits of the program should be more apparent this coming year when more specialized training courses can be offered. We believe the training program will allow us to take full advantage of the technological advances coming to our industry.



Edgar W. Crews received a Bachelor of Science degree in Electrical Engineering from Arizona State University in 1972. Before joining Western Electric in Phoenix, Arizona, in 1978, Mr. Crews worked for the Anaconda Company in several engineering positions. He is currently an electrical product engineer in plastic insulating. Mr. Crews is a member of Eta Kappa Nu and IEEE, and is currently participating in a Master of Engineering program at Clemson University.

AUTOMATED ELECTRICAL HARNESS MANUFACTURING

John W. Tarbox -- San Diego, California.

Tarbox Developments

This automated electrical harness manufacturing system described here is intended, thru Computer Controlled equipment, to lessen cost, improve quality and speed production in electrical harness manufacturing. It addresses the need to include wire marking; stripping; lugging; forming; tying and testing for a wide variety of gages and types of components. It sequences the operations of new but proven equipment--ink jet marking; robot wire end preparation; C-N/C forming and high speed assembly testing under the overall supervision of a host computer. It offers a number of choices of equipment and degrees of sophistication. It permits starting with a basic system of reasonable cost which is designed for future expansion with further economies.

Why automate?

The answer to this question comes to us in the United States from Taiwan, Korea, Mexico where manual labor costs are one tenth of ours. It comes from Japan who is automating; and currently at a rate much faster than us. Automation may reduce jobs in harness making but it will provide jobs in skilled manufacturing. And, if we don't compete through automation we will lose these jobs anyway--permanently!

Also there's Better Quality: Higher Productivity: Lower Cost.

Why then do we still find most harnesses are hand made?

That answer is easy. There has been no viable approach. No approach, that is, that accommodated the staggering variety of needs presented by wire gages ranging from 12 thru 28 with many different strandings and insulations --over 5000 varieties of terminals -- over 10,000 kinds of connectors; any geometric configuration coupled with a totally custom electrical configuration -- all of which requiring identification for assembly and maintenance. Steps within the overall assembly job have, indeed, been automated but there has been no answer to automating the whole. There is now!

The system described here has been made possible by developments in Computer Aided Design (CAD); in high speed printing (Ink Jets and Lasers); in Robots; in C-N/C machine controls; in high speed electrical and electronic testing; in automated bundle tying devicesplus some special ways of putting these all together. The next section describes this system.

The Wire Harness Assembly Center

First, let us review just what goes into the makeup of, say, an Aerospace equipment harness. A typical harness will use several different types of wire: single conductor, multi-conductor, twisted pair, shielded wire; it may use more than one color but the color in general is white; there will be several gages. Each wire will be numbered with its wire number. Then there will be a variety of terminals at the wire ends and each end must be correctly stripped of insulation before these terminals are applied. Stripping and lugging of the terminals require special tools matched to the wire and the terminal. Because of difficulty in applying numbering to certain wires numbered sleeves may be required adjacent to the end terminal. Pre-numbered shrink sleeving is typically used for this role.

From the collection pre-prepared wires the harness is next formed by running each wire, in turn, through its assigned path on the custom harness formboard. This is a tool made by locating forming pins and wire holding devices in the required pattern on a flat board. When all wires are run in the various trunks and branches are tied with lacing tape or plastic ties so that the harness may be removed from the formboard without losing its formed configuration.

We are not done. The next step is to insert the terminated ends correctly into their proper place in the connector. Then comes testing for correct continuity; final assembly of the connector strain relief shells, etc; addition of harness labels and, perhaps some extra protective wrapping. These final steps were taken only after the errors that showed up in the testing were corrected--not an easy task!

Industrial harnesses are usually somewhat simpler than Aerospace harnesses. Wire numbering may be omitted; wire color coding may be substituted; sometimes no wire identification is used. Wire end terminals are usually adapted well to automatic terminating tooling; connectors usually do not require the addition of an environment seal and connector assembly is therefore somewhat less of a chore.

Auto Assembly

Figure 1 outlines in schematic form the make-up of a basic Wire Harness Assembly Center. Figure 2 shows the components which extend the size and capabilities of this basic system. Refer first to Figure 1 -- System I.

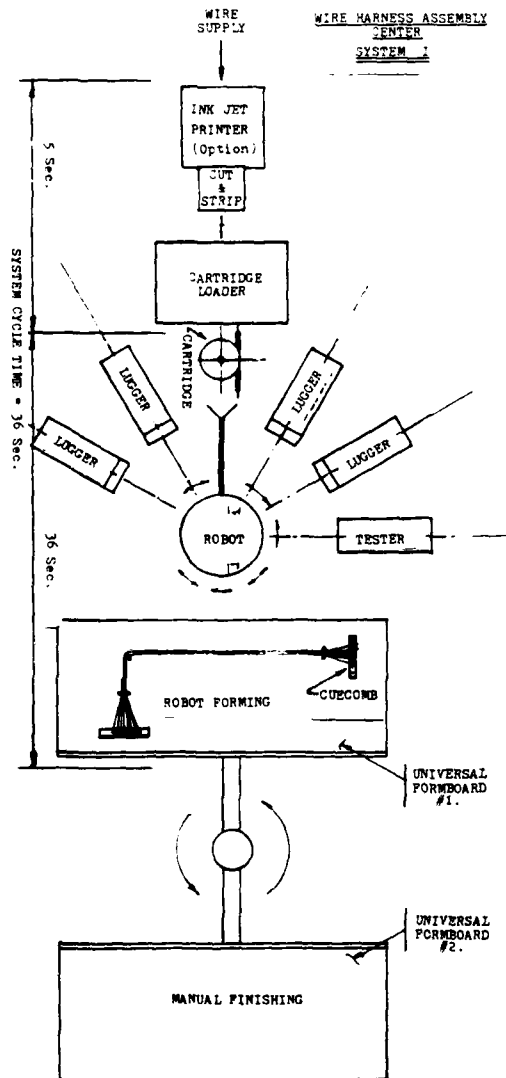


FIGURE 1.

In System I the wire feed to the printer, the first step in the harness making process, is initiated manually for each reel. Subsequent operations through harness forming are automatic.

From the printer the wire, now identified, passes thru the cut (cut and strip) module and is loaded into the cartridge by the action of the cartridge loader. The cartridge design is such that each end of the wire protrudes sufficiently to permit presentation to the strippers and terminal loggers for wire end termination which, in these systems, is completed prior to forming.

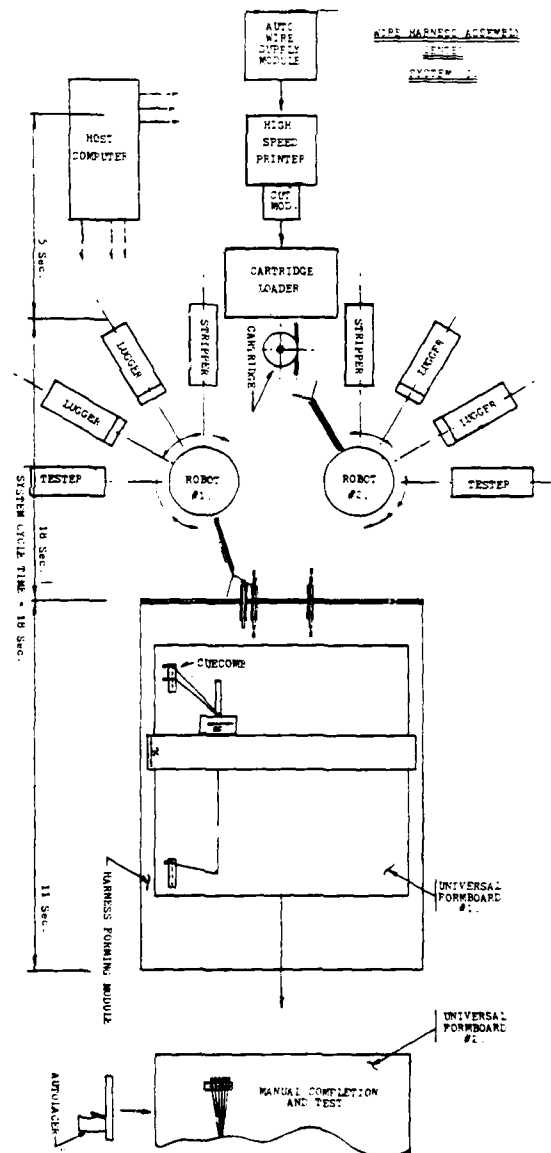


FIGURE 2

In the next operation the loaded cartridge is picked up by the Robot 'Hand' and is transported and presented to the lugging module selected to attach terminal #1. Following that action the Robot hand rotates the cartridge and presents the other end of the wire to the lugging module selected to attach terminal #2. The terminated wire is now ready for the forming operation.

In System I the Robot retains the cartridge, orients it and transports it through the manoeuvres needed to form the wire on the forming board. The cartridge design co-operates by providing precision payout of the wire into the gripping teeth of the 'Quecomb' wire grippers and around the forming pins which designate and maintain the correct forming pattern.

Operations subsequent to forming such as connector insertion, testing and tying of the harness are maintained as manual operations in System I. However, Robot precision in forming plus the guidance provided by the descriptive covers of the Quecomb system will add speed and reliability to these operations.

Wire Harness Assembly Center Modules

Printer: The printer required for this system must be capable of being programmed to number the wires in the sequence in which they are later to be formed. Also, it must operate with sufficient speed to keep up with the rest of the system. An Ink Jet wire marker marketed by American Jan is one suitable unit.

Cut or Cut-and-Strip Module: Since the wire cartridges are designed to handle individual wires a cut module capable of accurate length cutting of the various wire types used must precede cartridge loading. If wire types and stripping requirements can be handled by available 'in-line' strippers then the cut module may become a cut-and-strip module. If, however, wire types and strip lengths are too varied to permit practical use of in-line strippers then a module bank of powered 'end strippers' preceding the lugger line can be employed. The block diagram shows this alternative.

Wire Cartridge: This module has been designed specifically to meet the needs of this auto-wiring system. It co-operates with automatic loading from the cut or cut-and-strip module; prevents the wire from tangling; maintains control of the wire ends during wire end preparation (stripping, lugging, sleeving, testing) and provides for precision payout of the wire during the forming operation. Its configuration is such that it will handle a variety of wire types in lengths from one foot to several hundred feet.

Cartridge Loader: This module's role is to accept the numbered wire as it emerges from the cut module and load it with the proper protrusion of the wire ends into the wire cartridge and then park the cartridge ready for pickup by the robot.

Robot: The robot selected for use in System I is the V-15 Robot manufactured by the Cybotech Corporation of Indianapolis, Indiana, in a version specifically adapted for auto wiring. It incorporates a 'hand' capable of picking and parking the wire cartridge at the cartridge loader; presenting the cartridge correctly to the strippers, luggers, sleeves, testers; orienting the cartridge correctly during the forming operation.

Strippers: For those applications wherein currently available cut-and-strip modules are insufficient a bank of powered strippers of the end loading variety will be employed to cover the dimensional variations needed to match the wire and terminals used.

Luggers: A variety of terminal attaching (lugging) machines are available from the terminal manufacturers and/or from specialized tooling manufacturers. For robot operation the units selected should include automatic delivery of the terminals to the crimping dies. Since the luggers as now manufactured are designed to be operated by a human with feel and eyesight they will, for this application, be adapted for operation by robots without feel or eyesight.

Tester: This is a module specifically designed for auto wiring. It provides for both electrical and mechanical (pull) tests and checks both the integrity of the components and the quality of the operations up to this stage in the wiring process--in advance of harness forming and tying.

Forming: Forming of continuous strands of wire by C-N/C forming machines has been employed for some time. This system adds the forming of pre-prepped (end terminated) wire to that capability.

Quecombs: These are proprietary formboard accessories which provide for gripping and retaining the ends of the preterminated wires during machine forming. The Quecomb system, however, uniquely provides information needed by the technician responsible (in the basic System I) for the insertion of the wire ends into the connector. The user printed 'Quecovers' not only supply such information to the assembly technician but they also retain the wires in the comb in the array programmed and run by the robot during the wire forming process. This, typically, will be one wire per comb slot. Furthermore, Quecovers can provide information on wire runs, insertion and removal tools, manual stripping and lugging specifications, terminal, connector and wire part numbers for the final assembler and/or the maintenance technician inasmuch as the Quecomb/Quecover assembly is designed to remain with the harness for the remainder of its life. At the present time no alternate to this unique system exists.

Programming: Inasmuch as the Robot is the central operator of System I its auxiliary output commands are sufficient for initiating the operations of the printer and other modules. A host computer is not necessary.

Universal Formboard: This is a proprietary development of Adapt Developments, Santa Ana, California. It consists of a 2 foot by 3 foot module, joinable, like tiles, to make up larger boards. Each module contains 864 forming pins arrayed on 1 inch centers over the face of the module. At rest they are recessed within the unit. For forming they stand 2 inches high, perpendicular to the face of the formboard. Only an overlay which can be developed by hand or a graphics plotter is needed to control the setting pattern for the forming pins required. Set-up can be completed in a few minutes. No formboard storage is required. Grid patterns finer than 1 inch can be developed at any local area by means of slip-on accessories. The Luecomb system is designed to match to this formboard.

System II

Please refer to Figure 2.

System II adds both extra capability and size to System I. The Auto Wire Supply Module eliminates the processing interruptions which manual selection and feeding of a new color or type of wire to the printer causes. The Harness Forming Module added to System II provides for the forming of larger harnesses. This unit is sized to suit the user's needs--the largest one contemplated so far is 8 feet by 24 feet. In addition, the HFM makes practical the operation of a second robot to work in parallel with the first robot since both robots are relieved of the forming task. With cartridge loading and wire terminating proceeding simultaneously System II doubles the production rate of System I.

Wire Supply Module: Wire changeover taking longer than about 10 seconds will interrupt auto system operation. This module is intended to minimize such delays. Its role is to select the required wire supply package (reel or carton) from its store of such supplies and automatically feed wire from that package into the printer (or cut module if no printer is used).

Harness Forming Module (HFM): This unit is a Cybotech Gantry Robot, adapted to harness forming use. It interfaces with the wire end preparation robots by means of a parking rail which also provides a pooling area for cartridges in order to overcome production sequencing discontinuities.

Robot #2: This unit will be essentially the same as the robot used in System I. It will be sequenced to operate in co-operation with Robot #1 so that both robots can pick cartridges from the cartridge loader without colliding and, likewise, to park cartridges on the parking rail of the Harness Forming Module.

Autolacer: Available at this time is an 'Autolacer'. This is a device which carries its own supply of tying cord and has demonstrated the capability of lacing, automatically, a bundle of wires. In use now on industrial harnesses, it will, with modification, be applicable for use in aircraft applications. Designed for hand use it can be adapted for robotic operation. Alternatively, at least two varieties of 'guns' are available which are applicable for adaptation for robot use for the application of plastic bundle ties.

Host Computer: The more comprehensive role of System II dictates the need for a host computer to supervise the system's operation. The substantial benefits to be gained from computer manipulation of the mass of data needed to define each harness to be made on this system should be considered when sizing the computer system.

Circuit Tester: Subsequent to forming and, preferably, before tying the user may want to perform a complete circuit test for continuity and high potential (hi-pot) integrity. Several such testers, capable of operating at high speed, are available. An efficient, economical proprietary method of hooking up to these testers is available for use with this auto system.

Connector Assembly: This term is meant to describe the insertion of the wire end terminals correctly into the recess provided in the mating connector. A means for doing this by computer control is known to the author of this paper. It will provide for insertion at both ends of the wire being run; the mechanism is straight forward and most connectors can be worked. (Connectors requiring back-shell threading may be an exception.) System integration requires hardware which is additional to the forming equipment.

Proprietary considerations prohibit further disclosure.

Implementation

Planning Program: It hardly needs saying that the introduction of a Wire Harness Assembly Center such as is described in this paper must be preceded by a careful plan. The best plan will develop if two sets of experts are involved: the customer, who knows his needs and limitations and the supplier, who knows the system and the options. The result should be a permanent record which will provide by means of models, illustrations and text a comprehensive reference for the continuing use of concerned executives, engineers and technicians. It should set the timetable and provide the necessary background on the various system modules and their roles. It should include, during planning, key affected personnel so that, with their co-operation the plan lays the groundwork for shop integration. Disgruntled workers have many monkey-wrenches!

The author has a planning program outline available.

System I - Production Rates

OPERATION	TIME (Sec.)
1. Print Out Strip Cartridge Load	1
CARTRIDGE LOAD CYCLE TIME	1
2. Robot moves from park to pick position.	1
3. Robot picks cartridge.	1
4. Robot positions to lug end #1.	1
5. Lug end #1.	1
6. Robot positions to lug end #2.	1
7. Lug end #2.	1
8. Robot moves to tester.	1
9. Electrical and Pull Test.	1
10. Robot moves to start of forming cycle.	1
11. Forming cycle (Average)	10
12. Robot moves to park position.	1
13. Robot parks cartridge	1
TERMINATE - FORMING CYCLE TIME	10

TOTAL CYCLE TIME*.....30 sec wire or 100 wires/hour.

*Terminate + Forming proceed simultaneously with Cartridge Load

System II - Production Rates

OPERATION	TIME (Sec.)
1. Print/Out/Strip/Cartridge Load	1
CARTRIDGE LOAD CYCLE TIME	1
2. Robot moves from park to pick position.	1
3. Robot picks cartridge	1
4. Robot positions to lug end #1.	1
5. Lug end #1	1
6. Robot positions to lug end #2.	1
7. Lug end #2	1
8. Robot positions to tester	1
9. Test	1
10. Robot positions to and parks cartridge at HFM	1
11. Robot picks cartridge from HFM**	1
12. Robot moves to cartridge loader park position.	1
13. Robot parks cartridge at loader	1
TERMINATE + TEST CYCLE TIME (Ave)	10
FORMING Cycle Time approx.	10
14. HFM picks cartridge	1
15. High Speed Forming (Average)	1
16. HFM parks cartridge	1
FORMING CYCLE TIME	10

TOTAL CYCLE TIME ... 19 sec. wire or 100 wires/hr.

** Picks up a cartridge from a previous run
HFM = Harness Forming Module

Cost Savings Calculations -- SYSTEM I

Estimate manual rates now	14 min. wire.
Current technicians' wages w/overhead	\$ 24.00 hour.
Manual costs/wire = 14/60 x \$24.00	\$ 5.60/wire.
System I rate	100 wires/hour.
Assume 2 operators for System I.	\$ 48.00 hour.
Machine cost/wire = \$48.00/100	\$ 0.48/wire.
Estimated system utilization of 70%	
Adjusted machine cost/wire = 0.48/70 =	\$ 0.69/wire.
Estimate that 25% of current manual effort is still needed for such operations as loading, stuffing, connector assembly and manual costs remaining = .25 x 5.60 =	\$ 1.40/wire.
Total System I cost/wire	\$ 2.14/wire.

System I Savings	\$ 3.46/wire.
System I Savings/hour = 100 x 70% x 3.46 =	\$26.00 hour.
System I Potential Savings/year = 4 shifts 4000 x \$26.00 =	\$1,040,000.00

Cost to implement System I. (Budgetary estimate)

Program Plan	\$ 50,000.
Development & Hardware	50,000.
Company expense (estimated)	\$ 1,000,000.
Potential net savings in one year	\$ 1,040,000.00
Return on investment = $\frac{1,040,000.00}{1,000,000.00}$	104%

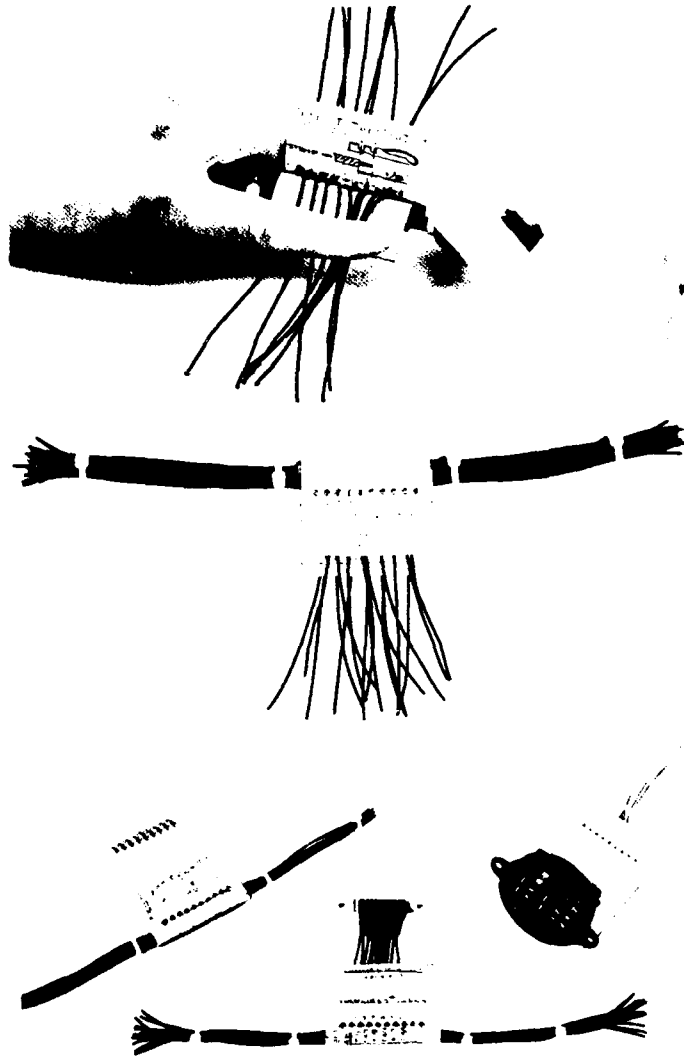
Cost Savings Calculations -- SYSTEM II

Estimate manual rates now	14 min. wire.
Current technicians' wages w/overhead	\$ 24.00 hour.
Manual costs/wire = 14/60 x \$24.00	\$ 5.60/wire.
System II rate	200 wires/hour.
Assume 3 operators for System II	\$ 72.00 hour.
Machine cost/wire = \$72.00/200	\$ 0.36/wire.
Estimated system utilization of 70%	
Adjusted machine cost/wire = .36/70 =	\$ 0.51/wire.
Estimate: 10% of current manual effort is still needed for such operations as loading, stuffing, etc.	
Manual costs remaining = .10 x 5.60 =	\$ 0.56/wire.
Total System II cost/wire	\$ 1.07/wire.

System II savings over manual	\$ 4.53/wire.
System II savings/hour = 200 x 70% x 4.53 =	\$634.00 hour.
System II Potential Savings/year = 2 shifts 4000 x \$634.00 =	\$2,536,000.00
Improvements: System II vs System I	\$1,496,000.00

Estimated Cost to Upgrade System I:

Development & Hardware	\$50,000.
Company supplied equipt.	50,000.
Company expense (estimated)	\$ 1,000,000.
Potential net savings System II vs I in one yr.	\$ 1,496,000.00
Return on additional investment = $\frac{1,496,000.00}{1,000,000.00}$	149.6%



"MAKE THE RIGHT CONNECTION"
CUECOMBS - FIGURE 3.

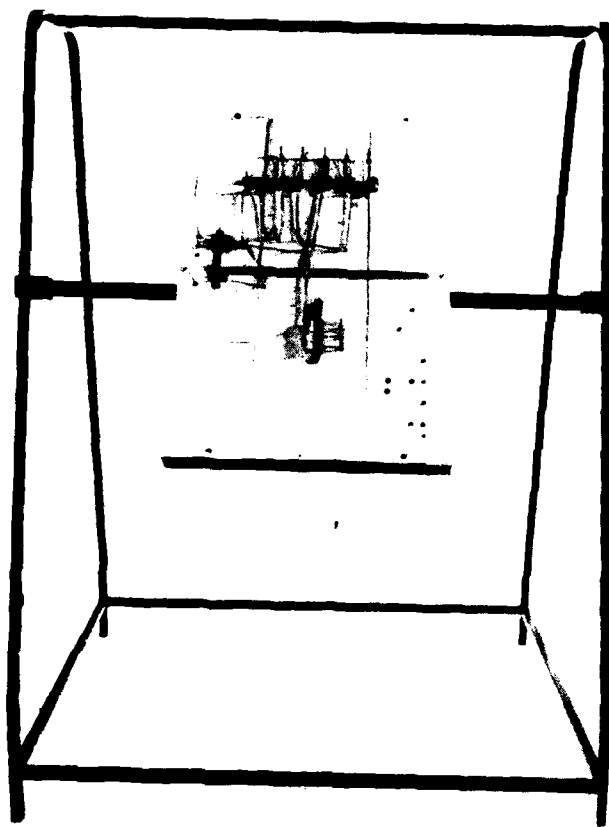
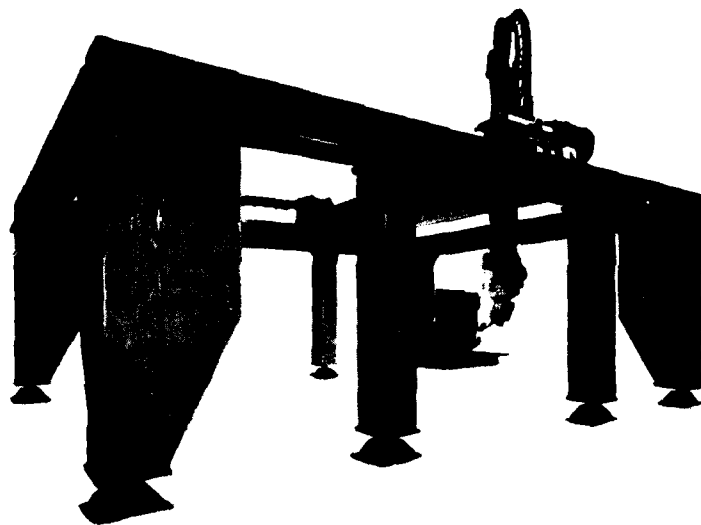


FIGURE 5



UNIVERSAL FORMBOARD - FIGURE 4.

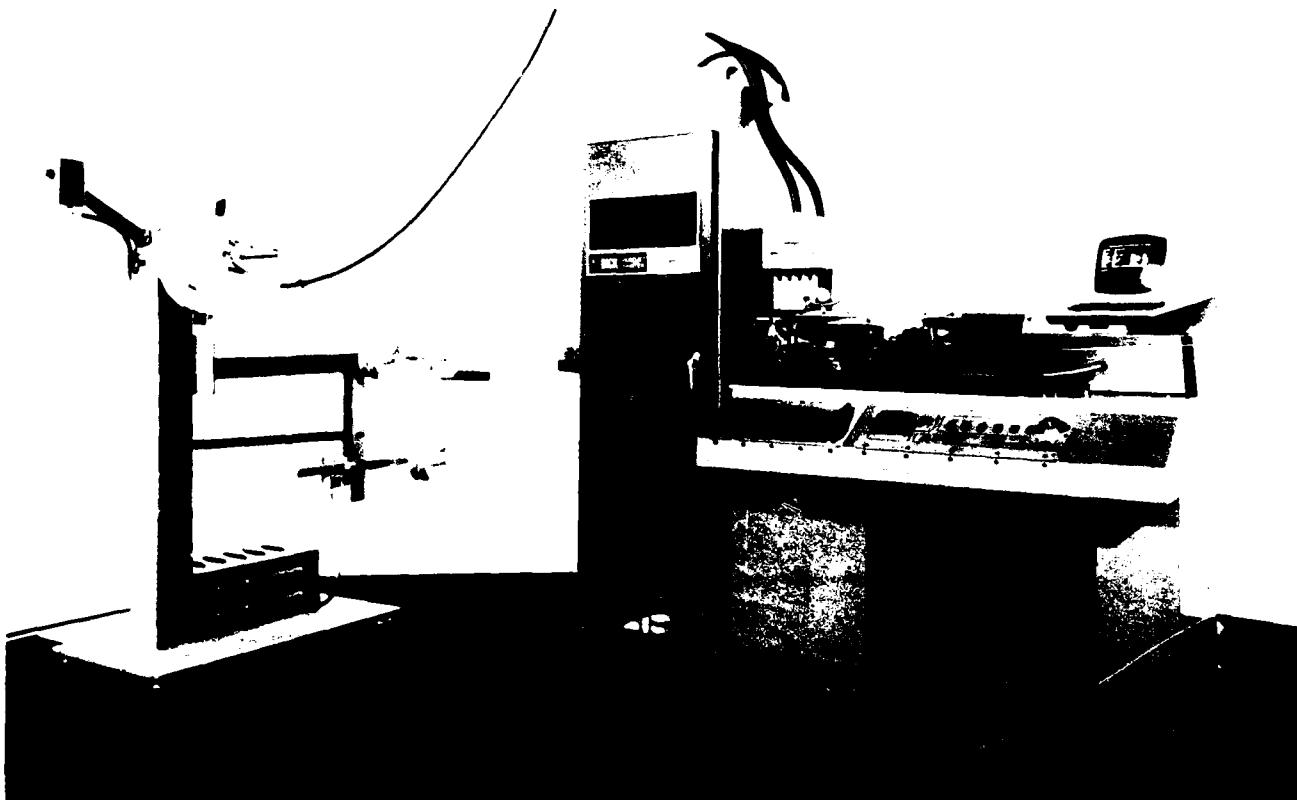


FIGURE 6



John Tarbox earned a degree in Mechanical Engineering some time ago which has given him a chance to add a good deal of practical experience in mechanical, electrical, electronic and systems engineering since then.

For the past 12 years, his main effort has been in the line of automating electrical wiring and he was active in the early developments at Boeing, Western Electric and Xynetics. The background for this paper on Automated Electrical Harness Manufacturing comes from that work updated with five years at the helm of a small company using a computer controlled wire forming machine of his own design in production of a wide range of industrial wire harness assemblies. John has a number of patents in this field--several applicable in the system to be discussed today.

METAL FORMING AND INSPECTION CONTROL FOR CABLE SHEATHING

W. D. Bohannon, Jr.

D. E. West

Western Electric
Norcross, GeorgiaAbstract

Development by Western Electric Company has resulted in a unique quality measurement system based upon the "percent take-up" and "build-up" of a cable sheath. Percent take-up is defined as the amount of useable metal remaining in the cable sheath after metal forming and Build-up is defined as the amount of spacing, due to the metal, between the polyethylene jacket and the conductor core. In the development of a quality control system, a direct relationship between the existing shop specifications and the new specifications involving build-up and percent take-up were established. With these requirements, the manufacturing window was effectively doubled and the quality level improved in cable products. Resulting parameters are measurable in all finished products and provide a quick feedback of cable quality guaranteeing a quality level exceeding the present standards (8X bend).

Introduction

In an examination of current cable specifications, one requirement reflects a standardization of performance testing. This requirement is the "Cable Bending Test". As stated in REA specification PE-89:

27. Cable Bending Test¹

27.1 All cables manufactured in accordance with the requirements of this specification shall be capable of meeting the following bend test:

27.1.1 A suitable length of cable shall be bent, with the shield overlap on the outside of the bend, in a 180° arc around a mandrel; straightened, bent 180° in the opposite direction, completing one cycle; the specimen shall be straightened, rotated 90°, and a second cycle of bending performed. The rate of bend shall be such that the test is completed within one minute. The specimen shall have been conditioned for a minimum of four hours at -20° +/- 2°C and shall be tested at this temperature, or immediately upon removal from the cold chamber where the sample has been conditioned, providing that the mandrel is

a non-conducting surface such as wood.

27.2 The mandrel diameter shall be as follows:

<u>Classification</u>	<u>Mandrel Diameter</u>
Non-Gopher	15X
Gopher	20X

27.3 The cable may be allowed to warm to room temperature before inspection. The bend area of the cable shall show no visible evidence of fracture of the jacket. After removal of the jacket, shield and armor, there shall be no visible evidence of fracture.

Though the mandrel diameters may vary (8X is used by WECo), it becomes apparent that this test is an acceptable standard which well correlates to the actual installation requirements (i.e., metal shield - armor construction).

With this final performance standard, the manufacturing engineer is faced with the problem of guaranteeing cable quality and developing the control system to do so. The maintainable level of quality in the product becomes directly related to the accuracy and the time constant of feedback data. Assuming adequate process stability, a quick concise quality measurement system is needed in order to precisely control metal forming process. Since the "bend test" requires four hours for sample stabilization, this is quickly denounced as a process control measurement.

The past method of process control used by Western Electric Company was based upon a relationship of two measurements: corrugation depth and corrugation count.

Corrugation Depth: Depth of corrugated metal prior to metal forming process.



Figure 1.

Corrugation Count: Number of corrugations per inch remaining after metal forming (averaged over 5" sample).

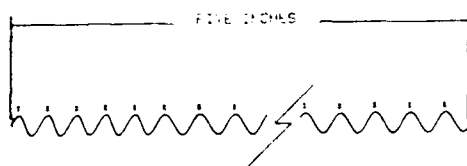
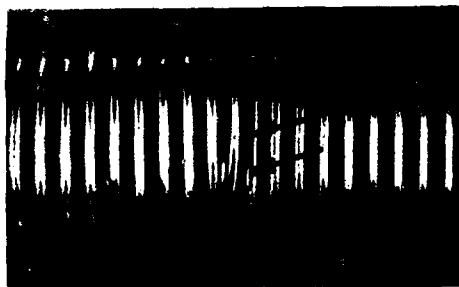


Figure 2.

This system appears to be adequate, but one fault in this measurement control system should be noted: The original corrugation depth measurement is destroyed in the metal forming process. This change makes it unavailable as an end product check point. When an effort was made by the WECO Cable and Wire PECC to improve cable sheath quality, this problem with the corrugation depth-count system was recognized as insurmountable. Since the specified corrugation depth was not measurable in the end product, the controlling parameter became corrugation count. This single variable was an inadequate control for guaranteeing uniform quality. It was deemed necessary to develop a new process control system.

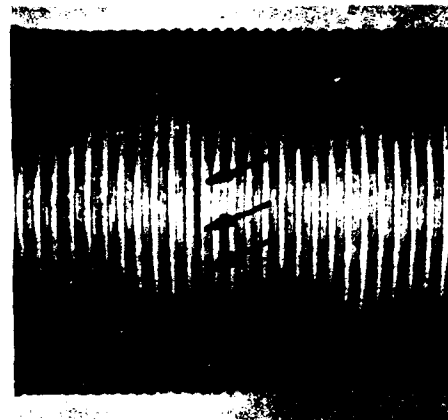
Solution Synthesis

The development of a new quality control system began with a study of cable failures. The primary objective was to identify the sheath failure mode (i.e., failure mode of corrugated metal(s) when subject to repetitive bend test cycles). The conclusion was that the cable fails in a compressive mode; therefore, the ultimate quality test would be a compressive test of the formed metal.



1" Diameter Buckle

Figure 3A.
(Ref. 2)



3" Diameter Buckle

Figure 3B.
(Ref. 2)

Prior to the search for a test method, certain design criteria were set to aid in its selection. Assuming an increase in the product quality control is required and the actual testing will be performed in the plant environment, the following criteria were established: The test must be quick, concise, reliable and durable. In the search and evaluation of "standard compressive tests", no unique test was found which met all the design criteria. Therefore, a decision was made to establish new control parameters.

To gain more understanding of the effect corrugation has upon metals, a number of experiments were undertaken. First, metal tapes were marked in 10" lengths. The tapes were corrugated (using 10 corr./in. rollers) into strips of various corrugation depths. Each tape was cut to 1-1/2" widths, then tensile tested on an Instron. The elongation versus force data were graphed.

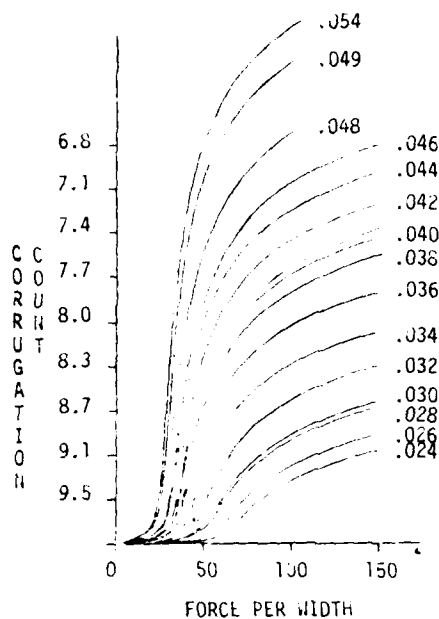


Figure 4 for Steel
(Ref. 2)

Such a graph is shown above. The following points are of significance:

1. The corrugated metal, in the initial stage of elongation, acts as a spring member.
2. The force required to form metal into a circular configuration exceeds this "spring region" capability.
3. Corrugation of metals has a "work hardening effect" on them due to corrugation stretch. The stretch is approximately 2% to 4%, depending on depth (see Figure 8).

From metal forming trials it was concluded that there exist two relationships of significance in the metal tape forming sequence. The first is an inverse relationship between tape width and minimum forming force. The second is a direct relationship of the tape width to the corrugation count required to prevent formed metal from springing open upon exiting the forming die.

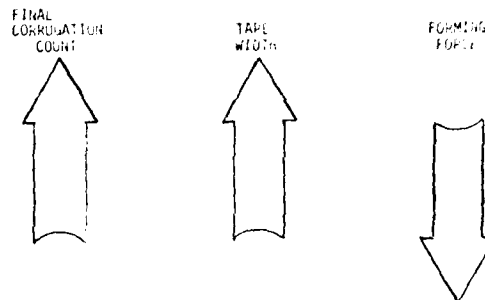


Figure 5.

It was concluded that in the final cable the only measurable parameters were the amount of metal in the corrugations, the final corrugation count and depth and the diameter over the formed metals. The studies outlined above indicated that a relationship exists among these parameters. It was decided to develop a quality control system around these parameters and relationships.

New Quality Control System

The quality control system is based upon two parameters: "Percent take-up" and "Build-up".

The first parameter, "Percent take-up", is defined as the amount of useable metal remaining in the cable after the forming process. The test procedure requires cutting a sample from the finished cable metal tape(s) of a specified length (L).

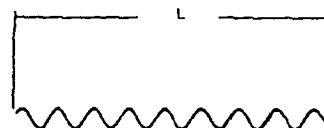


Figure 6.

A tensile force equal to the yield point for the raw material is applied to this sample (see Figure 8). (Note this is not the yield point of the corrugated material because it has been "work hardened" by the corrugation process.) The sample is then remeasured at some value $L + \Delta L$, ΔL being the elongation.

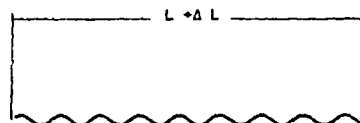


Figure 7.

The "percent take-up" is thus defined as $(\Delta L / L) \times 100\%$. This procedure leaves less than 1% of useable corrugation in the sample. However, this must be left in order to insure the metal does not yield while being straightened. These characteristics of the metal, before and after corrugation, are illustrated in Figure 8. This data is from the study conducted to verify the "percent take-up" measurement. It shows that this approach will insure ample amounts of corrugated metal in the cable to meet the "bend test".

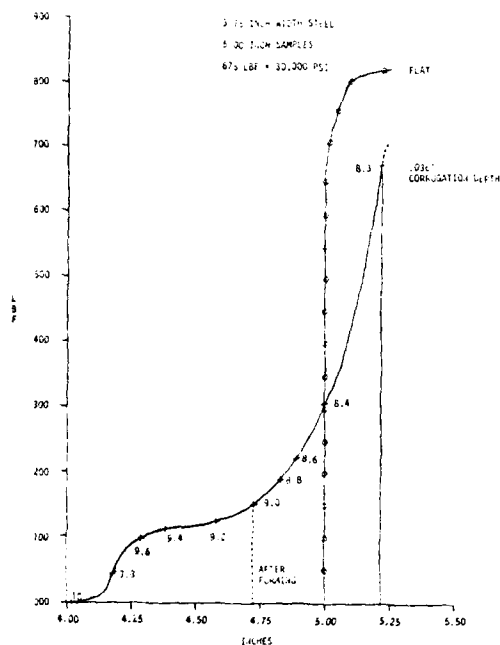


Figure 8.

The second control parameter is the "build-up" of the cable. Build-up is the amount of spacing, due to metal, between the polyethylene or PVC jacket and the conductor core. The measurement procedure is as follows: First, remove the jacket and measure the diameter over the metal (DOM). Next, remove the metal shield and/or armor. (Note: These pieces are then used in the aforementioned test for percent take-up.) Now measure the diameter over the core wrap (DOCW). Build-up is defined as diameter over metal minus the diameter over core wrap:

$$BU = DOM - DOCW$$

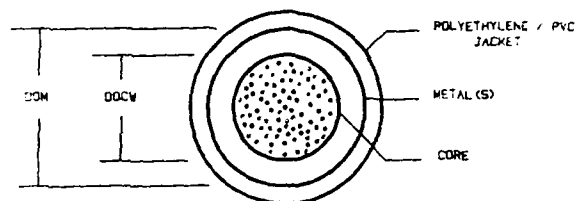


Figure 9.

The build-up control parameter serves two purposes. The first is as a check of forming equipment and proper tooling. The second and the most important is to assure proper control of the sheath buckling phenomenon. (See Ref. 3 for sheath buckling information.)

Establishment of Target Control Parameters

With the control parameters defined, a study⁴ was conducted to correlate percent take-up and build-up measurements with the 8X, 3 cycle test. The resulting target parameters were established to assure passing the bend test with 100% certainty.

Check of Solution

With the establishment of these target control parameters, an in-depth trial was conducted at Western Electric Atlanta Works. The intent of this study was to correlate the old control parameters (corrugation count and depth) with the new control parameters (build-up and percent take-up) and to compare the performance of each. In this study, a sample of each cable manufactured under the new specification was tested and stored for a one-year period for further testing. These cables were monitored during the installation process to identify cable sheath performance failures. Partial results of the study are in Figures 10-12.

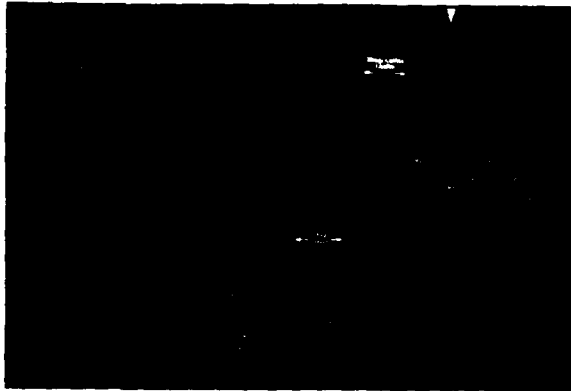


Figure 10.

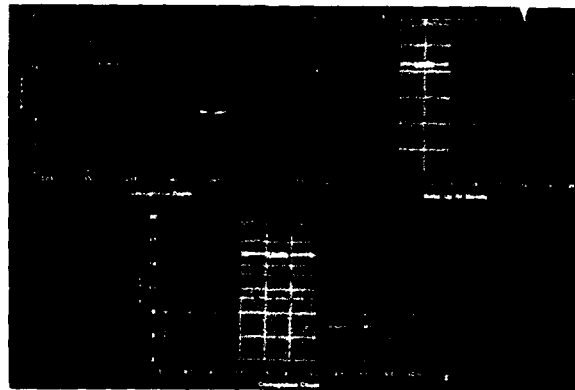


Figure 12.

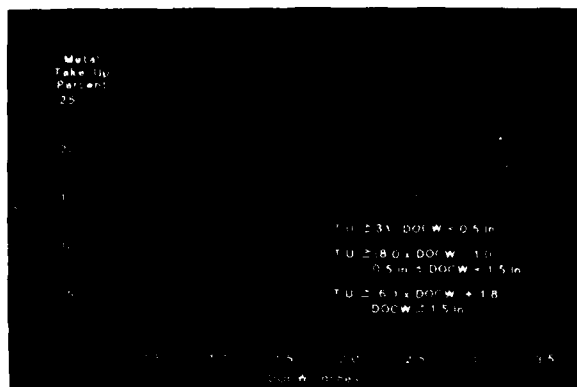
Note: "Shop requirements" are initialization parameters for the sheathing line operator to use in line set-up.

Results

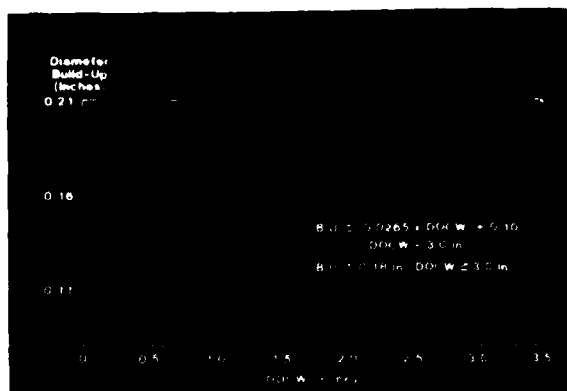
From the aforementioned trial results, two points should be highlighted. The first is that no defects or failures were reported on cables made during trials. The second is that the "manufacturing window" has essentially doubled as shown by Figure 11. (The old requirement was $.037 \pm .002$ inches depth and 9.1 minimum count which restricted manufacture to the right half of the curve.) With these positive results the final requirements were developed for implementation. These requirements are shown in Figures 13-16.



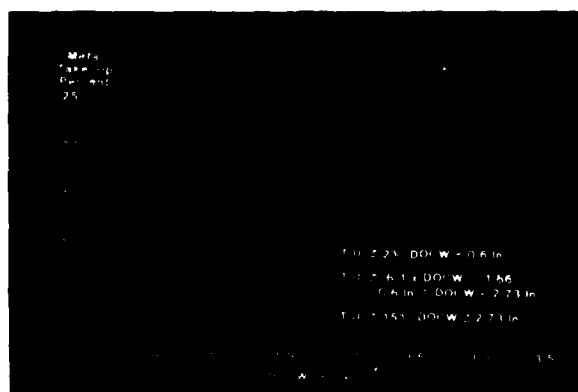
Figure 11.



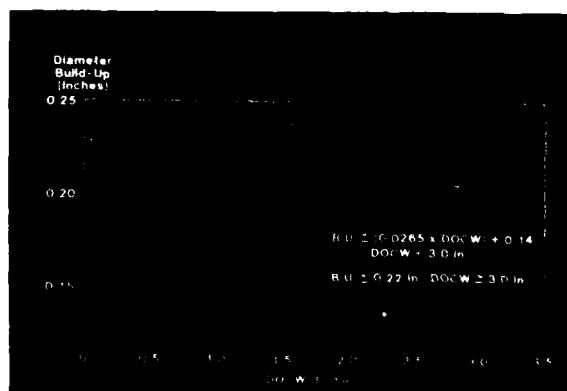
% Take-up, Steel
Figure 13.



Build-up, Single Metal
Figure 15.



% Take-up, Aluminum
Figure 14.



Build-up, Double Metal
Figure 16.

Conclusions

WECO has developed a quality control system which is comprised of two measurements: percent take-up and build-up. The resulting control system is superior to the old standard and is more reliable, concise and durable. The end requirements have doubled the manufacturing window and improved the overall quality level of WECO product. If compared to the "Bend Test", the percent take-up/build-up system yields:

1. A quantitative measurement of cable performance, not a pass-fail result.
2. Faster test time (5 minutes compared to 4 hours).
3. A test method which can be performed on any cable after manufacture, installation, etc., with results implicating facts about metal forming during manufacture.
4. A complete test of parameters which determine both bending performance and buckling performance.

The resulting system has completely resolved field complaints involving sheath performance failures. Therefore, it is recommended that this system be incorporated into REA and International Specifications.

Acknowledgements

The authors wish to acknowledge the work of Messrs. M. J. Swiderski, G. M. Yanizeski, and D. M. Mitchell, all of Bell Laboratories, for valuable contributions in developing this system. Also, Mr. J. J. Riordan, Atlanta Works, is acknowledged for cooperation in the use of his manufacturing facility in system prove-in.

References

1. "REA Telephone Specifications for Filled Telephone Cables with Expanded Insulation", REA Bulletin 345-39, PE-89, Washington, DC, 1981.
2. M. J. Swiderski - BTL, Atlanta - Unpublished studies, 1978.
3. G. M. Yanizeski, E. L. Johnson and R. G. Schneider, "Cable Sheath Buckling Studies and the Development of a Bonded Sheath", 29th International Wire and Cable Symposium, 1980.
4. D. M. Mitchell - BTL, Atlanta - Unpublished studies, 1978.



Bill D. Bohannon, Jr., is a senior staff engineer at the Western Electric Cable and Wire Product Engineering Control Center in Norcross, Georgia. He received his B.S. Mechanical Engineering degree from the Georgia Institute of Technology in 1947. He joined Western Electric in 1953 at Burlington, North Carolina and is presently a consultant in the field of special machines and manufacturing methods development.



Dan E. West is a development engineer at the Western Electric Cable and Wire Engineering Control Center in Norcross, Georgia. He received his B.S. degree in Mechanical Engineering from North Carolina State University in 1980. He joined Western Electric in 1980 and has been involved in the cable sheath metal forming and core wrap areas.

COMPUTERIZATION OF THE PULP WIRE
INSULATING PROCESS

V.L. LeNIR, W.A. CASCARANO, M.A. SHANNON*

NORTHERN TELECOM CANADA LIMITED
LACHINE, QUEBEC - KINGSTON, ONTARIO*
CANADAABSTRACT

A computerized feedback control system was developed at the pulp insulating stage as a first step to improve the uniformity of the pulp insulation. The objective is to assure a consistent average mutual capacitance of 83 ± 4 nF/mile and a capacitance deviation of better than 4% particularly for higher pair density type cables. The system consists of a microcomputer controlled diameter scanner and moisture measurement system for each pulp line. Control of oven temperatures and water applicator is effected at a central computer based on average values transmitted by the microcomputer. Better pulp insulation density control is achieved by increased sampling of weight per foot coupled with automatic regulation of pulp flow to each machine as a function of consistency. Significant improvements have been made in cable quality, and as a result of the continuous per wire monitoring capability of the system, the way is open for further improvement in capacitance deviation.

1. Introduction

The use of pulp insulated cables, which were originally designed for voice transmission, has been expanded to include applications involving higher transmission frequencies resulting in a need for tighter control of transmission parameters. They now have application in the field of exchange cables where the use of the DSL Rate PCM systems has proliferated. Even today pulp cables offer the telephone operating company considerable advantage in terms of cost and size, in addition to ease of failure detection and blocking characteristics in the case of water penetration. By comparison, foam insulated grease filled cables which meet the requirement of improved transmission characteristics incur a considerable penalty in terms of price and pair density.

This paper describes computerized feedback control system developed for the insulating stage of pulp cable manufacture in order to ensure the uniformity of the pulp insulation and thereby improve transmission characteristics.

2. Cable Parameters

All transmission characteristics including impedance, attenuation and crosstalk depend on the uniformity of the insulated conductors. A measure of the degree of uniformity can be obtained from the average mutual capacitance of the cable and the deviation of the capacitance of pairs within the cable.

Average mutual capacitance has traditionally been specified for the control of cable manufacture since it can be readily tested on the finished cable product.

DSL rate systems require an average mutual capacitance of cables of 83 ± 4 nF/mile with a narrow spread about the nominal, and a capacitance deviation of better than 4%. The existing installed pulp network does not always meet both of these requirements and hence problems have been experienced due to increased attenuation losses, and an increase in the cable generated noise level which necessitates shortened repeater spacings and/or selection of pairs for PCM applications.

The need for cables of consistent quality better suited to installation in PCM systems provided the impetus to the development and installation of a computerized control system on our pulp insulating lines.

3. Pulp Cable Manufacture

The various processes in the manufacture of pulp cables will be briefly reviewed to indicate the sources of variations in average mutual capacitance and capacitance deviation. Figure 1 shows the various manufacturing operations.

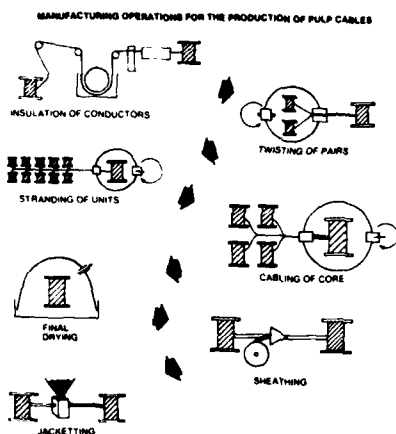


FIGURE 1

The bare conductors are first insulated on one of several 60-wire pulp insulating lines, and then twisted in pairs with twist lengths according to the color combination. The twisted pairs originating from one or more insulating lines are stranded together into units of 50 or 100 pairs which are cabled together and covered with a core wrap tape. The core is subsequently dried under vacuum in a "dome" drier shortly before sheathing.

For most applications the standard Stalpath sheath construction is used as shown in Figure 2.

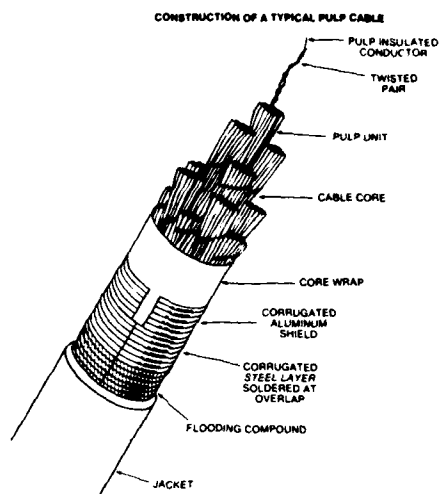
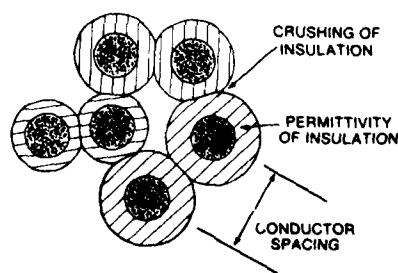


FIGURE 2

4. Mutual Capacitance

Referring to Figure 3, mutual capacitance mainly depends upon the spacing of the conductors of a pair and the dielectric constant of the insulation.

PARAMETERS AFFECTING MUTUAL CAPACITANCE



THE MUTUAL CAPACITANCE OF A PAIR DEPENDS PRIMARILY UPON THE SPACING BETWEEN CONDUCTORS AND THE PERMITTIVITY OF THE INSULATION.

FIGURE 3

The spacing between the conductors of a particular pair depends on the diameter of the individual insulated conductors and the amount of deformation occurring in subsequent processing. The dielectric constant of the insulation depends on the density of the pulp insulation and again upon the amount of deformation caused by machine tension and die sizes at twisting and stranding. The degree to which the insulation will accept permanent deformation also depends on the amount of moisture left in the insulation after the insulating process. These relationships are summarized in Figure 4.

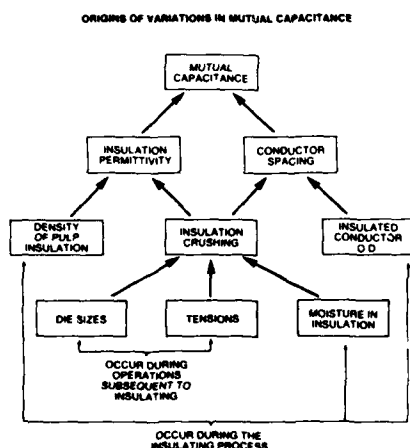


FIGURE 4

Therefore to ensure the uniformity of mutual capacitance from pair-to-pair it is necessary to start at the first manufacturing operation and to control the insulated conductor diameter, density of pulp and moisture content at the insulating process. Any non-uniformities created during insulating cannot be corrected during subsequent operations.

The integrated computer system, which controls all pulp machines simultaneously, is based on continuous monitoring of diameter and moisture of the pulp insulation and on a semi-automated control of weight/foot. Improved diameter control at this stage also simplifies selection of die sizes at subsequent operations. Further improvement in the average mutual capacitance level can be obtained by improving tension control at the twisting, stranding, and cable stages.

5. Pulp Insulating

Sixty wires are insulated simultaneously on each pulp machine at a speed in the order of 200 fpm (Figure 5).

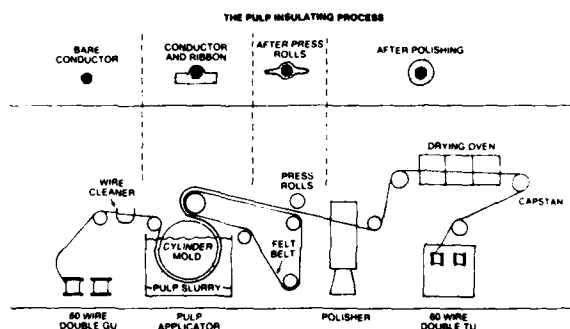


FIGURE 5

A flat ribbon of pulp is formed on the machine. Some of the water is squeezed out of the pulp ribbons by press rolls before they are wrapped around the conductors by high speed rotating polishing dies to form a continuous layer of pulp on each individual conductor. The insulated conductors are then passed through a three-zone oven to dry them prior to take-up on the process reels. During this operation a number of parameters are monitored and used along with the results of tests performed on completed reels of wire to make adjustments to the process. In these tests a sample of wire is taken from each of 10 reels and the average diameter, moisture, and

wieght per foot are obtained. Since reel changeovers occur every two or three hours depending on the wire gauge, and results of tests are dependent on the skill of the operator, manual control tends to be somewhat of an art.

6. Computer Controlled Pulp Insulating

The computer control system employs continuous monitoring of the pulp slurry consistency (pulp/water ratio) at the applicator vat, and monitoring of the diameter and moisture level of the insulated conductors via a microprocessor regulated system. In addition there is increased sampling of the pulp insulation weight/foot values. Automatic regulation of the process is carried out at a central facility with easy override by the operator should the process necessitate it. At the heart of the system is a Honeywell TDC 2000 industrial control computer where display and control programs reside. Figure 6 shows an overview of TDC 2000.

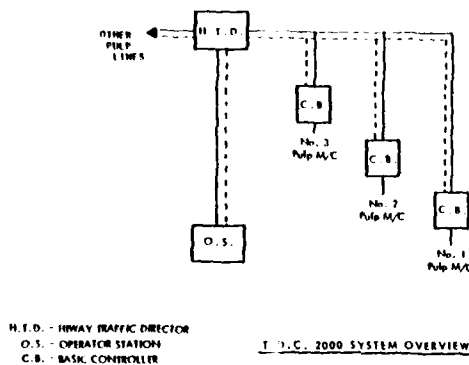


FIGURE 6

The TDC 2000 system consists of standard modular building blocks (Basic Controllers) linked together by a coaxial cable (the Data Highway) into an integrated structure. Each Basic Controller contains a micro-processor with its own "firm ware" and data base, and they are linked to the operating station (screen and keyboard). There is one basic controller per pulp machine (distributed control) and the operating station is backed up continuously by a "Data Entry Panel". The operating station displays for each basic controller (Figure 7) the following eight parameters for monitoring and control purposes:

Zone #1 temperature
Zone #2 temperature
Zone #3 temperature
Pulp flow
Average insulated wire diameter
Average moisture level
Water applicator pressure
Line speed



FIGURE 7

In addition the basic controller can store up to 72 hours of hourly averages of these parameters (Figure 8).

HOURLY AVERAGES									
GRP-002				LINE 2 OVERVIEW				15:30 11/10/82	
06:00	142	550	704	5.31	6.10	0.12	3.00	142	
07:00	141	550	705	5.33	6.11	0.13	3.00	142	
08:00	143	551	703	5.26	6.24	0.10	3.00	143	
09:00	145	551	701	5.21	6.23	0.06	3.00	143	
10:00	145	550	702	5.21	6.13	0.16	3.00	143	
11:00	145	549	702	5.21	6.15	0.11	3.00	143	
12:00	144	551	703	5.21	6.15	0.11	3.00	143	
13:00	144	551	699	5.23	6.20	0.16	3.00	143	
14:00	145	551	695	5.19	6.14	0.05	3.00	143	
15:00	145	551	699	5.11	6.13	0.16	3.00	143	
2TT1	DEGC	2TT2	DEGC	2TT3	DEGC	2FF1	GPM	2AA1	MOIST
ZONE 1	ZONE 1	ZONE 2	ZONE 2	ZONE 1	ZONE 1	ZONE 2	ZONE 2	ZONE 1	ZONE 1
SP/Y	145	550	700	5.10	6.00	0.00	3.00	143	
FW/X	145	549	699	5.08	6.23	0.07	3.00	143	
OUT 4	59.2	60.0	100.0	29.7	10.0	10.0	- 6.7		
A*	A*	A*	A*	A*	A	A	M		

FIGURE 8

The system is interlinked to the field monitors as shown in Figure 9. The user computer allows periodic printouts of diameter and moisture to be obtained as well as providing a means of historical data storage.

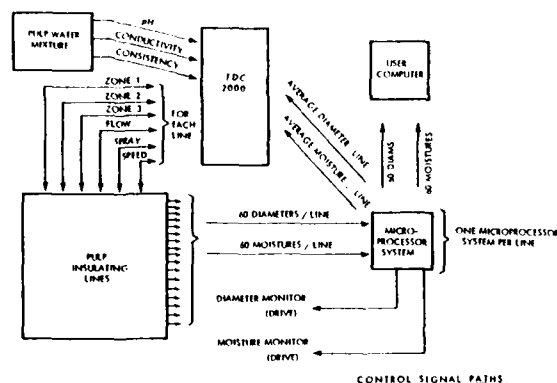


FIGURE 9

The control strategy used by the system is as follows.

The flow of the water/pulp mixture is regulated continuously according to the consistency of the mixture in order to introduce a constant rate of pulp fibers during the application of the pulp to the conductors. The level of flow is additionally changed by the operator according to the average weight/foot of insulation, manually measured at every reel changeover. The average diameter of the 60 wires is automatically measured by a Laser measurement system at the exit of the ovens - this is used to make automatic adjustment to the first zone temperature and to the water applicator pressure (located at the entrance to the ovens) thereby altering the degree of "blowing" out of the insulation when the moisture violently boils out. This combination of average diameter control and average weight/foot control translates into an effective pulp density control which directly influences the dielectric constant of the insulation. Finally the average temperature of the last two oven zones is regulated based on feed back from an on-line moisture monitor and thereby the average moisture level remaining in the insulated wires can be controlled.

Figure 10 shows a schematic representation of the control scheme.

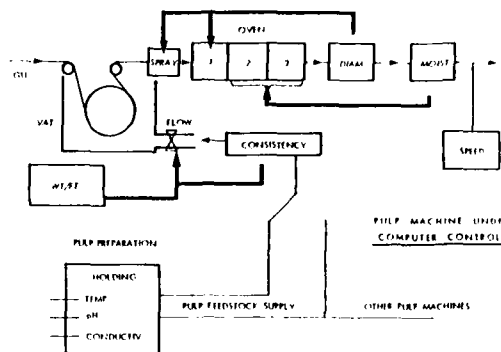


FIGURE 10

In addition to the control capability of the system, production reporting and continuous trending of process parameters allows rapid diagnosis of operating problems (Figure 11).

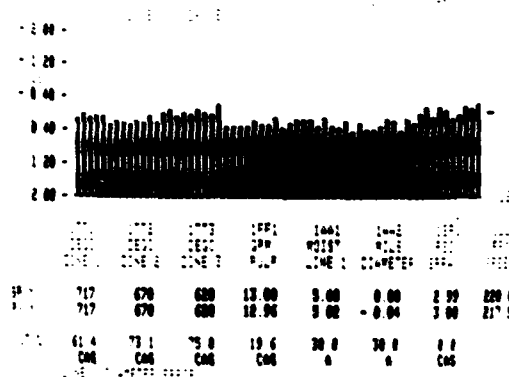


FIGURE 11

6.1 Diameter Monitoring System

The diameter measurement system is based on a laser diameter monitor mounted on a yoke and scanning horizontally over each of the wires in turn (Figure 12). The scanner is driven by a microprocessor system which positions the emitter over each wire successively, spending 10 seconds on each wire to obtain an average value per wire. At the end of the 60 wire traverse, the average of the 60 diameters is computed and transmitted to the TDC 2000 which updates the displayed value and uses it for regulation.

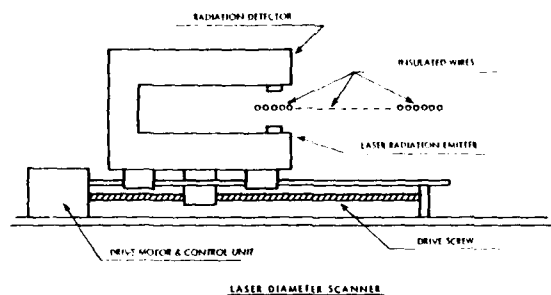


FIGURE 12

6.2 Moisture Monitoring System

A continuous feedback system is required to control pulp insulation moisture content. Equipment to perform this was developed based on the principle of a continuous insulation resistance measurement. There are 60 pairs of pulleys (as shown in Fig. 13), one pair

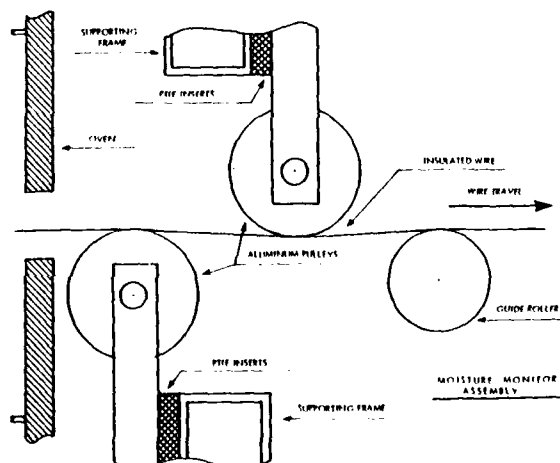


FIGURE 13

per wire, and the microprocessor drives a stepper switch to connect each pair of pulleys in turn to an electronic circuit which measures the insulation resistance across the pulp insulation from which a moisture level value is obtained. Each reading is taken over a 20 second time period permitting an average per wire to be obtained, and the overall average of the 60 wires is transmitted to the TDC 2000 at the end of each scan.

Figure 14 shows the diameter scanner and the moisture monitor pulley system.

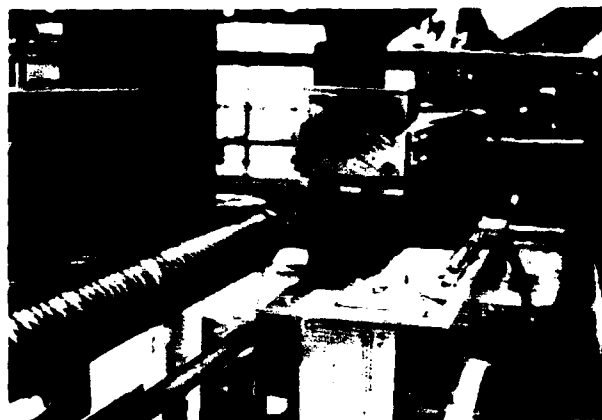


FIGURE 14

7. Improvements of Mutual Capacitance

The system has proven to be very effective in controlling the various parameters to tight tolerances. Typical average improvements of diameter, moisture and density spread were 50%, 40%, and 40%. The capability of producing pulp cables with a tight control of mutual capacitance over a wide range of pulp insulation densities has been established. This is of particular importance in producing a full line of pulp cables with increased pair count density.

In addition, the system, by its continuous wire to wire monitoring capability, permits some lateral control to be manually exercised over the process, and the way is open for a more sophisticated lateral control system to be implemented.

Summary

A computer system for the control of the pulp insulating process has been successfully developed and has demonstrated substantial improvement in the control of pulp insulating parameters under full production conditions. This coupled with manufacturing improvements to subsequent cable operations has been shown to produce cables which meet more stringent requirements for optimum DSL rate PCM applications.

Acknowledgements

The authors wish to thank W.E. Cowley who was a prime contributor in the development and implementation of the system and other members of the Cable R&D Laboratories as well as the members of the Manufacturing and Plant Engineering departments for their contributions to the success of this project and to the material contained within this paper.



Vic LeNir graduated from Manchester University, England with a B.Sc in Physics and received an M.Sc in Computer Science from London University in 1968. Since 1970 he has been a member of the R&D Staff of Northern Telecom Cable Division, Lachine, Quebec and has been involved in the application of computers to the wire coating process in the areas of mathematic modelling and computerized process control.



Wayne A. Cascarano holds a Master of Science degree in chemistry from Concordia University. He joined Northern Telecom in 1970, and is currently working in the Production Engineering department of Northern Telecom's Pulp Communications Cable Module. Mr. Cascarano has worked on several pulp cable development projects and is a member of ASTM and TAPPI.



Michael A. Shannon obtained a M.Sc in solid state physics from Sir George Williams University of Montreal, in 1975.

That same year he joined Northern Telecom's Cable Division, R&D Group where he was involved in simulation modelling and computerized process control.

Currently he is a staff member at the Kingston, Ontario Cable R&D facility and is acting as a project manager in the field of process control and new product development.

Development and Application of Optical Fiber
Composite Overhead Ground Wire (OPT/GW)

H. Nabeshima* K. Tsujimoto* T. Kobayashi**
O. Watanabe** K. Inada** A. Okazato**

* The Kansai Electric Power Co., Inc. Osaka, Japan
** Fujikura Ltd.
1440 Mutsuzaki, Sakura-shi, Chiba-ken, 285 Japan

Abstract

We have developed the optical fiber composite overhead ground wire and have applied the wire to the overhead power transmission line for the purpose of telecommunication systems and lightning observation system. The total system length is about 14 km. The optical fiber cable is inserted into the aluminum pipe settled in the center of the ground wire. Because there is a gap between the optical cable and the aluminum pipe, the optical fiber cable can be replaced to other optical cable without replacing the ground wire when larger capacity telecommunication system is needed or the fiber is failed due to some accident. Cabling, installation and jointing of the optical fiber composite overhead ground wire have been successfully carried out, and average loss of the ground wire and average splice loss using arc-fusion splicing have been obtained less than 0.7 dB/km and less than 0.1 dB, respectively.

1. Introduction

Optical fiber telecommunication systems have been recently applied to various fields because of the properties of low loss, wide bandwidth, no electromagnetic interference, small diameter and so on. Especially, it seems to be advantageous to realize optical fiber telecommunication systems using overhead power transmission lines which have been installed over long distance and wide area.

We have developed the optical fiber composite overhead ground wire to realize these systems. Considering to combine the optical fiber cable to the overhead ground wire, it seems to have many merits that the optical fiber cable inserted in to the overhead ground wire can be replaced with another optical fiber cable without replacing the ground wire when larger capacity telecommunication system is needed or the fiber is failed due to some accident. One of the peculiarities of our newly developed optical fiber composite overhead ground wire is replaceable of the optical fiber cable. Further, ground wire is exposed to severer conditions than usually used optical fiber cable such as

wider temperature range and larger strain. It is necessary that optical fiber cable combined to the ground wire must be withstand these severe conditions.

In this paper, development and properties of our newly developed optical fiber composite overhead ground wire are described and application of this ground wire is also reported.

2. Development of the optical fiber composite overhead ground wire (OPT/GW)

2-1 Design of the overhead ground wire

The overhead ground wire which is combined to the optical fiber has been designed considering the following matters.

(1) Weight, diameter, tensile strength and electric resistance should be almost equal to those of the conventional overhead ground wire.

(2) Straight and smooth aluminum pipe is settled at the center of the overhead ground wire in order to replaceable of the optical fiber cable.

(3) Inner diameter of this pipe is as large as possible.

(4) This pipe should be prevented from being collapsed by lateral pressure due to installation and clamping of the ground wire.

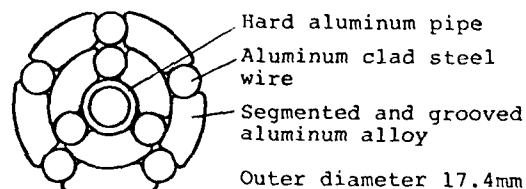


Fig. 1 Structure of the overhead ground wire in which optical cable is inserted

Fig. 1 shows the structure of the designed overhead ground wire considering these matters. Hard aluminum pipe with inner diameter of 3.8 mm is settled at the center of the wire. The aluminum pipe is manufactured by following methods. An aluminum tape is formed by roll forming into a pipe and continuously seamed by arc welding. This seamed pipe is drawn to a

designed diameter and hardness. In drawing process, plug is set in the pipe in order to get the smooth inner surface. Around the hard aluminum pipe, segmented and grooved aluminum alloys and round aluminum clad steel wires are stranded alternately with two layers. Because the alternately stranded alloys and wires compose a hard shell, the aluminum pipe in the center of the shell is prevented from being collapsed by lateral pressure due to installation and clamping.

Table 1 Characteristics of the overhead ground wires

Type	OPT/GW	Usual type
Tensile strength	11100kg	11150kg
Outer diameter	17.4mm	17.5mm
Weight	794.4kg/km	845.6kg/km
Resistance(20°C)	0.220Ω/km	0.293Ω/km

Table 1 shows the characteristics of the developed overhead ground wire as compared with conventional overhead ground wire. And fig. 2 shows the photograph of the both ground wires.

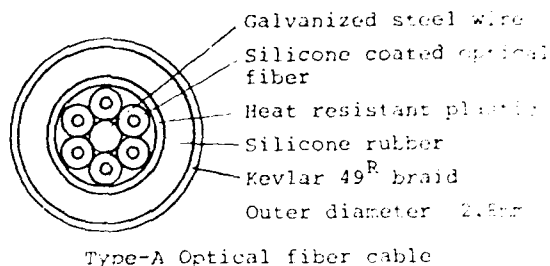


Fig. 2 Photograph of the overhead ground wires

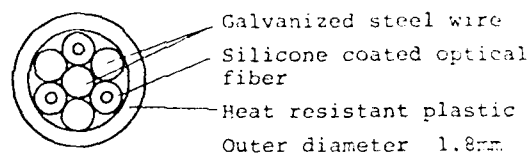
2-2 Design of the optical fiber cables

Graded index optical fibers are used for investigation of the optical fiber composite overhead ground wire. Core diameter and fiber diameter are 50 μm and 125 μm, respectively, and refractive index difference is 1%. Concerning the design of the optical fiber cable which is inserted into the overhead ground wire, the following matters are considered.

(1) Outer diameter of the optical fiber cable should be as small as possible for



Type-A Optical fiber cable



Type-B optical fiber cable

Fig. 3 Structures of the optical fiber cable inserted into the ground wire

the purpose of the replacement.

(2) Friction between optical fiber cable and aluminum pipe should be small.

(3) Optical fiber cable must withstand severe conditions of wide temperature range and large strain.

(4) Almost no loss increase of the fibers must be obtained during cabling and installation.

Fig. 3 shows the structures of designed optical fiber cables considering these matters. Type-A is designed mainly laying emphasis on withstanding wide temperature range. Optical fibers which are coated with silicone resin are stranded around a galvanvanized steel wire and heat resistant plastics are coated on the fiber strand. Furthermore, silicone rubber is coated on the stranded and coated fibers. Because silicone rubber does not melt at high temperature, this cable is not deformed at high temperature larger than 350°C in a short time, and transmission characteristics of the fiber is stable.

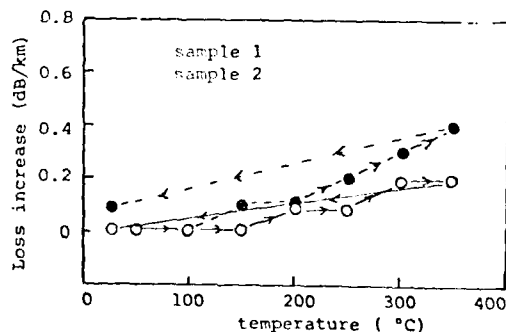


Fig. 4 Loss increase at high temperature of the Type-A optical fiber cable

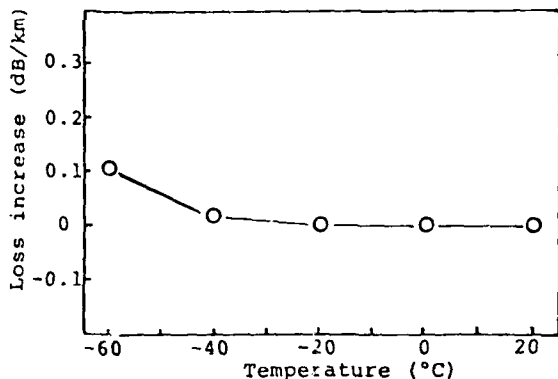


Fig. 5 Loss increase at low temperature of the Type-A optical fiber cable

Fig. 4 shows the loss increase of the optical cable at high temperature. This cable is also stable at low temperature as shown in fig. 5. For the purpose of the replacement of the optical fiber cable, Kevlar 49 are braided as a tension member and as reduction of the friction.

On the other hand, Type-B is designed mainly laying emphasis on replacement of the cable. Silicone coated optical fibers and galvanized steel wires as a tension member are stranded and coated with heat resistant and small friction plastic. This cable can not withstand higher temperature than that which is a melting point of the plastic. But using heat resistant plastic, this cable is stable at the temperature of 250°C in short time, as shown in fig. 6. Concerning replacement of optical cable, Type-B is expected to be easier than Type-A because diameter and friction of Type-B is smaller than Type-A.

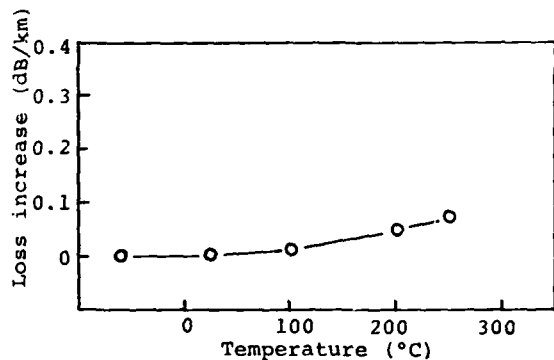


Fig. 6 Loss increase at temperature of the Type-B optical fiber cable

3. Insertion test of the optical fiber cable into the overhead ground wire

Insertion test of the optical fiber cable into the overhead ground wire was carried out for the purpose of prospecting to replace the optical fiber cable. Fig. 7 shows the outline of the insertion test. The overhead ground wire in which lead wire is settled was previously installed as shown in fig. 7. Two types of the optical fiber cables were used for the insertion test. Insertion length was about 400 m. In this test, pulling tension and loss increase of the optical fiber cable were measured.

Table 2 shows the results of the insertion test. Maximum pulling tensions of Type-A and Type-B are 13 kg and 6 kg, respectively. Loss increase of both cables are scarcely observed. As a result, both of the optical fiber cables are obtained to be replaceable. However, Type-B is more advantageous for long span insertion into overhead ground wire than Type-A unless required condition of the temperature is higher than 250 C.

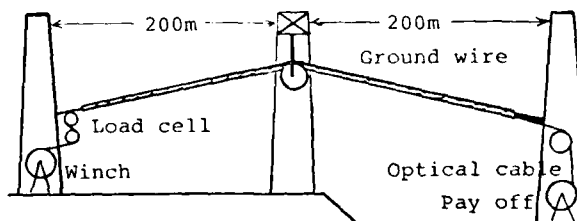


Fig. 7 Outline of the insertion test of the optical fiber cable

Table 2 Results of the insertion test of the optical fiber cables

Cable type	Type-A	Type-B
Pulling tension	13 kg	6 kg
Average loss increase of the optical fiber	0.01dB/km	0.02dB/km

4. Application of the optical fiber composite overhead ground wire

Various mechanical tests for the optical fiber composite overhead ground wire were carried out such as installation test, vibration test, galloping test, heavy load test, field test and temperature test, and good results have been obtained. After these tests, The ground wire has been applied to 500 kv overhead power transmission line (presently operating at 275 kv) for the purpose of the lightning system and

telecommunication test by Kansai Electric Power Company. This line is named Kada-Reinan line and is settled in the central part of Japan. The line is passing the mountainous area and exposed to severe meteorological conditions, especially in winter. The total system length is about 14 km. The construction of the ground wire was conducted in 1981. Type-A optical fiber cables have been mainly used for this application. The optical fiber cable was inserted during cabling process of the ground wire. Loss increase of the optical fibers during cabling were scarcely found. The installation of the ground wire was carried out by the conventional method in Japan without any problem. Fig. 8 shows the photograph of the installed optical fiber composite overhead ground wire. After installation, tensioning and clamping, loss increase of the fibers were scarcely observed. Fig. 9 shows the histogram of the loss of the fibers of the

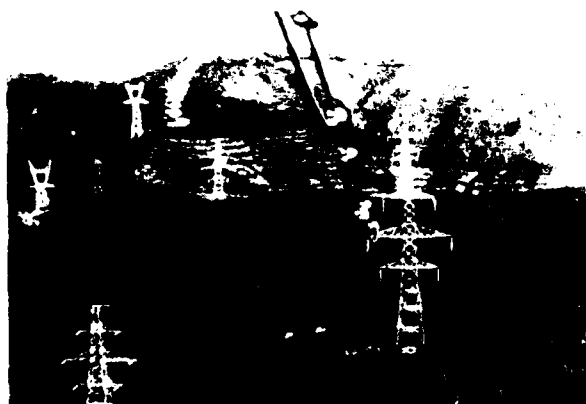


Fig. 8 Photograph of the installed OPT/GW

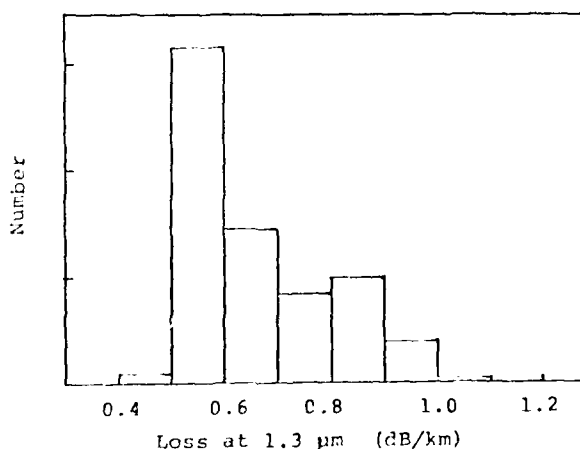


Fig. 9 Histogram of the loss of the OPT/GW

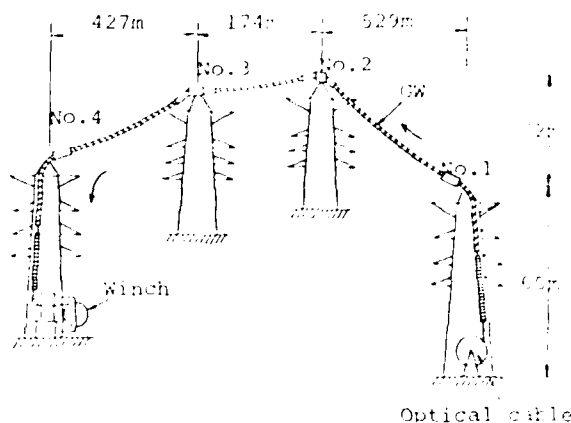


Fig. 10 Outline of the steel tower with the insertion of the optical fiber cable

installed ground wires. Average loss was found to be less than 0.7 dB/km at the wavelength of 1.3 μm.

Insertion of the Type-B optical fiber cable was also performed using this line. Fig. 10 shows the outline of the steel towers using the insertion of the optical cable. Fig. 11 shows the pulling tension of the insertion of the optical cable. Tension increased extremely at the no. 4 steel tower because of a bend of the ground wire at the top of the no. 4 steel tower.

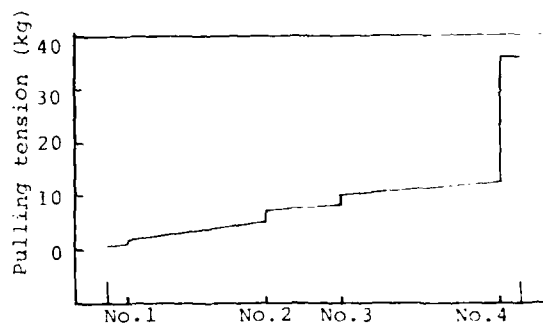


Fig. 11 Pulling tension of the optical fiber cable during insertion

Table 3 Transmission of the optical fiber cable at before and after insertion (Wavelength: 1.3 μm)

	Before insertion	After insertion
No.1 core	0.74 dB/km	0.74 dB/km
No.2	0.85	0.77
No.3	0.56	0.62
Average	0.72 dB/km	0.71 dB/km

However, except no. 4 steel tower, the optical fiber cable of 1.1 km long could be inserted at the small pulling tension. After insertion, loss of the fiber was observed not to increase as shown in table 3.

The jointing of the optical fiber composite overhead ground wire was performed at the top of the steel tower. Fig. 12 shows the jointing method at the top of the steel tower. After clamping, the ground wire was wound about two times in the steel tower and optical fiber cable was jointed. Optical fibers are spliced using arc-fusion splice machine which has a battery. Fig. 13 shows the splicing of the fibers at the top of the steel tower. In spite of the bad operating conditions at the top of the steel tower such as cold, windy, rainy and vibrated conditions, the arc-fusion splice was performed successfully and average splice loss was less than 0.1 dB.

After construction of the optical fiber composite overhead ground wire, loss change of the fibers have been observed. During about forty days, loss changes were observed less than 0.1 dB.

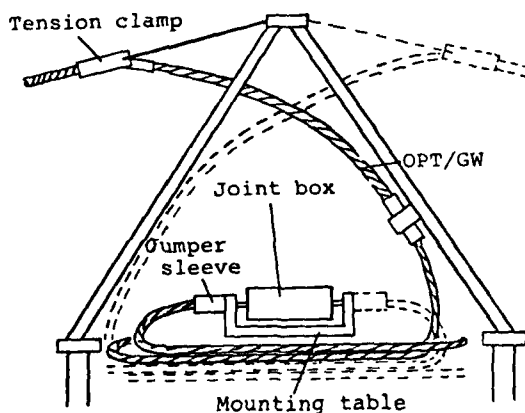


Fig. 12 Jointing of the OPT/GW at the top of the steel tower

5. Conclusion

We have developed the optical fiber composite overhead ground wire having a property that optical fiber cable can be replaced without replacing overhead ground wire. This ground wire has been applied to the live overhead power transmission line without any problem. We believe that optical fiber composite overhead ground wire will be one of the main telecommunication media.

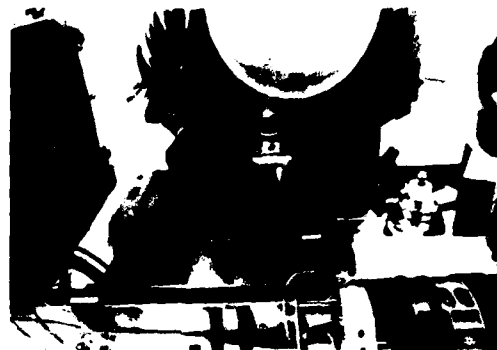


Fig. 13 Photograph of the arc-fusion splicing of the OPT/GW at the top of the steel tower

References

- (1) R. Yamauchi, et al., "Optimum structure of high density and low loss fiber units" 7th ECOC Sep. 1981
- (2) B. J. Maddock, et al., "Optical fibre communication using overhead transmission lines" CIGRE 35-01, 1980
- (3) H. Benndorf, et al., "Fiber-optic system for transmission of information of high voltage overhead power lines" CIGRE 35-09 1980



Hisashi Nabeshima was born in 1931. He received the B.S. degree in electric communication from Osaka University in 1953. In 1953, he joined the Kansai Electric Company Inc., Osaka, Japan, where he has been engaged in the investigation and design of telecontrol communication for power system. Since then, he served as a manager for research and development planning of Technical Research Center. Presently he is the Manager of Research Planning and the Telecontrol Communication R&D Group in Technical Research Center. Mr. Nabeshima is a member of the Institute of Electrical Engineers of Japan.



Kenzo Tsujimoto was born in 1937. He received the B.E. degree from Osaka University in 1960. In the same year, he joined the Kansai Electric Power Co., Inc., and has been engaged in design and construction of overhead transmission lines. Now he is the chief of Construction Transmission Section of System Engineering Department, and a member of J.I.E.E.



Koichi Inada was born in 1941. He joined Fujikura Ltd. after his graduation from Yokohama National University in 1963 and has been engaged in research and development of high frequency coaxial cable, leaky wave coaxial cable, super conducting cable, millimeter waveguide and optical cable. In 1976, he received Ph.D degree from Tokyo Institute of Technology. He is now a head of optical fiber and cable development section and a member of the Institute of Electronics and Communication Engineers of Japan and the IEEE of the U.S.A.



Toshiaki Kobayashi was born in 1947. He joined Fujikura Ltd. after his graduation from Tohoku University in 1971 and has been engaged in research and development of materials and constructions of the metallic cables and optical cables. He is now a senior engineer of optical fiber and cable section and a member of the Institute of Electronics and Communication Engineers of Japan.



Akira Okazato was born in 1945. He is received B.E. degree in electrical engineering from Kyoto University in 1968. In 1968, he joined Fujikura Ltd. and has been engaged in research, development and engineering of overhead transmission line, and now a assistant of engineering department of overhead transmission line division. He is a member of J.I.E.E.



Okosu Watanabe was born in 1945 and graduated from Musashi Institute of Technology with a B.E. degree in telecommunication engineering in 1968. He joined Fujikura Ltd. in 1968 and has been engaged in research and development of automatic telephone cable splicing machine, alarm system for telephone cable plant and optical fiber splicing. He is a member of IECE of Japan.

GAMMA IRRADIATION CHARACTERISTICS OF OPTICAL FIBERS

Kiyoshi Shibuya*, Kenji Yagi*, Norio Sugiyama*,
Takeshi Kojima* and Akitoshi Yoshinaga**

*Showa Electric Wire and Cable Co., Ltd.
**Toshiba Research and Development Center,
Toshiba Corporation

SUMMARY

The characteristics of optical fibers during 60 Co γ irradiation, i.e. the effect of dopant, OH content, dose rate and temperature were investigated. Moreover, the model which presumes the effect of long term use from the result of short term irradiation was investigated. The range of environment and a type of fiber which could be used for a long time was decided.

From experimental results, it became clear that the fiber which could be used in radiation exposed area was only pure silica core fiber. Moreover, the increase of transmission loss of pure silica core fiber was able to be explained from the model of color center formation by irradiation and from the dose rate dependence. The increase of transmission loss of pure silica core fiber used for a long time was presumed quantitatively. So we could find the guide of optical fiber cable design for long time use in radiation exposed area.

In addition, the degradation of mechanical strength by irradiation was investigated.

INTRODUCTION

Optical fiber is rapidly being developed to operate in nuclear environments because of its low loss and high bandwidth. For this purpose, it is essential to know how radiation affects transmission properties and mechanical strength of fibers. Optical communication systems used in an atomic power plant will be required to withstand exposure to nuclear environments. Although radiation-induced loss in optical fiber has been studied by some investigators^{1),2)}, more quantitative studies must be made on the growth and the recovery of radiation induced loss and the influence to mechanical strength. This report is concerned with the induced loss in various types of optical fibers during steady-state 60 Co gamma ray irradiation. We also describe the effects of ambient temperature, OH content in fiber and irradiation dose rate on the growth and recovery of radiation-induced loss, also

propose a model by which the lifetime of fiber can be estimated from accelerated irradiation.

SAMPLES AND IRRADIATION CONDITIONS

The samples are Ge-P doped silica core GI type fiber, Ge-B doped silica core GI type fiber, P doped silica core SI type fiber, pure silica core silicone clad fiber and pure silica core B-F clad fiber. All optical fibers were jacketed with nylon. Irradiated fiber length was 100 to 500 m. A experimental apparatus for measuring the radiation-induced loss in optical fiber waveguides is shown in Fig. 1.

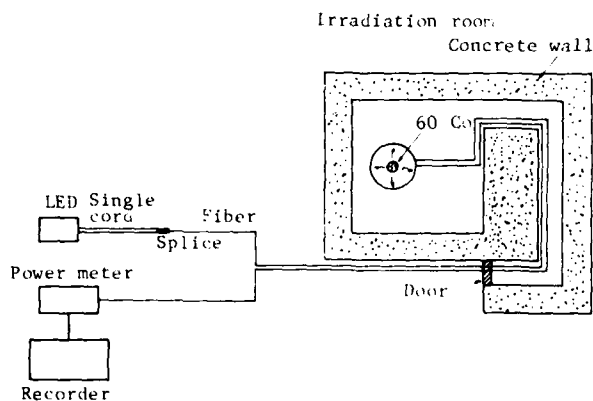


Fig. 1 The Experimental Apparatus

The apparatus consists of a light source and injection optics, the fiber, a constant temperature chamber, a source of radiation (60 Co) and a detector. The dose rate was determined by changing the distance between the radiation source and samples in the chamber. Samples and dose rate and total dose for each sample are listed in Table 1.

Table 1 Samples and Measurement Conditions

Fiber	Dose rate (R/H)	Total dose (R)	Wave-length (μm)	OH (ppm)	Remarks
Ge-P doped core GI type	30	5.0×10^3	0.84	-	
			1.26	-	
Ge-B doped core GI type	3	1.2×10^4	-	-	*1
P doped core SI type	30	5.0×10^3	0.84	-	
Pure silica core	3	1.2×10^4	-	-	*1
Silicon clad SI type	780	1.0×10^5	0.84	2	
	3	1.2×10^4	-	2	*1
	780	1.0×10^5	0.84	2	
Pure silica core	1.55×10^4	2.2×10^5	0.84	2	50°C, 80°C *2
B-F doped clad	2.3×10^4	3.2×10^5	0.84	2	
SI type	3.4×10^4	4.8×10^5	0.84	2	
	6.2×10^4	8.7×10^5	0.84	2	
	7.0×10^4	1.0×10^6	0.84	2	
Pure silica core	1.0×10^5	1.7×10^6	0.84	10	
B-F doped clad	3.0×10^5	5.0×10^6	0.84	10	
SI type	5.0×10^5	8.4×10^6	0.84	10	
	7.0×10^5	1.0×10^7	0.84	10	

*1: Intermittent irradiation for about 4,000 hours

*2: Irradiation at room temperature except 50°C and 80°C

RADIATION INDUCED LOSS IN FIBER

1. Ge-P doped silica core fiber

Fig. 2 shows radiation induced loss (at 0.84 and 1.26 μm) in the Ge-P doped silica core GI type fiber as a function of dose in situ steady state 60 Co irradiation.

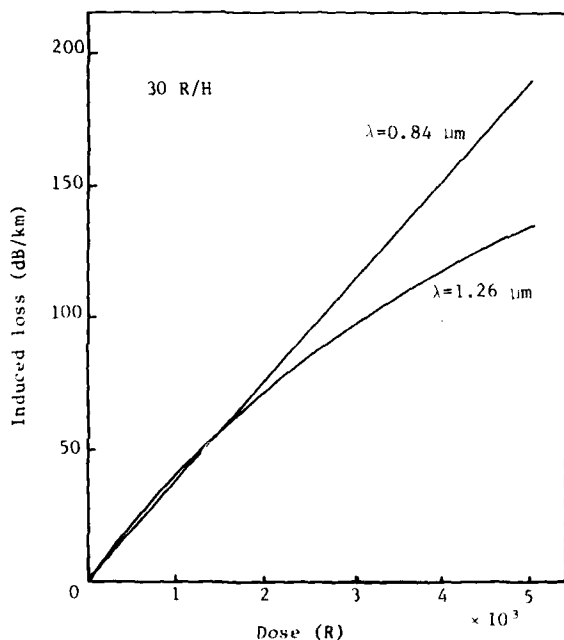


Fig. 2 Radiation-induced Loss (Ge-P Doped Core GI Type)

At 0.84 μm , the induced loss was great in spite of the low dose rate 30 R/H, and was proportional to the dose. The induced loss per unit dose was 0.03 to 0.04 dB/km/R. The induced loss at 1.26 μm grew in low dose range like at 0.84 μm , but was not proportional to dose in the high dose range.

Fig. 3 shows the recovery of the radiation induced loss in this fiber after irradiation. The additive loss remains 60 dB/km at 0.84 μm even after 7 weeks at room temperature.

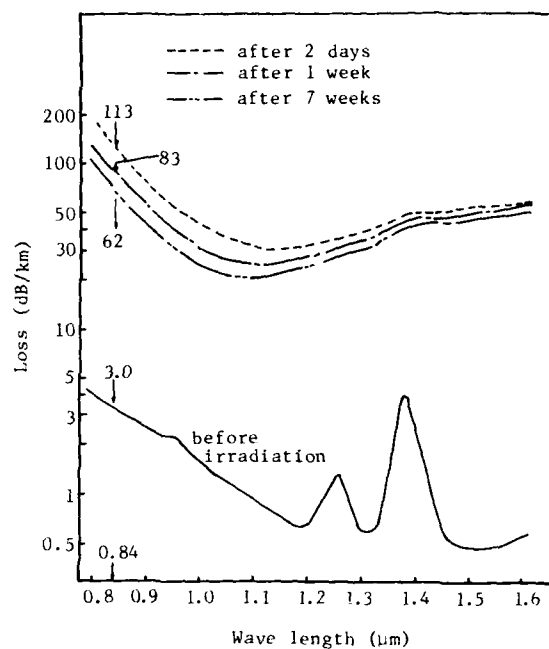


Fig. 3 Loss Spectra after Irradiation (Ge-P Doped Core GI Type)

2. Ge-B doped silica core fiber

Fig. 4 shows the loss spectra of the Ge-B doped silica core fiber to be irradiated for about 4,000 hours at 3 R/H. The radiation induced loss measured immediately after irradiation was 18 dB/km at 0.84 μm in spite of being as low as 3 R/H.

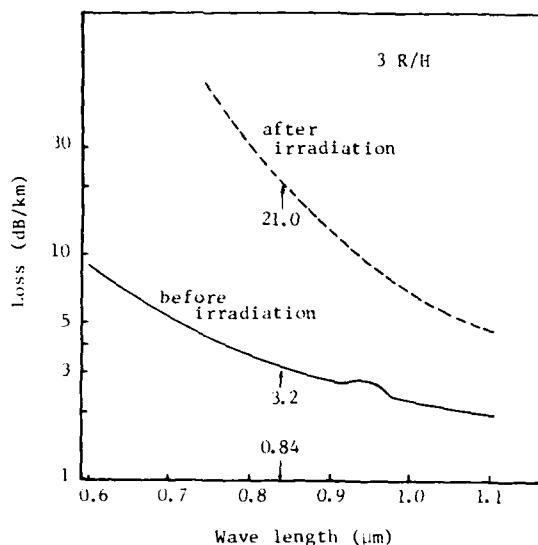


Fig. 4 Loss Spectra after Irradiation (Ge-B Doped Core CI Type)

3. P doped silica core fiber

Fig. 5 shows the radiation induced loss in the P doped silica SI type fiber.

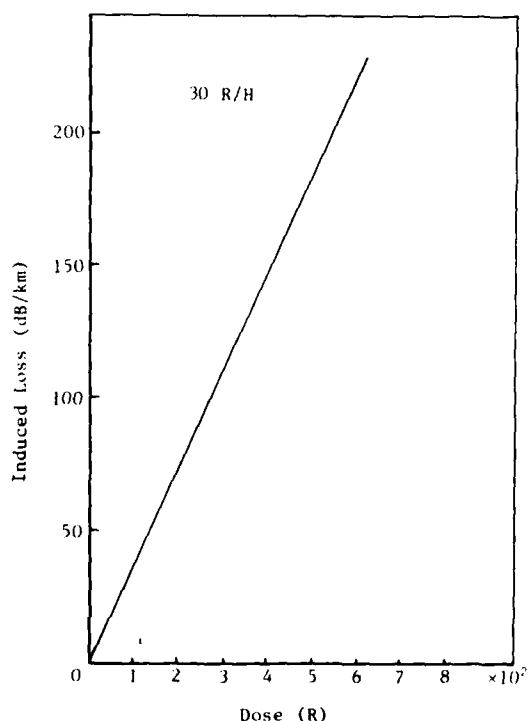


Fig. 5 Radiation-induced Loss (P Doped Core SI Type)

The induced loss is proportional to the dose and the induced loss per unit dose is 0.3 to 0.4 dB/km/R, which is about 10 times of that in Ge-P doped core fiber.

4. Pure silica core fiber

Ge, P or B increases the radiation sensitivity as described above, but the pure silica core fiber is considered to lower radiation sensitivity than a doped silica core fiber. Fig. 6 shows the radiation induced loss in pure silica core silicon clad fiber and pure silica core B-F doped silica clad fiber at 780 R/H dose rate. The induced loss is saturated at 3.5 dB/km in B-F doped silica clad fiber and at 4 dB/km in silicone clad fiber over dose of 7×10^3 R. The radiation-induced loss in B-F doped silica clad fiber after irradiation recovered to the level of before irradiation in about 3 weeks but in the case of silicone clad fiber, the additional loss is 0.7 dB/km in 7 weeks after irradiation. The degradation of the cladding silicon caused by irradiation attribute the additional loss. In the condition at dose rate of 3 R/H and radiation time of 4,000 H, the induced losses of both fibers were not detected.

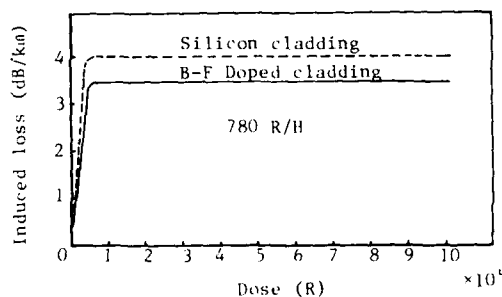


Fig. 6 Radiation-induced Loss (Pure Silica Core Fiber)

Fig. 7 shows the radiation induced loss at 0.84 μ m in the pure silica core B-F doped silica clad fibers with different OH contents at 7×10^4 R/H dose rate. The effect of OH content on the radiation response of pure silica core fiber is clearly evident in Fig. 7. The fibers which have a much lower OH content, have greater radiation sensitivity.

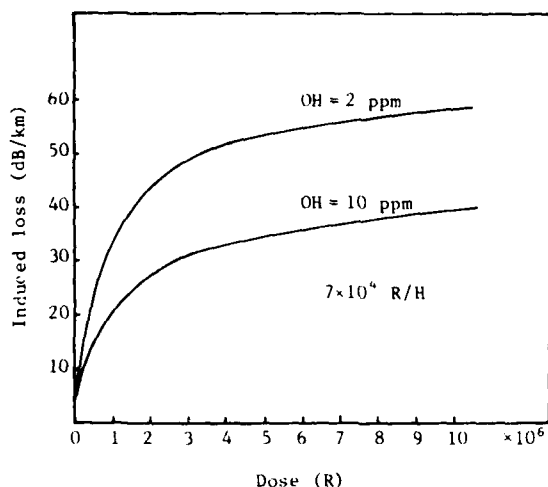


Fig. 7 Radiation-induced Loss (Pure Silica Core Fiber)

Fig. 8 shows the radiation induced loss in the pure silica core fiber with 2 ppm OH during irradiation at 6.2×10^4 R/H over the $0.6 \sim 1.1 \mu\text{m}$ wavelength range. A loss spectrum can be obtained following the irradiation by sweeping the wavelength with the monochromator. The induced loss measured at $0.84 \mu\text{m}$ seems to be primarily due to the tail of an intense induced absorption in the UV and visible.

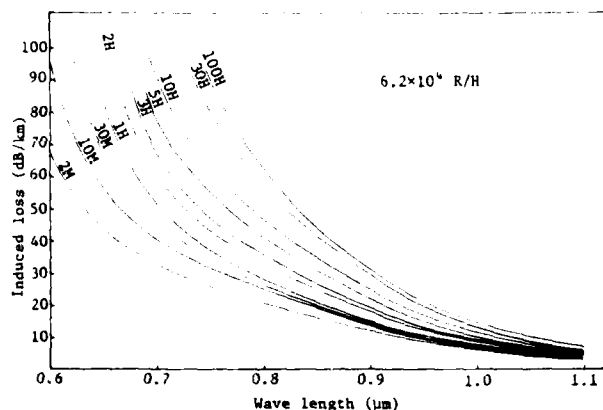


Fig. 8 Radiation-induced Loss Spectra during Irradiation

The growth and recovery of radiation induced loss depends upon the core glass composition and pure silica core fiber withstands exposure to radiation environments.

DOSE RATE DEPENDENCE OF RADIATION INDUCED LOSS

We quantitatively discuss the production of color centers in pure silica core fiber during steady state 60 Co irradiation, and estimate the lifetime of the fiber in the radiation environments.

1. Growth of radiation induced loss³⁾

Dotted line in Fig. 9 shows the radiation induced loss vs. time in pure silica core fiber at dose rates (1.55×10^4 , 2.3×10^4 , 3.4×10^4 and 6.2×10^4 R/H).

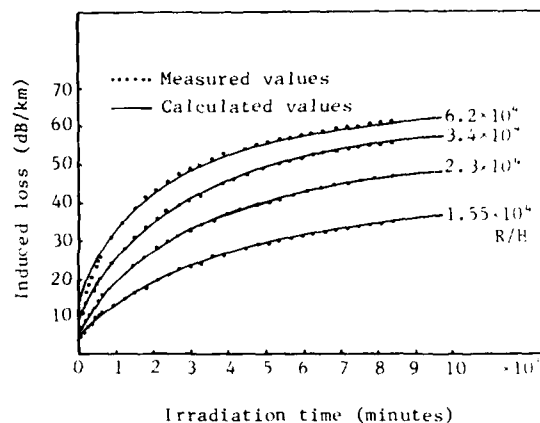


Fig. 9 Radiation-induced Loss of Pure Silica Fiber (OH 2 ppm)

The measured data in Fig. 9 (dotted lines) can be accurately fitted by the expression

$$\Delta\alpha = \alpha L t + \sum_i \alpha_i \{1 - \exp(-\lambda_i t)\} \quad (1)$$

Where, $\Delta\alpha$ is the induced loss and t the irradiation time. The fitting is accomplished by a computerized least-squares procedure. The constant (αL , α_i , λ_i) from the fit were listed in Table 2.

Table 2 The Coefficient of Equation (1) (OH 2 ppm)

	1.55×10^4 (R/H)	2.3×10^4 (R/H)	3.4×10^4 (R/H)	6.2×10^4 (R/H)
λ_1	5.1×10^{-4}	5.4×10^{-4}	6.9×10^{-4}	8.6×10^{-4}
λ_2	8.0×10^{-3}	8.7×10^{-3}	9.5×10^{-3}	1.1×10^{-2}
λ_3	1.4×10^{-1}	2.0×10^{-1}	2.5×10^{-1}	4.3×10^{-1}
α_L	1.5×10^{-3}	1.8×10^{-3}	2.1×10^{-3}	1.8×10^{-3}
α_1	17.50	26.04	30.81	33.69
α_2	0.96	1.60	1.77	5.52
α_3	4.45	5.15	6.12	6.55

2. Analysis of experimental results

The results presented in the previous section can be qualitatively understood on the basis of a simple kinetic model for color-center formation. Assume first that an initial precursor concentration P_{0i}

exist in glass before irradiation, and that additional precursors are created at a constant rate of K_i during irradiation. Second, assume that during irradiation, carrier trapping at precursors proceeds at a rate proportional to the number of empty precursor sites, with rate constant F_i . Finally, assume that both thermal untrapping and carrier recombination remove charges from precursor traps at rates proportional to the concentration of trapped charges, the respective rate constants being U_i and R_i . This leads to the equation

$$\frac{dN_i}{dt} = F_i(P_{oi} + K_{it} - N_i) - (R_i + U_i)N_i \dots (2)$$

Where N_i is the concentration of filled trapping sites of the i -th type. The simplest solution of (2) are obtained by assuming that each of the i components are independent. The solution, for $N_i = 0$ at $t = 0$, is

$$N_i = \frac{F_i}{F_i + R_i + U_i} \left[(P_{oi} - \frac{K_{it}}{F_i + R_i + U_i}) (1 - \exp - (F_i + R_i + U_i)t) + K_{it} \right] \dots (3)$$

If the observed absorption is assumed proportional to a linear combination of i -th different carrier trap concentration whose behavior is given by (3), growth curve expression of the from (1) are obtained immediately. Data obtained at different dose rates are consistent with the models discussed above. Assume that F_i , R_i and K_i are directly proportional to the dose rate ϕ , this leads to the expression for the λ_i coefficients

$$\lambda_i = A_i \phi + U_i \dots (4)$$

$$\alpha L = B \phi \dots (5)$$

Also, since α_i should be equivalent to the collision probability, it can be expressed as follows;

$$\alpha_i = \alpha_{oi} \exp(-C_i/\phi) \dots (6)$$

Where A_i , B , α_{oi} and C_i are intrinsic constants of core materials. λ_i , αL and α_i in Table 2 are shown in Fig. 10, 11 as function of dose rate ϕ . These relations in Fig. 10, 11 fit to the assumption (4), (5), (6).

From the above, the radiation induced loss during steady state 60 Co irradiation as function of dose rate and irradiation time can be expressed by the following;

$$\Delta \alpha = B \phi t + \sum_i \alpha_{oi} \exp(-C_i/\phi) \{ 1 - \exp - (A_i \phi + U_i)t \} \dots (7)$$

The induced loss at low dose rate for long irradiation time can be quantitatively estimated from equation (7).

The solid lines in Fig. 9 are based on values obtained by calculating equation (7) with A_i , B , C_i of Fig. 10, 11.

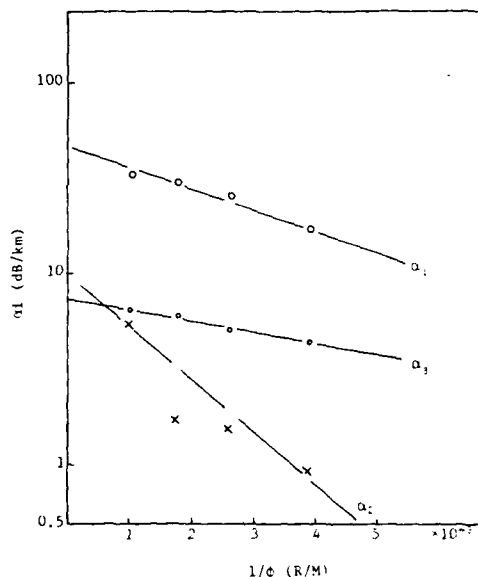


Fig. 10 Dose Rate Dependence of α_i (OH 2 ppm)

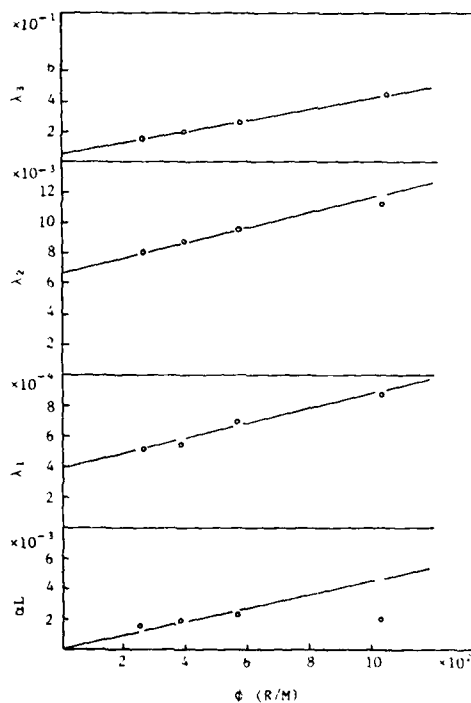


Fig. 11 Dose Rate Dependence of λ_i and αL (OH 2 ppm)

3. Effect of ambient temperature

The measured induced loss is influenced by experimental parameters such as temperature. In order to confirm the effect of ambient temperature during irradiation, the relation of the radiation induced loss vs. the irradiation time were measured at $50 \pm 2^\circ$ and $80 \pm 2^\circ\text{C}$. The dotted lines in Fig. 12 show the radiation induced loss at them.

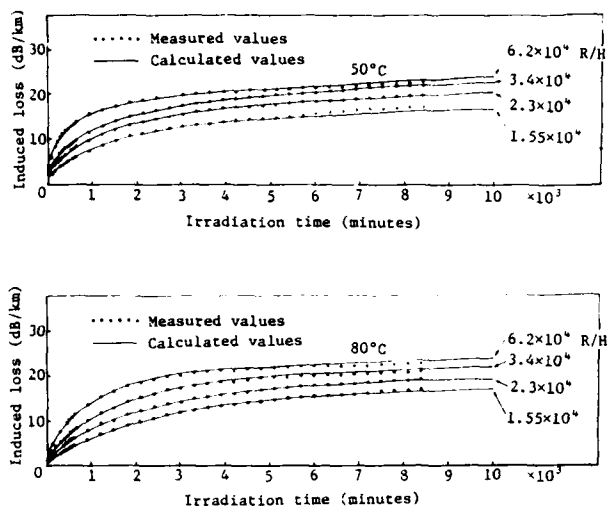


Fig. 12 Radiation-induced Loss of Pure Silica Core Fiber (OH 2 ppm, 50°C and 80°C)

The constants of equation (1) obtained from the dotted curve are shown in Table 3, Fig. 13, 14, 15. As is shown, if two identical fibers are irradiated at the same total dose and the same dose rate at different temperatures, the induced loss at low temperature is greater than that at high temperature. The solid lines in Fig. 12 are calculated values, obtained in the same way as in Fig. 9.

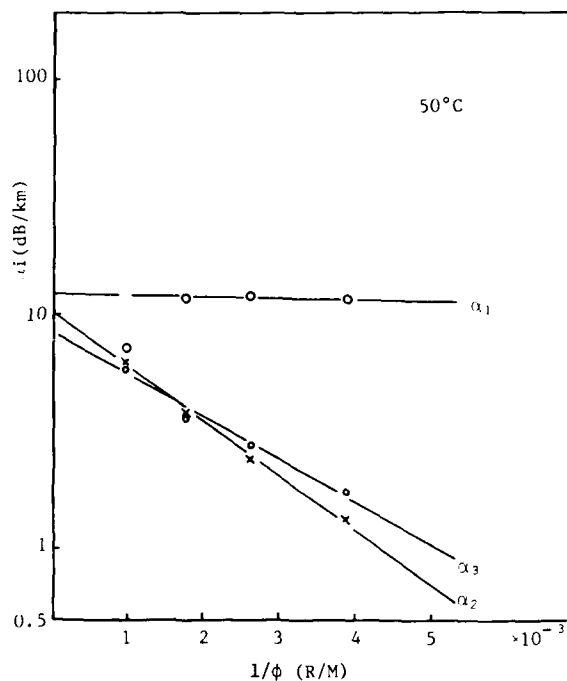


Fig. 13 Dose Rate Dependence of α_i (50°C)

Table 3 The Coefficient of Equation (1) (Temperature Effect)

	50°C				80°C			
	1.55×10^4 (R/H)	2.3×10^4 (R/H)	3.4×10^4 (R/H)	6.2×10^4 (R/H)	1.55×10^4 (R/H)	2.3×10^4 (R/H)	3.4×10^4 (R/H)	6.2×10^4 (R/H)
λ_1	4.9×10^{-4}	5.1×10^{-4}	4.9×10^{-4}	6.0×10^{-4}	3.1×10^{-4}	3.2×10^{-4}	3.0×10^{-4}	4.3×10^{-4}
λ_2	2.8×10^{-3}	2.9×10^{-3}	2.9×10^{-3}	3.5×10^{-3}	1.0×10^{-3}	1.6×10^{-3}	1.7×10^{-3}	1.8×10^{-3}
λ_3	3.1×10^{-2}	3.2×10^{-2}	3.5×10^{-2}	3.9×10^{-2}	7.0×10^{-3}	7.3×10^{-3}	5.7×10^{-3}	7.0×10^{-3}
α_L	2.3×10^{-4}	3.2×10^{-4}	4.1×10^{-4}	4.5×10^{-4}	0.3×10^{-5}	0.7×10^{-5}	1.0×10^{-5}	1.7×10^{-5}
α_1	11.83	12.01	11.55	7.15	15.71	16.30	16.38	14.18
α_2	1.35	2.45	3.82	6.30	0.86	1.95	4.02	5.09
α_3	1.75	2.81	3.61	5.90	1.66	2.32	3.41	4.90

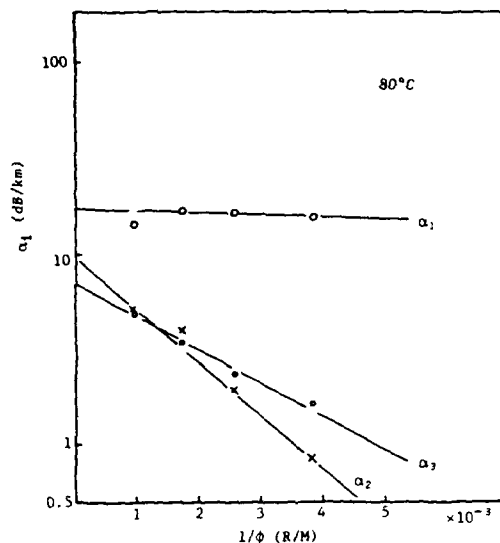


Fig. 14 Dose Rate Dependence of α_i (80°C)

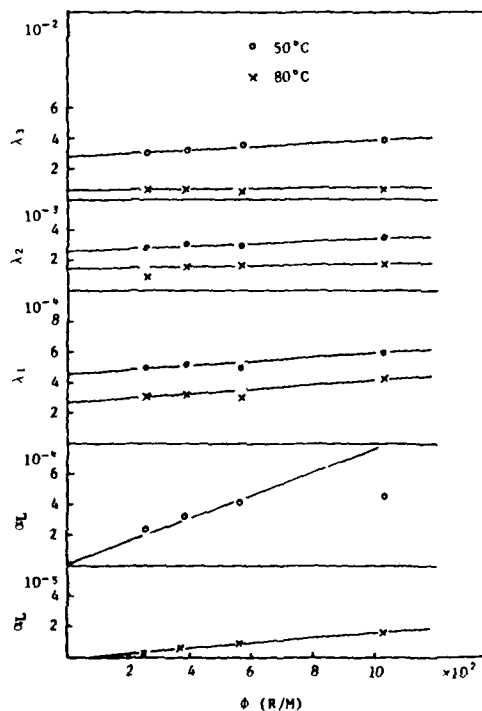


Fig. 15 Dose Rate Dependence of λ_i and α_L (50°C, 80°C)

4. OH content

As shown in Fig. 7, the induced loss changes with OH content in fiber. It is important to discuss the effect of OH content on the parameters λ_i , α_L and α_i for forecasting the induced loss for a long time. Data obtained by irradiating the 10 ppm OH content fiber, at dose rate 1×10^4 R/H, 3×10^4 R/H, 5×10^4 R/H and 7×10^4 R/H, at $0.84 \mu\text{m}$ are shown in Fig. 16 with dotted line. Table 4 lists the parameter calculated from the equation (1), and Fig. 17 and Fig. 18 show the dose rate dependence of above parameters. It seems that the OH content dominantly affects on α_L .

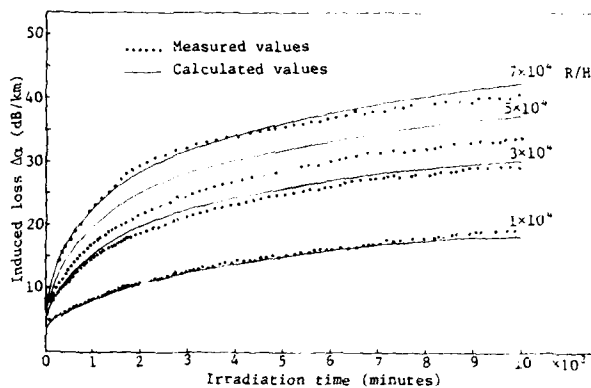


Fig. 16 Radiation-induced Loss of Pure Silica Core Fiber (OH 10 ppm)

Table 4 The Coefficient of Equation (1) (OH 10 ppm)

	$1 \times 10^4 \text{ R/H}$	$3 \times 10^4 \text{ R/H}$	$5 \times 10^4 \text{ R/H}$	$7 \times 10^4 \text{ R/H}$
λ_1	2.9×10^{-4}	3.3×10^{-4}	4.6×10^{-4}	3.0×10^{-4}
λ_2	2.0×10^{-3}	2.5×10^{-3}	3.2×10^{-3}	1.4×10^{-3}
λ_3	2.1×10^{-1}	7.1×10^{-1}	2.9×10^{-1}	3.3×10^{-1}
α_L	2.0×10^{-4}	5.0×10^{-4}	7.8×10^{-4}	1.1×10^{-3}
α_1	11.85	15.11	15.82	7.51
α_2	0.73	4.93	4.88	21.96
α_3	4.32	5.00	5.71	4.00

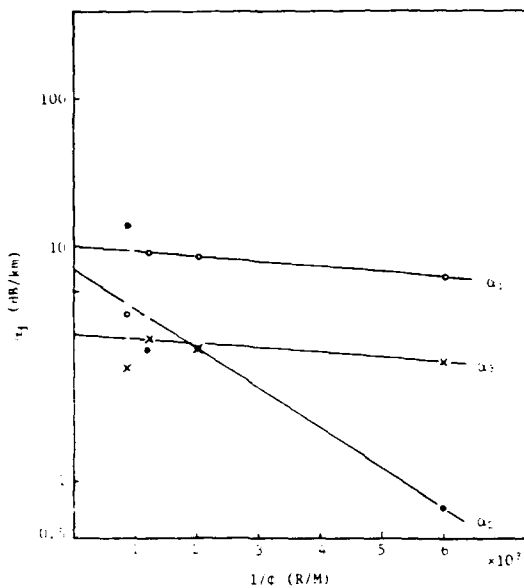


Fig. 17 Dose Rate Dependence of α_i (OH 10 ppm)

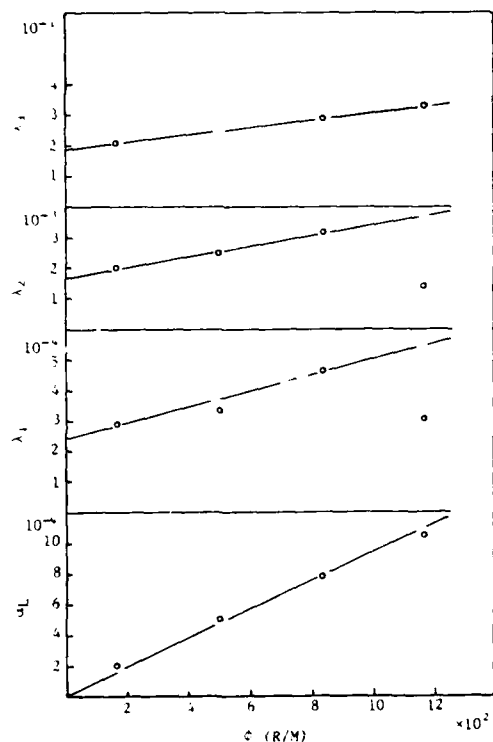


Fig. 18 Dose Rate Dependence of λ_i and α_L (OH 10 ppm)

5. Estimate of induced loss

The radiation-induced loss can be estimated for a long time at a low dose rate. For example, the induced loss during irradiation at 20 R/H are shown in Fig. 19.

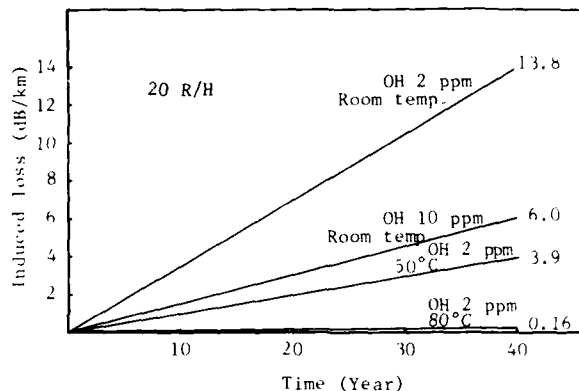


Fig. 19 Forecast of Radiation-induced Loss at Low Dose Rate

In the case of fiber containing 2 ppm OH, the radiation-induced loss at 50°C is only about one third of that at a room temperature, and the induced loss is almost negligible at 80°C. In the case of optical fiber containing 10 ppm OH, the radiation-induced loss is no greater than half of that of 2 ppm fiber.

We have thus been able to obtain a guide for installing optical fiber in radiation environment for a long time.

DECAY OF RADIATION-INDUCED LOSS

The radiation induced loss immediately begins to decrease once the γ -ray irradiation is terminated. Fig. 20 shows the decay curves of the induced losses in pure silica core fiber following the irradiation shown in Fig. 12 and 16.

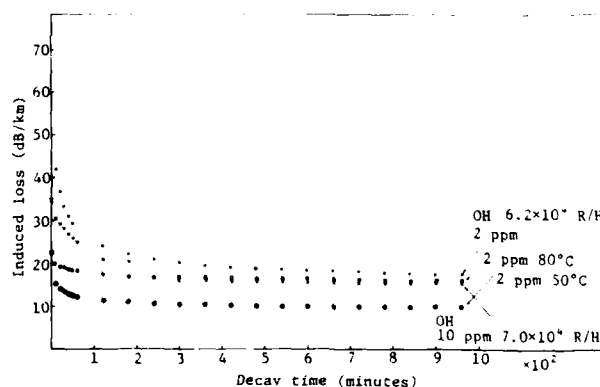


Fig. 20 Decay of the Induced Loss

All decay curves can be resolved into four decaying exponential components as given by the expression

$$\Delta_{ad} = \sum_{i=1}^4 \lambda_{di} \exp(-\lambda_{di} t) \dots\dots\dots (8)$$

Where Δ_{ad} is the induced loss at the time t and t the time after irradiation. The fitting procedure is similar to that mentioned above. Values of constants (λ_{di} , M_i) obtained from the fit are shown in Table 5.

The values of λ_{di} remain almost constant on all fiber, without depending on the dose rate, and $\lambda_{di}/\sum_{i=1}^4 M_i$ also is not changed

by the dose rate. The rate of a short lived component in induced loss is the majority. A long lived component is greater as the temperature rises and more OH is contained. From these results, equation (8) can be expressed in the following equation:

$$\Delta_{ad}/\Delta_{ao} = \sum_{i=1}^4 M_i \exp(-\lambda_{di} t) \dots\dots\dots (9)$$

Where, Δ_{ao} is the radiation-induced loss at the time when the irradiation is terminated, and M_i is the rate of i -th decaying exponential components. The relations of the standardized induced loss vs. decay time are shown in Fig. 21.

Table 5 The Coefficient of Equation (8)

OH 2ppm	$1.55 \cdot 10^{-1}$	$2.3 \cdot 10^{-1}$	$3.4 \cdot 10^{-1}$	$6.2 \cdot 10^{-1}$	Average	OH 10ppm	$1.0 \cdot 10^{-1}$	$3.0 \cdot 10^{-1}$	$5.0 \cdot 10^{-1}$	$7.0 \cdot 10^{-1}$	Average
λ_{d1}	$1.0 \cdot 10^{-3}$	$1.1 \cdot 10^{-3}$	$1.4 \cdot 10^{-3}$	$1.4 \cdot 10^{-3}$	$1.23 \cdot 10^{-3}$	λ_{d1}	$2.3 \cdot 10^{-3}$	$2.1 \cdot 10^{-3}$	$2.3 \cdot 10^{-3}$	$2.1 \cdot 10^{-3}$	$2.2 \cdot 10^{-3}$
λ_{d2}	$10.9 \cdot 10^{-3}$	$9.8 \cdot 10^{-3}$	$7.3 \cdot 10^{-3}$	$8.4 \cdot 10^{-3}$	$9.1 \cdot 10^{-3}$	λ_{d2}	$1.2 \cdot 10^{-2}$	$1.2 \cdot 10^{-2}$	$1.0 \cdot 10^{-2}$	$1.1 \cdot 10^{-2}$	$1.1 \cdot 10^{-2}$
λ_{d3}	$6.5 \cdot 10^{-3}$	$5.6 \cdot 10^{-3}$	$3.9 \cdot 10^{-3}$	$4.2 \cdot 10^{-3}$	$5.0 \cdot 10^{-3}$	λ_{d3}	$0.5 \cdot 10^{-2}$	$0.4 \cdot 10^{-2}$	$1.1 \cdot 10^{-2}$	$0.8 \cdot 10^{-2}$	$0.9 \cdot 10^{-2}$
λ_{d4}	0.61	0.44	0.22	0.24	0.378	λ_{d4}	0.32	0.22	0.1	0.26	0.23
M_1	0.47	0.40	0.37	0.34	0.395	M_1	0.53	0.46	0.46	0.44	0.47
M_2	0.25	0.23	0.21	0.19	0.22	M_2	0.16	0.16	0.21	0.21	0.18
M_3	0.22	0.24	0.24	0.26	0.24	M_3	0.18	0.15	0.21	0.21	0.19
M_4	0.06	0.13	0.19	0.22	0.15	M_4	0.13	0.22	0.12	0.13	0.15
OH 2ppm 50°C	$1.55 \cdot 10^{-1}$	$2.3 \cdot 10^{-1}$	$3.4 \cdot 10^{-1}$	$6.2 \cdot 10^{-1}$	Average	OH 2ppm 80°C	$1.55 \cdot 10^{-1}$	$2.3 \cdot 10^{-1}$	$3.4 \cdot 10^{-1}$	$6.2 \cdot 10^{-1}$	Average
λ_{d1}	$1.0 \cdot 10^{-3}$	$1.2 \cdot 10^{-3}$	$1.1 \cdot 10^{-3}$	$1.2 \cdot 10^{-3}$	$1.13 \cdot 10^{-3}$	λ_{d1}	$0.8 \cdot 10^{-3}$	$0.8 \cdot 10^{-3}$	$0.9 \cdot 10^{-3}$	$0.9 \cdot 10^{-3}$	$0.8 \cdot 10^{-3}$
λ_{d2}	$1.6 \cdot 10^{-2}$	$1.9 \cdot 10^{-2}$	$1.8 \cdot 10^{-2}$	$1.3 \cdot 10^{-2}$	$1.65 \cdot 10^{-2}$	λ_{d2}	$1.7 \cdot 10^{-2}$	$1.8 \cdot 10^{-2}$	$2.0 \cdot 10^{-2}$	$1.7 \cdot 10^{-2}$	$1.8 \cdot 10^{-2}$
λ_{d3}	$7.2 \cdot 10^{-3}$	$1.2 \cdot 10^{-2}$	$1.5 \cdot 10^{-2}$	$5.3 \cdot 10^{-3}$	$9.88 \cdot 10^{-3}$	λ_{d3}	$1.6 \cdot 10^{-2}$	$0.9 \cdot 10^{-2}$	$2.8 \cdot 10^{-2}$	$1.9 \cdot 10^{-2}$	$1.8 \cdot 10^{-2}$
λ_{d4}	$6.2 \cdot 10^{-3}$	$6.4 \cdot 10^{-3}$	$4.4 \cdot 10^{-3}$	$2.7 \cdot 10^{-3}$	$4.93 \cdot 10^{-3}$	λ_{d4}	1.22	1.06	0.62	0.94	0.96
M_1	0.69	0.65	0.60	0.54	0.62	M_1	0.86	0.83	0.83	0.77	0.818
M_2	0.14	0.16	0.20	0.16	0.165	M_2	0.08	0.11	0.11	0.12	0.103
M_3	0.09	0.11	0.13	0.13	0.113	M_3	0.04	0.02	0.06	0.07	0.048
M_4	0.08	0.07	0.07	0.17	0.098	M_4	0.02	0.03	0.02	0.04	0.03

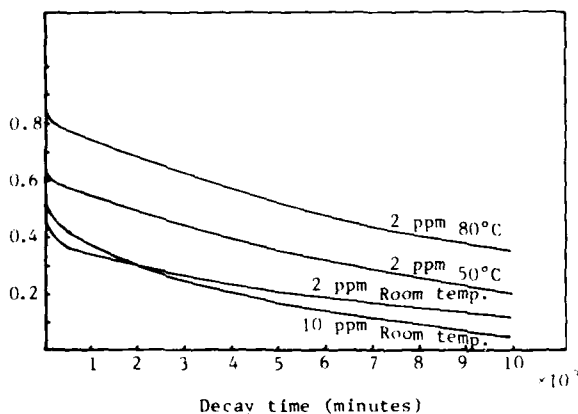


Fig. 21 Decay of the Induced Loss

MECHANICAL STRENGTH

It is important that we know mechanical properties of optical fiber in the radiation circumstance.

Fig. 22 is the Weibull diagrams of tensile strength of irradiated fiber and not irradiated fiber. In Fig. 22, optical fiber is 2 ppm OH content pure silica core fiber, radiation dose rate is 6.2×10^{-4} R/H and total dose is 8.7×10^6 R.

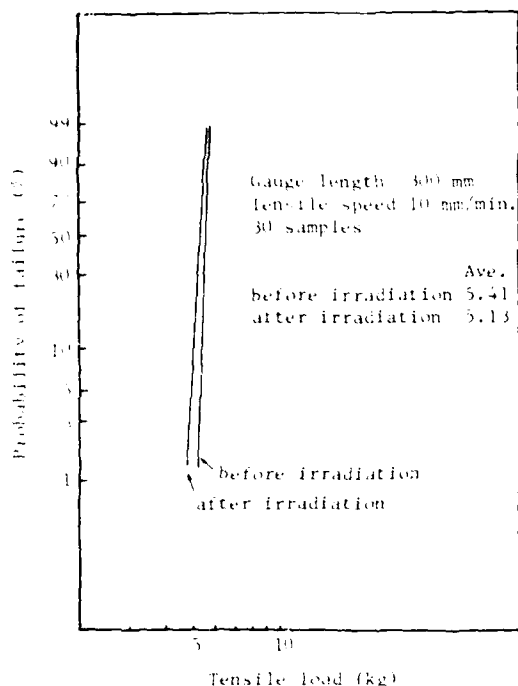


Fig. 22 Tensile Strength before and after Irradiation

Irradiated fiber display about 5% degradation compared with the not irradiated fiber. This degradation seems to be caused by the jacketing Nylon and the strength of the fiber itself may not be degraded.

SPLICED POINT

Investigation of irradiation effect on splicing loss and tensile strength of spliced point is as important as that to fiber strength. Splicing loss was measured as follows. Two optical fibers of 100 m length, one included 10 splicing points and other included no splicing point, were irradiated at the same time. Then induced losses at splicing points were estimated by comparing the induced losses of both fibers. Splicing loss per 10 points before and after 7.1×10^6 R irradiation is 0.201 dB and 0.204 dB, respectively (Table 6). Tensile strength is shown in Table 7.

Table 6 Splicing Loss before and after Irradiation

No.	Before irradiation (dB)	After irradiation (dB)
1	0.25	0.22
2	0.34	0.27
3	0.27	0.24
4	0.18	0.18
5	0.20	0.20
6	0.13	0.18
7	0.18	0.23
8	0.20	0.27
9	0.15	0.11
10	0.11	0.14
Ave.	0.201	0.204

Table 7 Mechanical Strength at Splicing Points before and after Irradiation

Before irradiation (kg)	After irradiation (kg)
3.3	3.1
2.3	3.5
2.8	2.3
2.1	3.4
2.1	2.8
1.9	3.1
2.0	3.1
2.8	3.2
2.3	2.9
2.6	2.8
Ave. 2.42	Ave. 3.02

Average tensile strength after irradiation is greater than before. This increase in tensile strength seems to be caused by the crosslinking of the epoxy resin that is used for reinforcement. From these results, we think that radiation did not affect to splicing point.

CONCLUSIONS

1. Fiber that can be used in irradiative circumstances is limited to pure silica core fiber only.
2. Increase of transmission loss in the infrared wavelength region caused by irradiation is mainly caused by an absorption band that is formed in UV and visible range.
3. Radiation-induced loss of pure silica core fiber can be explained using a model of color center formation by γ irradiation and it can be quantitatively assumed from the dose rate dependence.

4. It seems that the rate constants of the radiation-induced loss is reduced as the temperature rises.
5. OH contained in the core influences a long lived component of radiation-induced loss.
6. As to the mechanical strength, irradiation does not cause substantial degradation of glass itself up to irradiation of 8.7×10^6 R.
7. No problem is foreseen on the influence to spliced parts from irradiation of up to about 7×10^6 R.

REFERENCES

- 1) E. J. Friebele: "Optical fiber waveguides in radiation environments" Optical Engineering, Vol. 18, No. 6, 1979, pp. 552
- 2) E. J. Friebele, P. C. Schultz, and M. E. Gingerich: "Compositional effects on the radiation response of Ge-doped silica core optical fiber waveguides Applied Optics, Vol. 19, No. 17, 1980, pp. 2910
- 3) K. J. Swyler, W. H. Hardy II, and P. W. Levy: "Radiation induced coloring of glasses measured during and after electron irradiation" IEEE Transactions on Nuclear Science, Vol. NS-22, No. 6, 1975, pp. 2259



Kiyoshi Shibuya

Showa Electric Wire and Cable Co., Ltd.
4-1-1 Minamihashimoto,
Sagamihara, Kanagawa,
229, Japan

Kiyoshi Shibuya was born in 1947. He joined Showa Electric Wire and Cable Co., Ltd. after his graduation from Tohoku University in 1972. He has been engaged in research and development of aluminum conductors and super conductors. And he is engaged in research and development of optical fibers from 1976.



Kenji Yagi

Showa Electric Wire and Cable Co., Ltd.
4-1-1 Minamihashimoto,
Sagamihara, Kanagawa,
229, Japan

Kenji Yagi was born in 1942. He joined Showa Electric Wire and Cable Co., Ltd. after his graduation from Nagoya University in 1964. He has been engaged in research and development of dielectric material and semiconductor. And he is engaged in research and development of optical fibers from 1973.



Norio Sugiyama

Showa Electric Wire and Cable Co., Ltd.
4-1-1 Minamihashimoto,
Sagamihara, Kanagawa,
229, Japan

Norio Sugiyama was born in 1940. He joined Showa Electric Wire and Cable Co., Ltd. after his graduation from Keio University in 1963. He has been engaged in research and development of Extra High Voltage Cable and other Power Transmission Systems. And he is engaged in research and development of optical fibers from 1981.



Takeshi Kojima

Showa Electric Wire and Cable Co., Ltd.
4-1-1 Minamihashimoto,
Sagamihara, Kanagawa,
229, Japan

Takeshi Kojima was born in 1934. He joined Showa Electric Wire and Cable Co., Ltd. after his graduation from College of Tokyo Science in 1958. He has been engaged in research and development of Dielectric Material for Extra High Voltage Cable. And he is engaged in research and development of optical fibers from 1973.



Akitoshi Yoshinaga

Toshiba Research and
Development Center,
Toshiba Corporation

Komukai-Toshiba-cho,
Kawasaki, Kanagawa,
210, Japan

Akitoshi Yoshinaga was born in 1948. He joined Toshiba Corporation in 1972. He received his BE in 1970 and his ME in 1972 from Kyushu University. He has been engaged in research and development of glass fibers for optical communication. And he is presently engaged in research and development of the optical component for the optical communication system.

APPLICATION OF VAD FIBER CABLE TO COMMERCIAL FIBER OPTIC TRANSMISSION SYSTEM (FOTS)

M. Nishimura*, H. Horima*, O. Nishi*, H. Yokota*, S. Suzuki*, and M. Iwazaki**

*Sumitomo Electric Industries, Ltd.
1, Taya-cho, Totsuka-ku, Yokohama, 244, Japan

**Nippon Telegraph and Telephone Public Corporation
1, Uchisaiwai-cho, Chiyoda-ku, Tokyo, 100, Japan

Abstract

The VAD method for manufacturing graded-index fibers in mass production basis has been successfully developed. The losses of VAD fibers have been reduced to the values mainly determined by Rayleigh scattering loss, as the result of remarkable progress of dehydration technique. At the same time the bandwidths of VAD fibers have been also improved by profile controlling technique. Comparison of the bandwidths measured at plural wavelengths has revealed that the bandwidths of VAD fibers have the upper limits corresponding to theoretical prediction for perfect α -power profile.

Improvement of our cabling techniques has made it possible to manufacture optical fiber cables without impairing intrinsic transmission characteristics of VAD fibers. The length dependence of bandwidth of VAD fibers for long-spliced optical transmission lines has been also investigated, and γ coefficients have been found to be 0.7 at 0.85 μm and 0.6 at 1.3 μm . It will be demonstrated that commercial fiber optic wavelength-multiplexing transmission systems can be easily constructed by applying the VAD fiber cables.

1. Introduction

Remarkable improvement of optical properties on VAD graded-index fibers has been achieved and the VAD fiber of good quality has become easily obtainable as a result of successful development of dehydration and profile controlling techniques in some mass production basis.

Moreover, optical cables with high performances have also been manufactured by our successful cabling techniques without impairing intrinsic optical characteristics. VAD fibers and cables of more than 10,000 km fiber length with low loss and wide bandwidth has been shipped.

In this paper, the transmission characteristics of VAD fibers under mass production basis are described. Their wavelength dependence, especially the relation of transmission attenuation and bandwidth between at 0.85 μm wavelength and at 1.3 μm wavelength, is investigated. The length dependence of bandwidth for long-spliced optical transmission lines is also discussed.

2. Optical Transmission Achievement of VAD Fiber Cable

In 1981, commercial tests of inter-office trunk with medium capacity (32 Mbits/sec and 100 Mbits/sec) were carried out in twelve test sections around Japan by N.T.T. The test route length was a total of 107 km, and the total fiber length was about 2,700 km. Most of the fibers (about 80% of all) were produced by VAD method. In this section, the transmission characteristics of the total 935 km VAD fibers in the optical cables manufactured for the purpose of being used in the tests are described.

The principal specifications of the cables are summarized in Table I. The cable structure is shown in Fig. 1 [1]. Optical fiber units and five interstitial quads are arranged around a central strength member in one layer. Each unit consists of six tight-coated fibers and a central steel wire. The interstitial quads are used for transmission of repeater supervision and control signals, orderwire telephone signals during construction or maintenance and so on.

Figures 2 and 3 show the histograms of the transmission loss and the bandwidth, respectively, measured at 0.85 μm wavelength for the total 800 km VAD fibers in the cables using 0.85 μm wavelength band. The average unit length of the cables is

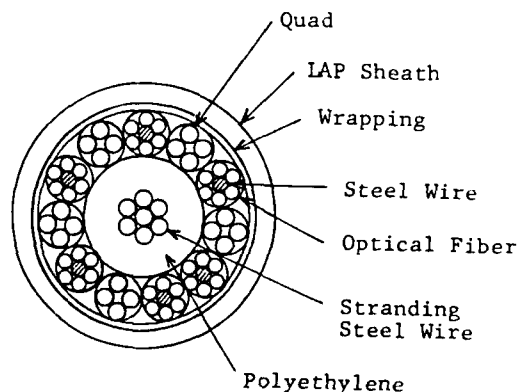


Fig. 1 Cable structure

Section		Kyoto Minami Kyoto Sanjo	Kyoto Sanjo Kamo	Uragami Nagayo	Sendai Aramaki	Gifu Kagamihara
Distance (km)		8.0	6.1	5.9	7.6	11.2
Wavelength (μm)		0.85	0.85	0.85	0.85	1.3
Transmission Speed (Mbits/sec)		32	32	32	32	100
Number of Fibers		36	36	12	24	12
Supply Fiber Length (km)		282.6	261.7	69.1	186.9	135.0
Average Cable Unit Length (m)		981	909	823	973	1125
Fiber Element Loss (dB/km)	90%	< 3.0	< 3.0	< 3.0	< 3.0	< 1.0
	100%	< 3.5	< 3.5	< 3.5	< 3.5	< 1.3
Fiber Element Bandwidth (MHz·km)	90%	> 500	> 500	> 500	> 500	> 800
	100%	> 300	> 300	> 300	> 300	> 600

Table I. Specifications of cables in the commercial tests

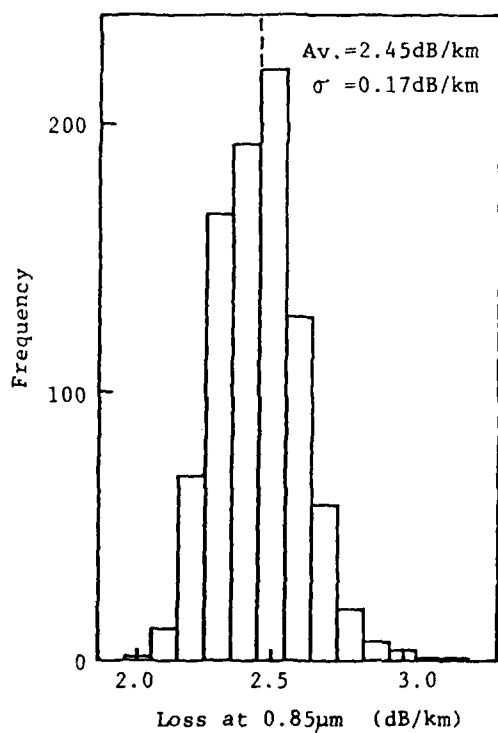


Fig. 2 Frequency distribution of loss of the VAD fibers in the cables produced for 0.85 μm wavelength band transmission systems. The total length of the fibers is 800 km.

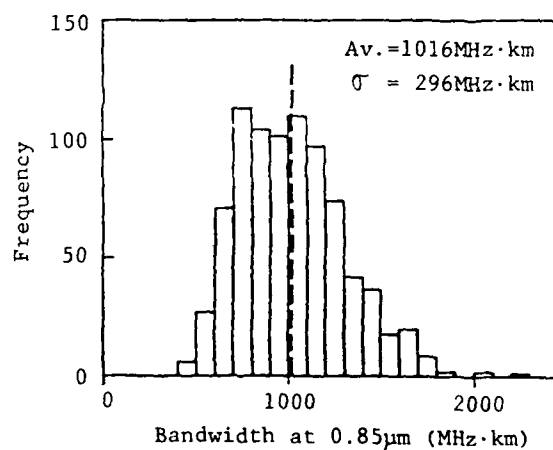


Fig. 3 Frequency distribution of bandwidth of the same fibers as in Fig. 2.

939 m, and the maximum is 1406 m. The average values and the standard deviation σ of the loss and the bandwidth are as follows:

Av. Loss (at 0.85 μm) = 2.45 dB/km σ = 0.17 dB/km
 Av. Bandwidth (at 0.85 μm) = 1016 MHz·km σ = 296 MHz·km

Figure 4 and 5 show the histograms of the transmission characteristics measured at 1.3 μm wavelength for the total 135 km VAD fibers in the cables using 1.3 μm wavelength band. The cable unit length is 1328 m at its maximum and 1125 m on the average. The achievements of them are summarized as follows:

Av. Loss (at 1.3 μm) = 0.53 dB/km σ = 0.083 dB/km
 Av. Bandwidth (at 1.3 μm) = 1279 MHz·km σ = 286 MHz·km

It is cleared that very high performance of the VAD fibers has been preserved even after the cabling process.

3. Wavelength Dependence of Transmission Characteristics

3.1 Transmission Loss

Figure 6 shows the measurement results of the spectral transmission loss of 108 pieces of VAD fibers which were randomly sampled from the total 972 pieces of fibers mentioned in the above section. The two curves represent the best data and the worst data respectively. The circles show the average losses at wavelengths of 0.85 μm , 1.2 μm , 1.3 μm and 1.55 μm with the error bars indicating the limits of $\pm 2\sigma$.

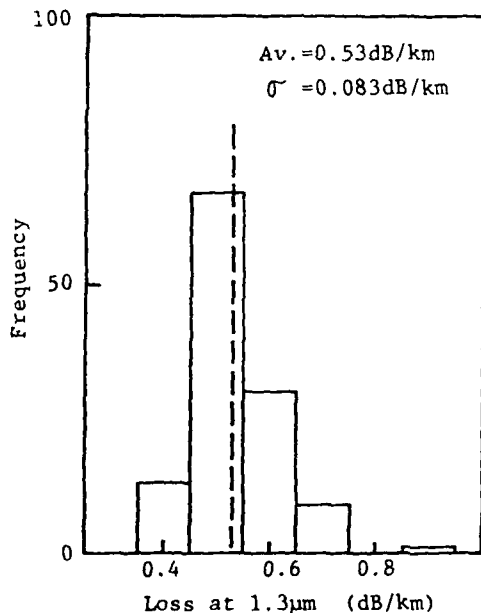


Fig. 4 Frequency distribution of loss of the VAD fibers in the cables produced for 1.3 μm wavelength band transmission systems. The total length of the fibers is 135 km.

The average losses at 1.2 μm and 1.55 μm wavelengths are 0.68 dB/km and 0.41 dB/km respectively. The former is 0.08 dB/km larger and the latter is 0.19 dB/km smaller than the average loss at 1.3 μm wavelength. Those three wavelength bands where very low loss can be achieved are suitable for long-span transmission systems and especially recommendable for wavelength-multiplexing transmission systems.

The spectral attenuation characteristics of graded-index fibers are expressed as the following well-known equation

$$\alpha(\lambda) = \frac{A}{\lambda^4} + B + C(\lambda). \quad (1)$$

The first and the third terms represent Rayleigh scattering loss and the remaining wavelength-dependent loss caused by OH-ion absorption and so on. The constant term B denotes the loss induced by structural imperfection of fiber. When $C(\lambda) = 0$, the transmission loss at 1.3 μm wavelength $\alpha(1.3)$ is related to $\alpha(0.85)$ as

$$\alpha(1.3) = \alpha(0.85) - A \left\{ \frac{1}{(0.85)^4} - \frac{1}{(1.3)^4} \right\} \quad (2)$$

or

$$\alpha(1.3) = \left(\frac{0.85}{1.3} \right)^4 \alpha(0.85) + B \left[1 - \left(\frac{0.85}{1.3} \right)^4 \right] \quad (3)$$

Rayleigh scattering coefficient A is predicted to be ranged from $A_{\min} = 1.0$ to $A_{\max} = 1.3$ (dB/km)·(μm)⁴, corresponding to the specified range of N.A. [2]

Distribution of $\alpha(0.85)$ and $\alpha(1.3)$ measured for the above-mentioned 108 pieces of fibers is mapped in Fig. 7. The lines A_{\min} and A_{\max} in Fig. 7 are derived from eq. (2), and the line $B = 0$ indicates the relation of eq. (3) with $B = 0$. When $C(\lambda)$ is negligible, the point determined by $\alpha(0.85)$ and $\alpha(1.3)$ is expected to be located in the region I which is bordered by the lines A_{\min} , A_{\max} and $B = 0$.

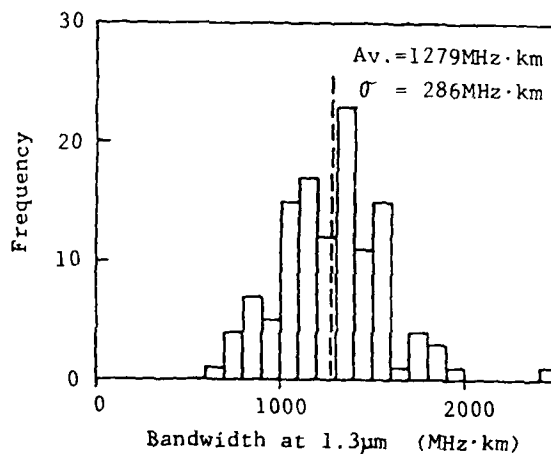


Fig. 5 Frequency distribution of bandwidth of the same fibers as in Fig. 4.

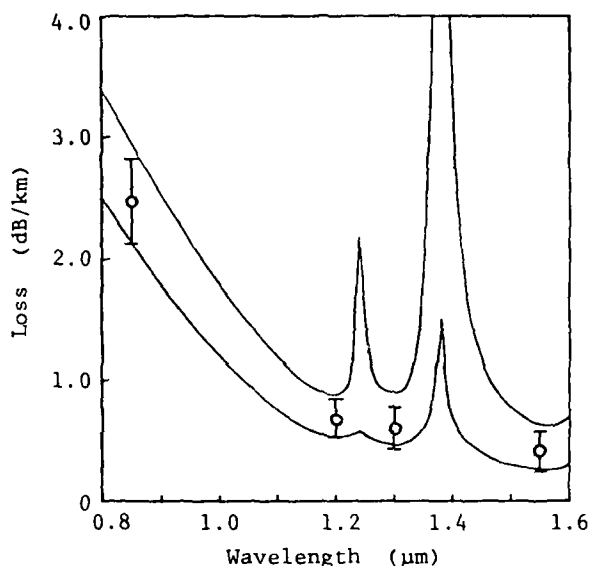


Fig. 6 Spectral loss of the VAD fibers. Two curves represent the best data and the worst data for randomly sampled 108 pieces of fibers. Circles and error bars denote the averages and the limits of $\pm 2\sigma$.

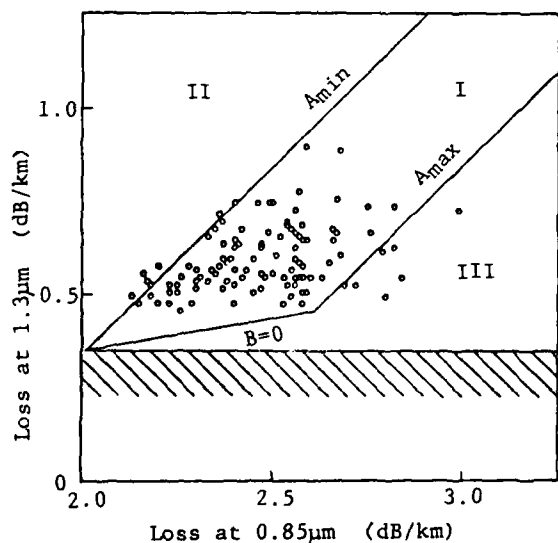


Fig. 7 Distribution showing the relationship between attenuations at 0.85 μm and 1.3 μm for the same fibers as in Fig. 6.

From Fig. 7, it is cleared that 87% of the fibers are located in the region I. 6.5% and 6.5% are in the region II and III, respectively. The fibers in the region II are characterized to have some amount of OH-ion absorption loss at 1.3 μm wavelength. Those in the region III are deduced to have the absorption loss at 0.85 μm wavelength caused by drawing defect and so on. However, those absorption losses are sufficiently small. It is concluded that the transmission losses of the VAD fibers are almost determined by Rayleigh scattering loss and that the excess loss is very small even after cabling.

3.2 Transmission Bandwidth

Distribution of the bandwidth at 0.85 μm , $B(0.85)$, and at 1.3 μm , $B(1.3)$, measured for 164 pieces of fibers sampled from the total 972 pieces used in the commercial tests is mapped in Fig. 8. The circles in Fig. 8 represent the fibers produced for 0.85 μm wavelength band transmission systems and the crosses for 1.3 μm wavelength band systems.

The relation between $B(0.85)$ and $B(1.3)$ was theoretically investigated for perfect α -power profiles by using WKB method[3]. The calculated results are also shown in Fig. 8 by broken curves with the profile exponent α as a parameter. From Fig. 8, it is cleared that though the points determined by $B(0.85)$ and $B(1.3)$ seem to be distributed randomly, they are almost bordered by the theoretical prediction.

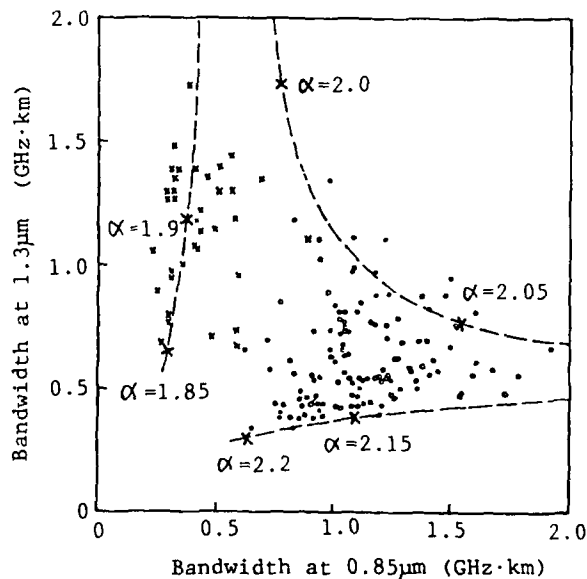


Fig. 8 Distribution showing the relationship between bandwidths at 0.85 μm and 1.3 μm for randomly sampled 164 pieces of VAD fibers. Circles and crosses represent the fibers used in 0.85 μm wavelength band and 1.3 μm wavelength band respectively. Broken curves show the theoretical prediction.

Figure 9 shows the spectral bandwidth measurement results of three VAD graded-index fibers by fiber Raman spectroscopy [4] and laser diodes. Fiber A and fiber C were manufactured under the profile control optimizing the profile exponent α for 0.85 μm wavelength band and 1.3 μm wavelength band, respectively. Fiber B has broad bandwidths at both wavelengths of 0.85 μm and 1.3 μm with the result that the profile has been optimized around 1.05 μm wavelength. Their spectral bandwidth characteristics have a single peak around each designed wavelength, suggesting that the profiles are well-controlled.

Taking such spectral characteristics into consideration, it is recommended that wavelength-multiplexing transmission systems should use wavelength bands close to each other, for example 1.2 μm and 1.3 μm or 1.3 μm and 1.55 μm , especially when broad bandwidths are required at both wavelengths.

4. Length Dependence of Bandwidth

The length dependence of bandwidth was investigated by the use of VAD fibers in order to design fiber-optic transmission systems with high quality.

The coefficient of length dependence of bandwidth γ for long spliced VAD fibers was estimated by comparing the measured value with calculated value of bandwidth. Figures 10 and 11 show the results at 0.85 μm wavelength and 1.3 μm wavelength respectively. From these figures, γ coefficient of VAD fibers is indicated to be about 0.7 at 0.85 μm and 0.6 at 1.3 μm .

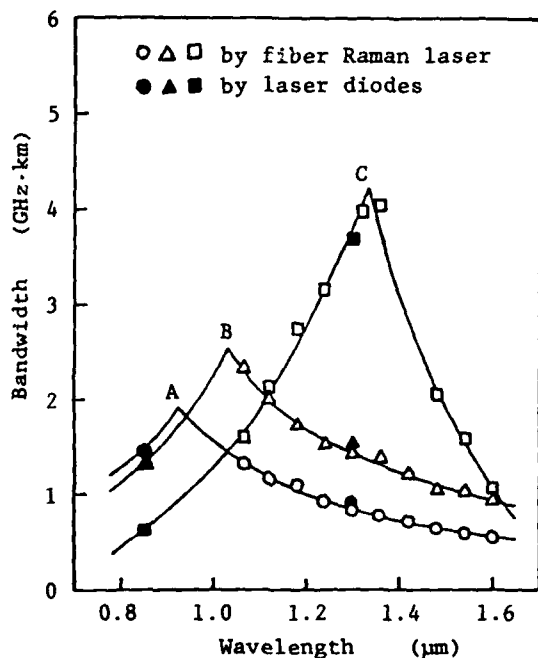


Fig. 9 Spectral bandwidth of VAD fibers.

In designing bandwidths of fibers from the system requirement, it is recommended to use the γ values of 0.7 to 0.8 over 0.85 μm wavelength band and 0.6 to 0.7 over 1.3 μm wavelength band, respectively, with a margin.

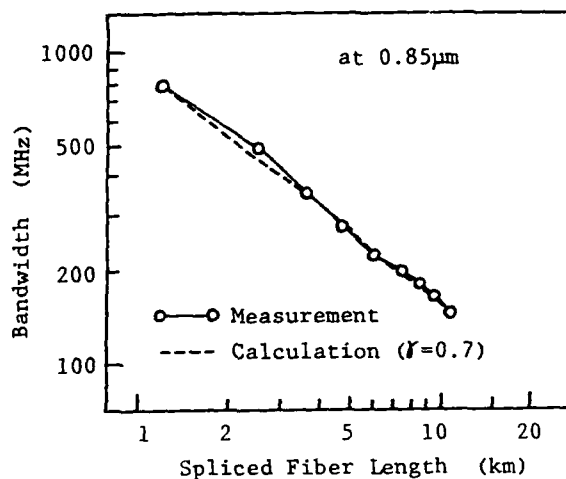


Fig. 10 Bandwidth of spliced fibers at 0.85 μm wavelength.

Each Fiber Length = 1.2 km
Av. Attenuation = 2.5 dB/km
Av. Bandwidth = 810 MHz·km^{0.7}

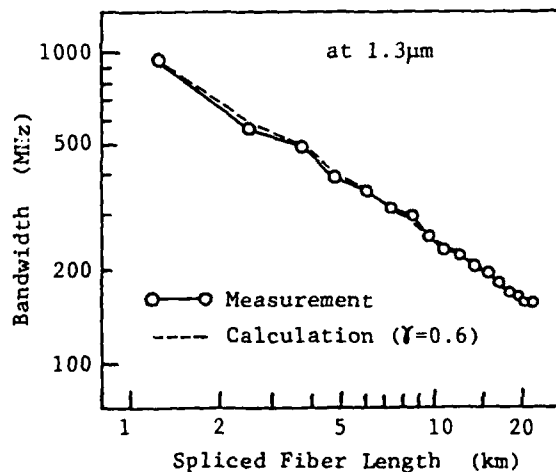


Fig. 11 Bandwidth of spliced fibers at 1.3 μm wavelength

Each Fiber Length = 1.2 km
Av. Attenuation = 0.60 dB/km
Av. Bandwidth = 1040 MHz·km^{0.6}

5. Conclusion

Transmission characteristics of VAD graded-index fibers in mass production basis were described. The VAD method has almost come to maturity to be able to produce fibers with low loss and broad bandwidth. Fiber optic transmission systems with high performances, including wavelength-multiplexing transmission systems, can be easily constructed by the use of the VAD fiber cables.

References

- [1] M. Iwasaki et al., "Graded-index optical fiber cables", Japan Telecommunications Review, Vol. 23, NO. 1, p. 139, 1981.
- [2] N. Shibata et al., "Optical-loss characteristics of high GeO₂ content silica fibers", Trans. IECEJ, Vol. E63, No. 12, p. 837, 1980.
- [3] D. Gloge and E.A.J. Marcatili, "Multimode theory of graded-core fibers", Bell Syst. Tech. Jour., Vol. 52, No. 9, p. 1563, 1973.
- [4] L. G. Cohen and C. Lin, "A universal fiber-optic (UFO) measurement system based on a near-IR fiber Raman laser", IEEE J. Quantum Electron., Vol. QE-14, p. 855, 1978.



Masayuki Nishimura

Masayuki Nishimura was born in 1956 and received a M.S. degree from Tokyo University in 1981. He joined Sumitomo Electric Industries, Ltd. in 1981, and has been engaged in research and development of optical fiber characterization. He is a member of the Institute of Electronics and Communication Engineers of Japan.



Hiroaki Horima

Hiroaki Horima was born in 1947 and received a M.S. degree from Osaka University in 1972. He joined Sumitomo Electric Industries, Ltd. in 1972, and has been engaged in research and development of multi-pair communication cables, CATV coaxial cables and optical fiber cables. He is a senior engineer of Fiber Optics Division of Sumitomo Electric Industries, Ltd., and is a member of the Institute of Electronics and Communications Engineers of Japan.



Osamu Nishi

Osamu Nishi was born in 1947 and received a M.E. in 1971 from Waseda University. He joined Sumitomo Electric Industries, Ltd. in 1971, and has been engaged in research and development of multi-pair communication cable, CATV coaxial cable and optical fiber cable. He is senior engineer of 1st Cable Engineering Section of Communication Division and is a member of the Institute of Electronics and Communications Engineers of Japan.



Hiroshi Yokota

Hiroshi Yokota received a B.S. degree in physical engineering from Tokyo University. He joined Sumitomo Electric Industries, Ltd. in 1975, where he has been engaged in research and development of optical fiber fabrication. He is a member of the Institute of Electronics and Communications Engineers of Japan.



Shuzo Suzuki

Shuzo Suzuki received a M.S. in 1972 from Tokyo University. He joined Sumitomo Electric Industries, Ltd. in 1972, and has been engaged in research and development of optical fiber and cable. He is a member of the Institute of Electronics and Communication Engineers of Japan.



Masatoshi Iwazaki

Masatoshi Iwazaki, Senior Staff Engineer of NTT's Engineering Bureau, is now engaged in developmental research planning on whole telecommunication outside plant, cables, telephone poles, ducts, terminal boxes and so on. He is a member of the Institute of Electronics and Communication Engineers of Japan.

TOLL MESSAGE LIGHTGUIDE TRANSMISSION NETWORK IN MANITOBA

* E. Byzio, H. K. Eastwood, K. K. Hau ** J. Petrin

* Canstar Communications,
Scarborough and Winnipeg, Canada ** Manitoba Telephone System
Winnipeg, Canada

ABSTRACT

This paper describes a large scale application of lightguide transmission to a multi-office toll message trunking network. Eight (8) city exchanges and six (6) rural dial offices are being interconnected with more than 130 km of lightguide cable containing up to 20 optical fibers. The system uses double window fiber manufactured by a Vapour Axial Deposition (VAD) technique and protected with a double coating of silicone and nylon.

INTRODUCTION

The "Toll Message Fiber Optics Transmission System" is a major project currently being implemented in Manitoba, Canada by the Manitoba Telephone System (M.T.S.). This network will connect Winnipeg exchanges and rural communities with the main switching offices in downtown Winnipeg. It will also form a part of the Trans-Canada Telephone System. The entire project, awarded to Canstar Communications will be completed and is scheduled to be in operation by the end of 1983. The initial subsystem is complete and has been in service since the summer of 1982.

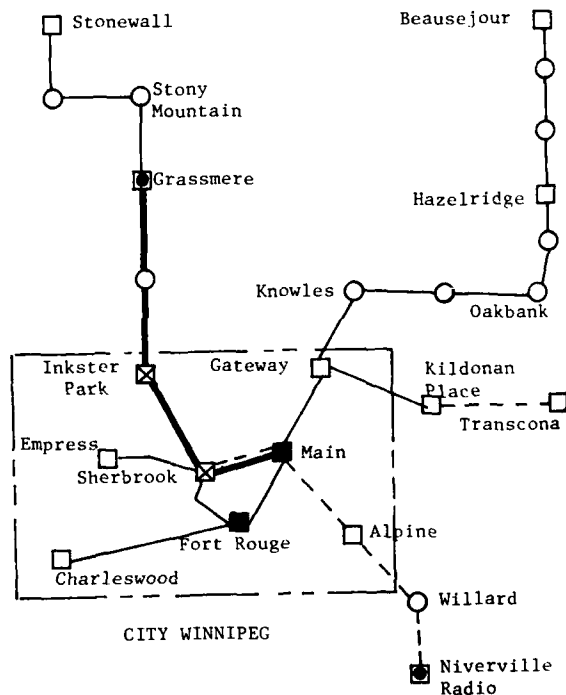
NETWORK

Structure

The network, as shown in Figure 1, is for toll grade message transmission at a 90 Mb/s line rate. It consists of nine subsystems and requires over 130 km of lightguide cable with fiber count from 6 to 20 optical fibers. It is the first lightguide system in Canada to operate at this bit rate and, to our knowledge, the first such system in North America to incorporate repeaters at spans over 9.0 km.

The initial requirement is for a Digital Entrance Link (DEL) to connect a new digital toll switch at the MAIN TOLL OFFICE in downtown Winnipeg to the digital microwave radio at GRASSMERE, 24 kilometers north of Winnipeg.

FIGURE 1 NETWORK ROUTE MAP



LEGEND:

- System Installed and Operating
- - - Cable Installed
- ... Future extension
- Repeater Location
- Terminal Location in Class 2 Toll Office
- ⊗ Terminal Location in Switch Office
- Terminal Location in Class 5 Office (Community Dial Office)
- ◼ Terminal Location in Microwave Radio Site

A further eight subsystems are required to carry Winnipeg interexchange traffic and to augment facilities between Winnipeg and surrounding communities. Drop-and-insert capability at the designated offices is accomplished by means of digital multiplex equipment at both the DS1 (1.5 Mb/s) and DS2 (6.3 Mb/s) bit rates.

The system is designed to operate at a wavelength of 850 nm with each fiber carrying DS3C (90 Mb/s) one-way traffic. The fiber provided however is also capable of operating at 1300 nm and provision has been made for wavelength division multiplex operation in the future. In this case the capacity can be expanded to carry almost 3000 voice channels per fiber.

Choice of 90 Mb/s Fiber Optic

As a transmission medium, fiber optics offers a number of definite advantages over competitive technologies. These include:

- high capacity
- RFI and EMI immunity
- cross-talk immunity
- long repeater spacing, close to the distance of inter-office trunk or wire line entrance links which range 10-15 km.
- ease of line-up and maintenance
- less congestion in underground conduit

Mainly, however, it is of prime importance to M.T.S. that the chosen technology proves economical over alternatives. Microwave radio for the GRASSMERE-MAIN DEL was a serious contender until it became apparent that costly tower modifications or new tower structures would be required. These costs contributed to elimination of microwave radio as a transmission medium. In addition, line-of-sight radio in the Winnipeg area is subject to the risk of propagation path blockage due to the highrise construction.

PCM metallic pair cable systems were a possibility on some of the interoffice spans, but were ruled out due to the comparatively short repeater spacing, and the very high traffic volume, that would involve large cables requiring too much space in the underground duct system.

Fiber optics proved to be the most appropriate technology for the project in terms of capacity, repeater spacing, and overall cost.

EQUIPMENT

The network requires five different types of equipment, namely: DM1-3 digital multiplex equipment, optical line terminating equipment (O-LTE), optical line repeating equipment (O-LRE), line protection switching equipment and centralized supervisory equipment. These are supplied by Nippon Electric Company (NEC).

The DM1-3 digital multiplex equipment is

designed to combine 7 low speed groups: each group can be made up of four DS1, two DS1C, one DS2 or two DS1 and one DS1C digital signal. A bit interleaving and positive-stuffing technique is employed to multiplex the asynchronous low speed digital streams into a single DS3 (45 Mb/sec) signal which satisfies the requirements of the DSX-3 cross connect. The low and high speed muldems are protected independently on a one-for-one basis.

The O-LTE is used for transmission of the DS3 signals over lightguide cable. Two asynchronous DS3 signals are multiplexed to form a DS3C (90.944 Mb/sec) digital signal incorporating overhead bits for line performance monitoring, and orderwire, supervisory and protection switching control signals. A Ga-Al-As double heterostructure laser diode is used in each optical transmitter converting the digital signal into a light pulse stream. The temperature-dependent output level of the laser source is stabilized using the light emitted from the back face of the diode in a negative feedback loop. In the optical receiver a silicon avalanche photodiode (APD) is used as the detector. An AGC circuit is used to accommodate a wide range of input power levels due to variations in link attenuation and to compensate for temperature sensitivity of the APD.

The O-LRE is a "three R" type repeater which provides reshaping, retiming and regenerating functions. It is used to retransmit the DS3C optical pulse trains which have been distorted after being passed through a lightguide transmission line. The equipment also provides a drop-and-insert of the supervisory signal for the repeater station.

The protection switching equipment between the DM1-3 and O-LTE is used to ensure reliable transmission against any trouble in optical line equipment and transmission lines. Each optical channel is continuously monitored for signal failure and high error rate. When the performance of a working channel is judged not to be acceptable, traffic is automatically switched to the standby channel by the protection switches at both ends.

To maintain stabilized service of the entire transmission network with high efficiency and a minimum of personnel, a centralized supervisory facility is employed. Local Supervisory Equipment (LSV) is installed at each local station to control communications with the central station and to transmit alarm data concerning the local station. Central Supervisory Equipment (CSV) is installed at the central station to collect alarm information from each LSV and monitor the operational status of each local station. The transmission path between each LSV and the CSV, established through the overhead bits, follows two parallel routes namely, one of the working 90 Mb/s optical lines and the standby optical

line. In the event that either line fails, centralized supervision can still be conducted.

LIGHTGUIDE CABLE

Fibers

Graded index VAD, directly strandable, (1) tight jacketed fibers were used for this project. The glass fibers are coated with a soft silicone material and covered with an extruded outer nylon jacket. (2) The typical structure and parameters of the fibers are illustrated in Figure 2 and Table 1. Each fiber is identifiable through the length of cable by means of the color coded nylon jacket and unit binders.

FIGURE 2

FIBER CROSS-SECTION

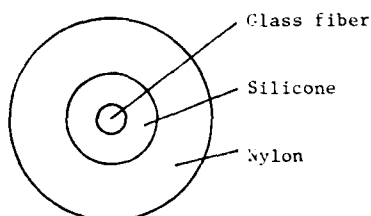


TABLE 1

GLASS FIBER	CORE	MATERIAL	DOPED SILICA GLASS
		NA	NOM. 0.20 ± 0.02
	CLADDING	DIAMETER	NOM. 50 ± 5 µm
		MATERIAL	SILICA GLASS
COATING	PRIMARY (BUFFER)	DIAMETER	NOM. 125 ± 5 µm
		MATERIAL	SILICONE RESIN
	SECONDARY (JACKET)	OUTER DIA.	APPROX. 0.4 mm
		MATERIAL	NYLON
		OUTER DIA.	0.9 ± 0.1 mm

Core Assembly

Figure 3 shows the concentric design used for 6 to 12 fiber cables. Fibers are stranded in a single layer around a central strength member consisting of an electrogalvanized, high tensile strength steel wire covered with a polyethylene jacket.

FIGURE 3

CONCENTRIC CABLE CROSS-SECTION

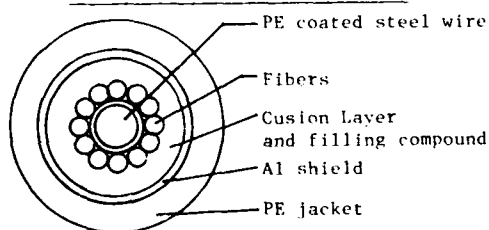
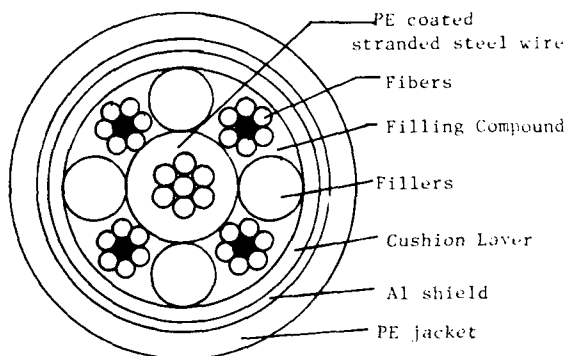


Figure 4 shows the unitized cable design with up to 24 fibers. Four units along with fillers are stranded around the central strength member. The central strength member consists of a 7 wire stranded electrogalvanized, high tensile strength steel wire covered with a polyethylene jacket. Each unit consists of a maximum of 6 fibers stranded around a unit strength member (copper-clad steel wire) and bound by a coloured binder. The cable core is filled with a petrojelly filling compound and protected with a cushioning layer of fibrillated polypropylene yarns and polyester tape(s). (3)

FIGURE 4

UNITIZED CABLE CROSS-SECTION



Sheath

Cables intended for duct and aerial installation are supplied with an Alpeth sheath consisting of a plastic-coated 0.2 mm aluminum shield applied longitudinally and smooth with an overlap and bonded to a low or medium density black polyethylene jacket.

Cables intended for direct burial installation are supplied with an additional GP sheath consisting of a 0.15 mm corrugated tin-coated steel tape applied longitudinally with an overlap and extruded black polyethylene jacket.

Transmission Requirements

The optical attenuation requirements of the cable were determined from a link margin calculation based on the system gain of the optical equipment (O-LTE and O-LRE). The example in Table 2 for the 9 km link from INKSTER to SEERBROOK results in a specified maximum cabled fiber attenuation of 2.8 dB/km.

For 90 Mb/s transmission the equipment used requires 90 MHz link bandwidth with no power penalty. The fiber bandwidth length product, B_L , requirement was estimated using a length exponent of 0.75 as follows:

$$B_L \text{ (MHz} \cdot \text{km)} = 90 \text{ (MHz)} L^{0.75} \text{ (km)}$$

TABLE 2

LINK MARGIN CALCULATION (9.0 km span)

INKSTER - SHERBROOK

System Gain	43.5 dB
Allowance for Future WDM	-6.0
Degradation & Future Splices	-5.5
Connector Loss (2x1.0 dB)	-2.0
Maximum Installed Cable Loss	30.0 dB
Splice Loss (13x0.3 dB)	-3.9
Net Maximum Cable Loss	26.1 dB
Maximum Cable Attenuation	2.9 dB/km
Cabled Fiber Specification	2.8 dB/km

For the 9 km link $B_L = 468$ MHz.km and the bandwidth specification was written to require a minimum link average of 450 MHz.km and a minimum individual bandwidth of 400 MHz.km.

The transmission requirements of cable for each subsystem are shown in Table 3. Factory test results for cables ready for installation in the INKSTER-SHERBROOK link are summarized in the following histograms. Figure 5 shows the distribution of fiber attenuation at both 850 and 1300 nm measured on shipping lengths of cable. A 500 m launch fiber was used to approximate the equilibrium mode distribution in the test fiber. Figures 6 and 7 show the 3 dB optical bandwidth length product, B_L , measured by a swept frequency technique using laser diode sources at 850 and 1300 nm respectively. A step-graded-step mode

scrambler connected to the input end of the fiber by a V groove splice ensured excitation of all propagating modes in the test fiber. Since finished cable lengths varied from 700 to 1700 m, depending on the site requirements, the measured bandwidth, B_m , was normalized for length using a length exponent of 0.8, i.e.

$$B_L \text{ (MHz.km)} = B_m \text{ (MHz)} L^{0.8} \text{ (km)}$$

FIGURE 5

CABLED FIBER ATTENUATION

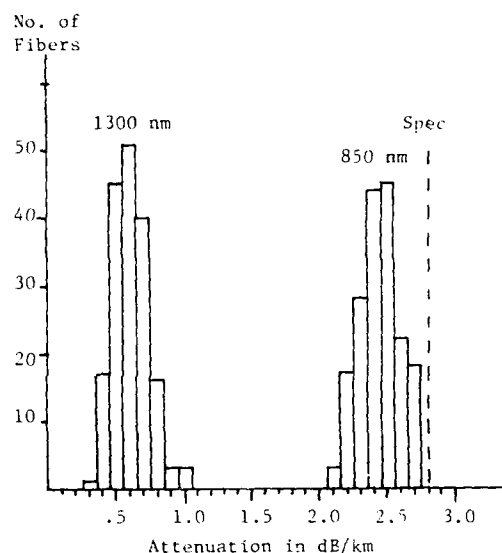


TABLE 3

SYSTEM	CABLE LENGTH (kms)	FIBER COUNT	CABLE PERFORMANCE @ 850 & 1300 nm		
			ATTENUATION MAX. (dB/km)	INDIVIDUAL BANDWIDTH MIN. (MHz.km)	LINK AVERAGE BANDWIDTH MIN. (MHz.km)
Grassmere-Inkster Park	12.7	12	3.6	300	350
Inkster Park-Sherbrook	9.0	16	2.8	400	450
Sherbrook-Main	2.3	20	3.6	250	300
Main-Fort Rouge	4.0	14	3.6	200	250
Sherbrook-Fort Rouge	2.1	12	3.6	250	300
Beausejour-Hazelridge	26.0	6	3.0	400	450
Hazelridge-Oakbank	11.0	6	3.6	300	350
Oakbank-Knowles	16.0	8	3.2	350	400
Knowles-Gateway	7.5	8	3.4	50	400
Gateway-Main	8.5	10	3.0	380	430
Fort Rouge-Charleswood	9.3	6	2.8	400	450
Stonewall-Stony Mountain	13.5	6	3.6	350	400
Stony Mountain-Grassmere	6.4	6	3.6	350	400
Gateway-Kildon Place	6.8	12	3.5	350	400
Empress-Sherbrook	3.4	10	3.5	350	400

AD-A125 662

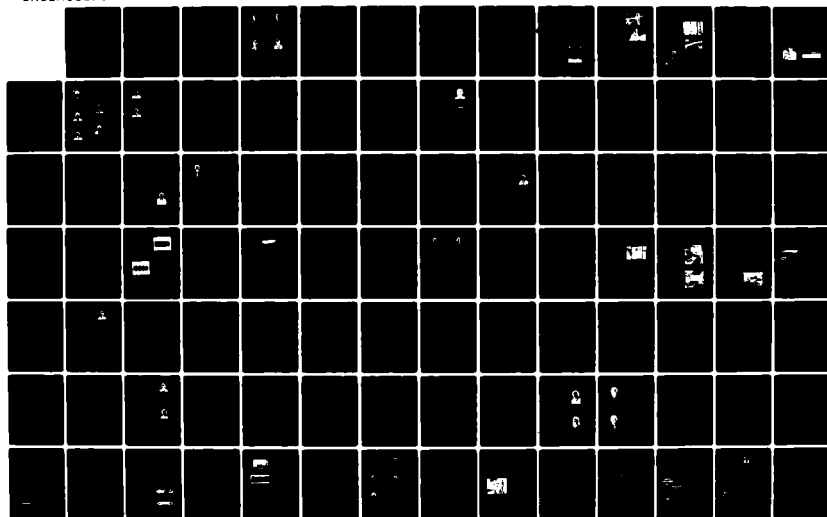
PROCEEDINGS OF THE INTERNATIONAL WIRE AND CABLE
SYMPOSIUM (31ST) HELD AT... (U) ARMY
COMMUNICATIONS-ELECTRONICS COMMAND FORT MONMOUTH NJ
NOV 82

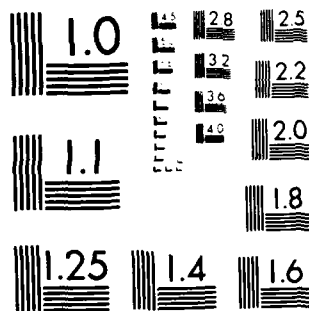
UNCLASSIFIED

F/G 20/6

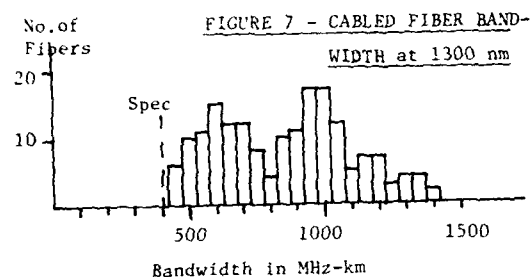
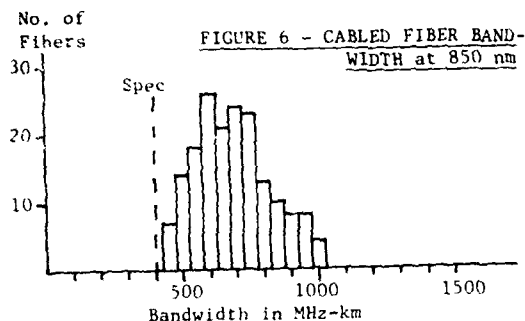
NL

216





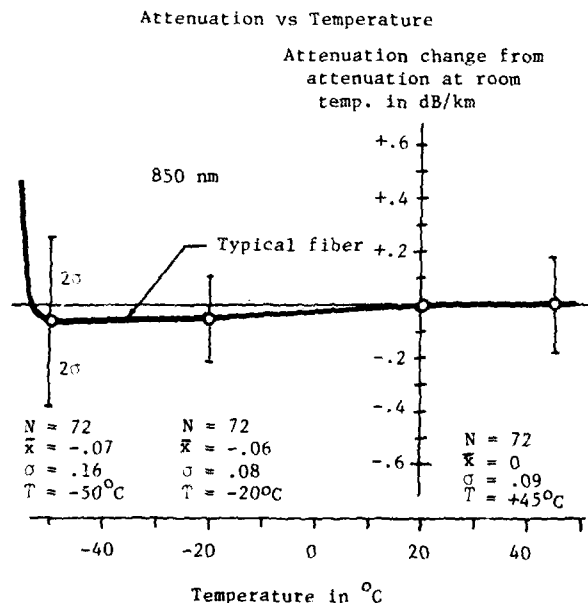
MICROCOPY RESOLUTION TEST CHART
NATIONAL BUREAU OF STANDARDS-1963-A



Temperature Performance Requirements

Cable for duct and buried installation are required to have an attenuation increase of less than 0.2 dB/km relative to the value at 20°C over the temperature range -20 to +35°C. The specification for aerial cable covers the temperature range -50 to +45°C but permits increases of up to 0.5 dB/km.

FIGURE 8



Test results on finished cable are shown in Figure 8. The solid curve shows the performance of a typical fiber in a pre-production cable of the final concentric design at 850 nm. This attenuation is essentially constant over the temperature range -50 to +70°C, however below -50°C the attenuation increases abruptly; due to buckling of the fibers inside the protective coating. There was no significant variation of temperature performance with source wavelength over the range 800 to 1500 nm. Quality Assurance measurements on sample cables from the production run show that the required temperature performance was achieved.

Physical and Mechanical Characteristics

Physical and Mechanical properties of cable are summarized in Table 4.

TABLE 4

	Concentric Cable	Unitized Cable
Cable diameter, mm	12.7	21.0
Cable weight, kg/km	180	400
Max. Pulling Tension, N	2000	3100

Mechanical Test

Results

Impact - 300 cycles at 1.5 Nm impact with 8.5 mm radius hammer	} No transmission change, no evidence of damage to cable structure
Flexing - 150 cycles of $\pm 90^\circ$ bend over a mandrel of 10 times cable diameter	
Crush Resistance - 1.5 kN crushing force between 10 cm jaws	
Torsional Strength - 10 cycles $\pm 90^\circ$ twisting of 3 m cable sample	
Tensile Load - 10 m gauge length, each end of cable sample wrapped 3 times around 30 cm diameter mandrel.	

Concentric Cable

2000N - No transmission loss
3560N - 5% transmission loss, output recovered after load was removed

Unitized Cable

4500N - No transmission loss

Processing Experience

Tight jacket fibers were directly stranded without any problems using conventional planetary stranding and cabling equipment with modified pay-off tension controls. Each cable length met the optical, thermal and physical requirements of the specification. The attenuation change throughout the stranding, cabling and sheathing process was within ± 0.2 dB/km from fiber attenuation prior to stranding for all manufactured lengths.

INSTALLATION

The lightguide cables were installed by MTS personnel with Canstar providing training and supervision for the first sub-system GRASSMERE-MAIN. By October 1982 the cable installation was complete as indicated on Figure 1.

Underground sections of cable were pulled into P.E. subducts with an inside diameter of 35 mm. Pulls of up to 1 km length were handled by a small electric winch without exceeding the tensile load rating of the cables. Buried sections of cable were ploughed to a depth of 1.07 m using two caterpillar tractors in tandem. A powered capstan ensured that the cable was not under tension as it entered the plough. This installation technique is very efficient in Southern Manitoba because of the terrain. In aerial sections the cable was doubly lashed to a 6.4 mm (1/4 inch) stranded steel messenger wire.

Splices were made using an arc fusion splicer equipped with a 3 axis manipulator and microscope for visual alignment of the fiber ends. The individual splices were protected with a reinforced sleeve, racked on a custom designed fiber organizer and housed in a conventional in-line lead sleeve enclosure.⁽⁴⁾ Each splice was inspected by optical time domain reflectometer. The average splice loss of 412 splices measured in this way was 0.26 with a standard deviation of 0.16.

Optical attenuation of the installed links was measured before attaching the terminal connectors using an 850 nm LED source and optical power meter. On the INKSTER-SHERBROOK link the end-to-end attenuation varied from 23.2 to 25.5 dB compared to a design target (Table 2) of 30 dB.

PERFORMANCE AND MAINTENANCE

The initial phase of the network was successfully completed and has been in service since the summer of 1982, following a test period of six months through a severe Manitoba winter. Various test results have shown a satisfactory performance of the transmission network. Bit error rate was maintained at better than 10^{-11} . The link loss safety margin exceeds the design value of 11.5 dB. No service failures have been reported. The lightguide network does not suffer from fading due to climate disturbances - a very real problem with the microwave systems. Its cable, being contained in cable ducts within the city, or buried is less vulnerable to disturbance.

System line-up and tests are much simplified compared with the microwave transmission system. A number of elaborate initial line-up and test procedures are eliminated, such as antenna orientation, RF return loss and interference tests. Envelope delay measurement and equalization are also not necessary because of the wide bandwidth of the lightguide. The lightguide

transmission line need simply the cable attenuation measurement to ensure required safety link loss margin for system degradation due to aging, temperature and additional splices.

The system and equipment do not need special maintenance only periodic inspection for performance and obvious defects. Combination of the following auxiliary equipment features provide easy maintenance and quick troubleshooting with a minimum of travel by maintenance personnel.

- Equipment modular design permits easy and fast replacement
- Detailed local alarms display
- Centralized supervision
- Equipment incorporates the test functions of signal local loopback and remote loopback to check faults and to identify the failed module.

CONCLUSIONS

This is the first application of 90 Mb/s lightguide transmission in a large scale toll message trunking network in Canada. It has demonstrated its suitability to this kind of application, especially in the environment of a large city, where underground conduits are crowded, repeaters not desired, microwave spectrum congested and line of sight insecure.

The tight buffered fiber used in the cable design can be cabled directly without application of prior protection such as a loose buffer as in the majority of present cable designs in North America. This reduces cost and improves the production rate. The tight buffered fibers also are much easier to handle during splicing and other installation operations. Further, the fibers, when suitably cabled, exhibit excellent performance over the wide temperature range encountered in North America.

REFERENCES

1. Continuous Fabrication Process for High-Silica Fiber Preforms.
T. Izawa, S. Sudo & F. Hanawa
Transaction of IECE of Japan
Vol. E. 62, No. 11, (1979) Pg. 779
2. Determination of Optimum Structure in Coated Optical Fiber & Cable Unit.
K. Ishihara, S. Mochizuki, N. Nakatani, N. Uchida, H. Hondo and Y. Sugawara
5th European Conference on Optical Communications Sept. 1979, Amsterdam, Holland.
3. Jelly-Filled Optical Fiber Cables.
Y. Kameo, H. Horima, S. Tanaka, Y. Ishida and Y. Koyamada
Proceedings 30th International Wire and Cable Symposium Pg. 236 Nov. 1981 Cherry Hill N.J.
4. New Reinforcement for Arc-Fusion Spliced Fiber.
M. Miyauchi, M. Matsumoto, Y. Toda, R. Matsuno and Y. Tokumaro
Electronics Letters Vol. 17, No. 24 (1981) Pg. 907



Edward Byzio received his bachelor of science in electrical engineering in 1971 from University of Manitoba. He joined Canada Wire Communication Product Division in 1972 as a design and development engineer of conventional telephone cable. Currently he is the Manager of Lightguide Cable Engineering, Canstar Communications Division of Canada Wire.



Keith Eastwood received his doctorate in physics from McMaster University, Hamilton, Ontario in 1964. He worked on material and device research at Northern Telecom from 1963 to 1970. From 1970 to 1976 he worked on the electrical and optical properties of thin films for Multistate Devices. In 1976 he joined Canada Wire's fiber optics program as Group Leader. Currently he is Fiber Optics Product Development Manager for Canstar Communications.

MAILING ADDRESS

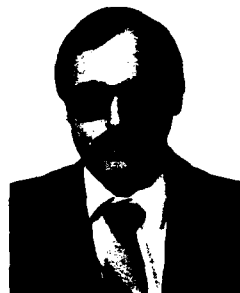
Canstar Communications
1395 Buffalo Place
Winnipeg, Manitoba, Canada
R3T 1L6



K. K. Hau graduated from the University of Waterloo, Canada, with a master of arts and science in electrical engineering in 1973. He joined Canstar Communications, a division of Canada Wire and Cable, in 1978 and since then has been involved with Fiber Optic Communication Systems. Prior to joining Canstar, he worked for Northern Telecom, Montreal, Canada as a microwave transmission engineer.

MAILING ADDRESS

Canstar Communications
1240 Ellesmere Road
Scarborough, Ontario, Canada
M1P 2X4



Jim Petrin graduated from Red River College in Winnipeg as a certified engineering technologist. He joined the Manitoba Telephone System in 1976 and currently holds the position of Job Manager and provisioner of radio, multiplex and fiber optic equipment. He is a member of Manitoba Society of Engineering Technologists.

MAILING ADDRESS

Manitoba Telephone System
Box 6666 B-401C
Winnipeg, Manitoba, Canada
R3C 3V6

OPTICAL FIBER CABLE FASTENED TO OVERHEAD GROUND
WIRE WITH LASHING ROD

K. Fuse, Y. Shirasaka, S. Kume, M. Kurokawa

Y. Obara, L. Kimata, M. Yoshizawa

The Furukawa Electric Co., Ltd.

6-1 Marunouchi, 2-chome Chiyoda-ku, Tokyo, Japan

Summary

This report deals with a new holding method of the optical fiber cable along the existing overhead ground wire as an optical fiber system utilizing power lines, which has been successfully developed by the authors.

The feasibility studies on such a holding method have never been proposed for the reason of:

1. Absence of the lightweight, small-sized optical fiber cable with mechanical properties durable to the holding.
2. Unfamiliarity to holding and installation methods.

This report is intended to discuss details of the system of the optical/ground wire separate type of high strength optical fiber cable newly developed by The Furukawa Electric Co., Ltd.

The features of the new system are detailed in the following.

- 1) Utilization of non-metal, FRP covered optical fiber cable.
- 2) Lashing rod separating method allowing use of the existing ground wire.
- 3) Development of new holding method.
- 4) Reliability testing.
- 5) Wide-range application.

1. Introduction

This paper describes the installation of the optical fiber cable developed by Furukawa Electric Co., Ltd. to an existing overhead ground wire. Conventional communications systems with power-transmission lines have employed power-line carrier systems and systems involving coaxial cable inserted in an overhead ground wire. Such systems have a considerable number of problems, such as high cost and poor quality due to the insufficient separation of communications signals from the high voltage of power conductors, or to noise induction from the transmission line. However, with the appearance of optical fiber it has become possible to use fiber communications in power transmission systems. Practical applications have been developed.

2. "FILA System" (Optical Fiber
Cable Fastened to Overhead Ground
Wire with Lashing Rod)

2.1 Optical Fiber System in Power Lines

The six methods shown in Fig. 1 are considered possible ways to use optical fiber in power lines as communications circuits and monitoring systems. However, methods (I) to (III) have been judged undesirable, because they all require extensive open areas limited to use for the installation of optical fiber cables. The power line method (V) is thought to be difficult to put into practice at present, although some have investigated its practical applications. The direct fastening or hanging of an optical fiber cable along a live power line can cause damage or deterioration of the optical fiber due to the tracking and various other causes.

On the other hand, the self-supporting method (IV) and ground wire method (VI) have great possibilities for practical use.

The self-supporting method can utilize existing power line pylons. It eliminates most of the problems such as susceptibility to lightning and tracking deterioration which arise in other methods. However, hanging optical fiber cables requires tension members, so that it is necessary either to install tension members or to use self-supporting optical fiber cables.

The facts that this method necessitates the use of optical fiber cables with a larger diameter and greater weight, and that the cables are subject to larger wind loads make the use of existing pylons with their insufficient structural strength impossible. Moreover, the length of the optical fiber cable to be hung can cause problems. It is a critical question whether or not the existing pylons can provide sufficient height for the optical fiber cable, in consideration of the height of existing power lines, as well as of the slugs and their vibration.

Consequently, practical employment of the self-supporting method requires extensive cable-installation areas, an optical fiber cable with a small diameter and light weight to minimize the force acting on the pylons, and an optical fiber cable of higher tensile strength. Practical use of the self-supporting method is anticipated, although the absence of optical fiber cables satisfying above-mentioned requirements has prevented its practical application thus far.

The overhead ground wire method (VI) detailed below is the method which has been most fully investigated to date.

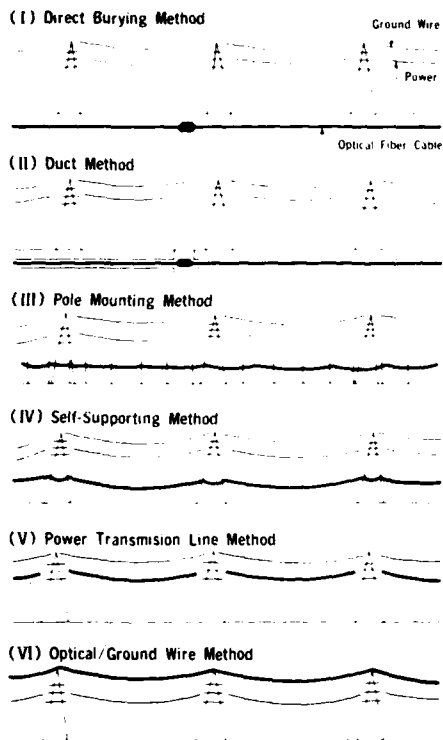


Fig. 1 Schematic Diagram of Optical Telecommunication System with Power line

2.2 Ground-wire Method

It can be said that at this point optical fiber integrated with ground wire is the method offering the greatest possibilities among the above six methods. It minimizes both the deterioration due to tracking and the area necessary for cable installation. This method will be realized as soon as a way to use existing ground wires becomes available. The following two types of ground wire can be supposed usable for this method:

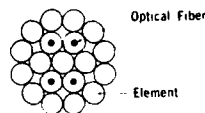
- (1) Optical fiber integrated ground wire (Integrated-type OPGW)^{1), 2)}
- (2) Optical fiber fastened ground wire (Separate-type OPGW)³⁾

The following methods, shown in Fig. 2, have been examined to insert optical fiber in the integrated-type OPGW: (1) substituting an aluminum pipe for one element cable of ground wire, (2) stranding a long spacer including optical fiber units with element cables of a ground wire, and (3) providing a hollow at the center of a ground wire. These methods for creating an integrated cable are accompanied by the following two problems.

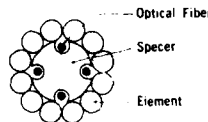
- (1) The method of replacing ground wire and the cost of the replacement become critical factors when an optical fiber cable is inserted in an existing ground wire, or when an existing ground wire is replaced by a new one, although the installation of a new groundwire/optical-fiber-cable system is accompanied by no such problem.
- (2) The method of pulling the optical fiber cable out of the ground wire, in regard to which there are a number of restrictions and a limited degree of freedom, becomes a tough problem in the connection of optical fiber cables.

Unlike the integrated system the other one involving the fastening of an optical fiber cable along a ground wire proves that the two problems mentioned above need not obstruct the practical application. The separate-type OPGW seems to handle the application of existing ground wires, which present the most serious problems for the integrated-type OPGW.

(I) Elemental Formula



(II) Spacer Internal Formula



(III) Central Integrated Formula

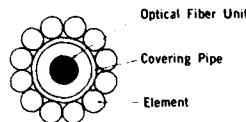


Fig. 2 Example of Optical/ground Wire Integrated Type

2.3 Separate-type OPGW

The separate-type OPGW is thus expected to prove greatly superior to the integrated-type OPGW. The reason the separate type has received little investigation is that the optical fiber cable to be used for it has the following specific requirements which must be satisfied if it is to be put to practical use:

- (1) The optical fiber cable must be within the allowable tensile strength range for the power-line pylon. Optical fiber cable with higher tensile strength, lighter weight, and smaller diameter becomes essential to minimize any loads, such as wind load, which

act on the pylon as a result of the installation of the optical fiber cable.

- (2) A new optical fiber cable must be developed which has stable transmission characteristics against the heating and elongation of a ground wire on the lightning.
- (3) The optical fiber cable must be installed in such a manner as to make various types of wind damage unlikely: galloping, aeolian vibration, wind howling, etc.
- (4) The optical fiber cable must have a sufficient mechanical strength to resist any external force possible in the cable installation. The subsequent chapters deal with a power-transmission line practically built for the evaluation of the design and installation of the attached ground wire in consideration of above-mentioned requirements.

3. Design

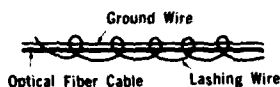
3.1 Fastening Method

Three fastening methods, shown in Fig. 3, have been considered for the installation of an optical fiber cable to an overhead ground wire:

- (a) Hanging method,
- (b) Lashing wire method,
- (c) Lashing rod method,

Adopted here is the lashing rod method (c), because methods (a) and (b) include several such problems in their systems, as will be described in Chapter 4. The lashing rod itself has sufficient gripping force and requires no particular restraining device in the passing-over and terminating sections around a pylon. In addition, this method is expected to limit the bad effects such as galloping and howling on the pylons and the environment.

(A) Lashing Wire Method



(B) Lashing Rod Method



(C) Hanging Ring Method



Fig. 3 Optical Fiber Cable Mounting Method to Ground Wire in Optical/ground Wire Separate Type

3.2 Cable Design (1-6)

A practical example of installation is here described, in which an OPCW is fastened to existing power lines. The power line has a rating of 132 kV acst, the main conductor cables employ ACSR "Hen," and the ground wire is GSW with a 50 mm² cross section.

The following factors should be noted in the design of the optical fiber cable fastened to this ground wire:

- (1) Small diameter (An objective O.D. is 6 mm or less.)
- (2) Light weight
- (3) Ordinarily employable over a temperature range of -30°C to 150°C.
- (4) No problems result even when the ground wire temperature is raised suddenly to 200°C or more.
- (5) No electrical conducting material is used.
- (6) Capable of containing four or more optical fibers.
- (7) Resists ground-wire vibrations such as aeolian vibration and galloping.
- (8) Good weather resistance
- (9) Protected against lightning

A small diameter and light weight are regarded as of major importance among these characteristics. The optical fiber cable must keep the existing ground wire within the designed tension allowance when fastened to the ground wire. For this reason, the optical fiber cable must be of light weight and small diameter when the icing up and wind force are considered. A light-weight optical fiber cable is also desirable for workability and safety in the cable installation, a process in which a drum containing the optical fiber cable is hung on the ground wire and moved along it. A small diameter optical fiber cable allows designing of a lighter drum without respect to a special high-strength design. Figure 4 shows an example of the optical fiber cable designed in line with the above-mentioned considerations and actually used. The OD of the optical fiber cable is 6 mm and the weight 55 kg/km. Ground wires are generally designed to tolerate temperature increases of: 1 up to 150°C, caused by induction current and 2 up to 200°C, caused by lightning. They are also provided with measures against icing up in winter.

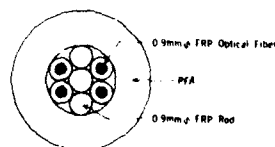


Fig. 4 Cross-section View of Optical Fiber Cable for "FILA System"

Ordinary optical fiber cables have a structure of fiber elements covered with thermoplastic resin either directly or in pipe-like form. This optical fiber is considered to be extremely difficult to manufacture into a cable with so small a diameter as 6 mm or so, because the fiber has a maximum service temperature of 100°C and requires heat-insulation and mechanical-protection layers on the fiber when used for an OPCW.

The newly developed FRP covered optical fiber has proven to be an optical fiber optimum for the "FILA System." Considering the facts that the FRP optical fiber shows no change in its transmission characteristics at temperatures even above 200°C if the time of the heat application (lightning etc.) developing this temperature is short.

The FRP optical fiber is not deformed when subjected to lateral forces from the lashing rods in cable installation.

The FRP optical fiber employs fluorocarbon resin (PFA)* as its covering material. This can resist lateral forces from the lashing rods at 150°C and has excellent weather-resistant and heat-resistant characteristics.

The process loss increase gives only a small change of approx. 2.5 dB/km for an LED light source whose wave-length $\lambda = 0.85 \mu\text{m}$, as shown in Fig. 5, throughout the period from the state of optical fibers to the completion of the cable installation.

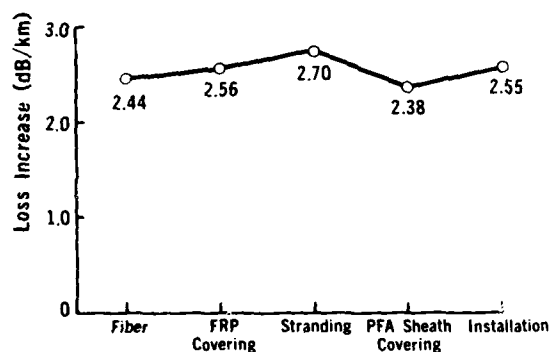


Fig. 5 Attenuation Loss Change between Optical Fiber Production to Installation

*PFA: Perfluoroalkoxy-modified tetrafluoroethylene

Table 1 Characteristics of Grand Wire

Ground wire	GSW 50 mm ²	
Composition	7/3.0	
Outside dia.	9.0 mm	
Weight	0.4 kg/m	
Elastic modulus	18,000 kg/mm ²	
Coefficient linear expansion	0.000012/°C	
Optical fiber cable	OD	6.0 mm
	Weight	55 kg/km
Lashing rod weight	44 g/rod	
Allowable max. tension	1,600 kg	

3.3 Examination of Sag/Tension Characteristics

The FRP optical fiber cable fastened to a ground wire of 50 mm² GSW has been tested for sag/tension characteristics.

Listed in Table 1 are the specifications of the ground wire used and the OD and weight of the lashing rods. The wind load is estimated at 60 kg/m² and the icing load is determined by 0.18 \bar{d} . Calculation of the sag/tension characteristics is then carried out on the ground wire with optical fiber cable under no-wind, wind, and icing conditions, respectively. The results of the calculations are shown in Figs. 6 and 7.

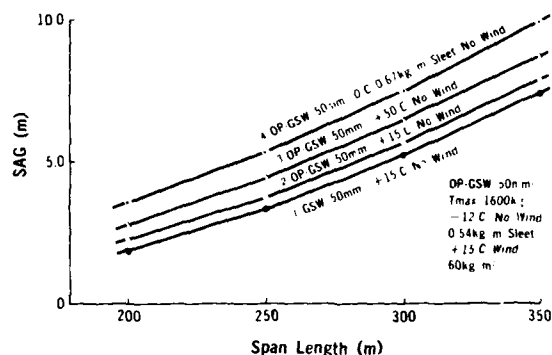


Fig. 6 OP-GSW 50 mm² Sag-tension Chart (1)

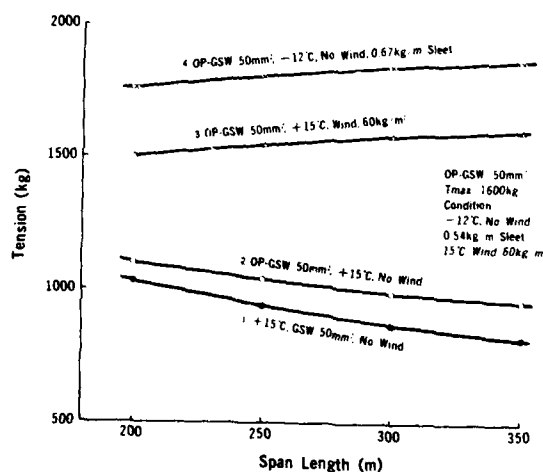


Fig. 7 OP-GSW 50 mm² Sag-tension Chart (2)

The sag/tension calculation uses the following equations:

$$f_2 \{ f_2 - (K - \alpha t E) \} = M \dots\dots 3.1$$

$$K = f_1 - \frac{(q_1 S)^2 S^2 E}{24 f_1^2} \dots\dots 3.2$$

$$M = \frac{1}{24} (q_2 S)^2 S^2 E \dots\dots 3.3$$

where:

- q_1 = load coefficient on initial condition
- q_2 = load coefficient on objective condition
- E = elastic modulus of wire
- S = span length
- f_1 = wire tension per unit area under initial conditions
- f_2 = wire tension per unit area under cable-installed conditions

In the calculation it is assumed that the optical fiber cable bears no partial share of the ground-wire tension, because the optical fiber cable is only fastened to the existing ground wire. The effect of ground-wire elongation in the 20° to 200°C range on the optical fiber cable is estimated by calculating the actual length of the ground wire at a temperature of 200°C on the assumption that the ground wire is heated by the flowing current by the flash-over in lightning. A strength check is made on supporting devices to ensure the safety of power lines. Under the most severe conditions the optical fiber cable increases the ground wire tension by approx. 300 kg. Although the sag in the ground wire increases by 0.3 m to 0.5 m due to the weight of the optical fiber cable in ordinary temperature conditions, this remains within the allowable range for clearance between the ground wire and the main conductor cable, causing no problem. The elongation of the ground wire at a high temperature of 200°C is estimated at 0.2% or less. This shows that the elongation of the ground wire detracts little from the long-term reliability of the OPGW.

4. Installation Processes

4.1 Fastening Optical Fiber Cable to Ground Wire

The installation process is one of the most critical of the techniques in the "FILA System." The existing ground wire is installed at higher levels of 20-40 m above the ground and with longer spans of 100-400 m. These give rise to two problems in methods of laying and fastening optical fiber cables. However, a full investigation has eliminated such difficulties in the "FILA System." There are three general methods of fastening of an optical fiber cable to ground wire. The lashing wire method, though mechanically feasible, contains higher possibilities of short-circuiting with power lines if the lashing wire should break. This method provides insufficient

grip force for an optical fiber cable. The hanging method is also not recommended because of the lack of an adequate grip force for the optical fiber cable and the application of localized pressure on the optical fiber cable.

The method employing lashing rods is therefore adopted; the lashing rod is non-continuous and gives sufficient grip force.

A new cable running method, outlined below, is attempted. It applies little tension to the optical fiber cable to be run, and takes advantage of the FRP optical fiber cable with a small OD of 6 mm and light weight of 55 kg/km. The cable laying method applied to the "FILA System" consists of the following processes as shown in Photo 1:

- ① The necessary length of FRP optical fiber cable is wound on a traveling drum (weighing only 22 kg) specially designed to allow it to be hung from the ground wire.
- ② The drum containing the optical fiber cable is hung from the ground wire and pulled along the wire with a pilot rope, laying the optical fiber cable as it goes.
- ③ A worker in a gondola follows the traveling drum and fastens the optical fiber cable to the ground wire with lashing rods at regular intervals.

The existing ground wire is made of 3.2 mm dia galvanized steel wires intertwined in a 1-6 array. The lashing rods are 2.4 mm in diameter and 75 mm long. They are spaced 25 cm apart. The cramping time is 50 to 60 min/100 m. The traveling drum and gondola are satisfactorily transferred across each pylon. A view of the cable laying process is shown in Photo 1.



Photo 1 A View of Cable Laying Process by Traveling Drum

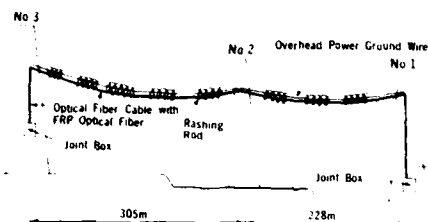


Fig. 8 Schematic Installation Diagram of Optical Ground Wire

4.2 Method of Passing Over and Terminating Cables Around Pylon

The optical fiber cable is protected by inserting it into *plafleky*® (a corrugated PE pipe covered with flexible PVC, made by The Furukawa Electric Co., Ltd.) which covers all passing over sections of the optical fiber cable at the pylon and all terminating sections from the top of the pylon to the point where the optical fiber cable is connected. This prevents the optical fiber cable from being damaged by the variety of maintenance operations performed on the pylon. Combining the *plafleky*® containing the optical fiber cable with the ground wire eliminates the generation of stress concentration. Optical fiber cable without *plafleky*® reaches its largest vibration amplitude near each pylon because of the tendency of the optical fiber cable to separate from the ground wire. The method of inserting the optical fiber cable into the *plafleky*® involves fixing the *plafleky*® to the connecting box beforehand and by pushing an end of the optical fiber cable into the *plafleky*®. No pull-rope is employed because of the small diameter and high degree of rigidity of the FRP optical fiber cable. Photos 2 and 3 show some states of the operation. The principal components involved in the installation are listed in Table 2.

Table 2 Tools and Accessories for Installation

Component	Specification
<i>Plafleky</i> ®	Self-extinguishing flexible conduit, 16 mm ID and 23 mm OD
<i>Hilum</i> ®	Jig for fixing <i>plafleky</i> ® (made by Negurosu Elec. Corp.)
Traveling Drum	Capable of continuous cable laying of 2 km max., 22 kg weight
Pilot Rope	For traveling drum traction ϕ mm dia.
Lashing Rod	For fixing the optical fiber cable, 2.4 mm dia and 750 mm long

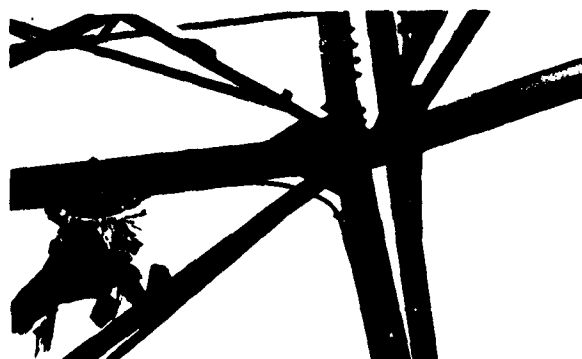


Photo 2 Terminating Cables Around Pylon



Photo 3 Terminating Cables Around Pylon

4.3 Post-Installation Checking

An optical fiber cable is installed across approx. 530 m, as shown in Fig. 8. A connection is provided below the No. 1 pylon, simulating an actual cable and its connection, and the optical fiber cable is drawn into a building where measurements are conducted. Two of four cores are return-connected to measure occasional changes in transmission loss. One core transmits the image signals from an ITV camera to the building, for monitoring icing and galloping.

5. Reliability Tests

The following outlines some representative examples of reliability tests which have been carried out. A number of evaluation tests for reliability of the Separate-type OPCW are needed because the Separate-type OPCW, unlike the Integrated type has an optical fiber cables outside the ground wire, which acts an arrester, and must ensure high reliability for a long time of the OPCW and power lines.

5.1 Lightning Test

The Separate-type OPCW must be provided with full protection against lightning. The following problems are assumed in lightning phenomena:

- (1) Problems accompanying the flashover caused by direct discharge of lightning to ground wire, (voltage, current, and arc).
- (2) Problems of current generation and arc involving the tower flash over.
- (3) Problems current of generation and arc involving the ground fault.
- (4) Problems involving the heat generation of the ground wire caused by induced currents.

An impulse test for the evaluation of the flash-over phenomenon is carried out in consideration of the possibility of dielectric breakdown in the cable sheaths due to a direct lightning strike. The testing method is as shown in Fig. 4, that is, an electrode is placed next to the optical fiber cable and impulse voltages — 1,000 kV, 2,000 kV, and 3,000 kV — are imposed on the electrode. Attenuation of light through the optical fiber is monitored.

An electrical discharge is shown in Photo 5. The results of the test show that the impulse voltage causes a discharge to the surface of the cable sheath in most cases, but damage to the cable itself is quite small. The attenuation increase remains within the range of the measurement error. The optical fiber cable used in this system ensures that it can withstand some 3,000 kV impulse voltage.

A current heating test is carried out to determine the critical temperature as a simulation of ground-wire heating due to the current of tower flashover. No attenuation increase is monitored in the optical fiber cable after 24 hours at 250°C. In this test, the optical fiber cable was subjected to heat shocks, repeated three times, involving heating of up to 200°C in a few minutes and cooling to normal temperature, with the attenuation continuously monitored.

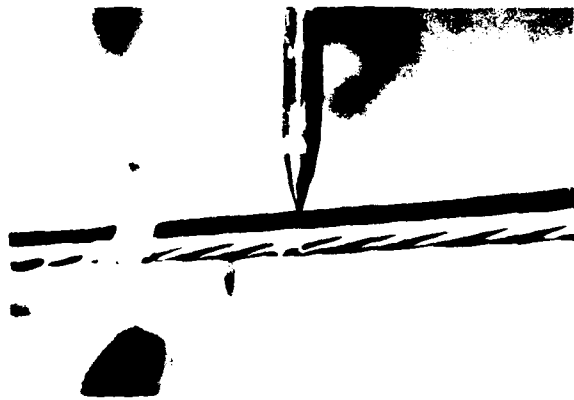


Photo 4 Impulse Test

Photo 6 shows a specimen for finding the temperature limit of the optical fiber cable heated in excess of the melting point (260°C) of the fluorocarbon resin PFA which is used as the sheath. It is recognized that the cable sheath has left deposits on the ground wire because of the heat, but no attenuation increase is detected. The PFA used for the cable sheath was selected in consideration of its good tracking properties and its excellence in both heat- and weather-resistance.



Photo 5 At the Time of the Arc in Impulse Test



Photo 6 A Optical Fiber Cable Heated in Excess of the Melting Point

5.2 Wind Damage Test

Damage from wind is along with the lightning test the other most important test. The following problems are listed as assumable from wind damage.

- (1) Fatigue of the ground wire due to Aeolian vibration.
- (2) Tension increase in the ground wire due to galloping.
- (3) Tension increase in the ground wire due to a wind load.
- (4) Environmental properties against howling.

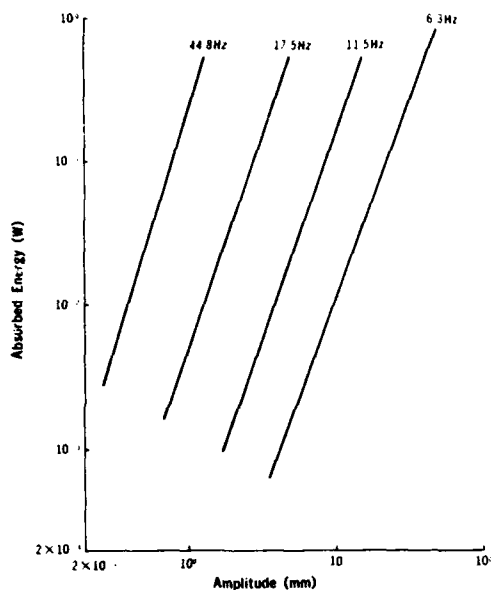


Fig. 9 Energy-absorption Characteristics of GW 50 mm²

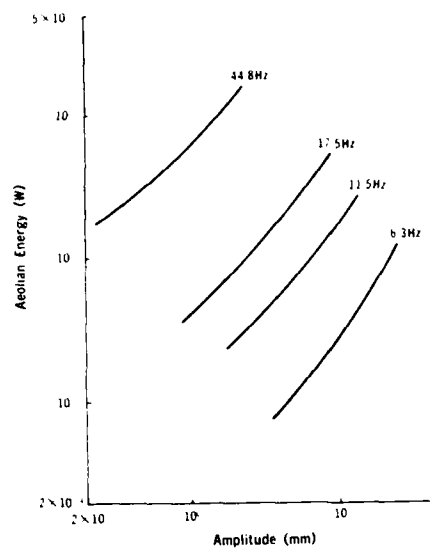


Fig. 11 Aeolian Energy Transmitted from Wind to the GW 50 mm²

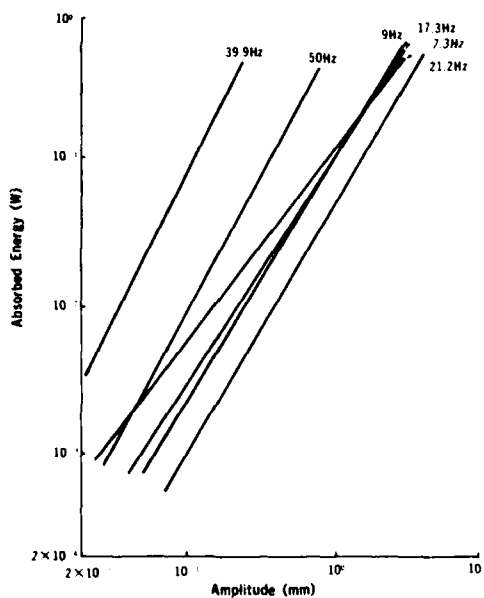


Fig. 10 Energy-absorption Characteristics GW 50 mm² with Optical Fiber Cable

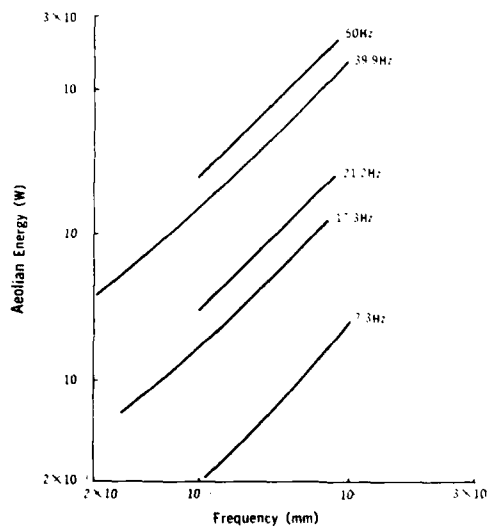


Fig. 12 Aeolian Energy Transmitted from Wind GW 50 mm² with Optical Fiber Cable

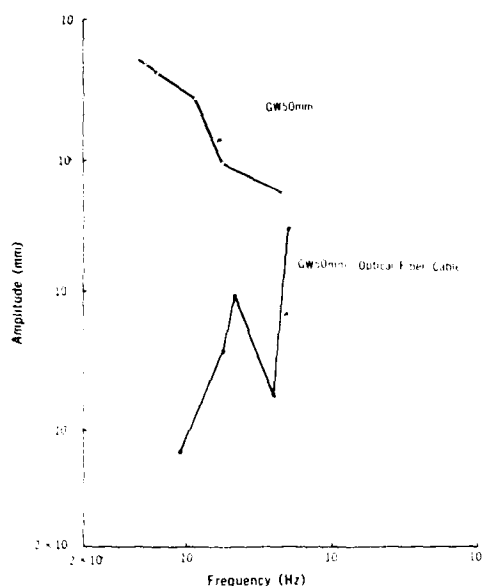


Fig. 13 Relationship between Vibrating Frequency and Amplitude of GW 50 mm²



Photo 7 Vibration Test

To evaluate problems (1), a comparison is made between the conditions of the 50 mm² ground wire with and without the fastened optical fiber cable. In the comparison the amplitude of the ground wire at each frequency is estimated using the energy balance method in which the energy difference is determined from the vibration (input) energy transmitted from wind to the ground wire and the energy consumed (absorbed) by the ground wire. Figures 9 and 10 show the energy-absorption characteristics of 50 mm² GW alone and 50 mm² GW with optical fiber, respectively, for each frequency. On the other hand, Figs. 11 and 12 indicate the Aeolian energy transmitted wind to the ground wire. Figure 13 shows the relationship between frequency and amplitude obtained from the energy balance point found on Figs. 9 or 10 and Figs. 11 or 12. Figure 13 apparently proves that no problem arises from the installation of the optical fiber cable, because the ground wire with the optical fiber cable shows a reduced amplitude from that of the 50 mm² GW alone. (However, the case in which an optical fiber cable is attached to the ground wire in positions where provision for vibration is required. Should be separately examined.) The overall view of the vibration test is illustrated in Photo 7, and the optical fiber cable fastened to 50 mm² GW in Photo 8.

No galloping and howling — problems (2) and (4) — can easily develop because of the structural design of the lashing rod with an S-Z turn. In spite of this, monitoring is maintained on the tension change, frequency of vibration, and attenuation on a 300 m single-spanned experimental line built in a place where galloping is especially likely to occur.

Problem (3) is as described in Article 3.3.

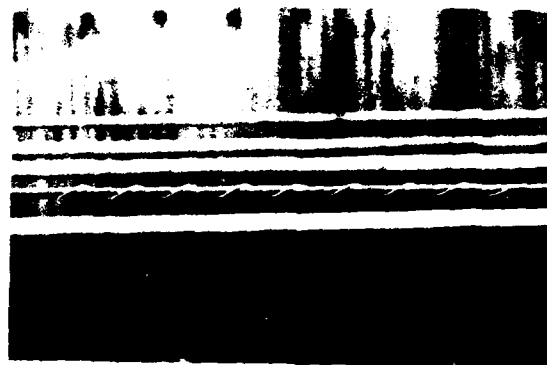


Photo 8 Optical Fiber Cable Fastened to Ground Wire with Lashing Rod

6. Conclusion

The "FILA System" (Separate-type OPCW) is possessed of the following advantages:

- (1) Non-metallic optical fiber cable using light-weight and small-diameter FRP optical fiber with excellent lateral-force resistance and durability.
- (2) Capability of installation with lashing rods allowing application to existing ground wires.
- (3) Economical installation processes with a newly developed traveling drum and gondola.
- (4) Versatility

However, further examination needs to be made on the obstacle effect from lightning strikes and on the long-term reliability, including weather resistance, because this system is quite new. Apart from this particular application, several experiments are under way to put this system to practical use by utilizing existing power lines. The new FRP optical fiber with higher strength has created this "FILA System," which is expected to increase the possibilities for the advent of new communications systems utilizing power lines.

Acknowledgement

The authors sincerely thank Mr. M. Ogai and M. Itho of the Furukawa Electric Co., Ltd. who had advised us earnestly in development of the FILA System. It should be stated that the development of FILA System was conducted with cooperation of Messrs K. Komura, T. Sasaki, M. Obara and Y. Matsuzaki of the Furukawa Electric Co., Ltd.

References

- 1) S. Kubota, et al., The Annu. Meeting of the IECE Japan 7-259 (1982)
- 2) N. Katuoka, et al., The Annu. Meeting of the IECE Japan 7-255 (1982)
- 3) M. Kurokawa, et al., The Annu. Meeting of the IECE Japan 7-257 (1982)
- 4) K. Fuse, et al., 30th IWCS Proceedings 147 (1981)
- 5) M. Ogai, et al., OFC'82 Technical Digest 46 (1982)
- 6) U. Shirasaka, et al., *ibidem* 7-391 (1982)



KENICHI FUSE
The Furukawa Electric
Co., Ltd.
6 Yawata-Kaigandori
Ichihara, Chiba
Japan

Mr. Fuse graduated from Keio Univ. 1971 with a M.Sc. degree in mechanical engineering. Then he joined The Furukawa Electric Co., Ltd. and has been engaged in research and development of plastic material and manufacturing methods for telephone cables.

Mr. Fuse is now assistant manager of Research & Development Section, Fiber Optics Division at The Furukawa Electric Co., Ltd. and a member of the Society of Rheology, Japan.

Mr. Kume graduated from Waseda Univ. 1980 with a B. Sc. in electronics and communication engineering. Then he joined The Furukawa Electric Co., Ltd. in 1980 and has been engaged in research and development of optical fiber cables.

Mr. Kume is now staff engineer of Cable and Apparatus Development Section, Fiber Optics Plant, Fiber Optics Division at Furukawa Electric Co., Ltd. and a member of the Institute of Electronics and Communication Engineering of Japan.



MICHIITOYO KUROKAWA
The Furukawa Electric
Co., Ltd.
5-1 Marunouchi
1-chome chiyoda-ku
Tokyo, Japan.

Mr. Kurokawa graduated from Osaka Univ. 1970 with B.Sc. in electric control engineering. Then he joined The Furukawa Electric Co., Ltd. and has been engaged in research and development of an image transmission system. Since 1980, he has worked on research and development of optical cables.

Mr. Kurokawa is now assistant manager of overseas engineering section of fiber optics division at The Furukawa Electric Co., Ltd.



YUSEI SHIRASAKA
The Furukawa Electric
Co., Ltd.
6 Yawata-Kaigandori
Ichihara, Chiba
Japan

Mr. Shirasaka graduated from Osaka Univ. 1980 with a B.Sc. in mechanical engineering. Then he joined The Furukawa Electric Co., Ltd. and has been engaged in research and development of plastic material and process for Fiber Optics.

Mr. Shirasaka is now staff engineer of Research & Development Section, Fiber Optics Division at The Furukawa Electric Co., Ltd.



YUICHI OBARA
The Furukawa Electric
Co., Ltd.
6 Yawata-Kaigandori,
Ichihara, Chiba
Japan

Mr. Obara graduated from Keio Univ. 1974 with a B. SC. in physical engineering then joined The Furukawa Electric Co., Ltd. and has been engaged in research and development of the accessories for the telecommunication systems.

Mr. Obara is now staff engineer of Transmission Apparatus Section, Fiber Optics Division at The Furukawa Electric Co., Ltd.



SHINICHI KUME
The Furukawa Electric
Co., Ltd.
6 Yawata-Kaigandori,
Ichihara, Chiba
Japan



LYUZO KIMATA
The Furukawa Electric
Co., Ltd.
610 Kiyotaki-cho
Nikko, Tochigi
Japan

Mr. Kimata graduated from Nagoya Institute of Technology 1972 with a B.Sc. in electrical engineering. Then he joined The Furukawa Electric Co., Ltd. and has been engaged in research and development of transmission line conductor engineering.

Mr. Kimata is now assistant manager to Research & Development of Overhead Transmission Line Conductor Section, Bare Wire Division at The Furukawa Electric Co., Ltd.



MASARU YOSHIKAWA
The Furukawa Electric
Co., Ltd.
6-1 Marunouchi,
2-chome, Chiyoda-ku
Tokyo, Japan

Mr. M. Yoshikawa graduated from Nihon Univ. 1966 with a B.Sc. in electrical engineering. Then he joined The Furukawa Electric Co., Ltd. and has been engaged in development of installation of power and telecommunication cables.

Mr. Yoshikawa is now chief engineer of Installation Division at The Furukawa Electric Co., Ltd.

EASY AND PRACTICAL EVALUATION OF OPTICAL FIBER'S SPLICES, GRADED INDEX-MULTIMODE, TO BE SET UP IN PLANT

J. Atín Balbás and J. Díaz Cortijo

Compañía Telefónica Nacional de España
Normativa Técnica
Lérida, 43, Madrid-20, SPAIN

Abstract

It has been obtained a single expression among magnitudes independently measured: core diameter and numerical aperture total maximum of the fibers to be spliced, and the loss of the arc fusion splice between them. This expression is suitable to be applied in junctions located in the proximity of the transmitter equipment, and whose optical and geometrical characteristics above mentioned are within of the tolerances of $\pm 3 \mu\text{m}$ and ± 0.02 respectively. Applying that expression it is possible: a) To foresee, with a fair approach, the real losses of the splices; b) To estimate a real acceptance range in the quality of splices to be made in plant, and c) To choose the best values of arc current and time operation to do fusion splices in accordance with the optical nature of the fibers.

1. INTRODUCTION

Since the use of the MCVD method in 1974, the reduction of optical fiber losses has reached an important success. Nowadays, optical fibers with losses of no more than 0.2 dB/Km^1 have already been experimentally obtained. As a consequence it is evident the importance to reduce the losses in splices among such fibers.

The insertion loss of an optical fiber splice (or connection), depends upon many factors, both extrinsic and intrinsic. Extrinsic factors are longitudinal, transverse and angular misalignments of the cores, quality of the ends, skill to make splices, choice of the suitable technique, etc. Intrinsic factors are mismatching of fiber parameters, such as core and cladding diameters, numerical aperture and index gradient.

Our present experiences² show us that with optical commercialized cables of 6 or 8 optical fibers operatives around 850 nm and with attenuation maximum coefficients of 3 and 4 dB/Km , it is not possible to obtain transmission sections with similar ($\pm 1 \text{ dB}$) losses, when the splices have been done between fibers with the same color code in their secondary coating.

Moreover, we could see that if we choice the fibers to be joined, using as criterium the more convenient sequence in attenuation coefficients, in order to equalize each transmission fi-

ber section in each splicing stage, the influence of the core diameter and numerical aperture tolerances (arc fusion procedure) associated to those fibers chosen, could give rise to losses between 0.1 dB and 0.3 dB . Although such values are usuals with multimode graded index of above-mentioned attenuation coefficients, we think they would be undesirable for lower coefficients.

The splices commented are located far from transmission equipment, that is for those where the incident fibers has reached their equilibrium lengths and the power modal distributions and emergence angles are around 60 or 70% of the core diameters and numerical apertures of the acceptant fibers. For these reasons, the mean causes of the losses in these splices are in the differences, point by point, between incident and acceptant refraction index profiles of the cores, produced by technological sources (no concentricity, different preforms, etc) or from extrinsic factors (inaccuracy alignment, incorrect handling, improper procedure, etc).

Moreover there are other kind of splices, those in the proximity of the transmission equipments, where the distance between launch end and the splice is shorter than the equilibrium length of the incident fiber. In these cases, the efficiencies are not only dependent of the inequalities of the geometrical and optical characteristics parameters of both fibers and their tolerances but there is a more emphasized dependence from the extrinsic factors, than in the splices above commented. Such influence is shown through the non repetibility of the losses and their standard deviations.

In this contribution we have centered the efforts on the latest kind of splices. We have reduced to the minimum the extrinsic sources of the losses through the repetition of the same splicing procedure made by an only person. So, we have minimized the non concentricity as a source of loss by a control of the best alignment between both cores through of the signal backscattered from the fibers confronted, before to apply the arc current. From these conditions, and taking into account that the tolerances of the geometrical and optical characteristics of fibers (graded index and multimode) are in line with those from CCITT, we propose a practical formulation to calculate the splice losses in terms of those characteristics.

2. EXPERIMENTAL PROCEDURE

The splices were carried out in one end of a commercialized optical cable, 350 m . long, containing six silica fibers (CVD Technology). Each of six fibers was spliced to five remaining

and the loss was measured for both transmission senses. This operation was made three times on the same cable end. Also, three splicing series of each fiber with itself were carried out by previously cutting 50 m from the original cable and splicing them later, figure 1 shows both situations.

The splices between different fibers (figure 1a) reached a total of 90, resulting from them 180 loss values. The splices made between the same fibers (figure 1b) reached a total of 18, and their loss values 36.

The 108 splices were made by a same procedure through the followings stages:

- Optical fibers ends preparation.
- Alignment and fixing of both ends.
- Prefusion.
- Fusion.

The measure of each splice was made in two steps:

- Splice preparation
- Measure of the losses in the two senses of propagation through the splice, by means of backscattered signals (OTDR).

Once finished all measures, we cut 2 m. of optical fibers in the same end of cable we had made the splices among different fibers, and it was measured each core diameter and numerical aperture total maximum.

The main aspects in the stages above-mentioned were the following:

- a. Control of : 1. The quality of the ends of fiber; 2. Their relative parallelism before the prefusion stage; and 3. The result of the final process of the splice. All these controls were made visually, through a microscope with zoom eyepiece (100 X) in two orthogonal directions respect to the common axis of fibers.
- b. Control of the final alignment before fusion stage; this operation was made in two steps. First was visual control with the same microscope used for preceding controls, but arranged to a lower magnification (20 X) and with an eyepiece with a special reticle in its focal plane, in such a manner to see in superposition the image of both fibers and the reticle. Second control was made after visual already commented and through the backscattered signal. Practically, this latest control was made to maximize the efficiency of the transparence of optical signal between fibers, and to determine quantitatively a beginning to the prefusion and fusion processes.
- c. The fusion machine allowed to establish the more convenient values of arc current intensity and time operations to made both processes: prefusion and fusion. The chosen values were the same for all the splices and were fixed in accordance with optical fibers manufacturer recommendations and a previous experience³. Such values were The following:

Prefusion : 12 mA during 240 mseg.

Fusion : 12 mA during 2500 mseg.

- d. Prefusion was made being both fiber ends separated between 50 and 70 μm , being the electrodes simetrically centered respect to these ends.
- e. Fusion was made in three stages : 1st - With the microscope in 100 X magnification, we placed both fibers, already optimized in alignment, separated nearly 20 μm , with the electrodes simetrically centered respect to them. 2nd - We connected the arc fusion current. 3rd - When both ends are in the "meltpoint", we produced two motions: first, an approximation to joint both "melt ends", and immediately, a separation to recuperate the original fiber diameter. The criterium used to reject one splice were: the presence of deformations nearly higher than $\pm 10\%$ respect to the fiber diameter, as soon as the presence of irregularities inner the fiber. Owing to these causes it was necessary to repeat 8 splices on the whole of 108.
- f. Taking into account the short distance (350 m) between the launch end and the splice, and in order to secure that the loss of each joint was produced, exclusively, by light propagating from core (incident) to core (acceptant), it has been placed a stripper to eliminate cladding modes on the same splice.
- g. The loss of the splice was measured by arc equipment (OTDR) from the signal backscattered from the splice. The measure was made on the screen of an oscilloscope in which it was possible to have a resolution of $\pm 0.03 \text{ dB}$. Figure 2 is a representation of backscatter signal, and the loss of the splice was calculated from:

$$P(\text{dB}) = 5 \log \frac{P_i}{P_A} \quad (1)$$

where P_i and P_A are backscatter signal levels between points close to the splice, P_i from incident core and P_A acceptant core.

- h. The core diameters (and their non circularities) have been measured from a microphotographic method. Microscopic Technique was of phase contrast (Nomarski Method) and it was appl. J on the ends of the fibers previously prepared. All the ends were simultaneously introduced (2s.) in hydrofluoric acid, and the photographs have been taken 12 hs later. Nomarski method with the same magnification (200 X), was also used to take a photography of a calibrated micrometer on the same film than the fibers had been taken. After a common developpe process, we measured core diameters on images of cores of 40 mm of diameters. From such procedure the precision obtained was $\pm 0.5 \mu\text{m}$.

- i. The total maximum numerical apertures were measured from far field technique with a precision of ± 0.003 . The samples of fibers had 2m long, and they were illuminated with small spot size ($\sim 10 \mu\text{m}$) and large aperture (0.6). The opposite end was in a stripper, in order to detect and measure light only propagated through the core, which it has been checked for each sample.

3. EXPERIMENTAL RESULTS

Table 1 shows the values of Core Diameters (D_{CO}) and total maximum Numerical Aperture (AN). Each D_{CO} value corresponds to an average of measures on three axis, from which we also have measured the respective non circularities, in this sense, none of the cores has shown values larger than 3.8 $\%$. In table 1 also is shown the averages (AV) and standard deviations (SD) for all the fibers.

Table 2 presents, for each sense of propagation, all the measures of the losses on each splice. Two last columns shows the averages (P), which will be the experimental values of the losses of the splices and their standard deviations (σ_P).

Table 3 is divided in five columns:

- 1st column defines each splice and the sense in which the loss has been measured, from incident (I) core to acceptant (A) core.
- 2nd column gives the values of X_{CO} defined from:

$$X_{CO} = \frac{D_{CO}(A)}{D_{CO}(I)} \quad (2)$$

where $D_{CO}(A)$ and $D_{CO}(I)$ are the core diameters of acceptant and incident fibers respectively, and accordance with measures in table 1.

- 3rd column gives an equivalent parameter of 2nd column, but respect to the numerical aperture from:

$$X_{AN} = \frac{AN(A)}{AN(I)} \quad (3)$$

- 4th column shows an interdependence parameter from the above defined X_{CO} and X_{AN} , through:

$$X = X_{CO}^2 \cdot X_{AN}^2 \quad (4)$$

5th column includes the values of the losses measured for each splice, $P(\text{dB})$ in accordance with the sense of propagation indicated in the 1st column. Each value of loss is an average among 6 measures on splices between different fibers, and among 3 measures for splices between each fiber with itself, (from Table 2).

Figure 3 shows a linear graphic representation of experimental points (P, X) from columns 4th and 5th of Table 3. On each point we have represented the experimental indetermination associated to P and X , $\pm 0.03 \text{ dB}$ and ± 0.05 respectively.

Independently of the true dependence law between P and X , we have found an interdependence defined from:

$$P_c(\text{dB}) = mX + P_{CO} \quad (5)$$

when $m < 0$ and $P_{CO} > 0$. This expression has been calculated as a linear regression of experimental values of $P(\text{dB})$ on experimental values of X , in agreement with Table 3. From now on, P_c will indicate calculated values of the losses.

Such correlation has been found for splices between different optical fibers as it is shown in Table 4. This Table presents five columns and must be interpreted in the following form:

- For the X values defined in the 1st column, there are N experimental points, (P, X), which linear correlation, of slope m and origin-ordinate $P_{CO}(\text{dB})$, have a correlation factor of r .

As Table 4 shows, there is an increment of r for the situation in which it is taken into account all the losses ($N=36$, $r=0.67$), to the situation in which are eliminated the losses of splices between each optical fibers and itself ($N=30$, $r=0.87$).

It is clear also that, if they are eliminated successively data of losses from splices between different fibers from $X=1$ in increasing steps (of 0.05 in our case), independently of the improvement of the correlation factor, there is a very small variation of m and $P_{CO}(\text{dB})$. Such circumstance is shown at the bottom of the same Table 4 for all the linear regressions with $r \geq 0.9$, where they are the average values \bar{m} and \bar{P}_{CO} with their respective standard deviations, $\sigma_{\bar{m}}$ and $\sigma_{\bar{P}_{CO}}$.

On taking these calculated average values as representatives of the variation of the losses of the splices respect to the parameter X , we have the expression:

$$P_c(\text{dB}) = -0.165X + 0.327 \quad (6)$$

and, if we calculate P_c for our experimental X , we can show Table 5 and Figure 4.

Table 4 presents, for all the splices between different fibers with their respective values of X , the losses measured P (dB) and calculated P_c (dB) from (6), and their relative differences ΔP (dB). Figure 4 compares graphically such values of losses through experimental points and the calculated correlation.

4. DISCUSSION AND CONCLUSIONS

Starting from graded-index-multimode optical fibers, with the same technological origin; and then, with the same nominal values in their core diameters and numerical apertures, it is possible to find a linear dependence between a quadratic ratio of mentioned characteristics and the losses of the splices between them, for points in the proximity of launch end. The only experimental conditions to obtain this dependence are to secure the good repetibility of the splice processes and the measure of their efficiencies.

This linear dependence takes the form:

$$P(\text{dB}) = mX + P_{co} \quad (7)$$

with $m < 0$ and $P_{co} > 0$. It must not be considered as a law of dependence for all the possible values of X , but as a experimentally useful dependence, with a good correlation factor, for fibers which core diameters and numerical apertures have the same nominal values with limited tolerances.

X is defined from:

$$X = \frac{(D_{co} \cdot AN)^2 \text{ of the acceptant fiber}}{(D_{co} \cdot AN)^2 \text{ of the incident fiber}} \quad (8)$$

If D_{co} and AN of the two fibers have the same nominal values (p.e. 50 μm and 0.2), their respective deviations will define the field of application of the practical dependence proposed. In such sense, it will be possible to calcul X_{max} and X_{min} from the characterizations of all the fibers, which is a normal control to the reception of the cables.

From this knowledge, the next step is to find a repetitive procedure to do good splices, which will be done splicing those fibers whose X values have extremes values. Through appropriate operations with different relations of arc current intensity and time of application, will be possible to find the minimum values of m and P_{co} . With a few splices more between different fibers with intermediate values of X will allow a better adjustment of m and P_{co} .

In order to use the expression (7) as an indicative to do splices in the field, it is important to take into account that the fusion machine, tools (manipulation to prepare ends fibers), etc. used in the laboratory must be the same than in the field, in order to secure the repetibility of each operation. This recommendation can be also extended on the technique used to measure the loss, because these kinds of splices (near to the launch end), can be checked with relative facility. On the contrary, if it is not possible to check the losses of the splices, the only rule to secure a good splice in the field is to operate under those conditions of repetibility. In this sense, the expression proposed can be useful.

In such sense, m gives us an indicative of the evolution of the losses P respect to X ; if P values are far from they expected it can suggest improper operation. Respect to P_{co} , it has not real significance as a loss, but it can be considered as a maximum value of loss to be accepted in the field.

Finally, and as a consequence of the measures, we have seen that splices, with values of X_{co} , X_{AN} and X closely to 1, from different optical fibers have important losses in front of splices that have been done between one fiber and itself. Table 2 complemented by Table 3 shows this comment. Assuming that the repetibility of each operation of splice was the main condition of this work, the only explanation we found is based in the mismatching of refraction index profiles.

Acknowledgements

The authors wish to thank Mr. Díaz de la Iglesia for their helpful comments and suggestions.

References

1. T. Miyashita, T. Miya and M. Nakahara: Digest of Topical Meeting and Optical Fiber Communication (Optical Society of America, Washington, D.C. 1979), paper PD1.
2. R. Díaz de la Iglesia and J. Atín Balbás: Attenuation and Dispersion of Multimode Fiber Optic Cables for PCM trunks, Proceeding of 30th IWCS, pp 62-69, 1981.
3. J. Atín Balbás and J. Díaz Cortijo: Influence of the geometrical and optical parameter in arc fusion splices (In Spanish). Actas de la 3ª Reunión Anual de la Comisión B de la URSI, Barcelona, Octubre 1981.

Mr. Atín Balbás is a P.H.D. from the Madrid University of Sciences. He has been a Scholarship of Scientific Research High Council up to 1970. In this year he joined the National Telephone Company of Spain, where from that date, is the Group Leader of Optical Communication in the C.T.N.E's Technical Standardization Department. He is an IEEE member and has given lectures and issued several works on this matter.



Mr. Díaz Cortijo has received his BSC in electronic physics in 1971 from the University of Madrid. He joined the National Telephone Company of Spain in 1972, where from that date, is working in Optical Communications of the C.T.N.E's Technical Standardization Department.



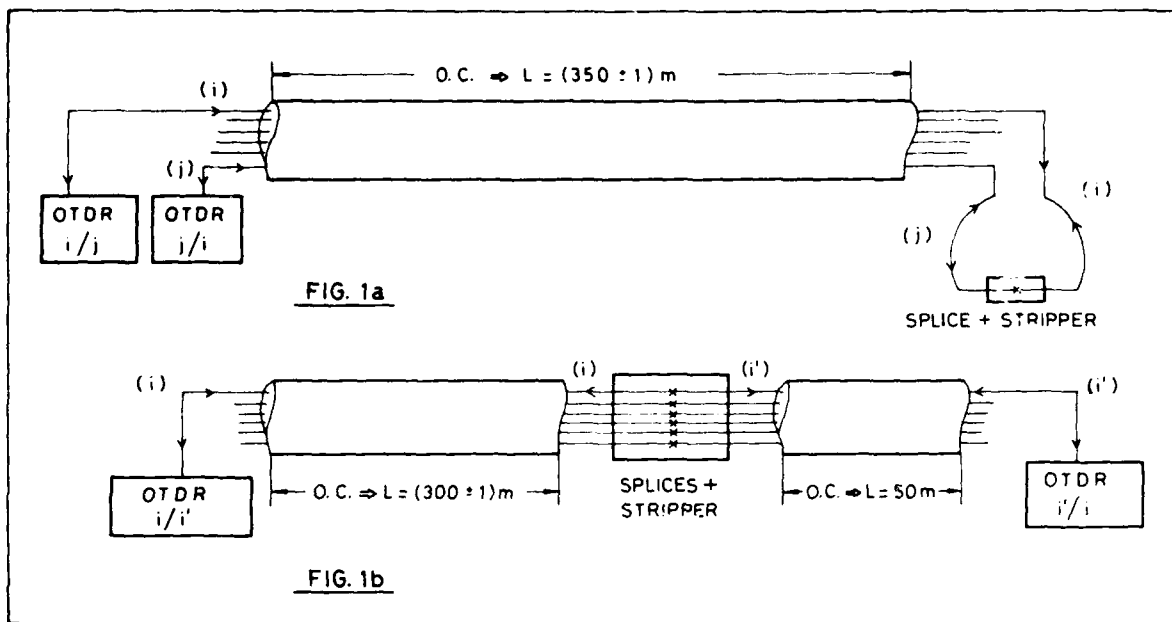
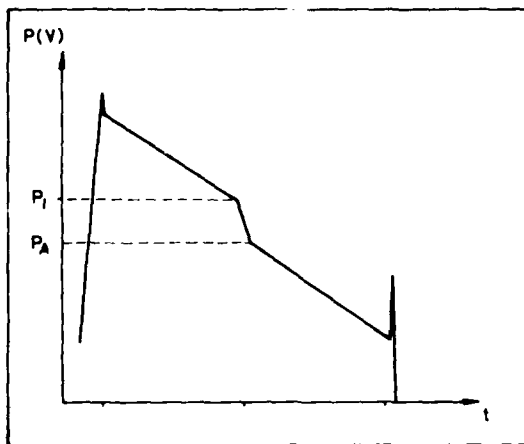


FIGURE 1
SPLICES AND MEASUREMENTS. 1a: different O.F.; 1b: The same O.F.



O.F.	1	2	3	4	5	6	AV.	S.D.
D_{co} (μm)	54.1	56.4	54.9	57.2	57.6	58.6	56.5	1.7
$A.N.$	0.23	0.17	0.21	0.22	0.2	0.23	0.21	0.02

NON CIRCULARITY OF CORES $\leq 3.8\%$

TABLE 1: CORE DIAMETERS AND NUMERICAL APERTURES

SPLICES		LOSSES						P	σ_p
1	2	0.2	0.26	0.2	0.26	0.26	0.2	0.23	0.03
1	3	0.2	0.23	0.23	0.2	0.23	0.2	0.22	0.02
1	4	0.2	0.16	0.26	0.16	0.2	0.16	0.19	0.04
1	5	0.16	0.13	0.2	0.26	0.16	0.2	0.19	0.04
1	6	0.13	0.13	0.16	0.13	0.23	0.16	0.16	0.04
2	1	0	0.03	0.03	0.06	0	0.03	0.03	0.02
2	3	0.13	0.16	0.16	0.13	0.16	0.16	0.15	0.01
2	4	0.03	0	0.06	0.03	0.08	0.03	0.04	0.03
2	5	0.06	0.03	0	0.09	0.1	0.09	0.06	0.04
2	6	0	0.03	0.03	0.03	0.09	0	0.03	0.03
3	1	0	0.09	0.2	0.13	0.2	0.21	0.14	0.08
3	2	0.16	0.2	0.23	0.23	0.26	0.26	0.22	0.04
3	4	0.03	0.03	0.06	0.09	0.09	0.09	0.07	0.03
3	5	0	0	0.13	0.09	0.13	0.2	0.09	0.08
3	6	0	0.03	0.03	0.13	0.05	0.16	0.07	0.06
4	1	0.2	0.2	0.2	0.2	0.2	0.2	0.2	0
4	2	0.3	0.2	0.25	0.3	0.23	0.3	0.26	0.04
4	3	0.18	0.2	0.13	0.2	0.26	0.23	0.2	0.04
4	5	0.16	0.16	0.2	0.16	0.2	0.16	0.17	0.02
4	6	0.16	0.13	0.06	0.23	0.09	0.1	0.13	0.06
5	1	0.16	0.13	0.2	0.16	0.13	0.16	0.16	0.03
5	2	0.23	0.26	0.2	0.23	0.23	0.23	0.23	0.04
5	3	0.2	0.16	0.16	0.23	0.2	0.2	0.19	0.03
5	4	0.13	0.06	0.1	0.16	0.16	0.13	0.12	0.04
5	6	0.09	0.1	0.06	0.2	0.13	0.13	0.12	0.05
6	1	0.2	0.2	0.16	0.16	0.2	0.26	0.2	0.03
6	2	0.23	0.23	0.23	0.23	0.26	0.26	0.24	0.01
6	3	0.18	0.2	0.16	0.2	0.16	0.26	0.19	0.03
6	4	0.2	0.09	0.1	0.2	0.09	0.06	0.12	0.06
6	5	0.21	0.13	0.16	0.13	0.23	0.13	0.15	0.05
1	1	0.06	0.03	0	0.03	0.03	0.03	0.03	0.03
2	2	0.06	0	0.03	0	0.03	0.06	0.03	0.03
3	3	0.09	0	0.03	0.03	0.06	0.03	0.04	0.05
4	4	0.09	0.03	0.03	0.06	0.03	0.06	0.05	0.03
5	5	0.09	0.03	0.06	0	0.09	0.06	0.06	0.03
6	6	0.06	0	0	0.03	0.03	0	0.02	0.03

TABLE 2 : TOTAL OF LOSSES MEASURED

SPLICE I A	X _{CO}	X _{AN}	X	P (dB)
6 2	0.96	0.76	0.50	0.24
4 2	0.99	0.77	0.58	0.26
1 2	1.04	0.74	0.59	0.23
5 2	0.98	0.85	0.69	0.23
3 2	1.03	0.81	0.70	0.22
6 5	0.98	0.87	0.73	0.17
6 3	0.94	0.91	0.73	0.19
4 3	0.96	0.95	0.83	0.2
1 3	1.01	0.91	0.84	0.22
4 5	1.01	0.91	0.84	0.17
6 1	0.92	1	0.95	0.2
1 5	1.06	0.87	0.85	0.19
6 4	0.98	0.96	0.88	0.12
4 1	0.95	1.05	1.00	0.2
5 3	0.95	1.05	1.00	0.19
1 1	1	1	1	0.03
2 2	1	1	1	0.03
3 3	1	1	1	0.04
4 4	1	1	1	0.05
5 5	1	1	1	0.06
6 6	1	1	1	0.03
3 5	1.05	0.95	1.00	0.09
1 4	1.05	0.95	1.00	0.19
4 6	1.02	1.05	1.15	0.13
5 1	0.94	1.15	1.17	0.16
1 6	1.08	1	1.17	0.16
5 4	0.99	1.1	1.19	0.12
3 1	0.99	1.1	1.19	0.14
3 4	1.04	1.05	1.19	0.07
3 6	1.07	1.1	1.36	0.07
5 6	1.02	1.15	1.38	0.12
2 3	0.97	1.24	1.45	0.15
2 5	1.02	1.18	1.45	0.06
2 1	0.96	1.35	1.68	0.03
2 4	1.01	1.29	1.70	0.04
2 6	1.04	1.35	1.97	0.03

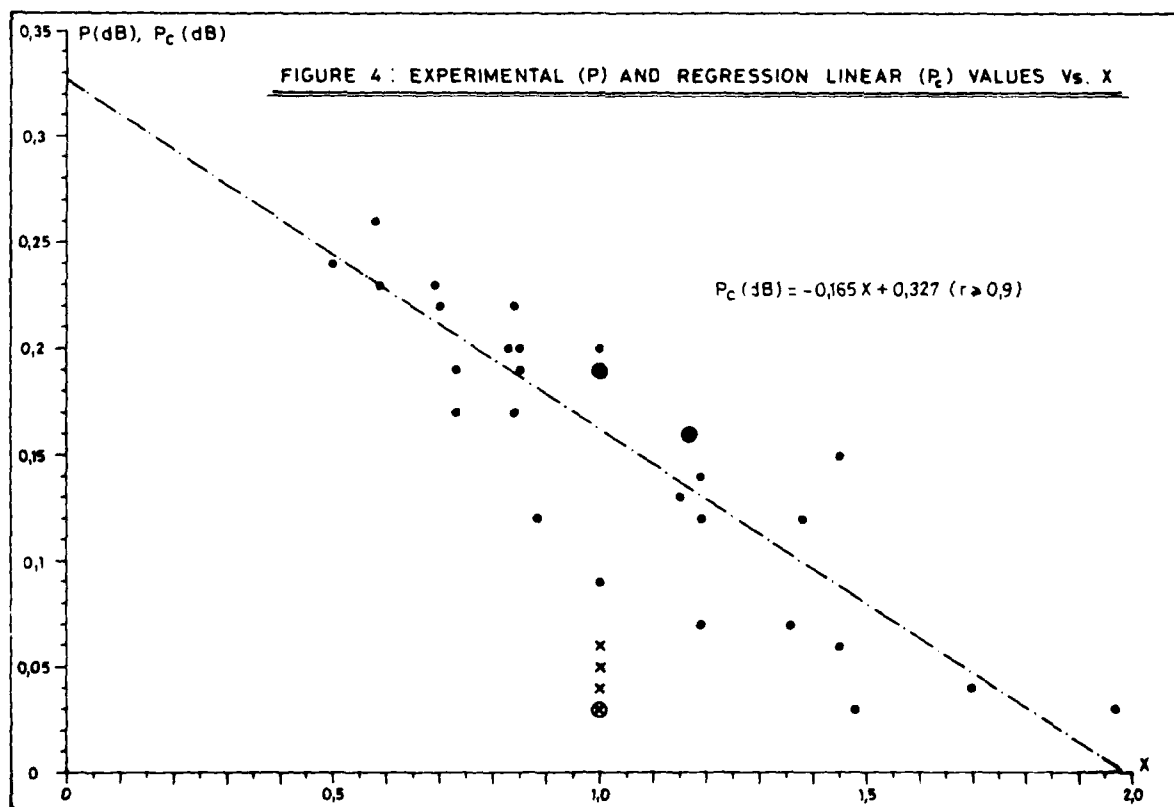
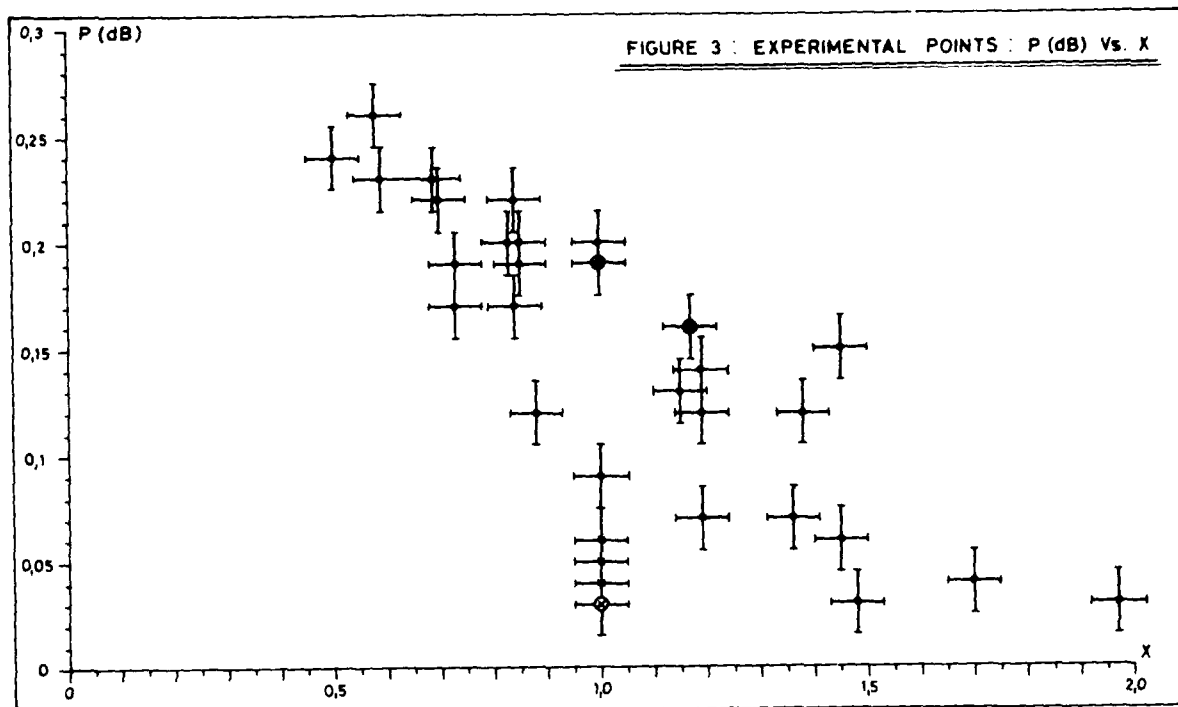
TABLE 3 : EXPERIMENTAL VALUES OF P(dB) AND X FROM EACH SPLICE

X	N	m	P _{CO} (dB)	r
ALL	36	0.155	0.296	0.67
DIFERENTS	30	0.164	0.325	0.87
* 1	26	0.163	0.323	0.90
0.95	26	-0.163	0.323	0.90
1.05				
0.9	26	0.163	0.323	0.90
1.1				
0.85	25	-0.163	0.329	0.91
1.15				
0.8	14	-0.163	0.324	0.93
1.2				
0.75	14	0.163	0.324	0.93
1.25				
0.7	12	-0.170	0.337	0.94
1.3				
0.65	10	0.167	0.331	0.93
1.35				
0.6	8	0.166	0.332	0.94
1.4				
CALCULUS FOR	\bar{m}	-0.165	0.327	P _{CO}
r ≥ 0.9	σ_m	0.003	0.005	$\sigma_{P_{CO}}$

TABLE 4 : CALCULATED VALUES OF REGRESSION LINEAR PARAMETERS FROM EXPERIMENTAL VALUES P AND X

SPLICE I A	X	P(dB)	P _c (dB)	ΔP (dB)
6 2	0.50	0.24	0.24	0.00
4 2	0.58	0.26	0.23	0.02
1 2	0.59	0.23	0.23	0.00
5 2	0.69	0.23	0.21	0.02
3 2	0.70	0.22	0.21	0.01
6 5	0.73	0.17	0.21	0.04
6 3	0.73	0.19	0.21	0.02
4 3	0.83	0.2	0.19	0.01
1 3	0.84	0.22	0.19	0.03
4 5	0.84	0.17	0.19	0.02
6 1	0.85	0.2	0.19	0.01
1 5	0.85	0.19	0.19	0.00
6 4	0.88	0.12	0.18	0.06
4 1	1.00	0.2	0.16	0.04
5 3	1.00	0.19	0.16	0.03
3 5	1.00	0.09	0.16	0.07
1 4	1.00	0.19	0.16	0.03
4 6	1.15	0.13	0.14	0.01
5 1	1.17	0.16	0.13	0.03
1 6	1.17	0.16	0.13	0.03
5 4	1.19	0.12	0.13	0.01
3 1	1.19	0.14	0.13	0.01
3 4	1.19	0.07	0.13	0.06
3 6	1.36	0.07	0.10	0.03
5 6	1.38	0.12	0.10	0.02
2 3	1.45	0.15	0.09	0.06
2 5	1.45	0.06	0.09	0.03
2 1	1.48	0.03	0.08	0.05
2 4	1.70	0.04	0.05	0.01
2 6	1.97	0.03	0.002	0.03

TABLE 5 : COMPARISSON BETWEEN CALCULATED AND EXPERIMENTAL VALUES



PAIR LAY DISTRIBUTION WITH REGARD TO FAR-END CROSSTALK IN SYMMETRIC TELECOMMUNICATION CABLE

Chaim Tencer and Antonio Tadeu Nogueira

Pirelli S/A - Cia. Ind. Brasileira
Santo André - SP - BrazilABSTRACT

The selection of the pair lay distribution to achieve satisfactory far-end crosstalk (FEXT) in symmetrical telecom cables is a problem which frequently has to be faced when dealing with machinery of already existing production lines. In this paper a solution to this problem, obtained by means of a semi-empirical formula relating the decoupling between critical pair combination to the FEXT is described. This solution has been computerised to simplify cable design work and details of the computer program are given.

In order to verify the validity of this approach a comparison has been carried out between predictions obtained from the theory and FEXT measurements made on more than 230 km of specially manufactured concentric and unit cable. The results, as shown in the paper, demonstrate a close correlation between theory and measurement and thus provide a satisfactory confirmation of the proposed design procedure.

experience and trial and error techniques. Apart from being inefficient this process does not allow any sort of optimisation.

The objective of the work reported here was therefore that of developing a design procedure which would generate automatically, given the series of lay lengths available, a reasonable number of possible lay distributions and so permit a certain degree of optimisation of crosstalk performance by enabling a selection of the best lay distribution from among those generated.

In the following sections of the paper a detailed description is given of the procedure developed, together with a comparison of the theoretical predictions of the method with the results of FEXT measurements carried out on a series of specially manufactured concentric cables or unit constructions in order to provide an experimental validation.

1.0 INTRODUCTION

The problem of selecting a lay distribution in a symmetrical pair telecom cable in order to meet far-end crosstalk (FEXT) requirements is one which presents itself to the design engineers wherever a new cable construction, differing from familiar types either in total number of pairs or in grouping arrangement, is requested.

Although a number of studies on symmetrical pair cable crosstalk have already been reported, they have been aimed either at understanding the fundamentals of the phenomenon or at designing lay distributions that while very satisfactory for FEXT are not always available with existing machinery. As a consequence it has apparently been common practice to rely on a combination of past

2.0 DESIGN CONCEPTS2.1 Theoretical Basis

In order to be able to assign lay lengths to specified pairs within a unit or concentric cable in such a way as to satisfy FEXT requirements for critical combinations (which according to REA and TELEBRÁS specifications are adjacent pairs, alternate and all pairs belonging to the centre and first concentric layer) it is necessary to have some way of estimating the pair-to-pair FEXT level. For this purpose the following semi-empirical expression has been used viz.

$$\text{Decoupling Factor} = A + B \log \left| \frac{1}{P_1} - \frac{1}{P_2} \right| \quad (1)$$

where A, B are constant determined empirically in prior work and P_1 and P_2 are the lay lengths of the pairs considered.

Once a given lay distribution has been selected it may be assessed in terms of a parameter which will be called the decoupling index. The decoupling index is the RMS value of the decoupling factors calculated using (1) above for all the critical coupling combinations in the unit or cable considered.

The decoupling index has the property of being able to predict at the design stage the cable's FEXT performance in terms of the selected lay distributions as will be seen in item 4.0.

The comparison between the decoupling indices of different lay distributions permits a certain optimisation of the FEXT performance for the series of lay lengths available.

2.2 Computer Program

In order to facilitate the application of the foregoing concepts to the design problem in hand, a computer program has been prepared. The input data necessary for its operation are the numerical values of the lay lengths available and the distribution of the pairs in the unit or concentric cable to be studied.

Starting with this information the computer program successively assigns lays from the series to each of the pairs, identifies the critical combinations and calculates their corresponding decoupling factors. The decoupling factors are then compared with limit values, set by the particular specifications employed, and accepted or rejected according to the positive or negative outcome of this comparison. In the case of a particular lay being rejected the program will go on to consider the next lay in the series. The program continues until a successful arrangement of lay is found, returning in the process to the beginning of the series if necessary. On finding a successful lay distribution the computer program calculates and stores the RMS value of the decoupling factors involved, i. e. the decoupling index. If a successful lay distribution is not found after having scanned through the entire series without having selected single lay length the program terminates the search with this particular permutation.

The whole of the above procedure is repeated for a number of permutations of the lay series and the optimum lay distribution is identified as the one with the best decoupling index.

The flowchart used in the preparation of the program was as follows:

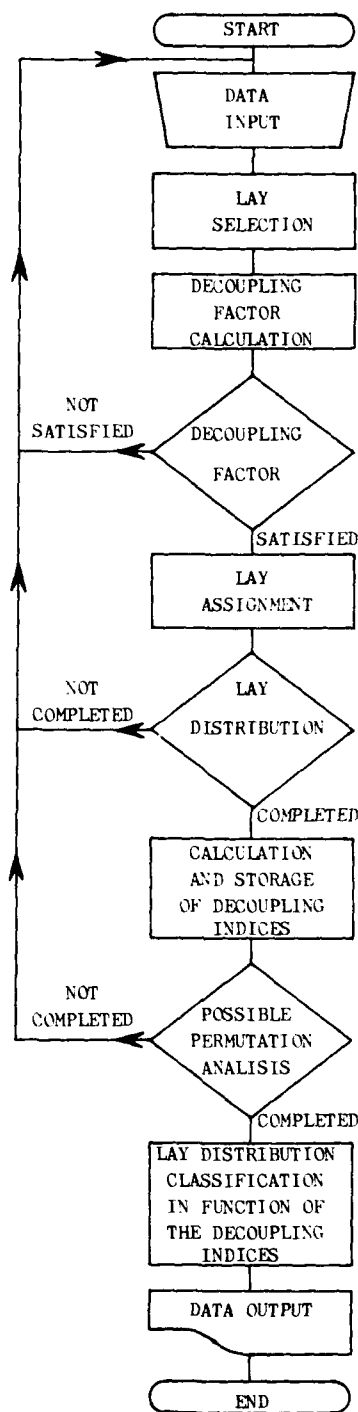


Fig. 1 - Computer Program Flowchart

3.0 EXPERIMENTAL VERIFICATION

3.1 General

In order to verify the new design procedure described in item 2.0 it was decided to compare the predictions made in specified examples with FEXT measurement made on the actual cables. To this end a 10 (2 + 8) pair concentric cable and 25 (3 + 9 + 13) pair unit cable were selected for investigation. Other constructional details were as follows: HDPE insulated 0.40 mm copper conductors protected with an Al/PE moisture barrier tape and PE sheath.

The production line chosen to manufacture the 10 pair cable had a series of 25 lays available while the 25 pair unit line had 32 lays.

FEXT measurements were all carried out at 150 kHz on each cable length and the relevant RMS values calculated according to TELEBRÁS and REA specifications.

Further experimental detail together with the results of the investigations on the two cable structures are given separately below in items 3.2 (10 pair cable) and 3.3 (25 pair units).

3.2 10 Pair Concentric Cable Construction

In this case the computer program generated 110 possible lay distributions with decoupling indices ranging from 0.150 to 8.432. From these 110 possible solutions, 6 lay distributions were chosen so that the range of decoupling indices was adequately covered. For each of the 6 lay distributions 15 cable lengths of 1 km were manufactured and on each length FEXT measurements were carried out as described in 3.1. The results are summarised in Table 1 and portrayed graphically in Fig. 2 where a linear relationship between FEXT and Decoupling Index is clearly demonstrated (correlation coefficient of 0.95).

LAY DISTRIBUTION №		1	2	3	4	5	6
DECOUPLING INDEX		0.150	8.088	8.800	8.750	8.000	8.432
FEXT (dB/km)	RMS, min	75.5	73.8	72.5	71.0	68.0	68.7
	$\overline{\text{RMS}}$	77.7	75.4	74.1	73.2	70.0	70.3
	RMS, max	79.0	77.2	76.8	75.5	72.8	71.0

Table 1 - FEXT of 10 pair experimental cable lengths at 150 kHz where,

RMS, min - is the minimum RMS value calculated for each lay distribution

$\overline{\text{RMS}}$ - is the average of the RMS values for each lay distribution

RMS, max - is the maximum RMS value calculated for each lay distribution

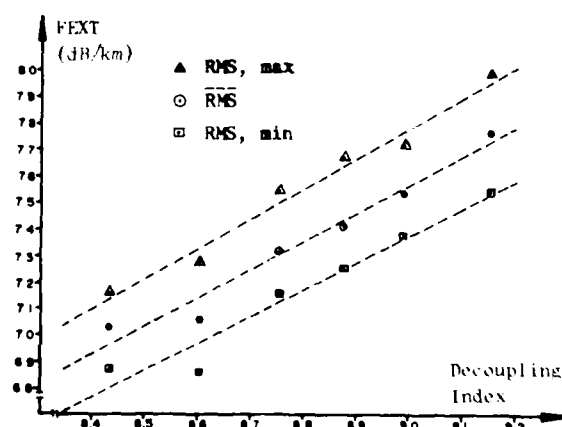


Fig. 2 - 10 Pair Cables: FEXT at 150 kHz versus Decoupling Index

3.3 25 Pair Unit Cable Construction

The computer program generated in this case only 12 possible lay distributions having a decoupling index range from 8.028 to 8.351. From these 12 lay distributions 5 were chose so as to cover the entire range and for each of these lay distributions 30 km of unit lengths were manufactured and subjected to FEXT measurements as previously described.

The test results are reported in Table 2 and also portrayed graphically in Fig. 3. Also in this case a well defined linear relationship (correlation coefficient 0.98) was obtained between the FEXT measurements and the corresponding decoupling indices.

LAY DISTRIBUTION No		1	2	3	4	5
DECOUPLING INDEX		8.028	8.700	8.002	8.499	8.351
FEXT (dB/km)	RMS, min	71.7	70.1	69.1	67.7	67.4
	$\overline{\text{RMS}}$	72.5	71.2	70.2	68.9	68.6
	RMS, max	74.2	71.0	71.2	69.8	69.5

Table 2 - FEXT of 25 pair unit experimental cable lengths at 150 kHz where,

RMS, min - is the minimum RMS value calculated for each lay distribution
 $\overline{\text{RMS}}$ - is the average of the RMS values for each lay distribution
 RMS, max - is the maximum RMS value calculated for each lay distribution

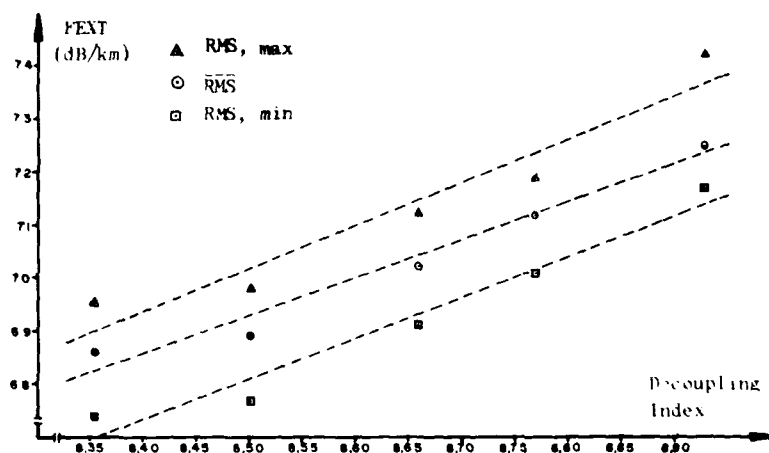


Fig. 3 - 25 Pair Unit: FEXT at 150 kHz versus Decoupling Index

4.0 CONCLUSION

The principal aspects of the work presented in this paper may be summarised as follows:

(1) A new design technique has been developed to enable certain optimisation of the FEXT performance in symmetrical pair telecom cables to be achieved for a given series of available twinning lays.

(2) This technique has embodiment in a computer program which automatically generates a number of lay distributions satisfying specified levels by a process which involves the selection of appropriate lays for each pair in the particular construction under study. This selection is made by comparing pre-set limit values for the "decoupling factor" of critical pair combinations with estimates obtained from the following formula:

$$\text{Decoupling Factor} = A + B \log \left| \frac{1}{P_1} - \frac{1}{P_2} \right|$$

where A, B are constants empirically determined in prior work and P_1 and P_2 are the pair lays under consideration. Each possible solution is then classified in terms of the decoupling index enabling the best lay distribution from amongst those generated to be identified.

(3) A completely satisfactory validation of the technique has been achieved by comparing predictions made for various concentric cable and unit constructions with experimental results of FEXT measurements carried out on specially manufactured experimental cables.

(4) As a consequence of item 3 above it may also be concluded that the validity of the computational procedure is independent of the formation of the cable or unit.

5.0 REFERENCES

1. "A STUDY INTO PAIRED CABLE CROSSTALK"
R.J.Oakley and R. Jaar
22nd IWCS - 1973
2. "TRANSMISSION TÉLÉPHONIQUE"
R.Croze, L.Simon and J.P.Caire
4th edition
3. "AN APPROACH TO CROSSTALK COUPLING REDUCTION OF PAIR TYPE CABLE"
Yotuya, Minematsu, Itah
23rd IWCS - 1974
4. "RELATING THE TWIST DETECTION MEASUREMENTS OF TWISTED PAIRS TO THEIR CROSSTALK PERFORMANCE"
H.W.Friesen
24th IWCS - 1975
5. "GEOMETRICALLY DECOUPLED BALANCED PAIRS"
D.P.Woodard
27th IWCS - 1978
6. "TEORIA DELLA TRASMISSIONE TELEFONICA"
D.Gagliardi
2nd edition



Chaim Tencer joined Pirelli Brasileira in 1973 and has been engaged in research and development of telecom cables. Degree in Electronic and Engineering from Mackenzie University (EEUM) - São Paulo. Presently he is the Telecom R and D Manager.



Antonio Tadeu Nogueira, degree in Electronic Engineering from University of São Paulo (USP) ; joined Pirelli in 1978. He is at present involved in telecom cable R and D.

AD P000551

CROSSTALK, INSERTION LOSS, SWEEP FREQUENCY ANALYSIS AND FIXTURING FOR TELEPHONE CABLES

JOSEPH S. GOLT, JR.

WESTERN ELECTRIC CO., INC.
BALTIMORE, MARYLAND

Crosstalk in a multipair telephone cable is defined as the amount of electrical signal from an energized pair that is induced or coupled to an unenergized pair. In this test, each pair is selected and energized and then all other pairs are, one by one, selected and any signal present is recorded. Any crosstalk set must also measure insertion loss as this value must be subtracted from the crosstalk loss measurement. Analyzing Sweep measurements can be very informative. For example, any deviation from the normal swept frequency response can help determine if the cable strander is operating properly. In addition, a low profile fixture has been developed which allows for shorter cable stub lengths. This paper will discuss all of these measurements plus the physical layout of the fixture.

Anyone who has used a telephone and heard a second conversation in the background has experienced the effect of crosstalk. Anytime two or more electrical signals get physically close to one another there may be unwanted coupling. Inside a telephone cable there could be hundreds of signals all within several inches of one another. Cable manufacturers attempt to construct their products so as to cancel any crosstalk. Pairs are twisted, bunched in groups, groups are twisted and perhaps oscillated. These techniques work quite well, however, the need to know how well inspires the desire to test. Most cables are tested for capacitance. Since capacitance and crosstalk are closely related one could gauge the crosstalk performance by observing capacitance data. This is done now in many applications. Nothing, however, can substitute for a direct measurement. The trend has been set to make more direct crosstalk measurements.

We have developed a system that will automatically test telephone cables for crosstalk. It can also make sweep frequency measurements and analyze the results. The connecting fixture also contains the necessary switching and is compact enough to get close to the reel hub. I will attempt to define the requirements for such a system and explain how we satisfied those requirements.

In crosstalk measurements there are two signals of interest. The send signal which emanates from an oscillator and is applied on the device under test. The receive signal comes from the device under test and is sent to a detector of some kind. Crosstalk can be measured in one of two ways: near end crosstalk (NEXT) and far end crosstalk (FEXT). In NEXT the send and receive signals are on different pairs at the same end of the cable. In FEXT the send and receive signals are on different pairs at opposite ends of the cable. Crosstalk can be defined as the voltage ratio of the send signal to the receive signal expressed in decibels.

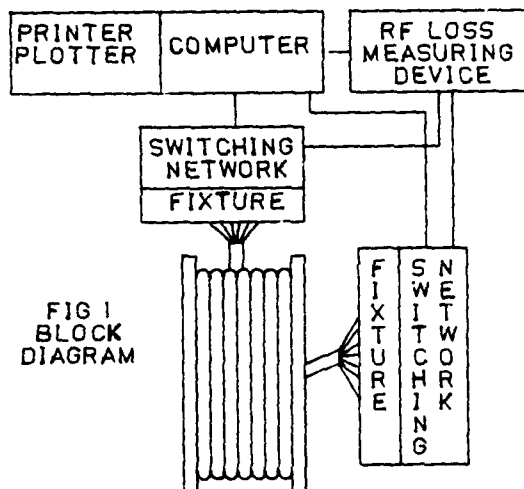
In FEXT there are two factors which affect the measured value of crosstalk. The insertion loss of each pair tends to attenuate crosstalk. Therefore, the insertion loss must be measured so it can be subtracted from the measured value. This is done by connecting the send and receive signals to opposite ends of the same pair. Another factor is length. The crosstalk signal on the receive end will increase logarithmically as the cable length is increased. We must therefore know the length and include it in our calculation. The exact structure of the equation can vary from one cable type to another but for locap cable used in T-2 carrier systems the equation is:

$$\text{FEXT} = \text{Measured value} - \text{Insertion Loss} + 10 \text{ LOG Length}$$

Certain cable types require a sweep frequency test. Since physically connecting both ends of the cable can be time consuming, sweep frequency can be performed subsequent to the crosstalk measurement. Whereas crosstalk is measured at a single discrete frequency, sweep measurements are, as the name implies done to examine how individual pairs respond to all frequencies between an upper and lower limit. The electrical connection is identical to the insertion loss hook-up.

Now that we have defined the measurements we can examine the requirements of a test system. There will be much control, calculation and printouts required, therefore, a rather high level processor of some kind is required. A device that can make RF loss measurements both at discrete and swept frequency is also needed. It must also be externally programmable, and relatively fast. There must be a switching system capable of making all

the necessary connections. It should be designed so as to maintain a constant characteristic impedance and provide high isolation between channels. It needs to be externally programmable by the processor. Finally, a fixture to physically connect to the cable is called for. It would be highly desirable to include the switching system and the fixture into one compact entity. Since cable manufacturers desire to make the stub ends as short as possible, the fixture should be maneuverable enough to get close to the hub of the cable. A block diagram appears in Fig. 1.



We selected a commercially available network analyzer. It satisfied all our measurement requirements and included a computer. The computer used a high level basic type language, had plenty of memory and a magnetic tape drive built in. A combination printer/plotter was selected in order to plot sweep frequency results. The computer controls the network analyzer via an IEEE-488 interface bus. A sixteen bit general purpose input/output interface was used to control the in-house designed switching system. A real time clock option also proved to be a valuable asset.

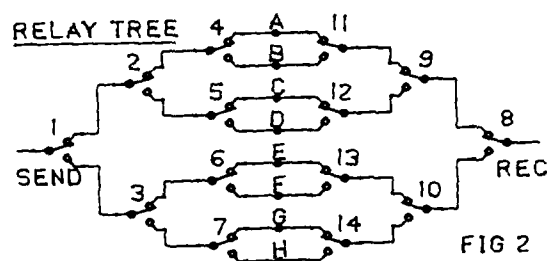
The Switching System

The switching system must meet the following requirements:

1. Be able to make the proper electrical hook-up for FEXT, NEXT, and insertion loss.
2. Maintain the proper level of characteristic impedance given the limits of frequency response (up to 13 Mhz), and provide high isolation between channels.
3. Lend itself to compact packaging.

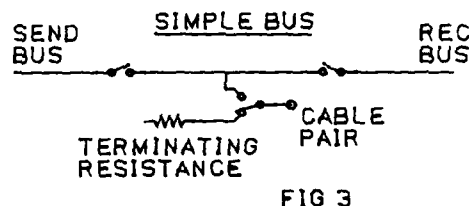
The "Relay Tree" and "RF Buss" are two techniques worth consideration. The schematic in fig. 2

depicts an eight pair in the "Relay tree" format. Each relay contact in this diagram represents the two wires in a twisted pair. For the sake of space we do not show another relay for each pair. This relay merely switches the pair into the switching network or rests on a terminating resistor. There will be an identical network for the other end of the cable. As an example, suppose we wished to set up for FEXT on pairs C and H. First, the relays (not shown) that disconnect the terminating resistor would be energized for both C and H on both ends of the cable. Next, relay 2 on the send end of the cable and relays 8, 10, and 14 on the receive end of the cable are energized. The crosstalk measurement can now be performed.

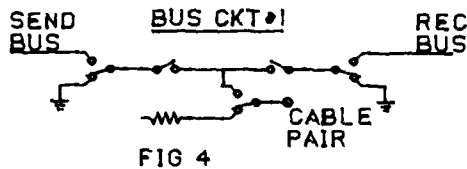


The "Relay Tree" technique satisfies requirement #1 in that all types of measurements can be set up. Requirement #2 is also met as there are no inherent problems in maintaining characteristic impedance or keeping isolation high. Requirement #3 is the downfall of "Relay Tree" switching. Typically an entire cabinet separate from the fixture may be needed to accommodate this method. This is not because of the number of components but rather the fashion in which they are laid out.

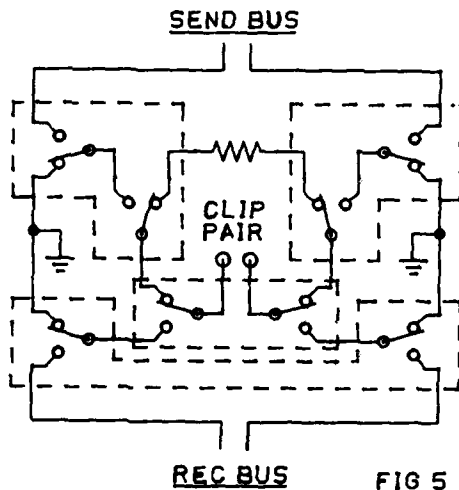
At first glance the circuit in fig. 3 looks like a simple way to achieve a bus type switching network. Each pair would have three relays. One would remove the pair from its terminating resistor, the other two would place the pair on either the send or receive bus. There is, however, stray capacitance across the relay contacts. The capacitance will couple the send signal onto the receive bus. This, of course, would erroneously add to any crosstalk in the cable. This circuit only shows one pair. As more pairs are added the capacitance adds and the coupling increases. With any appreciable number of pairs the isolation between the send and receive busses would be intolerably low.



Adding two more relays (fig. 4), whose normally closed contacts are grounded eliminates any coupling from the send to receive bus. This circuit has another advantage. If send and receive are called for on the same pair in the same fixture the test signal would short the send and receive busses. This can be useful if a self test algorithm is desired.



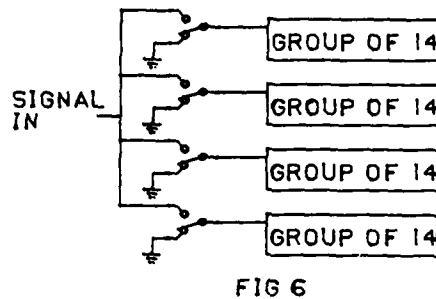
Since space was at a premium in our application we used the circuit in fig. 5. The logic required to select any given pair is also reduced. Notice that this drawing is complete, showing all relays and each side of the pair. This circuit satisfies requirement #1 in that all measurement configurations can be achieved. And as we will see later, this circuit lends itself to a tight compact layout. Isolation is also good as long as the grounding relays are used. That stray capacitance across the relay contacts can still be a problem, though, in maintaining characteristic impedance.



Each stray capacitor connects each side of the pair to ground. This, in effect, loads the bus with a small capacitive impedance. This tends to alter the characteristic impedance of the system. While singularly insignificant, many pairs in

parallel can create a large mismatch. This would cause unwanted reflections which would destroy any hope of an accurate measurement. We can circumvent this problem by selecting small groups of bus circuits.

It turns out that most units within a cable have fourteen pairs. This convenient number is low enough such that the additive effect of stray capacitance is not a serious problem. We now have a switching system as shown in fig. 6.



Our system, of course, uses exactly this type of switching. Very small relays were mounted on a printed circuit board. Each board was designed to connect fourteen pairs to either a send or receive bus. It would be mounted on the underside of the fixture. The clips that connect to the cable protrude through holes in the printed circuit board. The bus circuit relays are mounted as close as possible to the connecting clips. The layout for each pair consumes less than four square inches. The entire fourteen pair group can be mounted on an eight by eight inch board. Four of these boards were used to make a 56 pair fixture. The group select circuit board is mounted in a vacant portion of the fixture. It also contains the transformer that changes the 50 ohm coaxial from the network analyzer to the balanced impedance of the twisted pairs.

Since the boards mounted nearly flat against the rear of the fixture a low profile of 2.5 inches was achieved. The whole assembly rotates to expose doors at the rear. Opening the doors provides for easy maintenance access. The entire package mounts on a purchased roll around cart. This allows for easy maneuverability when attempting to connect to a short stub end. Special clips are used to connect to the cable. They will pierce the insulation during insertion. Thus, no pre-skinning of the cable is required.

Other Factors

Our measurement accuracy is in the $\pm .05$ db range. Therefore, the loss across relay contacts must be considered. Dry switching tends to degrade contact resistance or even worse the contact

resistance may change from one relay closure to another. This problem is solved by superimposing a DC current, at least 200 ma, in the RF measuring circuit. This can easily be done through a center tap on the matching transformer. In our equipment, every time a cable is tested a "Clean Relay" subroutine is called. It merely closes and opens the cleansing DC current through the relays and cable. This procedure helps maintain a stable and low contact resistance in our fixture.

The insertion loss of a pair is highly dependent on the resistance of the copper conductors. The resistivity of copper is temperature dependent. This implies that we must have a known constant temperature before testing a cable. We accomplish this by allowing the cable to stabilize in an air-conditioned test room for at least 24 hours. The cable temperature and ambient temperature are then assumed to be identical. The insertion loss is corrected for temperature by the equation:

$$\alpha_{75} = \frac{\alpha_T}{1 + (T - 75)K}$$

where T equals ambient temperature and K equals the temperature coefficient of the cable under test.

We can obtain ambient temperature by forming an elementary network with a resistor that is temperature dependent. A thermistor connected in series with a normal resistor forms a voltage divider. We calibrate the voltage divider by observing its response at several known ambient temperatures. We now use our network analyzer to measure the response of the voltage divider and interpolate the results to obtain ambient temperature.

Since we have a real time clock we can also monitor the integrity of the air-conditioned room. Every half hour the ambient temperature is taken. A running average of the previous 24 hours is updated. If there is a significant deviation from the mean the computer will not permit testing. A plot of the past 24 hours is available at the touch of a key. This procedure has helped us increase our confidence in the integrity of our measurement results.

SWEEP MEASUREMENT

Sweep measurement is really insertion loss response over a selected band of frequencies. The normal response to a sweep would be a nearly linear falloff. Deviations from this normal response can reveal some defects within the cable. For example, any discontinuity from the characteristic impedance would cause a reflection from that point. If there are equally spaced discontinuities the reflections would be additive at certain frequencies. This frequency would correspond to a half wavelength of the periodic discontinuity

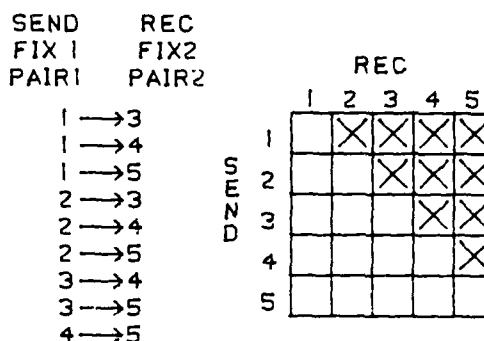
i.e.

$$\lambda = c/f \quad f = c/2d \quad c = \text{Speed of Light} \quad d = \text{Distance between defect}$$

Units within some of our cables are oscillated by the cable strander. When the unit is oscillated each pair comes close to the cable sheath every oscillation period. This slightly disrupts the characteristic impedance. Therefore, we observe a large spike in the frequency response at the half wavelength frequency. Our computer will set the start frequency of the sweep. The loss is measured and frequency increased until the stop frequency is reached. Now, via software, the computer will analyze the data looking for spikes. When a spike is located the computer will record its frequency and magnitude relative to what the normal response would be. By observing these results we can determine if the oscillation period is properly set on the stranding machine.

RELAY USAGE

When testing FEXT one is tempted to prescribe a switching algorithm as shown in fig. 7.



SWITCHING SEQUENCE
FOR A 5 PAIR CABLE
FIG 7

The send relays in fixture #1, pair #1, are energized. Then the receive relays in fixture #2 pairs 1 thru 5 are each energized long enough to allow the loss measurement to be made. Notice that only one half the matrix need be filled, i.e. we assume FEXT on 2-4 to be equal to FEXT on 4-2. This scheme obviously works, however, there is a disparity in relay usage. For every cable tested the send relays in fixture 1 pair 1 are energized one time, while the receive relays in fixture 2 pair 5 are energized 4 times. Furthermore, the send relays in fixture 2 and the receive relays in fixture 1 are not used at all. Our fixture has 56 pairs. If we used it only 10 times each day, in one year the receive relays for pair 56 would have been used 143,000 times. The send relays would log in only 2,600 actuations.

Software can correct this problem by rotating the switching algorithm every time a cable is tested. There are 8 different modes to choose from as tabulated in fig. 8.

SEND	REC	SEQUENCE	DIRECTION
FIX1	FIX2	S → R	FIRST TO LAST
FIX1	FIX2	S → R	LAST TO FIRST
FIX1	FIX2	R → S	FIRST TO LAST
FIX1	FIX2	R → S	LAST TO FIRST
FIX2	FIX1	S → R	FIRST TO LAST
FIX2	FIX1	S → R	LAST TO FIRST
FIX2	FIX1	R → S	FIRST TO LAST
FIX2	FIX1	R → S	LAST TO FIRST

FIG 8

Now, after 8 cables are tested all relays have been used approximately 56 times. In one year, at 10 cables per day all relays would be energized about 18,000 times. This technique has the potential to increase the usable lifetime of the switching fixtures by a factor of eight.

VSWR ON SHORT LENGTH

Each cable pair is designed to have a nominal characteristic impedance. Various factors including different twist lengths cause slight deviations from the nominal. Our system can only be set to one value of characteristic impedance. Therefore, when measuring insertion loss we will encounter slight mismatches as we switch from pair to pair. This will set up small Voltage Standing Wave Ratios (VSWR) whenever the test signal is present. If the cable is long the insertion loss is large enough to ignore the VSWR. On very short lengths, however, this effect can be significant. Proper software can help solve this problem.

Let's say our test frequency is 3 Mhz and the cable length is 700 feet. Using the formula $\lambda = c/f$ we determine the wavelength to be 328 feet. This means that there are $700 \div 328$ or 2.13 wavelengths on the cable. VSWR cycles every half wavelength, so we add and subtract a quarter wavelength. We can then calculate what frequency corresponds to $2.13 + .25$ and $2.13 - .25$ wavelengths. In this case we have 3.35 Mhz and 2.65 Mhz. If we set the network analyzer to sweep between these points we will observe the VSWR ripple on the normal falloff pattern. Now with similar techniques used in determining sweep frequency spikes, we can interpolate what the response would be without any VSWR. This value will more accurately represent the actual attenuation per mile of the cable.

ACKNOWLEDGEMENTS

I would like to thank several people for their significant contribution. Mr. L. M. Rackson lent his expertise in telephone cable manufacturing. Mr. C. L. Greenblatt contributed to the development of the switching network. Mr. J. L. Knapik helped in the mechanical design of the test fixture.

Mr. Golt is a Senior Development Engineer in the Test Set Development department at Western Electric. He has been in that organization for fourteen years and has participated in the design of other transmission measuring equipment. He graduated from the University of Maryland in 1968 with a BSEE Degree. He enjoys jogging, woodworking and is an avid tennis player.



COMPARATIVE STUDY OF ANALOG AND DIGITAL CROSSTALK MEASUREMENTS METHODS ON TELEPHONE CABLES

V. Abadía and J.L. Mariñosa

CABLES DE COMUNICACIONES, S.A.
ZARAGOZA (SPAIN)

ABSTRACT

The evaluation of a telephone cable capability for digital transmission has been traditionally based on analogical measurements of cable crosstalk. In this manner, from a single frequency measurement value, it is intended a prediction of the cable behaviour in all the transmission band.

In recent years it has been observed a tendency in some telephone administrations toward cable crosstalk characterization in a direct way, by means of digital measurements using real signals. In this study the analog and digital measurements methods are compared, from the points of view of accuracy of results and simplicity of operation. As a result of an extensive number of measurements performed in accordance with both methods, correction factors have been determined which should be added to the single frequency measurements results in order to compensate for the uncertainty introduced due to the incomplete knowledge of the curve of variation of crosstalk with frequency.

Finally some considerations about the applicability of digital method of measurements in the quality assurance area are discussed.

1 INTRODUCTION

When planning the introduction of a certain number of digital transmission systems in a multi-pair telephone cable, it is necessary a complete knowledge of the factors that place a limit to both the number of systems as well as the maximum distance between repeaters.

Besides the intrinsic NEXT and FEXT losses of cable, other sources of errors associated with the installation of the cable as reported by field measurements (1) should be taken into consideration such as crosstalk inside the repeater case and stub cable, repeater degradation, thermal noise, etc. The relative importance of each of these limiting sources or the fact that one of them becomes dominant lays on factors such as the utilization of one or two cables for each transmission direction, internal shield cable design, etc.

From a quality assurance point of view, the intrinsic crosstalk of cable is the only factor that can be controlled in the factory. Its measurement by different existing methods constitute

the object of this paper. Fig. 1 show the traditional schematic diagram of analogical measurements of NEXT and FEXT crosstalk.

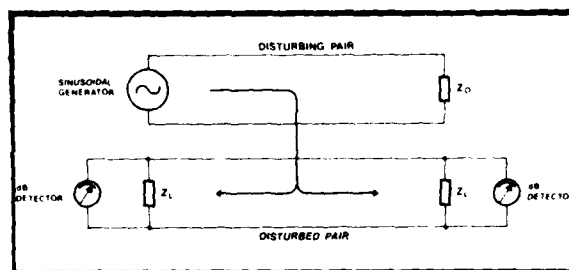


Fig. 1.- SINGLE FREQUENCY CROSSTALK MEASUREMENT.

All the studies dealing with the analytical computation of the magnitude of crosstalk noise for digital signal based on the crosstalk values obtained in single frequency measurements must always be based on a known frequency correction formula more or less valid about the variation of crosstalk with frequency. This hypothesis says that far end and near end crosstalk decrease with frequency at a rate of 6dB/octave and 4.5 dB/octave respectively.

It is a well known fact that the real variation of crosstalk outside the very low frequencies region is highly irregular. This phenomenon is especially emphasized in NEXT measurements due to the random length of the coupling ways originated by the unbalances distributed along the cable. This irregular variation is strongly exhibited in individual couplings but is more attenuated in the case of average, RMS or Power Sum values which include a great number of combinations. It becomes evident that by means of a single measurement at certain frequency of reference (generally at half the bit frequency) and assuming a theoretical variation of 6 dB/octave in FEXT and 4.5 dB/octave for NEXT the noise voltage analytically computed from this measurement is only an estimation of the real noise voltage when using as a disturbing signal a complex signal as is the case in actual pulse transmission. Fig. 2 depicts the afore said as an example.

Curve (1) of Fig. 2 represents a real variation of crosstalk with frequency for a pair to pair combination. While feeding the disturbing pair with an

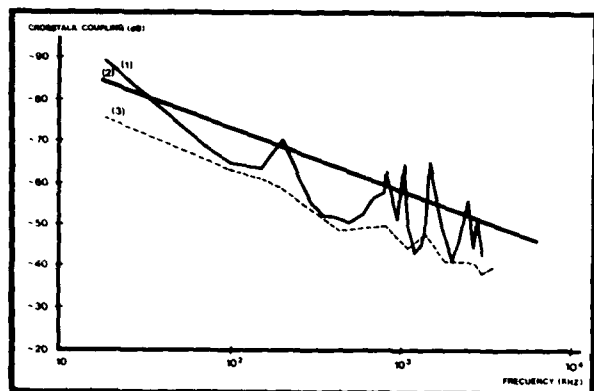


Fig. 2.- EXAMPLE OF VARIATION OF CROSSTALK WITH FREQUENCY.

actual PCM signal it was detected at the disturbed pair a mean noise power of -28 dBw. However from a single frequency measurement and assuming a linear decrease of crosstalk with frequency (on a log scale) represented by curve (2) a mean noise power of -38'6 dBw was computed following the steps explained in Appendix I.

Correlation improvement between both proceedings implies necessarily the extension of the number of selective measures to more than one point. This of course complicates enormously the test because of the multiplication of the time spent on performing it, which is especially characterized by the large amount of time required to cover all of the possible combinations between the pairs.

The additional number of selective measurements required to improve correlation depends on the dispersion of the statistical distribution of the mean value of crosstalk at each frequency. Crater and Cravis (2) established a variance of 5.56 dB in NEXT, but we have verified deviations up to 20 dB in some combinations.

As a final evidence the following test was carried out: A disturbed pair was selected from a 25 pair PIC cable and measured all possible noise contributions attributed by the other pairs. Crosstalk power transfer curves were defined by measuring 40 equally spaced points to obtain the integral in Appendix I in order to compute the expected value of power, which is then compared with the directly measured value using a RMS detector. Table 1 shows these results.

Comparison of column (2) with either column (3) or (4) shows two things: a) Single frequency values tend to be on the average somewhat optimistic. b) They suffer from uncertainty due to a rather low correlation coefficient ($\rho = 0.9$ in the example). Comparison of column (3) with (4) shows that a drastical increase in the number of selective measurements (40 points in the example) are needed to obtain a more reliable value.

TABLE 1.- CALCULATED AND MEASURED MEAN POWER CROSSTALK NOISE VALUES.

COMBINATION	CALCULATED		MEASURED
	SINGLE FREQUENCY	40 POINTS INTEGRATION	
Fig. 2 (1)	- 38'6	- 28'5	- 28'5
6/1	- 46'4	- 46'7	- 46'7
6/2	- 33'7	- 32'0	- 31'5
6/3	- 47'4	- 44'3	- 45'5
6/4	- 50'6	- 43'7	- 44'0
6/5	- 29'9	- 35'5	- 35'6
6/7	- 35'5	- 34'0	- 33'7
6/8	- 38'5	- 44'1	- 45'2
6/9	- 71'6	- 59'5	- 53'4
6/10	- 49'9	- 52'0	- 51'4
6/11	- 52'8	- 48'8	- 48'6
6/12	- 55'1	- 55'7	- 54'3
6/13	- 39'7	- 43'1	- 45'5
6/14	- 43'2	- 42'2	- 41'0
6/15	- 42'8	- 40'4	- 40'6
6/16	- 42'1	- 22'5	- 32'0
6/17	- 22'7	- 27'5	- 27'0
6/18	- 34'7	- 31'3	- 35'0
6/19	- 41'6	- 44'4	- 41'0
6/20	- 48'6	- 44'4	- 43'0
6/21	- 39'2	- 20'7	- 20'1
6/22	- 45'7	- 45'2	- 44'3
6/23	- 54'7	- 52'3	- 51'6
6/24	- 51'5	- 53'2	- 52'8
6/25	- 52'0	- 49'2	- 48'6

Curve (3) shows a 12 contributor power sum crosstalk variation. It is noted that the deviations with respect to a hypothetical mean value are much less pronounced, so that a single frequency measurements have a higher significance as an estimate of the mean value of crosstalk at all band frequencies.

Deviations as large as indicated are common on a pair to pair basis. The RMS method of crosstalk measurement, using a disturbing signal similar to that in a real system reveal itself much more accurate although it has other disadvantages that will be pointed out later.

2 CABLE TYPES EXAMINED AND EXTENSION OF MEASUREMENTS

Studies and measurements have been carried out on two different types of cables: pairs and quads because any empiric difference in its crosstalk - transfer functions might be expected. The following type of cables were selected:

- 2.1 25 and 50 pair cable, PE insulated, ϕ 0.9 mm, 52 nF/Km, unit type and concentric layers construction respectively.

2.2 28 quads filled cable, PE insulated,
 ϕ 0.9 mm, 38 nF/Km, and layer type
 construction.

In the paired cables a total of 2338 NEXT and FEXT measurements were made, both at a reference frequency (f_0) and making use of digital signals. In the quadded cable the number of pair to pair measures was 1104 in NEXT and FEXT. These measurements were made with a semiautomatic procedure in which the disturbed pair is manually selected and terminated with a balanced precision impedance. The others noise contributing pairs are automatically switched in 25 element blocks. During the execution of measurements the pairs not involved in the test (tertiary circuits) remained open at the near end, which proved to have no influence at all in the measurement frequency band.

Digital crosstalk measurements were performed for the 30 channel T1 transmission system of 2.048 Mbit. The reference frequency f_0 was 1.024 MHz corresponding to half the bit frequency.

3 MEASUREMENT TECHNIQUE

3.1 Digital measurement of crosstalk

The principal characteristic of this method is the ability of exciting simultaneously a certain number of systems, then measuring either RMS noise voltage or error rate as indicated in fig. 3.1 and 3.2. Moreover fig. 8 shows the case of error rate measurement under the simultaneous effect of near end and far end crosstalk.

The procedure of simultaneous disturbance cuts down the testing time but does not reveal the individual properties of each combination which is of great interest in the present work. The method followed will be then similar to that in the analogical technique selecting pair combinations in a sequential mode. Measuring diagrams are shown in fig. 3.

In figure 3 are shown two different configurations. Fig. 3.1 measures far end crosstalk in accordance with the characteristics of a real transmission channel. The point for noise detection may be the unbalanced one inside the equalizer (M) or 6 dB larger in the balanced regeneration section. In fig. 3.2 near end crosstalk noise voltage are measured on a symmetric load. In the latter case the amplification and shaping effect of the repeater does not exist, being required a greater sensitivity of detection.

The operating procedure described must yield in the cable the same effects that in a real case. In particular the following conditions must be satisfied:

- The noise power measured on a pair should be the same as that which would result in a real case. Actually the noise power induced in a pair is the resulting noise power when all the disturbing pairs work simultaneously.

The noise power measured in our case is the sum of noise powers induced by each disturbing pair individually. Due to the high harmonic content of the pseudorandom disturbing signal and their uncorrelation the principle of power addition works and can be assured that the measured power is that of the real case. Furthermore this point was experimentally verified.

- Due to the uncorrelation of the pulse sources feeding the pairs, the induced noise on any pair, has a instantaneous value following a normal distribution.

As will be noted later in paragraph 5 a statistical test was made to demonstrate the normal character of the induced noise. This is a relevant feature in order to calculate the error rate.

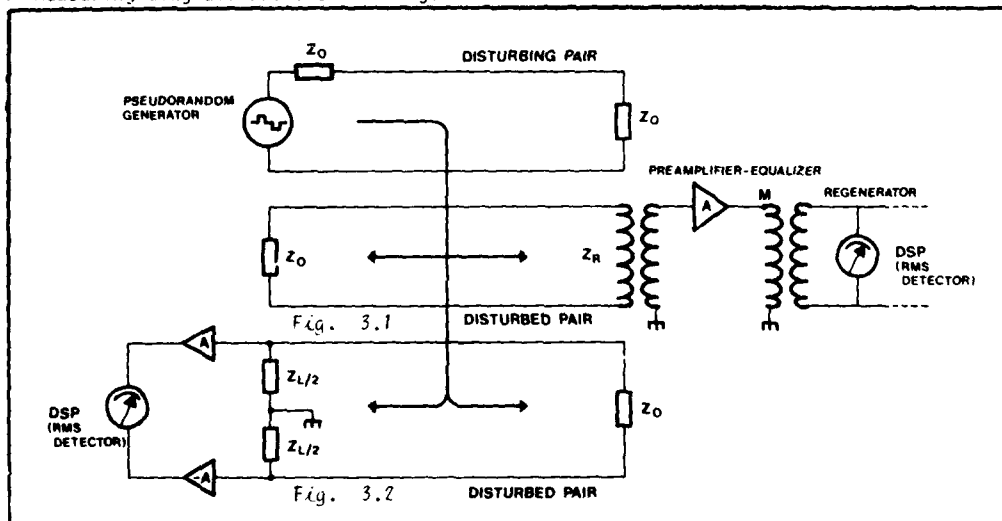


Fig. 3.- TWO POSSIBLE CONFIGURATIONS FOR DIGITAL CROSSTALK MEASUREMENTS

3.2 Components of digital crosstalk measurements assembly

3.2.1 Pseudorandom generator

The disturbing signal source generates a numerical sequence of 32767 elements with equal probability and HDB3 coded. The nominal pulse amplitude is $\pm 3V$, with an analytical power spectrum density $w(f)$ indicated in Appendix I. As is well known its graphical representation have a maximum at the Nyquist frequency (half the bit frequency). The energy contained at higher frequencies is low but offers an important contribution to the noise at the preamplifier input due to the high value of the coupling function at high frequencies. However the preamplifier-equalizer acts as a low pass filter limiting the measuring band to approximately 3MHz.

3.2.2 Preamplifier-equalizer

In fig. 3.2 is shown the terminal impedance as the measuring point of noise voltage. This is the usual procedure in the sinusoidal technique. In this case the filtering effect due to the regenerator does not exist. It could be argued that because of the low energy content at frequencies higher than the bit frequency there will be a linear correspondence between noise measurements performed using the regenerator and those without it, with the only difference that of the higher level of the former due to the amplification provided. Under those conditions using the regenerator might be avoided and correction of measured noise to actual noise would be made linearly to the preamplifier gain depending on the level of useful signal present.

Experimentally it has been verified that despite of the low content of energy of the pseudorandom signal at frequencies higher than the bit frequency there is a strong noise content from that region due to the large value of the coupling function in a frequency band in which the variation is highly irregular. This causes a correlation loss - between noise measurements performed with regenerator and without it (typical $\rho = 0$).

The method presented is then considered inadequate because it creates an additional uncertainty. Another problem arises in FEXT measurement because noise which is not amplified is difficult to measure over long lengths of cable.

The most realistic form of crosstalk measurement consist of using, prior pulse detection operation a filter reinforcing the noise spectrum around the reference frequency f_0 . For a better approximation to the real conditions of operation a normal regenerator for TNL system was employed. The first section is the preamplifier-equalizer which compensates line attenuation up to a maximum length (regeneration limit).

To avoid handling theoretical analytical expressions more or less accurate about channel shaping and form of the equalized pulse a complete characterization of preamplifier response was obtained resulting in the curves of fig. 4.

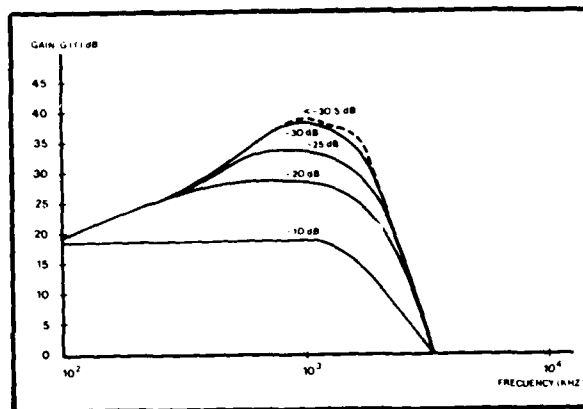


Fig. 4.- PREAMPLIFICATOR RESPONSE FOR VARIOUS SIGNAL LEVEL INPUTS.

Fig. 4 shows gain curves for different input levels. It is observed that for a level lower than the regeneration limit the sum of level and gain is constant (9dB) which means that the line loss is automatically compensated. From this graph we can also see that in the absence of useful signal and provided that the noise level does always exceed the range of regeneration, the response curve of interest will be the maximum gain curve.

By means of interval correlation an analytical expression $G(f)$ has been found for the maximum gain response curve that will be used for the computation of the effective noise voltage derived from crosstalk sinusoidal measurements.

It should be noted that except for when the measurement length equals the maximum repeater length the amplification level of crosstalk noise will be higher than in the case of signal presence.

This allows easy measurements on short lengths of cable without affecting the correlation being investigated. If we are primarily interested on the level of actual interference, correction can be done easily subtracting from the measured level in dBw the difference between the maximum and measuring lengths both in dB.

3.2.3 Digital Signal Processor (DSP)

The usual instrument to read the magnitude of crosstalk noise is a true RMS value voltmeter of enough wideband and sensitivity. To fulfill these conditions as well as others of experimental character a digital signal processor (DSP) was utilized for noise detection. The instrument offers the following advantages:

- High sensitivity that allows noise level detection up to -90dBw.
- Accuracy of reading can be fixed selecting the number of sampling points.

- c) The signal processing capability based on microprocessor can be used to investigate the statistical properties of crosstalk noise.

The operating mode of DSP lies on present signal sampling taking N points inside the period of the signal. These discrete values allows a direct computation of the power or RMS value of the sampled signal using the following formula:

$$\text{Power} = \frac{1}{T} \int_0^T u^2(t) dt = \frac{1}{NT} \sum_{i=0}^{N-1} u_i^2 T = \frac{1}{N} \sum_{i=0}^{N-1} u_i^2 \quad (1)$$

where:

- N : n° of samples.
 u_i : Instantaneous voltage sample i - order
 T : Time interval between samples

The time interval between samples should be enough to insure the independence of samples. This condition can be stated denoting that T must be larger than the reciprocal of the wideband of the measured signal. For the present application $T = 6 \mu\text{sec}$.

To obtain a measured value using (1) with the required tolerance N should be chosen large enough. In accordance to reference (3) N has been chosen 4096 points yielding a precision of ± 0.5 dB.

4. RESULTS OBTAINED: CORRELATION BETWEEN ANALOGICAL AND DIGITAL MEASUREMENTS

Up to now two possible methods of crosstalk measuring have been explained that have the same purpose: capability evaluation of a telephone cable for the PCM transmission.

This capability is given by the crosstalk noise power induced over any pair by the rest of the pairs which carry PCM signals. In the traditional analogical technique from the power sum measurement on each pair on analytical procedure (appendix I) is followed by which is deduced a computed expected value of noise power interfering the useful signal transmitted over the pair. That noise has an instantaneous voltage normally distributed and its RMS value determines a probability or error rate for the transmitted pulses.

We have also commented that alternatively to the indirect procedure represented by the analogical method we can perform a direct measurement of the mean power noise in a given pair. This is a realistic procedure consisting in feeding the interfering pairs simultaneously with pseudorandom sequences, and measuring the RMS value of the noise signal on the pair being evaluated. Instead of simultaneous excitation the disturbing pairs may be operated sequentially measuring the RMS value caused by each contributor separately. The summation on a power basis of the individual RMS values must be equal to the value obtained by simultaneous excitation.

The last method has been adopted in the present work because allows a pair to pair characterization. Nevertheless a quality assurance point of view it is a time consuming procedure.

When cable crosstalk measurements are completed by the two methods, calculated noise powers on each pair should be equal to the measured ones. A cartesian coordinates representation of measured values (y) versus computed (x) should be a straight line of slope unity.

Practical results show that computed values of noise power tend to be on the average some dBw larger than measured ones (absolute value), that is, they are somewhat optimistic. This makes the slope lower than unity. The reason lies on the fact that the selective measurement at f_0 is a biased estimator of the average value of the crosstalk curve at f_0 . Moreover the intrinsic uncertainty to the analogical measurements transform the straight line into a regression line with a correlation coefficient less than unity.

In Appendix I we prove that for a crosstalk value at frequency f_0 and length L_0 , the computed interfering noise power is given by:

$$P_F = F(f_0, L_0)_{\text{dB}} + 21 \text{ dBw} \quad (2)$$

$$P_N = N(f_0)_{\text{dB}} + 21.4 \text{ dBw} \quad (3)$$

or

$$P_F = F(f_0, L_0)_{\text{dB}} + 20.2 \text{ dBw} \quad (4)$$

$$P_N = N(f_0)_{\text{dB}} + 20.2 \text{ dBw} \quad (5)$$

In which:

$F(f_0, L_0)$: ECL FEXT in dB for a pair combination or power sum.

$N(f_0)$: NEXT in dB for a pair combination or power sum.

Relations (2) and (3) stand for pairs and (4) and (5) for quads.

The calculated values with (2) to (5) can be compared with those obtained by direct measurement. Given a certain RMS reading of V volts, the crosstalk noise power is:

$$P = 10 \log \frac{V^2}{Z_R} \text{ dBw}$$

In which Z_R represents the load impedance of regenerator having a nominal value of 120Ω .

$$P = 20 \log V - 20.8 \text{ dBw}$$

The RMS noise voltage may represent a single pair to pair value or a power sum from various interferers:

$$V = \sqrt{V_1^2 + V_2^2 + \dots + V_n^2}$$

The working procedure to achieve the correlation equations were made for each combination of crosstalk type (NEXT or FEXT) and cabling element (pair or quad) resulting in tables 2.1 to 2.4. For instance, in NEXT of a pair cable (table 2.1) the total number of individual measurements used in our comparative study were introduced to a special computed program that performed the following operations:

- a) Regression line fitting over all available absolute individual data (n). Computation of the linear coefficients (A_0, A_1), coefficient of determination (ρ) and standard error (S_1). In tables 2.1 to 2.4 these are included on file N = 1.
- b) Power sum groupings of size N. That is, - for each disturbed pair all possible grouping of N pairs have been taken, summing up on a power basis their computed and measured values at the same time.

A regression line is also fitted and determined the new coefficients.

Then the linear regression that correlate the computed absolute values (x) with the effectively measured (y) is:

$$y = A_1 x + A_0 + \xi$$

in which ξ is a random variable that gives the difference between the real y values and their estimates by the regression line given by:

$$\hat{y} = A_1 x + A_0$$

and

$$\xi = y - \hat{y}$$

The standard error of ξ is then:

$$S_N = \sqrt{\frac{\sum (y - \hat{y})^2}{n-2}} \quad (6)$$

This parameter is a direct indicator of the uncertainty that analogical measures have in themselves. For the most unfavorable case the calculated noise power P_F or P_N should be corrected according to the regression line equations and standard error:

$$\begin{aligned} P_F^* &= A_1 P_F + A_0 - K S_N \\ P_N^* &= A_1 P_N + A_0 - K S_N \end{aligned} \quad (7)$$

The constant K depends on the level of confidence required as well as the type of statistical

distribution of ξ .

We do not know the real distribution of ξ but assuming normality conduct to acceptable results.

Supposing that ξ follows a normal distribution of zero mean and a variance $\sigma_1^2 = S_1^2$ given by (6) then the variance of N interferers power sum can be expressed by the Wilkinson approximation⁽⁴⁾ for non truncated normal distributions:

$$\frac{\sigma_N^2}{N} = \frac{1}{\lambda^2} \log_e (1 + \exp(\lambda^2 \sigma_1^2)) - 1/N \quad (8)$$

$$1/\lambda = 10 \log_e.$$

In the last column of tables 2.1 to 2.4 are indicated the values of the standar error of estimation calculated by (8) for different N. A good approximation to real S_N can be observed.

The law of variation of σ_N are simply seen in the first approximation of (8)

$$\sigma_N \approx \frac{\sigma_1}{\sqrt{N}}$$

We can see by the above expression that as N gets larger the uncertainty parameter σ_N improves.

A normality criterion can be then used to assign a value for K in relations (7). For instance $K = 2.33$ for a confidence level of 99%.

In summary, given a disturbed pair and a certain number of interferers N, which represents a calculated noise power P in dBw, then with a 99% confidence level the actual interfering noise power (absolute value) shall not exceed:

$$P^* = A_1 P + A_0 - 2.33 \sigma_N$$

The goodness of fitting of the regression lines of tables 2.1 to 2.4 are given by the determination coefficient (ρ). In all cases ρ is near unity. The best correlation has been obtained in the case of FEXT and pairs.

TABLE 2.- LINEAL REGRESSION EQUATIONS OF
CROSSTALK NOISE POWER
y: MEASURED VALUES x: CALCULATED VALUES

TABLE 2.1
LINEAR REGRESSION EQUATIONS
FOR NEXT IN PAIR CABLE
 $y = A_1 x + A_0$

N° OF INTERFERERS N	A ₁	A ₀	ρ	S _N	σ _N
1	0.71	15.39	0.81	3.51	3.51
3	0.85	6.98	0.89	2.29	2.24
5	0.86	6.36	0.92	1.94	1.78
7	0.87	5.50	0.94	1.61	1.53
9	0.89	4.88	0.94	1.48	1.35
11	0.88	5.02	0.95	1.32	1.23
13	0.91	3.72	0.96	1.22	1.13
15	0.90	4.14	0.96	1.23	1.06

TABLE 2.2
LINEAR REGRESSION EQUATIONS
FOR NEXT IN QUAD CABLE
 $y = A_1 x + A_0$

N° OF INTERFERERS N	A ₁	A ₀	ρ	S _N	σ _N
1	0.69	11.8	0.82	3.44	3.44
3	0.76	7.6	0.87	2.29	2.19
5	0.74	7.6	0.88	1.76	1.74
7	0.77	6.3	0.92	1.43	1.48
9	0.78	5.4	0.90	1.24	1.32
11	0.69	8.3	0.83	1.12	1.19
13	0.66	9.4	0.82	0.93	1.10
15	0.66	9.4	0.82	0.93	1.03

TABLE 2.3
LINEAR REGRESSION EQUATIONS
FOR FEXT IN PAIR CABLE
 $y = A_1 x + A_0$

N° OF INTERFERERS N	A ₁	A ₀	ρ	S _N	σ _N
1	0.81	10.60	0.95	1.95	1.95
3	0.90	5.25	0.98	1.11	1.16
5	0.91	4.39	0.98	0.95	0.91
7	0.91	4.49	0.98	0.92	0.77
9	0.92	3.78	0.99	0.75	0.68
11	0.93	3.69	0.99	0.61	0.62
13	0.92	4.04	0.99	0.64	0.57
15	0.92	3.82	0.99	0.60	0.53

TABLE 2.4
LINEAR REGRESSION EQUATIONS
FOR FEXT IN QUAD CABLE
 $y = A_1 x + A_0$

N° OF INTERFERERS N	A ₁	A ₀	ρ	S _N	σ _N
1	0.75	10.90	0.89	2.74	2.74
3	0.86	3.66	0.97	1.25	1.69
5	0.90	1.79	0.97	1.11	1.32
7	0.93	0.26	0.96	1.10	1.12
9	0.92	0.85	0.97	0.86	0.99
11	0.93	0.24	0.98	0.69	0.90
13	0.95	-0.53	0.97	0.70	0.80
15	0.92	0.47	0.97	0.70	0.77

5. SIGNAL TO NOISE RATIO, ERROR RATE AND MARGIN OF ERROR

An important feature concerning crosstalk noise is their disturbing effect on the PCM transmission that is, the relationship between effective noise voltage and error rate.

The analytical procedure for computation of the error probability due to a noise power value is based on the normality of the statistical distribution of noise. Another supposition is the power addition of the various contributors of crosstalk over a given pair.

With the aid of the DSP some properties of crosstalk noise can be investigated. Fig. 5 shows picture of crosstalk noise due to a single interferer. In it can be observed a strong correlation between time instants and instantaneous noise voltage which means that at every time instant and their successive periods a different noise statistics one rates (normal distributions of noise with different variances).

A noise of this characteristic disturbing in the instant of pulse detection in a uncorrelated way gives rise to an error rate different depending on the phase of the sampling instants.

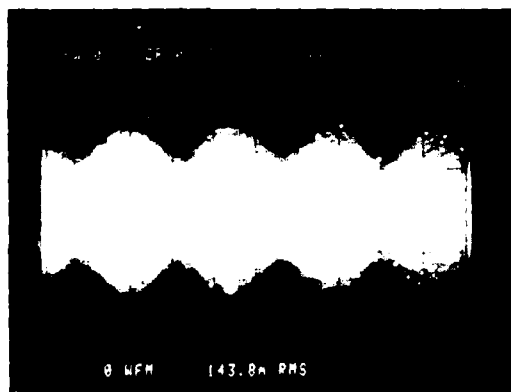


FIG. 5.- SINGLE INTERFERER NOISE PICTURE

In Fig. 6 is shown the result of the addition of a noise signal of similar magnitude due to another interferer excited by a pseudorandom signal source independent from that which originated Fig. 5.

In the last picture is clearly shown that the noise statistic is more independent of the time instants in which the useful signal is sampled at the decision process of regeneration.

It is reasonable to think that the uncorrelated addition of various crosstalk noise signals give as result a normal noise distribution. In

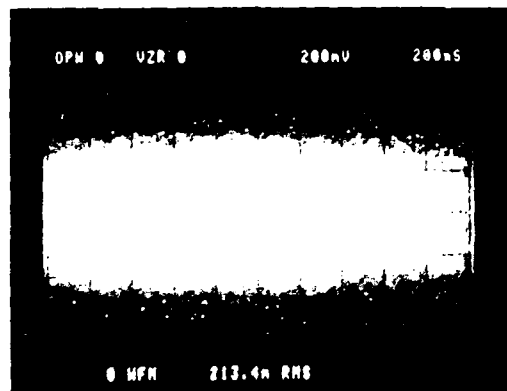


FIG. 6.- ADDITION OF TWO UNCORRELATED NOISE VOLTAGES.

these pictures are shown also the independent voltage samples that are used for the RMS computation of crosstalk noise. The samples also help to check the goodness of fitting to the normal distribution. The cumulative function constructed with the samples of noise signal proved itself to be entirely in accordance with the ideal normal cumulative function.

The noise picture of fig. 6 is the resulting noise addition contributed by two pairs excited by independent pseudorandom sources. If the contributions are NEXT type crosstalk noise the visual noise picture would be similar to that shown in fig. 6, although the disturbing sources were not independent, because unbalances are randomly distributed along the cable. However in the case of the addition of various NEXT noise contributions from a single disturbing source the noise picture would be similar to that indicated in Fig. 5 because the different crosstalk couplings along the cable sums up in phase at the terminal load.

In accordance with fig. 4 the peak power of transmitted signal at the decision point is:

$$S = 10 \log \frac{V_p^2}{120} = -11.2 \text{ dBw}$$

Suppose a disturbed pair whose total noise power level (power sum of P_N and P_F in dBw) is P_T . For a normally distributed noise the instantaneous power which is exceeded with a 10^{-7} probability is (⁵):

$$P_{10^{-7}} = P_T + 14.3 \text{ dBw}$$

The margin of error for a 10^{-7} error rate is then:

$$M_{10^{-7}} = S - P_{10^{-7}} - A$$

The term A is signal to noise ratio required for the amplifier to operate.

This formula shows that M_e should include a correction factor in the case that P_T have been calculated by means of single frequency measurements. The margin of error is then decreased accordingly to the magnitude of the standard error of estimation $S_N (\sigma_N)$.

6. DIGITAL MEASUREMENTS APPLICATION TO QUALITY ASSURANCE

6.1 Introduction

Up to this point we have mainly discussed conditions and measurements to apply in a regeneration section. Now it is necessary to adapt this type of measurement to manufacturing cable lengths.

From a quality assurance point of view two aspects are of most interest:

- Attainment of the best possible accuracy in the measurements, within reasonable economical limits. In the case of crosstalk the measurements performed should be representative of the cable behaviour when carrying a real signal.

From this point of view it has been proven the higher accuracy of measurements using digital signal. However employing a sinusoidal signal at a single frequency the measurements are more or less correlated depending on the number of interfering pairs.

- Quick performance and low cost of measurement equipment.

The method of error rate measuring do not seem to be the most suitable for separated cable lengths for two reasons. First it does not exist a simple relation between the total error rate required in a regeneration section and the maximum error rate of a separated length, consequently obtaining a limit in this case is not effective.

Second in short lengths the error rate direct measurements are not always possible.

Using the noise voltage measurement method a noise limit can be imposed on each length depending upon the ratio of the maximum regeneration length and the actual length of cable as per the following formula:

$$V_e = 1/L V_L 10^{\alpha(L-1)/20}$$

in which:

V_1 = Max. noise voltage in the measuring length -l- in mv.

V_L = Max. noise voltage in the regeneration section -L- in mv.

l = Reel length in Km.

L = Regeneration length in Km.

α = Cable attenuation in dB/Km.

Consequently it is concluded that from a quality assurance point of view it is more convenient to express the results in noise voltage.

6.2 Measurement configurations

Fig. 7 is the basic measuring arrangement. It is necessary as much pseudorandom generators as the number of interfering pairs, and the configuration is valid for both FEXT and NEXT noise measurement.

These configurations have the advantage of a fast execution whatever the number of pairs inclusive without the aid of a computer, but have the disadvantage of the high number of pseudorandom sources.

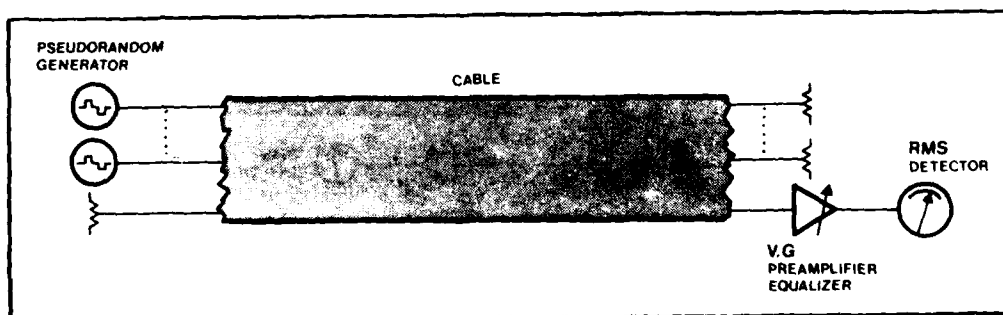


Fig. 7.- CONFIGURATION FOR CROSSTALK NOISE VOLTAGE MEASUREMENT.

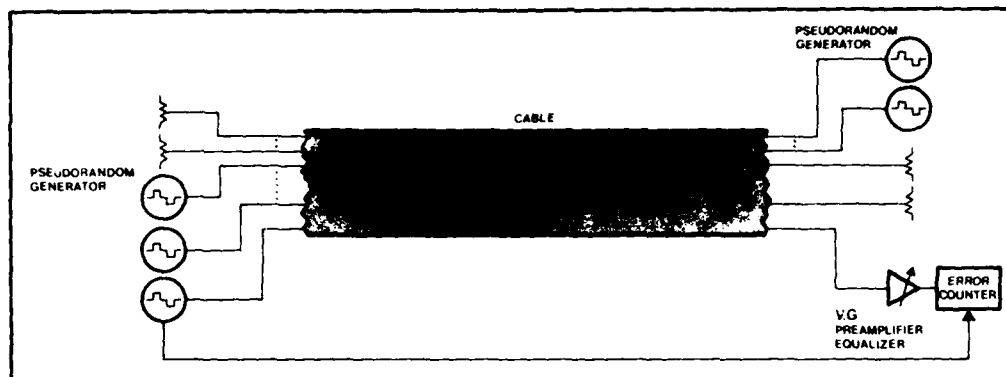


Fig. 8.- CONFIGURATION FOR ERROR RATE MEASUREMENTS.

A more simple and economical configuration - uses a single pseudorandom source and as many amplifiers as pairs (Fig. 9). However as has been indicated before, noise contributions from the pairs arrive in phase to the terminal impedance of disturbed pair in the far end. This configuration is not valid for FEXT crosstalk noise measurements but can be used in NEXT measurements.

The last configuration makes use of a computer and a single pseudorandom source (Fig. 10).

The principle of measurement is the same as the power sum crosstalk method in sinusoidal measurements. Total noise voltage on a disturbed pair results from the addition on a power basis of the voltage contributions from all the disturbing pairs.

The procedure of fig. 10 can take a longer time of testing due to the large number of combinations but has the advantage of being easily adaptable to any automatic crosstalk measuring equipment, replacing the sophisticated and expensive selective generator and detector by the simple and cheap pulse generator and RMS voltmeter.

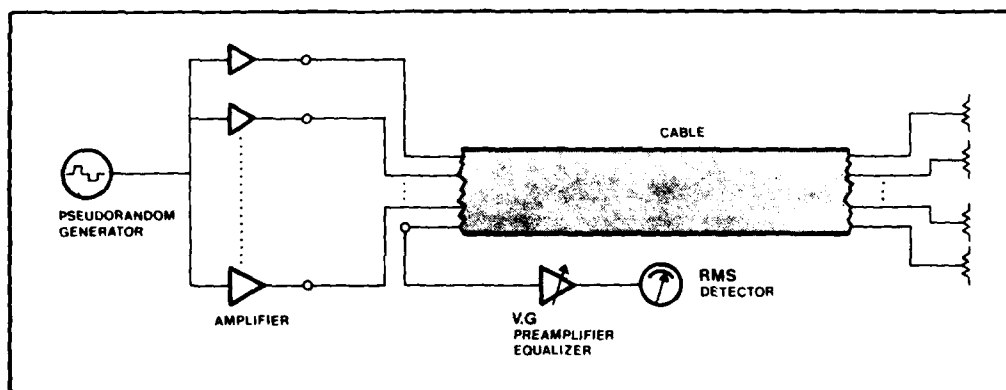


Fig. 9.- SIMPLIFIED CONFIGURATION FOR NEXT MEASUREMENTS.

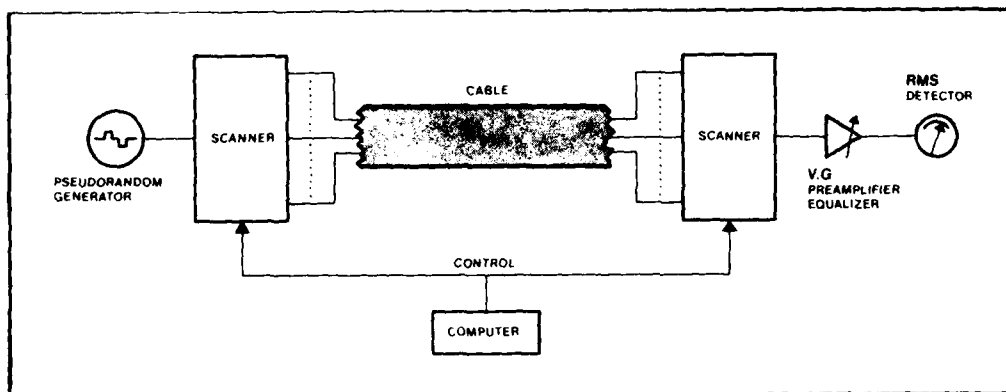


Fig. 10.- CONFIGURATION FOR AUTOMATIC CROSSTALK NOISE VOLTAGE MEASUREMENTS.

CONCLUSIONS

- Single frequency crosstalk measurements on a pair to pair basis have an appreciable error interval which may be up to 16dB in NEXT. In FEXT this interval decreases as well as for pairs when compared to quads.

When a certain number of pairs are simultaneously disturbing, the power sum has an uncertainty that decreases as the number of pairs increases.

- From a comparison with digital measurements using pseudorandom signal, it can be observed that the computed noise power obtained from single frequencies measurements tend to have, on the average, a higher absolute value (in dBW). The computed value should be linearly corrected by means of empirically determined regression equations for each crosstalk type and cabling element.
- The digital method of crosstalk measurement yields accurate results and requires simple instruments. However it has a lower sensitivity whereas the selective instruments commonly used in analog crosstalk measurements allows level measurements up to 20dB lower.
- In normal manufacturing shipping lengths noise voltages measurements are more convenient than direct error rate readings because with the first method a simple formula may be used for noise limits corrections depending on the measuring length.
- The digital crosstalk method with RMS reading is easily adaptable to a plant quality control. It can be adapted to an automatic measuring equipment using simultaneous or sequential excitation. The automatic procedure of sequential excitation has been used in this work to collect this data. At the present we have under development a new automatic system with simultaneous

excitation which allows a considerable measuring time reduction.

APPENDIX I

ANALYTICAL COMPUTATION OF THE MEAN CROSSTALK POWER NOISE

Graphically the basic crosstalk interference situation is shown in Fig. 3 for a single noise contributor.

In the case of FEXT, the pseudorandom signal of power spectral density $w(f)$ is transmitted over the disturbing pair having an attenuation characteristic $L(f)_{dB}$ couples to the disturbing pair through a FEXT transfer network $F(f)_{dB}$ and is amplified and equalized in the first section of the regenerator which has a response function $G(f)_{dB}$.

The FEXT noise power over the disturbing pair due to a single contributor is given by:

$$P_F = \int_0^B w(f) 10^{\frac{L(f)_{dB}}{10}} 10^{\frac{F(f)_{dB}}{10}} 10^{\frac{G(f)_{dB}}{10}} df \quad (9)$$

The analytical expressions for the various functions are:

Attenuation characteristic of line

$$L(f)_{dB} = -\alpha_0(f/f_0)^{1/2}$$

α_0 : attenuation at frequency f_0 and length L_0 in dB.

Equal level FEXT transfer function $F(f)_{dB}$

This function has not an exact analytical expression. To obtain an accurate noise power from (9) $F(f)_{dB}$ should be defined by enough number of points as was seen in table 1.

In the sinusoidal crosstalk measurement a sample is taken at frequency f_0 and length L_0 , obtaining a value $F(f_0, L_0)_{dB}$. A linear variation with frequency of 6dB/octave is then assumed:

$$F(f)_{dB} = F(f_0, L_0)_{dB} + 20 \log(f/f_0)$$

In the case of N contributors $F(f_0, L_0)_{dB}$ stands for the power sum:

$$F(f_0, L_0)_{dB} = 10 \log(10^{\frac{F_1}{10}} + 10^{\frac{F_2}{10}} + \dots + 10^{\frac{F_N}{10}})$$

Preamplifier-equalizer response

From fig. 4 has been obtained an analytical expression for $G(f)_{dB}$ by means of interval fitting of known regression functions. For the practical example:

$$G(f)_{dB} = \begin{cases} 40.5f^{0.311} & f < 1.024 \text{ MHz} \\ -5.55f + 45.4 & 1.024 \leq f < 1.7 \text{ MHz} \\ -24.5f + 77 & 1.7 \leq f \leq 3 \text{ MHz} \end{cases}$$

Spectral power density of pseudorandom signal

$$w(f) = \frac{2A}{Z_L} \frac{f_0}{\pi^2 f^2} \sin^2\left(\frac{\pi f}{4f_0}\right) (1 - \cos \frac{\pi f}{f_0})$$

A: Pulse amplitude 3V.

Z_L : Load impedance of pair. $Z_L \approx Z_0$ is the characteristic impedance of the pair.

$Z_L = 94 \Omega$ for pairs and $Z_L = 124 \Omega$ for quads.

By substitution of the various analytical functions in (9) results:

$$P_F = \int_0^B w(f) 10^{\frac{-\alpha_0(f/f_0)^{1/2}}{10}} 10^{\frac{F(f_0, L_0)}{10}} \left(\frac{f}{f_0}\right)^2 10^{\frac{G(f)}{10}} df$$

$$P_F = 10^{\frac{F(f_0, L_0)_{dB}}{10}} \cdot I$$

In dB:

$$P_F = F(f_0, L_0)_{dB} + 10 \log I \text{ dBw}$$

Integral I can be numerically calculated for $B = 3 \text{ MHz}$ resulting:

$$P_F = F(f_0, L_0)_{dB} + 21.0 \text{ dBw for pairs.}$$

$$P_F = F(f_0, L_0)_{dB} + 20.2 \text{ dBw for quads.}$$

The same steps can be followed in the case of NEXT. Here the dependency with length is not considered.

$$P_N = N(f_0)_{dB} + 21.4 \text{ dBw in pairs.}$$

$$P_N = N(f_0)_{dB} + 20.2 \text{ dBw in quads.}$$

ACKNOWLEDGMENT

The authors wish to thank the people of Cables de Comunicaciones S.A. for their helpful discussions and help in this work.

REFERENCES

- (1) T1 Carrier Characterization Field Measurements Results. T.C. Kanp, D.C. Leeper, A.K. Reilly, P.E. Scheffer. BSTJ. Vol 60, n° 6, August 1981, pp 965.
- (2) Engineering of T1 Carrier System Repeatered Lines. H. Cravis and T.V. Crater. BSTJ. March 1963, pp. 469.
- (3) Power Measurements. S. Cordray, D.L. Favin, D.P. Yorkgitis. BSTJ. Vol 60, n° 7, September 1981.
- (4) Some properties of Power Sums of Truncated Normal Random Variables. I. Nassell. BSTJ. November 1967, pp. 2109.
- (5) Crosstalk Considerations for a 48 Channel PCM Repeatered Line. Stevan D. Bradley. IEEE Transaction, Vol COM-23, n° 7. July 1975, pp. 725.
- (6) Mesure en Régime Numérique de la Diaphonie Sur Des Cables à Paires Symétriques. J. Boulvin, C. Beynié, G. Bargeton, A. Payant, B. Coutty, Centre National d'Etudes des Télécommunications. Décembre 1975.
- (7) Medida de Diafonia Digital y Comportamiento de los Regeneradores PCM contra Interferencias. P. Sorensen. Comunicaciones Eléctricas. N° 47/4 1972.



V. Abadía obtained his degree in Telecommunication Engineering in 1974 at the Universidad Politécnica de Madrid. He joined Cables de Comunicaciones, S.A. in Zaragoza, Spain, soon after his graduation and is now Manager of the Cable Design and Engineering Department.



J.L. Mariñosa received a degree in Technical Engineering from the Escuela Universitaria de Ingeniería Técnica de Telecomunicación de Alcalá de Henares. He joined Cables de Comunicaciones, S.A. in 1975 and is at present responsible for the Electrical Measurements Laboratory.

FIELD TESTERS FOR ASSESSING 1.5 AND 2.0 Mbit/s DIGITAL PERFORMANCE OF METALLIC-PAIR CABLES

I G Dufour - British Telecom, London, UK

Summary

The paper outlines the technical and planning requirements for providing 1.5 and 2.0 Mbit/s digital transmission on metallic-pair cables. It then describes how a need for test equipment to determine planning rules to maximise 2 Mbit/s working on existing (audio quad) cables has led to the development of testers with a wider application. A Digital Crosstalk Analyser, for detailed cable performance analysis and collection of planning rule data, and simple barrage testers for pre-commissioning tests are described. Both types of tester are suitable for testing metallic-pair cables at 1.5 or 2.0 Mbit/s.

Introduction

This paper describes factors relating to digital system provision on existing metallic-pair cables in junction (short-haul, inter-office trunk) networks. It relates these factors to field testing requirements and describes the use of digital cable testers.

Digital Provision in Junction Networks

In junction networks the most frequent requirement is for 1.5 or 2.0 Mbit/s transmission and there are 3 options for achieving this:-

- 1 Converting existing audio cables.
- 2 Providing new metallic-pair cables designed for digital transmission.
- 3 Providing optical fibre cables, usually with higher order multiplex.

All of these have their place in the planners repertoire.

Existing cables were designed and installed in an exclusively audio era but are capable of supporting significant numbers of digital systems. However, achieving maximum digital fills with minimum cost and difficulty calls for more knowledge of the digital performance of these older cables.

Metallic-pair cables designed for 2 Mbit/s working can be cheap to make and to install but their

attractiveness depends heavily on duct (conduit) availability and installation methods.

Optical fibres are so far only cost effective at high bit rates, say 34 Mbit/s and above, and so are not yet viable in the rural junction network where 2 Mbit/s is adequate, although this position is changing.

Existing Cables

Existing audio cables represent a large capital investment and cannot be ignored as a means of providing digital systems in spite of the many attractions of providing a new cable purpose designed for digital transmission. Typical situations where converting existing cables is cost-effective are on long rural routes and in city-centres. In both these cases duct-space is at a premium. Furthermore, the possibility of recovering cables to provide duct-space for a new cable is severely limited by practical considerations.

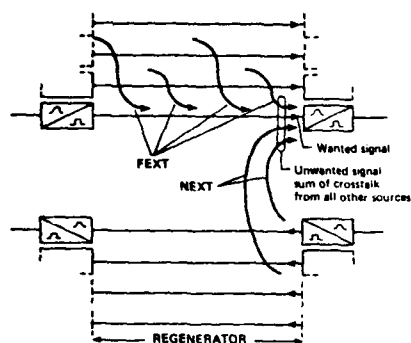
In the UK almost all existing junction cables are of star-quad construction.

Cable Characteristics Affecting Digital Performance

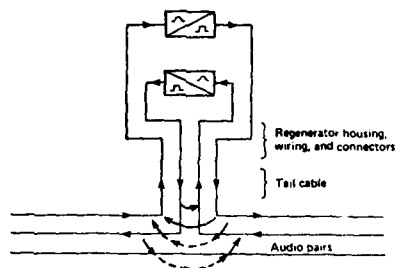
It is useful at this point to review the factors which affect digital performance. The key cable characteristics are insertion loss, near-end crosstalk (NEXT) and far-end crosstalk (FEXT). The main crosstalk paths are shown in Fig 1(a).

Fig 1(b) shows additional crosstalk paths, known as 3rd-circuit crosstalk (3CXT), which arise from particular jointing, tail cable and regenerator housing arrangements. The interrelationship of the key features and their effect on error-rate performance can be seen from Fig 2.

Figures 1 and 2 follow.



(a) NEXT AND FEXT



(b) 3 CXT (3rd circuit crosstalk)

FIGURE 1 CROSSTALK PATHS

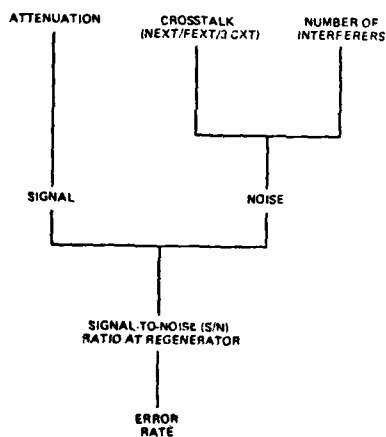


FIGURE 2 EFFECT OF CABLE CHARACTERISTICS ON ERROR RATE

Whatever cable types are employed locally it is necessary to quantify these characteristics and relate them to the line system being used in order to determine the digital capacity of the cable^{1,2}.

In determining the digital capacity of cables two approaches are possible: to treat each cable on its own or to characterise cables of a common type with a view to producing planning rules. In the UK the latter approach has been adopted but with a recognition that individual cables must be tested when they are outside the planning rule guidelines. Pre-commissioning tests are also required.

Planning Rules (Existing Cables)

The planning rules now used in the UK are derived from large amounts of crosstalk data obtained from measurements on many cables. Having characterised the network from a statistically valid sample, the number of systems that can be installed on any cable can be predicted, within certain confidence limits, such that an acceptable error ratio is not exceeded.

The rules allow the planner to trade-off regenerator spacing against cable-fill according to economic or operational considerations. They are expressed in terms of the probability of success; the published figures assume that 20% more pairs are intercepted than are actually required and that the number of systems shown will be achieved in 99 out of 100 routes. Of course, a high proportion of interceptions will prove capable of supporting more systems than the published figure. The actual capacity, after interception of pairs into regenerator housings, is then determined by the planner from an analysis pre-commissioning tests.

Summary of Testing Requirements

From the foregoing the following testing requirements have been identified:-

- Tests to characterise cables and produce planning rules. A large amount of crosstalk data is required so that the number of systems that can be installed on any cable can be predicted.
- Tests to confirm that the predicted capacity is actually achieved and to establish what extra capacity is available (pre-commissioning).
- Tests to troubleshoot cables where the predicted capacity is not achieved.
- Tests on cables, prior to interception of pairs, where the planning rules indicate that the required system fill cannot be achieved.

The paragraphs which follow describe the UK experience with test equipment to meet these needs.

Digital Testing Techniques

There are a variety of measurement techniques used to assess digital crosstalk performance: single frequency, swept frequency, band limited white noise, single digital source and multiple digital sources all provide useful data. However, of these, the digital source techniques are preferred in British Telecom because they correspond to the ultimate use of the pairs and are more easily related to digital system performance.

Of the digital source techniques the traditional margin test using an attenuator/error detector combination is largely unsuited to field applications.

For planning rule formulation cable crosstalk is best characterised by analysing many individual pair-to-pair combinations (ie sending a digital signal on one pair only and measuring on another).

The so called "barrage" test method, whereby all transmit pairs are loaded with send signals and the receive pair noise measured, is the most suitable for particular cable assessment, especially pre-commissioning tests.

Cable Characterisation

It was foreseen in the mid-1970s that the large number of 2 Mbit/s systems required for modernisation would cause problems on existing quad cables and that the planning rules which had satisfied lower circuit requirement demands would have to be revised. To do this it was decided to base the rules on the results of a substantial measurement program: but first a tester had to be designed for the purpose³. In order to allow many pair-to-pair measurements to be made without manual intervention it was a requirement to be able to connect many pairs to the tester and for the tester to test the combinations sequentially. As the most common regenerator housing in the UK contains regenerators for 36 digital line systems it was therefore a requirement for the tester to have 36 digital outputs. This would also allow the facility of sending on all transmit pairs at the same time to allow barrage noise to be measured on each received pair.

The solution chosen was to have 36 separate generators, each generator being driven by its own clock or from a common clock thus allowing plesiochronous or synchronous working to be simulated. In addition to the pseudo-random sequences it was decided to allow for the generators to be set to give an "all ones" pattern which, when encoded into HDB3 gives continuous mark reversals. This signal can be used for insertion loss measurements at approximately 1 MHz. The object of the measurements is to determine the amount of noise, resulting from crosstalk, at the decision point of a regenerator as this directly affects the required error rate (Figure 2). To do this it was decided to modify a proprietary regenerator to give access to the decision point and the agc control circuitry. Crosstalk noise at

the decision point is then measured by sampling and the information processed digitally to obtain the rms voltage of the crosstalk noise. As up to 36 receive pairs need to be measured a switching matrix is required to enable any one of them to be connected to the regenerator.

R92A Tester

A tester to meet the above requirements was designed, and made in small numbers, at the British Telecom Research Laboratories. The tester was named the R92A Tester and is shown in Figure 3.

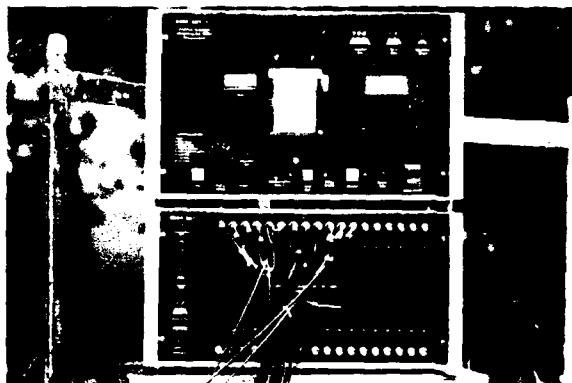


FIGURE 3 THE R92A TESTER

The signal generator and receive units are in separate cases. For NEXT (and 3CXT) measurements both units are used at the same site whereas for FEXT and insertion loss measurements the units are sited at the opposite ends of a regenerator section. In order to control the test sequences and allow individual pair-to-pair and barrage measurements to be made the switching of the transmit signals and of the receive unit was put under microprocessor control. A communication link is required between the 2 units (via a pair in the cable when units are separated).

The NEXT (and 3CXT) measurements which can be carried out with both units at one site are thus:-

- All pair-to-pair combinations using pseudo-random sequences.
- All pair-to-pair combinations using "all one" signals.
- Barrage measurements using pseudo-random sequences, plesiochronous.
- Barrage measurements using pseudo-random sequences, synchronous.
- Barrage measurements using "all one" signals, plesiochronous.
- Barrage measurements using "all one" signals, synchronous.

With units at opposite ends of the regenerator section, FEXT measurements can be carried out in the same variations listed for NEXT together with insertion loss and some other facilities included with minimum effort such as error rate monitoring and the amplitude distribution, sampled over a set period, of any extraneous noise on the cable.

The cable pair test results are recorded on magnetic tape (cassette) for later printing although a single reading LED display and a printer are provided for on-site inspection of a few readings.

The R92A testers were first used in 1979 and have since completed an extensive measurement program to characterise UK quad cables. The pair-to-pair measurements in particular have been used to formulate planning rules.

Digital Crosstalk Analyser (DCA)

Experience with the R92A tester confirmed the need for cable evaluation in the field. The main UK applications would be for debugging problem-cables and evaluating the digital performance of cables where the planning rule predictions show insufficient digital fill for the planners needs. For other administrations/telcos the ability to collect data for planning rules formulation would be a prime requirement.

Consideration was given to manufacturing more R92A testers. However, although the R92A proved valuable it had shortcomings. These were:-

- designed for use by specialists not normal cable test teams;
- little feedback to user during tests;
- results not available on-site: printout from cassette caused delay;
- insufficient digital output signals for large cables or assessing 3CXT effects;
- insufficiently rugged.

The DCA was therefore developed as an improved field tester based on the R92A. It has been jointly developed by British Telecom and Racal. The main features are the use of 144 bidirectional signal ports and a desk top computer controller to provide software control of functions and on-site computing power with operator feedback. The main measurement capability is as described earlier for the R92A Tester: viz NEXT, 3CXT and FEXT in pair-to-pair and barrage modes with pseudo-random and "all ones" signals. Also, for barrage, the option of plesiochronous or synchronous signals. However, the opportunity was taken to allow for 2 clock frequencies to allow measurements at 2048 kbit/s or 1536 (or, optionally, 1544) kbit/s to be made. A full technical specification is included as an appendix.

The software control of functions is very important as the test sequences and analysis of

data can be varied to suit user requirements. For instance, the 144 signal ports can be configured in any combination of transmit and receive. For UK use 72 transmit outputs and 72 receive paths are normal. Similarly, the analysis programs can be adapted to suit any cable type and regenerator housing configuration. In the UK the analysis is tailored to quad cables and 2 uni-directional regenerators in a single unit.

Prototypes of the DCA have already been employed for field tests (Figure 4) and production units are now being made.



FIGURE 4 THE DCA IN USE

The equipment is shown in more detail in Figure 5 from which it can be seen that the equipment comprises a DCA plinth unit, a power supply unit, the desk top computer controller and various connecting cords. For UK use British Telecom has selected the Hewlett Packard HP 85 computer.

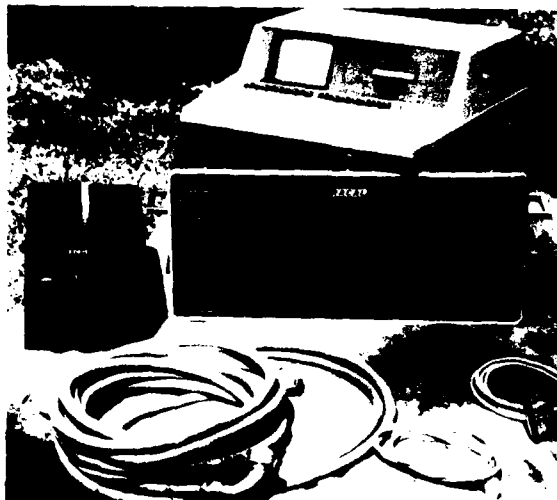
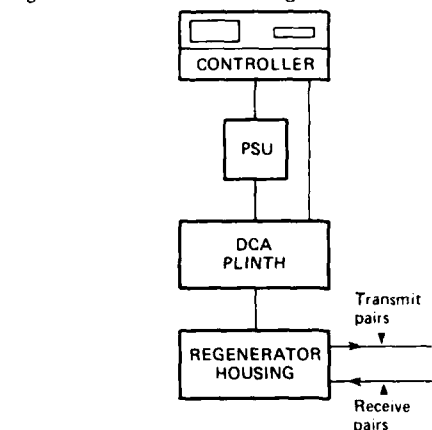
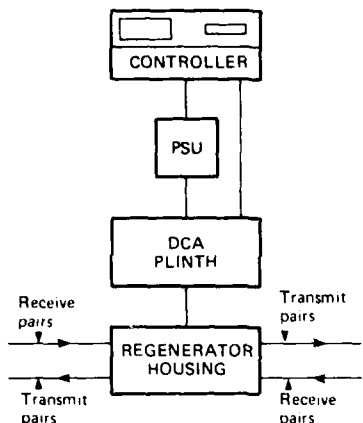


FIGURE 5 THE DCA

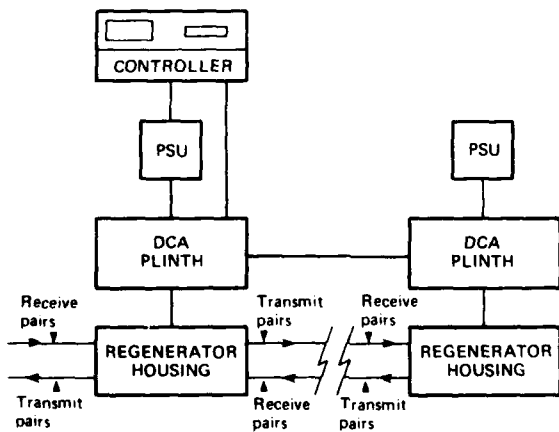
A single plinth unit is used for NEXT/3CXT measurements and 2 plinth units for FEXT and insertion loss measurements. Any plinth can be used in local or remote mode. Typical test arrangements are shown in Figure 6.



(a) NEXT ON ONE SIDE



(b) NEXT ON BOTH SIDES PLUS 3 CXT



(c) NEXT ON BOTH SIDES PLUS 3CXT AT CONTROLLER LOCATION PLUS FEXT

FIGURE 6 TYPICAL TEST CONFIGURATIONS WITH THE DCA

Once assembled and connected to the regenerator housing (or cable pairs) the operator selects the appropriate tests. The software designed for UK application gives the option of a standard test routine or the selection of any particular type of test on any specific pair or group of pairs.

A key feature of the standard test routine is a printout giving the optimum utilisation of pairs in a regenerator section to achieve maximum system fill. The particular combination of transmit and receive pairs to achieve the optimum is almost impossible to determine with other test methods.

Barrage Testing

It has already been explained that the planning rules are based on intercepting more pairs than are required and that statistically there is only one chance in 100 that the desired capacity will not be achieved. Nevertheless, there is an assumption that it is necessary to test the intercepted pairs to determine those which will actually support digital transmission. The R92A Tester and the Digital Crosstalk Analyser are unnecessarily complex for this purpose and a much simpler tester can be designed. The fundamental requirement is to be able to generate many pseudo-random transmit signals and to measure the resultant crosstalk noise on each receive pair. Three versions of such testers are already in use in the UK and a fourth variety will shortly be introduced.

The first version was constructed quickly using readily available parts: in particular an existing 8 output 2 Mbit/s HDB3 pulse generator, of which 2 were used, for the transmit section and an rms level meter for the receive side. The unit was powered by a lead-acid battery (24V). The main items needing construction were a receive amplifier, incorporating a filter to simulate the frequency sensitivity characteristics of a regenerator, a case, and the test lead for making connections to the regenerator housing. The Tester T63 was first issued to the field in 1980 and is shown in Figure 7.

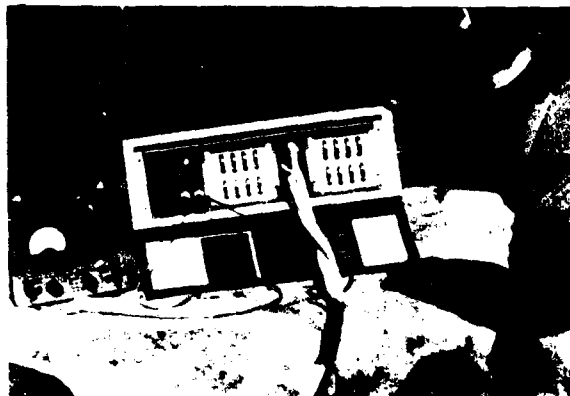


FIGURE 7 THE T63 TESTER IN USE

The next development was to increase the number of outputs by designing a new pulse generator with 18 outputs. This was of identical size to the former 8 output version and allowed upgrading of the earlier testers to 36 transmit signals.

Using standard items, intended for internal mounting, was accepted because of the need to produce a field tester quickly. For the longer term a more rugged, purpose designed, tester based on the established principles and experience of use was specified. In the meantime a commercial manufacturer produced a third version barrage tester (Tester T1019) based on the 36 output T63 but in a modified construction practice (Figure 8).

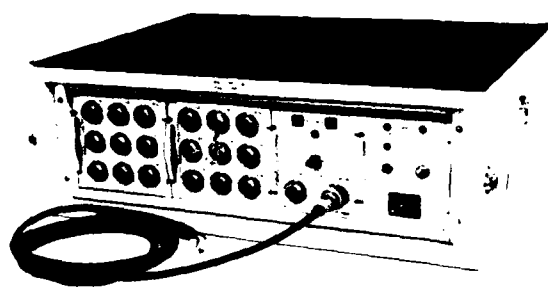
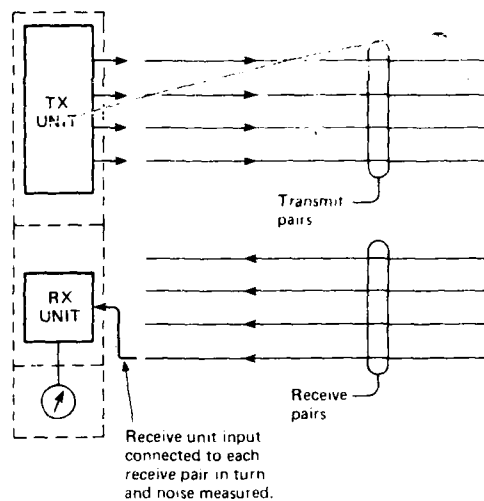


FIGURE 8 THE T1019 TESTER

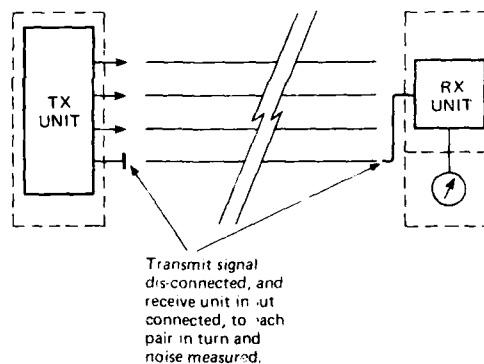
The next version will have several features not common to its predecessors:-

- the transmit and receive functions will be in separate cases;
- the transmit signals will be selectable between all 1536 kbit/s or all 2048 kbit/s (HDB3 encoded);
- the transmit signals can be individually disabled;
- the receive unit has a liquid crystal display of the true rms level of the incoming digital crosstalk noise;
- the receive unit also incorporates 2 transmit generators;
- the units are of robust construction;
- operation from battery or mains (eg from a generator).

All the versions follow the same basic principle shown in Figure 9.



(a) NEXT MEASUREMENT



(b) FEXT MEASUREMENT

FIGURE 9 PRINCIPLES OF BARRAGE MEASUREMENT

The main application of barrage testers in the field is as follows. After interception of the pairs into regenerator housings but before system commissioning the pairs are tested with a barrage tester. From the planning rules it is generally known which cable configurations are limited by NEXT and which by FEXT. When NEXT is the main consideration the tester is taken to each regenerator housing and tests are made first in one direction and then in the other. To test in one direction, all the transmit pairs are connected to the transmit signal outputs and each receive pair is connected in turn to the receive input of the tester. The measured readings are recorded. The maximum level of noise that allows a commissioning error rate of better than 1 in 10^{10} to be achieved has been established by

laboratory measurement for a range of line insertion losses measured at 1 MHz. This information is in nomogram form and for any known regenerator section line loss the minimum acceptable noise level can be established. The measured readings are then compared to this to provide an instant go/no-go result. Different nomograms apply to different line rates and the one used for the forthcoming 1.5 MBaud 4B3T (4 Binary 3 Ternary) line code will incorporate appropriate conversion factors to allow the actual readings from 1536 kbit/s HDB3 signals to be assessed.

For FEXT measurements similar considerations apply except that the transmit signals are remote from the receiver. In this application it is obviously wasteful to have a single unit for the transmit and receive sections as 2 must be used hence the requirement in future for separate units. FEXT measurements can be time consuming because of the need to remove transmit signals from each pair in turn as they are measured at the other end. It is therefore envisaged that the DCA will be used in its barrage mode where the number of FEXT measurements to be made is substantial.

A pleasing practical result of the very large number of barrage tests now carried out is that the published planning rules appear to have been correctly determined.

Transverse-screen Cables

Although beyond the main subject of this paper another experience in using the test equipment may be of interest. This is in connection with the development of a new range of small pair-count (20, 40, 60 and 80 pairs) transverse-screen cables purpose designed for 100% digital fills. The assessment of prototype cables was carried out using the R92A tester using pair-to-pair and barrage measurements.

Once the electrical and physical parameters had been determined and specified early production cable was subjected to rigorous testing, again with the R92A tester. Agreements with manufacturers allowed type approval to be given to avoid the need for costly digital testing in the factory.

Several installed cables have subsequently been tested with either the R92A tester or the T63 barrage tester to confirm that performance is being maintained in production.

The way in which an attempt was made to optimise attenuation, NEXT and FEXT for the current (2 Mbit/s HDB3) UK regenerators can be seen in Figure 10.

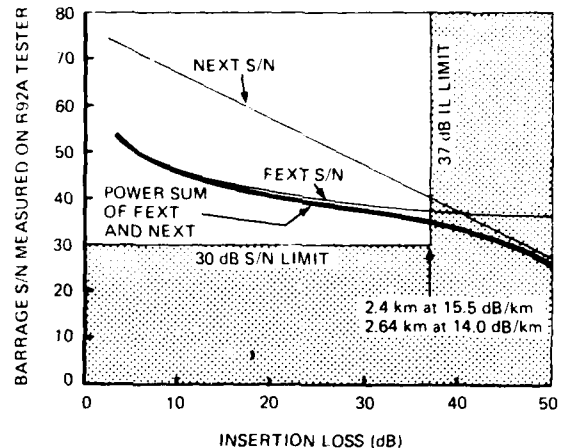


FIGURE 10 EVALUATION OF TRANSVERSE-SCREEN CABLE PERFORMANCE

The boundaries of performance are 37 dB insertion loss and 30 dB signal-to-barrage noise ratio measured on the R92A tester. (The latter figure is determined in the laboratory.) The graph shows the worst case readings from a sample of early production 80-pair cable. The optimum economic/technical performance would appear to be for the total barrage noise (NEXT plus FEXT) to pass through the intersect of the limits. Practical considerations, however, dictate that performance on the "safe" side of the limits is desirable and in practice regenerator sections have been restricted to the 2.0-2.2 km (1½ miles) range to allow trouble-free performance with simple installation techniques.

Conclusion

Administrations and Telcos throughout the world are now committed to extensive programs of digitalization. Maximising the use of existing cables, and hence investment, is a common preoccupation. This paper has described the problems and solutions from a British point-of-view with particular emphasis on field testers. The Digital Crosstalk Analyser is a powerful tester for characterising cable performance, debugging problem-cables and determining optimum system fills in particular cables. Its features are thought not to be available commercially elsewhere. Barrage

testers are simpler and cheaper and because of this have wider application for pre-commissioning tests. The latest British version incorporates the benefits of several years experience of earlier varieties.

Acknowledgements

Acknowledgement is made to the Director of the Transmission Department of British Telecom for permission to publish this paper.

References

- 1 HALL, R D and WHETTER, J. The Application of 2 Mbit/s Digital Line Systems to Symmetric Pair Cables. 2nd International Conference on Telecommunications Transmission, London, March 1981.
- 2 CATCHPOLE, R J and DYKE, P J. Design and Assessment of Primary PCM Line Repeaters. 2nd International Conference on Telecommunications Transmission, London, March 1981.
- 3 BORLEY, D. Digital Crosstalk Measurement. Electronics and Power, p737, September 1980.



Mr Dufour is Head of the Junction Plant Group in the Transmission Department of British Telecom Headquarters. He is responsible for plant used to provide transmission in the junction network and identifies the need for, sponsors the development of, and provides field implementation instructions for new items. The plant includes cables, transmission equipment and testers. He is a Chartered Engineer and a Member of the Institution of Electronic and Radio Engineers

I G Dufour
British Telecom, NE/T8.3.1
Lutyens House
Finsbury Circus
LONDON
EC2M 7LY

Tel: 01-357 4804

APPENDIX

TECHNICAL SPECIFICATION OF DIGITAL CROSSTALK ANALYSER

NUMBER OF PORTS

144 bidirectional

TRANSMITTED SIGNAL

2¹⁵-1 prbs and "all 1's"

CODING

HDB3

CLOCK FREQUENCY

2048 kHz and 1536 kHz or 1544 kHz

OPERATING MODES

Plesiochronous or synchronous

STATUS INDICATION

System status indicated by LEDs

Communications

Controller to local Plinth

Remote to local Plinth Operating frequency

Supply rails

OUTPUT DISPLAY

Dependent on desk top computer used (eg VDU, LED display, printer)

SIGNAL PROCESSING

Equalisation by regenerator input stage Range 5-37 dB at 1024 kHz

CONTROL SYSTEM

Overall system control by desk top computer.
Plinth Unit measurement functions controlled by microprocessor

OUTPUT LEVEL

6V pk-pk into 120 ohm

MINIMUM MEASURABLE CROSSTALK

-105 dB relative to transmitted signal

MEASUREMENT REPEATABILITY

± 1.5 dB

TERMINATION IMPEDANCE

120 ohm nominal input port

MEASUREMENT CAPABILITY

NEXT)Controller)
3rd cct XT)and)Controller
Impulsive Noise)1 Plinth)and
FEXT)2 Plinths
Insertion Loss)
Error Ratio)

SYSTEM SELF CHECK

Microprocessor system self test. Internal amplifier and regenerator gain calibration.

Cable connection integrity check. Signal source amplitude check.

OPERATION

Single measurement or pre-programmed measurement sequences under software control.

SYSTEM CONTROLLER TO PLINTH UNIT CONNECTION

Multipair umbilical 10 metres maximum length

PLINTH TO REGENERATOR HOUSING CONNECTORS OR CABLE PAIRS

Direct to UK Case Repeater No. 1A (connectors Plessey 74/10/1951/10 or McMurdo 700/3453/19) or via suitable test leads.

SOFTWARE

Controller

Overall system control

Data recording and analysis

Plinth Unit

Basic crosstalk measurement

Signal in/out control

Common measurement sequences

TEMPERATURE RANGE

Working -5°C to + 40°C

Storage -15°C to + 50°C

(Meets BS 2011 parts Ad and Ca)

POWER SUPPLIES

105, 115, 125, 220, 240 Volts AC

+10%, -15% 45-65 Hz

PLINTH UNIT

Size

Width 560 mm

Height 250 mm

Length 300 mm

Weight

22 kg

OPEN-CIRCUIT ADMITTANCE OF A TELEPHONE CABLE PAIR

J. A. Olszewski

R. J. Gerdes

General Cable International, Inc.
Edison, New Jersey

Continental Telephone Laboratories
Norcross, Georgia

Abstract

A simple delta form of open-circuit admittance diagram, representing a pair in a multi-pair telephone cable, has served well for many years both cable designers and cable users. Recent interest, however, in the mechanism of water entry into filled cable cores, has shown inadequacies of this diagram inasmuch as it could not pass the basic examination of a limiting case capacitances presented by water flooding of the cable core. Furthermore, this commonly accepted diagram cannot explain an apparent anomaly of a negative dissipation factor obtained from measurement of open-circuit wire-to-wire admittance of a moisture logged cable.

This paper proposes modifications of the pertinent open-circuit admittance components and shows that the modified circuit passes all the critical examinations, including explanation of the measured negative dissipation factor of the wire-to-wire branch.

Introduction

The commonly accepted simple delta form of open-circuit admittance (Y) or impedance ($Z = 1/Y$) diagram of a pair in a multi-pair telephone cable, namely TR-RG-GT, is shown in Fig. 1. It is apparently altered by moisture entry into the cable core so that it cannot pass the examination of the limiting case admittances or capacitances resulting from a complete cable core flooding condition.

Simple modification of this diagram, recognizing partial values due to the insulation and the cable core space medium, see Fig. 2, do not alleviate the problem, since it is readily apparent from Fig. 2 that upon water flooding, partials representing cable core space medium impedances tend to zero or the corresponding admittances tend to infinity. Thus, speaking in terms of capacitances, the use of the diagram of Fig. 2, will yield the following limiting capacitances at full water saturation of the cable core:

a) Wire-to-Wire

As $C_{gs} \rightarrow \infty$, wire-to-wire capacitance C_d will have to tend to $C_{di}/2$.

b) Wire-to-Ground

As $C_{gs} \rightarrow \infty$, wire-to-ground capacitance chain C_g will have to tend towards the value represented by C_{gi} in series with C_{gp} , or $C_g \rightarrow C_{gi}C_{gp}/(C_{gi} + C_{gp})$

c) Mutual

It follows from (a) and (b) that the mutual capacitance

$$C_m \rightarrow \frac{C_{di} + \frac{C_{gi}C_{gp}}{C_{gi} + C_{gp}}}{2}$$

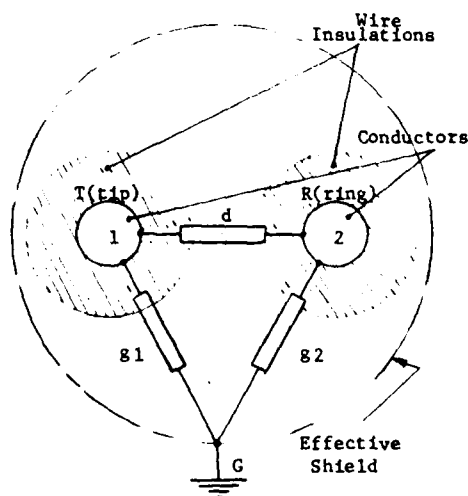


Fig. 1

In reality, however, it has been practically established by many experimenters^{(1),(2),(3)}, that with the water flooding of the cable core, wire-to-wire series capacitance chain C_d tends to zero, wire-to-ground series capacitances C_g tend to self capacitance C_s , or $C_{di} + C_{gi}$ per Fig. 2, while the mutual capacitance C_m , at full water saturation, becomes $C_s/2$.

It is clear therefore, that at the limiting conditions of complete cable core water flooding, the

simple delta diagrams of Fig. 1 or Fig. 2, do not reflect experimentally determined facts.

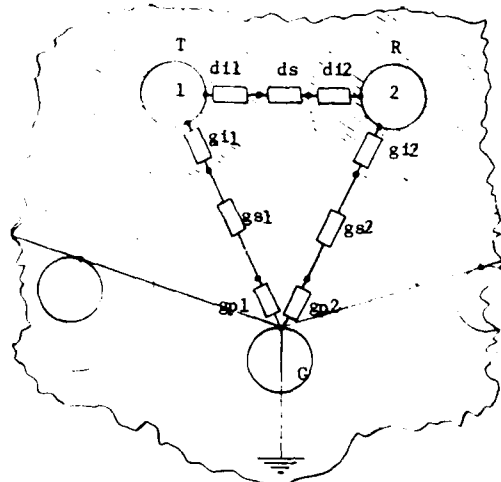


Fig. 2

Currently used delta diagram does not pass another critical examination. The experimenters have observed⁽⁴⁾ that the measured dissipation factor of the wire-to-wire chain Cd in the filled cables becomes negative upon moisture entry and increases in the negative direction with continued exposure of cable core to water, see Table 1. The same, seemingly odd, result is obtained by direct measurement of Cd using balanced bridges and through calculations from measured tip to ground, ring to ground, and tip plus ring to ground capacitances using unbalanced bridges. Referring back to Fig. 2, it is clear that water entry will increase both the capacitance and the dissipation factor constituting the admittance Yds. However, there is no apparent way that the latter can cause the dissipation factor of the series wire-to-wire chain to become negative.

All of the above observations point to the inadequacy of the currently accepted simple delta open-circuit diagram of a pair in a telephone cable.

Proposed Circuit and its General Analysis

The experimental results, see Table 1, and their preliminary discussion under "Introduction" point to the necessity of modification of currently used open-circuit pair diagram. It is proposed that this required modification can be represented by the addition of the branches AO, BO and CO, as shown in Fig. 3.

Table 1

1 kHz Capacitances and Dissipation Factors of Filled Cable in Water Immersion Tests at Room Temperature

Immersion Time, Days	Wire-to-Ground		Wire-to-Wire		Mutual	
	C, pF	tan δ	C, pF	tan δ	C, pF	tan δ
0	715.09	.00046	212.26	-.00023	569.81	.00025
47	733.20	.00225	208.24	-.00267	574.84	.00095
194	715.87	.00304	203.69	-.00539	579.63	.00103
607	778.74	.00451	195.77	-.00946	585.14	.00142
1290	793.82	.00682	192.58	-.01316	589.49	.00244

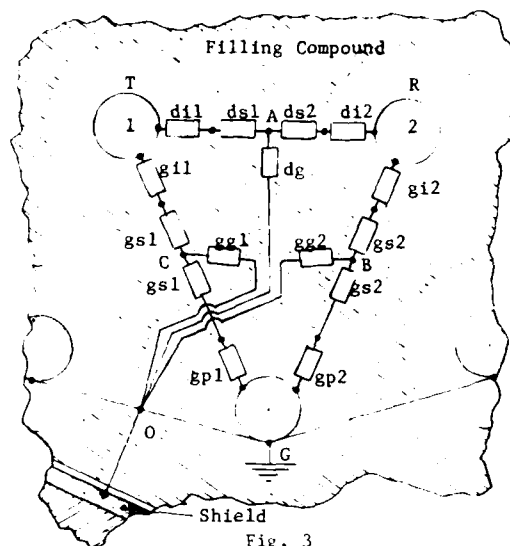


Fig. 3

Throughout this paper, the capacitance unbalance to ground is not considered since normal paired telephone cables have better than 1% balance. Thus, the admittance or the impedances shown in Fig. 1, for simplicity of subject analysis, were taken as

$$\begin{aligned} d_{11} &= d_{12} = d_i \\ d_{11} &= d_{s2} = d_s \\ g_{i1} &= g_{i2} = g_i \\ g_{s1} &= g_{s2} = g_s \\ g_{p1} &= g_{p2} = g_p \\ \text{and} \quad g_{g1} &= g_{g2} = g_g \end{aligned}$$

Thus, working for convenience with impedances, it can be seen that the proposed modified diagram of Fig. 3 can be reduced to that of Fig. 4 below.

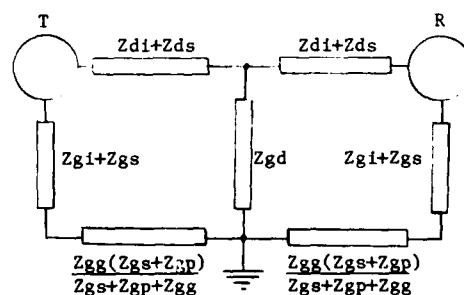


Fig. 4

It should be noted at this time that normally three admittances of a pair are determined by measurements at 1000 Hz (electrically short lines), i.e. Y1, of tip wire to ground G, Y2 of ring wire R to ground and Y3 admittance is measured with T and R wires together and ground G. Measured complex quantities are then used to determine the capacitance of interest, namely, wire-to-ground admittance Yg or the

capacitance chain C_g , wire-to-wire admittance Y_d or the capacitance chain C_d , and the mutual capacitance C_m or Y_m , i.e.

$$C_g = \frac{Y_s}{2} \quad (1)$$

$$C_d = \frac{Y_1 + Y_2 - Y_3}{2} \approx \frac{2Y_1 - Y_3}{2} \quad (2)$$

and

$$C_m = \frac{2Y_1 + 2Y_2 - Y_3}{4} \approx \frac{4Y_1 - Y_3}{4} \quad (3)$$

Measured real components are similarly treated to permit derivation of wire-to-ground, wire-to-wire and mutual conductances G_g , G_d and G_m respectively, namely

$$G_g = \frac{R_{Y3}}{2} \quad (4)$$

$$G_d \approx \frac{2R_{Y1} - R_{Y3}}{2} \quad (5)$$

and

$$G_m \approx \frac{4R_{Y1} - R_{Y3}}{4} \quad (6)$$

The validity of equations (2), (3), (5) and (6) is confirmed by the direct measurements of C_d , C_m , G_d and G_m using balanced measuring equipment.

Returning now to the circuit of Fig. 4, it can be seen that its wire-to-ground impedance, or Z_1 , is obtained when either tip T terminal or ring R terminal is taken to ground. Similarly, Z_3 impedance is that between terminal T and R shorted and the ground terminal G. It should be realized that $Z_1 = 1/Y_1$, while $Z_3 = 1/Y_3$.

Thus, since impedance $Z_1 \approx Z_2$, their circuit can be represented as shown in Fig. 5.

R or T

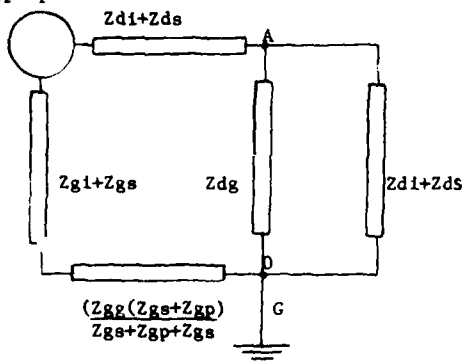


Fig. 5

and its value is

$$Z_1 \approx Z_2 = \frac{\left[Z_{di} + Z_{ds} + \frac{Z_{dg}(Z_{di} + Z_{ds})}{Z_{di} + Z_{ds} + Z_{dg}} \right] \left[Z_{gi} + Z_{gs} + \frac{Z_{gg}(Z_{gs} + Z_{gp})}{Z_{gs} + Z_{gp} + Z_{gg}} \right]}{Z_{di} + Z_{ds} + \frac{Z_{dg}(Z_{di} + Z_{ds})}{Z_{di} + Z_{ds} + Z_{dg}} + Z_{gi} + Z_{gs} + \frac{Z_{gg}(Z_{gs} + Z_{gp})}{Z_{gs} + Z_{gp} + Z_{gg}}} \quad (7)$$

Similarly, it can be shown that the pair-to-ground impedance diagram can be reduced to that shown in Fig. 6.

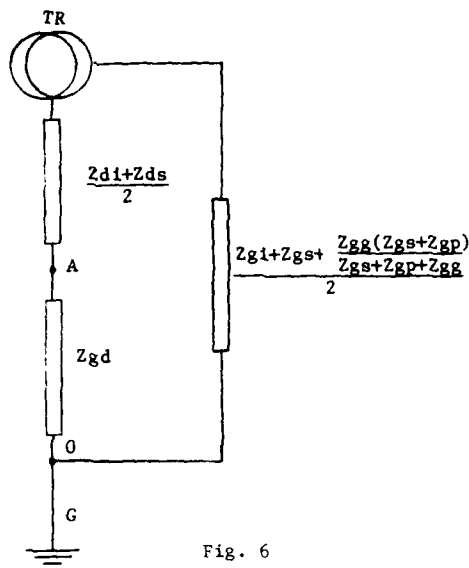


Fig. 6

while TR-AO impedance (Z_3) is

$$Z_3 = \frac{\left[Z_{di} + Z_{ds} + 2Z_{dg} \right] \left[Z_{gi} + Z_{gs} + \frac{Z_{gg}(Z_{gs} + Z_{gp})}{Z_{gs} + Z_{gp} + Z_{gg}} \right]}{2 \left[Z_{di} + Z_{ds} + 2Z_{dg} + Z_{gi} + Z_{gs} + \frac{Z_{gg}(Z_{gs} + Z_{gp})}{Z_{gs} + Z_{gp} + Z_{gg}} \right]} \quad (8)$$

Thus, it follows from equations (1), (2), (3), (7) and (8) that the open-circuit admittances of interest for the proposed diagram, i.e. Y_g , Y_d and Y_m , are as follows:

$$Y_g = \frac{Y_3}{2} = \frac{1}{2Z_3}$$

$$= \frac{Z_{di} + Z_{ds} + 2Z_{dg} + Z_{gi} + Z_{gs} + \frac{Z_{gg}(Z_{gs} + Z_{gp})}{Z_{gs} + Z_{gp} + Z_{gg}}}{Z_{di} + Z_{ds} + 2Z_{dg} + Z_{gi} + Z_{gs} + \frac{Z_{gg}(Z_{gs} + Z_{gp})}{Z_{gs} + Z_{gp} + Z_{gg}}} \quad (9)$$

$$= \frac{Z_{gs} + Z_{gp} + Z_{gg}}{(Z_{gi} + Z_{gs})(Z_{gs} + Z_{gp} + Z_{gg}) + Z_{gg}(Z_{gs} + Z_{gp})} + \frac{1}{Z_{di} + Z_{ds} + 2Z_{dg}}$$

$$\text{while } Y_d = \frac{Y_1 - Y_3}{2}$$

$$= \frac{Z_{dg}}{(Z_{di} + Z_{ds})(Z_{di} + Z_{ds} + 2Z_{dg})} \quad (10)$$

and consequently, under assumed pair balance conditions, the mutual admittance Y_m can be expressed as

$$Y_m = Y_d + Y_g$$

$$= 1/2 \left[\frac{Z_{gs} + Z_{gp} + Z_{gg}}{(Z_{gi} + Z_{gs})(Z_{gs} + Z_{gp} + Z_{gg}) + Z_{gg}(Z_{gs} + Z_{gp})} + \frac{1}{Z_{di} + Z_{ds}} \right] \quad (11)$$

Examination of equations (9), (10) and (11) shows that while Y_g and Y_d are a function of impedance Z_{gd} , the mutual admittance Y_m is not. This implies no current flow through Z_{dg} when mutual admittance is measured directly. Consequently, the mutual

impedance or admittance can also be calculated directly from the circuit shown in Fig. 4 when the value of Z_{dg} is assumed to be infinity, or an open-circuit. Examination of Figs. 3 and 4 indicates that the above conclusion is correct, since the application of +E to tip and -E potential to ring conductors or vice versa, has to result in zero potential at point A. Therefore, with point G also at zero potential, there is no current flow through Z_{dg} .

The primary interest equation (9), (10) and (11) contain seven unknowns, i.e. Z_{di} , Z_{ds} , Z_{dg} , Z_{gi} , Z_{gp} and Z_{gg} , but only four equations can be set up. These equations express Z_1 , Z_3 , Z_d and Z_m in terms of listed unknown partial impedances. Therefore, the individual partial impedances of a particular cable design cannot be determined. Bringing in engineering approximations, or assumptions, will allow setting up of additional required three equations, but all assumptions appear to be too risky for the subject study. This is particularly so because of implied study of changes with time. The electric field distribution with time of cable immersion in water is expected to change significantly and so will the measured values of impedances or admittances.

Limiting Capacitances with Water Flooding

With water flooding of the cable core, impedances Z_{ds} , Z_{dg} , Z_{gs} and Z_{gg} can be assumed to be practically equal to zero. Thus, general admittance equations (9), (10) and (11) of the proposed circuit reduce as follows:

$$Y_g = \frac{Z_{di} + Z_{gi}}{Z_{di} Z_{gi}} = Y_{di} + Y_{gi} \quad (9a)$$

which is equivalent to self-capacitance of the insulated wire.

$$Y_d = 0 \quad (10a)$$

while

$$Y_m = \frac{1}{2} \left(\frac{1}{Z_{gi}} + \frac{1}{Z_{di}} \right) = \frac{Y_{di} + Y_{gi}}{2} \quad (11a)$$

which, under assumptions made in this study, is equivalent to half value of self-capacitance.

Thus, the above shows that the admittances of the proposed circuit of Fig. 3 reduce to the experimentally established values under the limiting condition of complete water flooding of the telephone cable core.

Negative Conductance (Dissipation Factor) of Wire-to-Wire Admittance

The admittance studies of the cable pairs are normally conducted on electrically short lines and

therefore, equation (2), expressing the value of wire-to-wire admittance $Y_d = G_d + j\omega C_d$, is valid and is of particular interest. The special interest stems from the observation that its measured dissipation factor becomes negative soon after the filled cable sample with perforated sheath is immersed in water.

Referring back to the circuit diagram of Fig. 3 and equation (10), it is clear that Y_d is not represented by the series chain TR since in such a case its value would have been independent of Z_{dg} and would have been equal to $1/2 (Z_{di} + Z_{ds})$. Furthermore, the proposed diagram implies no direct wire-to-wire impedance or admittance and that in fact the link is a T-network, TR-AO. Equation (10) indicates that mathematically, the direct wire-to-wire admittance is a TR branch of an equivalent Δ -network transformed from the TR-AO T-network. The admittance transformation relationship in accordance with Fig. 3 is

$$TR_L = TA_T / (2TA_T + AO_T) = \frac{Z_{dg}}{(Z_{di} + Z_{ds})(Z_{di} + Z_{ds} + 2Z_{dg})}$$

Concentrating on Y_d , it follows that

$$Y_d = \left(\frac{Y_{di} Y_{ds}}{Y_{di} + Y_{ds}} \right)^{1/2} \left(\frac{2 Y_{di} Y_{ds}}{Y_{di} + Y_{ds}} + Y_{dg} \right) = \frac{Y_{di} Y_{ds}}{2 (Y_{di} + Y_{ds} + Y_{dg}) + \left(\frac{Y_{di}}{Y_{ds}} + \frac{Y_{ds}}{Y_{di}} \right) Y_{dg}} \quad (13)$$

Water entry into the filled cable core can be expected to increase real and imaginary parts of Y_{ds} and Y_{dg} , while Y_{di} , which is the admittance due to conductor insulation, can be assumed to have negligible or zero conductance in comparison with water affected Y_{ds} and Y_{dg} components. Thus, for electrically short cable pairs, the partial admittances can be expressed as

$$\begin{aligned} Y_{di} &= j\omega C_{di} \\ Y_{ds} &= G_{ds} + j\omega C_{ds} \\ Y_{dg} &= G_{dg} + j\omega C_{dg} \end{aligned} \quad \text{and} \quad Y_d = G_d + j\omega C_d$$

and equation (13) can be rewritten as follows:

$$Y_d = \frac{w^3 C_{di}^2 C_{ds}^2 - w G_{ds}^2 C_{di}^2}{w^2 (A+B)^2 + (G_{ds} C' - w^2 D)^2} - \frac{jw^2 2 G_{ds} C_{di}^2 C_{ds} [w(A+B) - j(G_{ds} C' - w^2 D)]}{w^2 (A+B)^2 + (G_{ds} C' - w^2 D)^2} \quad (14)$$

$$\text{where } A = \frac{G_{ds}^2 C_{dg}}{w^2}$$

$$\begin{aligned} B &= 2 G_{ds} C_{di} (C_{di} + 2 C_{ds} + C_{dg}) \\ &\quad - G_{dg} (C_{di}^2 + 2 C_{di} C_{ds} + C_{ds}^2) \\ &\quad - 2 G_{ds} C_{ds} C_{dg} \end{aligned}$$

$$C' = 2 Gds Cdi + Gds Cdg + 2 Cdg Cdi + 2 Gdg Cds$$

and

$$D = 2 Cdi^2 Cds + 2 Cdi Cds^2 + 2 Cdi Cds Cdg + Cdi^2 Cdg + Cds^2 Cdg$$

Expansion of the above shows that all G and C product terms in the numerator are 7th power while w component of each term varies in power from 1 to 5.

Since the conductance

$$G = wC \tan \delta \quad (15)$$

and the test frequency is normally 1000 Hz, while $\tan \delta$ of filled space medium in early stages of cable water immersion testing can be taken as 0.001 or less, then $w \tan \delta \ll 1$, or G is roughly of the same order of magnitude as C, and therefore, only the terms with highest power of w have practical significance. Thus, using the latter simplification, and also separating real and imaginary parts

$$Cd = \frac{w^4 Cdi^2 Cds^2}{w^2 (A+B)^2 + (Gds C' - w^2 D)^2} \\ (2 Cdi^2 Cds + 2 Cdi Cds^2 + 2 Cdi Cds Cdg + Cdi^2 Cdg + Cds^2 Cdg) \\ w^2 (A+B)^2 + (Gds C' - w^2 D)^2 \quad (16)$$

$$Gd = \frac{2w^4 Gds Cdi^3 Cds (Cdi Cds + Cds Cdg + Cdi Cdg)}{w^2 (A+B)^2 + (Gds C' - w^2 D)^2} \\ - \frac{w^4 Cdg Cdi^2 Cds^2 (Cdi + Cds)^2}{w^2 (A+B)^2 + (Gds C' - w^2 D)^2} \quad (17)$$

while, since $Gd = wCd \tan \delta_d$

$$\tan \delta_d = \frac{2Gds Cdi^3 Cds (Cdi Cds + Cds Cdg + Cdi Cdg)}{w Cdi^2 Cds^2 E} \\ - \frac{Cdg Cdi^2 Cds^2 (Cdi^2 + 2 Cdi Cds + Cds^2)}{Cdi^2 Cds^2 E} \quad (18)$$

$$\text{where } E = (2 Cdi^2 Cds + 2 Cdi Cds^2 + Cdi Cds Cdg + Cdi^2 Cdg + Cds^2 Cdg)$$

Equation (18), giving the loss tangent of the wire-to-wire capacitance Cd, is relatively complex and difficult to examine. It is clear though, that $\tan \delta_d$ will be negative if

$$2w \tan \delta_{dg} > \tan \delta_{ds} Cdi^3 Cds^2 (Cdi Cds + Cds Cdg + Cdi Cdg) \\ - w \tan \delta_{dg} Cdi^2 Cds^2 Cdg (Cdi + Cds)^2 < 0 \quad (19)$$

or

$$\tan \delta_{dg} > \tan \delta_{ds} \frac{2 Cdi (Cdi Cds + Cds Cdg + Cdi Cdg)}{Cdg (Cdi + Cds)^2} \quad (20)$$

It is assumed that at any time $\tan \delta_{dg} \approx \tan \delta_{ds}$, both values being characteristic of the filled space medium surrounding any given pair, and since initially, i.e. prior to cable immersion in water, $\tan \delta_d \approx 0$, therefore, also initially

$$\frac{2 Cdi (Cdi Cds + Cds Cdg + Cdi Cdg)}{Cdg (Cdi + Cds)^2} \approx 1 \quad (21)$$

but decreases with time of immersion to a value < 1 . Therefore, it follows from (21) that initially

$$Cdg \approx \frac{2 Cdi^2 Cds}{Cds^2 - Cdi^2} \quad (22)$$

and with time of immersion in water, when the dissipation factor $\tan \delta_d$ becomes negative, the value of capacitance Cdg becomes as shown below

$$Cdg > \frac{2 Cds}{\frac{Cds^2}{Cdi^2} - 1} \quad (23)$$

It is certain that Cds/Cdi ratio, and specially its square, increases rapidly with the longitudinal as well as transverse moisture ingress into the cable core. With time of immersion Cds has to increase primarily due to increase in SIC of filled space, while changes in electric field distribution result in decrease of Cdi. The latter causes the RHS of the inequality (23) to diminish in magnitude. Since Cdg also has to increase with moisture entry, the established constraints of the inequality are quickly satisfied. Of course, it is readily apparent that the value of the square of Cds/Cdi ratio is always greater than unity, since otherwise Cdg would be negative and this is a physical impossibility. Any further elaborations are judged to be potentially risky without the work of the field mapping.

Conclusions

1. New proposed open-circuit admittance diagram of a pair in the multi-pair telephone cable passes all the examinations including limiting case of complete water flooding of the cable core.
2. Negative $\tan \delta_d$ obtained in measurements is provable mathematically per assumed admittance diagram. It does not imply power generation or that the cable is an active device.
3. Negative $\tan \delta_d$ can occur only if $\tan \delta_{dg}$ is finite and positive. Conditions for this phenomenon were determined mathematically, and appear to be independent of the test frequency.
4. The petrolatum based filling compounds with high immunity to water ingress will show negative $\tan \delta_d$ by measurement only after prolonged time of immersion in water. Time to change from positive to negative value is proportional to filled cable immunity to water.

References

- (1) G.S. Eager, L. Jachimowicz, I. Kolodny and D.E. Robinson, "Transmission Properties of Polyethylene-Insulated Telephone Cables at Voice and Carrier Frequencies", AIEE Paper 59-778, 1959.
- (2) S. Verne, A.A. Pinching and M.R. Hagger, "Long-Term Stability of Fully-Filled Cables", 22nd International Wire & Cable Symposium, Atlantic City, N.J., 1972.
- (3) J.A. Olszewski, "Capacitance Relationships in Filled Telephone Cables and Equilibrium Predictions from Water Immersion Tests", 24th International Wire & Cable Symposium, Cherry Hill, N.J., 1975.
- (4) J.A. Olszewski, "Immunity to Water of Foam, Foam-Skin and Solid Insulated Filled Telephone Cables", 26th International Wire & Cable Symposium, Atlantic City, N.J., 1973.

AD P000555

TELECOMMUNICATION CABLES AND POWER FREQUENCY INDUCTION

Gustav Adolf Pettersson

Arne Ernbo

Retired from SWEDISH ADMINISTRATION OF
TELECOMMUNICATIONS

SIEVERTS KABELVERK
SUNDBYBERG SWEDEN

Abstract

In this paper the following aspects are treated

a) the necessity to pay attention to the earthing conditions of cable sheaths or screening wires when calculations are made concerning

→ the current in these conductors caused by induction from power lines

→ the electromotive force (emf) from induction in telecommunication circuits

→ the screening factor due to compensating effects from sheaths and screening wires

Formulae are derived in the general case when a sheath or a screening wire is terminated to earth by arbitrary impedances. For some special terminating impedances the formulae are arranged for practical use.

b) calculation of the screening factor of armoured cables, where the longitudinal impedance is not constant along the cable

c) calculation of the resulting screening factor from more than one screening wire

d) measurements in the field of propagation properties of cable sheaths or screening wires

e) wave propagation along two screening conductors

The mathematical treatment of this problem is not difficult. The numerical calculation is, however, rather complex.

Notations used

Index 1 is used for the inducing line

Index 2 is used for the cable sheath or the screening wire

Index 6 is used for the exposed telecommunication circuit

E_6 induced emf without screening, V

E_{62} induced emf with screening, V

e_2 field strength at the position of conductor 2, V/km

k_r, k_{rc} screening factors, i.e. E_{62}/E_6

i_1 inducing current, constant along the line, A

i_2 current in conductor 2, A

$z_2 = r_2 + jx_2$, longitudinal impedance, ohm/km

r_2 longitudinal resistance, ohm/km

Note:

$$r_2 = r_{2i} + \pi^2 f 10^{-4} + r_{2Fe} \text{ ohm/km}$$

$$\pi^2 f = 500 \text{ at } 50 \text{ Hz}$$

r_{2i} dc resistance, ohm/km

r_{2Fe} additional resistance due to losses in the armouring, ohm/km

$x_2 = x_{2i} + x_{2y}$, longitudinal reactance, ohm/km

x_{2i} = intrinsic reactance, ohm/km

Note:

$$x_{2i} = \mu_2 \cdot 2\pi f \cdot 0.05 \cdot 10^{-3} \text{ ohm/km}$$

If there is no armouring or if in the armoured case $i_2 = 0$ the relative permeability is 1.0 and at 50 Hz thus

$$x_{2i} = 0.0157 \text{ ohm/km}$$

x_{2y} extrinsic reactance, ohm/km

Note:

$$x_{2y} = 2\pi f (26.8 + \ln \frac{\rho}{r_2}) \cdot 10^{-4} \text{ ohm/km}$$

At 50 Hz

$$x_{2y} = 314 (22.9 + \ln \frac{\rho}{r_2}) 10^{-4} \text{ ohm/km}$$

μ_2 relative permeability

Note:

$$\mu_2 = \frac{x_2 - x_{2y}}{2\pi f \cdot 0.05} 10^3$$

At 50 Hz

$$\mu_2 = \frac{x_2 - x_{2y}}{15.7} \cdot 10^3$$

f frequency, Hz
 ρ resistivity of earth, ohm.m
r radius of conductor 2, mm
 γ_2 leakance to earth, ohm/km
 γ_2 propagation constant

Note:

$$\gamma_2 = \sqrt{(r_2 + jx_2) \gamma_2}$$

Z_2 characteristic impedance, ohm

Note:

$$Z_2 = \sqrt{\frac{r_2 + jx_2}{\gamma_2}}$$

z_{12} mutual impedance, ohm/km

z_{16} mutual impedance, ohm/km

z_{26} mutual impedance, ohm/km

L_2 length of conductor 2, km

L_6 length of conductor 6, km

0, x, a, b, L_2 coordinates along conductor 2, km

Z_{20} terminating impedance to earth for conductor 2 at $x = 0$

Z_{L_2} terminating impedance to earth for conductor 2 at $x = L_2$

Note:

In the chapter "Screening wires" some other notations are used.

Basic formulae

The current in a power line, especially under earth fault conditions, induces in an adjacent telecommunication line an emf, proportional to the current and to the mutual impedance. The current also causes a current in conductors, cable sheaths or screening wires in contact with earth. This latter current in its turn induces an emf in the telecommunication line. If it is assumed that the inducing line, the earthed conductor and the telecommunication line are parallel and that the compensation conductor is in very good contact with earth or directly earthed at its two ends, the following equations are valid (see fig 1).

$$0 = i_1 z_{12} + i_2 z_2$$

$$E_{62} = i_1 z_{16} L_2 - \frac{i_1 z_{12} z_{26}}{z_2} L_2$$

As seen from the equations, it is also assumed that the conductors 2 and 6 are of the same length L_2 .

If $z_{12} = z_{16}$ and the conductor 2 is in a position near the telecommunication line, the induced emf is

$$E_{62} = i_1 z_{16} L_2 \left(1 - \frac{z_{26}}{z_2}\right)$$

If there is no screening effect

$$E_6 = i_1 z_{16} L_2$$

The screening factor is

$$k_r = \frac{E_{62}}{E_6} = 1 - \frac{z_{26}}{z_2}$$

If conductor 2 is a cable sheath

$$k_r = \frac{r_{2i}}{z_2}$$

$$\text{i.e. } z_{26} = z_2 - r_{2i}$$

However, it is not permitted under all circumstances to make the above introduced assumptions concerning the contact between the screening conductor and earth. If the screening conductor is relatively short and when the earth resistivity is high, the calculations must be carried out in a way that takes the finite leakance into consideration.

The following system of equations is then used for the determination of the current i_2 .

$$-\frac{dv_2}{dx} = i_2 z_2 + i_1 z_{12}$$

$$-\frac{di_2}{dx} = v_2 \gamma_2$$

v_2 is the potential of conductor 2.

The solution of the differential equation system above is

$$i_2 = A e^{\gamma_2 x} + B e^{-\gamma_2 x} - \frac{z_{12} i_1}{z_2}$$

$$v_2 = -Z_2 (A e^{\gamma_2 x} - B e^{-\gamma_2 x})$$

The constants A and B are determined from the earth connexion conditions at the ends $x=0$ and $x=L_2$. The expression for i_2 in the general case, when the terminating impedances are Z_0 and Z_{L_2} respectively is

$$i_{2x} = -\frac{i_1 z_{12}}{z_2} \left(1 - \frac{\Delta_1}{\Delta} e^{\gamma_2 x} - \frac{\Delta_2}{\Delta} e^{-\gamma_2 x}\right)$$

where

$$\Delta = (Z_0 - Z_2)(Z_{L_2} - Z_2) e^{\gamma_2 L_2} - (Z_{L_2} + Z_2)(Z_0 + Z_2) e^{-\gamma_2 L_2}$$

$$\Delta_1 = Z_0 (Z_{L_2} - Z_2) e^{-\gamma_2 L_2} - Z_{L_2} (Z_0 + Z_2)$$

$$\Delta_2 = Z_{L_2} (Z_0 - Z_2) - Z_0 (Z_{L_2} + Z_2) e^{\gamma_2 L_2}$$

The emf induced by the current i_{2x} into the telecommunication circuit is

$$E_{6i_2} = z_{26} \int_0^{L_2} i_{2x} dx$$

Table 1 shows for the cases indicated below expressions for i_{2x} and E_{6i_2}

Case 1 $z_0 = 0 \quad z_{L_2} = \infty$

Case 2 $z_0 = \infty \quad z_{L_2} = \infty$

Case 3 $z_0 = z_2 \quad z_{L_2} = \infty$

Case 4 $z_0 = z_2 \quad z_{L_2} = z_2$

Case 5 $z_0 = z_2 \quad z_{L_2} = 0$

Case 6 $z_0 = 0 \quad z_{L_2} = 0$

For other cases the general formulae for i_{2x} and E_{6i_2} can be used.

The total induction from line 1 and conductor 2 in the telecommunication circuit, the induction being expressed as an emf, is

$$E_{62} = E_6 + E_{6i_2}$$

If the screening conductor and the exposed line have the same length the screening factor can be written as follows in the six cases.

Case 1

$$k_{rc} = k_r + \frac{z_{26}}{z_2 \gamma_2 L_2} \operatorname{tgh} \gamma_2 L_2$$

Case 2

$$k_{rc} = k_r + \frac{z_{26}}{z_2 \gamma_2 L_2} \operatorname{tgh} \frac{\gamma_2 L_2}{2}$$

Case 3

$$k_{rc} = k_r + \frac{z_{26}}{z_2 \gamma_2 L_2} \left[e^{-\gamma_2 L_2} (\cosh \gamma_2 L_2 - 2) + 1 \right]$$

Case 4

$$k_{rc} = k_r + \frac{z_{26}}{z_2 \gamma_2 L_2} (1 - e^{-\gamma_2 L_2})$$

Case 5

$$k_{rc} = k_r + \frac{z_{26}}{2 z_2 \gamma_2 L_2} (1 - e^{-\gamma_2 L_2})$$

Case 6

$$k_{rc} = k_r$$

Table 1

Case 1

$$i_{2x} = - \frac{i_1 z_{12}}{z_2} \left(1 - \frac{\cosh \gamma_2 x}{\cosh \gamma_2 L_2} \right)$$

$$E_{6i_2} = - \frac{i_1 z_{12} z_{26}}{z_2} \left(L_2 - \frac{1}{\gamma_2} \operatorname{tgh} \gamma_2 L_2 \right)$$

Case 2

$$i_{2x} = - \frac{i_1 z_{12}}{z_2} \left[1 - \frac{\sinh \gamma_2 x + \sinh \gamma_2 (L_2 - x)}{\sinh \gamma_2 L_2} \right]$$

$$E_{6i_2} = - \frac{i_1 z_{12} z_{26}}{z_2} \left(L_2 - \frac{2}{\gamma_2} \operatorname{tgh} \frac{\gamma_2 L_2}{2} \right)$$

Case 3

$$i_{2x} = - \frac{i_1 z_{12}}{z_2} \left[1 - e^{-\gamma_2 L_2} \sinh \gamma_2 (L_2 - x) - e^{-\gamma_2 (L_2 - x)} \right]$$

$$E_{6i_2} = - \frac{i_1 z_{12} z_{26}}{z_2} \left\{ L_2 - \frac{1}{\gamma_2} \left[e^{-\gamma_2 L_2} (\cosh \gamma_2 L_2 - 2) + 1 \right] \right\}$$

Case 4

$$i_{2x} = - \frac{i_1 z_{12}}{z_2} \left(1 - \frac{e^{-\gamma_2 L_2} e^{\gamma_2 x} + e^{-\gamma_2 x}}{2} \right)$$

$$E_{6i_2} = - \frac{i_1 z_{12} z_{26}}{z_2} \left(L_2 - \frac{1 - e^{-\gamma_2 L_2}}{\gamma_2} \right)$$

Case 5

$$i_{2x} = - \frac{i_1 z_{12}}{z_2} \left(1 - e^{-2\gamma_2 L_2} \frac{e^{\gamma_2 x} + e^{-\gamma_2 x}}{2} \right)$$

$$E_{6i_2} = - \frac{i_1 z_{12} z_{26}}{z_2} \left(L_2 - \frac{1 - e^{-\gamma_2 L_2}}{2 \gamma_2} \right)$$

Case 6

$$i_{2x} = - \frac{i_1 z_{12}}{z_2}$$

$$E_{6i_2} = - \frac{i_1 z_{12} z_{26}}{z_2} L_2$$

If the lengths L_2 and L_1 are not equal, the induced emf in the conductor 6 can be calculated by using the formulae under figure 2. The expressions for i_{2x} are given in the basic formulae.

Unarmoured cables

As an example a cable (type 1) with a diameter under lead of 57 mm and a lead thickness of 2.5 mm is chosen. The longitudinal resistance r_2 of the sheath is then 0.45 ohm/km and r_2 is 0.50 ohm/km. The longitudinal reactance is $x_2 = j 0.77$ ohm/km. The mutual impedance to the telecommunication circuit is $z_{26} = 0.05 + j 0.77$ ohm/km. The cable length is 10 km. The leakage values are chosen in the interval 0-1 mho/km. The propagation coefficient is

$$\gamma_2 = 0.22 + j 0.21 \text{ 1/km for } \gamma_2 = 0.1 \text{ mho/km.}$$

As seen from the first chapter of the paper the current i_{2x} can be written

$$i_{2x} = - \frac{i_1 z_{12}}{z_2} \cdot F(x)$$

For the Cases 1, 2, and 4 (mentioned before) the function $F(x)$ is calculated for $y_2 = 0.1$ mho/km. The result is found in figure 3.

The screening factor k_{rc} has been calculated for two cases (1 and 2) as a function of the leakage y_2 , when y_2 varies between 0 and 1 mho/km. The result is found in figure 4. A comparison with the k_r value shows that the ratio $k_{rc}:k_r$ in Case 1 has values between 2.05 and 1.14, while in Case 2 the corresponding values are 2.05 and 1.29 respectively.

It is fully evident that it is necessary to make the calculations of the screening effects in such a manner that the earthing conditions of the cable sheath are taken into consideration.

Armoured cables

The calculation of the screening factor for unarmoured cables is made under the assumption that the longitudinal impedance of the cable sheath is constant along the cable. For armoured cables which are so arranged that the current in the sheath is not constant the impedance varies as it depends on the current. This fact means a complication of the calculation. In this part of the paper we show how such a calculation can be fulfilled.

As an example we choose a cable with a lead sheath and armouring, which has a screening factor shown in figure 5. The diameter under lead is 16 mm and the thickness of the lead is 1.6 mm. The armouring consists of two tapes 20x0.5 mm. The cable type is designated 2 in this paper. The $r_2 x_2$ loop shown in figure 6 satisfies the k_r curve in figure 5. Figure 7 shows the dependence of r_2 and x_2 on the current i_2 , which varies with the field strength as indicated in figure 5. The calculation is made for two field strengths, 300 and 160 V/km. At the latter field strength k_r has its minimum. The cable length is supposed to be 5 km. The sheath is directly earthed at one end of the cable (coordinate $x=0$) and insulated from earth at the other end ($x=5$).

As a first step in the calculation procedure the current curve is derived as shown in the previous chapter for the following two cases with constant values of z_2 and a leakage $y_2 = 0.1$ mho/km.

e_2 V/km	z_2 ohm/km	$i_2 = F(x)$ A
300	4+j 5.5	Curve 1 figure 8
160	4+j 6.1	Curve 2 "-

The following currents and impedances are found

Co- ordi- nate x km	$e_2=300$ V/km		$e_2=160$ V/km	
	i_2 A	z_2 ohm/km	i_2 A	z_2 ohm/km
0.5	45	4+j 5.5	18.8	6.0+j 6.1
1.5	44	4+j 5.5	18.4	6.1+j 6.1
2.5	41	4.1+j 5.7	17.4	6.1+j 5.9
3.5	32	4.8+j 6.0	14.0	5.7+j 4.4
4.5	16	6.1+j 5.5	7.5	3.3+j 2.1

The cable is now divided in five elements each of 1 km length as indicated in figure 9.

The currents in the elements are derived by iterated current division and by use of the impedance values shown above. New curves are calculated and the result can be seen in figure 8, curves 3 and 4, and in the following two tables.

Field strength 300 V/km

Coordi- nate x km	i_2		z_{26} ohm/km
	i_{2Re} A	i_{2Im} A	
0.5	-28.2	j 34.3	1.75+j 5.5
1.5	-28.0	j 31.5	1.85+j 5.6
2.5	-26.0	j 26.0	2.15+j 5.8
3.5	-21.5	j 17.5	2.95+j 6.1
4.5	-12.0	j 7.0	3.75+j 4.3

Field strength 160 V/km

Coordi- nate x km	i_2		z_{26} ohm/km
	i_{2Re} A	i_{2Im} A	
0.5	-14.0	j 13.0	3.75+j 6.1
1.5	-14.0	j 12.5	3.75+j 6.1
2.5	-14.2	j 10.5	3.85+j 5.9
3.5	-15.2	j 7.5	3.85+j 5.8
4.5	-7.0	j 3.0	1.05+j 2.2

The screening factor can be written (after correction for the non constant current and for the varying longitudinal impedance of the sheath)

$$k_{rc} = \frac{5e_2 + \sum z_{26} (i_{2Re} + j i_{2Im})}{5e_2}$$

It is found

at $e_2 = 300$ V/km

$$k_{rc} = \left| \frac{1500 - 896 + j 392}{1500} \right| = 0.48$$

at $e_2 = 160$ V/km

$$k_{rc} = \left| \frac{800 - 495 + j 189}{800} \right| = 0.45$$

For the field strengths in question k_r is 0.33 and 0.26 respectively.

When comparing the two values given above one must observe that the compensating current decreases more slowly to the insulated end of the cable sheath if the field strength is 160 V/km than in the case when e_2 is 300 V/km as can be seen from figure 10.

In the chapter "Unarmoured cables" a formula is given for the calculation of k_r , when constant z_2 values are assumed and when the end conditions are the same as in the examples above.

$$k_{rc} = \frac{1}{z_2} (z_2 - z_{26} + \frac{z_{26}^2}{2L} \tanh \gamma_2 L)$$

This formula gives

$$k_{rc} = 0.50 \text{ at } e_2 = 300 \text{ V/km and}$$

$$k_{rc} = 0.42 \text{ at } e_2 = 160 \text{ V/km}$$

Screening wires

The emf reducing effects caused by screening wires can be calculated in the same manner that is used when the compensating conductor is a cable sheath. In the following it is supposed that the distance between the screening wire and the exposed telecommunication circuit is rather small. In this case the mutual impedance between the wire and the circuit can be written

$$z_{26} = \pi^2 f 10^{-4} + j 2 \pi f (12.98 + \ln \frac{\rho}{fa^2}) 10^{-4} \text{ ohm/km}$$

where a is the separation expressed in meters.

At 50 Hz

$$z_{26} = 0.05 + j 314 (9.07 + \ln \frac{\rho}{a^2}) 10^{-4} \text{ ohm/km}$$

As shown before the longitudinal impedance of the wire at 50 Hz is

$$z_2 = r_{2i} + 0.05 + j 0.0157 + j 314 (22.9 + \ln \frac{\rho}{r^2}) 10^{-4} \text{ ohm/km}$$

r being the radius of the screening wire in mm.

The term $j 0.0157$ represents the intrinsic impedance of the screening wire of for instance copper with $\mu_2 = 1$.

Thus the screening factor at 50 Hz is, if only one compensating conductor is assumed

$$k_r = \frac{z_2 - z_{26}}{z_2} = \frac{r_{2i} + j 0.45 + j 628 10^{-4} \ln \frac{r}{a}}{r_{2i} + 0.05 + j 0.73 + j 314 10^{-4} \ln \frac{\rho}{r^2}}$$

For example a 100 mm² copper wire gives the following screening factors, $\rho = 2500 \text{ ohm.m}$

Distance	1 m	0.4 m	0.2 m
k_r	0.42	0.36	0.33

It is assumed that there is no interaction from, for instance, a cable sheath. If there is a bundle of screening wires the calculation of the screening effect can be made in the following manner. The assumption is made that the wires are exposed to the same emf. See figure 11.

Three conductors are considered with the self impedances z_a , z_b and z_c . The mutual impedances are z_{ab} , z_{ac} and z_{bc} respectively. The currents are i_a , $k_b i_a$, and $k_c i_a$.

The three conductors are replaced by one conductor in which flows the current $i_a + k_b i_a + k_c i_a$ and having the longitudinal impedance z_2^+ .

The following equations are valid

$$i_a (z_a + k_b z_{ab} + k_c z_{ac}) = z_2^+ (1 + k_b + k_c) i_a$$

$$i_a (z_{ab} + k_b z_b + k_c z_{bc}) = z_2^+ (1 + k_b + k_c) i_a$$

$$i_a (z_{ac} + k_b z_{bc} + k_c z_c) = z_2^+ (1 + k_b + k_c) i_a$$

To be solved from the equations are k_b , k_c and z_2^+ .

The solution is

$$k_b = \frac{\Delta_b}{\Delta}$$

$$k_c = \frac{\Delta_c}{\Delta}$$

$$z_2^+ = \frac{z_{ab} + k_b z_b + k_c z_{bc}}{1 + k_b + k_c}$$

where

$$\Delta = (z_b - z_{ab})(z_c - z_{ac}) - (z_{bc} - z_{ab})(z_{bc} - z_{ac})$$

$$\Delta_b = (z_a - z_{ab})(z_c - z_{ac}) - (z_a - z_{ac})(z_{bc} - z_{ac})$$

$$\Delta_c = (z_b - z_{ab})(z_a - z_{ac}) - (z_{bc} - z_{ab})(z_a - z_{ab})$$

If the three conductors are arranged in an equilateral triangle and if $z_a = z_b = z_c$

$$k_b = k_c = 1$$

$$z_2^+ = \frac{z_a + 2z_{ab}}{3}$$

If the conductors are arranged so that $z_{ab} = z_{bc}$ and if $z_a = z_b = z_c$ (see figure 12).

$$k_c = \frac{\Delta_c}{\Delta} = 1$$

$$k_b = \frac{\Delta_b}{\Delta} = \frac{z_a - 2z_{ab} + z_{ac}}{z_a - z_{ab}}$$

$$z_2^+ = \frac{k_b z_a + 2z_{ab}}{2 + k_b}$$

In the same manner as the impedance z_2^+ a mutual impedance z_{26}^+ can be derived. The following equation is evident for three conductors

$$z_{a6} + k_b z_{b6} + k_c z_{c6} = z_{26}^+ (1 + k_b + k_c)$$

and thus

$$z_{26}^+ = \frac{z_{a6} + k_b z_{b6} + k_c z_{c6}}{1 + k_b + k_c} \quad (\text{see figure 13})$$

The screening factor caused by the bundle of conductors is

$$k_r = 1 - \frac{z_{26}^+}{z_2^+}$$

For two conductors is easily found that

$$k = \frac{z_a - z_{ab}}{z_b - z_{ab}}$$

$$z_2^+ = \frac{z_a z_b - z_{ab}^2}{z_a + z_b - 2z_{ab}}$$

and

$$z_{26}^+ = \frac{z_{a6} + k z_{b6}}{1 + k}$$

As a calculation example we choose three cases where the compensating conductors are of copper with a diameter of 10 mm, the cross section area being 78.5 mm² and the intrinsic resistance 0.22 ohm. The conductors are arranged as indicated in figure 14. The earth resistivity is 2500 ohm.m.

Case 1

$$z_a = 0.27 + j0.87 \text{ ohm/km}$$

$$z_{a6} = 0.05 + j0.63 \text{ ohm/km}$$

$$k_r = \left| \frac{0.22 + j0.24}{0.27 + j0.87} \right| = 0.36$$

Case 2

$$z_2^+ = \frac{z_a + z_{ab}}{2} = 0.16 + j0.75 \text{ ohm/km}$$

$$z_{26}^+ = \frac{z_{a6} + z_{b6}}{2} = z_{a6}$$

$$z_{a6} = 0.05 + j0.62 \text{ ohm/km}$$

$$\text{The distance } a-b = \sqrt{0.05} \text{ m}$$

$$k_r = \left| \frac{0.11 + j0.13}{0.16 + j0.75} \right| = 0.22$$

Case 3

The factor k_b can be written ($k_c = 1$)

$$k_b = 1 - \frac{z_{ab} - z_{ac}}{z_c - z_{ab}}$$

where

$$z_{ab} - z_{ac} = j628 \cdot 10^{-4} \ln \frac{0.4}{0.2} = j0.04 \text{ ohm/km}$$

$$z_a - z_{ab} = 0.22 + j0.24 \text{ ohm/km}$$

and thus

$$k_b = 1 - \frac{j0.04}{0.22 + j0.24} =$$

$$= 1 - 0.1 - j0.09 = 0.9 - j0.09$$

$$z_2^+ = \frac{2z_{ab} + (0.9 - j0.09)z_a}{2.9 - j0.09}$$

$$z_{26}^+ = \frac{2z_{a6} + (0.9 - j0.09)z_{b6}}{2.9 - j0.09}$$

$$\text{The distance } a-b = 0.08 \text{ m}$$

$$z_2^+ = 0.12 + j0.73 \text{ ohm/km}$$

$$z_{26}^+ = 0.03 + j0.64 \text{ ohm/km}$$

$$k_r = \left| \frac{0.09 + j0.09}{0.12 + j0.73} \right| = 0.17$$

Measurements of propagation properties

Method a: In series with a resistance R over a break in the cable sheath (or the screening wire) an emf E is applied. At a distance of about 1 km from the cable an earthing (1) is arranged. The following potentials and voltages are measured (see figures 15, 16, and 17).

$$P_2, P_3, P_4, V_{23}, \text{ and } V_{34}.$$

The point 4 along the cable may be chosen about 1 km from the break.

The characteristic impedance z_2 of the sheath is

$$z_2 = \left| \frac{P_3}{I_2} \right| \text{ ohm}$$

The phase angle of this impedance is determined by the expression

$$\cos \phi = \frac{P_3^2 + V_{23}^2 - P_2^2}{2V_{23}P_3}$$

Thus

$$z_2 = \left| \frac{P_3}{I_2} \right| (\cos \phi + j \sin \phi) \text{ ohm}$$

The potential P_4 can be written

$$P_4 = P_3 e^{-(\alpha + j\beta)l}$$

if l is the length of cable between the points 3 and 4.

The attenuation α is directly determined as

$$\alpha = \frac{1}{l} \ln \left| \frac{P_3}{P_4} \right| \text{ neper/km}$$

The phase angle between the potentials P_3 and P_4 is determined by the expression

$$\cos \phi_1 = \frac{P_3^2 + P_4^2 - V_{34}^2}{2P_3P_4}$$

Thus

$$\beta = \frac{1}{l} \beta_1 \text{ radians/km}$$

If there is interference from power installations the measurements can be carried out with a frequency somewhat deviating from the power line frequency. A frequency selective voltmeter must then be used.

The current i_2 is determined as

$$i_2 = \frac{V_{23}}{R}$$

By using a current transformer (CT) a check can be made that V_{23}/R is equal to i_2 .

It is necessary to introduce a series emf E as shown in figure 15, since in this case the conditions correspond to those which exist in the induction case. It is thus not permitted to arrange a remote earthing and apply an emf between this earthing and the cable. The current propagation along the cable in this latter case is quite different from the propagation that is valid in the series emf case.

Method b: In this case there is no break in the cable sheath (or on the screening wire).

Fig 18 shows the measuring arrangement.

In this case the phase angle (ϕ_2) between the currents i and i_2 must be determined.

This angle is given by (see fig 19)

$$\cos \phi_2 = \frac{i^2 + i_2^2 - i_3^2}{2ii_2}$$

The angle ϕ_3 between P_3 and V_{23} is determined by

$$\cos \phi_3 = \frac{P_3^2 + V_{23}^2 - P_2^2}{2V_{23}P_3}$$

and thus $\phi = \phi_2 + \phi_3$

$$Z_2 = \left| \frac{P_3}{i_2} \right| (\cos \phi + j \sin \phi)$$

The angle between the potentials P_3 and P_4 is determined by

$$\cos \phi_1 = \frac{P_3^2 + P_4^2 - V_{34}^2}{2P_3P_4}$$

and as with method a

$$\alpha = \frac{1}{l} \ln \left| \frac{P_3}{P_4} \right|$$

and

$$\beta = \frac{1}{l} \phi_1 \text{ radians/km}$$

If the measurement is made with direct current

$$Y_2 = \sqrt{r_{2i} Y_2} = \alpha_2$$

and thus

$$Y_2 = \frac{1}{l^2 r_{2i}} \left(\ln \frac{P_3}{P_4} \right)^2$$

for one conductor.

For two conductors in parallel (each with the resistance r_{2i})

$$Y_2 = \frac{2}{l^2 r_{2i}} \left(\ln \frac{P_3}{P_4} \right)^2$$

and for three conductors

$$Y_2 = \frac{3}{l^2 r_{2i}} \left(\ln \frac{P_3}{P_4} \right)^2$$

Observe that the potentials P_3 and P_4 are not the same in the three cases.

Short discussion concerning wave propagation and two interacting earthed conductors

This part is included in the paper in order to show the difficulties which meet the engineer, who has to solve this special situation. By using a computer, however, it seems that the problem can be treated.

A system of differential equations of the following type can be derived

$$-\frac{dv_2}{dx} = i_2^2 z_2 + i_3^2 z_{23} + i_1^2 z_{12}$$

$$-\frac{di_2}{dx} = v_2 (y_2 + y_{23}) - v_3 y_{23}$$

$$-\frac{dv_3}{dx} = i_2^2 z_{23} + i_3^2 z_3 + i_1^2 z_{12}$$

$$-\frac{di_3}{dx} = -v_2 y_{23} + v_3 (y_3 + y_{23})$$

The two conductors are both exposed to the same induced emf $i_1 z_{12}$.

The characteristic equation has two pairs of roots $\pm \gamma_2$ and $\pm \gamma_3$.

The two currents i_{2x} and i_{3x} can be written

$$i_{2x} = A_1 e^{\gamma_2 x} + A_2 e^{-\gamma_2 x} + A_3 e^{\gamma_3 x} + A_4 e^{-\gamma_3 x} - i_1 z_{12} \frac{z_3 - z_{23}}{z_2 z_3 - z_{23}^2}$$

$$i_{3x} = B_1 e^{\gamma_2 x} + B_2 e^{-\gamma_2 x} + B_3 e^{\gamma_3 x} + B_4 e^{-\gamma_3 x} - i_1 z_{12} \frac{z_2 - z_{23}}{z_2 z_3 - z_{23}^2}$$

The expressions for the voltages do not contain the last terms of the equations above. For example

$$v_{2x} = C_1 e^{\gamma_2 x} + C_2 e^{-\gamma_2 x} + C_3 e^{\gamma_3 x} + C_4 e^{-\gamma_3 x}$$

As all the constants A, B, and C must be independent of x, a relation between the various constants can be found. The values of the constants depend on the terminal conditions of the two conductors.



Gustav Adolf Pettersson
Orvar Odds väg 8
S-112 54 STOCKHOLM SWEDEN

G.A. Pettersson, born in 1907, graduated in 1932 from the Royal Institute of Technology, Stockholm, Sweden.

He is the retired Head of The Central Laboratory, Swedish Administration of Telecommunications. He has also been a member of The Swedish Power-Telecommunication Coordination Committee, Chairman of IVA (Royal Swedish Academy of Engineering Sciences) Commissions for studies of lightning and electrical properties of the Swedish soil, Chairman of the Commission of lightning questions within the Swedish National Committee of IEC, and participant of the work within Studygroup V of CCITT.



Arne Ernbo
Sieverts Kabelverk AB
S-172 87 SUNDBYBERG SWEDEN

Arne Ernbo, born in 1945, graduated in 1967 from the Technical University of Lund, Sweden, as Master of Science in Electrical Engineering. After four years' work at the same University, he received a Doctors' Degree in Electrical Measurements. In 1971 he joined the Telephone Cables Division of Ericsson, which was transferred to Sieverts Kabelverk in 1976. Until 1979 he was Head of the Transmission Laboratory. After working for two years at the Long Distance Division of Ericsson, he rejoined Sieverts Kabelverk in 1981. He is now Manager of the Telecommunication Cables Department within the Engineering Division of Sieverts Kabelverk.

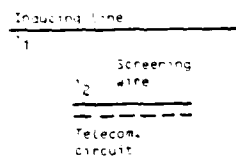
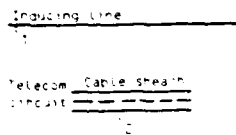


Figure 1. Arrangement of inducing line, telecom circuit and cable sheath/ screening wire.

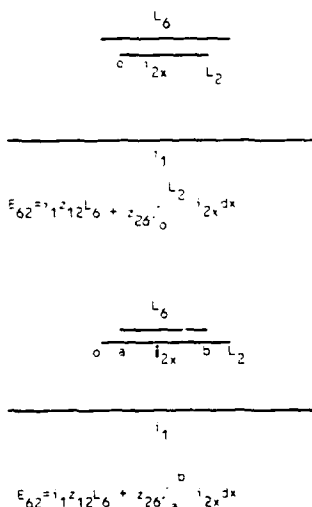


Figure 2. Telecom circuit and screen with unequal lengths.

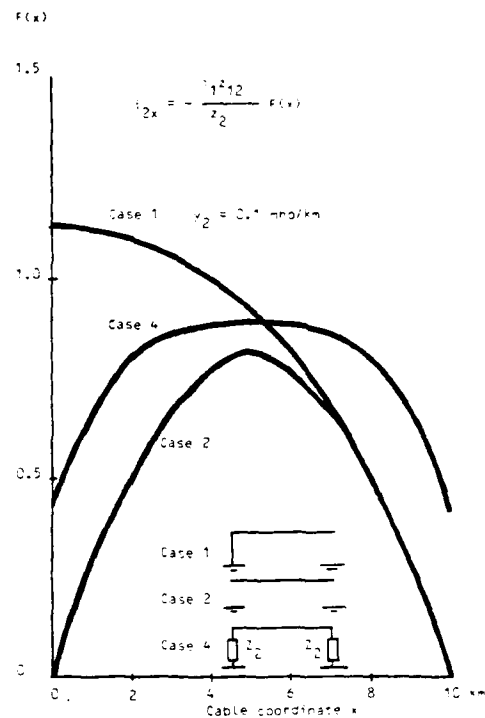


Figure 3. Current variation along cable with different terminations Cable type 1.

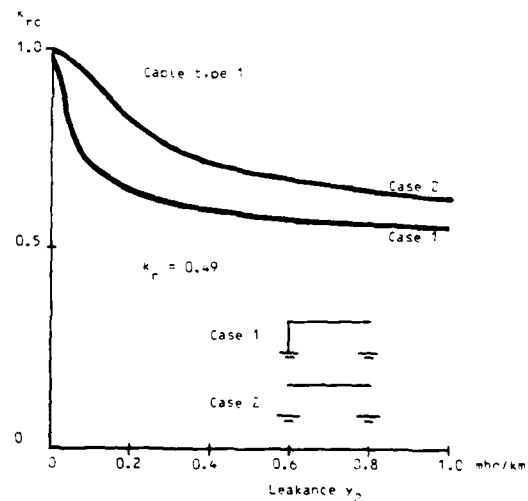


Figure 4. Corrected screening factor of cable type 1 with different terminations as a function of the leakance to earth.

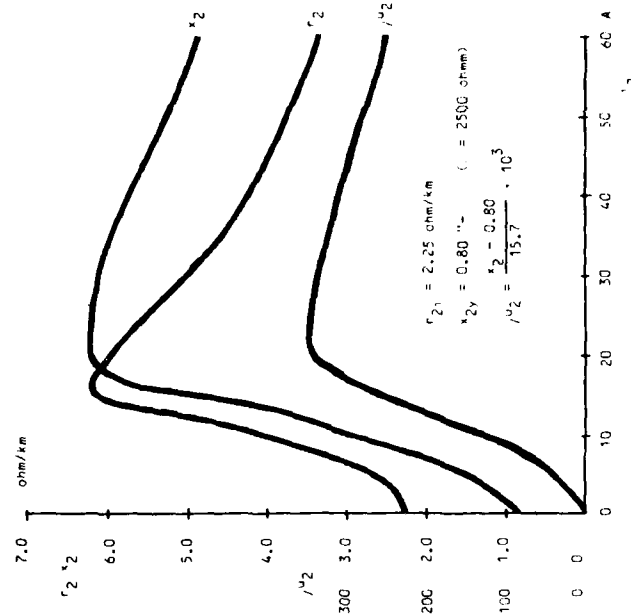
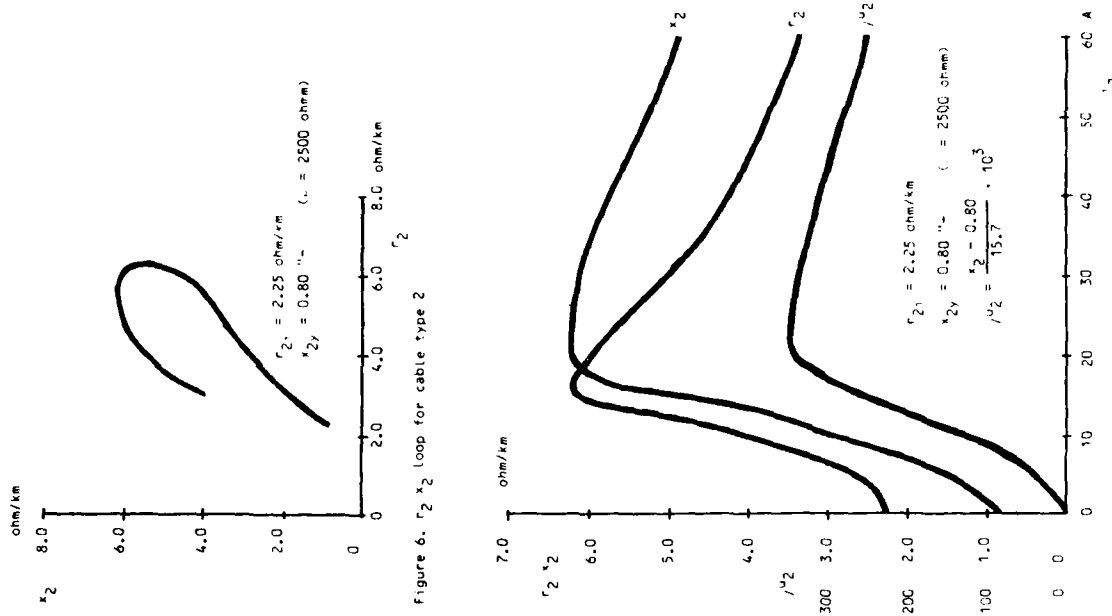


Figure 7. Longitudinal resistance and reactance
Relative permeability of sheath.

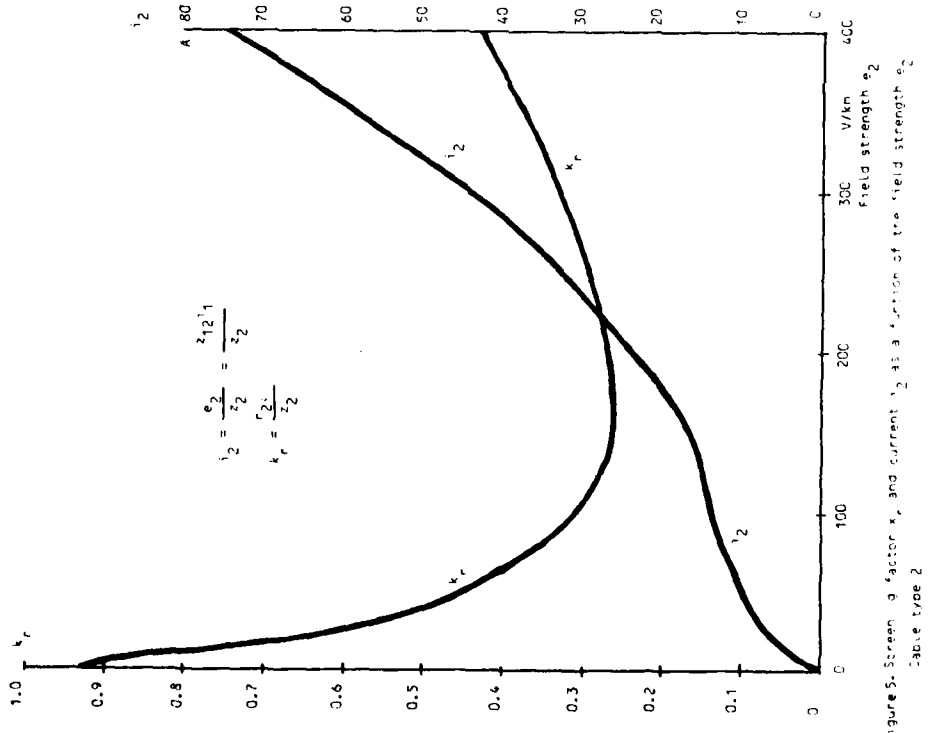


Figure 8. Screen g factor k_r and current I_2 as a function of the field strength H_2

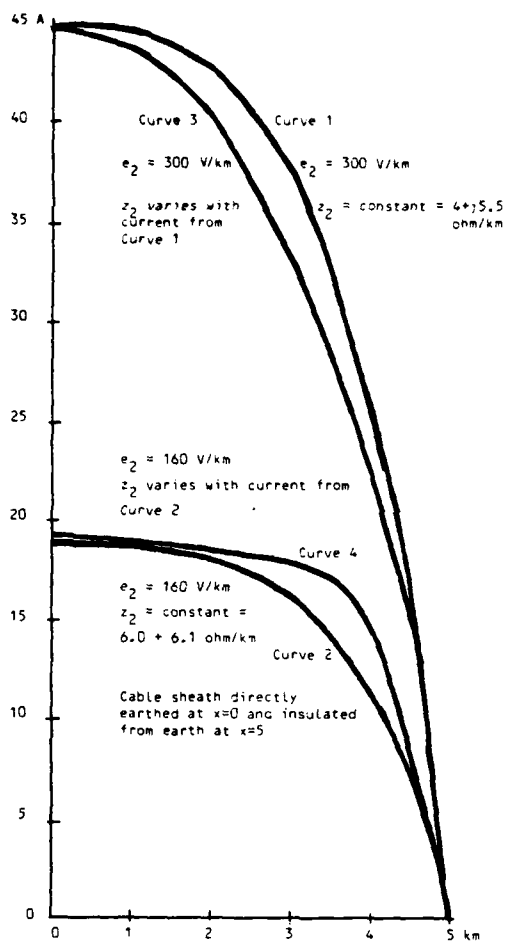


Figure 8. Current variation along cable
Cable type 2.

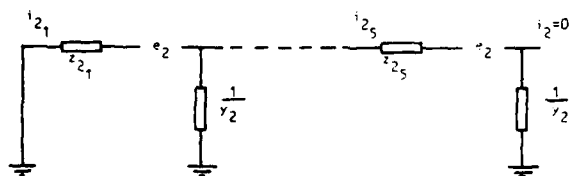


Figure 9. Cable length divided in 1 km elements

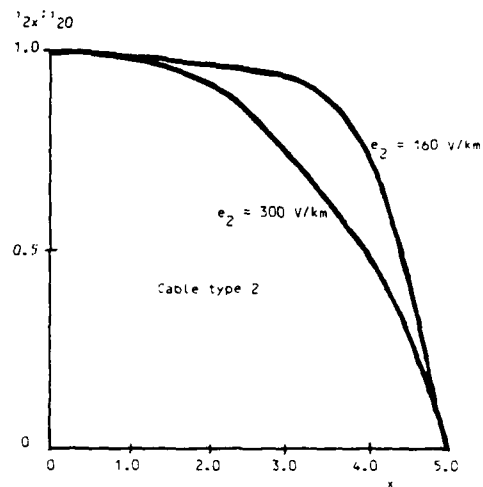


Figure 10. Relative variation of sheath current i_2
along cable (from curves 3 and 4, Figure 8.)

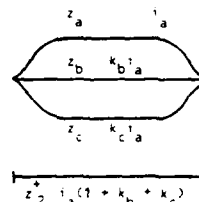


Figure 11. Three screening wires
replaced by one.

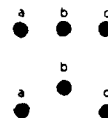


Figure 12. Arrangement of
screening wires

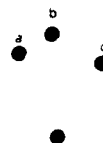
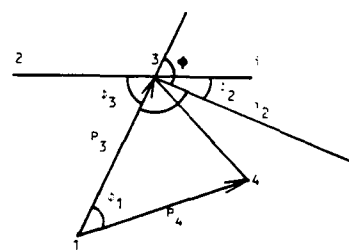
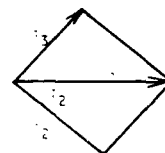
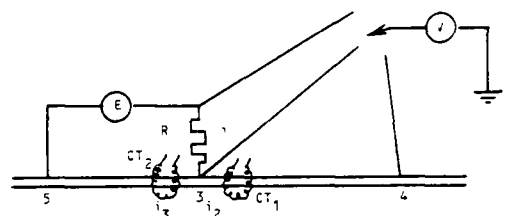
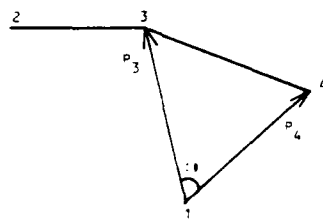
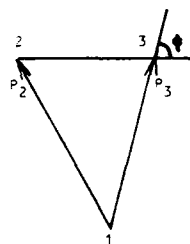
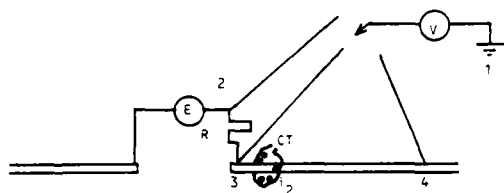
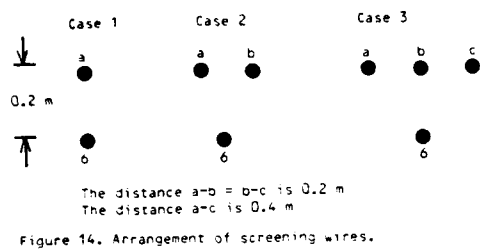


Figure 13. Arrangement of
screening wires



Fiber Optic Connection System

B. D. Campbell

P. M. Simon

J. T. Triplett

R. E. Tylor

Raychem Corporation
Menlo Park, CA

ABSTRACT

A fiber optic connection system based on the precise alignment of the fiber core is described. The system has the following features;

- a) optical power is launched into and detected from macrobends in the fibers to be spliced;
- b) the fibers are moved relative to one another until the optimum optical power ie. alignment is obtained;
- c) the fibers are locked in the aligned position by means of an ultraviolet polymerizable material.

The polymerizable material serves the triple function of bonding the fiber together, matching the index of refraction to minimize Fresnel losses and providing environmental protection.

Introduction

The two dominant splicing methods used in the world today are fusion splicing and physical positioning of the fiber within an alignment medium e.g. "V grooves". The strengths and weaknesses of the systems are well known. The methods are described in outline form here.

Fusion Splicing

Fusion splicing is a widely accepted means of connecting optical fibers in the field. The technique usually utilizes manual manipulation of the fiber under magnification to position the fiber ends. When aligned the fiber ends are fused by the application of an electric arc. Surface tension effects enhance the alignment.

Provided the fiber ends are well cleaned, free of impurities, well aligned and carefully fused high quality splices result. However, the fused splice is mechanically weak and requires environmental protection and support by mechanical means, potting, heat shrink tubing, etc. Additional problems can be foreseen when fiber of slightly different chemical compositions from different suppliers are required to be held together.

Physically Aligned Splices

All methods depend on the cladding alignment. The loss of the connection is therefore related to the concentricity of the cores within the respective claddings. Specification generally call out a one micron tolerance on cladding diameter and a 6% eccentricity of the core within the cladding.

All methods rely on an index matching medium to minimize losses. Mechanical strength is provided by mechanical means eg. crimping, adhesives or potting compounds.

As the use of optical fiber moves from trunk and toll to distribution plant, larger numbers of fibers will be encountered. It is likely that some form of factory pre-termination will result. Pre-termination will allow near perfect preparation of the fiber ends through polishing and similar methods and will favor a mechanical rather than a fusion splice. Additionally, the buffer may be left on the cladding up to the fiber end.

As the use of fibers increases the need for repairing damaged fiber will increase. A fast convenient method that could be used in an underground environment would be advantageous.

There is obviously a need for a fast, reliable splicing means that is versatile enough to join field prepared fibers or factory prepared fibers when the repair has to be performed in an underground environment.

Robotic Splicing

A new robotic splicing method based on the following principles is described:

- a) optical power is launched into and detected from macrobends in the fibers to be spliced;
- b) the fibers are moved relative to one another until the optimum optical power ie. alignment is obtained;
- c) the fibers are locked in the aligned position by means of an ultraviolet polymerizable material.

Fiber alignment can be accomplished most accurately by finding the maximum power transmission through the joint. This method is usually cumbersome however, since the optical power source must be distant from the site of the splice. The robot launches power into the core of the fiber adjacent to the fiber ends through a bend in the fibers. A LED is used to launch the power into the core at the macrobend. This system is shown in figure 1. The launching of optical power is accomplished through the buffer material.

The optical power is detected at a similar bending fixture at the opposite side of the joint by a PIN diode. The output of the PIN diode is amplified, digitized and becomes the input to a self contained microprocessor. The microprocessor output governs the position of the fibers by controlling the drive current to 2 voice coils. Each voice coil deflects a beam to align the fibers within 0.5 microns. The motion stage is schematically depicted in figure 2.

Splicing Robot Diagram

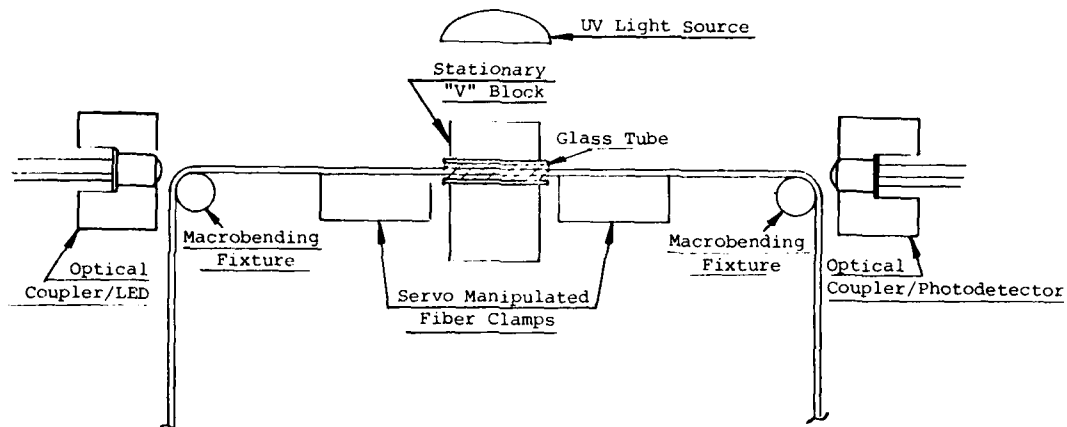


Figure 1
Fiber Motion Stage

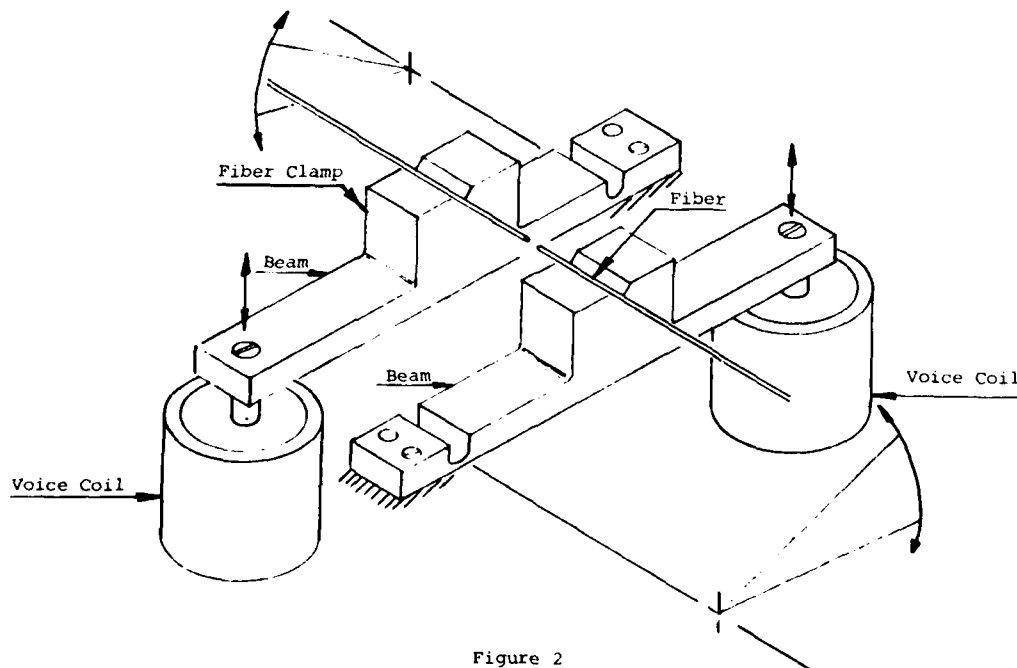


Figure 2

Insufficient optical power can result from an improperly prepared fiber end or foreign material at the intended fiber joint. Should the optical power passing through the joint be insufficient to align the fibers, the microprocessor will interrupt the program and display a reject instruction to the operator. In this manner a quality inspection of the joint is provided before completion of the joint.

The actual joint is secured by a UV curable, polymer material. The polymer has been formulated so that, in its liquid state, it may be supplied in a quartz tube retained therein by surface tension. The material serves to exclude contamination reaching the splice from the environment. In its cured state the material serves several functions:

1. Matches the index of refraction to eliminate fresnel losses;
2. Provides permanent positioning of the fiber ends;
3. Strain relieves and supports the joint;
4. Environmentally seals the joint from OH radical attack;
5. Provides axial load carrying capacity of at least 2½ pounds.

It is not necessary that the fibers be stripped of buffer material since the encapsulation of the fibers in the material forms the joint. The only reason that the buffer material is currently removed is to allow cleaving of the fiber ends. Were the ends of the fibers prepared by alternate means, such as factory grinding and polishing, robotic splicing would equal the time cycle achieved by preconnection.

TESTING

At the date of this paper a limited number of tests have been performed on splices made by the robotic technique. Preliminary results are summarized in Table I, below:

TABLE I

<u>Test</u>	<u>Results</u>
Axial Load	2.5lb
Attenuation	0.3db

Long term testing of material degradation in a wide variety of environmental influences is currently underway.

CONCLUSION

A new splicing concept has been described that should be suitable for use in underground environment for initial installation and repair on field and factory prepared fiber ends.

The method ensures fast, reliable core alignment coupled with low losses and mechanical and environmental protection.



Bruce D. Campbell received his bachelor of science degree in mechanical engineering (BSME) from Lehigh University in 1960 and a bachelor of law degree (LLB) from the University of San Fernando Valley, College of Law in 1968. Mr. Campbell is presently employed as a product design manager for the GETM division, Raychem Corporation, Menlo Park, California.



Phyllis M. Simon joined Raychem in 1978. She is currently employed in the development of fiber optic versions for Local Area Network Systems (LANS). She has been responsible for development of polymer material for use in the fiber optic splicing robot.



James T. Triplett has been working in Research and Development at Raychem for the past five years. He received his bachelors degree in mathematics from San Jose State University in 1974.



Richard E. Tylor has been working on fiber optics projects at Raychem since 1980. He was previously employed at Westinghouse Electric Corporation in Pittsburgh, PA. Mr. Tylor received his bachelors degree in electrical engineering at the University of Pittsburgh in 1975.

AD P000557

ON NEW CABLE ACCESSORIES FOR OPTICAL FIBER CABLE SYSTEM

M. Haraguchi, Y. Asano, Y. Tokumaru, T. Seike

Sumitomo Electric Industries, Ltd., Yokohama, Japan

Abstract

Recently, the optical fiber cable system has been utilized for telephone system in many countries. Therefore, it is getting very important to develop soon new cable accessories for the above system.

We have developed the jointing closures and the gas blocks with air-tightness, the tools for fusion splice with good operatability, the protection sleeve for fusion splice with high reliability, and others with economical cost.

This paper describes the idea of design, the results of performance testing, and the actual results about the jointing closures, the termination boxes, and the gas blocks from among our new products shown above. These results confirmed us that our new products can be installed practically in many countries.

1. Introduction

As the optical fiber cable systems are now applied to various kinds of fields, their cable accessories are too various. We have developed and produced many kinds of the cable accessories for above systems.

In Japan, the arc-fusion splice method for permanent splice of optical fibers and the heat shrinkable sleeve method for protection of the splicing are popular. We have developed cutter, fusion splice machine and fiber protection sleeve, and reported their results. (1)(2)(3)

In this paper, the gas block, the jointing closure, and the jointing or termination box are

described. The typical arrangement of those cable accessories is shown in Fig.1. In the development of the above ones, there are several considerable points for the treatment of the optical fibers. We have aimed at overcoming the targets shown below to develop:

- (1) Small size and light weight.
- (2) Available in any environmental conditions
- (3) Easy to operate
- (4) Economical

2. Gas block

2.1. Fundamental considerations

In the development of the gas block for optical fiber cable, it should be considered that the inner strain is loaded on the optical fibers in the gas block, and it causes the optical loss increase and the break of the optical fiber. We have no trouble with regard to the gas tightness to utilize the technique of the present copper cable gas block.

Prior to development, we took the three models shown in Fig.2 into consideration. Model 1 has the structure that the epoxy resin developed by us is molded around the optical fibers. When the model 1 is placed in the cold atmosphere, it causes the optical loss increase. Model 2 and 3 are improved on the model 1. The model 2 is reinforced by the compression member in the epoxy resin for the prevention of the loss increase. In the model 3, the epoxy putty mixed the inorganic filler is molded around the optical fibers for the prevention of the loss increase.

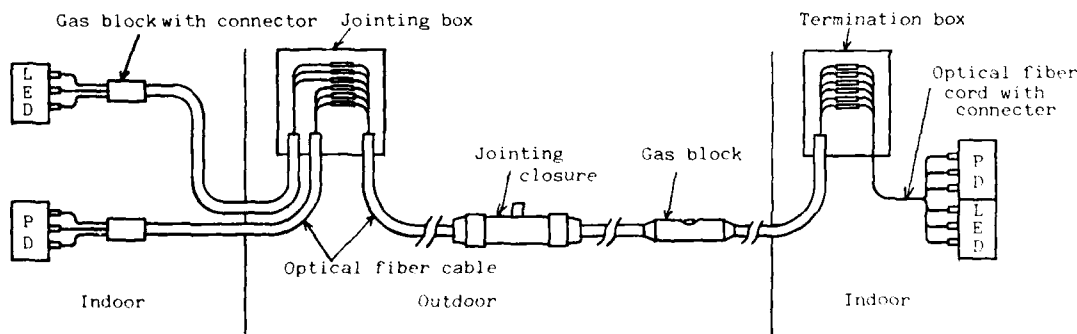


Fig. 1 Typical arrangement of optical fiber cable accessories

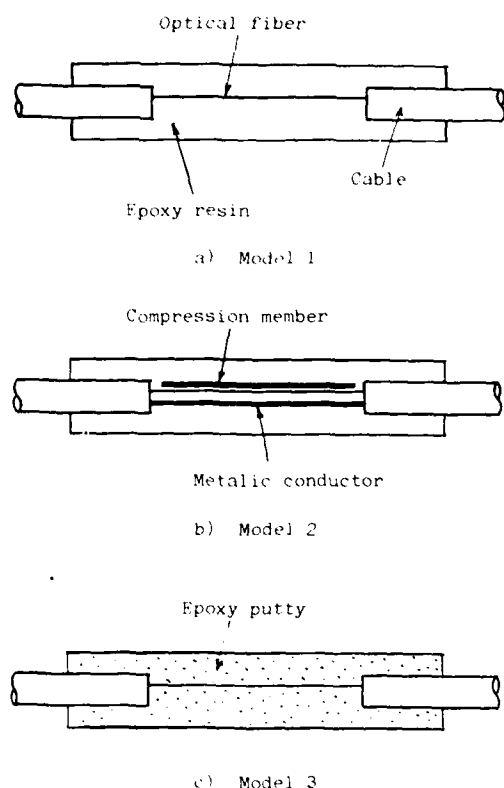


Fig. 2 Models of gas block

The temperature dependence of the loss increase in model 1, 2 and 3 is shown in Fig.3. The cable used in the test is 12 fibers cable with LAP sheath. We think the loss increase is caused by the micro bending, which is caused by the compressed deformation of the molding compound in the cold atmosphere.

So calculating simply the axially compressed by F.E.M., comparisons are made between the calculated stress and the actual loss increase. The conditions and results of the calculation by F.E.M. are shown in Fig.4, Table 1 and Table 2. The relation between the calculated axial stress and the actual loss increase is shown in Fig.5. From those data, those points shown below are made clear:

- (1) Loss increase is not caused if the calculated axial stress is kept under 10 kg/mm².
- (2) Position of the optical fibers in compound does not bring on loss increase.
- (3) In the model 2, the stable gas block independent of the ambient temperature is obtained by adding adequately the compression members in the molding compound.
- (4) In the model 3, the stable gas block is obtained by molding the epoxy putty reinforced the inorganic filler around the optical fibers.

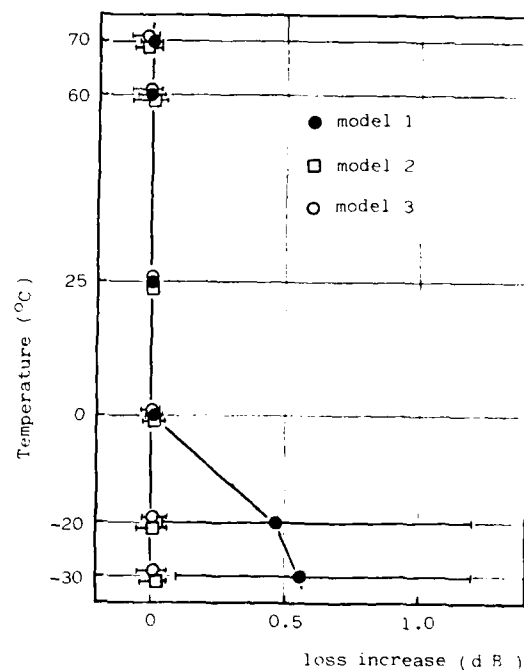


Fig. 3 Temperature dependence of loss increase in gas block model 1, 2 and 3.

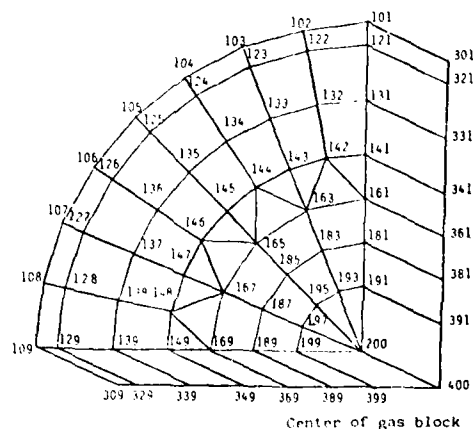


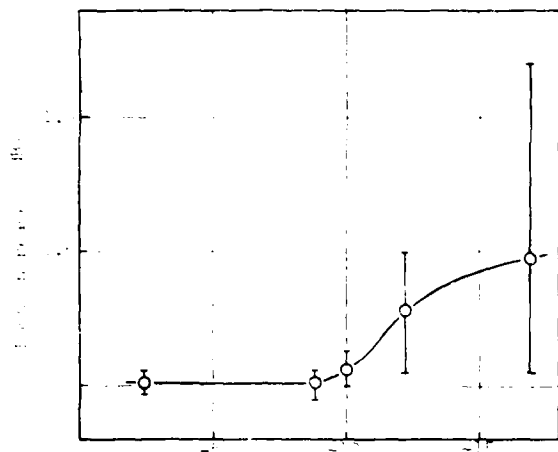
Fig. 4 Grid No. of division in F.E.M.

Table.1 Characteristic value of elements for F.E.M.

Element	Young's modulus (kg / mm ²)	Poisson's ratio	Linear expansibility (deg ⁻¹)	Outer diamater (mm)
1. Compression member	2.1×10^4	0.30	1.0×10^{-5}	0.9
2. Optical fiber	7.0×10^3	0.17	4.0×10^{-7}	0.125
3. Metallic conductor	1.25×10^4	0.34	1.6×10^{-5}	0.9 x 4
4. Epoxy resin	2.4×10^2	0.38	5.5×10^{-5}	—
5. Epoxy putty	3.2×10^2	0.36	8.1×10^{-5}	—

Table 2 Axial stress of fiber calculated by F.E.M.

Item No.	Compression member	Optical fiber	Metal conductor	Molding compound	Axial stress of optical fiber (kg/mm ²)	Remarks
1	—	Glid No 161 163 167 169	—	Epoxy resin	-16.8	Model 1
2	—	Glid No 161 163 167 169	165	Epoxy resin	-12.2	Model 1
3	Glid No 121 125 129	Glid No 161 163 167 169	165	Epoxy resin	-10.0	Model 2
4	Glid No 121 125 129	Glid No 181 183 187 189	165	Epoxy resin	-10.1	Model 2
5	Glid No 121 125 129	Glid No 131 133 137 139	165	Epoxy resin	-10.1	Model 2
6	Glid No 121 123 125 127 129	Glid No 161 163 167 169	165	Epoxy resin	-8.8	Model 2
7	—	Glid No 161 163 167 169	—	Epoxy putty	-2.4	Model 3



Axial stress : 100 kg/cm²

Fig. 5. Relation between axial stress and loss increase in gas block

2.2. Performance testing and field results

The performance testing and the field results of gas block model 2 and 3 are shown in Table 3. The sealed gas pressure is 1 kg/cm² at room temperature in the performance testing. The cables used in the testing are as follows.

Model 2:

- 60 fibers and 4 quads cable with LAP sheath
- 36 fibers and 4 quads cable with LAP sheath
- 12 fibers and 4 quads cable with LAP sheath

Model 3:

- 12 fibers cable with LAP sheath
- 3 fibers cable with LAP sheath

For the anti-impact, the buffer layer on the outside of the molding compound is made in the testing gas block.

2.3. Applications

The standard gas block is shown in Photo 1. The gas block with the gas valve and the multi-branched one with optical connectors are some of the applications. The gas block with the optical connectors is shown in Photo 2. This gas block with the flange for jointing the repeater housing are applied to the stub cable with gas block.



Photo 1. Standard gas block
(Diameter : 65 mm)
(Length : 450 mm)

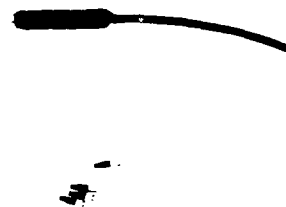


Photo 2. Gas block with connectors
(Diameter : 20 mm)
(Length : 120 mm)

3. Jointing closure

In jointing closure for optical fiber cables, we have developed heat-shrinkable jointing closure (HJC) and mechanical jointing closure (MJC). HJC is utilized for jelly-filled optical fiber cable. In this paper, MJC for the gas pressurization system is described.

3.1. Fundamental considerations

3.1.1. Structure

The size of the jointing closure for the optical fiber cable is large, because it is necessary to wind the spare length for splice around a bobbin.⁵⁾ In consideration of the handleability, the closure composed of one outer sleeve and two holders on the both ends of the sleeve is shown in Fig. 6.

The features of MJC are shown below:

- (1) Holders are separated type. Gas-tightness is obtained by adhesive sealing tape or cord set among the outer sleeve, the holders and the cable sheath. They are assembled with eight bolts.
- (2) Cable gripping force is obtained with screw on the inner surface of cable grips. The relation between the cable gripping force and the sticking depth of screw is shown in Fig. 7. We made the tensile strength of the aluminium tape of LAP sheath the minimum cable gripping force. The minimum force is 100 kg in 12 fibers cable with LAP sheath, and 115 kg in 36 fibers cable. Therefore, the sticking depth is required at 0.35 mm and above. The cable grips should be permitted to stick on the cable sheath as long as the optical fibers are not compressed laterally. Thus we decided the upper limit is 1.05 mm from Fig. 7.
- (3) The outer sleeve, the holders, and the sheath grips are mechanically assembled.

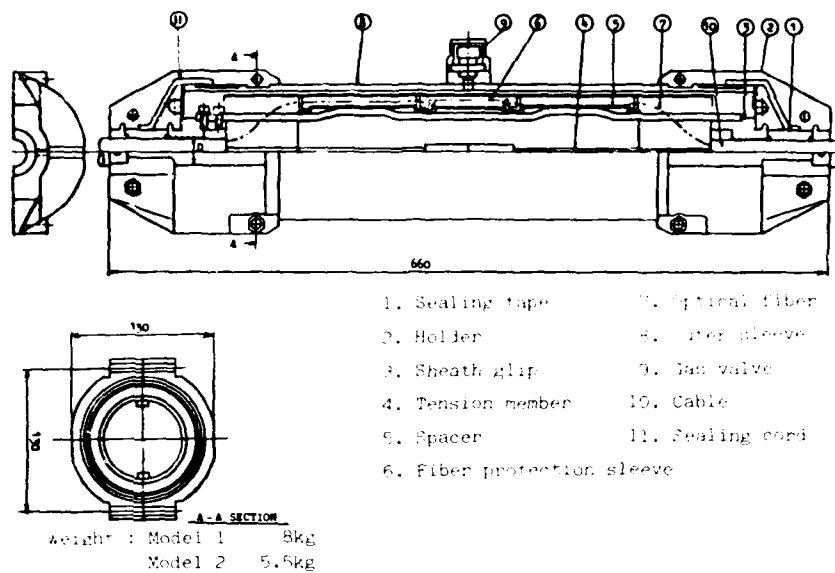


Fig.6 Mechanical jointing closure (MJC)

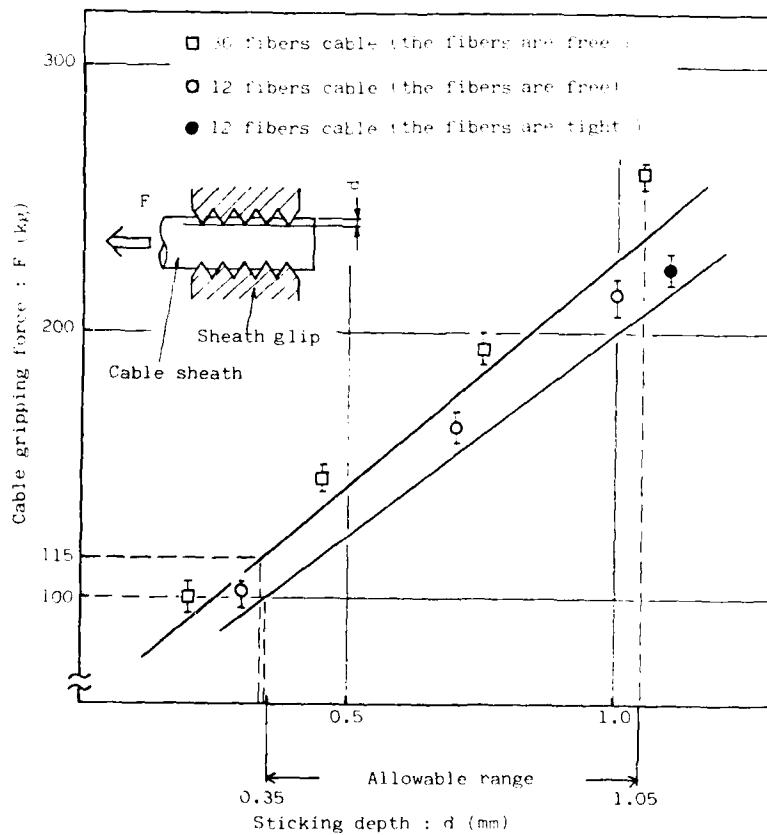


Fig.7 Cable gripping force vs. sticking depth

3.1.2. Selection of materials

In consideration of light weight and availability to any environmental conditions, we selected the materials and thought out two models shown below.

Model 1:

The outer sleeve and the cable holders are made of aluminium coated with epoxy resin. The environment test results of the coating are shown in Table 4. The electric insulation of the coating is shown in Fig.8. This appearance is shown in Photo 3.

Table 4. Environment test of model 1 coating resin

Solution & Oil	Temp.	Term	Results
10% HCl	60°C	A year	No failure No breakage at 2kV
10% H ₂ SO ₄	60°C	A year	
10% CH ₃ COOH	60°C	A year	
10% NaOH	60°C	A year	
10% NH ₄ OH	60°C	A year	
10% NaCl	60°C	A year	
CH ₃ COCH ₃	R.T.	A year	
Water	60°C	A year	
Sea water	60°C	A year	
Gasoline	R.T.	A year	
Kerosene	R.T.	A year	
Heavy oil	R.T.	A year	

Table 5. Environment test of MJC model 2 material

solution	Temp.	Term	Change ratio of tensile strength
3% H ₂ SO ₄	R.T.	A year	0%
5% CH ₃ COOH	R.T.	A year	0.6%
10% NaOH	R.T.	A year	-2%
10% NH ₄ OH	R.T.	A year	0%
10% NaCl	R.T.	A year	2%
CH ₃ COCH ₃	R.T.	A year	-4%
Water	R.T.	A year	0%
Gasoline	R.T.	A year	6%

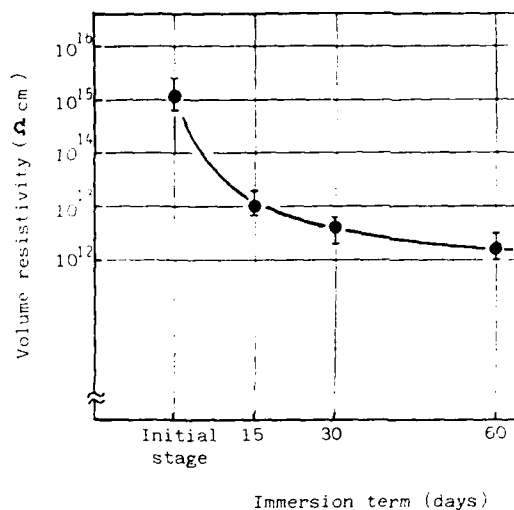


Fig 8 Volume resistivity change of coating resin on mechanical jointing closure model 1 in hot water (80°C) immersion test.

Model 2:

In consideration of anti-corrosion and mass production polyacetal resin is selected mainly. The environment test results of the material are shown in Table 5. It is not suitable for strong acid atmosphere. The holder is made of F.R.P. in consideration of pressure strain on assembly. This appearance is shown in Photo 4.



Photo 3. MJC model 1



Photo 4. MJC model 2

3.2. Performance testing and field results

The performance testing and field results in MJC model 1 and 2 are shown in Table 6. The sealed gas pressure is 1 kg/cm² at room temperature in the performance testing. The cables used in the testing are as follows.

- 60 fibers and 4 quads cable with LAP sheath
(outer diameter : 25 cm)
- 36 fibers and 4 quads cable with LAP sheath
(outer diameter : 25 cm)
- 12 fibers and 4 quads cable with LAP sheath
(outer diameter : 22 cm)

4. Jointing or termination box

We use the box type closure in the case of installation on the wall and request of frequent interconnecting.

4.1. Design

4.1.1. Treatment of spare length for splice

It is very important to treat compactly the spare length for splice and to take out easily a certain spare length for splice. In consideration of the economical cost, the method of treating spare length for splice on simple plate is adopted, and we thought out two models shown below.

Model 1:

Much spare length for splices is compactly treated on a plate shown in Fig.9 a). It is more economical.

Model 2:

Spare length for a splice is compactly treated on a plate, each plate is independently piled in the manner shown in Fig.9b). It is easier to take out a certain splice.

4.1.2. Outer housing

According to installed environment, we thought out two types as follows,

(1) Outdoor type

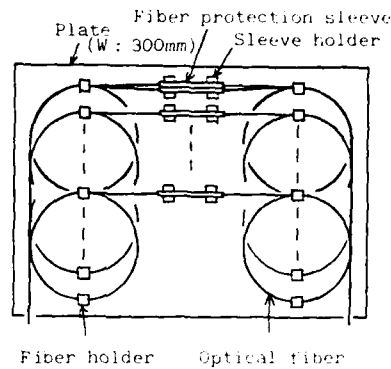
As water proof is required, rubber gascket is set between housing and lid. In entrance of cable, sealing tape is pressed mechanically, or epoxy putty is molded. In case of gas tightness, the rubber gascket is replaced with adhesive sealing cord. The outer housing is made of stainless steel in consideration of anti-corrosion.

(2) Indoor type

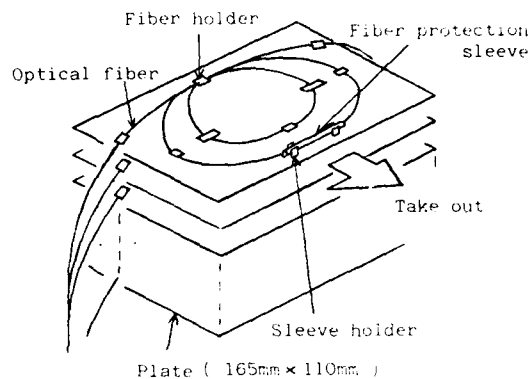
Simple rubber gascket is set between housing and lid. The entrance of cable or cord is treated by protection tape to protect dusts. It is economically made of steel plate.

4.2. Performance testing and field results

The performance testing and field results in



a) Model 1



b) Model 2

Fig 9 Treatment of fiber spare length for splice in jointing or termination box.

the jointing or termination box are shown in Table 7.

4.3. Applications

The termination box model 1 of indoor type is shown in Photo 5. The jointing box model 2 of outdoor type with gas tightness is shown in Photo 6. As shown in Photo 7, the storage plate of spare length is applicable to cord-to-cord connection.

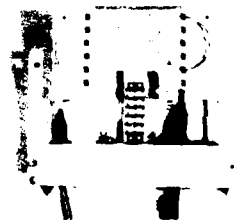


Photo 5. Termination box model 1 of indoor type

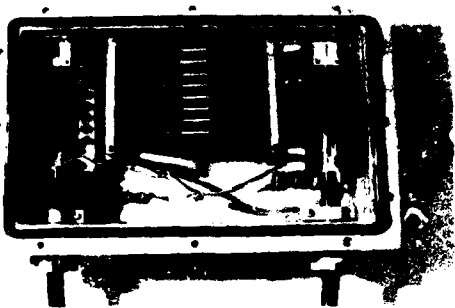


Photo 6. Jointing box model 2 of outdoor type with gas tightness

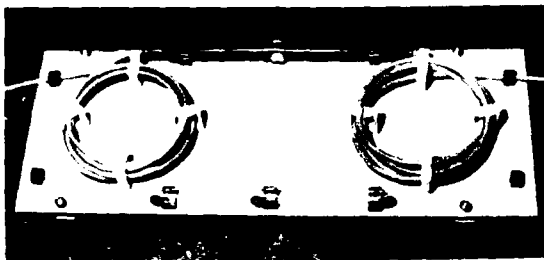


Photo 7. Plate for use with connection cord-to-cord

5. Conclusion

We have developed the gas block, the jointing closure, and the jointing or termination box for optical fiber cable system. From those results described above, we may conclude as follows:

Gas block

- (1) It is necessary that the axial stress of fiber calculated by F.E.M. is designed at 10 kg/mm^2 and below.
- (2) Therefore, we thought out two methods. One is to add compression members in molding compound (model 2) and the other is to mix filler in molding compound (model 3).
- (3) We take model 2 in case of fiber numbers not less than 12, and model 3 in case of fiber numbers not more than 12.

Jointing closure

- (1) Model 1 of aluminium coated with epoxy resin has excellent anti-corrosion and can be installed in any environment.
- (2) Model 2 of plastics is light weight, and can be easy to install.

Jointing or termination box

- (1) The type developed is compact, economical and superior in handability to take out.

As described above, we have developed main accessories in optical fiber cable systems, and can construct various systems from high grade to economical.

Table 3. Performance testing and field results of gas block model 2 and 3

Item	Conditions	Results
Thermal cycling	Thermal cycle : $-30 \sim +70^\circ\text{C}$, 3cycles a day Number of cycles : 100 cycles	No gas leakage No loss increase*
Vibration	Amplitude : 5mm Frequency : 10 Hz Number of cycles : 10^5 cycles	No gas leakage No loss increase*
Bending	Bending radius : 5 times cable diameter Number of bending : 5 times	No gas leakage No loss increase*
Impact	Weight : 6.5 kg Height : 1.3 m	No gas leakage No loss increase*
Stretching	Tensile load : 200kg	No gas leakage No loss increase*
Water immersion	Temperature : 60°C Depth : 50 cm Term : 60 days	No gas leakage No loss increase*
Field	Gas pressure : 150 kg/cm^2 Term : 3 years	No gas leakage No loss increase*

* No more than 0.1dB

Table 6 Performance testing and field results of mechanical jointing closure model 1 and 2

Item	Condition	Results	
		Model 1	Model 2
Thermal cycling	Thermal cycls : $-30 \sim +70^{\circ}\text{C}$, 3 cycles a day Number cycles : 100 cycles	No gas leakage No loss increase*	No gas leakage No loss increase*
Vibration	Amplitude : $\pm 5\text{mm}$ Frequency : 10Hz Number of cycles : 10^6 cycles	No gas leakage No loss increase*	No gas leakage No loss increase*
Bending	Bending radius : 6 times cable diameter Number of bending : 5 times	No gas leakage No loss increase*	No gas leakage No loss increase*
Impact	Weight : 1 lb (Machinist hammer) Height : 1 m	No gas leakage No loss increase* No cracking on resin coating	No gas leakage No loss increase* No cracking
Stretching	Tensile load : 200 kg	No gas leakage No loss increase*	No gas leakage No loss increase*
Water immersion	Temperature : 60°C Depth : 50 cm Term : 60 days	No gas leakage No loss increase*	No gas leakage No loss increase*
Field	Gas pressure : 650 kg/cm^2 Term : 3 years	No gas leakage No loss increase*	No gas leakage No loss increase*

*No more than 0.1dB

Table 7 Performance testing and field results of jointing or termination box

Item	Conditions	Results	
		Outdoor type	Indoor type
Thermal cycling	Thermal cycls : $-30 \sim +70^{\circ}\text{C}$, 3 cycles a day Number cycles : 100 cycles	No loss increase*	No loss increase*
Vibration	Amplitude : $\pm 5 \text{ mm}$ Frequency : 10 Hz Number of cycles : 10^6 cycles	No loss increase*	No loss increase*
Bending	Bending radius : 6 times cable diameter Number of bending : 5 times	No loss increase*	No loss increase*
Water immersion	Temperature : 60°C Depth : 50 cm Term : 60 days	No loss increase*	—
Field		No loss increase* for 3 years	No loss increase* for 5 years

* No more than 0.1dB

Acknowledgements

The authors wish to thank M. Sato, Y. Iigima, and Y. Toda of Sumitomo Electric Industries, Ltd., for their helpful comments and suggestions.

References

- (1) K. Sakamoto, et al., 4th ECOC, 296, 1978.
- (2) Y. Toda, et al., ICC Denver, 27.7, June, 1981.
- (3) M. Miyauchi, et al., Electron. Lett., 17, 1981, P907-P908.
- (4) Y. Kameo, et al., 30th IWCS, 236, 1981.
- (5) M. Hirai, et al., Review of the Electrical Communication Laboratories, 127, 1979, P966.

Authors



Masayosi Haraguchi
Sumitomo Electric
Industries, Ltd.
1, Taya-cho,
Totsuka-ku,
Yokohama,
Japan

Mr. Haraguchi graduated from Kagoshima Engineering High School 1961 in mechanical engineering. He then joined Sumitomo Electric Industries and has been engaged in design and product engineering of rubber and plastics products. He is a senior engineer of Communication Cable Accessories Engineering Section.



Yasuo Asano
Sumitomo Electric
Industries, Ltd.
1, Taya-cho,
Totsuka-ku,
Yokohama,
Japan

Mr. Asano received his B.S. degree in Mechanical Engineering from Waseda University in 1968. He joined Sumitomo Electric Industries in 1971 and has been engaged in development and design of connectors for coaxial cable and optical fiber cable. He is now a senior engineer of Communication Cable Accessories Engineering Section, and a member of the Japan Society of Mechanical Engineers.



Yuzo Tokumaru
Sumitomo Electric
Industries, Ltd.
1, Taya-cho,
Totsuka-ku,
Yokohama,
Japan

Mr. Tokumaru graduated from Oita Technical College 1970 in mechanical engineering. He then joined Sumitomo Electric Industries and has been engaged in development and design of accessories for communication cables. He is now an engineer of Communication Cable Accessories Engineering Section.



Takeo Seike
Sumitomo Electric
Industries, Ltd.
1, Taya-cho,
Totsuka-ku,
Yokohama,
Japan

Mr. Seike received the B.E. degree in precise engineering from Osaka University in 1975. He then joined Sumitomo Electric Industries and has been engaged in development and design of accessories for communication cables. He is now an engineer of Communication Cable Accessories Engineering Section.

OPTICAL AND MECHANICAL CHARACTERISTICS OF MICROFLAME
FUSION SPLICING OF OPTICAL FIBER

B. FERNANDEZ RONDAN; A. AGUILAR MORALES

Centro de Investigación de Standard Eléctrica, S.A.
Madrid
SpainSummary

A microflame fusion splicing technique has been statistically studied in order to evaluate the contribution on the splicing loss of fiber ends flatness, initial misalignment, final aspect of the splice, core/cladding deformations, impurities, air bubbles in the splices, fusion time and glass temperature. The mechanical resistance characteristics have been studied and compared with non spliced fibers, both with just fusion splices and with fusion followed by an annealing process. A splicing machine by a but: -oxygen miniature torch and an observing microscope was developed and used in the experiments. The tests were made in five groups of splices using multimode 50/125 micron diameters, 0.22 N.A. graded index fibers, on a cutting and splice basis, to evaluate the contribution of all aspects of the splicing process in the transmission loss. A conclusion of this work is that the reasonable splice quality, repetitivity and simplicity of the process make it a good and economic alternative for splicing of multimode fibers.

Introduction

Splicing optical fibers was considered in the past a critical factor, but nowadays, low loss splices are easily performed even in hard field environment. Among multitude of fiber splicing methods, direct fusion of the glass faces has been widely accepted, because of the simplicity, and high quality splices obtained with these methods. The fusion splice using high voltage electric arc machines are being much more used than the method using a flame machine. The purpose of this article is to propose that using the microflame fusion method can be a good and economic alternative to the arc fusion for field splicing of multimode fibers.

This microflame fusion splicing technique has been statistically studied in order to evaluate the contribution on the splicing loss of fiber cleaving quality,

final aspect of the splice, core/cladding deformations, impurities, fusion conditions, initial misalignment of the fibers and other special incidences. Also the mechanical resistance characteristics have been studied and compared with non spliced fibers, both with just fusion splices and with fusion followed by an annealing process.

Experiment Methodology

The experiment was initiated with a set of measurements organized in five groups of splices, followed by an analysis of the results. The first group of splices is a general statistical loss test analysis, including the study of the influence of different kind of splice defects in the splicing loss. The second group of splices was made to evaluate the dependence of the fusion conditions, such as the fusion time and the flame characteristics in the transmission loss. The third group of splices was made to establish the influence of the initial misalignment of the fiber ends to be joined on the splice loss. A fourth group of samples was selected among the former groups in order to study the core cladding distribution in the splice proximity and its influence on the loss. The fifth group of splices was used for a mechanical test studying the influence of the annealing process in the splice mechanical strength.

The tests were made on a cutting and splice basis, using standard multimode graded index fiber with an attenuation of 3.5 dB/Km at the wavelength of 850 nm a core/cladding diameters of 50/125 μ m respectively, and a numerical aperture of 0.22.

Each splice has been identified, and besides the transmission loss, other factors that can affect its quality has been noted in the measurement sheets, such as fiber ends cleaving quality; final aspect of the splice observed through the microscope; core uniformity; and other special incidences. Three different persons have participated in the measurement

in order to make independent the results from the operator skill.

In the analysis of results stage, the influence on the splicing loss of the splice conditions and incidences, was considered, obtaining statistical results in different conditions.

Splicing Method

The microflame fusion splicing machine used in this experiment was developed to make the splices in the first optical line installed in Spain in 1980. The special requirements of that installation (a railway tunnel with hard environmental conditions) claimed for the selection of an adequate splicing technique. The microflame method proved to be a good one.¹ Later on, the machine has been improved.

The machine^{2,3} (Fig. 1) is composed by an alignment and approaching device; a miniature welding torch; an observing microscope; and a platform supporting the



FIGURE 1: MICROFLAME FUSION SPLICING MACHINE. CLOSE-UP OF THE ALIGNMENT DEVICE WITH TWO FIBERS BEING SPLICED.

above assemblies, including a multiple fiber holder and a couple of optical cable holders for easy handling of optical cables. The aligning and approaching device has two V-grooved fiber supports capable of relative movements in three dimensions: an X-Y micromanipulator for fiber alignment, and fiber ends approximation by means of a sliding mechanism operated by a lever. The butane-oxygen microflame is obtained with the miniature torch being provided with a head with a special nozzle incorporating a 45° mirror. This head is fixed to the arm of the torch which has rotating movement in a vertical plane, to locate the mirror and the nozzle at working and resting

positions.

The thermal expansion caused in the faced fibers just at the beginning of the heating process is sufficient to provide the required pressure for joining both ends. When the fusion takes place, the surface tension of the softened glass causes the joint to tend to be uniform, giving the joining a final aspect of perfect continuity.

The process of a splice have been divided into seven steps: stripping the secondary and primary coating; cleaving the two fiber ends to be joined; aligning the two fiber faces; regulating the flame conditions; fire cleaning the fibers end; fusing the two fibers and splice annealing. All the conditions and incidences were easily observed through the splicing machine microscope without interrupting the process.

Although splice samples has been studied in detail with an interferential microscope, the fiber core uniformity was approximately observed during the splicing process because when the glass is at softening state the core can be seen through the machine microscope. For simplicity cleaving fiber ends was manually made with a diamond knife.

Splicing Loss Measurement Set-up

The block diagram is shown in Fig. 2. An 850 nm light emitting diode excited by a

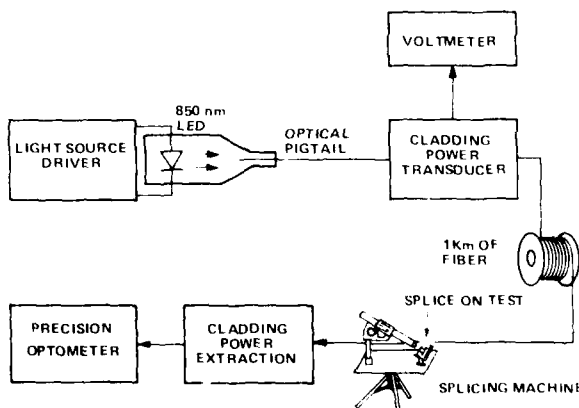


FIGURE 2: SPLICING LOSS SET-UP. HIGH PRECISION AND STABILITY IS OBTAINED DUE TO THE CONSTANT MONITOR OF THE REFERENCE LIGHT POWER.

controlled light source driver was used in the experiments. In the set-up used in this experiment, the reference signal has not been maintained accurately constant, but its small fluctuations have been monitored using a special cladding power transducer which extracts the light from

the cladding of a length of fiber and converts it in an electrical signal.^{4,5} The variations of the cladding detected light, measured by the voltmeter, has proven to be proportional to the core light power variations, so an indirect reading of the reference signal is obtained with this method. In order to have real conditions in the splice on test point, 1 Km of fiber was connected after the cladding power transducer device. The splice on test point was situated several meters before the end of this long fiber. Between the splice point and the precision optometer, a cladding power extraction device⁶ was placed. The calibration curve of the reference signal versus the cladding power was periodically checked. The resolution of this method is better than 0.005 dB.

General Statistical Loss Test

The first statistical test was made with 120 splices. Each initiated splice was finished and evaluated, even if specially bad conditions were detected during the process. Seven specially bad cases (5.8%) were detected: Two splices had a collapsed shape due to overheating; three splices with one of the fiber ends to be joined irregularly broken in the cleaving with the break covering more than 50% of the surface of the core; one splice had a small particle of the primary coating material between the faces to be joined; and one splice with an air bubble between the faces of the joint. All these defects were easily identified during the process by observing through the splicing machine microscope. These splices could have been easily remade if required in a regular splice process. These special cases have been eliminated in the statistical study.

The transmission loss histogram of Fig. 3 shows 0.11 dB mean loss with a standard

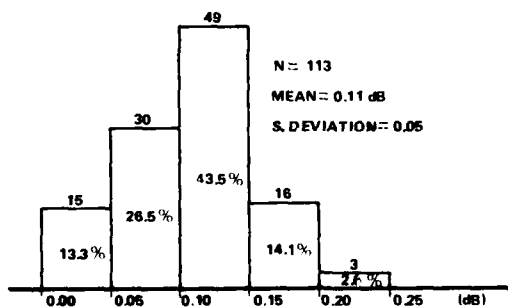


FIGURE 3: SPLICING LOSS GENERAL HISTOGRAM

deviation of 0.05, excluding the 5.8% specially bad splices, outside the normal distribution. 0.13 dB of mean loss are

obtained including all the 120 samples. Splices with similar peculiarities are grouped in table 1, in order to establish the contribution to the splicing loss of fiber cutting, splice deformation due to overheating and core misuniformity. In the group of good cleaving quality, a 74% have been obtained with perfectly flat faces, with a mean loss of 0.10 dB. The

Splice Subgroups	Perfect		Imperfect	
	%	dB	%	dB
Cleaving quality	74	0.10	26	0.14
External uniformity	91	0.10	9	0.17
Core uniformity	76	0.11	24	0.14

TABLE 1: Percentage and mean loss (dB) of splice subgroups with similar peculiarities

other 26% of the cuts have some defects affecting the flatness or the perpendicularity of the fiber ends, due to the manual cleaving method used for simplicity, averaging 0.14 dB of splice loss. In spite of easy selection of good quality cut during the process, it is not worth to perform a selection because cleaving defects increase the total average loss only in 0.01 dB (10%) approximately.

In 91% of the cases, the external aspect of a finished splice observed through the splicing machine microscope, looks like a perfect cylinder, being the splice in most of the cases imperceptible. (See photo b of Fig. 4).

In 9% of the cases some deformation is observed in the final aspect of the splice due to different reasons, being the most important the overheating due to either an excessive proximity of the flame or an excessive fusion time (see photo c of Fig. 4). In table 1 it can be observed that this kind of defect is the most sensible one to the splicing loss (0.17 dB). Although selection is also very easy in a current splicing process, it is not worth doing it due to the poor influence in the total splice loss (around 10%).

The core internal misuniformity of the joint in most of the cases is a consequence of a bad cleaving, because the core material with lower fusion temperature occupies the notch of the cutting defect. The influence of this defect in the mean loss is, as seen in table 1, similar to the cleaving quality subgroup, in percentage and in mean loss.

The results of this comparison supports the conclusion that no significant mean total loss exists with the optimum conditions splices, (except in the exceptional cases of a silicone particle or an air bubble in the splice, and cutting

defects affecting significantly the core of the ends of the fibers.

Splice Quality Dependence of Fusion Conditions

A second group of measurements were performed to establish how critical are the flame conditions and welding time in the microflame splicing process. This test was made with 20 splices on the basis of cumulative time increments of flame application in the sample on test, measuring the transmission loss in each increment. This increment of time was 5 seconds during the first 20 seconds and ten seconds later. Fig. 4 shows three curves of splices transmission loss as a function of cumulative fusion time. Curve 1 repre-

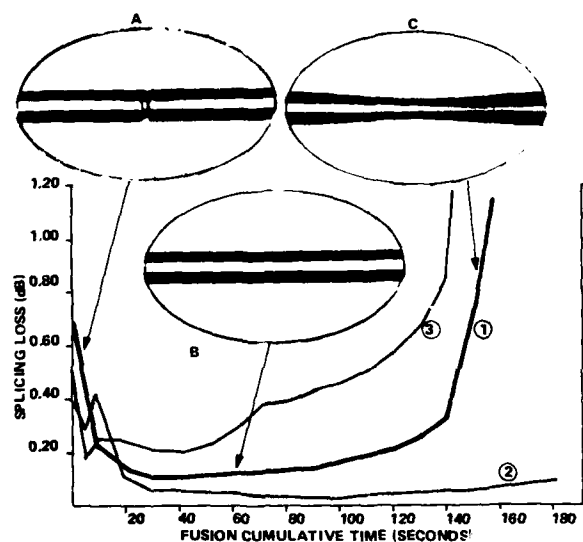


FIGURE 4: SPLICING LOSS DEPENDENCE OF FUSION TIME.
1) MEAN VALUE; 2) BEST CASE; 3) WORST CASE

sents the mean value of the loss and curves 2 and 3 are the best and worst case respectively. The mean curve indicates that between 15 seconds and nearly two minutes of fusion time the splice loss is maintained fairly near the minimum, and the aspect of the splice area is generally a perfect cylinder (photo b). Before 15 seconds, the losses are higher and the aspect is "unfinished" as indicated in photo a. After 1.5 minutes the loss smoothly increases and the fiber shows a slight narrowing as indicated in photo c. After 2.5 minutes to 5 minutes of applying the flame (depending on the sample considered), the splice zone is completely narrowed, the loss increases considerably and it separates in two parts.

In all the tests, the flame proportions of butane and oxygen were regulated to

obtain a good combustion, getting a blue dard-shaped flame. As the distance from the point of the torch nozzle to the splice point is fixed by the machine (6mm), the length of the flame is the factor that can affect the splice quality due to the glass temperature and in consequence the welding speed. The optimum length of the blue part of the flame was found to be of the order of 3 millimeters (a distance of about 3 mm from the point of the flame to the splice). Fifteen of the splices of this test were made in the optimum flame conditions, obtaining curves similar to number 2, with less splices loss and much less affected by the fusion time. The other five splices were intentionally made with a more than the usual flame size (of the order of 5 mm). The worst of these results is shown in curve 3. This case is slightly more sensible to the fusion time and the transmission loss are generally higher. Even in the worst fusion conditions, the quality of the splices is perfectly acceptable. It is remarkable that a flame length of more than 5 mm is difficult to obtain because it becomes extinguished due to the torch nozzle design.

Influence of Initial Misalignment

A third group of 50 splices was made and evaluated in order to establish the influence of the initial misalignment on the transmission loss. The initial misalignment of the fibers was visually measured through the machine observing microscope. The fibers are automatically self-aligned during the welding process due to the forces of the surface tension of the fused glass, and the external aspect of the finished splices is generally a perfect cylinder as in former tests. The test was made in 5 groups of 10 splices, each with an increment of misalignment of about 10% of the fiber external diameter. Fig. 5 shows the mean values obtained in each

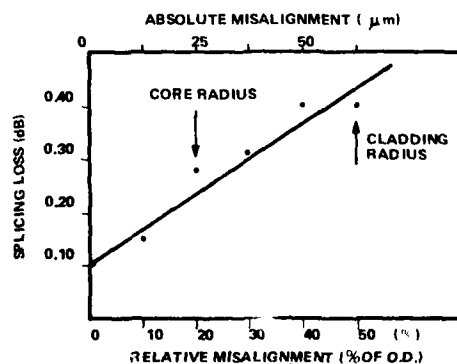


FIGURE 5: SPLICING LOSS VS INITIAL MISALIGNMENT

group and the least square linear approximation. In the graph it can be observed that with a misalignment of $62.5 \mu\text{m}$, corresponding to a 50% of the external diameter (or a 125% of the core diameter), the mean loss is only 0.4 dB. A core misalignment of 50% gives a mean loss of 0.23 dB. With a misalignment lower than 10% of external diameter (25% of core diameter) the loss increment is practically negligible. As a practical conclusion of this test, no very special care has to be taken in aligning very precisely the fiber ends to be joined, in the case of multimode fibers.

Interferential Microscope Analysis

A fourth group of special splice samples were selected of the former groups of tests in order to study the core/cladding distribution inside the splice, and to show how this material distribution is related to both the transmission loss and the incidences on the splice process. For this study an interferential microscope was used. Photographs of Fig. 6 were selected to show the most representative

cases. Transmission loss and splice conditions are indicated in the figure. In splices with a good cleaving quality and optimum splice conditions, a good core continuity made the splice nearly imperceptible (Fig. 6a). Poor cleaving quality is shown in Fig. 6b in which part of the core material, which has lower softening temperature, occupies the notch of the cladding due to the bad cut. Fig. 6c is a typical case of splice overheating, combined with a bad cleaving quality. Fig. 6d is one of the specially bad splices due to a particle of silicone in the faces of the fibers. This splice was intentionally made in order to study the effect. Other special case is shown in Fig. 6e. This rare case is an air bubble in the splice which blew out in the welding process. Fig. 6f shows one of the splices made with 50% of initial misalignment. It can be observed that the core material is shifted in self aligning process due to the surface tension.

Splice Annealing and Mechanical Strength

Finally a fifth group of 30 measurements were made applying after the fusion an annealing process consisting of smooth cooling by using the hot air arising from the flame, in the same splicing machine. The tension strength was measured and compared with non annealed splices, taking non splices fiber pieces as a reference. The annealed splices had a mean tensile strength of 460 gr. compared with 232 gr. for non annealed splices. The mean tensile strength non splices fibers was 804 gr.

A pneumatic mechanical strength tester, specially adapted for fiber tests was used in this experiment. The mechanical tests were performed with no mechanical protection of the splices.

Conclusion

This paper reports the evaluation of a manual method of splicing optical fiber by using a butane-oxygen welding machine.

The results of the evaluation are that this simple method is not very dependent of the operators skill. It has been analyzed the influence of cleaving, welding conditions and alignment, with the conclusions that no significative loss of quality can be observed taking the mean transmission loss as reference. Therefore it is found that no special automatic mechanisms of positioning and control are required to perform good splices. Besides the possibility of annealing and the simplicity of the machine makes this process a good alternative for high quality splicing for multimode fibers.

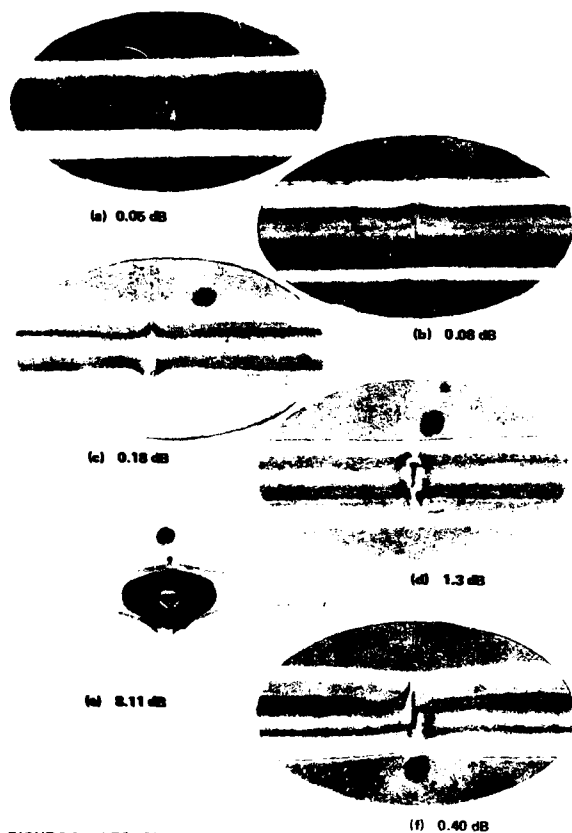


FIGURE 6: INTERFERENTIAL MICROSCOPE ANALYSIS. a) GOOD QUALITY; b) BAD CLEAVING; c) BAD CLEAVING AND OVERHEATING; d) SILICONE PARTICLE; e) AIR BUBBLE; f) 50% MISALIGNMENT.

Acknowledgements

The authors wish to thank Mr. L. Sanz for his valuable contribution in the design of the splicing machine, and to Mr. A. Ruiz and A. García Liz for assistance in the experimental work.

References

1. "Optical Fiber Technology: Transmission System for the Spanish National Railway". B. Fernández, A. Aguilar. Electrical Communication Vol. 56 No. 4, 1981.
2. "Welding Machine for Splicing Optical Fibers". B. Fernández, L. Sanz. Spanish Patent No. 253.398, Oct. 8, 1980.
3. "Improved Welding Machine for Splicing Optical Fibers". B. Fernández, L. Sanz. Spanish Patent No. 260.004, Aug. 12, 1981.
4. "Method to Create or Make Use of Areas of Energy Extraction in Optical Fibers". B. Fernández, A. Aguilar. Spanish Patent No. 476.609, Jan. 5, 1979.
5. "Optoelectronic Transducer for the Utilization of the Energy Extracted from the Cladding of an Optical Fiber". B. Fernández, A. Aguilar. Spanish Patent No. 491.784, May 23, 1980.
6. "Improvements in Optical Fiber References". A. Aguilar, B. Fernández. Spanish Patent No. 491.911, May 28, 1980.

Biographies



Baldomero Fernández Rondán was born in 1947 in Sanlúcar de Barrameda (Cádiz), Spain. After graduating from Madrid Polytechnic University with a degree in telecommunication engineering he joined CIISE* in 1974. During 1976 and 1977 he worked in the optical communication division of STI, Harlow, UK, on the design of the 140 Mbit s⁻¹ Hitchin-Stevenage optical transmission system. He is at present responsible for the CIISE optical communication group, which has developed and installed a number of optical fiber telephone and telemetry transmission systems.



Antonio Aguilar Morales was born in 1945. He received a BSc in electronic physics in 1968 from the University of Madrid, after which he worked for the Optics Institute of the Scientific Research Council, Madrid. He joined CIISE in 1972 as an engineer in the telecommunication planning division. During 1976 he worked at

STI on optical fiber manufacturing, measurements, and systems. Since 1977 he has been with the optical fiber group of CIISE, working on optical fiber technology and electro-optical devices.

(*) CIISE. Centro de Investigación de Standard Eléctrica, S.A.

ARC-FUSION SPLICE OF OPTICAL FIBER AND ITS RELIABILITY IN FIELD

Mitsuru Miyauchi*, Michito Matsumoto**, and Tadashi Haibara**

*Research & Development Bureau, N.T.T.
Musashino, Tokyo 180, Japan**Ibaraki Electrical Communication Lab, N.T.T.
Tokai, Ibaraki, 319-11, JapanAbstract

In practical optical cable transmission systems, efficient, stable, and reliable fiber splice techniques are required for optical transmission line construction. This paper describes design and performance of an arc-fusion splice machine, a fiber cutting tool, and a reinforcement for spliced portion. Field trial results on the splice are also discussed.

In order to assure long-term stability and reliability, stresses applied to fiber inside the reinforcement element due to fiber buckling, torsion and pushing out from the plastic coatings are clarified. It is also verified that proof testing with the proof stress of approximately 180 g is necessary for long-term durability of fiber against the applied stresses.

1. Introduction

Optical fiber transmission systems utilizing various advantages of fiber characteristics have been developed widely in many countries and institutes.¹ In practical optical cable transmission line construction, efficient, stable and reliable fiber splice techniques are required, and many kinds of splicing methods and techniques have been proposed.^{2,3} Among them, we have made a choice to use an arc-fusion splicing method in the viewpoint of workability and reliability in field. The important points required for the practical splice technique are as follows:

- 1) Simple and easy operation of splicing apparatus even for unskilled person in field.
- 2) Long-term reliability and stability for a spliced portion.

This paper mainly deals with multi-mode fiber splice, describing design and performance of a semi-automatic splicing apparatus using pre-fusion method⁴, a simplified cutting tool for fiber end-face preparation, and a reinforcement

method using heat shrinkable tube. Field test results show that low splice loss less than 0.1 dB on an average and high workability of about 4 minutes per one splice are achieved using the above mentioned components.

Furthermore, proof testing for spliced fiber before reinforcement is proposed to guarantee the life time of 20 years for the spliced portion.

2. Procedure for the optical fiber splice and requirements for the practical splice method

The splicing procedure for plastic coated fibers consists of the following processes;

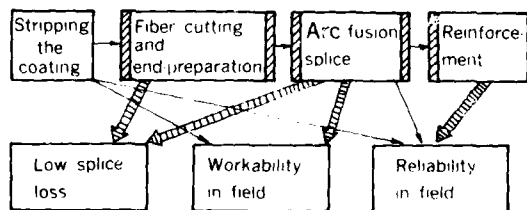
- 1) stripping and removing plastic coatings of optical fibers,
- 2) cutting the fibers with an appropriate length,
- 3) arc-fusion splicing of pair fibers.
- 4) reinforcement for the spliced portion.

Figure 1 shows relationships between the splicing processes and requirements for the practical splice especially in field.

Broad arrows indicate the strong and important relationships.

2.1 Low splice loss

As shown in Fig.1, fiber cutting and arc-fusion are the main items to achieve low splice loss. Factors to be considered are; (1) cutting condition to obtain good fiber end face, and (2) arc-fusion splice condition to attain low splice loss,



(this paper discusses about [1])

Fig.1 Relation between splicing procedures and requirements for the practical splice

AD-A125 662

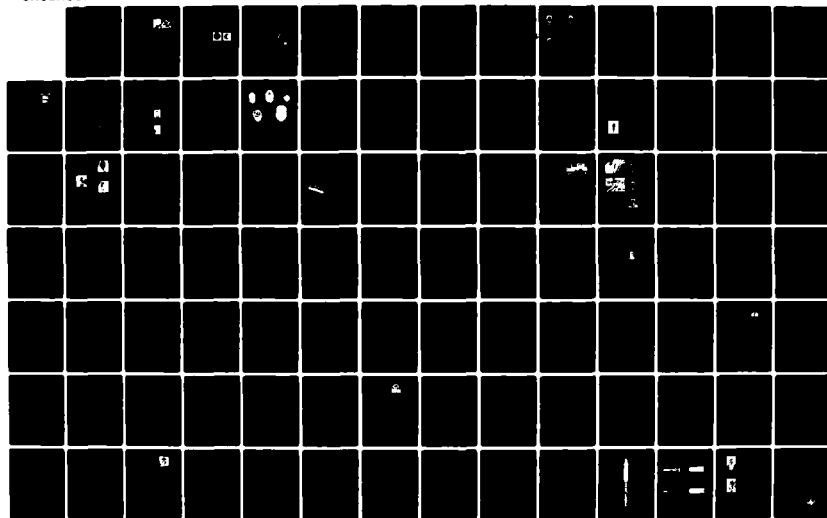
PROCEEDINGS OF THE INTERNATIONAL WIRE AND CABLE
SYMPOSIUM (31ST) HELD AT..(U) ARMY
COMMUNICATIONS-ELECTRONICS COMMAND FORT MONMOUTH NJ
NOV 82

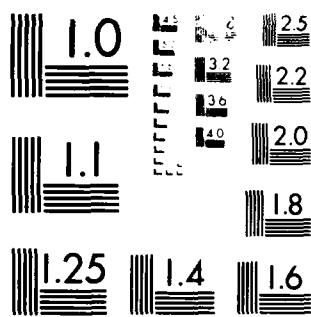
316

F/G 20/6

NL

UNCLASSIFIED





MICROCOPY RESOLUTION TEST CHART
NATIONAL BUREAU OF STANDARDS-1963-A

such as discharge voltage and time, pre-fusion time, and stuffing length for fibers to be spliced.

2.2 Workability

In the arc-fusion splice as well as other splicing techniques, workability is the most serious problem compared with that for the conventional metal wires. This is because almost all fiber splicing techniques require accurate axial alignment of fibers to be spliced, which is liable to depend on the skill of operators. Then, the automatic splice apparatus may be one of the solutions for the above problem.

2.3 Reliability

Reliability of the spliced fiber is mainly related to the reinforcement of the spliced portion. Optimum reinforcement method suitable for the layer structure of the presently used coated fiber must be examined to establish long-term reliability of the splice.

3. Optical fiber cutting tool

3.1 Requirements for a fiber cutting tool

Various types of fiber cutting tool based on the breaking method under tension⁵ have been used widely for fiber end-face preparation because of good cutting performance and simplicity in operation compared with the polishing method. The major target of the present investigation is to develop a more economical cutting tool, which can be used even by unskilled workers with good reproducibility. The following mechanisms must be provided for the tool;

- 1) A mechanism for blade pressure control to make a flaw in a specified amount on the optical fiber surface.
- 2) A guide mechanism to keep the cutting length constant.
- 3) A guide mechanism to set the optical fiber perpendicular to the blade.

3.2 Performance of the fiber cutting tool

Structure of the developed fiber cutting tool is shown in Fig.2. The size of the tool is about 2cm wide, 3cm deep, and 10cm long. The weight of the tool is only 90g. This small-size cutting tool of stapler type meets the above mentioned requirements in all respects, and is characterized in its simple operation throughout the cutting process as well as the good cutting performance. Figure 3 shows a histogram of breaking angle of fiber end face prepared by the cutting tool. The average breaking angle is found to be less than 1°. Cutting tests were repeated for

1000 times and the breaking angles were measured. The results for two cutting tools are shown in Fig.4, along with the data after the drop test from 5 meters.

The tests verify the stable operation of the tool.



Fig. 2 Fiber cutting tool

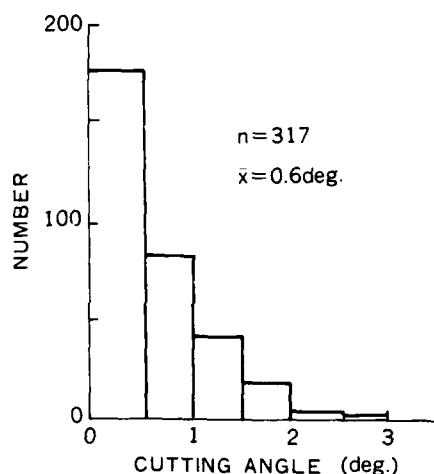


Fig. 3 Histogram of the fiber breaking angle

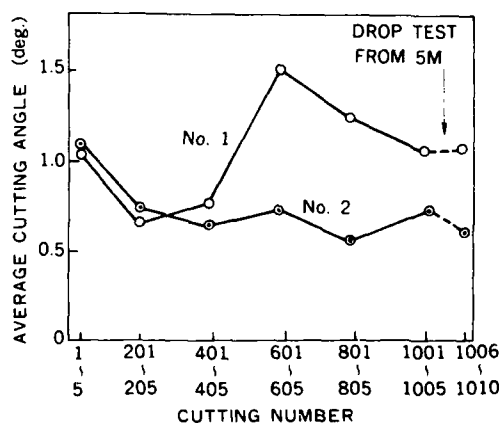


Fig. 4 Average fiber breaking angle as a function of the cutting number

4. Arc-fusion splicing apparatus

4.1 Development of a semi-automatic splicing

Major targets for the development of an arc-fusion splicing apparatus are; (1) low splice loss, (2) automatic alignment of fibers to be spliced, and (3) simple monitoring mechanism for the splice point.

The pre-fusion technique is useful for low loss fusion splicing of multimode fibers.

Figure 5 shows arc-fusion processes using the pre-fusion method. Fibers to be spliced are aligned with a small gap a few tens microns. Then, the arc-discharge is started and simultaneously fiber ends are pressed together under the continual arc-discharge. Photographs of a fiber end face before and after pre-fusion are shown in Fig. 6. It is found that the fiber core becomes a convex shaped due to pre-fusion, resulting in smooth contact of fibers to be spliced.

The fusion conditions such as pre-fusion time and stuffing length are important for low loss splice in this technique.

Figure 7 shows the dependence of splice loss on stuffing length H with various pre-fusion time t . It is apparent from Fig. 7 that the optimum stuffing length exists for each pre-fusion time.

Figure 8 shows the experimental relation between splice loss and pre-fusion time for fibers with imperfect end faces. The broken line indicates a tendency for fibers with good end face for comparison.

The pre-fusion is found to be especially useful for low loss splice when the fiber end faces are imperfectly prepared. The loss for the imperfect end face becomes nearly equal to that for the good end face by setting an appropriate pre-fusion time. As a result of these investigations, 0.3-0.4 sec pre-fusion time and about 30 μm stuffing length are found to be suitable to achieve low loss splice without failure.

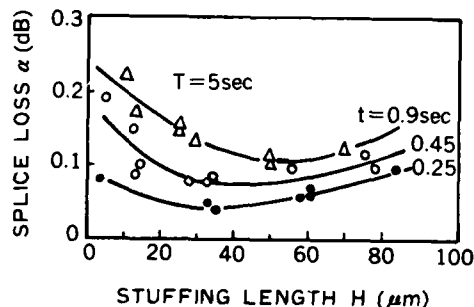


Fig. 7 Splice loss vs. stuffing length for various pre-fusion time

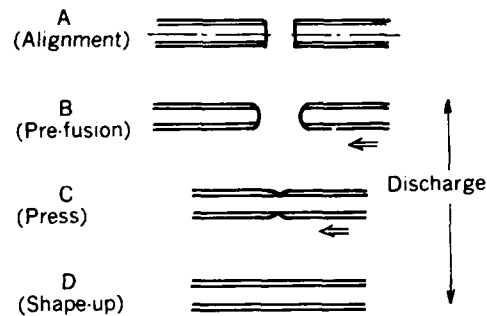


Fig. 5 Splicing process using the pre-fusion method

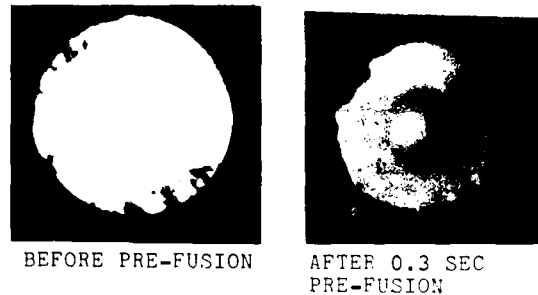


Fig. 6 Fiber end face before and after the pre-fusion

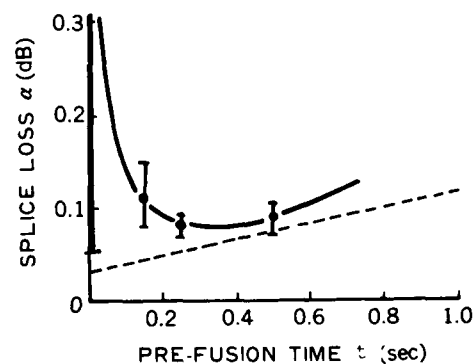


Fig. 8 Splice loss vs. pre-fusion time for fibers with imperfect end face

Automatic fiber alignment is necessary to improve working efficiency. Furthermore, splice loss tends to vary with the skill of worker especially for fiber setting on the apparatus. Thus, a slippery holder, by which the fiber alignment can be made with easy handling and with good reproducibility, is developed as described later.

In general, evaluation of fiber splice loss is made by the optical monitoring method using a light source and a detector. The method requires a certain amount of labor for the measurements, and much simpler method is necessary for the practical splice in field. For this purpose, a new method is adopted, where the splice point is observed by a microscope from two perpendicular directions using a mirror.

Most of the offsets between fibers before and after arc-fusion are visually checked. This monitoring mechanism markedly reduces the failure probability of splice, and also makes the splice loss estimation possible by checking geometrical deformation and imperfection of the splice point.

4.2 Performances of the arc-fusion splicing

In view of enhancement of operation efficiency and workability in the splice procedure, a semi-automatic splice apparatus has been developed. Figure 9 shows the splicing procedure of the machine. The procedure consists of the following five processes:

- 1) The optical fibers are set roughly on the fiber slippery holders.
- 2) The fibers are pushed deeply to butt fiber ends against a stopper.
- 3) The stopper is removed downwards and both fibers are automatically moved together with a distance required for the pre-fusion. Then, a mirror is placed between electrodes, permitting the observation of alignment and end-face conditions in two perpendicular directions.
- 4) Arc-discharge is started after the mirror is removed.
- 5) The fibers are fused and are pressed together with the predetermined stuffing length. The splice is finished in several seconds.

The processes 1) and 2) are made by an operator and other processes are made automatically. Figure 10 shows the photograph of the splice machine. Dimension of the machine is 22(W)*15(D)*19(H)cm³, and its weight is 4.7 kg excluding the microscope.

The splicing machines have been used in a field trial of trunk-line optical transmission systems using graded-index fiber cables. In the field trial, a total number of 840 splices have been made in manhole and on pole

Figure 11 shows a histogram of measured

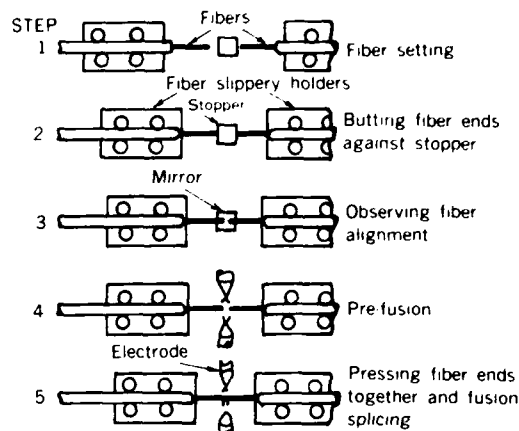


Fig. 9 Arc-fusion splice procedure



Fig. 10 Semi-automatic arc-fusion splicing machine

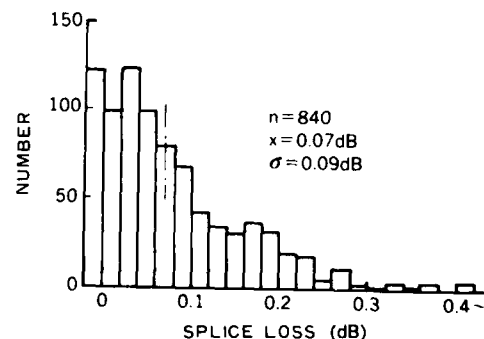


Fig. 11 Splice loss histogram in field for graded-index fibers.

splice losses. The loss measurement accuracy is estimated to be $\pm 0.02\text{dB}$.

It is found from Fig. 11 that the average splice loss is 0.07 dB and about 90 % of total splices exhibit the loss values smaller than 0.2 dB. No differences

in the splice loss and working efficiency are observed between the splices in manhole and on pole.

Figure 12 shows a histogram of the time required for the arc-fusion splice.

Average time is less than four minutes and about a half of the total splices is finished within two minutes.

In order to examine the usefulness of the visual checking method described in 4.1, splice operators have judged the splice to be successful or not by the microscopic observation of the splice point, without knowing the measured loss value. It is found that 99 % of the visual judgements meet those based on the loss measurements.

As a result, splice method without optical monitoring is considered fully practical and the method serves for simplification of splice procedure in field.

5. Reinforcement of a spliced portion

5.1 Requirements for a reinforcement method

The strength of the spliced portion is much reduced compared with that of the original fiber, due to removal of plastic coatings. For this reason, it is necessary to reinforce the fusion spliced portion.

In developing the reinforcement, optimum material and structure must be selected, so as to prevent fiber failure and fluctuation in reinforcement characteristic. It is necessary to clarify the stress applied to the fiber inside a reinforcement element for the optimum selection.

Fiber pushing out from the plastic coatings is one of the important factors to degrade the reliability of the reinforcement.

This pushing out results from the release of residual strain in plastic coatings. In Fig. 13, dependence of pushing out length on fiber length is shown for three-layer coated fiber shown in Fig. 14. It is found that the pushing out is remarkable under the heat-cycle test. This gives rise to fiber buckling and fiber break inside the reinforcement element.

Another factor affecting the reliability is a fiber torsion.

The torsion added to a coated fiber is propagated to the fiber end inside the reinforcement, because the fiber is not fixed tightly in nylon coating and buffer layer.

Figure 15 shows the relative torsion at fiber ends as a function of torsion applied to the coated fiber from outside under the heat-cycle test of 20 days. The torsion is propagated to fiber end inside the reinforcement element and this results serious stress in the spliced portion.

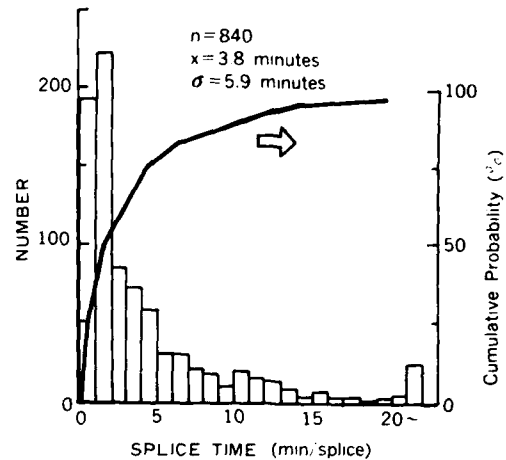


Fig. 12 Histogram of the arc-fusion splice time

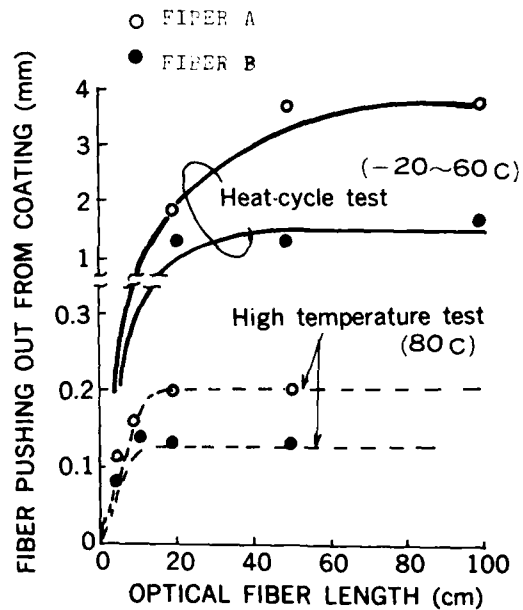


Fig. 13 Fiber pushing out from nylon coating under the aging tests for 20 days

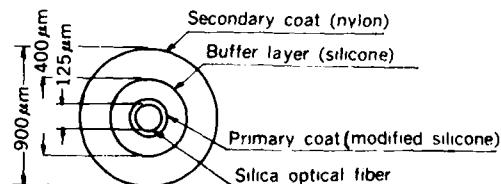


Fig. 14 Three-layer coated fiber structure

These stress due to fiber pushing out and torsion as well as the stress due to the thermal expansion are the main factors for fiber break in the reinforcement element.

Thus, the element must be designed to prevent these stresses applied to the fibers.

5.2 A new reinforcement element

Figure 16 illustrates the structure of a new type of reinforcement. The reinforcement is composed of a polyethylene (PE) shrinkable tube, an ethylene vinyl acetate (EVA) inner tube, and a steel rod both inserted in the PE shrinkable tube.

The EVA tube melts by heat and fixes the spliced fiber by shrinkage pressure of the PE tube. The steel rod contributes to increasing the tensile strength and also provides uniform pressure to the spliced fiber. In this method, it is important to avoid air bubbles and to prevent imperfect shrinkage during heating. Therefore, a heating apparatus is developed, where the heating is made at the tube center first, and the heating areas are moved gradually to the tube ends automatically.

Proof testing mechanism is also included in the apparatus in order to assure long-term reliability of the reinforced portion.

5.3 Characteristics of the reinforced portion

Figure 17 shows Weibull plots of the fiber breaking strength before and after reinforcement. Average strength of 2.3 kg is attained due to the reinforcement. Figure 18 shows the measured loss change against the temperature, where two-layer coated fiber without nylon coating (Refer to Fig 14) is used to evaluate the loss increase exactly at the reinforced portion. No loss increase is found in the temperature range of -30°C to 60°C . Even at a very low temperature of -70°C , the loss increase is only 0.02dB/splice.

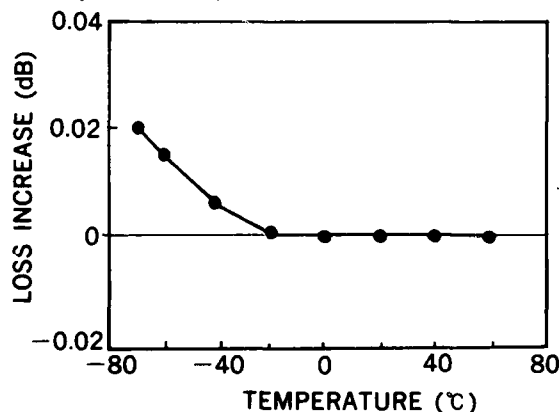


Fig. 18 Temperature dependence of loss increase for the reinforced splice portion

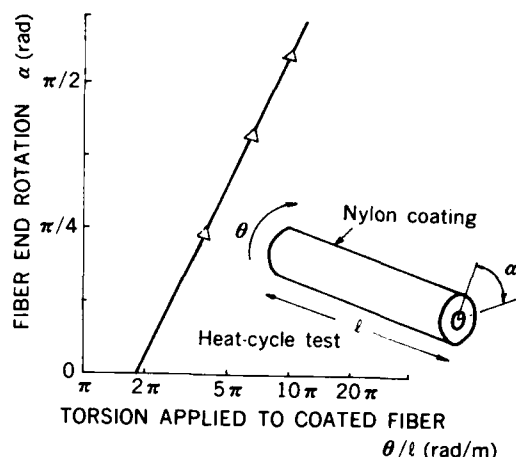


Fig. 15 Relation between torsion at the fiber end and torsion applied to the coated fiber under heat-cycle test

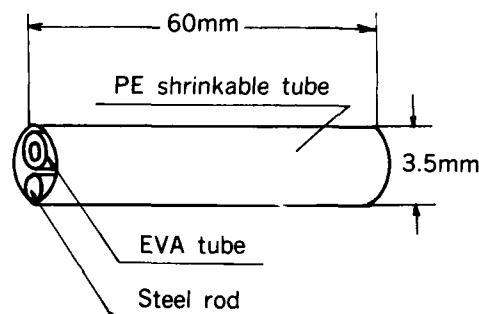


Fig. 16 Structure of a new reinforcement element

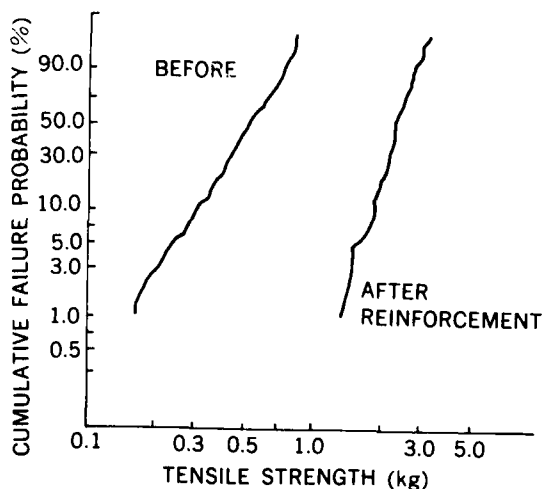


Fig. 17 Weibull plots of cumulative failure probability before and after reinforcement

The most important criterion for the reinforcement is the fiber failure probability at the reinforced portion during environmental tests. Heat-cycle test was made for splice specimens with a torsion of one turn, as shown in Fig. 19. The test condition was 4 cycle/day between -20°C and 60°C.

There was no fiber break for 200 samples after 40 days test. The tensile strength after the heat cycle test was not varied compared with that before the test.

5.4 Assurance for long-term reliability

In order to assure long-term reliability of reinforced portion, it is useful to reject the spliced fiber with low strength by proof testing. Various proof stresses were examined for spliced portion. Figure 20 shows Weibull plots of the fiber breaking strength before and after proof testing. It is clear that low strength spliced portion is removed by the proof testing.

When a spliced fiber after proof testing is subjected to a static stress σ_s , the failure probability F_s is expressed by⁶,

$$F_s = 1 - \exp \left[-N_p \cdot \frac{m}{n-2} \left(\frac{\sigma_s}{\sigma_p} \right)^n \frac{t_s}{t_p} \right] \quad (1)$$

where σ_p is the proof test stress, t_p is the proof test time, t_s is the failure time, N_p is the failure probability during the proof testing, n is the constant determined by a material and environment, and m is the constant related to the initial strength distribution. When the stress increases at a constant rate q , that is

$$\sigma = qt, \quad (2)$$

F_s becomes

$$F_s = 1 - \exp \left[-N_p \cdot \frac{m}{n-2} \cdot \frac{1}{(n+1)q} \cdot \frac{\sigma^{n+1}}{\sigma_p^{n+1} t_p} \right] \quad (3)$$

Solid curves in Fig. 20 show cumulative failure probability distribution calculated using Eq.(3). The measured results are found to be in excellent agreement with the calculated results.

When the stress applied to a fiber inside the reinforcement element is given, relation between the proof stress and failure probability after proof testing is obtained using Eq.(1). Figure 21 shows the relation between F_s and σ_p calculated for the reinforcement element described in 5.2, where σ_s is estimated as 5 kg/mm². Here, the following parameter values are used; $n=22$ (in dry atmosphere), $m=4$, $t_p=6$ sec, and $t_s=20$ years.

In Fig. 21, relation between N_p and σ_p is also shown. Splice workability in field is strongly affected by the value

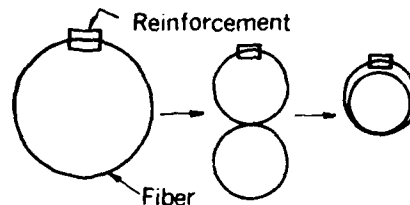


Fig. 19 Sample for heat-cycle test

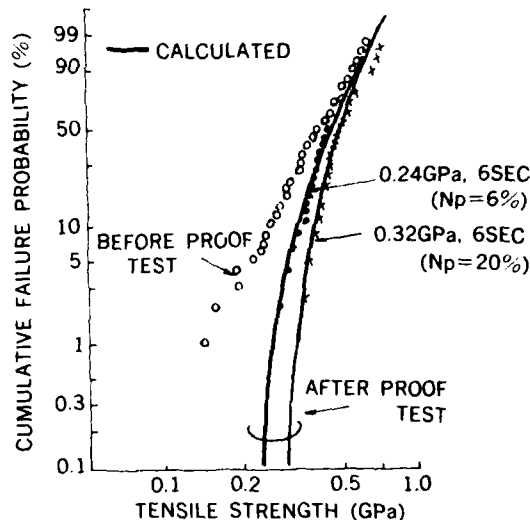


Fig. 20 Weibull plots of the cumulative failure probability for spliced fibers before and after proof testing

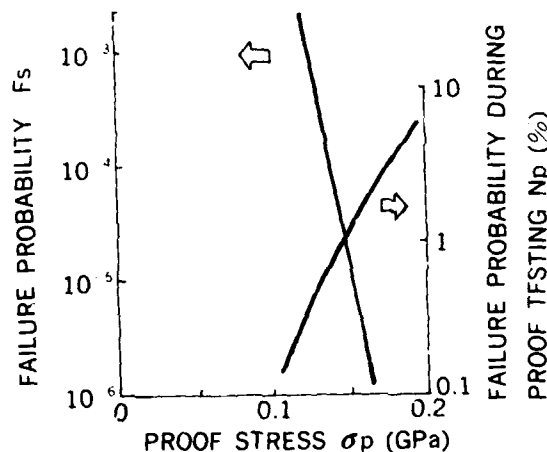


Fig. 21 Relation between F_s and σ_p , and that between N_p and σ_p . ($\sigma_s=5$ kg/mm², $n=22$, $m=4$, $t_p=6$ sec, $t_s=20$ years.)

of N_p . It is concluded from the figure that the failure probability for 20 years is suppressed below 10^{-5} and workability is not so degraded by the proof testing with the proof stress of 0.15 GPa (180 g for fiber with 125 μ m outer diameter).

6. Conclusion

We have investigated practical optical fiber splicing technique including an arc-fusion apparatus, a fiber cutting tool, and a reinforcement element for construction of stable and reliable fiber transmission lines. As a result, practical and high reliable splicing technique has been established as follows;

- 1) A stapler type cutting tool has been developed. The weight of the cutting tool is only 90 g. The average breaking angle for fiber end face is less than 1° .
- 2) A semi-automatic arc-fusion splicing apparatus has been developed. The apparatus is very compact and the main operation is made automatically. The optimum fusion conditions such as pre-fusion time and stuffing length have been determined for attaining low loss splice. In the field trial, average splice loss of 0.07dB is accomplished for graded-index fibers.
- 3) A new reinforcement method using heat shrinkable tube has been developed. The results for several reliability tests are found quite satisfactory.
- 4) Proof testing is applied for spliced portion and it is verified that the failure probability for 20 years is suppressed below 10^{-5} by the proof testing with the proof stress of 180 g.

These techniques are also applicable to the splice of single-mode fiber with some modifications, and we are now developing the single-mode fiber splicing techniques for long-haul high-bit-rate (e.g. 400Mb/s) optical transmission systems.

Acknowledgment

The authors wish to express their sincere thanks to N. Uchida for his useful discusses and guidance.

Thanks are also due to H. Fukutomi and N. Kozima for their encouragement.

Reference

1. T. Miki, M. Yamashita, "Commercialized 32MB/S & 100MB/S fiber optic transmission systems using 0.85 μ m & 1.3 μ m wavelength" 7th ECOC 1981, Bella Center, Copenhagen, Denmark, 15. 2-1.
2. G.C.Someda, Bell syst. tech. J. 52, 583(1973)
3. H.Murata, S. Inao and Y. Matsuda, in Digest of Topical Meeting on Optical Fiber Transmission (Optical Society of America, Washington, D.C., 1975)
4. M. Hirai, and N. Uchida, "Melt splice Multimode optical fibre with an electric arc", Electron. Lett. Vol.13, pp.123-125 (1977)
5. D. Gloge, P.W.Smith, D.L.Bisbee, and E.L.Chinnock, "Optical fiber end preparation for low-loss splice", Bell syst. tech. J. 52, No.9 (1973)
6. Y. Mitsunaga, Y. Katsuyama, Y. Ishida "Reliability assurance for long-length optical fibre based on proof testing" Electron. Lett. Vol. 17, No.16 P.567 (1981)



Mitsuru Miyauchi
Research & Development Bureau,
N.T.T.



Tadashi Haibara
Ibaraki Electrical
Communication Lab,
N.T.T.

M. Miyauchi, Staff engineer of Research & Development Bureau, N.T.T., is presently engaged in planning communication network. After joining ECL in 1973, he was engaged in the millimeter waveguide transmission system development and research on optical cable splices.

He received BS and MS degrees from Keio University in 1971 and 1973, respectively. He is a member of the Institute of Electronics and Communication Engineers of Japan.

T. Haibara, Engineer of Optical Transmission Line Section, Outside Plant Development Division, Ibaraki ECL, has been engaged in research and development of optical fiber splicing and its reliability. He joined ECL in 1981.

He received the BE and ME degrees in Precision Engineering from Hokkaido University in 1979 and 1981, respectively.

He is a member of the Institute of Electronics and Communication Engineers of Japan.



Michito Matsumoto
Ibaraki Electrical
Communication Lab,
N.T.T.

M. Matsumoto, Engineer of Optical Transmission Line Section, Outside Plant Development Division, Ibaraki ECL, is presently engaged in researching optical fiber splices. Since joining ECL in 1977, he has been engaged in the development of optical fiber splices.

He graduated from Kyushu Institute of Technology in 1975 and received his MS degree from Kyushu University in 1977.

He is a member of the Institute of Electronics and Communication Engineers of Japan.

AD P000560

FLAT MASS SPLICING PROCESS FOR CYLINDRICAL V-GROOVED CABLES

R.DELEBECQUE*

E.CHAZELAS**

D.BOSCHER***

*SAT-Département Câbles 41 rue Cantagrel 75013 PARIS-FRANCE

**SILEC-Service Applications Industrielles BP n°5-77130 MONTEREAU-FRANCE

***CNET-LANNION Route de Trégastel - 22301 LANNION - FRANCE

ABSTRACT

In France, among the loose structure cables, the V-grooved cylindrical element has emerged as the indisputable leader, and the mass-splicing process appears well adapted to it.

Although the cylindrical shape of the cable element naturally leads to the adoption of cylindrical splicing parts, the quality required in groove positioning and fiber coupling with this particular cylindrical approach has instigated SAT and SILEC to design a V-grooved flat splicing chip moulded from a polymer resin.

The essential advantage of this design is the simplicity of the mould allowing a flat chip to be produced easily and economically.

A special moulded plastic adaptor plate has been designed to transfer ten fibers from the cylindrical cable structure to the flat chip.

This paper describes the different splice elements, the mechanized splicing operation and a field splicing set-up. Histograms illustrating the results obtained over several hundreds of splices, are also provided.

This splicing process is currently being used in the wired city of BIARRITZ.

In conclusion, a concerted effort to achieve simplicity and efficacy in the splice component design and the splicing operation, has been made in order to ensure optimal reliability and cost effectiveness.

INTRODUCTION

To date, studies and practical applications carried out in France, have proven the indisputable advantages of loose structure cables (1) and mass splicing methods (2).

Thanks to its modularity, simplicity and mechanical and thermal characteristics, the cylindrical V-grooved element has emerged as the leader among the various fiber optic cable structures (fig.1). Moreover, it is well adapted to the simultaneous coupling of the fibers it carries.

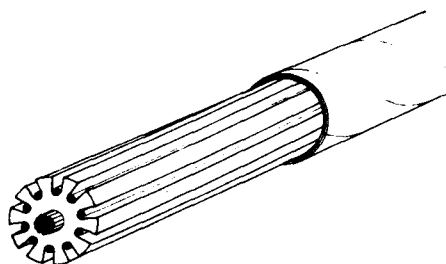


Fig. 1 10-FIBER CABLE ELEMENT

With a view to design simplicity and greater cost-effectiveness, the CNET (Centre National d'Etudes des Télécommunications) together with French industrialists have undertaken to investigate optical fiber cable technologies and to establish the most suitable splicing methods for each cable structure. In this perspective, the two sister companies SAT and SILEC have studied cables with a cylindrical V-grooved element produced by direct extrusion, and have obtained spectacular results attesting to the top-performance and moderate price of the design concept.

Concurrently, mass splicing of cylindrical grooved cables has been studied, and it is widely acknowledged that this splicing method offers several advantages (3), most notably with respect to quality (yielding results near those of the best individual fusion splices), rapidity and ease of handling and fine joint protection guaranteeing excellent resistance throughout time.

1.- ADVANTAGES OF THE FLAT CHIP MASS-SPLICING TECHNIQUE

It is already a well-known fact that the mass splicing method presents the advantage of processing all the fibers of a cable element simultaneously. In other words, the fibers do not undergo any individual operation during the splicing process, from the time they are removed from the grooved cable element until their faces are rectified to constitute the joint surface.

1.1.- The mass splicing procedure involves the following main operations :

- removal of the fibers to be spliced from the grooved element
- partial removal of the protective coating
- positioning and bonding of the fibers on each coupling half-chip
- fine grinding of the fibers and the half-chips on which they are bonded
- application of an index matching fluid
- joining of the cable elements prepared in this manner
- fitting of the outside protection envelopes.

1.2.- The cylindrical form of the grooved element carrying the fibers to be spliced, has naturally orientated design engineers towards cylindrical shaped fiber coupling elements. To achieve minimum transmission loss with mass splicing, the cylindrical parts supporting the fibers must be of excellent quality, both from a geometrical and dimensional point of view.

Moreover, the reference surfaces must exhibit a very slight degree of roughness.

1.3.- Flat chip mass splicing consists of a main splicing chip element (part on which the fibers are bonded) which is plane and parallelepipedic in shape. This splicing method was adopted because the manufacture and verification of this essential part involve simple and reliable procedures.

1.4.- The splicing chip (fig.2) is made of a cold-curable resin with two components with an 80 % silica content.

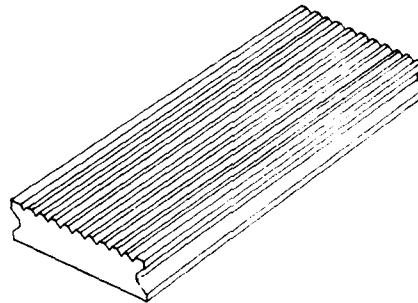


Fig. 2 FIBER SPLICING CHIP

This resin offers the advantage of having exceptional shrinkage characteristics, a low thermal expansion coefficient, excellent mechanical qualities and a very low moisture absorption factor. The mould is filled manually by means of a spatule. It is a parallelepipedic cavity whose bottom surface yields the grooves destined to receive the fibers. On either side of this mould, removable metal parts allow two side slots to be formed for accommodating the realignment cylinders. The mould cover itself does not play any decisive role in the definition of the specific forms of the splicing chip support.

Figure 3 shows that this mould can be easily manufactured using conventional machining methods.

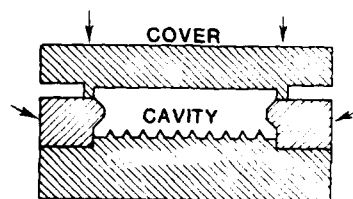


Fig. 3 CROSS -SECTION VIEW OF THE FIBER SPLICING CHIP MOULD

Moreover, as the moulding time is short, this process constitutes an economical means of producing top-quality parts.

1.5.- It is worthwhile to note that the term "top-quality" is not necessarily synonymous with "high precision". Indeed, when splicing optical fibers, their ends

must be aligned with considerable precision. This is, in fact, one of the advantages of this splicing process which allows high precision fiber alignment to be achieved without, however, requiring a highly precise splicing chip. By adopting a simple approach, consisting in using two half-chips, each taken from a single original casting which is reconstituted by applying realignment cylinders maintained in position by two clips (fig.4), the resulting assembly is without any play whatsoever. This unique process ensures fiber slot continuity from one half-chip to the other without calling for parts having tolerances identical to the precision required for the splice.

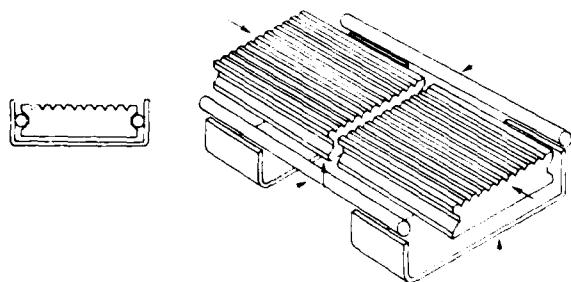


Fig. 4 SPlicing CHIP RECONSTITUTION PRINCIPLE

1.6.- The characteristics required of the fiber splicing chip are as follows :

- 1°) It must feature two bearing lines per fiber which are perfectly parallel to each other and separated by an angle α from 60 to 100° (fig.5).
- 2°) It must merely exhibit a surface quality in the fiber and realignment cylinder slots such that there is a maximum number of points of contact over the bearing lines.

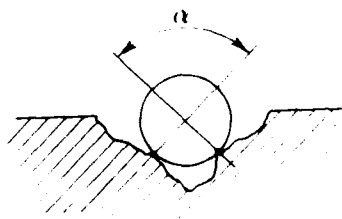


Fig.5 FIBER BEARING LINES

1.7.- It was, of course, necessary during the study stage and prior to adopting this type of flat splicing support definitively, to seek a simple solution for achieving the transfer from the cylindrical fiber arrangement of the V-grooved element to the coplanar fiber configuration of the splicing chip.

A fiber adaptor plate was therefore designed to be fitted to the cable element reinforcement rod. This moulded adaptor plate basically consists of grooves arranged so as to transform the circular position of the ten fibers into a coplanar disposition with the inter-groove distance on the adaptor plate corresponding to the inter-slot distance on the splicing chip. Figure 6 illustrates this process. In order to guide the fibers into the grooves of the adaptor, it is merely necessary to slide the elastic O-rings from their initial position on the cable element to their final position on the flat section of the adaptor.

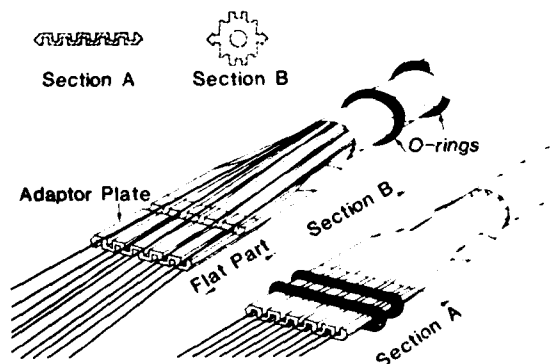


Fig. 6 FIBER COPLANAR ARRANGEMENT

Another interesting feature of this adaptor plate resides in the fact the cables may be layed in any way without having to worry about the clockwise or anticlockwise direction of the fibers. There are, in fact, two kinds of configuration adaptors available. They both have symmetrical shapes but differ in color.

Figures 7a and 7b provide simplified diagrams of the differences in configuration between the two adaptor plates.

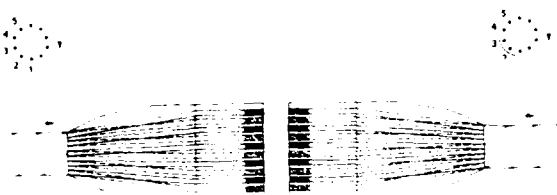


Fig. 7a ADAPTOR PRINCIPLE FOR CABLES LAID WITH THE SAME FIBER DIRECTION



Fig. 7b ADAPTOR PRINCIPLE FOR CABLES LAID WITH THE OPPOSITE FIBER DIRECTION

As can be seen, the use of two adaptors with the same fiber groove configuration and therefore, the same color, allows the fibers to be properly concorded with one another for the splicing operation when the two cables to be coupled have been layed in the opposite direction.

1.8.- Once the fibers are positioned in a coplanar arrangement, their coating is removed by a chemical process followed by a wiping operation (this process is well known). The flat end of each adaptor is bonded onto the end of the splicing half-chip, thereby fixing the fibers automatically into their slots. They are held in position during the bonding operation using mechanical fittings.

The fibers and half-chips undergo a single rectification pass on a machine specially designed for this purpose. It features a disk set with diamonds over two concentric areas with different granulometries. This allows a single rectification pass to be performed, consisting of a rough preliminary and finishing operation.

The above constitutes a brief summary of the flat-chip mass splicing technique for joining two cylindrical V-grooved optical fiber elements. Figure 8 provides a simplified diagram of a complete splice.

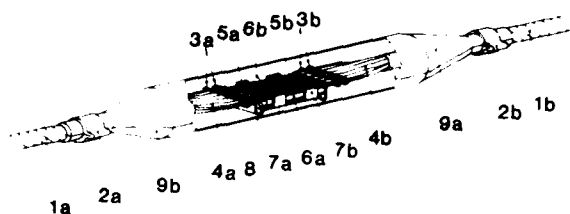


Fig. 8 10-FIBER MASS SPLICING

2.- SPLICE COMPOSITION

A splice consists of the following elements (listed in the order of their assembly) :

- two cable elements 1a and 1b to be joined
- two crimped collars 2a and 2b
- 2 x 2 elastic O-rings 3a and 3b
- two adaptor plates 4a and 4b
- two coupling half-chips 5a and 5b
- two realignment cylinders 6a and 6b
- two clips 7a and 7b
- a longitudinal clip 8
- two half-cases 9a and 9b

3.- SPLICING PROCESS

The splicing operation is performed in the following steps :

- Parts 2a, 2b, 3a and 3b are initially slipped onto the cable element.
- The tapes maintaining the fibers in the element grooves are removed over a length sufficient for enabling the fibers to be drawn out.
- The cable element is then cut and its inner rod exposed over a few millimeters in order to fit the adaptor plate onto the rod.
- The adaptor plates are then bonded onto the cable element reinforcement rod.
- The fibers are set in the coplanar arrangement by rolling the O-rings along the adaptor plates.

- The fibers are stripped of their coating by applying a dilating chemical agent followed by an overall wiping operation.
- The flat ends of the adaptors are bonded onto the ends of the coupling half-chips.
- The fibers are bonded in their slots on the coupling half-chips (see Note 1).
- The fiber ends together with the half-chips are fine-grounded so as to prepare the surfaces to be joined.
- They are ultrasonically cleaned.
- The two element ends fitted with their coupling half-chips are then joined using two cylinders and two side clips (an index matching fluid is applied between the two rectified faces).
- The longitudinal clip is fitted to maintain the position of the two half-chips applied one against the other.
- The two-part protective casing is applied and fitted onto the cable element by means of crimped collars.

Note 1 : When the operator is making a splice, he uses fiber chip supports fitted with a breaking initiator as shown in Figure 9. He merely has to separate the two parts by pressing lightly by hand.

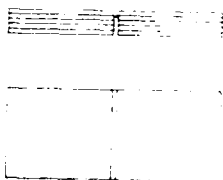


Fig. 9 CHIP SUPPORTS WITH A BREAKING INITIATOR

4.- SPLICING STATION

It is important to note that the operations are mechanized such that the operator needs no particular skill to perform the fitting, alignment and assembly operations required in making this mass splice.

He uses a specially designed splicing set-up as shown in Figure 10.

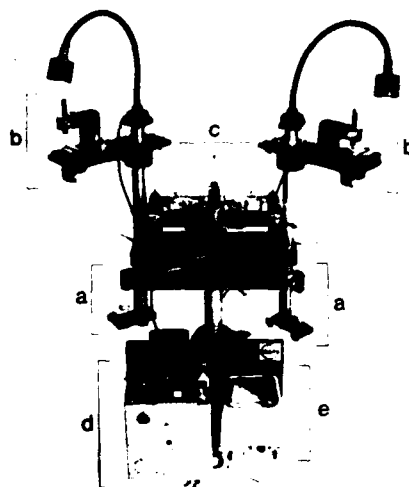


Fig. 10 FIELD SPLICING STATION

This equipment basically includes the following :

- two fiber stripping devices
- two tools for bonding the fibers onto the half-chips
- a device for holding, positioning and guiding the various splice elements (realignment cylinder, clips...)
- a special rectifying (grinding) machine
- an ultrasonic cleaning set-up.

The entire set-up is adjustable in height, thereby enabling the operator to work standing or seated.

5.- DURATION OF THE MASS SPLICING OPERATIONS

The time required for a single operator to splice the fibers of two single-element cables is approximately one hour.

However, other factors external to the splice operation itself such as work site conditions (loading, unloading, man-hole preparation, etc...) may be somewhat long.

Once access to the cable is achieved and the splicing equipment installed, the coupling of a 7-element cable and its protection is executed in one day (approximately 7 hours).

6.- EXPERIMENTAL RESULTS

Thusfar, our experiments have been performed on graded index fibers (50/125). The measurements are generally made using the backscattering method with a system manufactured by our company (known as the U 61 system).

6.1.- Laboratory Experiments

6.1.1.- A considerable number of splices have been made in our laboratories. They have been performed on fibers cut in two and then, mass-spliced together in order to establish the attenuation losses due to the splicing operation. The minimum length of fiber on either side of the splice was approximately 800 meters.

Figure 11 provides a histogram of these test results.

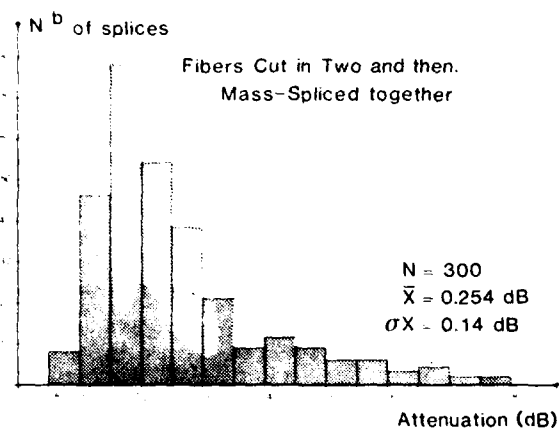


Fig. 11 HISTOGRAM OF LABORATORY MASS SPLICING RESULTS

6.1.2.- A series of experiments was performed on cable elements with fibers characterized by extreme dimensional variations limited by the following tolerances.

Cladding diameter : $125 \pm 2 \text{ } \mu\text{m}$
 Core : $50 \pm 3 \text{ } \mu\text{m}$
 Excentricity : $2.5 \text{ } \mu\text{m max.}$

Figure 12 illustrates the histogram of this series of experiments.

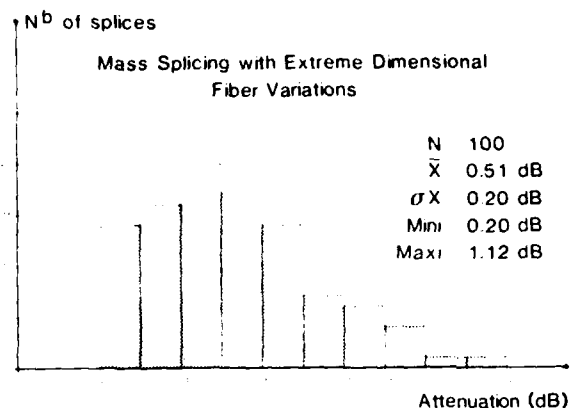


Fig. 12 HISTOGRAM OF LABORATORY MASS SPLICING RESULTS

6.2.- Field Experiments

6.2.1.- Field experiments have been performed on several sites. The first of these consisted in cutting a cable, and then coupling it by the mass-splicing method, which simply means that the fibers that were cut, were the same as those that were then spliced. The measurement results are provided in the histogram of Figure 13.

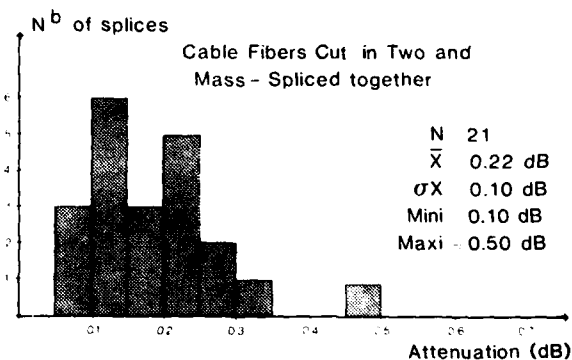


Fig. 13 HISTOGRAM OF FIELD MASS SPLICING RESULTS

6.2.2.- A second experiment consisted in splicing two cables from two different manufacturers (SAT and SILEC) containing fibers from different suppliers as well (FOI - CLTO - CORNING).

Each cable contained 7 elements with each element including 3 fibers. The 21 fibers were spliced according to the mass-splicing technique with the following combinations of fibers : FOI + CLTO, FOI + CORNING, CLTO + CORNING.

The measurements were performed at each cable end using the backscattering method and the mean values were calculated. The results are provided in the Figure 14 histogram.

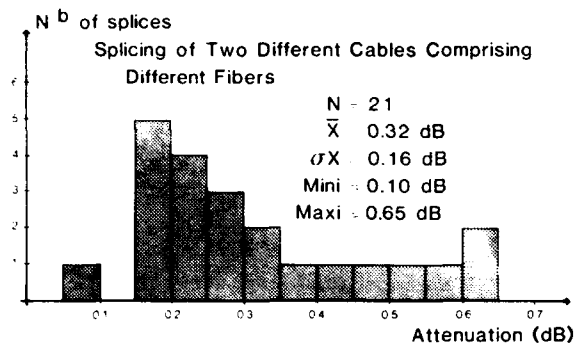


Fig. 14 HISTOGRAM OF FIELD MASS SPLICING RESULTS

CONCLUSION

The mass-splicing techniques developed thusfar have already proven particularly advantageous when coupling a large number of fibers contained in cylindrical V-grooved elements. The use of flat chips for the fiber splicing and adaptor plates for adapting the cylindrical element fiber arrangement to the flat chip position, results in a simplification of the fiber splicing technique, thereby reducing costs and greatly increasing reliability.

This process, developed more than a year ago, is currently being used, in particular, in the Biarritz project where 30 % of the fiber optic cables (3000 km of installed fibers) are to be spliced using this method.

- (1) - Low-loss optical fiber cable design and manufacture
 IWCSF - 1981 - D. BOSCHER -
 B. MISSOUT - P. CHERON -
- (2) - Experimental result on mass splicing techniques applied on optical fiber cables in the field
 IWCSF - 1981 - G. LE NOANE -
- (3) - Results on field operation of a mass splicing process
 ECOC - 1981 - A. BOUVARD - J.P. HULIN



Robert DELEBECQUE
 Société Anonyme des
 Télécommunications
 Département Câbles
 Paris - France

Robert DELEBECQUE studied mechanical and electrical engineering at CNAM (Conservatoire National des Arts et Métiers) from 1943 to 1948. He joined SAT in 1947 where he became involved in the development and manufacture of coaxial cables and electronic components. He is responsible, in particular, for SAT's part in the network engineering of the BIARRITZ project. He also heads study programs concerning optical cable connectors.



Elie CHAZELAS
 SILEC
 Service "Applications
 Industrielles"
 Montereau - France

Elie CHAZELAS graduated from the "Ecole Supérieure de Mécanique, d'Electricité et d'Electronique" de Paris in 1957. He is presently head of a SILEC division in charge of the development of connecting and jointing equipments for cables.



Daniel BOSCHER
 C.N.E.T.
 ROC/FCO - LANNION
 France

Daniel BOSCHER graduated from the "Ecole Nationale Supérieure des Arts et Métiers" in 1973. He joined the French Post Office in 1973. Since 1979 he is deputy manager of the optical fibers and Cables department at CNET.

TEST RESULTS OF MULTICHANNEL HERMAPHRODITIC OPTICAL
CONNECTORS DEVELOPED FOR THE US ARMYBY
Vasilios E. KalomirisU.S. Army Communications-Electronics Command
Fort Monmouth, New Jersey 07703

ABSTRACT

In order for the U.S. Army to benefit from the fiber optic technology, the Center for Communications Systems (CENCOMS) of the Communications-Electronics Command (CECOM) has supported a number of exploratory programs for the design and development of prototype six channel hermaphroditic butt-joint connector plugs and bulkhead receptacles required to meet the harsh conditions of the tactical field environment. In this paper, the requirements that a tactical connector should meet will be described. In addition, the test results obtained by uniformly testing the prototype connectors manufactured by Bell Northern Research, Hughes Aircraft Company TRW Eastern Research Laboratories, ITT-Cannon and ITT-STL (Pittsfield) will be reported. The prototypes manufactured by ITT-STL (Pittsfield) are of a two channel lens design and were delivered under the GAC-1 for use in operational testing of fiber equipment at Fort Benning and Fort Gordon, Georgia.

INTRODUCTION

Tactical fiber optic communications links require the use of cable assemblies in order to meet the rapid deployment and mobility requirements. The cable assemblies used by the Army consist of 0.3 or 1.0 km of ruggedized fiber optic cables terminated at each end with a hermaphroditic connector. The technical guidelines used in the development of the prototype tactical hermaphroditic connectors included the following requirements listed in Table 1.

TABLE 1
TACTICAL CONNECTOR REQUIREMENTS (1)

- o Hermaphroditic
- o Ruggedized
- o Repetitive Mating
- o Impact
- o Flex Strength
- o Tensile Strength
- o Shock
- o Simple (Assemble & Repair)
- o Vibration
- o Coupling Nut Rotation
- o Moisture Proof
- o Temperature Cycling
- o Thermal Shock
- o High & Low Temperature
- o Fluid Immersion
- o Salt Fog Proof

TABLE 1 (Cont)

- o Mud Proof
- o Field Cleanable
- o Sand and Dust
- o Insertion Loss 2 dB max
- o Reasonably Priced

At the time of initiation of the exploratory work for the development of tactical connectors standard methods were not available for use in the connector evaluation. In order to expedite the progress and development, a decision was made to allow the various manufacturers to use the available test equipment and known measurement procedures for the evaluation of the prototype connectors. At the time the prototype connectors were delivered it was considered necessary to uniformly evaluate them in order to select the best for use in tactical environment.

The most critical requirements were selected and included in the test plan that was to be followed throughout the evaluation. That is: (1) insertion loss, (2) repetitive matings, (3) temperature cycling, (4) strain relief flexing and (5) tensile strength. In addition to the above quantitative tests, a number of qualitative observations was made with respect to; (1) mating forces, (2) alignment ease, (3) mismating, (4) cleaning, (5) handling damage and (6) human factors. The test results are addressed in this paper.

OPTICAL CONNECTOR ENVIRONMENTAL AND
MECHANICAL REQUIREMENTS

One of the basic requirements that a tactical fiber optic connector has to meet is to be hermaphroditic so that when installed on cable assemblies it can mate with the connector at the adjacent cable end without the use of any special tool or interfacing part.

In addition the connector should be ruggedized in order to survive handling under rapid deployment in mobile situations. The connector shell shall also be rugged enough to withstand extensive compressive forces similar to those experimental when run-over by extra heavy vehicles.

The connector design must be simple enough in order to facilitate field assembly and repair by field technicians in a depot or a mobile van. Very basic, not complicated, ruggedized and inexpensive equip-



Top Row

Left BNR

Connector Plugs Tested

Middle ITT-CANNON

Right HUGHES

Bottom Row

Left ITT-STL

Right TRW

ment must be used.

Since the fiber optic links will be deployed in open terrain of highly variable climatic conditions, it is necessary that temperature cycling does not contribute to deterioration of the materials used to build the connector shell, fiber alignment ferrule, seals, cable strain relief, optical fiber, and epoxy used in assembling the connector. The temperature fluctuation used in a testing program should also simulate cable assembly performance during storage and transportation.

In situations where the cable assemblies are exposed to significantly low or high temperature environment, it is required that thermal shock performance of the connector not significantly contribute to the changes in performance of the cable assembly. The materials used in the connector have to be properly selected and should have compatible thermal expansion coefficients in order for the fiber to remain in the ferrule and not creep out of the ferrule.

The connector shell and face should be humidity and moisture proof so that the permeation of any liquid into the inside of the connector be precluded. It is known that once water reaches the inner portion of the connector its failure becomes unavoidable. It should also be noted that the materials used for the connector parts are corrosion proof and not subject to swelling due to absorption of oil or other lubricants. The optical surface as well as the connector shell should be capable of resisting the effects of dry dust (fine sand). It should be emphasized that the optical surface of the connector should survive this severe test.

The connector should also be designed to withstand immersion in certain fluids with which it may come in contact during its service life.

The materials used in making the connector shall be properly selected so that they inhibit fungus growth.

The connector shall be designed to pass the vibration test which simulates transportation as well as tactical environment conditions and rough handling. The material used for the coupling ring and connector shell shall be selected so that it does not flake due to mating and remating of the connector.

The optical surface of the connector shall be field cleanable without the need of a special tool kit or chemicals.

OPTICAL REQUIREMENTS (2)

The test plan followed for the uniform evaluation of the prototype connectors includes the following basic quantitative tests:

1. absolute insertion loss - normal mating
2. differential insertion loss - repetitive mating
3. temperature cycling
4. strain relief flexing

5. tensile stress

- cable to connector
- connector to connector

It should be emphasized that the connectors were installed by the connector developers on government furnished cable. Six fiber cables were used for TRW, BNR, HUGHES and ITT-CANNON. Two fiber cable was used for ITT-STL (Ptarmigan).

The ITT-STL (Ptarmigan) connectors had previously undergone field testing at Fort Benning and Fort Gordon, Georgia. All the other connector samples used in this program were new.

INSERTION LOSS MEASUREMENTS (3)

The insertion loss measurements were performed by establishing equilibrium mode distribution or steady state for both launch and receive conditions. This mode distribution also approximates the conditions expected in tactical deployment where the optical connectors will be used. Equilibrium mode distribution was achieved by using 1 km, six fiber cable preceding the connector under evaluation and an equilibrium mode filter following the connector. The mode filter consisted of a mandrel wrap followed by a mode stripper. The mandrel wrap was five turns around a 1.3 cm. o.d. mandrel. For the mode stripper, 8 cm of the fiber buffering were removed down to cladding, and the fiber covered by index matching oil. The purpose of the equilibrium mode simulator, following the connector, was to remove higher order modes that might be excited by the connector and splices.

Light emitting diodes (LEDs) and silicon PIN detectors operating at 850 nm were used in the instrumentation circuitry of each channel. The instrumentation included six transmitters and twelve receivers so that the connector insertion loss and the variations in transmitter power could be monitored at the same time.

ABSOLUTE INSERTION LOSS - NORMAL MATING

The insertion loss of the connectors as received is summarized in Table 2.

TABLE 2

CONNECTOR PROTOTYPES BY	AVERAGE INSERTION LOSS (dB)	STANDARD DEVIATION (dB)	SAMPLE SIZE
BNR	1.74	0.92	141
HUGHES	1.57	0.94	136
ITT-CANNON	3.42	1.67	136
ITT-STL	3.17	1.04	36
TRW	3.65	2.37	51

To simulate multiple deployment conditions, each connector half tested was connected as transmitting and as receiving side with every other connector half of that type. Each pair was mated and measured ten times and the readings averaged. Thus, each sample included in Table 2 represents 10 measurements of insertion loss.

DIFFERENTIAL INSERTION LOSS - REPETITIVE MATINGS

The connectors' mating durability and optical performance were evaluated by repeated matings of the same connector pair while measuring the insertion loss. The insertion loss was measured every 100 matings until 1000 matings were completed see Figure 1. The performance of the best and worst channel in the connector is shown. By performing this test, the mechanical durability, fiber alignment mechanisms and their influence on variations in insertion loss were assessed. The differential insertion loss results for the repetitive mating tests are summarized in Table 3.

TABLE 3
REPETITIVE MATING TEST
DIFFERENTIAL LOSS STATISTICS

	AVERAGE DIFFERENTIAL LOSS (dB)	STANDARD DEVIATION (dB)
TRW	1.28	2.02
BNR	-.05	.27
HUGHES	1.01	2.24
ITT-STL	.14 ¹	.30 ¹
ITT CANNON	.23 ¹	.49 ¹

¹DATA FROM BROKEN CHANNEL EXCLUDED

TEMPERATURE CYCLING

The prototype connectors were evaluated under temperature cycling conditions in order to determine variations in their optical and mechanical characteristics resulting from the exposure to temperature extremes. The temperature cycle included insertion loss measurements at 25°C, -55°C, 25°C, 85°C and back to 25°C. This cycle was repeated five times with the results summarized in Table 4. The differential insertion loss versus temperature cycle is shown in Figure 2. BNR and Hughes connectors were selected for this test because of their superior performance in the insertion loss test. The ITT-CANNON connector was added later because of the needs of another program.

TABLE 4
TEMPERATURE CYCLING TESTS
DIFFERENTIAL LOSS STATISTICS (dB)

	-55°C		25°C		85°C	
	\bar{x}		\bar{x}		\bar{x}	
BNR	0.43	0.25	↑0.29 ↓0.20	0.25 0.20	0.24	0.19
HUGHES	1.15	1.33	↑0.75 ↓0.37	1.24 0.84	0.27	0.91
ITT- CANNON	2.91	3.08	↑2.00 ↓0.91	2.45 1.79	0.70	1.88

↑ - rising temperature
↓ - falling temperature

Additional tests were performed in order to determine the effects of cable flexing on the connector's strain relief tie off, for effects of connector to connector tensile stress and for cable to connector tensile stress. Tables 5 and 6 show the average differential insertion loss versus flexing and tensile stress respectively.

The results showed no significant effects upon the optical and mechanical performance of any of the connectors.

STRAIN RELIEF FLEXING TESTS
DIFFERENTIAL LOSS STATISTICS

	Average Differential Loss (dB)	Standard Deviation (dB)
TRW	.00	.03
BNR	-.01	.03
HUGHES	.02	.09
PTARMIGAN	.05	.05
ITT	-.01	.09

TABLE 5

TENSILE STRENGTH TESTS
FIBER OPTIC CABLES
AVERAGE DIFFERENTIAL LOSS

	50 kg	100 kg	150 kg
BNR	-.03 dB	-.04 dB	-.01 dB
HUGHES	.03 dB	.05 dB	.06 dB

TABLE 6

QUALITATIVE TESTS

During sample preparation and testing there were certain observations made by the personnel responsible for the connector evaluation. The following qualitative tests were performed on the connectors in order to determine their characteristics.

- o mating forces
- o alignment ease
- o mismating
- o cleanability
- o handling damage
- o human factors
- o additional factors

MATING FORCES

It was determined that the hardest connector to mate was the ITT-STL (Ptarmigan) due to a very high compressive force. The required force to mate the connector is dependent on the spring constant of the spring used in the connector shell. This deficiency can be very easily corrected.

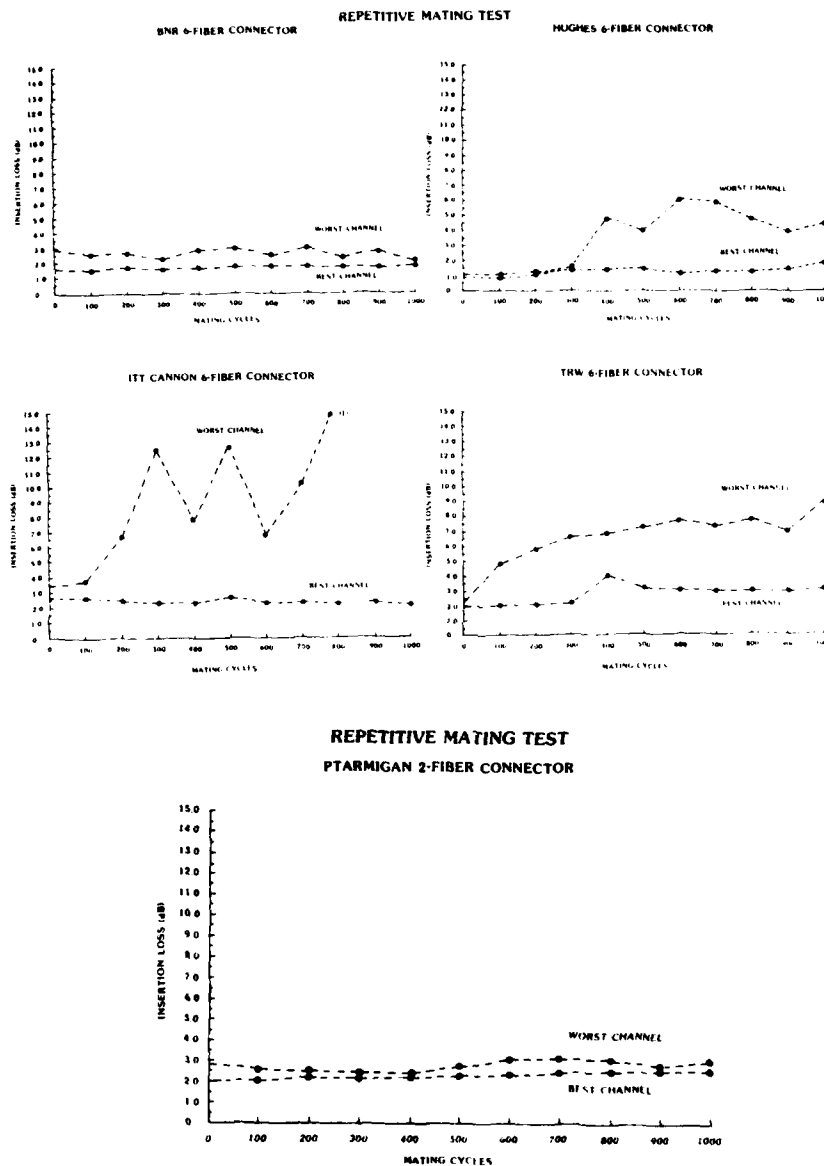


Figure 1. Insertion Loss (dB) vs Mating Cycles

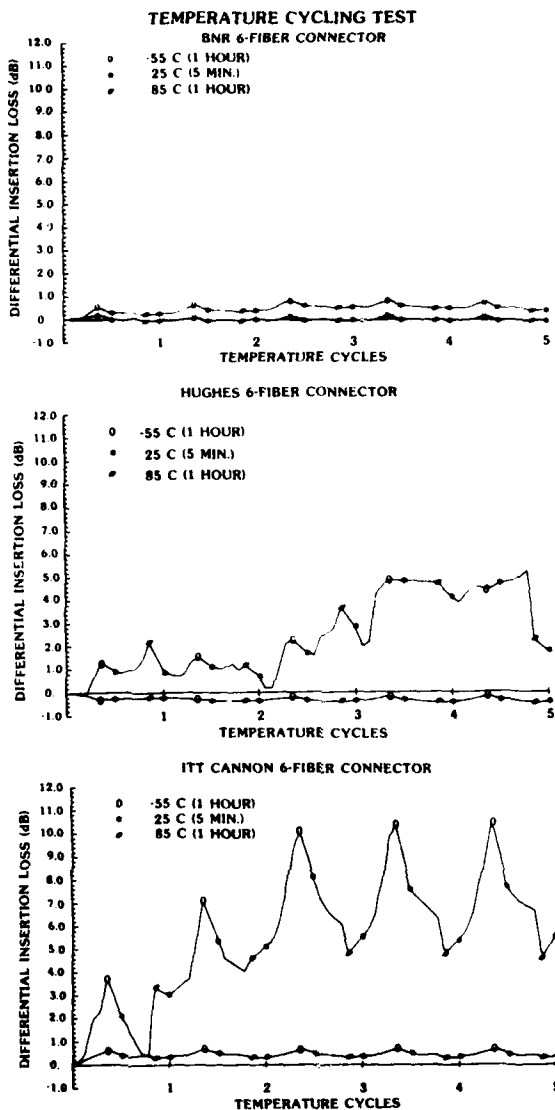


Figure 2. Differential Insertion Loss (dB) vs Temperature Cycle

ALIGNMENT FORCES

The connector developed by ITT-CANNON was considered as the easiest to align, visually or by touch, because of the two semi-cylinders on each half. The ITT-STL (Ptarmigan) is also easily aligned by its half-cylindrical sleeve on each half, but the locking lugs are more difficult to align than that of ITT-CANNON. The TRW connector is also easily aligned because of the particular shape and massive size of the connector halves. However, the locking rings must be tightened one after the other, which may be confusing. The BNR connector is the next most difficult to align even though the protruding bosses are of different shapes to prevent mismatching. The white dots were a good visual alignment indicator but alignment by touch was not possible. The most difficult to align was the Hughes connector because of the multiple alignment dots which have poor contrast in normal lighting, the similarly shaped alignment lugs (which made mismatching very easy) and the precise manipulation required of the coupling ring.

MISMATCHING CHARACTERISTICS

It was determined that the Hughes connector is the most easily mismatched by not completely tightening the coupling rings. The ITT-STL (Ptarmigan) because of the high force required, could be thought to be mated even though the locking was not completed. Also, the BNR could not be fully mated if the unused locking ring was not completely backed off the threads. The connector by ITT-CANNON could not be mismatched unless extreme force was applied to bend the alignment sleeves.

CLEANABILITY

The connector by ITT-STL (Ptarmigan), lens connector design, can be easily and quickly cleaned in the field. All the other connectors would require special tools, kits or use of liquids to be field cleanable.

HANDLING DAMAGE

The fibers in the four rod alignment guide employed in the TRW connector were prone to damage during handling since they are lying free in one of the cusps that the glass guide forms. The Hughes connector could be damaged by forcing a mismatching or dropping an uncovered connector half. The ITT-STL (Ptarmigan) and the ITT-CANNON half cylinder sleeves could also be damaged if dropped on a hard surface. The BNR connector appeared to be the least susceptible to handling damage.

HUMAN FACTORS

The multiple alignment dots, and their poor visibility in low light levels, made the Hughes connector potentially confusing to mate. The precise manipulation of the coupling rings was also a potential source of error. The TRW connector requires multiple turns of the coupling ring while pushing a somewhat difficult maneuver in tactical conditions. The high forces required to mate the

ITT-STL (Ptarmigan) connector can be frustrated to some personnel. The BNR connector also requires several turns to lock, but is small light weight and easy to mate. The ITT-CANNON is easily aligned, mated and tightened since it uses a proven military backshell for the connector.

ADDITIONAL OBSERVATIONS

The increased losses of the Hughes connector during the temperature cycling tests were caused by the gradual protrudence of all the fibers from the terminating ferrules as the fiber and buffer expanded and contracted. The epoxy used to hold the fiber in the ferrule tip did not retain the fiber in the ferrule during the temperature cycling. The ITT-CANNON connector lost one channel out of six during the temperature cycling tests when fiber broke just behind the watch jewel in the ferrule.

The ITT-CANNON and Hughes connectors had similar problems when flakes of metal from the guidesleeves were scraped off during repetitive matings and lodged on optical interface.

CONCLUSION

The test results obtained thus far under uniform testing conditions lead us to conclude that the evaluated prototype connectors are close to meeting the tactical requirements. Each connector design has desired advantages and in at least one area there is need for improvement.

The connector developed by BNR performed consistently during temperature cycling, repetitive mating and the best and worst channels performed consistently close throughout the evaluation. This shows that the ferrule used for the fiber alignment was precisely made and that the materials used for it were properly selected. The effects of the human factor in connector assembly seemed to have been minimized. The connector back shell is a special design for fiber optic applications which shows that there is always room for innovation.

The connector developed by Hughes exhibited insertion loss under normal conditions 0.17dB lower than the connector by BNR, but did not consistently perform during or after the repetitive mating or temperature cycling tests. The inconsistency in performance indicates that the fiber ferrule interface needs improvement possibly in the area of materials used in securing the fiber in the ferrule or possibly in connector assembly methods. The large deviation in performance between best and worst channel in the same connector shows that there is need for improvement and minimization of the human factor and or the technique used for fiber ferrule termination.

The above two butt-joint connectors are the most promising connector designs known today, closest to meeting the tactical connector requirements.

The lens connector developed by ITT-STL (Ptarmigan) has insertion loss higher than the BNR and Hughes connectors but is easily field cleanable. A field

cleanable connector with consistent performance can be easily considered for use in certain applications even though the insertion loss is higher than the known butt-joint connectors.

It is worth mentioning that the progress achieved today in the area of fiber optic connector for tactical applications is remarkable considering the rapid evolution of fiber optic technology. As a recommendation to both fiber and connector manufacturers it is necessary to emphasize that the U.S. Army will in the near future be purchasing tactical fiber optic cable assemblies not individual cables or connectors. Therefore, it would be to the advantage of every party concerned to increase the degree of cooperation in order to improve their respective products and expedite the advancement of this technology in addition to assisting in the timely fielding of tactical communication systems.

REFERENCES

1. V.E. Kalomiris, "Multichannel Hermaphroditic Connectors for Tactical Applications", Proceedings of FOC '81 West, San Francisco, CA, 1-3 Sep 1981, p. 96.
2. M.D. Drake, F. Gomes, M. Lesnick, G.W. Styskal and V.E. Kalomiris, "Uniform Evaluation of Multichannel Hermaphroditic Fiber Optic Connectors for Tactical Applications", Proc. of SPIE Tech Symposium on Fiber Optic Technology '82, Paper 355-10, 24-27 Aug 1982, San Diego, CA
3. J.D. Fridman, F. Gomes, L. Jou, G.W. Styskal, "Instrumentation for Multichannel Hermaphroditic Connector Evaluation", Proc. of SPIE Technical Symposium on Fiber Optic Technology '82, Paper 326-13, 28-29 Jan 1982, San Francisco, CA.

BIOGRAPHY



Vasilios Kalomiris is a project leader with the U.S. Army (CECOM), responsible for fiber optic cables and connectors. He is also currently involved in establishing a fiber optic test facility. Previously he worked for ITT/EOPD as a project engineer where he designed an air-layable cable. Prior to joining ITT, Vasilios was associated with General Cable Corp. R&D as a research engineer.

Projects included electronic equipment calibration, communications cable design, material evaluation and superconducting power cable development. A graduate of New York University (B.A., B.S., and M.S.) he is a member of the IEEE and the Technical Chamber of Greece (Society of Professional Engineers).

SHIELDING EFFECTIVENESS OF COMPOSITE METALS
AT VOICE AND CARRIER FREQUENCIES

Lyle E. McBride

Yury Trenkler

Richard G. Delagi

Texas Instruments, Incorporated
Attleboro, MassachusettsAbstract

Composite metals with both ferromagnetic and conductive layers are known to be more effective than monometals in attenuating electromagnetic fields at low and intermediate frequencies. Their usefulness, however, has been limited because available methods of analysis apply only to monometals and require different approximations in high and low frequency regions.

This paper describes a method using the Schelkunoff surface and transfer impedance characteristics of the component layers to determine the shielding effectiveness of the composite. The procedure applies to both "high" and "low" frequency cases, and can be carried out with the aid of a programmable calculator. Laboratory measurements of shielding effectiveness of several monometals and composites, over a frequency range of 50 Hz to 500 KHz, indicated satisfactory agreement between predicted and measured values. It is believed that the impedance method will be of value in selecting optimal materials and dimensions for cable shields.

Introduction

Clad metals have been used as cable shielding materials for a number of years, principally for the purpose of providing the mechanical strength of a ferrous layer while retaining the conductivity of copper (as in gopher-resistant telephone cable and distribution wire¹). However, the fact that a combination of magnetic and conductive layers can give rise to improved electromagnetic shielding properties was recognized by Schelkunoff in his fundamental paper on the theory of cylindrical shields².

In this work, the surface impedances and surface transfer impedance of thick and thin monometal shields were derived in terms of the geometric and electromagnetic parameters. In addition, a recursion relation was developed which permits the computation of impedances for composite shields, once the characteristics of the individual layers have been determined.

Several approximate expressions for the shielding effectiveness of monometals were derived in the same paper; however, rather than being obtained from surface impedance parameters, the shielding effective-

ness is expressed in terms of the intrinsic attenuation, phase shift and impedance of the metal, with a number of correction terms added to account for the effect of "electrically thin" shields (in which the attenuation in the metal is relatively small, so that re-reflection from inner to outer surfaces cannot be neglected).

At very low frequencies, all practical shields become "electrically thin"; in fact, the shielding effectiveness of non-magnetic conductors goes to zero, and the approximate expressions for shielding effectiveness are no longer valid. However, ferro-magnetic shields continue to exhibit effective shielding even at zero frequency (d-c), and another expression was derived to apply to this special case³.

The relations derived by Schelkunoff have been shown to be equivalent to those obtained by others⁴, and are recommended by current texts on shield design^{5,6}. Unfortunately, it is essentially impossible to use these relations to analyse the shielding effectiveness of composites; the ability of designers to employ multi-layered shields has been correspondingly limited. The inconvenience of having to decide in advance whether a given problem represents a "thick", "thin", or "zero-frequency" case probably also contributes to the general tendency to design shields by trial and error rather than by analysis.

An Impedance-based Method

Because even the approximate expressions for surface impedances involve complex trigonometric functions of complex arguments, their use in shielding computations was impractical before electronic calculators were available. Now, however, the impedances of multi-layer composite metals can readily be obtained by the use of a programmable calculator or desktop computer.

Although many problems (for example, determining the attenuation in a coaxial cable with copper clad inner and outer conductors) are readily solved once the surface impedance is determined, available expressions for shielding effectiveness required data that were not defined for composites. Since the surface impedance parameters are, by definition, ratios between E and H fields at the surface of the metal, and for cylindrical waves a similar impedance function can be defined in the dielectric outside the shield, an expression for shield effectiveness

can be derived in a manner analogous to that used by Schelkunoff in obtaining an expression for the surface impedance of composite metals (see Appendix). The resulting expression is:

$$S = 20 \log \left| \frac{2 Z_{ab} Z_w}{(Z_{aa} + Z_w)(Z_{bb} + Z_w) - Z_{ab}^2} \right| \quad (1)$$

where S is shield effectiveness in dB, Z_w is the radial wave impedance, Z_{aa} is the internal surface impedance, Z_{bb} is the external surface impedance, and Z_{ab} is the surface transfer impedance (the surface impedances, expressed in ohms per square, can be obtained from the thicknesses and electromagnetic properties of the metal layers comprising the shield⁸).

In most cases, the thickness of the shield is negligible compared to its radius of curvature, and the following simple expressions can be used to compute the impedances for monometal shields:

$$Z_w = i\omega\mu_0\rho \quad (2)$$

$$Z_{aa} = Z_{bb} = \frac{(1+i)}{\delta q} \coth \frac{(1+i)t}{\delta} \quad (3)$$

$$Z_{ab} = \frac{(1+i)}{\delta q} \operatorname{csch} \frac{(1+i)t}{\delta} \quad (4)$$

$$\delta = \sqrt{\frac{2}{\omega\mu g}} \quad (5)$$

where ω is the angular frequency of the wave, μ_0 is the permeability of free space, and μ , g and t are respectively the magnetic permeability, electrical conductivity and thickness of the shield. The dimension ρ , the effective radius of the wave in air, can be regarded as the distance from the pair of wires producing the wave to the shield. (We have assumed that the shield is thin enough so that the radius is the same on both sides of the shield.) The parameter δ is often called the depth of penetration in the metal.

Because the various impedances and hence the shield effectiveness can be determined for either monometals or composites by a combination of arithmetic and trigonometric manipulations of complex numbers, the solution of equation 1 can readily be programmed on any calculator designed to handle complex variables. Such devices did not, of course, exist when the original work on cylindrical shields was done; effectiveness was therefore expressed as a sum of logarithmic terms involving the basic (monometal) material parameters and not requiring the use of complex arithmetic.

To verify the validity of the impedance method in the case of monometals where $Z_{aa} = Z_{bb}$, equation 1 was rewritten in terms of the parameters used in reference 2. The result (see appendix) is:

$$20 \left(\log \frac{|k+1|^2}{4|k|} + \log e^{at} + \log \left| 1 - \frac{(k-1)^2}{(k+1)^2} e^{-2PT} \right| \right) \quad (6)$$

Equation 6 is equivalent to equations 114 through 119 of reference 2; its first two terms are

equivalent to (6-9) and (6-18) of reference 5 (whose Appendix C contains an approximation of the third term). Since the impedance method gives the same result as existing methods for monometals (although it appears to be more convenient to use) it should be valid for composites for which other methods are inapplicable.

Experimental Verification

To determine shielding effectiveness an apparatus was constructed including two coaxial coils, each 1.9 cm in diameter, separated by a distance of one centimeter. Midway between the two coils an opening was provided for the insertion of sheets of the metals to be tested (Fig. 1). One coil was excited at frequencies ranging from 50 to 500,000 Hz. and the attenuation of the signal in the second coil due to insertion of a metal shield was measured. The results were compared to the values calculated by means of equations 1-5 and recursion relations 94 and 95 of reference 2 on a TI-59 programmable pocket calculator. The dimension ρ was taken to be 0.5 cm; conductivity values were taken from the manufacturer's data sheets, and magnetic permeabilities estimated from the low frequency performance.

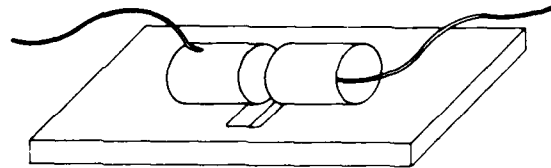


Fig. 1 - Test Apparatus

The various shields tested are listed in Table I; their measured and calculated shielding effectiveness curves are shown in figures 2 and 3.

Discussion of Results:

Correlation between measured values and the curves computed from equation 1 was good even for the magnetic composites. It was assumed in calculation that magnetic permeability remains constant at the low-frequency value throughout the test range. While data for magnetic materials usually show permeability decreasing with increasing frequency, the phenomenon may be largely due to eddy currents; these effects of conductivity are automatically included in equation 1.

A comparison of the various shields in the 50-500 Hz region indicates that low frequency attenuation is affected only by permeability and the amount of magnetic material present; copper is ineffective in

this range. On the other hand, conductivity becomes increasingly important at the higher frequencies: the copper clad iron (Clad #4) is almost 6 db less effective than iron clad copper (Clad #1) at 50 Hz, because it has only half the iron content; however, above about 100 KHz the high conductivity #4 exceeds #1 in attenuation. The combination of a ferromagnetic material with copper clearly provides more effective shielding than copper alone over the entire range of frequencies considered.

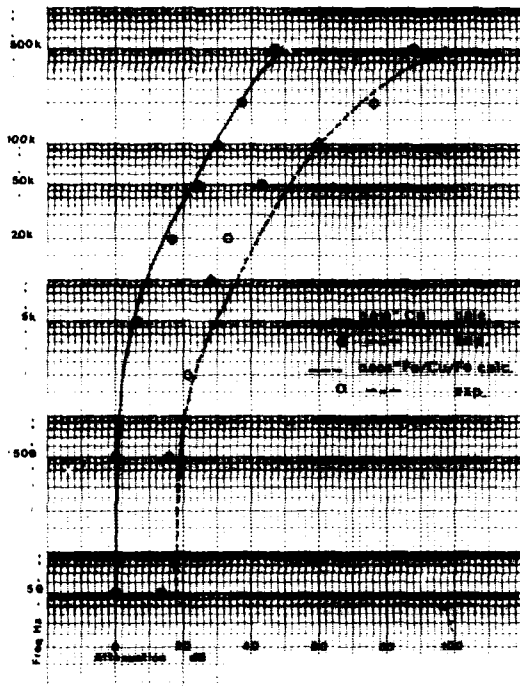


Fig. 2 - Attenuation Due to Copper and Silicon Iron Clad Copper Shields as a Function of Frequency

The results should be valid in predicting the crosstalk shielding ability of composite metals in small diameter telecommunications cables: the one centimeter separation between source and receiver is realistic, and the range of frequencies covers the bands commonly used for both voice and carrier transmission in paired-wire cables. The theoretical analysis based on equation 1 should, of course, be equally useable for other dimensions and frequencies.

The test conditions cover the entire gamut of "electrical thickness" from 50 Hz, where copper thickness divided by penetration depth (t/δ) is less than 0.03, to 500 KHz, where t/δ in magnetic material reaches 6. Thus the method appears to cover adequately both "thick" and "thin" shields, as well as the transition region in between.

TABLE I

Shield Material	Thickness--cm
Copper	.025
Clad #1: Silicon Core Iron "B" (33%) Copper (34%) Silicon Core Iron "B" (33%)	.020
Clad #2: Copper (33%) HyMu "80" (34%) Copper (33%)	.020
Clad #3: Copper (33%) High Permeability "49" (34%) Copper (33%)	.020
Clad #4: Copper (33%) Silicon Core Iron "B" (34%) Copper (33%)	.020

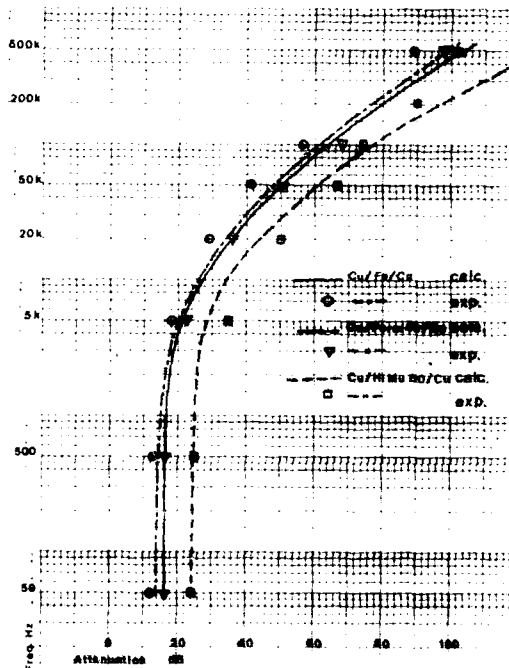


Fig. 3 - Attenuation Due to Copper Clad Magnetic Shields as a Function of Frequency

Conclusion

The impedance-based method of predicting shielding effectiveness appears to correlate well with test data for both monometallic and clad metal shields over the range of voice and carrier frequencies ordinarily transmitted by paired-wire telecommunications cables. Because it is straightforward and easily programmed this technique should prove useful to cable designers and others interested in evaluating metal shields at low and intermediate frequencies. While there is no theoretical reason why the method should not be used at megahertz frequencies, experimental verification will require further work.

Composite shields containing both conductive and ferromagnetic layers are much more effective than copper alone in the frequency range studied.

Appendix

Definitions:

- H_t = Magnetic field (transmitted)
- H_i = Magnetic field (incident)
- H_r = Magnetic field (reflected)
- Z_{aa} = Surface impedance (internal surface) in ohms per square
- Z_{bb} = Surface impedance (external surface)
- Z_{ab} = Surface transfer impedance
- Z_w = Radial wave impedance in dielectric (air)
- z_{hh} = Surface impedance presented to wave at external surface of shield (due to effect of shield plus wave impedance at internal shield surface)
- E_a = Electric field at internal surface (transmitted)
- S = Shielding effectiveness in db. = $20 \log \left| \frac{H_t}{H_i} \right|$

Derivation of equation 1:

For waves traveling from the outside toward the inside of the metallic shield,

$$E_a = Z_{ab}(H_i + H_r) - Z_{aa}H_t = Z_w H_t \quad (1a)$$

(by the definitions of the various impedances).

Therefore,

$$H_t = \frac{Z_{ab}}{Z_{aa} + Z_w} (H_i + H_r) \quad (2a)$$

Since the reflected wave is

$$H_r = H_i \frac{Z_w - z_{bb}}{Z_w + z_{bb}} \quad (3a)$$

$$H_i + H_r = H_i \frac{2Z_w}{Z_w + z_{bb}} \quad (4a)$$

Substituting the value of z_{bb} from eq. 93, ref. 2, gives

$$H_i + H_r = H_i \frac{2Z_w}{Z_w + z_{bb} - \frac{Z_{ab}^2}{Z_{aa} + Z_w}} \quad (5a)$$

Substituting (5a) into (2a) gives

$$H_t = H_i \frac{2Z_{ab}Z_w}{(Z_{aa} + Z_w)(Z_{bb} + Z_w) - Z_{ab}^2} \quad (6a)$$

so that the definition of S yields equation 1.

Derivation of eq. 6 from eq. 6a:

To translate equation 6a into the symbols used for monometals' shielding effectiveness in ref. 2, the following identities are recognized⁸:

$$Z_{ab} = \frac{Z_0}{\sinh \Gamma t}$$

$$Z_{aa} = Z_{bb} = Z_0 \frac{\cosh \Gamma t}{\sinh \Gamma t}$$

$$k = Z_w/Z_0$$

where Z_0 is the characteristic impedance of the metal, t is the metal thickness, k is the reflection coefficient, and Γ is the complex propagation constant in the metal.

Substitution of these identities into equation 6a, and replacing the hyperbolic trigonometric functions by their exponential forms yields

$$\frac{H_t}{H_r} = \frac{(k+1)^2 - (k-1)^2 e^{-2\Gamma t}}{4k e^{-\Gamma t}} \quad (7a)$$

from which equation 6 follows (α is defined as the real part of Γ).

Acknowledgements

The authors are indebted to Professor Donald W. Howe of Worcester Polytechnic Institute for valuable discussions and test work, and to Carpenter Technologies Corp. for the magnetic material samples used. HyMu "80" and High Permeability "49" are registered trademarks of Carpenter.

References

1. H. M. Hutson and K. W. Brownell, Jr., "Effective Rodent Shields and Cable Electrical Performance", 26th International Wire and Cable Symposium, 1977.
2. S. A. Schelkunoff, "The Electromagnetic Theory of Coaxial Transmission Lines and Cylindrical Shields", *Bell System Technical Journal*, 13, pp. 532-579, 1934.
3. S. A. Schelkunoff, *Electromagnetic Waves*, Van Nostrand Reinhold, 1943.

4. R. P. Buckingham and F. H. Gooding, "The Efficiency of Nonmagnetic Shields on Control and Communication Cable", IEEE Trans. on Power App. and Syst., PAS-89, pp. 1091-1099, 1970.
5. H. W. Ott, Noise Reduction Techniques in Electronic Systems, John Wiley and Sons, New York, 1976.
6. D. R. J. White, Electromagnetic Shielding Materials and Performance, Don White Consultants, Inc., 1975.
7. S. A. Schelkunoff, op. cit. (ref. 2), p. 573.
8. *ibid.*, pp. 557, 563, 564.



Lyle E. McBride is a Senior Member of the Technical Staff of Texas Instruments, Incorporated, and Manager of Applications Engineering, Wire Products Department. He received the B.E.E. degree from Cornell University in 1952, and the A.M. and Ph.D. degrees from Harvard University in 1961 and 1963 respectively.

He has been employed by TI since 1966; his current responsibilities include analysis of the electrical properties of clad metal strip and wire. He is a member of IEEE and the Society of Cable Television Engineers.



George (Yury) Trenkler is a Member of the Technical Staff, Advanced Development, Texas Instruments, Incorporated. He was born and educated in the U.S.S.R.

He has been employed by TI since 1965; his current responsibilities include the development of expanded clad metals and electronic systems. He holds 19 U.S. patents.



Richard G. Delagi is a Senior Member of the Technical Staff of Texas Instruments, Incorporated. He is Manager of Product Development for TI's Materials Division. His degrees are in Metallurgy and Mechanical Engineering (Columbia, 1951 and 1952).

Employed at TI since 1954, he has had various assignments in engineering, marketing, and product development. His patents include the areas of metallurgy, electrochemistry, electronics, magnetics and optics.

STRUCTURE AND CHARACTERISTICS OF CABLES FOR ROBOTS

T. Maezawa

A. Yoshizawa

E. Iwakabe

The Furukawa Electric Co., Ltd., Tokyo, Japan

ABSTRACT

The paper discusses a control cable which plays the role of nerve system of industrial robots. The new control cable (robot cable) uses a flexible stranded conductor, an ETFE (fluorocarbon resin) insulation, and a rubber or elastic PVC sheath. Two types of robot cable are introduced here, round type and curled type. The flexibility and elasticity of the robot cable were determined by bending test for the round type and by expansion-contraction fatigue test and robot simulation test (cylinder rotation test) for the curled type. The tests confirmed that this new cable is more durable than conventional control cables and proved that it is capable of following, within a limited wiring space, complicated movements (turning, bending, etc.) of a robot and usable in a broad range of applications as a cable of high reliability and flexibility which is an important requirement for in-robot wiring.

1. Introduction

While demand is increasing in the industry for higher productivity, higher product quality, and improved working environment, the development of industrial robots and the progress of robot technology have freed men from dangerous and soil-prone work and enabled them to do more advanced and intellectual work. At present, industrial robots are chiefly used in welding, painting, and assembling work, and most of them are independent computer-controlled automatic machines. The cable for these robots links the computer, "brain," to the machine, "limb." Compared to a human body, it is a blood vessel and a nerve and is therefore regarded as an important element of a robot system.

VCT (PVC cabtyre cable) has so far been used generally for robots. Especially for moving applications, one that passed the vibration test in electrical appliance and material control law has been considered desirable. It failed to produce satisfactory results, however, when used for industrial robots which are required to be highly reliable in performance.

This report clarifies the requirements for robot cables and introduces the construction and the distinctive features of round-

type and curl-type robot cables with significantly improved bending resistance and expansion-contraction property, developed after various evaluation tests.

2. Outline of industrial robots2-1. Classification of industrial robots

At present there are no established definitions for "robots." Individuals' concept of robots vary as they are discussed in all branches of industry. The robot cable that we developed is an information transmission cable for the playback robot, numerical-control robot, and intelligent robot specified by the Japan Industrial Robots Manufacturers' Association as in Table 1.

Classification	Definition
Automatic machine	Manual manipulator
	Fixed sequence robot
	Variable sequence robot
Robot	Playback robot
	Numerical control robot
	Intelligent Robot

Table 1 Classification and definitions of industrial robots

Industrial robots make full use of electronics technology which is now making rapid progress. In our study of robot cables to clarify their requirements, we selected the following five types of robots which are now in widespread use.

- 1) Spot welding robot
- 2) Arc welding robot
- 3) Painting robot
- 4) Assembling robot
- 5) Machining robot

2-2. Industrial robots and their cables

Cables used for industrial robots are closely related with

the uses, construction, and motion of the robots. The relations between the construction of the five robots in 1) ~ 5) of the preceding paragraph and cables are shown in Fig. 1 below.

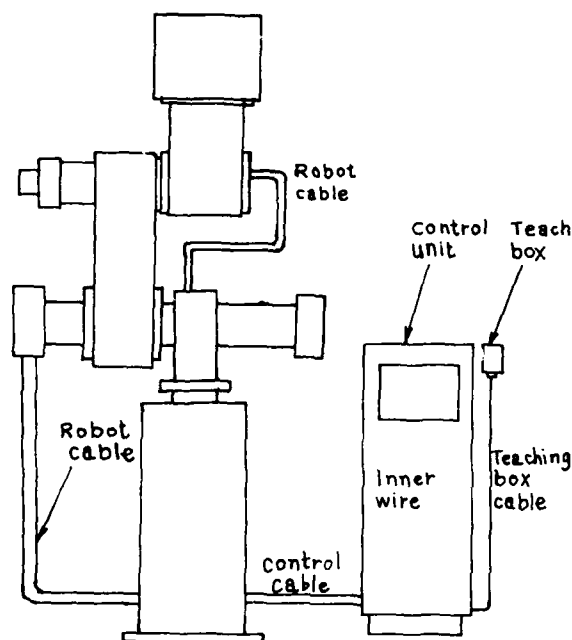


Fig. 1 Robot construction and cables

In the above figure, the teaching box is what is called "keyboard" which teaches a robot how to work. The control unit is the brain of the robot which memorizes work sequence, position, and other information, makes a comparative judgement with information from the robot, and gives instruction for controlled motion.

Cables used in robots are generally required to have excellent mechanical properties flexible and resistant to bending, expansion and contraction, though depending on the kind of robot for which they are used.

2-3. Movement of industrial robots

In the development of robot cables, it is very important to determine the form of their motion. We investigated the principal motion of the playback robot to have it reflected in the design of the cable used for it. Fig. 2 show the forms of robot motion.

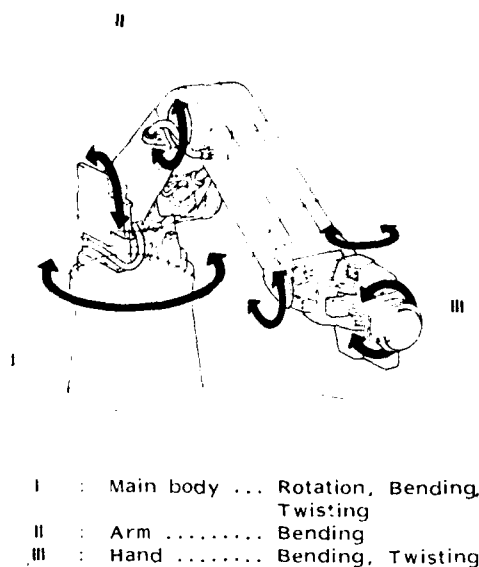


Fig. 2 Movement of Industrial Robot

The signals of position, speed, and other information are transmitted by the cable from the control unit to the robot and vice versa. They are analog and digital signals. Information-transmitting cables will be used increasingly as robots are made more intellectual.

As is learned from the robot motion in Fig. 2, robot cables are required to have excellent bending, twisting, and expansion-contraction properties where they are used at movable sections of robots. Small-diameter cables are also desirable for easy wiring in a limited space.

3. Cables for industrial robots

3-1. Design concept for robot cables

Judging from the motion of robots, high bendability and resistance to torsion are regarded as the essential properties required of robot cables. We therefore discuss here what stress is exerted in a cable and how its service life is affected when it is bent or twisted.

3-1-1. Bending strain and stress relaxation

When a cable is bent at a certain radius (R), it develops a compression inside and an elongation outside the bent part. Its conductor made up of wires stranded in a pitch diameter of (r) and with a pitch of (p) also receives such force. If the conductor is freely expandable and contractible, the strain occurs at the respective parts as shown in Fig. 3.

However, the range of elasticity of copper wires which make up the conductor is very limited so that the life of the con-

ductor is reduced much if given such a degree of expansion and contraction. Therefore the first consideration must be what type of motion is necessary for the cable to be bend without expansion or contraction of its conductor. Slipping phenomenon and diameter reducing phenomenon belong to such motion. Causing the stress relaxation motion with a low conductor stress produces a cable having a long service life in bending applications. Which of these stress relaxing phenomena should be used is determined by the working condition, number and size of cable conductors. They are shown in Table 2.

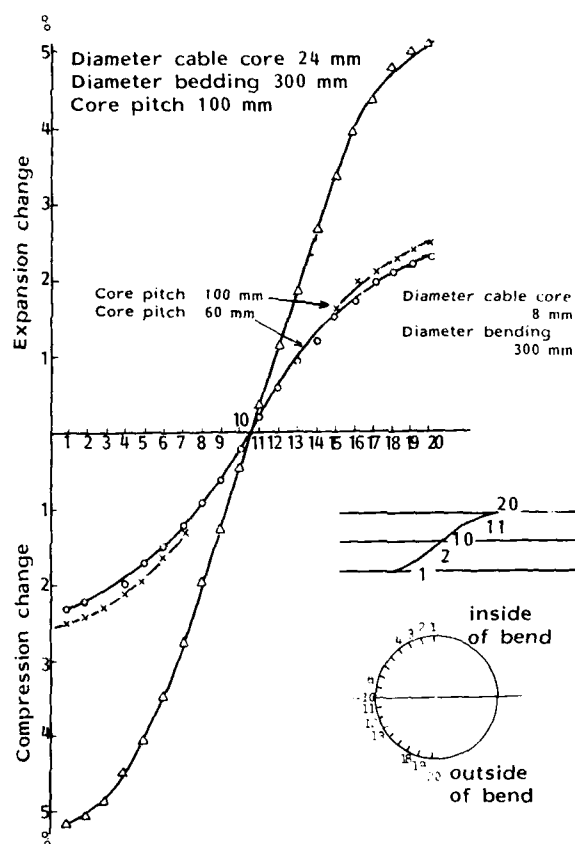


Fig. 3 Change of core length (Bend)

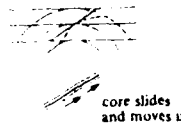
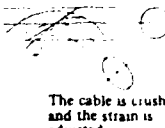
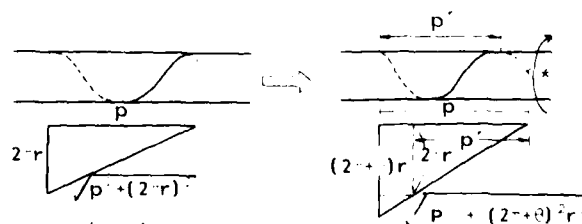
Item	Slipping phenomenon	Diameter reducing phenomenon
Stress relaxing behavior	 core slides and moves in one	 The cable is crushed and the strain is adjusted
Factor that determines the conductor stress	Slip resistance on the surface of insulated core	The conductor stress is determined by the compressing characteristic of the center filler of the cable.
Stress reducing means	The friction between the cores is reduced by the use of silicon oil, mica powder, etc.	The conductor stress is determined by the collapsibility of the center filler of the core.
Adaptability	The most fundamental stress relaxing method	Suitable for cables used for no-tension moving applications.

Table 2 Stress relaxation (Bend)

3-1-2. Torsional strain and stress relaxation

When a cable in which the cores are twisted in a pitch diameter of $2r$ and with a pitch of p is twisted at θ radians, it elongates as shown in Fig. 4. if its conductors are freely expandable and contractible.

Since the scope of elasticity of the conductors are very narrow, the expansion and contraction of the cores would greatly reduce the twisting life of the cable. For cables which sustain twisting, therefore, stress relaxation is necessary so that they are twisted without expansion and contraction of its conductors. Reduction in diameter is one of such motions. Causing these motions with a low conductor stress produces a cable having a long service life in twisting applications. The stress relaxing behaviors are shown in Table 3.



* Twisted to θ radians

Fig. 4 Change of core length (Torsion)

Stress relaxing behavior	In $\sqrt{P^2 + (2\pi\theta)^2} r^2$, r changes, adjusting the increment and decrement of θ .
Factor that determines the conductor stress	Collapsibility of the center filler of the core. Softness of the sheath
Stress relaxing means	The center filler is made soft. Stranding is done with care used to prevent "overlayer."
Adaptability	Stress relaxing behavior.

Table 3 Stress Relaxation (Torion)

3-2. Construction and features of robot cables

The newly developed robot cables are available in two types, curl type and round type, which are suitable for varied applications bending, twisting, expansion-contraction.

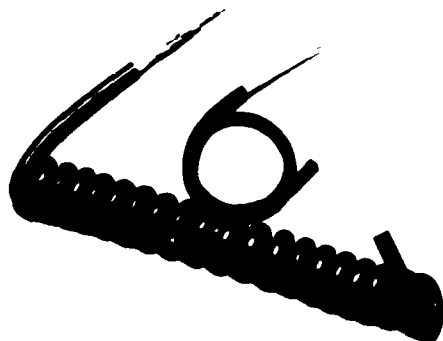


Photo 1. Curl-type robot cable and round type robot cable

The construction (core diameter, etc.) of a robot cable must be determined by the kind of robot for which it is used and the kind of signal to be transmitted by it. Electrically, the most suitable cable must be selected according to whether the transmission signal is analog or digital or whether the transmission system is parallel or serial. Needless to say, even more consideration must be given when the above different signals or signals of different levels are in the same cable. Table 4 shows the types of signals and standard forms of cable construction.

Signal	Remarks	Cable used
Low level analog signal	mV class signal	Multi-pair cable with an individual shield for each pair
	mV class signal	
High level analog signal	Other signals than above	Pair twisted cable with an overall shield for all pairs
	Other signals than above	
Digital signal (I)	High-speed pulse signal	Multi-pair cable with an individual shield for each pair
	High-speed pulse signal	
Digital signal (II)	Other signals than above	Multi-pair cable with an overall shield for all cores


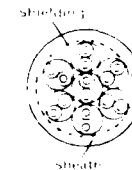
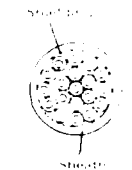
Cable construction	Multi-pair cable with an individual shield for each pair	Pair-twisted cable with an overall shield for all pairs	Multi-core cable with an overall shield for all cores
			

Table 4 Types of signal and cable construction

The mechanical requirements for robot cables are their capability to withstand movements as bending, expansion and contraction. The robot cables developed recently use forty 0.08 mm wire strands (0.2 sq.) and sixty 0.08 mm wire strands (0.3 sq.) for flexible conductors and ETFE (Ethylene-Tetrafluorethylene copolymer) insulation for a lower slip resistance to alleviate the stress of the conductor and for a lower deformation strain characteristic against the load that work on the core.

Table 5 shows the electrical properties of ETFE and Fig. 5 its cut-through characteristic.

Item	Unit	ETFE	FEP	TEF
Volume resistivity	$\Omega\text{-cm}$	$> 10^{16}$	$> 10^{18}$	$> 10^{18}$
Dielectric breakdown strength	KV/mm	16	20 ~ 24	16 ~ 24
ϵ (10^3 Hz)		2.6	2.1	< 2.1
ϵ (10^6 Hz)		2.6	2.1	< 2.1
$\tan \delta$ (10^3 Hz)		0.0008	< 0.0002	< 0.0002
$\tan \delta$ (10^6 Hz)		0.0005	< 0.0005	< 0.0002

Table 5 Electrical properties of ETFE

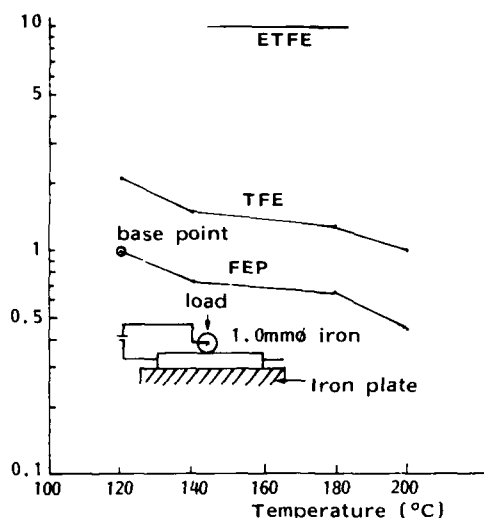


Fig. 5 Cut through characteristics (load-temperature)

4. Performance of robot cables

4-1. Rigidity

Considering the condition under which it is used, a robot cable must have a certain flexibility when used on the movable parts of robots. Within a certain limit, the more flexible the cable, the better. To determine this in quantitative terms, we tested the robot cable by the method shown in Fig. 6, in comparison with the conventional cable Fig. 7 shows the measured data. They indicate that the robot cable has an outstanding flexibility.

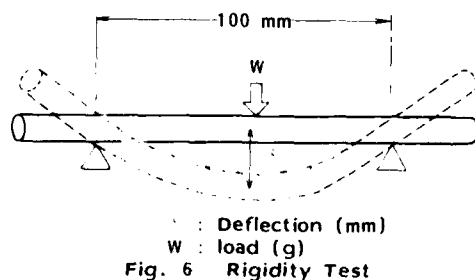


Fig. 6 Rigidity Test

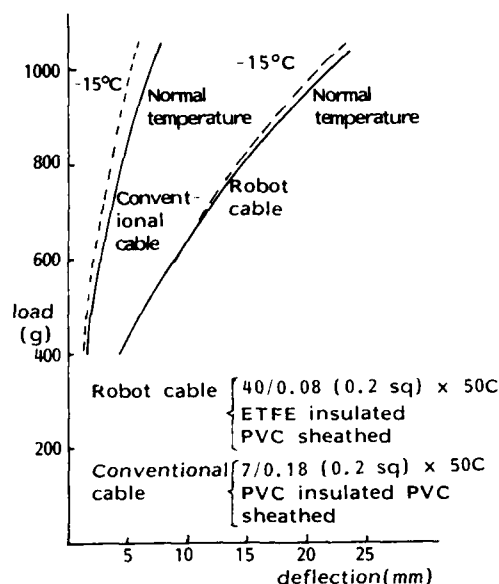


Fig. 7 Load-deflection characteristics

The cable proved to be capable of use where there are complicate bends or where wiring is changed very often.

4-2. Bending property

Various test methods have been worked out for evaluation of the bending property of robot cables. For comparison of robot cables with conventional cables, we trially made the following six types cables and evaluated their repeated bending property by three test methods shown in Figs. 8, 9, and 10. The cable was tested repeatedly until one of its cores is broken.

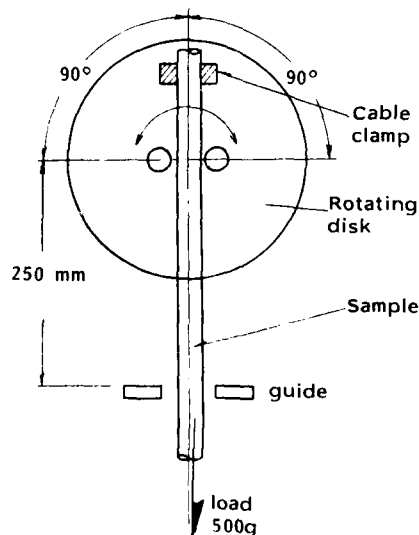


Fig. 8 Bending Test

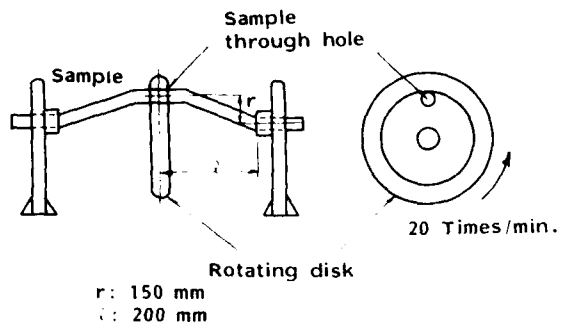


Fig. 9 Twisting Test

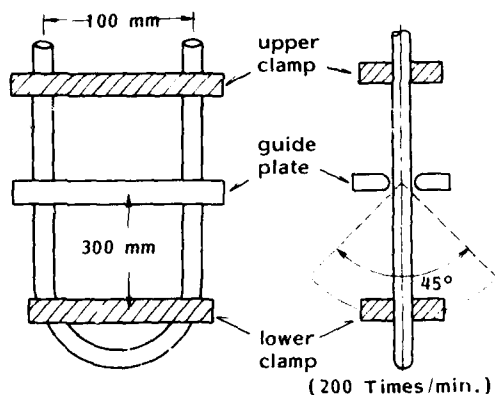
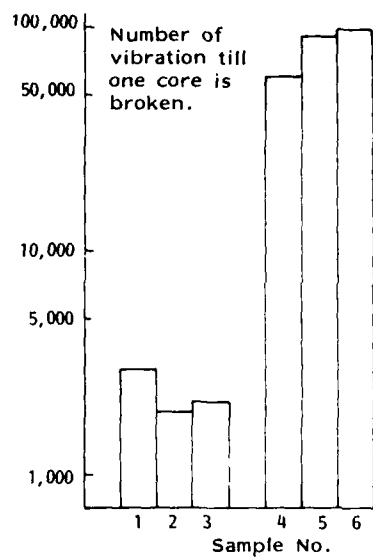


Fig. 10 Vibration Test

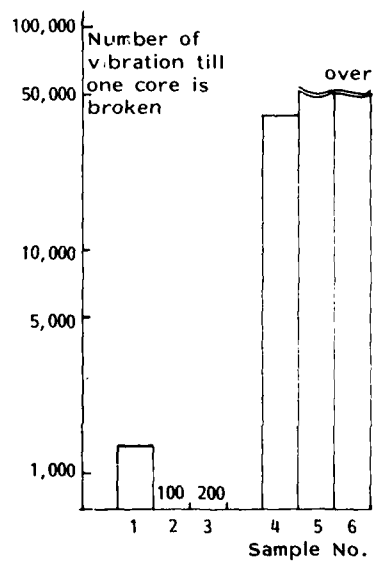
- Sample 1 7/0.1mm X 5 pair PVC insulated PVC sheathed cable
 Sample 2 30/0.08mm X 20 core PVC insulated PVC sheathed cable
 Sample 3 7/0.08mm X 50 core PVC insulated PVC sheathed cable with copper braided
 Sample 4 12/0.1mm X 10 pair ETFE insulated PVC sheathed cable with copper braided
 Sample 5 Robot cable
 Sample 6 30/0.8mm X 50 core ETFE insulated PVC sheathed cable
 Robot cable
 40/0.08mm X 50 core ETFE insulated PVC sheathed with copper braided.

The results of measurement taken on each sample are shown in Figs 11, 12, and 13.



Figures show the average value of three samples (n=3)

Fig. 11 Bending test result



Figures show the average value of three samples (n=3).

Fig. 12 Twisting test result

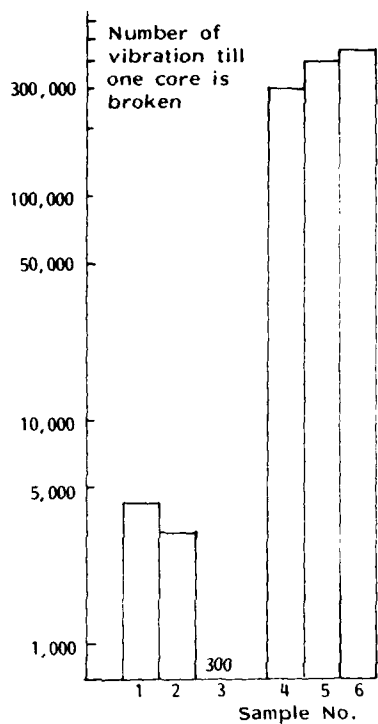


Figure show the average value of three samples (n=3)

Fig. 13 Vibration test results

The above results indicate an improved bending property over the conventional cables.

4-3. Expansion-contraction property

The curl type robot cable suitable for use for such parts of robots as make expanding and contracting motions is required to have a high degree of springiness that makes it follow the swift motions and also an improved service life. We made the following samples and evaluated their springing and expansion-contraction life properties.

- Sample I 40 wires/0.08mm X 20C ETFE insulated PVC sheathed cable (curled)
- Sample II 40 wires/0.08mm X 20C PVC insulated PVC sheathed cable (curled)

4-3-1. Spring property

The springiness required of the curl type robot cable was evaluated by measuring the distance (ℓ) between standard points by the method shown in Fig. 14. The results of measurement are shown in Fig. 15.

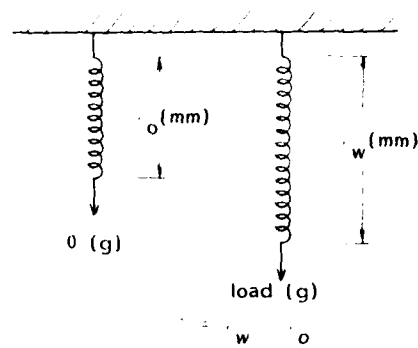


Fig. 14 Evaluation of spring property

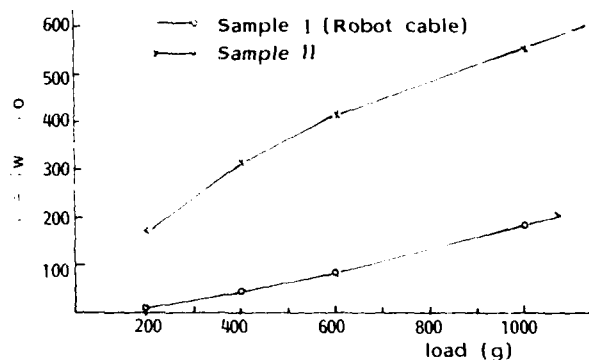


Fig. 15 Results of spring property

Next, the cable was elongated twice the length of its curled portion by the expansion-contraction tester (Fig. 16), with the arm to which the cable was attached making such number of rotations as shown in Table 6 at a rate of 23 rotations per minute. Then the length of the cable dangling under its own weight was measured. The results are shown in Table 6.

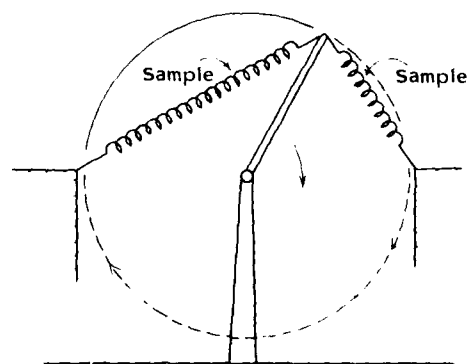


Fig. 16 Expansion Contraction Tester

Sample No.	Length of curled cable (mm) (initial)	Length of curled cable (mm) (20,000 rotations)	Length of curled cable (mm) (50,000 rotations)
Sample I	115	115 [0%]	120 [4%]
Sample II	121	134 [11%]	160 [32%]

[] shows percentage of expansion set

Table 6 Results of expansion contraction Test

4-3-2. Expansion-contraction life property (1)

The cable was elongated three times its curled length by the expansion-contraction tester shown in Fig. 16, and the number of expansions and contractions given up to the breakage of one core was measured. Table 7 shows the results of measurement.

Sample	Expansion-contraction frequencies up to wire breakage
Sample I	56853
Sample II	9834

Table 7 Expansion-contraction life property

4-3-3. Expansion-contraction life property (2)

Since the curl type robot cable is used at rotating part of in the robot body, Sample I was tested on a rotating tester shown in Fig. 16 and Photo 2 to see if it is usable there.

The samples were tested and proved to have a service life expectancy equivalent to more than 100,000 rotations.

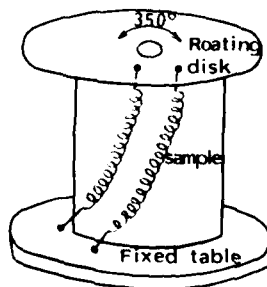


Fig. 16 Rotating Test Method

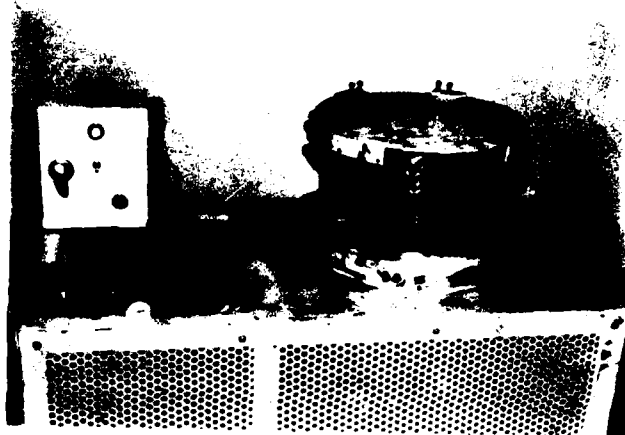


Photo 2 Roting tester

The test results showed that the curl type robot cable follows rapid expansion and contraction very easily, elongates little when expanded and contracted repeatedly, and has a long service life.

5. Electrical properties

There is no difference in electrical properties between robot cables and ordinary cables. They have the properties depending on their conductor size and insulating materials. Table 8 shows general properties of robot cables.

Construction of conductor (No./mm)	Electrical properties		
	Conductor resistance (Ω/km)	Insulation resistance ($\text{M}\Omega\cdot\text{km}$)	Dielectric strength ($\text{AC V}/\text{min}$)
30/0.08	125.0	10,000	500
40/0.08	91.0	10,000	500
60/0.08	65.0	10,000	500
100/0.08	37.5	10,000	500
150/0.08	25.0	10,000	500

Table 8 Electrical properties of Robot Cables

6. Uses (examples) of robot cables

Photos 3 and 4 show some practical example of use of robot cables improved in mechanical properties.



Photo 3

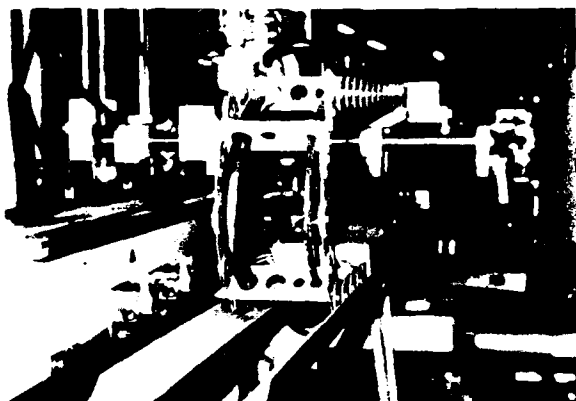


Photo 4

7. Summary

Industrial robots are fast finding extensive practical applications with the progress of electronics technology. As their motions are made faster and more sophisticated, cables used for them are required to be increasingly reliable in performance. At present there are no established methods for testing cables which sustain especially bends and twists while in use. In this report we introduced the development of a round-type and a curl type robot cable evaluated by various test methods. In consideration of current robot motions, and discussed their outstanding properties.

The development of these cables will be accelerated as the technology of industrial robots further advances. The application of optical fiber technology and fixed-point stoppage and position detection technology will be the center of future development.

I hope that this paper will contribute even a mite to such future development of robot cables.

REFERENCE

- 1) Cabtyre Cable for Travelling Machine, Furukawa Rev. 1980
- 2) Electronic Engineering 1979.



TAKAYOSHI MAEZAWA

The Furukawa
Electric Co., Ltd.
6-1 Marunouchi 2-chome
Chiyoda-ku
Tokyo, Japan

Mr. Maezawa, Manager, Engineering Section Products Division is engaged in the design and development of telecommunication wire and communication cable for the communication and data transmission systems.

He received his B.Sc in electric engineering from Keio Univ. in 1963.



AKIO YOSHIZAWA

The Furukawa
Electric Co., Ltd.
6-1 Marunouchi 2-chome
Chiyoda-ku
Tokyo, Japan

Mr. Yoshizawa Assistant Manager, Engineering Section of Electronic Appliance Wire & Products Division is engaged in the design and development of electronic appliance wire and communication cable for communication and data transmission systems.

He received his B.Sc in mechanical engineering from Nihon Univ. in 1970.



ETSURO IWAKABE

The Furukawa
Electric Co. Ltd.
6-1 Marunouchi 2-chome
Chiyoda-ku
Tokyo, Japan

Mr. Etsuro Iwakabe Assistant Manager, Engineering Section of Electronic Appliance Wire & Products Division is engaged in the design and development of electronic appliance wire and communication cable for communication and data transmission systems.

He received his B. Sc in electric engineering from Sagami Institute Univ. in 1970.

AD P000564

A CROSSTALK MODEL FOR CROSS-STRANDED CABLES

Nils Holte

Electronics Research Laboratory (ELAB)
Trondheim - Norway

ABSTRACT

A statistical model is presented which relates crosstalk both in cross-stranded and ordinary pair cables to cable geometry, assuming that crosstalk is mainly caused by irregular twisting.

Cable geometry of cross-stranded cables has been characterized by photographic measurements, and it is shown how variations in cable geometry is transformed into variations in coupling per unit length and finally into average near end and far end crosstalk.

The model has been compared to extensive crosstalk measurements for one specific type of cable, and it correctly predicts the variations of crosstalk with length, frequency, and twist periods of the cable. The model is suitable for optimizing twist periods, and it shows that twist periods of different pairs should be well separated. For existing cross-stranded cables crosstalk can be improved by choosing essentially shorter twist periods of all pairs.

1. INTRODUCTION

Crosstalk is a limiting factor for the use of PCM-systems in twisted pair cables. Today most pair cables in the telephone network are used for analog voice transmission, but the installation of PCM is increasing, and new transmission systems will be introduced, like for instance digital subscriber loops. Because the expected life time of the cables is 30-40 years from installation, the cables should be prepared for future use, and this motivated the Norwegian Telecommunications Administration to initiate work on improving crosstalk for existing types of pair cables.

Almost all telecommunication pair cables produced in Norway today are cross-stranded [1], a technique which was introduced to obtain uniform capacitance unbalances. The method also gives good crosstalk performance at higher frequencies [2].

Crosstalk is a complicated phenomenon and many attempts have been made to relate crosstalk to pair geometry. The first formulation of the problem was presented by Campbell [3] in 1907, and a valuable contribution has been made by Klein [4]. One of the major problems is that crosstalk can not be predicted from nominal cable geometry, but it is caused by random deviations from nominal geometry. Thus deterministic approaches failed, and the first successful statistical approach was made by Cravis and Crater [5], which explained the length and frequency variations of crosstalk by assuming that the coupling functions were stochastic processes. Friesen [6] showed that near end crosstalk in a specific cable can be successfully calculated from knowledge of the twist angles throughout this cable. By describing the geometrical variations statistically, a model was presented (Holte [7]) which relates crosstalk directly to cable geometry. This model was suitable for predicting and improving crosstalk in starquad cables [16]. In this paper the model is refined and extended to cross-stranded cables. Ordinary pair cables will be a special case.

The paper begins in the next section with establishing a geometrical model of a cross-stranded cable, supported by geometrical measurements. In the following sections it is shown theoretically how geometrical variations are translated into electrical parameters, coupling per unit length, and finally into crosstalk. In the last sections the model is adjusted to match the measured crosstalk variations in cross-stranded cables, and potential crosstalk improvements are discussed.

2. CABLE GEOMETRY

An accurate characterization of cable geometry is of vital importance for predicting crosstalk. Nondestructive measurements of cable geometry have been demonstrated by Friesen [6], but a simple and straightforward method is to cut a cable into uniform pieces, photograph the cross sections and digitize the conductor coordinates.

Such a photographic measurement has been carried out for 70 meters of low capacitance, cross-stranded cable, which was cut into sections of length 50 mm [8].

2.1. Deviations from ideal twisting

The twist angle of a pair can be written

$$\varphi_i(x) = s_i x + \phi_i(x) \quad (1)$$

$s_i = \frac{2\pi}{p_i}$ is the twist frequency of pair i in rad/m

p_i is the twist period of pair i

$\phi_i(x)$ is the deviation from ideal twisting.

We assume that $\phi_i(x)$ is a stationary Gaussian stochastic process having zero mean. It proves difficult to estimate the autocorrelation function of ϕ_i because ϕ_i tends to be unbounded. For crosstalk calculations, the twist differences between adjacent cross sections in the cable is important, and we choose to characterize:

$$\eta_i(\tau) = \phi_i(x+\tau) - \phi_i(x) \quad (2)$$

η_i will be stationary and Gaussian and will have zero mean. Its variance is estimated from the geometrical measurements:

$$s_i(\tau) = E[\eta_i^2(\tau)] \quad (3)$$

The measured variances are shown in Fig. 1 for different twist periods.

There is a systematical difference between different pairs for small τ due to the torsion stiffness of the pairs. For long twist periods, the two conductors are almost parallel and they can be rotated independently, but for short twist periods the two pairs will be held together so that the torsion stiffness is increased.

For larger τ there are only moderate differences between s_i of different pairs, and the differences do not vary systematically with the twist periods. For the longest τ shown in Fig. 1 s_i has been estimated from only 100 independent samples which gives $\pm 15\%$ standard deviation on the measured s_i . Hence realistic confidence intervals for different pairs will overlap.

The information that can be extracted from this measurement is that s_i increases approximately linearly with τ , all pairs having almost the same slope. This means that the deviation from ideal twist angle is modelled as a Wiener-Lévy process [17]. Some minor corrections to this model may be introduced for small τ .

The conductor diameter including insulation is two times greater in the cable used for geometrical measurements than the

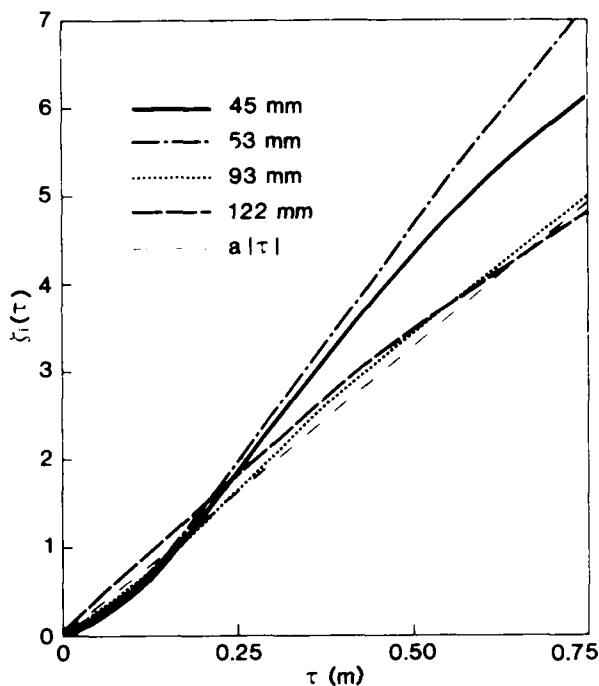


Fig. 1. Variance of difference in twist deviation between two cross sections with distance τ for different twist periods.

cable used for measurements and calculations of crosstalk in later sections. The diameters of the copper conductors of the cables are almost equal. If the deviation from ideal twisting depends primarily on the relative size of the pairs, the results of this section can be applied to the other type of cable by scaling the twist periods by factor 2, and in this case the longest twist periods will be most relevant for further calculations. However the relative difference in copper diameter causes relative differences in stiffness which complicates the scaling, and the results obtained here must be applied with some care.

From the nature of the twisting process one would expect that the accumulated twist deviation is bounded. The deviation from ideal twisting is generated mainly by the mechanical interaction in the stranding point where the different pairs are forced together to form a 10-pair group. However the pairs are twisted with constant speed, and if the twist deviation ϕ_i becomes too large, the torsion stiffness of the pair will tend to reduce the deviations. This feedback is governed by the torsion spring defined by the pair between the twisting point and the stranding point. The cross-

stranding machinery is twisting 10 pairs and stranding them to a group in one operation. The length of the torsion spring is several meters, so that the feedback effect will not be visible in Fig. 1, and crosstalk will not be influenced. For conventional cables which are twisted and stranded in different operations this may be different.

As shown in section 5 the most important parameter of the twist deviations is the Fourier transform of

$-\zeta_1(\tau)$ which is denoted $G(s)$. Calculating $G(s)$ for the curves in Fig. 1 gives the result shown in Fig. 2.

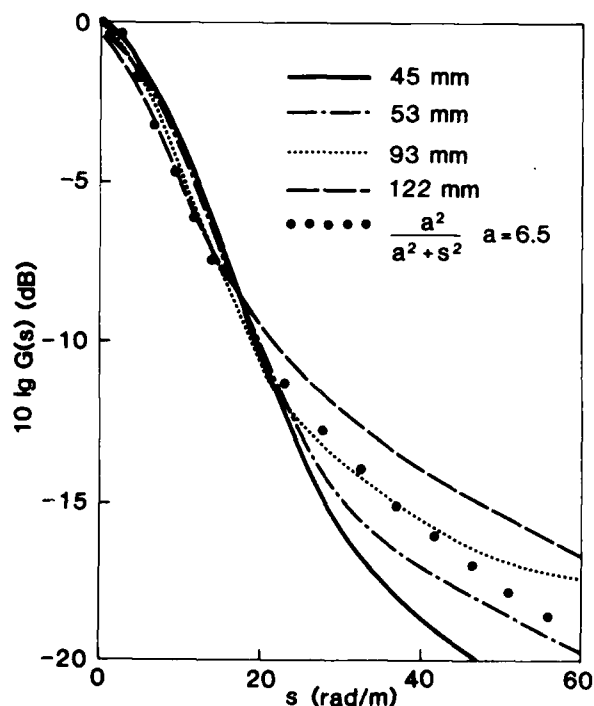


Fig. 2. Fourier transforms of $-\zeta_1(\tau)$ for different twist periods.

For small twist frequencies s the curves are almost coinciding, but there is a systematical variation with the twist period of the pair at larger s .

Large $G(s)$ means large crosstalk, and the most important region of Fig. 2 is for $s < 20$ rad/m. The straight broken line in Fig. 1 with slope $a = 6,5 \text{ m}^{-1}$ corresponds to the heavily dotted line of Fig. 2 and represents a fair analytical approximation that can be used for all pairs in this type of cable.

2.2. Stranding effects

An often used model for the cable geometry is that each pair rotates around a fixed point in the cable cross section so that the pairs may just touch each other as demonstrated in Fig. 3.

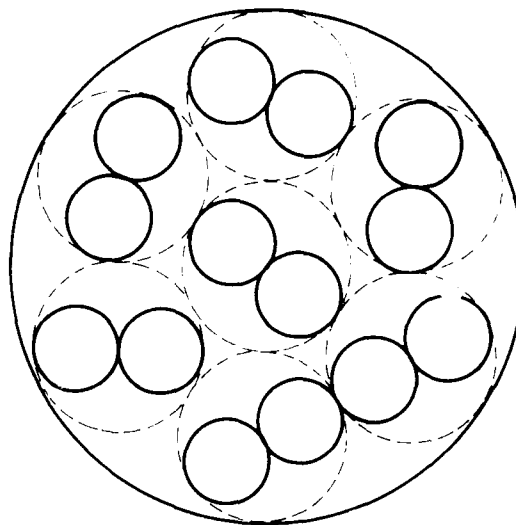


Fig. 3. Idealized cross section of 7-pair cable.

This model is a fair approximation for starquad cables, but for pair cables the measured cable (group) diameter is considerably smaller than shown in Fig. 3. In practical cables the pairs are packed together so that the cross section is minimized.

According to section 2.1 the deviations from ideal twisting show relatively small variations from one cross section to another (50 mm apart). The movements of the mid-points of each pair around their equilibrium positions showed very little correlation from one 50 mm interval to another. Consequently the pairs seem to have greater torsion stiffness than stiffness against bending, and the twisting process is treated independently from the movement of the pairs within the cross section.

As a model for the movement of the pairs within the cross section we use an algorithm described in [9]. Different cross sections are treated independently. By means of an iterative algorithm the pairs are moved within a circular shield having the empirically measured diameter until the overlap between pairs is minimized. The twist angles of the pairs are held constant during the movements.

2.3. The cross stranding process

In the cross-stranding process [1] the twisted pairs are running through individual dies in a matrix as shown in Fig. 4.

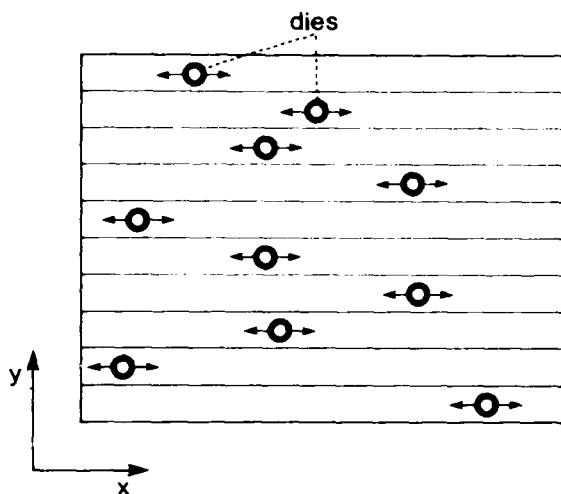


Fig. 4. Cross-stranding matrix.

The position of dies in the x-direction is changed according to signals from a noise generator. After passing the matrix the pairs pass two rollers, and the group is wrapped together by binder tape. The purpose of the cross-stranding equipment is to make the mutual distance for all pair combinations almost equal in average. It is rather complicated to translate the positions of the dies to pair positions within the group. Thus one of the main purposes of the geometrical measurements was to find out how the pair positions really change in practical cross-stranded cables.

Inspection of the measurements showed that almost all cross sections had two pairs in the center and 8 pairs in the outer layer as shown in Fig. 5. The different positions are numbered as shown in the figure.

The measurements showed that the pairs remained in the same positions for several succeeding cross sections (in some cases up to 3 m). The point where any of the pairs change their positions is denoted an interchange. A cumulative distribution of the distance between interchanges is shown in Fig. 6. The average distance between two interchanges is 412 mm and the average number of pairs taking part in each interchange is 3.5. There will be a greater distance between points where two distinct pairs changes their relative positions.

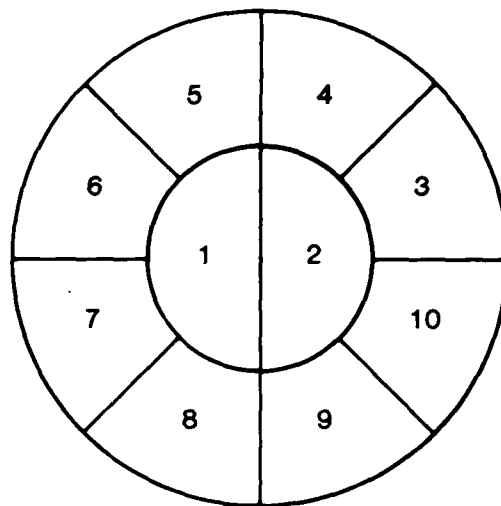


Fig. 5. Pair positions in a 10-pair group.

These results show that the position of the pairs are changed in a rather abrupt manner and that a cross-stranded cable may be regarded as sections of a conventional pair cable connected in cascade, having random splicing in the cross sections.

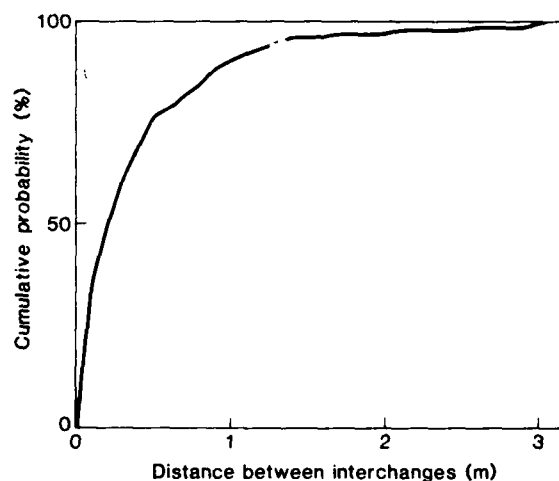


Fig. 6. Cumulative distribution of the distances between pair interchanges in a cross-stranded 10-pair group.

All pairs have the same type of stochastic motion in the x-direction in the matrix, but there are constant distances

between the pairs in y-direction. Correlating the distance between pairs in y-direction in the matrix and measured average pair to pair distance in the cable gives the result shown in Fig. 7.

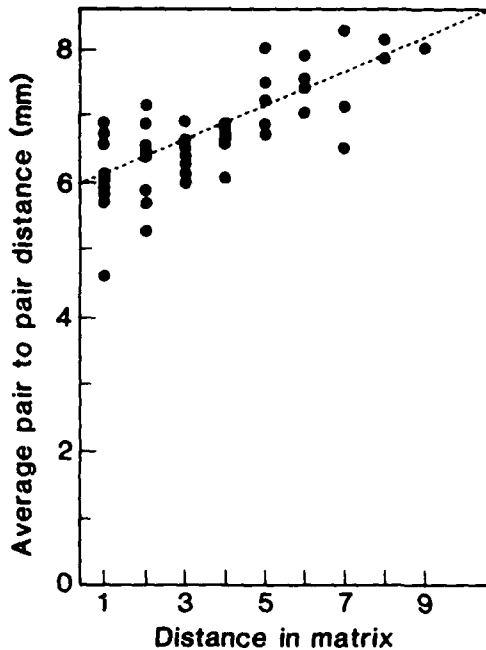


Fig. 7. Average pair to pair distance as a function of distance in cross-stranding matrix.

The figure shows that adjacent pairs in the matrix will have short separation also in the final cable. The statistical material is somewhat too small to give an accurate model of the variation, but using the broken line of Fig. 7, the most distant pairs will have 25% greater average separation than the nearest. This represents a nonideal property of the cross-stranding process, but it will not necessarily result in poorer crosstalk performance, because the effect of twisting and the effect of different distance in the cross-stranding matrix may be combined. However, it is important to allocate distinct dies in the matrix to each of the pairs.

3. IMPEDANCE AND ADMITTANCE MATRICES

In order to calculate crosstalk, the geometrical characterization of the cable must be translated into an electrical characterization in form of impedances and admittances.

Piecewise parallel conductors and homogeneous permittivity between conductors are assumed. The per unit length capacitance matrix of each cross section is calculated by means of a method given by Singer et al [10] which simulates the surface charge on each conductor by concentrated line charges inside each conductor.

In most cables permittivity varies across the cross section. More realistic methods are available at the cost of increased computing time. Clements et al [11] calculate the capacitance matrix of dielectric-coated cylindrical conductors, and Lenahan [12] describes a method for calculating cables having parallel wires coated with two layers of insulation (foamed skin).

For lossless and parallel conductors and homogeneous permittivity, the per unit length inductance matrix of the wires is proportional to the inverse capacitance matrix as shown by Klein [4]:

$$L = \mu_0 \epsilon C^{-1} \quad (4)$$

C is the per unit length capacitance matrix of the wires

μ_0 is the permeability of vacuum

ϵ is the permittivity of the insulation

Losses can be taken into account by Wheeler's incremental inductance rule [13], [14].

4. COUPLING FUNCTIONS

The coupling between different pairs in the cable can be described by the Generalized Telegraph Equation:

$$\frac{d}{dx} \underline{I} = -\underline{Y} \underline{U} \quad (5)$$

$$\frac{d}{dx} \underline{U} = -\underline{Z} \underline{I}$$

\underline{I} is a vector containing the currents of each conductor.

\underline{U} is the voltages of each conductor (relative to the shield).

\underline{Y} is the admittance matrix of the cable per unit length,

\underline{Z} is the impedance matrix of the cable per unit length.

Crosstalk is calculated by solving this equation. An exact solution is possible only for special cases as for instance parallel wires (Rice [15]). Since both harmonical and stochastic variations of \underline{Y} and \underline{Z} are present in the model, approximations must be used.

At the frequencies of interest ($f < 10$ MHz) the coupling is so weak that the influence of the disturbed pair on the disturbing pair can be neglected.

The lossy elements of Z and Y are small compared to the capacitive and inductive parts for $f > 100$ kHz so that losses can be neglected for the calculation of cross-talk coupling. Dimensionless, lossless, per unit length coupling functions for the near end and far end direction respectively are defined by Klein [4]:

$$\kappa_N = \frac{1}{2} \left(\frac{C_{ij}}{C} + \frac{L_{ij}}{L} \right) \quad (6)$$

$$\kappa_F = \frac{1}{2} \left(\frac{C_{ij}}{C} - \frac{L_{ij}}{L} \right) \quad (7)$$

C_{ij} and L_{ij} are per unit length mutual capacitance and inductance between pair i and j .

C and L are per unit length capacitance and inductance of all pairs (equal).

4.1. Fourier series expansion of coupling functions

A more convenient analytical expression for the coupling function between two pairs is desired.

For this purpose a conventional group having parallel pairs is considered. The coupling function varies with the twist angles of the pairs. For ideal twisting the coupling function between pair i and j can be expressed as a Fourier series:

$$\kappa(x) = \sum_{k=1}^{\infty} c_k \cos(s_{Fk}x + \varphi_{ok}) \quad (8)$$

where

$$s_{Fk} = ns_i + ms_j$$

n, m are integers

c_k are Fourier coefficients

φ_{ok} are phase angles at $x=0$

The two dominating terms have twist frequencies $s_{F1} = s_i - s_j$ and $s_{F2} = s_i + s_j$. Higher order terms have at least 20 dB lower amplitudes and may be neglected.

This representation of the coupling function will be valid also when deviations from ideal twisting is present. The paranthesis in (8) contains a linear combination of the twist angles. The deviations from ideal twisting will be added inside the paranthesis and cause phase modulation of each term in the series.

The two dominating Fourier coefficients have been calculated for a 10-pair unit like the one shown in Fig. 5. The result is shown in Table 1.

5. NEAR END CROSSTALK

Using the weak coupling assumption, near end crosstalk (NEXT) can according to Klein be expressed:

$$N = js \int_0^l \kappa_N(x) e^{-2sx} dx \quad (9)$$

$\gamma = \alpha + j\beta$ is the propagation constant of the pairs.

l is the length of the cable.

We assume that crosstalk is caused by only the first term of the Fourier series if all pairs are twisted in the same direction. We will return to this assumption in the end of this section. The interchanges of pair positions are assumed to take place at distinct points in points in the cable. The coupling factor can be formulated:

$$\kappa_N(x) = c_n \cos(sx + \varphi(x)) \quad (10)$$

$$l_{n-1} < x < l_n \quad n = 1, N$$

where

$$s = s_i - s_j \quad (11)$$

Table 1. Fourier coefficients of near end and far end coupling functions.

Pair positions	Near end coupling		Far end coupling	
	-20 lg c_1	-20 lg c_2	-20 lg c_1	-20 lg c_2
Adjacent pairs (1-2 and 3-4 in Fig. 5)	35.0	23.4	35.7	37.6
Pairs with one pair in between (3-5, 4-6,...)	37.9	36.3	39.5	38.1
Pairs with two pairs in between (3-6, 4-7,...)	42.6	41.0	43.0	41.4
Diagonally positioned pairs (3-7, 4-8,...)	42.8	42.3	43.0	42.6

$$\varphi(x) = \varphi_i(x) - \varphi_j(x) \quad (12)$$

φ_i is the deviation from ideal twisting in pair i

c_n is the Fourier coefficient of length interval n

ℓ_n is the position of an interchange

Consequently:

$$N = j\beta \sum_{n=1}^N \int_{\ell_{n-1}}^{\ell_n} c_n \cos(sx + \varphi(x)) e^{-2\alpha x - 2j\beta x} dx \quad (13)$$

The cross-stranding process and the random twisting are assumed to be uncorrelated. Calculating average near end crosstalk power, we first take the expectation with respect to random twisting:

$$p' = \langle N N^* \rangle = \beta^2 \sum_{n=1}^N \sum_{m=1}^N c_n c_m \int_{\ell_{n-1}}^{\ell_n} \int_{\ell_{m-1}}^{\ell_m} \langle \cos(sx + \varphi(x)) \cdot \cos(sy + \varphi(y)) \rangle e^{-2\alpha(x+y) - 2j\beta(x-y)} dy dx \quad (14)$$

$\langle \rangle$ denotes expectation with respect to the twisting process

* denotes complex conjugation.

Manipulating the expression inside the expectation gives:

$$\begin{aligned} \langle \cos(sx + \varphi(x)) \cos(sy + \varphi(y)) \rangle &= \\ \frac{1}{2} \langle \cos \varphi_+ \rangle \cos s(x+y) &+ \frac{1}{2} \langle \sin \varphi_+ \rangle \sin s(x+y) \\ + \frac{1}{2} \langle \cos \varphi_- \rangle \cos s(x-y) &+ \frac{1}{2} \langle \sin \varphi_- \rangle \sin s(x-y) \end{aligned} \quad (15)$$

where

$$\begin{aligned} \varphi_+ &= \varphi(x) + \varphi(y) \\ \varphi_- &= \varphi(x) - \varphi(y) \end{aligned} \quad (16)$$

Both φ_+ and φ_- will be Gaussian with zero mean. Because sine is an odd function, both the sine terms of (15) will be zero. The first term of (15) will have random phase angle and does not contribute to the integral.

Denoting the expectation of $\cos \varphi_-$ by R , yields:

$$\begin{aligned} R(x-y) &\triangleq \langle \cos \varphi_- \rangle = \\ \frac{1}{2\pi\sqrt{\xi}} \int_{-\infty}^{\infty} \cos z e^{-\frac{z^2}{2\xi}} dz &= e^{-\frac{\xi}{2}} \end{aligned} \quad (17)$$

where

$$\xi = \xi(x-y) = \langle [\varphi(x) - \varphi(y)]^2 \rangle \quad (18)$$

For uncorrelated deviation from ideal twisting in different pairs, ξ can be related

to the measured deviations in the two pairs by:

$$\xi(\tau) = \xi_i(\tau) + \xi_j(\tau) \quad (19)$$

Combining (14), (15) and (17) and changing variables $u = x+y$ and $v = x-y$ gives:

$$p' = \frac{\beta^2}{4} \sum_{n=1}^N \sum_{m=1}^N c_n c_m \int_{R_{nm}} \int e^{-2\alpha u - 2\beta v} R(v) \cos sv \, du dv \quad (20)$$

R_{nm} are the transformed ranges of integration.

From the results of section 2.1 we observe that $R(v)$ is essentially different from zero only for v less than a fraction of a meter. Thus the integration limit with respect to v can be extended to infinity. The length of the cross-stranding intervals are approximately one meter in average. Thus the major contributions to p' are caused by terms having $n=m$. Neglecting the boundary effects between the integration ranges gives:

$$p' = \frac{\beta^2}{4} \sum_{n=1}^N c_n^2 \int_{\frac{2\ell_{n-1}}{2\ell_n}}^{\frac{2\ell_n}{2\ell_{n-1}}} e^{-2\alpha u} \int_{-\infty}^{\infty} R(v) e^{-2\beta v} \cos sv \, dv \, du \quad (21)$$

This means that $c_n \cdot c_{n+1}$ has been replaced by c_n^2 and c_{n+1}^2 in small regions near the borders between integration ranges. According to Table 1, c_1 shows moderate variations for different pair positions, so that this simplification will cause only small approximation errors in the final result after averaging with respect to cross-stranding.

To simplify the result we introduce the Fourier transform of $R(v)$ which is denoted $G(s)$, and where s is given in angular twist frequency:

$$G(s) = \int_{-\infty}^{\infty} R(\tau) e^{-s\tau} d\tau = \int_{-\infty}^{\infty} e^{-\frac{\xi(\tau)}{2}} e^{-s\tau} d\tau \quad (22)$$

Integrating (21) with respect to u and introducing (22) gives:

$$p' = \frac{\beta^2}{16\alpha} \left[G(s+2\beta) + G(s-2\beta) \right] \cdot \sum_{n=1}^N c_n^2 \left(e^{-4\alpha \ell_{n-1}} - e^{-4\alpha \ell_n} \right) \quad (23)$$

Averaging with respect to cross-stranding leads to:

$$p = \frac{3\overline{c^2}}{16\alpha} \left[1 - e^{-4\alpha} \right] \left[G(s+2\alpha) + G(s-2\alpha) \right] \quad (24)$$

$\overline{c^2}$ is the expectation of c_n^2 with respect to the cross-stranding process.

For cables of length greater than a few hundred meters the term $e^{-4\alpha}$ becomes negligible. For the frequencies of interest ($f < 10$ MHz) α is negligible compared to the twist frequencies. Average near end crosstalk power between two pairs i and j can now be expressed:

$$p = \frac{3\overline{c^2}}{8\alpha} G(s_i - s_j) \quad (25)$$

The result shows the same 15 dB/decade frequency variation as calculated by Cravis and Crater [5] for conventional pair cables, which corresponds to measurements of both conventional and cross-stranded cables.

In Fig. 2 it was shown that $G(s)$ has its maximum at $s=0$ and decreases monotonically with s . Consequently the twist periods should be essentially different for all pairs. Short twist periods are disadvantageous because of reduced production efficiency, and too long twist periods can not be tolerated because the pairs will split and cause other crosstalk mechanisms than described here. According to (25) a uniform distribution of twist frequencies over the permissible range of variation will be optimum if c^2 and $G(s)$ are equal for all pair combinations.

Calculation of near end crosstalk caused by the second term in the Fourier series (the sum of twist angles) will produce the same result as (25) but with the difference of the twist frequencies replaced by the sum $s_i + s_j$, and that $\overline{c^2}$ means an average of c_2 instead of average c_1 . For typical cross-stranded cables having twist periods in the range 60-90 mm, the largest $s_i - s_j$ will be 35 rad/m and the smallest $s_i + s_j$ will be 140 rad/m.

Extrapolating the results of Fig. 2 indicates that $G(s)$ is at least 10-15 dB greater for the difference term than for the term no. 2. Table 1 shows that $\overline{c^2}$ may be up to 10 dB lower for the difference term for pairs having short average separation. This means that the term containing the sum of twist angles may be almost equal in magnitude for the pairs having best near end crosstalk performance. Thus for accurate calculations the second term should be taken into account. However for the critical pair combinations having small differences in twist frequency, the difference term will be dominating.

6. FAR END CROSSTALK

From Klein [4], equal level far end crosstalk (ELFEXT) can be expressed:

$$F = j \int_0^l F(x) dx \quad (26)$$

In the same way as for near end crosstalk it is assumed that only the difference term of the Fourier series contributes to crosstalk. This is a much better approximation for far end crosstalk because c_1 and c_2 are almost equal in magnitude as shown in Table 1. Using the same expression for $F(x)$ as given by (10) yields:

$$F = j \sum_{n=1}^N \int_{n-1}^n c_n \cos(sx + \phi(x)) dx \quad (27)$$

For a given set of cross-stranding intervals, the average far end crosstalk power will be:

$$q' = \langle F \cdot F^* \rangle = \frac{1}{2} \sum_{n=1}^N \sum_{m=1}^N \int_{n-1}^n \int_{m-1}^m \langle \cos(sx + \phi(x)) \cdot \cos(sy + \phi(y)) \rangle dy dx \quad (28)$$

Carrying out the same steps as for near end crosstalk gives:

$$q' = \frac{1}{4} \sum_{n=1}^N \sum_{m=1}^N c_n c_m \int_{R_{nm}} \cos sv R(v) dv du \quad (29)$$

Using the same approximations as for near end crosstalk:

$$q' = \frac{1}{2} \sum_{n=1}^N c_n^2 \left(\frac{1}{n} - \frac{1}{n-1} \right) \int_0^\infty \cos sv R(v) dv = \frac{1}{2} \sum_{n=1}^N c_n^2 \left(\frac{1}{n} - \frac{1}{n-1} \right) G(s) \quad (30)$$

Averaging with respect to cross-stranding gives:

$$q = \frac{1}{2} \overline{c^2} G(s_i - s_j) \quad (31)$$

The result shows the experienced 20 dB/decade frequency variation and 10 dB/decade length variation as calculated by Cravis and Crater [5]. It also shows that far end crosstalk in principle varies in the same way with twist periods as near end crosstalk.

7. COMPARISONS WITH MEASUREMENTS

Crosstalk measurements have been carried out on a 45 nF/km, .6 mm, subscriber cable, having from 30 to 150 pairs in 10-pair cross-stranded units. Both near end and far end crosstalk were measured for all pair combinations within 56 different 10-pair groups and for 41 combinations of adjacent 10-pair groups. All measurements were carried out as single frequency measurements at $f = .35, 1$ and 4 MHz. The measurements were scaled according to the results of sections 5 and 6 to 1 MHz and 1 km. Then crosstalk for each specific pair combination was averaged on a power basis over all cables and frequencies. This gives estimates for each pair combination having a standard deviation of approximately .5 dB.

It is important that crosstalk is not averaged directly on a dB-basis because the estimates will be biased and have considerably greater variance. A few very good crosstalk values will contribute strongly to the dB-average and this is undesirable because the part of the distribution having poorest crosstalk values is of major interest.

The geometrical measurements were carried out for a previous cable design, and we do not have a comprehensive set of both crosstalk measurements and geometrical measurements for the same type of cable. Thus crosstalk can not be directly calculated from the geometrical measurements, but the parameters of the model will be calculated from the crosstalk measurements so that deviations between measurements and calculations are minimized.

7.1. Crosstalk between adjacent 10-pair cross-stranded groups

Different adjacent 10 pair groups will have a random relative orientation. Consequently, the average pair to pair distance between the two groups will be constant, and the coefficients c^2 of (25) and (31) will be equal for all pair combinations. Thus crosstalk between adjacent groups should depend only upon the twist frequencies. Correlating measured crosstalk versus the difference in twist frequency gives the plots in Figs 8 and 9.

The result of Fig. 2 indicates that deviations from ideal twisting is statically almost equal in all pairs. If this was the case also in the new cable and our approximations are valid, the points of Figs. 8 and 9 should gather around a smooth curve. However, the variations are greater than can be expected from the statistical uncertainty of the measurements. It is a tendency that pairs having long twist periods show crosstalk values poorer than the average.

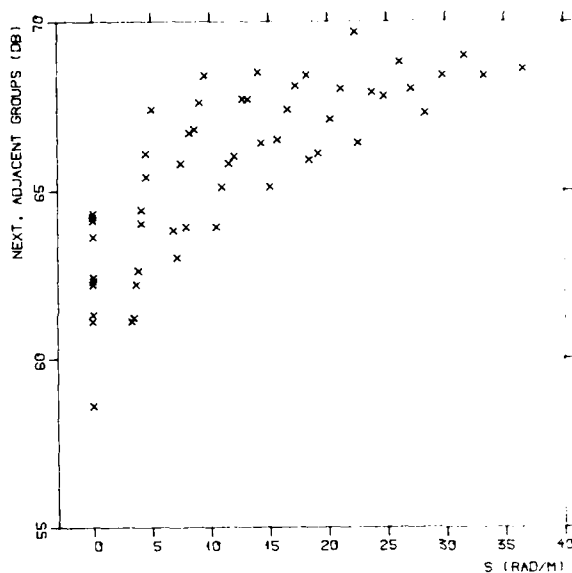


Fig. 8. Near end crosstalk for different pair combinations of adjacent groups versus twist frequency difference.

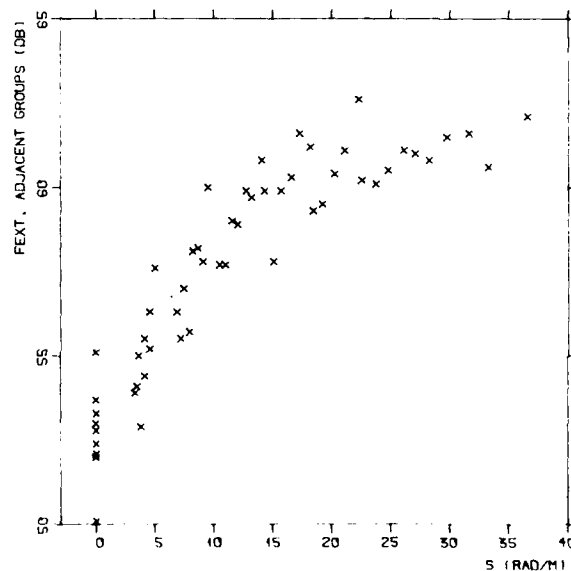


Fig. 9. Far end crosstalk for adjacent groups versus twist frequency difference.

The average curves of Figs. 8 and 9 have considerably steeper variation in dB than the curves of Fig. 2. The deviations from the model may have different reasons as listed below:

- The term in the Fourier series containing the sum of twist angles may contribute significantly to crosstalk. According to the geometrical measurements this effect should be important only for the largest values of s for near end crosstalk (Fig. 8). However the observed results may be caused by a $G(s)$ having less steep variation with s than measured in Fig. 2.
- The deviation from ideal twisting may vary significantly with the twist periods.
- Unbalances due to the pair interchanges in the cross-stranding process may cause crosstalk.
- The terms c_i of the coupling factors may have significant amplitude variations along the cable, caused by the complicated mechanical interaction between the pairs.
- The pairs having the longest twist periods will have the weakest forces keeping the pairs together, and this may cause variations in the distance between the conductors of a pair.

The crosstalk measurements do not contain sufficient information to reveal the cause of the discrepancy. This can be done only by means of new geometrical measurements. However, it is a preliminary aim to predict the crosstalk variation with twist periods. It is assumed that the deviation from ideal twisting can be modelled by

$$\epsilon_i(t) = a \cdot t \quad (32)$$

where a is equal for all pairs.

In addition an additive empirical term is introduced to explain the poorer crosstalk for long twist periods. Average near end crosstalk power can then be expressed:

$$p = \frac{p_0^2 c^2}{8} \left[\frac{2a}{(s_i - s_j)^2 + a^2} + k \left(\frac{p_i p_j}{p_0^2} \right)^n \right] \quad (33)$$

Average equal far end crosstalk power will be:

$$q = \frac{p_0^2 c^2}{2} \left[\frac{2a}{(s_i - s_j)^2 + a^2} + k \left(\frac{p_i p_j}{p_0^2} \right)^n \right] \quad (34)$$

k and n are empirical constants

$p_0 = 100$ mm is a reference twist period.

The parameters c^2 , a , k and n were optimi-

mized to reduce the mean square deviation from the measured crosstalk values. For convenience, independent optimizations were carried out for near end and far end crosstalk. The results are shown in Table 2.

Table 2. Parameter values found by minimizing deviations from measured crosstalk between adjacent groups.

Parameter	Near end crosstalk	Far end crosstalk
$-10 \lg c^2$	48.6 dB	46.8 dB
a	5.17 m^{-1}	4.44 m^{-1}
k	.693	.175
n	2.48	1.66

The value of a should be expected to be the same for both near end and far end crosstalk. However, the difference is moderate and demonstrates the uncertainty of the calculated parameters due to the statistical uncertainty of the crosstalk estimates. The calculated values of a are also in relatively good agreement with the geometrical measurements, thus indicating that the model for the deviations from ideal twisting (32) is correct.

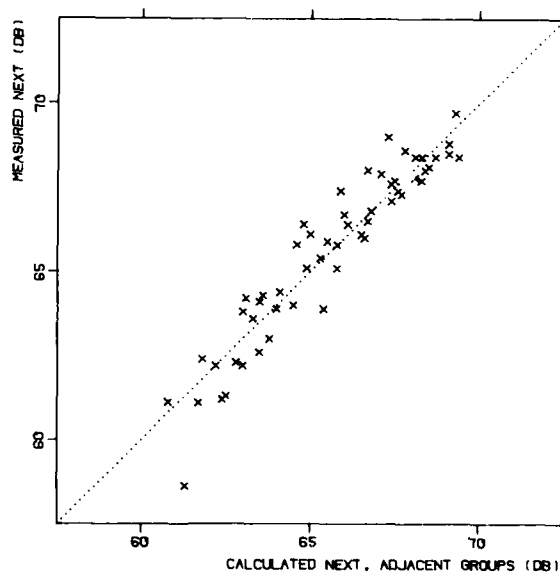


Fig. 10. Correlation between calculated and measured near end crosstalk between adjacent cross-stranded groups for different pair combinations.

For the parameters shown in table 2 the correlation between calculated and measured crosstalk will be as shown in Figs. 10 and 11.

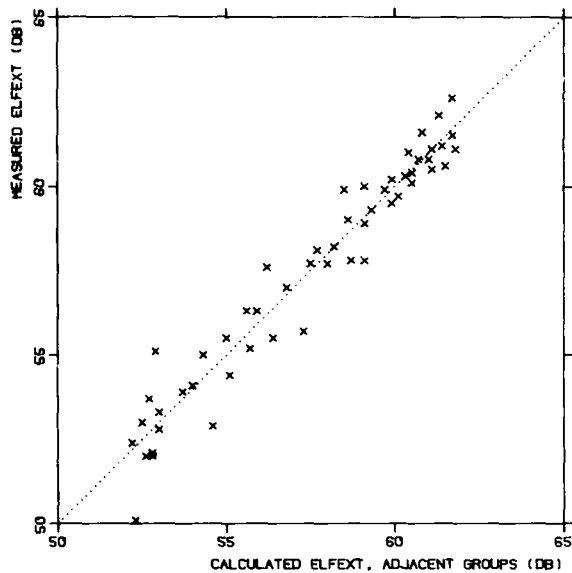


Fig. 11. Correlation between calculated and measured far end crosstalk between adjacent cross-stranded groups.

Except for a few points of Figs. 10 and 11, differences between calculations and measurements correspond to the variance of the measured crosstalk. Thus by introducing an empirical correction to the model, it has successfully been described how crosstalk varies with twist periods in a cross-stranded cable.

7.2. Crosstalk within 10-pair cross-stranded groups

As shown in the geometrical measurements, the average pair to pair distance varies as a function of the separation in y-direction in the cross-stranding matrix. Consequently the parameter \bar{c}^2 will also be a function of the distance in the matrix. The variation of crosstalk due to nonideal twisting should according to (25) and (31) be the same for pairs in different groups and pairs within a group. Thus by taking the difference between crosstalk of adjacent groups and crosstalk within groups for each pair combination, an estimate for the variations of \bar{c}^2 is obtained which is shown in Figs. 12 and 13.

For small distances in the matrix the crosstalk difference has somewhat greater variations than can be expected from the

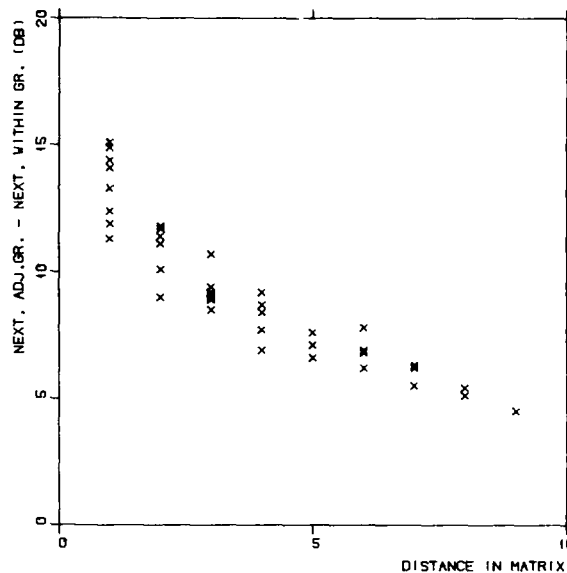


Fig. 12. Difference between near end crosstalk in adjacent groups and crosstalk within groups versus pair to pair distance in the cross-stranding matrix.

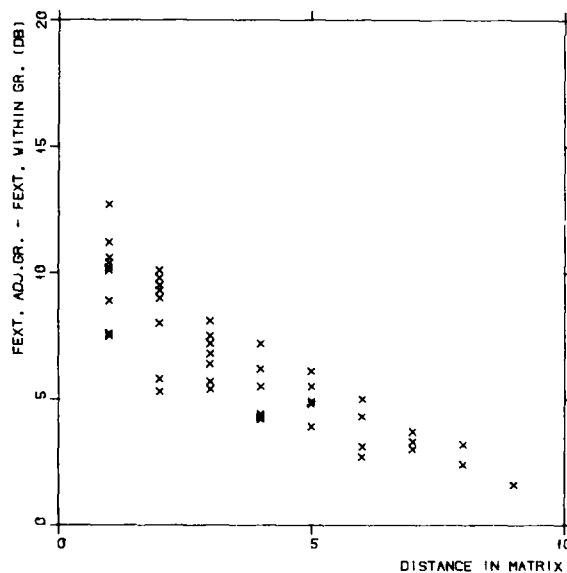


Fig. 13. Difference between far end crosstalk in adjacent groups and crosstalk within groups versus pair to pair distance in the cross-stranding matrix.

uncertainty of the crosstalk measurements, but the crosstalk variations of Figs. 12 and 13 can almost entirely be explained from the distances in the cross-stranding matrix.

Fitting a smooth curve through Figs. 12 and 13 gives the values of $\overline{c^2}$ for pairs within a group shown in Table 3.

Table 3. Average Fourier coefficients $\overline{c^2}$ for pairs within a 10-pair unit.

Distance in y direction in cross-stranding matrix	Near end cross-talk	Far end cross-talk
	$-10 \lg \overline{c^2}$	$-10 \lg \overline{c^2}$
1	35.5	36.5
2	37.7	38.7
3	39.2	40.2
4	40.3	41.3
5	41.2	42.2
6	42.0	43.0
7	42.7	43.7
8	43.3	44.3
9	43.8	44.8

The range of variations of the Fourier coefficients of Tables 1 and 3 are almost the same. This means that the relative distances between pairs in the cross-stranding matrix are almost maintained in the final cable and that this variation is even stronger than in the geometrical measurements shown in Fig. 7. This may be caused by a misadjustment of the cross-stranding machine during the production of the cables used for crosstalk measurements.

The pairs having the largest separation have slightly smaller Fourier coefficients in Table 3 than calculated for diagonally positioned pairs in Table 1. This means that the methods used for calculating capacitance and inductance matrices probably underestimates the shielding effect caused by the other pairs in the cable when calculating the coupling for two well separated pairs.

Using $\overline{c^2}$ in Table 3 and the other parameters found from crosstalk between groups, the correlation between calculations and measurements for crosstalk within groups is as shown in Figs. 14 and 15.

The deviations between calculations and measurements are slightly greater than in Figs. 10 and 11 because the parameters have been matched to measurements of pairs in adjacent groups. By adjusting the parameters to measurements within groups,

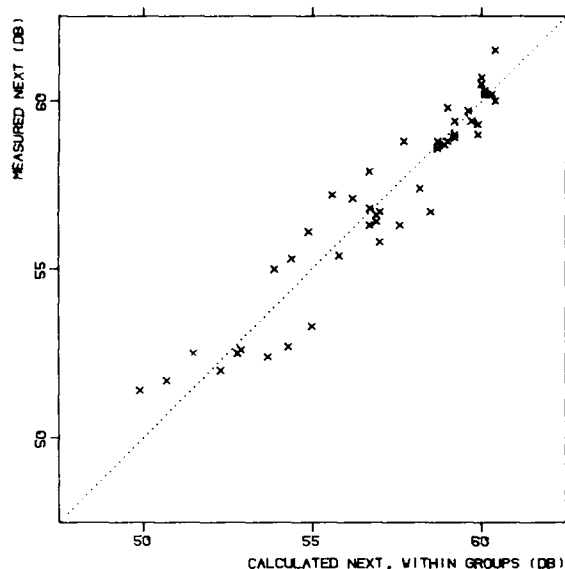


Fig. 14. Correlation between calculated and measured near end crosstalk within 10-pair cross-stranded groups.

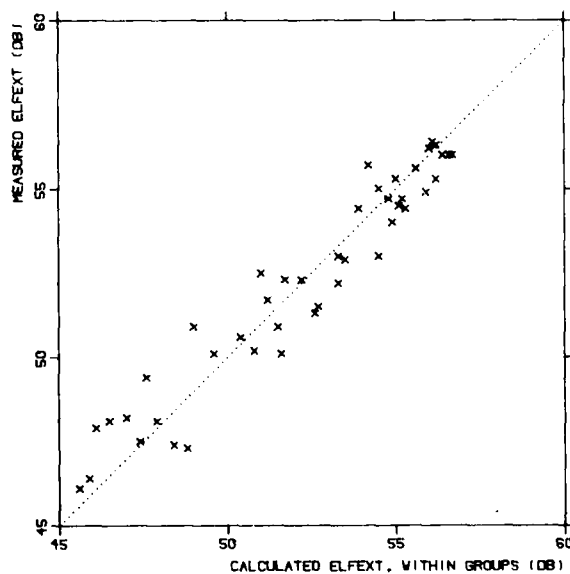


Fig. 15. Correlation between calculated and measured far end crosstalk within 10-pair cross-stranded groups.

this difference could be removed. However, Figs. 14 and 15 show good correlation between calculations and measurements, and by introducing the empirical term in (33) and (34) a model has been obtained which predicts the variations of crosstalk with twist periods for pairs within a 10-pair cross-stranded group.

8. IMPROVEMENT OF CROSSTALK

In this paper it has been described how crosstalk varies with twist periods for a given cable design and a given adjustment of the existing cross-stranding machines. The results of section 7 primarily explain how crosstalk will change if only the twist periods are changed, keeping all other parameters constant, and possible improvements of crosstalk will be discussed for this case. Further improvements may be obtained by modifications of machinery and cable design, so that the parameters of the model are changed, but this is not addressed here.

For PCM use of cross-stranded cables it will be convenient to put the two directions of transmission in separate groups. In this case near end crosstalk between adjacent groups will be critical. As shown by (33), two pairs in adjacent groups having equal twist periods will have poorest crosstalk performance. Using different sets of twist periods in different groups is inconvenient from a production point of view, and the possible crosstalk improvement of this approach will be negligible. According to (33) the term caused by nonideal twisting will remain constant for pairs of equal twist periods, but the empirical term is almost eliminated by choosing essentially shorter twist periods. By reducing the longest twist period from 90 to 70 mm the crosstalk of the poorest pair combination will be reduced by 2 dB. Thus a moderate reduction of crosstalk between adjacent groups can be obtained by only changing the twist periods.

For crosstalk within a 10-pair unit the model predicts larger possible crosstalk improvements. Average crosstalk of the poorest pair combination is used as a measure of crosstalk quality. This gives a good and simple indication of crosstalk performance, but power sum distributions will be more accurate.

To obtain a quick estimate we assume that \bar{c}^2 is equal for all pair combinations and start with a cable having uniformly distributed twist frequencies over the interval corresponding to twist periods from 60 to 90 mm. The critical pair combinations are pairs having adjacent twist periods. A 3 dB improvement of near end

crosstalk may be obtained by choosing optimum twist periods over the interval 55-90 mm, and a 6 dB improvement is predicted for twist periods 40-80 mm. The measurements have been carried out only for twist periods greater than 60 mm so that the predictions above are extrapolations from the model which must be used carefully. For essentially shorter twist periods, other crosstalk mechanisms may be present, for instance because the assumption of piecewise parallel conductors is violated. However, the model clearly indicates that shorter twist periods must be used to improve crosstalk.

9. CONCLUSION

A statistical model has been presented which makes it possible to calculate crosstalk in cross-stranded cables on the basis of the cable geometry. Ordinary pair cables can be handled as a special case. The model is suitable for frequencies from 100 kHz to 10 MHz. It is shown that crosstalk in pair cables is mainly caused by irregular twisting of the pairs.

Crosstalk depends strongly upon the twist periods, and pair combinations having small differences in twist periods will have the poorest crosstalk performance. The model will be a helpful tool for selecting optimum twist periods in a cable.

Extensive crosstalk measurements have been carried out for 45 nF/km, .6 mm, cross-stranded subscriber cables. After introducing minor empirical corrections, the model correctly predicts the variations of both near end and far end crosstalk for different pair combinations in this type of cable. It is shown that improvements of crosstalk can be obtained by choosing essentially shorter twist periods of all pairs.

ACKNOWLEDGEMENT

This work has been sponsored by Norwegian Telecommunications Administration, Research Establishment, and the author wishes to thank them for the permission to publish it. He also wishes to thank Standard Telefon og Kabelfabrikk A/S (STK) and A/S Norsk Kabelfabrikk (NK) for providing crosstalk measurements and measurements of cable geometry.

REFERENCES

- [1] S. Nordblad, Multi-paired cable of nonlayer design for low capacitance unbalance telecommunications networks, IWCS, 1971, pp 156, 163.
- [2] The Norwegian Telecommunications Administration, Measurement report for 700 pair cross-stranded subscriber cable, Oslo, June 1977. (In Norwegian).
- [3] G.A. Campbell, Dr. G.A. Campbells memo-randa of 1907 and 1912, BSTJ, October 1935, pp 558, 572.
- [4] W. Klein, Die Theorie des Neben-sprechens auf Leitungen, Springer Verlag, Berlin, 1955.
- [5] H. Cravis and T.V. Crater, Engi-neering of T1 Carrier System Repea-tered Lines, BSTJ, March 1963, pp 431-486.
- [6] H.W. Friesen, Relating the twist detection measurements of twisted pairs to their crosstalk performance, IWCS, Cherry Hill, 1975, pp 150, 157.
- [7] N. Holte, A statistical model for calculation of crosstalk in a balan-ced pair cable, IWCS, Cherry Hill, 1976, pp 25, 31.
- [8] N. Holte, Measurements of cable geo-metry in cross-stranded cables by photographic methods, internal project memo, March 1978. (In Norwegian).
- [9] N. Holte, Calculation of crosstalk in balanced pair cables by means of simulation, IWCS, Cherry Hill, 1977, pp 428, 439.
- [10] H. Singer et al., A charge simulation method for the calculation of high voltage fields, Paper T 74085-7, IEEE PES Winter Meeting, New York, 1974.
- [11] J.C.Clements et al., Computation of the Capacitance Matrix for Systems of Dielectric-Coated Cylindrical Con-ductors, IEEE Trans. on Electro-magnetic compability, No 4, 1975.
- [12] T.A. Lenahan, The theory of uniform Cables, Part II: Calculation of charge components, BSTJ, Apr. 1977, pp 611, 625.
- [13] H.A. Wheeler, Formulas for the Skin Effect, Proc of the IRE, Sept. 1942, pp 412, 424.
- [14] V. Alessandrini et al., The skin effect in multiconductor systems, Int. J. Electronics, 1976, Vol 40, No 1, pp 57, 63.
- [15] S.O. Rice, Steady state solutions of transmission line equations, BSTJ, April 1941, pp 131, 178.
- [16] N. Holte, Calculation of crosstalk by statistical methods, ELAB report STF44 F77118, Trondheim, Feb. 1977 (In Norwegian).
- [17] A. Papoulis, Probability, Random Variables, and Stochastic Processes, McGraw-Hill, 1965.



Nils Holte
ELAB
N-7034 Trondheim-NTH
Norway

Nils Holte was born in Norway in 1946. He received the M.Sc. degree in 1971 and the Dr.ing. degree in 1976, both from the University of Trondheim, Trondheim, Norway.

From 1970 to 1974 he was an assistant Professor at the University of Trondheim, working on computer aided design of LC-filters. Since 1975, he has been at ELAB, except in 1979 when he was employed at A/S Elektrisk Bureau. His main interests are crosstalk in balanced pair cables and digital transmission systems.

AD P000565

IMPEDANCE IRREGULARITIES IN TELEPHONE NETWORKS

Leo M. Chatter

DCM INTERNATIONAL CORP.
San Leandro, California U.S.A.

ABSTRACT

Telephone companies of the world are having network problems due to impedance mismatch and impedance irregularities in their telephone network. This is caused to a large extent by tolerances on the primary parameters and on unbalances of the circuits in telephone cables. This results in reflections and standing waves which affect voice frequency and carrier frequency telephone transmission. This paper highlights these irregularities and recommends specific values and tolerances which would considerably reduce the impedance mismatch between telephone cables and telephone cables connecting to switching, transmitting and receiving equipment.

INTRODUCTION

Although U. S. telephone companies have more rigid telephone cable specifications than most of the other countries of the world, the trend in the U. S. and other countries is to reduce telephone network losses through more rigid telephone cable specifications. These specifications reduce the measurement values and tolerances and increase the measurement parameters; thereby improving the transmission characteristics by reducing impedance mismatch losses.

1. THE TELEPHONE NETWORK

A telephone circuit consists of three essential parts: A source of energy, a medium for which it is desired to transmit energy to a receiving device and the receiving device itself, which usually converts the electric energy into some more useful form. In a telephone connection the transmitter may be considered as the source of energy. The cable from the speaking party to the listening party with all of its associated switching equipment and connections is the transmission medium and the telephone receiving at the distant end is the third part of the transmission system or the device which converts small electric currents into audible vibration of air called sound waves. A signal which is transmitted is subject to various influences that deteriorate its quality from the source via the conversion equipment and the transmission facilities to the receiving terminal. The most significant of these influences are IMPEDANCE IRREGULARITIES resulting in loss due to reflections and noise due to unbalances and

crosstalk. Since the transmission characteristics of a cable are indicated by its characteristic impedance (Z_0) and the propagation constant (γ), which in the case of homogeneous lines are determined by the four-line primary constants (resistance, R ; inductance, L ; conductance, G ; and capacitance, C), every irregularity in the homogeneous line represents a discontinuity with partial reflection of the energy. These discontinuities which affect the transmission quality result from the interconnection of lines with differing impedances and from internal irregularities in the line.

2. CHARACTERISTIC IMPEDANCE (Z_0)

Since impedance mismatch between cables and impedance irregularities within cables are so important, let's determine the characteristic impedance of a transmission line in terms of the primary parameters RLGC.

The fundamental transmission characteristics of the twisted pair transmission line are determined by four basic properties known as the primary parameters of the line. These are the Resistance of the conductors, R ; the Inductance of the conductors, L ; the capacitance between the two conductors, C ; and the leakage resistance or conductance between the conductors, G . These four qualities combine to give the line a value of impedance; R and L are series parameters and C and G are shunt parameters. In terms of these parameters, a multi-section uniform network simulating the transmission line may be represented by Figure 2-1.

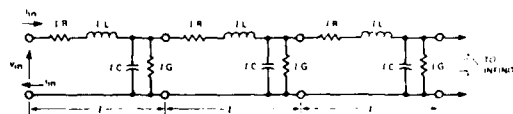


Fig. 2-1 Series Connected Sections to Approximate a Distributed Transmission Line

What amount of input current i_{in} is needed to produce a given voltage V_{in} across the line as a function of the primary parameters $R L C G$ of the transmission line? Combining the series terms R

and L together simplifies calculation of the series impedance Z_S as follows:

$$Z_S = (R + j\omega L) \quad \text{Eq. 2.1}$$

Likewise, combining C and G produces a parallel impedance:

$$Z_P = \frac{1}{(G + j\omega C)} \quad \text{Eq. 2.2}$$

Based on equations 2.1 and 2.2 we can represent Fig. 2-1 as Fig. 2-2.

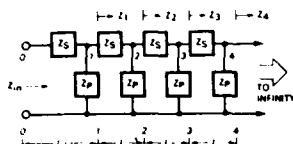


Fig. 2-2 Impedance Network

Since it is assumed that the impedance network is infinite in length, the impedance looking into any cross section should be equal, that is, $Z_1 = Z_2 = Z_3$, etc. Therefore we now represent Fig. 2-2 as Fig. 2-3:

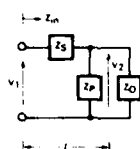


Fig. 2-3 Characteristic Impedance

Z_0 is the characteristic impedance of the line and Z_{in} must equal this impedance; $Z_{in} = Z_0$. From Fig. 2-3

$$Z_{in} = Z_S + \frac{Z_0 Z_P}{Z_0 + Z_P} = Z_0 \quad \text{Eq. 2.3}$$

multiplying both sides by $(Z_0 + Z_P)$ collecting terms and using the quadratic formula we get

$$Z_0 = \frac{(R + j\omega L)}{2} \pm \frac{1}{2} \sqrt{(R + j\omega L)^2 + 4 \left[\frac{R + j\omega L}{G + j\omega C} \right]} \quad \text{Eq. 2.4}$$

As the section length l is reduced, all the parameters (RLGC) decrease in the same proportion. This is because RLGC are constants for a given line. As l approaches zero, the terms in Eq. 2.4 which contains l as a multiplier will become negligible when compared to the last term, $(R + j\omega L / G + j\omega C)$ which remains constant as l approaches zero. Therefore, Eq. 2.4 can be written as

$$Z_0 = \sqrt{\frac{R + j\omega L}{G + j\omega C}} = \sqrt{Z_S Z_P} \quad \text{Eq. 2.5}$$

As Equation 2.5 shows, the value of characteristic impedance is dependent solely on the primary parameters of the line and the frequency. At any given frequency, therefore, this impedance has a fixed value for any given type of line regardless of the length of the line or what may be connected to the line.

The characteristic impedance of a transmission cable is thus very important for impedance matching. If the impedance of one cable connected to another is different, some of the energy applied to the line will be reflected from the connection point back to the source. This represents a loss of power, but if the impedance of both cables is the same, all of the energy applied to the line will pass to the load with designed line attenuation. If the impedance of the load connected to the line is different from the characteristic impedance of the line, some of the energy applied to the line will be reflected from the load back to the source with a loss of power; but if the load impedance is the same as the line's characteristic impedance (Z_0) all the energy applied to the line will be absorbed by the load.

2.1 Propagation Constant (Phase Shift and Propagation Velocity)

Referring to Fig. 2-3 there will be some phase shift and loss of signal of V_2 with respect to V_1 because of the reactive and resistive parts of Z_S and Z_P . Each small section of the line (l) will contribute to the total phase shift and amplitude reduction if a number of sections are cascaded as in Fig. 2-2. It is important to determine the phase shift and signal amplitude loss contributed by each section because the velocity of propagation effects voice intelligibility. If different frequencies arrive at the ear at different times, the voice may not be recognizable.

Using Fig. 2-3 V_2 can be expressed as

$$V_2 = V_1 \left(\frac{Z_P Z_0}{Z_P + Z_0} \right) \left(\frac{1}{(Z_S + Z_P Z_0) / (Z_0 + Z_P)} \right) \quad \text{Eq. 2.6}$$

or,

$$\frac{V_2}{V_1} = 1 + Z_S \left[\frac{1}{Z_0} + \frac{1}{Z_P} \right] \quad \text{Eq. 2.7}$$

In terms of γ , the per unit length constant we can show a reduction in amplitude and the change in phase per unit length of the section by

$$\gamma_l = \alpha_l + j\beta_l \quad \text{Eq. 2.8}$$

and since

$$V_2 = V_1 e^{-\alpha_l} + V_1 e^{-j\beta_l} \quad \text{Eq. 2.9}$$

where $V_1 e^{-\alpha_l}$ is the signal attenuation and $V_1 e^{-j\beta_l}$ is the change in phase from V_1 to V_2 . By combining equations taking \log_{10} substituting Eq. 2.5

for Z_0 and using the \log_{10} series expansion we can obtain

$$\gamma_z = \sqrt{\frac{Z_s}{Z_p}} = z \sqrt{(R+j\omega L)(G+j\omega C)} \quad \text{Eq. 2.10}$$

and then dividing by the section length

$$\gamma = \sqrt{(R+j\omega L)(G+j\omega C)} \quad \text{Eq. 2.11}$$

The propagation constant in terms of the line primary parameters R L C G. If the resistive components R and G are further neglected by assuming the line is reasonably short, Eq. 2.11 can be reduced to read

$$\gamma_z = jB_z = j\omega L \sqrt{LC} \quad \text{Eq. 2.12}$$

dividing by j and z

$$B = W \sqrt{LC} \quad \text{Eq. 2.13}$$

Eq. 2.13 shows that the lossless transmission line has very important properties. Signals introduced into the line have a constant phase shift per unit length with no change in amplitude. This progressive phase shift along the line actually represents a wave traveling down the line with a velocity equal to the inverse of the phase shift per section. This velocity is

$$\gamma = \frac{W}{B} = \frac{1}{\sqrt{LC}} \quad \text{Eq. 2.14}$$

The larger the LC product of the line, the slower the signal will propagate down the line. A time delay per unit length can also be defined as the reciprocal of γ

$$\delta = \frac{1}{\gamma} = \sqrt{LC} \quad \text{Eq. 2.15}$$

and total propagation delay for a line of length z as

$$T = z\delta = z \sqrt{LC} \quad \text{Eq. 2.16}$$

The propagation constant is very important because it contains the attenuation and phase of the input signal down the line and thus affects the intelligibility of the transmission.² This signal represents the sum of the original signals fourier (continuous) spectrum because both the attenuation and the propagation velocity of these fourier components increase with frequency. The resultant signal shape at that point down the line depends greatly on the winners of the race to get to that point. The high frequency components with their faster propagation velocity arrive first, but the increased attenuation minimizes their effect. The low frequency signals arrive later, but then re-

duced attenuation allows them a greater influence on the resultant signal.

2.2 Variations in Z_0 , $\alpha(\omega)$ and Propagation Velocity as a Function of Frequency

The variations in the primary line parameters as a function of frequency (Fig. 2-4) have a significant influence on the secondary parameters of Z_0 , $\alpha(\omega)$ and γ (Fig. 2-5 and Fig. 2-6).

Reviewing Figs. 2-4 to 2-6 (plotted from Eq. 2.2 to 2.6) indicates that inductance drops approximately 27% from 10 kHz to 20 MHz. The capacitance is very stable with frequency showing no change from 0.1 kHz to 10 MHz (providing a frequency stable dielectric system such as polyethylene is used). Resistance increases approximately 80% from 10 kHz to 12 MHz and the conductance increases approximately 100 times from 100 kHz to 12 MHz. These RLGC changes cause the characteristic impedance to become purely resistive above 100 kHz since the reactive part of Z_0 goes to zero.

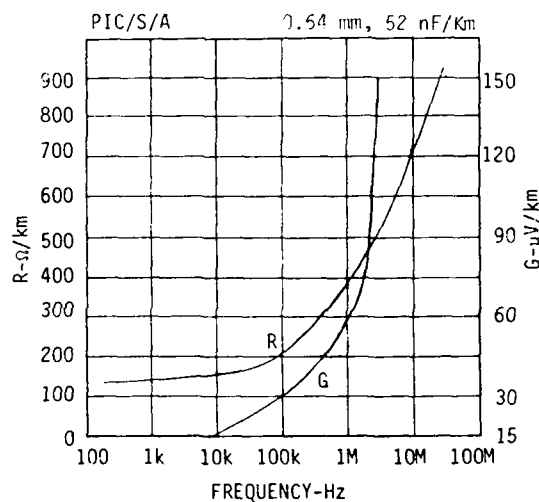


Fig. 2-4 R and G vs Frequency

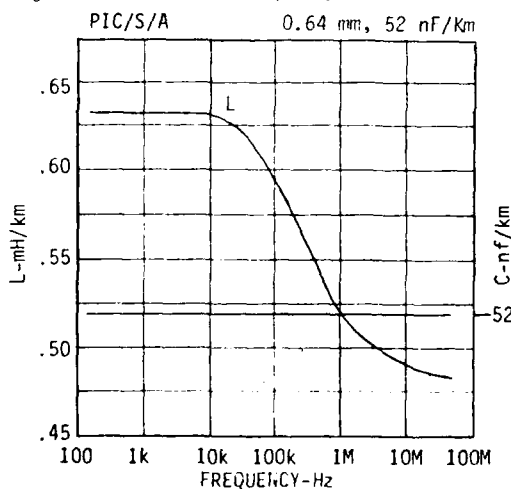


Fig. 2-5 L and C vs Frequency

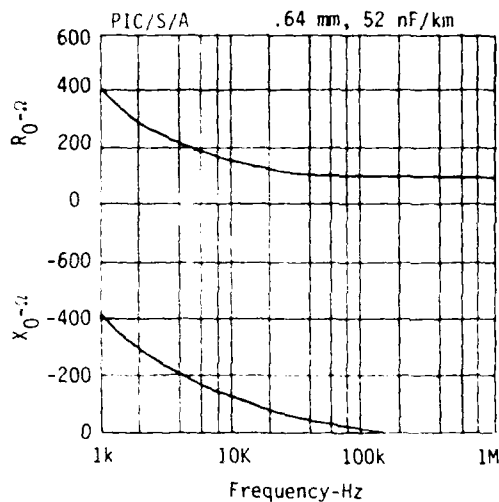


Fig. 2-6 $Z_0 = (R_0 + jX_0)$ vs Frequency

Typical behavior of the line attenuation as a function of frequency is shown in Fig. 2-7. This attenuation is the real part of the propagation constant of Eq. 2.3 as shown in Eq. 2.4. The change in resistance is the primary contributor to the attenuation increase as a function of frequency, due to the skin and proximity effects. The attenuation curve is plotted from Eq. 2.4 which is expanded from 2.1 to eliminate the imaginary quantities.

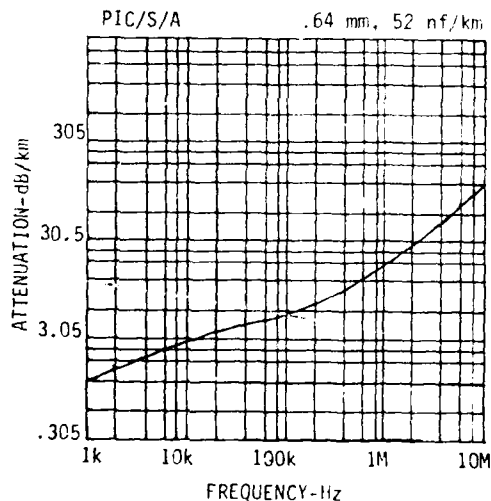


Fig. 2-7 Attenuation vs Frequency

NOTE: PIC/S/A = Polyethelene Insulated Conductor, Solid, Air Core.

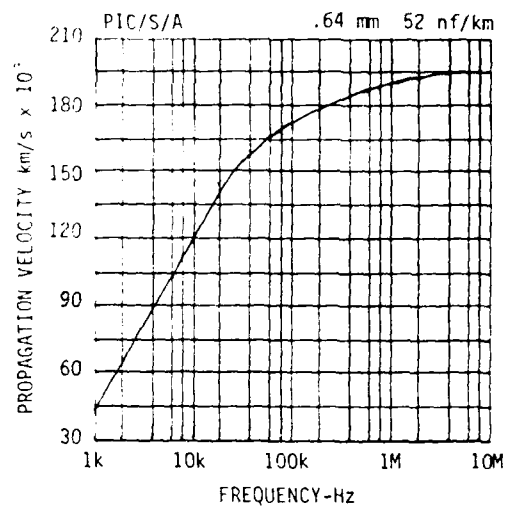


Fig. 2-8 Propagation Velocity vs Frequency

The variation of the propagation velocity as a function of the signal frequency as shown in Fig. 2-5 is called "dispersion". The resistance of the line results in signal attenuation and the attenuation also varies with frequency. Attenuation and dispersion cause the frequency components of a signal, at some point down the line, to be quite different from the frequency components of the signal applied to the input of the line. Thus, at some point down the line the frequency components add together to produce a wave shape that may differ significantly from the input wave shape.

Impedance irregularities even when they are small can cause phase changes which can cause unintelligible transmission.

3. ECHO AND SINGING FROM IMPEDANCE IRREGULARITIES

Echo, as the name implies, refers to a phenomenon whereby a part of the signal energy traveling in one direction reverses its direction of travel due to an impedance irregularity and returns toward the point from which originated. This, of course, is very annoying in communication circuits because a talker may hear his own words after some delay or a listener may hear the same words a second time, again after some delay.

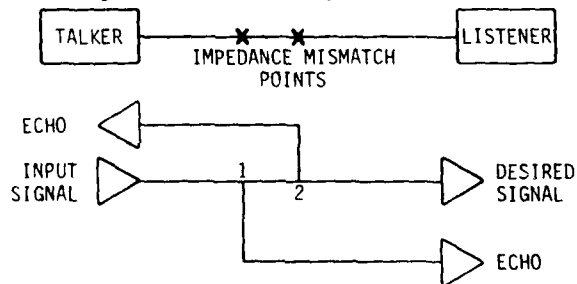


Fig. 3-1 Echo from Impedance Irregularities

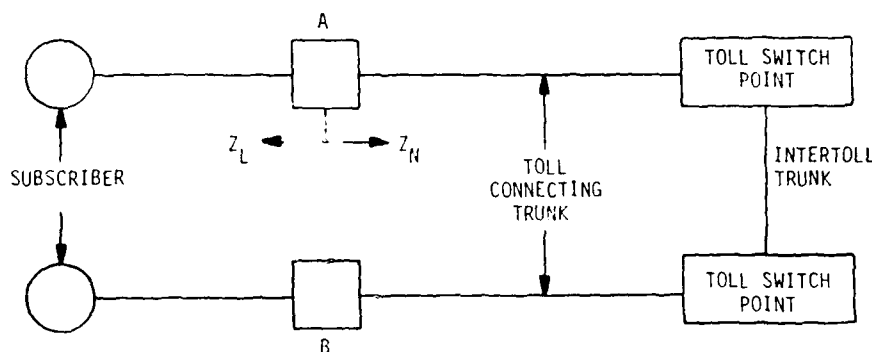


Fig. 3-2 Return Loss in Toll Networks

Since the echo signal is energy which returns to the point of origin, the magnitude of a reflected signal at the point of impedance discontinuity is generally expressed in terms of "return loss". Return loss is a function of the impedances which produce the reflection. In Fig. 3-2 the return loss at junction A between the subscriber loop and the toll connecting trunk is given by

$$\text{Return Loss (dB)} = 20 \log_{10} \frac{Z_L + Z_N}{Z_L - Z_N} \quad \text{Eq. 3.1}$$

Where Z_L is the impedance looking toward the subscriber loop, and Z_N is the impedance seen looking toward the toll.

The frequency range over which talker echo may be significant extends from about 500 hertz to 2500 hertz. Listener echo results when the talker echo signal is again reflected and the impedance discontinuity generates a secondary echo signal which travels towards the listener.

A singing (high frequency sound) condition may occur at frequencies outside the talker echo frequency gain mentioned above because the impedance match between interconnected circuits is poorer at these frequencies resulting in poorer return losses. The voice frequency bands which are significant with regard to singing are from 200 to 500 hertz and from 2500 to 3500 hertz. Losses at the junction between the toll connecting trunk and the subscriber loop generally are much poorer than those at the junctions between intertoll trunks making the loop/toll connecting trunk interface the predominant source of signal reflection. This is caused because generally cables of the same conductor type and characteristic impedance are used in junctions between intertoll trunks, but cables of different conductor diameters and types are used between the connecting trunk and subscriber loops.

3.1 Digital and Analog Carrier Line Losses

In digital transmission systems, one of the most serious problems is crosstalk. Crosstalk is basically a type of noise and as such its absolute level is not important. What is important is the relationship between the crosstalk noise and the desired signal; that is, the signal to noise ratio (S/N). Since the most important feature of digital transmission lines is the ability to reconstruct the transmitted pulse train after it has traveled through a dispersive and noisy medium, the signal to noise ratio is of utmost importance. The digital transmission process is performed by regenerative repeaters which have the basic functions of equalization, timing, and regeneration. Fig. 3-3 shows the different stages of a PCM signal as it goes through a complete repeater section including a regenerative repeater. A perfectly shaped signal is transmitted by repeater "A" but at the input of repeater "B" the pulse stream is distorted and corrupted by noise. In repeater "B", the input signal is amplified and equalized to compensate for the characteristics or absence of a pulse in the signal. Finally, according to the decision made, a well-shaped noiseless signal is generated and transmitted. In the ideal situation the output stream of repeater "B" is an exact replica of the output stream of repeater "A". In practice, if the interference is sufficiently large at the decision time, the repeater will make a wrong decision and an error will occur. These errors introduce noise into the decoded analog signals and have to be kept at a very low rate of occurrence. In a digital system, the error rate for pulse detection increases rapidly as the pulse power relative to the noise decreases; that is, if the signal to noise ratio is too low, the detector can mistakenly decode a pulse as no pulse or vice versa. Table 3-1 shows this relationship for a binary system indicating that at about 20 dB there is a threshold about which the error rate changes significantly even for moderate changes in signal to noise ratio. The acceptable error rate for different systems has been established as values between 10^{-6} and 10^{-7} which happen to coincide with the 20 dB threshold in the signal to noise ratio.¹

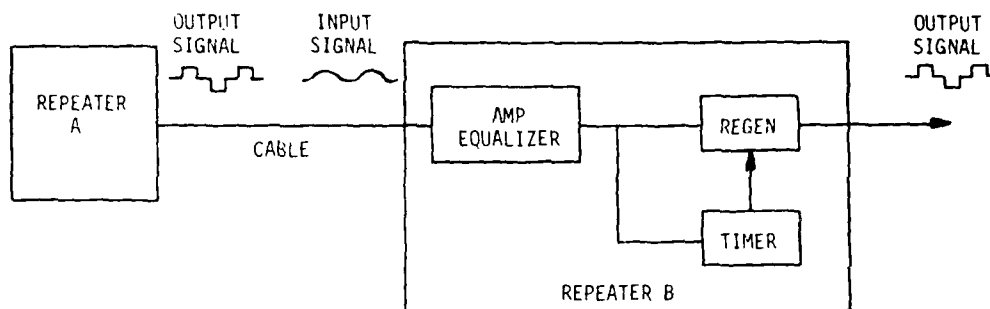


Fig. 3-3 Digital Generator

Table 3-1 Binary T-1 (1.5 Mb/s) S/N vs Error

S/N RATIO dB	ERROR PROBABILITY	ONE ERROR EVERY
23.0	10^{-12}	8 days
22.0	10^{-10}	2 hours
21.0	10^{-8}	1 minute
19.6	10^{-6}	1 second
17.4	10^{-4}	10^{-2} second
13.3	10^{-2}	10^{-4} second

The excellent behavior of PCM signals in a noisy environment can be appreciated when this 20 dB requirement is compared to the 60 dB signal to noise ratio required by analog carrier systems for toll quality transmissions. It must be noted, however, that even a small degradation of PCM signal beyond the threshold has catastrophic results in the error rate as opposed to analog transmission where the degradation is only on a dB per dB basis.

3.2 Total Losses in the Transmission System

We have seen that there will be attenuation losses on the line in any practical case. Unless the impedance of the sending circuit is exactly equal to the sending end impedance of the line and the impedances of the interconnecting lines, and unless the receiving circuit is exactly equal to the impedance of the receiving end of the line, there will be other losses known as impedance mismatch or reflection losses at these junction points.⁵

Fig. 3-4 represents a simple transmission system in which a sending circuit having an impedance Z_S is connected at points 1 and 2 to a line of length l of characteristic impedance Z_0 and propagation constant γ ; which in turn is connected at points 3 and 4 to a receiving circuit of impedance Z_R . Let us assume that the line is long enough so that both its sending end and receiving end impedances are equal to its characteristic impedance Z_0 . Considering the junction at 1-2, the ratio of the current I_0 entering the line to the I_0' that would enter the line if Z_S were equal to Z_0 is

$$\frac{I_0}{I_0'} = \frac{2 Z_S Z_0}{Z_S + Z_0} \quad \text{Eq. 3.2}$$

Similarly, the reflection loss at 3-4 may be determined from Eq. 3.3.

$$\frac{I_R}{I_R'} = \frac{2 Z_0 Z_R}{Z_0 + Z_R} \quad \text{Eq. 3.3}$$

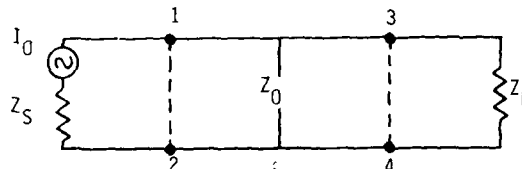


Fig. 3-4 Mismatch Losses

Note that for no reflection loss the impedances at each side of the junction points must be identical. The total loss in the transmission system (assuming an effectively infinite line) is now equal to the sum of the two reflection losses determined by Eqs. 3.2 and 3.3 plus the loss in the line itself expressed as $e^{-\gamma l}$.

Where e = naperien log
 γ = propagation constant
 l = line length

If, as is usually the case, the line is not electrically infinite in length, the sending and receiving end impedances will be somewhat different from Z_0 because of the different impedances connected to the distant ends. Any such differences will, of course, reduce the accuracy of the reflection losses as calculated from the equations given above. An exact general expression for the total loss of the system, however, may be written as follows:

$$\frac{I_R}{I_R'} = \frac{Z_S Z_R}{2 \sqrt{Z_S Z_R}} \times \frac{2 \sqrt{Z_0 Z_S}}{Z_0 + Z_R} \times e^{-\gamma l} \times \frac{(Z_0 + Z_R)(Z_0 + Z_S)}{(Z_0 + Z_R)(Z_0 + Z_S) - (Z_0 - Z_R)(Z_0 - Z_S)e^{-2\gamma l}} \quad \text{Eq. 3.4}$$

Here the first three terms represent the two reflection losses as above and an inverse term correcting for the fact that Z_S is not equal to Z_R ; the fourth term $e^{-\gamma l}$, represents the line attenuation and phase shift; and the final term represents an interaction factor which takes care of the fact that the line may be so short, the impedance looking into it from either end is not Z_0 . Examining the equation will show that this interaction factor will approach 1 as the length of the line is increased because $e^{-\gamma l}$ becomes very small. Similarly, if $Z_S = Z_R$, the first term of the equation becomes 1.

As can be seen from Eq. 3.4, the larger the number of mismatches, the larger the system loss.

$\frac{I_R}{I_T}$ for Eq. 3.4 can be converted to dB loss as follows:

$$\text{dB} = 20 \log \frac{I_R}{I_T} \quad \text{Eq. 3.5}$$

4. NOISE SUSCEPTIBILITY AND CROSSTALK

We have seen that when lines of unequal impedances are connected or are not terminated in the proper characteristic impedance there will be reflections at the far end. Also, reflections will occur every time the uniformity of the line is disturbed. This is caused by variations in resistance, inductance, conductance, and in particular, capacitance, insulation faults, and poor connection faults. In addition to these losses there are other losses resulting from the manufacturing process which affect the intelligibility of the telephone circuit. These are caused by unbalances in the cable pairs which not only affect the uniformity of the limit but which make the lines susceptible to induction from other sources such as power line harmonics, ground noise, noise voltage, etc.

The degree of balance in a communication circuit determines how susceptible the circuit will be to induced noise voltages. A perfectly balanced metallic communication circuit is one in which the series impedance for both sides of the line is equal, the shunt impedance of both sides of the line to ground is equal and the impedance between each side and any other metallic circuit is also equal. In addition, the series impedances and shunt impedances of the circuit itself must be well balanced with respect to ground and with respect to other nearby circuits. A good cable specification will include requirements which are designed to insure good balance between the pairs in the cable and between each pair and ground. These requirements include measuring:

1. Capacitance Unbalance
 - Pair to Pair
 - Pair to Shield
 - Pair to Ground
2. Resistance Unbalance

These unbalances are direct results of the manufacturing process.

Pair to pair capacitance unbalances are very significant in voice frequency crosstalk, with a noticeable effect at carrier frequencies. Pair to shield, pair to ground, and resistance unbalances cause susceptibility to power line harmonics resulting from frequencies over and above the original 50 to 60 Hz. Most voice frequency noise is due to induction from power lines and is important because of the highly sensitive telephone system and the human auditory system to 50 or 60 Hz harmonics. For 60 Hz power sources, the harmonics would be multiples of 60 Hz such as the 9th and 10th harmonic or 540 or 600 Hz, etc., which interfere with the voice frequency range; for 50 Hz the 10th, 11th and 12th harmonic.

At carrier frequencies, CUPG and RU increases the far end crosstalk coupling loss as a function of increasing length at the same frequency or increasing frequency at the same length. Accordingly, it is very important that when measurements are made to qualify cables to specifications that both low and high frequency measurements be made at the same time.

To reduce the far end crosstalk degradation at high frequencies and to reduce long repeater spacings requires a higher degree of manufacturing control over the capacitance and dimensions of the insulated conductors at extrusion. New methods of manufacturing more uniform insulated conductors on a computer controlled insulating line are required to achieve lower CUPG values. A further reduction in far end crosstalk and near end crosstalk at carrier frequencies is possible by optimizing pair twist lengths.⁶

Many telecoms try to balance unbalanced circuits by using transposition and capacitors. Both these methods are of some help but not desirable because balancing consists basically in compensating a given unbalanced with an equal unbalanced of opposite sign. We should point out that when a current passes through an unbalance, it undergoes a phase shift which is determined only by the nature of this unbalance. This current, when traveling over the disturbed circuit, is subject to the propagation conditions on this latter circuit, i.e., its phase shifts through angle α per unit of length. The result is that a given unbalance cannot be cancelled by an equal unbalance of opposite sign which is located at a fairly long distance from the first relative to the wavelength. This is because the two unbalance conditions set up currents on the disturbed circuit which are no longer in phase. Compensation is possible in certain cases but this would apply only to a single frequency. The manufacture of cables with very low unbalances is more desirable.

5. PAIR CABLE DESIGN AND THE MANUFACTURING PROCESS

We have determined that impedance mismatch between cables and irregularities within the cable cause losses in the telephone network. Because of the interrelation between the cable design and the manufacturing process it is important to specify the proper electrical parameters with tight tolerances and to make sufficient measurements to prove the quality of the cable.

Design of the cable to provide the proper electrical characteristics of multipair telephone cables by rigorous mathematical methods is not possible because of the complex physical configuration of the cable pairs. For this reason, methods of an empirical nature must be used and correlation achieved between the design and the manufacturing process to arrive at the most desirable transmission properties. In other words: how do we adjust the dimensions of the conductors and the insulation system so as to obtain the desired resistance, inductance, capacitance and conductance of the cable pairs, from which we get the propagation constant γ and the characteristic impedance Z_0 ?

For first approximation we can use complex calculations to determine the geometry of the cable which produce the desired RLGC characteristics, both for voice and carrier frequencies. Then test the cable to see if we achieved the desirable transmission properties. If not, we adjust the geometry and retest and reiterate this process until we achieve the desired results. Then during the production process we continually monitor the results to ensure meeting specifications.

5.1 Manufacturing Process

The manufacturing process for telephone cable is a continuous high speed process with many process tolerances which affect the FLGC parameters. Consider that wire is drawn, annealed and insulated at 1200 to 2500 meters per minute; the insulated conductors are twisted together into pairs or quads at 450 to 600 meters per minute; the pairs or quads are stranded together at 120 to 240 meters per minute; cores are made at 90 to 150 meters per minute; and sheathing and jacketing is performed up to 45 meters per minute. This is the economics of telephone cable manufacturing: how circular can the wire be, how concentric is the insulation over the conductor, how accurate are the twists, how precise is the pair positions in each cable, how accurate is the core twist or oscillation, how stable is the sheath and jacket.

This high speed complex process has many variables and how these variables affect the geometry and the RLGC constants is shown in Fig. 5.1. To control these variables, the manufacturer must continuously monitor the process as well as the finished product by measurements of the cable's electrical characteristics to ensure they meet specifications.

PROCESS	PROCESS VARIABLE	GEOMETRIC EFFECT	RLGC EFFECT
Rod Breakdown	Grooves, Impurities	d	R
Wire Drawing	Impurities, Pockets, Circularity, Diameter	d, DOD, S	R
Extruding	Temperature, Diameter, Eccentricity, Color, Impurities, Blow, Dispersion, Expansion, Material, Speed, Cooling, Faults	DOD, S, ϵ	R, G, C
Twisting	Uneven tension, High tension diameter, Twist lay, Twist stability, Interaxial space wraparound, Faults	A, d, S	R, L, G, C
Stranding	Oscillated lay, High tension spiraling, Unit layup stability binder material, faults	A, d, S, D	R, L, G, C
Cabling	Oscillated or spiral twist lay spiraling, Unit layup stability, Binder material, Core wrap material, Rip cord material, Identification tape material, faults	A, S, D, ϵ	L, G, C
Inner Jacket	Material, Temperature, Conductivity, Carbon black	S, D, ϵ	L, G, C
Sheathing and Jacketing	Closing diameter, overlap smooth, Corrugated, Coating	A, S, D	L, G, C

d = conductor diameter
DOD = diameter over dielectric
S = interaxial spacing
D = effective shield diameter
A = gap between conductors

R = resistance
G = conductance
C = capacitance
L = inductance
 ϵ = Dielectric System Constant

Fig. 5-1 Manufacturing Variables

6. TRANSMISSION LOSS VS IMPEDANCE MISMATCH

We can now see that at voice and carrier frequencies that each mismatch results in transmission loss. Fig. 6-1 is a curve relating transmission loss in (dB) to impedance mismatch Z_1/Z_2 . If we can determine the number of planned mismatch losses per network, Fig. 6-1 can provide the number of dB lost in that circuit.

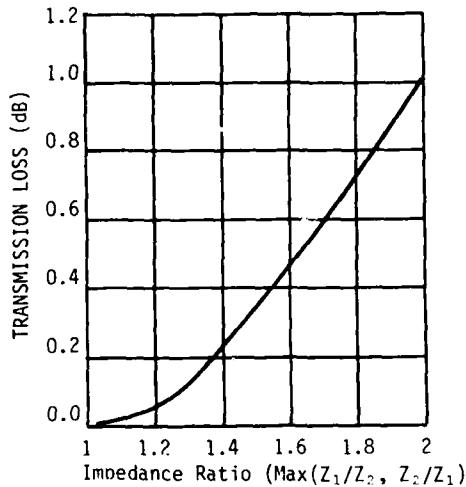


Fig. 6-1 Transmission Loss vs Impedance Mismatch

6.1 Characteristic Impedance (Z_0) Variations Vs R and C

Characteristic impedance (Z_0) variations as a function of Resistance (R) and Capacitance (C) tolerances per existing specifications can be determined from Fig. 6-2.

Figures 6-2 and 6-3 show how the characteristic impedance of telephone cable is sensitive to the fundamental cable parameters R and C, and to the cable fill. In the calculations upon which the figures were based, the variation in C was assumed to be caused entirely by variations in the conductor spacing, so L as simultaneously varied in inverse proportion to C.

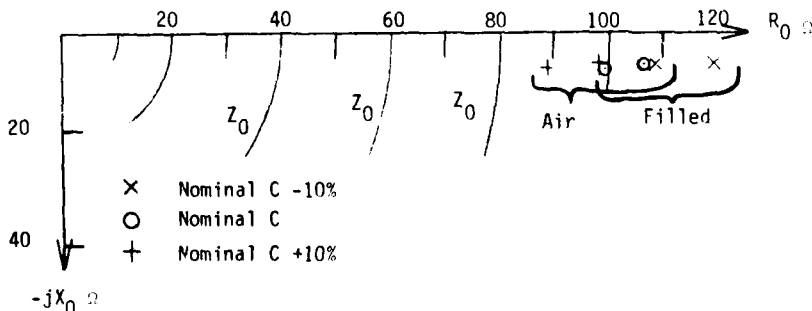


Fig. 6-2 Characteristic Impedance of PIC Solid Insulation, Air Core and Filled, 52 nF/Km .644mm Cable at 771 kHz

Figure 6-2 shows the cables at a typical carrier frequency. At this frequency, small changes in resistance do not greatly affect the impedance, so these were left off the graph. The graph shows, however, that the characteristic impedance is sensitive to variations in mutual capacitance. The graph also shows that differences in insulation type can also affect the characteristic impedance significantly.

Figure 6-3 shows the cable characteristic impedance at a typical voice frequency. The graph in this case shows the reciprocal effect on impedance of varying R and C. Decreasing R by a small percentage affects characteristic impedance at voice frequencies about the same as increasing C by that same percentage. Furthermore, these variations affect mainly magnitude, with very little effect on the phase.

7. SPECIFYING ELECTRICAL PARAMETERS

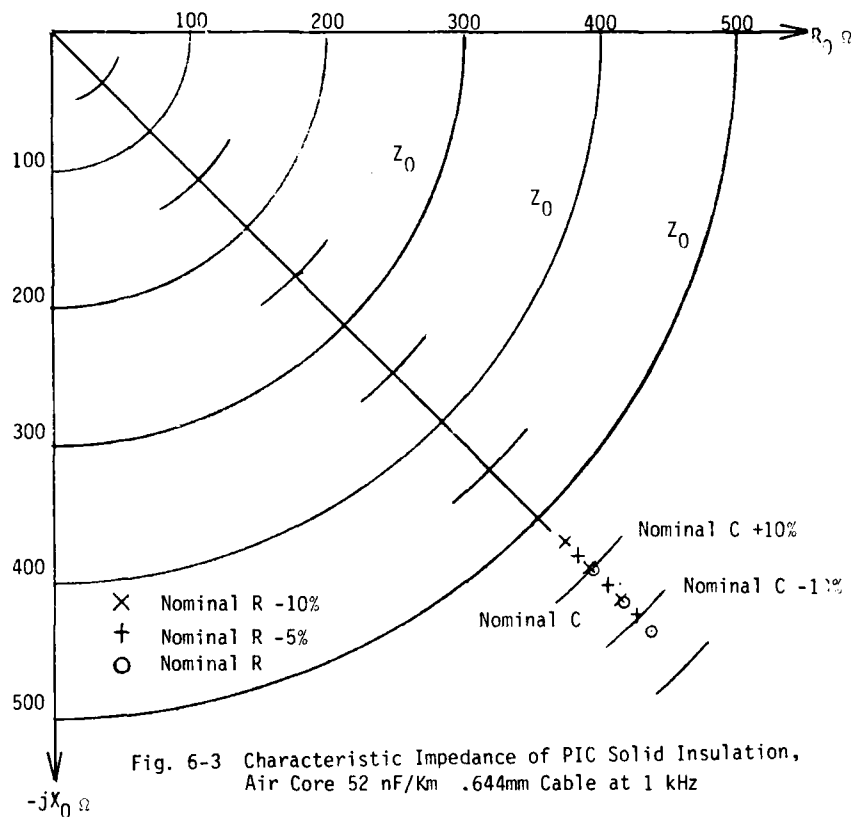
We have shown that problems in the telephone network result from the non-homogeneity of the telephone cables caused by deficient RLGC line characteristics resulting from the following:

- Ground Unbalances
- Resistance Unbalances
- Capacitive Coupling
- Inductive Coupling
- Crosstalk Coupling
- Noise Voltages
- Impedance Variations
- High Frequency Second Order Effects
- Dielectric Constant Effect

These deficiencies result from the manufacturing process and in order to control them the following electrical parameters must be specified for measurement:

Voice Frequency Cables

1. Resistance of each conductor
2. Resistance unbalance of each pair
3. Mutual capacitance of each pair
4. Capacitance unbalance, pair to ground
5. Capacitance unbalance, pair to pair
6. Conductance
7. Insulation resistance
8. Dielectric strength
9. Shield resistance



Voice Frequency Cables for Growth to Carrier Frequencies and Carrier Frequency Cables

1. Conductor Resistance
2. Resistance unbalance of the pair
3. Mutual capacitance of the pair
4. Capacitance unbalance, pair to ground
5. Capacitance unbalance, pair to pair
6. Conductance
7. Attenuation
8. Equal level far end crosstalk
9. Near end crosstalk, outer end
10. Near end crosstalk, inner end
11. Insulation resistance
12. Dielectric strength
13. Shield resistance
14. Screen resistance

There are two methods for measurement of mutual capacitance: the bridge method and the ramp method. If the bridge method is used, then the dissipation factor and the conductance must be measured in order to determine the dielectric loss and the shung leakage. Measurements should also be made at 100, 800, 2500 and 4000 Hz in order to determine the frequency dependence of the dielectric which affects the voice frequency band dispersion and propagation velocity thereby creating impedance irregularities. Bridge measurements are limited to the following pair lengths beyond which lengths correction factors must be added:

Conductor Diameter (d)	Length (L)	d	L
mm	m	mm	m
1.3	7000	0.5	2000
0.9	4500	0.45	1800
0.64	2500	0.4	1500
		0.32	1000

If the ramp method is used, the measurement of conductance or dielectric loss is not required since cables with poor dielectrics or high conductance will automatically fail the mutual capacitance test and so it should because variations in CM in the voice or carrier frequency band causes impedance irregularities in the transmission. Ramp measurements can be made in pairs up to 30,000 meters in length.

7.1 Values and Tolerances

Table 7-1 lists the recommended values and tolerances for the low frequency measurements. Table 7-2 lists the recommended values and tolerances for the high frequency measurement.

TABLE 7-1 SPECIFICATION VALUES AND TOLERANCES

MEASUREMENT PARAMETER	CONDUCTOR DIAMETER							
	0.41		0.51		0.64		0.91	
R @ 20°C IND MAX Ω /Km	144.4		90.2		57.1		28.5	
CABLE AVG (MAX-AVG) %	3		3		2		2	
IND (MAX-AVG) %	4		4		3.5		3	
RU (CABLE AVG) U%	1.5		1.2		1		1	
(IND) U%	4.0		3.0		3		3	
HIGH VOLTAGE DC 3 SEC	PIC/S/A		PIC/S/A		PIC/S/A		PIC/S/A	
	PIC/F/F PIC/S/F		PIC/F/F PIC/S/F		PIC/F/F PIC/S/F		PIC/F/F PIC/S/F	
CONDUCTOR-CONDUCTOR KV	2.4	2.8	3	4	3.6	5	4.5	7.0
CORE TO SHIELD KV	10	15	10	15	10	15	10	15
CORE TO SCREEN KV	5							
SHIELD RESISTANCE Ω /Km	$R = 6.25/D$, D = Outside Diameter of Shield in cm							
SCREEN RESISTANCE Ω /Km	25							
CM nF/Km	52 \pm 2							
CM DEVIATION RMS %	2							
CUPP IND MAX PF/Km	125							
MAX RMS PF/Km	35							
CUPG IND MAX PF/Km	2000							
AVG MAX PF/Km	500							
CUPS IND MAX PF/Km	1500							
AVG MAX PF/Km	250							
G M Mi Micromho/Km	2							
INSULATION RESISTANCE 1 MIN (100-500V)	25000							

PIC/S/A = Polyethylene Insulated Conductor/Solid/Air core

PIC/F/F = Polyethylene Insulated Conductor/Foam/Filled

PIC/S/F = Polyethylene Insulated Conductor/Solid/Filled

TABLE 7-2 VALUES AND TOLERANCES

ATTENUATION

Tolerance +5%-10% @ 20°C \pm 1°C

CONDUCTOR DIAMETER		PIC/S/A			PIC/S/F			PIC/F/F		
		dB/Km			dB/Km			dB/Km		
		FREQUENCY kHz			FREQUENCY kHz			FREQUENCY kHz		
MM	AWG	150	772	1576	150	772	1576	150	772	1576
0.91	19	4.4	10.4	14.7	4.0	8.6	12.7	4.4	10.4	14.7
0.64	22	6.2	14.6	20.4	5.7	12.4	17.8	6.2	14.6	20.4
0.51	24	8.3	18.5	25.4	7.5	15.4	23.1	8.3	18.5	25.4
0.41	26	11.4	22.3	32.5	10.9	19.5	26.5	11.4	22.3	30.5

Table 7-2 VALUES AND TOLERANCES
(Continued)

POWER SUM FEXT
(50 PAIR UNITS)

FREQUENCY kHz	AVERAGE dB/Km	WORST PAIR dB/Km	GRAND dB/Km
150	61	57	53
772	49	44	40
1576	43	39	35
3152	37	33	29
6304	31	27	23

POWER SUM NEXT
(dB)

FREQ. kHz	WITHIN 25 PAIR GROUP			BETWEEN ADJACENT 25 PAIR GROUP			ACROSS SCREEN 50 PAIR GROUP		
	AVG dB	WORST PAIR	GRAND dB	AVG dB	WORST PAIR	GRAND dB	AVG dB	WORST PAIR	GRAND dB
150	65	59	55	73	64	60	107	103	99
772	54	48	45	61	52	48	101	96	87
1576	49	43	39	56	47	43	96	90	84
3152	44	38	34	51	41	37	92	86	82
6304	39	34	32	46	36	33	89	80	74

Table 8-1 Statistical Parameters

Measurement Parameter	Statistical Evaluation	Measurement Parameter	Statistical Evaluation
Conductor Resistance & Resistance Unbalance	Minimum Individual Maximum Individual Average Standard Deviation Histogram	Attenuation	Minimum Individual Maximum Individual Average Standard Deviation Histogram
Cable Capacitance	Minimum Individual Maximum Individual Average Standard Deviation Percent Deviation Histogram	Crosstalk: ELFEXT I/O FEXT ONEXT INEXT	Minimum Individual Maximum Individual Average RMS Standard Deviation Mean minus Standard 1% Worse Than Value Deviation Histogram
Capacitance Unbalance: Pair to Ground Pair to Shield Side to Earth Side to Ext. Earth	Minimum Individual Maximum Individual Average Standard Deviation RMS Histogram	POWER SUM WITHIN & BETWEEN GROUPS	Relative Power Sum Individual Power Sum Average Power Sum Grand Power Sum
Capacitance Unbalance: Pair to Pair Within Quad Adjacent Quad	Minimum Individual Maximum Individual Average RMS Histogram	Conductance	Minimum Individual Maximum Individual Average Standard Deviation Histogram

8. TEST DATA FROM MANUFACTURERS

The proof of the design and manufacturing process is in the final test results on the finished cable. In addition to verification against the values and tolerances of the measurements specified, additional statistical specifications materially aid in controlling the cable characteristics. These additional statistical parameters are listed in Table 8-1.

The minimum and maximum individual values control the range of the particular measurement. The average value controls the quantity of high and low values. The RMS value controls the magnitude of the high and low values. The standard deviation, on the other hand, controls the magnitude of the variations around the average, thereby controlling the dispersion of the data. The desirable situation is to have the smallest standard deviation possible. The histogram is a means of showing the manufacturer and the user of the dispersion of values on a frequency distribution basis.

8.1 Power Sum

Working with data in decibels is equivalent to working with the logarithm of the data. Because the crosstalk data follows a log-normal distribution when expressed as a power ratio, it follows a straight normal distribution when expressed in dB. This normal distribution has a mean and standard deviation that is easy to calculate from a limited sample size. Thus, many of the world's specifications are written in terms of the near-end standard deviation of the normal distribution. From such a standard, it is possible to specify that no more than a certain fraction of the individual crosstalk combination will be worse than a specified value.

Unfortunately, the crosstalk performance of a cable pair is not governed by the average of the logarithm of the crosstalk power, but by the total crosstalk power coupled into that pair. Because of the highly skewed and dispersed nature of the crosstalk distribution, the crosstalk power sum will be dominated by one or two of the worst crosstalk combinations involving that pair. However, these same crosstalk combinations that contribute nearly all the crosstalk power to the pair under test contribute only slightly to the mean and standard deviation when statistics of the logarithms of the data are taken. Conversely, the aggregate of data that contributes almost nothing to the power sums will contribute almost everything to the mean and standard deviation of the log data.

If the statistics of the log data conformed exactly to the normal distribution, the power sum statistics could be predicted accurately; but the crosstalk data is not that perfect. The statistics of the log data are slightly skewed in such a way that the low-side (when the crosstalk loss data is expressed in dB) tail does not extend as far as the Gaussian model (with log variate) predicts.

Because the low-side tail of the actual distribution is shorter than that for the normal distribution, modifications have been made to create a distribution that predicts the worst-case values and the power sums better. The most common modification involves truncating both tails of the normal distribution. The trick is determining where to truncate, because the truncation point varies in an unknown way with binder size, frequency, crosstalk mechanism, and so on. Another model that has been proposed is the gamma distribution with a log variate. This distribution has a shortened lower-end tail that fits the experimental data (on a log scale) fairly well at the expense of misfitting the rest of distribution.

In any case, until a truly satisfactory non-empirical model for crosstalk performance is found, enough crosstalk data must be taken to validate the predictions of the existing empirical models.⁸

8.2 Individual Power Sum (IPS) Within a Group (W)

The performance of a given cable pair is based upon the total crosstalk power injected into that pair. If

m_{ij} = the crosstalk loss between pair i and pair j in dB, then the individual power sum in dB for crosstalk within a group is given by the formula:

$$IPS_i(W)(dB) = -10 \log_{10} \left[\sum_{\substack{j=1 \\ j \neq i}}^n 10^{-(m_{ij}/10)} \right]$$

where n is the number of pairs in the group.

Eq. 8.1

8.3 Individual Power Sum (IPS) Between Groups (B)

For the case when i and j are in different groups,

$$IPS_i(B) \text{ dB} = -10 \log_{10} \left[\sum_{j=1}^n 10^{-(m_{ij}/10)} \right]$$

Eq. 8.2

where n is the number of pairs in the group containing pair j .

It should also be noted in each case that each summation occurs over a single group, so there is an individual power sum associated with each pair-group combination.

8.4 Grand Power Sum (GPS) Between Groups (B)

The idea of individual power sums can be expanded in several directions, one which is determining the whole crosstalk power coupled from one cable group to another. The result of such a calculation is a single number that can be used as an indicator of the crosstalk isolation between the two groups. This grand power sum is given by Eq. 8.3:

$$GPS(B) \text{ dB} = -10 \log_{10} \left[\sum_{i=1}^n 10^{-IPS_i(B)/10} \right]$$

Eq. 8.3

where the individual power sums are calculated by Eq. 8.1 and the summation is over all the pairs in the disturbed group. The final result of the above calculation is in dB, so it is really the logarithm of the total crosstalk power multiplied by a constant.

The grand power sum can also be calculated directly from the crosstalk data by Eq. 8.4:

$$\text{GPSUM(dB)} = -10 \log_{10} \left[\sum_{i=1}^h \sum_{j=1}^k 10^{-m_{ij}/10} \right] \quad \text{Eq. 8.4}$$

where m_{ij} is the crosstalk between pairs i and j in dB, h is the number of pairs in the group containing pair j .

Eq. 8.4 assumes that pairs i and j are in different groups.

Eq. 8.4 gives some insight into why the grand power sum makes such a good figure of merit. The grand power sum, when expressed as a power ratio, differs by a multiplicative constant from the average of all the crosstalk power ratios for all the pair combinations across the two groups. This comes as no surprise; the sum of any group of numbers differs from the mean only by a multiplicative constant equal to the number of data points. The grand power sum is thus $h \cdot k$ times the average crosstalk power, or h (or k , depending upon which power sums are being averaged) times the average of the individual power sums. When the grand power sum is expressed in dB, the multiplicative constant turns into an additive constant. In fact,

$$\text{GPS (dB)} = \text{RMS (dB)} - 10 \log_{10} h - 10 \log_{10} k \quad \text{Eq. 8.5}$$

where RMS(dB) is the average of the individual crosstalk power ratios, expressed in dB.

8.5 Grand Power Sum (GPS) Within a Group (W)

The idea of grand power sum can also be extended to crosstalk within a group, but the calculation is a little different. Because of the overlap between the disturbing and disturbed pairs, care must be taken to avoid counting the same datum twice in the summations. For the within-group case, the grand power sum is the sum over all possible pair combinations of the individual power ratios. In other words,

$$\text{GPS(W)dB} = -10 \log_{10} \left[\sum_{i=1}^h \sum_{j=i+1}^n 10^{-m_{ij}/10} \right] \quad \text{Eq. 8.6}$$

Note especially the index on the same summation in Eq. 8.6. With this index, the power sum is analogous to the between-group case of group A coupling into group B. The summation,

$$\sum_{i=1}^n \sum_{\substack{j=1 \\ i \neq j}}^n 10^{-m_{ij}/10} \quad \text{Eq. 8.7}$$

would have been analogous to group A talking to group B plus group B talking to group A in the between-group case. In fact, each crosstalk term is added twice in Eq. 8.7--once as m_{ij} and again as m_{ji} . The summation in Eq. 8.7 add up to twice the grand power sum (before conversion to dB). Eq. 8.7 also is the sum of the individual power sums. Therefore, the grand power sum is half the sum of the individual power sums. In other words,

$$\text{GPSUM(dB)} = -10 \log_{10} \left[\frac{1}{2} \sum_{i=1}^n 10^{-\text{IPSUM}_i(\text{dB})/10} \right] \quad \text{Eq. 8.8}$$

$$= -10 \log_{10} \left[\sum_{i=1}^n 10^{-\text{IPSUM}_i(\text{dB})/10} \right] + 10 \log_{10} 2 \quad \text{Eq. 8.9}$$

The constant $10 \log_{10} 2$ is approximately 3 dB.

The within-group grand power sum is a good indicator of the crosstalk performance of the group as a whole, but the individual power sums are of more importance to the cable manufacturers, and possibly to the cable user as well. However, to better illustrate the individual pair coupling, another indicator can be used. This is the Relative Power Sum which can be obtained by use of Eq. 8.11. The Average Power Sum (Eq. 8.10) can be used to determine the relative power sum for each pair.

8.6 Average Power Sum (APS)

$$\text{APSj(dB)} = \frac{1}{n} \sum_{j=1}^n (\text{IPSj}) \quad \text{Eq. 8.10}$$

Relative Power Sum (RSP)

$$\text{RPSj(dB)} = \text{APSj(dB)} - \text{IPSj(dB)} \quad \text{Eq. 8.11}$$

These relative power sums can be plotted against their respective pair numbers in order to form a pictorial representation of each pair's variation of their power sum. This is shown in Fig. 8.1. In reviewing Fig. 8.1 we find that the relative near-end and far-end crosstalk power sums at carrier frequencies follow the same variation from pair to pair, but are of different magnitude. This indicates that the sources of both near-end and far-end crosstalk at these frequencies are the same. Figure 8-1 indicates that the within-unit and between adjacent-unit power sums follow the same variation from pair to pair. Therefore, any change resulting in an improvement in the within-unit crosstalk should also lead to an improvement in the adjacent unit crosstalk.

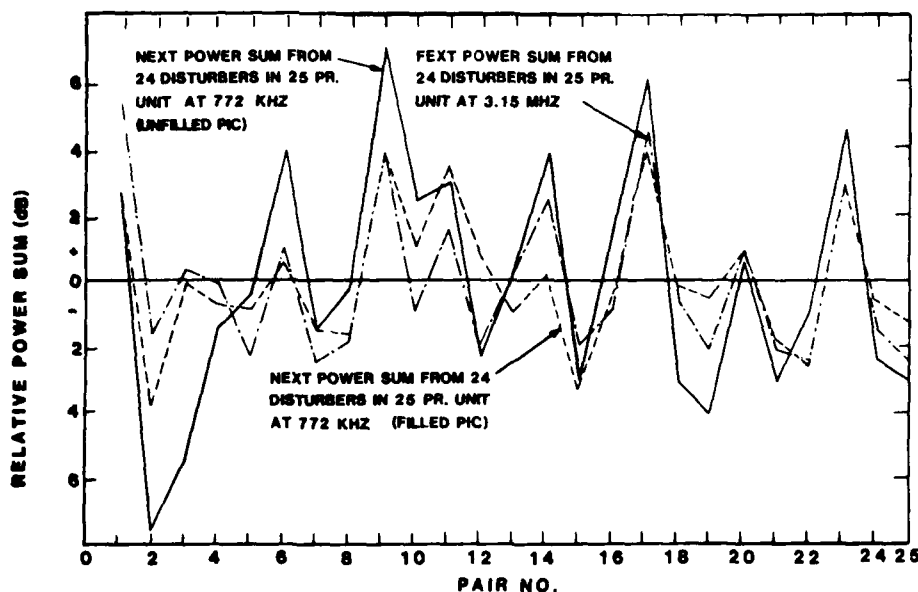


FIG. 8.1 PAIR TO PAIR POWER SUMS

Correlation of power sums with the crosstalk effects of twist lengths indicates that it is possible to gain significant improvements in crosstalk quality of cables by correct twist length selection and correct twist angles.

Before the manufacturers start using the power sums, the user's specification must be revised so that power sums are specified instead of the average of the individual crosstalk values in dB. This is important because improving the individual power sum of the worst pair would not necessarily improve the crosstalk average and might even worsen it. In any case, improving the worst pairs would make the tail of the crosstalk histogram even shorter than it presently is, making predictions based upon the log-normal distribution even worse than they are now. The performance of the cable will have improved, but the mean and standard deviation will hardly change. Recommended power sum values are shown in Table 7-2.

8.7 Pair Grand Power Sum (PGPS)

There is another grand power sum which should be considered. This power sum is the sum of the crosstalk power ratios of all active pairs in the cable talking to a given disturbed pair. In other words, all the individual power sums for a given cable pair are added to give a grand power sum for that pair. Eq. 8.4 and 8.5 give the Grand Power Sums, between groups and within groups. This grand power sum is for the entire cable and will be called the Pair Grand Power Sum (PGPS_i) as expressed in Eq. 8.12.

$$\text{PGPS}_i \text{ (dB)} = -10 \log_{10} \left[\sum_{j=1}^k 10^{-\text{IPS}_{ij}/10} \right] \quad \text{Eq. 8.12}$$

The pair grand power sum is exactly what the final user needs to evaluate crosstalk performance, because it is this number that determines the crosstalk power coupled into the pair in question. In screened cables, the active pairs for near-end crosstalk will be all those on the opposite side of the screen from the pair under test. Similarly, the active pairs for far-end crosstalk will be all of those on the same side of the screen.

9. TELEPHONE ADMINISTRATIONS' CONTROL OF THE PRODUCT

Telephone administrations can only control the product through rigid comprehensive specifications with manufacturer's test data to verify compliance with the specifications. In addition, telephone administrations may sample test each procurement to verify the manufacturer's test data.

Specifications should be evolved over a period of time. In order to improve the product, the specifications should have values and tolerances to be met at the country's current level of development with projected values and tolerances to be met at some future date. This would permit the cable manufacturer of that country to improve their manufacturing process and adjust the cable's dimensions to meet the transmission requirements. Statistical techniques must be developed over a period of time on a solid data base. Both the manufacturer and the telephone administrations can use these techniques to quality telephone cables.

10. CONCLUSION

To ensure satisfactory transmission in telephone networks requires that the installed plant have the transmission characteristics for which it was designed. To obtain these transmission characteristics, telephone administrations must prepare adequate cable specifications with the necessary electrical parameters to be measured and with values and tolerances on these measurements that will permit the network to meet its net loss requirements.

With the proper values and tolerances specified, unbalances must be maintained at minimum values since they contribute to increasing the network losses and the unintelligibility on communication circuits. For both analog and digital carrier systems, specific crosstalk requirements must be specified. For PCM systems specific signal to noise ratios must be met in order to ensure repeater span objectives and power sum calculations as recommended.

Accordingly, with good specifications and verifiable test data, network loss objectives can be achieved.

REFERENCES

1. Transmission Properties of Polyethylene Insulated Telephone Cables at Voice & Carrier Frequencies, G.S. Eager, Jr., L. Jachimowicz, AIEE General Meeting, Seattle, WA, U.S.A., June 21-26, 1959, Paper No.
2. Understanding Transmission, E.W. Riley, J.E. Acuna, Engineering Seminar No. 1, Anaconda Co., 1976.
3. Transmission Properties of Filled Thermoplastic Insulated and Jacketed Telephone Cables at Voice & Carrier Frequencies, L. Jachimowicz, J.A. Olszewski, International Conference on Communications, June 19-21, 1972, Philadelphia, PA, U.S.A.
4. Cable Design Considerations for Digital Transmission Systems, P.D. Kish, Northern Telecom, Ltd. Outside Plant Seminar, 1976.
5. Bell Telephone Labs Transmission Systems for Communications, Fourth Edition Copyright BTL, Feb., 1970.
6. Computerized Automatic Measurement of Telephone Cables, Leo M. Chattler, Pacific Coast Meeting, Wire Association International, Los Angeles, CA, Feb. 5, 1979.
7. Shielded Cable System, S.P. Mead vs. Patent No. 2,086,629, April 14, 1936.
8. Computerized Statistical Quality Control of Telephone Cables, Leo M. Chattler, International Wire Symposium Proceedings, Nov. 1980.



Leo M. Chattler received his B.S. degree in Aeronautical Engineering from the University of Illinois and his M.S. degree in Electrical Engineering from the University of Maryland. He was in Naval Aviation, U.S. Navy, Aeronautics & Electrical Design with Chance-Vought Aircraft, V.P. and Division Manager with Northrop Aircraft, President of Advanced Technologies Corporation, a subsidiary of Beckman Instruments and General Manager of Beckman's Electronics Instrument Division. He was associated with Western Electric, REA and many U.S. and international cable companies and telephone administrations on special projects. He is currently President and General Manager of DCM International Corporation and has been active in the development of equipment for telephone administrations and cable industry.

He has four patents issued and three patents pending in connection with his work.

POWER SUM CROSSTALK OF PIC CABLES
AS A FUNCTION OF CABLE DESIGN

J. J. Refi

Bell Laboratories
Norcross, Georgia 30071

ABSTRACT

A previous study of the crosstalk performance of the various designs of plastic insulated conductor (PIC) cables used in the Bell System (air core and waterproof, solid and expanded insulations, 19 through 26-gauge, 83 nF/mile and low capacitance) showed that the mean power sum far-end crosstalk (FEXT) of these various designs is a function of their average pair twist helix angle.^[1] The present paper extends this previous work to other forms of power sum crosstalk such as worst pair FEXT, within unit worst pair near-end crosstalk (NEXT), and within unit mean NEXT.

Unlike mean FEXT, average twist helix angle alone does not adequately explain the variations that occur in worst pair FEXT, worst pair NEXT, or mean NEXT. A slightly more complicated regression model that includes a measure of the skewness of the twist helix spectrum improves the fit to these data substantially.

The analyses in this paper further show that not only is the frequency scaling of mean FEXT a function of average twist helix angle (as found in the previous paper), but that the frequency scalings of worst pair FEXT, worst pair NEXT and mean NEXT also depend on average twist helix angle.

Linear regression equations are presented that can be used to calculate the mean and worst pair FEXT and NEXT performance of most copper PIC cables used in the Bell System. In addition, as long as pair twist schemes are judiciously chosen, these equations can also be used to predict the crosstalk performance of new cable designs simply from their diameter over dielectric, average twist frequency, and median twist frequency.

1. INTRODUCTION

Because the crosstalk performance of multipair cables restricts the maximum number of digital carrier systems which those cables will support, it has become increasingly desirable to know the crosstalk properties of the various cable designs. One way to obtain this information is by actually measuring crosstalk on the various cables and, over the years, many such measurements have been made. While such data are extremely useful, their value can be enhanced if they reveal systematic patterns that depend on particular features of the cable design.

In a previous paper,^[1] we showed that the mean power sum FEXT of the various designs of copper PIC cables used in the Bell System is a function of their average pair twist helix angle. Cables with small average pair twist helix angles were shown to have stronger crosstalk coupling than cables with large average pair twist helix angles. Consequently, 26-gauge solid insulation air core cable, which has the smallest helix angle of any standard PIC cable, has the strongest (worst) mean FEXT coupling. At the other extreme, 19-gauge solid insulation waterproof cable has the largest helix angle and also the weakest (best) mean FEXT coupling. The crosstalk spread between these two designs is about 6 dB at 0.15 MHz.

The present paper extends the previous work to: (1) worst pair power sum FEXT, (2) within unit worst pair power sum NEXT, and (3) within unit mean power sum NEXT. As in the previous paper, empirical crosstalk data are examined using linear regression analyses to find a functional relationship between crosstalk performance and particular features of the cable design.

2. CROSSTALK MEASUREMENTS

Over the years many Bell System cables have been measured for crosstalk on a Computer Operated Transmission Measurement Set (COTMS).^[2] Normally, 50 consecutive pairs are connected to a pair fan-out and the 1225 pair-to-pair crosstalk combinations are measured at several frequencies. The power sum crosstalk of each pair is then calculated by summing the pair-to-pair couplings into that pair on a power basis. Statistical parameters such as means and standard deviations are then computed and reported for both the pair-to-pair and the power sum crosstalk distributions.

3. CROSSTALK AND CABLE TYPES EXAMINED

3.1 Crosstalk

Insofar as power sum crosstalk is the summed power of the crosstalk couplings from many pairs, power sum crosstalk statistics tend to be less affected by cable-to-cable variations than pair-to-pair statistics. Because of this robustness, power sum (as opposed to pair-to-pair) crosstalk data on the various cables were studied. Power sum means and worst pairs for FEXT and within unit NEXT were examined at five frequencies—0.15, 0.772, 1.6, 3.15 and 6.3 MHz. Because some cables were not measured at all five frequencies and because some of the measurements appeared to be gross outliers, the number of measurements* used to obtain the regression equations ranged from 35 to 53 depending on the particular crosstalk type and frequency.

As mentioned in Section 2, COTMS measurements are normally made on 50 pair groupings. Therefore, all the data presented here are for 50 pair groups except for 25 pair cables in which case the data are for all 25 pairs in the cable.

3.2 Cables

Cable designs in the data base represent almost all standard 83 nF/mile copper PIC cables, i.e., air core and waterproof, solid and DEPIC (dual expanded plastic insulated conductor)^[3] insulations, and 19 through 26-gauge conductors. In addition to these standard cables, data were also examined on some "special" cables such as ICOT[†] cable (24-gauge DEPIC, 52 nF/mile for air core, and 60 nF/mile for waterproof),^[4] MAT[†] cable (25-gauge DEPIC, 64 nF/mile, air core),^[5] DUCTPIC[†] cable (26-gauge DEPIC, 83 nF/mile, air core),^[6] an experimental 28-gauge cable, and two experimental 26-gauge low capacitance cables. These cables are termed "special" because they use shorter twist lengths and have a different twist spectrum than the standard cables. In addition, ICOT, MAT and the 26-gauge low capacitance cables have lower mutual capacitances than the standard 83 nF/mile.

The various cables ranged in length from 700 to 5400 feet with the average length being 2000 feet.

4. TWIST HELIX ANGLE

Let's review the finding of the previous paper that mean FEXT is a function of average twist helix angle.^[1] This relationship is of the form

* The term "measurements" will be used instead of "cables" because several measurements may have been made on different units in a single cable.

[†] Trademark of Western Electric

$$XT = b_0 + b_1 \times DOD \times \text{avgTF} \quad (1)$$

where

DOD = diameter over dielectric, and
avgTF = average twist frequency.

The DOD x avgTF product in this equation measures the average twist helix angle of the twisted pairs in a cable. For example, Figure 1 shows that the helix angle, θ , of a twisted pair is proportional to the product of its diameter over dielectric (DOD) and twist frequency (TF) where TF is the reciprocal of twist length. Because twists with large helix angles require more mechanical energy to deform than twists with small helix angles, pairs with large helix angles have greater mechanical stability. This greater mechanical stability helps resist twist deformation during manufacture thereby producing more perfect twists which in turn are more likely to produce better crosstalk.^{[1] (b)}

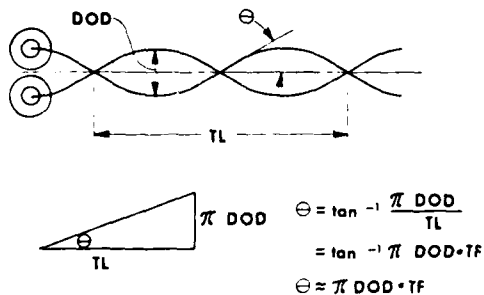


Figure 1. The helix angle, θ , of a twisted pair is proportional to the pair's diameter over dielectric (DOD) and twist frequency (TF).

Although all the pairs in a given cable have the same DOD, the pairs have several different (usually 25) twist frequencies and therefore different twist helix angles. We shall use the average twist helix angle of the pairs in a cable as a measure of the uniformity of the pairs in that cable.

Table 1 lists the average TF, DOD, and average helix angle* for each PIC cable design. The average twist frequencies span a 42% range (from 0.2827 to 0.4018 twists/inch) whereas the DOD's span a 242% range (from 21.6 to 74 mils). Consequently, DOD differences among cable designs have a greater effect on helix angle than twist frequency differences.

Table 1 Average Twist Frequency, Diameter over Dielectric and Helix Angle of Standard and "Special" Cables										
cable	AWG	avgTF (twists/in)	air core				waterproof			
			DEPIC		solid		DEPIC		solid	
			DOD (mils)	DOD x avgTF	DOD (mils)	DOD x avgTF	DOD (mils)	DOD x avgTF	DOD (mils)	DOD x avgTF
Standard	19	0.2827	-	-	60	17.0	63	17.8	74	20.9
"	22	0.3007	-	-	43	12.9	45	13.5	52	15.6
"	24	0.3270	-	-	34	11.1	36	11.8	42	13.7
"	26	"	-	-	27	8.8	29	9.5	33	10.8
ICOT	24	0.4018	49	19.7	-	-	49	19.7	-	-
MAT	25	"	35	14.1	-	-	-	-	-	-
DUCTPIC	26	"	24.5	9.8	-	-	-	-	-	-
26 locap	26	"	39	15.7	-	-	39	15.7	-	-
28 AWG	28	"	-	-	21.6	8.7	-	-	-	-

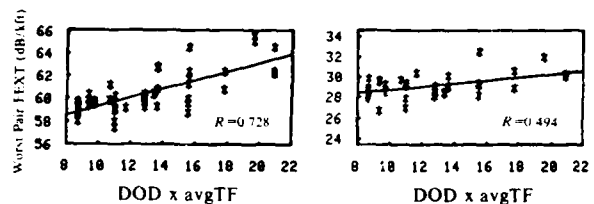
* Although average helix angle equals $\pi \times DOD \times \text{avgTF}$, the term "helix angle" will be used more loosely in this paper to mean "DOD x avgTF."

5. FAR-END CROSSTALK

5.1 Worst Pair FEXT

Insofar as mean FEXT has been previously shown to be a function of average twist helix angle,^[1] we first examine the possibility that worst pair FEXT might be also.

Figure 2 shows a plot of worst pair FEXT versus average helix angle at 0.15 and 6.3 MHz. Although the correlation coefficient is a respectable 0.728 at 0.15 MHz, it decreases to a mere 0.494 at 6.3 MHz. This decrease is due not to an increase in the scatter of the points about the line (the residual standard error is smaller at 6.3 MHz than at 0.15 MHz), but rather to a smaller slope at the higher frequency.



(a) 0.15 MHz; 44 measurements (b) 6.3 MHz; 35 measurements

Figure 2. Worst pair power sum FEXT vs. the product of diameter over dielectric (DOD) and average twist frequency (avgTF).

Because of the small explanatory value of helix angle at the higher frequencies, other linear regression models were examined. After evaluating many possibilities, the following model was chosen:

$$XT = b_0 + b_1 \times DOD \times \text{avgTF} + b_2 \times DOD \times (\text{medTF} - \text{avgTF}) \quad (2)$$

where

medTF = median twist frequency.

This new model explains a reasonable proportion of the crosstalk variation both at low and high frequencies and is only slightly more complicated than the simple helix angle model. The new model is identical to the helix angle model (equation (1)) except that a second explanatory variable (shown in bold above) has been added. We can obtain an insight into the significance of this new variable by looking at the twist frequency spectra of the pairs used in the various cable designs. Figure 3 shows these four spectra.

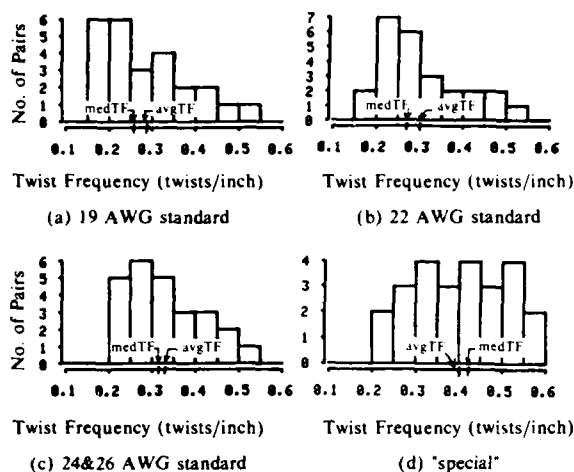


Figure 3. Histograms of the 25 twist frequencies used in standard and 'special' cable designs. Average twist frequencies (avgTF) and median twist frequencies (medTF) are shown.

Notice from Figure 3(a) that 19-gauge standard cable contains many pairs having small twist frequencies (long twist lengths), but only a few pairs having large twist frequencies (short twist lengths). In other words, the twist spectrum is skewed toward small twist frequencies. Since computation of an average is very sensitive to a few points having extreme values, the average twist frequency is pulled toward the few pairs having large twist frequencies. Contrastingly, since the median is insensitive to a few pairs having extreme values, the median twist frequency more closely represents the bulk of the data. The difference between the median TF and the average TF serves as a measure of the asymmetry of the twist frequency spectrum. Multiplying this difference by DOD as in equation (2) provides a measure of the asymmetry of the twist helix angle spectrum. When medTF-avgTF is positive, the spectrum is skewed toward large helix angles whereas when medTF-avgTF is negative, the spectrum is skewed toward small helix angles.

Figure 3 shows that the three twist spectra for standard cables are all skewed toward small helix angles whereas the twist spectrum for the 'special' cables is just slightly skewed toward large helix angles.

The difference between medTF and avgTF that we have been describing as skewness is not the same as the strict mathematical definition of skewness defined as⁽⁹⁾

$$\text{skewness} = \frac{m_3}{m_2^{3/2}} \quad (3)$$

where

$$m_3 = \frac{\sum_{i=1}^n (x_i - \bar{x})^3}{n-1} = \text{third central moment of the } x_i, \text{ and}$$

$$m_2 = \frac{\sum_{i=1}^n (x_i - \bar{x})^2}{n-1} = \text{second central moment of the } x_i = \text{variance.}$$

To see if using the strict mathematical definition of skewness would be superior to using medTF-avgTF, the skewness of each of the four twist spectra was calculated from equation (3) and used

instead of medTF-avgTF in equation (2). The degree of correlation with worst pair FEXT stayed essentially the same. Insofar as medTF-avgTF carries more physical meaning than equation (3), we shall use equation (2) in the remainder of this paper and shall refer to DOD x (medTF-avgTF) as helix angle skewness. Table 2 lists the median twist frequency and the helix angle skewness for the cable designs in Table 1.

Table 2 Median Twist Frequency and Twist Helix Angle Skewness of Standard and 'Special' Cables						
cable	AWG	medTF-avgTF (twists/inch)	DOD x (medTF-avgTF)			
			air core		waterproof	
			DEPIC	solid	DEPIC	solid
Standard	19	-0.0269	-	-1.61	-1.69	-1.99
	22	-0.0304	-	-1.31	-1.37	-1.58
	24	-0.0145	-	-0.49	-0.52	-0.61
	26	-	-	-0.39	-0.42	-0.48
ICOT	24	0.0097	0.48	-	0.48	-
MAT	25	-	0.34	-	-	-
DUCTPIC	26	-	0.24	-	-	-
26 locap	26	-	0.38	-	0.38	-
28 AWG	28	-	-	0.21	-	-

We now fit equation (2) to the worst pair FEXT data at each of the five frequencies. Table 3 shows the results.

Table 3 Linear Regression Equations for Worst Pair Power Sum FEXT of Standard and 'Special' Cables						
frequency (MHz)	Worst Pair FEXT (dB/kft) = $b_0 + b_1 \times \text{DOD} + b_2 \times \text{DOD} \times (\text{medTF} - \text{avgTF})$					
	b_0	b_1	b_2	correlation coef.	residual std. error	no. of msmts.
0.15	55.0	0.493	1.26	0.847	1.03	44
0.772	43.0	0.394	1.24	0.777	1.07	49
1.6	36.9	0.404	1.51	0.863	0.84	45
3.15	31.6	0.362	1.26	0.776	1.01	48
6.3	26.4	0.286	1.15	0.731	0.83	35

Notice from Table 3 that the coefficients of the helix angle term (b_1) tend to decrease as frequency increases. This tendency is statistically significant and has been observed previously for mean FEXT.⁽¹⁾ Contrasting with these decreasing values for b_1 , the coefficients of helix angle skewness (b_2) seem to fluctuate randomly. For example, the standard errors for b_2 are about 0.22, suggesting that even the smallest and largest values of b_2 (i.e., 1.15 and 1.51) are not statistically different at the 5% level of significance. Hence, b_2 can be taken as a constant value regardless of frequency. In Section 5.3, we will use this information regarding the frequency behavior of b_1 and b_2 to consolidate the five individual equations in Table 3 into one concise equation for worst pair FEXT that can be used at any frequency between 0.15 and 6.3 MHz.

One last observation from Table 3. The residual standard errors listed in the table serve as an estimate of the standard deviation of the data about the regression equation. Since these standard errors are approximately one, about 95% of the worst pair FEXT values in the data base lie within $\pm 2 \times 1 = \pm 2$ dB of the regression surface.

5.2 Mean FEXT

Having seen in the previous section that equation (2) fits the worst pair FEXT data better than equation (1), we question whether this might also be true for mean FEXT. Appendix A shows that at 0.15 MHz, the simple helix angle model given by equation (1) is just as good as the two variable model given by equation (2). However, at 6.3 MHz the two variable model explains 5.7% more of the crosstalk variation than does the simple model and this

improvement is statistically significant. Because of this improvement, we will retain the two variable model in the rest of our analyses. Table 4 presents the linear regression equations when equation (2) is fitted to the mean FEXT data at each of the five frequencies.

Table 4 Linear Regression Equations for Mean Power Sum FEXT of Standard and 'Special' Cables						
frequency (MHz)	Mean FEXT (dB/kft) = $b_0 + b_1 \times \text{DOD} \times \text{avgTF} + b_2 \times \text{DOD} \times (\text{medTF} - \text{avgTF})$					
	b_0	b_1	b_2	correlation coef.	residual std. error	no. of msmts.
0.15	58.2	0.543	0.30	0.934	0.73	44
0.772	46.6	0.410	0.21	0.870	0.82	48
1.6	40.6	0.424	0.57	0.865	0.84	46
3.15	35.3	0.371	0.44	0.837	0.82	48
6.3	29.0	0.376	0.56	0.868	0.75	39

Once again, just as for worst pair FEXT, the standard errors for b_1 and b_2 in Table 4 are such that b_1 can be considered to be decreasing with frequency whereas b_2 can be considered a constant. We shall use this information in the following section to consolidate the five equations into one concise equation for mean FEXT.

5.3 Consolidating the Mean and Worst Pair FEXT Equations

The previous paper showed that because b_1 in equation (1) decreases as frequency increases, mean FEXT frequency scaling is not a constant for all cables, but rather is a function of the cable's average twist helix angle. Our observations in Sections 5.1 and 5.2 regarding the behavior of the b_1 and b_2 coefficients suggest the same to be true for the two variable model (equation (2)). If this were the case, then the five equations for either mean or worst pair FEXT can be expressed in an equation of the form

$$\text{XT} = b_0 + b_1 \times \text{DOD} \times \text{avgTF} + b_2 \times \text{DOD} \times (\text{medTF} - \text{avgTF}) - (b_3 + b_4 \times \text{DOD} \times \text{avgTF}) \log_{10} f. \quad (6)$$

Table 5 gives the results of fitting equation (6) to the mean and worst pair FEXT data. These equations consolidate the ten equations in Tables 3 and 4 into two—one for mean FEXT and one for worst pair FEXT.

Table 5 Consolidated Mean and Worst Pair Power Sum FEXT Regression Equations (0.15 to 6.3 MHz)								
FEXT (dB/kft) = $b_0 + b_1 \times \text{DOD} \times \text{avgTF} + b_2 \times \text{DOD} \times (\text{medTF} - \text{avgTF}) - (b_3 + b_4 \times \text{DOD} \times \text{avgTF}) \log_{10} f$								
crosstalk	b_0	b_1	b_2	b_3	b_4	corr. coef.	residual std. error	no. of msmts.
Mean	44.0	0.444	0.48	17.8	0.118	0.997	0.83	225
Worst Pair	40.6	0.406	1.32	17.8	0.106	0.996	0.97	221

Examining Table 5 we see that the b_3 are identical (17.8) for both mean FEXT and worst pair FEXT and that the values of b_1 and b_4 for mean FEXT are similar to the corresponding values for worst pair FEXT. We show in Appendix B that the data support the validity of these simultaneous equivalencies and that we can therefore obtain two new equations in which b_1 , b_3 , and b_4 are forced to have the same values in both the mean and worst pair equations. Table 6 lists these equations.

Table 6 Consolidated Mean and Worst Pair Power Sum FEXT Regression Equations (forced to have similar b_1 , b_3 and b_4 coefficients) (0.15 to 6.3 MHz)								
FEXT (dB/kft) = $b_0 + b_1 \times \text{DOD} \times \text{avgTF} + b_2 \times \text{DOD} \times (\text{medTF} - \text{avgTF}) - (b_3 + b_4 \times \text{DOD} \times \text{avgTF}) \log_{10} f$								
crosstalk	b_0	b_1	b_2	b_3	b_4	corr. coef.	residual std. error	no. of msmts.
Mean	44.2	0.423	0.38	17.8	0.113	0.996	0.90	446
Worst Pair	40.4	-	1.36	-	-	-	-	-

95% of the mean and worst pair FEXT values in the data base fall within $\pm 2 \times 0.90 = \pm 1.8$ dB of the value predicted by the regression equations in Table 6.

Insofar as b_1 , b_3 and b_4 are the same for both mean FEXT and worst pair FEXT, the difference between mean FEXT and worst pair FEXT is given by

$$\text{Mean-Worst Pair FEXT} = 3.8 - 0.98 \times \text{DOD} \times (\text{medTF} - \text{avgTF}). \quad (7)$$

From Table 2, the $\text{DOD} \times (\text{medTF} - \text{avgTF})$ product ranges from 0.48 for ICOT cable to -1.99 for 19-gauge solid insulated waterproof cable. Substituting these values into equation (7) shows that worst pair FEXT ranges from 3.3 dB less than mean FEXT for ICOT cable to 5.8 dB less than the mean for 19-gauge waterproof cable. In other words, the power sum FEXT distribution for 19-gauge waterproof cable has a larger standard deviation than for ICOT cable.

Although the value of 0.996 for the correlation coefficient in Table 6 appears comfortably high, it is somewhat misleading because it accounts not only for the crosstalk variation with cable design, but also the crosstalk variation with frequency. If we remove the frequency effect and examine only the portion of the regression equation that pertains to cable design, then we find that mean FEXT has a correlation coefficient of 0.873 and worst pair FEXT has a correlation coefficient of 0.805 with cable design.

6. NEAR-END CROSSTALK

By now we might suspect that the two variable model containing average helix angle and helix angle skewness as explanatory variables might also be a good model for both mean and worst pair NEXT. Indeed this turns out to be the case. Even after many alternate models were tried, the same two variable model is about as good as any and better than most. Consequently, we shall discuss the results using this model.

6.1 Worst Pair NEXT

Table 7 gives the results of fitting the two variable model given by equation (2) to the worst pair NEXT data at each of the five frequencies.

Table 7 Linear Regression Equations for Worst Pair Power Sum NEXT of Standard and 'Special' Cables						
frequency (MHz)	Worst Pair NEXT (dB/kft) = $b_0 + b_1 \times \text{DOD} \times \text{avgTF} + b_2 \times \text{DOD} \times (\text{medTF} - \text{avgTF})$					
	b_0	b_1	b_2	correlation coef.	residual std. error	no. of msmts.
0.15	55.4	0.308	1.24	0.772	1.13	49
0.772	45.4	0.162	0.89	0.599	1.00	50
1.6	41.7	0.086	1.24	0.592	1.30	50
3.15	37.1	0.078	1.05	0.578	1.08	52
6.3	33.3	0.025	1.36	0.633	1.32	49

Just as for FEXT, the standard errors for b_1 and b_2 in Table 7 are such that b_1 can be considered as decreasing with frequency and b_2 can be considered constant. We will use this information later in Section 6.3 to consolidate the five individual equations into one concise equation.

6.2 Mean NEXT

Table 8 lists the linear regression equations for mean NEXT at each of the five frequencies.

Table 8 Linear Regression Equations for Mean Power Sum NEXT of Standard and 'Special' Cables						
frequency (MHz)	Mean NEXT (dB/kft) = $b_0 + b_1 \times \text{DOD} \times \text{avgTF} + b_2 \times \text{DOD} \times (\text{medTF} - \text{avgTF})$					
	b_0	b_1	b_2	correlation coef.	residual std. error	no. of msmts.
0.15	58.6	0.383	1.06	0.773	1.10	52
0.772	48.3	0.253	0.72	0.687	0.92	53
1.6	44.5	0.178	0.85	0.657	0.88	48
3.15	40.5	0.154	0.95	0.624	0.95	52
6.3	36.6	0.114	0.98	0.590	1.05	49

Once again b_1 can be considered as decreasing with frequency and b_2 can be considered a constant.

6.3 Consolidating the Mean and Worst Pair NEXT Equations

The coefficients for helix angle and helix angle skewness in Tables 7 and 8 behave the same as they did for FEXT in Section 5.3. Consequently, the frequency scaling of worst pair and mean NEXT is not a constant for all cable designs, but rather is a function of the cable's average helix angle. Therefore, NEXT at any frequency can be modeled (as was done for FEXT) by equation (6). Table 9 gives the results of fitting equation (6) to the mean and worst pair NEXT data. These two equations consolidate the ten equations in Tables 7 and 8 into two.

Table 9 Consolidated Mean and Worst Pair Power Sum NEXT Regression Equations (0.15 to 6.3 MHz)								
NEXT (dB/kft) = $b_0 + b_1 \times \text{DOD} \times \text{avgTF} + b_2 \times \text{DOD} \times (\text{medTF} - \text{avgTF}) - (b_3 + b_4 \times \text{DOD} \times \text{avgTF}) \log_{10} f$								
crosstalk	b_0	b_1	b_2	b_3	b_4	corr. coef.	residual std. error	no. of msmts.
Mean	47.2	0.236	0.92	13.6	0.166	0.988	0.998	254
Worst Pair	44.1	0.152	1.15	13.6	0.177	0.984	1.16	250

We see from Table 9 that b_3 is identical (13.6) for both mean and worst pair NEXT. In addition, the two values for b_2 are close to one another as are the two values for b_4 . We show in Appendix C that the data support the assumption that these coefficients are simultaneously equivalent. However, the b_1 's cannot be taken as being similar. This differs from the FEXT case where the b_2 's were found to be different, but the b_1 's the same.

Table 10 presents the equations for mean and worst pair NEXT when b_2 , b_3 and b_4 are forced to have the same values in both equations.

Table 10 Consolidated Mean and Worst Pair Power Sum NEXT Regression Equations (forced to have similar b_2 , b_3 and b_4 coefficients) (0.15 to 6.3 MHz)								
NEXT (dB/kft) = $b_0 + b_1 \times \text{DOD} \times \text{avgTF} + b_2 \times \text{DOD} \times (\text{medTF} - \text{avgTF}) - (b_3 + b_4 \times \text{DOD} \times \text{avgTF}) \log_{10} f$								
crosstalk	b_0	b_1	b_2	b_3	b_4	corr. coef.	residual std. error	no. of msmts.
Mean	47.2	0.246	1.03	13.6	0.171	0.993	1.08	504
Worst Pair	44.2	0.142	1.03	13.6	0.171	0.993	1.08	504

95% of the mean and worst pair NEXT values fall within $\pm 2 \times 1.08 \approx \pm 2.2$ dB of the value predicted by the equations in Table 10.

Insofar as b_2 , b_3 and b_4 are the same for both mean NEXT and worst pair NEXT, the difference between the mean and worst pair NEXT equations is given by

$$\text{Mean} - \text{Worst Pair NEXT} = 3.0 + 0.104 \times \text{DOD} \times \text{avgTF} \quad (8)$$

From Table 1, the $\text{DOD} \times \text{avgTF}$ product ranges from 8.7 for the 28-gauge experimental cable to 20.9 for 19-gauge solid insulated waterproof cable. Substituting these into equation (8) shows that

worst pair NEXT is 3.9 dB less than mean NEXT for the 28-gauge cable, but 5.2 dB less than the mean value for the 19-gauge cable. In other words, the power sum NEXT distribution for 19-gauge waterproof cable has a larger standard deviation than for the 28-gauge cable.

As with FEXT, although the value of 0.993 for the correlation coefficient in Table 10 appears comfortably large, it is misleading because it reflects not only the variation of crosstalk with cable design, but also the crosstalk variation with frequency. If we remove this frequency effect and examine the regression equation only as it pertains to cable design, then we find that mean NEXT has a correlation coefficient of 0.664 and worst pair NEXT has a correlation coefficient of 0.597 with cable design.

7. COMPARISON OF FEXT AND NEXT EQUATIONS

Table 6 gave the final equations for FEXT and Table 10 for NEXT. We rewrite these equations again here:

Table 11 Consolidated Power Sum Crosstalk Regression Equations (0.15 to 6.3 MHz)						
XT (dB/kft) = $b_0 + b_1 \times \text{DOD} \times \text{avgTF} + b_2 \times \text{DOD} \times (\text{medTF} - \text{avgTF}) - (b_3 + b_4 \times \text{DOD} \times \text{avgTF}) \log_{10} f$						
crosstalk	b_0	b_1	b_2	b_3	b_4	residual std. error
FEXT						
Mean	44.2	0.423	0.38	17.8	0.113	0.82
Worst Pair	40.4	*	1.36	*	*	0.97
NEXT						
Mean	47.2	0.246	1.03	13.6	0.171	1.01
Worst Pair	44.2	0.142	*	*	*	1.17

The b_3 and b_4 coefficients are frequency scaling terms and these terms indicate that crosstalk frequency scalings are a function of the particular cable design. For example, FEXT frequency scalings range from 18.8 dB per decade for the 28-gauge cable to 20.2 dB per decade for 19-gauge solid insulated waterproof cable. These are from 1.2 dB less to 0.2 dB more than the traditional 20 dB per decade rule. Similarly, NEXT scalings range from 15.1 dB per decade for the 28-gauge cable to 17.2 dB per decade for 19-gauge solid insulated waterproof cable. These are from 0.1 dB more to 2.2 dB more than the traditional 15.0 dB per decade rule.

At 1 MHz, the frequency scaling term in the equations in Table 11 become zero and we are left with only the design dependent terms (plus a constant). At this frequency, b_1 (the coefficient of the helix angle term) is largest for mean and worst pair FEXT, smaller for mean NEXT, and smallest for worst pair NEXT. This suggests that at 1 MHz, increasing the average twist helix angle of a cable design improves mean and worst pair FEXT three times as much as worst pair NEXT.

The b_2 coefficient is largest for worst pair FEXT and smallest for mean FEXT. Consequently, skewing the helix angle spectrum toward large helix angles (short twist lengths) improves worst pair FEXT 3.6 times as much as it improves mean FEXT.

The residual standard errors in Table 11 show that mean FEXT can be predicted with the greatest precision whereas worst pair NEXT has the least precision. This implies that unidentified factors influence worst pair NEXT much more than they affect mean FEXT.

The crosstalk and frequency scalings for all the standard and "special" cable designs were computed at 1 MHz using the equations in Table 11. Table 12 gives the FEXT results and Table 13 gives the NEXT results.

cable	AWG	XT Type	air core				waterproof			
			DEPIC		solid		DEPIC		solid	
			XT (dB/kft)	Scaling (dB/dec)	XT (dB/kft)	Scaling (dB/dec)	XT (dB/kft)	Scaling (dB/dec)	XT (dB/kft)	Scaling (dB/dec)
Standard	19	Mean	-	-	50.8	19.7	51.1	19.8	52.3	20.2
		Worst Pr	-	-	45.4	*	45.6	*	46.5	*
"	22	Mean	-	-	49.2	19.2	49.4	19.3	50.2	19.6
		Worst Pr	-	-	44.1	*	44.2	*	44.8	*
"	24	Mean	-	-	48.7	19.0	49.0	19.1	49.8	19.3
		Worst Pr	-	-	44.4	*	44.7	*	45.4	*
"	26	Mean	-	-	47.8	18.8	48.0	18.9	48.6	19.0
		Worst Pr	-	-	43.6	*	43.8	*	44.3	*
ICOT	24	Mean	52.7	20.0	-	-	52.7	20.0	-	-
		Worst Pr	49.4	*	-	-	49.4	*	-	-
MAT	25	Mean	50.3	19.4	-	-	-	-	-	-
		Worst Pr	46.8	*	-	-	-	-	-	-
DUCTPIC	26	Mean	48.4	18.9	-	-	-	-	-	-
		Worst Pr	44.9	*	-	-	-	-	-	-
26 locap	26	Mean	51.0	19.6	-	-	51.0	19.6	-	-
		Worst Pr	47.6	*	-	-	47.6	*	-	-
28 AWG	28	Mean	-	-	48.0	18.8	-	-	-	-
		Worst Pr	-	-	44.4	*	-	-	-	-

cable	AWG	XT Type	air core				waterproof			
			DEPIC		solid		DEPIC		solid	
			XT (dB/kft)	Scaling (dB/dec)	XT (dB/kft)	Scaling (dB/dec)	XT (dB/kft)	Scaling (dB/dec)	XT (dB/kft)	Scaling (dB/dec)
Standard	19	Mean	-	-	49.7	16.5	49.8	16.6	50.3	17.2
		Worst Pr	-	-	45.0	*	45.0	*	45.1	*
"	22	Mean	-	-	49.0	15.8	49.1	15.9	49.4	16.3
		Worst Pr	-	-	44.7	*	44.7	*	44.8	*
"	24	Mean	-	-	49.4	15.5	49.6	15.6	49.9	15.9
		Worst Pr	-	-	45.3	*	45.3	*	45.5	*
"	26	Mean	-	-	49.0	15.1	49.1	15.2	49.4	15.4
		Worst Pr	-	-	45.0	*	45.1	*	45.2	*
ICOT	24	Mean	52.5	17.0	-	-	52.5	17.0	-	-
		Worst Pr	47.5	*	-	-	47.5	*	-	-
MAT	25	Mean	51.0	16.0	-	-	-	-	-	-
		Worst Pr	46.6	*	-	-	-	-	-	-
DUCTPIC	26	Mean	49.8	15.3	-	-	-	-	-	-
		Worst Pr	45.8	*	-	-	-	-	-	-
26 locap	26	Mean	51.4	16.3	-	-	51.4	16.3	-	-
		Worst Pr	46.8	*	-	-	46.8	*	-	-
28 AWG	28	Mean	-	-	49.6	15.1	-	-	-	-
		Worst Pr	-	-	45.6	*	-	-	-	-

8. CONCLUSIONS

Analyses of the power sum crosstalk performance of the various standard and "special" copper PIC cable designs show that:

- At frequencies near 0.15 MHz, the variation in mean power sum FEXT from one cable design to another is adequately explained by the cable's average twist helix angle. At high frequencies (6.3 MHz), however, the addition of a helix angle skewness term significantly improves the explained variation.
- Average twist helix angle alone does not adequately explain the variation in worst pair power sum FEXT, worst pair power sum NEXT, or mean power sum NEXT. A model that contains both average helix angle and helix angle skewness terms substantially increases the explained variation.
- FEXT and NEXT frequency scalings are a function of the average twist helix angle of the cable design. Mean and worst pair FEXT scalings range from 18.8 to 20.2 dB per

decade and these are from 1.2 dB less to 0.2 dB more than the traditional 20 dB per decade rule. For NEXT, scalings range from 15.1 to 17.2 dB per decade and these are from 0.1 dB to 2.2 dB more than the traditional 15.0 dB per decade rule.

The regression model used in this paper is an extension of the one used previously to model mean FEXT. The new model includes not only average twist helix angle as an explanatory variable, but also the difference between median twist frequency and average twist frequency as a measure of the skewness of the twist helix angle spectrum. These two variables suggest that crosstalk depends not only on the location of the twist helix angle spectrum, but also on its shape.

The regression equations in Tables 3 and 4 can be used to calculate respectively the expected worst pair and mean FEXT performance of standard or "special" copper PIC cables at any of the five specific measurement frequencies. Similarly, the equations in Tables 7 and 8 can be used to calculate worst pair and

mean NEXT performance. Alternately, rather than use these equations at the specific measurement frequencies, one can use the consolidated equations in Table 11 at any frequency from 0.15 to 6.3 MHz.

The equations in Table 11 were used to calculate the crosstalk performance of existing cable designs at 1 MHz and the results appear in Tables 12 and 13. These equations can also be used to predict the crosstalk performance of new designs. As long as pair twists are judiciously chosen and spaced within the twist spectrum, one can use these equations to predict crosstalk using only three design parameters—diameter over dielectric (DOD), average twist frequency (avgTF), and median twist frequency (medTF).

References

1. Refi, J. J., "Mean Power Sum Far-End Crosstalk of PIC Cables as a Function of Average Twist Helix Angle," 29th International Wire and Cable Symposium, *Proceedings*, pp. 111-116, November 1980.
2. Anderson, R. E., "Computer Controlled Cable Measurements," 21st International Wire and Cable Symposium, *Proceedings*, pp. 188-192, December 1972.
3. Mitchell, D. M., "Material Savings by Design in Exchange and Trunk Telephone Cable, Part I: Waterproof Cable with Dual Insulation," 23rd International Wire and Cable Symposium, *Proceedings*, pp. 216-221, November 1974.
4. Nutt, W. G. and Savage, J. P., "Multipair Cables for Digital Transmission," National Telecommunications Conference, *Conference Record*, pp. 21.1.1 through 21.1.5, December 1978.
5. Webster, G. H., "Material Savings by Design in Exchange and Trunk Telephone Cable, Part II: Metropolitan Area Trunk Cable," 23rd International Wire and Cable Symposium, *Proceedings*, pp. 222-225, November 1974.
6. Nantz, T. D., "An Increased Pair Density Underground Feeder Cable," 27th International Wire and Cable Symposium, *Proceedings*, pp. 187-190, November 1978.
7. Strakhov, N. A., "Crosstalk in Multipair Cable—Theoretical Aspects," National Telecommunications Conference, *Conference Record*, pp. 8B-1 through 8B-7, November 1973.
8. Holte, N., "Calculation of Crosstalk in Balanced Pair Cables by Means of Simulation," 26th International Wire and Cable Symposium, *Proceedings*, pp. 428-439, November 1977.
9. Kempthorne, O. and Folks, L., *Probability, Statistics and Data Analysis*, The Iowa State University Press, 1971, p 21.

Appendix A

Comparing the Simple Helix Angle and Two Variable Models for Mean FEXT

We wish to compare the amount of mean FEXT variation explained by equation (1) to the amount explained by equation (2).

A.1 0.15 MHz

From Table 4, we see that equation (2) has a multiple $R^2 = 0.872$ at 0.15 MHz. (Multiple R^2 is the square of the correlation coefficient.) In other words, equation (2) explains 87.2% of the mean FEXT variation. Fitting equation (1) to the same data produces a multiple $R^2 = 0.863$. Since equation (1) is a subset of equation (2), equation (1) can be considered a reduced

model and equation (2) the full model. We can therefore compare the results of the two models statistically by using the F test of the form*

$$\hat{F} = \frac{(R_p^2 - R_q^2)/(p - q)}{(1 - R_q^2)/(n - p - 1)} \quad (A-1)$$

with $p - q$ and $n - p - 1$ degrees of freedom, where

R_p^2 = multiple R^2 of the full model,
 R_q^2 = multiple R^2 of the reduced model,
 p = number of explanatory variables in the full model,
 q = number of explanatory variables in the reduced model, and
 n = number of observations.

For our situation we have

$$\hat{F} = \frac{(0.872 - 0.863)/(2 - 1)}{(1 - 0.872)/(44 - 2 - 1)} = 2.88.$$

At the 5% level of significance, the value of F for 1 and 41 degrees of freedom can be found from standard tables of the F distribution and equals 4.08. In other words, 95% of the sample values for R_p^2 and R_q^2 will have F values less than 4.08. Since 2.88 is less than 4.08, our value of 0.863 for R_q^2 is not significantly different from the value of 0.872 for R_p^2 . We therefore conclude that for mean FEXT at 0.15 MHz, the helix angle model is not significantly different from the two variable model.

A.2 6.3 MHz

From Table 4, we see that equation (2) has a multiple $R^2 = 0.753$ at 6.3 MHz. Fitting equation (1) to the same data yields an $R^2 = 0.696$. Substituting these values into equation (A-1) we get

$$\hat{F} = \frac{(0.753 - 0.696)/(2 - 1)}{(1 - 0.753)/(39 - 2 - 1)} = 8.31.$$

At the 5% level of significance, F for 1 and 36 degrees of freedom equals 4.11. Since 8.31 is greater than 4.11, we conclude that for mean FEXT at 6.3 MHz, the helix angle model is significantly different from the two variable model.

Appendix B

Testing Whether Selected Coefficients for Mean FEXT are the Same as for Worst Pair FEXT

We wish to show that the values for b_1 , b_3 and b_4 for mean FEXT in Table 5 are not significantly different from their values for worst pair FEXT in the same table.

Table 5 lists two equations—one for mean FEXT and one for worst pair FEXT. These two equations can be expressed in a single equation as

$$XT = b_0 + b_5T + (b_1 + b_6T) \times DOD \times \text{avgTF} + (b_2 + b_7T) \times DOD \times (\text{medTF} - \text{avgTF}) - [b_3 + b_8T + (b_4 + b_9T) \times DOD \times \text{avgTF}] \log_{10} f \quad (B-1)$$

where

$T = 0$ for mean XT, and
 $T = 1$ for worst pair XT.

* Chatterjee, S. and Price, B., *Regression Analysis by Example*, John Wiley and Sons, 1971, p. 66.

In order for b_1 , b_3 and b_4 to be the same for both mean FEXT and worst pair FEXT, b_6 , b_8 and b_9 must be equal to zero. In this case, (B-1) reduces to

$$XT = b_0 + b_5T + b_1 \times \text{DOD} \times \text{avgTF} + (b_2 + b_7T) \times \text{DOD} \times (\text{medTF} - \text{avgTF}) - (b_3 + b_4 \times \text{DOD} \times \text{avgTF}) \log_{10} f. \quad (\text{B-2})$$

Equation (B-2) is a submodel of equation (B-1). We can therefore compare the two models using the same procedure as in Appendix A. Fitting equation (B-1) to the mean and worst pair FEXT data yields an $R^2 = 0.99324$. Fitting equation (B-2) to the same data produces an $R^2 = 0.99320$. Substituting these values into equation (A-1):

$$\hat{F} = \frac{(0.99324 - 0.99320)/(9-6)}{(1 - 0.99324)/(446-9-1)} = 0.860.$$

At the 5 % level of significance, F for 3 and 336 degrees of freedom equals 2.63. Since 0.860 is less than 2.63, we conclude that there is no significant difference between equations (B-1) and (B-2).

Evaluating equation (B-2) for mean and worst pair FEXT ($T = 0$ and $T = 1$) produces the results given in Table 6.

Appendix C

Testing Whether Selected Coefficients for Mean NEXT are the Same as for Worst Pair NEXT

We wish to show that the values for b_2 , b_3 and b_4 for mean NEXT in Table 9 are not significantly different from their values for worst pair NEXT in the same table. We shall show this by using the same method as in Appendix B.

Table 9 lists two equations—one for mean NEXT and one for worst pair NEXT. Both equations can be expressed as a single equation having the form given by equation (B-1). For b_2 , b_3 and b_4 to be the same for both mean NEXT and worst pair NEXT, b_7 , b_8 and b_9 must be equal to zero. In this case, (B-1) reduces to

$$XT = b_0 + b_5T + (b_1 + b_6T) \times \text{DOD} \times \text{avgTF} + b_2 \times \text{DOD} \times (\text{medTF} - \text{avgTF}) - (b_3 + b_4 \times \text{DOD} \times \text{avgTF}) \log_{10} f. \quad (\text{C-1})$$

Fitting equation (B-1) to the mean and worst pair NEXT data yields an $R^2 = 0.98665$. Fitting equation (C-1) to the same data produces $R^2 = 0.98653$. Substituting these values into equation (A-1):

$$\hat{F} = \frac{(0.98665 - 0.98653)/(9-6)}{(1 - 0.98665)/(504-9-1)} = 1.48.$$

At the 5 % level of significance, F for 3 and 494 degrees of freedom equals 2.62. Since 1.48 is less than 2.62, we conclude that there is no significant difference between equations (B-1) and (C-1).

Evaluating equation (C-1) for mean and worst pair NEXT ($T = 0$ and $T = 1$) produces the results given in Table 10.



James J. Refi
Bell Laboratories
2000 Northeast Expressway
Norcross, Georgia 30071

Mr. Refi began work with Bell Laboratories in 1966 at the Baltimore Laboratory as a Member of Technical Staff. He has worked on land coaxial cable, multipair cable, international cable specifications, and has authored papers on T2-LOCAP cable, pair unbalance phenomena, lightning surges in telephone cable, and crosstalk. He is currently engaged in optical fiber bandwidth studies.

Mr. Refi received his B.S.E.E. from Villanova University in 1966 and the M.S.E.E. from the Polytechnic Institute of Brooklyn in 1968. He is a member of I.E.E.E., Tau Beta Pi, and Eta Kappa Nu.

AD P000567

INSTANTANEOUS CABLE SEALING TECHNIQUE: THEORY AND TYPICAL APPLICATIONS

Roger H. Keith, P.E.

TelComm Products Division/3M
St. Paul, Minn.

ABSTRACT

Prestretched tubing is made from an elastomeric sleeve, factory expanded onto a core which supports it. Unwinding the core applies the sleeve, collapsing it onto the cable or connection with continuing shrink force throughout its service life.

Unlike heat shrink and two-part seal systems, no source of heat or energy, wet or hot adhesives are needed in most uses, and the action is immediate on initiation of core collapse, freeing results from operator technique. The seal is made at once, even in rain, snow, immersion or zero visibility.

Tube materials and shrink characteristics are given with practical product sizes and capacities. Environmental tests show excellent protection of CATV coax connectors, suggesting solution of many fiber optics splice/connect problems. Uses for communications battery clamps, case gland seals, cable splices, and plenum cable sheath repair are shown. Molded sleeves allow special shapes; multiple cores and various materials are possible. New designs hold cable pressures or apply torque prestress to lock twist and bayonet connections.

INTRODUCTION

After a successful history of service in power cable splicing and insulation, the advantages of prestretched tubing are being applied to communications uses with unique benefits and expanded design concepts as a result. Prestretched tubing provides a useful set of alternative features for the covering and sealing of a cable splice, connection or case entry.

Traditionally, a heat shrink material provided the best way to perform many of these tasks, but it has drawbacks resulting from variations in operator technique, fire and burn hazards, difficulties in getting good heat coverage in cramped quarters, and possible damage to surrounding installations during application that limit its use in some conditions.

Prestretched tubing offers a continuous, seamless tubular seal at a competitive cost, easily applied without tools or formal training, using no heat and almost instantaneous in activation. Contrast this with tools, heat, adhesives, and mechanical clamps or wet mastics or sealers which must be mixed or applied to close a cable connection or case gland,

and the accompanying training, skill, application and setting time of traditional sealing methods.

In the event of removal of the tubing, prestretched material is normally bonded by continuing shrink forces alone, and no adhesive cleanup is required.

PRODUCT FORM, MANUFACTURE, AND USE

The simplest prestretched tube construction consists of a cut length of extruded elastic tubular sleeve, diametrically expanded in the factory over a longer rigid cylindrical core which holds it in the expanded condition as shown in Figure 1. The core is

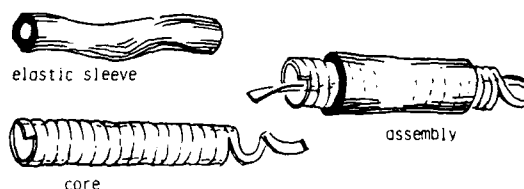


Figure 1. PRESTRETCHED TUBE ASSEMBLY

made by spiralling an interlocking polypropylene extruded ribbon which is then periodically tacked to hold the core in shape during manufacture and storage. The core construction is detailed in Figure 2. A tail end of the extrusion is left as a pull, and is used in the application of the prestretched

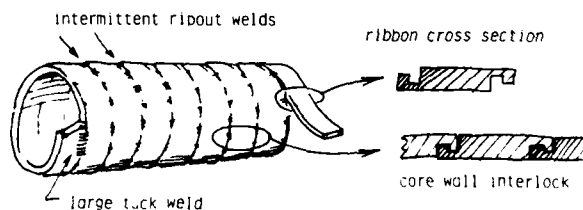


Figure 2. CORE DETAILS

tube. Figure 3 shows the procedure:

First, the tube assembly is chosen which has an elastic sleeve with a relaxed internal diameter somewhat smaller than the outside diameter of the cable to be covered. This assembly is slipped over one of the cables to be joined, and slid to one side while the connection is made. The prestretched

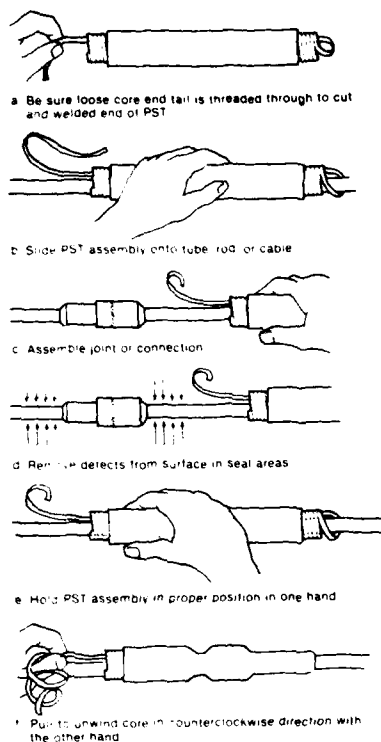


Figure 3. INSTALLATION TECHNIQUE

tube assembly is moved over the splice, and the pull tail of the core is unwound with a spiralling motion around the core. The pull of the tail rips out the intermittent welds of the spiral ribbon, collapsing the core and withdrawing it as a long tail from the opposite end. The elastic sleeve progressively shrinks as the core collapses, seeking its original unstretched size.² Since the cable outer diameter is larger than the relaxed sleeve ID, the elastic sleeve exerts a continuing, firm shrinkdown force, and this force perseveres for the life of the connection. The appearance of a prestretched tube, cutaway after application to show this effect, is shown in Figure 4.

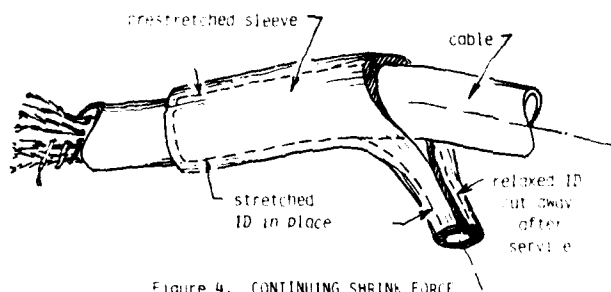


Figure 4. CONTINUING SHRINK FORCE

This action is unlike that of heat shrink tubing, which requires the application of heat from a torch

or hot air gun to release locked-in stresses; heat shrink material does not continue to exert significant shrink forces after heat is removed. In contrast, the prestretched tubing remains an elastic, low modulus material throughout its service life as well as during application, and can adjust to cable movement, environmental dimension changes, and flexing and stressing of the finished assembly without relinquishing its persistent grip on the cable or connector. This property of prestretched tubing allows it to form an excellent watertight seal without the use of adhesives or mastics to bond to most cable sheath surfaces and materials.

SLEEVE MATERIALS AND PROPERTIES

The choice of an elastomeric material for the prestretched sleeve requires a compound having low permanent set, good cut, tear, and abrasion toughness, high elongation and ultimate strength, and good environmental inertness. Silicone, Neoprene[™], and EPDM synthetic materials have these characteristics and special formulations and manufacturing techniques have been developed especially for this use to maximize these properties, control uniformity, and insure freedom from inhomogeneities or defects which could cause failure of the sleeve during manufacture, storage, or use.

Prestretched products are remarkably free from mechanically-related defects during their service life, since this unique product actually sees higher stresses during manufacture and storage than in usual service, and any tearing defect tendencies are dramatically exposed during the manufacturing process!

Table 1. HIGH STRETCH ETHYLENE PROPYLENE RUBBER:
TYPICAL PROPERTIES

Color	Black
100% Modulus ASTM D 412-75	0.90 MPA (125 psi)
300% Modulus ASTM D 412-75	3.50 MPA (500 psi)
Ultimate Tensile ASTM D 412-75 Original	9.00 MPA (1300 psi)
Ultimate Elongation ASTM D 412-75 Original	650%
Angle Tear ASTM D 624C-73 Original	29.KN/m (160 ppl)
Shore A Hardness ASTM D 2240-75	43
Ozone Resistance 70 Hz. @ 150 PPM ASTM D 518-61	No cracking
Dielectric Strength ASTM D 149-75 Original @ 1.78mm	12.8 MV/m (326 V/mil)
22 Hr. in H ₂ O at 90°C	8.5MV/m (216 V/mil)

Table I shows typical properties of the EPDM compounds developed for this use. Originally, expanded:relaxed ID ratios of 2.0:1 were the highest that could be reliably employed, but these can be increased to a core size of 2.5:1 for many applications, due to improvements in formulation and processing care. Recently, a high strength EPDM material has been developed which permits a 4.0:1 expansion of the extruded rubber sleeve on its core.

As the elastomer sleeve is stretched onto the collapsible core during manufacture, the longitudinal stresses induced by the hoop forces pull the tube slightly inward along its axis, making it about 15% shorter than its relaxed cut length after being stretched 2 to 3 times its original ID onto a core. In shrinking, the tube approaches its original length as it is applied. This can be modified by the degree of diametrical relaxation, and also by changes in operator technique in either pulling or pushing the tube assembly along the cable as the core tail is pulled and unwound. This lays the rubber down in a slight longitudinal tension or compression with its friction to the cable jacket holding it in place.

A programmable routine for the TI-59 printing calculator has been developed to represent the typical sleeve length and wall thickness variation that can be expected for given stretch and relaxation ratios of the sleeve (see Appendix.) This calculation assumes incompressibility of the bulk elastomer, and is of value to a designer in approximating the as-applied length of a given cut sleeve if a very close tolerance must be kept for length on-cable. Conversely, it provides a first approximation to the specifier for a cut length to give a desired special result. In most cases, however, the 10 to 20% change in length is simply allowed for by using a slightly overlength sleeve as-cut for the desired in-place coverage.

PRODUCT DIMENSIONS AND CAPABILITIES

The most common type of prestretched tube consists of a straight extruded hollow EPDM rubber tube on a single wound polypropylene core, with the sleeve having an inside diameter of 0.14 to 1.5 inches. Larger sizes of rubber sleeve can be used, but collapsing forces on the core can be large and limit the degree of stretch that can be employed, independent of the stretch ratios attainable in smaller sizes with a given elastomer formulation.

Wall thicknesses are typically 0.12 to 0.24 inches; this is "heavy wall tube," particularly in the smaller sizes. The devices can be made from just an inch or so up to several feet long.

Some commonly available sizes for communications use are shown in Table II, along with their "application range." This range first describes the smallest diameter that the tube can be applied to, for which a lasting shrink force will maintain an effective seal in typical service. This represents about 40% stretch over the as-extruded ID, and al-

Table IIa. PRESTRETCHED TUBES, EPDM RUBBER SLEEVE
GENERAL COMMUNICATIONS USE

Type	Application Range	Sleeve Relaxed ID	Wall	Cut Length
620-4	0.34-0.72 in	0.24 in	0.15 in	4.0 in
620-7				7.0
622-4	0.44-0.95 in	0.32 in	0.16 in	4.0 in
622-6				6.0
622-9				9.0
622-11				11.0
626-4	0.71-1.63 in	0.50 in	0.18 in	4.0
626-6				6.0
626-12				12.0
626-16				16.0
630-4	1.16-2.67 in	0.84 in	0.18 in	4.0
630-6				6.0
630-18				18.0

Table IIb. PRESTRETCHED TUBES, EPDM RUBBER SLEEVE
CATV COAXIAL CABLE USE

Short \underline{S} Tubes: Terminations to Taps, Amplifiers, Splitters
Long \underline{L} Tubes: Coaxial Cable Splice Connectors

Type	Cable Diameter Outer Conductor	Application Diameter Environmentally Exposed	Length
4626S	Drop Wire	0.27 - 0.60 in	3.0 in
4626L			6.0
4627S	0.412 in	0.50 - 1.12	7.0
4627L			13.0
4628S	0.500	0.58 - 1.23	7.0
4628L			14.0
4629S	0.625	0.69 - 1.50	7.0
4629L			12.0
4630S	0.750 & 0.875	0.71 - 1.50	7.0
4630L			14.0
4631S	1.00	0.88 - 1.80	7.0
4631L			15.0

lows for slight residual permanent set, loss of contracting force over years of storage or service, and an additional margin to create the interference between the cable or connector OD and the sleeve ID which generates the inward sealing action. The maximum diameter of accommodated range may approach the largest stretch that the rubber composition can allow, but is always somewhat smaller, lessened by the thickness of the core tube and a clearance, typically 0.12 to 0.18 inches, for pulling of the core ribbon tail between the core ID and the cable or connector OD. Environmental and mechanical requirements for the stretch tube often pose additional limitations on a practical upper diameter in many services.

The table shows a series of prestretched tubes sized specifically for CATV and similar coaxial cable connector protection. The large stretch ratios which these devices can accommodate allows specification of a single product size for many sizes, shapes, and makes of connectors manufactured for a given size of cable, despite rather large variations in the size of hex bushings and nuts used by different makers.

SHRINK FORCES

The magnitude of the inward shrink force exerted by a sleeve can be measured experimentally by inflating a section of the tube and measuring its diameter. This represents a dynamic equilibrium between the air pressure inside the tube, tending to expand it, balanced by the contacting force of the elastomer sleeve, as shown in Figure 5.

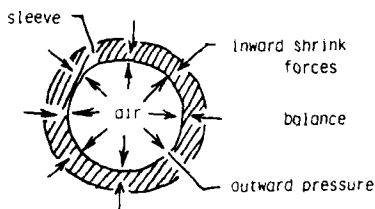


Figure 5. CROSS SECTION OF INFLATED SLEEVE

A series of copper tubes of various diameters was prepared, with test gauges and a regulated air supply, in order to determine these pressure forces.

The apparatus is shown in Figure 6. A hole near the center of each tube allowed air to bleed under pre-stretched sleeves attached to the tubes.

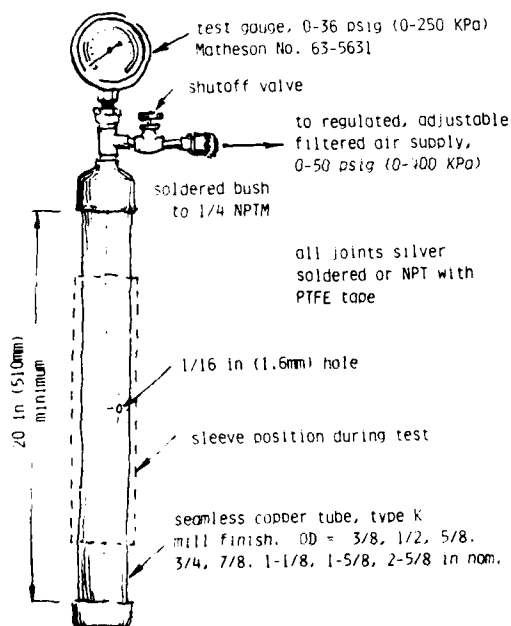


Figure 6. TEST APPARATUS

Before an inflation test series was begun, the internal air pressure was raised until the rubber sleeve just barely lifted off the copper tube due to internal pressure, and the pressure was noted. At this pressure, the sleeve is held in a near-fric-

tionless air bearing condition, with the internal pressure forming a thin, moving sheet of air which runs from the hole in the copper tube, under and out each end of the sleeve. This frictionless state was used to precondition the sleeve and remove residual stresses which might have been imposed in loading it onto its core, or in application to the copper tube. By rotating and sliding the sleeve up and down the tube, and then lowering the air pressure until the sleeve once again grabbed and locked onto the copper tube, unwanted stresses were relieved and the sleeve was held in this condition.

The sleeve was then secured to the copper tube using worm screw hose clamps, protecting the sleeve under the clamps with several wraps of Type LR telephone tape.

The rubber sleeve was marked at regular intervals along its length to provide stations for diameter measurements. The internal pressure was advanced for 10 minutes by step increments of 2 psi, and bi-axial diameter measurements of the rubber sleeve were taken at each pressure, for each station. At the maximum permissible expansion for a given tube, the pressure was held for 10 minutes, then reduced in 2 psi increments until the tube was firmly seated with diameters being recorded at the end of each 10 minute period.

Typical results of a test are shown in Figure 7, relating diameter and internal pressure for an EPDM sleeve applied to a copper tube very close in size to its relaxed ID. The curve represents increasing diameter with increasing pressure, and at the extreme in pressure, a slight increase in diameter results as the pressure is held constant, due to the relaxation of the 10-minute remnants of permanent set. This same phenomenon is responsible for the hysteresis loop formed as pressure is reduced. The spacing between the upward and downward pressure change data is small, indicating the excellent recovery of this EPDM compound, amounting to a small fraction of an inch at most.^{3,4}

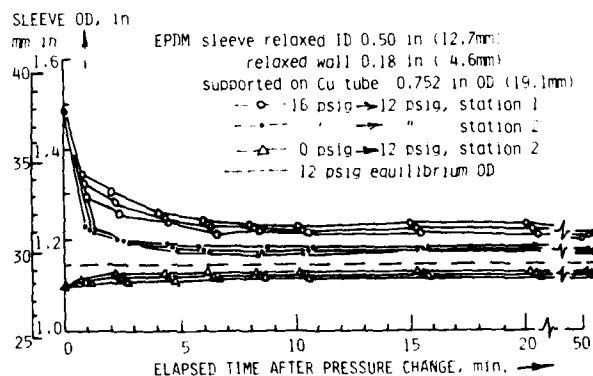


Figure 7. SLEEVE DIAMETER CHANGE, STEP PRESSURE INPUT

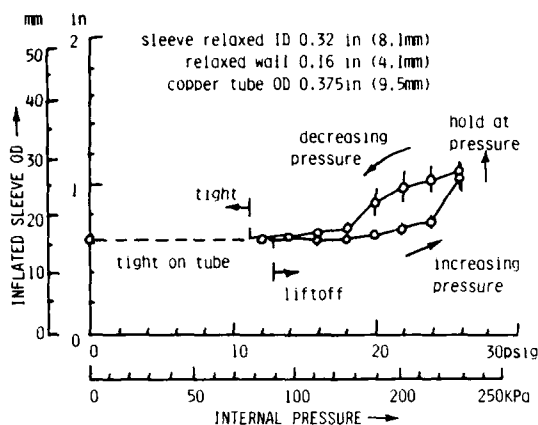


Figure 8. EPDM SLEEVE OD & INTERNAL PRESSURE

A better idea of the extent of this time dependence of relaxation is shown in Figure 8, which graphs the change in diameter with time for a typical rubber sleeve, after preconditioning at pressure for at least an hour, first in response to a step increase in pressure from 0.00 to 12.00 psig, then in response to a step decrease from 16.00 to 12.00 psig. These curves indicate maximum and minimum limits of what might be expected as a diameter measurement after a very long time under these conditions. In this case, the tube almost immediately reacts to a change in internal pressure, coming to well within 10% of its expected equilibrium diameter in two minutes or less. This agrees with results obtained with dumbbell specimens in uniaxial stress-strain, and indicates the rapidity with which these sleeves develop their full shrink-down force, and thus the speed with which they can be placed in service after application.

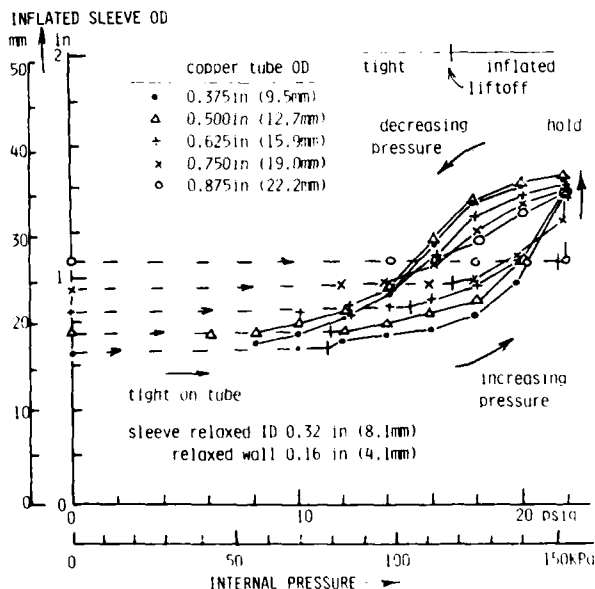


Figure 9. EPDM SLEEVE OD & INTERNAL PRESSURE

When similar sleeves of the same size are applied to copper tubes of different diameters, a family of curves such as that shown in Figure 9 is obtained. The curve for each diameter of tube is essentially the same at higher pressures, but has a different line of entry representing the prestretch of the sleeve on the copper tube. The copper tube holds the sleeve in an unvarying stretched condition at low pressures, until the internal pressure exceeds that corresponding to a sleeve diameter in excess of the copper tube diameter. At that point, the sleeve lifts off and follows the general curve for an unsupported sleeve. This verifies the prediction of liftoff pressures and shrink forces for a given applied diameter and set of conditions, from a general sleeve curve.

ENVIRONMENTAL EXPOSURE

Impressive results are obtained on environmental test of prestretched tubing applied to coaxial cable connectors. The bare connectors are not completely weatherproof, and may also be subject to tampering, vandalism, or mechanical damage as they are applied to military use, home distribution, and industrial cable TV applications. It is also desirable to extend their use to severe chemical environments, immersion, or direct burial. The application of a prestretched tube is a simple, no-tools way of buttoning-up these connectors in any kind of weather, and broadening their application.

Fiber optics connections may have poor environmental resistance without a covering, but are subject to immediate stress and possible failure during application of a heat shrink tube.⁵ The data for protection of coaxial connectors suggests that similar protection by prestretched tubing, without the trauma of heat application, may extend to fiber optics as well.

Tables III, IV, and V indicate the excellent results obtained in response to very severe environmental exposure of prestretched tubing on many common types of coaxial cable connectors. The effects of water

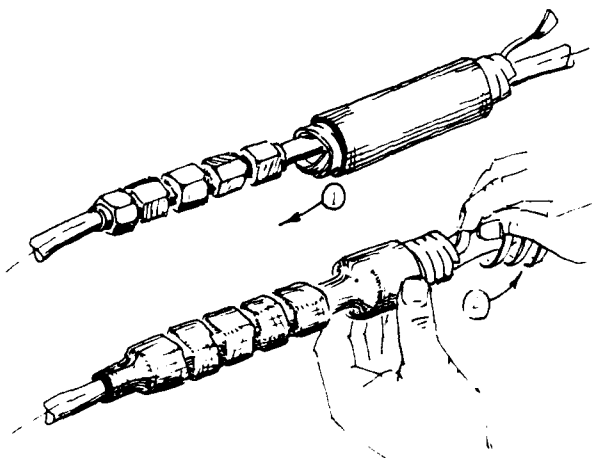


Figure 10. APPLICATION TO CATV COAX CONNECTOR

immersion to significant pressures have also been tested: the action of water head serves only to press the applied sleeve more tightly to the cable. Tests of insulation leakage were terminated successfully at 150 foot head, the limits of the apparatus, and deeper exposures are planned.

Table III. PRESTRETCHED TUBING ON CATV COAXIAL CONNECTORS

Environmental Ageing:

A. Hot Storage: packaged, store in 130°F air 20 days. Inspect for degradation, then B or C:

B. Cold Impact: Install on type 6 drop wire or type L 0.412, 0.500, 0.750 inch connectors. Condition 2 hr -40°F. 3 impacts of 3 ft-lb with 1 inch OD steel cylinder. Inspect.

C. Hot Age: Install as above, age 148°F air 6 months. Inspect. Results: All pass. No visible degradation or measurable hardness change.

Table IV. PRESTRETCHED TUBING ON CATV COAXIAL CONNECTORS

Insulation Resistance: 500 v DC on outer conductor, to water bath immersion (except to wet sand in freeze-thaw test) after 1 hour conditioning at room temperature:

A. WATER SOAK: 3 mo room temp, 2 ft water head

Size, in	Type	Insulation resistance, ohms			
		Initial	2 wk	1 mo	3 mo
RG-6	G	3×10^{13}	1×10^{12}	8×10^{11}	8×10^{10}
	P	1×10^{13}	9×10^{11}	1×10^{12}	3×10^{10}
0.412	P	1×10^{13}	5×10^{11}	3×10^{11}	2×10^{10}
	P	8×10^{12}	5×10^{11}	3×10^{11}	5×10^{10}

B. TEMPERATURE CYCLE: -20°F to +140°F air, 2 cy/day, 3 mo

Size, in	Type	Insulation resistance, ohms			
		Initial	2 wk	1 mo	3 mo
RG-6	G	3×10^{11}	2×10^{11}	5×10^{10}	2×10^{10}
	P	3×10^{11}	2×10^{11}	5×10^{10}	3×10^{10}
0.412	P	2×10^{11}	1×10^{11}	8×10^{10}	5×10^{10}
	P	3×10^{11}	1×10^{11}	5×10^{10}	1×10^{10}

C. FREEZE-THAW CYCLE: Imbed in wet sand, -20°F to +140°F, 2 cycles/day, 3 mo

Size, in	Type	Insulation resistance, ohms			
		Initial	2 wk	1 mo	3 mo
RG-6	G	1×10^{13}	3×10^{11}	4×10^{11}	1×10^{11}
	P	1×10^{13}	1×10^{11}	3×10^{11}	1×10^{11}
0.412	P	1×10^{13}	1×10^{11}	2×10^{11}	1×10^{11}
	P	1×10^{13}	1×10^{11}	2×10^{11}	2×10^{10}

D. HIGH HUMIDITY: Age 6 mo +120 to 130°F, 95%rh.

Size, in	Type	Insulation resistance, ohms				
		Initial	2 wk	1 mo	3 mo	6 mo
RG-6	L	2×10^{12}	4×10^{11}	1×10^{12}	4×10^{12}	1×10^{12}
	L	1×10^{12}	1×10^{11}	2×10^{11}	1×10^{12}	1×10^{12}
0.412	L	7×10^{11}	8×10^{10}	1×10^{10}	2×10^{12}	4×10^{12}
	L	1×10^{12}	3×10^{10}	1×10^{10}	1×10^{12}	2×10^{11}

E. SALT SPRAY: ASTM B-117 salt fog chamber, 6 mo

Size, in	Type	Insulation resistance, ohms				
		Initial	2 wk	1 mo	3 mo	6 mo
RG-6	G	8×10^{12}	3×10^{13}	3×10^{11}	1×10^{10}	4×10^{11}
	P	1×10^{13}	3×10^{10}	2×10^{11}	1×10^{10}	5×10^{11}
0.412	P	1×10^{13}	2×10^{11}	1×10^{11}	2×10^{10}	1×10^{12}
	P	1×10^{13}	2×10^{11}	1×10^{11}	1×10^{11}	1×10^{12}

Table V. PRESTRETCHED TUBING ON CATV COAXIAL CONNECTORS

Environmental Agents:

A. OZONE: Install on "G" connectors on cable, RG-6, 0.412, 0.500, 0.750 in. ASTM B-1149 chamber, 100 F Zipper ozone, 164 hrs. Inspect under 4x magnification for crazing, cracks. Results: Excellent physical condition.

B. HUMID/CONDENSATION: Install on connectors on cable, sizes as above, WFOH weatherometer 3 cycles/day (1.5 hr +140°F, then 1.5 hr condensation 100% rh +122°F). Inspect visually.

Set	Type	Hrs Exposure	Results
I	L	123	No observed degradation
II	L	50	Slight chalking, one sample only
III	G	296	Slight chalking, one sample only

C. CHEMICAL STABILITY: Install on "G" connectors on cable, sizes as above. Expose by immersion 36 hrs. Examine. Immerse in room temp water 1 hr and determine 500 V DC insulation resistance. Water conductor to bath.

Material	Conc.	Temp	Effect	Insul Res, ohms
Sulfuric Acid	3 by vol	+100°F	none	2×10^{11} minimum
Sodium Hydroxide	0.2 Normal	+100°F	none	2×10^{11} minimum
Sodium Chloride	5 by wt	+100°F	none	2×10^{11} minimum
Acetic Acid	5 by wt	+100°F	none	2×10^{11} minimum
Sodium Carbonate	0.1 Normal	+100°F	none	1×10^{11} minimum
No. 2 Commercial Fuel Oil	-	room	severe softening and swelling	1×10^{11} minimum
No. 2 Commercial Fuel Oil	-	48 hr water soak		5×10^{11} minimum

BATTERY CABLE CLAMP PROTECTION

Another application which has created interest in prestretched tube is the sealing of the joint where a battery cable for communications supply joins the battery post clamp or lug. This is a weak point where flexing of the cable insulation can pull it away from the cast-on lead clamp, causing a void where battery acid mist can wick in and accumulate. This passage opens to the point where bare copper contacts the lead clamp, and capillary transfer of acid is a frequent cause of galvanic corrosion and rapid mechanical or electrical failure. This hidden location is practically impossible to inspect and difficult to repair.

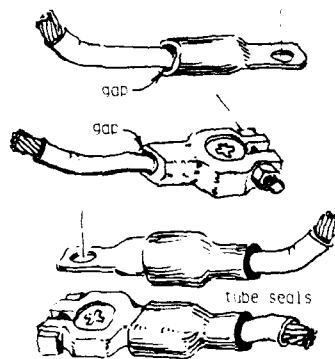


Figure 11. BATTERY CLAMP SEALS

A prestretched tube has been proposed as an ideal solution to the problem, as shown in Figure 11. Its continuing shrink force gives a watertight seal on

both the cable and clamp shank. While allowing limited flexing of the cable, it aids in preventing kinking at the shank end and thus helps prevent insulation gap from forming as well as restricting copper strains in service. The sleeve is compatible with silicon and no-ox greases common in battery work, and can be retrofitted to batteries in service with little risk since neither heat nor flame is needed to apply it.

The EPDM material of most prestretched tubes is superbly immune to attack by sulfuric acid electrolyte. One large use of the EPDM sleeve material requires it to be employed above, below, and "at the waterline" immersed in electrolyte of 30-year life float service telephone batteries. It was qualified for this service by accelerated high temperature ageing in electrolyte, followed by examination of the rubber, and also IR analysis of the electrolyte and potentiometric verification that its anodic and cathodic behavior in lead cell service are undisturbed.⁶

CABLE SPLICES: MOLDED SLEEVE, DOUBLE CORES

The durability and toughness of the coverage which can be obtained with a prestretched tube is exemplified by medium voltage mine power cable splice service. Although this application is neither new for prestretched tube nor a communications application, it demonstrates the service history which has been accumulated for this type of product and points out how custom features can be developed for a given use.

Mine power cables supply medium voltage electricity to loaders, undercutting machines, pumps, shovels, and locomotives, being run over roads, floors, ledges, and tracks in open pit and deep cuttings. The cables are dragged over rough rock surfaces, and run over by heavy vehicles, must be reeled and unreel, are almost always damp and frequently immersed in acid mine waters or exposed to the elements. In this service a Neoprene sleeve is used for oil and grease resistance. The sleeve is a molded, rather than extruded part, which allows the design to have tapered slim ends for the splice cover for snag resistance as the cable is dragged or reeled.

This prestretched tube assembly has another unusual feature, a double pull core. Two cores are mounted in tandem inside the sleeve, each with its own pull tail extending to one end, with the two starting ends butted together at the center, as shown in Figure 12. This configuration allows the orderly dress

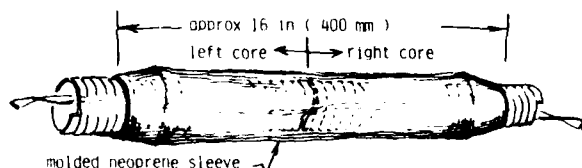


Figure 12. MINE CABLE SPLICE PRESTRETCH TUBE

of the core tail, in spite of a long, 16 inch coverage of the cable splice by the double tapered sleeve. Each core need be pulled only half that distance, and entangling of the ribbon tail is minimized.

Another application of the double pull is to a situation in which a splice or paired connectors have a protrusion or "nose" which could catch the pull of a core tail, as shown in Figure 13. With a double core, the pull of the ribbon tail always passes from a larger to a smaller diameter and snagging is prevented.

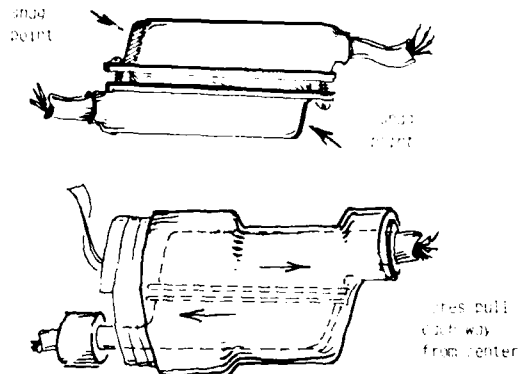


Figure 13. SLEEVE WITH DOUBLE PULL CORE COVERS CONNECTOR PAIR

SPECIAL SLEEVE DESIGNS

If a molded sleeve is used, non-cylindrical parts such as transitions, and even multiple breakouts can be designed. Figure 14 shows a molded cable seal especially made to fit the crotch area of a 3-phase cable with shaped sectors, sealing and insulating the breakout of separate phases from the cable group. The body is molded, then the major diameter is stretched over a large core, and the three small breakouts at the other end are stretched over their own small cores.

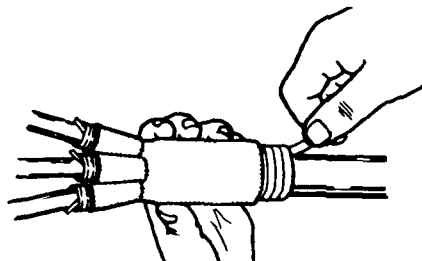


Figure 14. PRESTRETCH CABLE BREAKOUT

The seal is applied by first splaying the individual cables, slipping the molded sleeve over the three small sectors until it bottoms, then pulling first the large core and then the three small cores.

PLENUM CABLE SHEATH REPAIR

A proposed application would employ silicone rubber prestretched tubes with tapered ends to repair Teflon™ plenum cable sheath defects. Plenum cable is unlike many other telephone cables: the majority is laid on a false ceiling or pulled through air ducts with generous clearances, frequently admitting the craftsman as well as the cable. Many of the usual cable pulling problems are never seen, and thus it may allow a thickened section at a repair or splice, or even connectors on-run.

The Teflon material does not lend itself well to economic stripping and re-extrusion if a sheath defect is found. The Teflon cannot be easily recycled so there can be considerable scrap penalty for pinholes or poorly fused sections of sheath.

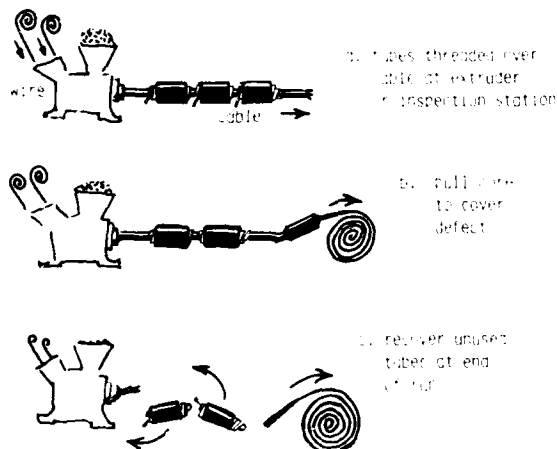


Figure 15. PLENUM CABLE SHEATH REPAIR

Figure 15 shows how this might be overcome: Prestretched tubes would be threaded over the wires at the extruder nozzle, at the beginning of a sheath extrusion run, or at the inspection station if a rehabilitation or inspection spooling of completed cable is being performed. During extrusion of sheath to specification, the completed cable passes through the cores of the tubes held in readiness. If a defect is found, a tube is collapsed over it. The elastic force of the sleeve forms a tight grip on the Teflon sheath, bypassing problems with adhesives or chemical bonding that is marginal in effect or difficult to perform. If defects are not found which would use all the prestretched tubes, the remaining ones are not wasted: they can be slipped off the tail end of the run and rethreaded as part of the complement of the next length.

RECENT DEVELOPMENTS

Two new configurations of tube show promise to allow the use of prestretched cable splice and connector covers for pressurized seals and locking of twist connectors. Both of these designs use elastomer sleeves of conventional design, but loaded onto their cores in a novel way:

PRESSURE RETENTION

A prestretched tube which can hold pressure is made by cuffing each end of the rubber sleeve inward when it is placed on its core. The appearance of the finished product is shown in Figure 16. On pulling the core tail, the entire sleeve, cuffs and all, is transferred onto the splice or connection.

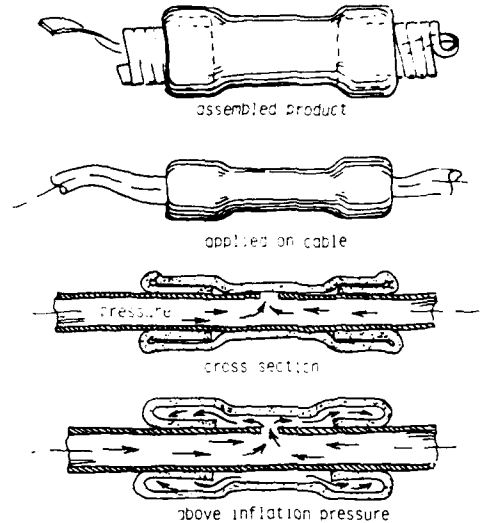
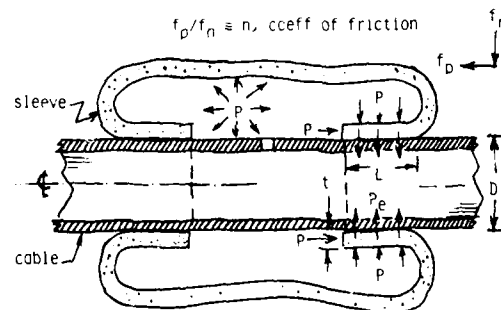


Figure 16. CUFFED SLEEVE RETAINS PRESSURE

In use, the cuffed sleeve is held in place normally due to the shrink action of its elastomeric material. But when the liftoff force of the sleeve is exceeded by an internal pressure such as a cable fill, the center part of the sleeve will expand, and the cuffs on the end will stay attached to the cable. Increasing pressure inflates the sleeve, but the interior cuffs grip the cable ever more tightly, sealing like a tubeless tire onto a wheel rim or a valve leather in a pump.



to retain cuff ag. liftoff:

extrusion force < lifting forces = n (new shrink + elastic shrink)

$P \times \text{cuff edge area} \geq n (P + P_e) \times \text{cuff surface area}$

$P(\pi(D+2t)^2/4 - \pi D^2/4) \geq n(P + P_e) \pi LD$

$P(Dt + t^2) \geq \pi LD(P + P_e)$

typically: $D=1.0''$ $t=0.18''$ $L=2''$ $n=0.3$ $P_e=10\text{psi}$

$0.66, n \approx 6.28P + 62.8 : \text{Q.E.D.}$

Figure 17. CUFFED PRESTRETCHED TUBE FORCE BALANCE

Figure 17 indicates the forces involved, an extruding force against the cross section of the cuff tending to force the cuff outwards, opposed by the internal pressure and its frictional tangential resultant, plus the elastic shrink force of the cuff material.

Applications to typical cable surfaces show excellent tolerance to surface roughness, scratches, and kinks. The forgiveness of a tubeless tire bead and the steel rim it seals to are a good analogy of the practical roughnesses the system tolerates well.

The low modulus of the sleeve, as compared with that of applied heat shrink tubing, allows excellent penetration and sealing into many surface irregularities and eliminates many leaks that might otherwise develop due to differential flexing under mechanical and thermal action. Leaktight seals are easily accomplished on ordinary mill finish galvanized steel water pipe without special surface preparation or adhesive sealants.

On the other hand, knurls, threads, or deep longitudinal scratches in the cuff area that the sleeve will not fill can be a source of leaks if not closed with a sealing filler or tape. Greases or oils are not recommended for this purpose, since the pressure retaining action of the cuff is dependent on friction to the cable sheath. Typical practice specifies a 2 inch cuff at each end of the sleeve, which translates into a critical coefficient of friction far below what can be expected on most materials, but which might be defeated by a heavy coat of good lubricant applied in error.

In any case, the seal is developed along a very short section of each end, and even if a good seal is not obtained at one end of a cuff or another, the balance of the cuff will hold the pressure. A long, long sealing area does not seem to be needed to insure a tight closure, in contrast to typical practice with an adhesively bonded shrink tube.

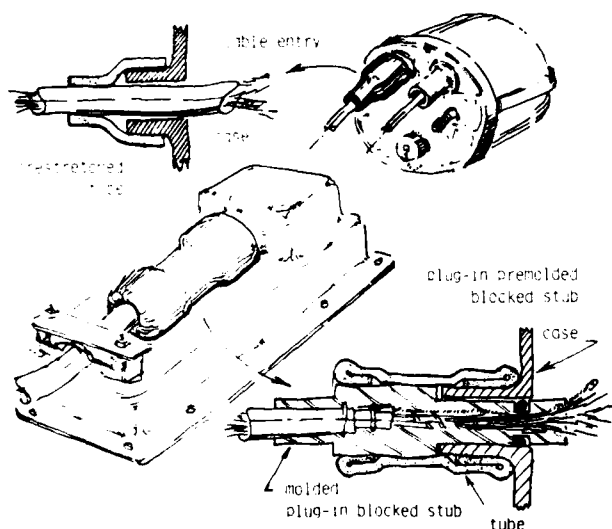


Figure 18. APPARATUS CASE/REPEATER CABLE ENTRY

Considerable interest is being found in using a cuffed sleeve to seal the entry of a cable to a repeater housing, load coil, or other pressurized case, bridging the gap between the cable and the case snout, shown in Figure 18. Preliminary tests show extremely good leak seals being obtained, and a simple, easy to learn application practically eliminates the risk of damage to cable or housing. The system could also allow the prestretched tube to act as a mold for the pour of a cable stub block and seal to the case. A separately poured or molded end^{7,8} might have other advantages: If a stub is separately plugged from the apparatus case, then inventories of combinations can be reduced. Leak prevention of cable plug and case to plug become separately detectable and correctable. Stubs can be inserted to respond to service orders in a short time, rather than being built to maintain a large inventory.

TORQUE PRESTRESS

A cover to produce torque prestress is formed if the elastic sleeve is mounted on its core in a torqued condition. When applied, this tube will give a torque load to the connector or joint under it, just as it gives a continuing shrink force which provides an environmental seal. This torque action can be used to prevent vibration or thermal loosening of lock nuts and rings on connectors, and prevent the problems of unlatching of bayonet and twist-to-lock plugs and sockets. Cable twist from coilup or reel spill has inspired designs of locks and seals^{9,10} to insure the integrity of these connectors. Figure 19 shows how a torque prestretched tube satisfies

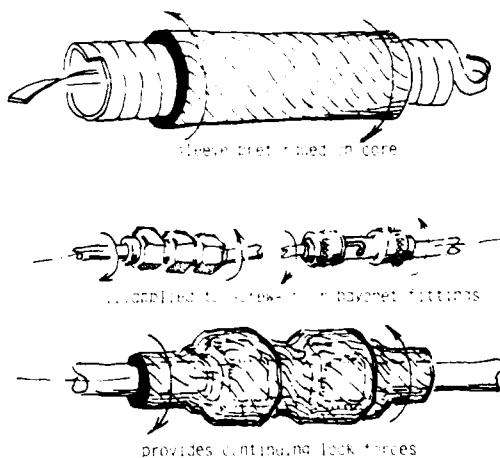


Figure 19. TORQUE PRESTRESS TUBE

both the unlatching problem and also seals the entire assembly from cable to cable, including the cord grommeting as well as the plug/socket interface.

CONCLUSION

A history of past service in rigorous power cable uses has recently been extended to a variety of communications connectors, splices, and case entries. New product forms and abilities show promise of even broader future use. The simple dependable action of prestretched tubes to seal onto cables and connectors of many types makes them particularly valuable in a wide spectrum of environmental situations. Recent interest in CATV and similar coaxial cable connector protection indicates that optical and other emerging communications systems may find additional matches of their unique properties with exacting system requirements.

ACKNOWLEDGEMENT

We are indebted to J.B.Baldasty and F.M.Miller of Western Electric Purchased Products Engineering, and J.H.Ball, H.Dinh, F.M.Farrell, D.R.Goff, J.R.Miller, R.L.Pannemann, P.R.Schaetzel, and many others of 3M for their contributions making this paper possible.

REFERENCES

1. Moisson, M. "The Use of Test & Field Data in Designing Splice Closures" Figs 9,10 p.144 Int'l Wire & Cable Symp Proc. 1980.
2. Sievert, J.A. U.S.Patent 3,515,798, Jun 2, 1970
3. Lenk, R.S. "Deformation in the Solid State - Large Stress" Ch 15 in Polymer Rheology, Appl. Sci. Publ, London, 1978 ISBN: 0-85334-765-4 "Cyclic Stress" Ch 16, Ibid.
4. Pohrt, J. "Critical Strain" Ch 17-20, in Lenk, R.S., Ibid.
5. Large, S.F. "Splicing Techniques for Tactical Optical Fiber Systems" pp 223-5 Int'l Wire & Cable Symp Proc. 1980.
6. "Electromechanical Compatibility Test" Mfg Std 17000 Sect 1241, Lead Acid Battery Use, W.E.
7. Charlebois, L.J. U.S.Patent 4,322,573 March 30, 1982.
8. Ibid, & Huszarik, F.A. "Low Pressure Molding for Encapsulation of Cable Splices" Int'l Wire & Cable Symp. Proc. 1980.
9. D'Amato, M.J. U.S.Patent 4,241,969 Dec 30, 1980
10. Hoffman, E.G. U.S.Patent 4,274,692 Jun 23, 1981



Roder H. Keith is a Senior Product Development Specialist with Elform Products Division/3M Laboratories, in St.Paul, Minn. He received a B.S.C.E. degree from U.of Dayton in 1954 and did graduate work at U.of Cincinnati, receiving his Ohio P.E. in 1962. He performed aerospace materials testing and apparatus design with U.Dayton Research Institute before coming to 3M in 1970, where he has developed new product concepts and materials for Industrial Specialties, Structural Products, and TelComm Division of 3M. He is registered in Ohio and Minnesota, and a past chairman of the Dayton sections of ISA and AIChE, and the Twin City AIChE.

APPENDIX

SLEEVE STRETCH DATA PROGRAM for TI-59 Programmable + PC-100C:

Program assumes incompressible elastomer sleeve (density does not change with stretch.) XL+ and RS entered as x t and B' represent known value of length change at a given stretch ratio for the sleeve material, and are entered as data. RS is printed out as "calculations" as the particular stretch ratio for the given diameters entered as data. Any consistent units may be used.

KEY	SYMBOL	FUNCTION	Rnn location
A	ID R	ID relaxed	01
	OD R	OD relaxed	11
B	T R	T wall, relaxed	02
C	L R	Length, relaxed	03
D	R L	Length ratio = LS/LR	09
E	DATA	Initiate	
A'	ID S	ID stretched	06
	OD S	OD stretched	12
	T S	T wall, stretched	13
B'	XL+	% length increase	07
x t	R S	Stretch Ratio LS/LR	10
C'	L S	Length, stretched	08
D'	R S	Diameter Ratio IDS/IDR	04
E'	CALC	Calculate	
		Input RS known	t
RST R/S		Fix Digits	00
		not used	05

Flags on the data entry will automatically cue the proper calculations for the data entered. The program will always calculate ODR, ODS, TS, & LR. It will also calculate:

1) RD & LR:

To Initiate: enter fix digit and press **RST R/S** or press **E**
to initiate with automatic Fix 4.
Prints fix digit n as "PST n PLCS DATA"

Data: enter ID R, press A ID S, A' T R, B
L S, C %L+, x L R S, B'

To Calculate: Press **E'** Prints RD, ODR, RL, LR, ODS, TS.

2) ID S, LS:

To Initiate: as above

Data: enter ID R, press A R D, D' L R, C
T R, B %L+, x L R S, B'

To calculate: Press **E'** Prints IDS, ODR, RL LS, ODS, TS.

LABELS	047 06 6	123 05 5
004 99 PPT	048 69 DP	124 04 04
012 11 A	049 04 04	125 43 PCL
092 16 A'	050 43 PCL	126 02 02
114 12 B	051 00 00	127 71 SBP
131 17 B'	052 69 DP	128 99 PPT
178 42 STO	053 06 06	129 92 PTN
189 12 C	054 69 DP	130 76 LBL
198 19 C'	055 00 00	131 17 B'
207 14 D	056 98 ADV	132 42 STO
224 19 D'	057 01 1	133 10 10
243 15 E	058 06 6	134 32 INT
247 10 E'	059 01 1	135 42 STO
258 87 IFF	060 02 2	136 07 07
266 35 L L	061 03 3	137 76 LBL
246 28 SIN	062 07 7	138 42 STO
256 39 COS	063 01 1	139 06 6
415 28 LOG	064 03 3	140 01 1
429 86 STF	065 69 DP	141 02 2
443 24 CE	066 01 01	142 07 7
MODE 23 LINE	067 69 DP	143 04 4
EFFOPR FLASH	068 05 05	144 07 7
	069 00 0	145 06 6
	070 92 PTN	146 03 3
	071 76 LBL	147 69 DP
	072 11 A	148 04 04
PROGRAM	073 42 STO	149 43 PCL
479.59	074 01 01	150 07 07
000 61 GTO	075 02 2	151 71 SBP
001 00 00	076 04 4	152 99 PPT
002 13 13	077 01 1	153 03 3
003 76 LBL	078 06 6	154 05 5
004 99 PPT	079 00 0	155 00 0
005 58 F10	080 00 0	156 00 0
006 40 IND	081 03 3	157 03 3
007 00 00	082 05 5	158 06 6
008 69 DP	083 69 DP	159 69 DP
009 06 06	084 04 04	160 04 04
010 22 INV	085 43 PCL	161 43 PCL
011 58 F10	086 01 01	162 10 10
012 92 PTN	087 71 SBP	163 71 SBP
013 47 CMC	088 99 PPT	164 99 PPT
014 42 STO	089 86 STF	165 86 STF
015 00 00	090 00 00	166 01 01
016 01 1	091 92 PTN	167 92 PTN
017 05 5	092 76 LBL	168 76 LBL
018 42 STO	093 16 A'	169 16 A'
019 07 07	094 42 STO	170 42 STO
020 01 1	095 06 6	171 03 03
021 93 3	096 02 2	172 02 2
022 05 5	097 04 4	173 07 7
023 42 STO	098 01 1	174 00 0
024 10 10	099 06 6	175 00 0
025 01 1	100 00 0	176 02 2
026 42 STO	101 00 0	177 05 5
027 09 09	102 03 3	178 69 DP
028 69 DP	103 06 6	179 04 04
029 00 00	104 69 DP	180 43 PCL
030 02 2	105 04 04	181 02 02
031 03 3	106 43 PCL	182 71 SBP
032 03 3	107 06 06	183 99 PPT
033 06 6	108 71 SBP	184 86 STF
034 02 2	109 99 PPT	185 04 04
035 07 7	110 86 STF	186 92 PTN
036 69 DP	111 02 02	187 76 LBL
037 01 01	112 92 PTN	188 16 A'
038 69 DP	113 76 LBL	189 42 STO
039 05 05	114 12 P	190 08 08
040 03 3	115 42 STO	191 02 2
041 03 3	116 02 02	192 07 7
042 02 2	117 02 2	193 00 0
043 07 7	118 00 0	194 00 0
044 01 1	119 00 0	195 00 0
045 05 5	120 00 0	196 11 11
046 03 3	121 02 2	

197 69 DP	247 03 3	297 01 2
198 04 04	248 02 2	298 95 5
199 43 PCL	249 01 1	299 42 STO
200 03 03	250 06 6	300 12 12
201 71 SBP	251 00 0	301 03 3
202 99 PPT	252 00 0	302 07 7
203 86 STF	253 01 1	303 00 0
204 05 05	254 05 5	304 00 0
205 92 PTN	255 69 DP	305 02 2
206 76 LBL	256 04 04	306 69 DP
207 14 D	257 43 PCL	307 04 04
208 42 STO	258 11 11	308 43 PCL
209 04 04	259 71 SBP	309 12 12
210 02 2	260 99 PPT	310 71 SBP
211 05 5	261 43 PCL	311 49 PPT
212 00 0	262 07 07	312 91 F 1
213 00 0	263 55 5	313 76 LBL
214 02 2	264 01 1	314 28 LOG
215 07 7	265 00 0	315 87 IFF
216 69 DP	266 02 2	316 02 02
217 04 04	267 95 5	317 27 LNO
218 43 PCL	268 55 5	318 43 PCL
219 04 04	269 19 19	319 06 06
220 71 SBP	270 43 PCL	320 06 06
221 99 PPT	271 10 10	321 95 5
222 86 STF	272 42 STO	322 43 PCL
223 76 LBL	273 01 1	323 01 01
224 16 A'	274 54 54	324 95 5
225 42 STO	275 15 15	325 19 D'
226 09 09	276 01 1	326 61 GTO
227 03 3	277 43 PCL	327 15 15
228 05 5	278 12 12	328 76 LBL
229 99 PPT	279 75 75	329 87 IFF
230 60 0	280 01 1	330 05 05
231 00 0	281 54 54	331 24 CE
232 01 1	282 95 5	332 43 PCL
233 06 6	283 15 15	333 07 07
234 43 PCL	284 01 1	334 95 5
235 09 09	285 45 45	335 43 PCL
236 71 SBP	286 15 15	336 04 04
237 99 PPT	287 14 D	337 95 5
238 86 STF	288 87 IFF	338 19 C'
239 03 03	289 04 04	339 61 GTO
240 02 02	290 92 STF	340 43 PCL
241 92 PTN	291 87 IFF	341 04 CE
242 76 LBL	292 05 05	342 24 CE
243 15 E	293 510	343 43 PCL
244 04 4	294 31 P 5	344 06 06
245 81 PBT	295 76 LBL	345 95 5
246 76 LBL	296 12 SIN	346 43 PCL
247 10 E'	297 43 PCL	347 02 02
248 22 INV	298 08 08	348 02 02
249 87 IFF	299 55 5	349 95 5
250 00 00	300 43 PCL	350 61 GTO
251 23 LNO	301 04 04	351 14 D
252 87 IFF	302 95 5	
253 01 01	303 13 13	
254 87 IFF	304 76 LBL	
255 71 SBP	305 29 COS	
256 42 STO	306 43 PCL	
257 76 LBL	307 11 11	
258 87 IFF	308 12 12	
259 98 ADV	309 56 56	
260 00 0	310 43 PCL	
261 69 DP	311 01 01	
262 04 04	312 12 12	
263 01 1	313 95 5	
264 05 5	314 43 PCL	
265 01 1	315 03 03	
266 02 2	316 55 5	
267 02 2	317 43 PCL	
268 07 7	318 08 08	
269 01 1	319 08 08	
270 05 5	320 85 85	
271 69 DP	321 43 PCL	
272 01 01	322 06 06	
273 69 DP	323 12 12	
274 05 05	324 95 5	
275 87 IFF	325 14 D	
276 02 02	326 42 STO	
277 28 LOG	327 12 12	
278 43 PCL	328 03 03	
279 01 01	329 02 2	
280 65 65	330 01 1	
281 43 PCL	331 06 6	
282 09 09	332 00 0	
283 95 95	333 00 0	
284 16 A'	334 01 1	
285 76 LBL	335 06 6	
286 35 10	336 04 04	
287 43 PCL	337 04 04	
288 01 01	338 43 PCL	
289 95 95	339 12 12	
290 02 2	340 71 SBP	
291 43 PCL	341 99 PPT	
292 15 15	342 15 15	
293 02 02	343 43 PCL	
294 95 95	344 56 56	
295 42 STO	345 55 55	
296 11 11		

PRESSURE BLOCKING OF FILLED CABLE

Richard J. Pokorny
George W. Frost

3M/TelComm Div.
St. Paul, Minnesota

Abstract

Polyurethane adhesion to filled cable conductor insulation has been extensively studied in our Laboratories. As a result of these investigations, a novel proprietary resin has been developed which has excellent adhesion to grease contaminated conductor insulation. Our studies have also been concerned with the application of this resin to a factory and field method for pressure blocking filled cable. During the course of developing a filled cable pressure blocking technique some potential sources of air leakage were discovered which appear to be inherent in the basic cable construction. These findings have contributed to the development of a suitable method for blocking filled cable.

Introduction

Plastic insulated cable filled with a waterproof compound was introduced to the telephone network in 1968 as a means of minimizing water problems in buried applications. It has proved to be effective, and today virtually all new buried construction uses filled cable.

The petroleum jelly compounds used for filling cable have, however, caused problems such as craft objections to working with sticky substances, difficult cable handling in cold weather due to cable stiffness and increased cable size and weight. These problems have been resolved to acceptable levels through design and material improvements and new operating procedures. However, an effective method of pressure blocking filled cable has not been developed, primarily due to the inadequate adhesion of present blocking compounds to grease contaminated conductor insulation.

Pressure blocks in filled cable are necessary at transition points between pressurized and filled cables, especially when pulp insulation is present because cable filling compounds and pulp insulation are not compatible. Pressure blocks in filled cable are also necessary on filled cable stubs between cross connecting terminals and pressurized feeder and distribution cables. The present common practice for providing these pressure blocks is to install a short preblocked section of air-core plastic insulated cable. This practice imposes the economic penalties of an additional splice in addition to the inventory costs inherent in maintaining a stock of plugged cable stubs in all necessary cable sizes.

This paper describes the development work that has been done to date in the search for a cost effective method of pressure blocking filled cable. Included in this effort is the development of a unique new polyurethane compound that exhibits significantly improved adhesion to grease contaminated plastic insulation and application techniques that have achieved excellent pressure blocking performance and are adaptable to field and factory practices.

Pneumatic Characteristics of Filled Cables

Laboratory tests have confirmed that there is a need for a block on filled cable since air will eventually leak down filled cable. For example, a 1200 pair, 46 meter filled cable was placed under 0.7 kg/cm² air pressure at room temperature. Air leaked out the other end of this cable after 30 days. The air displaces the grease, works its way down the cable and produces a core leak.

Filled cable also has another possible leak path, between the conductor and its insulation. Cable fillers do increase the weight and diameter of polyethylene insulation on aging.^{1,2,3,4,5} This swelling loosens the insulation on the copper conductor and creates an air gap at the conductor/insulation interface. Since air can enter this gap at the cut ends of wires in a splice or through pin holes in the insulation, this will often produce an air leak in a pressure dam. This leak path is unavoidable. Since the encapsulating compound has no access to the conductor, it cannot block this leak.

In order to determine what effect cable fillers have on air leakage between the conductor and insulation, 19 AWG PIC insulated conductors were immersed in cable filler at 70°C. After three weeks, air flow was observed between the conductor and insulation. Control samples that had not been immersed in grease exhibited no leakage. The consequence of this leakage down the conductors is a air leakage path that is not a factor in PIC or pulp cable blocks.

Further investigation of this air path was performed by making core blocks on various filled cables. These blocks were constructed near the cable ends with the blocking compound surrounding the insulated conductors and with the conductor ends protruding from the blocking compound. Air pressure at 0.7 kg/cm² was then applied to the still exposed cut ends of the wires. After 50 cycles from -40°C to +60°C the air leakage between the conductors and insulation was measured. Initially, short lengths (2-3 m) were used. Most samples leaked at a rate less than 2 cc/min. (see Table I). One sample, a 400 pair, 22 AWG, greased filled, solid insulation cable had a very high leak rate (70 cc/min). A 15.2 m piece of this same type of cable was cycled and used to investigate the leak rate as a function of length. This cable was shortened by one meter increments, the corresponding leak rate determined, and the data plotted on semi-log paper (Figure 1). The data fits the equation: $\log(\text{conductor leak rate}) = 2.13 - 0.080 \times (\text{length in meters})$. A second 400 pair, 24 AWG, initially 12 meters long, cable from a different manufacturer produced a similar equation: $\log(\text{conductor leak rate}) = 1.19 - 0.063 \times (\text{length in meters})$. Both of these equations fit the data with a correlation coefficient of 0.99 and also have very similar slopes. These equations show essentially that the leak rate decreases rapidly (logarithmically) with conductor length. This result indicates that for long cable runs there will be a very low conductor/insulation leak rate.

A second experiment was performed to determine the effect of splice connectors on the air leakage along the conductor/insulation interface. The 400 pair, filled cable sample having the highest insulation leak was cut into three equal pieces. The end of the first cable section was terminated with modular connectors, the end of the second cable section was terminated with discrete connectors while the third cable section was left as a control with the cut wire ends exposed.

These samples were cycled 50 times from -40°C to +60°C and the leak rate measured. The data show that modular connectors decreased air flow by two thirds and discrete connectors reduced it by half in comparison with the control. These results indicate that in a normal splice air leakage by this mechanism will be significantly reduced.

In summary, even though it has been shown that cable filling compound swells polyethylene insulation and thereby creates a new leakage path, this is not a significant problem in blocking filled cable. The combined effects of pneumatic resistance over long runs of cable and the restriction by splice connectors act to diminish this leakage rate to a negligible value.

Blocking Compound Development

Conventional polyurethanes used in blocking communication cables are two-part materials. One part (the isocyanate) generally contains a prepolymer consisting of an aromatic or aliphatic isocyanate. The other part (the polyol) can consist of polyether, polyester, or polybutadiene polyols. Also there can be included in the formulation various plasticizers, fillers, and additives. The two parts are mixed together and injected into the block and react to form a thermosetting, crosslinked polyurethane resin.

Polyurethanes ordinarily have fairly low adhesion to polyethylene and even lower adhesion to grease-coated polyethylene surfaces. Resins formulated with an aliphatic hydrocarbon isocyanate and polyol have improved adhesion to polyethylene due to a lowered surface tension that provides better wetting. However, even this formulation technique will not produce a satisfactory level of adhesion to grease contaminated conductor insulation.

We discovered that the inclusion of long chain hydrocarbon, mono-functional alcohols in the resin formulation provides high

adhesion to filled cable insulation. These alcohols serve several purposes: First, since they are surfactants, they improve the ability of the polyurethane to wet out hydrocarbon greases and polyethylene. Secondly, they act as internal plasticizers which eliminate the need for common plasticizers that reduce adhesion by producing weak boundary layers on the surface of the resin. At the same time, since they are internal plasticizers, they improve the compound's physical strength (toughness).

A resin was formulated combining these features in one proprietary composition.⁶ This material has several physical properties which are important for pressure blocking filled cable:

1. Low viscosity (900 cps mixed) for good compound penetration into the core conductors.
2. High adhesion to grease-coated polyethylene insulation: almost an order of magnitude greater than standard polyurethane blocking compounds.
3. High modulus (175 kg/cm²) and high elongation (250%) for good resistance to air flow and high toughness.
4. Good hydrolytic stability (7 days, 100°C, 1.8% wt. gain).
5. Good dry heat aging (21 days, 115°C, 2.4% wt. loss).

This combination of properties (adhesion, strength, and stability) provides a compound with superior ability to block filled cable.

Even a resin with very high adhesion to filled cable may not be able to contend with all of the grease present in a block. In order to determine the extent of grease removal necessary to achieve a reliable pressure block and the effect of grease on the compound itself, different amounts of cable filling material were dissolved in the unreacted compound. Then insulated conductors from a filled cable, both cleaned and uncleaned, were encapsulated to a depth of 5 cm in the mixed, contaminated encapsulating resin. The results of pull out tests are given in Table II.

This compound retains its high adhesion to conductor insulation even in the presence of grease as can be seen by the 55 N adhesion to greasy wires versus 75 N for those degreased, a decrease of only about 25%. Even with this excellent adhesion, however, once the compound contains over 5% grease, adhesion to conductor insulation drops quickly. This decrease is due to the degree of solubility of grease in the resin and the ultimate reduction in strength and adhesion of the resin due to plasticization by the

grease. Since grease concentration in actual field applications can easily reach these levels, it is necessary to separate the conductors sufficiently (as in a splice) or at least partially to clean the conductors of cable filling compound. Both of these methods reduce the percentage of grease in the compound and thereby improve adhesion.

Filled Cable Studies

Degreasing

An investigation into the cleaning of filled cable was performed to better understand the controlling factors. A Baron and Blakeslee Model BH.220 vapor degreaser with 1,1,1-trichlorethane solvent was used for degreasing. Grease-filled and polymer-filled, 900 pair, 22 and 26 AWG cable were prepared by removing 1.25 m of sheath and tying off 25 pair groups. After cleaning, the insulated conductors were encapsulated to a depth of 5 cm. in the high adhesion resin. After curing, the wires were pulled to measure the degree of adhesion. Results were averaged over all samples. The high adhesion compound was compared to a common industry blocking compound.⁷ For cleaned wires the high adhesion compound yielded a pull out force of 45 N (with many wires breaking) while the reference compound yielded a pull out force of only 24 N. Therefore, the high adhesion compound offers better adhesion to both cleaned and uncleaned filled wire. It was also discovered that adhesion to cleaned, polymer-filled, foam skin wires (47 N) was better than for cleaned, grease-filled, solid insulation wires (36 N). Waiting one hour or 24 hours after degreasing had no effect on adhesion. Apparently, degreasing solvents are either not absorbed by the insulation or have no detrimental affect on adhesion. As might be expected, it took longer to completely degrease 22 AWG than 26 AWG cables (17 min. vs. 10.5 min.). Also, polymer-filled cable took somewhat longer to clean than grease-filled cable (15 min. vs. 12.5 min.). In summary, vapor degreasing is a quick and effective method of cleaning filled cable which removes the bulk of the filler and promotes adhesion to the insulated conductors.

Kit Studies

Using the information that was compiled during the laboratory studies a method was devised for blocking filled cable. All samples were tested by cycling 50 times from -40°C to +60°C under 0.7 kg/cm² air pressure. The initial design (Figure 2)

consisted of simple poured blocks, installed on the ends of several 400 and 900 pair vapor degreased cables. It was learned that poured blocks having less than 20 cm. of conductor coverage failed upon cycling while blocks with 30 cm. or more of coverage usually held. This is expected, since on vapor degreased 900 pair cable, grease extends out 5-10 cm. from the sheath opening. This grease cannot be removed by vapor degreasing, since it continues to flow out the cable as it is cleaned. Therefore, actual clean conductor coverage is reduced by this length so that a longer, initially cleaned conductor length is necessary to effect a successful block.

Additional blocking studies suggested that pressure on the resin during injection and curing might be beneficial in making a plug. In air core PIC or pulp cable, pressure helps to force the resin down the cable. In filled cable, however, this is not possible. To determine whether pressure affects blocking performance, uncleaned and vapor degreased cables were encapsulated with the high adhesion compound. Samples were pressurized at atmospheric pressure, and 1.0 kg/cm², 2 kg/cm², and 4 kg/cm² above atmospheric pressure while the resin cured. The results demonstrate that for both cleaned and uncleaned wires, pressure was beneficial although pressures above 1 kg/cm² increased the benefit only slightly. As a result of these findings, several blocks were constructed by applying pressure according to the methods diagrammed in Figure 3.

The first sample was a remake of the design shown in Figure 2 but with a pressure boot over the end. This allowed the application of 1 kg/cm² air pressure while the resin cured. After cycling this sample leaked rather badly (56 cm³/min). The failure mode of this sample appeared to be along the inside of the closure. This design will be investigated further. The second design (Figure 3 (A)) utilized an open sheath blocking kit with an end seal at the splice end. A tube was used to connect to the splice case. After cycling, this sample performed well by exhibiting only a 1 cm³/min. leak. The most recent design evaluated is diagrammed in Figure 3 (B). In this design the compound is wrapped in a sheath of plastic and overwrapped with vinyl and rubber tape. The tape provides constricting pressure as well as serves as an outer sheath. This method may be craft sensitive, however it has worked very well. So far, three samples have been cycled and all three had less than 1 cm³/min. air leak.

Conclusion

The development of a new polyurethane compound having high adhesion to filled cable conductor insulation has provided the ability to block filled cables. An air leak path between the conductor and insulation was discovered but has been found to be negligible in practical, long run situations. Vapor degreasing was studied and identified as a very effective cleaning method. Finally, methods were developed to block filled cable, samples of which have successfully gone through temperature cycling. These samples have core leaks below presently acceptable industry standards for air core PIC cable.

References

1. S. Verne, R.T. Puckowski, and J.M.R. Hagger, "Compatibility of Polyolefine Insulation and Hydrocarbon Fillers in Telephone Cable", Proceedings of 19th International Wire and Cable Symposium, 1970, pp. 280-287.
2. L.M. Molleda and E. Used, "Filled Cable for Aerial Installation", Proceedings of the 25th International Wire and Cable Symposium, 1976, pp. 158-173.
3. M. Tenzer and J.A. Olszewski, "Analysis of Long Term Stability of Expanded Insulations in Filled Cables", Proceedings of the 28th International Wire and Cable Symposium, 1979, pp. 244-253.
4. C. Gieniewski and L.L. Blyler, Jr., "Effects of Waterproofing Cable Fillers on Some Physical Properties of Polyethylene Cable Materials", Proceedings of the 30th International Wire and Cable Symposium, 1981, pp. 270-279.
5. R.D. Parker and R.W. Tarwater, "Analysis of the Long Term Performance of Expanded Insulation in Waterproof Cable", Proceedings of the 30th International Wire and Cable Symposium, 1981, pp. 280-285.
6. R. J. Pokorny, U.S. Patent 4,329,442.
7. F.M. Farrell, M. Filreis, J.D. Groves, and H.K. Kapell, "Economics and Performance considerations of Telephone Cable Plugging", Proceedings of 23rd International Wire and Cable Symposium, 1974, pp. 403-413.

Table I

Conductor/Insulation Leak Rates

	<u>Sample No.</u>					
	<u>1</u>	<u>2</u>	<u>3</u>	<u>4</u>	<u>5</u>	<u>6</u>
Manufacturer	<u>A</u>	<u>B</u>	<u>B</u>	<u>B</u>	<u>C</u>	<u>D</u>
Pair Count	400	400	400	400	900	900
Gauge (Awg)	22	26	22	26	22	22
Grease or Polymer Filled	G	G	G	P	G	G
Solid or Foam-Skin Insulation	S	F	F	F	S	S
Sample Length (m)	2	3	3	3	3	3
Conductor/Insulation Leak Rate cc/min. after 50 temperature cycles	68	1.6	1.3	0	0.1	0

Table II

Adhesion of Grease Contaminated Resin to Clean and Uncleaned Filled Cable

Grease in Resin	20% Modulus	Pullout Force of 22AWG Wires	
<u>% of Total Weight</u>		<u>Uncleaned</u>	<u>Cleaned</u>
0	175 kg/cm ²	55 N	75 N
5	135 kg/cm ²	45 N	75 N
10	100 kg/cm ²	25 N	55 N
20	65 kg/cm ²	15 N	30 N

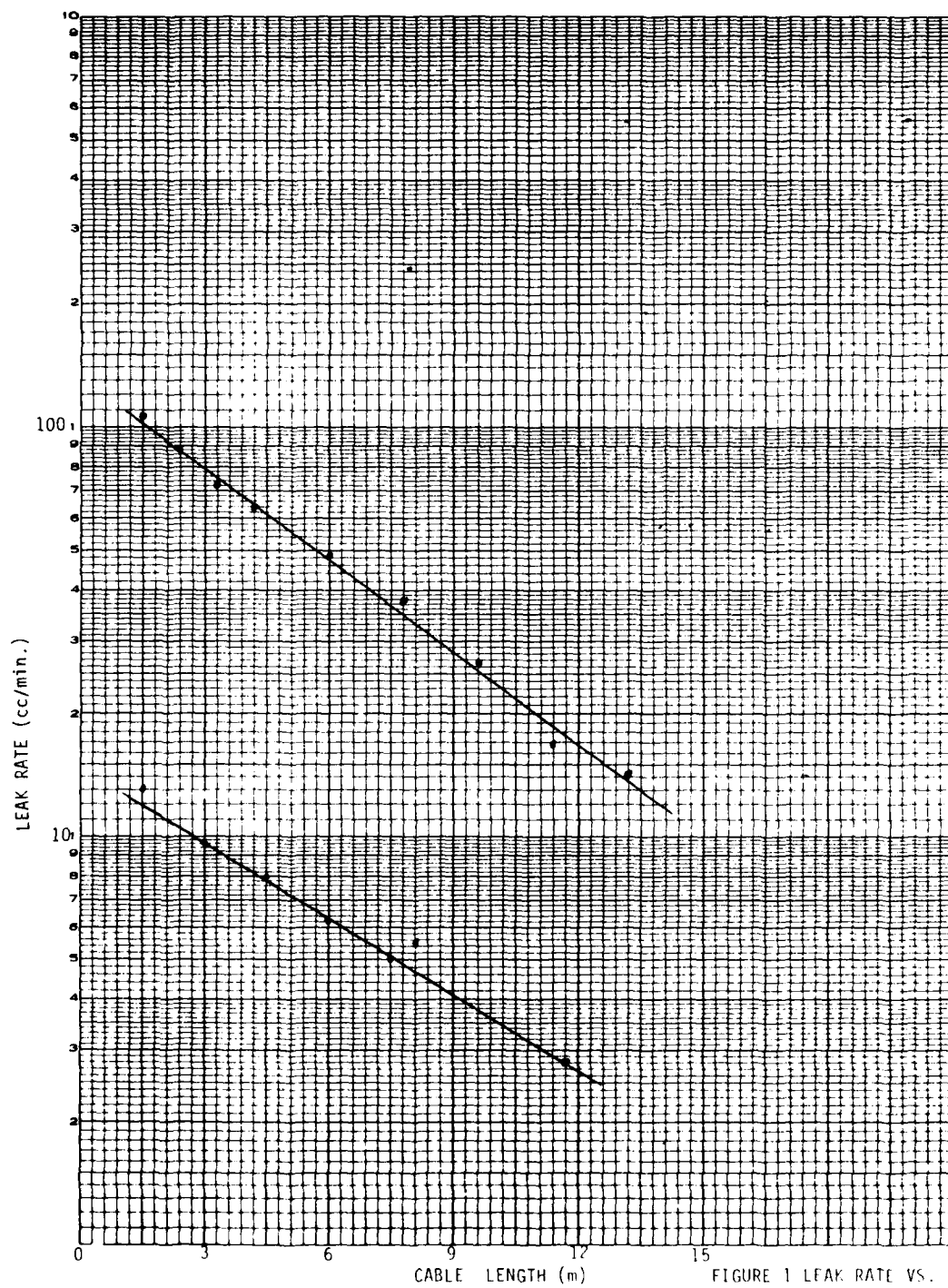
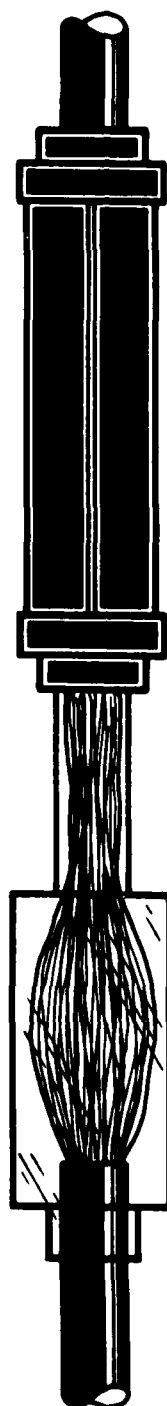


FIGURE 1 LEAK RATE VS.
CABLE LENGTH



SPLICE
CASE

TUBE

CLOSURE

FIGURE 2. BLOCKING KIT

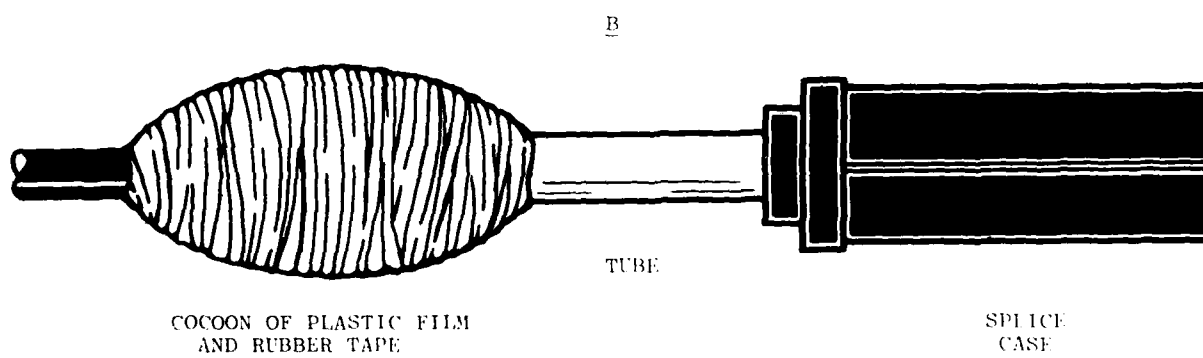
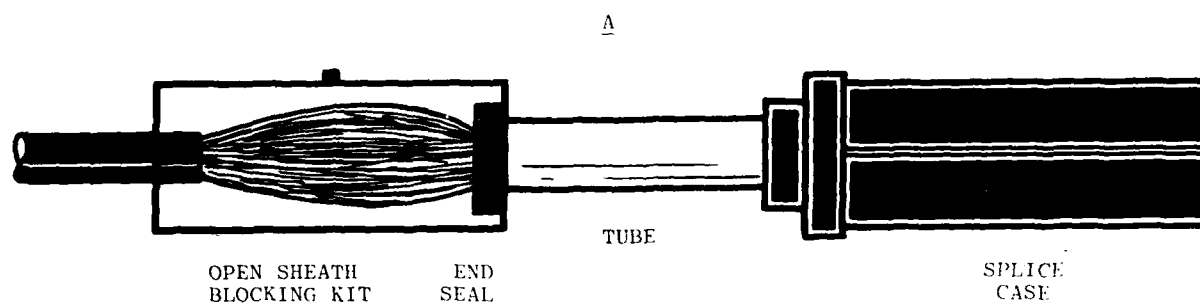


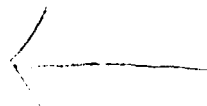
FIGURE 3. BLOCKING KITS



Richard J. Pokorny graduated from the University of Minnesota with a BS Chem degree in 1976. He joined 3M's analytical group and in 1978 transferred to TelComm Products Division. Since that time he has worked on encapsulating resins and coatings.



George W. Frost graduated from the University of Wisconsin in 1973 with a BS Chem degree. He came to 3M's Traffic Control Products Division and worked on reflective sheeting and pavement markings. In 1982 he joined TelComm Products Division and has been working on packaging film development and blocking cables.



SHIELD BONDING TERMINAL FOR BURIED SERVICE WIRE

by

David Lane
 Bob Young
 AMP Incorporated
 Winston-Salem, NC

Abstract

The rapid growth of buried service wire use in the telecommunications industry has increased the demand for a reliable, low cost means for splicing new or damaged buried service wire. Splicing kits of various types for this purpose have been available for several years. Each type has been subject to varying degrees of craftsman sensitivity at installation and reliable long term performance of the shield interface.

For the most part, until recently the shield bonding devices consisted of either a split bolt and nut arrangement or a screw secured clamping arrangement. Neither of these devices provided a satisfactory follow-up feature to compensate for long term creep of the plastic components within the cable.

This paper describes a unique stored energy clamping device which provides long term creep compensation. The device consists of two identical U-shaped spring steel pieces which fit and latch together hermaphroditically to apply and maintain spring force at four points for large area shield to shield interface. This shield bonding device is easily manufactured at low cost, can be installed without tools, is independent of craftsman sensitivity, and will accommodate the range of wire sizes most commonly used.

The initial and primary purpose for the development of this Shield Bonding Terminal was for use in the new buried service wire splice kit now in production. Subsequent testing of the Terminal indicated that it has significant additional potential for terminating the shield with either solid or braided copper grounding conductors.

Introduction

Widespread use of buried service wiring in the telephone industry in recent years has brought about a much higher demand for splicing apparatus. Splices are used in initial construction as well as in repairing damaged cables. A variety of commercial splices have been available for this purpose. Most of the available types had at least one undesirable characteristic such as poor long term shield bonding reliability, sensitivity to craftsman technique, and/or containing a two-part encapsulation sealant which is messy and difficult to properly apply.

A study of the various buried service splice problem areas revealed that the greatest need was for a low cost, easily applied cable shield bonding terminal with long term reliability. This study resulted in the development of a splice that meets this need and various other needs of the industry.

The new splice is less dependent on craft skill, has self-contained one-part sealant, and provide long term, large interface area cable shield bonding capability.

In most of the previous splices, shield bonding was accomplished by means of a split bolt and nut or other screw secured clamping arrangement. Such screw secured devices depended upon the craftsman's feel for tightness and provided little or no follow-up feature to compensate for long term effects of temperature changes and creep of plastic components within the cable.

The new Bonding Terminal described in this paper is a unique stored energy clamping device. It is easily manufactured at low cost, can be installed without tools, and will accommodate the range of wire sizes most commonly used, including Bell 5-pair cable. Subsequent testing of this terminal revealed that it has significant additional potential for other termination applications.

Design Objectives

The initial goal was to design a radically new shield bonding terminal with the following parameters:

- One size to fit all commonly used cable sizes.
- Stored energy clamping to compensate for long term plastic creep.
- Positive grip to provide good strain relief.
- Easy to install without tools.
- Low cost.

Terminal Description

During development, several methods for engaging and latching the 2 piece Terminal were evaluated. The terminal concept in its final form is unique in its simplicity (Figure 1) and ease of application. It consists of two identical U-shaped

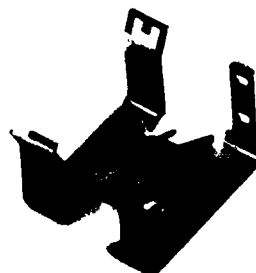


Figure 1. Clamp.

AD-A125 662

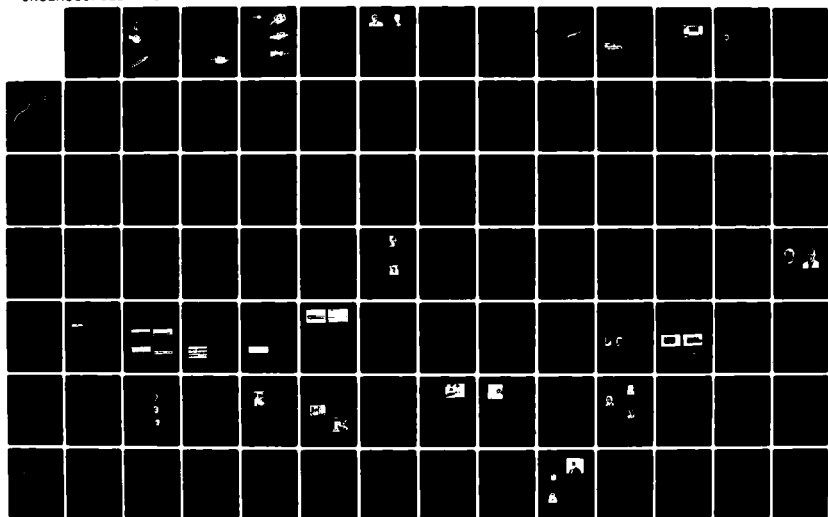
PROCEEDINGS OF THE INTERNATIONAL WIRE AND CABLE
SYMPOSIUM (31ST) HELD AT..(U) ARMY
COMMUNICATIONS-ELECTRONICS COMMAND FORT MONMOUTH NJ
NOV 82

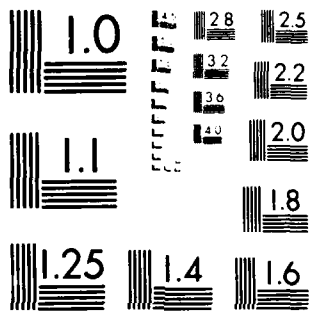
F/G 20/6

NL

4/6

UNCLASSIFIED





MICROCOPY RESOLUTION TEST CHART
NATIONAL BUREAU OF STANDARDS 1963-A

spring steel clips which fit and latch together hermaphroditically (Figure 2) to apply spring force at four points on the cable shields (Figure 3)



Figure 2. 2 Mated clamps.

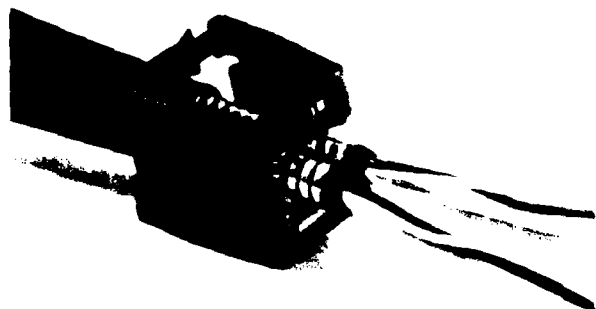


Figure 3. Mated clamps on end of cable.

The Terminal clips are stamped and formed in a progressive die from SAE number 1050 carbon steel strip. Figure 4 shows a progression sample in which can be seen the stamping and forming sequence and connecting carrier strip. The clips are heat treated by Austempering to Rockwell C hardness of 45-48 for the desired spring property. The clips are then zinc plated followed by a chromate conversion for long term corrosion protection.

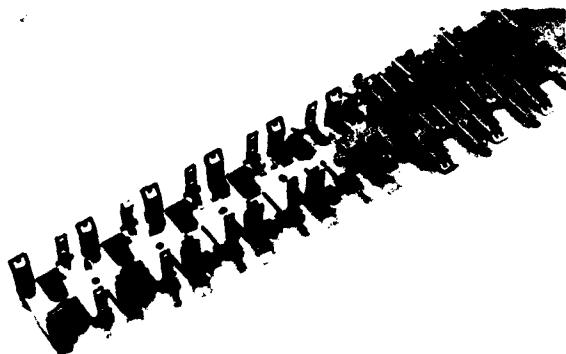


Figure 4. Stamping progression.

The clips can be applied without tools. This is accomplished by engaging the legs as shown in Figure 2 inserting the cable ends, and compressing the two clips together until the latches engage in the closed position as shown in Figure 3. Other than checking for 4-point latching, the craftsman has to make no other determination for proper tensioning. The Terminal can be easily removed by unlatching with a small or medium size screw driver or similar tool.

The primary function of the Terminal is to apply high spring force to a large shield interface area. The primary electrical contact is the direct shield to shield interface. The terminal clips themselves provide a secondary electrical path.

The clips apply the contact force through two cantilevered tongues on each clip. When two mated clips are compressed and latched onto the prepared cable ends (Figure 3), the directly opposed pairs of tongues contact the exposed shields and are deflected. Such deflection plus slight additional deflection of the clip body provide the stored energy to compensate for creep of the plastic components within the cable. This stored energy is adequate to insure the desired long term integrity of the shield bond. In addition, the Terminal provides positive strain relief for the cable splice.

Testing

Numerous tests were performed to determine the long term reliability and capability of the terminal as a bonding device. Two of the most significant tests and their results and two less significant tests are described here.

Current Carrying Capability

This test consisted of the application of DC current through the shield interface and measuring the temperature rise at the approximate center of the interface and on the shield away from the interface. The temperature was measured and recorded at both points at 5 second intervals throughout the test period. Figure 5 shows the testing arrangement.

The following two types of shields were tested:

1. Corrugated, 5 mil bronze shielded, 2 pair, 22 AWG cable;
2. Smooth, copolymer-coated 8 mil aluminum shielded, 2 pair, 24 AWG cable.

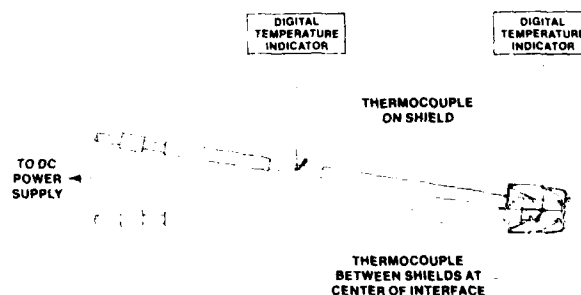


Figure 5. Test arrangement.

The testing current and time periods were as follows:

	Test No.	Current (amp)	Period (sec.)
Bronze shield	1	50	60
	2	100	60
	3	200	30
Aluminum shield	1	50	60
	2	100	30
	3	150	30

Test Results

Maximum temperature rise, °F:

	Test No.	On Shield	In Interface
Bronze shield	1	40.0°	23.4°
	2	147.7°	79.6°
	3	369.7°	153.6°
Aluminum shield	1	25.5°	35.2°
	2	68.0°	100.9°
	3	157.5°	190.5°

See Table 1 and Figures 6 and 7 for the recorded data and data plots.

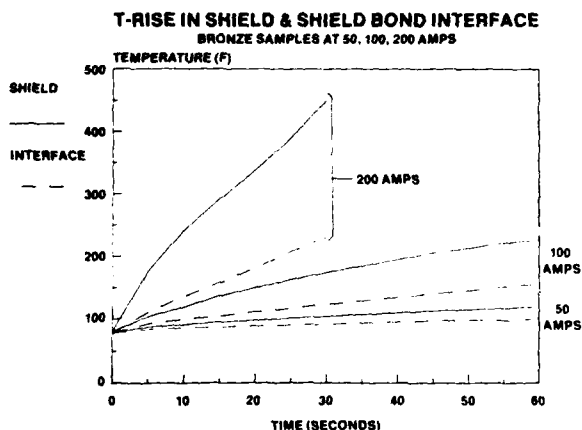


Figure 6. Temperature rise for bronze shield.

For the bronze shield, a comparison of the temperature rise on the shield and within the interface indicates that, for shields of this material, the shield interface has a greater current carrying capability than the shield itself. This is apparently the result of the large area of direct contact between the shields combined with the heat sinking provided by the clamp.

A comparison of the data for the aluminum shield shows that the temperature rise in the interface was somewhat greater than on the shield for the current levels and periods used in the tests. It is apparent from a closer study of the data that extrapolation indicates that for longer periods the temperature difference at the interface and on the shield would remain approximately constant.

The difference between the performance of the bronze and aluminum shield bonds appear to be the result of incom-

T-RISE IN SHIELD & SHIELD BOND INTERFACE ALUMINUM SAMPLES AT 50, 100, 150 AMPS

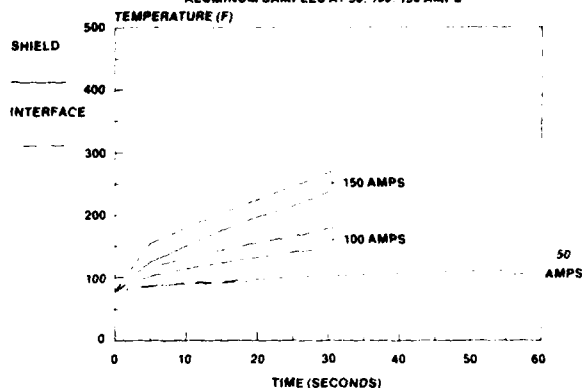


Figure 7. Temperature rise for aluminum shield.

plete removal of the copolymer material from the aluminum shield in the bonding area.

There was evidence of deterioration of the cable insulation during the higher temperature portions of the tests. The high shield temperature caused significant smoking, melting, and/or shrinking of the insulation. The shield bond remained intact and exhibited no evidence of deterioration throughout all tests.

Results of this testing indicate that the clamping device will maintain a secure bond during periods of high current exposure.

Large Conductor Splice Performance

Testing was done to determine the capability of the terminal for use as a clamp for splicing number 6 AWG solid copper grounding conductors. This test consisted of subjecting spliced conductors to a constant current of 1000 amps (DC) for 20 seconds or until failure occurred. Figure 8 shows a splice prepared for testing.

In all samples tested the splice remained intact throughout the test period, and in each case the conductor failed within 15 to 20 seconds, by melting and parting at one or more points away from the splice. Figure 9 is a photograph of a typical sample after testing. No damage to the terminal clips was apparent in any of the tested splices. The results indicate that the heat sinking characteristics of the terminal provided efficient cooling and protection of the splice integrity.

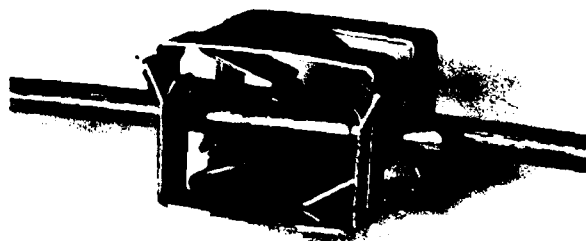


Figure 8. AWG #6 splice.



Figure 9. Tested sample of AWG #6 splice.

Other Testing

Tensile testing was performed to determine the pull force the splice would withstand before damage to the cable occurred. Bronze shielded 2 pair cable was used in this testing. It consisted of the application of a pull-out force of either one cable end or both cable ends with the splice housing restrained in a fixed position. The single cable ends withstood a force of 55 to 65 pounds before damage occurred. When both cable ends were pulled, a force of 85 to 95 pounds was required to cause damage.

Measurements of the connection resistance of the shield interface were made to evaluate the detrimental effect of environmental conditions. Completed splices were subjected to environmental tests such as thermal cycling, thermal cycling in high relative humidity, and water immersion. Comparison of connection measurements made before these tests with those made after the tests provided an indication of the degree of deterioration of the shield bond. The initial resistance measurements through the splice assembly averaged 5.7 milliohms with a range of 5.6 to 5.8 milliohms. After the environmental testing the resistance measurements average 5.9 milliohms with a range of 5.6 to 6.3 milliohms. A comparison of these before and after readings shows that the average resistance change was only .2 milliohms and a maximum change of .7 milliohms.

Applications

The Shield Bonding Terminal was designed and developed for use in the buried service wire splice for the telecommunications industry. The terminal concept has received considerable attention because of its simplicity, performance, ease of application, and low cost. Evaluation tests have proven that it will effectively and reliably perform not only its intended function but also perform other functions as well.

Examples of other applications for this terminal are as follows:

Figure 8 shows the terminal used for splicing number 6 AWG solid copper grounding conductors.

Figure 10 shows a method for branching or tapping number 6 AWG conductors.

Figure 11 shows an application in which the terminal is used to bond a cable shield to a number 6 AWG solid conductor.

Figure 12 shows that the terminal can be used to bond a cable shield to a braided grounding conductor.



Figure 10. Branching or tapping AWG #6 conductor.

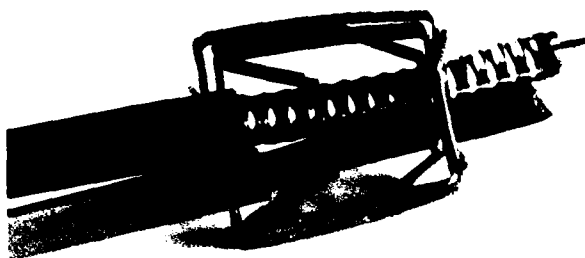


Figure 11. AWG #6 conductor bonded to shield.

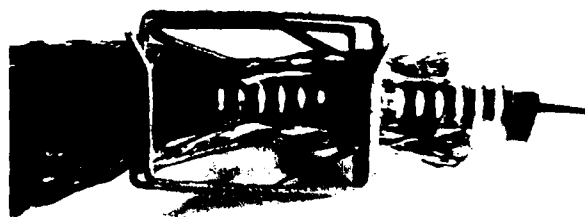


Figure 12. Braided GRD conductor bonded to shield.

**Table 1. High Current Test Measurements
Temperature Rise Data Summary**

BRONZE

Current =	Shield			Interface		
	50 Amps	100 Amps	200 Amps	50 Amps	100 Amps	200 Amps
Seconds = 0	80.0	80.3	80.3	78.2	77.3	77.5
5	87.3	104.0	176.5	83.8	92.4	111.1
10	91.0	119.3	241.5	85.7	99.3	135.7
15	95.3	137.0	291.0	87.4	105.3	158.3
20	98.0	150.3	337.5	88.9	111.8	182.0
25	101.5	163.0	389.5	90.5	117.3	206.9
30	104.3	174.5	450.0	92.1	123.2	231.1
35	107.0	185.0	—	93.8	128.8	—
40	110.0	195.3	—	95.2	134.4	—
45	113.0	206.0	—	96.9	140.2	—
50	115.5	213.8	—	98.5	145.7	—
55	117.5	222.0	—	98.0	151.5	—
60	120.8	228.0	—	101.6	156.9	—

ALUMINUM

Current =	50 Amps	100 Amps	150 Amps	50 Amps	100 Amps	150 Amps
	Amps	Amps	Amps	Amps	Amps	Amps
Seconds = 0	80.8	79.5	80.0	77.9	77.9	77.9
5	86.3	101.5	123.5	85.1	115.1	154.4
10	89.5	113.4	150.0	90.7	131.4	179.3
15	91.5	123.3	175.0	93.4	143.4	203.0
20	93.3	132.0	197.0	97.0	155.7	224.8
25	95.5	140.0	214.5	99.8	165.4	246.4
30	96.5	147.5	237.5	102.4	178.8	268.4
35	98.5	—	—	104.4	—	—
40	100.5	—	—	106.3	—	—
45	102.0	—	—	107.9	—	—
50	103.5	—	—	109.7	—	—
55	104.8	—	—	111.5	—	—
60	106.3	—	—	113.1	—	—

Temperature given in degrees Fahrenheit.

Table 1. High current test measurements.



Bob Young

AMP Telecom Division
3800 Reidsville Road
Winston-Salem, NC 27102

Bob Young is a Product Manager in the Telecom Division of AMP Products Corporation. He joined AMP Incorporated in 1968 in Field Sales and for the last ten (10) years has been involved in Sales and Marketing Outside Plant Products to the telephone industry. Prior to joining AMP, he was a Member of the Technical Staff of North American Rockwell Corporation.



David Lane

AMP Incorporated
3800 Reidsville Road
Winston-Salem, NC 27102

David Lane is a Product Development Engineer in the Communication Products Division of AMP Incorporated. He received his B.S. Degree in Mechanical Engineering in 1950 from North Carolina State University. Prior to joining AMP in 1978, he was a Member of the Technical Staff of Bell Laboratories, Incorporated for 25 years.

AD P000570

OUTDOOR CONNECTOR WITH ADVANCED WEATHER RESISTANCE

M. Meyerstein

Bell Northern Research, Ottawa, Canada

Abstract

A persistent problem for telephone operating companies has been low insulation resistance and noisy circuits in outdoor cross-connect terminals. This is due to impurities in condensed moisture which forms conductive bridges between nearby electrical contacts. In fact, a performance monitoring program of connectors in the outdoor environment showed that in periods of high humidity, 100 per cent of the contacts in a 25-pair connector can become noisy. So when, in 1979, a new connector system was introduced for in-building cross-connecting, special features were incorporated into the connector design with a view to outdoor operation. This paper describes these features and additional techniques which include filling the connector with a resilient gel, housing it in a moisture-shedding retainer and using a hydrophobic compound which is extruded over the cable wire ends. Reliability testing shows that the use of these features has produced an outdoor cross-connect system with exceptionally good weather resistance.

Introduction

The Outdoor Cross-connect Interface

Telephone signals are carried from central offices on cables (feeder cables) which usually have a large pair-count. At some point in the loop, they are connected to smaller cables (distribution cables) which serve individual areas within a community. In the past, the cables were connected together using permanent cable splices. In recent years however, due to increasing urban development and population mobility, the need has arisen for a system which facilitates frequent changes to the cross-connection arrangements. This has resulted in the introduction of the outdoor cross-connect interface, frequently referred to as the serving area interface (SAI) or jumper wire interface (JWI).

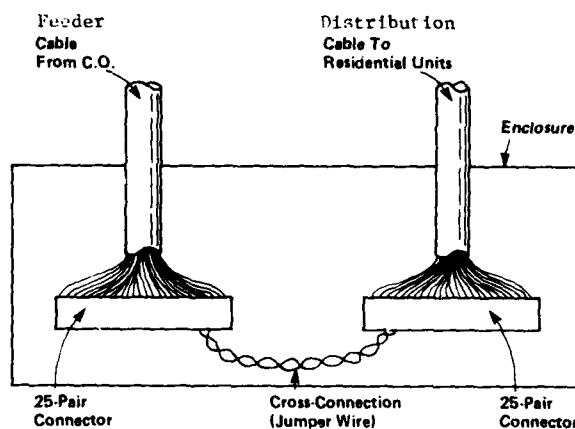


Figure 1
Schematic View of an Outdoor
Cross-connect Interface

As shown in Figure 1, the feeder cables from the central office are terminated onto 25-pair connector blocks. Distribution cables are terminated onto a separate bank of connectors, and the two are cross-connected by running removeable jumper wires between connectors. In this manner, spare distribution pairs can be provided for future use, but costly feeder pairs can be allocated as and when required.

Existing Products

Typical cross-connect terminals for SAI's fall into two categories; binding post and quick-clip. On a binding post connector, wires are connected to threaded posts by screw terminals. The wires must be stripped before connection can be made. In a quick-clip connector, special contact elements (Insulation Displacement Contacts) cut through the insulation and make contact with the conductors. Whilst both types have been on the market for some years, the latter is more compact and simpler to use than the former and is a more recent development.

Problems with Outdoor Cross-Connections

The Major Source of Trouble

Many telephone companies have experienced persistent problems concerning the reliability of outdoor connectors, and in 1978 Bell-Northern Research¹ undertook a program of connector performance monitoring in the field to determine the causes. The main source of trouble was found to be low insulation resistance (IR) between adjacent contacts on the connectors.

It has been determined that if the insulation resistance between tip and ring can be maintained above 100 megohms, then good telephone transmission is possible. If the IR falls to 1 megohm then the user will hear noise on the line and at 0.1 megohms or less, the line is unacceptably noisy, or even unserviceable. In an outdoor cross-connect interface this problem is caused by water which condenses onto the connectors. This water, containing dissolved impurities from the air and the surface of the connector, forms a conductive bridge which reduces the IR between adjacent terminals. The extent of the problem is influenced by the location of the installation, the environment inside the interface and, of course by the design of the connectors and the enclosure.

The Frequency of Trouble

The connector performance monitoring program included measurements of the frequency of occurrence of noise in various types of cross-connect interface from 1978 until 1982. Figure 2 shows the results for ground-mounted installations of standard design located in Ottawa.

Type of Connector	Sample Size (Pairs)	Percentage of Noisy Terminals				
		May 1979	June 1979	July 1979	Aug. 1979	Sept. 1979
Quick-clip	25	68	84	0	64	0
Binding post	24	29	50	0	12	0

Figure 2 (source: reference 2)
Percentage of Terminals Noisy for More than 15 Minutes, May to August 1979

As can be seen, a very large percentage of terminals, both binding post and quick-clip, became noisy at some time during the period shown in Figure 2. A noisy terminal is designated at one whose IR value falls below 100 megohms, as is explained above.

Figure 3, showing the accumulated hours of noise in three months on one 25-pair quick-clip connector and one 25-pair binding post connector, demonstrates the severity of this problem. The impact on the operating company, due to a large number of trouble calls from customers, would be highly significant during such periods.

Connector Type	Duration of Noisy Circuits, hours		
	July 1980	Aug. 1980	Sept. 1980
Binding Post 24 Pairs	2	2	12
Quick-clip 25 Pairs	25	25	0

Figure 3
Hours of Noisy Circuits, July to September 1980, Location: Ottawa

The Need for a New Approach

The conclusion reached was that the cabinets could not be expected to provide internal humidity control which was better than ambient. In fact it was frequently observed that environmental conditions caused perfectly sealed cabinets to have an internal environment which was worse than vented cabinets. This situation is exacerbated by small quantities of precipitation which enter the cabinets when the doors are opened, and then become sealed in when the doors are closed again.

The solution to the problem of noisy circuits caused by the situation described above is to build into the connectors themselves enough protection against condensation such that they would not be affected by such conditions as may prevail inside the cabinet. The cabinet would then be relied upon to provide physical protection and to shield the contents against rain and snow, etc.

It became obvious, therefore, that a connector system with a better resistance to condensed moisture would be a useful innovation in the field of Outside Plant.

The Solution: A New Connector

Designed for a High I R

In 1979 a new 25-pair connector was introduced³ for use on indoor cross-connect installations. Although it was initially used indoors, the requirements for future outdoor applications were taken into account by designing the connector to have an inherently high I R in an adverse environment.

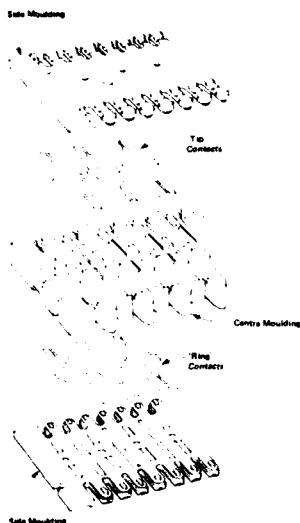


Figure 4
Exploded View of 25-pair Connector

Figure 4 shows some of the features which were designed into the connector. Firstly, the contact elements are separated by the plastic centre moulding; all of the upper contacts are tips and all of the lower contacts are rings. The connector is also designed to have a "quiet front" which has the advantage that there is no direct path between contacts across the surface of the connector. Lastly, each contact is separated from its neighbours by internal plastic ridges, ultrasonically welded to the opposite face of the connector. This configuration forms pockets in which the contacts are contained. All of these features act in concert to greatly lengthen the path which moisture must take in order to bridge between contacts, thus increasing the IR in a condensing atmosphere.

With this approach, therefore, action was taken at the design stage to combat the problem of noisy lines in outdoor cross-connect interfaces.

Enhanced Environmental Protection

In addition to designing the plastic body of the connector in the most effective manner, several additional features have been incorporated in order to further enhance its environmental protection, thus producing a connector system specifically intended for outdoor use.

Internal Protection: In order to prevent moisture from entering the connector or from reaching the contact interfaces, the connector is filled with a resilient, conformal gel.

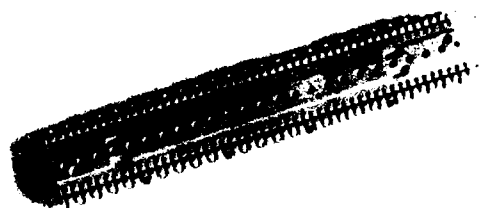


Figure 5
External View of Outdoor Connector

The gel is injected (by the manufacturer) into each of the 50 contact pockets. This ensures that each contact is completely encapsulated by the gel. The gel was chosen with several requirements in mind, including the resistance to thermal degradation, its chemical inertness, its high dielectric strength, its hydrophobic nature which causes moisture to bead on its surface rather than forming a continuous film, and its ability to remain soft at low temperatures. This ensures that the gel does not impede normal operations such as terminating wires, testing of circuits, etc. It also has a high resistance to migration, which is important for handling and using the connector.

External Protection: The connector is protected against the accumulation of water on its external surfaces by housing it in a plastic moulded retainer, as shown in Figures 6 and 7.

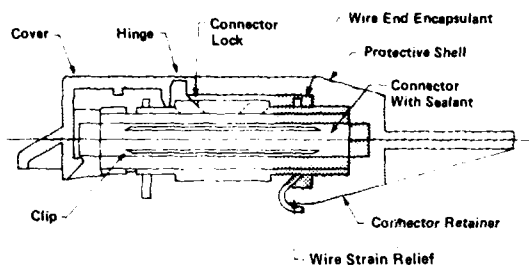


Figure 6
Cross-section through an Outdoor
Connector and Retainer

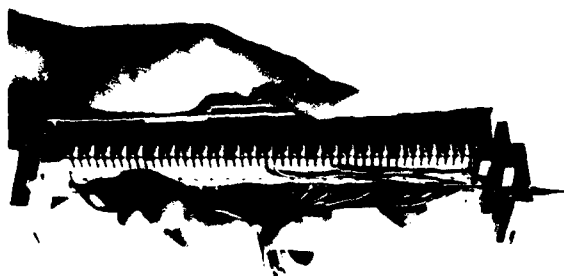


Figure 7
Connector/Retainer Assembly

The retainer is filled with an inert hydrophobic compound, which, when the connector is inserted into the retainer, extrudes over the cut ends of the cable wires and the surfaces of the connector in the base of the retainer. A flexible cover is provided which allows access to the front of the connector for the installation of jumper wires. This cover is moulded integrally with the body of the retainer, using a "living hinge" which eliminates the possibility of water leaking in through a hinge opening. The hinged cover is spring-loaded which solves the problem of

moisture ingress due to covers being left open.

Wire Arrangement: The wires enter the connector from underneath, so that moisture cannot run down them into the contacts, as happens with other connection systems where the wires enter from above. Also, it is impossible to have wires running from one contact over the top of other contacts, which would form an easy path for moisture to track across, causing low I R

The Results

Salt Fog Testing

Test Method: The proof of the pudding is in the eating, and so the effectiveness of the design features described above was verified by a program of reliability testing. A good test for simulating a life-cycle in a condensing environment is the ASTM B117 standard salt-fog test, in which fully wired connector assemblies are subjected to a mist of five per cent sodium chloride solution. This test has been augmented by energizing all tips and rings with a potential difference of 48 volts DC, which provides a more severe test condition than with non-energized contacts. Any condensation which occurs between contacts or wire-ends will, under these conditions, cause a rapid degradation of insulation resistance. The I R between each contact and all the others in the connector electrically joined together is measured periodically during the test, and any reading falling below 100 megohms is regarded as a failure.

The testing of I R between one contact and all the others together is a very severe test condition which detects low I R due to leakage from one contact to any others in the connector. This produces a potentially lower I R than that obtained merely by measuring between the tip and ring of each pair individually. This represents a very realistic situation where in the field, leakage or capacitive unbalance in the circuit can occur between any combination of contacts if water bridges them - not just the tip and ring of a pair.

Test Criteria:

Over a period of several years, using data from the connector performance monitoring program, a correlation was made between failure rates in the field and those in the salt-fog tests. It was found that one hour in the salt-fog chamber produced failure rates similar to one month in the field, for a large proportion of the environmental conditions encountered therein. Thus, a salt-fog test of 240 hours duration equates to a life in the field of 20 years.

Test Samples: Three types of connector were tested, two samples of each type being used. Production samples of a commercial binding post connector, a commercial quick-clip connector, and the new connector described in this paper were tested, all connectors being of the 25-pair modular variety. The connectors were all mounted in the salt-fog chamber and wired according to the manufacturer's recommended procedures, but they were not placed in a cabinet. With this setup, it was therefore possible to compare the environmental protection of the new connector with that of two existing types of connector.

Test Results

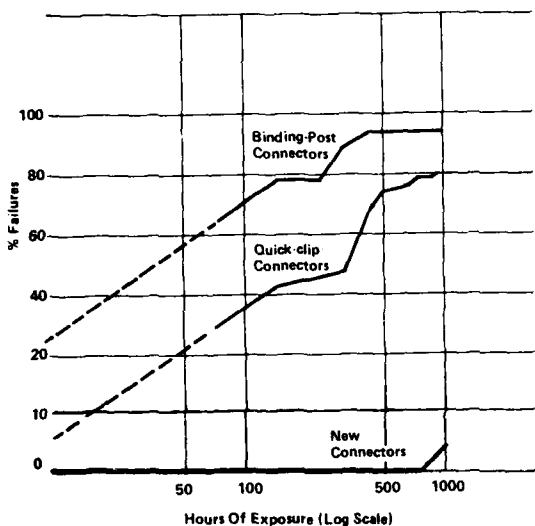


Figure 8

Percentage of Failed Contacts vs. Time of Exposure to Salt-fog. New Connector, Commercial Binding-Post and Commercial Quick-Clip

Figure 8 shows the results of the salt-fog test on the three types of connector. The results dramatically illustrate the improvement in reliability achieved by designing a connector which has an efficient system of environmental protection. The new connector obviously has a much greater life expectancy than the other types of connector which were tested along with it.

Other Tests

The reader should be aware that salt-fog testing was by no means the only form of testing to which the connector was subjected. In fact, a very comprehensive program of reliability testing was conducted on the connector and its associated hardware before the product was released onto the market. The program included such tests as thermal cycling, durability, heat-aging, and many other tests which are commonly used in the connector industry.

The Cabinets

Environmental Features

A family of cabinets has been designed as part of the new outdoor cross-connect system. These cabinets, ranging in size from 600 to 3000 pairs also have features designed into them to improve their environmental protection.

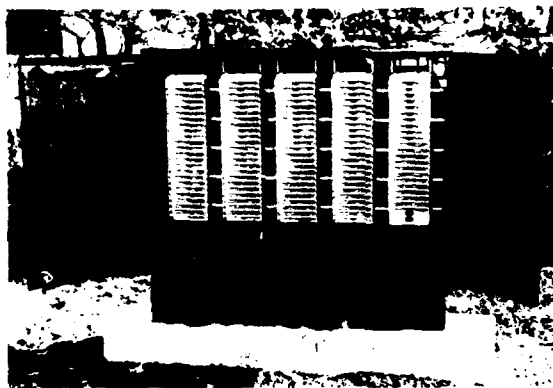


Figure 9

3000-pair Outdoor Cross-connect Cabinet

Figure 9 shows a 3000-pair ground-mounted cabinet with its doors open. The base is a separate structure, sealed off from the cabinet shell, thus preventing moist air from the ground or improperly sealed ducts from entering the cabinet and condensing therein. The cabinet also has a double-skinned top designed to reduce radiative heat loss at night, thereby reducing condensation inside the cabinet. The cabinet is well ventilated, in order to encourage a fresh supply of ambient air to flow through the cabinet, and to prevent the humidity from building up to condensation conditions, the vents being designed to resist the entry of snow and rainfall.

The contribution of these features is being assessed as part of BNR's connector performance monitoring program.

Conclusion

Northern Telecom has developed a new outdoor cross-connect system which has a highly efficient means of environmental protection. Tests indicate that the reliability of the system in a condensing environment greatly surpasses that achieved hitherto by other systems.

Production of this new system began in late 1981 and it was standardized by Bell Canada in early 1982. The system is currently undergoing field trials with several North American telephone companies.

References

- 1 "Connector Performance Monitoring in the Outdoor Cross-connect Environment", L.E. Martin, et al, I.W.C.S. Proceedings, 1980.
- 2 "Connector Performance Monitoring in the Outdoor Environment", J.D. Lee. Proceedings of the National Electronics Conference, 1981.
- 3 "New In-building Distribution Terminal Eases Installations", B.T. Osborne, Telephone Engineer and Management, August 15, 1980.
- 4 "The BIX Outdoor Cross Connect System", M. Meyerstein et al. Telesis magazine, to be published December 1982.



Michael V. Meyerstein
Bell-Northern Research
Ottawa, Canada

Michael Meyerstein, a native of Leicestershire, England, received his B.Eng. honours degree in mechanical engineering from the University of Liverpool in 1971. Since then he has worked on the development of electrical connectors and the thermal design of nuclear power reactors and computer disk drives. Since 1979 he has been a member of scientific staff at Bell-Northern Research, where he has been involved with the design of electrical connector systems.

AD P000571

A NEW CLAMP-ON TAP FOR COAXIAL DATA NETWORKS

by
James Fetterolf
AMP Incorporated
Harrisburg, PA

Abstract

This paper discusses the coaxial cable tapping requirements of local area networks and describes a new type of tap that meets these requirements. The new tap combines the reliability of rf connectors with the installation ease of a static probe tap. Interaction of the unique probes enable the tap to clamp onto unstripped cable eliminating the extensive installation time required by traditional coaxial connectors.

Typical applications of the tap are described and the relative advantages are explored for two methods of installation. The direct penetration method is quick and simple but is highly "cable-dependent" whereas the cable drilling technique produces a reliable tap over a wider variety of cables and introduces less capacitance loading.

Complete physical and electrical characteristics of the tap are presented with special attention to cable/tap compatibility. Data is presented demonstrating the effects of cable materials, design, and tolerances upon overall performance.

The equipment, procedure, and philosophy for a cable penetrability test is disclosed, and typical test results are presented.

Introduction

A local area network allows data-generating and data-receiving equipment to communicate over the data bus promoting distributed processing by permitting large and small computers, peripherals, and other intelligent equipment stations. A typical network, such as that illustrated in Figure 1, can contain up to 256 stations operating at speeds of 5 to 10 megabaud over a coaxial cable bus 1,000 feet long.

The growth of these networks brings the need for a fast and reliable means of tapping cable to add stations. Although traditional rf connectors, such as "N" Series, offer high performance (when carefully applied by a skilled technician) the cable must be cut to install them. Cutting the cable requires that the entire network must be shut down simply to add a station. To avoid loss of critical data, a shutdown requires scheduling with all network users.

In an effort to avoid disruptive shutdowns, static probe taps such as that shown in Figure 2 have been used. These taps use a single probe to make contact with the cable's center conductor. While the tap is easily applied and does not require the network be shut down, long-term reliability is a concern, especially considering the needs of data processing. The probe presses against one side of the center conductor. Since there is no mechanism (other than the tensile characteristics

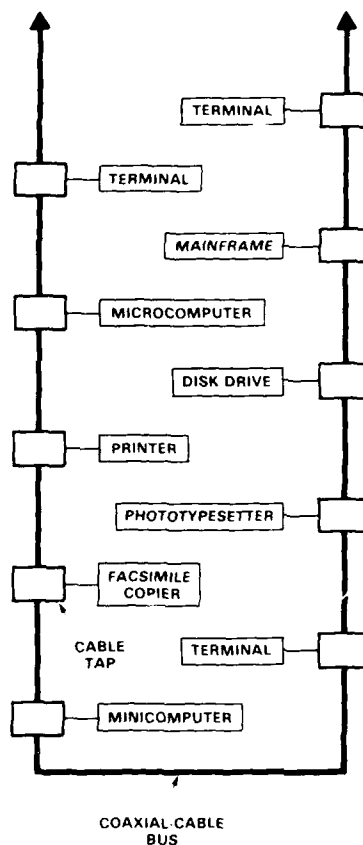


Figure 1 A typical local network.

of the wire) to hold the conductor against the probe, the conductor could eventually drift away from the probe resulting in intermittencies, or complete loss of contact.

A New Approach

Designed to meet the demand for a more reliable tap in CATV applications, the AMP Coaxial Tap has undergone a series of refinements during development to produce a new and more logical solution to the problem of reliably tapping coaxial cables. As indicated by Figure 3, this tap can be installed without cutting the cable. Some cables can be tapped with no preparation, while others require an additional step. In either case, the tap can be installed while the network is operating and total installation time is brief.

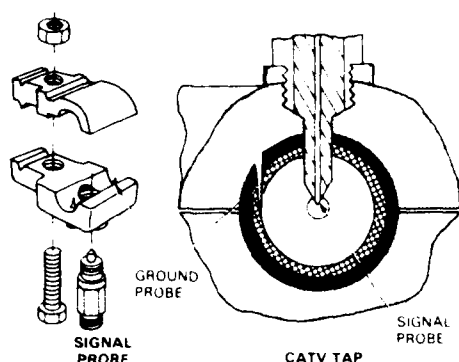


Figure 2. Static probe coaxial tap.

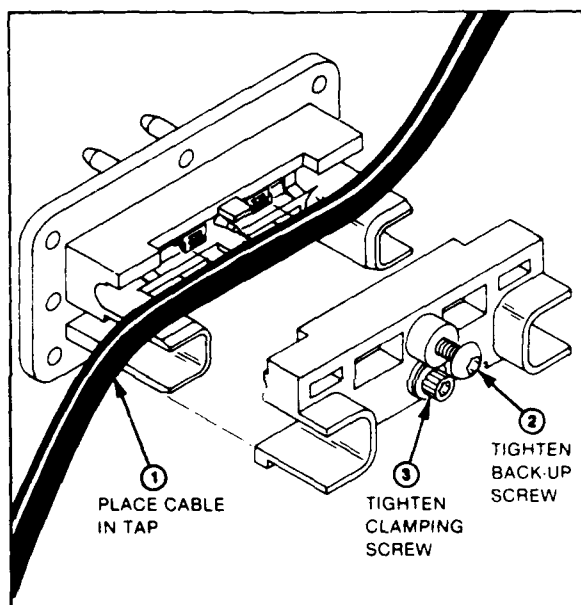


Figure 3. Installation of active probe coaxial tap assembly.

The two halves of the tap body locate the cable and grip the jacket to provide strain-relief.

The center conductor is captured between two probes as shown in Figure 4 to establish the signal connection.

Both probes are insulated and do not make electrical contact with the shield of the coaxial cable. The stationary probe achieves electrical contact to the center conductor, and the spring-loaded back up probe maintains the force for long-term reliability. The second spring-loaded probe overcomes the shortcoming of static probe taps, which use a single non-compliant probe and tends to push the center conductor deeper into the dielectric material. Both probes are designed to pierce the cable and forcefully trap the center conductor. A minimum amount of metal enters the cable, to minimize impedance discontinuities at the termination. Actual capacitive

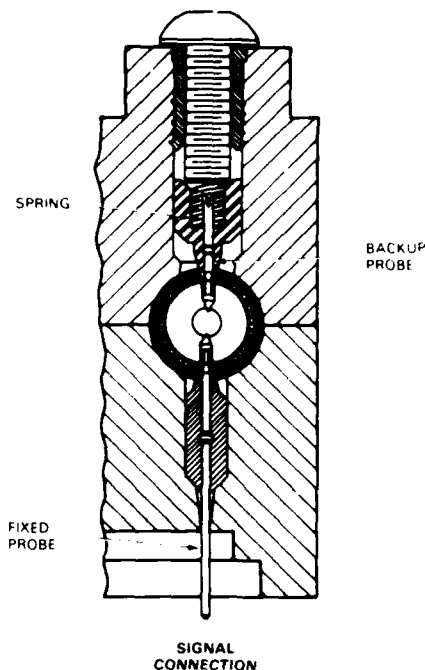


Figure 4. Active probe coaxial tap.

loading is less than 3 pF for undrilled cable and 2 pF for drilled cable.

Four pair of redundant ground probes pierce the cable jacket unassisted to establish the shield connection as shown in Figure 5. The cable curvature and plastic cavity design cause the permanent deformation necessary to "crimp" the braid strands between compliant prongs.

Two ground posts and a single post protrude into the PCB cavity in the tap. These posts allow simple removal of the transceiver module from the tap body without removal of the tap from the coaxial cable bus. A variety of standard disconnects are available to couple the PCB to the remote digital device.

The major electrical and mechanical specifications for the tap are listed in Table 0.

Table 0. Specifications for AMP Coaxial Tap

Operating Cable Voltage (max)	50 Vdc or $V_{ac_{rms}}$
Operating Tap Voltage (max)	600 Vdc or $V_{ac_{rms}}$
Capacitance (max)	3 pF (on drilled cable)
Contact Resistance (max)	50 m Ω
Contact Current Rating (max)	1 A
Insulation Resistance (min)	5 G Ω
Cable Retention (min)	150 lb
Cable Torque Resistance (min)	20 in.-lb
Operating Temperature	0 to 50°C
Storage Temperature	-30 to 80°C

In a system such as this, the cable serves as more than

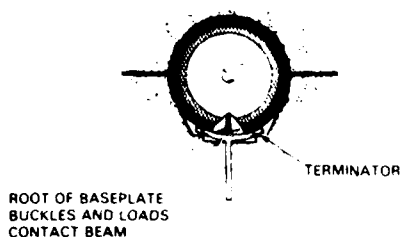


Figure 5. Shield connection.

the medium for data transmission; it also functions as an important part of the electrical and mechanical connection. To be used with the AMP Coaxial Tap, coaxial cables must meet the following material requirements:

Center Conductor — Solid annealed copper of the wire size required by the particular tap.

Dielectric: Plastic, such as polyethylene or Teflon® TFE or FEP.

Shield: Braid or foil, with up to four layers. The outer layer must be braided, tin-plated copper 32 through 36 AWG.

Jacket: Plastic. The outer diameter must be between 0.370 and 0.410 inch to ensure the cable will be firmly held by the tap.

Cable Compatibility

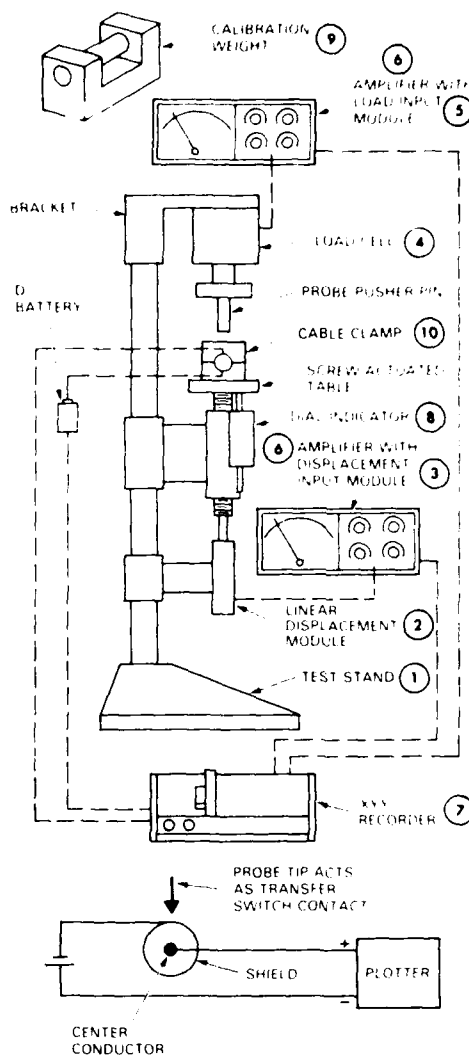
The AMP Coaxial Tap was initially designed for use with RG-8 cable. As EMI requirements became more stringent, network designers began demanding cables with better shielding performance. This resulted in the use of braid-foil, braid-foil-braid, and braid-foil-braid-foil combinations. As might be expected, some of these cables are better suited to direct penetration than others. A penetrability test was devised to determine which cable configurations could be reliably tapped by direct penetration.

Penetrability Testing

The penetrability test measures penetration force versus probe travel and indicates the presence (or absence) of shorts between the shield and center conductor providing a "signature analysis" of the sample cable for direct penetration tapping.

Figure 6 is a diagram of the test setup and a list of recommended equipment. The cable is placed in a special test fixture that simulates a tap. A single probe is in the top section of the fixture. The cable-clamp fixture rests on a linear displacement transducer; above the fixture is a pressure transducer used to measure penetration force of the probe. As the probe displaces the cable materials, an X-Y plotter graphs probe travel versus penetration force. It also plots an electrical circuit used to detect shorts through circuit continuity. The resulting graph is used to determine whether the tap can be applied without drilling the cable.

Figure 7 is a typical penetration-test graph. As the probe enters the cable and encounters the shield, the force increases. When the probe ruptures the shield, the force required drops until the probe reaches the center conductor, at



EQUIPMENT	MANUFACTURER AND MODEL
1 Test Stand	Hunter CTM
2 Linear Displacement Module	Daytronic DF 160
3 Displacement Input Module	Daytronic Type 70
4 Load Cell	Daytronic 152A (100 lb)
5 Load Input Module	Daytronic Type 71
6 Amplifiers (2)	Daytronic 300D
7 XY Recorder	Hewlett Packard 7046A
8 Dial Indicator	Federal DB15
9 Calibration Weights	
10 Cable Clamp	

Figure 6. Penetration test setup.

which time it increases again. The line across the top of the graph represents the electrical circuit. The circuit consists of a battery, cable, probe and plotter. The cable shield and center conductor are connected in series in the circuit. When the shield is shorted against the center conductor by the metal probe tip, the circuit to the plotter is connected; the line on the chart will show a sharp drop until the shunt is opened.

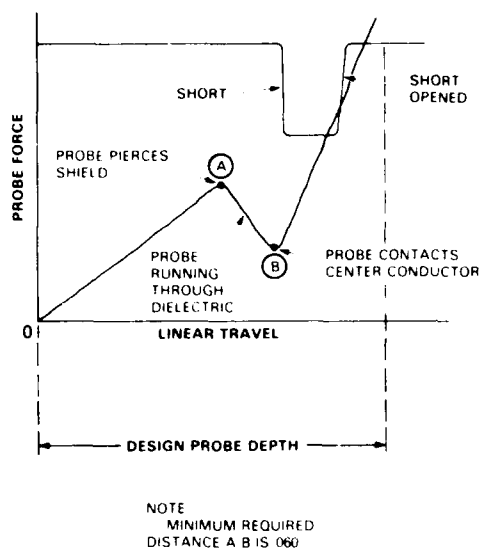


Figure 7. Graph for penetration test.

Typical penetration graphs, and representations of the condition responsible for them, are shown in Figure 8.

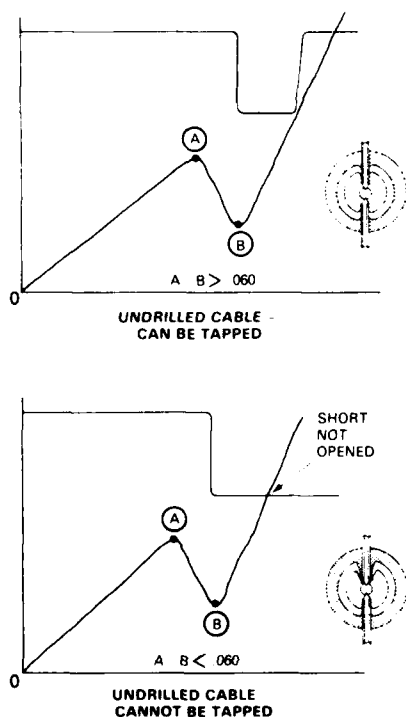


Figure 8. Typical penetration graphs.

Cable samples that can be consistently penetrated without sustained shorts indicate a cable that is suitable for direct

penetration. As a result of extensive penetrability testing the following general recommendations (Table X1) have been established.

Table X1. Cable Requirements for Direct Penetration

Cable part	Materials	Remarks
Conductor	Solid annealed copper	No plating required
Dielectric	Solid or foamed polyolefin (polyethylene, etc.) Solid or foamed fluoropolymer (Teflon*, etc.)	Foam plastics <i>cannot</i> be used if the cable has a double-layer shield (on 50-Ω cable).
Shield	Up to two layers — one braid and one foil Braid: tin-plated copper 32 through 36 AWG	Outer layer must be braid. Foil should have less than 10% elongation.
Jacket	Polyolefin, fluoropolymer, or polyvinyl chloride (PVC)	Outer diameter must be between .370 and .410 inch.

When a cable cannot be tapped satisfactorily by direct penetration, it is usually because parts of the shield are dragged inward by the probe to short against the center conductor. Even in instances where shorts do not occur, it is possible that deformation of the shield can be great enough to excessively increase capacitive loading by the tap. These restrictions significantly limit the number of coaxial cable types that can be used effectively with local area networks using this tap.

Since these conditions often exist with cables that offer the desired qualities of low capacitance and high shielding performance, and because of network designers' interest in a reliable tap that can be applied without interrupting the bus, an improved method of applying the tap was developed. This improved method includes drilling the shielding level of the cable with an insulated bit.

Drilling

Although drilling involves an extra operation in tapping a cable, it has several advantages. It maintains consistent capacitance values and eliminates the possibility of the probes dragging the shield inward to short against the center conductor. Drilled multi-braided cables present much less capacitive loading than undrilled cables — typically 2.0 pF versus 5 pF.

The tap is applied in two steps. First, a drilling fixture is placed on the cable. The fixture has two clamps that firmly hold the cable and prevent its twisting. A drill guide fits into the fixture and snaps over the cable. The guide has a drill hole in each side to guide the drill bit. A specially insulated bit is used; the insulation isolates the cable conductors from the drill motor and acts as a stop on the drilling depth. The purpose of drilling is to locally *remove the shield* to provide a clear path for the center-conductor probes. Figure 9 shows the drilling fixture.

After the cable is drilled, the plastic drill guide is removed from the cable and strap fixture. *The fixture is left on the cable.*

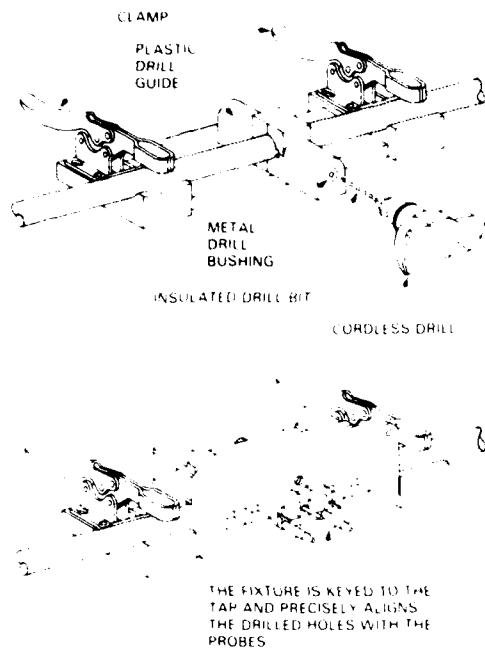


Figure 9. Drilling fixture.

The strap fixture is keyed to the tap. When the tap is placed on the fixture, the probes are precisely aligned with the drilled holes in the cable.

Completing the tap is simply a matter of tightening the same two screws that are used for direct penetration tapping and removing the drilling fixture. The probes and shield terminators establish electrical connections with a drilled cable in the same manner as they do with direct penetration. A penetration test performed on drilled cable yields the test results shown in Figure 10.

Typical tapping times are less than three minutes.

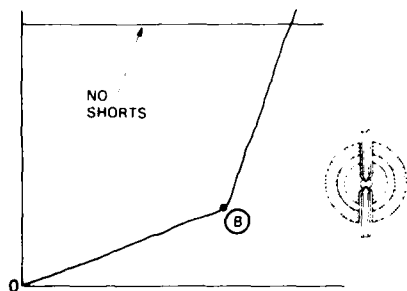


Figure 10. Penetration profile of drilled cable.

Concentricity

During penetrability testing, it became apparent that the results for many cable samples did not follow the patterns established by other samples with the same configurations.

Further investigation disclosed that this was caused by a lack of concentricity within the cable. Therefore, even if the cable meets the material requirements indicated in Table X1 performance with direct penetration cannot be assured unless penetrability tests are conducted using samples of the cable to be tapped.

An ideal coaxial cable is concentric, with all layers having a common axis. In a real cable, manufacturing tolerances introduce some eccentricity into the cable. For the tap to work properly, eccentricity must be within certain limits. For example, if the center conductor is sufficiently off center, the probes may bend or may completely miss the center conductor during tapping. Three equations have been devised to ensure that the cable falls within the eccentricity limits required by the tap. Figure 11 shows the eccentricity requirements.

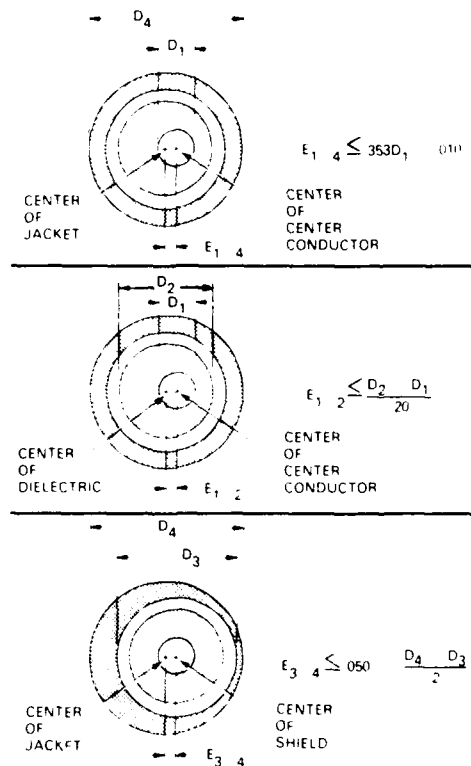


Figure 11. Cable eccentricity limits.

Center-Conductor-to-Jacket — The difference between the center of the center conductor and the center of the jacket must be less than or equal to the following:

$$E_{1-4} \leq .353 D_1 - .010''$$

where D_1 is the diameter of the center conductor.

Center-Conductor-to-Dielectric — The difference between the center of the center conductor and the center of the dielectric must be less than or equal to the following:

$$E_{1-2} \leq \frac{D_2 - D_1}{20}$$

where D_1 is the diameter of the center conductor and D_2 is the diameter of the dielectric.

Shield-to-Jacket — The difference between the center of the shield and the center of the jacket must be less than or equal to the following:

$$E_{3-4} \leq .050'' - \frac{D_4 - D_3}{2}$$

where D_3 is the outer diameter of the shield and D_4 is the diameter of the jacket.

An Example — The cable must meet all three concentricity requirements as demonstrated in Figure 12.

1. Center Conductor
2. Dielectric
3. Shield
4. Jacket

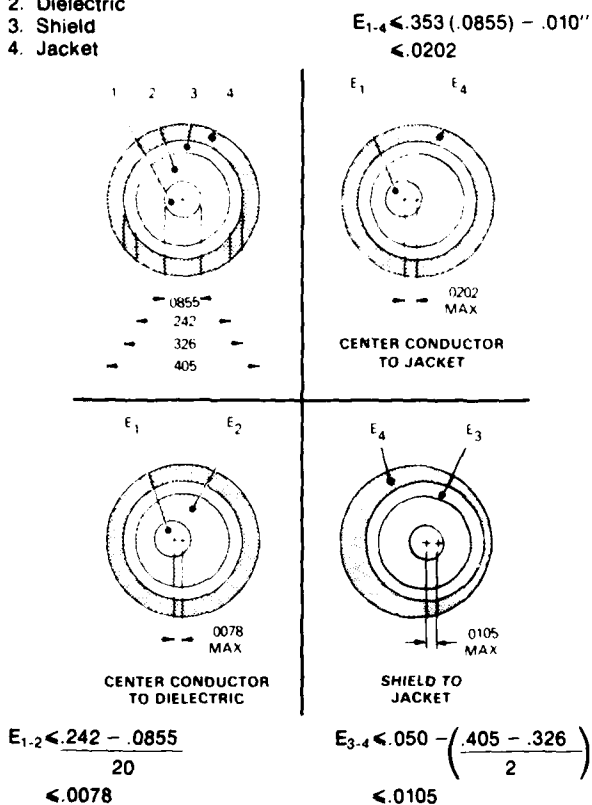


Figure 12. Eccentricity examples.

Conclusion

The AMP coaxial tap provides an efficient, reliable means of tapping a coaxial cable in a local area network. The performance of this tap depends on certain physical characteristics of the cable on which it is applied. Although the cable drilling technique described in this paper overcomes many of the limitations imposed by cable geometries and materials it cannot compensate for cables wherein the jacket, shield, dielectric, and center conductor are not sufficiently concentric. We know of no tapping method available today that will compensate for highly eccentric cable constructions.

DROPWIRE LEAKAGE DUE TO A FAULTY CONNECTOR: A GENERAL MODEL
BASED ON RADIATION FROM A CIRCUMFERENTIAL SLOT

Thomas N. Lovern II* and Chalmers M. Butler**

*Comm/Scope Company
Catawba, North Carolina
**Department of Electrical Engineering
University of Mississippi
University, Mississippi

Summary

In this paper we consider the elementary but important case of excitation in which the leakage from the coaxial cable is caused by a partially disconnected connector. The coax center conductor is assumed to be continuous but the connector outer fitting is assumed to be unscrewed, effectively leaving a gap in the outer conductor of the coax. It is through this circumferential slot that electromagnetic energy reaches the exterior region. In general, the current induced on the exterior surface of the outer coaxial conductor is strongly dependent upon where this gap is located along the length of the coax, and, in turn, exterior fields depend directly upon this surface current. Therefore, in this investigation, the exterior fields are computed for numerous values of the displacement of the faulty connector from the center of the finite-length coaxial cable. The effects of length and radius of coax outer conductor, height of coax above ground, frequency and the nature of the internal fields (voltage and current) are considered.

Introduction

In an expanding CATV network, an understanding of system R.F. radiation is of increasing importance. In the cable system environment, it is often difficult to empirically separate the effects of various connectors, cable arrays, etc. Understanding the electromagnetic leakage of individual components is, therefore, of practical value. The purpose of this paper is to describe the results of an investigation of the field exterior to a coaxial cable caused by the presence of a hole or a gap in the coax outer shield. The analytical techniques employed are outlined and representative data are presented.

The intensity and characteristics of the field radiated and that leaked by a coaxial cable depend upon numerous parameters: the length and radius of coax outer conductor; height of the coax above ground; frequency; the nature of the internal fields (voltage and current); and the nature of the means by which the internal energy leaks to the region exterior to the coaxial shield. In this paper we consider the elementary but important case of excitation in which the leakage from the coaxial cable is caused by a partially disconnected

connector. The coax center conductor is assumed to be continuous, i.e., the center pin and its female counterpart make good contact, but the connector outer fitting is assumed to be unscrewed, effectively leaving a gap in the outer conductor of the coax. It is through this circumferential slot formed by the gap in the outer coaxial shield that electromagnetic energy reaches the exterior region. In general, the current induced on the exterior surface of the outer coaxial conductor is strongly dependent upon where this gap is located along the length of the coax, and, in turn, exterior fields depend directly upon this surface current. Therefore, in this investigation, the surface current is computed for numerous values of the displacement of the faulty connector from the center of the finite-length coaxial cable and exterior fields are determined therefrom.

The coaxial cable resides a specified distance above the earth and is taken to be parallel to the earth's surface. For the purposes of analysis, the outer conductor of the coax, as well as the surface of the earth, are assumed to be ideal conductors, and the radius of the coax is assumed to be very small relative to the height of the coax above ground. The assumptions of small radius-to-height ratio and the idealness of the coax shield introduces little error except in those locales where earth conductivity is extremely low, allowing displacement current to become comparable to conduction current.

Subject to the idealizations discussed above, an integro-differential equation is developed and solved for the current which is induced on the exterior surface of the outer conductor of the coax. The forcing function in this integro-differential equation is the field in the gap caused by the incompletely fastened connector. In turn, the field in the gap is related to the excitation and terminations inside the coaxial cable, thus enabling one to relate the solution of the integro-differential equation to the quantities normally known for a coax.

For numerous conditions of interest of excitation, the integro-differential equation is solved for the exterior shield current and, from knowledge of this current, the field radiated by the coax is computed. Near fields and far-zone radiated fields are calculated, and they are presented as functions of the parameters of interest discussed above. It is observed that the strength of the exterior field is far greater for certain cable lengths than it is for other lengths.

Formulation

The general problem to be considered here is illustrated in Fig. 1, where one sees a finite length PEC wire of radius a oriented along the z axis a distance d above the ground (yz plane).

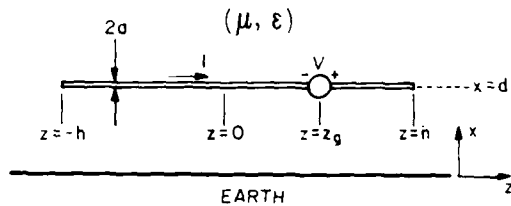


Fig. 1. Wire above ground.

The ground is assumed to be of infinite extent and perfectly conducting. This allows one to employ image theory in the construction of an equivalent model shown in Fig. 2. In particular, we introduce an image wire of the same dimensions as the original. The image voltage source is equal and opposite to the original, the image and its source are located in a medium (μ, ϵ) a distance d below the air-earth interface, and the image wire is parallel to the original wire. This reduces

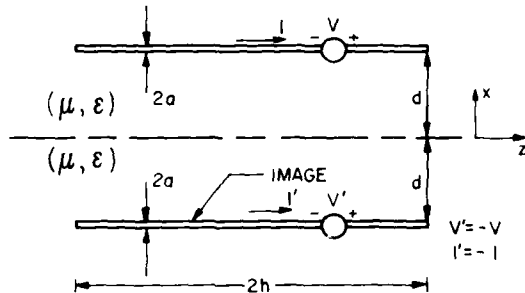


Fig. 2. Wire and its image.

the problem to one of two coupled voltage-fed parallel wires in infinite homogeneous space (μ, ϵ) . Due to the symmetry of the structure and the sources, the current on the image wire must be equal to but opposite in direction from the current on the original wire. This means that

$$I(x) = -I'(x) \quad (1)$$

so $I'(x)$ is known as a function of $I(x)$.

Finding the currents I and I' requires solving a boundary value problem. For this particular problem the boundary conditions require that the total electric field tangential to and on the surface of both PEC wires be zero. We define $E_1^s[I_1; \underline{r}]$ as the electric field at a point \underline{r} due to current I_1 on wire 1, $E_2^s[I_2; \underline{r}]$ as the electric field at \underline{r} due to current I_2 on wire 2, and $E^i(\underline{r})$ as the known electric field at \underline{r} resulting from electromagnetic energy radiating from the gap in the outer conductor of the coax. The field $E^i(\underline{r})$ is directly responsible for the current I_1 and I_2 . The total electric field is the sum of that produced by I_1 , that produced by I_2 and of the incident field:

$$\underline{E}_{\text{TOTAL}} = \underline{E}_1^s[I_1; \underline{r}] + \underline{E}_2^s[I_2; \underline{r}] + \underline{E}^i(\underline{r}) \quad (2)$$

Under the thin-wire assumptions, only the z components of the fields are significant in the satisfaction of the boundary conditions. If we further define $E_{ab}^s[I_b; z]$ as the z component of the electric field due to I_b (evaluated on the surface of wire a) and $E_a^i(z)$ as the z component of the incident electric field evaluated on wire a , then the boundary conditions are given by

$$-E_{11}^s[I_1; z] - E_{12}^s[I_2; z] = E_1^i(z) \quad , \quad z \in (-h, h) \quad (3a)$$

$$-E_{21}^s[I_1; z] - E_{22}^s[I_2; z] = E_2^i(z) \quad , \quad z \in (-h, h) \quad (3b)$$

If we set E_{12}^s to zero, then (3a) would be the equation for a single isolated wire in free space. Similarly, if we set E_{21}^s to zero, then (3b) would be the equation for a single isolated wire in free space. The terms E_{11}^s and E_{22}^s are referred to as "self" terms while E_{12}^s and E_{21}^s are referred to as "coupling" terms.

In general, E^s , the electric field at the surface of a PEC body, is given by

$$\underline{E}^s(\underline{r}) = j\omega \underline{A}(\underline{r}) + \nabla \phi(\underline{r}) \quad , \quad \underline{r} \in S \quad (4)$$

where \underline{A} is the magnetic vector potential and ϕ is the electric scalar potential due to the currents and charges on the wires. The vector \underline{r} locates the observation point. Considering our geometry in cylindrical coordinates, we find that only the z component of the vector potential survives, and that E_z^s from Eq. (4) is simply

$$E_z^s = j\omega A_z + \frac{d}{dz} \phi \quad (5)$$

where J_z is the z -directed surface current density, where

$$A_z = \frac{\mu}{4\pi} \int_{-h}^h J_z(z') \int_{-\pi}^{\pi} \frac{e^{-jkR}}{R} a d\phi' dz' \quad (6)$$

and where

$$\phi = \frac{1}{4\pi\epsilon} \int_{-h}^h q(z') \int_{-\pi}^{\pi} \frac{e^{-jkR}}{R} a d\phi' dz' \quad (7)$$

R is the distance from the source point (a, ϕ', z') to the observation point (a, ϕ, z) . Both points are on the cylindrical surface of the wire. Since all quantities are ϕ independent we can set $\phi = 0$ without loss of generality and for convenience we can define a total current I as

$$I(z) = 2\pi a J_z(z) \quad (8)$$

The surface charge density q is related to I by the continuity equation:

$$\frac{d}{dz} I(z) = -j2\pi a \omega q(z) \quad (9)$$

It is convenient to replace J_z and q in (6) and (7) with their equivalents from (8) and (9):

$$A_z(z) = \frac{\mu}{4\pi} \int_{-h}^h I(z') K(z-z') dz' \quad (10a)$$

and

$$\phi(z) = j \frac{\eta}{4\pi k} \int_{-h}^h \frac{d}{dz'} I(z') K(z-z') dz' \quad (10b)$$

where

$$K(z-z') = \frac{1}{2\pi} \int_{-\pi}^{\pi} \frac{e^{-jkR}}{R} d\phi' \quad (11a)$$

in which

$$R = [(z-z')^2 + 4a^2 \sin^2(\phi'/2)]^{1/2} \quad (11b)$$

Finally, insertion of A_z and ϕ of (10) into (5) yields

$$E_z^S[I; z] = j \frac{\eta}{4\pi k} \left\{ k^2 \int_{-h}^h I(z') K(z-z') dz' + \frac{d}{dz} \int_{-h}^h \frac{d}{dz'} I(z') K(z-z') dz' \right\} \quad (12)$$

Self Terms

For the self term, $-E_{11}^S[I_1; z]$, Eqs. (11) and (12) apply directly:

$$-E_{11}^S[I_1; z] = j \frac{\eta}{4\pi k} \left\{ k^2 \int_{-h}^h I_1(z') K(z-z') dz' + \frac{d}{dz} \int_{-h}^h \frac{d}{dz'} I_1(z') K(z-z') dz' \right\} \quad (13)$$

As a result of symmetry $-E_{22}^S[I_2; z]$ is identical to $-E_{11}^S[I_1; z]$ with I_1 replaced by I_2 . $E_{11}^S(E_{22}^S)$ is the electric field due to $I_1(I_2)$ on wire 1 (wire 2); hence, the expression "self term."

Coupling Terms

Consider $E_{12}^S[I_1; z]$ which is the electric field on wire 1 due to current on wire 2. The expression for E_{12}^S is analogous to equation (12):

$$-E_{12}^S[I_1; z] = j \frac{\eta}{4\pi k} \left\{ k^2 \int_{-h}^h I_2(z') K_{12}(z-z') dz' + \frac{d}{dz} \int_{-h}^h \frac{d}{dz'} I_2(z') K_{12}(z-z') dz' \right\} \quad (14)$$

where

$$K_{12} = \frac{1}{2\pi} \int_{-\pi}^{\pi} \frac{e^{-jkR_{12}}}{R_{12}} d\phi' \quad (15)$$

R_{12} is the distance from a point on the surface of wire 2 to a point on the surface of wire 1. If $d > 5a$, then

$$R_{12} = \sqrt{(z-z')^2 + 4d^2} \quad (16)$$

and K_{12} simplifies to

$$K_{12} = \frac{e^{-jkR_{12}}}{R_{12}} \quad (17)$$

Similarly,

$$-E_{21}^S[I_1; z] = j \frac{\eta}{4\pi k} \left\{ k^2 \int_{-h}^h I_1(z') K_{21}(z-z') dz' + \frac{d}{dz} \int_{-h}^h \frac{d}{dz'} I_1(z') K_{21}(z-z') dz' \right\} \quad (18a)$$

where K_{21} is given by

$$K_{21} = \frac{e^{-jkR_{21}}}{R_{21}} \quad (18b)$$

and is found due to symmetry to be the same as K_{12} of (17).

Combining (13), (14), and (18) with (3), we have the final coupled equations:

$$j \frac{\eta}{4\pi k} \left\{ \left[k^2 \int_{-h}^h I_1(z') K(z-z') dz' + \frac{d}{dz} \int_{-h}^h \frac{d}{dz'} I_1(z') K(z-z') dz' \right] + \left[k^2 \int_{-h}^h I_2(z') K_{12}(z-z') dz' + \frac{d}{dz} \int_{-h}^h \frac{d}{dz'} I_2(z') K_{12}(z-z') dz' \right] \right\} = E_1^i(z), \quad z \in (-h, h) \quad (19a)$$

and

$$j \frac{\eta}{4\pi k} \left\{ \left[k^2 \int_{-h}^h I_1(z') K_{21}(z-z') dz' + \frac{d}{dz} \int_{-h}^h \frac{d}{dz'} I_1(z') K_{21}(z-z') dz' \right] + \left[k^2 \int_{-h}^h I_2(z') K(z-z') dz' + \frac{d}{dz} \int_{-h}^h \frac{d}{dz'} I_2(z') K(z-z') dz' \right] \right\} = E_2^i(z), \quad z \in (-h, h). \quad (19b)$$

For leakage through the thin circumferential slice in the coax outer conductor, the classic slice generator source model is ideally suited. Therefore, the incident fields of (19) for the wire and its image (Fig. 2) are $E_1^i(z) = V \delta(z-z_g)$ and $E_2^i(z) = -V \delta(z-z_g)$, where V is the strength of the potential difference across the thin slice or gap in the coax outer conductor, z_g is the displacement of the gap from the wire center, and $\delta(\cdot)$ is the familiar delta function. The location of the source generator is illustrated in Fig. 1.

Numerical Solution of the Integro-Differential Equations (19)

Eqs. (19) have been solved numerically by the method of moments [1,2]. Only the highlights are presented here with emphasis on the features relevant to solving (19). The currents I_1 and I_2 are approximated as piecewise linear functions so they can be represented by means of

$$I_1(z) = \sum_{n=1}^N I_n^{(1)} \Lambda_n \quad (20)$$

where Λ_n is the n th triangular pulse and $I_n^{(1)}$ is the unknown weighting coefficient of Λ_n . (Representative Λ_n 's are illustrated in Fig. 3.)

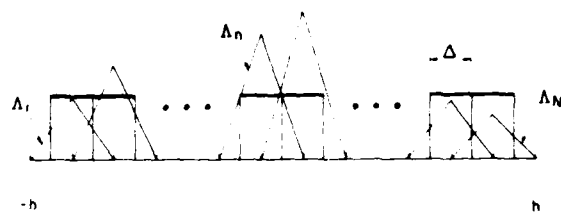


Fig. 3. Piecewise linear (triangular) expansion functions and pulse testing functions for a wire.

Rectangular pulses Π_m are used as testing functions where

$$\Pi_m = \begin{cases} 1 & , z \in (z_m - \Delta/2, z_m + \Delta/2) \\ 0 & , \text{otherwise} \end{cases} \quad (21)$$

Δ is the length of the $N+1$ segments into which the length $2h$ is partitioned ($\Delta = \frac{2h}{N+1}$). Pulse testing functions and Δ are depicted in Fig. 3.

We now outline briefly the pulse testing/triangle expansion scheme. Representing I_1 and I_2 in (19a) by the piecewise linear approximation of (20) and testing the resulting equation with Π_m of (21) for $m=1,2,3,\dots,N$ leads to

$$\sum_{n=1}^N I_n^{(1)} Z_{mn}^{(1)} + \sum_{n=1}^N I_n^{(2)} Z_{mn}^{(2)} = V_m^{(1)}, \quad m=1,2,3,\dots,N \quad (22a)$$

on wire 1 where

$$Z_{mn}^{11} = j \frac{\eta}{4\pi k \Delta} \left\{ k^2 \Delta^2 \int_{z_{n-1/2}}^{z_{n+1/2}} K(z_m - z') dz' + \int_{z_{n-1}}^{z_n} [K(z_{m+1/2} - z') - K(z_{m-1/2} - z')] dz' - \int_{z_n}^{z_{n+1}} [K(z_{m+1/2} - z') - K(z_{m-1/2} - z')] dz' \right\}, \quad (22b)$$

$$Z_{mn}^{12} = j \frac{\eta}{4\pi k \Delta} \left\{ k^2 \Delta^2 \int_{z_{n-1/2}}^{z_{n+1/2}} K_{1,2}(z_m - z') dz' + \int_{z_n}^{z_{n+1}} [K_{1,2}(z_{m+1/2} - z') - K_{1,2}(z_{m-1/2} - z')] dz' - \int_{z_n}^{z_{n+1}} [K_{1,2}(z_{m+1/2} - z') - K_{1,2}(z_{m-1/2} - z')] dz' \right\}, \quad (22c)$$

and where

$$V_m^{(1)} = \int_{z_m - \Delta/2}^{z_m + \Delta/2} E_1^1(z) dz = \begin{cases} 1 & , z_g : (z_m - \Delta/2, z_m + \Delta/2) \\ 0 & , \text{otherwise} \end{cases} \quad (22d)$$

In (22), $z_p = -h + p\Delta$, where p may be $m, n, n+1/2$, or $n-1/2$. The same procedure may be applied to (19b) to arrive at

$$\sum_{n=1}^N I_n^{(1)} Z_{mn}^{21} + \sum_{n=1}^N I_n^{(2)} Z_{mn}^{22} = V_m^{(2)}, \quad m=1, 2, 3, \dots, N, \quad (23)$$

with corresponding definition of terms. Due to the symmetry of the wire plus its image, one can show that $V_m^{(2)} = -V_m^{(1)}$, $Z_{mn}^{22} = Z_{mn}^{11}$, and $Z_{mn}^{21} = Z_{mn}^{12}$.

(See remark following (18).) By solving the two coupled algebraic equations (22a) and (23), one determines the sets of coefficients $I_n^{(1)}$ and $I_n^{(2)}$ which in (20) allow one to approximate I_1 and I_2 with high accuracy.

It is instructive to write (22a) and (23) as a pair of matrix equations,

$$\begin{bmatrix} Z_{mn}^{11} \end{bmatrix} \begin{bmatrix} I_n^{(1)} \end{bmatrix} + \begin{bmatrix} Z_{mn}^{12} \end{bmatrix} \begin{bmatrix} I_n^{(2)} \end{bmatrix} = \begin{bmatrix} V_m^{(1)} \end{bmatrix} \quad (24a)$$

$$\begin{bmatrix} Z_{mn}^{21} \end{bmatrix} \begin{bmatrix} I_n^{(1)} \end{bmatrix} + \begin{bmatrix} Z_{mn}^{22} \end{bmatrix} \begin{bmatrix} I_n^{(2)} \end{bmatrix} = \begin{bmatrix} V_m^{(2)} \end{bmatrix}, \quad (24b)$$

or as a single matrix equation,

$$\begin{bmatrix} Z_{mn}^{11} & Z_{mn}^{12} \\ Z_{mn}^{21} & Z_{mn}^{22} \end{bmatrix} \begin{bmatrix} I_n^{(1)} \\ I_n^{(2)} \end{bmatrix} = \begin{bmatrix} V_m^{(1)} \\ V_m^{(2)} \end{bmatrix} \quad (25)$$

in which $[Z_{mn}^{22}] = [Z_{mn}^{11}]$ and $[Z_{mn}^{21}] = [Z_{mn}^{12}]$ are explicitly incorporated. A more convenient form is

$$\begin{bmatrix} Z_{mn} \end{bmatrix} \begin{bmatrix} I_n \end{bmatrix} = \begin{bmatrix} V_m \end{bmatrix} \quad (26)$$

with obvious definitions of matrices. From (26), the matrix $\begin{bmatrix} I_n \end{bmatrix}$ of current coefficients is seen to be

$$\begin{bmatrix} I_n \end{bmatrix} = \begin{bmatrix} Z_{mn} \end{bmatrix}^{-1} \begin{bmatrix} V_m \end{bmatrix} \quad (27)$$

from which one has the coefficients needed in the piecewise linear approximation of I_1 and I_2 .

Obviously, the matrix $\begin{bmatrix} Z_{mn} \end{bmatrix}$ and its inverse can be quite large for long wires which require many pulses for an accurate representation of the current. The symmetries peculiar to our problem, however, allow for a reduction in the order of the matrices in (26). Matrix folding techniques [2] enable one to

reduce $\begin{bmatrix} Z_{mn} \end{bmatrix}$ from $2N \times 2N$ to $N \times N$, which is clearly a significant savings in computer resources.

Radiated Field

From knowledge of the current on the wire, determined by solving (19) by means of the procedure discussed above, one can determine the field radiated by the wire above ground. We compute in this section the far-zone electric and magnetic fields and the near-zone electric field on the surface of the earth. In general \underline{E} and \underline{H} are computed by means of

$$\underline{H} = \frac{1}{\mu} \nabla \times \underline{A} \quad (28a)$$

and

$$\underline{E} = -j\omega \underline{A} - \nabla \phi \quad (28b)$$

where \underline{A} and ϕ are the vector and scalar potentials due to the sources induced on the wire plus its image. For a point located in space by \underline{r} which is distant from the wire compared to its radius a , \underline{A} and ϕ are

$$\underline{A}(\underline{r}) = \frac{\mu}{4\pi} \int_{-h}^h I(z') \left\{ \frac{e^{-jk|\underline{r}-\underline{r}'|}}{|\underline{r}-\underline{r}'|} - \frac{e^{-jk|\underline{r}-\underline{r}'_1|}}{|\underline{r}-\underline{r}'_1|} \right\} dz' \quad (29a)$$

and

$$\phi(\underline{r}) = j \frac{\eta}{2\pi k} \int_{-h}^h \frac{d}{dz'} I(z') \left\{ \frac{e^{-jk|\underline{r}-\underline{r}'|}}{|\underline{r}-\underline{r}'|} - \frac{e^{-jk|\underline{r}-\underline{r}'_1|}}{|\underline{r}-\underline{r}'_1|} \right\} dz' \quad (29b)$$

where

$$|\underline{r}-\underline{r}'| = \sqrt{(x-d)^2 + y^2 + (z-z')^2} \quad (30a)$$

and

$$|\underline{r}-\underline{r}'_1| = \sqrt{(x+d)^2 + y^2 + (z-z')^2} \quad (30b)$$

In (29) I is I_1 the current on the wire above ground but, since I_1 and I_2 are related, the subscripts are dropped for convenience.

Far-Zone Field

In the far zone, $r \gg h$ and $r \gg 2h$. As a result,

$$\frac{e^{-jk|\underline{r}-\underline{r}'|}}{|\underline{r}-\underline{r}'|} \approx \frac{e^{-jk(r-r'(\hat{r} \cdot \hat{r}'))}}{r} \quad (31a)$$

and

$$\frac{d}{dz'} \frac{e^{-jk|\underline{r}-\underline{r}'|}}{|\underline{r}-\underline{r}'|} \approx \frac{d}{dz'} \frac{e^{-jk(r-r'(\hat{r} \cdot \hat{r}'))}}{r} \quad (31b)$$

so

$$\frac{e^{-jk|\underline{r}-\underline{r}'|}}{|\underline{r}-\underline{r}'|} \approx \frac{e^{-jk|\underline{r}-\underline{r}'_1|}}{|\underline{r}-\underline{r}'_1|}$$

$$\frac{e^{-jkr}}{r} \left[-j \sin(kd \sin \theta \cos \phi) e^{jkz' \cos \theta} \right] \quad (32)$$

where θ and ϕ are the angles of a spherical coordinate system centered at $(0,0,0)$ and oriented in the usual way. Substituting (32) into (29a) and performing the operation indicated in (28a), one obtains

$$\underline{H} = -2k(\hat{z} \times \underline{r}) \sin(kd \sin \theta \cos \phi) \frac{e^{-jkr}}{4\pi r} \int_{-h}^h I(z') e^{jkz' \cos \theta} dz' \quad (33)$$

Replacing I by its piecewise linear representation from (20), one may write the magnetic field in terms of the coefficient I_n determined from the numerical solution:

$$\underline{H}_\phi(r, \theta, \phi) = -2k \Delta \sin \theta \sin(kd \sin \theta \cos \phi) \cdot \frac{e^{-jkr}}{4\pi r} \sum_{n=1}^N I_n e^{jkz_n \cos \theta} \quad (34)$$

where $\underline{H} = H_\phi \hat{\phi}$. Knowing H_ϕ one computes E_ϕ simply from $\underline{E}_\phi = \eta \underline{H}_\phi$ in the far zone.

Near-Zone Field

Due to the presence of the ground at $x=0$ in the yz plane, which is taken to be ideal, E_x and E_z are zero on this plane ($x=0$) and $E_x(0,y,z)$ is twice the x -directed E -field radiated by the current in open space (no ground plane present). So, to determine $E_x(0,y,z)$, we compute radiation from I alone and double the x component of E -field. Since on the ground E_x is the total E -field, since E_y and E_z are very small near the earth, and since major interest lies in the field on the ground, we choose E_x on the ground to present as a characterization of near field behavior.

The x component of the E -field due to I alone in open space is computed by $-\frac{\partial}{\partial x}$: where $\frac{\partial}{\partial x}$ now is (29b) with the second term in the braces set to zero. Hence,

$$E_x(0,y,z) = -j \frac{\eta}{2\pi k} \int_{-h}^h \frac{d}{dz'} I(z') \left\{ \frac{\partial}{\partial x} \frac{e^{-jk|\underline{r}-\underline{r}'|}}{|\underline{r}-\underline{r}'|} \right\}_{x=0} dz' \quad (35)$$

from which it follows that

$$E_x(0,y,z) = -j 2 \frac{\eta d}{k} \int_{-h}^h \frac{d}{dz'} I(z') g(y,z;z') dz' \quad (36)$$

where

$$g(y,z;z') = \left(\frac{1}{D^2} + \frac{j k}{D} \right) \frac{e^{-jkD}}{4\pi D} \quad (37a)$$

in which

$$D = \sqrt{d^2 + y^2 + (z-z')^2} \quad (37b)$$

Replacement of I in (36) by its piecewise linear approximation (20) allows one to arrive at

$$E_x(0,y,z) = -j 2 \frac{\eta d}{k} \sum_{n=1}^N I_n [g(y,z;z_{n-1/2}) - g(y,z;z_{n+1/2})] \quad (38)$$

which is E_x in terms of the coefficients I_n determined from the solution procedure described above.

Loading of the Coaxial Cable

In Fig. 4 is illustrated a transmission line model of the coax in Fig. 1. A known load is assumed to exist at the end at $z=h$ and a faulty connector at $z=z_g$, and we wish to know the input impedance Z_{in} of the section of coax at $z=-h$. The series impedance seen by the line at z_g is the impedance Z_A computed for the radiating section of the coax. By standard transmission line theory one can readily show that

$$Z_{in} = Z_0 \frac{Z_s^+ + Z_s^- e^{-j2k_c z_g}}{Z_s^+ - Z_s^- e^{-j2k_c z_g}} \quad (39)$$

where Z_0 and k_c are the characteristic impedance and propagation constant, respectively, of the coax and where

$$Z_s^\pm = Z_0 \left\{ \frac{Z_A}{Z_0} + \frac{Z_L + Z_0 + (Z_L - Z_0)e^{-j2k_c(2h-z_g)}}{(Z_L + Z_0) - (Z_L - Z_0)e^{-j2k_c(2h-z_g)}} \pm 1 \right\} \quad (40)$$

Z_A is determined from the numerical solution method discussed above and the value of Z_L is available from knowledge of the terminal conditions at $z=h$ (open circuit, short circuit, or otherwise). Knowing Z_A and Z_L one computes Z_{in} from (39) and (40).

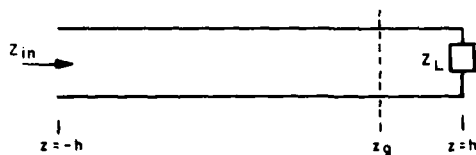


Fig. 4. Transmission line model with load Z_L at $z=h$ and with leaky connector at $z=z_g$.

Results and Discussion

In view of the large number of variables to consider such as coax length, height above ground, excitation, location of excitation on the cable, and radius of the coax, a complete characterization of the problem would result in far more data than could be reported here. For this reason, in the presentation of the results below, we confine ourselves to an overview of some of the possible combinations of parameters. In particular, we discuss only the influence of coax length and the location of excitation on the cable.

In Figs. 5-9 is illustrated the magnitude of the current induced on the outside of the coax due to the electromagnetic energy that reaches the exterior region through the circumferential gap. In all cases the gap voltage is 1 Volt, the height above ground is 5 meters and the coax radius is .0022 meters which is representative of a standard RG59 coaxial cable. The medium is taken to be free space and the earth is modeled by a PEC plane of infinite extent. The excitation wavelength is 6 meters (50 MHz). The current exhibits the expected features. The largest value occurs for the 3m wire (half-wavelength) with $z_g=0$ (center fed). The current excited on a wire that is an odd multiple of a half-wavelength is smaller but is still quite significant. The current on a center-fed drop wire that is an integral multiple of one wavelength (6m) is even smaller. Maximum current in these cases occurs when the distance from the gap to the wire end becomes half wave-length.

It is clear from Figs. 5-9 that the magnitude of the current and its variation along the wire are strongly dependent on the two variables $2h$ and z_g considered. The significance of this can not be overstated since the leakage field depends directly on $I(z)$ as shown in earlier sections. In addition, the variation in the current at the gap in the coax due to wire length and z_g results in a wide variation in the value of Z_A and, therefore, in the input impedance of the coax. In Table 1, Z_A is given for each case considered in Figs. 5-9. These values of Z_A can be used in Eqs. (39) and (40) to compute the loading Z_{in} at the input ($z=-h$) of the coax caused by the faulty connector.

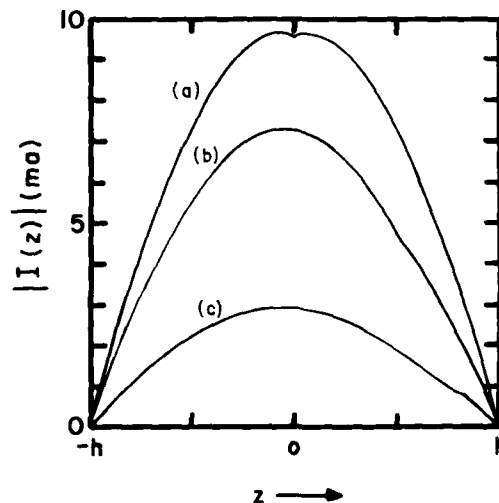


Fig. 5. Magnitude of current on 3m wire above earth ($2h=3m$, $a=.0022m$, $f=50MHz$, $d=5m$): (a) $z_g=0$, (b) $z_g=.75m$, (c) $z_g=1.25m$.

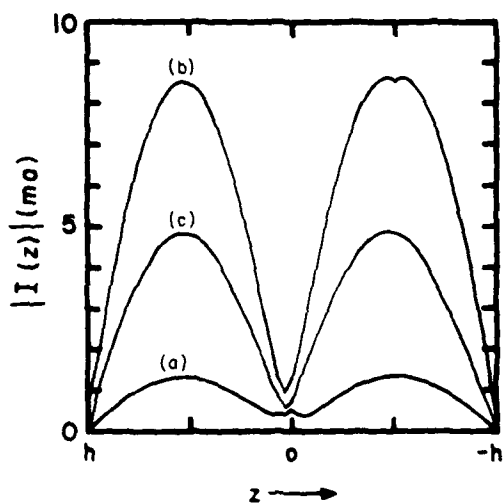


Fig. 6. Magnitude of current on 6m wire above earth ($2h=6m$, $a=.0022m$, $f=50MHz$, $d=5m$): (a) $z_g=0$, (b) $z_g=1.5m$, (c) $z_g=2.5m$.

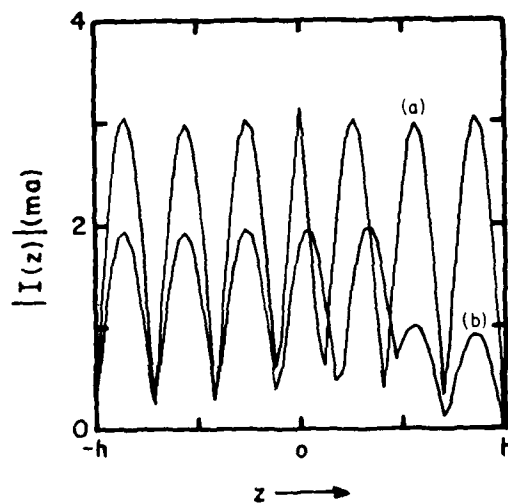


Fig. 8. Magnitude of current on 20m wire above earth ($2h=20m$, $a=.0022m$, $f=50MHz$, $d=5m$): (a) $z_g=0$, (b) $z_g=4.7m$.

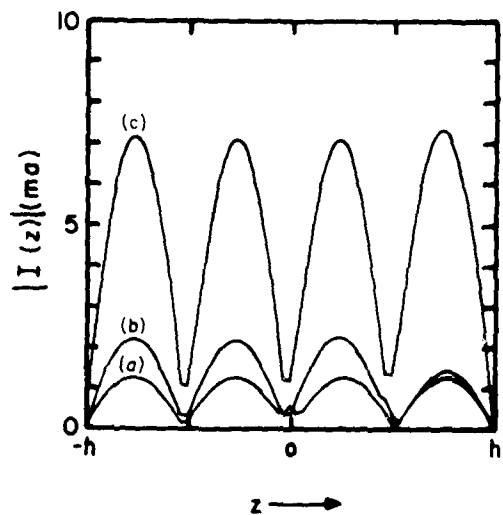


Fig. 7. Magnitude of current on 12m wire above earth ($2h=12m$, $a=.0022m$, $f=50MHz$, $d=5m$): (a) $z_g=0$, (b) $z_g=2.82m$, (c) $z_g=4.94m$.

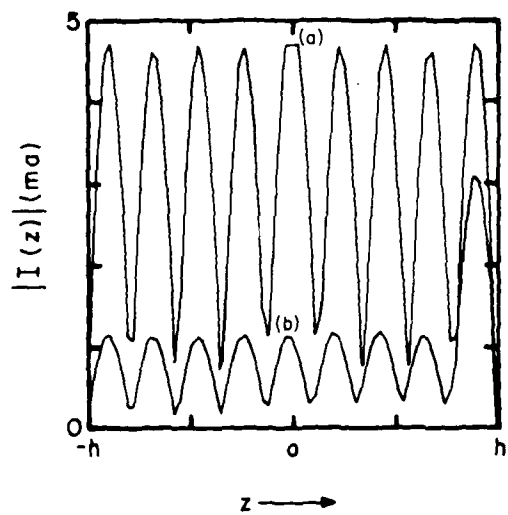


Fig. 9. Magnitude of current on 27m wire above earth ($2h=27m$, $a=.0022m$, $f=50MHz$, $d=5m$): (a) $z_g=0$, (b) $z_g=10.8m$.

Table 1
Driving Point Impedance Z_A of Gap-Fed Drop Wire

2h	case a	Z_A (Ohms) case b	case c
3m	(116.8,-230.1)	(222.1,-629.7)	(1391,2534)
6m	(2686,2476)	(131,-151)	(475,-7484)
12m	(2523,2236)	(1550,2794)	(161.2,-658)
20m	(851,343.3)	(1495,-12162)	-----
27m	(246,-424.8)	-----	(116.8,-5734)

In Figs. 10-11 is illustrated the normalized magnitude of the magnetic field, H_ϕ , in the far field for a 27m wire above the earth. The normalization factor, $\frac{e^{-jkr}}{r}$, determines the manner in which the magnetic field falls off with distance. The most striking feature of the far field is its complex structure which is quite unlike what one would expect for a short wire very close to the ground. In fact, for all of the wire structures considered in this paper, where the distance between the wire and its image is greater than a wavelength, the far field is very lobate.

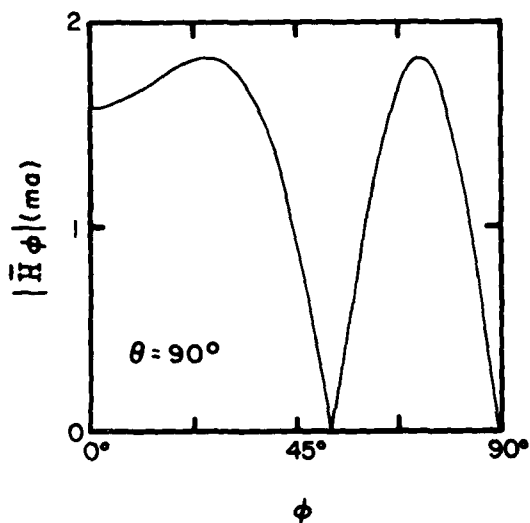


Fig. 10. Normalized magnitude of H_ϕ in the far field for 27m wire above the earth (refer Fig. 9, case (a)): $\theta=90^\circ$, ϕ varies from 0° to 90° .

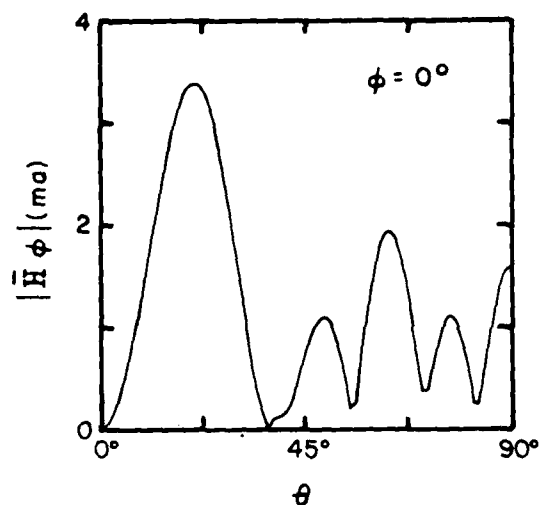


Fig. 11. Normalized magnitude of H_ϕ in the far field for 27m wire above the earth (refer Fig. 9, case (a)): $\phi=0^\circ$, θ varies from 0° to 90° .

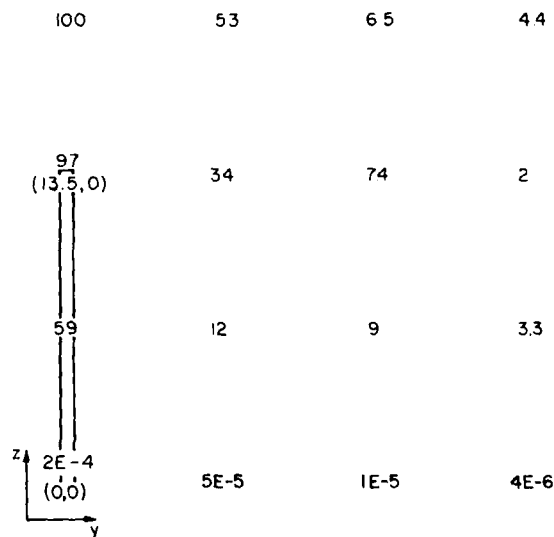


Fig. 12. Relative magnitude of $E(0,y,z)$ in the near field for one quadrant for 27m wire above earth (refer Fig. 9, case (a)).

In Fig. 12 is presented a map of the electric field, $E_x(0,y,z)$, in the near field for a 27m wire above earth. Only one quadrant is shown. The other three quadrants can be deduced by inspection since the current on the wire for this case is symmetric about the center. The magnitude of the electric field at points (y,z) is normalized so that the greatest field strength is "100."

Summary

In this paper the current induced on the exterior surface of a coaxial cable due to a circumferential gap is determined and the resulting exterior fields are computed. It is determined that the current and, therefore, exterior fields are strongly dependent on wire length and gap location and that, in general, both the near and far field patterns have complex structures.

It should be noted that the representation of a dropwire in a CATV network by an isolated wire is a rough approximation at best. However, the purpose of this paper is to convey the theoretical scope of the problem and to gain insight into the effects of various parameters and the relative importance in leakage from a coaxial cable. To this end, the use of an isolated wire as an approximation is acceptable.

References

1. Harrington, R.F., Field Computation by Moment Methods, Macmillan, New York; 1968.
2. Butler, C.M., D.R. Eilton, and A.W. Glisson, Jr., "Fundamentals of numerical solution methods in electromagnetics—short course notes," University of Mississippi, University, MS 38677; March, 1982.

Biographical Sketches

Thomas N. Lovern II was born in Corpus Christi, TX, on December 28, 1951. He received his Ph.D. degree in physics from the University of Virginia in 1979. He is currently employed by Comm/Scope Co. in Catawba, NC, where he is engaged in the application of numerical solution methods in electromagnetics to problems relevant to CATV systems.

Chalmers M. Butler was born in Hartsville, SC, on July 31, 1935. He received the B.S. and M.S. degrees from Clemson University and the Ph.D. degree from the University of Wisconsin. From 1962 to 1965, he was an associate professor at Louisiana State University. Since 1965 he has been a professor of electrical engineering at the University of Mississippi.

Dr. Butler is a member of Sigma Xi, Tau Beta Pi, Phi Kappa Phi, Eta Kappa Nu, the Institute of Electrical and Electronic Engineers (IEEE), and Commissions B and F of the International Union of Radio Science (URSI). He is presently serving his third three-year term as associate editor of the IEEE Transactions on Antennas and Propagation. He has also served as National President of Eta Kappa Nu, as Chairman of the Research Unit and Vice President of the Southeastern Section of the American Society for

Engineering Education. He has served on the Administrative Committee of the IEEE Professional Society on Antennas and Propagation and as Vice-Chairman of US Commission B of URSI. Presently, Dr. Butler is a member of the Board of Directors of the Electromagnetics Society and is the Chairman of US Commission B of URSI. In 1974, he received the Western Electric Fund Award for contributions to engineering education and was the recipient of the 1977-78 School of Engineering Outstanding Teacher Award at the University of Mississippi.

Dr. Butler was a US Delegate (elected) to the Eighteenth General Assembly of URSI, Lima, Peru, in 1975, to the Nineteenth General Assembly in Helsinki, Finland, in 1978, and to the Twentieth General Assembly in Washington, D.C., in 1981. He organized, invited speakers, and chaired a special session on numerical methods in electromagnetics for the Nineteenth General Assembly. Dr. Butler served for three years as a IEEE Professional Society on Antennas and Propagation National Distinguished Lecturer.

THERMODYNAMIC INTERACTIONS, MECHANICAL PROPERTIES AND
PROPERTY RETENTION IN POLYMERIC WIRE COATINGS

H.P. Schreiber

and

J. Chacklund

Department of Chemical Engineering
Ecole Polytechnique, Box 6079,
Station A, Montreal (Que.) H3C 3A7

Cable Division
Northern Telecom Inc.
Lachine (Que.) Canada

The influence of thermodynamic interactions among components on the mechanical properties and the aging characteristics of wire coating compositions was evaluated. The systems considered involve plasticized PVC, and CaCO_3 fillers. Inverse gas chromatography (IGC) was the vehicle for the measurement of interaction parameters, and express the strength of "specific" (acid-base) interactions among the components of the coating over a broad range of temperatures. It was shown that the volumes of plasticizers retained by the PVC correlate with the measured interaction parameters. Similarly, the interaction parameters identify a CaCO_3 filler preferred for reinforcing rigid PVC, and a different CaCO_3 filler for use in given PVC-plasticizer combinations. The mechanical properties of filled PVC (up to 40 phr CaCO_3), and particularly the ultimate properties of the compounds, correlate with the interaction concepts, as do property retention data after accelerated aging of the compounds at 100°C . It is concluded that component interaction parameters may provide useful guidelines to the formulation of coating systems with superior properties and reduced property losses due to aging.

INTRODUCTION

Optimizing the properties of polymer compounds used as wire and cable coatings remains a high priority objective. One approach to the desired optimization lies in understanding the influence of thermodynamic interactions among the components of a polymer coating on its properties, and then selecting materials with satisfactory miscibility ("compatibility"). This principle is generally recognized in the organic coatings field, but its embodiment is hampered by experimental difficulties encountered in the measurement of meaningful thermodynamic interaction parameters. The most widely used quantity, the solubility parameter¹, is an unsatisfactory compromise in too many cases.

Clarifying the role of thermodynamic interactions is the subject of the present paper, which is concerned with the performance of filled, plasticized PVC compounds, formulated for wire coating applications. In this work, we approach the problem of interaction thermodynamics through the experimental method referred to as inverse gas chromatography (IGC). IGC has been developed in recent years as a rapid, convenient tool for the determination of thermodynamic interactions between

a polymeric, or solid, stationary phase and vapor at very high dilution^{2,3}. Subsequent work in our laboratories^{4,5} has extended the concept to make possible evaluating the interaction between two solids, or a solid and a liquid component in the stationary phase. The primary experimental datum in IGC, a specific retention volume V^0 , can be measured over wide temperature ranges⁶ and over the entire composition range in polymer blends or polymer-plasticizer combinations. Thus, IGC has the ability to supply experimental information (V^0), which can be directly related to the free energy of mixing the components of interest over composition and temperature ranges important in industrial uses of polymeric systems.

An additional concept used in this work is due to recent proposals of Fowkes et al.^{6,7}. These workers suggest that miscibility in polymer compounds is strongly related to acid-base interactions. Thus, high "compatibility" should occur when strong acid and base interactions are involved in a formulation. Poor compatibility would be associated with the use of materials which are all either acids or bases. In the IGC experiments conducted here, the vapors were chosen so as to represent typical acid and base probes. In this manner, the V^0 data at once assign an acid-base character to the polymer, the plasticizers and the fillers used, and make possible a test of the relevance of acid-base thermodynamic interaction concepts to the performance of formulations implicated here. That performance, finally, was evaluated through stress-strain curves and by monitoring property retention following controlled, accelerated aging cycles.

EXPERIMENTAL

i) Materials

The PVC sample used was an Exxon Canada Ltd. homopolymer with a K value of 67. The resin was blended with 3 phr dibasic lead stabilizer prior to any exposure to elevated temperatures.

Plasticizers involved were di-isooctyl-phthalate (DiOP), dioctyl sebacate (DOS) and trioctyltrimellitate (TOTM). All of these were commercial grades, used as received. Two fillers were used in this work. Both of these were precipitated CaCO_3 , one sample₂ (CaCO_3)_A having a specific surface area of 5.5 m^2 , the other (CaCO_3)_B with an area of 21.2 m^2 .

To compound these ingredients, a Brabender Plasticorder was employed. Blends generally containing 20 or 40 phr plasticizer, and 20 and 40% wt. of filler were made at 190°C and 50 r.p.m.

ii) Procedures

Gas chromatography: Standard procedures for the preparation of polymer or filler stationary phase columns have been described in detail^{4,8}. In this work, polymer and plasticized PVC columns were prepared by coating these materials onto 60/80 mesh chromosorb W support from solutions in THF. Pure plasticizers were slurried with excess support to make a free-flowing powder suitable for column preparation. The CaCO_3 samples were tumble blended with 5 times their weight of glass beads prior to packing. The various IGC columns and their compositions are given in Table I.

IGC experiments were conducted with t-butanol as the characteristic acid probe and t-butyl amine as the base. Retention times and volumes were measured in triplicate in the temperature range 30°-90°C, with a repeatability of $\pm 2\%$. A normalized acid-base interaction number, Ω , was defined for each material using the V_g^0 results, and

$$\Omega \equiv (V_g^0)_a / (V_g^0)_b \quad (1)$$

By this convention $\Omega < 1$ for acidic stationary phases (since, hypothetically, $(V_g^0)_a$ would be small), and $\Omega > 1$ for basic solids^{8,9}, as $(V_g^0)_b$ diminishes.

Compounding and property evaluation: As already noted, all compounding was done on a Brabender instrument to give vinyl stocks containing 20 and 40 phr plasticizer, and 20 or 40% filler, by weight of polymer. These materials were compression molded at 170°C, and molds were used to cut specimens for stress-strain testing. These were carried out on an Instron Tester, at 30°C, 70% R.H. and a jaw separation speed of 0.5 cm. min⁻¹. Data reported are the averages of 5 determinations. Retention of mechanical properties on aging was monitored by storing similar tensile specimens in desiccators under N_2 , and placing these into air ovens at 100°C, for up to 2 weeks.

RESULTS AND DISCUSSION

i) Chromatographic data

For convenience the chromatographic results are summarized in terms of the Ω parameter defined above. Results are given in Table II. A number of striking inferences may be drawn from this tabulation.

i) It is clear that PVC is a strongly acidic substrate, at least in terms of the hypothesis underlying this work. Each of the plasticizers in turn falls well above $\Omega = 1.0$, hence each is an effective base, again in terms of the Lewis acid-base concepts involved here^{6,7}. Thus, each of the plasticizers appears capable of significant acid-base interaction with PVC, thereby contributing to the "compatibility" of each pair.

ii) Using the 30°C data as a useful reference, there are significant differences in the Ω values of the three plasticizers. Comparing cols. 2, 8 and 14 TOTM is the most "basic" of the three, while DOS is least so. Provided the strength of polymer-plasticizer interactions is correctly reflected by the Ω values, then the compatibility of the three with PVC should rank in the descending order: TOTM > DOP > DOS. Inspection of Table II shows that this "compatibility order" is maintained in the investigated temperature range.

iii) The Ω values are somewhat T-dependent, and the variation is such as to reduce the differences between acidic and basic materials. Thus, for the acidic PVC, Ω tends to increase with temperature toward unity, while for the plasticizers Ω shows a slight decrease. This implies that the degree of "compatibility" between polymer/plasticizer pairs is also temperature dependent, and that, in general, the plasticizers are more highly compatible at lower temperatures. In other words, these plasticizers seem "better" at use temperatures than at temperatures used for compounding.

iv) The Ω values for the CaCO_3 fillers (cols. 20, 21, Table II) are distinct, suggesting that different surface finishes had been applied to these commercial products. On the present basis of rating, the surface of $(\text{CaCO}_3)_A$ is mildly acidic, that of $(\text{CaCO}_3)_B$ is mildly basic.

The inferences of Ω values also may be illustrated more specifically. As an example, in mixed PVC-plasticizer columns, Ω increases with increasing plasticizer content, the variation at 30°C being shown graphically in Figure 1. In each case, an initial, gradual increase in Ω is followed by a much sharper increase at higher plasticization levels. Evidently, the vapor probes, which are sensitive to the surface composition of the solid, detect a predominance of plasticizer molecules at these compositions. Assuming a total uncertainty of 10% in the Ω values for plasticized polymers, the Ω of pure DOP and DOS is attained in the vicinity of 70-75phr of the former and near 60 phr of the latter plasticizer. The case of TOTM is less certain, but a similar occurrence may be inferred near the 85 phr composition. Apparently, then, there are critical volumes (V_c) for each PVC-plasticizer pair, below which the polymer and plasticizer are more or less randomly distributed, but above which an excess of plasticizer migrates to the surface. These V_c values appear to correlate qualitatively with the strength of thermodynamic interactions as expressed by Ω , again decreasing in the order $(V_c)_{\text{TOTM}} > (V_c)_{\text{DOP}} > (V_c)_{\text{DOS}}$. In view of the temperature dependence of Ω , V_c should decrease with rising temperature. This finding may have significant value in the formulation of plasticized compositions and in interpreting performance variations of plasticized compounds at different use temperatures.

In a second example, an attempt is made to express the magnitude of acid-base pair interactions quantitatively in terms of Ω . No

theoretical basis exists for defining the correct approach, but it is reasonable to select the ratio of Ω values as a possible procedure. The concept is illustrated in Figure 2 by bar graphs of pair interactions at 30°C, involving the three plasticizers. The data in Figure 2 are typical of the entire T. range studied, though of course, the absolute values of Ω ratios will decrease at higher temperatures.

Two inferences in particular seem called for from Figure 2. One concerns the relative magnitudes of PVC interactions with $(\text{CaCO}_3)_A$ and $(\text{CaCO}_3)_B$. Clearly, the latter pair is considerably more strongly coupled, the Ω ratio being some 40% greater than the corresponding datum for PVC- $(\text{CaCO}_3)_A$. Since strong thermodynamic interactions are a requisite for wetting and adhesion at component boundaries, $(\text{CaCO}_3)_B$ should be the better reinforcing filler for rigid PVC, or for formulations containing very small amounts of plasticizer. Interfacial wetting is also an important criterion for dispersing solids in a polymer matrix, hence $(\text{CaCO}_3)_B$ should also be more readily dispersed in PVC than the less basic filler sample.

The second inference touches on the probable interaction balance in three-component systems involving PVC, and the present plasticizers and fillers. Clearly, in any 3-component system, the dominant pair interaction will be between polymer and plasticizer. Plasticizer/filler interactions appear to be relatively weak, but $(\text{CaCO}_3)_A$ appears to interact more significantly with either DOP or DOS than is the case with $(\text{CaCO}_3)_B$. Hypothetically, then, these fluids will be more successful in wetting and dispersing the former filler, and this should result in more homogeneous compounds than when $(\text{CaCO}_3)_B$ is involved. The balance of interaction forces among the component pairs is therefore more evenly distributed in systems with $(\text{CaCO}_3)_A$ than with $(\text{CaCO}_3)_B$. It is not immediately evident whether this will have any bearing on the mechanical or physical properties of filled, plasticized PVC formulations; an empirical response to these questions is therefore called for, and provided, in part, in the following section.

ii) Mechanical properties

Many performance parameters can be drawn from stress-strain relationships; in the present case the initial modulus (μ_i) and the elongation at rupture, ϵ_b , were chosen to represent mechanical properties at small and at large deformations. These parameters are known to correlate with use properties of polymers¹⁰.

A selected overview of μ_i data is given in Figure 3. This must lead to the conclusion that acid-base (thermodynamic) interactions, at best, play a minor part in determining mechanical performance at low deformational stress. While μ_i varies somewhat with plasticizer choice, the differences are not sufficient to permit a link with Ω concepts. The presence of CaCO_3 obviously affects μ_i , and differences in the performance of the two fillers slightly favor $(\text{CaCO}_3)_B$. These

differences again are slight, however, and more likely reflect the discrepancy in specific surface areas of the two solids.

The characteristics at high deformation are entirely different, however. As shown by the bar graphs of Figure 4, the elongation at rupture appears to be sensitive to the thermodynamic forces under discussion. This is true in unfilled as well as in filled compounds. The elongation of control, unfilled materials, both at 20 and 40 phr plasticization, increases in the same order as Ω ratios for the corresponding pairs, i.e. TOTM > DOP > DOS. Further, the initial ϵ_b datum is slightly but reproducibly greater for compounds with $(\text{CaCO}_3)_A$ than with $(\text{CaCO}_3)_B$, both at 20% and 40% loadings (Figures 4A and 4B, respectively). This is consistent with expectations stated above, that on the basis of Ω ratings, $(\text{CaCO}_3)_A$ should be capable of forming more homogeneous multi-component blends than the more basic filler in this pair.

The relationship between thermodynamic interactions (in this case of the acid-base type) and the mechanical properties of complex polymer compounds is extended by the aging behavior of present specimens. The pertinent evidence is given in the parts of Figure 5, part A showing the per-cent ϵ_b retained by control samples aged at 100°C. In Figure 5B the excess property loss due to the presence of filler is shown, again as function of exposure time. The excess property loss $\Delta\epsilon_b$ is calculated from

$$\Delta\epsilon_b = (\epsilon_b)_{pl-f} - (\epsilon_b)_{pl} \quad (2)$$

where $(\epsilon_b)_{pl}$ is the % elongation retained after given aging by the plasticized control, and $(\epsilon_b)_{pl-f}$ is the property for the corresponding filled, plasticized compound. For clarity, only the compounds at 40 phr plasticizer and 40 wt.% filler are represented in 5B, but the pattern of results at other loading levels follows that shown. It is evident that in each case, the addition of CaCO_3 filler accelerates property loss in the compounds. Equally, however, the performance of compounds with $(\text{CaCO}_3)_A$ is superior, elongations at break after two weeks' aging being significantly greater than those for specimens with $(\text{CaCO}_3)_B$. Hypothetically, loss of elongation is attributable to the loss by evaporation of plasticizer. Since the vapor pressures of the three plasticizers at 100°C rank in the order DOP > DOS > TOTM, it is understandable that the % retained elongation in unfilled, plasticized compounds reflects that order. In order to vaporize, plasticizer molecules must migrate to a free surface, however. The effect of fillers may then be interpreted as providing additional free paths for plasticizer transport from the bulk to the surface of specimens. Evidently, $(\text{CaCO}_3)_B$ provides much greater opportunity for the necessary diffusion process. In the present context, this is attributed to the "mis-match" in interaction potentials of the materials involved. Since, according to the evidence of Ω ratios (Figure 2), this mis-match is more severe for $(\text{CaCO}_3)_B$ than when $(\text{CaCO}_3)_A$ is involved, the pattern of data in Figure 5 is consistent with expectation.

An additional point of consistency seen in Figure 5 is the relatively low excess loss of property incurred in DOS-based, filled compounds. Of the three palsticizers used here, DOS is the least "compatible" with PVC, but the interaction balance in 3-component systems is more equally matched in DOS-containing mixtures than when either DOP or TOTM is employed. We might therefore expect these combinations to produce more homogeneous compounds with relatively superior property retention than others in this comparison. For the present, a lack of theoretical guidance to a quantitative expression of interaction force balances in multi-component systems, does not permit further development of this point. Additional work is being directed to this objective, and to further developing the usefulness of interaction concepts as a guide to the formulation of compounds tailored to meet desired performance norms.

CONCLUSIONS

- . Inverse gas chromatography is a convenient, relatively simple experimental method for the measurement of acid-base (thermodynamic) interaction properties of polymers, fillers, plasticizers etc. involved in wire and cable coatings.
- . Acid-base interaction criteria are involved in determining the plasticizer volume which can be absorbed by PVC,
- . Acid-base interaction criteria may be useful in the selection of reinforcing fillers (e.g. CaCO_3) for PVC,
- . Elongation at break of filled, plasticized PVC compounds correlates with the balance of interaction forces among the components of the formulation,
- . Property retention after high-temperature exposure also seems dependent on interaction force balances in the compounds,
- . Acid-base interaction criteria may be useful in formulating compounds with superior property balances and durability.

Acknowledgment

The support of this research by Cable Division, Northern Telecom Inc. is greatly appreciated. Additional support was received from the Natural Sciences and Engineering Research Council of Canada.

References

- (1) A.F.M. Barton, Chem. Rev. 75, 731 (1975).
- (2) O. Olabisi, L.M. Robeson and M.T. Shaw, in Polymer-Polymer Miscibility, Ch. 3, Academic Press, New York (1979).
- (3) J.M. Braun and J.E. Guillet in Progress in Gas Chromatography, J.H. Purnell, Ed., Wiley Interscience, New York (1976).
- (4) C.S. Su, D. Patterson and H.P. Schreiber, J. Appl. Polym. Sci. 20, 1025 (1976).

- (5) D. Deshpande, D. Patterson, H.P. Schreiber and C.S. Su, Macromolecules 7, 530 (1974).
- (6) F.W. Fowkes and S. Maruchi, A.C.S. Polymer Preprints 37, 606 (1977).
- (7) R.S. Drago, G.G. Vogel and T.E. Needham, J. Am. Chem. Soc. 93, 6014 (1971).
- (8) M. Lamba and H.P. Schreiber, Eur. Polym. J. 16, 211 (1980).
- (9) R.L. Patrick, Ed. "Treatise on Adhesives and Adhesion", Marcel Dekker, Inc., New York (1966).
- (10) L.E. Nielsen, "Mechanical Properties of Polymers and Composites", Marcel Dekker, Inc. New York (1974).

H.P. Schreiber was educated at the Universities of Manitoba and Toronto. He has been active in research on polymer rheology, solution properties and composite materials first as Research Scientist in C-I-L, Inc. and since 1973, as Professor of Chemical Engineering in Ecole Polytechnique. He has published over 110 papers in these fields and holds numerous patents.

J. Checklund was educated at Strathclyde University and at McGill University where he obtained the Masters Degree in Chemical Engineering. He has been associated with the Materials Department of Northern Telecom Ltd since 1973, and is currently Department Manager.

TABLE I

COMPOSITION OF IGC COLUMNS

Col. No.	1 ^a	2 ^b	3	4	5	6	7	8	9	10	11	12	13	14	15	16	17	18	19	20 ^c	21 ^c
PVC	7.9	-	100	100	100	100	100	-	100	100	100	100	100	-	100	100	100	100	100	-	-
DOP	-	100	23	41	67	73	95	-	-	-	-	-	-	-	-	-	-	-	-	-	-
DOS	-	-	-	-	-	-	-	100	27	44	53	61	70	-	-	-	-	-	-	-	-
TOTM	-	-	-	-	-	-	-	-	-	-	-	-	-	100	18	38	57	63	75	-	-
(CaCO ₃) _A	-	-	-	-	-	-	-	-	-	-	-	-	-	-	-	-	-	-	-	0.931	-
(CaCO ₃) _B	-	-	-	-	-	-	-	-	-	-	-	-	-	-	-	-	-	-	-	-	0.815

a) PVC concentration expressed as % polymer by weight of coated support.

b) In cols. 2-19 all compositions expressed as phr.

c) Wt. of filler expressed in grams

TABLE II

SUMMARY OF IGC DATA EXPRESSED
AS Ω PARAMETER

Column No.	Ω at			
	30	50	70	90°C
1	0.33	0.40	0.46	0.50
2	2.70	2.61	2.61	2.55
3	0.52	0.58	0.59	0.64
4	0.97	1.06	1.04	1.10
5	2.41	2.29	2.20	2.20
6	2.58	2.70	2.55	2.50
7	2.73	2.57	2.44	2.49
8	2.06	1.99	1.94	1.90
9	0.77	0.80	0.83	-
10	1.55	1.61	1.66	-
11	1.72	1.72	1.81	-
12	1.89	2.06	2.00	-
13	1.99	2.08	1.96	-
14	2.88	2.81	2.80	2.76
15	0.46	0.49	0.51	0.52
16	0.75	0.80	0.82	0.80
17	1.33	1.40	1.44	1.46
18	1.64	1.66	1.68	1.63
19	2.26	2.20	2.18	2.18
20	0.82	0.80	0.79	0.79
21	1.33	1.20	1.17	1.19

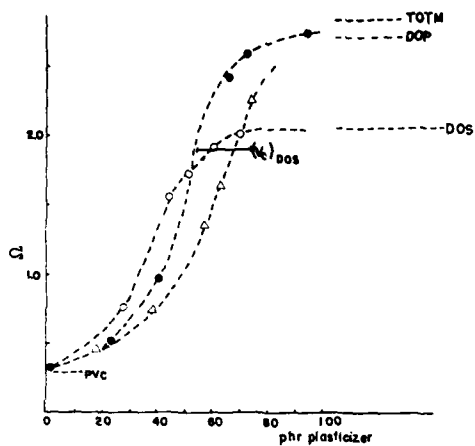


Figure 1: Relation of interaction parameter with critical plasticizer volume in PVC.

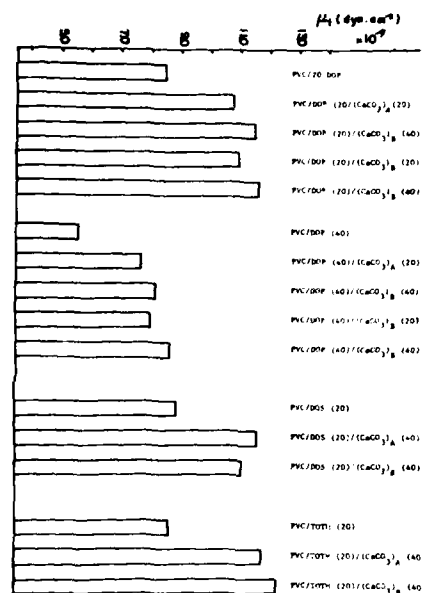


Figure 3: Initial modulus of filled, plasticized PVC: Effect of filler type and concentration.

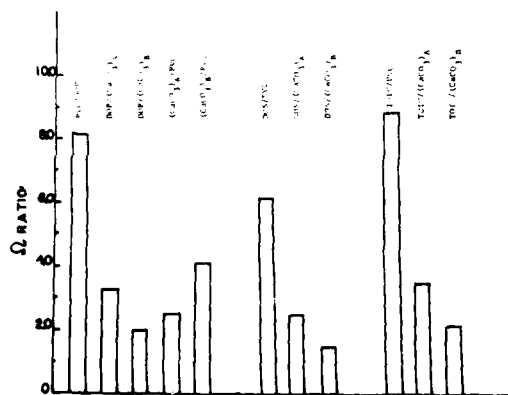


Figure 2: Apparent pair interactions in filled, plasticized PVC compounds. (30° data base)

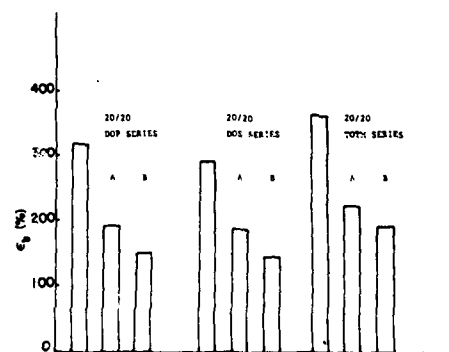


Figure 4A: Elongation at break for PVC compounds; 20% load level.

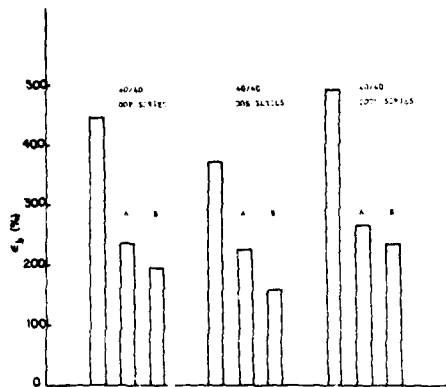


Figure 4B: As in Figure 4A; 40% load level.

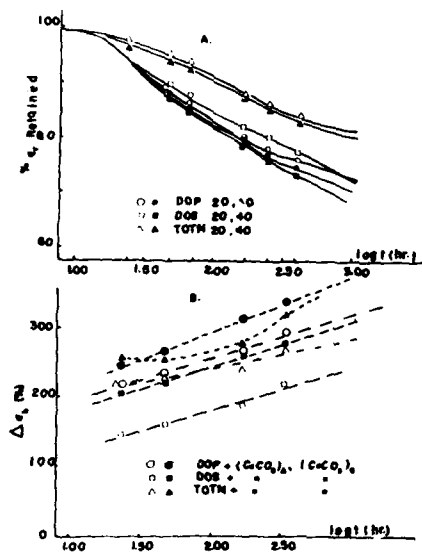


Figure 5: A. Retention of elongation following aging at 100°C; sensitivity to interaction effects.
B: Excess property loss due to presence of fillers in PVC aged at 100°C; sensitivity to interaction effects.

AD P000574

INVESTIGATION OF PREMATURE DEPLETION OF STABILISERS FROM SOLID POLYETHYLENE INSULATION

B.L. Board

H.J. Ruddell

Telecom Australia
Melbourne,
Australia.

ABSTRACT

Early failure of solid polyethylene insulation jointed in above ground closures is a serious field problem in Australia in cables made between 1965-74. Analysis has confirmed thermal oxidation as the cause, resulting from inadequate initial stabilisation and rapid depletion of antioxidant in service. No failures have been reported in more recent insulation incorporating the current primary antioxidant/metal deactivator systems, as used in many other countries. However, these systems are also depleted prematurely, and current polymers are unlikely to provide the expected life. Several factors cause this depletion of stabilisers, including rapid migration to the polymer surface due to insolubility at all service and polymer storage temperatures, substantial extrusion losses, elevated service temperatures and reaction with colourants. The use of a secondary antioxidant appears beneficial, and triple component stabilisation systems, with components chosen for their excellent solubility and oxidative stability, are being evaluated.

INTRODUCTION

Polyethylene insulated and sheathed telephone cable was introduced in Australia in 1956. It featured solid low density polyethylene (LDPE) insulated copper conductors in an unfilled core, and was used initially in sizes up to 100 pairs in the subscribers distribution network only. Solid polyethylene insulation is currently used in Australia in all unfilled distribution cables, which remain the standard cables for all aerial and urban underground distribution installations, and in some tail cables. (Cellular polyethylene insulation is used on filled cables, the standard cables for the buried rural subscriber and minor trunk networks, and on unfilled underground pressurised junction and subscriber main cables.)

In the earlier years following its introduction, many field problems occurred as a result of extrusion pinholes in the insulation. However, the oxidative stability was never questioned, and insulation cracking was not reported until the mid-1970s. The initial failures occurred in exposed (i.e. non-sheathed) insulation in above ground joints. Further reports and analysis suggested thermal oxidation as the cause, and the stabilising system used in the approved insulants was changed in order to overcome the problems.

However, the number of reports of insulation cracking in the earlier cables continued to increase, revealing that a major problem existed.

As these reports came from most areas of Australia, Telecom Australia decided to carry out a national field survey to characterise the extent and features of the problem. In conjunction with this survey, a comprehensive laboratory investigation was undertaken to determine the causes and extent of stabiliser losses in insulation, including the earlier failed insulation, current production insulation, and developmental insulations containing various experimental stabiliser systems.

HISTORY OF INSULATION CRACKING PROBLEMS

Insulants Used In Australia

The various solid polyethylene insulants used by Telecom Australia from 1956 to the present are listed in Table 1. Trade names of stabilisers have been used for convenience; their chemical names are listed in Table 6. There is some uncertainty about the stabilisation of the early polymers, and at least some insulant was imported prior to 1963/64. Prior to 1976, Santonox R, in low concentrations, was the principal if not the sole stabiliser in all insulants.

Overseas Experience Of Thermal Cracking

The phenomenon of embrittled solid polyethylene insulation in above ground pedestals was first observed in the USA in 1970 in the Bell network and some independent networks¹⁻³. Their conclusions were that the embrittlement of insulation occurring after 6-10 years' exposure in above ground jointing pedestals was due to the depletion of antioxidant by copper-catalysed air-oxidation at the elevated temperatures existing within the enclosures. It was also considered that the oxidation process was accelerated by the presence of a processing aid and the pigment titanium dioxide (TiO_2) in the polymer, and by a reduction in the concentration of antioxidant by migration and by dissolution in water condensed within the pedestal.

As a result, modifications were made in 1972 to the Bell System solid polyethylene resins for insulation of air-core cables. The stabilisation system was changed from a single primary (phenolic

TABLE 1 SOLID POLYETHYLENE INSULATION COMPOUNDS USED BY TELECOM AUSTRALIA

Period	Supplier/ Local (L) or Imported (I)	Polymer Density (kg/m ³)	MFI (g/10 min.)	Stabiliser System	Nominal Stabiliser Concentration	Comments
1956-60	UCAL/I?	918	2	Santonox R	< 0.05%	
1961-63/64	UCAL/I?	918	2	Santonox R Nonox WSP	< 0.05% = 0.1%?	
1963/64-66	UCAL/L ICI/L	919 923	0.3	Santonox R	0.05%	Provided a higher Mol. Wt. polymer
1966-76	UCAL/L ICI/L	926-928	0.3	Santonox R	0.05%	Density increased to overcome pinholes
1976-82	ICI/L	926	0.3	Irganox 1010 Eastman Inh. OABH	0.1% 0.1%	Introduced to overcome thermo- oxidative cracking
1977/78-82	UCAL/L	927	0.3	Irganox 1035* Irganox MD1024	0.1% 0.1%	

UCAL = Union Carbide Australia Ltd

ICI = ICI Australia Pty Ltd

* = Small concentrations of in-house processing stabilisers also incorporated.

type radical scavenger) antioxidant, Santonox R, to a system with both a primary antioxidant, Irganox 1010, and a copper deactivator, Eastman Inhibitor OABH, to improve the thermo-oxidative resistance of the polymer⁴. The polymer was changed from a 920 kg/m³ density resin to one with a density of 950 kg/m³ to improve physical properties of the insulation such as abrasion resistance⁵. Alternative metal deactivators Irganox MD 1024 and Ube MD have since been approved. The above two component stabiliser system is also used in the foam skin DEPIC insulation of filled cables. It is understood that these changes have resulted in an improvement in life expectancy of exposed insulation at joints.

Reports of similar insulation degradation in REA-sponsored cable networks⁶ followed soon after the initial Bell reports. Many of the independent US telephone companies and their cable suppliers followed the Bell lead and introduced similar changes to their stabiliser systems.

The Australian Experience

Some of the initial faulty joints observed in Australia in the mid 1970s were returned from the field for inspection. A preliminary analysis showed the embrittled unsheathed insulation to be depleted of Santonox R, consistent with the American findings. In order to arrest the manufacture of potentially faulty insulation, it was considered essential that the stabilising system be changed immediately. No detailed laboratory investigations were conducted at that time. Instead, as the symptoms of the degradation appeared identical to those observed several years earlier by Bell, Telecom Australia decided

to adopt a similar stabilisation system. In mid 1976 this change was implemented. In fact, different stabilisation systems were adopted by the two Australian polymer suppliers as is shown in Table 1, to suit their base polymers. These respective systems have been used since then for both the solid and cellular insulants. However, in contrast to the Bell policy, no change was made to the density of the solid polyethylene.

Since that time, observations of cracked insulation have continued to be reported from many parts of Australia in increasing numbers. The 1978/79 national fault analysis system reported about 2700 faults in above ground joints due to degraded insulation. These reports showed a geographic dependence roughly consistent with the thermal environment. Such data, together with the field reports from various Australian States, prompted a decision in 1980 to investigate the problem in detail and determine its severity and any specific features.

NATIONAL SURVEY OF CRACKED INSULATION

The field survey⁷ was conducted in late 1980 in all States except Western Australia. Joints were selected in both known trouble areas and in areas selected at random. Thus the survey showed some bias towards deteriorated plant.

The above ground joints⁸ inspected included the standard above ground jointing post (a free-standing galvanised steel enclosure similar to the REA channel-type housing⁶), the pole-mounted untailled terminal box (a black LDPE closure for drop wire feeding) and various local custom housings. Some underground openable joints (non-encapsulated plastic distribution joints housed in pits) were also examined.

Of the 200 joints surveyed, involving 216 cables, the following conclusions were drawn, many supporting earlier US observations ^{1,3,4,6}.

- i. 31% of all above ground joints exhibited some cracked insulation.
- ii. no degradation was observed in the small number of underground joints inspected.
- iii. the jointing post and untailled terminal box had similar incidence of embrittled insulation.
- iv. all failures observed were in the end length from which the cable sheath had been removed. No cracking was in sheathed sections.
- v. pole-mounted joints facing east, north, and west showed higher fault incidence than those facing south.
- vi. failures were observed in all but the most southern State. Thus all failures occurred north of 38° south latitude. However, in the hottest State surveyed, Queensland, 54% of joints were faulty. Correspondingly, the cooler areas showed failure rates less than the overall survey average. The results of ii-vi indicate clearly that the degradation is temperature-related.
- vii. all insulation failures occurred in cables manufactured between 1965 and 1974 (see Figure 1). This graph suggests that age in itself is not a critical factor.
- viii. the failures showed a dependency on colour. Table 2 presents the failure data according to the insulation colour. This is separated into two periods during which different colour codes were used. Shown are the percentages of the total cracked wires accounted for by each colour, and also these percentages corrected for the frequency of the respective colours in the colour code concerned (i.e. weighted percentages). The

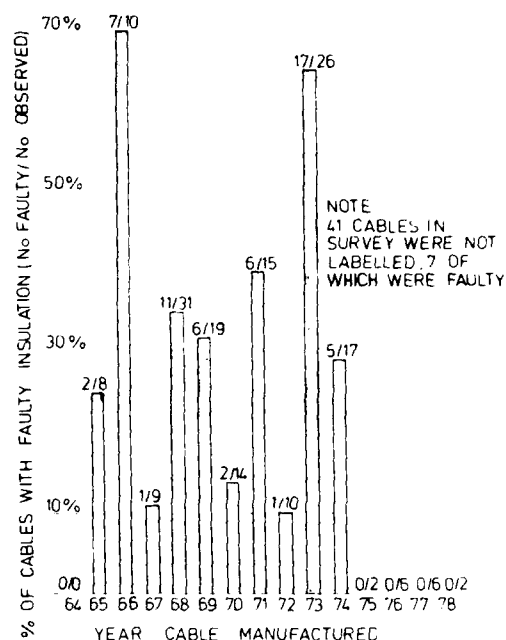


FIGURE 1 DISTRIBUTION OF INSULATION FAULTS FROM FIELD SURVEY ACCORDING TO YEAR OF MANUFACTURE

results show that white and grey exhibit by far the highest failure rate, and black is virtually fault-free. The 1965-69 period also showed considerable blue faults ². It is probable that the blue pigment used during the 1965-69 period contained free copper and was responsible for the considerable number of faults in blue insulation.

- ix. some joints displayed both cracked and uncracked insulation and, upon analysis, showed no antioxidant remaining in either state. Only the cracked insulant exhibited a decrease in molecular weight.

TABLE 2 INSULATION CRACKING ACCORDING TO COLOUR (FIELD SURVEY DATA)

YEAR OF MANUFACTURE	MEASURE DETAILS	INSULATION COLOUR								TOTAL
		WHITE	RED	BLUE	ORANGE	GREEN	BROWN	GREY	BLACK	
1965-67	Number of Failures	35	3	9	1	4	3	9	2	66
	% of Total Failures	53	4.5	14	1.5	6	4.5	14	3	100
	Rel. Freq. in Colour Code	5	5	1	1	1	1	1	5	
	Weighted % of Total Failures	21	2	26	3	12	9	26	1	100
1968-74	Number of Failures	241	30	14	13	8	4	106	-	416
	% of Total Failures	58	7	3	3	2	1	25	-	100
	Rel. Freq. in Colour Code	5	5	2	2	2	2	2	-	
	Weighted % of Total Failures	38	5	5	5	3	2	42	-	100

- x. excessive failures were observed in joints where the obsolete practice of twisting the two legs of a pair together tightly at the base of the joint had been carried out.
- xi. the use of grease-filled sleeves appeared to give some protection to the insulation.
- xii. tin-plated copper conductors used in the tails of in-joint loading coils also showed cracked insulation.
- xiii. partial fading of insulation in some joints suggests that photochemical oxidation may be a contributory factor (neither type of joint is completely sealed against light entry). However, the survey indicated that it is at most only a secondary factor.

It is apparent in the limited samples seen that no cracking was observed in insulations incorporating the current stabilisation systems.

As a result of this survey, a detailed laboratory program was undertaken to investigate the causes and the extent of stabiliser losses in pre-1976 insulation, in post-1976 insulation incorporating the two current stabiliser systems, and in insulation containing various experimental stabiliser systems.

LABORATORY ANALYSIS OF PRE-1976 CABLE INSULATION

The results shown in Table 3 were obtained on insulation from a 1970 cable submitted from Toowoomba, Queensland because the joint had severely cracked insulation. Tests conducted on all colours of both the exposed (cracked joint area) and unexposed (uncracked under sheath) insulations revealed levels of antioxidant concentration so low as to offer no protection to the polymer against oxidation. This finding is consistent with the field experience that joints fail in less than two years after being remade from insulation previously protected by the sheath.

TABLE 3 COMPARISON OF EXPOSED AND UNEXPOSED INSULATION OF 1970 CABLE

Insulation Colour	Unexposed Insulation		Exposed Insulation	
	OIT	Residual	OIT	Residual
	t 190°C	Santonox R	t 190°C	Santonox R
	minutes	% m/m	minutes	% m/m
White	6	0.0043	<1	<0.0005
Grey	5	0.0034	<1	<0.0005
Green	6	0.0044	<1	<0.0005
Brown	8	0.0021	<1	<0.0005
Blue	7	0.0089	<1	<0.0005
Orange	9	0.0029	<1	<0.0005
Red	6	0.0051	<1	<0.0005

The period of cable manufacture in which the insulation is prone to the above type of premature failure by cracking was clearly identified in the field survey (Figure 1) as being 1965-1974. It was therefore of interest to determine what difference exists between cables made during this period and those made prior to 1965. Short lengths of cable were subsequently obtained for many of the years between the introduction of plastic cable in 1956 and up until 1975. Table 4 shows the results of the tests conducted on the white insulated wire taken from beneath the sheath at least two metres from the end of all cables.

Year of Manuf.	Stabiliser Type Present	Stabiliser Concentration			Pigtail Test F +	OIT ² t 190°C Al ₂ O ₃
		Initial by XRF*	Residual by HPLC	WSP		
		SR %	SR %	WSP %	days	minutes
1956	SR	0.020	<0.001		10	<1
1958	SR	0.023	<0.001		9	1
1961	SR&WSP	0.022	<0.001	0.046	146	17
1962	SR&WSP	0.019	<0.001	0.054	45	33
1963	SR&WSP	0.027	0.015	0.038	45	37
1963	SR&WSP	0.029	0.015	0.039	41	34
1966	SR		0.014		6	8
1966	SR	0.038	0.008		16	11
1966	SR	0.034	0.004		33	6
1967	SR	0.034	0.005		14	10
1968	SR	0.034	0.006		14	14
1969	SR	0.026	0.003		22	15
1969	SE	0.041	0.008		15	18
1970	SR	0.024	0.004		15	6
1972	SR	0.029	0.001		20	9
1973	SR	0.033	0.003		16	7
1974	SR	0.038	0.004		40	<1
1975	SR	0.042	0.012		45	2*

* Calculated from total sulphur concentration determined by ICI Australia Operations Pty Ltd using X-ray fluorescence techniques. It includes sulphur present on the insulation surface (i.e. the insulation was not wiped).

+ The F₂ value approximates the 20% failure point. For a more precise definition refer to Reference 4.

SR = Santonox R

WSP = Nonox WSP, now known as Permanox WSP(PU).

TABLE 4 CHARACTERISTICS OF UNEXPOSED (WHITE) INSULATION TAKEN FROM UNDER SHEATH OF FIELD CABLES

The cables had been manufactured by three cable companies using polyethylene from two local and one Japanese supplier. Consequently it was reasoned that no blame could be placed on any one of the cable or polymer manufacturers. Also, as faults were found in cables made in 1965, the consequent change made to the polymer density in 1966 cannot be considered a cause of failure.

The stabilising systems used in the polymer were identified by thin layer chromatography (TLC) and the remaining stabiliser concentration in the insulation determined by high performance liquid chromatography (HPLC)³. Santonox R, a sulphur-containing antioxidant, was found to be present in all insulations and its initial concentration (i.e. that at the time of compounding the

polyethylene) was calculated from the total sulphur concentration, as determined by a quantitative X-ray fluorescence technique. This method is able to account for all sulphur present, be it in the form of unused Santonox R or its breakdown products. The determination showed Santonox to be present initially in very small amounts, frequently far below the stated nominal concentration of 0.05% at the time of polymer manufacture. The residual Santonox R concentrations in all samples were extremely low.

Another major finding from the cable analysis was the presence of the mixed stabilising system of Santonox R and Nonox WSP in insulation made between 1961-1963. These insulations were in good condition 19-21 years after manufacture, as demonstrated by excellent pigtail test⁹ and oxidation induction times (OIT)¹⁰ when compared with the results for insulation made many years later. The amount of Nonox WSP remaining in the insulation ($\geq 0.04\%$) was very high compared to that of Santonox R ($\approx 0.015\%$). Unfortunately, no analytical technique is available to ascertain the concentration of Nonox WSP at the time of polymer manufacture in the same way as was possible for Santonox R.

STABILISER DEPLETION

As the Santonox R component of the double antioxidant system was lost from the insulation to the same extent as in the straight Santonox R systems, the better quality of the insulation containing the double system must have been due to the Nonox WSP component alone. It was at first thought that this may have been a result of its better chemical efficiency and that smaller amounts were consumed in protecting the polymer during processing and service life. However, thermal analysis conducted on LDPE containing these antioxidants did not support the above hypothesis as the oxidation induction time (OIT) for Nonox WSP was found to be only about half that of Santonox R⁸, in general agreement with previously published data¹¹.

In view of the effectiveness of Santonox R in controlling oxidation, investigations were conducted to ascertain if the losses of Santonox R were the result of reactions with other additives or due to other causes, since depletion of an antioxidant from polyethylene can occur by both chemical and physical processes^{12,13}. The additives requiring study included pigments/opacifiers and their coatings, metals present as the conductor or as contaminants in the polymer from the production process, and other possible components of the colour and stabiliser masterbatches, including dispersants and low molecular weight polyethylene base polymers. Losses incurred during the processing of polymer compound to insulation on wire and during the storage of stabiliser masterbatch and compounded polymer prior to processing were also investigated.

ANTIOXIDANT LOSSES PRIOR TO PROCESSING

As mentioned previously, the polymer was considerably understabilised at the time of compounding. The familiar problems of ensuring that the specified levels of antioxidant are included in the compound have been considerable over the years. Recent improvements in measurement technique and equipment¹⁴ and greater understanding of stabiliser behaviour have done much to overcome the uncertainties.

However, it has not been generally appreciated that a significant loss of stabilisers can occur from the stabiliser masterbatch or from the insulant from the time of manufacture through to extrusion. It is suggested that the loss may be particularly rapid from the masterbatch itself due to the high concentrations of stabilisers there, but no attempt has yet been made to verify this. However, the occurrence of losses from the compound during storage has been verified.

The results in Table 5 show that the concentration of some antioxidants in polymers stored in a laboratory at room temperature, whether in the dark or exposed to light, diminishes at an alarmingly fast rate.

TABLE 5 LOSS OF ANTIOXIDANT FROM POLYETHYLENE STORED IN THE LABORATORY

Sample No.	Antioxidant	Time period stored months	Loss during storage	
			in dark %	in light %
1	Santonox R	28	47	
2	Santonox R	28	38	
3	Irganox 1010	37	54	
4	Irganox 1010	37	46	
5	Irganox 1010	37	47	
6	Irganox 1010	37	52	
7	Irganox 1010	38	57	
8	Irganox 1010	12		24 #
8	Irganox 1010	21		39 #
8	Irganox 1010	42		69 #

Ref. 15

It is suggested that the major cause of such rapid loss under relatively moderate conditions is migration of the antioxidant to the polymer surface, where it is lost to the system. Stabiliser migration, and investigations to identify high solubility stabilisers, are discussed in detail later in this paper.

ANTIOXIPANT LOSSES DURING PROCESSING

Stabilisers are added to polymers for various reasons, one of which is to protect the polymer during processing. In the insulating process, the polymer is subjected to very high shear stress and temperature conditions. The amount of stabiliser consumed in chemical protection or lost by physical means (volatilisation) depends to a very large extent on the extrusion machine and operating conditions^{14,16}.

In order to determine whether the loss of the primary antioxidant was significant in cables supplied to Telecom Australia, an analysis was carried out in 1979 of samples of insulated wire and insulant pellets obtained from all three Australian cable manufacturers using the current approved commercial compounds. It was found that the loss of antioxidant was as high as 45%, with an average loss of 26% for all samples. The cellular insulant (MDPE) generally exhibited much higher losses than the solid compounds. Sheath samples were similarly analysed and the loss of stabiliser (Santonox R) averaged 15%.

In late 1980, an investigation was conducted with the three Australian cable manufacturers using four specially prepared compounds, each incorporating a different secondary antioxidant in addition to the normal dual component stabiliser system, to ascertain the effect of the additional antioxidant in controlling the loss of the primary antioxidant during extrusion. The results, shown in Figure 2, reveal that an average of 34% of the primary antioxidant was lost, with the maximum being 54%. Also, it can be seen that, with each manufacturer, less primary antioxidant was lost when BHT or PEPQ was included as the third component than was lost from the other two triple stabilised compounds.

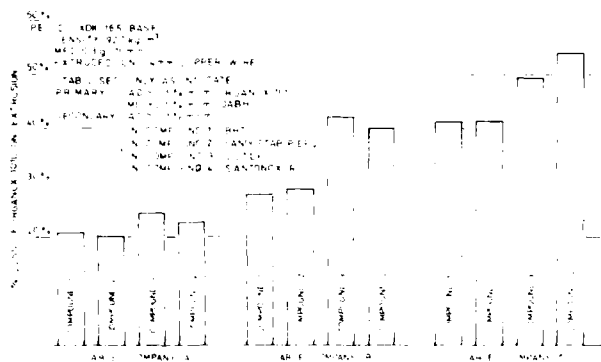


FIGURE 2 LOSS OF ANTIOXIDANT (IRGANOX 1010) INSULATION EXTRUDED BY DIFFERENT CABLE COMPANIES (1980/81).

In 1981, samples of granules and insulation (HDPE, stabilised with Irganox 1010/Irganox MD 1024) were obtained from a Japanese cable manufacturer for a similar evaluation to verify that the considerable processing losses were not a local phenomenon. Although the solid insulation showed quite acceptable losses of antioxidant (~15%), the cellular insulation showed losses of 46%. The losses of the metal deactivator were considerably higher in both cases.

That extruder losses were not being monitored by any of the overseas cable companies visited by one of the authors during 1981 was therefore a great surprise. The assumption being made by manufacturers was that an adequate proportion of a nominated concentration of stabiliser in an approved polymer would always be present after processing!

Because of the magnitude of these extrusion losses, the use of a secondary antioxidant was proposed. It is now accepted generally that an effective primary antioxidant of high molecular weight and low volatility in combination with a metal deactivator in appropriate concentrations are required in order to obtain even moderate insulation lifetimes^{2,9,12,17}. However, the need for a secondary antioxidant (hydroperoxide decomposer) is not widely accepted. In addition to interrupting the degradative cycle associated with the decomposition of the hydroperoxides in the on-going oxidation mechanism, an effective secondary antioxidant should also limit the consumption of the primary antioxidant during extrusion, and prevent crosslinking of radical formations or chain scission, thus maintaining acceptable insulation surface finish and mechanical properties¹⁷⁻²⁰.

The results in Figure 2 are in general agreement with those of Swasey¹⁹. In that work, BHT was found to be as good a processing stabiliser as the phenols, whilst DLTDPP proved ineffective. However, PEPQ performed extremely well in evaluations, showing a marked synergistic effect on both processing stability and long term stability when used in conjunction with a phenolic antioxidant. BHT showed no such synergism with the phenols. Some of the organic phosphites have also demonstrated considerable synergism with the phenols in extending processing stability²⁰.

In spite of more recent investigations demonstrating that processing losses at Company C can be reduced to 10-15% with reduced extruder shear and tighter machine controls, such as improved temperature profiles, it is believed that the use of an effective secondary antioxidant is worthwhile. For the reasons given and also because BHT can discolour the polymer and has no long term stability due to its volatility, Sandostab PEPQ was chosen as the secondary antioxidant for use in compounds for the migration evaluations of developmental stabiliser systems.

Our studies have demonstrated the need to specify not only the stabiliser type, but its content in the polymer after processing onto wire. This must be of a level sufficient to provide a minimum life of 40 years under all service conditions. To meet this requirement, the cable manufacturer must ensure optimum extrusion conditions for compounds containing a sufficient extra amount of stabiliser to provide the specified concentration after processing.

MIGRATION OF STABILISERS

The performance of an antioxidant in protecting polyethylene from oxidation is a function of its solubility in polyethylene over the service temperature range, its tendency to diffuse or migrate out of the polymer, its chemical effectiveness in countering the degradation reactions, its volatility, and of the polymer itself. Moisan²¹ claims that the solubility is the most important property in determining the long term stability. Predictably, solubility and migration are intimately related.

Migration of antioxidants from polyethylene has been studied by many people^{3,11-13,21,22} but as stated by Roe²² it appears that the "physical depletion of additives from polyolefins has not been given the proper attention that it deserves". The migration of stabilisers from low and medium density polyethylene was investigated by us as a function of both temperature and time, initially using moulded plaques and later using insulation on copper wire.

Relationship between migration and temperature

The degree to which a stabiliser diffuses to the polymer surface is related to its solubility in the polymer¹¹, and hence is dependent upon temperature.

The relationship between migration and temperature was studied using a 919 kg/m³ density polyethylene (UCAL DFDL 6005 unstabilised) as the base resin into which the stabilisers given in Figure 3 were incorporated in masterbatch form on a two-roll mill. 0.5 mm thick plaques were pressed at 165°C from the crepe produced. The plaques were aged in air-circulating ovens at temperatures of 23, 40, 60, 80 and 100°C each for 28 days. The amount of exudate on the plaque surfaces was determined before and after ageing at each of these temperatures by immersing the plaque, 30 times in 30 seconds, in acetone (containing 10% v/v dimethyl formamide when determining the migration of Eastman Inhibitor OABH) followed by a wash and finally a wipe with cotton-wool wetted with a fresh amount of the same solvent type. The stabiliser content in the "wash" was determined by HPLC and the amount of stabiliser migration expressed as a percentage of the total stabiliser initially present in the sample.

The results are presented in Figure 3 from which it can be observed that Nonox WSP and Eastman Inhibitor OABH did not migrate at any test temperature and that maximum migration occurred at 60°C for 4 out of the 5 stabilisers that did show migration tendencies.

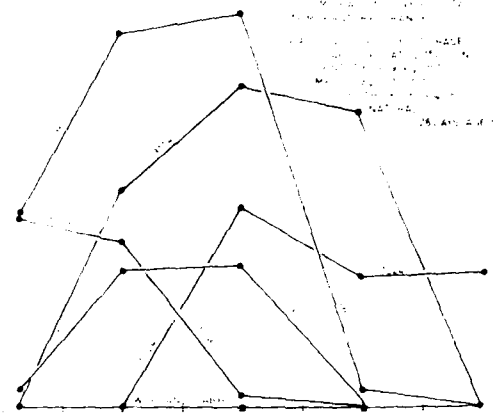


FIGURE 3 MIGRATION OF STABILISERS AFTER 28 DAYS AT VARIOUS TEMPERATURES.

It should be noted that the above results are based on stabiliser concentrations of approximately 0.1% in LDPE. Different concentrations may result in different migration behaviour, this being determined by the solubility of the stabiliser in the polymer. Once the concentration exceeds the solubility limit of that stabiliser at a particular temperature, the stabiliser will exude until eventually it does not exceed that limit at that temperature (see Figure 6).

The maximum value at 60°C for Santonox R agrees with Howard's conclusion³ that migration of Santonox R is most prominent in the region of approximately 50-70°C. 60°C is also close to the maximum temperature found in current above ground joint enclosures. Although it was recognised that 60°C favoured Irganox 1035 which migrates at lower temperatures, it was considered to be the temperature best suited for a single point determination. The investigation of the relationship between migration and time was therefore conducted at this temperature.

Relationship between migration and time

This study was conducted in two parts. Firstly, an investigation was carried out of the migration behaviour of 4 primary antioxidants and 2 metal deactivators from 0.5 mm thick plaques of 919 kg/m³ polyethylene. Each antioxidant was used in a set of 3 systems: either as the sole antioxidant or combined with each of the two metal deactivators. The secondary antioxidant,

Sandostab P-EPQ, was added to the systems containing the metal deactivators. Various colour masterbatches were used within each system, making a total of 39 plaques evaluated. Measurement of any migrated primary antioxidant or metal deactivator was determined before and after ageing at 60°C for 36 and 72 days, by the same technique as described earlier. No attempt was made to determine Sandostab P-EPQ, as energy dispersive X-ray analysis techniques indicated Sandostab P-EPQ was not present on the surface of the plaques before or after either ageing period, and it was therefore assumed to be non-migratory.

The most important results⁸ arising from the plaque tests were that Nonox WSP, Irganox 1035, and Eastman Inhibitor OABH showed negligible migration at 60°C even after 72 days, whilst Irganox MD 1024 migrated rapidly. Santonox R and Irganox 1010, used on their own, also migrated readily. However, in combination with other stabilisers, the migration of Santonox R decreased whilst that of Irganox 1010 increased. Except for those stabilisers that migrated very rapidly, the quantity of exudate detected after 72 days ageing was often approximately double that for the 36 day period. The addition of colour masterbatch appeared to have no effect on the migration behaviour of any system.

The second part of the study was to ascertain if the geometry, polymer morphology, or copper wire contact altered the behaviour pattern of the stabilisers. The same 4 antioxidants as before, combined with Eastman Inhibitor OABH and Sandostab P-EPQ, were incorporated into the two approved 926/7 kg/m³ base polyethylenes and extruded as insulation on wire. Also evaluated were the two currently used solid insulating grade polyethylenes from the same two companies (see Table 1). As before, the incorporation of various colour concentrates was followed, making a total of 32 insulated wires examined.

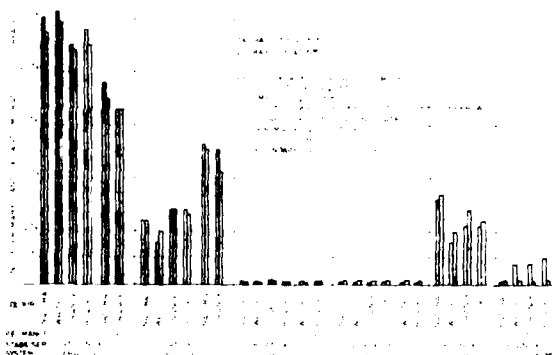


FIGURE 4 MIGRATION OF PRIMARY ANTIOXIDANT FROM POLYETHYLENE INSULATED WIRE CONTAINING VARIOUS STABILISING SYSTEMS

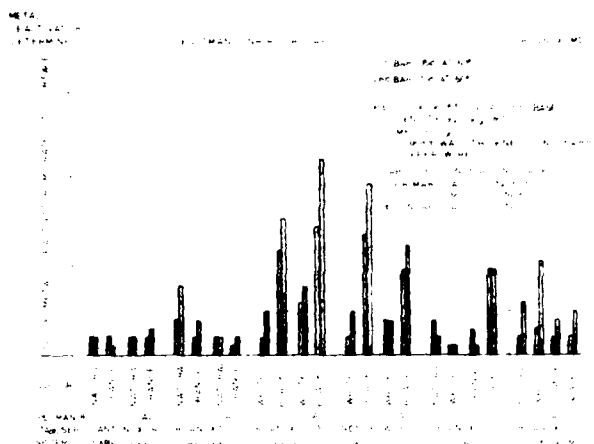


FIGURE 5 MIGRATION OF METAL DEACTIVATOR FROM POLYETHYLENE INSULATED WIRE CONTAINING VARIOUS STABILISING SYSTEMS

The results for migration from the insulation are given in Figures 4 and 5. When compared with the plaque results, several differences are apparent for which no technical explanations can yet be offered, although the different polymer densities of the plaques and insulation may be a factor. The significant differences are (i) an increase in the migration of Santonox R when in the presence of Eastman Inhibitor OABH, (ii) migration of Eastman Inhibitor OABH from black insulation and (iii) a decrease in the loss of MD 1024 when combined with Irganox 1035.

In contrast to Figure 4 which expresses the percentage of antioxidant rejected by the polymers during ageing at 60°C, Figure 6 shows the amount of antioxidant retained in the same two polymers after several months at 60°C. These values are in good agreement with the solubility data of Moisan¹¹ determined at the same temperature.

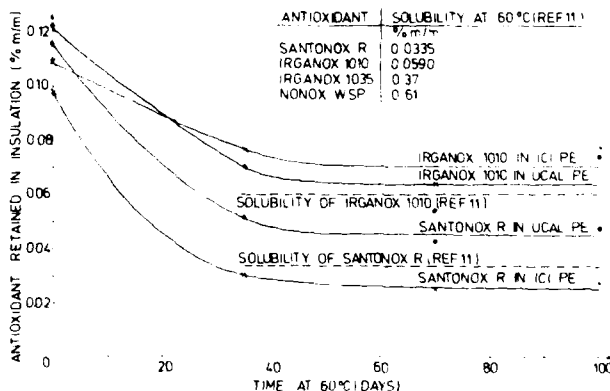


FIGURE 6 PERCENT ANTIOXIDANT RETAINED BY INSULATED WIRE AGED AT 60°C

Accelerated Ageing Testing

The migration results have demonstrated a major reason for inaccuracies in life prediction when accelerated ageing tests (OIT, oxygen uptake, pigtail, or elongation testing) are conducted at temperatures well above the actual service temperatures ^{3,12,18}. Hence any accelerated ageing test of insulation containing migratory stabilisers must incorporate a pre-conditioning program of forced migration ²³ prior to ageing, carried out at that temperature within the service temperature range at which maximum migration occurs for the particular stabiliser system used. This ensures that the stabiliser concentration at the commencement of the ageing test does not exceed the effective net concentration during initial service. With non-migratory stabilisers, the forced migration step becomes unnecessary.

Some ageing tests have been completed on insulated wire containing several of the above stabiliser systems. These samples were pre-conditioned at 60°C for 70 days, then the surfaces were wiped prior to ageing at 100°C. Three measures of degradation have been used in these tests: OIT (on straight insulation), cracking stability (on insulation pigtails), and elongation at break (on straight insulation). These measures have yielded inconsistent results. No pigtails cracked, even after prolonged ageing such that the elongation and OIT values of similarly aged samples were both drastically reduced to unacceptable levels. Also, the elongation and OIT results did not correlate: although the OIT reduced with age, many samples with low elongation showed much higher OIT values than did other samples with greater elongation. This was true where the samples were different base polymers, and where the samples were of the same base polymer but incorporated different stabiliser systems.

This was also observed in the field samples listed in Table 4: the OIT and pigtail results showed no uniform correlation with the residual antioxidant concentrations or with each other.

When a joint is re-entered, the insulation is subjected to dynamic stressing, and it must be elastic to survive. Pigtail tests do not imitate this stressing. Consequently, pigtail tests can give optimistic results, as observed above.

Elongation appears the most realistic measure of degradation, as it involves the transient stressing of the aged material. It is particularly appropriate for HDPE testing as it is claimed ²³ that such polymer cracks before it oxidises.

Figure 7 shows the results of ageing tests performed on MDPE base polymers from two suppliers containing two different stabiliser systems. The different performances of the stabiliser systems can be observed. However,

the most substantial difference is that one polymer appears to be clearly superior to the other. This may be due to polymer morphology - molecular weight distribution, type and number of branch chains, degree of unsaturation etc. - and/or metal contamination. Further work is being performed to explore the polymer contribution to ageing performance as well as the stabiliser system and colour contribution.

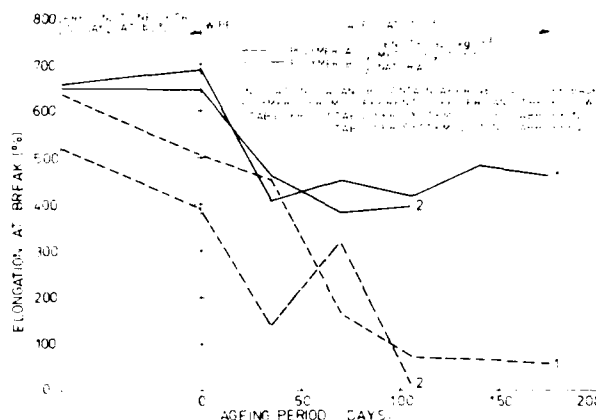


FIGURE 7 ACCELERATED AGEING OF EXPERIMENTAL STABILISER SYSTEMS

DEPLETION OF ANTIOXIDANTS BY PIGMENTS AND OTHER POLYMER ADDITIVES

The field survey data on colour dependency of failure (Table 2) indicated that white and grey insulation were the most readily degraded colours, accounting for more than 75% of all failures (after weighting the results to allow for the relative frequency of appearance of the colours in the colour code). As all colour concentrates have been obtained almost exclusively from the one manufacturer since 1956, the only possible difference between the white and grey insulation and the other colours was the TiO₂ content. This was 40% and 30% for white and grey respectively compared to an average value of 10% for green, orange, blue and brown. Red and black contained no TiO₂ prior to 1974.

It is well documented ²⁴⁻²⁶ that reactions occur between primary antioxidants ² (phenols, amines) and the reactive hydroxyl groups of TiO₂ pigment created as a result of the manufacturing process. These hydroxyl groups are on the edges of the surface crazing of the TiO₂ particles ²⁷. Attempts to reduce the reactivity of the hydroxyl sites by applying 3 nm thick coatings of various metal hydrous oxides has been only partially successful since the coatings are never completely homogeneous. However, these coatings are also believed to react with antioxidant ³. No zinc or zirconium oxide coatings have been used in the

titanium pigments supplied (from one manufacturer only) for Telecom masterbatches to date. Silicon and aluminium oxide coatings have, however, been employed extensively in these coatings, together with some organic coating compounds in post-1967 pigment. Generally, the cable industry has not recognised that such reactions occur, and they should be considered when selecting pigments and antioxidants.

Thus, in the faults surveyed, it is highly probable that a Santonox R/TiO₂ reaction occurred. Since the white and grey insulations have greater loadings of TiO₂ than the other colours, higher reaction losses of Santonox R resulted. This left a lower concentration of Santonox R available to protect the polymer against oxidation, causing earlier degradation. Conversely, the good performance of black insulation (pre-1968 cables) could be attributed to the absence of TiO₂, since the small amount of carbon black present would have provided little protection from oxidative attack.

It is believed that the other inorganic pigments used in masterbatches, particularly heavy metal pigments, may also react with antioxidants in a similar manner to TiO₂, though possibly at a slower rate². In addition, at least some of these pigments are coated with similar hydrous oxides to those on TiO₂ to improve stability. These coatings also prevent agglomeration of the finely divided small pigment particles. Thus these coatings, too, can consume the stabiliser/s.

Siloxane is also commonly used as a lubricant or dispersing agent in pigment manufacture, and metal stearates are often used in colour masterbatch preparation to aid dispersion of the particles throughout the polymer on which the masterbatch is based. Metal stearates and siloxane react with phenolic antioxidants^{24,25}. Fortunately, no metal stearates or other lubricants, including low molecular weight PE waxes, are used in either Telecom's colour masterbatches or stabiliser masterbatches. Only a minimal amount of siloxane (<0.5%) is present in the currently used titanium pigment.

Active metals can also be present in the insulant as catalyst residues of the polymerisation process, and can degrade the insulant stability¹⁶. However, the approved Australian insulants are produced by processes in which the catalyst residue levels are not considered significant.

CORRECTIVE FIELD PRACTICES AND HARDWARE

The obvious and possibly most effective solution to thermal degradation of insulation is to place all cable joints underground. However, this is not attractive in many Australian rural areas for several reasons. Therefore alternative techniques need to be considered to minimise degradation in both existing and new above ground installations.

Since the laboratory analysis confirmed that sheathed insulation adjacent to a degraded joint is virtually exhausted of antioxidant, little

benefit is gained by stripping back the sheath and remaking the joint. It appears necessary to replace the affected cable/s back to the nearest underground joint. This may be a new underground joint installed at the base of the pole or jointing post to limit the length of cable to be replaced. Encapsulation of joints, whether degraded or satisfactory, is not an option as complete encapsulation is not practiced in Australia.

Colour - related changes are also being considered. These include the adoption of a colour code based on the susceptibility of the colours to oxidation, the reduction of masterbatch concentrations to a minimum level required for correct colour identification, the acceptance of some degree of translucency in the insulant colours, and the relaxation of the colour standard limits specified on production insulation. Understandably, however, decisions on these aspects cannot be made until the analytical work planned for colour masterbatches and pigments is completed and the most suitable masterbatches for our insulants are identified.

The field survey indicated that the insulation cracking was temperature related. Loss of antioxidant by physical and chemical processes mentioned previously is also temperature dependent. Therefore temperature recording sites were established recently to measure the thermal conditions of joints over an extended period. The recording sites are near Mt. Isa, Queensland (a HOT DRY climate, 21st parallel south latitude) and at Melbourne, Victoria (a TEMPERATE MOIST climate, 38th parallel south latitude) (Köppen's Climatic Classification). These climates reasonably bracket the range of climates encountered by the cable network in Australia. The limited data⁸ indicate that temperatures up to 15°C higher and 10°C higher than ambient shade temperature are reached inside the standard terminal box and jointing post respectively, the difference increasing with the ambient temperature. However, the use of white plastic covers or overcovers on these enclosures reduced the maximum temperatures inside the joints substantially. They also reduced the daily temperature fluctuations, thus verifying their insulating effect. No further significant reduction appears to be gained by venting the white covers, though some small improvement is obtained by venting the standard enclosures. Therefore, the design and use of white covers is being examined. Rigid PVC pipe overcovers are already a standard item for use on above ground jointing posts in some rural areas to prevent cable damage during grass fires. However, they are unlikely to be considered suitable for use in suburban locations.

The use of aliphatic polyurethane and butyl rubber insulation restoring sprays²⁸ and restabilising sprays²⁹ are not considered viable treatments. The mechanism of stabiliser migration to the insulation surface is likely to prevent restabilisation by spraying. At best, these approaches will extend the life of non-cracked

insulation by a relatively short time. Additionally, their use raises significant occupational safety and health concerns for field staff.

Thick foam cover bags for joints are claimed⁶ to provide some thermal protection to the insulation. However, moisture condensation in the bag and periodic low insulation resistance - related faults can be a feature of these bags.

SUMMARY

Insulation of Cables Manufactured prior to 1976

Our investigations have shown that the premature degradation of the polyethylene insulation of cables manufactured during the period 1965-1974 has been confined to installations in above ground joint enclosures, and was caused by thermo-oxidation, resulting primarily from insufficient and hence ineffective antioxidant (Santonox R) content. The low concentration of antioxidant detected experimentally has been caused by a number of interacting factors. The nominal 0.05% concentration in the unprocessed compound has been shown to be clearly too low for the intended application, even if the claimed concentration was ever present in the finished product. Our measurements indicate that the true figure since 1963 was on average about two thirds of the claimed value. It is also now clear that further Santonox R losses must have occurred during storage and extrusion, leading to a further reduction of at least 20% and perhaps as high as 50%. It is therefore not unreasonable to assume that the Santonox R concentration in the finished insulation was only about 0.02%.

Under the temperatures existing in above ground temperature enclosures, it has been demonstrated that Santonox R rapidly migrates to the polyethylene surface. Furthermore, reactions with heavy metal pigments and their coatings in the insulation colourants can lead to further significant losses, in particular with those colours containing a high concentration of TiO_2 .

Consequently, it is evident that little or no Santonox R remained in the insulation after a relatively short time to provide protection against the normal oxidative attack. Once the available antioxidant had been used up, by reaction or exudation, the oxidative chain reaction proceeded under the catalytic action of the metal conductor and the acceleration in the reaction rate due to elevated temperatures in the enclosures, to the stage where severe cracking of the insulation occurred.

However, with Nonox WSP it has been shown that losses due to migration are negligible. Therefore any reduction in antioxidant concentration in the 1961-63 cables was probably caused by depletion in performing its expected function as a primary antioxidant. Thus the tendency of Nonox WSP not to migrate enables it to provide protection against oxidative attack for a much longer time span than does Santonox R, even though thermal analysis data suggests Nonox WSP to be inferior.

Insulation of Cables Manufactured after 1976

As described, two new stabilisation systems were introduced in 1976/77, both systems containing an antioxidant as well as a metal deactivator, both at 0.1% m/m, with the aim of improving thermal oxidative stability. Since then we have found that both Irganox 1010 and Irganox 1035 migrate significantly at service temperatures. Irganox MD1024 gave similar results for plaques but, for as yet unexplained reasons, exhibited low migration for a small sample of insulated wires. Eastman Inhibitor OABH showed a low tendency to migrate except in black coloured polyethylene. As these new systems have been in service for only a short time, no faults have yet been reported from the field, and it is still expected that insulation containing these systems will last longer than the Santonox R-containing insulation. However, our results indicate that both systems will tend to lose their primary antioxidant. Also, the possible rapid loss of Irganox MD 1024 in one system could lead to early depletion of the primary antioxidant. Consequently the insulation containing either of these systems is still unlikely to achieve the specified 40 year service life, particularly in the hotter regions.

Future Insulation

Based on the studies carried out to date, it is believed that the following actions will prevent premature stabiliser depletion:

- a. ensure that an adequate amount of stabiliser is present in the polymer after extrusion of insulant on wire. The processing losses must be allowed for in determining the required level of stabiliser in the polymer compound before extrusion.
- b. select stabilisers from those known to exhibit low volatility and little or no tendency to migrate over the entire service and storage temperature range when present in the required concentrations.
- c. choose a stabiliser system which will counter all possible thermal oxidation mechanisms. This can be achieved by the inclusion of suitable efficient primary and, possibly, secondary antioxidants as well as a metal deactivator.
- d. ensure that the stabiliser concentration is not significantly depleted by reactions with other additives, i.e. colourants. Limit the concentrations of reactive additives where possible.
- e. reduce the temperature inside the joint enclosure, as this will extend the insulant life due to the reduction in the stabiliser depletion rate. The optimum solution is to locate all joints underground. Where this is impossible or impractical, the use of white reflective covers on above ground joints appears effective.

To date only a limited number of stabilisers have been evaluated in the laboratory, and of these the system of Permanax WSP (PQ), Eastman Inhibitor OABH and Sandostab P-EPQ appears to provide the best protection for our existing solid medium density polyethylene, the choice of components being in line with (b) and (c) above. Compounding and processing trials of the solid MDPE insulant containing the above stabiliser system at minimum concentrations of 0.09%, 0.09%, 0.05% respectively are currently in progress.

Further studies are planned to investigate other antioxidants and metal deactivators, particularly those of high solubility, in order to pinpoint the most efficient system for each base polymer and the optimum component concentration levels. Furthermore, a parallel study is required to identify the optimum stabilising system for cellular polyethylene insulation in both filled and unfilled cables. Finally, much remains to be done to characterise the reactivity of the various masterbatch pigments and their coatings, and the possible replacement of TiO₂ and other metal pigments by alternative non-metallic pigments. Such work will also necessitate a review of the current colour code and colour standards.

Through these combined and multiple actions Telecom Australia expects to achieve a minimum 40 year service life for all future cables under the most severe operating environments.

TABLE 6 CHEMICAL IDENTIFICATION OF STABILISERS

Trade Name	Manufacturer	Chemical Name
Santonox R	Monsanto Co	4,4' - Thiobis (6-tert-butyl-3-methylphenol)
Irganox 1010	Ciba-Geigy Ltd	Tetrakis {methylene-3, (3,5-di-tert-butyl-4-hydroxyphenyl) propionate} methane
Irganox 1035	Ciba-Geigy Ltd	2,2' - Thiodiethyl-bis{3-(3,5-di-tert-butyl-4-hydroxyphenyl) propionate}
Permanax* WSP (PQ)	Vulnax International Ltd	2,2' - Dihydroxy-3,3'-bis (1-methylcyclohexyl) - 5,5' - diphenylmethane
Goodrite 3114	Goodrite Chemicals	Tris (3,5-di-tert-butyl-4-hydroxybenzyl) isocyanurate
Eastman Inhibitor OABH	Eastman Chemical Products Inc	Oxalic acid - bis(benzylidene hydrazide)
Irganox MD 1024	Ciba-Geigy Ltd	1,2-Bis{3-(3,5-di-tert-butyl-4-hydroxyphenyl) propionic acid} hydrazide
Sandostab P-EPQ	Sandoz Ltd	Tetrakis (2,4-di-tert-butylphenyl) 4,4'-biphenylenediphosphonite
BHT	-	2,6-Di-tert-butyl-4-methylphenol
DLTDP	-	Dilauryl thiodipropionate

* Formerly known as Nonox WSP

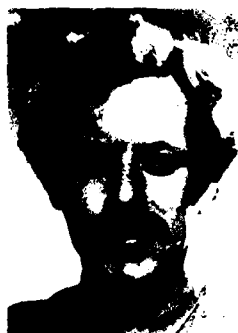
ACKNOWLEDGEMENTS

Many people in Telecom Australia assisted in the field surveys and laboratory evaluations. Their help is gratefully acknowledged. Special acknowledgement is given to all the staff of the Polymer Section of the Research Department for the development of the analytical techniques and the design and execution of the many experiments involved. Thanks are also given to BTP Tioxide Limited, BXL Plastics Limited, ICI Australia Operations Pty Ltd and Union Carbide Australia Limited for supplying valuable information and/or materials, and to Austral Standard Cables Pty Ltd, Olex Cables Ltd, and Pirelli-Ericsson Cables Ltd for the supply of the variously stabilised samples of insulated conductor. The permission of the Chief General Manager, Telecom Australia, to publish this paper is acknowledged.

REFERENCES

- 1 B.B. Pusey, M.T. Chen, W.L. Roberts, Proc. 20th Int. Wire & Cable Symp., 209, (1971).
- 2 W.L. Hawkins, M.G. Chan, G.L. Link, Polym. Eng. Sci., 11, 377 (1971).
- 3 J.B. Howard, Proc. 21st Int. Wire & Cable Symp., 329 (1972).
- 4 H.M. Gilroy, Proc. 23rd Int. Wire & Cable Symp., 42 (1974).
- 5 M.G. Chan, Proc. 23rd Int. Wire & Cable Symp., 34 (1974).
- 6 L. Ance, J.P. McCann, 23rd Int. Wire & Cable Symp., 82 (1974).
- 7 D. McInnes, E.T.C. Cole, Report of Field Survey to Telecom Australia Committee on Deterioration of Polyethylene Insulation, Engineering Department, Headquarters, Telecom Australia, 1981.
- 8 H.J. Ruddell, D.J. Adams, B.A. Chisholm, Plast. in Telecommun., 3rd Int. Conf., (1982).
- 9 Australian Standard 1049-1983.
- 10 E. Kokta, Proc. 24th Int. Wire & Cable Symp., 220 (1975).
- 11 J.Y. Moisan, Plast. in Telecommun., 2nd Int. Conf., 26.1 (1978).
- 12 H.E. Bair, Annu. Tech. Conf. - Soc. Plast. Eng., 19, 106 (1973).
- 13 H.E. Bair, R.J. Roe, C. Gieniewski, Annu. Tech. Conf. - Soc. Plast. Eng., 20, 412 (1974).
- 14 J. Fech, A. de Witt, Proc. 29th Int. Wire & Cable Symp., 327 (1980).
- 15 A.C. Anderson, ICI Australia Operations P/L, Private Communication, 22 May 1980.

- 16 G.A. Schmidt, L.A. Bopp, Proc. 29th Int. Wire & Cable Symp., 331 (1980).
- 17 J.M. Farber, W.H. Brown, A.DiBattista, P.P. Klemchuk, Proc. 21st Int. Wire & Cable Symp., 361 (1972).
- 18 J.B. Howard, H.M. Gilroy, Polym. Eng. Sci., 15, 268 (1975).
- 19 C.C. Swasey, Proc. 25th Int. Wire & Cable Symp., 68 (1976).
- 20 Ciba Geigy Ltd., Basle, Switz., "Irgafos 168 in Combination with Irganox Antioxidants", Technical Information Bulletin, July 1978.
- 21 J.Y. Moisan, R. Lever, Eur. Polym. J., 18 (1982) (to be published).
- 22 R.J. Roe, Org. Coat. Plast. Chem., 132 (1974).
- 23 G.A. Schmidt, Proc. 22nd Int. Wire & Cable Symp., 11 (1973).
- 24 R. Solvik, W. Wu, L. Krebaum, Mod. Plast., 78 (1974).
- 25 D. Holtzen, Annu. Tech. Conf. - Soc. Plast. Eng., 22, 488 (1976).
- 26 BTP Tioxide Ltd. Technical Service Report D8745GC (1976).
- 27 W. Hughes, Congr. FATIPEC, 10, 67 (1970).
- 28 J.W. Shea, Proc. 21st Int. Wire & Cable Symp., 70 (1972).
- 29 F.R. Wight, Proc. 28th Int. Wire & Cable Symp., 112 (1979).



B.L. Board
Lines Construction Branch
Engineering Dept. HQ,
Telecom Australia
28/570 Bourke Street
MELBOURNE VIC 3000
AUSTRALIA

Bruce Board graduated in Electrical Engineering (Electronics and Communications) from the University of Queensland, Australia in 1971. Following graduation, he worked as an external plant field engineer for Telecom Australia. In 1974 he joined Bell-Northern Research, Ottawa, Canada where he was responsible for the development and engineering of optical fibre systems in the outside plant. This included fibre cable design and specifications and all fibre outside plant hardware and practices. In 1978 he returned to Australia and joined the Engineering Development Division of Telecom Australia Headquarters. He is currently Senior Engineer, Cable Design, responsible for the development and introduction of all new cable materials and new paired cables and optical fibre cables into the Telecom Australia network.



H.J. Ruddell
Polymer Section
Research Dept.
Telecom Australia
770 Blackburn Road
CLAYTON VIC 3168
AUSTRALIA

Hec Ruddell joined Telecom Australia Research Laboratories in 1955 as a Chemist after 19 years in private industry in the field of oils, general chemistry, rubbers, and plastics. In 1966 he was promoted to set up the Polymer Section which is responsible for the investigation, development and application of all plastics, rubbers, and adhesives in communications equipment. He was actively associated with the early manufacture and installation of plastics cable, including the development and formulation of epoxy resins and the epoxy resin field pack, the design of joints and the recent developments in filled cable, optical fibres, and stabilisation of polyethylene. Mr Ruddell has been an Associate Member of The Plastics Institute of Australia since 1959, and was awarded a Fellowship of that Institute in 1982.

AD P000575

BLENDING OF A BLOCK COPOLYMER THERMOPLASTIC RUBBER FOR SPECIFIC WIRE AND CABLE APPLICATIONS

A. C. Levy and R. Sabia

Bell Laboratories
Norcross, Georgia 30071

ABSTRACT

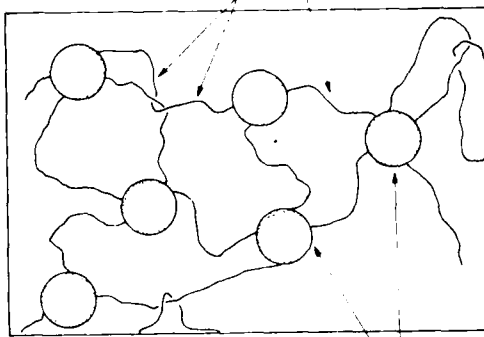
Thermoplastic rubbers based on styrene block copolymers have been modified with selected oils, waxes, and other additives to obtain various compounds for wire and cable applications. Included in these developments are a low modulus coating for optical fibers, a filling compound for optical cable, a flame retardant filling compound for service wire and a sealing compound for connectors. The design considerations and properties of these compositions are described.

1.0 INTRODUCTION

Communication cable and apparatus are exposed to adverse aerial, buried and underground environments. The conventional approach to keep water out of cables is pressurization with its attendant high first costs and maintenance problems over its lifetime. Another approach used with multipair PIC cable is to physically block the water by filling all interstitial spaces with hydrophobic materials. The latter approach is now widely favored by the Bell System Operating Companies. With the success of this approach, the use of water blocking materials has been extended to service wires, cable stubs, connectors, splice cases and, most recently, lightguide cables.

In this paper, thermoplastic rubbers (SEBS) having rigid polystyrene end-blocks and a flexible, saturated mid-block of ethylene/butylene copolymer are shown to have wide use in wire and cable applications. A schematic of the structure of these materials is given in Figure 1. Between the glass transitions of the polystyrene end-blocks, 90-100°C, and the rubber mid-block, -65°C, the material acts as if it were crosslinked. Above the polystyrene phase glass transition temperature, the material can be processed as a thermoplastic. The saturated rubber makes it an ideal choice for applications requiring high temperature processing and/or long term environmental stability. The structure of the end and mid-blocks makes it possible to do selective blending

ETHYLENE BUTYLENE MIDBLOCKS FORM RUBBER PHASE



RIGID POLYSTYRENE ENDBLOCKS FORM
PHYSICAL CROSSLINKS OR DOMAINS

FIGURE 1. DIAGRAMMATIC REPRESENTATION OF A
THERMOPLASTIC RUBBER STRUCTURE

with other materials to optimize physical properties such as modulus, adhesion, toughness, melt viscosity, etc.

One such composition is the FLEXGEL* cable filling compound,^{1,2} which exhibits improved characteristics³ over petrolatum based materials. Selected properties of a typical composition are reported in Table I. This paper deals with four different applications. Specific compositions were developed which have been commercially introduced. In order of increasing rubber content they are:

- a connector sealant,
- a fire resistant filling compound for buried service wire,
- a lightguide cable filling material, and
- a low modulus buffer coating for optical fibers.

*A trademark of Western Electric

TABLE I
CHARACTERIZATION OF AN OIL EXTENDED
CABLE FILLING COMPOUND

Composition		
Materials	Parts by Weight	
SEBS	6	
Polyethylene	4	
White Mineral Oil	90	
Stabilizer	0.2	
Properties		
Parameter	Value	Method of Test
Viscosity at 130°C, cps	18	ASTM D2664, Brookfield
Drop Melting Point, °C	94	ASTM D127
Slump Temperature		
60°C	Pass	
70°C	Fail	
Penetration, dmm,		ASTM D217
at 80°	124	
at 0°F	93	
Tensile Strength, psi	112	ASTM D1708, 100mm min.
Elongation at Break, %	158	ASTM D1708, 100mm min.
Tear Strength, lb/in.	0.80	ASTM D624, die C, 100 mm min
Oxidative Stability, wires		RTL Test
at 110°C	4.5	
at 180°C	50	
Dielectric Constant 41MHz	2.27	ASTM D150
Dissipation Factor 41MHz	0.0000	ASTM D150
Volume resistivity, ohm-cm	1.2x10 ¹⁷	ASTM D257

2.0 CONNECTOR SEALANT

To provide moisture resistance in the wire joining of PIC insulated conductors, a grease-like material is used as a sealant in the waterproof codes of connectors. Various suppliers have used sealants based on petrolatum, silicone chemistry, etc. One material, referred to as PEPB compound, is based on low molecular weight polyethylene (PE) waxes and polybutene (PB) oils.

The PEPB material has functioned well in the application. However, as in the case of the cable filling compounds based on petrolatum, several properties were considered marginal. For example, in the application of molten PEPB compound to the connector, its set-up as it cools is too slow for optimum sealant placement. If the sealant is not properly distributed in the connector, the water resistance of the connector is degraded. Also, a compound with a lower modulus than the PEPB formulation is desirable to allow easier connector assembly at low temperatures. In addition, a compound less grease-like than PEPB sealant is desirable for craft acceptance. Finally, the PEPB sealant tends to form an oily interface with an oil extended, low tear strength (reenterable) polyurethane encapsulant used in splice cases.³ The concern here is that the oily interface can potentially provide a water path to the connector.

A logical alternative to the PEPB sealant is a material similar to the FLEXGEL compound since the latter (1) does

not form an oily interface with the polyurethane encapsulant as used in a closure, and (2) has excellent low temperature properties. The FLEXGEL compound is also less greaselike than the PEPB formulation.

2.1 Laboratory Evaluation

The laboratory evaluations of new formulations involved the determination of material properties such as viscosity, slump, cone penetration, low temperature modulus and encapsulant compatibility. Selected formulations were used to fill connectors and conduct electrical tests.

The improved sealant material is referred to as PETR where PE refers to the polyethylene wax component and TR to the thermoplastic rubber. The properties of the PETR and PEPB formulation are compared in Table II and Figure 2.

TABLE II
CONNECTOR SEALANT MATERIALS

PROPERTIES	Sealant	
	PETR	PEPB
Modulus at 20°F and 1 hertz (dynes/cm ²)	1.5 x 10 ⁸	5.0 x 10 ⁸
Cone Penetration, 0.1" dmm at room temperature (ASTM D217)	160-190	110-155
Volume Resistivity, ohm-cm (ASTM D257)	10 ¹⁷ Min.	10 ¹⁷ Min.
Compatibility with Polyurethane Encapsulant ³	Yes	No

³Splice case tests.

Table II indicates that PETR formulation exhibits higher penetration and increased compatibility with the polyurethane encapsulant. The low temperature modulus data in Table II show PETR sealant to be significantly less stiff, and this was reflected in lower filled connector pressing forces at 20°F.

Figure 2 indicates that lower processing temperatures are possible for PETR. With a lower processing temperature and the viscosity profile at temperatures below the knee in the curves, one would expect PETR to set-up faster than PEPB. Such has been the observation in actual filling operations.

The electrical testing of assembled connectors (with conductors) was done per AT&T's "Product Criteria for Communication Cable Wire Joining Systems," Issue 1,

October 1975. The final composition met or exceeded connector requirements for temperature cycling (-40 to 140°F, 95% RH), dielectric strength and water immersion. Low temperature pressing of filled connectors and compatibility with the reenterable encapsulant were also evaluated and found to be improved.

Since the PETR formulation has been demonstrated to meet the requirements for a sealant for modular connectors and is in several respects superior to the PEPB compound, it is now used exclusively in the 710 connectors supplied by Western Electric.

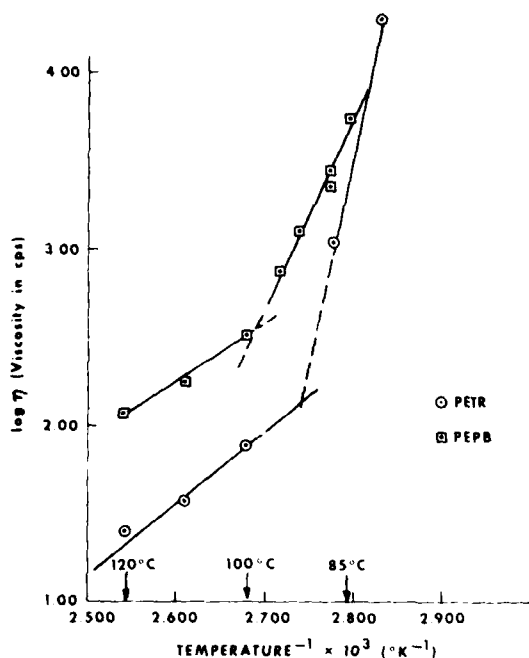


FIGURE 2. VISCOSITY vs. TEMPERATURE⁻¹ FOR FILLING MATERIALS

3.0 FLAME RETARDANT FILLING COMPOUND

Buried service wire is a critical component of the loop plant, and its water resistance is an important design feature. Since service wire may enter customer's premises, no compromise of its fire resistant properties by the water filling compound is permitted.

A water and flame resistant service wire has been available for years. The water resistance of this design has been reported⁵ and a short term water resistance test has been described.⁶ Flame resistance was measured using the UL 83 test. The water and flame resistant fill-

ing compound exhibited a high dielectric constant but was acceptable because the wire is designed for use in relatively short lengths and at voice frequencies.⁵

In order to function satisfactorily in buried service and distribution wires, a new design objective required that the filling compound exhibit a dielectric constant below 2.38. In developing a suitable compound, a second objective was reduced tack for easier handling. Both objectives were met while retaining the flame resistance of the existing compound by modifying the FLEXGEL formulation.

3.1 Laboratory Evaluation

The high dielectric constant of flame retardant compound is due to the use of halogenated compounds as additives. The dielectric constants of chlorinated paraffins are typically greater than 5, Table III. Of interest is the observation that the dielectric constant of the materials in Table III, covering a narrow chlorine content range, decreases with molecular weight (as measured by the viscosity), Figure 3. One sample is off the curve. A possible explanation is that the latter liquid is based on a significantly different material; for example, linear rather than branched paraffins. The remaining materials may be based on similar paraffins with structure differences explaining the increasing dielectric constant. Extending the curve in Figure 3 to higher molecular weight materials (chlorinated waxes) should further reduce the dielectric constant.

TABLE III

PROPERTIES OF LIQUID CHLORINATED PARAFFINS

Material	Nominal Viscosity, Sus @210°F	Nominal Chlorine Content, %	Dielectric Constant @ 1 KHz
A	63	54	7.96
B	75	70	5.41
C	90	62	6.63
D	190	70	5.84
E	200	68	5.77
F	250	67	5.31
G	530	70	4.80

In Table IV, blends using liquid (G in Table III) and solid chlorinated paraffins (waxes) of the same chlorine content are compared. The wax exhibits lower dielectric constant. The table shows that a dielectric constant of less than 2.38 is readily attainable. However, lot to lot variations in the dielectric constant of the chlorinated wax gave a spread of 0.05 units. Thus, the new compound would have to have a nominal value of 2.33 or about

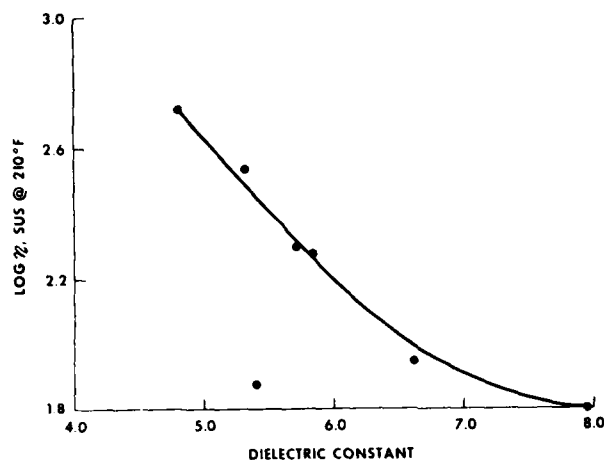


FIGURE 3 THE CHANGE IN DIELECTRIC CONSTANT WITH VISCOSITY

20% chlorinated wax to insure compliance. If the chlorine content is too low, a reduction in flame retardancy to unacceptable levels results. A 20% chlorinated wax content approaches this level. The addition of antimony oxide, which is synergistic with chlorine in a fire situation, gave the required safety factor without degrading the dielectric constant. Tests show that under manufacturing conditions proper dispersion of the insoluble antimony additive is maintained.

TABLE IV
DIELECTRIC CONSTANT OF BLENDS BASED ON LIQUID
AND SOLID CHLORINATED MATERIALS

Chlorinated Material, %	Dielectric Constant @ 1 MHz	
	Liquid ⁺	Solid
35	2.82	2.38
30	2.72	2.37
25	2.63	2.34
20		2.33

⁺G in Table III

The second objective, reduced tack, was achieved by substituting 20 parts of the chlorinated paraffin wax for the mineral oil in the FLEXGEL compound. The final formulation had the improved handling properties desired and the predicted dielectric constant of 2.33. This material has also exhibited improved processing characteristics and is now used exclusively in Western Electric's buried service and distribution wires.

4.0 LIGHTGUIDE CABLE FILLING MATERIAL

In this development, the following materials objectives were identified:

- compatibility with cable materials,
- compatibility with existing processing know-how,
- water resistance performance,
- craft acceptability,
- high temperature resistance to flow, and
- low relaxation modulus, to minimize added loss, over the temperature of interest, -40 to 170°F.¹

With the exception of the last item, the above objectives have been previously investigated and found to be met by the FLEXGEL compound. Modification of the FLEXGEL compound for the lightguide application is discussed below.

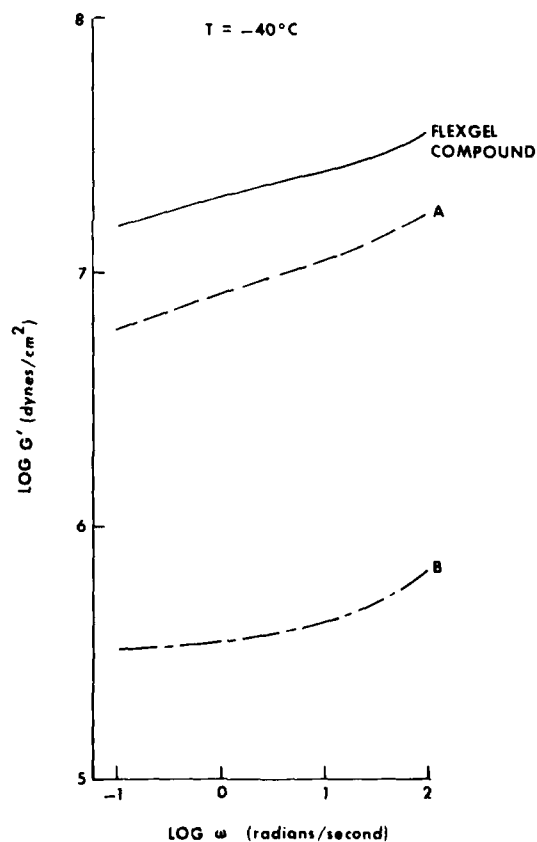


FIGURE 4. SHEAR MODULI OF VARIOUS FILLING COMPOUNDS

4.1 Modification of FLEXGEL Compound

In general, the modulus of materials increases as the temperature decreases. Since fiber optic cables are being designed for an environment ranging from -40 to 170°F, the initial characterization was done at -40°F. Figure 4 presents the value of $G'(\omega)$ (the dynamic shear modulus) as a function of frequency for the standard FLEXGEL formulation. The material is rubber-like at this temperature in the frequency range studied.

To reduce the modulus below that of FLEXGEL, the level of rubber can be reduced. Alternatively, the polyethylene wax can be removed. Without the polyethylene, the high temperature properties are degraded. If the latter approach is chosen, the high temperature properties can be restored as discussed below.

To compensate for the loss of polyethylene, a higher molecular weight block copolymer rubber was used at a higher level. The resultant compound formulations and properties as blended with two different pour point oils is given in Table V along with that for FLEXGEL compound. The higher viscosities for the new blends, A and B, reflect the higher rubber content as well as the use of a higher molecular weight rubber. Moduli data for the blends in Table V are shown also in Figure 4. As expected, the moduli at -40°C for A and B are less than those of FLEXGEL compound, reflecting the omission of the polyethylene wax. It is also important to note that the choice of oil is critical to minimizing the modulus. One would expect, based on the pour points of the oil, that Blend B would exhibit a lower modulus than A but possibly not to the extent observed. Other formulations with and without polyethylene additives were characterized and determined to be useful blends.⁷

TABLE V
MODIFIED CABLE FILLING COMPOUND

	FLEXGEL	A*	B**
Viscosity at 266°F (130°C), cps	30	42	56
Slump Temps, °C			
Pass	65	50	50
Fail	70	60	60
$G'(\omega) \times 10^{-6}$ (dynes/ cm ² @ 10 ³ rad/sec)		16.2	0.62

*Based on an oil with a nominal pour point of +10°F.

**Based on an oil with a nominal pour point of 0°F.

Blend B has been extensively evaluated in lightguide cable. In conjunction with use of dual coated fiber, performance with respect to added loss both in cable as manufactured and in environmental cycling has been excellent.⁸

5.0 LOW MODULUS THERMOPLASTIC HOT MELTS FOR OPTICAL FIBER COATING

Optical fibers require protective coatings in order to preserve fiber strength and to protect the fiber from microbending induced optical loss. The coating is generally applied in-line with fiber drawing by passing the fiber through a reservoir containing the coating material and having an exit orifice which has been sized to apply some desired thickness of the material. With this technique a coating with a viscosity less than 10,000 centipoises at the application temperature is preferred. Classes of materials which have been applied to optical fibers by this technique include UV curables, thermal curables, such as silicone resins, solvent based materials and thermoplastic hot melts.

Properties of the coating material which influence the ability to preserve fiber strength are toughness, abrasion resistance, thickness and adhesion to the fiber. In general, an increase in any of these properties reduces the susceptibility of the fiber to mechanical damage.

Brockway et al.⁹ have shown that microbending sensitivity is related to the product αEA of the coating where α is the coefficient of thermal expansion, E is the modulus and A is the cross sectional area. In practice and for a given design, the modulus in controlling so that a reduction in the coating modulus decreases microbending sensitivity. Thermally cured silicones with moduli below 10⁷ dynes/cm² (140 psi) have been used as coating where low sensitivity to microbending is required. Unfortunately a low modulus also means low toughness and abrasion resistance, perhaps too low for adequate protection of the fiber. For this reason, a secondary coating is often placed over the primary silicone.

5.1 Laboratory Evaluation

A limitation of silicones is that they exhibit limited pot lives due to their curing behavior. We have developed a thermoplastic hot melt based on a block copolymer rubber which, like silicones, exhibits low modulus down to -40°C, yet has significantly greater toughness than the silicones and exhibits long pot life. To accomplish this, significant deviations from the FLEXGEL formulation were

required. The rubber content was increased by several factors and resins which reinforce the styrene domains were added.⁷ The role of the various additives on the low temperature modulus was characterized. Formulations useful as primary coatings were developed. Critical factors such as blocking (fiber sticks together) and adhesion to the polyester tape used in making ribbons were considered. Typical properties of two formulations are given in Table VI. Note principally the low moduli at -40°C. Of immediate interest was coating A since it has the potential as both a primary and a secondary coating. It was characterized extensively as a material and as a coating.

TABLE VI
COATING MATERIAL FOR OPTICAL FIBERS

	A Primary or Secondary Coating	B Primary Coating
Oxidation Induction Time at 210°C (min)	30	30
Viscosity at 190°C (cps)	4800	1190
Toughness (psi)	970	
T-Peel Adhesion (kg/cm) to polyester	1.6	
Ring and Ball Softening Point (°C)	135	
30 Minute Tensile Relaxation Modulus x 10 ⁻⁸ dynes/cm ² , (psi) at 25°C	8 (120)	2.4 (20)
at -40°C	80 (1200)	10 (140)

5.2 Microbending Loss of Coated Fibers

Coating A was evaluated on optical fiber drawn from germanium phosphosilicate preforms. A UV curable material with a 30 minute tensile relaxation modulus of $\sim 6 \times 10^9$ dynes/cm² at 23°C and $\sim 3 \times 10^{10}$ dynes/cm² at -40°C was used as the secondary coating. Both coatings were applied in-line with drawing. In all the tests, fiber coated with the UV material only was used as a control.

Ribbons were manufactured, one with each coated fiber type. Each ribbon consisted of 12 fibers sandwiched continuously between two layers of a polyester pressure sensitive coated tape. The added loss due to ribbon fabrication was within the measurement error. The average thermal added loss of the fibers in each ribbon was determined. The data¹⁰ shown in Table VII indicate a much lower sensitivity to microbending for the dual coated fiber.

Based on these results and other data, dual coated fibers with a hot melt buffer coating are preferred for use in filled lightguide cables.

TABLE VII
ENVIRONMENTAL LOSS

Coated Fiber Type	Added Loss at 0.82 μ m (dB/km)			
T(°F):	-40	-11	11	75
Control (UV)	0.24	0.12	-0.01	0
Dual (Hot Melt/UV)	0.07	-0.05	-0.03	0

6. CONCLUSIONS

Thermoplastic rubbers having rigid polystyrene end-blocks and a flexible, saturated mid-block of ethylene/butylene copolymer have been evaluated for several wire and cable applications. In specific developments, selective blending of the rubber with modifiers was used to optimize physical properties. Successful formulations have been introduced in products for use by the Bell System Operating Telephone companies.

ACKNOWLEDGEMENT

The various developments described were made possible by the efforts of numerous coworkers at Bell Laboratories and Western Electric. Their cooperation and good will is sincerely appreciated.

REFERENCES

1. U.S. Patent 4,176,240
2. U.S. Patent 4,259,540
3. D. M. Mitchell and R. Sabia, Proceedings of the Twenty-Ninth International Wire and Cable Symposium, 1973.
4. M. Brauer and R. Sabia, Proceedings of the Twenty-fourth International Wire and Cable Symposium, 1975.
5. N. J. Cogelia, et al, Proceedings of the Twenty-second International Wire and Cable Symposium, 1973.
6. W. C. Reed, Proceedings of the Twenty-eighth International Wire and Cable Symposium.
7. Patent applied for.
8. B. R. Eichenbaum et al, Proceedings of the Thirty-first International Wire and Cable Symposium, 1982.
9. G. S. Brockway, et al, "An Analysis of the Environmental Behavior of Fiber-Optic Ribbons," Proceedings of the Sixth European Conference on Optical Communication, York, U.K., September 16-19, 1980.

10. L. L. Blyler, et al, "A New Dual-Coating System for Optical Fibers," Proceedings of the Eighth European Conference on Optical Communication, Cannes, France, September 21-24, 1982.



A. C. Levy is a graduate of the Georgia Institute of Technology (B.S., M.S., Ph.D.). He was employed by the Film and Fiber Division of E. I. DuPont prior to joining the Transmission Media Laboratory of Bell Telephone Laboratories in 1976. Since 1976 he has been active in the development of materials for conventional and lightguide cable applications.



Raffaele Sabia, a graduate of St. Francis College of Brooklyn (B.S.) and Polytechnic Institute of Brooklyn (Ph.D.), was employed by the Polymer Chemical Division of W. R. Grace prior to joining Bell Telephone Laboratories in 1963. Since 1963 he has been active in the research and development of materials for application in the wire and cable area. Since 1967 he has been supervisor of the Chemical Engineering Group in the Transmission Media Laboratory.

BEHAVIOUR OF ZINC-COATINGS ON STEEL TAPES IN ARMOURED CABLES

A.M.J.M. Claassens, A.T.M. Grooten, J. Rozendaal

NKF Kabel B.V., Waddinxveen, The Netherlands

ABSTRACT

Telecommunication cables are often supplied with armounging tape for protection against electromagnetic interference and mechanical damage. From corrosion point of view zinc-coated steel tape is applied.

Examination of the zinc-iron equilibrium phase diagram combined with testing of samples in a mikroscope revealed that differences in nature of brittle zinc-iron intermetallic compounds can lead to blistering of the zinc-layer of normal hot-dip zinc-coated steel tape. Two new routine tests are developed to obtain a quick insight in nature and adherence of zinc-layers.

A much better solution for adherence problems is application of continuous zinc-coated slitted steel sheet (according to the Sendzimir process). The adherence of this material is inherently better due to the almost complete absence of intermetallic compounds.

Corrosion tests are carried out on coaxial cables (Bamboo-construction) to determine the effect of zinc-absence on cutting faces of Sendzimir zinc-coated steel. These tests include both newly developed laboratory tests and comparative test in soil. Theoretical explanations are given for surprising results of tests. Differences in nature of zinc-layers between Sendzimir zinc-coated and conventional hot-dip zinc-coated steel tape (almost pure zinc vs zinc-iron compounds) proved to have greater influence on attack of steel armounging tape by underground corrosion than the presence of zinc on cutting faces.

1. INTRODUCTION1.1. Cable protection demands

The requirements for safe and troublefree operation of telecommunication cables can be divided into two areas. First the primary electrical demands including resistance of conductors and insulation, mutual capacitance, attenuation and cross-talk. Besides these the secondary demands relating to environmental influences threatening the primary functions or the security of the telecommunication system.

Among these environmental influences are electromagnetic interference, biological attack (rodents, termites, fungi), mechanical violence (heavy: human; light: vibration, shift, temperature) and physical/chemical attack: soil corrosion, hydrocarbons, acids, ultra-violet radiation and lightning.

The combined demands for a low electrical reduction factor and protection against mechanical damage lead to the application of flat steel tape as interlocking armour or flat armour. Although this steel tape normally is protected against soil corrosion by a polyethylene outer sheath, the possibility of sheath damage by installation, rocks, rodents and dig-ins makes a second protection by for instance a zinc-layer on the steel tape necessary. According to ASNI/ASTM A 459-71¹ up till recently at NKF steel tape has been applied, first slitted to the required size and then zinc-coated at all surfaces including edges.

1.2. Construction of bamboo coaxial cables

NKF uses zinc-coated flat steel armouring tape, applied as two overlapping helical layers, in a wide range of cable types. In this paper special attention will be given to our research on armoured bamboo cables. These cables are used for high frequency transmission. It is a coaxial cable to be used for e.g. CATV networks.

The construction of the cable (seen from insight to insight) is for the bamboo-three type 2: (figure 1).



FIGURE 1 CATV BAMBOO-CABLE

- Solid electrolytic copper inner conductor.
- Dielectric consisting of polyethylene discs covered by a polyethylene tube. Together this makes the dielectric look like a bamboo cane.
- A longitudinally applied copper foil as outer conductor.
- A polyethylene sheath, extruded directly over the outer conductor.
- The actual armouring consisting of two overlapping layers of zinc-coated steel tape.
- A polyethylene outer-sheath.

The name of the different cable types (Bamboo-three, Bamboo-six, etc.) indicates the attenuation (dB/100 m) at 20°C and a frequency of 230 MHz.

2. HOT-DIP ZINC-COATED (HDZC) STEEL TAPE

Generally speaking there are many advantages when using zinc-coatings as corrosion barrier for a steel substrate.

- It provides an effective and pinhole-free barrier between the corrosive environment and the steel substrate.
- Zinc has a rather good intrinsic corrosion resistance by the formation under certain circumstances of a water-insoluble zinc-patina.
- Compared with other application-methods for metal coatings, such as electrodeposition, flame-spraying or cladding, zinc can very easily be applied by hot-dipping the steel in a molten metal bath due to the low melting point of zinc.

2.1. Phase-diagram Zinc-Iron

Due to the hot-dip process the zinc layer on HDZC-steel tape is composed of three intermetallic zinc-iron compounds covered by a top layer of pure zinc. The nature of these layers is determined by the zinc-iron equilibrium phase-diagram.

Figure 2 shows this diagram, recently modified by Gellings and Bastin³. Going from iron to zinc we meet the following intermetallic compounds:

EQUILIBRIUM PHASE-DIAGRAM ZINC-IRON (Zn-RICH PART)

ACCORDING TO GELLINGS AND BASTIN

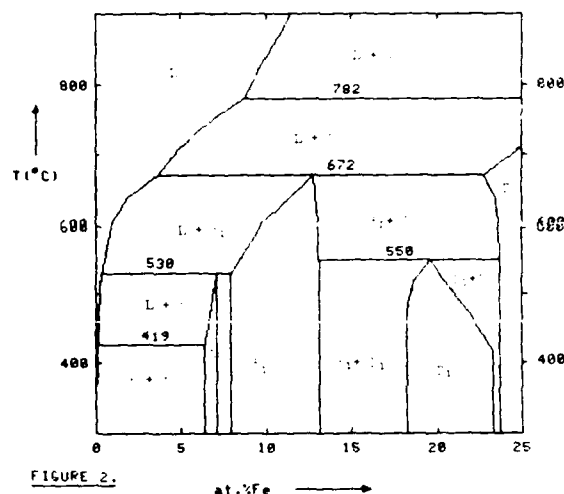


FIGURE 2.

- The gamma (Γ)-phase with a bodycentered cubic (bcc) structure ($a=0,895$ nm);
- The recently discovered gamma-1 (Γ_1)-phase with a face centered cubic (fcc) structure ($a=1,7963$ nm) and a peritectic decomposition temperature of 550°C. This phase only occurs in diffusion layers and is not created in zinc coating processes.
- The delta-1 (δ_1)-phase with a complex hexagonal structure ($a=1,285$ nm, $c=5,735$ nm).
- There does not exist a separate δ_k -phase (iron-rich and compact) nor a δ_p -phase (zinc-rich and palissade-structure, as proposed by Ghoniem⁴).
- The zeta (ζ) phase with a monoclinic structure and a peritectic melt-temperature of 530°C.
- The intermetallic layers are covered with pure eta (η) zinc with a hexagonal structure ($a=0,260$ nm, $c=0,494$ nm).

2.2. Microphotographs of HDZC-steel

Figure 3 shows a micro-photograph of a metallographic sample of normal HDZC-steel tape. From bottom to top it consists of the steel-substrate, a thin gamma-layer, a mixture of delta- and zeta-layers and a rather thick zinc-layer. The total thickness of the hot-dip layer amounts to 35 microns.

For the zinc-coated steel tape applied to the Bamboo coaxial cables (and to a lot of other cable types) a thickness of the zinc-layer of 3 to 12 microns gives adequate protection⁵. To achieve a layer of a given thickness the steel tape is wiped off after the galvanizing process as can be seen in Figure 4. This results in the pure zinc top-layer being almost completely absent and the coating consisting mainly of zinc-iron intermetallic compounds. Because of the egg-shell finish this is called mat HDZC-steel tape.

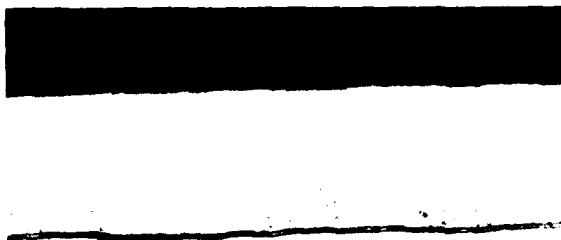


FIGURE 3.

MAGNIFICATION: 400X
SAMPLE: NORMAL HOT-DIP ZINC-COATED STEEL TAPE

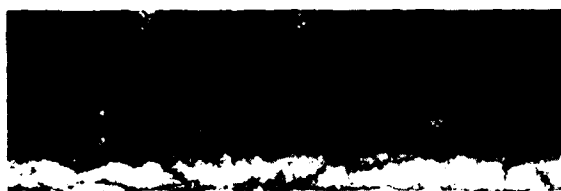


FIGURE 4.

MAGNIFICATION: 400X
SAMPLE: WIPED HOT-DIP ZINC-COATED STEEL TAPE

Besides the earlier mentioned advantage, there is on the other hand for cable armouring one disadvantage in the application of normal or mat HDZC-steel tape. Due to the hard and brittle nature of the zinc-iron alloys there is always the risk of blistering of the zinc layer. Figure 5 shows a dramatic example of a blister in a zinc layer which was displaced during hot moulding under pressure of this metallographic sample.

2.3. Example of a cable with a blistered zinc layer

During the manufacturing of cables blistering of the brittle alloys can be caused by the inevitable deformation of the steel tape or by thermal effects during extrusion of the outer sheath. Figure 6 shows an armoured Bamboo-six cable with mat HDZC-steel armour. The polyethylene outer sheath has been removed to reveal the blistered zinc-layer.

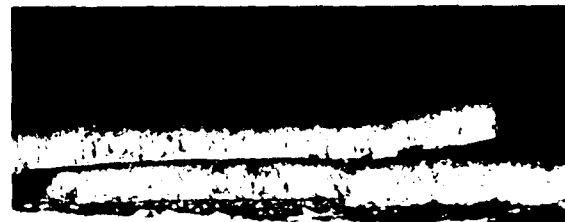


FIGURE 5.

SAMPLE: WIPED HOT-DIP ZINC-COATED STEEL TAPE
DAMAGED DURING PREPARATION DUE TO
BRITTLE ALLOY-LAYER
MAGNIFICATION: 400X



FIGURE 6.

BAMBOO-6 CABLE WITH BLISTERED HOT-DIP
ZINC-COATED STEEL TAPE
PE OUTERSHEATH IS REMOVED

2.4. Multiple bend test

Two new routine tests were developed to obtain a quick insight in the nature and the adherence of zinc layers. The most simple starting point is the normal bend test (single bending over 180° around a mandrel with prescribed diameter according to international standards 1,6. The outcome of this test, however, appears not to give any guarantee for trouble-free manufacture. Differences between troublesome and trouble-free lots of HDZC-steel tape can be found after multiple bending of the samples. The histogram of figure 7 shows that only after two or three bends there can be seen some difference between parcels with a well respectively a badly adhering zinc-layer. The difference between two similar lots of 50x0,8 mm steel tape can be seen from figure 8. At the left the samples with blistering after three bends, at the right the samples with no problems after bending.

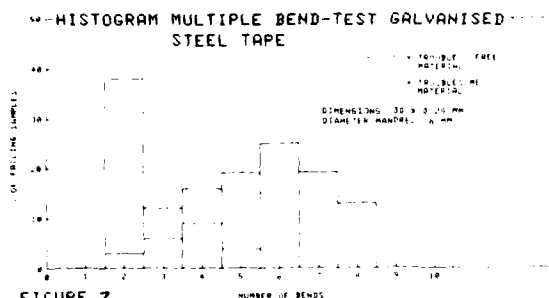


FIGURE 7



LEFT: TROUBLE-SOME HOT-DIP ZINC-COATED STEEL TAPE (50 X 0 80 MM)
RIGHT: TROUBLE FREE MATERIAL
FROM TOP TO BOTTOM: 1, 2 AND 3 BENDS WITH MANDREL DIAMETER 8 MM

FIGURE 8.

2.5. Electrode-potential during zinc-stripping

It is quite clear that due to the brittle nature of the intermetallic compounds the adherence of the zinc-layer is determined by the occurrence and the thickness of the various alloys. We have developed a quick electrochemical method to examine the composed zinc-layer. This method was derived from the standard method for the determination of the mass of zinc-coating by zinc-stripping in an acid solution 7.

The electrochemical potential of the sample is measured during zinc-stripping in a hydrochloric acid solution, from which in this case the SnCl_3 must be omitted.

According to the galvanic series of metals 8,9 every metal has a certain electrode-potential when placed in an electrolyte. Noble metals have higher potentials than active metals. The potential of zinc (Zn) is about -1100 mV with respect to a Saturated Calomel reference Electrode (SCE), iron (Fe) takes a higher potential: about -500 mV (SCE). The zinc-iron alloys have intermediate potentials. During zinc-stripping the potentials at every moment will be determined by the particular layer being dissolved at that moment and thus, depending upon the thicknesses of the various layers, the potential will change stepwise. The same result can be achieved by anodic stripping of the sample with the aid of an imposed current. The advantage of the earlier mentioned method, however, is that due to the longer dissolving time of alloys compared with pure zinc minor differences between the alloy-layers of various samples can more easily be demonstrated.

Figure 9 shows the results for the same samples as shown in the bend test of figure 8. The left curves are recorded in a more concentrated hydrochloric acid than the right ones, thus reaching shorter stripping times. The difference between the "good" and the "bad" samples is a thicker gamma-layer, being responsible for a higher blistering risk.

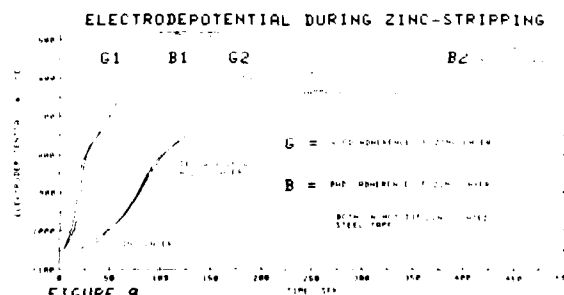


FIGURE 9

The hot-dip zinc-coating process is inherently prone to create intermetallic layers of varying thickness and thus to differences in adherence.

3. SENDZIMIR ZINC-COATED (SEZC) STEEL TAPE

3.1. Nature of the zinc-layer

The best solution to cope with adherence problems is the application of a totally different type of zinc-coated steel on which the alloy layers are almost completely absent. More than 95% of the total zinc-layer should consist of pure zinc to achieve an inherently better adherence. A material satisfying these demands is continuously zinc-coated steel sheet, produced according to the Sendzimir process or related methods (SEZC-steel tape). In the Sendzimir process a steel sheet with unlimited length is led through a tunnel-furnace.

The iron-oxides at the surface are all oxidized to Fe_2O_3 . In the end part this oxide is reduced with the aid of the cracking gases of ammonia (N_2 and H_2) to iron (Fe). The outlet of the tunnel-furnace is placed in the bath of molten zinc so that no reoxidation of the metal can occur. The zinc-bath is composed of high purity zinc (99,99%) to which is added 0,16-0,20% aluminium. Combined with a short residence time in the zinc-bath this prevents almost completely the growth of inter-metallic compounds. During the process only a 0,1-0,5 micron gamma-layer is built up.¹⁰



FIGURE 10.

MAGNIFICATION 400X
SAMPLE SENDZIMIR ZINC-COATED STEEL TAPE

The zinc-coated steel sheet next is slitted to the required size. The cutting faces of the steel tape produced in this way are not covered with zinc.

The consequences of this fact for the corrosion behaviour of the steel tape are thoroughly discussed in chapter 4. Figure 10 shows the microstructure of SEZC-steel tape, which consists of the steel substrate, a thin alloy-layer and a thick pure zinc layer. The total thickness amounts to 15-20 microns.

3.2. Differences in the properties of the zinc-layer between HDZC-steel tape and SEZC-steel tape.

SEZC-steel tape is tested with the newly developed quick reference methods, in order to compare this material with HDZC-steel tape.

Due to the thick pure zinc-layer the electrode-potential of SEZC-steel tape during zinc-stripping remains at a constant value during a finite time (fig. 11). Next an abrupt increase occurs with a little stop at the alloy-potential to reach the electrode-potential of the equilibrium reaction $Fe \rightleftharpoons Fe^{2+} + 2e$ which takes place at the steel substrate. For HDZC-steel the potential starts rising immediately from the starting point exhibiting a few more or less pronounced flexure-points which indicate the boundaries between the various alloy-layers.

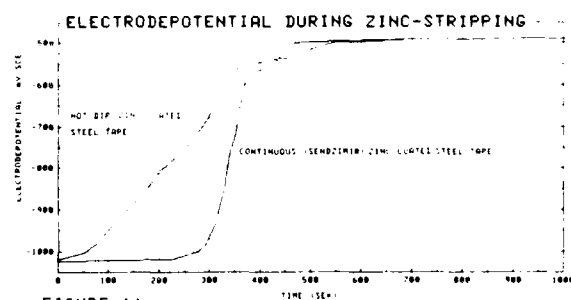


FIGURE 11

Comparative bending tests have been performed on 25 x 0.30 mm steel tape, which is applied to armoured Bamboo-three cables. Figure 12 shows at the left side HDZC-steel with a blistered zinc-layer after three bends around a mandrel of 3 mm diameter. At the right side fig. 12 shows SEZC-steel that has been bended for more than 10 times. The steel tape is broken but nevertheless there is no blistering of zinc.



FIGURE 12.

LEFT: WIPED HOT-DIP ZINC-COATED STEEL TAPE
3 BENDS WITH MANDREL DIAMETER 3 MM
ZINC BLISTERS VISIBLE

RIGHT: SENDZIMIR ZINC-COATED STEEL TAPE
MORE THAN 10 BENDS UNTILL CRACKING
OF STEEL SUBSTRATE
NO BLISTERING OF ZINC

DIMENSIONS: 25 X 0.30 MM

4. THEORY OF CORROSION TESTING

4.1. General principles

The very good adherence of the zinc-layer is all important in the application of SEZC-steel tape as cable armour. On the other hand the corrosion resistance of the material must be at least equal to the mat HDZC-steel tape used earlier.

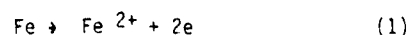
Especially the uncovered cutting faces of SEZC-steel tape, which might be unsufficiently cathodically protected by the surrounding zinc-layers, asked for a thorough investigation with respect to corrosion behaviour. For that reason new cable corrosion tests, both laboratory tests and tests in soil, were developed. These tests revealed to be applicable to the corrosion problems of all metallic cable components and are not limited to the research described in this paper.

All tests are based upon the modern electrochemical theory of aqueous corrosion ^{8,14}. This mainly consists of the two hypotheses of the mixed-potential theory:

- Any electrochemical corrosion reaction can be divided into partial oxidation (anodic) reactions (the dissolution reactions of the corroding metals) and the corresponding reduction (cathodic) reactions (hydrogen formation or oxygen reduction).

- There can be no net accumulation of electrical charge during an electrochemical corrosion reaction. It follows that during the corrosion of an isolated metal sample immersed in an electrolyte the total rate of oxidation must be equal to the total rate of reduction.

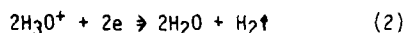
The mixed-potential theory can be explained further very well with the aid of logarithmic polarization curves. Figure 13 shows at the vertical axis the electrochemical potential and at the horizontal axis the logarithm of the absolute value of the electrical current densities. Corrosion of iron basically can be interpreted as proceeding of the anodic dissolution reaction:



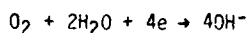
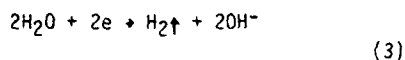
at the metal-electrolyte interface. The Fe^{2+} -ions diffuse into the electrolyte. The liberated electrons form the electrical corrosion current, which flows through the metallic electrode.

At the equilibrium (non-corrosion) potential the oxidation rate is equal to the corresponding reduction rate ($\text{Fe}^{2+} + 2e \rightarrow \text{Fe}$), so no net reaction occurs. For corrosion to occur there must be at least one separate cathodic reaction, with its own reversible equilibrium potential, which increases the potential of the iron-anode. This is called polarization and it results in a net corrosion current.

The nature of this cathodic reaction depends upon the corrosive environment. In acid solutions hydrogen formation will occur:



In neutral and alkaline solutions the corrosion rate will be dominated by one of the following cathodic reactions:



In practice due to the low acidity of most soil type oxygen reduction instead of hydrogen evolution will govern the corrosion process.

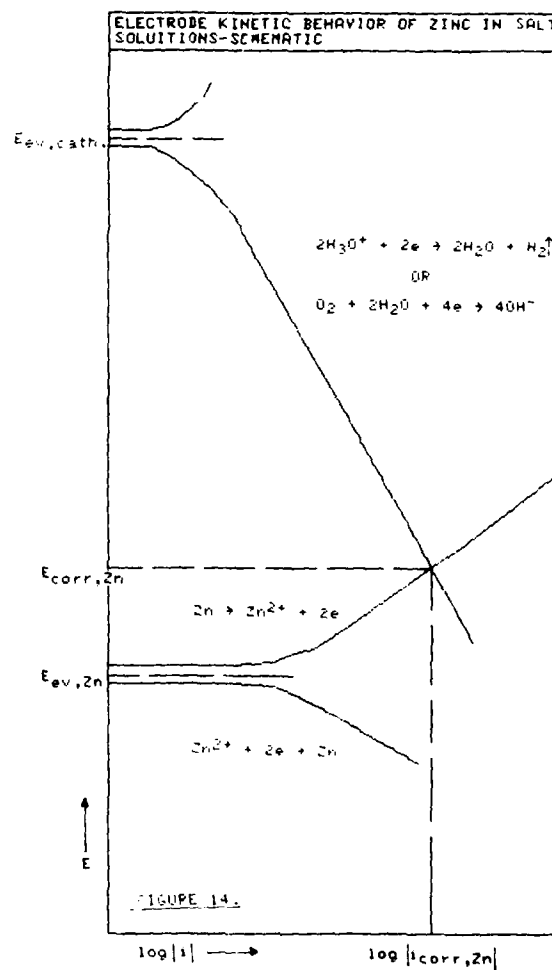
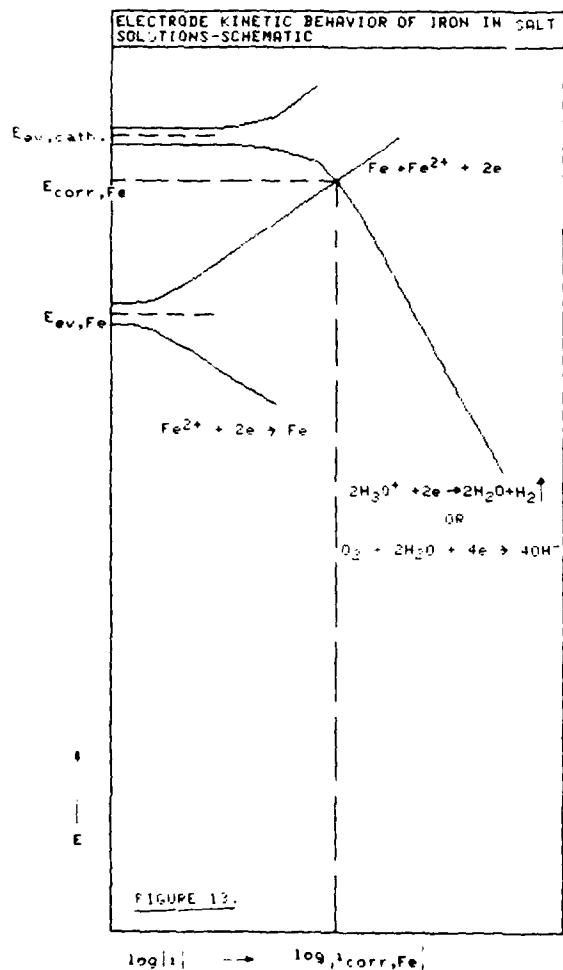
Following the second hypothesis of the mixed-potential theory the iron will take a corrosion-

potential (E_{corr}) at which the total rate of oxidation is equal to the total rate of reduction. Neglecting two minor partial reactions the following equation yields:

$$i_{\text{a,Fe}} + i_{\text{c,O}_2} = 0 \quad (4)$$

At this stationary state cathodic polarization of the O_2/OH^- -reaction and anodic polarization of the Fe/Fe^{2+} reaction will occur. The corrosion current density (i_{corr}) equals $i_{\text{a,Fe}}$ (figure 13). It appears that there is a linear relation between the potential and the logarithm of the current density provided that the potential is not too close to the equilibrium potential. The slope of the curve is called the Tafelconstant (β).

Figure 14 shows the situation for zinc-corrosion. Compared with iron the following differences are important:



- The equilibrium-potential of zinc is more negative because zinc has a greater tendency to dissolve.
- The hydrogen evolution rate at the zinc surface is smaller.

Nevertheless the corrosion-potential of zinc is more negative and the corrosion current density larger when compared with iron.

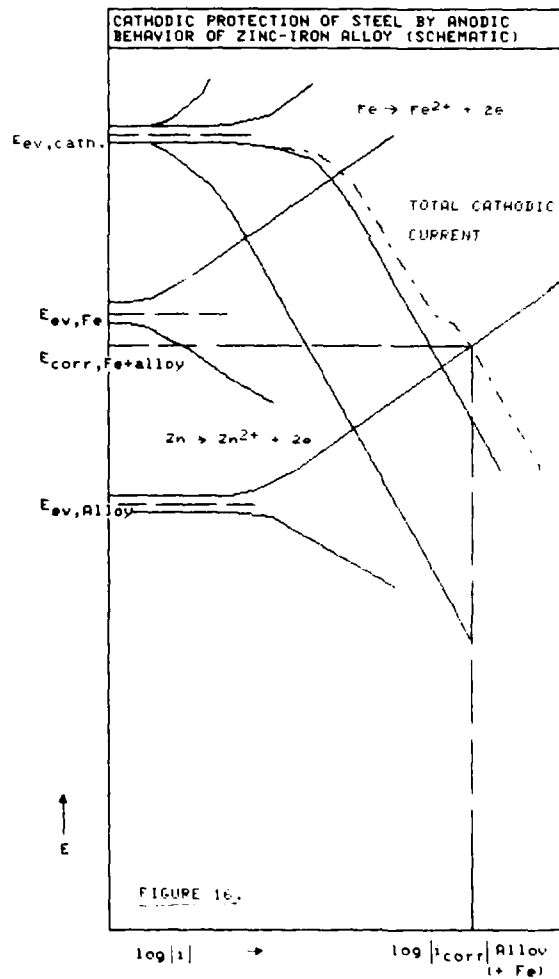
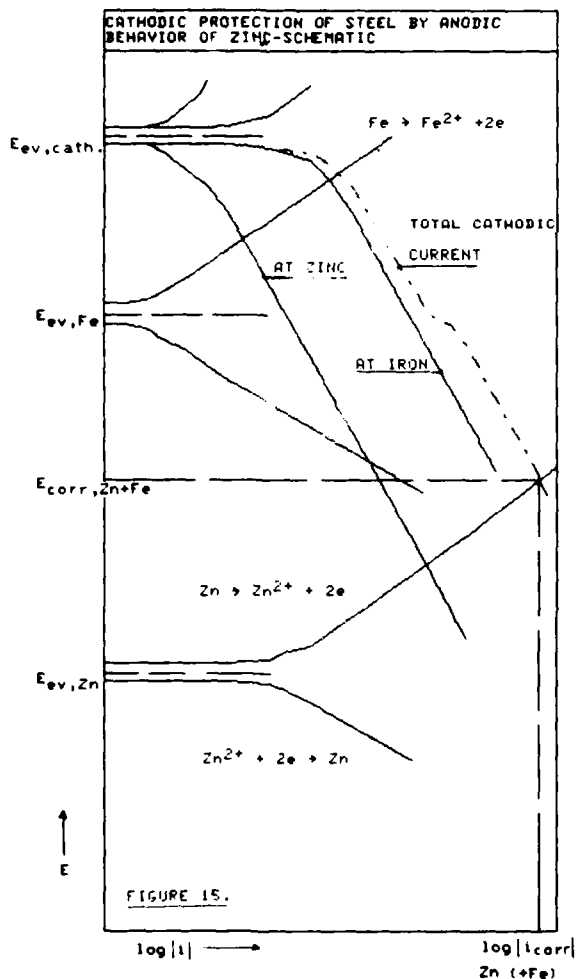
4.2. Cathodic protection

The principles of the mixed-potential theory can also be used very well to explain the mechanism of cathodic protection of a steel substrate by a zinc-layer, acting as sacrificial anode ¹⁵.

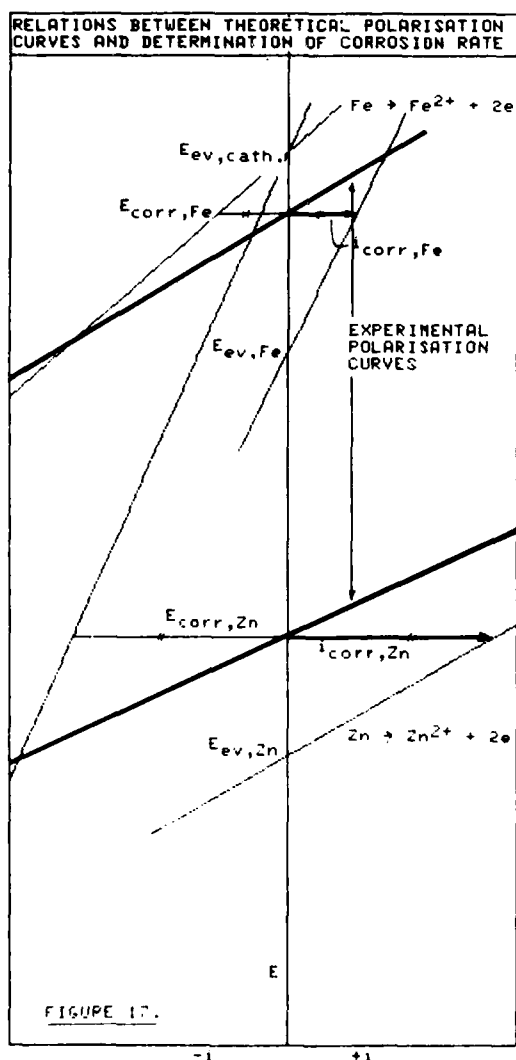
In that case there must be an electrical contact between the iron-electrode and the

zinc-electrode. Both metallic parts take the same electrode-potential and no net electrical charge can be accumulated (figure 15). The anodic current (dissolving of zinc) is equal and opposite to the sum of all cathodic currents. The corrosion-potential belonging to this situation is more negative than the iron equilibrium-potential.

Therefore no anodic dissolution can take place at the iron surface, prohibiting any corrosion attack. The anodic corrosion current at the zinc surface is increased, compared with the uncoupled situation. Being the active metal of the galvanic couple, zinc is attacked due to galvanic corrosion.



So the pure zinc-layer on SEZC-steel tape provides a very effective cathodic protection for the underlying steel and the uncovered cutting faces. Mat HDZC-steel tape, however is covered with an alloy-layer. The equilibrium potential of this compound-layer can be found between that of pure iron and pure zinc (figure 16) (compare the zinc-stripping curves of figure 9). Therefore in this case the corrosion-potential is nearer to the equilibrium-potential of iron, so that the latter is less effectively protected, as will be explained later. The corrosion current of the zinc-layer, however, is smaller.



4.3. Measurement of the anodic corrosion current

When trying to measure the anodic corrosion current of an iron or zinc sample one is faced with the problem that an anodic corrosion current is always accompanied with a cathodic current, resulting in no net current exchange. So the anodic corrosion current can only be measured indirectly by the application of an external overvoltage with the aid of a potentiostat, thus increasing the potential of the sample artificially. In this way an external current can be measured, the net difference between the current densities of the simultaneously occurring anodic and cathodic reactions. The relation between the externally applied overvoltage and the measured current gives the experimental polarization curve. Figure 17 shows schematically the situation for both iron and zinc. In this figure at the horizontal axis the current densities now has been plotted linearly.

A mathematical equation can be derived describing the polarization curve which represents the relations between the applied overvoltage (η), the measured current (I) and the unknown corrosion current (I_{corr}):

$$I = I_{corr} (\exp(\eta/b_a) - \exp(-\eta/b_c)) \quad (5)$$

$$\eta = E - E_{corr}$$

Here b_a and b_c are constants, related to the Tafel constants which characterize the local anodic and cathodic reactions β_a and β_c by:

$$b_{a,c} = \beta_{a,c} / \ln 10 = \beta_{a,c} / 2,303 \quad (6)$$

Methods have been developed⁸ to experimentally determine these constants.

A few methods are known to derive from equation (5) practically applicable analysis techniques. The classical linear polarization technique of Stern and Geary¹⁶ assumes that the experimental polarization curve becomes linear as $\eta \rightarrow 0$.

If $\eta \rightarrow 0$ equation (5) can be rewritten as:

$$I = I_{corr} \left(\frac{1}{b_a} + \frac{1}{b_c} \right) \eta \quad (7)$$

or assuming a linear curve:

$$I_{corr} = \frac{b_a \cdot b_c}{b_a + b_c} \left(\frac{dI}{dE} \right)_{E_{corr}} = \frac{B}{R_p} \quad (8)$$

Here R_p is the slope of the polarization curve at the corrosion-potential. R_p is often called polarization resistance.

A similar method is to evaluate the current at a fixed overvoltage. Then from equation (8) can be derived:

$$I_{corr} = I \cdot K \quad (K \text{ supposed to be constant}) \quad (9)$$

This method is applied in some commercial available corrosion rate meters and for instance used by Choo ¹⁷. This one-point method can be quite useful if qualitative corrosion rates are required. Fluctuations in the corrosion-potential will however always result in a more reliable indication of i_{corr} from multiple current measurements at various overvoltages.

A new method based upon curve fitting, which does not assume a linear polarization curve, is recently developed by Leroy ¹⁸. He states: "the best value of I_{corr} is the value for which the sum of the squares of the deviations of the measured currents (I_j) from the predicted (equation (5)) is a minimum". In mathematical terms this yields:

$$\frac{d}{dI_{corr}} \sum_{j=1}^n (I_j - I_{corr} \{ \exp \eta_j / b_a - \exp -\eta_j / b_c \})^2 = 0 \quad (10)$$

or

$$I_{corr} = \frac{\sum_{j=1}^n (I_j (\exp \eta_j / b_a - \exp -\eta_j / b_c))}{\sum_{j=1}^n (\exp \eta_j / b_a - \exp -\eta_j / b_c)^2} \quad (11)$$

In this method no graphical exploration of the polarization curve has to be done, as is the case with the linear polarization technique. Digitally recorded overvoltage and current values can be directly evaluated with the aid of a simple computer program based upon equation (11).

Values of the Tafelconstants B_a and B_c have been published ¹⁸. Although these values differ from case to case Leroy has proven that a deviation between real and assumed values is of minor influence upon the value of the corrosion current, when calculated according to the curve fitting method. In our calculations the following values of the Tafelconstants are used: $B_a = 30$ mV and $B_c = -120$ mV.

4.4. Comparative corrosion current measurements

To get an impression about the reliability of the analysis techniques mentioned above comparative measurements were performed. A special polarization cell suited for flat specimens is used. In this cell a circular spot with a well-known diameter is exposed to the electrolyte. This cell also can be used very well to record the potential zinc-stripping curves mentioned earlier.

Two experimental polarization curves, recorded with a Wenking POS 73 potentiostat at uncoated bare steel and SEZC-steel respectively, in a 0,05M Na_2SO_4 -solution, are shown in figure 18. In accordance with figure 17 it can be seen that the corrosion-potential of zinc is more negative. Moreover the slope of the polarization curve at the corrosion-potential reveals a larger corrosion current for zinc.

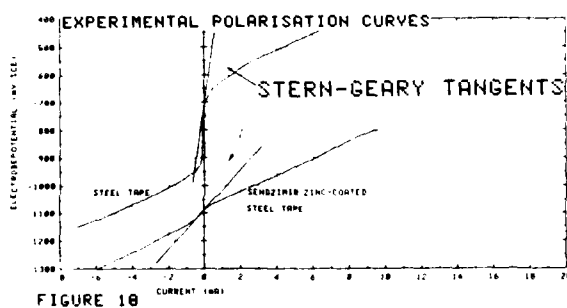


Figure 19 shows the corrosion rates of uncoated bare steel tape in various corrosive environments. Comparing weight loss results with two important electrochemical methods it can be seen that the Leroy-method gives slightly better results. Added to the easy handling made us decide to generally adopt this method for the calculation of corrosion currents.

COMPARISON OF CORROSION RATE MEASUREMENTS			
ON STEEL ABRADED TAPE SAMPLES MEASURED IN POLARIZATION CELL AND PLANT SPECIMENS			
	WEIGHT LOSS	STERN AND GEARY	LEROY
0.01 N H_2SO_4	0.09	0.081	0.11
0.05 N H_2SO_4	0.14	0.094	0.14
0.1 N H_2SO_4	0.11	0.067	0.12
1.0 N H_2SO_4 + 1% $NaCl$	0.4	2.5	5.0
1.0 N H_2SO_4 + 10% $NaCl$	5.5	2.5	5.4

FIGURE 19

5. LABORATORY CABLE CORROSION TESTS

5.1. Cable corrosion test construction

Generally speaking the most reliable corrosion test results are achieved on complete cable samples, due to the complex nature of corrosion attack. When testing an isolated sample one always will change unintentionally some parameters like oxygen content or ion concentration as compared with the real cable situation. Therefore a new cable corrosion test equipment has been developed in which simultaneously six complete cable samples with a length of approx. 50 cm can be tested, in combined exposure and electro-chemical testing. Figure 20 shows a general overview. Important parameters of the electrolyte can be measured, artificial gasflow can be applied and provisions have been made for electro-chemical measurements at different metallic cable parts. With these techniques a quick and continuous determination of corrosion parameters is possible. Besides they are unevitable when testing complete cable samples because weight loss determination can not be applied. All tests are carried out at room temperature.

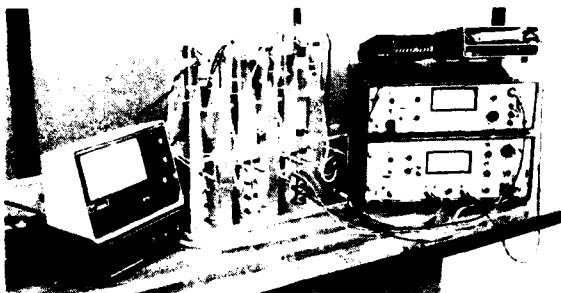


FIGURE 20: GENERAL OVERVIEW OF THE CABLE CORROSION TEST EQUIPMENT. LEFT: TEST EQUIPMENT AND CABLE SAMPLES. RIGHT: TEST EQUIPMENT AND CABLE SAMPLES. CENTRE: TEST EQUIPMENT AND CABLE SAMPLES. RIGHT: TEST EQUIPMENT AND CABLE SAMPLES.

5.2. Corrosion-potential during exposure test

The effective protection of the steel-substrate by a zinc-coating is depending upon the time the corrosion-potential of the armour tape is controlled by the zinc corrosion-potential. Therefore the corrosion-potential has been recorded during exposure of several cable samples in the test tubes. In this way similar curves are recorded as the zinc-stripping curves described earlier. In the first place two Bamboo-three cable samples with an artificial circumferential outersheath damage of 4 cm length were tested in a 0.05 M

Na_2SO_4 solution (specific conductivity:

11 mS cm^{-1}). The corrosion-potential of the cable sample armoured with SEZC-steel maintains the value of the zinc-corrosion potential, even after nearly all the zinc at the damaged spot has been dissolved. The potential of the sample armoured with mat HDZC-steel changes quickly, resulting in a diminished cathodic protection (fig. 21). In both cases the total thickness of the zinc-layer is 20 microns.

ELECTRODEPOTENTIAL DURING CORROSION-TEST



FIGURE 21

Next two parameters were explored more in detail, the corrosive environment and the dimensions of the sheath damage.

Test solutions:

- Tap-water (pH = 6.75; specific conductivity = 0.66 mS cm^{-1})
- 2.5% NaCl + 2.5% Na_2SO_4 (pH = 7.8; spec. cond. = 60 mS cm^{-1})

Sheath damages:

- 2 mm length
- 25 mm length
- 50 mm length including zinc removal of 25 mm.

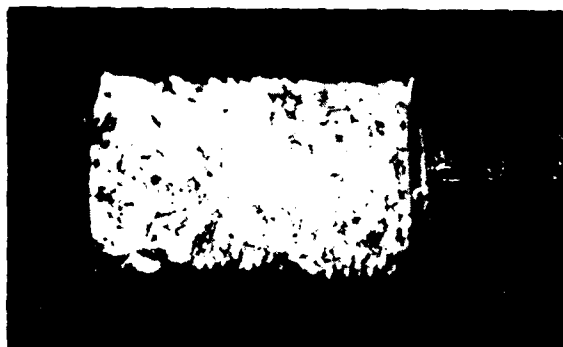
Figure 22 shows the results. The most important conclusions are:

- The corrosion-potential does change faster in the low-conducting tap-water than in the salt solution, because the higher electrolyte resistance decreases the contribution of the protecting zinc-reaction.
- The corrosion-potential of SEZC-steel exhibits under all circumstances a more negative value revealing a cathodic protection behaviour which is at least as good compared with that of mat HDZC-steel.
- The influence of the size of the sheath damage is rather small. It decreases in the course of time for the mat HDZC-steel samples placed in the low-conductive tap-water and increases for all samples placed in the salt solution.

FIGURE 22

Figure 23 shows some photographs of cable samples, from which can be concluded that SEZC-steel

exhibits less attack of the steel substrate than mat HDZC-steel.



SEZC-Steel Tape. Exposure Time: 100 days.
TEST-SOLUTION: 0.05 M Na_2SO_4



MAT HDZC-Steel Tape. Exposure Time: 100 days.
TEST-SOLUTION: 0.05 M Na_2SO_4



SEZC-STEEL TAPE. EXPOSURE TIME: 175 DAYS.
TEST-SOLUTION: TAP-WATER
25 MM DAMAGE, PE-OUTERSHEATH REMOVED AFTER TEST.

FIGURE 23.



MAT HDZC-STEEL TAPE. EXPOSURE TIME: 175 DAYS.
TEST-SOLUTION: TAP-WATER
25 MM DAMAGE, PE-OUTERSHEATH REMOVED AFTER TEST.

5.3. Corrosion current measurements on cable samples

At regular time intervals the corrosion currents of the samples mentioned have been measured and, assuming a certain active metal area, the corrosion rate has been calculated. To this end the experimental polarization curves were recorded and analysed following the previously described Leroy-method. Figure 24 shows some data, recorded after 75 days of exposure. The conclusions are:

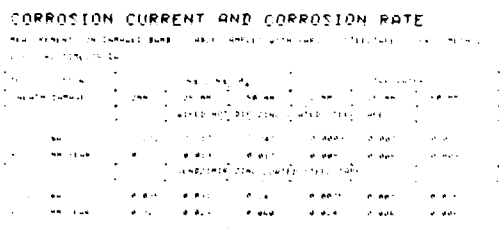


FIGURE 24

- The corrosion rate in the low-conducting tap-water is about 2 to 10 times smaller than in the salt solution.
- The apparently higher corrosion rate of the samples with a small sheath damage reveals a larger active surface area expanding under the undamaged sheath.
- A well performing cathodic protection needs a large zinc corrosion rate. Indeed at SEZC-steel a higher corrosion rate is measured compared with mat HDZC-steel.

6. CABLE CORROSION TESTS IN SOIL

6.1. Assessing soil properties

To affirm the laboratory corrosion tests some tests in soil have been carried out on complete cable samples buried in soils with well-known properties. To assess the aggressiveness of different soil-types several parameters can be used, varying from the water-content to the presence of oxygen or organic acids 19,20. Two commonly applied methods are selected. The soil resistivity measurement using the Wenner four-electrode method 21 and the redox-potential of an inert platinum electrode 22. Based upon available data two test-sides have been selected with largely divergent soil resistivities. The soil parameters were measured during 10 months. They depend to some extent on the time of year, temperature and rainfall. Results are shown in the following table. Test-location no. 1 can be classified as moderately aggressive, test-location no. 2 as non-aggressive.

test-location no.	soil resistivity (Ωm)			redox-potential (mV NHE)		
	min.	mean	max.	min.	mean	max.
1	3.3	7.3	11	223	258	291
2	5560	8080	10700	248	308	358

6.2. Corrosion-potential during soil tests

Bamboo-three cable samples, with a length of 10 meters and armoured with SEZC-steel and mat HDZC-steel respectively, were buried at the two test sides. Different outersheath damages were applied:

- a circular incision every 0.5 meter
- a 100 mm damage including zinc removal for 35 mm every 1.5 meter
- the outersheath removed over 4 meter length

The corrosion-potential was recorded, being the controlling parameter for the corrosion behaviour. In this case the reference-electrode is a Cu/CuSO₄ field-electrode with its potential being 73 mV more noble than the value of the calomel electrode.

Figure 25 shows the results. In the non-aggressive test-location SEZC-steel acts better than mat HDZC-steel for all damages tested. The potential of SEZC-steel has a value between -850 and -900 mV vs. the Cu/CuSO₄ electrode, after approx. 25 weeks of exposure. The potential of mat HDZC-steel has a value between -550 and -600 mV. This corresponds with the corrosion-potential of the steel substrate, which no longer is protected. Visual inspection of the samples does not reveal however any significant attack.

In the moderately aggressive test-location no. 1 there is only difference between both types of zinc-coated steel in case of the incision damage. The value of the potential is about 175 mV more negative for SEZC-steel tape.

Generally speaking both laboratory and soil tests show that SEZC-steel tape has a better or exceptionally equivalent corrosion resistance compared with mat HDZC-steel tape.

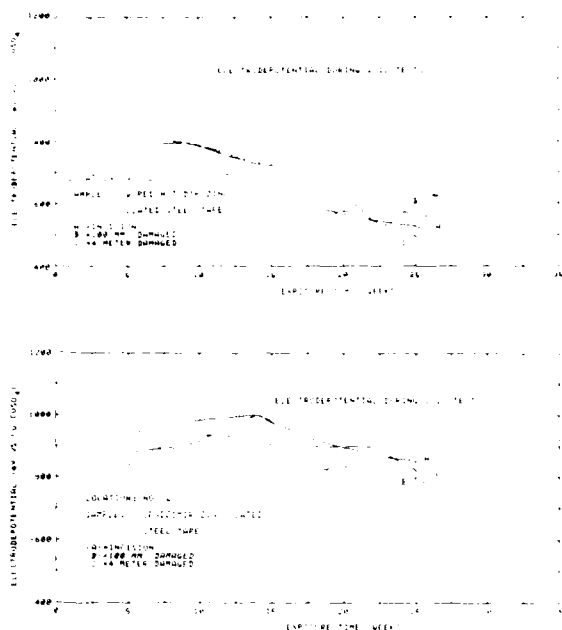


FIGURE 25

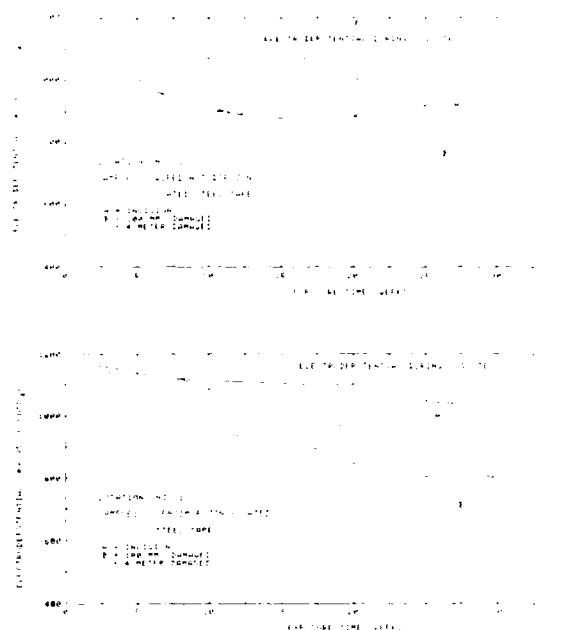
7. DISCUSSION

Once a sheath has been damaged soil water will enter the cable at the damaged spot and migrate along the crevice between outersheath and armour tape. The oxygen near the sheath-opening is replenished by diffusion from the surrounding soil water, so an oxygen concentration gradient is established. The water near the sheath opening is oxygen-rich compared to water between jacket and armour tape.

According to Choo ¹⁷ there are two important mechanisms which can explain enlarged corrosion attack of metallic cable components in case of sheath damage, besides the normal aqueous corrosion:

- Galvanic corrosion due to dissimilar metals. This has been thoroughly discussed in chapter 4.2. The reverse of galvanic corrosion is cathodic protection by e.g. a sacrificial zinc-layer.
- Galvanic corrosion due to differential aeration. The area of the metal exposed to a higher oxygen concentration is cathodic to the area in a lower concentration.

A critical situation arises if bare steel is exposed to the soil water, as a result of the almost complete dissolution of the zinc-layer at the damaged spot or in case of severe mechanical damage of the zinc-layer. The steel then is pro-



ected by a combined action of the two mechanisms: differential oxygen aeration and cathodic protection by the neighbouring zinc-layer.

At the bare steel the cathodic oxygen reduction can take place very easily, whilst the zinc-layer under the sheath dissolves at an ever increasing distance from the damaged spot, maintaining by this undersheath attack the corrosion-potential at a constant zinc-corrosion value.

As seen in both laboratory and soil tests in course of time the electrode-potential increases to that of the steel-substrate. SEZC-steel exhibits this behaviour less pronounced than mat HDZC-steel, revealing a better cathodic protection. The potential-increase is caused by a few cooperating circumstances. This can be explained with the aid of the theoretical logarithmic polarization curves in case of undersheath attack. Figure 26 shows these curves for SEZC-steel (compare figure 15).

- The zinc equilibrium-potential is increased by an increased zinc-ion concentration near the anodic spot. The zinc-ions are hindered to diffuse away in the electrolyte due to the covering PE outersheath. The Nernst equation gives the relation between concentration and electrode-potential:

$$E_{\text{ev,Zn}} = E_{\text{o,Zn}} + \frac{RT}{2F} \ln(\text{Zn}^{2+}) = E_{\text{o,Zn}} + \frac{0.059}{2} \log(\text{Zn}^{2+}) \quad (12)$$

Here:

$E_{\text{eq,Zn}}$ is the zinc equilibrium-potential

$E_{0,\text{Zn}}$ is the zinc standard-potential

$[\text{Zn}^{2+}]$ is the zinc-ion concentration

z is the number of reacting electrons of one atom

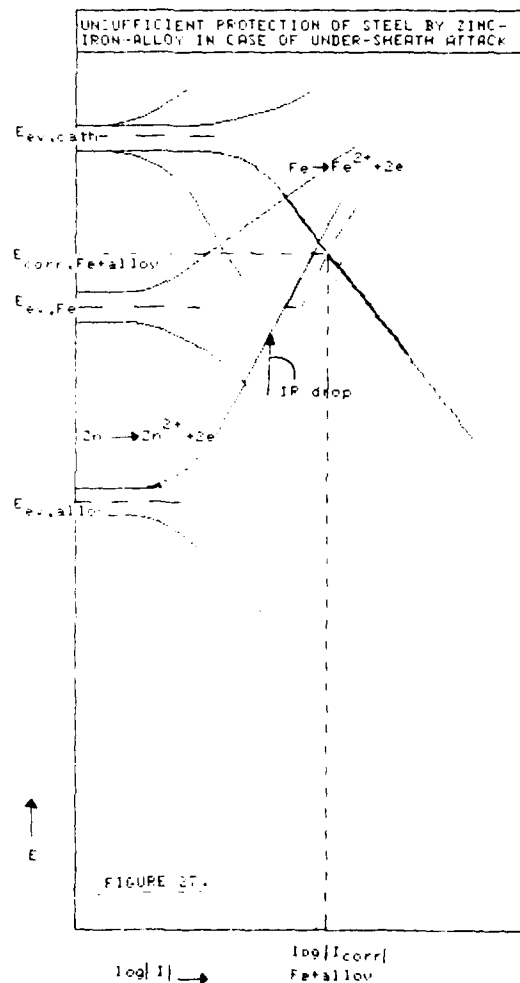
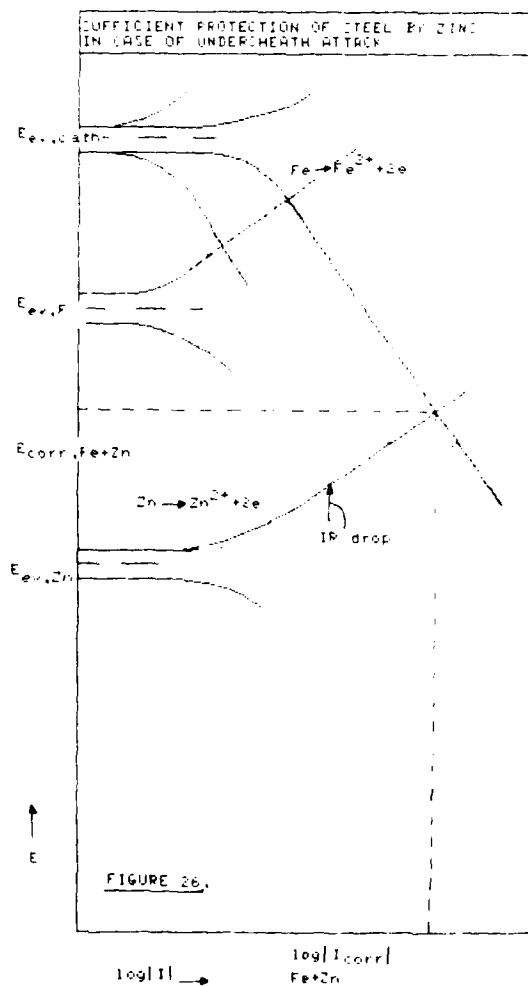
For each tenfold increase in zinc-ion concentration, the zinc equilibrium-potential increases by 30 mV, because $z=2$ for zinc.

- During the corrosion reaction the cathodic area will increase, because an ever increasing area of bare steel has to be protected. This results in an increasing cathodic current, while current densities do not change. A larger cathodic current will raise the (corrosion) potential, at which cathodic and anodic current (which is increased as well) are equal.

- The IR-drop will increase during the corrosion process due to the increasing distance between anodic and cathodic places.

The IR-drop decreases the potential difference between anodic and cathodic regions, thus increasing the corrosion-potential. The electrolyte with a low specific conductivity will have the most influence. This agrees with test results.

Figure 27 shows the theoretical situation for undersheath attack of mat HDZC-steel. The same circumstances raise also in this case the corrosion-potential. The equilibrium-potential of the zinc-iron alloy is however less negative, so the corrosion-potential can pass the iron equilibrium-potential. This results in attack of the steel-substrate, due to the anodic iron dissolution reaction which can take place now.



GENERAL CONCLUSION

The general conclusion of the research on zinc-coated steel tape is that the application as cable armour tape of slitted steel sheet covered with a zinc-layer mainly consisting of pure zinc has considerable advantages: The zinc-layer will by no means blister and the steel-substrate including the uncovered cutting faces are well cathodically protected by the pure zinc-layer.

ACKNOWLEDGEMENTS

The authors wish to thank A.P. de Bruijn for collecting data, P. Blaak for the photographs and A.H. Hofland for typing.

REFERENCES

1. Standard specification for zinc-coated flat steel armouring tape.
ANSI/ASTM A 459-71 (reapproved 1975).
2. Bamboo cables for television distribution systems. NKF Kabel B.V. Telecommunication Cable Systems (1979).
3. P. Gellings, Z. Metallkunde, 71 (1980) H2 p.70-75.
4. M.A. Ghoniem and K. Löhberg, Metall, 20 (1972) p. 1026.
5. Netherlands Postal and Telecommunication Services, Draft specification no. 139 (1979).
6. Charakteristische Merkmale für feuerverzinktes Bandstahl, Deutsche Verzinkerei Verband (1978).
7. Standard Methods of test for weight of coating on zinc-coated iron or steel articles, ASTM A 90-69 (reapproved 1973).
8. M.G. Fontana, N. Greene, Corrosion engineering 2nd ed. (1978).
9. Z.D. Jastrzebski and J.D. Wood, Syllabus Industrial Corrosion (1980).
10. Continu thermisch verzinkt staalband, J. van Eijnsbergen, pt-p.33 (1978) no.4 p. 193.
11. Standard specification for general requirements of zinc-coated iron or steel sheets, ASTM A 525-67.
12. Continuous hot-dip zinc-coated carbon steel sheet, ISO 3575 (1976).
13. Hot-dip zinc-coated strip and sheet of mild unalloyed steels, DIN 17162 (1977).
14. Syllabus Corrosie en bescherming tegen corrosie, W.A. Schultze, TH-Delft, The Netherlands (1972).
15. Handbuch des Kathodischen Korrosionsschutzes, W.v. Baekmann, Verlag Chemie (1980).
16. M. Stern and A.L. Geary, J. Electrochem. Soc., 104, 56 (1957).
17. T.S. Choo. "Corrosion studies on shielding materials for Underground Telephone Cables, Part I: Development of Test Methodology", 24th International Wire and Cable Symposium (1975).
18. R. Leroy, Corrosion, 31, 5 (1975) p. 173-177.
19. Recommendations concerning the construction, installation and protection of telecommunication cables in public networks, CCITT, Geneva (1977).
20. Underground corrosion, ASTM STP 741 (1981).
21. Field measurement of Soil resistivity Using the Wenner Four Electrode Method, ANSI/ASTM G 57-78.
22. Handbook on Corrosion Testing and Evaluation, W.H. Ailor, John Wiley & Sons (1971), p. 576.

Ad M.J.M. Claassens was born in 1930 in the Netherlands. He is a graduate of the higher Technical College of Dordrecht and he holds a degree in chemistry from the Technical University of Eindhoven. He joined NKF KABEL B.V. in 1967 where he now is manager of the Materials Laboratory.



Albert T.M. Grooten was born in 1952. He holds a degree in Metallurgy from the Delft University of Technology (Netherlands). He joined NKF KABEL B.V. in 1978, where he is an development engineer, working in the areas of corrosion research and development of materials for industrial cables. He is a member of the CCITT Study Group VI.



Jan Rozendaal was born in 1959 in the Netherlands. He obtained a Chemical Engineering degree from the Higher Technical College in Rotterdam and joined NKF KABEL B.V. in 1981 as a member of the Materials Laboratory. His main concern is the development of instrumental analysis techniques.



AD P000577

TEST PROCEDURES FOR DETERMINATION OF THE RADIATION RESISTANCE
OF CABLE MATERIALS

E.L. Ney
(Siemens AG, Telecommunications Cables, Munich, West Germany)

H.Rost and R.H. Knoch
(Siemens AG, Telecommunications Cables, Neustadt/Cob. West Germany)

ABSTRACT

Test procedures and devices are described, which are used to determine the behavior of materials for telecommunication cables under the influence of high energy radiation.

Radiation sources are Electron v.d.Graaf-Generator and Co-60 rods.

The samples are exposed to radiations of various dose rates as plates or cables respectively.

To test also specimens under more real service conditions a cell was equipped to measure transmission properties of cables during the radiation at elevated temperature.

Some results of our investigations are discussed and demonstrated by graphs.

Descriptions are very different and whoever gains improvements in material development wouldn't publish how.

Therefore our company is engaged since some years developing compounds for cables, which can be used in nuclear power stations. During these activities the radiation resistance of the cable materials were perpetual the dominant question. We determined this radiation resistance in various kinds. The procedures are described in the following.

2. TEST PROCEDURES

The investigations, which are not yet finished, are to divide in three chapters:

- . short term irradiation in laboratory (see 2.1.)
- . long term irradiation in laboratory (see 2.2.)
- . tests in technical facilities (see 2.3.)

1. INTRODUCTION

The service conditions of cables installed in reactor stations and nuclear power plants demand high quality materials of very special requirements.

Such cables must be flame retardent, i.e. they must extinguish by themselves and must not lead farther a fire. They must not in the case of fire drip off burning particles and they must not generate corrosive gases. They must withstand in the Loca-Test *) the simultaneous influence of heat, steam and pressure. They must meet usual electrical requirements and last not least they must be radiation resistance in a high degree. Because the security of the population as well as technical equipments are dependent on the quality of the cables and wirings the requirements are of a very high level in this special branch.

In the field of formulations and choice of the materials for those cables publications and the technical literature is not of great help. The national pre-

2.1. Short term irradiation in laboratory

The radiation source is a v.d.Graaf-Generator, which is regulated to 2 MV beam voltage and a dose rate of 9 ... 90 MGy/h.

Because the electron beam has on the sample surface only a 1.5 ... 2 cm diameter it oscillates with a frequency of $f = 10$ Hz to cover the complete width of the samples.

With this equipment the materials are irradiated as plates or tapes. The specimens are about 8 ... 10 cm wide and up to 1 m long. They are moved under the oscillating electron beam by some kind of carriage with a max. speed of 40 mm/s.

To get a homogeneous electron distribution in the sample material the samples

*) Loss of coolant accident

with a ~ 2 mm thickness are put on graphite and covered by 1 mm PE plates.

Remarkable is the increase of the material temperature of 4 K/10 Gy dose, i.e. during the absorption of 200 kGy dose the temperature increases for 80 K.

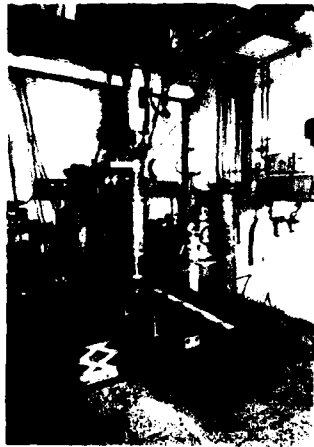


Fig. 1 Laboratory equipment for short term irradiation of materials with β -rays. The v.d.Graaf-Generator is located in the floor above. Before the rear wall the vacuum pump system is to see. Specimens are put on the graphite surface of a carriage to move them under the ray window

By repeated moving back and forth under the electron beam every wanted radiation dose can be applied. A typical radiation dose for our investigations is $1.5 \text{ MGy} \approx 150 \text{ Mrd}$ and exposition times of 1 ... 10 min.

2.2. Long term irradiation in laboratory

In the field of long term irradiation there are several test possibilities, which we used and still do so. The radiation sources are Co-60 rods that means gamma-sources. The Co-60 gammas have two energy levels: 1.17 MeV and 1.33 MeV, which can be taken to the mean value of 1.25 MeV.

Co-60 has a half-life of $T/2 = 5.25 \text{ a}$. This must be taken into account for the dose rates and the doses in long term experiments.

The irradiation procedures with Co-60 sources are all on principle equal. They

differ more in economical aspects. The equipments consider the number and the shape of the samples (cables or plates) and whether the wanted dose shall be accumulated within weeks, months or years.

2.2.1. Test equipment "1" for long term irradiation

The smallest test equipment used is a Co-60 source of 2 cm diameter, which consist of 1 mm pellets. According to the smallness it is called a point source. Point sources are of geometric conditions well to overlook.

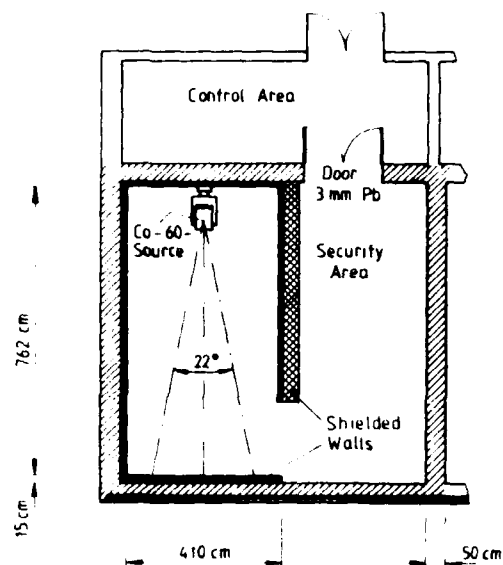


Fig. 2 Room arrangement with Co-60 point source

The source has had an initial activity of 3.78 kCi and a dose rate at 1 m distance of $\sim 42 \text{ Gy/h}$, which now decreased in the meantime to $\sim 30 \text{ Gy/h} \approx \sim 3 \text{ krd/h}$.

The distance between source and samples is to vary from 0.12 m to 6 m. The opened source radiates in a bevel angle of 22° . This narrow angle and the limited possibility for the distances limit also the useful diameter of the area for experiments.

Distance m	Radiation Cone Diameter m	Dose Rate	
		Gy/h	krd/h
0.2	0.078	1050	105
1	0.39	42	4.2
2	0.78	10.5	1.05
6	2.35	1.17	0.117

Tab.1 Relations at test equipment "1" between source-samples distances, irradiated area and dose rate (Co-60 activity 3.78 kCi)

With this equipment it is easy to fix cables of 25 m length on each side of a wooden board for irradiation. Such an experimental procedure makes it possible to measure electrical transmission dates during the irradiation.



Fig. 3 Co-60 test arrangement "1". On the left side the Co-60 point source box is to see. In 6 m distance a cable specimen is fixed on a wooden board. In the course of rays are sample holders made of aluminium partially isolated by foamed plastic

The Co-60 gammas have a great penetration power. Therefore it is allowed to install in the course of rays some cases. All outfits consist of aluminium or plastic. We test in these cases chiefly materials on the base of PE and SiR.

2.2.2. Test equipment "2" (plates) for long term irradiation

The second long term irradiation station is intended for plates and has a higher efficiency. The gamma source consists of 2 x 16 Co-60 rods, which are circular straight situated in two levels

superimposed and combined in a cylindrical container with an outer diameter of 21 cm. The source is placed in the center of a well shielded room and radiates radially except an angle of $\sim 20^\circ$ in which is located the controlling mechanism for the rods.

The Co-60 gamma source has had an initial activity of ~ 10 kCi and gave off dose rates from 5 kGy/h $\hat{=}$ 500 krd/h at 1 mm distance to 3 Gy/h $\hat{=}$ 0.3 krd/h at 1.80 m distance additional 5 cm lead shield.

Advisable the specimens are plates in size $\sim 15 \times 15$ cm². With regard to the gamma-radiation the thickness is not critical and is in our trials 1 ... 1.5 mm. Eight plates are combined to a package. In order to prevent potential metal electrolytic influences during the long term experiments the plates are fixed on rods without touching any metal. To make sure a not hindered circulation of air the plates will be kept in a certain distance by plastic spacer.

Irradiation occurs at room temperature. Only direct on the source surface a material heating up to 50 ... 40°C is to be expected. The room has a change of air of 6/h. The amount of ozone is to neglect.

With this source we irradiate materials up to two years. The accumulated doses depend on the likewise wanted dose rates. That means total doses 10 ... 2000 kGy $\hat{=}$ 5 ... 200 Mrad.

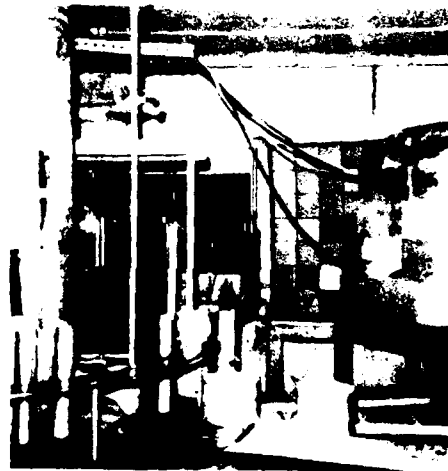


Fig. 4 Sample arrangement in test procedure "2" for plates

This radiation source is especially suitable for simultaneous investigations of several materials for comparison, with which one must be sure that all samples will be processed identically.

Such a test program is shown in the following table:

Dose rate		Exposition time			Total dose	
Gy/h	krd/h	a	m	d	kGy	Mrd
1	0.1	1	+	11	50	5
10	1	1	+	11	500	50
100	10			5 + 15	2000	200
2000	200			1 + 12	2000	200
5000	500			27	2000	200

Tab. 2 Program for material irradiation. Exposition times for wanted total doses at given dose rates

To get the smallest dose rate a lead screen of 5 cm in front of the samples in the farthest position (1.80 m) is required. For the maximum dose rate the test pieces must be attached directly on the Co-60 container. Therefore this irradiation represents an extreme test, with which the material will be stressed by radiation and additionally by mechanical bend, perhaps ozone attack and thermal influence of $\sim 40^\circ\text{C}$.

In these investigation series the productivity and capacity of the following laboratories order the frequency of intermediate value collection, the number of samples and the plurality of materials.

2.2.3. Test equipment "3" (cables) for long term irradiation

2.2.3.1. Test procedure in concrete floor cavities. Another long term irradiation test equipment in laboratory style is intended for comfortable cable examinations.

In the concrete floor of a laboratory hall are hollowed out cavities. These floor cavities ~ 30 cm diameter and ~ 65 cm height are closed by a concrete stopper plug equipped with three labyrinth passages. The passages are assigned for the cable sample and for the ventilation of the experiment space.

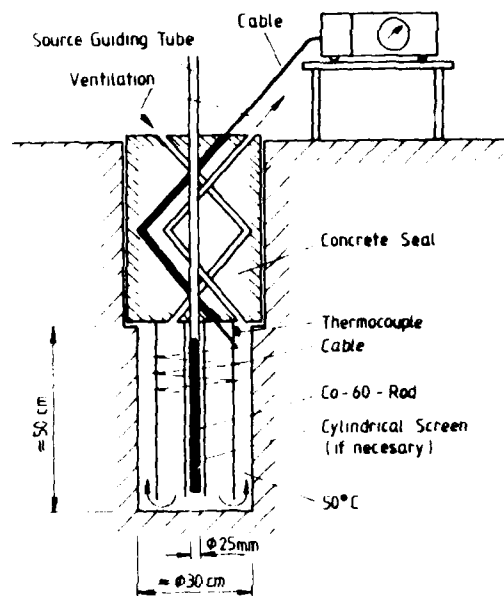


Fig. 5 Sketch of a concrete floor cavity

We installed two floor cavities for

$$\begin{aligned} 1 \text{ Gy/h} &\hat{=} 0.1 \text{ krd/h} \\ 10 \text{ Gy/h} &\hat{=} 1 \text{ krd/h.} \end{aligned}$$

To gain exact results the Co-60 rods were individual activated in a reactor to the requested dose rates.

The Co-rods consist in these cases of Co-granules in a double-walled protective covering. The complete rods have an outer diameter of 25 mm and a useful length of ~ 0.75 m.

In each floor cavity 45 m cable length can be wrapped on a cylindrical device. We installed in both of them three cables 15 m each because we guess this as the minimum for a reliable measurement of electric transmission properties. In addition short pieces of cables can be stored in the cavities to have samples available during the long term test for examinations in other laboratories.

By external controlling using the ventilation the samples are heated at $50^\circ\text{C} \pm 5 \text{ K}$. Doing this the great heat capacity of the cavity walls is remarkable as well as the heating of the specimens by the absorbed radiation (4 K/10 Gy).

2.2.3.2. Test procedure in a "hot cell". A farther trial is carried out at a dose rate of $0.5 \text{ kGy/h} \approx 50 \text{ krad/h}$. According to this dose rate the irradiation runs for a shorter time. Due to internal reasons we perform this test not in a concrete floor cavity but in a so-called hot cell. A hot cell is a laboratory cabinet with the internal dimensions $1.8 \times 1.8 \times 1.6 \text{ m}^3$, i.e. a little more than 5 m^3 .

The Co-60 source is fitted in the center of this cell. The cable specimens are placed around it as a loop with defined diameter.

By lamps, heat radiators, gamma-radiation and ventilation the test object is warmed at $50^\circ \text{C} \pm 5 \text{ K}$. The cabinet has an air change of $\sim 17/\text{min}$. The hot cell has wall tubes and one can the cables measure during the irradiations. Also in this test procedure 1 m cable pieces are in the irradiation chamber for intermediate testing without any change in the other cable arrangement.

In this test procedure we have at present three cable types, two telecommunication cables and one power cable. The telecommunication cables are 4 pair 0.8-Cu conductor cables with 9.5 and 11 mm outer diameter. The power cable is a 4 core 1.5 mm^2 Cu cable with an outer diameter of 14 mm.

The tests are projected for two years and they have the following schedule:

Dose rate		Exposition time			Total dose	
Gy/h	krad/h	a	m	d	kGy	Mrd/h
1	0.1	7			5	0.5
		1 + 2			10	1
		2			17.5	1.75
10	1	6 + 28			50	5
		1 + 1 + 21			100	10
		1 + 8 + 20			150	15
		2 + 3 + 15			200	20
500	50	20 h			10	1
		2.5			30	3
		8			100	10
		21			250	25
		1 + 17			500	50
		2 + 23			1000	100
		4 + 5			1500	150
		5 + 17			2000	200

Tab. 3 Program for cable irradiation. Exposition times for wanted total doses at given dose rates

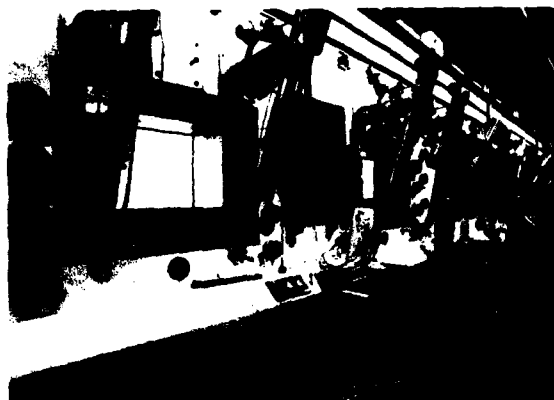


Fig. 6 Front view of hot cells, a test procedure for irradiation of cables by Co-60 sources

2.3. Tests in technical facilities

Often investigations of cables or cable materials are to carry out under special conditions for which laboratory procedures are not sufficient.

In other cases results from the laboratory must be compared with measures of the real practice. Such comparisons show whether laboratory test procedures are representative of service conditions. For this it is necessary for the cable maker to cooperate with atomic energy research facilities or nuclear power plants. For a cooperation like this one example may be given:

It is well known, that plastics can change their properties by irradiation with high energy radiation. The amount of such variations is not only given by the total absorbed dose, but also by the dose rate for accumulation of the total dose. We call this the dose rate problem.

In the containment of a nuclear power plant are installed many cables at many places and at nearly each of them there is to find out a different dose rate. To gain an opinion on the realistic irradiation stress of installations in the containment it is necessary to deal with dosimetric tasks. We do this in team-work with the power plant division of our company.

We fixed on the main pipe of the coolant loop of a pressurized water reactor by means of a belt cable samples. To install this test we used the regular service period when the reactor was turned off during the test run of the plant. We leaved the specimens for one year in the working plant before checking them.



Fig. 7 Cable samples are fastened by a belt on the pipe of the main coolant loop in a nuclear power plant

In the same manner it is possible to do with dosimeter to measure the local dose in different ways.

These are tests in technical facilities from the coolant loop to the fuel decay storage pond.

3. EXAMINATIONS

3.1. Measurements

The measurements in these trials meet just the same properties usually used in the cable industry. Out of one plate are formed eight dumb-bells and measured in a machine the ultimate elongation and the tensile strength at break. In this way material brittleness is registered carefully. We use also plates to measure (but not so often) the electric values dielectric number, loss factor $\tan \delta$ and specific resistance.

In the cases of cable tests during the irradiation, by open-circuit short circuit measurement the following properties are known:

- . Mutual capacitance
- . dissipation factor $\tan \delta$
- . ohmic resistance
- . inductance
- . characteristic impedance and
- . insulation resistance.

Also with cables after irradiation stress the variations are registered of mechanical characteristics of jackets and insulations.

In comparative experiments of several materials with initial measurements, some intermediate test series and final values the individual checks will sum up quickly to some thousand.

3.2. Dose rate dependence

Usually we take the ultimate elongation as the critical value for degradation of irradiated plastics. In the range of lower dose rates takes the decrease of the ultimate elongation place at remarkable lower total doses than in case of higher dose rates. This can be shown with the example of a tested XLPE.

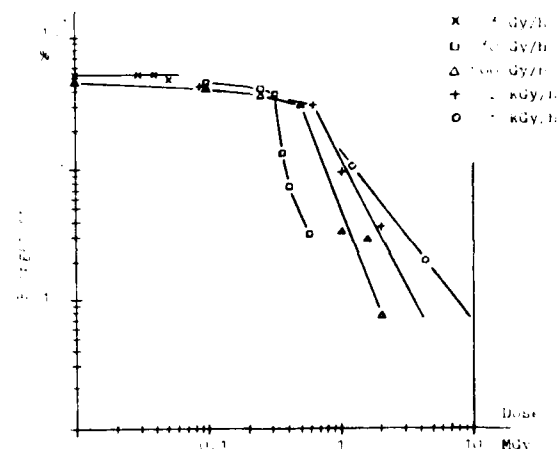


Fig. 8 Decrease of elongation at break in dependence on different dose rates with XLPE

The succession of materials given by the amount of a certain effect (e.g. decrease of the elongation to 50 %) is not a fixed one. There are materials, which show in their properties a considerable dose rate dependence and other polymers with a less one. When varying the dose rates material can in this aspect change their succession places. That means a good material after high dose rate irradiation is not necessarily also a good material after a low dose rate irradiation. It follows consequently by these investigations for the choice of materials for containment cables not to neglect the influence of the relative harmless radiation

doses of a reactor working under normal conditions. One must know the dose rate influence of the material properties for every day service and the Loca-case.

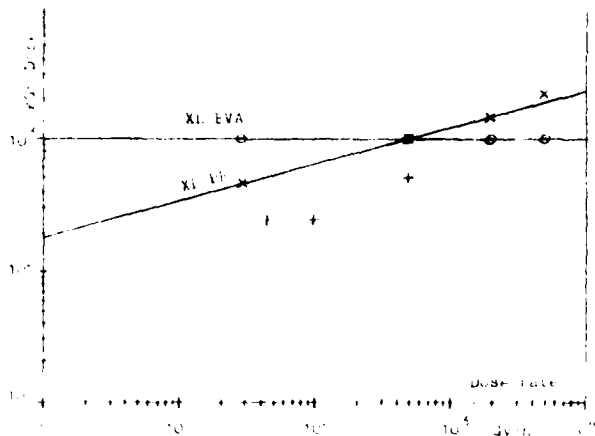


Fig. 9 Injurious doses for elongation decrease to 50 % (abs.) of two cable materials in dependence on the dose rate. (+ ETFE)

3.3. Acceleration of irradiation tests

Investigations were started to check the possibility for acceleration of the irradiation tests with XLPE-compounds and SiR. To make the oxidative attack more intensiv the oxygen partial pressure was elevated (pure oxygen) as well as the test temperature (70° C). Measured were the ultimate elongation and the tensile strength at break of the samples as characteristics easy determinable. With XLPE in one run was measured also the Young's modulus at 100° C. These tests are very time consuming because one needs results at low dose rates for comparison but accumulated to reasonable doses. Some insights of our efforts are given in the following:

- It is not allowed to shorten the radiation exposition time by increasing the dose rates and to accumulate high doses in short time. In this way one will reach even with weak materials good measure results at high doses. Competent in the material influence is not only the absorbed radiation dose but also the mutual action of irradiation and oxygen. This reaction needs time at least for the diffusion of oxygen into the plastic.
- The ultimate elongation shows in these cases a more significant distinction

than the tensile strength at break.

- The elevation of the oxygen partial pressure from air to pure oxygen is not helpful.
- The elevation of the test temperature to 70° C and consequently the increase of oxygen diffusion into the plastic gain better distinctions of the test results.

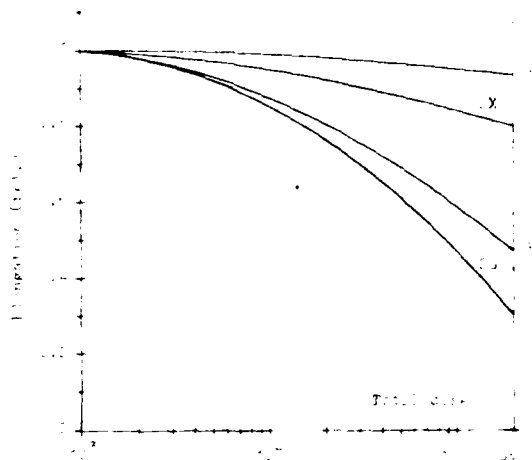


Fig. 10 Decrease of ultimate elongations of two cross-linked materials at different temperatures dependent on the total dose

4. CONCLUSION

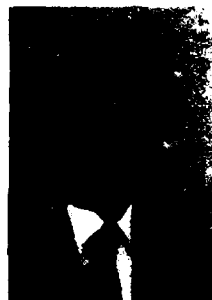
The paper reports test procedures by which in the cable industry material alterations caused by high energy radiation can be measured.

The test equipments differ for cable tests respectively plate tests. As radiation sources work a v.d.Graaf Generator and Co-60 sources of diverse shapes. As major characteristics the variations of ultimate elongation and tensile strength at break of the materials are measured. Also the examinations of electric transmission datas of cables are possible during the irradiation.

The dose rate dependence of property variations is a material specific one and of special importance.

ACKNOWLEDGEMENTS

The investigations described in this paper were carried out by several laboratories and they have been a real team work. Therefor the authors wish to express their thanks to all those colleagues who were cooperating in this field.



Heinrich Rost
Siemens AG
NK E TA 11
Postfach 1520
D-8632 Neustadt



Ernst L. Ney
Siemens AG
NK E TA
Postfach 7000745
D-8000 München 70

Heinrich Rost was born in 1946 in Weismain, Germany. He received his Dipl.Phys. degree in 1975 from the University of Erlangen-Nürnberg. He also received his doctorate in Physics from the same institution in the field of nuclear physics. In 1980 he joined Siemens AG as a research engineer in the telecommunication cables division.

Ernst L. Ney was born in 1925 in Danzig. He studied Chemistry at the Universities of Würzburg, Germany and Innsbruck, Austria and hold a PhD in Chemistry. He joined in 1961 the electric and electronic components division of Siemens AG. He changed to the Siemens telecommunication central labs in 1968. Since 1970 he has been with the development department of telecommunication cables division and is now responsible for general technology.



Roland H. Knoch
Siemens AG
NK E KN
Postfach 1520
D-8632 Neustadt

Roland H. Knoch was born in 1947. He studied at the Fachhochschule Coburg, Germany and graduated in 1972 in Electrical Engineering. Then he joined the telecommunication cables division of Siemens AG in Neustadt/Coburg, Germany. Since 1978 he has been engaged in the development of telecommunication cables.

AD P000578

SUSPENSION LIGHT ABSORPTION MEASUREMENT OF WEATHERABLE PVC COMPOUNDS

P. C. Warren

Bell Laboratories
Murray Hill, New Jersey

Abstract

A rapid and reproducible method to measure the effective carbon black concentration in weatherable vinyl compositions has been developed. Instead of the usual difficult preparation and manipulation of a thin film of plastic, the compound is simply dissolved in tetrahydrofuran before making the traditional light absorption measurement. The black particles remain in suspension and absorb light just as if they were immobilized in a polymer matrix. The test accurately identifies carbon black that is too large a particle size, poorly dispersed, too low a concentration, etc., all of which detract from the UV resistance of finished product. The only compounds that are incompatible with the new technique are those that are insoluble or those that contain significant amounts of inorganic materials that scatter rather than absorb light.

Introduction

1. *History*

A significant fraction of the capital investment of the telecommunications industry lies in aerial wire and cable, where individual components are expected to provide trouble-free, outdoor service for several decades. Early cable designs utilized lead sheaths or rubber jackets to protect insulated wires from the harmful effects of sun, wind and rain but these materials created expensive, short-lived and/or weighty constructions that would be entirely unsatisfactory in the extensive network of today. The timely developments of such thermoplastics as polyethylene (PE) and plasticized polyvinyl chloride (PVC) in the late 1940's offered inexpensive, durable substitutes for metal or rubber cable jackets but their inherent resistance to the weather, particularly to the higher energy portions of the sun's spectrum, was extremely poor. Were it not for the relatively small amounts of finely divided carbon black that protect these vulnerable materials from sunlight, we might be using prohibitively expensive cables today. Instead, virtually all of the modern exposed cable plant is covered with black plastic that satisfies the design lifetime requirement 20-40 years outdoors. Indeed, a black polyethylene sample placed in a Florida exposure site in 1941 and retrieved some forty years later is still mechanically viable and would be satisfactory today as a cable covering.¹

Carbon black attenuates the ultraviolet portion of sunlight by absorbing the energy and reemitting it at longer wavelengths.² Comprehensive studies throughout the 1950's and early 1960's showed that the amount, dispersion, particle size and type of carbon black all played a role in the effectiveness with which the pigment protected the organic matrix. For instance, it is now established that about 2% of a well dispersed, 20 nm particle size channel black will guarantee immunity of polyethylene jacketed cable to ultraviolet light.³ With the many sizes and varieties of blacks currently available and the difficulty in dispersing these small

particles into polymers, combined with the fact that the additive is normally incorporated by a compounder who has exclusive control over the amount introduced, it is no wonder that a considerable effort has been expended over the years in devising methods to measure the quality and quantity of the pigment in PE and PVC plastics.

Two techniques to measure the quality of black compositions were devised in the middle 1950's. One was based on microscopic observation of a thin film of polymer to assess the homogeneity of dispersion.⁴ This method was essentially qualitative and depended on a subjective comparison with an observational standard of an acceptable blend of carbon black in the base polymer. A second method relied on absorption of single wavelength light, again through a thin film.⁵ This measurement, based on Beer's Law, provided a quantitative evaluation that could be incorporated into specifications and used to accept or reject material. The light absorption test received a relatively large development effort primarily because the single quantitative determination avoided individual measurements of particle size, concentration, type and dispersion of carbon black; it was eventually standardized as ASTM D3349 in 1974.⁶

2. *The Problem*

While PVC compositions were originally used indoors, a substantial amount of vinyl jacketed cable is now used outside, including drop wire, urban and rural wire, and some coaxial cables. Like PE, the primary protection from ultraviolet light for both resin and plasticizer relies on preferential absorption by carbon black. The measurement of the quality of this screen was also borrowed from PE experience, namely, light attenuation by a thin film of black plastic. From the very beginning it became obvious that there were problems with the test, most of which focused on the poor reproducibility of results from laboratory to laboratory. Some of them can be illustrated along with a brief discussion of the procedure.

Initial sample preparation requires a very thin, compression molded film of the order of one-half of one-thousandth of an inch that must be absolutely pinhole-free. Usable films of this thickness demand accurately ground steel plates and excellent operator skill. The film is lifted off the plate and onto small hoop which supports it inside the spectrophotometer. The transfer is difficult because of static clinging and often results in torn or unevenly stretched films. A further error in the method lies in different numbers being obtained from different spectrophotometers. Also, too thick a film requires a modification in the procedure; the light must be reduced in the reference beam in order to give a readable absorbance, a change which always compromises sensitivity and accuracy. Finally, the film thickness must be accurately measured since the absorbance is proportional to path length, but only an indirect technique based on the weight of the tiny film is possible.

3. *Suspension Method*

PVC is readily soluble in tetrahydrofuran (THF), as are most of the

organic compounds present in flexible PVC formulations. The experiment consists of simply dissolving a small PVC sample in THF, diluting to a known volume and measuring the absorbance. Development of the method required control experiments to determine (1) the stability of the various solids suspensions over time, (2) the accuracy of the method in determining unacceptable compounds that contain poor black dispersions, too large a median particle size or too small an amount of the pigment, (3) the reproducibility of the method from experiment to experiment, from instrument to instrument and from laboratory to laboratory, and (4) the ease with which this test may be carried out relative to the present film method.

Procedure

1. Apparatus

A. Spectrophotometer

Any instrument that is sensitive at the wavelength of measurement^a and meets the requirements of ASTM E60 is sufficient.

B. Two matched, glass cells with 45x12.5x12.5 mm outside dimensions that can be sealed to prevent solvent evaporation are required. The cells should have a 10.0 mm path length and must not absorb significantly at the measurement wavelength.^b

C. Magnetic stirrer and Teflon coated stirring bar

D. 100 mL volumetric flask and stopper

E. 25 mL graduate

F. Tetrahydrofuran (THF), analytical reagent, stabilized

G. Analytical balance, capable of 0.1 mg accuracy.

2. Calibration

A. Stirring bar volume

Fill the 25 mL graduate about 10 mL with water and record the volume to the nearest 0.1 mL. Slide in the stirring bar and read the new volume to 0.1 mL. The difference between the two readings is the volume of the stirring bar.

B. Spectrophotometer

Using the dark current adjustment set the meter to 0% transmittance. Establish 100% transmittance by adjusting the slit width at the specified wavelength using pure THF solvent as the reference.

3. Procedure A

Approximately 0.05 g of PVC compound, weighed to the nearest 0.1 mg, is added to the volumetric flask, as are the magnetic stirring bar and about 50-75 mL THF. The flask is placed on the magnetic stirrer and allowed to gently stir until the PVC compound is dissolved (usually 15-20 minutes are required). After assurance that all the material is homogeneously distributed throughout the liquid (easily checked by holding the flask up to the light and looking for any remaining undissolved material), the volume is diluted to the mark with THF, stoppered and briefly shaken to mix all components. The solution/dispersion is decanted into one of the cells and its percent transmission (relative to a pure THF solvent reference) at the specified wavelength is recorded. For maximum accuracy the reading should be made within 10 minutes of filling the cell.

4. Procedure B

Follow instructions as exactly outlined in Procedure A. Instead of discarding the sample, allow the sample cell to remain undisturbed

for 24 hours. Then remeasure the suspension absorbance and record it along with the initial absorbance. If the delayed measurement is less than 80% of the initial reading, the suspension method should not be used and the ASTM D3349 thin film method will take precedence.

Results and Discussion

1. Theory

The well known relationship defined by Bouguer, Beer and Lambert showed that light is attenuated exponentially when absorbed:

$$(1) \quad A = \ln \frac{I_0}{I} = \epsilon bc$$

where A = absorbance

I_0 = incident light intensity

I = light transmitted through the medium

ϵ = extinction coefficient

b = thickness of the PVC film, mm

c = concentration of absorbing material, wt. %

An apparent absorption coefficient^c is calculated by normalizing the experimentally observed A to constant film thickness:

$$(2) \quad \left(\frac{1}{b}\right) \ln \left(\frac{I_0}{I}\right) = \epsilon c$$

This function is sufficient to categorize an unknown sample because the amount of carbon black and the quality of its dispersion tend to compensate for one another. For example, use of larger particle size and/or poorly dispersed additive will offer sufficient weathering protection if there is enough of it; alternatively, only a minimum amount is needed if a fine particle size is well homogenized throughout the plastic. The above measurement will characterize both cases.

The PVC solution path length can be transformed to an equivalent film thickness by calculating the volume fraction of the solution that is PVC:

$$(3) \quad b = \left(\frac{w}{\rho}\right) \frac{1}{V}$$

where λ = solution path length, mm

w = weight PVC compound, g

ρ = density PVC compound, g/mL

V = volume PVC/THF solution, mL

Substituting into (2), converting I_0 and I to 100 and T (percent transmission), respectively, changing to base 10 logarithms and subtracting the volume (V_s) of the stirring bar yields:

$$(4) \quad \text{Apparent Absorption Coefficient} = \frac{2.3\rho(V - V_s)\log(100/T)}{w}$$

2. Calibration

The suspension method was compared to the film method by measuring apparent absorbance coefficients of 0 to 4.0 phr (parts per hundred of resin), in 0.5 phr increments, of a 28 nm particle size furnace black mixed into the PVC formulation described in Table I. Figure 1 shows that both methods give straight line dependences on carbon black concentration, the identical slopes indicating that each phr of carbon black increases the apparent absorption coefficient by a little over 100. The curve does not go

^a Unless otherwise specified, the wavelength will be 375 nm

^b Helma Series III, Type OS Teflon-stoppered glass cells have been found adequate and are available from most laboratory supply houses

^c The term 'apparent absorption coefficient' is used because transmission is a function of light scattering as well as true absorption

through zero in either case because suspended inorganic fillers such as antimony oxide, clay, lead stabilizers, etc., scatter light slightly. Also, the parallel lines are not superimposed on one another, apparently because there is a greater interaction of light with reflective filler particles in the liquid suspension than in the solid polymer film. Highly filled materials cause significant error due to this phenomenon and therefore are not compatible with the suspension technique; such samples are easily identified by monitoring the stability of the suspension.

3. Suspension Stability

An important characteristic of the suspension absorption method is that it requires a reasonably stable suspension of particles in PVC/plasticizer/THF solution. Figure 2 shows the change in apparent absorbance values of the same PVC compound with various levels of carbon black added. The nonblack sample gave an original apparent absorbance of 88 but dropped to 90% of that number within 15 minutes; furthermore it was halved in the next 3.5 hours. The 2.5 phr black pigmented formulation gave an initial value of 326 which dropped only 2% after the first hour.

Since inorganic fillers such as calcium carbonate, silica, clay, antimony oxide, lead stabilizers, alumina hydrate, etc. are relatively large (1-10 μm diameter) and heavy (2.5-7 specific gravity) they tend to settle fairly rapidly. Carbon black, on the other hand, is much finer in size (0.01-0.05 μm diameter) and somewhat lighter (1.8 specific gravity) and forms reasonably stable suspensions. Consequently, PVC compounds with a high proportion of well dispersed black relative to filler will give unchanging numbers by the solution method, but highly filled compounds that exhibit high apparent absorbance coefficients (due to scattering rather than absorption) will not be constant with time.

Unsuccessful attempts were made to separate the inorganic reflective fillers from the absorptive blacks by filtration, centrifugation and sedimentation. The last technique appeared to be the most promising, but the inorganic particles that settled out tended to also transport some carbon black to the bottom of the cell. As a result, artificially low apparent absorption coefficients were obtained. The sedimentation process is valuable, however, in identifying those compounds that contain excessive amounts of filler. The sample is left in the spectrophotometer cell and remeasured 24 hours later. If the delayed reading is less than 80% of the original result, too many reflective particles are present for an accurate reading and the alternate ASTM D3349 thin film method should be used.

4. Reproducibility

Table 2 summarizes an experiment that uses a black PVC formulation with weights differing by almost an order of magnitude. The percent transmissions ranged from 9% to 69%, yet the apparent absorbances were all within one percent of each other. This result is consistent with the straight line dependence shown in Figure 1 and affirms the accuracy of Beer's Law in suspension measurements.

Table 3 compares the results of the suspension method on three spectrophotometers, a single beam Bausch and Lomb Spectronic 20, a single beam Beckman Model B, and a double beam Cary 219. The numbers are all within 5% of one another, an excellent reproducibility compared to reported film test deviations on various instruments.⁵

5. Round Robin

An informal round robin was organized to better ascertain the accuracy and reproducibility of the new method. The nine laboratories that participated used a variety of single and double beam spectrophotometers, including the Beckman B, Beckman DB, Beckman 5280, Beckman DB-G, B&L Spectronic 20, HP 8450A

and Cary 15. Five samples were submitted for testing (labelled only as numbers one through five), each consisting only of a slight variation of the composition detailed in Table 1.

Sample one, the control, was a drop wire formulation containing 2.5 phr (1.35%) 28 nm furnace black. Sample two contained 2.0 phr (1.08%) of the identical black, simulating a slightly deficient pigment loading. Sample three had an identical black concentration as the control but was purposely made with a poor dispersion; instead of introducing the black in the form of a masterbatch it was simply added as powder to the base formulation on a two-roll mill. Sample four represented a less effective carbon black, consisting of a larger 49-60 nm particle size material with a similar concentration and dispersion as the control. Sample five was very deficient in black pigment, containing only 1.0 phr (0.54%) 28 nm furnace black, but also included 50 phr (27%) of a surface treated, 1.0 μm calcium carbonate diluent.

Table 4 summarizes the results of the interlaboratory study. All numbers reported for each sample were obtained in duplicate; the reproducibility of these numbers were within $\pm 3.5\%$ except for the highly filled sample. The standard deviations of the averaged results were somewhat higher, falling somewhere between 5 and 9%, again with the exception of the highly filled sample. Most important, the test easily identified all problems that were incorporated into the samples, and so appears reasonably accurate. For example, based on the value of 324 obtained for the control, and taking into account that about 90 of this number is due to light interaction with nonblack portions of the formulation (as shown by the 0 phr black reading in Figure 1) the expected absorption of sample two would be $(324-90)(2.0/2.5)+90=267$, which compares well with the actual 278 result.

Samples one and five were also measured by Procedure B, which requires a reading 24 hours after the spectrophotometer cell was filled. The control formulation value was reduced to 86% of the original apparent absorption coefficient, while that of filled sample was lowered to 26% of its initial number. Based on arguments presented earlier in the discussion, sample five shows too high an apparent absorption coefficient (since the delayed reading is less than 80% of the original). The traditional thin film method is better suited to this sample for an accurate prediction of weathering performance.

Conclusions

A method has been devised that measures the light absorption of black PVC compounds intended to stand up to the weather as outdoor cable jackets. It is applicable to all PVC materials that are soluble, and excludes only those that are crosslinked or are highly extended with inorganic fillers. The new procedure eliminates many of the errors that are inherent to the ASTM D3349 film method. The reproducibility of the suspension technique is better than film method and an informal round robin showed it to accurately portray the effective black content of the material.

Acknowledgement

The author would like to thank J. E. Adams, J. L. Williams, S. Kaufman of Bell Laboratories, M. F. Marx, E. Sauer and J. F. R. Dixon of Western Electric; J. R. Taylor, J. Gonzalez and W. Hampton of B. F. Goodrich; F. Roesler, P. A. Ketterer and R. J. Bowblis of Tenneco; and R. H. Colvard of Columbian Chemicals for their participation in the round robin.

References

1. H. M. Gilroy, private communication
2. J. F. Ambrose, *Bell Laboratories Record*, 247 (July, 1957).
3. J. B. Howard and H. M. Gilroy, *Polym Eng Sci* 9, 286 (1969).
4. R. M. Schulken, Jr., G. C. Newland and J. W. Tamblin, *Mod. Plast* 35, 125 (1958).
5. J. B. Howard, *Polym Eng Sci*, 6, 1 (1966)
6. 1981 Annual Book of ASTM Book of Standards, American Society for Testing Materials, Part 36, pp. 829-834.



Paul C. Warren is a Member of Technical Staff at Bell Laboratories, Murray Hill, N.J. He received an A.B. degree in chemistry from Wesleyan University and a Ph.D. in organic chemistry from Cornell in 1969. His current interests at Bell Labs have centered on structure/property relationships and high temperature performance of plasticized PVC, with special emphasis on the wire and cable application.

Table 2

Reproducibility of Suspension Absorption Test

Initial Wt. Black PVC Compound, ^b g	Percent ^a Transmission	Apparent Absorption Coefficient
0.0879	9.0	356
0.0578	20.5	357
0.0354	37.5	360
0.0135	69.1	356

^aBausch and Lomb Spectronic 20, 400 nm

^b2.5 phr furnace black incorporated into the compound described in Table 1.

Table 3

Apparent Absorption Coefficient^a

Table 1		Wavelength, nm	B&L 20	Beckman 8	Cary 219
Additive	Concentration (phr)	375	-	357	376
PVC homopolymer	100	400	340	342	357
Dialkyl phthalate plasticizer	62	450	308	310	301
Tribasic lead sulfate stabilizer	5	500	281	283	297
Inorganic fillers	13				
Carbon black pigment	variable				

^a0.0624 g PVC Compound (2.5 phr furnace black) in 98.7 mL THF

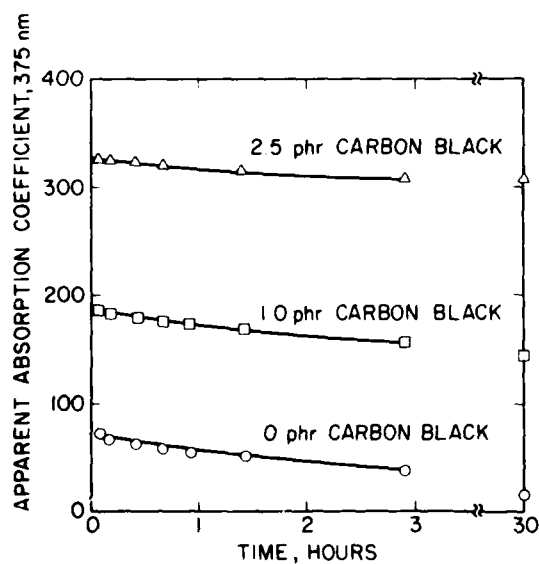
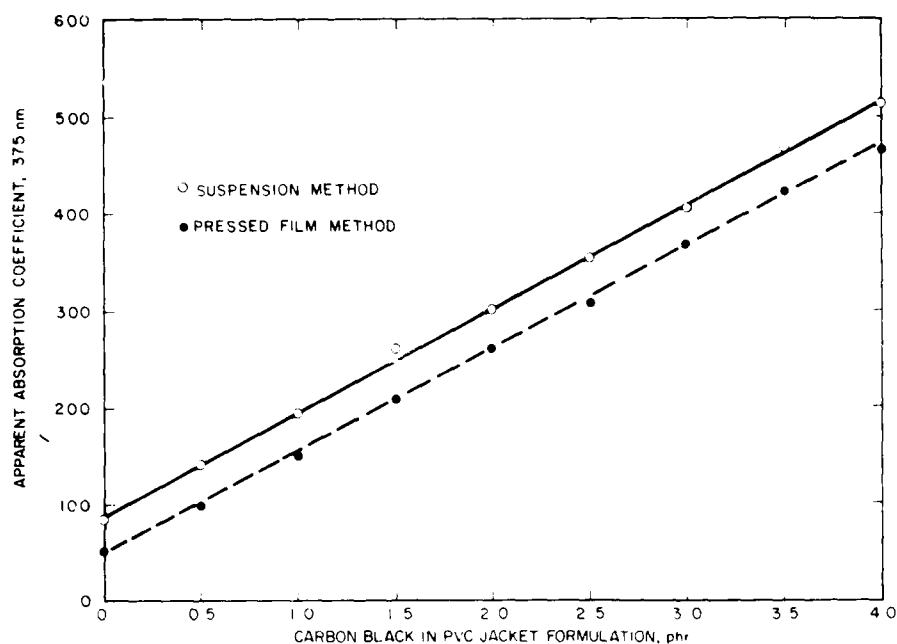


Table 4

No.	Description	Ave. Deviation of Duplicates	Average Apparent Absorption Coefficient	Std. Deviation of Results
1	Control (Table 1)	+ 2.6%	324	+ 5%
1 (24 hr)	Control (Table 1)	1.4%	278	5%
2	Reduced Black	1.4%	274	5%
3	Poor Black Dispersion	3.0%	210	7%
4	Large Particle Black	3.4%	198	9%
5	CaCO ₃ filled	1.3%	84	13%
5 (24 hr)	CaCO ₃ filled	17.2%	84	33%

Viscoelastic Analysis of Shrinkback

C. R. Taylor H. M. Dillow C. J. Aloisio

Bell Laboratories, Norcross, Georgia 30071

At processing temperatures most polymers exhibit a considerable amount of elastic behavior which is time dependent. When a molten polymer is deformed into a desired shape and rapidly cooled during processing, orientation is locked into the product. The amount and nature of the orientation will depend on processing conditions. For instance the primary orientation in drawn fiber and wire insulation is longitudinal. There is then the possibility of this orientation being recovered during the lifetime of the product with an ensuing change in physical dimensions. For instance, a fiber may become shorter, exposing copper conductor at the end of the wire. It is necessary to characterize a polymer product for shrinkback performance over its lifetime of use. The basic physical principles of shrinkback will be presented along with the application of the principles to quantitatively characterize shrinkback in a wire insulation product.

Introduction

The occurrence of dimensional changes in plastic parts fabricated by various means are a function of both time and temperature. The class of dimensional variations for which the terminology shrinkback is applied are strongly time dependent and often in a direction opposite from that expected from thermal expansion. The thermal expansion effects, analogous to those that one observes in non-polymeric materials, may be considered essentially independent of time in situations characterized as unconstrained. In plastics applications, the phenomenon of shrinkback is also referred to as internal stresses, orientation, and residual stresses/strains. The number of different terms used to describe this phenomenon is probably an indication of the degree of confusion that exists in attempts to characterize this behavior.

The importance of shrinkback may be seen by the variety of applications in which it has an impact on performance. In lightguide applications, levels of shrinkback in the order of one percent can adversely affect the environmental performance of cables¹ and splices.² Common blow-molded products, such as bottles, exhibit shrinkback due to orientation locked in during processing³ that reflects on the dimensional stability of the part. The shrinkback in polyester magnetic tapes limits the track densities.⁴ Approaches to improve the performance of such tapes have involved annealing⁴ and lamination.⁵ Even paper used in copiers exhibits shrinkback that can adversely affect performance.^{6,7} In the conventional cable business shrinkback has been a cause for concern both in jacketing^{15,16} and insulation.

Interest in shrinkback as a means of measuring the degree of orientation of polymer films and fibers has been high for many years.⁸⁻¹⁴ With few exceptions,¹³ there has not appeared to have been a recognition that shrinkback or viscoelastic recovery can be treated analytically and experimentally as well-known viscoelastic effects.

In this paper the general principles for the quantitative characterization of shrinkback are presented. Then the approach is applied to shrinkback in tape. Finally, a composite insulation is examined within the framework of the proposed viscoelastic analysis.

Shrinkback Model

A. Viscoelastic Effects

When a polymer melt is deformed the long chain molecules of which it consists are oriented due to their inability to instantaneously rearrange their configurations to conform to the new shape. This results in a time dependent stress in the material which decays as a function of time, i.e., the orientation decays as a function of time due to molecular motion.

The time dependent stress, σ , can in general be described by a set of entropic moduli, E_i , and associated time constants, τ_i , for decay by molecular motion. The stress is given by

$$\sigma(t) = T(t) \epsilon = \left(\sum E_i e^{-t/\tau_i} \right) \epsilon \quad (1)$$

where $E(t)$ is the time dependent Young's relaxation modulus and ϵ is the strain in extension on a length of material. If stress relaxation is allowed to occur at a given temperature under a constant strain for a length of time and the stress is subsequently released the polymer does not return immediately to its original length, but undergoes prolonged recovery which is essentially described by equation (1). The relaxation-recovery process is shown diagrammatically in Figure 1 and represents the essence of the shrinkback phenomenon. In general the manufacturing conditions will involve a complicated temperature and stress-strain history followed by rapid cooling to ambient temperature. Shrinkback or recovery then occurs over a period of time at the environmental temperatures encountered in the application. As will be seen below there is an equivalence between time and temperature for polymers that will allow long range shrinkback predictions to be made.

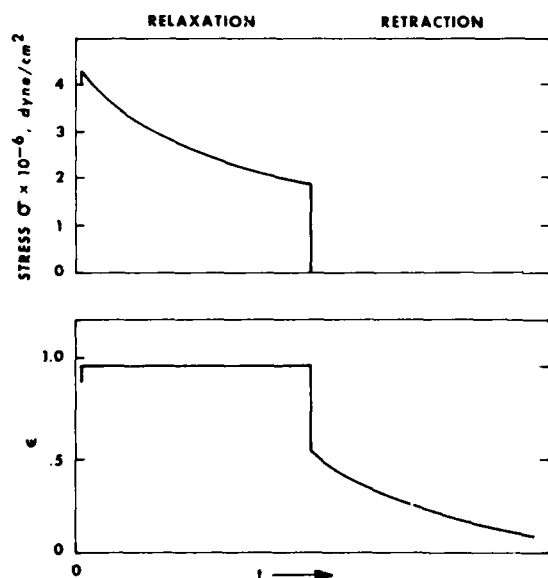


FIGURE 1. TIME PROFILE OF A STRESS RELAXATION EXPERIMENT IN SIMPLE EXTENSION FOLLOWED BY RECOVERY.

B. Thermal Effects

It is found for many different polymers that the main effect of changing temperature on equation (1) is to change all the relaxation times, τ_i , by the same factor, i.e.,

$$a_T(T) = \frac{\tau_i(T)}{\tau_i(T_0)} \quad \text{for any } i, \quad (2)$$

where the temperature is changed from a reference temperature, T_0 , to temperature T . This effect is known as time-temperature superposition¹⁷ since the result in equation (1) is to effectively change the time scale by the factors $1/a_T$, i.e.,

$$\sigma(t, T) = \sigma(t/a_T, T_0). \quad (3)$$

The shift factor $a_T(T)$ will apply to the change in time scale with temperature for any viscoelastic process. The temperature dependence of a_T can therefore be determined from readily performed oscillatory mechanical experiments and used in more complicated experiments such as shrinkback.

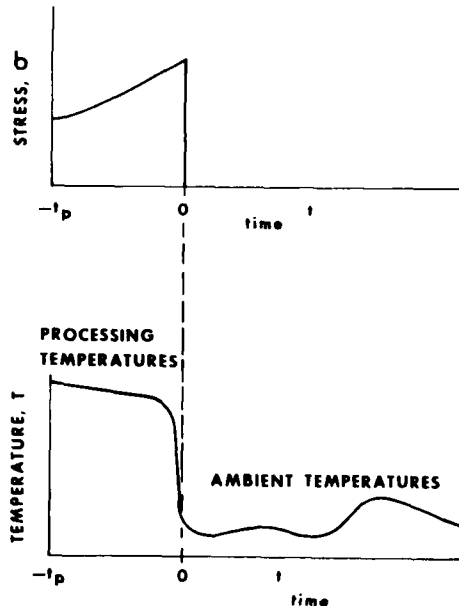


FIGURE 2. ORIGIN OF SHRINKBACK.

As mentioned above shrinkback occurs because of orientation of the long polymer molecules introduced during manufacturing. This process is described diagrammatically in Figure 2 for a general polymer undergoing extrusion or fiber drawing. The orientation occurs as a result of axial stresses applied during fabrication at a high temperature where the material is rubbery followed by a rapid cooling which "locks in" the orientation by dramatically slowing the recovery (as will be seen by the temperature dependence of a_T).

C. Shrinkback Experiment

In order to experimentally probe shrinkback a test is performed as diagrammed in Figure 3. It is assumed that up to time zero all the material has been subjected to the same temperature and stress-strain conditions. Shrinkback can be measured quantitatively as the percent recovery of the insulation in terms of the initial length L_0 , at $t=0$ and length at time t , $L(t)$, i.e.,

$$\% \text{ Recovery} = \% \text{ Shrinkback} = \frac{L_0 - L(t)}{L_0} \times 100 \quad (4)$$

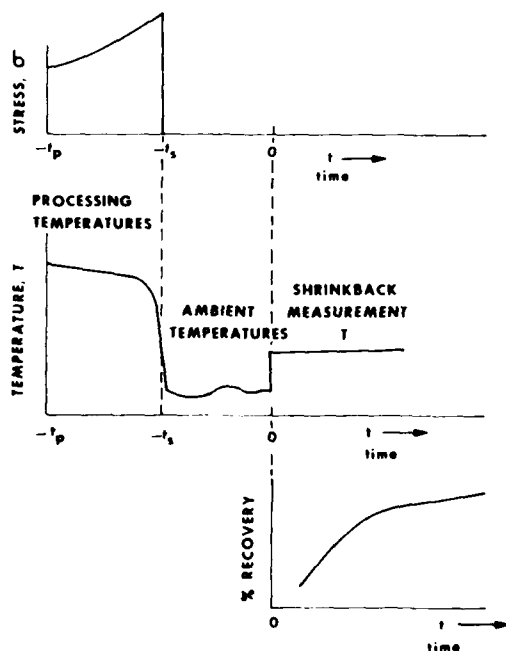


FIGURE 3. SHRINKBACK EXPERIMENT

Equation (4) can be written in terms of strain as,

$$\% \text{ Recovery} = [\epsilon(0,T) - \epsilon(t,T)] \times 100 / [\epsilon(0,T) + 1] \quad (5)$$

where $\epsilon(0,T)$ is the strain on the insulation at $t=0$ (the beginning of the shrinkback experiment), and $\epsilon(t,T)$ is the strain at time t . The strains are defined relative to some unstrained initial length. The % shrinkback will therefore shift with temperature in the same manner as $\epsilon(t,T)$. In order for the shrinkback experiments depicted in Figure 3 to shift with temperature according to the a_T factors from viscoelastic measurements, the following relation must hold.

$$\epsilon(t,T) = \epsilon(t/a_T, T_0) \quad (6)$$

where T_0 is an arbitrary reference temperature. This is shown to be true below.

In order to facilitate the analysis the time scale of Figure 3 is redesignated as shown in Figure 4. The strain $\epsilon(t,T)$

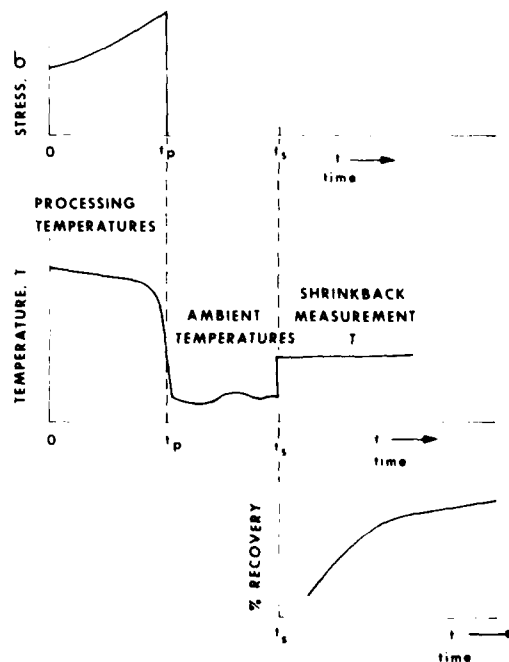


FIGURE 4. SHRINKBACK EXPERIMENT WITH TIME SCALE REDEFINED

can be given in terms of the creep function, $D(T_0, t)$, by

$$\epsilon(t, T) = \int_{-\infty}^t D(T_0, \xi(t) - \xi(t')) \frac{d\sigma}{dt'} dt' \quad (7)$$

where σ is the stress and

$$\begin{aligned} \xi(t) &= \int_0^t \frac{dt''}{a_T(T(t''))} \\ \xi(t') &= \int_0^{t'} \frac{dt''}{a_T(T(t''))} \end{aligned} \quad (8)$$

As can be seen from the stress history of Figure 4, the integral of (7) becomes,

$$\epsilon(t, T) = \int_0^{t_p} D(T_0, \xi(t) - \xi(t')) \frac{d\sigma}{dt'} dt' \quad (9)$$

and since $t' < t_p$ in this integral

$$\begin{aligned} \xi(t) - \xi(t') &= \int_0^{t_p} \frac{dt}{a_T(T(t))} + \int_{t_p}^{t_s} \frac{dt}{a_T(T(t))} \\ &= \frac{t - t_s}{a_T(T)} + \int_0^{t'} \frac{dt}{a_T(T(t))} \end{aligned} \quad (10)$$

This calculation gives $\epsilon(t, T)$ with $\xi(t) - \xi(t')$ given by equation (10). The same calculation may be made for $\epsilon(t, T_0)$ in which case

$$\begin{aligned} \xi(t) - \xi(t') &= \int_0^{t_p} \frac{dt}{a_T(T(t))} + \int_{t_p}^{t_s} \frac{dt}{a_T(T(t))} \\ &= \frac{t - t_s}{a_T(T)} + \int_0^{t'} \frac{dt}{a_T(T(t))} \end{aligned} \quad (11)$$

since $a_T(T_0) = 1$. In changing the shrinkback experimental temperature from T to T_0 the only term that changes is that involving $t - t_s$. This time variable, $t - t_s$, is the time measured during shrinkback as given in Figure 3 and equation (6). It is seen from equations (10) and (11) that

$$\epsilon(t - t_s, T) = \epsilon[(t - t_s)/a_T, T_0] \quad (12)$$

which proves that equation (6) is true.

If viscoelastic data is available in the form of master curves at a reference temperature, T_0 , and accompanying $\log a_T$ and $\log V_T$ information the following equations may be used to calculate the various viscoelastic properties as a function of time and temperature:

$$\begin{aligned} \sigma(t, T) &= \frac{1}{V_T} \sigma(t/a_T, T_0) \\ E(t, T) &= \frac{1}{V_T} E(t/a_T, T_0) \\ E'(\omega, T) &= \frac{1}{V_T} E'(\omega a_t, T_0) \\ E''(\omega, T) &= \frac{1}{V_T} E''(\omega a_t, T_0) \end{aligned} \quad (13)$$

Applications

A. Polyethylene Terephthalate (PET)

Commercial PET, typical of that found in adhesive tape and yarns, was measured in an oscillatory tension mode using the Rheovibron instrument. The data were reduced to a master curve using previously described techniques of time-temperature superposition. The results are given in Figure 5 as master curves of the storage

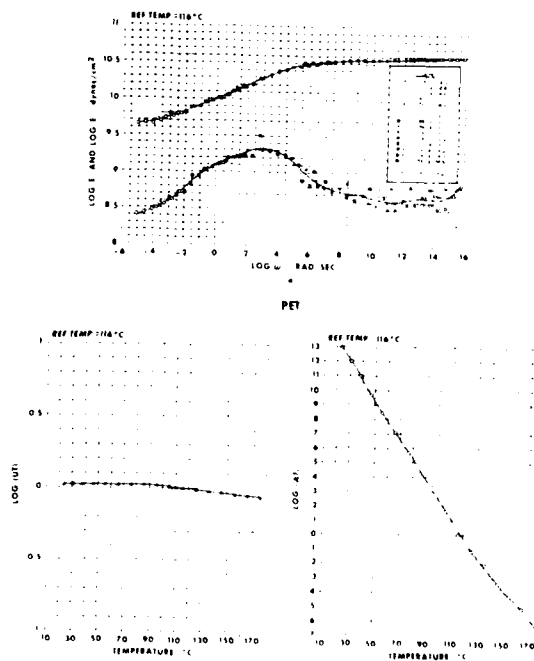


FIGURE 5. COMPOSITE MASTER CURVES OF E' AND E'' VERSUS REDUCED FREQUENCY AT 116°C

modulus $E'(\omega)$ and loss modulus $E''(\omega)$ versus reduced frequency at a reference temperature of 116°C . The master curves give the mechanical behavior of the PET over the frequency range shown at 116°C and the curves can be transformed by horizontal shifts along the log frequency axis (and small vertical shifts, $\log V_T$) to provide the mechanical behavior at other temperatures as shown in Equation 13. It is important to realize that the shifting of the time scale with temperature in Figure 5c will be the same for any viscoelastic process whether it be adhesion, friction or shrinkback.

Shrinkback experiments of the type described by Figure 3 were made on a PET tape. The shrinkback results at different temperatures were superposed to form a master curve with the $\log a_T$ horizontal shifts obtained from the mechanical results of Figure 5. The master curve for the tape is shown in Figure 6.

B. Semirigid Polyvinyl Chloride (PVC)

An insulation grade PVC was measured in an oscillatory shear mode using the Rheometrics Thermal Mechanical Spectrometer. Using the same data synthesis techniques as applied to the PET, the master curves of storage modulus $G'(\omega)$ and loss modulus $G''(\omega)$ shown in Figure 7 were ob-

tained. The data reduction required only the horizontal shift ($\log a_T$) included in Figure 7.

C. PET Yarn Reinforced PVC Insulation

A PVC insulation with PET yarn reinforcement has been under study as a possible replacement for a PVC-textile insulated wire. The wire is commonly used in central offices to make connections between equipment bays. Manufacturing inefficiency has been the main driving force to replace the PVC-textile insulation. The composite PVC/PET insulation exhibited tensile strength, heat resistance, abrasion resistance and cut through strength comparable to the PVC-textile insulation but was more efficient to manufacture. The one property in which the replacement failed was shrinkback.

The standard shrinkback quality control test for this central office wire is performed on six inch lengths of wire. The insulated wires are placed in an oven at 250°F (121°C) for one hour. If the amount of conductor exposed at both ends is less than 12/64ths of an inch the samples pass. Exposure lengths of 24/64ths of an inch were observed for the PVC/PET insulation.

In order to assess the significance of the quality control results on long time

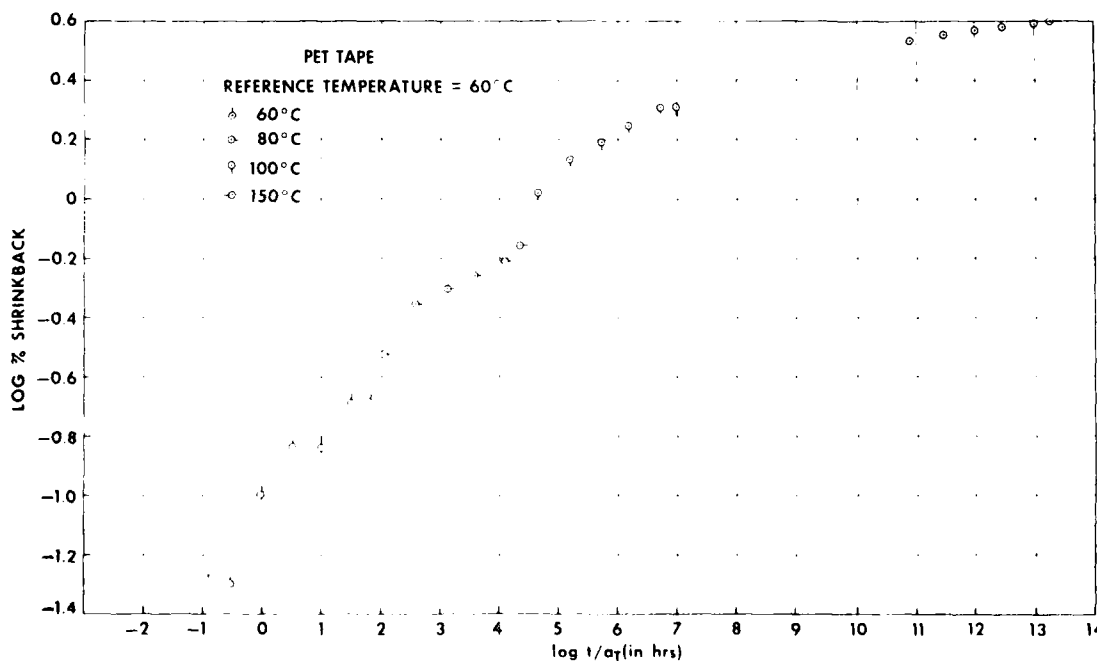


FIGURE 6. MASTER CURVE OF SHRINKBACK VERSUS REDUCED TIME FOR TAPE AT 60°C

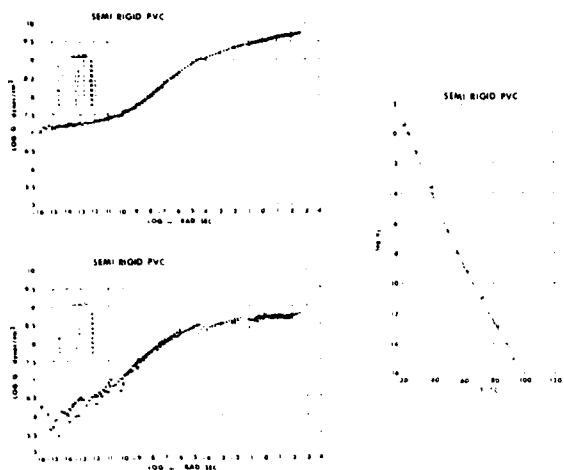


FIGURE 7 COMPOSITE MASTER CURVES OF G' AND G'' VERSUS FREQUENCY AT 25°C.

performance the shrinkback test was performed at four different temperatures and the conductor exposure measured as a function of time. The results for 60°C, 80°C, 100°C and 121°C are presented in Figure 8. If the shrinkback is dominated by the PET yarn the curves of Figure 8 should form a master curve using the $\log a_T$ values from Figure 5C. This is the case as shown in Figure 9 for a reference temperature of 60°C. Entering the $\log \% \text{ shrinkback}$ scale at 0.5 (the value corresponding to 12/64ths of an inch) one finds that it would take in excess of 20 years to observe such a level of shrinkback in a six inch length of conductor.

The dominance of the PET yarn in the shrinkback of the composite insulation was supported by the results of two additional tests. In one, a conductor with PVC alone indicated no shrinkback in the standard quality control test. In the second, PET yarn exposed to 121°C yielded a shrinkback value about the same as for the composite insulation.

While the shrinkback master curve of Figure 9 indicates acceptable long time performance with respect to the quality control test samples, longer length samples exhibit increasing percent shrinkback as shown in Figure 10. Therefore reduction in the inherent shrinkback of the PET yarn prior to incorporation into the composite insulation would be required to further insure satisfactory performance in the field.

Summary

Shrinkback problems involving any combination of plastics, type part geometry

and manufacturing process may be analyzed using the techniques presented here. This viscoelastic analysis permits quantification of the acceleration factors ($\log a_T$) produced by various thermal exposure. Application to the shrinkback of a PVC/PET composite insulation revealed the importance of the inherent shrinkback of the PET yarn.

Acknowledgements

The authors would like to express their gratitude to R. P. DeFabritis for some of the laboratory measurements and G. S. Brockway for help with the derivations.

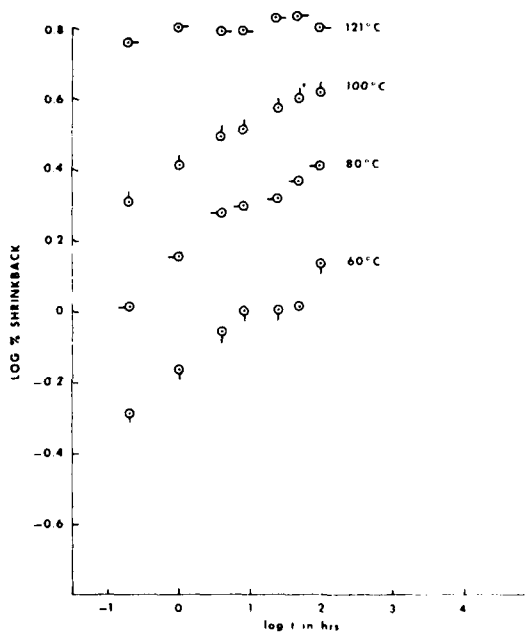


FIGURE 8 ISOTHERMS OF SHRINKBACK ON 6 INCH LENGTHS OF PET YARN REINFORCED PVC INSULATED WIRE

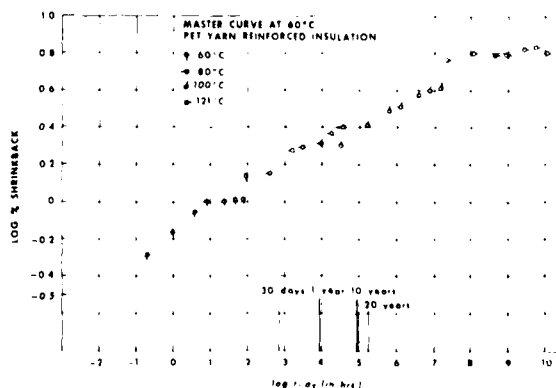


FIGURE 9 COMPOSITE CURVE OF PERCENT SHRINKBACK VERSUS REDUCED TIME AT 60°C

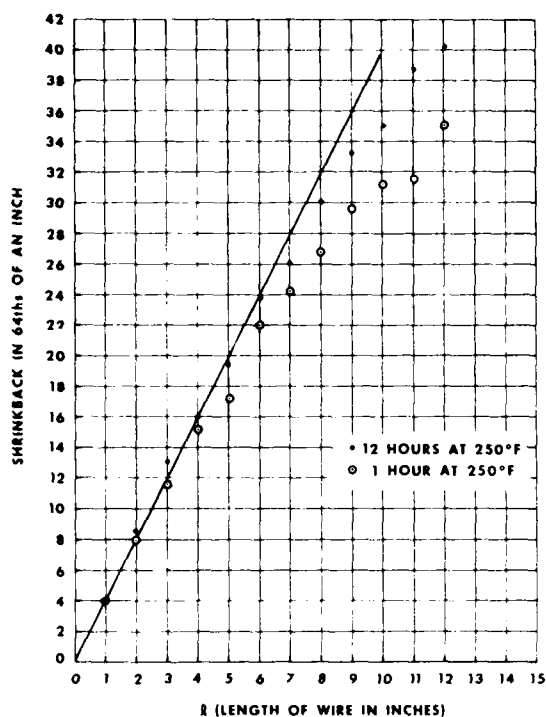


FIGURE 10. SHRINKBACK AT 121°C AS A FUNCTION OF WIRE LENGTH. SOLID LINE CORRESPONDS TO CONSTANT PERCENTAGE OF SHRINKBACK (6.3%).

References

1. G. S. Brockway, P. F. Mahr, and M. R. Santana, "An Analysis of the Environmental Performance of Fiber-Optic Ribbons," Sixth European Conference on Optical Communication, University of York, United Kingdom 16-19, September 1980.
2. A. H. Cherin, P. J. Rich, C. J. Aloisio and R. R. Cammons, "A Vacuum-Assisted Plastic Repair Splice for Joining Optical Fiber Ribbons," Bell System Technical Journal, 58, No. 8, (October 1979), pp. 1825-1838.
3. H. Frank and W. Wangler, "Shrinkage of Blow-Molded Polyethylene Hollow Bodies: The Effect of Processing Conditions," Verpackungs-Rundschau, 10, pp. 1382-1392.
4. B. F. Blumentritt, "Annealing of Poly(ethylene terephthalate)-Film-Based Magnetic Recording Media for Improved Dimensional Stability," IBM J. Res. Develop., 23, No. 1, (January 1979) pp. 56-65.
5. B. F. Blumentritt, "Laminated Films with Isotropic In-Plane Properties," IBM J. Res. Develop., 23, No. 1, January 1979, pp. 66-74.
6. L. K. Agbezuge, "Internal Stress Levels in Xerographic Papers," Polymer Engineering and Science, June 1981, 21, No. 9, pp. 534-537.
7. L. K. Agbezuge, "Numerical Determination of Internal Stress and Viscoelastic Parameters for Xerographic Papers," Polymer Engineering and Science, June 1981, 21, No. 9, pp. 538-541.
8. K. Imada, T. Yamamoto, K. Shigematsu, M. Takayanagi, "Crystal Orientation and Some Properties of Solid-State Extrudate of Linear Polyethylene," Journal of Material Science, 6, (1971), pp. 537-546.
9. T. Nakayama and N. Inoue, "Mechanical Testing and Structural Characterization of Hydrostatically Extruded Polymers. I. Effects of Hydrostatic Extrusion on Subsequent Mechanical Behavior," Bulletin of the JSME, 20, No. 144, June 1977, pp. 688-695.
10. N. J. Capiati and R. S. Porter, "Dimensional Changes in Ultradrawn Polyethylene," J. Polymer Sci.: Polymer Physics Edition, 15, (1977), pp. 1427-1434.
11. P. Barham and A. Keller, "A Criterion for Distinguishing Between Polymer Fibers of Fundamentally Different Origin," Polymer Letter Edition, 13, (1975), pp. 197-202.
12. M. P. C. Watts, A. E. Zachariades, R. S. Porter, "Shrinkage as a Measure of the Deformation Efficiency of Ultra-Oriented High Density Polyethylene," Journal of Materials Science, 15 (1980), pp. 426-430.
13. D. Hansen, W. F. Kracke and J. R. Falender, "Shrinkage of Cold Drawn Polyethylene and Polypropylene," AM CHEM SOC-Division Polymer Chem., 10, No. 2, (1969), pp. 1044-1050.
14. M. Spajer and J. P. Goedgebuer, "Interferometric Studies of the Dimensional Variations of Silicone Elastomers," Optics and Laser Technology, April 1979, 11, pp. 100-102.
15. K. Ogawa, "Laminated Aluminum-Polyethylene Sheath Cable," Japan Telecommunications Review, 1970, pp. 130-133.

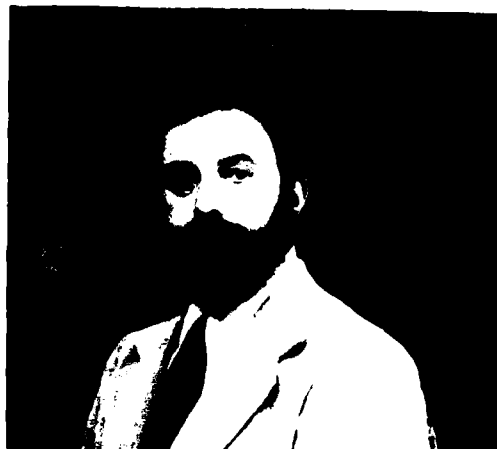
16. H. Fukutomi, "Improved Laminated Aluminum-Polyethylene Sheath Cable," Japan Telecommunications Review, July 1973, pp. 204-207.
17. J. D. Ferry, "Viscoelastic Properties of Polymers," 2nd edition, John Wiley and Sons, Inc., New York 1970.



Carl Taylor is a Member of Technical Staff at Bell Laboratories in Norcross, Georgia, where he works in the Plastics Engineering and Characterization Group. He received his B.A. degree from The College of Wooster in Ohio and Ph.D. from The University of Wisconsin in Madison. He is a member of The Society of Plastics Engineers, ASTM, The Society of Rheology, The American Chemical Society and Sigma Xi.



Harry Dillow is a Member of the Technical Staff of Bell Laboratories in Norcross, Georgia. His current assignment in the Cable and Wire Department involves the design and development of building entrance cables and central office wire and cable. He received a BSE (Electrical) degree from Johns Hopkins University.



Charles J. Aloisio, Jr. earned a B.S. in Electrical Engineering from Newark College of Engineering and an M.S. and Ph.D in Engineering from the School of Aeronautics, Astronautics and Engineering Sciences at Purdue University.

Currently he is the Technical Supervisor of the Plastics Engineering and Characterization Group for the Bell Laboratories in Atlanta, Georgia. During his 30 year career with Bell Laboratories, he has been investigating the mechanical and electrical characteristics of plastics, and the relationship between processing and the resulting properties of plastics.

He is a member of the Society of Plastics Engineers and the American Physical Society (Division of High Polymer Physics). Dr. Aloisio has also lectured in the Georgia Institute of Technology Graduate Program.

AD P000500

CHARACTERIZATION OF RUGGEDIZED FIBER OPTIC DUAL WAVELENGTH CABLES

P.S. Venkatesan and K. Korbela

General Cable Co., Edison, N.J.

ABSTRACT

This paper summarizes the design, manufacture and evaluation, including cable installation, of dual window (850 nm and 1300 nm) optical fiber cables utilized in the MX missile command control and communication test instrumentation system at Vandenberg Air Force Base. Qualification tests on the finished cables were performed on test equipment especially designed to meet Military Standards DOD 1678. The cables were subjected to impact, tension, compression and low temperature flexibility, while concurrently monitoring optical fiber power levels at 850 and 1300 nm. Temperature cycling, water penetration, water tightness, shock and vibration characteristics of the cables were also obtained. The test equipment employed and the results obtained are discussed herein.

INTRODUCTION

In the early part of 1981, GTE Sylvania Systems Division, as a prime contractor of MX Missile Command, placed an order with General Cable Company to design and manufacture ruggedized, gopher resistant, six fiber dual wavelength optical cables in two kilometers (6560 feet) lengths. The cables were to meet specific optical and mechanical specifications. The optical parameters; attenuation, bandwidth and numerical aperture, were to be measured in accordance with Electronic Industry Association's standard procedure. The mechanical tests; tensile strength, impact, compression and low temperature flexibility, performed on specially designed equipment built to meet DOD 1678, were conducted while monitoring the fiber power levels at 850 nm and 1300 nm wavelengths. Environmental tests designed to characterize the cable for its temperature cycling, water penetration, water tightness, vibration and shock were also performed.

The reasons for the selection of fiber optic cable by the MX Missile Command in lieu of conventional metallic cables are typically because of its following positive attributes.

1. Immunity from electromagnetic and crosstalk interference.

2. No electrical ground loop and short circuit problems.
3. Smaller size and less weight.
4. High strength and greater flexibility.
5. Safe for use in combustible areas because of no electrical arcing and no electrical hazard when cut or damaged.
6. Secure against signal leakage and tapping.
7. Low attenuation and large bandwidth which results in long repeater spacing.

CABLE DESIGN

To meet the stringent environmental and mechanical loading requirements and to provide reliable long term stability, the cable design selected employed tight buffered fibers in silicone gel filled loose tubes. The tubes were stranded around an epoxy glass central member with filling compound in the interstices of the core in order to prevent water entry and flow. The inner jacket was reinforced with Kevlar (R)* which is the cable's strength member. A longitudinally folded corrugated steel tape (coated on both sides for corrosion protection) and an outer polyethylene jacket overall provided gopher protection.

The optical, mechanical and environmental requirements which the cable design had to meet are given in Table I. Figure 1 shows a schematic of the design of the six fiber steel tape armored cable. The customer's specification required two dummy filler tubes to maintain the core geometry of an eight fiber cable fabricated by another subcontractor.

Loose Tube Fiber Fabrication:

The optical fibers used in the fabrication of these cables had a core diameter of 50 μ m (.002 inches), a cladding diameter of 125 μ m (.005 inches), and an overall buffer coated diameter of 500 μ m (.020 inches). The coating was comprised of a dual inner soft and outer hard UV cured urethane acrylate. This dual tight buffer coating over the bare glass fiber, (1) preserved the intrinsic high tensile strength of glass, (2) avoided strength degradation during subsequent cable operation, storage and

* Registered trademark of E.I. DuPont Company.

installation and (3) reduced microbending² losses during cabling. These tight buffer coated fibers were placed in loose buffered tubes. The loose buffering material selected was a hard, smooth and flexible plastic. The oversize cavity of the plastic tube was filled with a moisture resistant thickstropic silicone gel material. Excess fiber length inside the loose tube is controlled to an optimum value.

Stranding:

Six loose tube buffered fibers, along with two dummy filler tubes were stranded around an epoxy fiber glass central member. During stranding a water-proof petroleum jelly was applied to the core. A polypropylene ribbon binder and polyester tape were wrapped over the loose tube core for containment.

The selection of an epoxy glass fiber composite rod as the central member provided three major advantages; (1) dual sharing of tensile loads between the center and perimeter strength members, (2) enhanced antibuckling properties to reduce kinking induced fiber damage and (3) a compatible temperature expansion/contraction coefficient of the center rod and fibers.

Jackets:

A Kevlar reinforced inner polyethylene jacket was used to provide the needed cable strength to withstand the tensions of installation. A corrugated steel tape was applied longitudinally over the jacketed cable. A thermoplastic flooding compound was applied to both sides of the steel tape for corrosion protection. A final jacket of black polyethylene was extruded over the steel tape. The corrugated steel tape design provided cable flexibility in addition to resistance against gopher attack.

OPTICAL CHARACTERIZATION OF CABLED FIBERS

Attenuation:

Fiber attenuation at 850 and 1300 nm was measured using the cut-back method. A block diagram of the set-up is shown in Figure 2. All optical components were mounted on a common optical bench. The output of the tungsten light source passed through a mechanical chopper providing a frequency which eliminated ambient light interference, through the adjustable numerical aperture compound lens system and the appropriate filter. The beam of light was launched into a reference fiber at 0.1 numerical aperture. The reference fiber provided steady state power distribution (equilibrium) conditions at its output. The output was coupled to the fiber under test for maximum input. The power output (P_o) at the end of the test fiber received from the photodiode detector was read at the power meter. The detection technique used the principle of phase lock single beam approach using a lock-in amplifier. Without disturbing the coupling, the fiber under test was cut approximately 2 meters (6.56 feet) from the coupling, (see Figure 2, Point A) and the input power P_i was read

at the output of the short length. The attenuation was determined by:

$$\text{Attenuation (dB/km)} = \frac{10 \log \frac{P_o}{P_i}}{L}$$

where L = length of test fiber in kms.

Bandwidth:

Fiber bandwidth was measured using the frequency domain technique. A schematic of the measurement set-up is shown in Figure 3. A sweep frequency generator was used to modulate CW laser diodes with emission wavelengths of 850 nm and 1300 nm. The output of the laser diode was coupled to the fiber under test. The far-end fiber output was fed to a photodiode detector and to the spectrum analyzer for screen display. A silicon avalanche photodiode detector was used for 850 nm and a germanium avalanche photodiode detector for 1300 nm wavelengths. The bandwidth of the fiber is the frequency at which the electrical power level has decreased by 6 dB from the power level at "zero" frequency.

Numerical Aperture:

The numerical aperture was determined from the measurement of the radiation angle. The radiation angle of the fiber was measured using the output of the far field intensity pattern at 5 percent intensity, (see Figure 4). A two meter length of fiber was used for this measurement. A tungsten light source with optical focusing lens and filters were used to create a monochromatic constant radiance spot larger than the fiber core diameter. The spot was focused on the cleaved end face of the fiber under test. A cladding mode stripper was used at both ends of the fiber. The output end of the fiber was mounted for proper alignment of the end face normal to and coincident with the axis of rotation of the detector. The detector, by means of a motor, was rotated through an arc sufficient to detect the output radiation pattern. A pen recorder was used to record the angular position of the detector and the detected power output with respect to the specimen axis. From this output trace, the angle at which the detector output drops to 5% of its maximum power was noted and sine of this angle gave the numerical aperture. Typical optical data are given in Table II.

MECHANICAL CHARACTERIZATION

Impact:

The purpose of this test was to determine the ability of the cable to withstand impact loads. An apparatus shown in Figures 5 and 6 was built to DOD-1678 specifications. Basically this apparatus permitted 150mm (6 inches) free fall of a specified hammer mass with a cylindrical shaped striking surface 12.5 mm (0.5 inches) radius x 50 mm (2 inches) long onto the clamped fiber optic cable sample. The hardness of the striking

hammer was R₁₀₀. Impacting was affected at 30 cycles per minute by means of a cyclic arm and an electric motor.

Prior to mechanical testing, the cable specimen, approximately 7 meters (23 feet) long was preconditioned for 48 hours at $50 \pm 5\%$ relative humidity and $23 \pm 2^\circ\text{C}$, then removed and clamped in the test apparatus. A 7 meter (23 feet) length of cable was needed to allow for power monitoring. Three of the six fibers in the cable were each connected to 850 nm transmitters and receivers and the remaining three to 1300 nm transmitters and receivers. Initial power level outputs were noted. The cable lengths were then impacted by a 9 kg (19.8 lbs.) hammer at 30 cycles a minute and the power level outputs at 850 and 1300 nm monitored. The change in attenuation of the cable was determined from measured change in power output at the end of the test. The power level as a function of the number of impacts were recorded. Typical graph of power change versus number of impacts are given in Figure 7. The cable easily met the specific requirement of a maximum 0.5 dB change after ten impacts.

As the number of impacts increased, the cable jacket indented and this indentation transferred to the fiber causing microbending which resulted in increased attenuation. The increase in fiber attenuation was a function of the toughness of the cable jacket, number of impacts, weight of the hammer, the drop height and the position of the fiber in the cable. After many impacts, the jacket ruptured and the fiber was subjected to a large amount of compression and ultimate fracture.

Tension:

The tensile test on the fiber optic cable was performed to determine its ability to withstand tensile loading. In addition to the customer's specification, the following parameters were measured:

- Percent of broken fibers versus tension.
- Change in radiant power versus tension.
- Ability of cable strength member to withstand tensile loads.

MX requirements called for a maximum power level change of 0.2 dB under 272 Kgms (600 lbs.) load.

A 9090 Kgms (20,000 lbs.) Instron tensile testing machine was used. Circular mandrel grips with a minimum diameter of 25 cms (10 inches), shown in Figures 8 and 9 were specially designed to grip the cables. Prior to testing, the cable specimen, 30 meters (98.4 feet) in length, required for connectorizing to monitors and wrapping over mandrel grips was preconditioned for 48 hours at $50 \pm 5\%$ relative humidity and $23 \pm 2^\circ\text{C}$. The cable was removed from the conditioning chamber and wrapped 5 times around the mandrel grips and clamped. A center to center distance between mandrels of 45 cms (18 inches) was used. An extensometer with a gauge length of 25 cms (10 inches) was attached to the sample. Three

fibers in the six fiber cable were each connected to the 850 nm transmitter and receiver units. The remaining three were connected to the 1300 nm units. The fiber power level outputs under zero load were noted. The cable was loaded at a crosshead speed of 1.25 cms (0.5 inches) per minute to various values and the power level output recorded. The load was removed and the recovered power level output recorded. This procedure was repeated until fibers or cable failed. The power level output versus tension was used to determine the cable attenuation change under tensile load.

Variation of fiber power level output versus tensile load and its recovery on release of load is shown in Figure 10. It can be observed that there is practically no change in power level output up to a load of 363 Kgms (800 lbs.). This behavior indicates that there is no microbending of fiber up to this stress level. Above this, the cable jacket material begins to deform transversely causing microbending of the fiber resulting in power level drop. The recovery of the power level when the load is released is a function of the resiliency of the jacketing material. On further increase of the load, the Kevlar strands break. After the break of the Kevlar strands, the plastic jacket elongates until fiber failure and loss of power.

Compression:

A 15 meter (49 feet) length of cable sample was conditioned at $23 \pm 2^\circ\text{C}$ and $50 \pm 5\%$ relative humidity for 48 hours. At the end of the conditioning period it was removed and mounted between two steel compression plates 10 cms (4") long by 5 cms (2") wide, which were placed in an Instron testing machine so that the cable sample was subjected to 10 cms (4") compression, (see Figure 11). The mounting of the cable was such that there was no lateral motion of the cable in the fixture. Three of the six fibers of the cable were each connected to the 850 nm power level monitoring system and the remaining three to the 1300 nm system. The transmitted optical power outputs were measured under no load. The cable was then subjected to various compression loads at a crosshead displacement rate of 0.125 cms (0.05 inches) per minute. The transmitted power level was measured and the cable was then unloaded. This procedure was repeated for incremental loads until fiber failure.

A plot of fiber power level output versus compression load and the power level recovery on release of compression load is shown in Figure 12. It should be noted that the cable met the MX specifications of less than 0.5 dB power level change under 181 Kgms (400 lbs.) of load. It is to be observed that up to about 363 Kgms (800 lbs.) the fiber is well insulated from the load by the cable components. Beyond this load, the cable jacket deforms and the load is transmitted to the fiber causing its deformation and consequently microbending and optical transmission loss. Even when the compression load increased to 4545 Kgms (10,000 lbs.) the recovered power level showed only a 3 dB loss which confirms the ruggedness of the cable.

Low Temperature Flexibility:

This test was used to determine the ability of a fiber optic cable to withstand bending at the specified temperature.

A 15 meter (49 feet) long cable sample was conditioned for 48 hours at $23 \pm 2^\circ\text{C}$ and $50 \pm 5\%$ relative humidity and attached to the low temperature flexibility apparatus shown in Figure 13. A 17.5 kg (38.5 lbs.) mass was attached to each end of the cable. Three of the six fibers were each attached to a 850 nm optical power level monitoring system and the remaining three attached to a 1300 nm wavelength monitoring system and the transmitted power measured. The chamber was cooled to the specified temperature of 0°C for 20 hours. The cable, while in the cold chamber, was then wrapped two turns over a 15 cms (6") diameter mandrel (ten times cable diameter) at a rate of two turns per minute. The cable sample, still wrapped on the mandrel, was allowed to return to room temperature, and the cable jacket examined for splitting or cracking at 10X magnification. Within one hour after reaching room temperature the cable specimen was straightened and the transmitted power through the six fibers at 850 nm and 1300 nm wavelengths measured. Results are shown in Table III.

ENVIRONMENTAL CHARACTERIZATION

Temperature Cycling:

This test was performed to determine the effect of temperature cycling on cable attenuation. The temperature cycling effect is defined as the difference in fiber attenuation (dB/km) before and after temperature cycling.

Fiber attenuation was measured at 850 and 1300 nm at 20°C . The cables were temperature cycled for a total of 10 cycles in a Tenney environmental chamber. One cycle consisted of $+20^\circ\text{C}$ to -40°C to $+60^\circ\text{C}$ to $+20^\circ\text{C}$. (Figure 14). The holding time at the temperature extremes was 8 hours and the time for temperature change from one extreme to the other was 4 hours. At the end of ten cycles, the attenuation was measured at both wavelengths at 20°C . The cables were visually examined for any splitting or cracking of jacket or fiber buffering. Results are reported in Table IV. MX requirements are not more than 0.5 dB/km change after temperature cycling for 10 cycles.

Water Penetration:

A two meter (6.56 feet) specimen of the finished cable was subjected to a water penetration test as follows: A water tight enclosure was applied to one end of the cable with the closure end placed under a three feet head of water. (A schematic of the test apparatus is shown in Figure 15). A small amount of Zyglo colorant was added to the water. The cable sample was supported horizontally with the other end open to atmospheric pressure. After subjecting the cable sample to the hydrostatic pressure head for 24 hours, it was examined for evidence of water incursion.

Water Tightness:

A two meter (6.56 feet) section of a cable was subjected to a hydrostatic pressure head of 3.05 meters (ten feet) of water (colored red by adding a small quantity of Zyglo) with both the cable ends open to atmosphere for a period of 24 hours. At the end of the test period, the cable was cut open and examined for evidence (red coloration) of water incursion. A schematic of the test apparatus is shown in Figure 16. This test was performed to determine if there were any flaws or pinholes in the cable jacket.

Shock:

The shock test was designed to test the cable and the cable reel for dynamic shock stress produced by the environment expected in handling, transportation and service use.

A reeled cable was dropped (free fall) 3 times from a height of 45 cms (18 inches) onto a 5 cms (two inch) plywood surface backed by concrete. The drops were made with the reel flanges in different positions with the horizontal plane, namely, normal, parallel and at 45 degrees. Attenuation at 850 nm and 1300 nm were measured before the drops and after completion of test. The cable reel was examined for any damage. Results are reported in Table V.

It is observed that the attenuation value generally decreased after shock. We believe this decrease is associated with the stress relaxation of the optical fiber in the tube and a probable redistribution of fiber oscillations inside the tube.

Vibration:

The vibration test was performed to determine if the cable could withstand dynamic vibrational stresses and to insure that performance degradations or malfunctions would not result from the service vibration environment.

The attenuation of optical fibers in a reeled cable was measured at 850 and 1300 nm prior to subjecting the cable to the vibration tests. The reel was wrapped with 24 gauge sheet metal and banded with metal bands. It was then secured on the vibration table and tested as per MIL-STD-810C, Method 514, Procedure X, Curve A_x for equipment transported as secured cargo except that low frequency displacement was maintained at 0.80 inches. (Figure 17). The reel was vibrated for 84 minutes in each of the three mutually perpendicular axes. The reel was cycled seven times from 5 - 200 - 5 Hz in twelve minute cycles at an approximate rate of 1 octave per minute. Attenuation of the optical fibers was measured at the end of the test. Results are shown in Table VI. Figure 18 shows the vibration test axes and cable reel fastened to the vibration table (x-x axis).

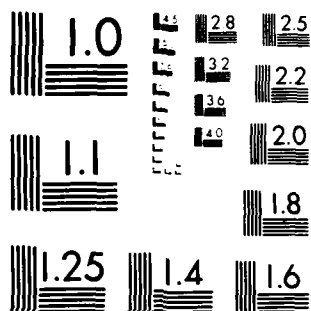
Although the attenuation did not decrease as in the shock test, the results are approximately similar to the shock data and it can be assumed that the

UNCLASSIFIED

NOV 82

5/6

NL



MICROCOPY RESOLUTION TEST CHART
NATIONAL BUREAU OF STANDARDS 1963-A

mechanism described in the shock test is operational here also.

INSTALLATION

The cables were installed by direct burial. Six optical fiber cables were simultaneously buried at a depth of 1.2 meters (48 inches) using conventional plowing equipment. Prior to installation, cables were checked for continuity and their attenuation measured using an OTDR. One cable reel was placed on the plowing rig. The remaining five cables were laid on the ground along the installation route by simultaneous pay-off from a 12 meter (40 feet) flat bed trailer.

The five cables which had been placed on the ground and the cable on the plowing rig were passed over cable guides and threaded through the plowing chute. The rate of plowing averaged approximately 20 meters (66 feet) per minute. Approximately two sections, each 2 kilometers (6560 feet) long, were installed in a day or a total of 24 kilometers (15 miles) of cable.

Excess lengths of cable were accumulated at each splicing location. Individual fibers were spliced by means of electric arc fusion welding and housed in a 15 cms (six inch) diameter splice case. A fiber organizer, designed by GTE Sylvania, for orderly handling and placement of fiber during and after splicing was contained in the splice case. Also, provisions in the splice case had been made to tie off the strength member. To prevent any moisture ingress into splice case, the internal cavity was filled with a re-enterable encapsulating compound.

No problems were encountered and a successful installation at a steady rate of plowing was accomplished. It can be safely stated that even though an additional number of cables were installed together, the fiber optic cable design for the rugged requirements of direct burial permitted safe installation by means of conventional plowing techniques and equipment.

ANALYSIS AND CONCLUSIONS

We have successfully fabricated ruggedized dual wavelength fiber optic cables in two kilometer (6560 feet) lengths and characterized their mechanical and environmental behavior at 850 and 1300 nm wavelengths on test equipment designed to meet DOD 1678 specifications. Power level output that was obtained at 850 nm versus those at 1300 nm did not show any significant differences which indicated that it might not be necessary to characterize the cable at 1300 nm in addition to 850 nm for its mechanical and environmental performance. During impact testing we observed that the fiber power level output was a function of the position of the fiber in the cable. The fiber that was in the direct line of impact underwent the most attenuation, whereas, the one that was positioned at 90 degrees to it the least attenuation. Certain fibers were in direct line of loading compared to others and their power level output showed the

most attenuation. Therefore, results presented in this paper are the maximum change in power level output of the fiber in the cable. The cables were found to easily meet the MX specifications.

ACKNOWLEDGMENT

The authors acknowledge the help of and useful discussions with various personnel in the GTE Sylvania Systems Division.

REFERENCES

1. "Military Standard Fiber Optic Test Methods and Instrumentation", published by Naval Air Engineering Center, Lakehurst, New Jersey.
2. D. Gloge, Bell System Technical Journal, Vol. 54, 243 (1975).

TABLE IA
MX CABLE SPECIFICATIONS

<u>Fiber Count</u>	<u>Maximum Attenuation dB/km</u>		<u>Minimum Bandwidth MHz-km</u>		<u>Cable O.D.</u>	<u>Max. Weight</u>
	<u>850 nm</u>	<u>1300 nm</u>	<u>850 nm</u>	<u>1300 nm</u>	<u>Inches (Max.)</u>	<u>LBS./km</u>
6	3.5	2.0	400	400	0.75	660

TABLE IB
MX CABLE - MECHANICAL SPECIFICATIONS

<u>Designation</u>	<u>Minimum Number of Test Samples</u>	<u>Test Procedure</u>	<u>Specifications</u>
Tensile Loading	4	DOD 1678	600 lbs. with \leq 0.2 dB change in power level output.
Compressive Strength	4	DOD 1678	400 lbs. with \leq 0.5 dB change in power level output.
Impact	4	DOD 1678	9 kg dropped 10 times from 15 cm height with \leq 0.5 dB change in power level output.
Low Temperature Flexibility	4	DOD 1678	2 turns over 6 inch diameter at 0°C with \leq 0.5 dB change in power level output.

TABLE IC
MX CABLE - ENVIRONMENTAL SPECIFICATIONS

<u>Designation</u>	<u>Minimum Number of Samples</u>	<u>Test Procedure</u>	<u>Specifications</u>
Temperature Cycling	4	10 cycles of +20, -40, +60, +20°C	\leq 0.5 dB/km attenuation change before and after cycling.
Water Penetration	4	2 meter sample subjected to 3' water pressure head.	No water penetration in 24 hours.
Water Tightness	4	Surface of 2 meter section of cable subjected to 10 feet water pressure head.	No water incursion in 24 hours.
Shock	2	MIL STD. 810, Method 510, Procedure II.	\leq 0.5 dB/km change before and after drops.
Vibration	2	MIL STD. 810C, Method 514, Procedure X, Curve AX.	\leq 0.5 dB/km change before and after vibration.

TABLE II

TYPICAL OPTICAL FIBER DATA OF MX CABLE

Fiber No.	Color	Attenuation dB/km		Bandwidth MHz-km		Numerical Aperture
		@ 850 nm	1300 nm	@ 850 nm	1300 nm	
1	Red	2.87	1.14	936	624	0.18
2	Orange	2.50	1.01	554	867	0.19
3	Yellow	2.47	1.26	1213	640	0.20
4	Green	2.50	1.00	815	728	0.20
5	Blue	2.45	0.97	763	1180	0.20
6	Violet	2.77	1.06	485	954	0.20

TABLE III

LOW TEMPERATURE FLEXIBILITY TEST RESULTS

Specimen No.	Temp.	Weight	Power Level before Winding	Power Level after Winding	No. of Turns	dB Change	Power Level After Return to 21°C Wound	Straight	Remarks
1	0°C	17.5 kg	1.245	1.245	2	0	1.212	1.210	Mandrel dia.=6". Sample conditioned 24 hrs. at 0°C before winding over mandrel two turns. No. splitting or cracking of cable insulation visible at 10X magnification.
2	0°C	17.5 kg	1.454	1.454	2	0	1.446	1.445	
3	0°C	17.5 kg	1.735	1.734	2	0	1.730	1.730	
4	0°C	17.5 kg	1.202	1.199	2	0	1.208	1.206	
5	0°C	17.5 kg	2.212	2.209	2	0	2.283	2.282	
6	0°C	17.5 kg	3.681	3.679	2	0	3.595	3.597	

Requirement: Maximum 0.5 dB change at 0°C after winding.

TABLE IV

MX CABLE - TEMPERATURE CYCLING RESULTS

Fiber No.	Color	No. of Cycles	Attenuation dB/km before Cycling		Attenuation dB/km after Cycling		Change in Attenuation	
			850 nm	1300 nm	850 nm	1300 nm	850 nm	1300 nm
1	Red	10	3.2	1.4	3.2	1.8	0	+0.4
2	Orange	10	2.7	1.7	2.6	1.8	-0.1	+0.1
3	Yellow	10	2.7	1.4	2.4	1.4	-0.3	0
4	Green	10	2.8	1.8	2.6	1.9	-0.2	+0.1
5	Blue	10	2.7	1.1	2.6	1.3	-0.1	+0.2
6	Violet	10	2.7	1.2	2.5	1.4	-0.2	+0.2

TABLE V
MX CABLE - SHOCK TEST RESULTS

Sample	Drop Distance	No. of Drops	Attenuation (dB/km) Before Shock		Attenuation (dB/km) After Shock		Change in Attenuation	
			850 nm	1300 nm	850 nm	1300 nm	850 nm	1300 nm
1 km reel	18"	3	2.79	1.73	2.68	1.48	-0.11	-0.25
			3.00	1.49	2.79	1.17	-0.21	-0.32
			2.71	1.76	2.58	1.32	-0.13	-0.44
			2.69	1.76	2.70	1.27	0.01	-0.49
			2.89	1.81	2.84	1.52	-0.05	-0.29
			2.64	1.98	2.56	1.51	-0.08	-0.37
2 km reel	18"	3	3.24	1.80	3.17	1.43	-0.07	-0.37
			2.61	1.80	2.70	1.71	0.09	-0.09
			2.40	1.46	2.49	1.29	0.09	-0.17
			2.57	1.90	2.68	1.80	0.11	-0.10
			2.57	1.30	2.63	1.07	0.06	-0.23
			2.49	1.38	2.48	1.18	0.01	-0.20

TABLE VI
MX CABLE - VIBRATION TEST RESULTS

Cable	Attenuation (dB/km) Before Vibration		Attenuation (dB/km) After Vibration		Change in Attenuation	
	850 nm	1300 nm	850 nm	1300 nm	850 nm	1300 nm
1 km reel	2.87	1.14	2.78	1.13	-0.09	-0.01
	2.50	1.01	2.62	1.20	0.12	0.19
	2.47	1.26	2.51	1.30	0.04	0.04
	2.50	1.00	2.49	1.02	-0.01	0.02
	2.45	0.97	2.46	1.01	0.01	0.04
	2.77	1.06	2.83	1.14	0.06	0.08
2 km reel	2.33	1.18	2.70	1.46	0.38	0.28
	2.77	1.11	2.62	1.14	0.15	0.03
	3.00	1.14	2.98	1.50	-0.02	0.36
	2.68	1.14	2.62	1.03	-0.06	-0.11
	2.59	0.99	3.09	1.33	0.50	0.34
	2.64	1.50	2.70	1.46	0.06	-0.04

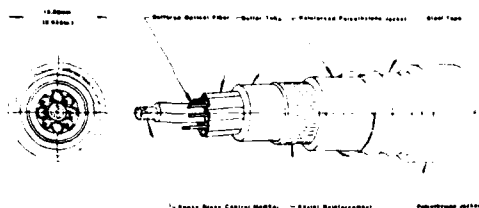


FIGURE 1

Schematic of the Design of 6 Fiber Armored MX Cable.

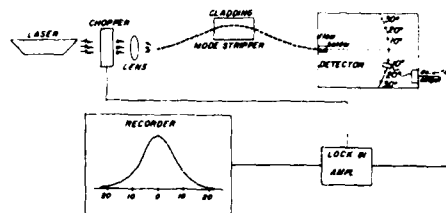


FIGURE 4

A Schematic Instrumental Set-Up to Measure Fiber Numerical Aperture.

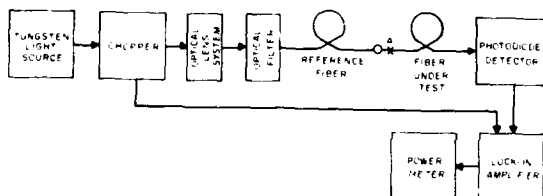


FIGURE 2

A Block Diagram of Set-Up for Fiber Attenuation Measurement.



FIGURE 5

Photograph of Impact Testing Apparatus

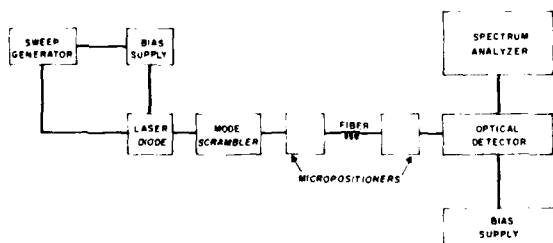


FIGURE 3

Block Diagram of Set-Up for Bandwidth Measurements by Frequency Domain Technique.

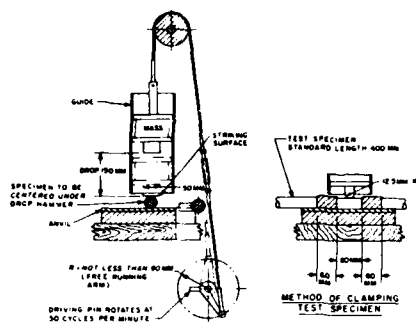


FIGURE 6

A Schematic of Impact Testing Apparatus

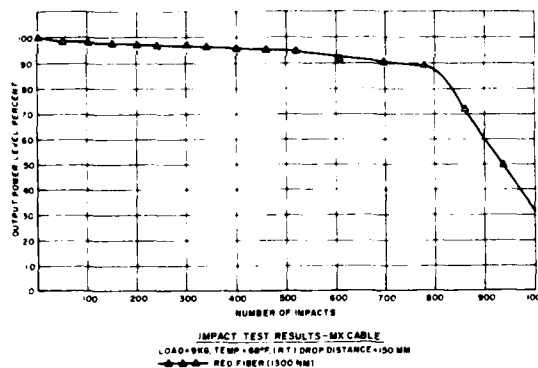


FIGURE 7

Typical Impact Characteristics of 6 Fiber MX Cable.

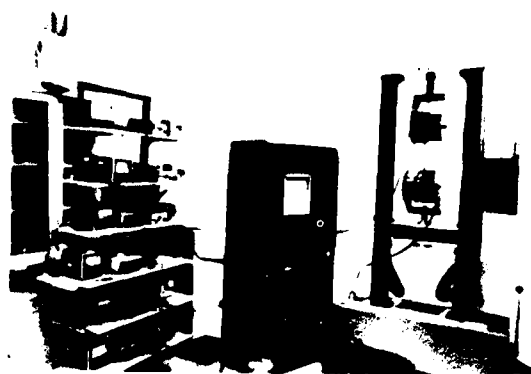


FIGURE 8

Photograph of Tensile Testing of an MX Cable with Fiber Connected to 850 and 1300 nm Power Level Monitors.

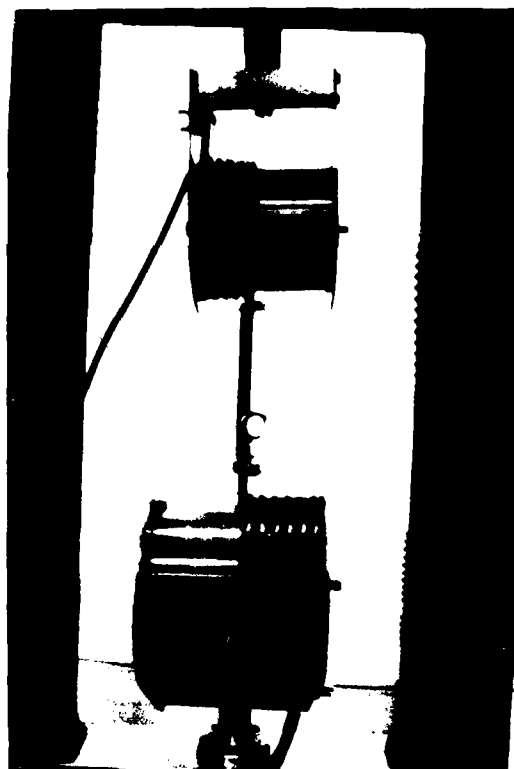


FIGURE 9

A Close Up View of Mandrel and Cable Grips.

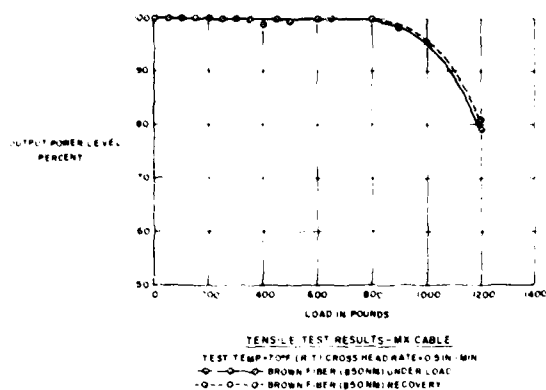


FIGURE 10

Typical Tensile Test Results on 6 Fiber MX Cable.

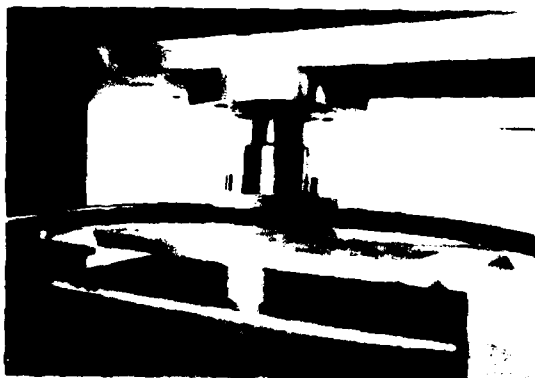


FIGURE 11

Photograph of Compression Test on MX Cable.

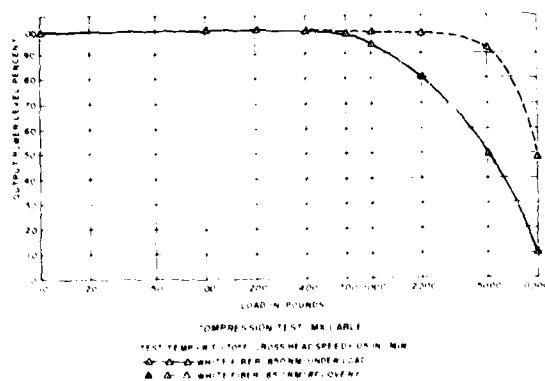


FIGURE 12

Typical Compression Test Results on 6 Fiber MX Cable.

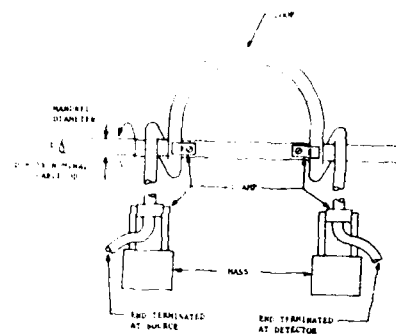


FIGURE 13

A Schematic of Low Temperature Flexibility Test fixture per DOD 1678.

ENVIRONMENTAL TEMPERATURE TEST CYCLES (2)

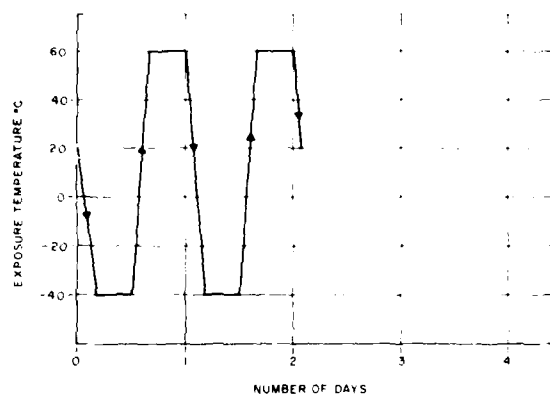


FIGURE 14

Environmental Temperature Test Cycle.

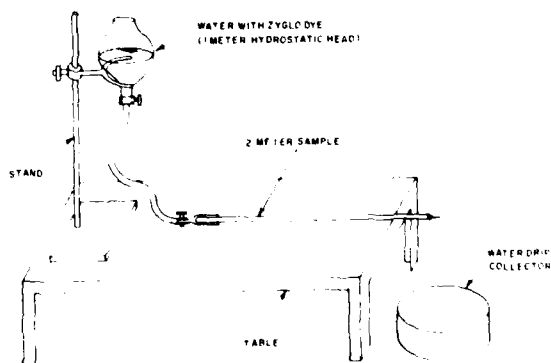


FIGURE 15

A Schematic of Water Penetration Test Apparatus.

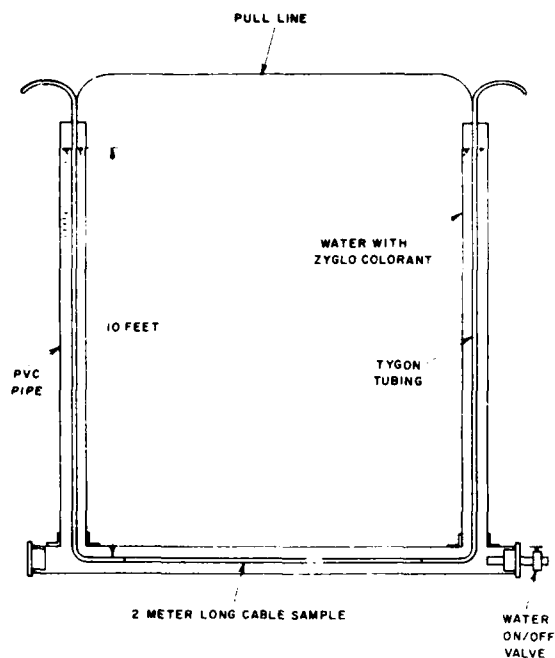


FIGURE 16
A Schematic of Water Tightness Test Apparatus

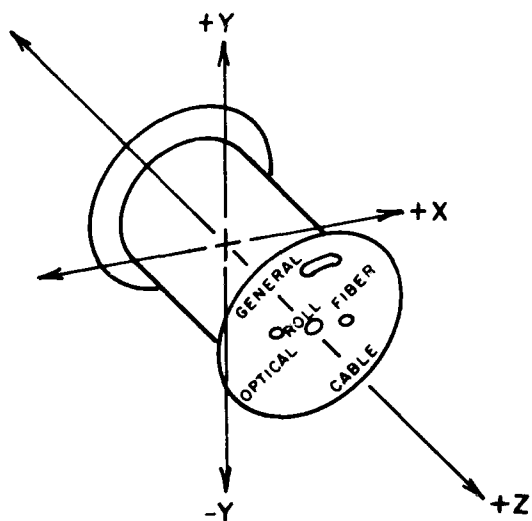


FIGURE 18A
Diagram of Vibration Test Axes.

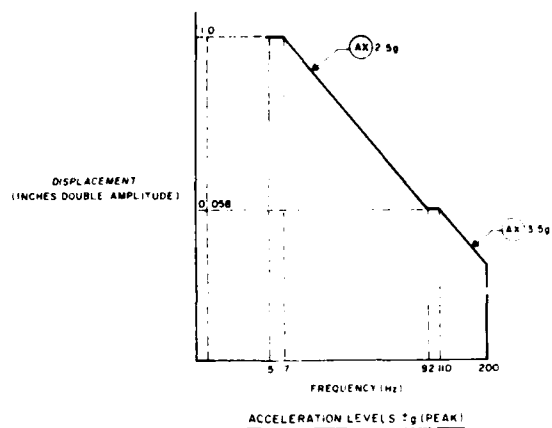


FIGURE 17
Displacement Versus Frequency Curve for Vibration Test



FIGURE 18B
A Photograph of Cable Vibration Test Set-up.



Perry Venkatesan joined General Cable Company in 1977. He is currently a Research Staff Specialist in the Fiber Optics Division. Dr. Venkatesan has been involved in optical, mechanical and environmental characterization of fiber optic cables of varied designs. His previous work included optical fiber preform fabrication and fiber drawing. Before joining General Cable he worked at Western Electric Research Center in Fiber Optics Division and Metal Forming Division at Princeton, New Jersey.

EDUCATION:

PhD in Metallurgy from Columbia University in the City of New York.



Mr. Kenneth Korbelak has been with General Cable for eight years and is currently a field engineer. He was responsible for the fusion splicing of the Kennedy Space Center fiber optic cable installation in 1977 and received a citation award for fusion welding from NASA. He also was involved in the design and fabrication of the environmental chamber permitting fusion splicing in manholes. He holds several patents, including a patent for the fiber organizer. He is presently pursuing a degree in Electrical Engineering from Middlesex College (N.J.).

A REFINED TIGHT DESIGN DUCT CABLE FOR LOW LOSS MONOMODE FIBRE

*P.G. Hale,[†]D. Delme Jones,*M.M. Ramsay,[†]J.N. Russell,*J.G. Titchmarsh,[†]R.C. Townsend

* Standard Telecommunication Laboratories Limited, Harlow, Essex.

[†] Standard Telephones & Cables, Headquarters, 190, The Strand, London.SUMMARY

This paper discusses design, manufacturing and installation experience with a simple tight design cable for use in ducts. The small outside diameter and low weight, of 7.5 mm and 60 kg/km respectively, allow it to be manufactured and installed in lengths in excess of 2 km and the design, including fibre axial compression optimised through optical strain measurements, provides large safety margins against fibre failure under tensile loading. Both multimode and monomode cables have been cabled with zero incremental loss. Under contract with British Telecom a total of 15.6 km of monomode cables were produced. Laboratory operation over 62.4 km at 320 Mb/s was demonstrated and they were installed and spliced to give mean attenuations of 0.49 and 0.33 dB/km at 1.3 and 1.55 μ m wavelengths respectively.

INTRODUCTION

Over the last decade STL, and more recently its parent company STC plc, have been involved in the development of a range of optical fibre cables. One of the main cable types was designed for duct installation in PTT applications. The philosophy in designing this cable has been to utilise the small size of the transmission medium to allow the cable itself to be kept small in size with associated benefits of ease in handling both during manufacture and installation. It is the aim of this paper to demonstrate that with this approach we have been able to maintain the high initial performance of the fibre through the production stages and installation. The key features are described with reference to both monomode and multimode fibres and it is shown that this simple cable design formed an excellent vehicle for development in a recent experimental monomode system.

FIBRE PACKAGING

The fibre is packaged in two tightly filled layers of silicone rubber and nylon 12 as shown in Fig. 1.

The silicone primary coating is applied on-line with fibre pulling and provides immediate protection against surface damage and a soft buffer layer which forms one element of the protection against microbending. The nylon secondary coating is

applied in a separate extrusion process and provides the higher modulus element of the protection against radial and axial forces during cabling. An analysis of the effectiveness of this hard/soft coating combination in buffering the fibre against externally applied radial forces has been reported by a number of authors, and they show¹ that our empirically determined coating thicknesses are not far from an optimum. Both fibre types use a fibre o.d. of 125 μ m and silicone thickness of about 50 μ m. The multimode fibre has a nylon o.d. of 1.0 mm and the monomode 0.85 μ m.

One feature of nylon which makes it particularly suitable for tight extrusion coating of fibres is its low melting viscosity which minimises shear forces on the fibre and minimises sensitivity to tooling detail. X-ray analysis has shown no signs of orientation in this coating² but other parameters have been found to be sensitive to the conditions used to cool the extrusion coating and some of these are shown in Table 1.

Incremental losses at room temperature due to the coating process are low, but temperature testing shows the increments at -40°C to increase with the speed at which the nylon was cooled after extrusion. A further parameter which changes is the axial compression³ which the coating produces in the fibre. Fig. 2 shows the way in which this changes as the water cooling trough is moved down the extrusion line.

Air cooling, which we have found to give the better low temperature performance is thus also giving higher axial compression. This experience is apparently at variance with the generally accepted theory that low temperature incremental losses are due to collapse of the fibre into helical bends under axial compressive strains induced by coating shrinkage.⁴ We believe that while this is true the better adhesion which we see and the minimising of voids between primary and secondary coatings⁵ gives an improved package stability which more than outweighs the higher compression.

CABLE DESIGN AND MANUFACTURE

The cable designs for both monomode and multimode are almost identical, differing only slightly in size because of the different nylon coating diameters. A configuration used for a monomode cable is shown in Fig. 3.

A total of ten packaged fibres, and fillers as required, are helically stranded around a central strength member of deformed steel strand coated with nylon. The steel has an o.d. of 1.83 mm and a stranding lay length of 150 mm is used. The strands are held in place by a PETP tape wrap. The cable is completed by the application of an APL (aluminium plastic laminate) longitudinally wrapped tape and a low density polyethylene extruded sheath. In addition to the philosophy referred to in the introduction of producing a size of cable commensurate with the fibre, we have also favoured the "tight" approach where the various components are in close contact ensuring that they maintain their correct relative positions through a range of static and dynamic load conditions. In such a structure there are obvious dangers of producing high local contact stresses and microbending losses. The fibre packaging is, as already discussed, designed to minimise these, but it has also been found important to minimise radial pressures within the cable structure. Both fibre stranding pay-off tensions and the PETP wrapping tension are controlled at 1 N and the sheath is applied by a tubing technique. The APL tape, whose primary purpose is to provide a water barrier also forms a tubular barrier against radial forces during and after sheath extrusion.

OPTICAL PERFORMANCE

Monomode

Using the techniques discussed above about 24 km of cable, each incorporating 4 monomode fibres, were produced under a contract with BREL (British Telecom Research Laboratories).⁶ Fig. 4 shows the spectral loss changes during cable processing. At longer wavelengths where the evanescent fields in the cladding are becoming more significant a bend edge can be seen. This is most prominent at the secondary coating stage where the fibre is wound in multiple layers on small diameter reels, but is almost completely absent under the more controlled bend conditions of the cable. Moreover at the designed operating wavelengths of 1.3 and 1.55 μm incremental losses are extremely low and well controlled as can be seen in Table 2.

Multimode

When operating away from mode cut-off wavelengths a properly designed monomode fibre is relatively insensitive to microbending losses, but in a multimode fibre under equilibrium conditions there are always modes close to cut-off and it is consequently more difficult to control incremental losses during cabling. Table 3 shows the losses achieved at the various stages in cabling ten multimode fibres.

CABLE STRENGTH

The cable is designed to have sufficient strength to protect the fibre during the most severe lead/time envelope, which may be experienced during installation. The designed peak installation load is 1200 N that is the weight of 2 km of cable

The steel strength member ensures a cable elongation of $\sim 0.25\%$ at this load which should be compared to the 0.6% strain proof-test applied to the packaged fibre. Even with this safety margin, under the more pessimistic assumption of static fatigue fibre failure is possible, but the probability is very low and this is borne out by the installation results. A further margin of safety is also provided by the compressive strain induced by the nylon coating as described earlier in the paper.

INSTALLATION

It is of particular interest that the installation programme has been carried out in very diverse weather conditions. Temperatures have been as low as -20° centigrade and as high as $+20^\circ$ centigrade and cable drum lengths ranging from 1 to 2.7 km have been used.

Multimode Cable

Early in 1980 the first multimode optical cables were drawn into ducts between Croydon and Vauxhall in the south of London. These and subsequent routes are shown in Table 4.

On the first optical cables to be pulled a duct, a winch was used for some of the section which recorded the pulling tension on the draw rope and limited the pull on the rope to a pre-defined figure. This method was discontinued after the first few pulls for a more conventional method of using a capstan winch but the method provided some useful data for planning subsequent installations.

The pulling tension on the cable depends on the length and occupancy of the duct and on these early routes the occupancy varied from zero to a maximum of 50%. In the empty ducts cable pulls were relatively simple and pulling tensions were understandably low. Although the cable was designed for a maximum pulling tension of 1200 N, the pull on the rope was limited to 1000 N.

As a capstan winch is more commonly used for cable installation, after the first few lengths were drawn into duct by the variable tension winch, a standard capstan with polypropylene draw rope with a stretch factor of 15% was used. Although the variable tension winch limited the pull on the draw rope, it is the pull on the cable itself which needs to be protected and a mechanical fuse (see attached figure) was developed with a breaking strength that can be adjusted by selection of a shear pin. This fuse was set to 1000 N and proved extremely effective and reliable. The shear pin was renewed for each pull.

A small swivel specially designed with a thrust ball race was used throughout the cable pulling operations with the optical cable threaded through the eye of the swivel, looped back over a length of 1 metre and lashed tightly throughout its length. This method of anchoring the cable proved very effective and was not modified throughout these

operations. The design of this type of cable ensures that pulling tensions are transferred from the outer sheath to the other constituent parts of the cable over about 4 metres of cable.

When pulling long lengths of cable into duct with a high occupancy factor some of the cable was pulled by hand. Where ducts were not in line at a man-hole turning wheels were used if necessary and when a cable pull became too difficult or tensions were likely to exceed 1000 N the cable was flected alongside the manhole in a figure of eight. The cable would then be fed into the next duct section as necessary.

Throughout the cable installation programmes all the pulling techniques described above were used and all the known hazards in cable installation experienced and successfully overcome.

Monomode Cable

During 1982 15 km of monomode cable was installed between the research establishment of British Telecom and Ipswich utilising the installation methods described above, that had been so successful with the multimode fibre cable.

In all 10 drums of cable were installed between the 2 terminals, 9 of them in duct and 1 within the precincts of the research establishment. The average length of cable installed was rather greater than in previous installations, the longest length being 2.7 km. Also duct occupancy, which had been no more than 50% in previous routes, was as high as 85% on this route. Because of this the cable had to be manhandled rather more than previously.

As on previous routes a mechanical fuse set at 1000 N was used to protect the cable.

Splice losses are of particular concern in monomode systems and extensive trials were carried out on these cables before installation. In all some 200 splices were made with an average splice loss at 1.3 μm of 0.11 db and 0.08 db at 1.55 μm .⁷ When these cables were spliced in the field slightly but not significantly lower losses were found.

Conclusion

It can be seen from the above that in a relatively short period of time confidence in installing optical cables has progressed markedly. The average length of cable pulled into duct has increased and fibre splicing and jointing has become a routine matter. More importantly, it has been demonstrated that monomode cable of this design can be pulled into duct, spliced and jointed by installation personnel. Although it must be recognised during training that splicing operators need to be very patient with a natural aptitude for the manipulating skills required for this type of operation, such operatives are not uncommon.

MONOMODE SYSTEM TRIALS

Several system experiments have been performed using these cables. First, before installation, all the cabled fibres were spliced together in the laboratory and transmission at 1.3 μm with a modulation rate of 320 Mb/sec was established through the full 62.4 km. In this experiment a bit error rate of less than 1 in 10^9 was found with a signal margin of several db. After installation and field splicing, workers at BTRL reported⁸ 565 Mb/sec. operation at 1.3 μm over the same length with a margin of 1 db for the same bit error rate. Finally the fibres were spliced to a further 31.5 km of cabled fibre that had been installed earlier and operation at 1.52 μm at a modulation rate of 155 Mb/sec. was demonstrated over the total length.

CONCLUSION

This paper has presented design, manufacture and installation experience on a tight cable design for a duct environment. This simple, low weight cable is capable of maintaining the integrity of high grade multimode and monomode fibre to allow their use in commercial systems.

REFERENCES

- 1 D. Gloge, Bell Syst. Tech. Jour., 54, 243, (1975)
- 2 S.R. Barnes, P.C. Hale, J.N. Russell and S.V. Wolfe, Sect. 15-1, Proc. Plastics in Telecommunication III, London, Sept. 1982
- 3 R. Kashyap, M.H. Reeve, S. Hornung, J.N. Russell and J.G. Titchmarsh, Proc. of 3rd Int. Conf. on Optics and Optical Fiber Comm., San Francisco, April 1981
- 4 T. Yashiro and M. Takeshima; ACS Organic Coatings and Plastics Chemistry, 40, 87 (1979)
- 5 M. Rokunohe, T. Shintani, M. Yajima and A. Utsumi; Comm. VI-4 Proc. 2nd ECOC, Paris, Sept. 1976
- 6 J. Irven, G.J. Cannell and J.G. Titchmarsh; Comm. AVII-6, Proc. 8th ECOC, Cannes, Sept. 1982
- 7 J.S. Leach, G.J. Cannell, A.J. Robertson and P. Gurton; Elec. Lett., 18, 697 (1982)
- 8 I.W. Stanley, R.C. Hooper and D.W. Smith, Comm. AXIV-1, 8th ECOC, Cannes, Sept. 1982

AUTHORS

Dr. P. G. Hale graduated with an honours degree in Engineering Science and Economics from the University of Oxford in 1973. After a short period with Instron Limited he returned to the University of Oxford where he gained a D.Phil. on the subject of the metal coating of optical fibres in 1979. He joined STL in 1980 as a Research Fellow in the Optical Fibre Cable Group.

David Delme Jones obtained an HNC from Watford before joining the Medical Research Council. He is a Member of the British Computer Society and of the British Institute of Management. In 1963 he joined Hawker Siddeley Dynamics as a System Analyst, later transferring to STC's Data Systems Division. After a period at Tech. HQ he became Manager of the optical fibre cable manufacturing department.

Murray M. Ramsay obtained a B.Sc. from University College, London in 1952. He is a Fellow of the Institute of Physics. He joined STL in 1962 and was a founder member of the team set up in 1966 to study optical communication systems. He acted as consultant to EOPD Roanoke when in 1973 work on optical fibre communication was started there. He later returned to STL and is currently Chief Research Engineer for optical fibre cables.

John N. Russell graduated with an honours degree in Applied Physics from University College, London in 1970; since then he has worked for Standard Telephones and Cables plc. where he has been engaged in development of optical fibre cables.

Jim G. Titchmarsh obtained a B.Sc. in Physics from Bristol University in 1964 and an M.Sc. in Solid State Electronics from Manchester University in 1966. He then joined STL to work on thin film deposition techniques. After a period working on plasma panel displays he started work in the optical fibre area and is currently Head of the Optical Cable Technology department.

Ronald C. Townsend obtained a B.Sc.(Eng) from London University in 1947. He then joined STC's Transmission Engineering Department where he worked on the development of open wire and coaxial cable systems. From 1949-52 he managed an STC project in Syria and later returned to Transmission System Planning. After a time in Export Marketing he was appointed Installation Manager in 1977 and is currently responsible for the installation of all digital, analogue and optical cable systems.

TABLE 1 Effect of Cooling Regime On Fibre Package Parameters

COOLING REGIME	INCREMENTAL LOSS dB/km		NYLON DENSITY Kg/m ³	NYLON YOUNG'S MODULUS GN/m ²
	-40°C	+70°C		
AIR COOL	0.0	0.25	1015.6	0.96
HOT(80°C) WATER QUENCH	20	0.2	1010.2	0.85
COLD WATER QUENCH	36	0.25	1003.9	0.74

TABLE 2 Summary of Fibre/Cable Parameters

	No. in sample	Attenuation dB/km	
		1.3 μ m	1.55 μ m
Primary fibres	55	0.44	0.27
Total length 267 km		0.04	0.055
Cabled fibres	56	0.43	0.28
Total length 97 km (14 x 4 fibre cables. 24.3 km)		0.04	0.08
Incremental loss	52	-0.007	+0.028
	32	Core diam 8.7 μ m.	Δn 5.05 x 10 ⁻³
	36	n 0.33	n 0.33 x 10 ⁻³
	20	Zero dispersion wavelength	1.32 μ m
		OH absorption peak @ 1.39 μ m	2.4 dB/km

TABLE 3 Optical Results: Multimode Cable C351
Length 1090 m

STRAND	ATTENUATION (dB/Km)				
	N.A.	PCF*	SCF†	CORE	CABLE
1	0.22	2.6	2.7	2.8	2.7
2	0.23	3.0	3.1	3.2	3.0
3	0.22	3.0	3.1	3.2	3.2
4	0.22	3.0	3.0	-	3.0
5	0.23	3.1	3.0	3.1	3.0
6	0.23	2.7	2.7	2.8	2.8
7	0.22	2.8	2.9	2.9	2.8
8	0.20	2.7	3.0	2.9	2.8
9	0.23	3.0	3.1	3.1	3.1
10	0.22	3.0	2.9	2.9	2.9
MEAN VALUES		2.89	2.95	2.99	2.93

* PCF = Primary Coated Fibre

† SCF = Secondary Coated Fibre

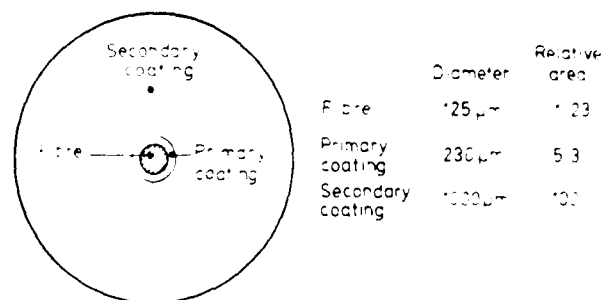


Fig. 1 Packaged fibre construction

TABLE 4 Cable Installation

SYSTEM	CABLE TYPE	CABLE DRUMS	TOTAL LENGTH (Km)	LONGEST DRUM LENGTH (Km)	DUCT OCCUPANCY		NUMBER OF FLEETINGS
					MEAN (%)	MAX. (%)	
Croydon - Vauxhall	Multi-mode	16	15.5	1.04	3	50	16
Vauxhall - Faraday	"	4	4	1.1	30	50	7
Aberystwyth - Ponterwyd	"	21	19.7	1.2	20	40	12
Aberdeen - Kingswells	"	12	12.22	1.5	20	45	9
Ipswich - Martlesham	Mono-mode	10	15.8	2.7	40	85	24

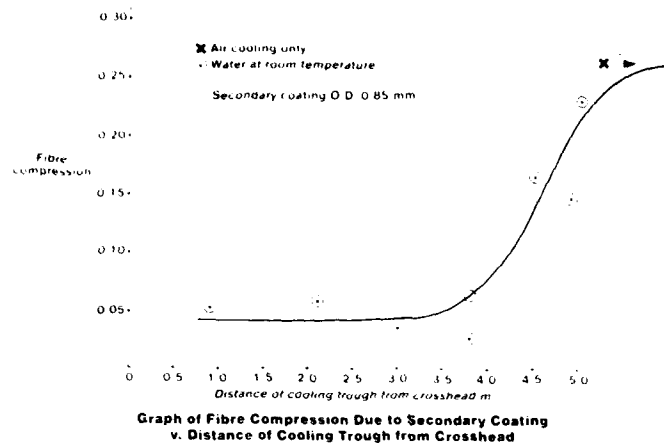


Fig. 2

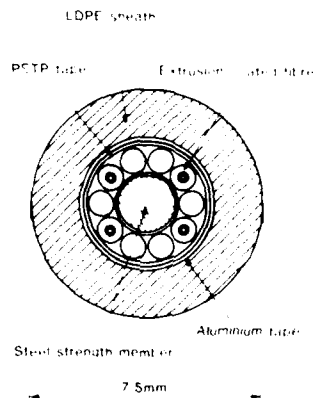


Fig. 3 Schematic cable structure

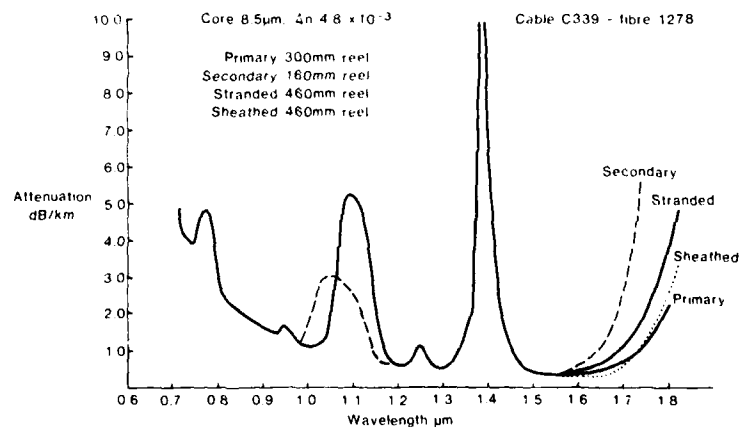


Fig. 4 Spectral attenuation changes during cable processing

DESIGN CONSIDERATION FOR JACKETING
FIBER OPTIC CABLE

M.M. Rahman and G.M. Davidson

Pirelli Cables Inc.
Surrey, British Columbia, CanadaAbstract

Fiber optic cable is vulnerable to its environment more than conventional metallic cables. In addition to the required mechanical properties, adequate moisture and rodent protection are necessary, especially in direct burial applications.

In such application optical fibers can experience stress due to moisture freeze-up and the small diameter of the cable makes it an easy prey for rodents. All these protections can obviously be achieved by designing layers of jackets, each of which has its own function. The major drawback of such construction though is not only economic but also performance.

In this paper a jacketing concept is discussed whereby two layers of jackets - moisture protection through corrugated steel and polyethylene can be replaced by a single jacket comprising longitudinally formed steel tape bonded to polyethylene.

Introduction

The thermal coefficient of expansion of glass is lower than that of metal by an order of magnitude and lower than that of jacketing materials by two orders of magnitudes.

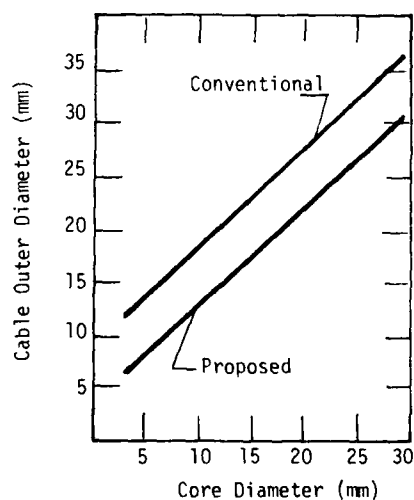
Material	Coefficient of expansion $\times 10^{-6} \text{ cm/cm}^\circ\text{C}$	Modulus of elasticity kg/mm^2
Glass fiber	0.8 - 1.7	7000
Steel	11 - 18	19000
Aluminum	22 - 25	7000
Nylon	80 - 100	125
Polypropylene	80 - 100	110
Polyurethane	100 - 200	25
Polyethylene (LD)	100 - 200	17

The performance of fiber optic cable core depends largely on two properties of its protecting materials-namely modulus of elasticity and thermal coefficient of expansion. Ideally, the coefficient of thermal expansion and contraction of the composite

cable should be as low as that of glass. Mechanical properties should be such as to protect the cable core during installation and against the environment. Once the cable is installed the main environmental concerns are temperature, water and rodents. Adequate moisture protection can be achieved through metal barrier and/or fully filled cable core whereas rodent protection can be achieved only through steel armouring. The common practice for designing cable with both moisture and rodent protection is to jacket a cable core with bonded aluminum-polyethylene and then cover with a corrugated and longitudinally formed steel tape and polyethylene. Sometimes a flat steel tape is helically applied instead of corrugated and longitudinally formed steel tape. The corrugation or helical taping is done to increase the flexibility of cable especially for large diameter cables commonly found in copper cable. This type of moisture and rodent protection not only increases the diameter and the weight of the cable but also decreases the strength to weight ratio and increases the thermal coefficient of expansion.

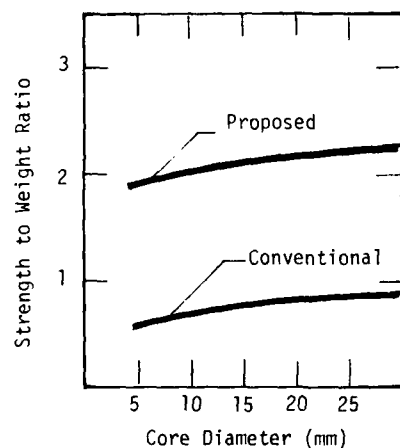
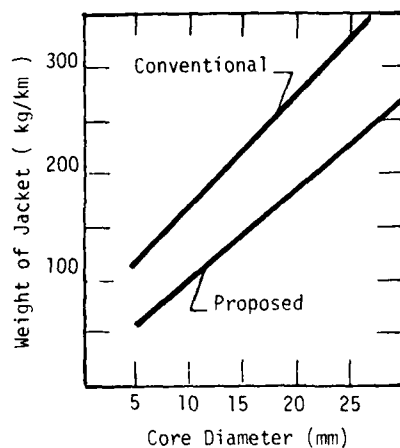
A single bonded steel and polyethylene jacket can provide all the advantages of bonded aluminum and polyethylene as well as the corrugated steel and polyethylene jacket and still reduce the diameter, coefficient of thermal expansion, processing costs and increase the strength to weight ratio.

Diameter and Strength to Weight Ratio



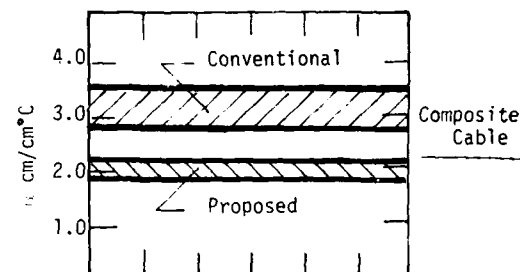
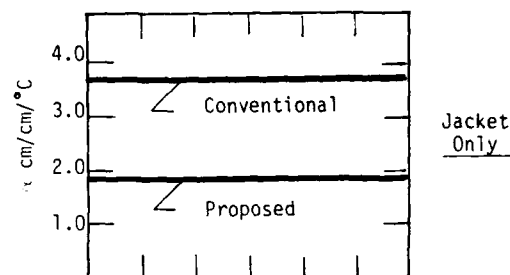
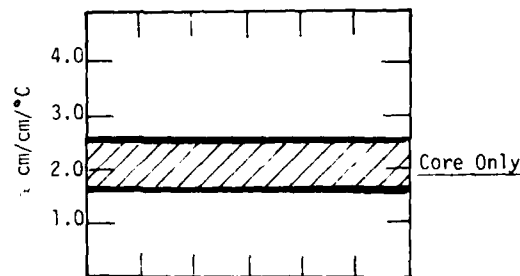
One of the biggest advantage of optical fiber cable is the smallness of the glass fiber itself. Although it needs sufficient protection the diameter of the packaging need not necessarily be increased.

The omission of the corrugated steel and polyethylene jacket not only reduces the weight of the cable but also increases the strength to weight ratio, as steel tape has a higher modulus of elasticity than aluminum. This decrease in weight and increase in strength to weight ratio is important as longer lengths of optic cable are manufactured and installed. Today, a fiber unit length of 2 to 3 km is a reality but it is expected that in the near future fiber lengths of 3 to 5 km will be available.



Coefficient of Thermal Expansion

Typical coefficient of thermal expansion for fiber optic cable core varies from 1.7 to 2.6×10^{-5} cm/cm/°C. Conventional moisture protection and gopher protection will increase this coefficient to 2.8 - 3.5×10^{-5} cm/cm/°C. This means for every 0.1 percent of contraction or expansion of the



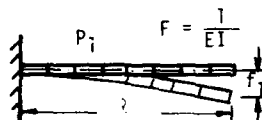
composite cable a reduction of 23 to 10°C in temperature performance. A bonded steel/polyethylene jacket increases this coefficient of expansion to 1.85×10^{-5} cm/cm/°C if the core has 1.7×10^{-5} cm/cm/°C originally and to 2.1×10^{-5} cm/cm/°C if the core has 2.6×10^{-5} cm/cm/°C. This means for every 0.1 percent of contraction or expansion of the composite cable a deterioration of 5°C for the cable core with lower coefficient of expansion and improvement of 9°C for cable core with higher coefficient of expansion ie. and average of 18 to 19°C improvement with a single bonded steel / polyethylene jacket.

Flexibility, Crush Resistance

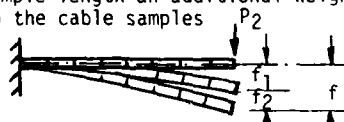
Cables need to be flexible enough so that they can be installed easily. Typical bending radii a cable undergoes during installation is the guide pulley ($R > 150$ mm) in duct installation and the cable chute of the plow ($R > 400$ mm) in direct burial installations. In practice the bending performance of the cable is also characterized by its ability to bend around a mandrel having radius equal to 10, and 15 times the diameter of the cable for static and dynamic loading respectively.

Two tests were performed on the cable jacket to determine the flexibility and bending characteristics of the cable. Flexibility (F) is inversely proportional to the bending resistance or stiffness and can be determined from a simple experiment. Stiffness is a product of modulus of elasticity and moment of inertia. In other words:

$$F = \frac{1}{EI}$$

$$f_1 = \frac{P_1 l^3}{8EI}$$


Since the weight of the cable (P_1) is not enough to get a sufficient deflection for 600-1000 mm sample length an additional weight (P_2) was added to the cable samples

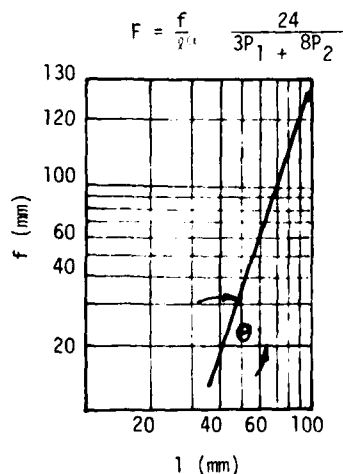


$$f = f_1 + f_2 = \frac{P_1 l^3}{8EI} + \frac{P_2 l^3}{3EI}$$

Therefore,

$$F(\text{flexibility}) = \frac{1}{EI} = \frac{24}{l^3} \frac{f}{3P_1 + 8P_2} \text{ cm}^{-2} \text{ kg}^{-1} \text{ s}^2$$

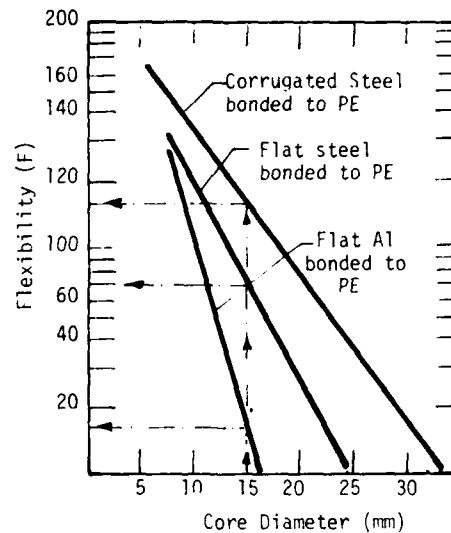
In reality a cable has a different structure than an ideal stab. Therefore, the above formula must be correct with a factor α .



$$\alpha = \frac{\log(f_1/f_2)}{\log(l_1/l_2)}$$

or $\alpha = \tan \theta$

Stiffness or flexibility of different cable types as determined above, are compared in the following diagram.



The bending properties of the jacket were also determined from $\pm 90^\circ$ bend test over bending radius of 10 D. The results are as follows:

Cable Type	Observation
Flat steel bonded to polyethylene	No damage for cycles > 10 times

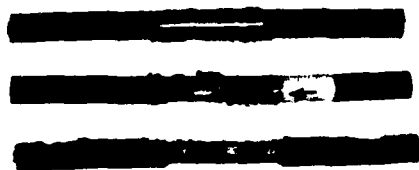
Gopher Protection

The life of cable exposed to nature is often limited by gnawing rodents particularly pocket gophers and squirrels. Cable in the field can experience significant gopher damages often as long as six years. Cables smaller than 55mm outside diameter particularly those under 25mm diameter are easily attacked by plains gophers. Biting pressure of 1268 kg/cm² and an average of 1.5 bites per second are quite common. All these actions of nature make fiber optic cables absolutely vulnerable when installed outside.

Tests and experience have shown that only metals such as steel or bronze can give adequate protection against gophers. Single cable jackets consisting of longitudinally formed steel tape and bonded to polyethylene were tested for gopher resistance. Tests were carried out according to the procedure described in AS&M National Research and Standards Vol. 9, No. 23, except that specimens were positioned horizontally across a 2 inch square hole. The results are as follows:

Sample	Damage Category *							
	0	1	2	3	4	5	x	
Bonded steel/polyethylene Cable O.D. = 11 mm Steel thickness = 0.15mm Jacket thickness = 1.2mm	-	-	9	1	-	-	2.1	

* 0=no damage; 1=jacket scratched; 2=jacket penetrated; 3=armour penetrated; 4=core damaged; 5= cable severed.

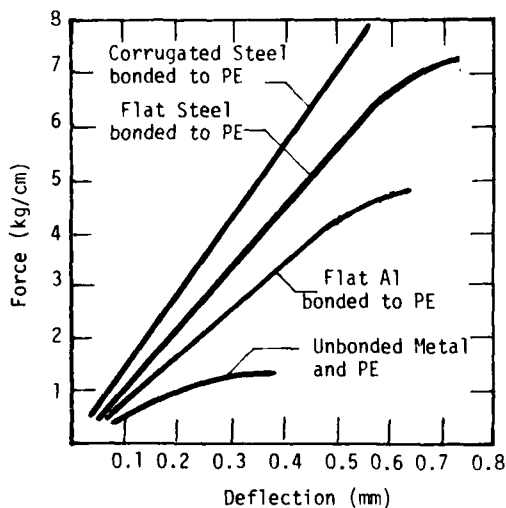


Cable samples after being exposed to Gopher bites.

The typical average gopher resistance required according to industry standards is 2.7

Crush Resistance

Crush resistance of jacket depends very much on the bonding of polyethylene to metal. 250mm long samples were subjected to force between two flat plates. Force applied on two axis show that if the bonding at the over lap is poor, the crush resistance is considerably lower. Typical crush resistance of different samples are shown in the following diagram.



Conclusion

Advantages of fiber optic cable like smallness and long lengths can be improved by protecting it with a single jacket. A single jacket composed of bonded steel tape and polyethylene also improves the temperature performance, strength to weight ratio and protects the core against moisture ingress and gopher bites while at the same time it is flexible enough for all installations and handling.

References

1. J.R. Osterfield et al - - An optical fiber link in mountainous environment, Proceedings from 29th International Wire and Cable Symposium.
2. K. Locher - - Verfahren zur Messung der Flexibilität von Litzen, Kabeln und Leitungsschnüren. ETH Dätwyler A.G., Altdorf.
3. N.J. Cogelia et al - - Rodent biting pressure and chewing action and their effects on wire and cable sheath. Proceedings from 25th International Wire and Cable Symposium.



Mir Mujibar Rahman graduated in mechanical engineering from Bangladesh and completed his Dipl. Ing. from Technical University of Darmstadt in W. Germany. After working one year as Research Assistant in TU Berlin, he worked for Siemens W. Germany from 1968-1971 and for Siemens Austria from 1972-1976. He managed fiber optics cable development program for Canstar from 1977 to 1980. In 1981 he joined Pirelli Cables Inc. Currently, he is Engineering Manager of Fiber Optics.



Grant M. Davidson received a Bachelor of Applied Science Degree in Engineering Physics from the University of Toronto in 1964. He joined Pirelli Cables Inc. in 1974. At present he is Manager Engineering Communications Products.

DEVELOPMENT OF NONMETALLIC, LOOSE-GROOVE SPACER-TYPE OPTICAL FIBER CABLE

O. Ichikawa, K. Sakamoto, Y. Saitoh

Sumitomo Electric Industries, Ltd. Yokohama, Japan

Summary

Nonmetallic optical fiber cables, due to their noninductive characteristics, are highly suitable for use in strong electromagnetic fields such as in electric power facilities. However, conventional nonmetallic optical cables required improvement of their tensile strength, waterproofness, and transmission loss vs. temperature characteristics before they could be put to effective use. This has now been accomplished with the development of a new construction that houses three-layer-coated optical fibers separately in a grooved plastic spacer. The spacer has helical grooves on its outer surface in which the optical fibers are laid, and then the fibers are covered with a plastic housing. The spacer is formed around an FRP strength member by direct polyethylene extrusion through a specially shaped rotary die to create a unitary structure. An optical fiber is housed in a slack condition in the center of each groove by means of a new line speed control method which detects slight groove pitch changes and by means of an air jet housing method that eliminates subjection of the fiber to external forces. Various evaluation tests show that the new cables maintain stable transmission loss vs. temperature characteristics over a wide temperature range. The optical fibers receive adequate protection against mechanical forces, and the addition of a waterproofing agent in the grooves provides the waterproofness necessary for outdoor use. Economical production is expected since the cables are light-weight and small in diameter, thus meeting the specifications of small-core optical cables.

Introduction

A vast range of applications for nonmetallic optical fiber cables making good use of their noninductance to electricity, such as computer links, robot control, induction-free observation and control in power plants, and temporary communications for emergency telephones, field telegraphs, and so on, can be expected. However, conventional types of nonmetallic optical fiber cables have many problems for practical use such as high elongation, low tensile strength, inadequate waterproof properties, and poor temperature stability of transmission loss. Therefore, development of cables solving these problems has been desired. The authors have developed nonmetallic optical fiber cables having three-layer-coated optical fibers separately housed within helical-grooves of a spacer formed

around an FRP strength member by direct polyethylene extrusion through a specially shaped rotary die.

This helical-grooved spacer structure has many advantages for the optical fibers: it relieves them from elongational strain under high tension, increases their resistance to compressive strain under high-compressive load, and mitigates the effect of microbends in a wide temperature range. It is therefore possible to make nonmetallic optical fiber cables having excellent transmission loss stability and long-term reliability when subjected to mechanical force and large variations in temperature. Furthermore, nonmetallic optical fiber cables with adequate waterproof properties are easily obtained by filling the grooves of the spacer with jelly compound. Since the new cables contain relatively few optical fibers, standardization of their structure is possible, and thus economical production can be expected.

This paper describes manufacturing techniques and evaluates the characteristics of the helical-grooved plastic spacer, nonmetallic optical fiber cables.

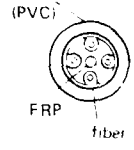
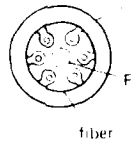
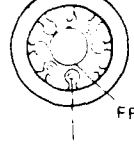
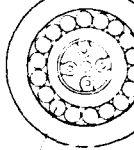
2. Cable Structure

The structures of the newly developed non-metallic, spacer-type optical fiber cables are shown in Table 1. Each cable houses three-layer-coated optical fibers separately in a grooved plastic spacer. The grooved spacer is formed by extruding polyethylene over the central FRP strength member through a specially shaped rotating die. The spacer is covered with a plastic outer sheath after fiber laying.

The new cables are classified into three sizes containing four (Cable I), six (Cable II), and eight (Cable III) optical fibers. Each size comes in both a jelly-filled (JF) type for outdoor use and an air-core (AC) type for indoor use. Cable IV is a self-supporting aerial optical fiber cable armored with Kevlar ropes around a 4-fiber JF-type Cable I and then covered with polyethylene. The optical fibers housed in the helical grooves are large-core fibers (core/cladding: 100/140 μ m) or standard-core fibers (core/cladding: 50/125 μ m).

A standard three-layer-coated optical fiber, with two room-temperature-vulcanized silicone resin coats (total dia.: 0.4mm) and a nylon coat (dia.: 0.9mm), is utilized. The new cables have excellent handling (such as splicing) characteristics since

Table 1. Cable Specifications

Item	Type	I	II	III	IV
Number of fibers		4	6	8	4
Core diameter (mm)		50 125	50 125	50 125 100 140	50 125 100 140
Core dia (mm)		1	1	1 2	1 2
dia (mm)		0.9	0.9	0.9	0.9
dia (mm)		7.0	8.5	10.0	13.0
weight (kg/km)		35	55	80	125
Cable construction					

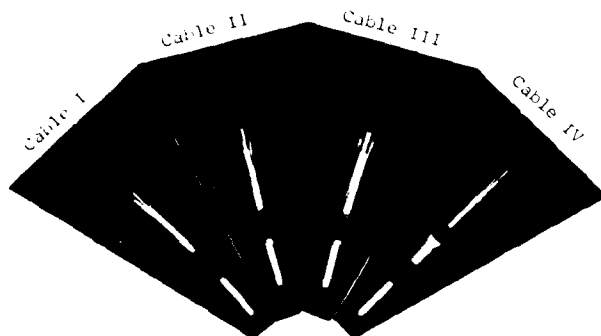


Photo 1. New Optical Fiber Cables

their outer coat consists of nylon.

Cables I, II, and III are designed so the cable can withstand tension corresponding to the weight of a 1km-long cable during installation in the conduit. For Cable IV, the strength member is

designed for withstanding wind pressure of 110kg/m² when the cable is in aerial use strung between towers 1km apart. Photo 1 shows the new optical fiber cables.

3. Cabling Techniques

The helical-grooved plastic spacer is formed around the FRP strength member by direct polyethylene extrusion, thereby creating a unitary structure. A specially shaped rotating die is used for extrusion to produce grooves in helical design. In this process, the pitch of the helical grooves is easily uniformed simply by keeping the supply speed of the FRP and the rotating speed of the die constant. In all of the new cables, the pitch of the helical grooves is the same.

A new fiber-laying device has been developed to eliminate the external force acting on the optical fibers as they are laid in the grooves due to slight fluctuations of the groove pitch and the fiber tension when pulled from the supply reel.

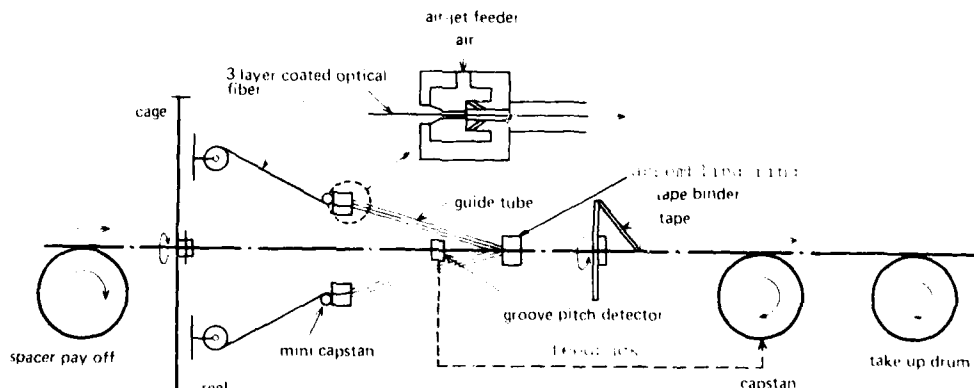
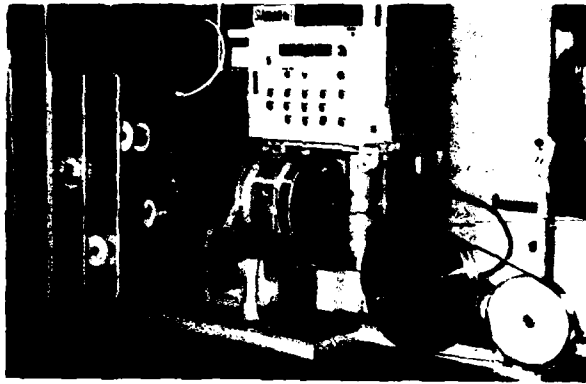
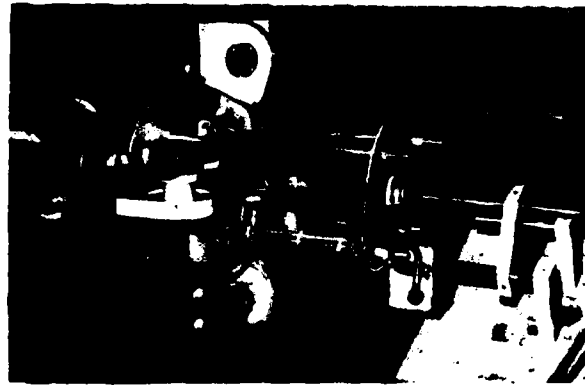


Fig. 1. Cabling line



(a) Cabler



(b) Equipment for housing fibers in grooves

Photo 2 New Fiber-Laying Device

Figure 1 and Photo 2 show the new fiber-laying device. In the fiber-laying process, the three-layer-coated optical fibers are pulled off reels set on a cage rotating at constant speed, utilizing mini-capstans fixed to the cage, and are fed into the grooves by means of an air-jet housing method. Therefore, the optical fibers are housed in a slack condition in the center of the helical grooves with no residual strain. The speed of the main capstan is precisely controlled, based on continuously detected signals of helical-groove angles utilizing a pitch detector located just before the assembling ring, so that the optical fibers will be laid in the center of individual grooves without being subjected to external force resulting from groove-pitch irregularities.

The transmission losses of cabled optical fibers were less than 1.0 dB/km at long wavelength ($\lambda = 1.3\mu\text{m}$) and 3.0 dB/km at short wavelength ($\lambda = 0.85\mu\text{m}$). No significant transmission loss increase in the cabling process was observed. The JF-type cable can be easily manufactured by filling epoxy compound into the grooves as the fibers are laid.

4. Characteristics

Temperature characteristics, mechanical properties, and waterproof properties of the new JF-type cable were evaluated.

4.1 Temperature characteristics

Transmission loss stability with variation in temperature was experimentally evaluated for Cables I, II, and III. Transmission loss variation due to change in temperature was measured utilizing the continuous monitoring system shown in Figure 2. The four optical fibers in a 500m sample cable were fusion spliced together to form an approximately 2km-long test sample, which was then placed in the temperature-test chamber. Fluctuation of light output was controlled within 0.002dB by keeping both the light sources (LED) and dummy fibers (500m) in another test chamber, in which temperature was kept at a constant 20°C. Measuring accuracy of the transmission loss of the spliced optical fiber was kept within 0.01dB by placing the optical fiber splices outside the chamber. Therefore, the measuring accuracy of the entire system was also within 0.01 dB. The tem-

perature pattern of the test chamber was set at an 8-hr cycle of -30°C and 70°C .

Figure 3 shows the transmission loss variation vs. temperature characteristics of cabled fibers. Figure 3(a) compares the transmission-loss variation of the 4-fiber Cable I vs. the 6-fiber Cable II when both use a standard-core fiber. The transmission loss variations are so little (within 0.04dB/km) that the spacer is considered to be practicable and free of significant variations in structure. Figure 3(b) shows the transmission loss variations of a Cable III using a large-core fiber in comparison with a Cable III using a standard-core fiber. In the higher temperature range, the transmission loss increase of the large-core fiber (less than 0.03dB/km) was slightly less than that of the standard-core fiber. This is presumed to result from the difference in microbending effect between the fibers. The modulus of elasticity in bending of the large-core fiber was larger than that of the standard-core fiber. Therefore, microbending of the large-core fiber was less than that of the standard-core fiber. Figure 3(c) compares the transmission loss variation for long ($1.3\mu\text{m}$) vs. short ($0.85\mu\text{m}$) wavelengths for the standard-

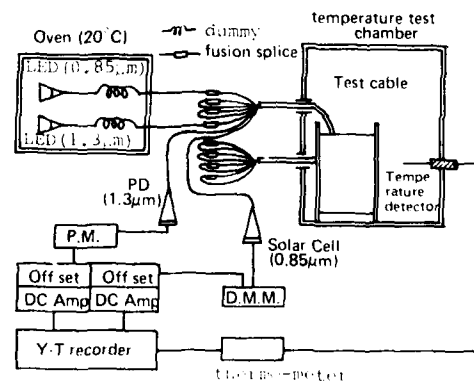


FIG. 2 System for Measuring Transmission Loss vs. Temperature

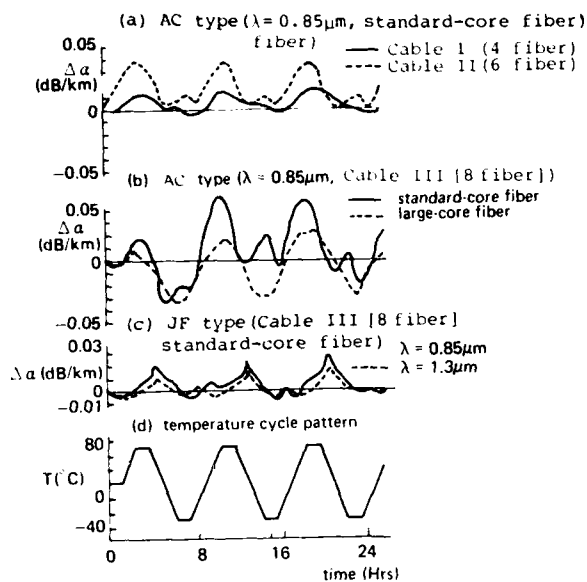


Fig. 3 Transmission Loss vs. Temperature

core fiber housed in a JF-type Cable III. The transmission loss increases when the temperature changes from 70°C to -30°C. The increases in transmission loss for both long and short wavelengths were small: 0.035dB/km and 0.025dB/km, respectively. It can be recognized from Figure 3(a) and Figure 3(b) that transmission loss of the JF-type cable is more stable than that of the AC-type cable in a wide temperature range from -30°C to 70°C. The jelly compound restricts the movement of the fiber in the groove. Therefore, micro-bending of the fiber in the JF-type cable is less than that in the AC-type cable. Figure 3(d) shows the temperature cycle.

It is clear from this test that housing the three-layer-coated optical fibers in the grooves of the spacer is very effective to diminish micro-bending and that the transmission loss of the housed fiber is more stable with temperature than the three-layer-coated optical fiber itself.

4.2 Mechanical properties

The mechanical properties of the new cables were evaluated by using the test methods shown in Table 2. Transmission loss variation of the cabled fibers during the mechanical test was measured by the continuous monitoring system shown in Figure 4. The measuring accuracy of this system was within 0.005dB.

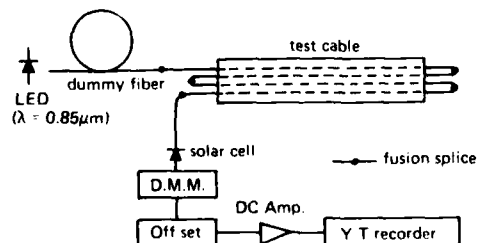
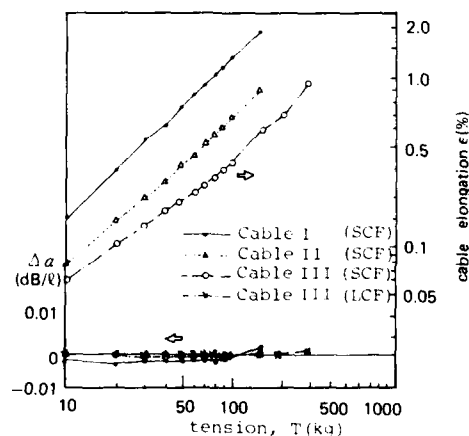


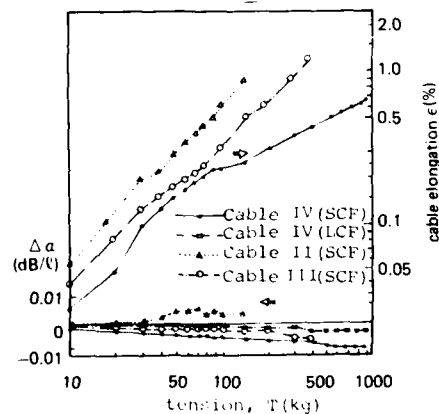
Fig. 4 Setup for Measuring Transmission Loss Variations

(1) Tension test

Figure 5 shows the transmission loss variation of the optical fiber and the elongation of the cable when tensile load was applied to both ends of the cable. No significant increase of transmission loss was observed in any of the new cables under tension corresponding to 1% cable elongation. The permissible tension was defined to be the tensile load corresponding to 0.5% elongation. The permissible tension was 30kg in Cable I, 95kg in Cable II and 200kg in Cable III. These values correspond to the tensile load in the case when the whole tensile load is placed only on the FRP (Young's modulus: 5500kg/mm²). In Cable IV armored Kevlar rope makes the cable's resistance to withstand tension so high that the permissible tension was 700kg. The ratio of elongation to tension of Cable IV decreased at higher tensile loads. This is presumed to be the result of a tension-sharing phenomenon between FRP and Kevlar rope in a transition period in which the role of main tension member shifts from the FRP to the Kevlar rope as the tension increases.



(a) AC type



(b) JF type

SCF: standard-core fiber

LCF: large-core fiber

Fig. 5 Tension Property (ℓ = 3m)

Table 2 Mechanical and Waterproof Tests

test	content	method
mechanical properties	tension sample length : 1.5 m measuring length : 1 m tension : to breakpoint of epoxy-putty mold evaluated items : transmission loss variation, cable elongation	
	minimum bend bending diameter : 20, 15, 10, 8, 6, 4, x d (cable O.D.) bending angle : 360 °C evaluated items : transmission loss variation, noncircularity	
	cyclic bend bending diameter : 10 x d bending angle : ±180 °C bending cycle : 30 cycles evaluated items : transmission loss variation, noncircularity	
	compression compression board : 50 mm square metal plate compression load : to 1000 kg evaluated items : transmission loss variation, noncircularity	
	twist twist length : 300 mm twist angle : groove direction 1,200 deg/m opposite direction 400 deg/m evaluated items : transmission loss variation, twist torque	
	impact impact energy : 1, 3, 5 x 1b-m dropping object : 25 mm diameter column drop method : different points, 5 times evaluated items : transmission loss variation, noncircularity	
	vibration sample length : 1 m vibration amplitude : ±5 mm vibration cycle : 10 Hz, 1 million cycles evaluated item : transmission loss variation	
waterproof properties	pulling-on-mandrel sample length : 2.5 m bending length : 1.5 m bending diameter : 150 mmφ tension : load corresponding to 0.5% elongation bending cycle : 30 cycles evaluated items : transmission loss variation, noncircularity	
	penetration sample length : 1,000 mm initial water height : 1,200 mm aging time : 24 Hrs evaluated item : water-flow from cable end	
	dripping sample length : 100 mm setting : perpendicular, 24 hrs evaluated item : dripping of jelly compound	

*Both ends of cable molded with epoxy-putty resin

(2) Minimum bending test

Figure 6 shows the relationship between bending diameter and transmission loss variation of the optical fiber and noncircularity of the cable. The permissible bending diameter was defined to be the bending diameter at which the transmission loss increase reached 0.005 dB. The permissible bending diameter was less than six times the cable diameter in the standard-core fiber and four times in the large-core fiber.

(3) Cyclic bending test

Figure 7 shows maximum transmission loss increase per cycle and noncircularity of the cable during 30 bending cycles utilizing a mandrel (10 times the cable diameter). No significant residual transmission loss increase was observed after straightening the cable in each cycle. The maximum transmission loss increase was less than 0.005dB in all of the new cables. This cable structure was thus confirmed to be very stable for bending.

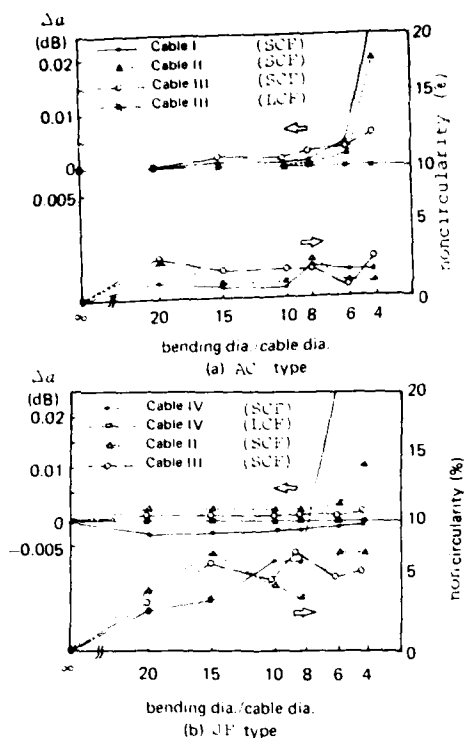


FIG. 6 Minimum Bending Property

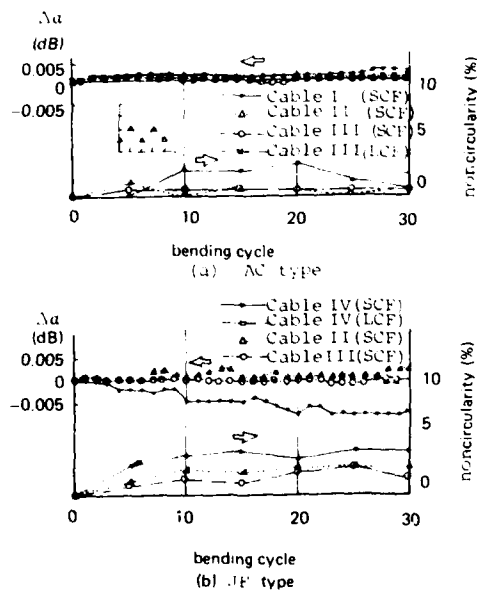


FIG. 7 Cyclic Bending Property

(4) Compression test

Figure 8 shows the transmission loss variation of the optical fibers and the noncircularity of the cable when compressive load was placed on the cable

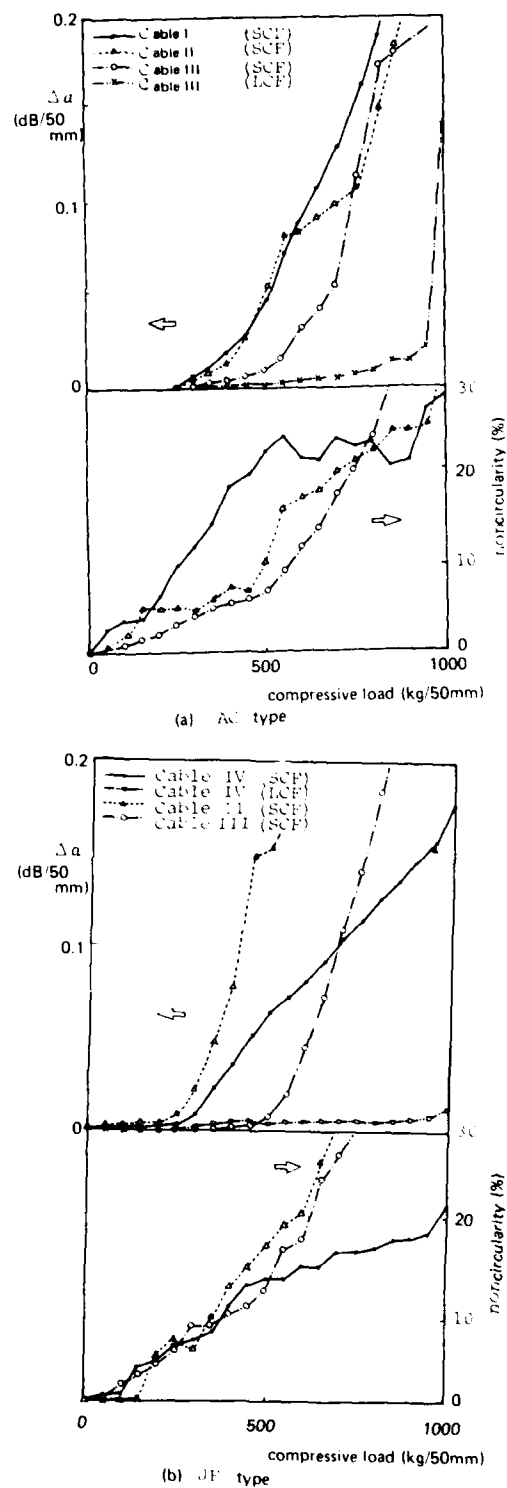
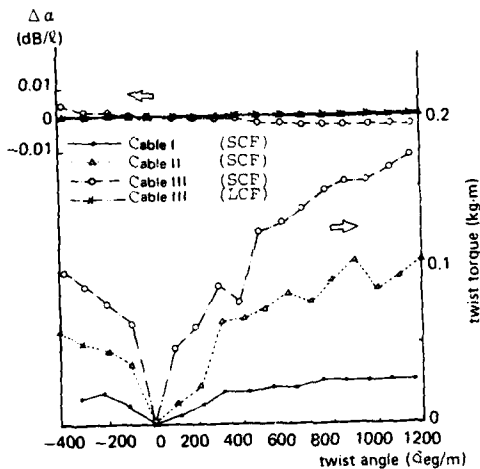


Fig. 8 Compression Property

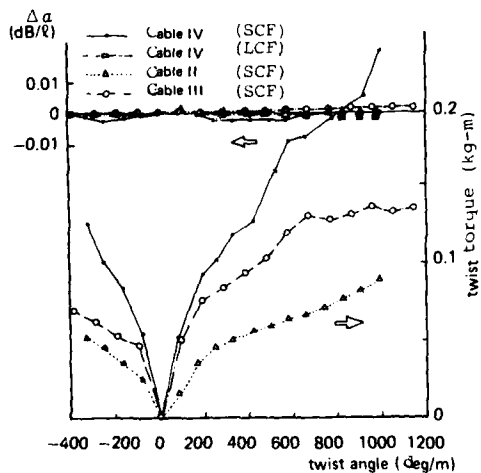
utilizing two metal plates (50mm square). The permissible compressive load was defined to be the compressive load at which the transmission loss increase reached 0.05 dB. The permissible compressive loads of AC-type Cables I, II, and III utilizing standard-core fibers were respectively 500, 500, and 700kg/50mm. The noncircularity of the AC-type cables under the permissible compressive load was between 10% to 20%. The permissible compressive load of the large-core fiber cable was remarkably improved in comparison with that of the standard-core fiber cable. The transmission loss vs. compressive load of the JF-type cable was as good as that of the AC-type cable.

(5) Twist test

Figure 9 shows the effect of twist angle on the transmission loss variation of the optical



(a) AC type



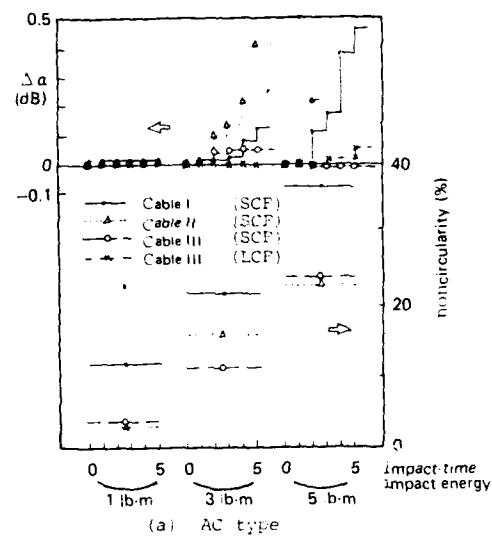
(b) JF type

Fig. 9 Twist Property ($\lambda = 0.6\mu\text{m}$)

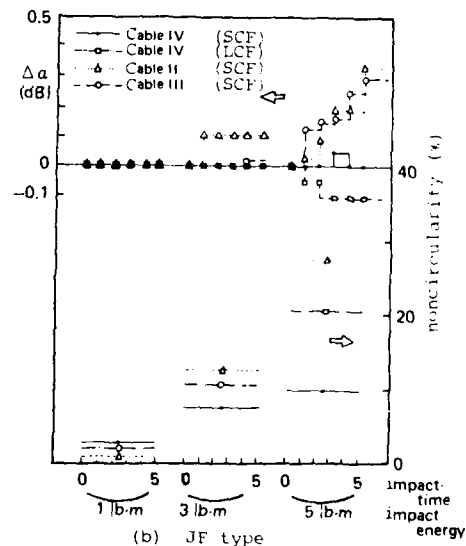
fiber and twist-torque of the cable. The transmission loss variation was too small to be recognized in a wide range of twist angles, from 1 turn/m in the opposite groove-direction (negative direction) to 3 turns/m in the groove-direction (positive direction). Little difference in transmission loss vs. twist properties was recognized among the various fibers or cables (AC type and JF type). The helical groove of the spacer was thus confirmed to stably protect the three-layer-coated optical fiber from damage caused by twisting.

(6) Impact test

Figure 10 shows the transmission loss variation of the optical fiber and the noncircularity of the cable when 25mm-diameter columns with a mass of 1 lb, 3 lb, and 5 lb were naturally dropped



(a) AC type



(b) JF type

Fig. 10 Impact Property

five times on different spots from 1m height. The permissible impact energy was defined to be the impact energy at which the transmission loss increased by 0.05dB at the instant of impact and no residual transmission loss was recognizable. The permissible impact energies of AC-type Cable I, II, and III with standard-core fibers were respectively about 11J-m, 11J-m, and 31J-m. The non-circularities of the cables for these permissible impact energies were against between 10% to 20%. The cabled large-core fiber was found to be stronger against impact than the cabled standard-core fiber. The transmission loss vs. impact property of the JF-type cable was more stable than that of the AC-type cable.

(7) Vibration test

A 1m-long cable was horizontally laid. One million cycles of vertical vibration with an amplitude of 5mm were applied to the middle of the sample at 10Hz. No significant transmission loss variation was observed during the vibration test.

(8) Pulling-on-mandrel test

A 2.5m-long cable was bent around a 150mm-diameter mandrel at 90 degrees under tension corresponding to 0.5% elongation. A 1.5m section of the cable was then pulled back and forth at that angle on the mandrel for 30 cycles. Figure 11 shows the transmission loss variation of the fiber after each cycle and the noncircularity of the cable at 5-cycle intervals. Transmission loss increase of the standard-core fiber in the JF-type cable was less than 0.01dB under the bending and

pulling. The transmission loss vs. bending/pulling property of the AC-type cable was better than that of the JF-type cable. The spacer was thus confirmed to protect the three-layer-coated optical fiber from the various stresses of bending, elongation, and compression resulting from the bending and pulling.

By these mechanical tests, the spacer-type cable was found to be effective in protecting the optical fiber from various kinds of external force.

4.3 Waterproof test

The results of examination of long-term reliability of the JF-type cable were already reported[1]. Waterproof properties of the JF-type cable were evaluated, based on the methods shown in Table 2.

(1) Water penetration test

A 1m-long cable was horizontally laid. A watertight enclosure was placed over the sheath at one end and filled with water to 1.2m height over the sample. There was no water leakage from the other end of the sample after 24 hrs in any of the new cables.

(2) Jelly dripping test

A 10cm-long cable was vertically placed and kept at 55°C for 24 hrs. Both ends of the sample remained open. There was no jelly dripping at all in JF-type cables.

From these tests, all of the new JF-type optical cables were found to have adequate waterproof properties and to be suitable for outdoor applications such as aerial use.

5. Conclusion

Transmission loss vs. temperature property, mechanical properties, and waterproof properties of newly developed nonmetallic, loose-groove optical fiber cables were evaluated. The cable properties were confirmed to be satisfactory for actual use of the cables. The new cables have many advantages such as small size, transmission loss stability under various mechanical forces and temperatures, and so on. A vast range of applications in fields where electromagnetic interference exists can be expected for these high-quality optical fiber cables for indoor or outdoor use. The simple but versatile grooved spacer is suitable for cable standardization and useful for economical production of the small-core optical fiber cable, especially cables containing relatively few optical fibers.

References

- [1] Y. Kameo, H. Horima, S. Tanaka, Y. Ishida, and Y. Koyamada, "Jelly-Filled Optical Fiber Cables", 30th I.W.C.S., Nov., 1981.

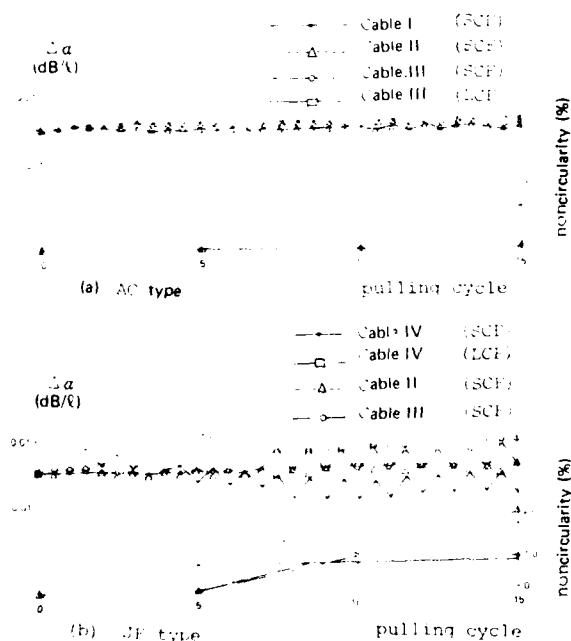


Fig. 11 Pulling-on-Mandrel Property ($d = 5m$)



Yasunori Saitoh
Sumitomo Electric
Industries, Ltd.
1, Taya-cho,
Totsuka-ku,
Yokohama, Japan

Yasunori Saitoh received his B.S. degree in Electrical Communication Engineering from Tohoku University in 1969. He then joined Sumitomo Electric Industries and has been engaged in research and development of high frequency transmission lines including fiber optics. Mr. Saitoh is a senior engineer of R & D Group, and a member of the Institute of Electronics & Communication Engineers of Japan.



Katsuji Sakamoto
Sumitomo Electric
Industries, Ltd.
1, Taya-cho,
Totsuka-ku,
Yokohama, Japan

Katsuji Sakamoto finished the Mechanical Engineering Course of Tsurumi Industrial High School in Kanagawa Prefecture in 1962. He then joined Sumitomo Electric Industries and has been engaged in development and design of manufacturing processes of communication cables. Mr. Sakamoto is a senior engineer of Yokohama R & D Group.



Osamu Ichikawa
Sumitomo Electric
Industries, Ltd.
1, Taya-cho,
Totsuka-ku,
Yokohama, Japan

Osamu Ichikawa received his B.S. degree in Electrical Communication Engineering from Tohoku University in 1980. He then joined Sumitomo Electric Industries and has been engaged in research and development of optical fiber and cables. Mr. Ichikawa is a member of Yokohama R & D Group, and a member of the Institute of Electronics & Communication Engineers of Japan.

AD P000584

SELF-SUPPORTING METAL FREE OPTICAL FIBRE CABLE FOR LARGE SPAN LENGTH

W. Schmidt, K. Kimmich, S. Metz

Standard Elektrik Lorenz AG, Stuttgart, Germany

Abstract

A self-supporting optical cable has been developed for very large span length. This cable has an inner core with up to four optical fibres and an outer glass fibre reinforced plastic suspension unit. A thin PE sheathing increases the outer diameter up to 10 mm. This metal free cable is developed for span length up to 500 m from pole to pole. Considering wind-, ice load and the large span length, very high tensile strength is needed. Tensile strength for the FRP element is more than 50 kN, resistance to vibration and temperature cycling show good performance in the cable. The tests are carried out with special suspension clamps also used for the mounting poles. The cable contains up to four optical fibres tight jacketed with PA 12; attenuation values of 3.5 dB/km at 850 nm have been obtained in the cable. Electric utilities will be main users of this aerial type communication cable installed along the HT poles.

Introduction

Electric power companies have a need for communication facilities for the effective operation of their own networks. As the conventional copper cables can be influenced by the high voltage power lines, high shortcircuit currents or lightning, optical fibre cables get more and more interest because of their interference immunity.

The low attenuation high capacity of transmission is an other attractive advantage of the optical fibre. Of special interest is the use of fibres in high voltage overhead lines inside a metal free self-supporting optical communication cable. The cable must be able to bridge span length up to 500 m from pole to pole and to withstand wind and ice load. These cables are very economical for the electric power companies because of the use of the existing poles, and to

avoid structural work below ground level.

Cable design

Known designs

Messenger wire: In this common type of cable the wire is installed first (it could be identical with the earth conductor), and then the optical cable is lashed onto the messenger wire. The wire consists of stranded steel ropes, and the optical cable can be a normal type without extra strengthening elements. (1) Fig. 1.

Figure Eight: In principle the same design as the messenger wire, but the supporting element is coupled together with a common PE plastic sheath. The supporting element can be a steel wire or a Kevlar element (1). This cable is only used for short span length. Fig. 2.

Combined Cable: In the axis of a metal conductor the optical section is integrated. The metal elements of the power cable surrounding the optical section are used as the supporting elements. (2) Fig. 3.

Self-supporting: The strength members of this type of cable are located in the cable axis or combined with the cable jacket. These designs create problems for installation with the clamps and the tension coupling of all elements. (3) Fig. 4.

New construction

The decision was made to take a self-supporting cable and a metal free version with an outer strength member. Fig. 5. The outer strength element should be able to be gripped by installation clamps and keep the core free of tension. The cable core contains two optical fibres. These fibres are graded index fibres with a core of 50 μm and a cladding of 125 μm , NA = 0.2. Above the soft silicone buffer as a primary coating is the tight Nylon jacketing. These fibres are all temper-

ature tested in cycles from room temperature down to minus 40 degrees centigrade and up to 70 degrees centigrade.

The two coated fibres are stranded together with two fillers in a short pitch and taped with a thin tape. A layer of glass rovings stranded with very long pitch is used as a cushion. The cable core is covered with two more tapes of a diameter of about 3.0 mm. The FRP strength member has an outer diameter of 8 mm. This is needed to get the cross section for the 44 mm² to withstand the long span length. A final polyethylene sheath of one millimeter thickness on the FRP gives a protection against UV-radiation and corrosive gases. The construction of this cable is so designed that the inner cable core can move in the FRP pipe and slip on the glass filaments during temperature changes.

The data of this cable are the following:

- outer diameter with PE sheath 10 mm
- outer diameter of RP 8 mm
- inner diameter of RP 3 mm
- weight with sheathing 0.1 kg/m
- supporting cross section 44 mm²
- Young's modul (E-modul) 55000 N/mm
- breaking load (clamps) 55 kN
- thermal expansion coefficient $0.7 \cdot 10^{-6} / ^\circ\text{C}$
- minimum bending radius 60 cm
- typical manufacturing length 2000 m

Cable fabrication

This special designed cable needs some fabrication steps as stranding, buffering, FRP-laying and sheathing. But this metal free version compared with a metal cable is easier to handle because there is no need for shield and steel armouring. One of the problems during cable production is the slow stranding speed due to the very short pitch and the small cable diameter. All fibres are secondary coated with Nylon 12 and on-line proof tested with 5 N over the full length during extrusion process. For the stranding of the elements a special machine with sensitive brakes is used. It is important to have the same back load on each fibre or filler especially if there is no central element.

In the second step 12 thin glass rovings are stranded in a long lay length with the same machine around the four elements. Two thin tapes are wound around the rovings for closing the cable core to the FRP strength element.

The load supporting part of the cable is produced in a special developed process,

where glass strengthening fibres saturated with polyester resin are put around the cable core. The hardened resin gives a relatively stiff behaviour to the cable which, however, is an advantage in its later environment. The cable can be wound on the drum with a core diameter of 120 cm. The sheathing process is made on a conventional cable sheath machine. For uniform running through the cross head of the extruder the brake of the pay off drum has to be put on very hard, and a special caterpillar for calming the cable under tension has to be put between capstan and cross head. With these arrangements the 1 mm wall thickness of the PE-sheathing can be extruded smoothly on the FRP.

Measurements

The fibres used for fabrication length are selected by the temperature cycling test ($-40^\circ\text{C} < T < 70^\circ\text{C}$). Only fibres with an attenuation change of $\Delta\alpha < 0.5 \text{ dB/km}$ are considered suitable. During fabrication process, the fibre loss is measured in each cabling step. The measurement is done by means of the backscatter technique, whereby not only the amount of the attenuation, but also its possible faults and irregularities over the production length can be detected. In production lengths up to 2000 m the following measurement results were achieved:

fibre		cable	
prim.coated	second.coated	stranded	sheathed
2.2 dB/km	2.5 dB/km	2.8 dB/km	3.2 dB/km

Mean values of fibre loss in different production steps.

Special tests

In order to check the temperature behavior in the final cable, a temperature cycling test was carried out. For this purpose a cable length of 890 m was spooled on a wooden drum with a core diameter of 120 cm. The temperature cycling program was the same as applied for the fibres. Beginning with room temperature of $+20^\circ\text{C}$, the cable was cooled down to -40°C , whereby the temperature equilibrium was checked by optical transmission of a fibre. After going back to $+20^\circ\text{C}$, the cable was warmed up to $+70^\circ\text{C}$ and then the cycle was finished at $+20^\circ\text{C}$. The whole temperature program was carried out in a large temperature chamber and tested over a period of some ten days. A typical course

of the temperature behaviour of the cable is shown in Fig. 6.

Cable accessories and environmental tests

It was not intended to develop new cable accessories for installation, rather to rely as much as possible on approved - maybe slightly modified - conventional types.

Tensile forces which have to be applied at certain poles are taken up by dead-end clamps made of preformed rods, whereas suspension of the cable can be accomplished by similar preformed rods. Both types of accessories are made of corrosion-resistant materials, are field mountable and easy to handle without any tool. As a pre-requisite for field installation mechanical tests described below have been performed where both accessories and the cable have been tested.

- Tensile load test (short term)
Slowly increasing pulling stress has been applied to dead-end clamps at both ends of 10 m cable samples.
Result: breaking load > 50 kN (10 samples).
 - Tensile load test (long term)
Constant stress of various degree has been applied on 3 m samples with dead-end clamps.
Result: No material fatigue at 70 % of breaking load (35 kN) with 2 samples after 1 year period.
 - Vibration test
30 m cable samples fitted at both ends with dead-end clamps and in between with a suspension clamp have been subjected to vibrations under the following conditions:
tensile load 10 kN
vibration frequency 22 Hz
(resulting in standing waves with 3 knots)
oscillation angle $\pm 30^\circ$
number of vibrations > 25×10^6
(typical number during lifetime in excess of 20 years).
- During this test light transmission through the fibres was monitored and no fibre break occurred. The cable was then inspected for mechanical flaws which, however, were not observed. Subsequent tensile tests showed unchanged performance with respect to unstressed samples (i.e. breaking load > 50 kN).

- Installation test
The cable has been pulled between 3 poles across two 50 m spans using conventional equipment, i.e. force- and speed controlled winch. Cable grip with swivel, drum with breaking shoe and wheels of 80 cm O.D. positioned

on top of the poles. Parameters like varying pulling speed (10 ... 30 m/min) and tension, also pulling jerks up to 5 kN have been introduced which, according to the hired specialist, will never be exceeded in real field installations. For cable jointing, which is being done 3-5 m above ground, a water-tight splice housing was developed consisting of two Al-half shells. Cable inlet and outlet are at the same side of the housing which is mounted in such a way that they are directed toward the top of the pole. Splicing of the fibres is performed by arc fusion.

Field installation for an electrical utility company

A 4.4 km link between two switching stations has been installed on a 220 kV HT line supported by 11 poles with max. span length of 385 m. A typical pole construction and the position of the aerial cable within the shaft is shown in Fig. 9. The sag of the optical cable is smaller ($\approx 2.5\%$) than that of the HV conductors and calculated such as to avoid clashing in case of lateral swinging by wind. Typical parameters of the 385 m span are:

Temperature °C	sag/m	tensile strength/N
- 20	7.9	3020
+ 20	8.7	2780
+ 40	9.0	2670

with vertical ice loading (0.6 kg/m) and, lateral wind loading (0.5 kg/m) according to VDE-regulations. The longest cable section bridging 5 poles was 1426 m, the shortest 280 m between two adjacent poles. Installation was smoothly without problems and to the satisfaction of the workers.

Overall link attenuation after splicing is 17.3 dB and 17.7 dB, respectively. Optical characteristic will now be monitored for half a year, before a PCM 30 system (2Mb/s) will be connected by mid 1983.

Conclusion

It has been shown that a metal free optical fibre cable can be constructed and fabricated which is capable to bridge very long span length at high tensile forces. Attenuation and dispersion values show very suitable results for applications at electrical utility companies. Regarding the transmission characteristics this all-dielectric design makes full use of the specific fibre advantages, i.e. non-interference. From the installation point of view this cable

is easy to handle due to its low weight, small dimensions, which also results in small additional loading on the poles.

References

1. U. Oestreich, G. Zeidler, P. Bark, Fibre Optic Cable for Aerial Application, 29th International Wire and Cable Symposium, Proceedings Nov. 1980.
2. H. Benndorf, H. Doering, H. Dagefoerde and Th. Pfeifer, Fiber-optic for Transmission of Information on High Voltage Overhead Power Lines, International Conference on large High Voltage Electric Systems, Sept. 1980.
3. O.L. Bishop, J.C. Smith, Installation of a Fibre Optic System in an Electric Power Station, 28th International Wire and Cable Symposium Proceedings, Nov. 1979.
4. H. Haag and G. Thoennessen, Selbsttragendes Luftkabel mit Lichtwellenleitern für eine 220 kV Freileitungsstrecke, Elektrizitäts-wirtschaft, Jg. 80 (1981), Heft 26



Siegfried Metz was born in Stuttgart, Germany, in 1941, where he also enrolled in the Technical University and got a M.S.E.E. degree in 1966. Until 1969 he held the position of a research assistant at the University of Florida's Nuclear Engineering Department. In 1970 he earned a Ph.D. degree in electrical engineering at the University of Stuttgart where he was then appointed as research assistant in the field of optoelectronics. He joined SEL, Cable Division, in 1978 and today is project manager of optical cable systems. He is a member of VDE, NTG and DGaO.



Wolfgang Schmidt was born in 1944. He studied physical engineering at the Ingenieurschule Wedel/Hamburg. After graduation in 1970 he started working at Farbwerke Hoechst, where he has been engaged in R&D-activities for plastics. In 1972 he joined Standard Elektrik Lorenz AG in Stuttgart, starting with R&D for plastic sheathing materials of wires and cables. Since 1975 he is responsible in the development of optical fibre cables.



Klaus Kimmich was born in 1942. He received his Dipl.-Phys. degree from the Technische Hochschule Stuttgart in 1969 and thereafter joined SEL Kabelwerk. From 1969-1978 he was engaged in developing conventional cables and cabling processes. In 1978 he joined the department of optical fibres and cables, where he is responsible for measurements since 1980.

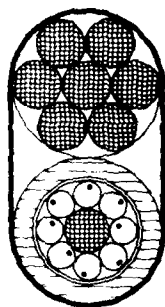


Fig. 1 Messenger Wire

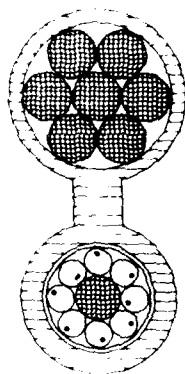


Fig. 2 Figure 8-Design

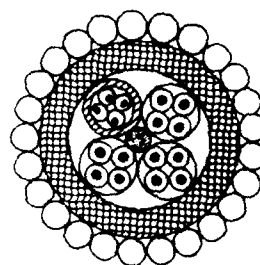


Fig. 3 Combined Cable

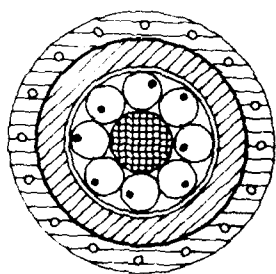


Fig. 4 Self-Supporting Cable

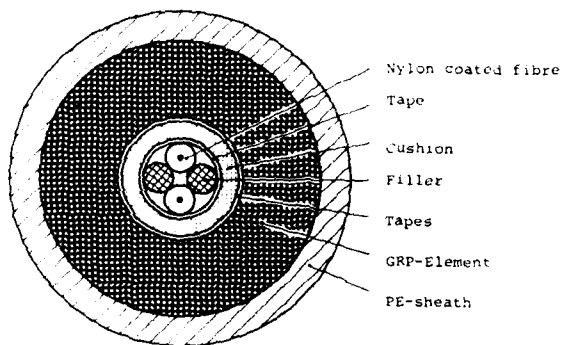


Fig. 5 New Designed Cable

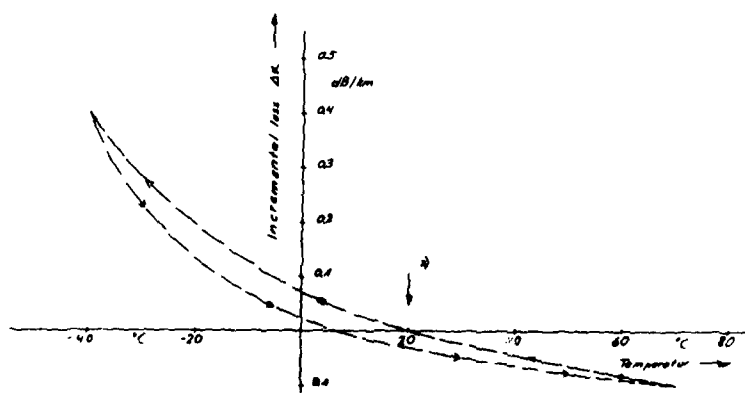


Fig. 6 Temperature cycling diagram of a cabled fibre
(* $\Delta\alpha = 0$ dB/km at + 20 °C)



Fig. 7 Dead -end Clamps

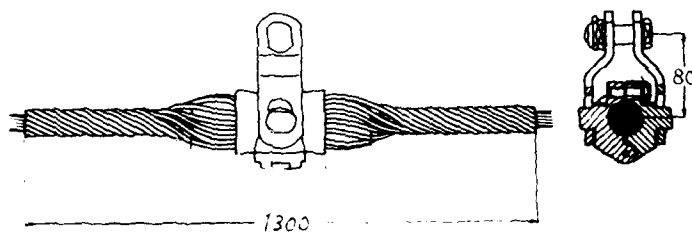


Fig. 8 Suspension Clamp

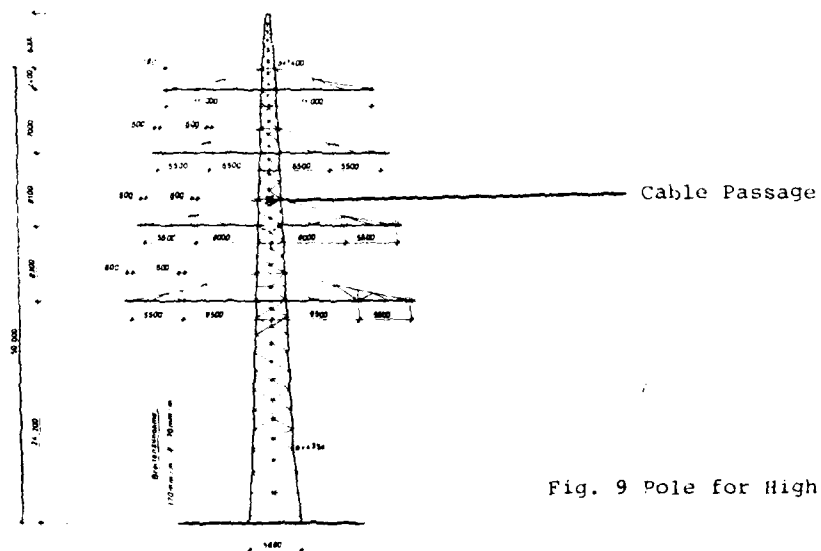


Fig. 9 Pole for High Voltage Cables

AD P000305

DESIGN AND PERFORMANCE OF A FILLED,
HIGH-FIBER-COUNT, MULTIMODE OPTICAL CABLE

B. R. Eichenbaum, M. R. Santana,
L. D. Tate, and R. Sabia

Bell Laboratories
2000 Northeast Expressway
Norcross, Georgia

Abstract

In order to avoid the use of pressurization in optical fiber cables, a filled, water-blocking optical fiber cable was developed. It consists of a stacked-ribbon core surrounded by a crossply-reinforced sheath. The ribbon core is filled with a newly formulated filling compound which remains very soft at temperatures as low as -40°F yet retains anti-slump properties at high temperatures. Cables were made and tested for cabling added loss and for environmentally induced added loss in a thermal cycling mode from -40°F to 190°F . Mechanical tests were performed to ascertain the resistance of the cables to damage from impact, bending, and twisting. In every manner, the cables performed on a par with equivalent aircore cables with cabling added loss typically 0.1 dB/km . Also, pneumatic-resistance tests proved the water-blocking capability of the filling.

fiber cable which reduces trunk outside-plant maintenance and has mechanical and optical performance similar to equivalent aircore cables.

Optical Cable Design

Design Considerations

The cable uses a modification of a crossply sheath described in an earlier paper and shown in Figure 1. Its response to tensile, bending, impact, and twist loads are well characterized, and it has performed well in the field.

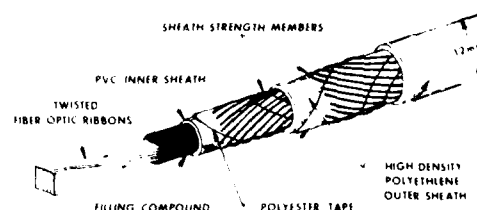


FIGURE 1 FILLED LIGHTGUIDE CABLE

Introduction

The intrusion of water into optical cable presents two hazards to reliable transmission. If the water freezes, the ice may distort fibers next to it and result in microbending loss.¹ If the water carries in other contaminants, they may hasten the aging of or react with cable materials and likewise distort the cable structure and induce microbending loss. One way of inhibiting water intrusion is to pressurize the cable with dry air. The drawback here is that it complicates outside-plant maintenance.

Experience with polyethylene-insulated copper cable has shown that filling the voids between wires with a water-blocking agent effectively inhibits longitudinal water migration. Then, in case of a breach in the sheath, water intrusion is limited. In this paper we describe a continuously filled, multimode optical

Installation and service conditions of the filled version will be basically the same as those for the aircore version. The considerations that led to the stacked-ribbon core geometry for the aircore cable of the earlier paper are still valid, e.g., ease of mass array splicing and high spatial efficiency. In the filled cable, the remaining room in the core is filled with an oil-extended rubber which blocks longitudinal migration of water.

By its very nature, fibers in filled cable are in more intimate contact with the cable than in aircore cable. This presents both materials and processing challenges. Contact forces on the fibers are more pervasive in filled cable and this enhances the potential for microbending loss. To lessen the contact forces, a very soft filling compound is needed. It must remain soft at the lowest service temperatures yet resist flow at

elevated temperatures. It must also process well during cable manufacture. A new compound (a modification of FLEXGEL) was formulated at Bell Laboratories to meet these requirements at low cost and is reported on in another paper at this Symposium³. To further minimize the influence of even this very soft material, we used thin-layer, dual-coated^{3,4} optical fibers which are currently being used in the Bell System standard lightguide trunk transmission system, designated FT3.⁵ The thin coating is particularly valuable in this high-space-efficiency optical cable.

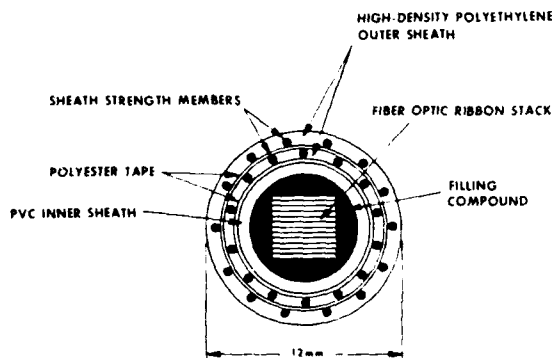


FIGURE 2. FILLED CABLE CROSS SECTION

Sheath Design

Figures 1 and 2 show exploded and cross-sectional views of the sheath design, respectively. The filled core is surrounded by a tube-extruded inner sheath of poly(vinyl chloride) (PVC). Over this, a polyester tape is applied which is in turn covered by reinforcing wires and a pressure-extruded, high-density polyethylene (HDPE) layer. This sequence of polyester tape, reinforcing wires, and pressure-extruded HDPE layer is repeated to complete the cable. The two layers of wires have opposite lay directions, and their lay lengths are adjusted to eliminate the tendency to twist under a tensile load. This sheath differs from the air-core crosply design described earlier² both in the elimination of a thermal wrap under the inner sheath and in the substitution of PVC for HDPE as the inner-sheath material. Details of the sheath design rationale and its tensile, bend, impact, and twist performance are given in Table I. The nominal weight has increased to 92 lb/kft from the aircore value of 80 lb/kft.² Both weight and tensile stiffness will vary slightly depending on fiber content.

Table I

Property	Value*	Comments
Number of fibers	12-144	Ribbon structure
Outside diameter	0.48 in.	
Weight	92 lb/kft	
Tensile stiffness	1800 lb/%	
Tensile load	600 lb	Assumes 5×10^4 psi fiber proof-test level and safety factor
Bend radius	9 in.	Includes a safety factor
Single impact	30 ft-lb	0.25-inch radius striking mandrel
Cyclic impact	400 cycles	5 ft-lb impact, 0.5-inch radius striking mandrel
Cyclic twist	2000 cycles	$\pm 90^\circ$ of twist in 66 in., simultaneously rolled over a 7-inch-diameter pulley
Cycle bend	2000 cycles	$\pm 90^\circ$ bend over a 4.9-inch radius

*The criterion for the ratings is no sheath and/or fiber damage at 23°C.

Differential Length

The fractional difference in length between unstrained core and unstrained sheath we call differential length, ϵ_{DL} . If the core ribbons were shorter than the sheath, there would be a positive ribbon strain when no external load is applied to the sheath. In such a case we denote $\epsilon_{DL} > 0$. We designed this cable with $\epsilon_{DL} < 0$ so that we incur no load-rating penalty from built-in fiber strain. If ϵ_{DL} is made too negative, transmission characteristics suffer as a result of microbending losses when the core ribbons buckle excessively to make up for their excess length. A variety of ϵ_{DL} 's were tested to arrive at a design window. The cabling loss performance and environmental loss performance of the cables were measured using ϵ_{DL} as a parameter.

Cable Performance

Cables were made using fibers having a graded-index core with a diameter of 50

μm , a cladding diameter of 125 μm , and a Δ = 1.3%. Dual coatings were used having a thermoplastic primary layer and a thermoset secondary layer. Overall coating thickness was approximately 0.24 mm. The core of each cable contained four ribbons. The core is designed to allow a maximum of twelve ribbons.

TABLE II
ADDED LOSS,
FIBER \rightarrow CABLE

CABLE #	ϵ_{DL}	0.82 μm ADDED LOSS (dB/km) ± 0.1
1009	-0.01%	0.13
1010	-0.03%	0.06
1005	-0.08%	0.13

Cabling Added Loss

Table II shows cabling added loss incurred when going from the fiber stage to the cabled condition with differential length as a parameter. In all three cases the ribbon is longer than the sheath so that various degrees of buckling are present. However, the performance remains essentially constant over the range $-0.08\% < \epsilon_{DL} < -0.01\%$. That the minimum added loss occurred in cable #1010 is not considered experimentally significant.

Environmental Added Loss

Table III shows the environmental added loss measured over the temperature range from -40°F to $+190^\circ\text{F}$ including an extended (720-h) high-temperature exposure at 190°F to simulate aging. In environmental testing of optical cables, the low-temperature performance is particularly notable since all the structural components of the cable contract more than the optical fibers. The fibers are then in compression and microbending losses tend to result from fiber buckling. Furthermore, it has been shown that polymeric shrinkage from relaxation of processing-induced strains (shrinkback) can occur at elevated service temperatures.⁶ At a subsequent low-temperature exposure, the mechanical effects of thermal contraction

TABLE III
ENVIRONMENTAL ADDED LOSS
(dB/km) (± 0.05)

TEMP. ($^\circ\text{F}$)	REEL # (ϵ_{DL}) \rightarrow	# 1005 (-0.08%)	# 1009 (-0.01%)	# 1010 (-0.03%)	# 1010 (-0.03%)
	(TEST POSITION)	(FLOOR)	(FLOOR)	(FLOOR)	(REEL)
75 (REFERENCE)		0	0	0	0
-40		0.10	0.11	0.14	0.12
+15		-0.03	-0.01	-0.01	-0.06
75		-0.01	-0.03	-0.04	-0.06
190 (AFTER 720 hr.)		0.03	0.08	0.06	-0.01
75		-0.04	0.00	-0.03	-0.10
-40		0.26	0.23	0.38	0.17
+15		-0.01	0.02	0.05	-0.08
75		-0.06	-0.01	-0.01	-0.05

and shrinkback are additive and result in a severe but realistic test of the transmission stability of the cable.

To be able to distinguish between the effect of thermal contraction and the effect of combined thermal contraction and shrinkback, we cycled the cables as shown in Table III. An initial low temperature excursion to -40°F and $+15^{\circ}\text{F}$ checked solely the response to thermal contraction. After aging at 190°F for 30 days, the second set at -40°F and $+15^{\circ}\text{F}$ measured the response to combined thermal contraction and shrinkback. All exposures other than the one at $+190^{\circ}\text{F}$ were for two days.

The cables shown on Table III are the same three as in Table II except that cable #1010 was cut into two 0.5-km sections. The samples on the floor in three-meter-diameter loops were able to respond fully to thermal dimensional changes while the one on the reel was relatively constrained. In any field environment, there is always some constraint on dimensional changes imposed by either the messenger wire in aerial installations or friction from the duct or earth in underground and buried installations. Therefore, the reel response may be considered indicative of field performance at the respective temperatures. The floor response, though unrealistically severe in terms of in-service effects, provides us with an enhanced sensitivity for comparing one cable to another.

The most severe response came when the effects of maximum thermal contraction and shrinkback were simultaneous, at the second -40°F exposure. We view this temperature as an extreme minimum for aerial plant while the $+15^{\circ}\text{F}$ level is representative of an extreme minimum temperature for underground and buried plant. No experimentally significant change is seen for any of the samples at $+15^{\circ}\text{F}$ either before or after aging.

Fluid Migration

In order to expedite testing of the water-blocking ability of the cable filling, a low-pressure pneumatic-resistance test is employed. Two psi of air is applied to the core at one end of a 30-cm length. In the many such samples tested, no air has evolved from the core at the other end. When one considers the difference in viscosity between water and air and the average hydrostatic pressure gradients one may expect from elevation variations, successfully passing this test implies resistance to long term, pressure-driven water migration. Furthermore, the almost 100% fill essentially prevents any possible deleterious effects of capillary

water transport by eliminating places where water may accumulate.

Summary

We have described the design and performance of a filled, high-fiber-count multimode optical cable. This design, an outgrowth of an earlier aircore crossply design, is being used in the Bell System standard FT3 lightguide trunk transmission system. It performs optically and mechanically on a par with the aircore crossply design over the entire outside plant thermal environment. Its water-blocking capability reduces trunk outside plant maintenance.

Acknowledgements

Many people at Bell Laboratories made contributions to the success of this project. Special thanks go to T. B. Eaton for mechanical testing and M. Y. Smith and L. L. Swift for optical and environmental testing.

References

1. H. Horima, T. Yamanishi, S. Tanaka, H. Kumamaru, T. Nakahara, and K. Ishihara, "Jelly-Filled Optical Cable," *Fiber and Integrated Optics*, 3 (1980) pp. 149-163.
2. P. F. Gagen and M. R. Santana, "Design and Performance of a Crossply Lightguide Cable Sheath," *Proc. 28th International Wire and Cable Symposium*, (1979) pp. 391-395.
3. A. C. Levy and R. Sabia, "Blending of a Block Copolymer Thermoplastic Rubber for Specific Wire and Cable Applications," *31st International Wire and Cable Symposium* (1982).
4. L. L. Blyler, Jr., A. C. Hart, Jr., A. C. Levy, M. R. Santana, L. L. Swift, "A New Dual-Coating System for Optical Fibers," *Eighth European Conference on Optical Communication, Cannes, France*, (1982).
5. M. I. Schwartz, "Design and Performance of the FT-3 Lightguide Trunk Transmission Medium," *Proc. International Conference on Communication, Denver, Colorado*, (1981), Paper 6.1.
6. G. S. Brockway, P. F. Mahr, and M. R. Santana, "An Analysis of the Environmental Behavior of Fiber-Optic Ribbons," *Proc. Sixth European Conference on Optical Communication, York, United Kingdom*, (1980), Paper 12.1.



Bernard R. Eichenbaum received a B.S. degree in Physics from City College of City University of New York in 1963 and M.S. and Ph.D. degrees from New York University in 1965 and 1969. Since 1972 he has been employed by Bell Laboratories at Norcross, Georgia, where he is a member of the technical staff in the Lightguide Technology Department. He has worked on optical fiber cables and coatings.



Louis D. Tate is a member of the technical staff in the Lightguide Cable Group. Since joining Bell Laboratories in 1960 he has worked on microwave circuit design, telephone apparatus design and design of cabling machinery and associated control circuitry, his current activity. He has three patents on telephone equipment.



M. R. Santana (Manuel) is supervisor of the Lightguide Cable Group. The group is responsible for developing a family of lightguide cables for the Bell System lightguide communications systems.

Since joining Bell Labs in 1970, he has been involved in multipair cable development and in lightguide cable design, analysis and testing. Manuel has a Bachelor of Science degree in Electrical Engineering from the University of Hartford and a Master of Science degree in Electrical Engineering from Georgia Institute of Technology. He is a member of the IEEE and of Kappa Mu, and his hobbies include varied sports activity.



Raffaele Sabia, a graduate of St. Francis College of Brooklyn (B.S.) and Polytechnic Institute of Brooklyn, (Ph.D.), was employed by Polymer Chemical Division of W. R. Grace prior to joining Bell Telephone Laboratories in 1963. Since 1963 he has been active in the research and development of materials for application in the wire and cable area. Since 1967 he has been supervisor of the Chemical Engineering Group in the Transmission Media Laboratory.

FLAME RETARDANT HALOGENFREE THERMOPLASTIC TELECOM INDOOR WIRING

H.G. Dageförde, W. Berchem, H.A. Mayer

AEG-Telefunken Kabelwerke AG
West Germany, Mönchengladbach 2Abstract

Flexible telecommunication cables and jumper wires are packed and formed as multipaired units in switching and main-repeater stations.

Due to high values of electronic equipment, telecommunication systems and buildings, the following properties are required in case of fire:

- all cable and wire components contain no halogens
- no flame propagation, self extinction, no dripping
- low smoke density, reduced toxicity, calorific values.

Electrical and mechanical properties are to be similar to PVC cables on the whole.

The approach discussed here makes use of non-crosslinked, thermoplastic materials which can be processed in existing, conventional extrusion lines economically.

The new thermoplastics are suitable for insulation and sheathing, as a substitute for some plastics. Typical and standardized cable designs and their properties are shown.

Introduction

Outbreaks of fire in telecommunications systems are on the increase since many years. In accordance with the state of technical development, these systems are wired-up with PVC-insulated cables and conductors. Damage compensations paid out to commercial policy holders by the fire insurance companies have increased by a factor of about four during the last 10 years¹. Secondary damage is greater by a factor of 10 to 20 compared with the primary fire damage, usually caused by the presence of PVC.

In a fire, one kilogram of PVC can discharge the same quantity of hydrogen chloride to the environment, as is contained in a liter of hydrochloric acid.

In Switzerland, the statistical average amount of damage compensation paid out by the insurance companies amounts to about 66 DM per year per head of the population².

Modified PVC materials designed for reduced release of HCl, were unable to achieve any significant solution.

But the problem was fixed at the first attempt by the development of flame-retardant crosslinked materials which do not contain halogens. This first generation of halogen-free flame-retardant crosslinked cables was introduced in 1980^{3,4,5,6}.

The crosslinked (flame-retardant, halogen-free, insulation materials show some disadvantages compared with the conventional thermoplastic materials (which, however, drip, burn and/or release corrosive gases in the case of fire), such as: larger diameter, more difficult insulation, low-contrast color coding and considerably higher manufacturing costs.

A second generation of halogen-free cables and conductors was reported at the IWCS 1980^{3,4}. These used non-crosslinked, now thermoplastic materials with flame-retardant properties. In the case of fire, these materials do not drip, produce almost no smoke and they pass the stringent fire-tests. Therefore thermoplastic halogen-free materials have been promoted to serial production, with a whole range of new cable designs resulting therefrom.

The further development of this new generation of cables is presented here. As far as the properties of the insulation and sheath materials are concerned, these new cables are at least equal to conventional cables in performance. The materials concerned are non-crosslinked and can be extruded by conventional means.

Tasks and Requirements

The increasing packing density in switching stations are continually being reduced in size, aggravates the potential danger of PVC fires, so that the desires for telecommunications systems are summed-up as follows:

"Low cost wiring material with no drip or halogen release in the case of fire. It should not propagate flame and must itself extinguish. The flame density must be low. The electrical performance and installation procedure should differ as little as possible from that of previous material."

It is not a primary requirement imposed on these cables and wiring materials, that they shall provide special emergency duty capabilities in the case of fire. It is certainly possible to meet such a condition, but this would call for special constructional measures in particular cases.

Some of the new materials possess "inherent emergency duty capabilities", i.e. in the case of flame exposure caused by external fire, they show a longer time delay before mutual electrical contact between the circuits appears.

The approach adopted to fulfil low cost requirements with crosslinked expensive materials and procedures, i.e. to avoid the use of crosslinking or energy sources (high-energy radiation, thermal energy, vulcanization).

The materials were required to be similar to thermoplastics such as PVC or polyethylene (flame-retardant), i.e. approximately equivalent electrical performance was called for, with low toxicity and no release of corrosive gases.

The oxygen index is a measure for the flame retardancy and self-quenching. It should lie in the region of 30% for insulation of conductors and 35 and 40% for cable sheath materials.

Thermoplastic Materials

So far almost exclusively polyethylene and PVC have been used for standardized and for installation cables. Recently new thermoplastic flame-retardant materials have been introduced for halogen-free cables, apart from crosslinked materials¹⁴.

Particularly the insulation materials have been improved in the meantime. A whole range of such materials has been established.

Tables 1 and 2 list the chief properties of these materials, which are mainly based on special flame-retardant compounds of polyolefines or ethylene-copolymers with aluminium hydroxides, which release water when exposed to fire:

- Wall Insulations
- HXFR: crosslinked compounds which are referenced here for comparison.
 - HFR-2 (POAH) is a group of thermoplastic materials with high performance electrical characteristics, for use as insulation wall of cable conductors. (Types A and B)
 - HFR-3 (POAH) is a thermoplastic material with electrical characteristics similar to PVC, but with improved behaviour in the case of fire and enhanced emergency duty capability (circuit integrity).
 - HFR-4 (PPOmod.) is a modified polyphenylene oxide

Table 1

Halogen-Free, Flame-Retardant Insulating Materials

Properties in case of fire	HXFR	HFR-2	HFR-3	HFR-4
Basic Material	X-POAH	POAH	POAH	PPO mod.
Oxygen Index	28	30	45	35
Halogen	0	0	0	0
Pyrolysis Products (800°C, 1.2 hr)				
pH			> 4	
Conductivity $\mu S/cm$			< 4	
Tensile Strength N/mm^2 min. typ.	5	5	5	5
Elongation at break	160	250	150	150
Heat Compression $\leq 5\%$ at 150°C	150	80	80	150
Tensile Strength & Elongation min. Retention aft. 7d/80°C	70		75	15
Flame Test IEC				
IEC 20 191 WGI2			passed	
VDI 0472 Flame A			7	passed
Calorific Value MJ/l	25	26	21	40
Temperature Rating VDE 0303 (25 000 hrs)	90	70	80	70
Gold-Wrap-Test		-25		-15
Volume Resistivity $\Omega \cdot cm$ at 20°C	$\geq 10^{11}$	$\geq 10^{11}$	$\geq 10^{11}$	$\geq 10^{11}$
70°C	-	$\geq 10^{11}$	$\geq 10^{11}$	$\geq 10^{11}$
90°C	$\geq 10^{11}$	-	-	-
Dielectric Constant 20°C	3,6	4	6	2,6
Dielectric Loss Factor 800 C 20°C				
20°C	0,02	0,05	0,07	0,01

Notes: 1) Winding test passed at 1 day

2) Test result variable depending on conductor diameter and wall thickness; critical in the range of 0,3-0,5 mm

Explanations: H = Halogen-free

FR = Flame Retardant

X = Crosslinked

POAH = Polyolefin-copol.-Al-Hydroxide

PPO = Polyphenylene oxide

The table 2 compares the thermoplastic non-crosslinked compound HM2 with a crosslinked compound HXMI¹.

The behaviour of the new thermoplastics in a fire is at least as good as that of crosslinked materials, but cables with sensitive internal structure made of polyethylene can be sheathed therewith without suffering thermal damage as would be the case with thermal vulcanization, for example CV (continuous vulcanization).

In the meantime the thermoplastic compound type HM2 has been proved satisfactory also for electric power cable constructions with XL-PE or EPR insulation. HM-2 has also been used for accessories such as sleeves.

A range of new telecom cables which pass severe flame tests have been successfully constructed with HM-2. These do not drip and produce little smoke in fire.

Table 2
Thermoplastic, Highly Flame Retardant
Compound HM2 for Sheathing
(Compared with Crosslinked HXMI)

Properties in case of fire		HXMI	HM2
Basic Material		X-POAH	POAH
Oxygen Index	%	40	45
Halogen	%	0	0
Pyrolysis Products (600 °C, 1.2 hr)	pH	>4	>4
Conductivity (VDE 0472 Part 813)	$\mu S/cm-1$	<40	<40
Tensile Strength (20 °C, VDE 0472)	N/mm ²	7-9	7-8
Elongation at Break	%	>150	>150
Temperature Rating (VDE 0303 25000 hrs)	°C	90	90
Heat Compression $\leq 50\%$ (on Cable)	°C	~100	~100
Calorific value	MJ/l	22	21
Smoke Density on Cable Optical Test Integrated in Oven Test VDE 0472/5408 °C	%	<10	<10
Cold-Wrap-Test ≤ 12.5 mm	°C	-15	-10
Elongation at -15 °C	%	≥ 20	≥ 20

Explanations: H = Halogenfree, highly flame retardant, based on POAH
X = Crosslinked
M = for Sheathing

Cable Constructions

Halogen-free cables have been come into use in electric mains systems as:

- o indoor installation cables, as an equal performance substitute for conventional standard types (national specification¹⁰).
- o special cables for certain specific applications

The letter "H" (for halogen-free) in the cable designation guarantees that this cable meets the test conditions of German industrial standards^{11,12} and that it has the following properties with respect to fire:

halogen-free, non-dripping, little smoke;
almost toxicologically harmless

Fig.1 shows some halogen-free cables with "improved characteristics in the case of fire", conforming to the standard types range of specification VDE 0815 (draft). They are manufactured using thermoplastic material and show the following features, among others:

- ① I-HH 10x2x0,6, star-quad with unit stranding, ring marking; installation cable up to 100 conductor pairs. No metallic shield.
- ② I-H(St)H 10x2x0,6, conductor pairs in layer stranding; installation cables up to 100 conductor pairs. Static metallic shield.
- ③ IE-LiH(St)H 8x2x0,5 mm², conductor pairs in unit stranding, 8 conductor colours in each unit, bunched conductors, as electronic installation

cables up to 80 conductor pairs. Static metallic shield.

- ④ IE-H(St) 8x2x0,8, conductor pairs in unit stranding, 8 conductor colours in each unit, solid copper conductors, as electronic installation cables up to 80 conductor pairs. Static metallic shield.

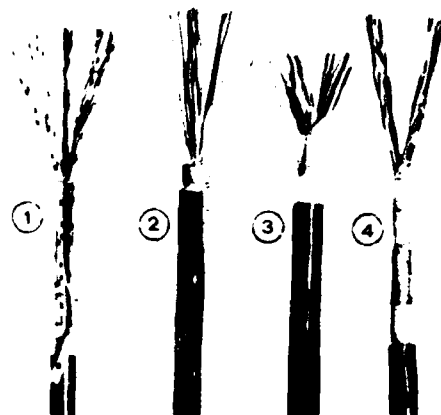


Fig. 1
flame-retardant halogen-free standard cables

Fig.2 shows some special cables for particular applications. So far these cables have not been type-standardized, but with their "improved characteristics in the case of fire" they fully conform to the requirements of the specification^{10,11}.

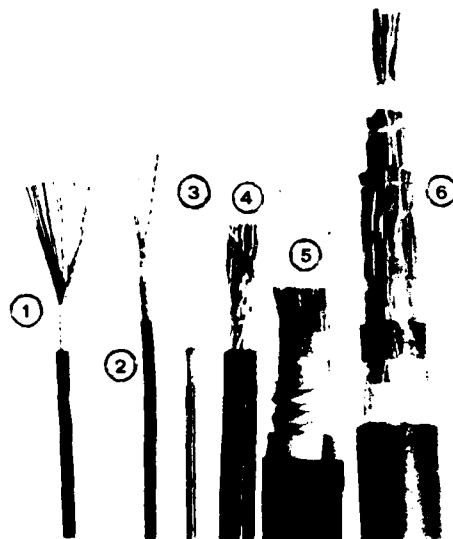


Fig. 2
flame-retardant halogen-free special cables

The cable sheath made of POAH compound (HM2) is common to all these special cables. In all cases the insulation of the cable core consists of halogen-free material, but has been selected to suit the particular application.

Features:

- ① I-2YH 10x2x0,6, star-quads in bunch stranding with polyethylene wall insulation. No metallic shield. Intended as high performance signal transmission installation cables, e.g. for radio frequency signals.
- ② IE-HCH 4x2x0,8 in pair stranding. Multicolour ring marking. Intended as computer system cables with copper wire braiding shield.
- ③ Coaxial cable similar to RG62 (MIL). Hose/helical construction.
- ④ PCM distribution cable, 60 double conductors in star-quad stranding in units, colour coding according to PTT standard, polyethylene conductor-wall-insulation.
- ⑤ AJ-PLDHH 50x2x1,4 F, as trackside long-distance cable for underground railway sections. Conductors with paper insulation. Corrugated aluminium sheath with halogen-free fill mixture and POAH layer sheath. This cable passes a 3 hour emergency running test (circuit integrity) according to¹³.
- ⑥ I-HH(St)H 7x2x1,4/84x2x0,8 Bd as data / telecommunications cable for mains protection systems.

Electrical Data

The electrical and transmission performance data in normal operating condition correspond to those of conventional cables, with a tendency to be even better^{14,15}.

Installation procedure

Soldering operations are greatly facilitated, because the higher thermal stability of the conductor insulation avoids thermoplastic melting due to thermal conduction of the copper conductor during soldering operations. Stripping techniques followed by cold contacting (e.g. wire wrap and termpoint techniques) are possible in separate procedure steps: stripping first, then contact establishment. Combined work procedures still require modification by the US equipment manufacturers.

Press-contacting procedures by piercing through the insulation sheath are possible using currently customary methods.

Behaviour in the case of fire

Tests carried out on single conductors

The fire test behaviour of halogen-free flame-retardant insulation materials in thin layers on connecting wires and cable conductors is about the same in principle as that of PVC insulation, i.e. about equivalent flame tests are passed, but without the negative secondary effect such as liberation of corrosive decomposition products, generation of smoke or toxic hazards.

As is already known from work with PVC-insulated wires, the results obtained for flame retardancy tests on single conductors depend on the geometric dimensions, i.e. on the conductor diameter and the

insulation layer thickness. This is true too for conductors insulated with halogen-free flame-retardant materials.

For example, the test according to VDE 0472/804 with test flame A, or IEC 331, is passed in the case of large dimensions, but conductor diameters less than 0,8 mm and insulation layers thinner than 0,6 mm prove critical. For this reason it is contemplated in WG 12 to devise special tests in particular for small dimensions, for example a test based on the draft version of IEC TC 20/191/WG12 in which the test wires are positioned at an angle of 60° with the bunsen burner held at right angles thereto. The flame exposure time is 5 seconds, whereby the burned region must not extend as far as the 75 mm mark if the test is to be considered passed.

Taking the testing method at present under discussion, the results already presented in Table 1 were obtained. It is evident therefrom that these results do not depend directly on LOI.

The behaviour of bunched telecommunications conductors towards fire

Thick vertical or horizontal bunches of conductors are present in telecommunications switching stations. Each individual conductor consists only of a copper conductor surrounded by an insulation sheath. Such bunches of conductors lack the common protective sheath which provides additional fire resistance for a cable. Non-sheathed bunches of conductors are found as patching trunks or as cable ends from which the sheath has been stripped off to permit distribution of the individual core conductors onto soldering tagstrips, wiring harness or other term. devices.

In switching stations these unprotected conductors are exposed to the same fire conditions as the cables. Thus the fire behaviour of various conductor types has been investigated in a shaft furnace (Fig. 3). In each test, 16 adjacent conductors were exposed to the ignition flame.

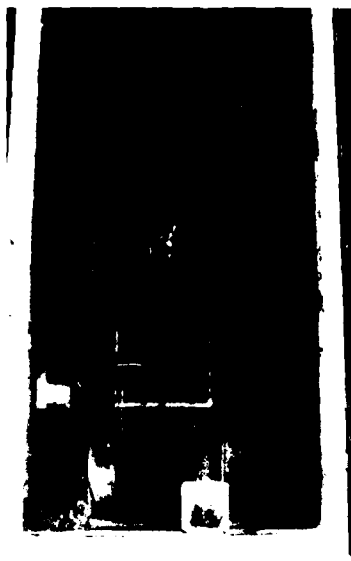


Fig. 3 Bunched telecommunications conductors in shaft furnace test

POAH(B) = Polyolefine-copolymer-aluminiumhydroxide
 POAH(A) = polyolefine-copolymer-aluminiumhydroxide
 (both material type HFR2)
 PPO = Polyphenylene oxide

Copper conductor diameter = 0,8 mm
 Insulation layer thickness = 0,3 mm

The burnt length as a function of the burning time is shown in Fig.4 for various thermoplastic conductor insulation materials. An unambiguously evident point of "self extinction" was found only for PPO conductor insulation material.

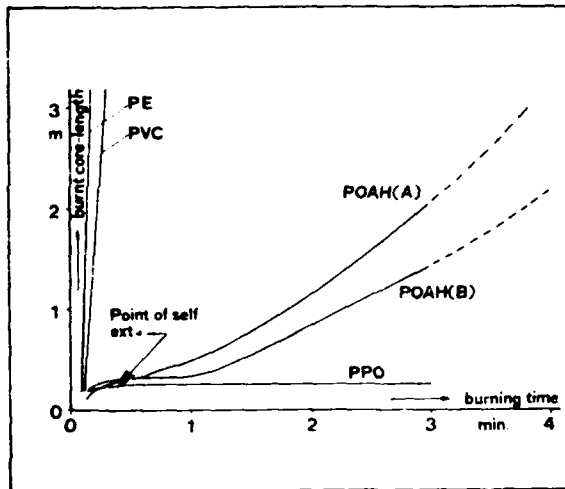


Fig. 4
 Burnt length of bunched conductors in the vertical shaft furnace test as a function of burning time

Tests on cables, individually and bunched

The great advantages of the new halogen-free compounds, in particular the thermoplastic ones, compared with PE, PVC and halogen-containing elastomers, are clearly manifest in fire tests carried out on cables. This is true for tests made on single cables with the Bunsen burner (IEC 332; VDE 0472/804, test type A or B) as well as in particular for the grouped configurations (IEEE-383, and in the vertical shaft furnace test according to VDE 0472/Part 804, test type C).

The new thermoplastic materials pass such severe tests even under difficult conditions (such as certain constructions with non-flame-retardant insulation materials based on PE, XLPE or EPR), whereas PVC-insulated cables do not pass these tests and liberate large amounts of smoke and corrosive gas when exposed to fire.

The test results are shown in Table 3.

Table 3
 Fire test results of cables in the vertical shaft furnace test

Material	Test type	Flame	Smoke	Corrosive gas
PE	A	Pass	Pass	Pass
PVC	A	Fail	Fail	Fail
POAH(A)	A	Pass	Pass	Pass
POAH(B)	A	Pass	Pass	Pass
PPO	A	Pass	Pass	Pass
PE	B	Pass	Pass	Pass
PVC	B	Fail	Fail	Fail
POAH(A)	B	Pass	Pass	Pass
POAH(B)	B	Pass	Pass	Pass
PPO	B	Pass	Pass	Pass
PE	C	Pass	Pass	Pass
PVC	C	Fail	Fail	Fail
POAH(A)	C	Pass	Pass	Pass
POAH(B)	C	Pass	Pass	Pass
PPO	C	Pass	Pass	Pass

Smoke Density

To determine the smoke density produced in the combustion test, a photometric measurement is carried out above the shaft furnace (VDE 0472/804/C) according to Fig.5, in the exhaust air flue. This procedure has been defined in a factory specification¹⁴. An international specification is under consideration. The readings obtained by this method (percentage light transmission) show good reproducibility when the airflow rate is held constant. Ambient light does not interfere¹⁷.

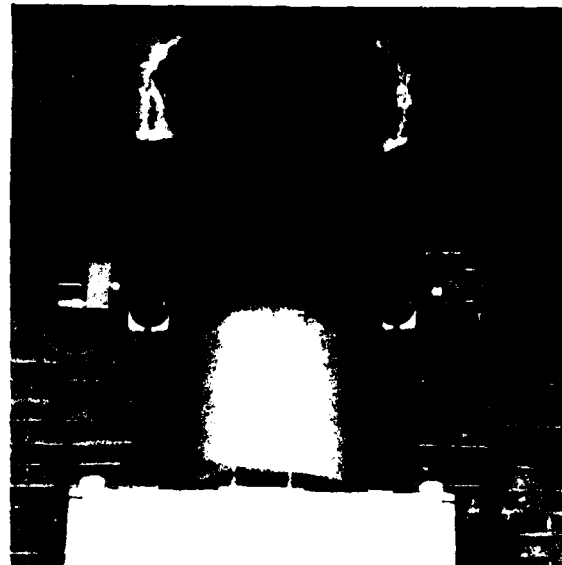


Fig. 5
 Smoke density determination on the vertical shaft furnace

Fig. 6 shows the smoke density as a function of time, recorded for a PVC-insulated cable and for an equal performance halogen-free cable.

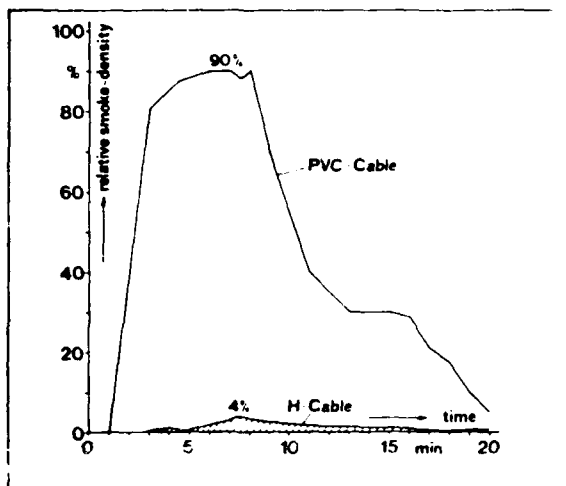


Fig. 6

Smoke density as a function of time during the combustion test

Non-corrosive nature of the combustion gases

Halogen-free materials must not release any corrosive gases when they are exposed to fire. This is verified according to VDE^{10,3} by exposing the materials to 800 °C temperature in a current of air. The pH-value must not drop below 4 in this test, and the electrical conductivity must not rise above 100 µS/cm. This requires that the materials shall not contain any appreciable amounts of sulphur, phosphorus or nitrogen compounds which form acid or otherwise corrosive decomposition products when exposed to fire.

Low toxicity

Hot combustion gases are always deleterious for lung respiration. As far as cooled combustion gases present in a room are concerned, it is important to avoid or at least greatly reduce toxic components. By virtue of the freedom from halogen compounds, caustic components are missing in the combustion gases. In the case of smouldering fires, carbon monoxide also requires special attention as possibly produced toxic component. Production of carbon monoxide is reduced to a minimum for the compounds with metal hydroxides.

Pyrolysis products are generated at 600 °C in a procedure which has been standardized according to DIN⁸ and they are checked according to DIN⁹. Very direct assessments are possible on the basis of biological tests carried out by a medical research institute¹³, in which the survival of test animals was observed by monitoring certain physiological para-

meters (percentage of carboxyhaemoglobin in the blood). These neutral test results now exist for the indoor cables discussed in this paper and certify for their negligible toxic risk.

Electrical transmission performance during flame exposure

For electric power cables, various specifications define functional integrity in the case of fire as "capability of sustaining an applied voltage between the cable conductors". This feature of "insulation conservation" corresponds to the actual functional task of an electric power cable.

Indoor communications system cables, however, must satisfy a more diversified range of expected performance requirements, such as:

- Dielectric strength greater than 60 Volts conductor-conductor (exchange battery circuit, calling current)
- Insulation resistance between conductors at least 10 kΩms (non-diversion of the microphone energizing current)
- Crosstalk-attenuation (voice circuit integrity)
 - for PCM : about 20 dB
 - for analog signals: about 50 dB
- Increase of line attenuation factor less than 5 dB

Fulfilment of these or similar requirements over a given period of time (20 minutes contemplated as standard, but 2 hours also being considered) is actually required only for communications cables with emergency running specifications (circuit integrity).

The standardized indoor installation cables presented in this paper do not have any constructional features which guarantee particular emergency running times. Nevertheless, these cables have some "inherent emergency running characteristics" in accordance with the use of suitable materials.

The evaluation of 10 combustion tests (VDE 0472-804/Test C) on cable type I-H(St)H 8x2x0,8 with POAH material (see above, "Cable Constructions") showed, that 73,5% of the conductor pairs were still functioning after 20 minutes flame exposure.

Fire Ballast

In interior installations cables run adjacently to horizontal or vertical bunches. The devastating effects of cable fires have been adequately described in the published literature. Suitable test procedures (e.g. VDE 0472, Part 804) simulate cable bunch fires. By "fuse cord" behaviour, cable runs can propagate the fire to other sections of the system. Two material-specific causes lead to this fire behaviour:

- The specific calorific value of one liter (1000cm³) of cable material.
- The fuse cord effect, i.e. self-sustained flame propagation along the cable after extinction of the original source of ignition.

The volume-specific combustion values (specific caloric values) for some thermoplastic non cross-linked cable insulation materials are listed in the following table 4 of approximate values:

Abbreviated Material Designation	Material Type	Used for	Combustion value MJ/l
PE	Polyethylene	Conductors Sheath	44
PVC	Polyvinylchloride	Conductors Sheath	30/27
PPO	Modified polyphen- ylene oxide	Conductors	40
POAH(HFR2)	Polyolefine copo-	Conductors	27
POAH(HFR3)	lymer aluminium	Conductors	22
POAH(HM2)	hydroxide	Sheath	21

Caloric value

Material	Caloric value (MJ/g)	Category
core 25 MJ/1	~6.5	Economical halogenfree cable
jacket 23 MJ/1	~6.5	
core PE	~6.0	
jacket POAH	~6.0	
core 40 MJ/1	~5.8	Optimum, halogenfree cable
jacket 23 MJ/1	~5.8	
core PPO	~5.5	
jacket POAH HM2	~5.5	
core PE	~8.0	Wallthickness imm.
PVC	~4.5	
core POAH 2	~4.5	
jacket POAH	~4.5	
core POAH 2	~3.5	
jacket POAH	~3.5	
core POAH 2	~6.5	Wallthickness imm.
jacket POAH HM2	~6.5	

Waltthickness imm.

Calorific values per meter of cable 80x2x0,6
insulation wallthickness 0,2 mm and 0,3 mm
cable type according to VDE 0815 I-YY resp. I-HH

Calorific value per meter of cable

1-HH with 0.3mm Ins

1-YY with 0.2mm Ins

1-HH with 0.2mm Ins

Copper diameter - 0.6mm

Specific calorific values for

PVC - cores - 30 MJ/l

PVC - jacket - 27 MJ/l

H - cores - 26 MJ/l

H - jacket - 21 MJ/l

0 20 40 60 80 100 Pairs

- International Wire & Cable Symposium Proceedings 1982 407

To determine the actually releasable thermal energy, the potential cable fire ballast values must be multiplied by so-called combustion factors (s) which are less than or at most equal to one.

Combustion factor for:

PVC and PE cables $s = 1$
H cables in vertical runs $s \sim 0.3$ to 0.6
H cables in horizontal runs $s \sim 0.1$ to 0.3

Vertical positioning of cable bunches leads to the more serious conditions in the case of fire. The thermal energy of the external supporting fire and the initiated local cable combustion ballast are additive in this case. The total heat rises and flows around the higher cable sections, so that the cable extinguishes at greater distance from the source of ignition, than in the case of horizontal cable positioning.

Behaviour in moisture environment

The specifications for indoor installation telecommunications cables (VDE 0815/1982) call for different conductor insulation and cable sheath materials according to the nature of the operating location environment:

Operating location environment	A	B	C
	dry, damp in/under plaster	dry, damp in/under plaster	dry damp in/under plaster
	permanent outdoor installation	permanent outdoor installation	-
	short distance buried run	-	-
Material type	PE	PVC	"halogen-free"

This classification according to the operational environment (A, B and C) is conditioned by the property of the utilized plastic material, to absorb and pass-through water vapour from the immediate environment, i.e. by the fact that moisture can permeate through the cable sheath into the core of the cable.

Water vapour permeation measurements carried out on membrane-type films as well as on complete cable sheaths for various installation materials, have led to the following typical results in mutual agreement.

Material	PE	PVC	"halogen-free"	
water vapour permeability	1	25	33	times the diffusion rate

Unrestricted installation buried in the ground, with undefined environmental moisture, can be achieved in cable engineering only by using metallic barriers for water vapour (aluminium layer sheath, corrugated metal sheath, etc.). In such constructions, intimate union between the metallic layer and the overlying plastic sheath is always achieved by suitable choice of sheath material and manufacturing technique. Only by this means is it possible to obtain the required moisture exclusion factor of 200 or greater, as compared to solid PE-sheath.

The same technique as for PE can be used for extrudable non-crosslinked halogen-free cable sheath material of the kind described above. In this manner it is possible to manufacture halogen-free cables on conventional sheathing plant. The moisture exclusion factor of these cables is at least 200.

Halogen-free cables with high moisture exclusion factors are installed in industrial plant where the individual buildings are scattered over the factory premises and the halogen-free indoor cables can also be buried underground for direct mutual link-up of the various stations without numerous transition sleeves for a system using separate indoor and underground cables.

Moisture exclusion factors of at least one thousand are achieved in practice. Such halogen-free indoor cables are fully equivalent to normal underground cables with regard to prevention of water permeation.

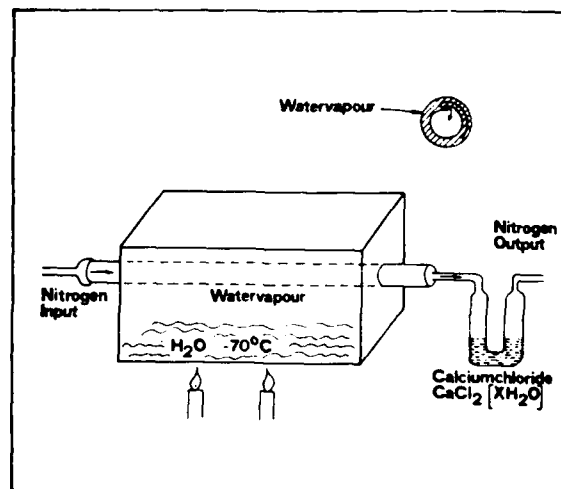


Fig. 9
measuring arrangement "Moisture Exclusion Factor"

The integrated aluminium layer sheath advantageously enhances the inherent emergency running behaviour to give longer emergency running times in the case of fire.

Manufacturing

The new cable materials can be processed in conventional extrusion lines (15 to 25 D, with water-cooling through) as customarily used for PVC and PE.

No plant capital investments are necessary for vulcanization and crosslinking, such as boilers for CV-lines. The absence of such work steps saves energy (such as high pressure steam).

It is a distinct advantage that typical telecommunications cables cores with their many thinly insulated conductors do not need to be exposed to the heat and pressure stresses resulting from sheath vulcanisation processes. Thus high-performance or special cable cores with PE, cellular PE, foam skin PE, fused discs, etc. as required for PCM, carrier frequency or coaxial cables for indoor purposes, can be protected too by highly flame-retardant sheaths without impairing their geometry and signal transmission performance.

Radiation-induced crosslinking of the protective sheath material is a procedure which is used occasionally. Such irradiation is not required for the new cables discussed in this paper. This constitutes a further cost saving factor because equipment for generating high energy radiation is not required.

The costs for crosslinking activators and crosslinking agents are avoided too. Powerful drives are required for processing on the extruder plants. The screws should produce a low compression.

Optimization of the screw design is recommended for best extrusion quality and high ejection rates. For specific requirements, special low compression two-zone screws have been developed¹⁴.

Fields of Application for Cables

The generic term "indoor" refers to enclosed regions in general, for which escape of combustion products is restricted, i.e. this term is not limited to buildings.

Indoor installations are involved for the following applications:

Application fields	Utilizer
Commercial and industrial	Power stations, hospitals, warehouses, electronic data processing stations, telecommunications centers
Public	Department stores, multistorey buildings, hotels, theatres, railways
Traffic	Railways
Ships	Merchant and naval surface vessels, submarines, offshore installations

Application fields

Application fields	Utilizer
Tunnels	Underground railways, traffic control installations
Underground mining	Ventilation shafts, feed shafts, mining safety installations, ore and cable mining
Towers	Transmitter towers, airport control towers

Halogen-free safety cables are now being used predominantly in the application fields listed above, where staff safety requirements are an important factor and a high concentration of equipment value exists.

Conclusions

Halogen-free safety cables for indoor telecommunication systems are now past the stage of primary development. They have been standardized in a first national specification. In order not to hinder further technological advances and fulfilment of economic requirements in this field, the standard specification has deliberately not yet stipulated the material type and is so far confined to a general framework of safety and signal transmission performance requirements. These general requirements can be fulfilled:

- o On the one hand by using crosslinked materials of the first generation
- o On the other hand by using the newer second generation non-crosslinked thermoplastic materials.

In this report the "second generation material" has been discussed with respect to its suitability for standardized indoor cables. Standard specification cables have been realized therewith which pass severe fire tests, do not drip in the case of fire, are self-quenching and produce little smoke and no halogen compounds in the combustion smoke. They involve negligible toxic risk and their electrical performance is at least equal to that of conventional cables. Since no crosslinking process steps are required during manufacture, the improved economic consideration for these cables are another factor promoting their extensive use. This is another contribution towards improved safety in the "plastics age".

Acknowledgements

The authors wish to express their thanks for and to acknowledge the contribution made by Mr. B. Ivanfy, Mr. W. Munro, Mr. D. S. Parmar in the development of these new thermoplastic compounds and the special screws for extrusion of these materials. Our thanks are also due to Mr. G. Hög for his work in designing and testing the cables.

References

1. Journal "Spiegel" Nr. 3/1981
2. Guzwiler, M. "Brandsicherheit: Risikobeurteilung im Kunststoffbetrieb" Swiss Plastics, 4 (1982), Nr. 15
3. Mayer, H.A., Hug, G. "New Generation of Nonhalogenated, Flame Retardant Compounds and Cables" Proceedings of the 29th IWCS, Cherry Hill, Nov. 1980
4. same authors, AEG-KABEL-Mitteilungen 3/1981
5. Mayer, H.A. "Material Conception for Halogenfree Cables"
Goedecke, H. "Design of Halogenfree Cables" Symposium Haus der Technik, Essen 26.Okt.1980
6. Harbort, H. "New Flame Retardant Halogenfree Cables for Nuclear Power Plants" 29th IWCS, Cherry Hill, Nov.1980
7. De Munck, Bury, Simpson, Devoldere: "A New, Non-halogenated, Flame Retardant Wire Insulation Based on Polyphenylene Oxide" 29th IWCS, Cherry Hill, Nov. 1980
8. German Standard DIN 53 436, 1979, Part 1 and 2 "Erzeugung thermischer Zersetzungsprodukte von Werkstoffen unter Luftzufuhr und ihre toxikologische Prüfung"
9. Herms, C.D. "Brandtechnische Anforderungen an elektrische Kabel und Leitungen für Grubenbetriebe des Steinkohlenbergbaus." Journal Glückauf, 118 (1982) Nr.1
10. VDE Specification 0472/Teil 813 "Testing of cables, wires and flexible cords; Corrosivity of combustion gases"
11. Werknorm AEG-KABEL, SR21-6.81 + DIN 53 437, 11.66
12. VDE Specification 0472/Teil 804/Prüfart C "Testing of cables, wires and flexible cords; Behaviour under fire condition"
13. VDE Specification 0472/Teil 814 "Testing of cables, wires and flexible cords; functional endurance of electric cables, when exposed to a flame-source"
14. Ivanfy, B., Mayer, H.A., Parmar, D.S.: Patents Pending
15. German Standard, DIN 4102
16. Einbrodt, H.J. "Toxizitätsprüfungen an Kabeln und Leitungen" Symposium Haus der Technik, Essen, Okt.1980
17. Goedecke, H.P., Schuppe, W.D. "Halogenfreie Kabel und Leitungen mit besonderen Eigenschaften im Brandfall." Elektrizitätswirtschaft 81 (1982) "1/2"
18. VDE Specification 0815, Draft, "Wiring cables for telecommunication- and information processing systems", Juni 1982



H.G. Dageförde is head of development- and designing-department of communications cables section in AEG-TELEFUNKEN KABELWERKE. He took his degree as Dipl.-Ing. (high.freq. and electronics) of the Technical High School Aachen and joined Kabelwerk Duisburg in 1952. He was engaged in testing, quality control, engineering and installation.



Walter Berchem. 1963 he joined Rheinische Draht- und Kabelwerke, Köln, including Kabel & Draht Co, Mannheim. 1976 - 1980 SEL (Köln), mainly in materials and technology. 1980 he joined AEG-TELEFUNKEN KABELWERKE as head of materials and technology



Hans A. Mayer. 1951 - 1956 he studied industrial chemistry and obtained his degree as a Dipl.-Ing. He was than 5 years in the plastic & rubber industry and 3 years in the chemical industry as Head of quality control and central laboratories. In 1965 he joined AEG-TELEFUNKEN KABELWERKE. As Obering. he was head in R & D materials and process engineering, now head of cable technical labs.

Address:

AEG-TELEFUNKEN KABELWERKE AKTIENGESELLSCHAFT
2 - 14 Bonnenbroicher Straße
4050 Monchengladbach 2, W.-Germany

AD P000587

LARGE SCALE FIRE TESTS OF BUILDING RISER CABLES

S. Kaufman
J. L. Williams

E. E. Smith

L. J. Probyla

Bell Laboratories
Norcross, Georgia

Bell Laboratories*
Norcross, Georgia
and

Ohio State University
Columbus, Ohio

Underwriters Laboratories
Northbrook, Illinois

Abstract

The National Electrical Code requires that riser cables have sufficient fire resistance so they will not spread fire from floor to floor in a shaft. Fire tests were conducted as the initial task in developing a test method for determining compliance with the Code. The tests provided data on the flame propagation characteristics of riser cables in a simulated riser shaft, the design of which was based on information from a field survey. The data indicated that with a large ignition source, simulating burning combustibles in a shaft without fire stops, some cables propagated fire from floor to floor; others, utilizing newer fire resistive materials, did not exhibit the same propensity to promulgate fire.

Introduction

Riser cables have a potential for spreading fire in buildings. In order to reduce this potential to an acceptable level, the National Electrical Code¹ requires that communications cables "in a vertical run in a shaft shall have a fire-resistant covering capable of preventing the carrying of fire from floor to floor." Although the intent of the Code is quite clear, the Code does not specify the means of determining compliance; it neither specifies a test method nor requires "listing" of cables by a recognized testing laboratory.

In order to clarify the Code, the Telephone Group has proposed the following for Section 800-3(b) of the 1984 National Electrical Code.

"Communications wires and cables, both metallic conductor and optical fiber types, in a vertical run in a shaft shall be listed as having fire-resistant characteristics capable of preventing the carrying of fire from floor to floor."

*Summer (1980) Employee

The important change sought by this proposal is the requirement that a recognized testing laboratory such as Underwriters Laboratories determine that the cables do not spread fire from floor to floor. In order for Underwriters Laboratories to List or Classify cables as meeting this requirement, a standardized fire test must be adopted. A program to develop a standardized test has been initiated. The program consists of several tasks to develop and analyze applicable tests conditions and assess the feasibility and need for the test. The initial task consisted of conducting fire tests to provide data on the flame propagation characteristics of riser cable in a simulated riser shaft. This paper reports the data obtained in carrying out this task.

This task was carried out in two phases. The first phase consisted of a field survey of telephone cable riser shafts. A cross section of buildings built from 1973-1980 in several geographical areas of the country were visited to determine field conditions such as shaft size, number of cables, size of floor openings and materials stored in the riser closets.

The second phase consisted of full scale fire testing. The information obtained from the field survey was used to design a fire test facility which modeled a riser shaft and to choose typical cable configurations. The tests were carried out jointly by Bell Laboratories and Underwriters Laboratories at the fire test facility in Bell Laboratories, Chester, New Jersey.

Field Survey

Bell Laboratories, assisted in part by Underwriters Laboratories, conducted a survey of seventeen buildings in Atlanta, Chicago, Miami and New York. They ranged in size from a 4 story library in Atlanta to the World Trade Center in New York and the Sears Tower in Chicago, both 110 stories. The riser shafts in these buildings are a series of vertically aligned

rooms connected by holes or slots for the passage of cable.

Various holes and slots were encountered (Figure 1). Holes, many of them fire-stopped, were found in approximately two-thirds of the buildings. The slots in the remaining third were usually 1 foot deep by 2 feet wide. Fire stopping of the slots occurred infrequently. In several cases the shaft was shared with other utilities. The typical size of a shaft devoted exclusively to telephone usage was 4 to 5 feet by 8 to 10 feet. The number of riser cables in the shaft generally varied from 1 to 5, with the exception that the largest buildings had up to 12 cables in a slot. Many of the shafts were used for storage of materials such as office supplies, Christmas decorations, files and paint.

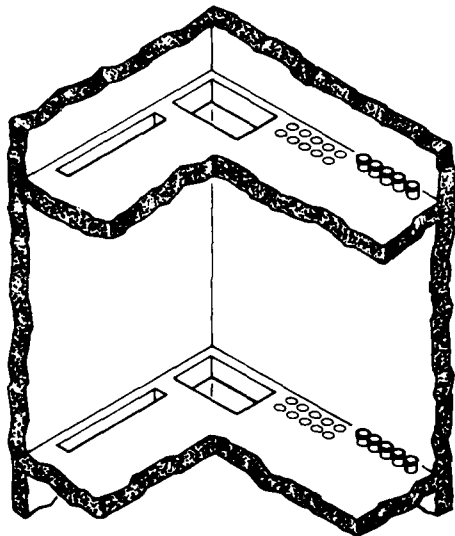


FIGURE 1. FLOOR PENETRATIONS - ELONGATED SLOT, REGULAR SLOT, 4 INCH HOLES AND 4 INCH HOLES WITH PIPE SLEEVES.

Fire Test Facility

A four by eight by twelve foot high compartment (Figure 2) simulating a section of a riser shaft was constructed inside the Bell Labs large scale fire test building. The compartment had one by two foot slots, one directly above the other. Slots were chosen for cable penetration rather than the more commonly used holes because a large slot will allow fire to propagate from floor to floor more readily than a small hole. Likewise, fire stops were not used. Three full size (2700 pair) cables were selected as a representative cable loading.

A propane burner was chosen to simulate a fire from stored materials. The burner was located on the floor of the shaft adjacent to the cable slot (Figure 3). The flow rate of propane was adjusted so that the ignition fire was not large enough to cause fire propagation from floor to floor in the absence of cables, while it was large enough to impose a radiant flux sufficient to cause rapid ignition on a significant amount of cable. Simply put, the ignition source could not be too large nor too puny.

Construction Details

The frame of the test facility was constructed with Unistrut® channel iron. The corner in which the slots are located was lined, floor to ceiling, with high temperature ceramic fiber insulation board extending four feet from the corner. The top four feet of all walls were also lined with this board. The remaining lining was 1/2 inch gypsum wall board, as was the four foot high draft shield above the ceiling slab.

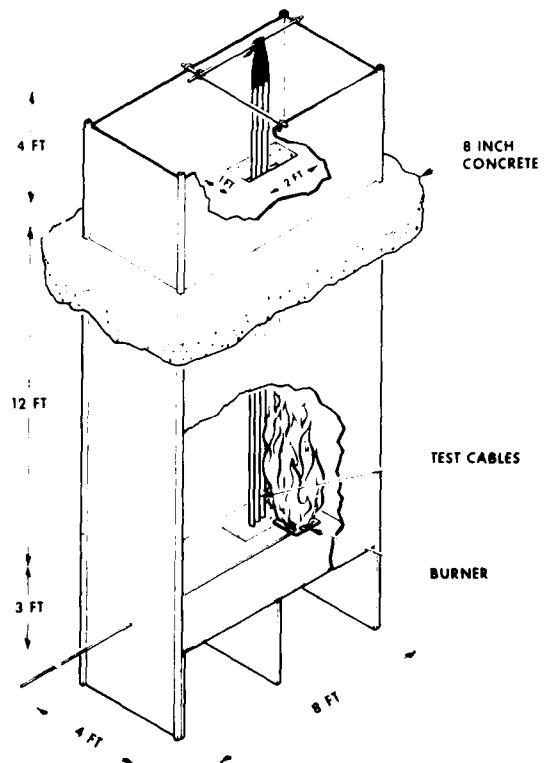


FIGURE 2. FIRE TEST FACILITY - SIMULATED RISER SHAFT



Figure 3. Photograph of the inside of the fire test facility during a calibration test. The ignition source, approximately four feet high, is adjacent to the slot.

A four by six foot high access door was put in the eight foot side adjoining the slot. In the wall opposite the access door, a two by two foot Pyrex® glass observation window was installed to allow observation of the fire.

Thermocouples were arranged to measure the temperature of gases leaving the compartment through the upper slot; the temperature and temperature distribution in a horizontal plane three inches below the top slab; the vertical temperature distribution along the center line of the compartment; and the temperature distribution along the cable, one inch from the surface of the center cable.

The temperatures of the gases in the slot were used to assist in determining if flame had propagated from floor-to-floor. Temperatures of 400°C or higher were used as an indication of flame passage through the slot.

Burner

Propane gas was fed through a 1/2" pipe ended in a 1/2" pipe elbow with the opening pointed to the center of a dispersion plate supported 3" above the floor. A propane flow of 0.1 m³/min at 25°C provides a heat input rate of approximately 145 kW which is roughly equivalent to the average rate of heat release of a 20 pound wood crib over the first 10 minutes after ignition.

The "steady state" upper layer temperatures in the compartment were not affected by placement of the burner. The burner was placed adjacent to the slot as near the cable as possible. Adjustment of the lower duct in the flow opening was necessary to eliminate cross flow of air in order to get a stable, vertical-rising plume. Orientation of the burner and cable was critical since the radiant heat received by the lower section of the cable was determined by the relative position of the cable and plume. Even though the cables were heated by radiant and convective heat from the ignition source, flames from the ignition source did not impinge on the cable. To provide a positive ignition source similar to the small flame associated with flying flaming embers in a trash fire, a small pilot flame was introduced to the surface of the cable in the area facing the source fire at two minutes after the source fire was started.

Selection of Test Conditions

Operating conditions for full-scale testing were selected, based on the following considerations. The fire source should be: 1) located to simulate a fire of stored materials, i.e., flames not impinging on the cable, but close enough that the radiant heat flux from the source fire will reach 30 kW/m² over a significant area of each cable in order to insure rapid ignition, 2) of an intensity to raise the temperature of gases coming through the upper slot close to, but not exceeding, the flash ignition temperature of wood, approximately 250°C.² When temperatures through the slot exceed 250°C and wood products are in the upper compartment, fire could spread through the slot even if cable were absent.

Calibration tests using steel pipe in place of cable showed that a propane flow rate of 0.1 m³/min meets the temperature criteria yielding a temperature of approximately 230°C of the gases issuing from the upper slot (Figure 4). Heat flux radiometer measurements of propane flames of the size used here have shown that the radiant heat flux to adjacent surfaces exceeds 30 kW/m².

The selection of the number of cables (3) was based on typical numbers of cable found in the field study and the number required to give inter-cable radiation under fire exposure. A set of preliminary tests conducted using one, two and three cables showed that during the first 10 to 15 minutes when the initial cable burning occurred, and then subsided, the cable's contribution to the total fuel load was not of major significance.

Cables Tested

Three different types of riser cables were used in these tests: 1) vintage 1960 cable with pulp insulated conductors and a bonded alvyn sheath that was state-of-the-art in fire resistance in 1960, 2) vintage 1980 cable with pulp insulated conductors and a bonded alvyn sheath that is state-of-the-art in fire resistance today, and 3) a new riser cable³ with flame retardant plastic insulated conductors and the same sheath as the 1980 vintage pulp insulated conductor cable. In bonded alvyn sheath the corrugated aluminum shield is adhesively bonded to the vinyl (PVC) jacket.

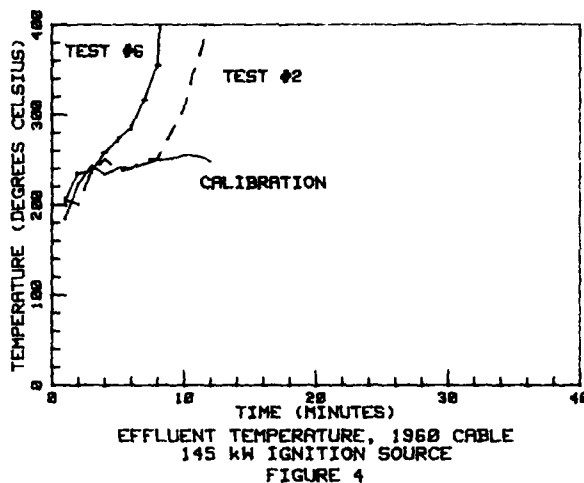
Both pulp insulated cables were full size (3-1/4 inch diameter, 2700 pairs), while the plastic insulated cable contained 1800 pairs. The 1960 vintage PVC jacket compound contained antimony trioxide flame retardant and had an oxygen index of 25%. The 1980 vintage PVC has an oxygen index of 31% and is similar to the compound used for inside wiring and switchboard cable jacket.⁴ The new riser cable has a dual insulation of foamed polyethylene with a PVC skin as described by Dillow and Dougherty.³

Results

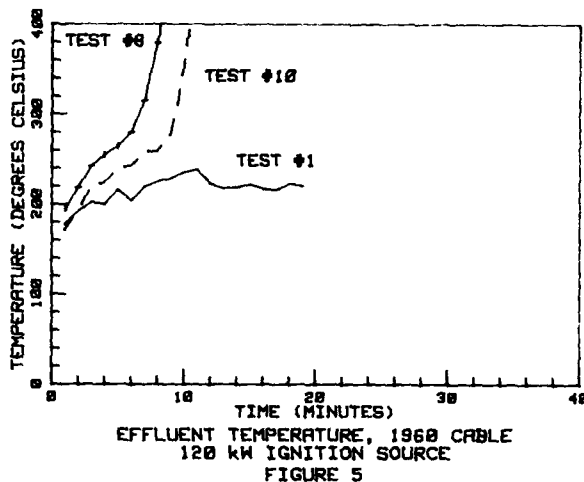
1960 Vintage Cable

Two tests on three 5 metre lengths of cable were conducted at a heat input rate of approximately 145 kW. In approximately 10-12 minutes the flame had propagated the entire length of the cables and passed through the 1 x 2 foot opening in the top of the test building. The average temperatures of the effluent gases out the upper slot versus time are illustrated in Figure 4. Temperatures over 400°C are indicative of flame passing through the slot.

Three tests were conducted using a heat input rate of approximately 120 kW. At this lower rate, two samples carried flame through the opening in approximately 9-12 minutes while the maximum flame height on the third sample was less than nine feet. The average temperatures of the effluent gases versus time are shown in Figure 5. Even though the temperature trace of the third sample terminates at 19

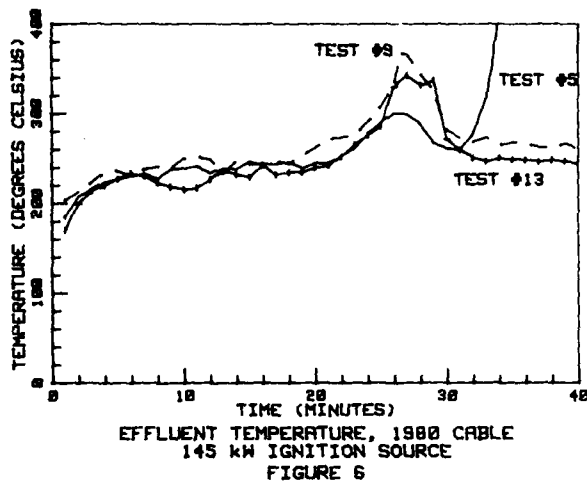


minutes, the test was conducted for a total of 40 minutes. Over the last 21 minutes the temperature remained fairly constant (200-240°C).



1980 Vintage Cable

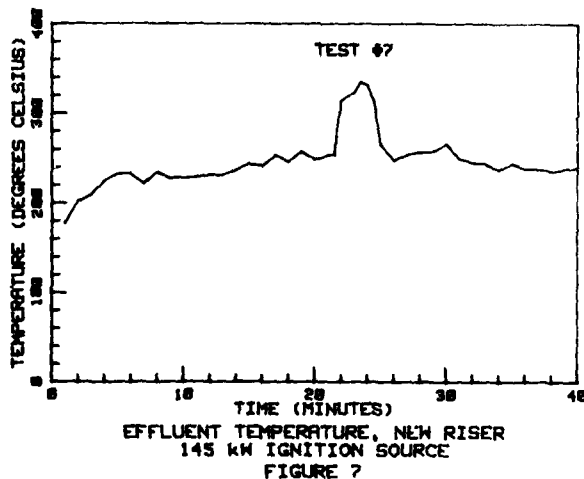
A total of six tests were conducted on this type of cable at a heat input rate of 145 kW. In five of the six tests, the maximum height of flame varied between six and ten feet. Anomalous flame travel was noted in one test in which the flame propagated through the opening (12 feet) and the effluent gas temperature exceeded 400°C. The typical temperature behavior (including the sixth sample) of three of these tests are shown in Figure 6.



Even though the temperature of the effluent gases of the sixth sample did not show a major temperature difference from the other tests during the first 30 minutes of the test, a review of the complete temperature profile shows that the temperatures near the cables in the lower portion of the fire compartment during this test were 400 to 500°C hotter than any other test. A review of the data and the video tapes do not indicate the reason for this temperature difference.

New Riser Cable

Since the diameter of this 1800 pair cable was only 2.5 inches, four 5 metre lengths of cable were used in the test in order to keep constant the surface area of cable jacket which was heated by the ignition source. As shown by the plot of the effluent gas temperature in Figure 7, this cable performed similarly to the 1980 vintage pulp cable, which is consistent with the cables having identical sheaths.



The test results for all cables are summarized in Table I.

TABLE I

Cable	Heat Release Rate kW	Maximum Outlet Temp. (°C)
1960	120	Over 400 @ 8 min.
Pulp	120	Over 400 @ 10 min.
Riser	120	240 @ 11 min.
	145	Over 400 @ 8 min.
	145	Over 400 @ 12 min.
1980	145	270 @ 25 min.
Pulp	145	295 @ 27 min.
Riser	145	365 @ 27 min.
	145	Over 400 @ 34 min.
	145	250 @ 8 min.
	145	345 @ 27 min.
New Riser	145	335 @ 23 min.

Summary

Fire tests on riser cables were conducted as the initial task of a program to develop a standardized test method for determining compliance with the Code. The tests provided data on the flame propagation characteristics of riser cables in a simulated riser shaft without fire stops. With an ignition source that was large, but insufficient to cause propagation of fire from floor-to-floor without cable, early vintage cable propagated fire from floor-to-floor whereas cables with newer fire resistant materials did not exhibit the same flame spreading characteristics.

This investigation was undertaken for the purpose of providing information for the development of a test method, and has not resulted in Classification, Listing, Recognition or Follow-Up Service of any product or material by Underwriters Laboratories.

Acknowledgements

The authors thank W. N. Butler, V. P. DiLullo, W. S. Dombrowski, and J. Simpson of Bell Laboratories, Chester, New Jersey, and S. G. Ebling of UL, for their assistance in this program.

References

1. National Electrical Code 1981 Edition, National Fire Protection Association, No. 70-1981 Section 800-3(b).
2. C. J. Hilado, editor, Flammability Handbook for Plastics. 2nd edition, Westport, Conn., Technomic Publishing Co., 1974, p. 48.
3. H. M. Dillow, T. S. Dougherty, "New Color Coded Dual Insulated Riser Cables," Proceedings of the 30th International Wire and Cable Symposium, 1981, p. 318.
4. S. Kaufman, C. A. Landreth, "Development of Improved Flame Resistant Interior Wiring Cables," Proceedings of the 24th International Wire and Cable Symposium, 1975, p. 9.



Stanley Kaufman is the Supervisor of the Metallurgy and Fire-Resistant Plastics Group at Bell Telephone Laboratories in Norcross, Georgia. He received a B.S. in Physics from the City College of the City University of the City of New York, and a Ph.D. in Chemistry from Brown University. Before joining Bell Laboratories in 1970, he was a research scientist at the Uniroyal Research Center.



Edwin E. Smith was born in Sugarcreek, Ohio and received his academic degrees in Chemical Engineering at the Ohio State University; his Ph.D. in 1949. Major fields of interest include flammability research and industrial pollution control. He is a member of the American Institute of Chemical Engineers, American Chemical Society, National Fire Protection Association, and ASTM.



J. L. Williams, a graduate of Johns Hopkins University of Baltimore (B.S.), was employed by the Glen L. Martin Company prior to joining Bell Laboratories in 1962. Since 1980 he has been involved in the development of fire tests and fire testing of flame-retardant plastics. Prior to joining the Fire-Resistant Plastics Group he was active in the research and development of materials and methods for use in the outside plant.



L. J. Przybyla is an Engineering Team Leader in the Fire Protection Department of Underwriters Laboratories, Inc. He has been involved in large scale fire testing and the development of fire test methods for wire cable. He attended the University of Illinois, Chicago Circle and received a B.S. in Engineering in 1972.

A NEW FLAME RESISTANT, HIGH TEMPERATURE,
CROSS-LINKED POLYPROPYLENE COMPOUND INSULATED WIRE

Hideo Suzuki

Tadao Katahira

Nobuyasu Sato

Kazuji Ishi

Fuikura Ltd.
Sakura-shi, Chiba-ken, 285, JapanAbstract

Polypropylene, although possessing inherent mechanical toughness and a high crystalline melting point, is generally seen to be an unsuitable material for an irradiated cross-linkable polyolefine, primarily because of poor resistance to degradation of the polymer by irradiation and oxidation.

We have developed a flame resistant irradiated cross-linked polypropylene insulation.

There are two principal steps in developing flame resistant irradiated cross-linked polypropylene insulation. One is the application of a functional monomer to prevent the degradation of polypropylene by radiation dose, the other is the blend of thermoplastic elastomer to improve the elongation property of cross-linked polypropylene.

The resultant cross-linked polypropylene insulated wire meets the requirements of the U.L.VW-1 flame test and U.L. rated 150 °C wire specifications.

This insulation is superior to cross-linked polyethylene insulation in mechanical properties at the rated temperature, for instance, tensile strength and the U.L. penetration test.

This paper discusses the flame resistant polypropylene compound for irradiated cross-linking and the properties of its insulated wire developed by our company.

Introduction

For many years the wire industry has worked to upgrade the high temperature performance of low cost insulating materials.

One technique that has been developed is cross-linking by irradiation, such as cross-linked polyethylene and cross-linked polyvinylchloride. This achievement has been generally applied not only to hook-up wires but also to products in other fields, for example, shrinkable tubes and highly expanded plastics.

It is well known the thermal properties and mechanical properties of polymers are

improved by cross-linking.

Recently the wire industry has been required to upgrade the flame resistance of low cost insulating materials as well as mechanical and thermal properties. For imparting excellent flame resistance to a polymer, large amounts of flame retardants are added to the polymer and these additives reduce the mechanical properties of the insulation. Even cross-linked polymers are not excluded from deterioration of their mechanical properties by adding flame retardants.

There are some cases where cross-linked polyethylene insulation or cross-linked polyvinylchloride insulation while possessing excellent flame resistance does not meet the severe requirements of mechanical and thermal properties. These problems especially occur when insulation thickness is thin.

For this reason it has been necessary to develop new flame resistant cross-linked insulations which have more excellent mechanical and thermal properties than the properties of flame resistant cross-linked polyethylene (FRXLPE) insulation or cross-linked polyvinylchloride (FRXL PVC) insulation.

Polypropylene, although possessing inherent mechanical toughness and a high crystalline melting point, is generally seen to be an unsuitable material for an irradiated cross-linkable polyolefin, primarily because of poor resistance to degradation by irradiation and oxidation. But polypropylene is essentially classified as a polymer of cross-linking type.

If a cross-linked polypropylene insulation could be developed, it is forecast that cross-linked polypropylene would have better mechanical and thermal properties.

From the view point of utilizing excellent characteristics in polypropylene, we have studied the cross-linking of polypropylene and developed a flame resistant irradiated cross-linked polypropylene (FRXL PP) insulation.

This cross-linked polypropylene insulation is designed to meet the requirements of the U.L.VW-1 flame test and U.L. rated 150 °C wire specifications.

Our investigation, and the resulting data will be discussed in three phases:

1) Basic components of the flame resistant polypropylene compound for irradiated cross-linking; 2) Irradiated cross-linking of flame resistant polypropylene; 3) Physical properties of FRXLPP insulation, and the comparison of FRXLPP insulation and FRXLPE insulation in some mechanical characteristics.

A brief explanation of each will reveal some of the FRXLPP insulation properties.

Basic components

A flame resistant polypropylene compound for irradiated cross-linking is composed of many components. These components should be used in a proper combination in consideration of their workability.

Basic components are described here.

Polypropylene

Polypropylene is essentially classified as a polymer of the cross-linking type as shown in Table 1.

Table 1

Classification of radiation effect on polymers

Types Radical	Cross-linking types	Degradation types
-H	Polyethylene	—
-CH ₃	Polypropylene	Polyisobuthylene
-C ₆ H ₅	Polystyrene	Polymethylstyrene
-C(=O)OCH ₃	Polymethylacrylate	Polymethylmethacrylate
-C(=O)NH ₂	Polyacrylamide	Polymethacrylamide
-Cl	Polyvinylchloride	Polyvinylidenechloride
-OR	Polyvinylalylester	—

We have tried to cross-link several kinds of polypropylene which have different molecular designs, but the difference of efficiency of cross-linking has not been observed among the various types.

Common polypropylene has been selected for the base polymer of FRXLPP insulation and this polypropylene is ethylene copolymer of the isotactic type.

Table 2 shows the physical properties of the polypropylene used in FRXLPP insulation.

Table 2

Polypropylene used in FRXLPP insulation

Density g/cm ³	Melt index g/10min	Tensile strength kg/mm ²	Elongation %
0.91	1.5	3.2	600

Flame retardants

FRXLPP insulation is designed to meet the requirements of the U.L.VW-1 flame test. Vertical flame tests are often employed to evaluate the flame resistance characteristics of wire insulation on a more critical basis. Tests of this type are more severe than the horizontal method. Many kinds and different additive quantities of flame retardants were investigated to get the FRXLPP insulation capable of meeting the requirements of the U.L.VW-1 flame test.

The combination of a halogen containing additive and antimony trioxide was found to be most effective in imparting excellent flame resistance to the FRXLPP insulation.

Stabilizers

Polypropylene has poor resistance to degradation by oxidation because of its molecular structure, and the break down by oxidation is accelerated when copper makes contact with polypropylene.

Therefore the stabilizers for polypropylene should be carefully tested so as to maintain a long life for the insulation at high temperatures. As there are few documents on stabilizers for cross-linked polypropylene at high temperature, several kinds of stabilizers have been tested in order to clarify the ageing resistance of cross-linked polypropylene containing these stabilizers.

Antioxidants and copper inhibitors were added to polypropylene as stabilizers. Alkylated phenol and ester containing sulfur, as Distearyl thiodipropionate, are generally used in an antioxidant system. It is well known that ester containing sulfur has a synergistic effect on antioxidant action with alkylated phenol. In case of FRXLPP insulation the same synergistic effect has been observed, too.

Table 3 shows several kinds of antioxidants and copper inhibitors used in the experiments. Many combinations of these antioxidants and copper inhibitors were tested and the stabilizer system of FRXLPP insulation has been selected from the results of accelerated ageing tests.

Table 3

Antioxidants and copper inhibitors used in the experiments

Antioxidants	Tris[β -(3,5-di-t-butyl-4-hydroxy-phenyl)propionyl-oxyethyl]isocyanurate
	Tetrakis[methylene-3(3,5-di-t-butyl-4-hydroxyphenyl)propionate]methan
	2,2-Thio[diethyl-bis-3(3,5-di-t-butyl-4-hydroxyphenyl)propionate]
	1,3,5-Tris(3',5'-di-t-butyl-4-hydroxybenzoyl)isocyanurate
	Distearyl thiodipropionate
	Bis[2-methyl-4-(3-n-alkylthiopropionyloxy)-5-t-butylphenyl]sulfide
	1,3,5-trimethyl-2,4,6-tris(3,5-di-t-butyl-4-hydroxybenzyl)benzene
Copper inhibitors	Tris-(2-methyl-4-hydroxy-5-t-butylphenyl)butane
	3-(N-Salicyloyl)amino-1,2,4-triazole
	N,N'-dibenzal-(oxalyl dihydrazide)
	Isophthalic acid bis(2-phenoxypropionyl hydrazide)
	Commercial copper inhibitor of undisclosed structure

There were several undesired stabilizers which resulted in disadvantages to FRX LPP insulation. They produced the following: 1) Changes in the color of the insulation; 2) Foaming of insulation; 3) Inhibition of cross-linking.

Irradiated cross-linking of polypropylene

There were many reports or patents concerned with cross-linking of polypropylene, but only the foamed polypropylene is used practically.

The point at issue of cross-linking polypropylene is its low resistance to degradation by oxidation. Therefore preventing degradation by oxidation should be paid attention at the process of irradiation in order to get cross-linked polypropylene which can be used practically.

We have studied two methods to put cross-linked polypropylene to practical use. One is the addition of a functional monomer and the other is the blending of a thermoplastic elastomer.

Functional monomer

Degradation of polypropylene takes precedence over cross-linking when it is irradiated in air. The irradiated raw polypropylene changes into a brittle material which produces few gel at our initial investigations.

The acceleration of cross-linking is important to prevent the degradation of polypropylene because cross-linking should take precedence over degradation.

We have investigated the introduction of functional monomers as a accelerator of cross-linking for the purpose of preventing the degradation of polypropylene. This technique is the same one as used in cross-linking of polyvinylchloride.

Table 4 Functional monomers

TMPTA	Trimethylolpropane triacrylate
TMPTM	Trimethylolpropane trimethacrylate
TEGDM	Tetraethylene glycol dimethacrylate
TAC	Triallyl cyanurate
DAP	Diallyl phthalate
TEGDA	Tetraethylene glycol diacrylate

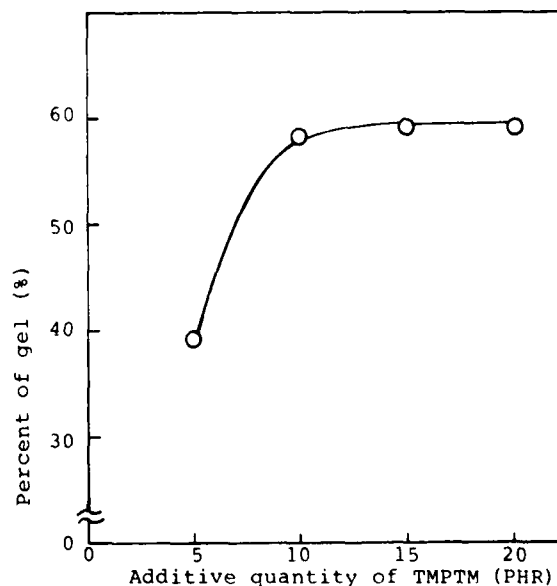


Figure 1 Relation between the percent of gel of polypropylene and the additive quantity of TMPTM

Table 4 shows the functional monomers used in the investigation.

The functional monomer which was most effective was TMPTM. It had many active groups and was more effective in accelerating the cross-linking of polypropylene than the others investigated.

Figure 1 shows the relation between the percent of gel of polypropylene and the additive quantity of TMPTM. It is clear from Figure 1 that the relation between the percent of gel and the additive quantity of TMPTM begins to reach equilibrium when the additive quantity of TMPTM amounts to 10 parts of TMPTM per 100 parts of polypropylene. This means that the proper additive quantity of TMPTM is in the range of 10-15 parts of TMPTM per 100 parts of polypropylene.

Thermoplastic elastomer

The relation between the radiation dose and the elongation of cross-linked polypropylene insulation is shown in Figure 2.

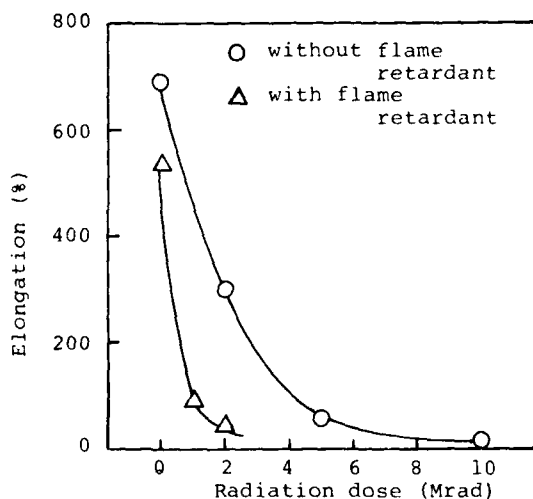


Figure 2 Relation between the radiation dose and the elongation of cross-linked polypropylene insulation

There are the two relations in Figure 2. One is the that between the radiation dose and the elongation of cross-linked polypropylene insulation which does not contain any flame retardant. The other is between the radiation dose and the elongation of cross-linked polypropylene insulation which contains flame retardants to meet U.L.VW-1 flame test.

As shown in Figure 2, the elongation of cross-linked polypropylene insulation decreases significantly with the radiation dose. In the case of cross-linked polypropylene insulation containing flame retardants, the deterioration of elongation was especially noticeable.

It is clear from the results of Figure 2 that the improvement of the elongation property of flame resistant cross-linked polypropylene insulation is needed to be used practically as insulation. We have investigated the need to add a kind of polymer having elasticity in polypropylene to improve the elongation property of FRXL PP insulation.

Table 5

Polymers used in the blend with polypropylene

EVA	Ethylene-vinylacetate copolymer
EEA	Ethylene-ethylacrylate copolymer
SEBS	Styrene-ethylene-butylene-styrene block copolymer
EAO	Ethylene-olefin copolymer

Table 5 shows several kinds of polymers used in the blend with polypropylene.

We have studied the relation between the radiation dose and the elongation of several kinds of FRXLPP insulations consisting of the polymer blends of each of those polymers with polypropylene.

Every polymer, as shown in Table 5, has resulted in an improvement in the elongation property of FRXLPP insulation. Especially SEBS has had a great effect.

Figure 3 shows the relation between the radiation dose and the elongation of FRXLPP insulation consisting of the blend of SEBS with polypropylene. It is recognized from Figure 3 that SEBS has a great effect on the improvement of the elongation property of FRXLPP insulation.

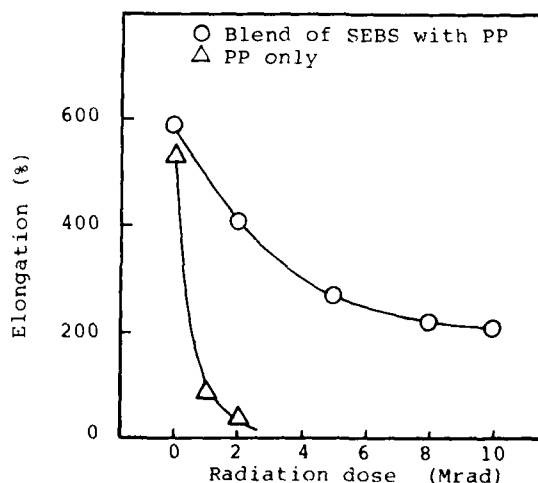


Figure 3 Effect of SEBS on the elongation of FRXLPP insulation

FRXLPP insulation has to maintain its excellent characteristics at high temperature over a long time. We have studied the heat resistance of several kinds of FRXLPP insulations consisting of the polymer blends of each of those polymers as shown in Table 5 with polypropylene.

Table 6

Percent of retentions of elongation of FRXLPP insulations

Polymer blends	EVA with PP	EEA with PP	SEBS with PP	EAO with PP
Elongation %original	5	10	85	5
After 7 days at 180°C				

Table 6 shows the percent of retentions of elongation of several kinds of FRXLPP insulations consisting of polymer blends after heat ageing at 180°C for 7 days. It can be seen from the results in Table 6 that only the polymer blend of SEBS with polypropylene is able to resist heat ageing at 180°C for 7 days. It is important that the polymer used in the blend with polypropylene has itself good resistance to heat ageing.

From the above mentioned results, SEBS has been selected as the polymer for blending to improve the elongation properties of FRXLPP insulation.

Physical properties of FRXLPP insulation

We measured the physical properties of FRXLPP insulation to explain its characteristics. At the same time, we measured the physical properties of FRXLPE insulation to explain the different physical properties between FRXLPP insulation and FRXLPE insulation.

These are summarised in the results and discussion.

Testing specimens

Table 7 shows the testing specimens. We prepared the specimens of FRXLPP insulated wire to meet the requirements of U.L. rated 150°C wire specifications, based on the above mentioned study. Also the specimens of FRXLPE insulated wire selected in this case meet the requirements of U.L. rated 150°C wire specifications.

Testing methods

Table 8 shows the testing methods.

They conform with the test methods for U.L. specifications.

Several measurements were carried out, employing temperature as the parameter.

Table 7 Testing specimens

	Insulation thickness	Conductor
FRXLPP insulated wire	0.8mm	AWG 22
	0.4mm	
FRXLPE insulated wire	0.8mm	AWG 22

Table 8 Test methods

Item	Method
Tensile test	U.L.-62
Tensile test after heat aging	U.L.-62
Tensile test after oil immersion	U.L.-62
U.L. flexibility test	U.L.-62
Heat shock test	U.L.-62
Cold bend test	U.L.-62
Vicat softening point	ASTM D-1525
Torsion test	ASTM D-1043
Slow compression test	U.L.-62
Deformation test	U.L.-62
Penetration test	U.L.-62
Cutting test	CSA standard
Flame test	U.L.-62 (VW-1)
Conductor corrosion	U.L.-62
Dielectric strength	U.L.-62

Table 9 Results of U.L. rated 150°C wire test methods

Item		Specification	Results		
			FRXLPP		FRXLPE
			t=0.8	t=0.4	t=0.8
Unaged	Tensile strength (kg/mm ²)	> 1.05	1.6	1.5	1.3
	Elongation (%)	> 150	240	240	270
After 7day air oven at 180°C	Tensile strength (% original)	> 70	100	110	120
	Elongation (% original)	> 65	85	82	85
After 96 hr oil immersion at 100°C	Tensile strength (% original)	> 50	62	60	54
	Elongation (% original)	> 50	55	62	56
VW-1 Flame test			Pass	Pass	Pass
Cold bend test (-10°C x 1hr)		No crack	None	None	None
Heat shock test (180°C x 1hr)		No crack	None	None	None
Flexibility test after air oven aging		No crack	None	None	None
Deformation test at 180°C		> 50	63	58	58
Conductor corrosion			None	None	None
Dielectric strength test (2000v x 1min)	Unaged	No break down	NB	NB	NB
	Aged	No break down	NB	NB	NB

Results

1) The results of U.L. test methods

Table 9 shows the results of tests which are published as the specifications of U.L. rated 150°C wire. Both FRXLPE insulation and FRXLPP insulation meet all items. They were tested over a short period of time, but wire must have resistance against longer ageing. To extrapolate heat resistance over a long time, we took two Arrhenius' plots; one about the U.L. flexibility test and the other, the percent of retention of elongation after heat ageing.

The Arrhenius' plot of flexibility test is given by plotting the times when the cracks in the specimen's surface is caused by wrapping a specimen around the mandrel at the certain temperatures.

The Arrhenius' plot of the percent of retention of elongation after heat ageing is taken by plotting the times when the percent of retention of elongation after heat ageing shows 65 %.

Figure 4 and Figure 5 shows the

Arrhenius' plot of both.

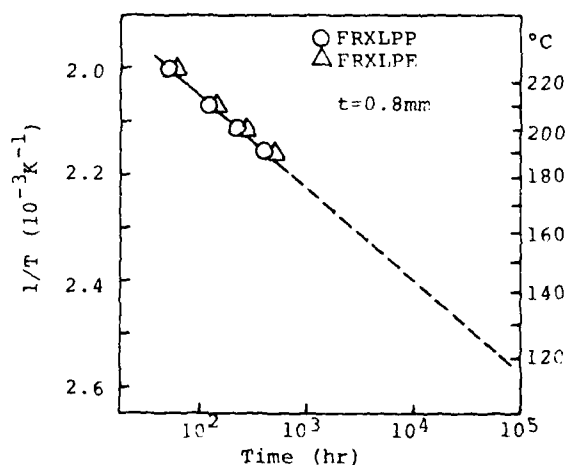


Figure 4 Arrhenius' plot of U.L. flexibility test

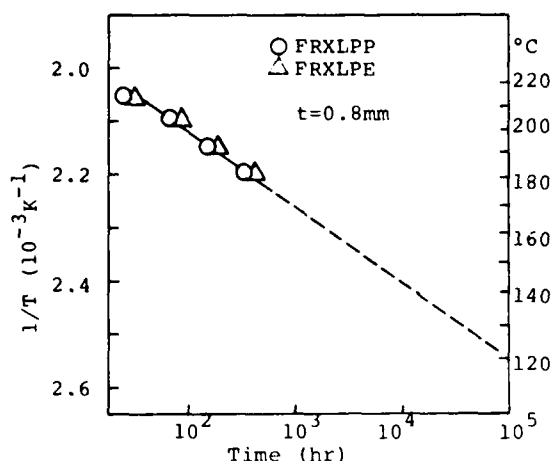


Figure 5 Arrhenius' plot of percent of retention of elongation

As both FRXLPE insulation and FRXLPP insulation show similar curves of Arrhenius' plots, the heat resistance of each is almost on the same level.

According to these results, it is presumed that the useful life of FRXLPP insulation is about 5000 hours at 150°C, and about 40000 hours at 125°C.

As polypropylene is relatively brittle at low temperatures, a cold bend test was carried out in detail at temperatures which are lower than required by U.L. specification. Table 10 shows the results of the cold bend tests at -30°C and -60°C.

Table 10 Results of the cold bend test

Temperature	FRXLPP		FRXLPE
	t=0.8mm	t=0.4mm	t=0.8mm
-30°C	No crack	No crack	No crack
-60°C	No crack	No crack	No crack

The FRXLPP insulation did not crack as badly as the FRXLPE insulation. It is recognized that the blended elastomer has the effect of improving of low temperature brittleness of polypropylene.

2) Vicat softening point, Torsion test

To explain the characteristics of FRXLPP insulation, the Vicat softening point and the apparent modulus of rigidity were measured.

Table 11 shows the Vicat softening points. In this case, the temperatures at which a flat-ended needle penetrated the insulation to a depth of 0.5 mm were measured.

ured.

Each of the resultant softening point is almost equal to those of polyethylene and polypropylene. Therefore, these results show that the Vicat softening point depends on its own basic polymer even in cross-linked materials. Several properties mentioned later changed significantly beyond the softening point.

Table 11 Vicat softening point

	FRXLPP		FRXLPE
	t=0.8mm	t=0.4mm	t=0.8mm
Temperature (°C)	121	—	81

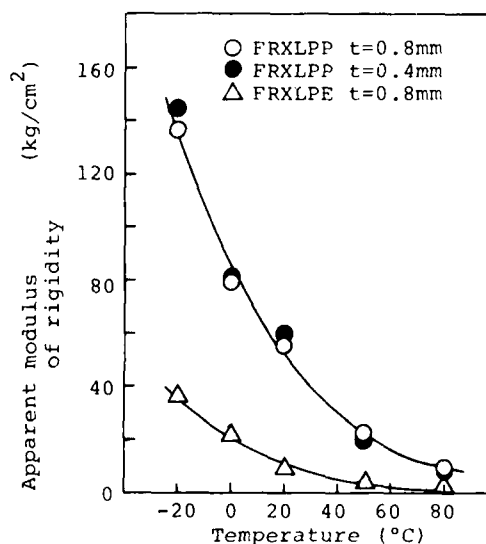


Figure 6 Relation between the apparent modulus of rigidity and temperature

Figure 6 shows the relations between the apparent modulus of rigidity and temperature. The apparent modulus of rigidity were measured by means of insulations. It is recognized from these results that the apparent modulus of rigidity of FRXLPP insulation is higher than that of FRXLPE insulation, and, the lower temperature falls, the larger the difference becomes.

These results show that the mechanical strength of FRXLPP insulation is greater than FRXLPE insulation. This characteristics depends on the polypropylene used in FRXLPP insulation. Higher Vicat softening point and apparent modulus of rigidity are the characteristics which distinguish FRXLPP insulation from the other materials of insulation.

It is expected from these results that FRXLPP insulation will have an excellent tensile properties and deformation resistance.

3) Tensile properties

Figure 7 shows the change of tensile strength with temperature. Figure 8 shows the change of elongation with temperature.

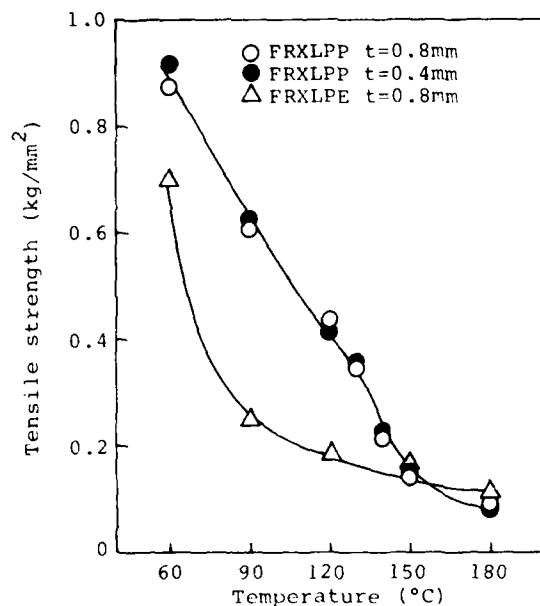


Figure 7 Change of tensile strength with temperature

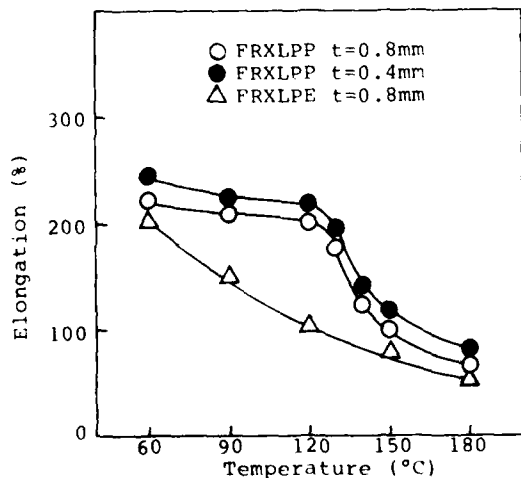


Figure 8 Change of elongation with temperature

The tensile strength of FRXLPP insulation is higher than that of FRXLPE insulation in the temperature area below 150°C. The elongation of FRXLPP insulation does not change in the temperature area below 130°C, although the difference of elongation of both insulation is small in the temperature area above 150°C. It is recognized from the above mentioned results that the tensile properties of FRXLPP insulation are excellent at high temperatures and this characteristic disappears in the temperature area above 150°C.

4) Slow compression test

To investigate the compression resistance of FRXLPP insulation at room temperature, a slow compression test was carried out. Table 12 shows the results of slow compression tests. As can be seen, FRXLPP insulation has an excellent compression resistance and the 0.4 mm thickness of FRXLPP insulation is almost equal to that of 0.8 mm of FRXLPE insulation in the compression resistance.

Table 12 Results of the slow compression test

Radius of edge		FRXLPP		FRXLPE
		t=0.8mm	t=0.4mm	t=0.8mm
1.6mm	kg	38.4	18.2	21.6
0.15mm	kg	17.7	6.7	9.7

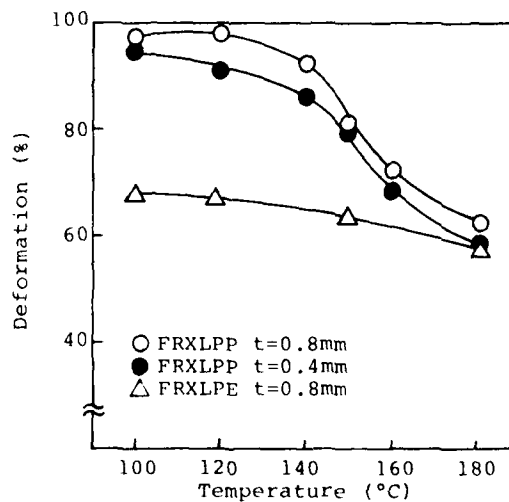


Figure 9 Relation between the percent of deformation and temperature

5) Deformation

Figure 9 shows the relation between the percent of deformation and temperature. It is recognized that the percent of deformation of FRXLPP insulation is higher than that of FRXLPE insulation in the wide temperature area. Although there is a change at the near softening point, the percent of deformation of FRXLPP insulation is about 20 % higher than that of FRXLPE insulation below 150°C.

6) Penetration resistance

As the results of slow compression tests and deformation tests have shown the excellent properties in FRXLPP insulation, we investigated the penetration resistance with a sharp edge at high temperatures. This test carried out by employing the methods of the U.L. penetration test and CSA cutting test.

Figure 10 and 11 shows the results of the U.L. penetration test and the CSA cutting test. FRXLPP insulation shows excellent properties in each test. It should be noticed that the penetration resistance of 0.4 mm thickness FRXLPP insulation is equal to that of 0.8 mm FRXLPE insulation. The excellent mechanical strength of FRXLPP insulation at high temperature is clearly explained by these results.

The above mentioned physical properties of FRXLPP insulation meet the requirements of U.L. rated 150°C wire specifications. It is recognized that the mechanical properties of FRXLPP insulation, for example, tensile property, slow compression, deformation and penetration, are superior to those of FRXLPE insulation, especially in high temperatures. Because of these reasons, it is possible to make a insulation thickness thin according to demand.

Conclusion

Our flame resistant cross-linked polypropylene insulation has been developed on the basis of extensive research concerned with many components, such as polypropylene, flame retardants, stabilizers and other factors. Especially important factors were the introduction of a functional monomer and a thermoplastic elastomer.

The resultant product exhibits an optimum balance of electrical, thermal, flame resistance and mechanical properties. This flame resistant cross-linked polypropylene insulated wire meets the requirements of the U.L. VW-1 flame test and U.L. rated 150°C wire specifications.

It is especially worthy of notice that the flame resistant cross-linked polypropylene insulation is superior to the flame resistant cross-linked polyethylene insulation in mechanical properties from low temperature to high temperature.

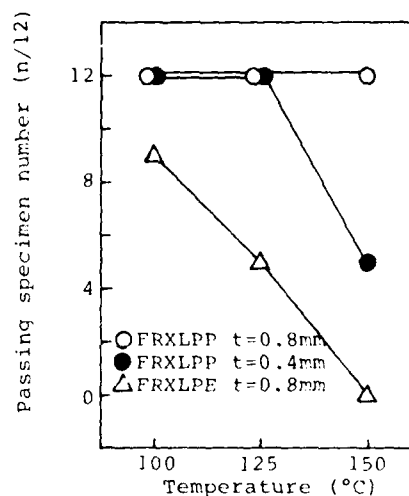


Figure 10 Results of the U.L. penetration test

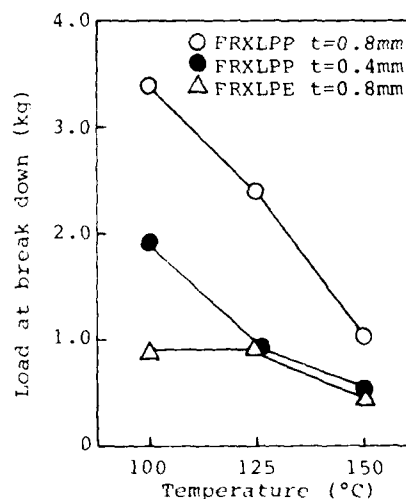


Figure 11 Results of the CSA cutting test

Especially the resistance to compression or deformation of FRXLPP insulation is superior to these properties in FRXLPE insulation. For that reason, the primary advantage of applying the FRXLPP insulation is that the insulation is smaller in diameter than that of FRXLPE insulation in the same rated wire.

Therefore it will find broad acceptance in motor leads, appliances, hook-ups and all industries which want new materials having excellent mechanical properties.

Acknowledgement

Many members in Fujikura Ltd. have made important contributions to our study. The authors wish to acknowledge them and especially express deep appreciations for much advice of Mr. S. Tanaka and Mr. A. Tsujikawa.

References

1. W. A. Salmon and L. D. Loan, Journal of Applied Polymer Science, Vol. 16, 671 1972
2. Miller, A. A., Industrial and Engineering Chemistry, Vol. 51, 1271, 1959
3. J. W. Lyons, The Chemistry and Uses of Flame Retardants, John Wiley and Sons, Inc., New York, 1975
4. Hawkins, Degradation and Stabilization of Polymers, Applied Science Publishers, 60, 1975
5. M. Ishibashi, T. Yamamoto, A. Mogi, Proceedings of the 27th International Wire and Cable Symposium, 213, 1978



Hideo Suzuki
Senior Engineer

Telecommunication Cable Research & Development Department. Fujikura Ltd.
1440, Mutsuzaki, Sakura-shi, Chiba-ken, 285, Japan

Mr. Suzuki received the B. E. degree in polymer chemistry from Gunma University in 1971 and joined Fujikura Ltd.. He is responsible for the development of plastic materials and polymer processings. He is a member of The Society of Polymer Science, Japan.



Tadao Katahira
Engineer

Telecommunication Cable Research & Development Department. Fujikura Ltd.
1440, Mutsuzaki, Sakura-shi, Chiba-ken, 285, Japan

Mr. Katahira received the B. E. degree in polymer chemistry from Tohoku University in 1977 and joined Fujikura Ltd.. He is responsible for the development of plastic materials and polymer processings. He is a member of The Society of Polymer Science, Japan.



Nobuyasu Sato
Chief

Telecommunication Cable Research & Development Department. Fujikura Ltd.
1440, Mutsuzaki, Sakura-shi, Chiba-ken, 285, Japan

Mr. Sato received the B. E. degree in Telecommunication Engineering from Tohoku University in 1966 and has been engaged in development of telecommunication cables. He is a member of The Institute of Electronics and Communication Engineers of Japan.



Kazuji Ishi
Assistant Manager

Telecommunication Cable Engineering Department. Fujikura Ltd.
1-5-1, Kiba, Koto-ku, Tokyo, Japan

Mr. Ishi received the B. E. degree in Telecommunication Engineering from Yokohama National University in 1969 and has been engaged in engineering of electronic and telecommunication cables. He is a member of The Institute of Electronics and Communication Engineers of Japan.

AD P000589

A COMPREHENSIVE SMALL SCALE SMOKE TEST

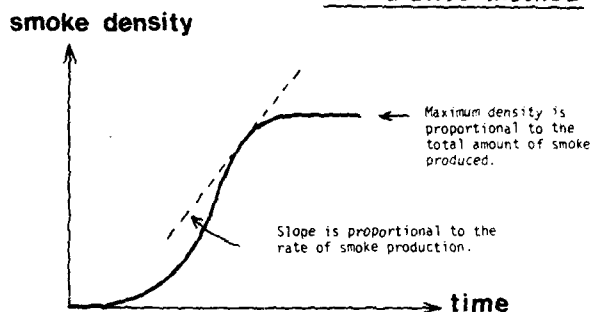
R.H. Whiteley

Raychem Ltd., Swindon, England

Abstract

A small scale smoke test method is described. The test involves the pyrolysis or combustion of a small sample of material (~ 200 mg) in a flow of pre-heated dry air. The optical density of the resulting stream of smoke is continuously monitored. The temperature of the pyrolysis oven can be varied in the range 200°C to 900°C which corresponds to a range of radiant heat flux of 0.3 Wcm⁻² to 8.5 Wcm⁻². A microcomputer is used to process the data generated, to produce smoke versus time plots, smoke versus temperature plots, and '3D' plots of smoke evolution versus time versus temperature to illustrate the overall smoke producing characteristics of materials.

Cumulative Method



Dynamic Method

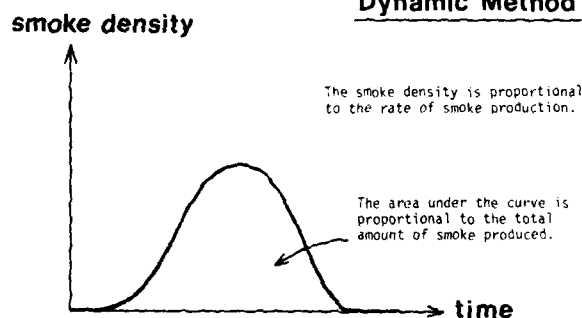


FIGURE 1 - Representative smoke plots

The Measurement of Smoke

A number of methods have been developed¹ and they all use one of two measurement techniques; gravimetric or optical. Gravimetric methods involve determining the mass of smoke particles deposited on a filter. Optical methods, which are much more common, involve the measurement of the fraction of light obscured by the smoke evolved and are of two types - cumulative and dynamic. In the former, smoke accumulates in a chamber and the density of the smoke is monitored over a period of time. In the latter, measurements are made by monitoring the density of smoke in a gas stream. The general shapes of smoke density versus time plots for cumulative and dynamic measuring methods are illustrated in Figure 1.

Light attenuation through smoke follows the Beer-Lambert law which states

$$I = I_0 e^{-\epsilon c l} \quad \dots \quad (1)$$

where

- I_0 = incident light intensity
- I = transmitted light intensity
- ϵ = extinction coefficient
- c = concentration
- l = light path length

This can be rewritten as

$$\log_{10} (I_0/I) = \frac{2.303}{\epsilon c l} \dots \dots \dots (2)$$

The decrease in light transmission with increasing concentration of smoke therefore follows a logarithmic law and so it is more useful to express the amount of smoke in terms of optical density, D,

$$D = \log_{10} (I_0/I) \dots \dots \dots (3)$$

since D is proportional to concentration, whereas transmission is not,

$$\% \text{ trans.} = \frac{I}{I_0} \times 100 \dots \dots \dots (4)$$

Table 1 illustrates the relationship between these two quantities.

TABLE 1 - Percent Transmission and Optical Density

trans.	D
100	0
10	1
1	2
0.1	3
0.01	4

A further quantity, specific optical density D_s , can be defined by the equation

$$D_s = D \times \frac{V}{\ell m} \dots \dots \dots (5)$$

where

V = volume of smoke
 ℓ = light path length
 m = mass of sample

In a dynamic method it is useful to calculate the specific optical density of all the smoke produced from the sample, i.e. obtain a measure of the total smoke, S , produced by the material under test. This is found using the equation

$$S = f/\ell m \times \int D \cdot dt \dots \dots \dots (6)$$

where

f = gas flow
 $\int D \cdot dt$ = the area under the optical density versus time curve.

When defined in this way S , like D_s , has units of area per unit mass e.g. $\text{cm}^2 \text{g}^{-1}$. An alternative definition of specific optical density is sometimes used,

$$D_s' = D \times \frac{V}{\ell A} \dots \dots \dots (7)$$

where

A = the area of the sample exposed to the heat source.

and in this case D_s' is dimensionless.

Test Methods

Table 2 lists some of the numerous smoke tests now being used. All the tests in the list are optical and most are of the dynamic type. There are large variations between the tests e.g. the sample size ranges from 200 mg (NF T 51-G73) up to a 24 ft long board (E84) and the heat sources vary from small radiant heaters (e.g. E662) to a 5000 BTU/min gas flame (E84).

Probably the most commonly used small scale apparatus is the NBS smoke chamber (ASTM E662) which is of the cumulative optical type - see Figure 2.

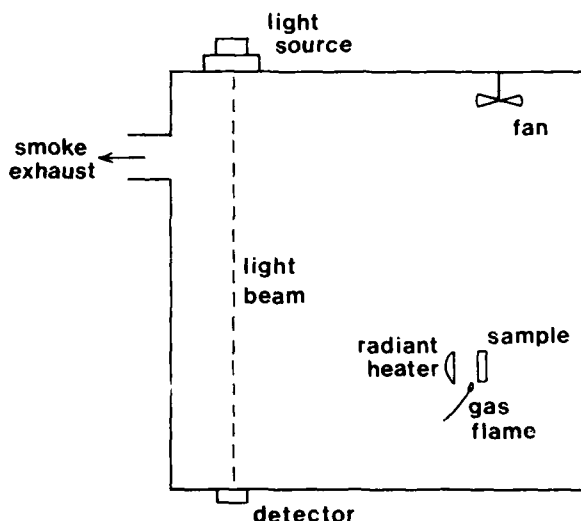


FIGURE 2 - Schematic diagram of the NBS smoke chamber.

There are however several disadvantages in using the NBS chamber ;

- Only one level of radiant heat flux is commonly used (2.5 Wcm^{-2}) which corresponds to a relatively low temperature ($\sim 475^\circ\text{C}$).
- The test method is rather slow.
- For the routine screening of materials a relatively large sample is required for each test - typically 15 - 30 g.
- Many samples melt and drip away from the radiant heat source and therefore give unreliable results.

TABLE 2 - Smoke Tests - Current and Under Development (from ref. 1)

Country/ Institution	Test Reference	Test* Type	Smoke Measurement	Unique/ Multipurpose (x)
Australia	AS 1530 Part 3	D	Optical	M (flammability)
Canada	CAN 4, S 102	D	"	U
France	NF-T51-073	D/C	"	U
Germany	DIN 53437/ 53436	D	"	U (smoke & toxicity)
Japan	JIS A1321 : Part 3	C	"	U (also measures toxicity)
Netherlands	NEN 3883	D	"	M (flashover)
Scandinavia ⁽¹⁾	Nord test NT FIRE 004	D	"	M (heat release)
UK	BS/DD 36	C	"	U
	BS 5111	D/C	"	U
USA	E84	D	"	M (flame spread)
	E268	D	"	M (flame spread)
	E162	D	"	M (flammability)
			plus gravimetric	
	E662	C	Optical	U
	D 2843	D/C	"	U
ISO ⁽²⁾	DTR 5924	C	"	U
UK ⁽²⁾	BS DD/70 + DD36 (See DTR 5924)	C	"	U

* Test types :

Dynamic
Cumulative
Dynamic/Cumulative

X Primary objective of the test

- (1) Denmark, Finland, Norway & Sweden
having corresponding internal
specification and own reference to the test.
(2) Under development.

For these reasons we have developed the apparatus described in this paper in order to complement and supplement data obtained from the NBS chamber.

The requirements we wanted were as follows :

- a range of radiant heat fluxes, with a maximum of at least 8 Wcm^{-2} .
- small sample size.
- relatively rapid measurements.
- elimination of the dripping problem.

A range of radiant heat fluxes was regarded as being particularly important because it has been shown that some materials produce very low smoke in the NBS chamber when exposed to a radiant heat flux of 2.5 Wcm^{-2} but when the heat flux is raised smoke emission can increase very considerably^{2,3}.

The Apparatus

The apparatus, illustrated in Figure 3, is based on the French standard NF T 51-073⁴ and is of the dynamic optical type.

Dry air passes at a rate of 3.5 l min^{-1} through a pre-heater (250°C) into a silica tube which is heated by an annular furnace.

The sample, typically 200 mg, is in a small metal boat in the middle of the tube. The temperature at the sample is measured by a thermocouple located just behind the boat. The temperature can be varied between 200°C and 900°C corresponding to measured radiant heat fluxes of between 0.3 and 8.5 Wcm^{-2} - see Figure 4.

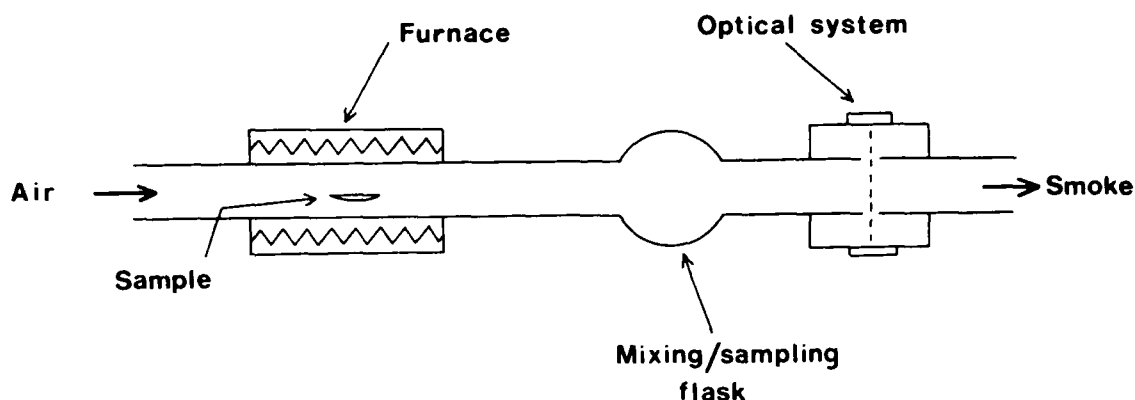


FIGURE 3 - Schematic diagram of the apparatus

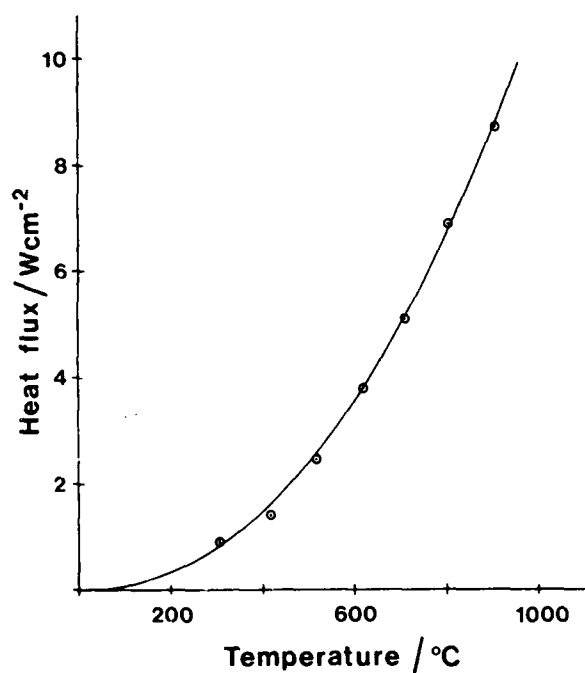


FIGURE 4 - Heat flux measurements

Smoke from the sample passes into a mixing/sampling chamber and then into a photometer which measures the light obscuration produced by the smoke. A silicon photodiode detector (United Detector Technology Inc. 'PIN-10 AP') is used with a filter so that its spectral response matches that of the human eye. The signal from the photodiode is recorded as a function of time on a pen recorder and, together with the output from the thermocouple, is fed to a microcomputer for analysis.

Raw Data Corrections

The flow rate of air through the apparatus of 3.5 lmin^{-1} was measured at 25°C and 1 atmosphere pressure. When the pre-heater and furnace are on, the temperature of the gases passing through the photometer is higher than 25°C * so the actual flow of smoke through the photometer is greater than 3.5 lmin^{-1} and is given by the equation ;

$$f/\text{lmin}^{-1} = \frac{3.5 \times (T_{\text{photometer}}/^{\circ}\text{C} + 273)}{298} \quad (8)$$

The measured O.D. values are therefore corrected to take this effect into account.

The pressure in the photometer was found not to vary with temperature and to be about 1mmHg above atmosphere pressure. A correction for pressure variation is therefore not needed. No corrections are made for variations in atmospheric pressure.

The start of a run is taken as the time when the sample is loaded into the pyrolysis tube. However, when smoke is first produced from the sample it takes 2.5 seconds to reach the photocell so this time lag has to be subtracted from the microcomputer timings.

A small flow of air ($20 \text{ cm}^3 \text{ min}^{-1}$) passes into the photocell in order to minimise soot deposition. Nevertheless some deposition does still occur and this causes a gradual shift in the 100% transmission baseline. The microcomputer is therefore programmed to apply appropriate corrections to eliminate this effect.

* The relationship between the photometer temperature and the temperature measured at the sample boat was found, empirically, to be

$$T_{\text{photometer}}/^{\circ}\text{C} = \frac{(T_{\text{sample}}/^{\circ}\text{C})}{30} + 29 \quad (9)$$

Total Smoke, Half Smoke Time, and Smoke Index

The total smoke, S , evolved from a material was defined in equation 6, and is one of the important parameters which is measured by the apparatus. However, the hazards associated with smoke in fires are not only related to the total amount of smoke that may be evolved from a material, but also to the time taken for that smoke to be evolved. For this reason the time taken for half the total smoke to be evolved (half-smoke time, $t_{1/2}$) is calculated, and a smoke index combining these two factors is also calculated using the formula;

$$S.I. = S/t_{1/2} \quad \dots\dots\dots (10)$$

Procedure

For any one material and furnace temperature, three samples are usually tested. The computer calculates average optical density-versus-time, and sample temperature-versus-time plots and also calculates the means and standard deviations for S , $t_{1/2}$ and S.I. These data are recorded on disc and are also output to an x/y plotter in a form similar to those shown in Figure 5.

Results

High Density Polyethylene [HDPE]

Figure 5 A illustrates the data obtained with an uncrosslinked high density polyethylene at 400°C. The samples pyrolysed without undergoing self-ignition and the smoke evolved was in the form of a grey aerosol. In Figure 5 B we see what happened at 550°C. Here the samples self-ignited after about 20 seconds and black sooty smoke was produced for a short time.

Because the results are stored by the computer it is relatively easy to measure smoke plots of this type over a wide range of temperatures and then to generate a composite "SD" plot illustrating the overall behaviour of a material. Figure 6 shows such a plot for HDPE. Several features are immediately apparent, e.g.

- Smoke is produced more rapidly as the temperature increases.
- There is a clear difference between the pyrolysis region, below the self-ignition point ($T_{ig} \sim 420^\circ\text{C}$), and the combustion region, above T_{ig} .
- Above T_{ig} the smoke plots are all similar.
- The temperature at which smoke starts to be produced, T_0 , is about 295°C .

Some of these features are more easily appreciated if the total smoke, S , is plotted against temperature - see Figure 7. Here the discontinuity between flaming ($>T_{ig}$) and non-flaming ($<T_{ig}$) degradation is clear. Below T_{ig} , S rises rapidly with increasing temperature from zero at $\sim 295^\circ\text{C}$.

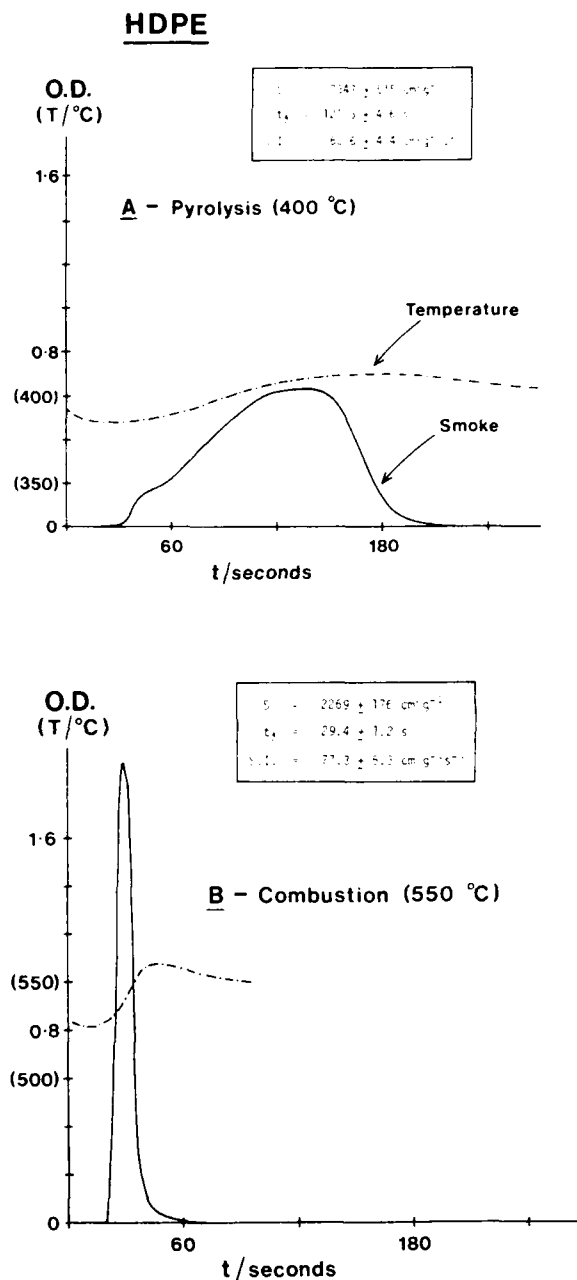


FIGURE 5 - Typical smoke v. time plots

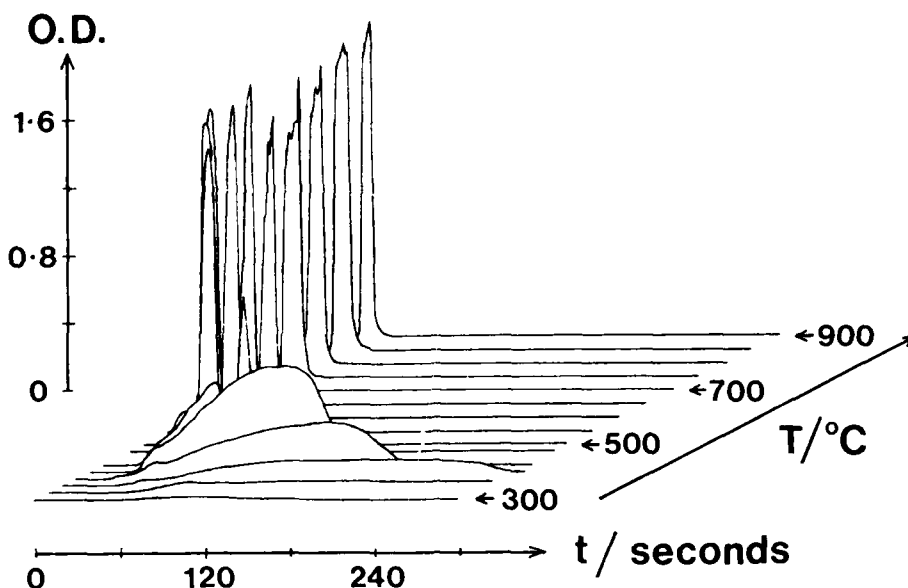


FIGURE 6 - '3-D' Smoke plot, HDPE

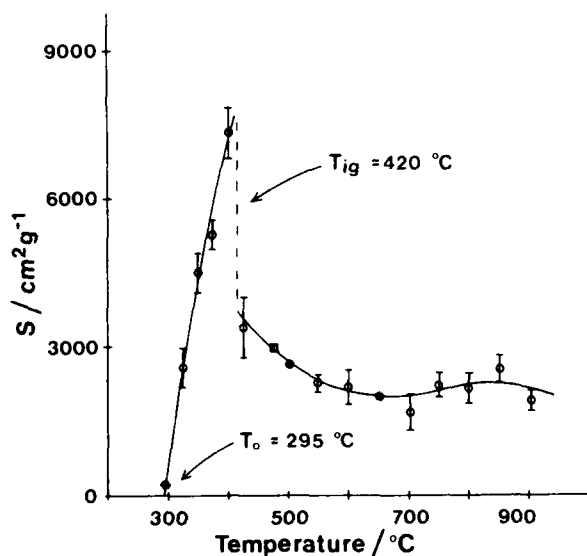


FIGURE 7 - S v. T Plot, HDPE *

* Error bars represent \pm one standard deviation (\bar{s}) from the mean, where

$$\bar{s} = \left\{ \frac{\sum (x - \bar{x})^2}{n-1} \right\}^{\frac{1}{2}}$$

(T_0) up to $7500 \text{ cm}^2\text{g}^{-1}$. Above T_{ig} , S gradually decreases from $3500 \text{ cm}^2\text{g}^{-1}$ to $2000 \text{ cm}^2\text{g}^{-1}$ at 900°C .

Edgerley and Pettett have suggested that a useful measurement is the area under a total smoke-versus-temperature curve⁵. Such a measurement would represent the smoke potential of a substance in a situation where all temperatures in the chosen range were equally represented. A sensible range would be from 200°C to 900°C since 900°C is the upper limit of our apparatus and no substance that we have tested to date produces smoke below 200°C , the lower limit of our apparatus.

We can then define a quantity \bar{S} by the equation

$$\bar{S} = \frac{1}{T_2 - T_1} \int_{T_1}^{T_2} S.dT \dots\dots\dots (11)$$

where

$$T_2 = 900^\circ\text{C} \text{ and } T_1 = 200^\circ\text{C}$$

\bar{S} is then the average total smoke value between 200°C and 900°C . For HDPE \bar{S} is $2340 \text{ cm}^2\text{g}^{-1}$.

Figures 8 and 9 illustrate how $t_{\frac{1}{2}}$ and S.I. vary with temperature for HDPE.

An average smoke index $\bar{S.I.}$ can be calculated in the same way as \bar{S} , and for HDPE,

$$\bar{S.I.} = 99.6 \text{ cm}^2\text{g}^{-1}\text{s}^{-1}$$

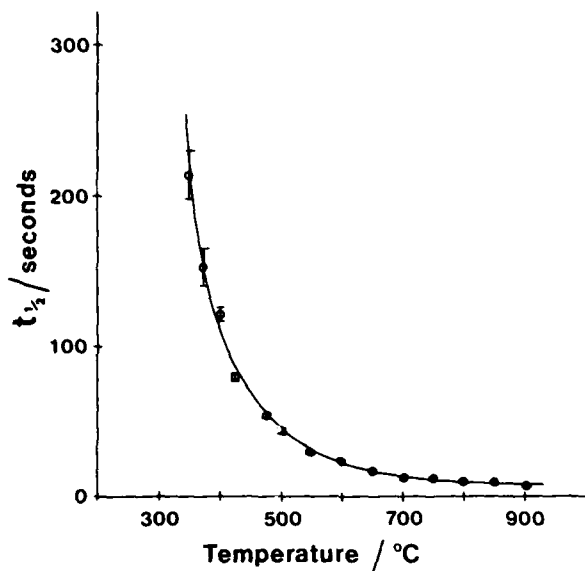


FIGURE 8 - $t_{1/2}$ v. T Plot, HDPE

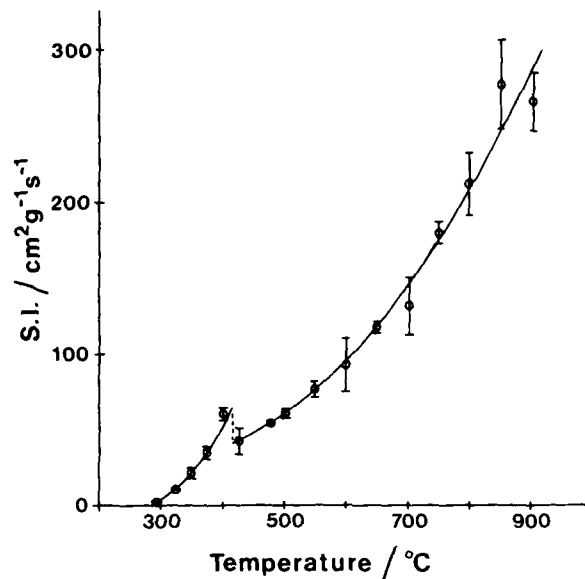


FIGURE 9 - S.I. v. T Plot, HDPE

Poly(phenylene-ether-ketone), [PPEK]

In Figures 10 to 13 we can see how the various plots discussed above differ for a commercial poly(phenylene-ether-ketone), a 'high-performance' polymer. Again several features are immediately apparent from the '3-D' plot (Figure 10) ;

- . overall smoke production is lower than for HDPE
- . $t_{1/2}$ decreases rapidly as the temperature increases from 500°C to 600°C.
- . T_{ig} is $\sim 500^\circ\text{C}$.
- . Above T_{ig} ($\sim 625^\circ\text{C}$) smoke production varies very little.

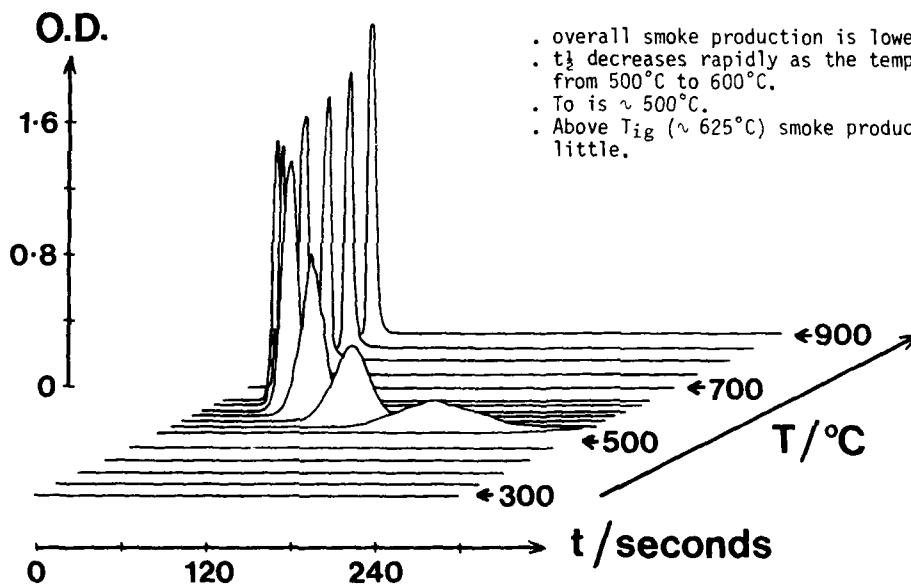


FIGURE 10 - '3-D' Plot, PPEK

The total smoke-versus-temperature plot (Figure 11) again shows a discontinuity at T_{ig} . Below T_{ig} , S rises from zero at 505°C to a maximum value of $\sim 2500 \text{ cm}^2\text{g}^{-1}$. Above T_{ig} , S is roughly constant at $\sim 1500 \text{ cm}^2\text{g}^{-1}$. S is $794 \text{ cm}^2\text{g}^{-1}$, and $S.I.$ is $33.3 \text{ cm}^2\text{g}^{-1}\text{s}^{-1}$.

The behaviour of another poly(phenylene-ether-ketone) to which we had added a small amount of a smoke suppressant is also illustrated in Figures 11 to 13. The smoke hazard from this material is not significantly different below T_{ig} , but in flaming conditions above T_{ig} it is substantially reduced. S is $491 \text{ cm}^2\text{g}^{-1}$ and $S.I.$ is $14.5 \text{ cm}^2\text{g}^{-1}\text{s}^{-1}$. These data serve to emphasise the usefulness of these measurements, as the difference in the smoke producing potential of these two materials would not be evident from small scale tests which use relatively low radiant heat fluxes, such as the NBS smoke chamber.

A - a commercial PPEK
B - a smoke suppressed PPEK

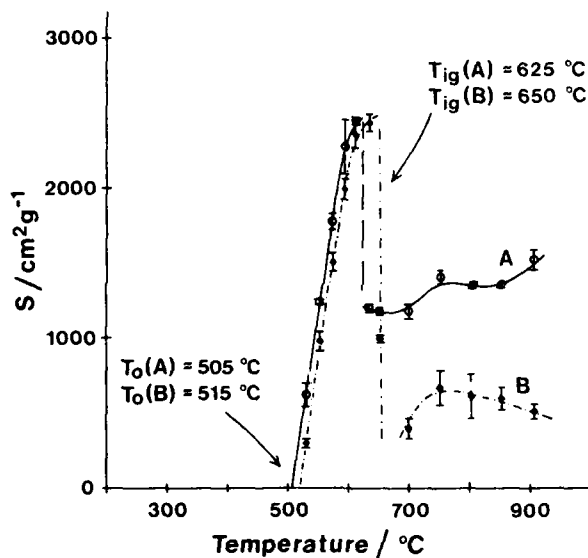


FIGURE 11 - S v. T Plots, PPEK

A Halogen-free Flame Retarded Cable Jacket Compound.

Figures 14 to 17 illustrate the behaviour of a halogen-free flame retarded cable jacket compound. The '3-D' plot shows that the material produces low levels of smoke over the whole temperature range. As in the previous examples there are two distinct regions - pyrolysis and combustion. In the pyrolysis region S rises from zero at 340°C to a maximum of $1500 \text{ cm}^2\text{g}^{-1}$ at 425°C and then falls to $\sim 900 \text{ cm}^2\text{g}^{-1}$ at just below T_{ig} (525°C). In the combustion region S rises slightly from $240 \text{ cm}^2\text{g}^{-1}$ just above T_{ig} to $320 \text{ cm}^2\text{g}^{-1}$ at 650°C .

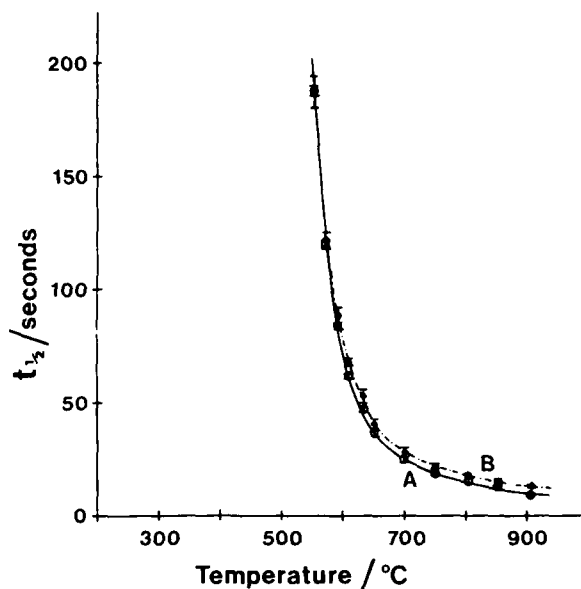


FIGURE 12 - $t_{1/2}$ v. T Plots, PPEK

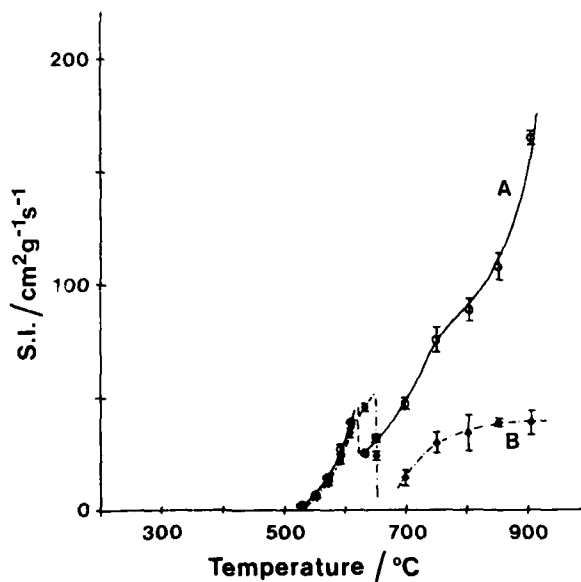


FIGURE 13 - $S.I.$ v. T Plots, PPEK

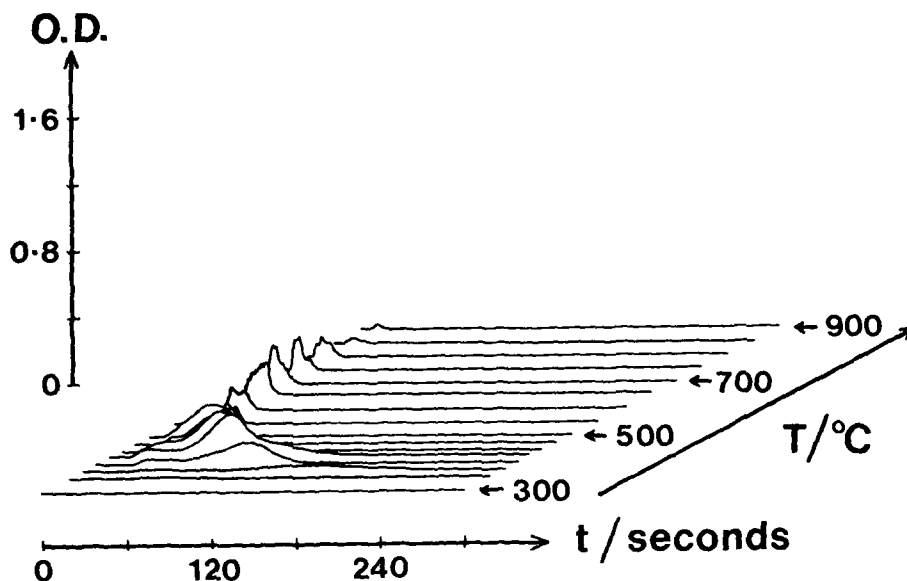


FIGURE 14 - '3D' Smoke plot, FR Cable Jacket

and then falls to less than $40 \text{ cm}^2\text{g}^{-1}$ above 850°C . S is $303 \text{ cm}^2\text{g}^{-1}$ and $S.T.$ is $9.6 \text{ cm}^2\text{g}^{-1}\text{s}^{-1}$. A summary of properties is given in Table 3 together with the corresponding data obtained from the other materials discussed above.

Conclusions

The apparatus described gives useful smoke data rapidly and reproducibly using small samples.

Temperature, and hence radiant heat flux, has been shown to have a major effect on smoke generation. Results show that the measurement of smoke production at one particular temperature or heat flux could be misleading.

References

1. Malhotra H.L., Rogowski B.F.W. and Raftery M.M., 'Smoke tests - a critique' Conference on Smoke and Toxic Gases from Burning Plastics - QMC Industrial Research and the Fire Research Station, London, Jan. 1982.
2. Edgerley P.G. and Pettett K., Fire and Materials 4 (2), 104, 1980 'Further variations of smoke density with heat flux'.
3. Brown L.J.Jr., Federal Aviation Administration Report No FAA-RD-79-26, 1979. 'Smoke emissions from aircraft interior materials at elevated heat flux levels using modified NBS smoke chamber'.
4. AFNOR NF-T51-073, September 1977.
5. Edgerley P.G. and Pettett K., Fire and Materials 2 (1), 11, 1978 'The effect of pyrolysis and combustion temperatures on smoke density'.

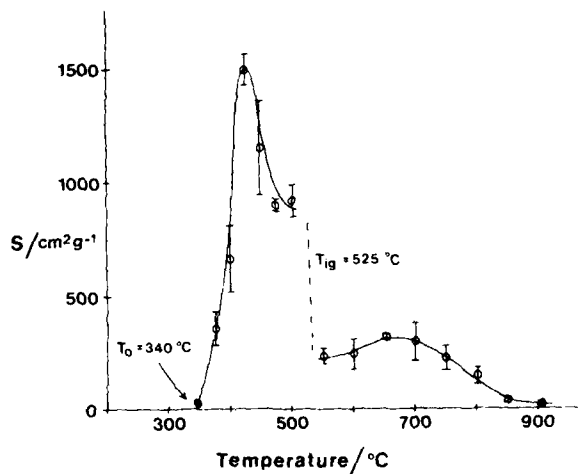


FIGURE 15 - S v T Plot, FR Cable Jacket

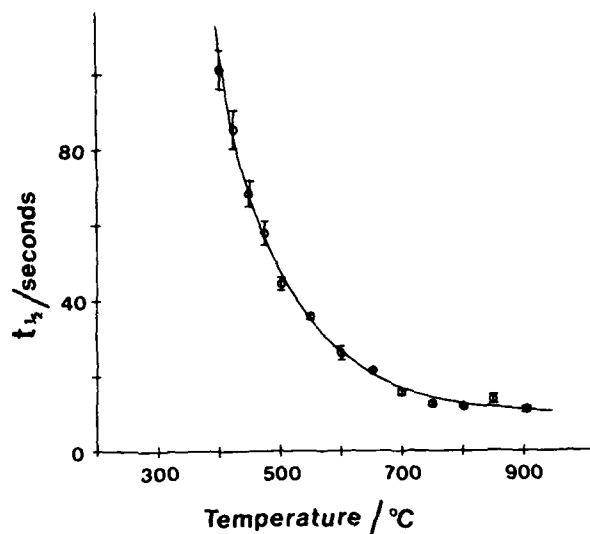


FIGURE 16 - $t_{1/2}$ v T, FR Cable Jacket

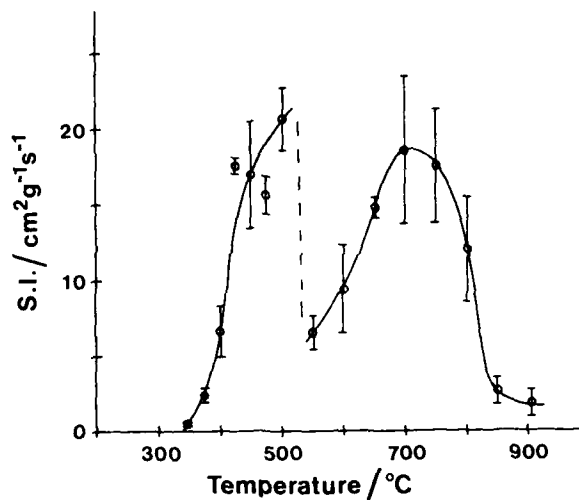


FIGURE 17 - S.I. v T, FR Cable Jacket

TABLE 3

Smoke Properties - Comparative Data

	HDPE	PPEK A	PPEK B	Halogen free FR cable jacket
\bar{S} / cm^2g^{-1}	2340	794	491	303
$\bar{S.I.}$ / $\text{cm}^2\text{g}^{-1}\text{s}^{-1}$	99.6	33.3	14.5	9.6
T_0 / $^{\circ}\text{C}$	295	505	515	340
T_{ig} / $^{\circ}\text{C}$	420	625	650	525
Maximum \bar{S} / cm^2g^{-1}	7500	2500	2500	1500
T at maximum \bar{S} / $^{\circ}\text{C}$	415	620	645	425
Maximum S.I. / $\text{cm}^2\text{g}^{-1}\text{s}^{-1}$	270	175	40	21
T at maximum S.I. / $^{\circ}\text{C}$	900	900	900	520



Richard Whiteley was born in Yorkshire, England in 1947. He received B.Sc. and Ph.D. degrees in Chemistry from Exeter University in 1974 and 1977 and joined Raychem in 1980. He is a Senior Technologist in the Materials Technology Group within Corporate R & D, Swindon, and is involved in the development of low hazard wire and cable products.

AD P000500

A NEW CONSTRUCTION OF HALOGEN-FREE FLAME RETARDANT INSULATED WIRE WITH DOUBLE LAYERS

S. Yamamoto, M. Nishimura, A. Satou, H. Nakae and S. Fujimura

The Furukawa Electric Co., Ltd.

6-1 Marunouchi 2-chome, Chiyoda-ku, Tokyo Japan

Summary

A few halogen-free materials with highly flame retardant properties have been so far reported for cable use, but none of them have been developed for insulated wires to attain UL Std.62 VW-1 Flame Test.

The authors were successful in developing a halogen-free insulated wire by using a combination of the newly developed halogen-free highly flame retardant material and double layers construction. The new construction consists of the outside layer of a highly flame retardant special ethylene-vinyl acetate copolymer and the inside layer of common polyolefin. These double layers are simultaneously extruded through the fixed die to cover a conductor and then crosslinked by an electron accelerator. This insulated wire, passing flame tests like IEEE-383 or UL Std.62 VW-1 and having excellent mechanical and electrical properties that satisfy LOCA Test requirements in IEEE-323, finds not only a particular application to nuclear power plants, but also other wide applications to appliance wires in general use because of the capability of continuous 40,000 hour service at 110°C and high oil resistance. In addition to the inherent halogen-free composition, surprisingly the observed CO generation was one-fifth that of natural polyethylene and no black smoke was produced in combustion.

1. Introduction

To protect peripheral equipment from corrosive gaseous HCl and prevent formation of black smoke and toxic gases during combustion of halogen compounds, a few halogen-free materials with highly flame retardant properties have so far been studied for cable use in nuclear power plants, underground railways and ships. For internal wiring in appliances, however, halogen-free insulated wires that pass the flame test of UL Std.62 VW-1 have not been developed. Flame retardant XL-PVC or XL-FRPE insulated wires now in use produce halogen gases when the wires are used at high temperature for a long term, thereby corroding the periphery equipment. Amplifier relay circuits, which are liable to excessive temperature rise, pose an especially difficult problem.

To obviate such problems, halogen-free compounds can be used for insulation. These prevent the corrosion of equipment due to halogen compounds. However, if an attempt is made to achieve the VW-1 grade with ordinary polyolefine or polyolefine copolymer by using aluminum hydrates, it is necessary to impregnate aluminum hydrates of 2-3 times the polymer. The natural consequence is that the superior mechanical and electrical properties inherent to the polymer will be substantially reduced, thus making it unusable as an insulation material.

We have overcome this problem by developing wires of crosslinked double-layer insulation construction:

- 1) an outer layer of a newly-developed special ethylene-vinyl acetate copolymer (Special EVA) which is highly flame retardant and yet has a brittleness temperature as low as -20°C, and
- 2) an inner layer of common polyolefine with excellent mechanical, water-resistant and electrical properties.

Properties of Special EVA and test results of wires for appliance wiring and for general wiring of trial manufacture are presented in this paper.

2. Properties of Special EVA

2.1 Non-corrosive Special EVA

Non-corrosive Special EVA contains no halogen compounds. Consequently, it does not corrode metals.

The results of tests using the ASTM D2671 Corrosion Testing Method A are shown in Table 1. XL-PVC and XL-FRPE do corrode metals.

Table 1. Corrosive Property

(ASTM D 2671)			
Materials	DT	Condition	Result
XL-PVC	29	180 C X 17 hr	Fail
XL-FRPE	29	180 C X 17 hr	Fail
XL-EVA Spec	48 min	180 C X 17 hr	Pass

* Crosslinked PVC
* Crosslinked Flame Retardant PE
* Crosslinked Special EVA

2.2 Smokelessness

The smoke optical density, C_s max., and the gases produced by combustion of various materials are shown in Table 2. Special EVA produces scarcely any smoke and transmits about 90% or more of light. Also, its CO generation is one-fifth that of flammable polyethylene.

Table 2. Smoke Optical Density and Gas Formation

Materials	OI	Smoke Optical Density (C_s max.)	Gas (mg/g)		
			HC#	CO	CO ₂
XL-PVC	29	4.8	290	100	900
XL-FRPE	29	3.2	180	200	1200
XL-EVA Spec.	48 min.	0.2	0	34	850
XL-PE	18	0.02	0	170	1250

*** None-flame-retardant PE

Method:

- Determination of smoke optical density, C_s max., by JIS D1201 (1973). The concentrations of smoke produced by combustion of materials at the OI value of 0.5 higher than that of each material were obtained with the device shown in Fig. 1.

$$C_s \text{ max} = \left(\frac{2.3}{L} \right) \log_{10} \left(\frac{100}{T_{\min}} \right)$$

where: C_s max = smoke optical density (maximum light reduction coefficient per lm)

L = light path length, 0.5m

T_{\min} = minimum transmission rate at the time of maximum smoke emission, %.

- Determination of gases produced by combustion. A 0.5g specimen is placed in the heating oven shown in Fig. 2 and kept at 800°C for 30 min. Halogen is trapped by a sodium hydroxide solution. This is expressed as the amount of HCl according to the silver nitrate method described by JIS K0107 (1967). The other gases are analyzed separately by gas chromatography. The heating conditions are 800°C x 10 min.

$$S = 36.5 \times \frac{0.1 \cdot f(B-A) \cdot 1000/50}{W}$$

where: S = quantity of HCl produced, mg/g

A = consumption of 0.1N ammonium thiocyanate solution, ml

B = quantity of 0.1N ammonium thiocyanate solution consumed by a blank test, ml

2.3 Mechanical, Electrical and Flame Retardant Properties

The mechanical, electrical and flame retardant properties of crosslinked Special EVA are shown in Table 3. The tensile strength is 0.6 kg/mm² - less than half that of PVC - however, it has

Fig. 1 Oxygen Indexer and Smoke Optical Density Measuring Device

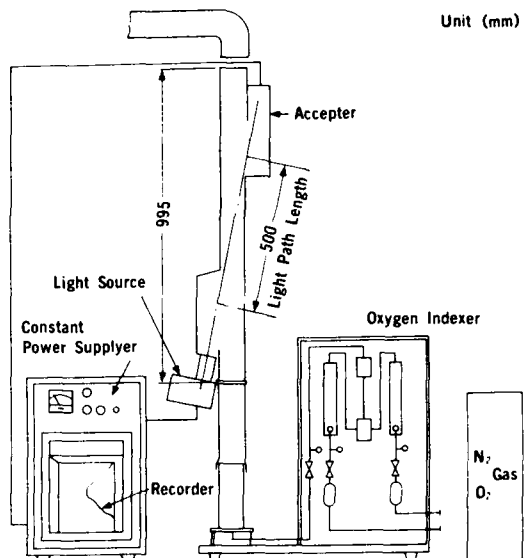
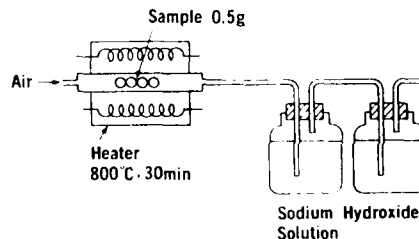


Fig. 2 Halogen Gas Sampler



excellent oil resistance and heat-aging properties. As a plastic offering such high flame-retardant properties as OI 48, UL 94V-0, by addition of aluminum hydrates, it retains excellent mechanical properties, such as a 550% elongation at rupture and a brittleness temperature as low as -20°C.

Table 3. Properties of Special EVA

(Crosslinked by Radiation)

Test	Units	Method	Typical Value
Tensile Strength, min.	kg/mm ²	JIS K6723	0.6
Elongation at Rupture, min.	%	JIS K6723	550
Air Oven Aging, 168 hr at 150 C			
Tensile, min. Retention	%	JIS K6723	90
Elongation, min. Retention	%	JIS K6723	85
Oxygen Index, min.		JIS K7201	48
Brittleness Temperature	C	JIS K6723	-20
Immersion in ASTM Oil No 2			
4 days at 100 C		UL62	
Tensile, min. Retention	%		120
Elongation, min. Retention	%		105
Heat Distortion, 121 C, 2kg. max.		UL62	5
Volume Resistivity	Ω-cm	JIS K6760	1.1 × 10 ¹¹
Flammability		UL94	V-0

3. Trial Manufacture and Evaluation of Wires with Double-layer Insulation for Appliance Wiring

Special EVA is applicable only to particular low-voltage wires because of its low tensile strength and low dielectric strength $\sim 1.1 \times 10^{13} \Omega \cdot \text{cm}$. Therefore, the possibility of making up for these deficiencies in mechanical strength and electrical properties with a separate polymer was investigated. The inevitable conclusion was that the application of a polymer blending technique would degrade the excellent flame retardant properties of Special EVA with no appreciable improvement in its electrical properties.

Thus, a double-layer insulation configuration employing a polymer with excellent mechanical and electrical properties around the conductor was investigated. As the inner layer insulation an ordinary LDPE with tensile strength of 2.3 kg/mm², elongation of 750% and M.I. 0.3 was adopted.

In the manufacture of this double-layer insulation wire, a double-layer fixed die originally developed by The Furukawa Electric Co., Ltd.⁽⁴⁾ was employed and then crosslinked by an electron accelerator.

The construction of the trial manufacture sample is shown in Fig. 3, and the layout of the fixed die in Fig. 4.

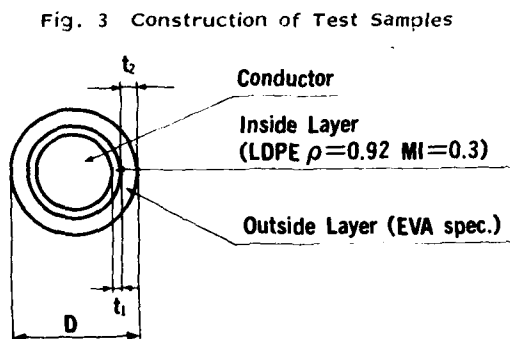
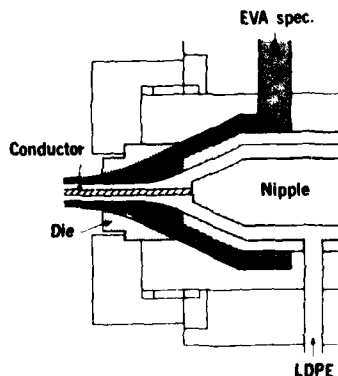


Fig. 4 Fixed Die for Double Layers Extrusion



3.1 Details of trial manufacture samples

By adopting three sizes of typical conductors commonly used as appliance wires, and varying the insulation thickness of the LDPE inner layer and special EVA outer layer, respectively, 25 kinds of wires were manufactured on a trial basis. Table 4 shows the construction of each sample.

Table 4 Test Sample Description

Sample No.	Conductor		Thickness of Inside Layer (t _i) mm	Thickness of Outside Layer (t _o) mm	Outer Diameter mm	Inside Layer Ratio (t _i /(t _i +t _o))
	Type	Diameter mm				
1	0.4ϕ Copper	0.4	0	0.20	0.80	0
2			0.07	0.18		0.1
3			0.03	0.17		0.15
4			0.04	0.16		0.2
5			0.05	0.15		0.25
6			0.07	0.13		0.35
7			0.09	0.11		0.45
8			0.10	0.10		0.5
9			0.13	0.07		0.65
10			0.15	0.05		0.75
11			0.17	0.03		0.85
12	20/0.18 Strand Tinned Copper	1.0	0.10	0.40	2.0	0.2
13			0.15	0.35		0.3
14			0.20	0.30		0.4
15			0.25	0.25		0.5
16			0.30	0.20		0.6
17			0.35	0.15		0.7
18			0.40	0.10		0.8
19	17/0.26 Strand 2.0mm Tinned Copper	1.8	0.10	0.50	3.0	0.17
20			0.15	0.45		0.25
21			0.20	0.40		0.33
22			0.25	0.35		0.42
23			0.30	0.30		0.5
24			0.35	0.25		0.58
25			0.40	0.20		0.67

3.2 Measurement Results

3.2.1 Elongation and tensile strength

Figure 5 shows a typical stress-strain curve. The tensile test of the insulation was conducted at a pulling speed of 500m/min on a gauge mark of 1 inch in accordance with UL 62.

Figures 6 and 7 show the elongation and tensile strength values, respectively.

The elongation of PVC or XLPE required by UL 62 is over 100%. However, since all samples show elongations of over 350%, all satisfy the standard.

The tensile strength requirement under UL 62 is more than 1500 psi (1.05kg/cm²), so the inside layer ratio should be set to 0.25 or more.

3.2.2 UL 62 VW-1 flame test

In the UL 62 VW-1 flame test, with natural or propane gases as a gas source, a flame of a given length is applied to the wire such that the flame's blue core touches the wire 5 times for 15 sec each time. The testing device is shown in Fig. 8.

The judgment factors are:

- 1) The specimen should not flame longer than 60 sec after any application of flame.
- 2) No more than 25% of the kraft paper should be burned or charred.
- 3) The absorbent cotton should not be burned.

The test results for each wire are shown in Fig. 9, the 0.5mm² wire is most flammable, and

its inside layer ratio should be maintained at 0.3 or less.

3.2.3 Dielectric breakdown strength and insulation resistance

After a 1 hr immersion in water, all 30 m long wires were subjected to measurements of dielectric breakdown strength and insulation resistance. The results are shown in Figs. 10 and 11.

A dielectric breakdown strength at 3500V/min or more is sufficient for practical applications. This wire, with a breakdown strength of over 8,000V when the inside layer ratio is 0.1, is adequate for practical use.

The assured insulation resistance is 250M Ω ·km or more for common PVC and 2500M Ω ·km or more for FR-PE. The assured range of this double-layer insulated wire is 1000M Ω ·km or more.

3.2.4 Optimal inside layer ratio

The worst wire in terms of flammability properties is 0.5mm² conductor wire. If the inside layer ratio is raised above 0.4 for 0.5mm² wire, the wire is disqualified for VW-1.

However, if the inside layer ratio is reduced to the extreme, the tensile strength will fall below 1.05kg/mm². Consequently, a ratio somewhere around 0.3 is optimal.

Further, in the case of ϕ 0.4 and 2.0mm², an inside layer ratio as low as 0.5 is permissible. Of course, a larger inside layer ratio affords higher tensile strength and better electrical properties.

3.2.5 Typical properties of double-layer insulated appliance wires

A comparison was made between the major properties of the double-layer insulation and the PVC insulation UL style 1007. The results are shown in Table 5. The double-layer insulated wire is far superior in air-oven aging and oil-resistance properties and is adequate for use as the UL 105°C rating grade.

Table 5 Comparison of Properties with PVC Wire

Test	Halogen Free Flame Retardant Insulated Wire with Double Layers (Sample No. 1)	UL1007 (None Crosslinked PVC)	UL Value (105°C)
T.S.	1.15kg/mm ²	1.75	1.05
El.	580 %	250	100
Air Oven Aging	150°C 2 days		
	T.S. Retention	94 %	75
	El. Retention	94 %	65
	150°C 1 day		
	T.S. Retention	90.6 %	110.2
	El. Retention	87.2 %	55
150°C 2 days	T.S. Retention	92.5 %	
	El. Retention	87.2 %	
	El. Retention	87.2 %	
Immersion in Oil ASTM No. 100 C 100 C 100 C	T.S. Retention	94 %	123.3
	El. Retention	109 %	68.8
Heat Distortion (UL167) 120°C 200g	40 %	11.0	50
Resistance to Self Solder (MIL W 16878 D)	Pass	Pass	
Heat Shock	Pass (150°C 1hr)	Pass (146°C 1hr)	
Cold Bend	Pass (-10°C)	Pass (-10°C)	

Fig. 5 Stress-Strain Curve of Insulation with Double Layers

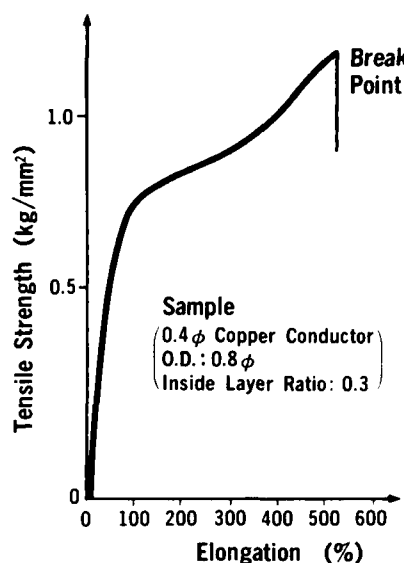


Fig. 6 Elongation of Insulation

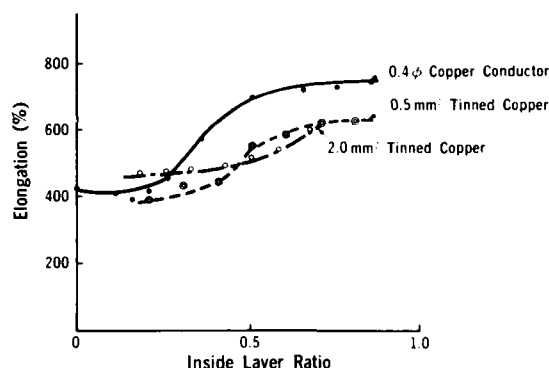


Fig. 7 Tensile Strength of Insulation

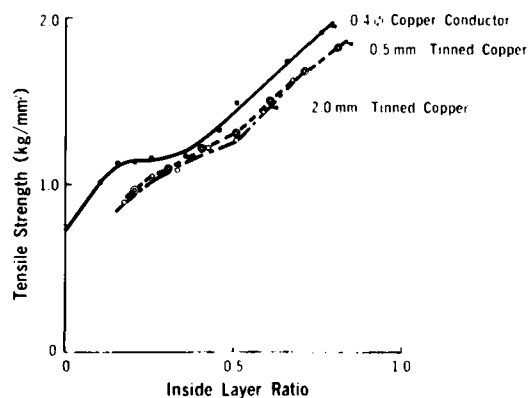


Fig. 8 Flame Test Device For UL62 VW-1

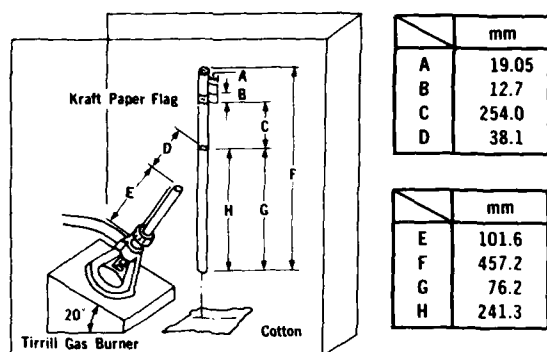


Fig. 9 Flammability of Wire

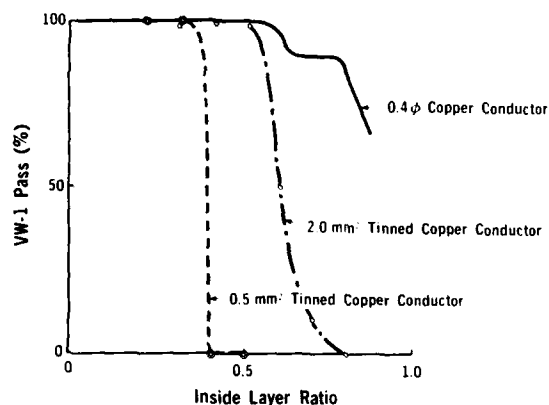
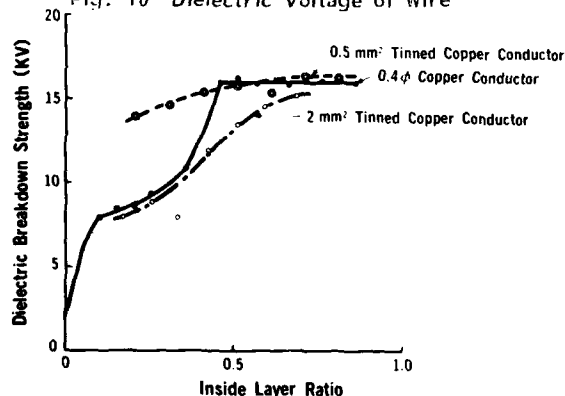


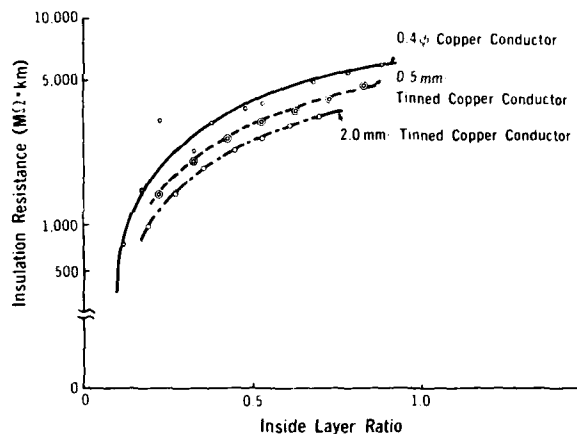
Fig. 10 Dielectric Voltage of Wire



4. Application to Wires for General Wiring

Unlike appliance wires, general wiring cables require water resistance as well as flame retardance satisfying the requirement for laying cables in vertical trays in IEEE 383. Furthermore cables used in nuclear power plants should clear the LOCA test. A test was made to determine whether halogen-free double-layer insulation can satisfy these requirements.

Fig. 11 Insulation Resistance of Wire



4.1 Sample

Assuming a 600V rating, the sample shown in Table 6 was manufactured on trial for evaluation.

4.2 Measurement Results

The measurement results are shown in Table 7. Since the LOCA test would take 100 days if it were conducted in exact conformity with IEEE 323, a short-term evaluation method based on IEEE 323 was employed.

The LOCA test conditions are shown in Fig. 12. The halogen-free double-layer insulated wires passed the IEEE 383 flame test as well as the water-resistance and LOCA tests which were considered difficult for XL-PVC or XL-EPPE wires to clear.

Table 6 Dimensions of Test Sample

Conductor	0.3 ϕ
Inside Layer Ratio	0.55
Outer Diameter	2.1 ϕ

Table 7 Properties of Double-layer Insulated Wire

Test	Method	Units	Typical Value	Requirements of UL44 Class XL Thermosets
Tensile Strength	UL44	kg/mm	105	105
Elongation	UL44	%	450	150
Capacitance & Stability Factor	UL44			
Specific Inductive Capacity after 24hr	UL44		4.8	5
Capacitance at 14days		%	100	110
Capacitance at 24hr		%	100	104
Capacitance at 7days				
Stability Factor at 14days			0.09	1
SF at 14days			0.283	0.5
SF at 24hr				
IEEE383 Vertical Tray Flame Test	IEEE383		Pass	—
LOCA Test	Based on IEEE323		Pass	—

[illegible]

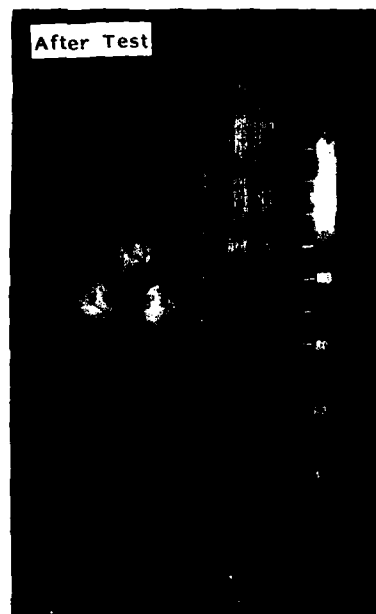
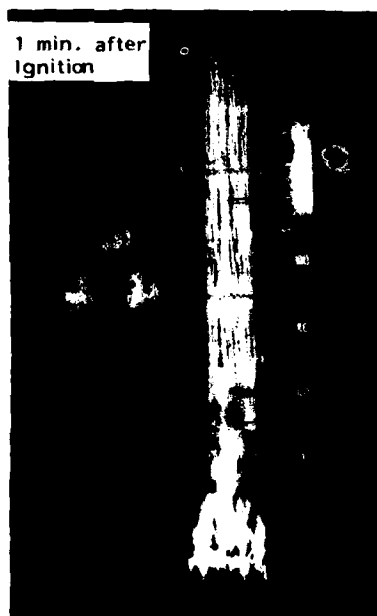
A crosslinked halogen-free, double-layer insulated wire that supersedes PVC, XL-PVC, and XL-FRPE insulated wires for appliance wiring was developed. This wire has non-corrosive properties and high flame retardance satisfying UL 62, VW-1. Furthermore, the halogen-free, double-layer insulated wire for general wiring has passed all the water resistance test under UL 44, the vertical-tray flame test under IEEE 383 and the LOCA test based on IEEE 323. The newly developed halogen-free, double-layer insulation is applicable to appliance wires for continuous use over 40,000 hours at 110°C, control and power cables for general use such as buildings, subways, and ships, and cables and wires for nuclear power plants. In addition to the inherent halogen-free composition, surprisingly the observed CO generation was one-fifth that of natural polyethylene and no black smoke was produced in combustion.

- 1) H. A. Mayer, G. Hög, 29th IWCS Proceedings 253 (1980)
- 2) H. Harbort, 29th IWCS Proceedings 263 (1980)
- 3) U. Ueyama, et al., Fire Vol. 29 No.3 120 Japan (20 June 1979)
- 4) K. Fuse, 27th IWCS Proceedings 62 (1978)



Conductor: 2.0 mm²
O.D.: 3.0 mm
Inside Layer Ratio: 0.42

Conductor: 0.86
O.D.: 2.4 mm
Inside Layer Ratio: 0.35





SHOJI YAMAMOTO
The Furukawa Electric
Co., Ltd.
6-Yawata-Kaigandori,
Ichihara, Chiba
Japan

Mr. Yamamoto graduated from Hakodate Technical College in 1972, where he majored in Industrial Chemistry. Then he joined The Furukawa Electric Co. Ltd. and has been engaged in research and development of flame retardant plastics and manufacturing methods for foamed plastic insulation.

Mr. Yamamoto is now a member of the Material Research Department of the Telecommunication Laboratory.



MASAO NISHIMURA
The Furukawa Electric
Co., Ltd.
6-Yawata-Kaigandori,
Ichihara, Chiba
Japan

Mr. Nishimura graduated from Kyoto University 1969 with M.Sc. in Applied Chemistry. Then he joined The Furukawa Electric Co., Ltd. and has been engaged in research and development of plastic materials and manufacturing methods for cable.

Mr. Nishimura is now a assistant manager of the Research and Development Department, Fiber Optics Division at the Furukawa Electric Co., Ltd. and a member of the Institute of Electronics and Communication Engineers of Japan.



ATUO SATO
The Furukawa Electric
Co., Ltd.
6-Yawata-Kaigandori,
Ichihara, Chiba
Japan

Mr. Sato graduated from Sibauro Institute University in Electrical Engineering in 1976. Then he joined The Furukawa Electric Co., Ltd. and has been engaged in development of tape heaters and manufacturing methods for flexible print circuit.

Mr. Sato is now a staff engineer of the Electric Appliance Wire and Product Division at

The Furukawa Electric Co., Ltd.



HIROYUKI NAKAE
The Furukawa Electric
Co., Ltd.
The Central Research
Laboratory
9-15, 2-chome, Futaba,
Shinagawa-ku, Tokyo
Japan

Mr. Nakae graduated from Kyoto University in 1966 with M.Sc. in Chemistry. Then he joined The Furukawa Electric Co., Ltd. and has been engaged in research and development of plastic composite materials.

Mr. Nakae is now a member of The Chemical Society of Japan and The Ceramic Society of Japan.



SYUNICHI FUJIMURA
The Furukawa Electric
Co., Ltd.
5-1-9 Higashiyawata,
Hiratsuka,
Japan

Mr. Fujimura graduated from Osaka University in synthetic chemistry in 1971. Then he joined the Furukawa Electric Co., Ltd. and has been engaged in research and development of plastic materials for nuclear power cable.

Mr. Fujimura is now a member of the Research and Development Division of the Hiratsuka Research Laboratories.

AD P000391

BANDWIDTH CHARACTERIZATION OF FIBER WAVEGUIDE
SYSTEMS WITH FUSION-SPLICED MULTIMODE GRADED-INDEX FIBERS

Eugene W. Riley

Anaconda-Ericsson, Inc.
Overland Park, Kansas 66204

Abstract

Fiber splice losses and the effect of splices upon the overall loss of built up connections have received considerable attention in the literature from both a theoretical and experimental viewpoint.¹ The methods for determining system bandwidth from measurements on individual fiber lengths, and the effect of splices upon system bandwidth, on the other hand, still is a subject of much debate. In this paper, several different approaches found in the literature are reviewed, some results from bandwidth measurements made at 850 nm on built-up system lengths of telecommunications grade, multimode, graded-index fibers using both time domain and frequency domain measurement techniques are presented and the effect of fusion splices upon bandwidth is examined. The accuracy of the often-used approximate method of bandwidth determination from pulse broadening measurements assuming a Gaussian shaped fiber transfer function also is evaluated.

Introduction

When a communication system consists of conventional transmission media, such as balanced cable pairs or coaxial cable, systems engineers confronted with the task of predicting system performance face no appreciable difficulty. Armed with typical transmission parameters per unit length for such facilities, and statistical bounds on these parameters, one can mathematically extrapolate the data using established procedures, to define, with reasonable accuracy, the overall system parameters. Connectors and splices within the system are essentially transparent (i.e., have little or no effect upon the transmitted signal). The same cannot be said of communication systems configured from multimode graded-index optical waveguides.

To provide some insight into the reasons for this difference, let us consider the following analogy. Suppose we were to use, as a single transmission path, a cable consisting of a parallel arrangement of a large number of dissimilar individual conductors,

each with its own propagation characteristics and each subject to mutual electromagnetic interference coupling to and from the others. We would, in order to define the frequency response of such a transmission path, be required to investigate: (1) how the input power divides among the various conductors, (2) the effect upon the transmitted power of electromagnetic coupling between the conductors, and (3) the effect of the propagation characteristics of each conductor upon that portion of the signal power carried by it. To complicate things even further, if, at connectors or splices, there occurred a "redistribution" of power among the various conductors, this would have to be accounted for in a built-up system. The simple task described above then would become much more complex. This is essentially the problem the systems engineer faces when designing a lightwave system using multimode, graded-index optical waveguides.

As the name implies, a multimode optical waveguide is a single transmission facility wherein the input signal is transmitted over many parallel transmission paths (or modes), each with its own power input characteristics, each subject to electromagnetic power coupling (here called distributed mode coupling) to and from the others along a length of the waveguide, and each with its own axial propagation constant. Furthermore, a redistribution of power amongst the modes (here called lumped mode coupling) may occur at points where the fibers are joined by splices or connectors. The bandwidth performance of a built-up system, because of the situation described above, will at least be influenced by the following factors:²

1. Mode Coupling - the exchange of power among modes
 - (a) distributed
 - (b) lumped
2. Differential mode delay - The variation in propagation delay that occurs because of the different group velocities of the modes
3. Differential mode attenuation - The variation in attenuation among the propagating modes.

It has been shown^{3,4,5} that in order to accurately predict the frequency response of systems incorporating multimode fiber waveguides, it is necessary to combine the powers flowing in the different mode groups using rather complex mathematical procedures - too complex to be mutually beneficial to most fiber waveguide cable suppliers and users - which take into account the factors mentioned above. A considerable amount of research effort has been expended during the past few years to develop simple yet accurate methods of defining, measuring and using the propagation characteristics of multimode fibers to predict system performance. In spite of this effort, and even though the application of multimode fiber for communications is well into its second decade, it was stated as recently as within the last year that "accurate prediction of the waveguide bandwidth from measurements on individual fibers within a link is still very much a problem".⁶ Since it is this problem which we will be addressing in this paper we begin by repeating here, as a point of reference, the generally accepted definitions of fiber bandwidth and fiber transfer function and we discuss the accepted measurement procedures for them.

Fiber Bandwidth and Fiber Transfer Function

Fiber bandwidth is defined as follows²:

"The lowest frequency at which the magnitude of the fiber transfer function decreases to a specified fraction of the zero frequency value. Often the specified value is one-half the optical power at zero frequency".

This is usually designated by BW (3 dB₀) and referred to as the 3 dB optical bandwidth. In the above the transfer function is defined as²:

"The complex function, $H(f)$, equal to the ratio of the output to input of the device as a function of frequency. The amplitude and phase responses are, respectively, the magnitude of $H(f)$ and the phase of $H(f)$. Note 1. For an optical fiber, $H(f)$ is taken to be the ratio of output optical power to input optical power as a function of modulation frequency. Note 2. For a linear system, the transfer function and the impulse response $h(t)$ are related through the Fourier transform pair, a common form of which is given by

$$H(f) = \int_{-\infty}^{\infty} h(t) \exp(i2\pi ft) dt$$

and

$$h(t) = \int_{-\infty}^{\infty} H(f) \exp(-i2\pi ft) df$$

where f is frequency".

One almost universally accepted method of measuring the fiber transfer function and fiber bandwidth is the following:⁷ The fiber is excited, under carefully controlled conditions, with an optical pulse of short time duration and narrow spectral width. After transmission through a length of fiber the pulse is detected at the output. The input and output pulses are transformed from the time domain to the frequency domain, to obtain the fiber transfer function, using the Fourier transform techniques described above. The 3 dB optical bandwidth then is determined from the transfer function in accordance with the foregoing definitions. The procedure outlined here is referred to as a "time-domain" measurement of the fiber transfer function and fiber bandwidth. The measurement of the characteristics directly in the frequency domain by sinusoidally modulating the light source also is an accepted procedure⁸ and is referred to as a "frequency-domain" measurement.

Although these procedures are suitable for determining the bandwidth performance of a length of fiber (be it an individual length or a concatenation of individual lengths) they provide no information on how data taken on individual fibers may be used to determine, in advance of measurement, what frequency response may be expected to be achieved in a concatenated length. It has become common practice to calculate system bandwidth from bandwidth data obtained on individual fibers using an assumed length-dependency factor (γ) and the following expression:

$$(BW_S)^{-1/\gamma} = \sum (BW_i)^{-1/\gamma}$$

where, BW_S = system bandwidth in MHz
 BW_i = measured bandwidth of i -th fiber

When the concatenated lengths and measured bandwidth-length products do not differ significantly the following approximate formula may be used:

$$BW_S = \frac{\overline{BW}}{L^\gamma}$$

where, \overline{BW} = the average bandwidth-length product in MHz-km
 L = system length in kilometers

γ -factors used for systems capable of operating near 850 or 1300 nanometers (single window) range from about 0.7 to 0.8, while for systems capable of operating near both 850 and 1300 nanometers (double window) γ usually is assumed to be 0.9.

Recognizing that the above is an approximate method, many researchers have invested considerable time and effort recently to develop more accurate alternate procedures. In the following section, we review some of the more recent approaches suggested in the literature for predicting and/or optimizing system bandwidth.

Suggested Approaches

The fiber transfer function defined above is a single composite function of frequency which simultaneously accounts for the power flow in all modes. The relationship between output power and input power is expressed by a single equation of the form,

$$P_o(f) = H(f) P_i(f)$$

Holmes⁶ has shown that the solution of the coupled power flow equations for mode groups is represented by M-dimensional matrices, where M is the maximum number of mode groups in the fiber. He investigated the case wherein the modes are divided into low and high order groups, yielding a matrix equation of the form,

$$\begin{bmatrix} (P_l)_o \\ (P_h)_o \end{bmatrix} = \begin{bmatrix} H_{ll} & H_{lh} \\ H_{hl} & H_{hh} \end{bmatrix} \times \begin{bmatrix} (P_l)_i \\ (P_h)_i \end{bmatrix}$$

The elements of the 2 x 2 power transfer matrices were determined for two 1.1 km fibers by group mode filtering and application of the transfer function measurement procedure outlined in the previous section. The frequency response of the 2.2 km length formed by splicing the two fibers was predicted using the transfer matrix model. The splice was accounted for in the calculations by means of a splice matrix of the form,

$$\begin{bmatrix} 1. & -c \\ c & 1. - c \end{bmatrix}$$

Very good correlation between the measured and computed frequency response was reported for a splice coupling coefficient $c = 0.5$.

Rodhe⁹ has described a method for obtaining a matrix transfer function for a two-mode fiber which accounts for mode coupling, differential mode delay and differential mode attenuation. This method, which utilizes least-square optimization to obtain the matrix transfer function, requires only the measurement of the transfer function and index profile.² Of course, since the matrix equations are M-dimensional, computation time will increase as the maximum number of modes, M, increases, but no additional measurements would be required. The length dependence of the matrix transfer model was investigated and very good correlation between measured and calculated results was observed. The model did not include the effect of splices but it appears that a splice matrix, such as that proposed by Holmes could be easily added. Application of the model to a concatenated length with a larger number of modes should be of interest.

Ohashi and colleagues¹⁰ derived a mode transfer matrix which accounts for mode coupling at a fusion splice. A 2 km length of multimode graded index fiber was cut at the midpoint and repeatedly respliced, the splice loss and 3 dB₀ bandwidth being measured each time. A strong relationship between splice loss and bandwidth was observed. For fibers with similar index profiles the bandwidth increased with splice loss due to increased mode coupling. The slope of the curve was quite steep in the range of 0 to about 0.4 dB splice loss, but approached an asymptotic limit beyond this interval. The total increase in bandwidth in the interval from 0 to 0.25 dB splice loss was approximately 10%. For fibers with dissimilar index profiles, on the other hand, the bandwidth decreased as splice loss increased. Bandwidths calculated for several values of splice loss using the mode transfer matrix model were in very good agreement with the experimental results. A continuous 10 km length of fiber also was investigated. One kilometer sections were cut, consecutively, from the output end and the bandwidth was measured on the remaining section. The fibers then were respliced in reverse order and the bandwidth was remeasured after each splicing operation. The bandwidth increase due to mode coupling at the splices again was found to be about 10% (corresponding to $\gamma = 0.96$ for a 10 km system) and the correlation between measured data and that calculated using the transfer matrix model was very good.

Love¹¹ has investigated the possibility of system bandwidth optimization and prediction by considering modal delay equalization in terms of peak bandwidth performance as a function of wavelength. Two fibers with peak bandwidths of 1.0 GHz-km and 2.5 GHz-km at approximately 800 nm and 1450 nm, respectively were spliced. Calculations predicted that the peak bandwidth of the concatenated length would be 1.86 GHz-km at about 1100 nm. The measured result was in very good agreement with the predicted value. This method shows excellent promise for optimizing system bandwidth by judicious placement of the fibers in the built-up connection. It does, however, require spectral bandwidth measurements on the individual fibers rather than a single measurement at a proposed operating wavelength. Love has also shown that for operation near the wavelength corresponding to peak bandwidth, the bandwidth decreases with length according to the square root law ($\gamma = 0.5$) up to approximately a limiting length l_s which is quite long for fibers in current production. Operation at or near the peak bandwidth wavelength is, therefore, very desirable; or, stated another way, manufacture of fibers with peak bandwidth wavelengths near the proposed operating wavelength is highly desirable.

Tanifuji¹² investigated, both analytically and experimentally, the effect upon modal delay compensation of deviations from a power law function for the index profiles of spliced fibers. A model for the index profiles based on a polynomial representation rather than a square law representation was developed. Concatenated bandwidths (assuming no lumped mode coupling at splices) were predicted using the model and results were verified experimentally. Comparison also was made to predicted bandwidths using the power law model for the index profiles. It was concluded that fibers for which the index profiles deviate from a power law function exhibit much lower levels of modal delay compensation than would be predicted using a power law representation for the profiles, but that the polynomial representation is capable of predicting the frequency response within about 5%.

Wright and Nelson¹³ investigated lumped mode coupling effects at splices for a segment consisting of three spliced fibers wherein each fiber had a twin-peaked impulse response. Twin-peaked Gaussian models of the impulse responses were developed which demonstrated good correlation with the measured responses when 50% modal power coupling at the splices was assumed. Eleven additional fibers were spliced to the 3-fiber segment, bandwidth being measured as each additional fiber was added. Measured bandwidth showed a linear length dependence out to about 8 km. Bandwidth calculated from the twin-peaked Gaussian model of the fiber transfer function also exhibited linear length dependence when 50% mode coupling at splices was assumed. However, when a single Gaussian pulse was used to model the impulse response the bandwidth varied approximately as $L^{0.8}$ with 50% mode coupling. Since this agreed with results reported by Suzuki and colleagues¹⁴, it was concluded that an assumption of at least 50% mode coupling at splices is not unreasonable. Furthermore, this appears to be in agreement with the results obtained by Holmes wherein very good correlation was obtained between computed and measured results when a coupling factor of 0.5 was assumed.

Lowe and colleagues¹⁵ investigated the effect of splicing a fiber with low bandwidth into a link with four other fibers having much higher bandwidth. The fibers were 2.0 km long and measurements were made at 1300 nm. It was shown that the overall frequency response was virtually independent of the position of the low bandwidth fiber in the link, but that the system bandwidth decreased drastically at the point of insertion of the high dispersion fiber. The additional fibers spliced beyond this point had negligible influence on the system bandwidth. Most interesting, however, was the fact that the end-to-end frequency response, at least out to the frequency corresponding to the 3 dB bandwidth, was pre-

dicted with reasonable accuracy by decibel addition of the frequency responses of the individual fibers. This, by far, is the simplest and most useful means of determining system frequency response from measurements on individual fibers, assuming it can be shown to be a valid approach in the general case. It was stated that the fibers used in this investigation had similar index profile characteristics; therefore, modal delay compensation may have been negligible. The average measured bandwidth for the five individual fibers was 464 MHz and the average bandwidth measured on the concatenated lengths was 108 MHz. Assuming two kilometer individual lengths this corresponds to a γ -factor of 0.93 which is in good agreement with the results published by Ohashi¹⁰. The calculated bandwidth using dB addition was 119 MHz, corresponding to a γ -factor of 0.89.

Experimental Results

The results reported herein were obtained from measurements made on 6-fiber cables of the filled, loose-tube, helically-laid design with an effective fiber bending radius of 10.5 cm. The fibers were optimized for transmission in the 820 to 880 nm band. Measurements were made at 850 nm using standard launch conditions. A mode scrambler was employed to establish steady state launch conditions for both the time domain and frequency domain measurements.

A 2126 meter length was cut into two lengths of 1049 and 1077 meters. Bandwidths were measured on the individual fibers using the time domain measurement procedure. The cables were respliced and the bandwidth measurements repeated. Results are shown in Table I.

Table I
Bandwidth in MHz
850 nm

Fiber	Measured				Calculated	γ
	1049r	1077m	2126m*	2126m**	2126m***	
1	650	860	328	363	378	1.05
2	842	862	440	451	426	0.92
3	668	806	377	387	369	0.94
4	666	778	337	407	361	0.84
5	784	767	333	374	388	1.05
6	743	551	279	326	323	0.99

*Initial measurement; **spliced measurement
*** $\gamma = 1.0$ assumed.

It is seen that the bandwidths for the spliced length exceeded those for the original length in every case. Although the average percent increase (11%) is in close agreement with the results reported by Ohashi¹⁰, the variation among the six fibers is quite large (2.5 to 22%). The expected bandwidths assuming $\gamma = 1.0$ were calculated and also are shown in Table I, along with the

values of γ required to yield the measured results. The measured transfer functions were compared to a Gaussian curve passing through the 3 dB₀ frequency point as shown in Figure 1. The Gaussian approximation generally underestimated the magnitude of the transfer function at frequencies below that corresponding to the 3 dB₀ point as shown by curves A.

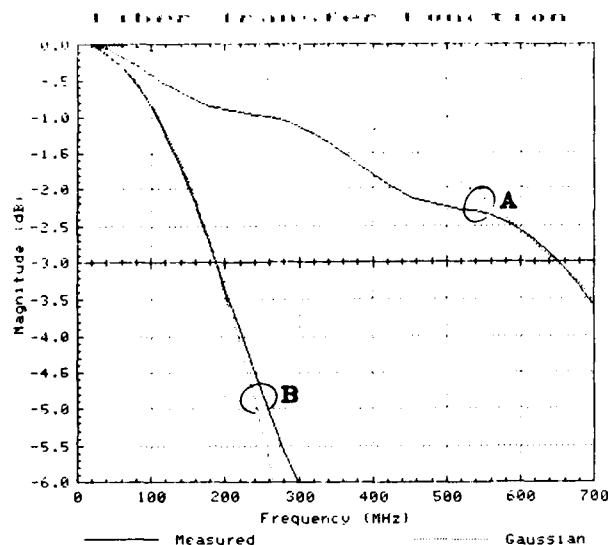


Figure 1. Transfer Function and Gaussian Approximation. A. Fiber No. 1, 1049 m; B. Four-fiber concatenation, 4196 m

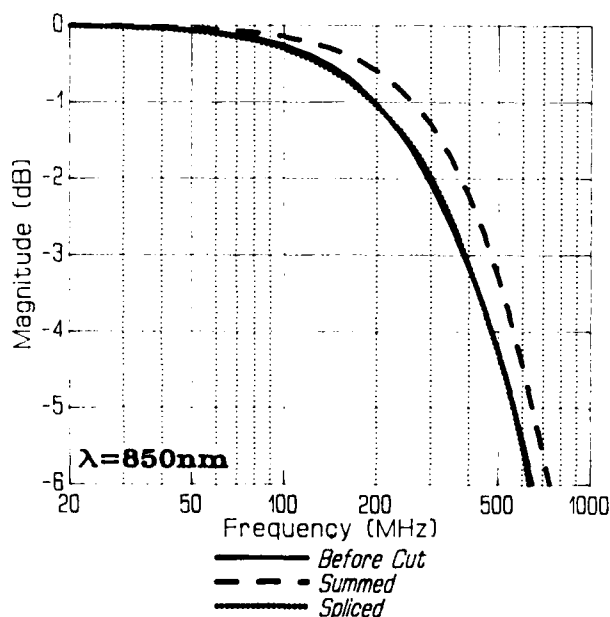


Figure 2. Measured vs. Calculated Transfer Functions. Fiber No. 3

An attempt was made to predict the frequency responses of the respliced fibers using point-by-point addition of the individual frequency responses. The measured 3 dB₀ bandwidths differed from the calculated values by amounts ranging from 12% to 36%, the computed result being an overestimate in each case.

Figure 2 shows typical results obtained on fiber number 3 which exhibited 21% difference between measured and computed values. The responses for the computed curves were within one dB of the measured values at the 3 dB₀ frequency in all cases.

Five of the fibers in the 1049 meter length of cable were fusion spliced as shown in Figure 3.

650	411	273	188					
<u>1</u>	x	<u>2</u>	x	<u>3</u>	x	<u>4</u>	x	<u>5</u>
685		404		279		184		

Figure 3. Concatenated Fibers and Measured Bandwidth in MHz

Results obtained from bandwidth measurements made on the concatenated lengths at 850 nm using the time domain technique are shown in the upper level of the figure. We were unable to obtain meaningful bandwidth results beyond 5 km due to limitations in the measurement setup; however, longer concatenations were evaluated using the frequency domain measurement technique.

Length dependency factors γ were calculated for each concatenation and are shown in Table II. Calculated system bandwidths based on $\gamma = 1.0$ also are shown.

Table II

Concatenated Measurements - Time Domain

Concatenation	Length (m)	Bandwidth in MHz		γ
		Calc.	Meas.	
		$\gamma = 1.0$		
1-2	2098	373	411	.87
1-3	3147	240	273	.89
1-4	4196	177	188	.96

The measured bandwidths ranged from 6 to 14% higher than those calculated using $\gamma = 1.0$ which is in good agreement with results reported by Ohashi¹⁰. The Gaussian approximation to the transfer function was excellent for the four-fiber concatenation as indicated by Curves B in Figure 1.

An attempt again was made to predict the frequency responses for the concatenated lengths using point-by-point addition of the indi-

dual fiber responses. Results are shown in Figure 4. Except for the two-fiber concatenation, the results were uncorrelated.

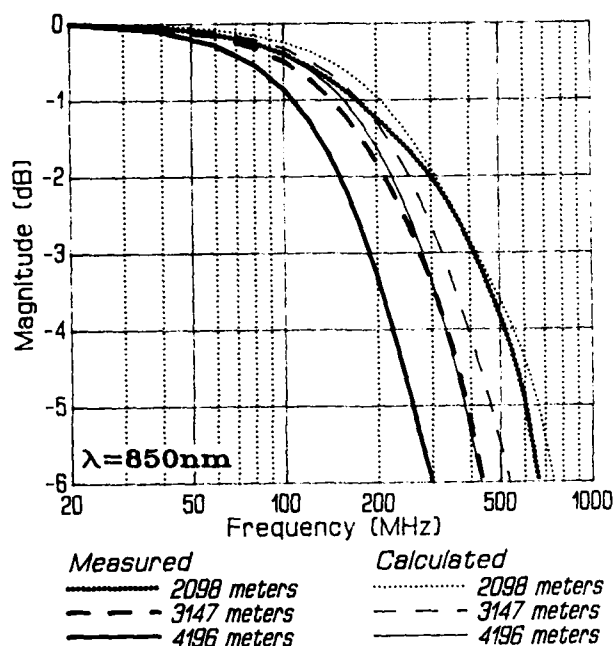


Figure 4. Measured Vs. Calculated Transfer Functions. Concatenated Lengths

The spliced fibers then were cut back leaving approximately two meters of fiber beyond each splice. Bandwidths were again measured at the points where the fibers were cut and results are shown in the lower level of Figure 3. It is seen that the bandwidth changes at the splice were negligible except for the first splice.

The measurement sequence described above was repeated for concatenated lengths up to 8448 meters using frequency domain measurement

techniques. Results are summarized in Table III. Differences between time domain and frequency domain results, on those lengths for which both methods were employed, ranged from 3 to 7%. It is again seen that changes in bandwidth across the splices are negligible.

Calculated system bandwidths using bandwidths measured on the individual fibers in the time domain and an assumed $\gamma = 1.0$ also are shown as well as values of γ required to yield the results measured in the frequency domain.

Personick¹⁶ showed that, as a result of mode coupling, the shape of the transfer function of a fiber (or a concatenated length of fibers) approaches a Gaussian form when the length is sufficiently long. Under these conditions the 3 dB₀ bandwidth can be calculated from the simple formula,

$$BW (3 \text{ dB}_0) = \frac{440}{\sqrt{T_2^2 - T_1^2}}$$

where T_1 and T_2 are the widths in nanoseconds of the Gaussian input and output pulses at one-half the pulse height (full-width, half-maximum). The denominator in the above expression is the pulse dispersion expressed in nanoseconds and is assumed to vary linearly.

Many industry specifications for fiber waveguide cables specify minimum bandwidth as determined by the above relationship. This, however, is a gross approximation for typical reel lengths (1-2 km). Figure 5 shows a comparison of bandwidths determined as above at 850 nm on 106 fibers approximately 1.1 kilometers long and those obtained by Fourier transform techniques described in reference 7. The solid line represents the above formula; the dashed line, the least squares fit to the plotted data. The differences range from -28.0% to +29.2% which agrees closely with results reported previously on a

Table III

Concatenated Measurements
Time Domain and Frequency Domain

Concatenation	Length (m)	Bandwidth in MHz					
		Measured		Frequency Domain		Calculated $\gamma = 1.0$	Derived γ -factor
		Time Domain Before Splice	Time Domain After Splice	Frequency Domain Before Splice	Frequency Domain After Splice		
1-2	2098	411	404	385	360	373	0.96
1-3	3147	273	279	265	265	240	0.91
1-4	4196	188	184	200	205	177	0.91
1-5	5245	-	-	180	190	144	0.87
1-6	6294	-	-	160	168	121	0.85
1-7	7371	-	-	120	125	106	0.94
1-8	8448	-	-	95	-	96	1.00

small sample.¹⁷ The application of this method to reel lengths of cable should be abandoned in favor of the referenced EIA method.

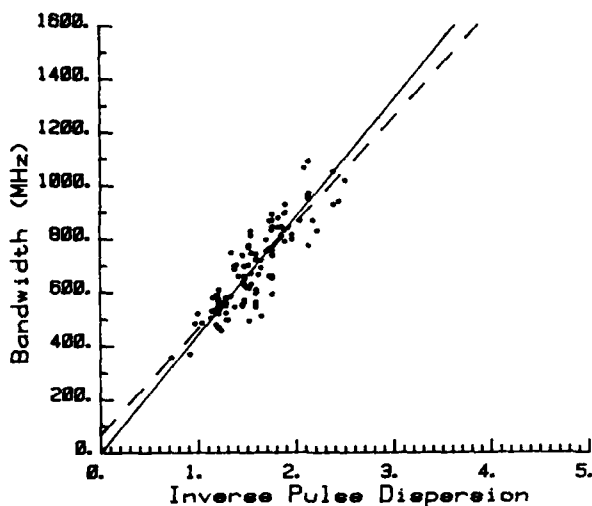


Figure 5. Measured Bandwidth Vs. Measured Pulse Dispersion

Conclusions

Although a number of different methods for predicting and/or optimizing system bandwidth have been suggested, none have yet been developed to the point where they are simple to apply. Most require measurements beyond those normally performed by cable manufacturers to determine compliance with industry specifications; e.g., differential mode delay, profile characterization, spectral bandwidth, etc. Some require predetermination of fiber positions within a link to obtain differential mode delay compensation. Until one or more of these methods emerges as superior and becomes commonplace, the technique based on the use of length dependence factors, γ , and random positioning of fibers appears to be the most suitable method. We were unable to consistently obtain satisfactory results by using individual fiber transfer function addition.

Standardization of γ -factors to be employed, as a function of system length and operating wavelengths, is, however, desirable. It has come to our attention recently that γ -factors in the range 0.6 - 0.7 are being used in some instances at both 850 and 1300 nm.

Considering the previously published results cited in the review, the experimental results, and the quality of fibers being manufactured today, there appears to be no justification for using γ -factors below 0.9 unless one or more of the differential mode delay compensation methods is employed. The conclusions based on measured results are, of course, only valid for 850 nm transmission on multimode, graded-index fibers and system lengths up to about 8 km; longer lengths may

give different results for the γ factor. Note also that the effect of a standard launch must ultimately be related to the optical source excitation actually used in a system (assuming that the sources are not preconditioned to emit standard launch) if these data are to be useful in the design of practical optical waveguide transmission systems.

Bandwidth measurements using either time-domain or frequency-domain techniques should be considered equally acceptable. However, the often-used method of calculating bandwidth from measured pulse dispersion assuming Gaussian shaped waveforms should be abandoned except possibly for long concatenated systems.

Acknowledgement

I wish to express appreciation to Messrs. Dave Williams, Paul Brand and John Hellmer for their assistance in the measurements and assimilation of the data.

References

1. A.H. Cherin and J.F. Dalglish, "Splices and Connectors for Optical Fibre Communications", Telecommunications Journal, Vol. 48, 1981.
2. Optical Waveguide Communications Glossary, NBS Handbook 140, U.S. Government Printing Office, Washington, D.C., 1982.
3. D. Gloge, "Optical Power Flow in Multimode Fibers", Bell System Technical Journal, Vol. 51, 1972, p. 1767.
4. R. Olshansky, "Mode Coupling Effects in Graded-Index Optical Fibers", Applied Optics, Vol. 14, 1975, p. 935.
5. K. Kitayama, S. Seikai and N. Uchida, "Impulse Response Prediction Based on Experimental Mode Coupling Coefficient in a 10-km Long Graded-Index Fiber", IEEE Journal of Quantum Electronics, Vol. QE-16, 1980, p. 356.
6. G.T. Holmes, "Estimation of Concatenated System Response Based on Measured Transfer Functions for Low and High Order Modes", Proceedings of Seventh European Conference on Optical Communication, Copenhagen, Denmark, 1981.
7. Pulse Distortion Measurement of Multimode Optical Fiber Information Transmission Capacity, FOTP-51, Electronic Industries Association, 2001 Eye Street, N.W., Washington, D.C. 20006.
8. Frequency Domain Measurement of Multimode Optical Fiber Information Transmission Capacity, FOTP-30, Electronic Industries Association, 2001 Eye Street N.W., Washington, D.C. 20006.

9. P.M. Rodhe, "An Experimental Study of a Matrix Transfer Function for Optical Fiber", Proceedings of Seventh European Conference on Optical Communications, Copenhagen, Denmark, 1981.
10. M. Ohashi, K. Kitayama, and S. Seikai, "Mode Coupling at Arc-Fusion Splices in Graded-Index Fibers", IEEE Journal of Quantum Electronics, Vol. QE-18, 1982, p. 274.
11. W.F. Love, "Bandwidth Spectral Characterization of Modal Compensation in Multimode Optical Fibers", Proceedings of Seventh European Conference on Optical Communication, Copenhagen, Denmark, 1981 - "Statistical Time Delay Equalization in Multimode Optical Fibers", Topical Meeting on Optical Fiber Communication (OFC 82), Phoenix, Arizona, 1982, p. 26. "Time Dispersion in Optical Fibers", Laser Focus, June 1982, p. 113.
12. T. Tanifuji, "Exact Analysis of Intermodal Dispersion Compensation in Spliced Graded-Index Optical Fibers", IEEE Journal of Quantum Electronics, Vol. QE-18, 1982, p. 844.
13. J.V. Wright and B.P. Nelson, "Bandwidth Studies of Jointed Multimode Fibres", Proceedings of Seventh European Conference on Optical Communication, Copenhagen, Denmark, 1981.
14. S. Suzuki et al, "Characteristics of Graded Index Fiber by VAD Method", Proceedings of Fifth European Conference on Optical Communication, Amsterdam, 1979.
15. R.S. Lowe, F.P. Kapron and R. Yip, "Prediction of Link Baseband Response from Individual Fiber Responses", Topical Meeting on Optical Fiber Communication (OFC 82), Phoenix, Arizona, 1982, p. 28.
16. S.D. Personick, "Time Dispersion in Dielectric Waveguides", Bell System Technical Journal, Vol. 50, 1971, p. 843.
17. D.L. Franzen and G.W. Day, "Measurement of Optical Fiber Bandwidth in the Time Domain", National Bureau of Standards, Technical Note 1019, February 1980, p. 51.



Eugene W. Riley
Anaconda-Ericsson, Inc.
TelcomCable Product
Engineering Center
Overland Park, Kansas

Mr. Riley was born in Wilmington, Delaware. He received the B.E.E. degree from the University of Delaware in 1958 and the M.S. degree in mathematics from Northern Illinois University in 1968.

From 1958 to 1960, he was employed by the Rural Electrification Administration as a Staff Engineer in the Telephone Engineering and Operations Division. He joined Anaconda Wire and Cable Company, now Anaconda-Ericsson, Inc., in October 1960. In 1967, he was named Senior Transmission Engineer in charge of the Transmission Engineering Section of the Communications Division. He was transferred to Overland Park, Kansas in 1975 and at that time was promoted to Manager, Systems and Applications Engineering. Since August, 1981, he has held the position of Chief Engineer at the Company's TelcomCable Product Engineering Center.

Mr. Riley is a member of the Communications Society of IEEE, its Transmission Systems Committee and is chairman of the Susceptibility Subcommittee.

AD P000592

PURE-SILICA CORE OPTICAL FIBER AND FIBER CABLE FOR RADIATION FIELDS

H. TANAKA

T. HIRASHIMA

T. SHINTANI

DAINICHI-NIPPON CABLES, LTD.
TOKYO, JAPANABSTRACT

Using ^{60}Co gamma ray and fast neutron flux from a research reactor, in situ measurements of radiation-induced optical attenuation have been conducted to characterize the radiation response of pure-silica core fibers and doped-silica core fibers. It has been revealed that pure-silica core fibers fabricated by Modified Rod-in-Tube method have much higher radiation resistivity than Ge/P- and B/F/P-doped-silica core MCVD fibers. Among the pure-silica core fibers, high-OH content grade has shown the highest resistivity in short wavelength region, whereas OH-free grade is useful in long wavelength region. Radiation hardening was observed in the high-OH content fiber during the test by long-term irradiation on pure-silica core fibers. The temperature dependence of radiation-induced attenuation was also observed; the higher the temperature of the environment, the smaller the radiation-induced attenuation. For application in radiation and high voltage fields, an optical fiber cable of the flame-retardant non-metallic type was developed. The cable passed IEEE-383 flame test and showed no degradation in mechanical strength after a 10^7 rad irradiation.

1. INTRODUCTION

Technological improvements and the growth of successful applications are leading to expanded use of fiber optics in all industries. Systems in radiation fields such as atomic power plants, vessels with nuclear power engine, or artificial satellites are no exception where the advantageous features of silica optical fibers are well used.

However, certain problems still remain to be solved for the application of optical fibers to such a radiation field. The most serious problem is that the transmission efficiency is deteriorated by exposure to radiation. This deterioration is complicatedly affected by various factors such as glass composition, nature and energy level of radiation source, ambient temperature, wavelength and power of signal carrier.

Influence of radiation on mechanical properties of optical fibers and cables is another problem to be clarified to build reliable optical transmission systems.

Included in this paper first are experimental results obtained by ^{60}Co and fast neutron flux irradiation tests on several kinds of silica

fibers. Second, we describe the radiation response of pure-silica core fibers fabricated by Modified Rod-in-tube method¹⁾, in particular, their outstanding radiation resistance. Also reported are test results on flame-retardant non-metallic optical fiber cable developed for use in radiation and high voltage fields.

2. RADIATION RESISTANCE OF SILICA OPTICAL FIBERS

Dopants for controlling refractive index are added to the core and/or the cladding. Such dopants include Ge and P usually employed to give a higher refractive index and B and F for affording a lower refractive index. In discussing the radiation resistance of silica optical fibers, it is important first of all to compare and examine the radiation response of fibers with different core dopants, because the core composition mainly governs the optical properties.

2.1 ^{60}Co GAMMA RAY IRRADIATION TEST

Table 1 lists the tested fibers. Fiber 1 fabricated by Modified Rod-in-Tube method is a step-index type pure-silica core fiber whose core consists of synthetic silica glass without any dopants. Fibers 2 and 3, fabricated by MCVD method, are both of the graded-index type with different dopants. Fiber 2 contains B, F and P, and Fiber 3 contains Ge and P.

No.	Fabrication Method	Composition of core glass	Refractive index profile
1	MRT	SiO_2	Step
2	MCVD	$\text{SiO}_2 + \text{B/F/P}$	Graded
3	MCVD	$\text{SiO}_2 + \text{Ge/P}$	Graded

Table 1. Test optical fibers

Figure 1 shows the attenuation induced at room temperature by ^{60}Co irradiation and measured in situ, and the subsequent recovery. The light sources for the measurements were high-radiance light-emitting diodes (LED, $\lambda=0.88 \mu\text{m}$). Marked

differences are seen in Figure 1 in radiation resistance between the pure-silica core fiber and the doped-silica core fibers. Fiber 1 not only exhibits much less radiation-induced attenuation but also recovers very rapidly. This reveals that the pure-silica core fiber has higher resistance to ^{60}Co irradiation.

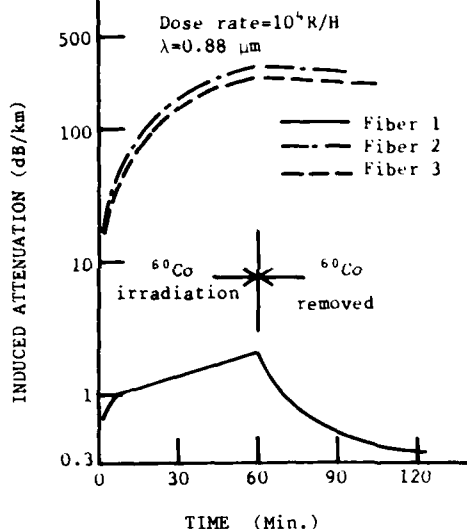


Figure 1. Radiation response of silica optical fibers during ^{60}Co irradiation

2.2 FAST NEUTRON FLUX IRRADIATION TEST

The fibers listed in Table 1 were also tested for attenuation induced by fast neutron flux using a research reactor (YAYOI, University of Tokyo) and LED's ($\lambda=0.88\ \mu\text{m}$) as the light sources. Figure 2 shows the attenuation as measured *in situ*. The flux density was varied stepwise by regulating the reactor output as depicted in dotted lines. The flux density of fast neutron was $6 \times 10^8\ \text{n/cm}^2/\text{sec}$. at a reactor output of 2 kW. As shown in Figure 2, the pure-silica core fiber has the highest radiation resistance also to fast neutron flux, whereas there is a noticeable difference between the two types of doped-silica core fibers. The B/F/P-doped-silica core fiber suffers more attenuation, presumably because dopant B has a large absorption cross-section for the neutron. In other words, optical fibers containing boron in the core appear useful as neutron sensors.

Figures 3a and 3b show the spectral loss characteristics of the pure-silica core fiber (Fiber 1) and the B/F/P-doped-silica core fiber (Fiber 2). The radiation-induced attenuation of Fiber 1 increased with decreasing wavelength below about $1.0\ \mu\text{m}$. As well known in investigation of radiation effects on silica glass, such behavior of induced attenuation is mainly due to color centers produced

in the glass matrix by irradiation, and giving rise to light absorption in the ultraviolet wavelength region. On the other hand, Fiber 2 displays great radiation-induced attenuation over a wider spectral region.

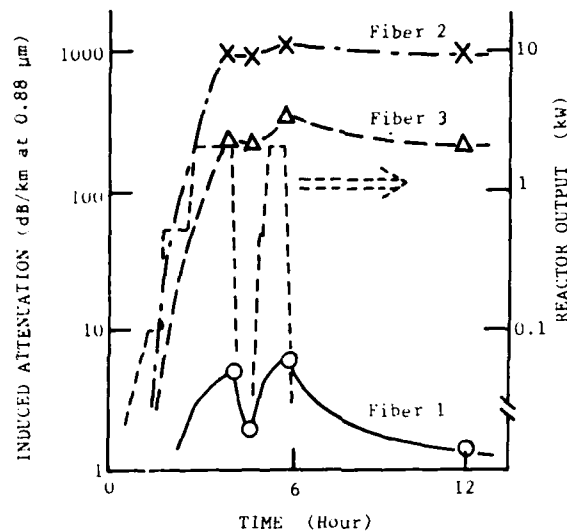


Figure 2. Radiation response of silica optical fibers during fast neutron flux irradiation

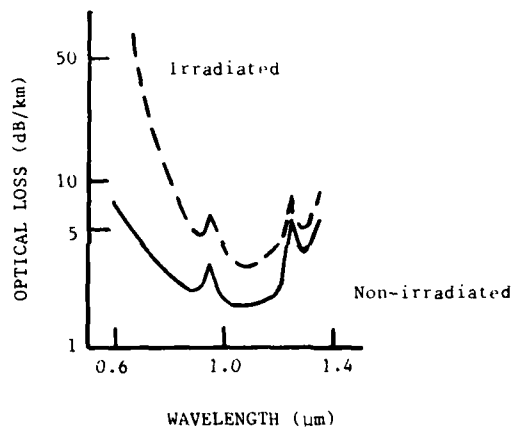


Figure 3a. Spectral loss characteristics of Fiber 1

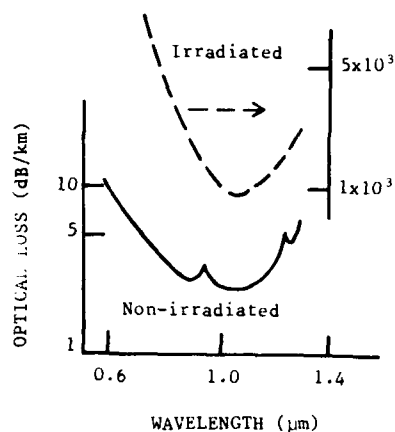


Figure 3b. Spectral loss characteristics of Fiber 2

3. RADIATION RESPONSE OF PURE-SILICA CORE FIBER

Low-loss, silica-core MRT fibers, developed primarily for medium- or long- distance communications, have also found various other applications, for example, to high-power laser guides, light guides and image guides. Among silica glasses commercially available, Diasil[®], synthetic silica glass manufactured by Mitsubishi Metal Corp., was used for the cores of MRT fibers tested, while the cladding glass was prepared by the current MCVD method.

3.1 EFFECT OF CORE GLASS

Figure 4 shows the initial spectral loss characteristics of three types of pure-silica core fibers. Fiber A, with a core of low-OH content (2 ppm OH) exhibits transmission losses almost comparable to the theoretical loss characteristics of silica glass determined by the Rayleigh scattering and ultraviolet absorption, except an OH absorption peak at a wavelength of 0.94 μm. The fiber B with a core of high-OH content (200 ppm OH) characteristically has absorption peaks at 0.88 μm, 0.72 μm and 0.94 μm. Fiber C comprising core glass produced in the unusual atmosphere in the presence of an excess of oxygen characteristically has a loss peak around 0.6 μm. These three types of fibers have the same parameters (core diameter/fiber diameter = 100 μm/150 μm, NA = 0.18).

Figure 5 shows the attenuation induced by *in situ* ⁶⁰Co irradiation. LED light sources (λ=0.88 μm) were used for the measurements. Figure 5 reveals that even pure-silica core fibers differ in radiation resistance owing to the difference in the core glass formula. Since Fiber C having a loss peak at 0.6 μm is highly sensitive to gamma ray irradiation, it is not suitable for use in radiation environments. Fiber A and Fiber B, although different only in OH content of the core, differ greatly in radiation resistance. The

induced attenuation of Fiber A gradually increases with dose, while that of Fiber B initially increases greatly followed by a recovery and further by a gentle increase. Thus, the curve of Fiber B indicates two transient modes of radiation-induced attenuation, further showing that the fiber experiences both damage and recovery during irradiation.

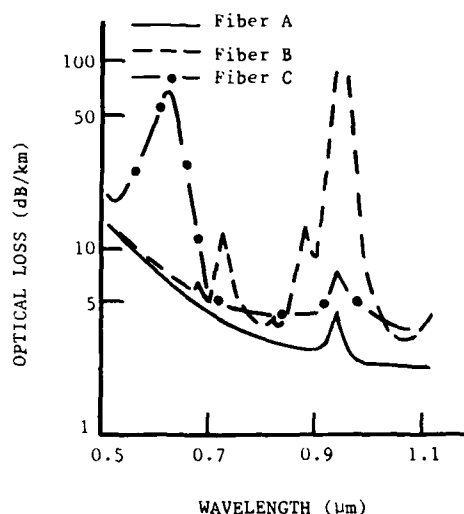


Figure 4. Spectral loss characteristics of three types of pure-silica core fibers

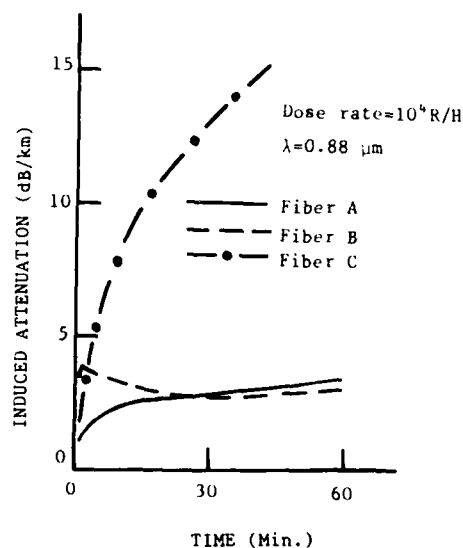


Figure 5. Radiation response of pure-silica core fibers during ⁶⁰Co irradiation

3.2 DOSE DEPENDENCE

Figure 6 shows the attenuation increases of Fibers A and B by ^{60}Co irradiation at 10^4 , 10^5 and 10^6 rads. As evidently indicated in this figure, Fiber B shows better radiation resistance as compared with Fiber A, with a remarkable difference in resistance between the two fibers at a higher dose. This difference can be attributed to that of recovery/damage rate. In order to ascertain the effect of the OH content, the radiation-induced attenuation was measured *in situ* for higher doses using a ^{60}Co source. The test results revealed that the attenuation increase in the high-OH content fiber was only 60 dB/km for an exposure of 8.4×10^7 R, while that of the low-OH content fiber exceeded 100 dB/km even for an exposure of 2×10^7 R.

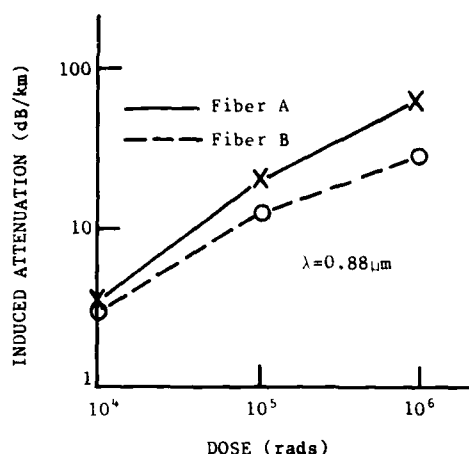


Figure 6. Dose dependence of pure-silica core fibers in ^{60}Co irradiation

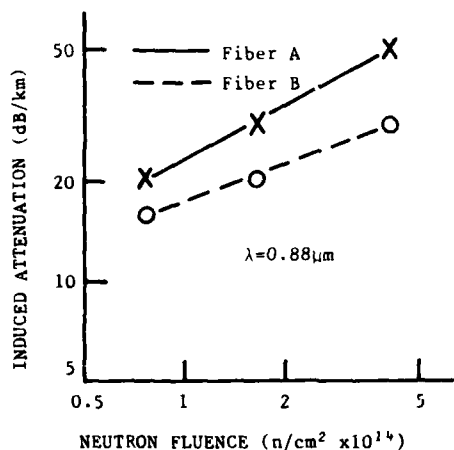


Figure 7. Neutron fluence dependence of pure-silica core fibers

A similar test was conducted to investigate the effect of OH radicals on fast neutron flux irradiation. The result is shown in Figure 7, which indicates a tendency similar to that seen in Figure 6. Unlike gamma ray, neutron flux had been expected to alter the molecular structure of glass to thereby vary the refractive index, because of its direct interaction on the nucleus. To examine this, refractive index differences, Δn , were measured on the non-irradiated and the irradiated ($\sim 10^4$ n/cm 2) fibers. There was no significant difference between the measured values.

3.3 LONG-TERM RADIATION EFFECT

While we have discussed short-term induced attenuation, namely transient radiation-induced attenuation, as determined by *in situ* measurements, now we will discuss long-term or permanent radiation-induced attenuation which is important to evaluate the availability of optical fiber for practical use. For this purpose, long-term irradiation tests were conducted for a year on both low-OH fiber (Fiber A) and high-OH fiber (Fiber B). The fibers were irradiated at room temperature intermittently with ^{60}Co , and attenuation was measured twenty-four hours after every irradiation to eliminate short-term recovery effect. The light source was a fiber monochromator of $0.85 \mu\text{m}$ in wavelength. The output power was as low as several nanowatts so that photobleaching effect²⁾ can be neglected. The results are plotted in Figure 8, which shows a marked difference between Fibers A and B. The recovery seen in high-OH content Fiber B can be regarded as a result of the radiation-induced hardening effect which was reported by Sigel et al.³⁾

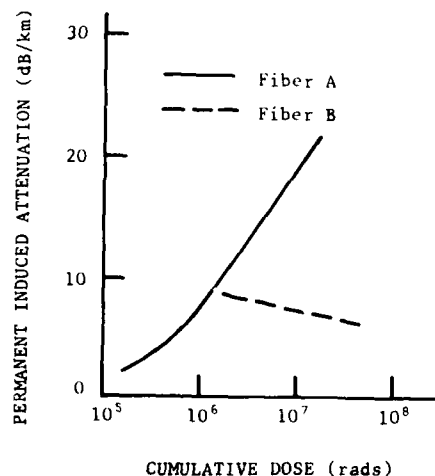


Figure 8. Permanent induced-attenuation vs. cumulative doses

3.4 TEMPERATURE DEPENDENCE

The radiation response of pure-silica core fibers is sensitive to the ambient temperature. The temperature dependence of *in situ* measured radiation-induced attenuation of Fibers A and B is shown in Figure 9. Evidently, the higher the temperature of the environment, the smaller the radiation-induced attenuation; this can be explained by the geminate recombination theory. According to this theory, trapped electrons generated by irradiation are excited to the conduction band by thermal energy and become free electrons. These electrons move freely in the glass matrix, and recombine with positive holes, resulting in a structural recovery. The probability of the recombination of electrons and holes increases at higher temperatures. Thus, fiber heating is effective for giving an improved radiation resistivity.

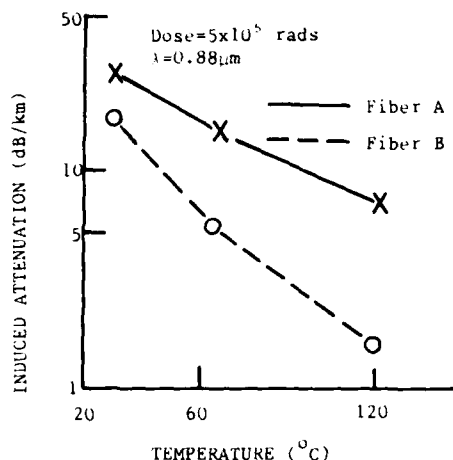


Figure 9. Temperature dependence of induced attenuation in ^{60}Co irradiation.

3.5 RADIATION RESISTANCE OF OH-FREE PURE-SILICA CORE FIBER

Second generation optical communication systems using OH-free Ge/P-doped fibers are introduced into use with carrier wavelengths in the 1.2 - 1.6 μm region where silica optical fibers have more attractive transmission properties. These doped fibers, however, are not suitable for systems in radiation fields. Therefore we have developed OH-free pure-silica core fiber with high radiation resistance for use in the long wavelength region.

Figure 10 shows the spectral loss characteristics of this type of fiber (core diameter/fiber diameter = 100 μm /150 μm , NA = 0.20). With a minimized OH content, the fiber has a minimum loss of below 1.0 dB/km.

Figure 11 shows the induced attenuation at 0.63 μm , 0.83 μm and 1.31 μm of this fiber as measured *in situ* using a He-Ne laser and laser

diodes as optical sources. The input light power values for the fiber specimens were adjusted to almost the same level (about 400 μW). It is seen that the OH-free pure-silica core fiber has excellent radiation resistance in the long wavelength region where the transmission loss is also low. Fortunately, the wavelength region where the minimum transmission loss becomes minimum coincides with the region where the minimum radiation-induced attenuation is minimum. The newly developed OH-free pure-silica core fiber is therefore satisfactorily applicable to long-distance optical systems in environments which are likely to involve exposure to radiation.

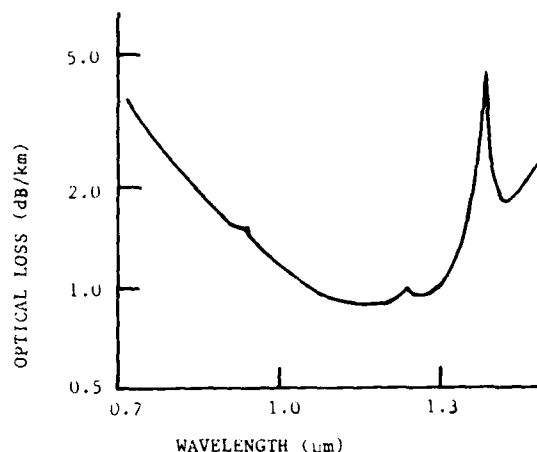


Figure 10. Spectral loss characteristics of OH-free pure-silica core fiber

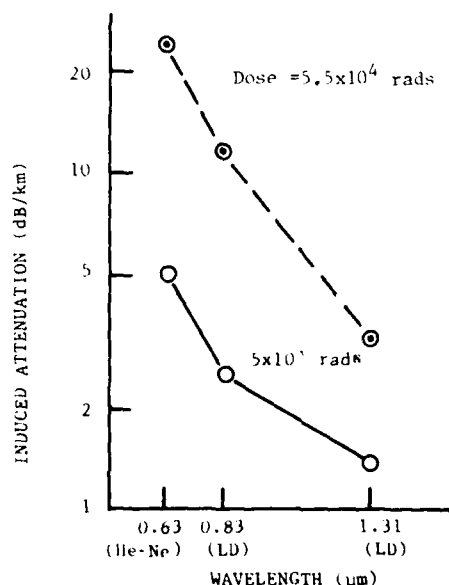


Figure 11. Induced attenuations of pure-silica core fiber at various laser wavelengths in ^{60}Co irradiation

4. THE FLAME-RETARDANT NON-METALLIC OPTICAL FIBER CABLE FOR RADIATION FIELDS

4.1 FLAME-RETARDANT NON-METALLIC OPTICAL FIBER CABLE

For applications in radiation and high voltage fields as in atomic power plants, we have developed a pipe spacer type non-metallic fiber cable with a flame-retardant PVC sheath. The cable, shown in Figure 12 in cross-section, comprises optical fibers having a core diameter of 100 μm , a fiber diameter of 150 μm , and a nylon jacket of 0.9 mm in diameter. Each fiber is protected with a nylon pipe spacer from lateral pressure. An FRP rod having a diameter of 1.6 mm is employed as the central strength member. The flame-retardant PVC sheath used for overall protection is 3.5 mm in wall thickness. Table 2 shows the optical properties of the fibers in completed cable, which were found to be free of any degradation due to cable fabrication.

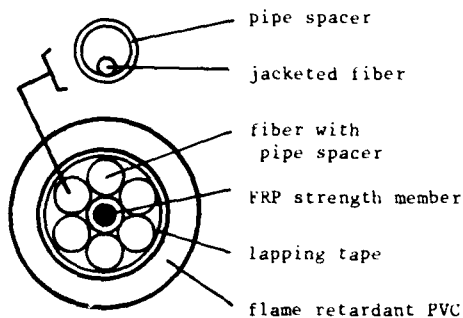


Figure 12. Cross-section of the non-metallic optical fiber cable

OPTICAL LOSS	6 dB-DOWN BAND WIDTH	TEMP. VARIATION OF ATTENUATION
2.1 dB/km at 0.85 μm	28 MHz · km	± 0.1 dB/km, -20-60°C

Table 2. Optical properties of the non-metallic fiber cable

4.2 MECHANICAL PROPERTIES OF IRRADIATED CABLE

Figure 13 shows the stress and strain characteristics of the cable measured before and after an irradiation (10^7 rads). No significant change was observed. For a bending test, specimens were taken from the irradiated cable and bent through ± 180 degrees repeatedly five times around a

mandrel of 180 mm in diameter. No damage was found in any specimen.

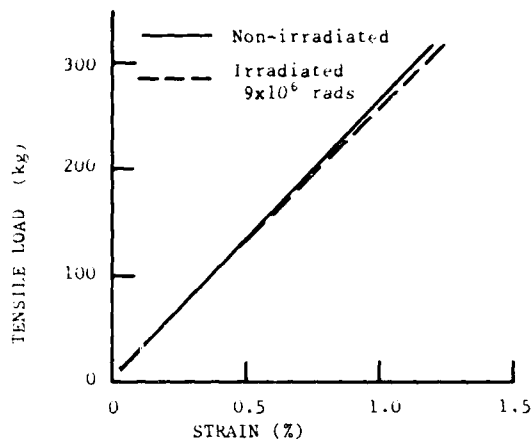


Figure 13. Stress and strain characteristics of irradiated and non-irradiated cable

4.3 FLAME RETARDANCY TEST

The optical fiber cable given in para. 4.1 was tested for flame retardancy according to IEEE 383. Figure 14 shows the cable under the flame testing. The cable specimens were burnt for twenty minutes with a ribbon gas burner at a flame temperature of 820 °C. The cable self-extinguished in 12 minutes after the ignition of the burner due to the presence of the thick flame-retardant PVC sheath. Thus the cable was found acceptable according to the IEEE 383 standard.

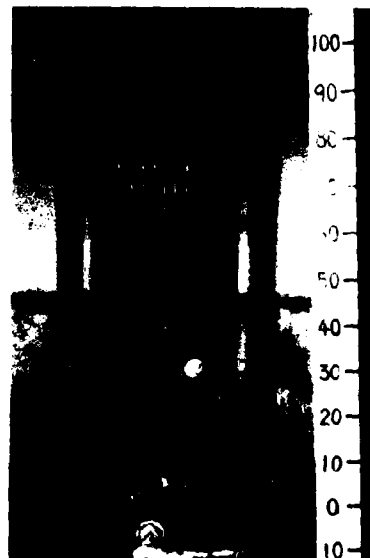


Figure 14. Flame testing of the cable

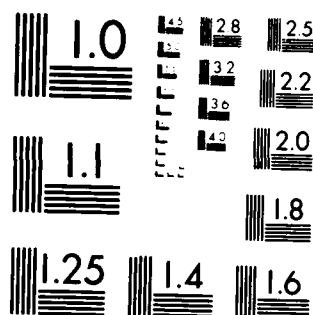
UNCLASSIFIED

PROCEEDINGS OF THE INTERNATIONAL WIRE AND CABLE
SYMPOSIUM (31ST) HELD AT..(U) ARMY
COMMUNICATIONS-ELECTRONICS COMMAND FORT MONMOUTH NJ
NOV 82 F/G 20/6

F/G 20/6

NL

END
DATE
FILMED
- 3
DTIC



MICROCOPY RESOLUTION TEST CHART
NATIONAL BUREAU OF STANDARDS 1963-A

5. CONCLUSIONS

Radiation-induced attenuation measurements were conducted on various silica fibers. Pure-silica core fibers had much higher radiation resistance than doped-silica core fibers.

High-OH content pure-silica core fiber was useful in the region of short wavelengths, whereas OH-free fiber showed a better radiation response in the long wavelength region.

For applications to atomic power plants, we developed a non-metallic fiber cable with good flame retardancy.

ACKNOWLEDGEMENTS

The authors would like to thank T. Nishitani and K. Kurihara of Japan Atomic Energy Institute, Assist. Prof. M. Nakazawa of University of Tokyo, and S. Okamoto of Radiation Center of Osaka Prefecture for their helpful discussions and encouragement.

REFERENCES

- 1) A. Utsumi, T. Sagawa, T. Shintani, R. Kobayashi and T. Sugawa, "Modified Rod-in-Tube method for low-loss step-index optical fiber", in Digest of Optical Fiber Communication (Optical Society of America, Washington, DC), paper WF 1, 1979.
- 2) E.J. Friebele and M.E. Gingerich, "Photo-bleaching effects in optical fiber waveguides", Applied Optics, Vol. 29, 3448, 1981.
- 3) M.S. Maklad, G.W. Bickel and G.H. Sigel, Jr., "Radiation response of low loss silicone clad silica fiber", in Digest of Optical Fiber Transmission II (Optical Society of America, Washington, DC), paper TuD 8-1, 1977.



Hiroyuki Tanaka
DAINICHI-NIPPON CABLES, LTD.
4-3, Ikejiri, Itami,
Hyogo Pref.,
664, Japan

Mr. Tanaka, chief Engineer of Optical Communication Department, is engaged in development of optical fiber cables. He received his M.S. degree in Electrical Engineering from Osaka University in 1971. He is a member of the Institute of Electronics and Communication Engineers of Japan.



Toshihiro Hirashima
DAINICHI-NIPPON CABLES, LTD.
4-3, Ikejiri, Itami,
Hyogo Pref.,
664, Japan

Mr. Hirashima, Staff Engineer of Optical Communication Department, is engaged in development of optical fiber cables. He received his M.S. degree in Electrical Engineering from Doshisha University in 1975. He is a member of the Institute of Electronics and Communication Engineers of Japan.



Takeshi Shintani
DAINICHI-NIPPON CABLES, LTD.
4-3, Ikejiri, Itami,
Hyogo Pref.,
664, Japan

Mr. Shintani, Manager of Optical Communication Department, is engaged in development of optical fiber cables. He received his B.S. degree in Electrical Communication Engineering from Osaka University in 1960. He is a member of the Institute of Electronics and Communication Engineers of Japan.

RADIATION EFFECTS OF OPTICAL SILICA FIBER AND RADIATION HARD OPTICAL TRANSMISSION

T. Suematsu

K. Sanada

H. Yoshida

Fujikura Ltd.
Tokyo JapanSUMMARY

Optical fiber is expected to apply for computer communication and CAMAC control systems of JT-60 (Japan Atomic Energy Research Institute TOKAMAK-60). No electromagnetic interference and high speed transmission of electrical signals are required for the project control. Radiation hard optical fiber makes more wide applications. This paper discusses radiation effects on silica fiber of graded-index Ge-P doped fiber, step-index borosilicate clad pure silica core fiber and graded-index borosilicate fiber.

These fibers were exposed to X-ray radiation, γ -ray radiation and neutron flux radiations. Step-index pure silica core fiber is naturally the most radiation hard among them. The fiber followed low induced attenuation window in the 0.9 - 1.1 μ m range.

Radiation hard fiber-optic link is proposed by the choice of step-index pure silica core fiber in the 0.9 - 1.1 μ m range.

INTRODUCTION

Radiation test to silica fibers were conducted by typical 3 sources. They are silica fiber of graded-index Ge-P doped fiber (A fiber) known as usual communication fiber, step-index borosilicate clad pure silica core fiber known as better radiation hard fiber (B fiber) and graded-index borosilicate fiber (C fiber). Now, graded-index borosilicate fiber is chosen for influence of boron dopant to radiation characteristics. These fibers were exposed to X-ray radiation, γ -ray radiation and neutron flux radiation.

1. Fibers under test

Initial characteristics of fibers under test are shown in Table 1. The manufacturing process of these fibers is Vapor-phase Axial Deposition (VAD) or Modified Chemical Vapor Deposition (MCVD). That is, graded-index Ge-P doped silica fiber is made by the former, step-index borosilicate clad pure silica core fiber and graded-index borosilicate fiber are by the latter.

Table 1. Initial characteristics of fibers under test

Optical fiber	Sign	Construction data				Fiber attenuation (dB/Km) at (0.85 μ m/ 1.3 μ m)	Fiber bandwidth (MHz-Km) at (0.85 μ m/ 1.3 μ m)	Testing level	
		NA	Core dia. (μ m)	Clad- ing dia. (μ m)	Nylon jacket dia. (mm)			Before radiation	Under radiation
Graded-index Ge-P doped silica fiber	A	0.25	80			2.0	185	10	
Step-index borosilicate clad pure silica core fiber	B	0.15	52	125	0.9	0.5	16	100	
Graded-index borosilicate fiber	C	0.10	57			1.8	170	100	

2. Radiation source and method

Radiation source and method for the test are shown in Table 2.

Table 2. Radiation source and method

Radiation source	Equipment	Acceleration method	Target	Operation output
X-ray	Linear accelerator	RF traveling	Tungsten	5-18 MeV \times 1 mA
	Handy X-ray generator	Potential difference	Tungsten	30 KeV \times 1 mA
γ -ray	^{60}Co	-	-	14904 Ci
Neutron flux	Linear accelerator	RF traveling	Lead	5-18 MeV \times 1 mA

3. Testing item

Transmission and mechanical characteristics of fibers were measured and the items are as follow.

- (1) Continuous fiber attenuation measurement under radiation by Light emitting diode (LED) source.
- (2) Fiber attenuation versus wavelength before and after radiation.
- (3) Infrared absorption spectrum of glass rod before and after high γ -ray radiation.
- (4) Fiber bandwidth before and after radiation.

- (5) Tensile strength before and after high γ -ray radiation.
- (6) Fiber induced attenuation of step-index pure silica core fiber under differently rated γ -ray radiation.

Fig.1 shows one example of continuous attenuation measurement by LED source (1) and Table 3 shows testing conditions of radiation sources.

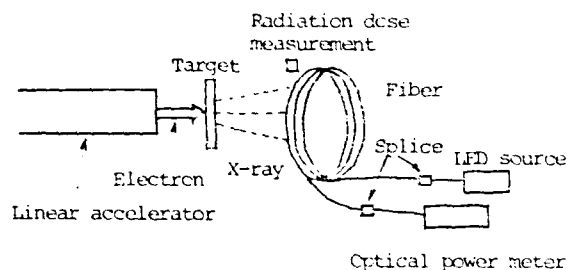


Fig.1 One example of continuous attenuation measurement by LED source

Table 3 Testing conditions of radiation sources

Radiation source	Radiation rate (Rad/hour)	Fiber attenuation at 0.85 μ m		Fiber attenuation versus wavelength	
		Exposure time (min.)	Dose (Rad)	Exposure time (min.)	Dose (Rad)
X-ray	1.3×10^4	10	2.5×10^2	10	1.75×10^2
	1.3×10^2	5	48		
γ -ray	1.3×10^2	10	1.3×10^2	120 hours	1.3×10^3
				10 min.	
Neutron flux	6.5×10^9 neutrons/cm ² -sec	10	1.3×10^2	10 min.	1.3×10^2
X-ray	1×10^4		1.3×10^2	10 min.	1.3×10^2

DATA OBTAINED

1. Continuous fiber attenuation measurement by LED source.

Fig.2 to Fig.5 shows induced attenuation of fibers versus exposure time under radiation. Fig.2 shows the characteristics by low X-ray radiation of 80 KeV energy. This means remarkable difference of induced attenuation and the inclination on the rising curve from A fiber to B fiber or C fiber.

Fig.3 shows the characteristics by high X-ray radiation of 10 MeV energy. Different induced attenuation curve is obtained from B and C fiber compared low energy with high energy radiation.

Fig.4 shows the characteristics under γ -ray radiation. This means, compared with Fig.2 and Fig.3, remarkable difference of induced attenuation curve because of high radiation rate. Therefore induced attenuation of B fiber was saturated after 5 minute radiation, however that of A fiber was not saturated in case of high γ -ray radiation.

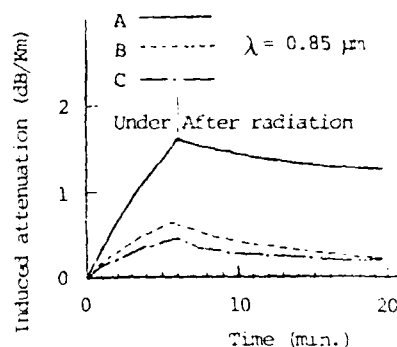


Fig.2 Induced attenuation under X-ray radiation of low energy

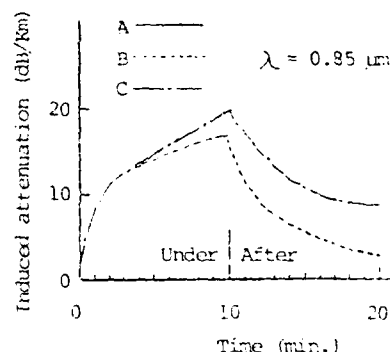


Fig.3 Induced attenuation under X-ray radiation of high energy

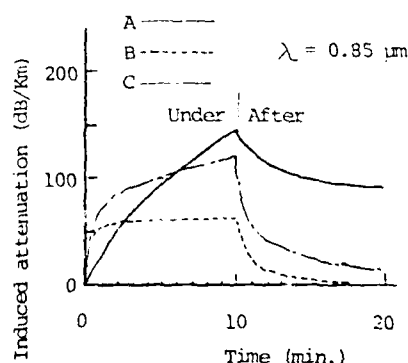


Fig.4 Induced attenuation under γ -ray radiation

In addition, it was found that recovery process after radiation of A fiber is different from that of B fiber.

Color center having more than 2 differential disappearance speed is produced by radiation. Consequently it is assumed that the number of color center having fast disappearance

speed of B or C fiber is more than that of A fiber. And many number of color center of A fiber are assumed to be produced because induced attenuation of that was not saturated under high radiation.

Fig. 5 shows the characteristics under neutron flux radiation. This means induced attenuation of A fiber is increased straightly by radiation and recovery speed of A fiber is very slow than that of B or C fiber. In Fig. 5, X-ray is followed with neutron flux radiation, however induced attenuation of C fiber is less than that in Fig. 3 notwithstanding high X-ray radiation.

As a result, it was found that reaction speed of color center is greatly influenced by radiation energy in addition to rate and dose.

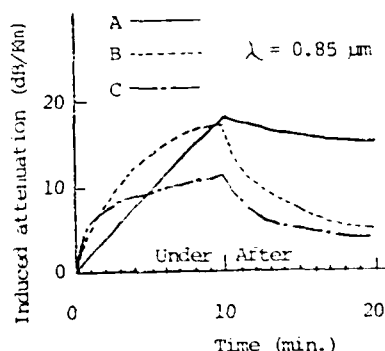


Fig. 5 Induced attenuation under neutron flux radiation

Table 4 shows induced attenuation followed by relative radiation dose of these fibers by different radiation source or energy. This means that of any fiber is high by X-ray, neutron flux and γ-ray source in order. Attenuation change of A fiber is low, however that of B or C fiber is decreased extremely with exposure time become long.

Table 4 Induced attenuation followed by relative radiation dose

Optical fiber	Sum	Exposure time (min.)	X-ray		γ-ray	Neutron flux (with X-ray)
			Low energy	High energy		
Graded-index Ge-P doped silica fiber	A	1	0.050		0.002	0.004
		5	0.035		0.001	0.004
		10			0.001	0.005
Step-index borosilicate clad pure silica core fiber	B	1	0.019	0.032	0.003	0.010
		5	0.014	0.012	0.001	0.006
		10		0.007	0.0004	0.003
Graded-index borosilicate fiber	C	1	0.013	0.032	0.004	0.012
		5	0.010	0.012	0.001	0.004
		10		0.008	0.001	0.002

Unit: dB/km

2. Fiber attenuation versus wavelength before and after radiation

Fig. 6 to Fig. 8 shows fiber attenuation versus wavelength before and after radiation by monochromator method. This means that the curve of attenuation versus wavelength of these fibers is almost identical to any kind of radiation source, furthermore minimum attenuation window of A fiber is in the 1.0 - 1.2 μm range and that of B or C fiber is in the 0.9 - 1.1 μm range. B fiber is also the most radiation hard identical to the case of continuous attenuation measurement.

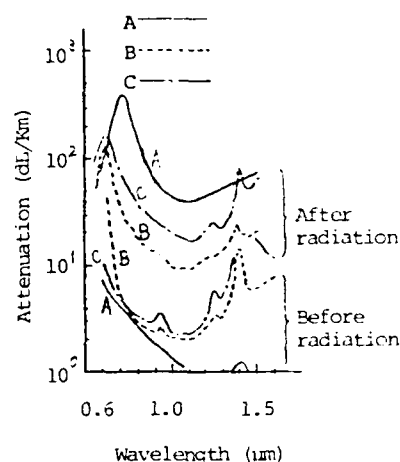


Fig. 6 Attenuation versus wavelength before and after X-ray radiation

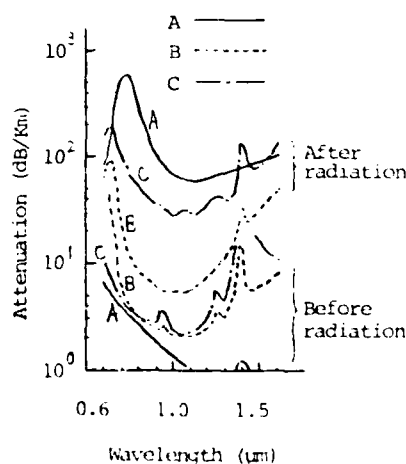


Fig. 7 Attenuation versus wavelength before and after neutron flux radiation

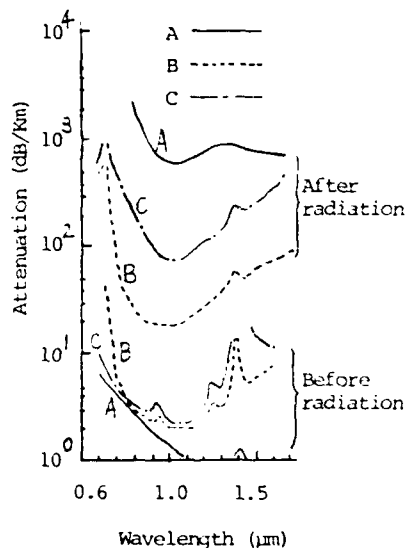


Fig. 8 Attenuation versus wavelength before and after γ -ray radiation

Peaked wavelength of absorption of these fibers is at around $0.72 \mu\text{m}$ in A fiber, $0.65 \mu\text{m}$ in B fiber and $0.63 \mu\text{m}$ in C fiber respectively. The characteristics involve that peaked wavelength of absorption shifts slightly to shorter wavelength to dope boron in fiber core.

These Fig. give that attenuation at long wavelength is increased extremely followed by radiation dose, the slope of the characteristics is similar and it shifts parallel. Minimum attenuation window shifts to shorter wavelength followed by radiation dose increased. The measurement of absorption attenuation of various glass rods at longer wavelength indicates the cause of induced attenuation at long wavelength.

3. Infrared absorption spectrum of glass rods before and after high γ -ray radiation.

Glass rods under test are doped mother rod of A fiber, synthetic silica rod and quartz rod respectively, and absorption spectrum was measured before and after high γ -ray radiation (1.0×10^6 Rad/hour rate, 1.2×10^8 Rad dose). Doped mother rod became discolored to light-brown color, quartz rod to pale purple and synthetic silica rod not to at all.

Infrared absorption was measured continuously by same method of lapping both ends of 2 pieces of same length (5 cm) from same rod before and after radiation. Data obtained from these rods is shown in Fig. 9.

Induced attenuation in kilometer gives 3000 dB/Km at $2.6 \mu\text{m}$ and 4800 dB/Km at $3.0 \mu\text{m}$ of synthetic silica rod, or 2600 dB/Km at $2.6 \mu\text{m}$ and 4100 dB/Km at $3.0 \mu\text{m}$ of doped mother rod from the remainder of transmittance before from after radiation.

It is assumed that induced attenuation at long wavelength caused to increase absorption attenuation from elastic vibration of

Si-O ion at $3.2 \mu\text{m}$ by radiation, in addition same absorption spectrum below $2.6 \mu\text{m}$ of quartz rod before and after radiation caused relatively low induced attenuation by radiation from very high absorption of OH ions.

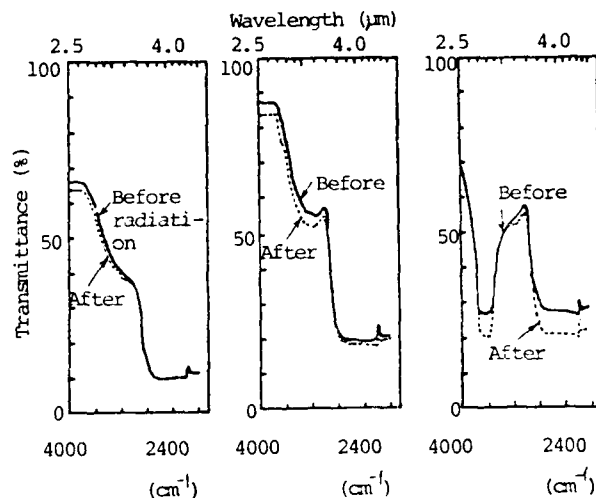


Fig. 9 Infrared absorption spectrum of silica rods before and after high γ -ray radiation

4. Fiber bandwidth before and after radiation

Fiber bandwidth was measured by frequency sweeping method. Fig. 10 shows bandwidth characteristics before and after X-ray radiation.

This means bandwidth characteristics is hardly changed by radiation. In addition, similar effects have also been observed under γ -ray or neutron flux radiation.

It is assumed that the electromagnetic wave of X-ray or γ -ray have effects to density or structure of glass, however bandwidth characteristics is expected to change by index change because neutron energy or flux influence on density or structure of glass. As a result, this experimental neutron flux caused no change to bandwidth characteristics.

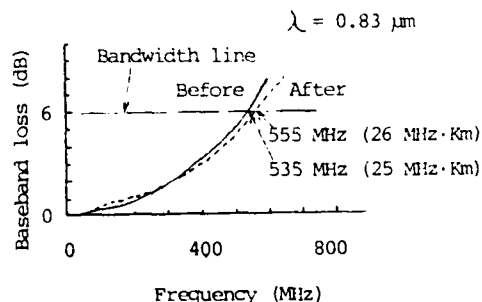


Fig. 10 Bandwidth before and after X-ray radiation

5. Tensile strength before and after high γ -ray radiation

The span length was 300 mm and the pulling speed of the test was 5 mm/min. Table 5 shows breakdown strength of these fibers before and after high γ -ray radiation. This means no difference of strength among fibers and less strength after than before radiation. However it is assumed tensile strength of optical fiber itself was hardly changed because all fibers were broken at the clamp edge caused from degraded Nylon jacket by radiation.

Table 5 Tensile strength before and after high γ -ray radiation

Optical fiber	A		B		C	
	Before radiation	After radiation	Before	After	Before	After
Data (Kg)	9.8	5.3	7.0	5.3	5.3	5.3
	9.8	5.0	7.0	5.2	7.0	5.3
	5.8	5.7	5.1	5.2	5.2	5.2
	5.3	5.3	5.0	5.2	5.2	5.2
	5.6	5.3	5.2	5.3	5.3	5.3
	5.7	5.8	5.3	5.0	5.0	5.4
	5.7	5.0	5.3	5.3	5.3	5.3
	5.8	5.4	5.2	5.3	5.3	5.3
	5.7	5.3	5.2	5.2	5.2	5.2
	5.6	5.3	5.3	5.3	5.3	5.4
Average (Kg)	5.7	5.6	5.2	5.5	5.3	5.7
Dispersion (Kg)	1.07	0.36	0.25	0.28	1.11	0.24

6. Fiber induced attenuation of step-index pure silica core fiber by differently rated γ -ray radiation.

The data shows that step-index pure silica core fiber (B fiber) is the most radiation hard and induced attenuation is caused from radiation rate and dose. Induced attenuation of B fiber was measured by different radiation rate under γ -ray radiation for various radiation environment.

The result is shown in Fig.11. This means the curve of induced attenuation is different by radiation rate and becomes to saturate when radiation rate become higher. It is expected induced attenuation of B fiber is below 10 dB/Km at 0.85 μ m when radiation rate is below 10 Rad/hour under γ -ray radiation environment.

PROPOSED OPTICAL CABLE FOR JT-60 PROJECT

The choice of optical fiber is decided by installation environment. There are usual and radiation environment in JT-60 area. Flame retardant and nonmetallic optical cable is proposed for computer communication and CAMAC control systems of JT-60 project to superior reliable system. Furthermore radiation hard optical fiber cable is expected to apply for the system under radiation environment. Flame retardant and nonmetallic optical cable is developed as shown in Fig.12, Fig.13 and Table 6. Fig.12 shows cut view of 4 fiber cable. Fig.13 shows cross section of the cable.

Table 6 shows construction, transmission characteristics and mechanical characteristics.

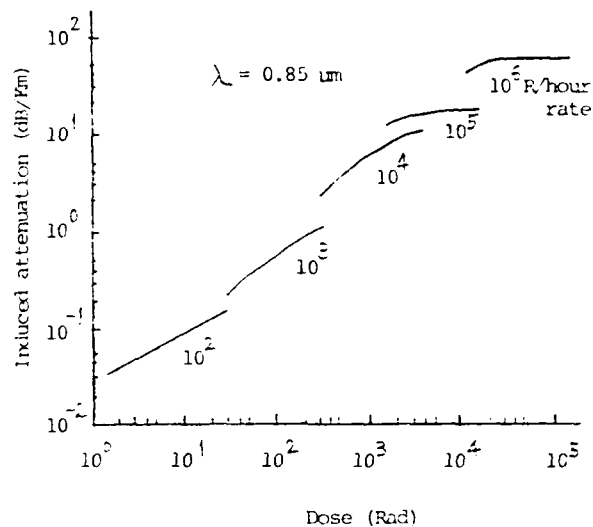


Fig.11 Induced attenuation of step-index borosilicate clad pure silica core fiber by differently rated γ -ray radiation

Fig.12 Cut view of flame retardant and nonmetallic 4 optical fiber cable

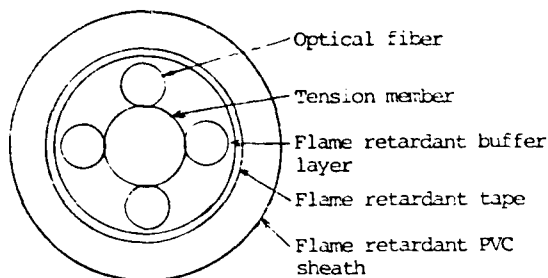


Fig.13 Cross section of the cable

Table 6 Characteristics of the cable

Optical fiber	Graded-index doped silica fiber
Core dia. (μm)	90
Cladding dia. (μm)	125
Nylon jacket dia. (mm)	0.9
NA	0.25
Tension member	FRP
Approx. overall dia. (mm)	11
Approx. net weight (Kg/Km)	120
Fiber attenuation (dB/Km at 0.85 μm)	1.5 max.
Fiber bandwidth (MHz/Km at 0.85 μm)	200 max.
Tensile strength (Kg)	100 max.
Bending radius (mm)	120 min.
Vertical tray frame test	Passing of IEC-183

CONCLUSION

Transmission and mechanical characteristics have been studied by 3 kinds of silica fibers under different radiation source and energy. The result gives following evidence.

1. Continuous fiber attenuation measurement by LED source.

Graded-index doped silica fiber has remarkable different curve of induced attenuation from radiation source and many number of color center which is produced than step-index pure silica core fiber or graded-index borosilicate fiber. Color center have more than 2 reaction speed from recovery process after radiation.

2. Fiber attenuation versus wavelength before and after radiation.

Induced attenuation curve of these fibers is identical each other under any kind of radiation and minimum attenuation window of each fiber is in the 0.9 - 1.1 μm range. Boron dopant degrade slightly radiation hard characteristics than pure silica. The wavelength of minimum attenuation shifts to shorter wavelength followed by radiation dose increased. This is caused by absorption attenuation increased at infrared from infrared absorption spectrum of

glass rod.

3. Tensile strength before and after high γ-ray radiation

Tensile strength of optical fiber is hardly changed under high γ-ray radiation.

Radiation hard fiber-optic link is proposed by the choice of step-index pure silica core fiber in the 0.9 - 1.1 μm range. Superior radiation hard optical fiber will be developed by making clear the mechanism of radiation effects.

Further support for the development is expected to apply widely for nuclear plant or nuclear fusion plant.

ACKNOWLEDGEMENT

The authors wish to express our sincerely thanks to Mr. E. Toyoda, Mr. S. Yoshizawa and Mr. S. Hayashi of Toshiba Corporation for their continuous encouragement.

REFERENCES

1. K. Sanada and H. Osanai, No.946, '78 National Convention of IECE of Japan
2. N. J. Kreidl, Nucleonics, Vol.14, No.3, '56
3. K. Inada, Vol.63, No.11, The Journal of IECE of Japan, '80
4. K. Arakawa, K. Shimada, E. Toyoda, S. Yoshizawa, S. Hayashi, K. Sanada, T. Suematsu and H. Yoshida, EIM-82-26, IEE of Japan, '82



TETSUYA SUEMATSU was born in Nagoya, Japan on 1938. He received B. E. degree from Nagoya University in 1961.

He joined Fujikura Ltd. in 1961 and has been engaged in research and development of nuclear plant cables since 1980.

He is a member of the Institute of Electrical Engineers of Japan



KAZUO KANADA was born in Tokyo on 1946.

He received B. E. degree from Science University of Tokyo in 1971.

He joined Fujikura Ltd. in 1971 and has been engaged in research and development of optical fibers.

He is a member of the Institute of Electronics and Communication Engineers of Japan.



HATSUHO YOSHIDA was born in Tokyo on 1948.

He received B. E. degree from Waseda University in 1971.

He joined Fujikura Ltd. in 1971 and has been engaged in research and development of optical fibers.

He is a member of the Institute of Electronics and Communication Engineers of Japan.

DESIGN AND TEST RESULTS OF AN OPTICAL-FIBER SUBMARINE CABLE

Y. EJIRI M. NUNOKAWA K. FURUSAWA Y. NIRO

KDD Research and Development Laboratories
1-23 Nakameguro 2-chome, Meguroku, Tokyo 153, JapanSummary

This paper describes the design and the test results of an experimental optical-fiber submarine cable. It includes the outline of the cable structure, loss changes during the cable manufacturing and chiefly clarifies the mechanical behavior of the cable under sea water pressure.

Introduction

An optical-fiber submarine cable system is expected to realize the digital transmission of higher capacity with more economical basis compared with the coaxial submarine cable systems of conventional type. A long haul transmission of color television signals will become possible through a submarine cable system. It may be said that this system, together with the satellite communications will be the trunk line for international digital communication in the future.

Recently, various optical-fiber submarine cable structures¹⁻⁵ have been proposed and developed in several countries. An optical-fiber submarine cable system requires to have the cable manufactured in a length longer than several tens of kilometers in continuation while containing optical-fibers inside. It must withstand deep sea water pressure. It should also be capable of being laid on and recovered from a deep sea bottom. Further, it is also required to have a stable operation assured for more than 20 years once it is laid on the sea bottoms.

An optical-fiber submarine cable is a composite structure comprising several member parts. Therefore, it is an important work for realizing an optical-fiber submarine cable with high reliability to clarify the mechanical properties of each of the member parts.

This paper describes a design of an optical-fiber submarine cable used for a long haul submarine cable system under the development at present as well as the test results obtained by experimental cables.

In particular, the description is made as to the results of theoretical and experimental analyses of the hydraulic pressure characteristics which are of a particular importance for an optical-fiber submarine cable.

Optical-fiber submarine cable design

The typical design requirements for an optical-fiber submarine cable for a long haul deep sea system aimed at the transoceanic cable system are shown in Table 1.

An optical-fiber submarine cable with the cross-section as shown in Fig. 1 was manufactured as a trial product, and the manufacturability as well as the mechanical and optical characteristics were evaluated.

Optical-fiber unit design

Six single mode optical-fibers contained at the core of the optical-fiber submarine cable are stranded around a center steel wire and embedded into a soft silicone rubber as shown in Fig. 1⁶. This structure is adopted for the purpose of reducing microbending loss as small as possible when tension, bending, hydraulic pressure and other external forces are applied on the cable.

Cable design

A small-diameter, thick-walled aluminum pipe by assembling three pieces of wire whose cross-section is fan-shaped is used for protecting the optical-fibers from external forces. It is not stranded but only assembled together. The outside diameter of the optical-fiber unit is selected somewhat smaller than the inside diameter of the aluminum pipe. However, they are partially making contact to each other and have enough frictions to avoid slippage of the optical-fiber unit from the aluminum pipe when tension is applied on the cable. A layer of strength members made of 16 high tensile strength steel wires is stranded around the aluminum pipe. Relatively long length of lay is adopted for the high tensile strength steel wires with the aim of restraining the untwisted torque as small as possible. Outside the high tensile strength wires, a copper tube is formed around and swaged in such a way that the aluminum pipe, the high tensile strength wires, and the copper tube are integrated together resulting in a mechanically stable composite body. The aluminum pipe and the copper tube are used as the electrical power supply line for the optical-fiber submarine repeaters. Lastly, the polyethylene insulator and the jacket are extruded and the

outside diameter of the cable is 26 mm ϕ .

Hydraulic pressure characteristics of the cable

Inside diameter change of aluminum pipe

An optical-fiber submarine cable is structured by the compound materials of the optical-fiber unit, the aluminum pipe, the high tensile strength wires, the copper tube, and the polyethylene insulator. It is important for grasping the transmission characteristics of the optical-fibers to know how much the inside diameter of the aluminum pipe contracts under the hydraulic pressure.

When the inside diameter of the aluminum pipe is decreased by hydraulic pressure, the capacitance between the center steel wire and the aluminum pipe will be changed. By measuring the amount of such capacitance change, we can know the change of the inside diameter of the aluminum pipe. Provided C is the initial capacitance between the aluminum pipe and the center steel wire of the optical-fiber unit, and that ΔC is the capacitance change due to hydraulic pressure, the equation (1) is derived.

$$\frac{\Delta C}{C} = - \frac{\frac{2\epsilon\delta}{(d_2 + 2\delta)} \cdot E}{\left\{ E \cdot l_1 \left(\frac{d_2 + 2\delta}{d_2} \right) + l_2 \left(\frac{d_2}{d_1} \right) \right\}} \quad (1)$$

where,

- ϵ ; Dielectric constant of fiber-unit (3.02)
- d_1 ; Outside diameter of center steel wire of optical-fiber unit (0.40 mm ϕ)
- d_2 ; Outside diameter of optical-fiber unit (average 2.76 mm ϕ)
- $d_2 + 2\delta$; Inside diameter of aluminum pipe (2.95 mm ϕ)
- $2(\Delta\delta)$; Inside diameter change of aluminum pipe

The calculation result obtained by substituting the values in the equation (1) is shown in Fig. 2.

The hydraulic pressure test equipment is shown in Fig. 3. The hydraulic pressure up to 1600 kg/cm² can be imposed on the cable sample of 6m long.

The measuring accuracy of capacitance measurement system is less than 0.05 pF. So, a, minute change of the inside diameter of the aluminum pipe as small as 0.23 μ m can be measured.

Measurement results and discussions

Hydraulic pressure was applied on the optical-fiber submarine cable and the change of the inside diameter of the aluminum pipe was obtained by calculating the measurement results of capacitance change.

The measurement results are shown in Fig. 4. The measurements were executed on two

cable samples both of which showed practically similar characteristics. There is a remarkable difference between the inside diameter change at the low hydraulic pressure region of about 600 Kg/cm² or lower pressure and that at the hydraulic pressure region higher than 600 Kg/cm².

Low hydraulic pressure region The aluminum pipe is made by assembling three pieces of wire whose cross-section is fan shaped. However, the deformation of the inside diameter of the pipe when hydraulic pressure below about 600 Kg/cm² is applied is practically the same as the characteristics of an perfect aluminum pipe of the same wall thickness and expressed by the equation (2) within the range of elasticity provided that the longitudinal fit surfaces of the aluminum pipe divided in three parts are making contact to each other.

$$u(a) = - \frac{2P(1-\nu^2)}{E} \cdot \frac{k^2}{(k^2-1)} \cdot a \quad (2)$$

where,

- $2a$; Inside diameter of pipe (2.95 mm ϕ)
- ν ; Poisson's ratio of pipe (0.33)
- E ; Young's modulus of pipe (7300 Kg/mm²)
- k ; Ratio of outside diameter to inside diameter (2.37)
- P ; Pressure
- $u(a)$; Radial displacement of the inner wall of pipe

Plotting the calculation results of the equation (2) in Fig. 4, it is found that the measured values at low hydraulic pressure region lower than 600 Kg/cm² make good coincidence with the calculated values.

On the basis of the results described above, we may say that, within the range in which the stress of the aluminium pipe is lower than the yield point of aluminium, the aluminium pipe can act as the major resisting structure against hydraulic pressure.

High hydraulic pressure range At a high hydraulic pressure region exceeding the yield point of aluminium, on the other hand, it is assumed that the high tensile strength wire provided with the highest Young's modulus among the components of the cable is making the largest contribution to the resistibility against hydraulic pressure. In other words, the conglomerate of high tensile strength wires may be assumed as a hydraulic pressure resisting cylinder. When a hydraulic pressure is imposed on a cable, the state of the high tensile strength wires contacting to each other changes and it is assumed that the high tensile strength wires slightly move to the direction of the cable center. The rough estimation of such displacement of the high tensile strength wires toward the cable center can be done based upon the contact theory of Hertz. Provided here that a hydraulic pressure q is imposed on the external side of the high tensile strength wires as shown in Fig. 5,

it is assumed that the initial line contact which is assumed between two adjacent high tensile strength wires will change to the plane contact when hydraulic pressure is increased. In this way, when the contact area of the high tensile strength wires to each other increases and the distance between the centers O_2 and O_3 of the high tensile strength wires is reduced, the centers of the high tensile strength wires O_2 and O_3 shift respectively to O_2' and O_3' along O_1O_2 and O_1O_3 on Fig. 5. The displacement e ($=O_2O_2'=O_3O_3'$) is obtained by the equation (3) from their geometrical relation.

$$e = \frac{(a+b)\delta}{2b} \quad (3)$$

On the other hand, the decreased distance between two high tensile strength wire centers, can be approximated by the equation (4) according to the Hertz's theory.⁷

$$\delta = \frac{2(1-\nu_s^2)}{\pi E_s} \cdot \frac{X}{\left\{ \frac{2}{3} + 2\ln\left(\frac{4b}{w}\right) \right\}} \quad (4)$$

where,

$$w = 2.15 \sqrt{Xb/E}$$

$$X = (a + 2b)q \quad (q = 8 \text{ kg/mm}^2)$$

ν_s : Poisson's ratio of high tensile strength wires (0.3)

E_s : Young's modulus of high tensile strength wire (21000 kg/mm²)

$2b$: Diameter of high tensile strength wires (1.70 mm ϕ)

The equation (3), however, gives only an approximation as to the displacement of the high tensile strength wires. So, for the purpose of executing more precise calculation, the displacement e of the tensile strength wires is calculated by the non-linear finite element method⁸ in which the Coulomb's Law of Friction is applied on the contact surface of the mesh shown in Fig. 6. According to the calculation, the displacement e of the tensile strength wire toward the cable center caused by the hydraulic pressure 800 kg/cm² is 21.5 μ m. This result is a little less by 1.9 μ m or so than the value calculated by the simplified equation (3).

The calculated results of FEM for the range of 0 kg/cm² through 800 kg/cm² are added on Fig. 4 by shifting the starting point of pressure by 800 kg/cm² or so to the right. Fig. 4 showed that, as to a high hydraulic pressure region between about 900 kg/cm² through about 1300 kg/cm², the measurement results of the inside diameter change of the aluminum pipe coincides well with the calculated results by FEM. As to the result of investigation described above, it is found out that

(1) at a low hydraulic pressure region lower than about 600 kg/cm², the aluminum pipe acts as the major hydraulic pressure resisting structure.

(2) at a high hydraulic pressure region higher than about 600 kg/cm², on the other

hand, the aluminum pipe enters into a plastic region.

(3) at a intermediate hydraulic pressure region between 600 kg/cm² through 1300 kg/cm², the high tensile strength wires act as the major structure for resisting hydraulic pressure.

(4) at a high hydraulic pressure region higher than about 1300 kg/cm², the high tensile strength wires shows also a plastic region.

(5) deformation of the inside diameter of the aluminum pipe caused by hydraulic pressure of 800 kg/cm² is about 10 μ m or less.

Examples of other test results

Cabling loss

The loss change of the optical fibers in the trial cables measured after each cabling processing stage is shown in Fig. 7. The changes are within 0.02 dB/km.

Tensile characteristics

Cable elongation and rotation The breaking strength of the trial cables was about 8 tons. Fig. 8 shows the elongation and rotation characteristics of the long length cable of 122 m.

According to Fig. 8, the elongation of the cable shows practically a linear relation with the tensile force up to 4 tons, and the cable is within the elastic region.

The rotation caused by tensile force, on the other hand, increases parabolically with the tensile force.

Loss changes

Fig. 9 shows an example of loss changes against the tensile force measured by utilizing the long size test piece of the experimental cable of 122 m long. The loss measurement was made on the overall fiber length of about 0.5 km which consisted of four 122 m long single mode fibers spliced in a loop. The stability of the measuring instrument is 2 mdB/5 hours.⁹ The test results showed that the optical loss increased practically in proportion with the tensile force with a small hysteresis. The change of loss by 4 ton tensile force to the cable is so small as 6 mdB/km. It is assumed that this small loss change is due to the cable structure in which the optical fibers are embedded into a soft silicone rubber in such a way that the microbending loss is difficult to develop.

Conclusion

The design of the optical fiber submarine cable being developed at present as well as the test results executed on the trial product have been described. In particular, it has become clear by the measurement of capacitance between the center steel wire of the optical fiber unit and the aluminum pipe that the behavior of deformation of the aluminum pipe due to hydraulic pressure differs according to the following three hydraulic pressure regions: low hydraulic pressure region lower than 600 kg/cm²

where the aluminum pipe acts as the major resisting structure against hydraulic pressure, high hydraulic pressure region higher than 1300 kg/cm² where the high tensile strength wires show a plastic deformation, and the intermediate region between these two hydraulic pressure where the high tensile strength wires act as the major resisting structure. Further, such results well agreed with the theoretical investigation. It was clarified that the contraction of inside diameter of the aluminium pipe due to hydraulic pressure of 800 kg/cm² was smaller than 10 μ m. So that, a contraction of aluminium pipe will give only a small effect on the transmission characteristics of optical fiber.

It is considered that, in the future, it will be necessary to promote the development of fibers of high strength and to evaluate the long term characteristics with higher precision for the purpose of realizing the highly reliable optical fiber submarine cable.

Acknowledgments

The authors would like to thank to Drs. H.Kaji, H.Teramura, K.Amano, and C.Ota for their encouragements and Drs.Y.Namihira, K.Tatekura for their contributions in experiments. Also, the authors wish to thank to Nippon Telegraph and Telephone Public Corporation for their cooperation.

References

- (1) K.Amano, "Under Sea Cable Technology", in IEEE Trans. on Microwave Theory and Techniques, vol. MTT-30, No.4, pp.543-550, April, 1982.
- (2) R.F.Gleason, R.C.Mondello, B.W.Fellows, and D.A.Hadfield, "Design and Manufacture of an Experimental Lightwave Cable for Undersea Transmission Systems", International Wire and Cable Symposium, pp.385-389, Nov.14-16, 1978.
- (3) P.Worthington, "Installation of a Trial Optical Fiber Cable Designed for Transoceanic Submarine Telecommunications Systems", ibid, pp410-417, Nov.18-20, 1980.
- (4) G.Le.Noane, M.Lenoir, "Submarine Optical Fiber Cable Development in France", International Communication Conference, pp.7.D.4.1-7.D.4.3, June, 1982.
- (5) H.Fukutomi, N.Kojima, F.Ashiya, and Y.Negishi, "Submarine Optical Fiber Cable Development", ibid, pp.7.D.1.1-7.D.1.5, June, 1982.
- (6) H.Yamamoto, Y.Ejiri, K.Tatekura, M.Nunokawa, and Y.Nihiro, "Design and Experimental Model of Fiber Unit for Optical Submarine Cable", Paper of technical group, IECE Japan, TG-CS 81-27, May, 1981.
- (7) R.J.Roark, W.C.Young, "Formulas for Stress and Strain", 5th ed., McGraw-Hill
- (8) Y.Ejiri, M.Nunokawa, K.Furusawa, and Y.Nihiro, "A Study on Mechanical Properties of An Optical Fiber Submarine Cable", Paper of technical group, IECE Japan, TG-CS 81-157, Jun., 1982.
- (9) Y.Namihira, H.Wakabayashi, and H.Yamamoto, "High-Stability Measuring Equipment for Very Small Variations of Optical-Fiber Loss", Electronics Letters, 4th Feb., 1982, vol.18, No.3, pp.124-126.

Table 1 Design requirements for optical-fiber submarine cable

Items	Objectives
Maximum Sea Depth	8,000 m
Maximum Water Pressure	800 kg/cm ²
Tensile Strength	≥ 8 ton
Cable Modulus	> 9 km
Sinking Velocity	≥ 1,000 m/h
Allowable Minimum Bending Radius	≤ 1m
Number of Fibers	Max 6
Maximum Power	± 6kV
Feed voltage	± 6kV
DC Resistance	≤ 0.5Ω/km

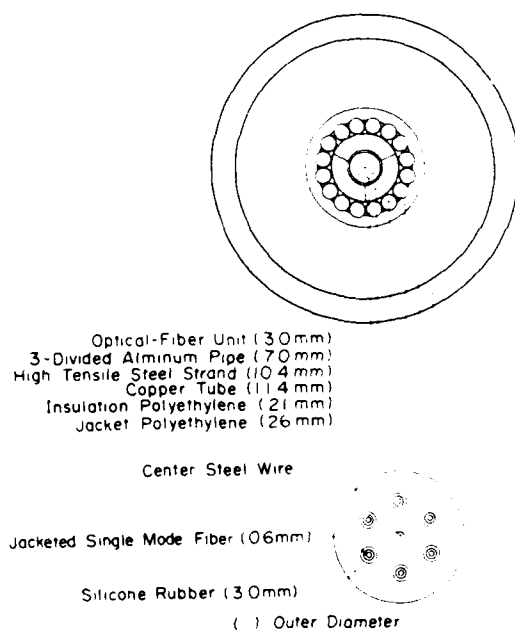


Fig.1 Cross-section of experimental optical-fiber cable and optical-fiber unit

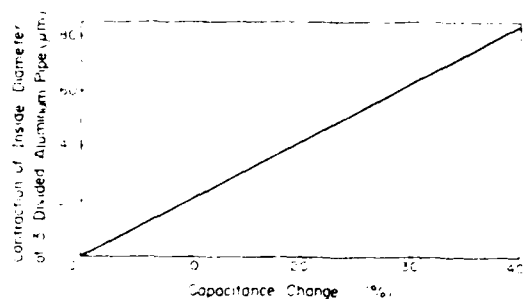


Fig.2 Relation of capacitance change between aluminum pipe and center steel wire of fiber unit

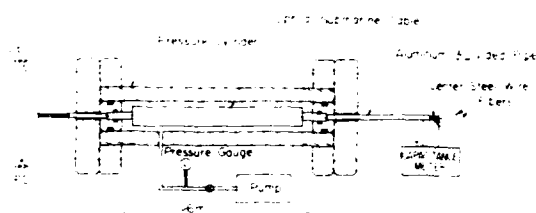


Fig.3 Outline of water pressure test equipment

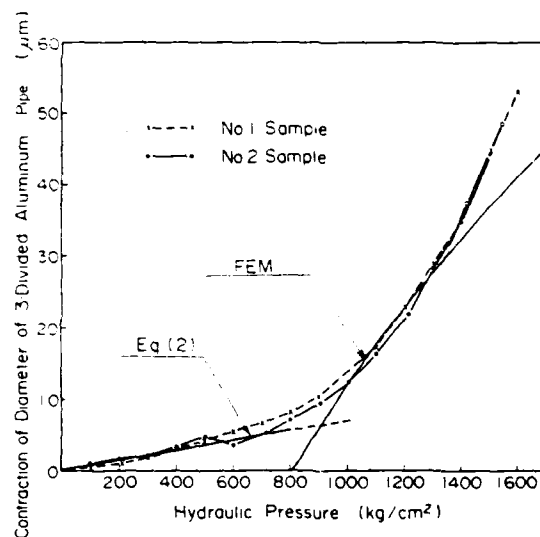


Fig.4 Relation of contraction of aluminum pipe under hydraulic pressure

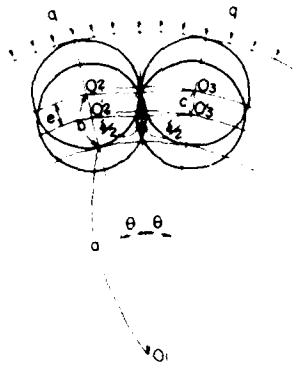


Fig.5 Schematic of contact of strand

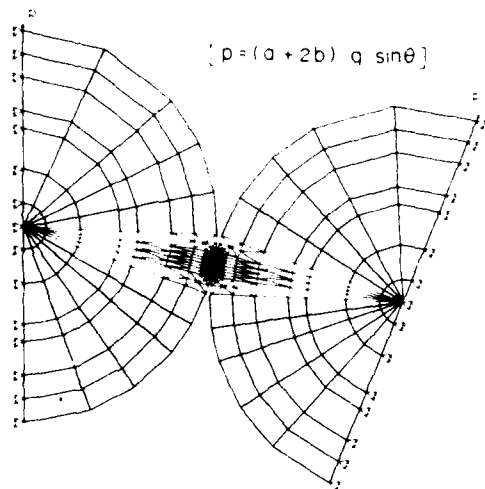


Fig.6 Mesh of strand for FEM

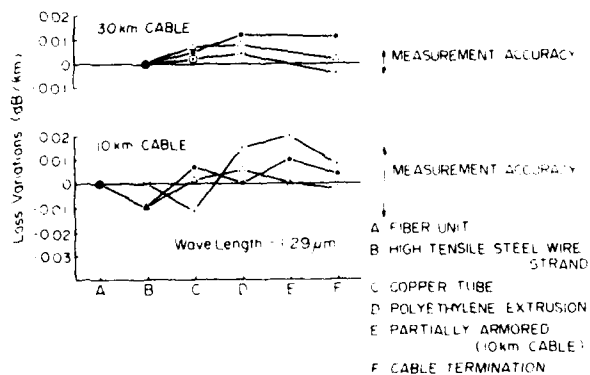


Fig.7 Fiber loss changes of field trial cables

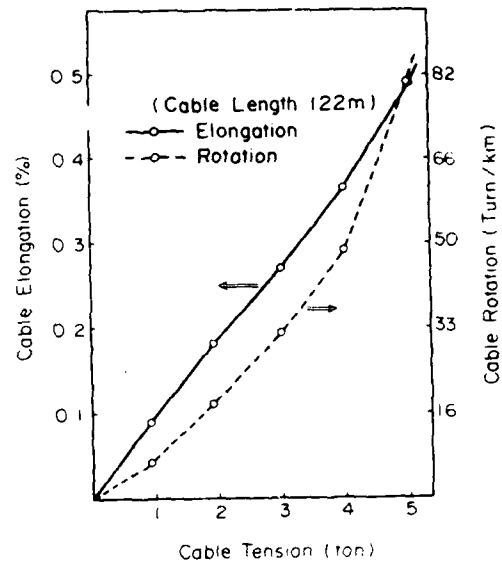


Fig.8 Typical elongation and rotation of experimental optical-fiber submarine cable

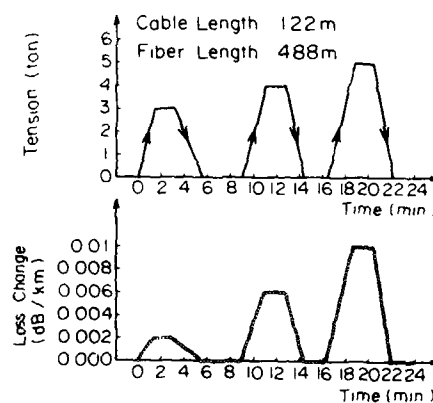


Fig.9 Example of optical-fiber loss changes vs. cable tensile strength



Yoshihiro Ejiri received his B.S. in Mechanical Engineering in 1971 and M.S. in Communication Engineering in 1973 from the University of Electrical communication. He has been a research engineer of the Cable Communication System Laboratory since he joined KDD Laboratories after graduation. Recently he has been engaged in the development of optical-fiber submarine cables and cable terminations and repeater housings.



Kahei Furusawa received his B.S. in the Mechanical Engineering from Nippon University. He joined KDD in 1953. He has been engaged in the development of repeater housings and cable terminations of submarine coaxial cable systems. Now he has been responsible for repeater housings including cable terminations of optical-fiber submarine cable systems. Recently he has been responsible for the construction of the long length cable test equipment.



Makoto Nunokawa received his B.S. in 1968 and M.S. in 1970 in Electrical Engineering from Waseda University. He joined KDD Laboratories and engaged in the research and development of coaxial submarine cable systems, especially in the undersea equalization design and electrical characterization of coaxial submarine cables. Recently, he has been working on the development of optical-fiber submarine cable systems and responsible for the cable design. He is now an assistant to manager of the Cable Communication System Laboratory.



Yasuhiko Niino received his B.S. in Electrical Communication from Musashi Institute Technology in 1964. After graduation he joined KDD as a member of submarine cable construction section. He has been engaged in the development of the submarine coaxial cable systems since 1971 in KDD Laboratories. He is presently managing a group with responsibilities for development of the optical-fiber submarine cable systems in KDD Laboratories.

AD P000595

COMPUTER CONTROLLED
OPTICAL TIME DOMAIN REFLECTOMETER
MONITORING OF LIGHTGUIDE CABLE INSTALLATIONS

Arthur F. Judy, Robert E. Fangmann
Michael J. Swiderski

Bell Laboratories
2000 Northeast Expressway
Norcross, Georgia 30071

Abstract

A computer controlled Optical Time Domain Reflectometer was used to monitor and measure fiber loss during the first Bell System installation of lightguide cable using standard plowing methods. The tests showed that the plowing operation had no measurable effect on fiber loss.

Introduction

During the first week of June 1981, five lightguide cables were plowed in by AT&T Long Lines with Bell Laboratories' assistance. This was the first attempt by Bell System craft to plow such cables. Special Optical Time Domain Reflectometer (OTDR)¹ tests verified that the plowing had no measurable effect on fiber loss.

Cable Installation

The five cables, totaling 3 km were part of Long Lines' 16 km Orlando-Windermere FT3 route. The cable was a standard Bell System design with six 12-fiber ribbons enclosed in a crossply sheath.² No additional sheath protection was used.

The system will initially operate at the FT3 rate (45 Mbit/sec at 825 nm). In addition the cable is capable of future upgrading to the FT3C rate (90 Mbit/sec).

The plowing equipment (Figure 1) consisted of a Caterpillar D8 tractor and a standard plow equipped with a dual chute for simultaneously placing the lightguide cable and a spare plastic duct. A few days before the cable plowing operation, the route was preplowed to disclose buried obstructions and check the tractor's traction. The cable plowing operation was performed using standard cable plowing methods and was trouble-free.



FLOWING EQUIPMENT

Test Equipment and Procedure

The test equipment consisted of a Western Electric 191A OTDR interfaced to an HP85 computer. Using sample and holds, the OTDR averages the reflected signal from two locations in the fiber. The computer sets

the two locations, the number of measurement repeats (from 2^1 to 2^{14}) and calculates loss from the two measured signals. This system measures fiber loss with a resolution of 0.01 dB and has a long term repeatability (2 σ) of 0.06 dB. When compared on one hundred sixteen 0.5 km-fibers in the lab, OTDR loss measurements at 819 nm had high correlation ($R=0.97$, $\sigma=0.08$ dB/km) with transmission loss measured at 831 nm (Figure 2). In Orlando an OTDR was used for measuring loss because it only required connection to one end of the cable. This, with its ability to selectively measure the loss between any two points in a fiber, allowed the determination of both the location and magnitude of any fiber loss changes while a cable was being plowed.

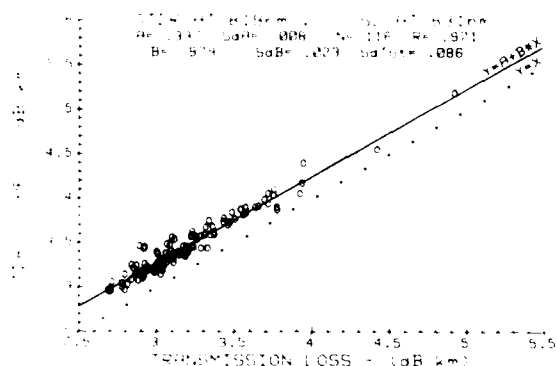


FIGURE 2

The test equipment was located in a temperature controlled van and was connected to the lightguide cable by one of two fanout/test-ribbon assemblies (Figure 3). Standard array connectors were used for the cable connection. The two fanout/test-ribbon assemblies were used to permit monitoring of any of the 12 fibers in each of two ribbons. The fanouts provided quick access to the individual fiber ends within the test van. The test ribbon served two functions, it placed the monitored fibers out beyond the test set connection echoes, and provided a conveniently long lead from the test van to the installed cable end.

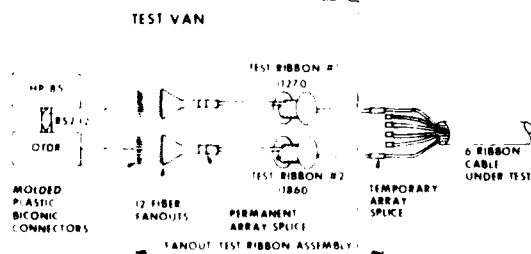


FIGURE 3 ORLANDO WINDERMERE TEST ARRANGEMENT

The OTDR was programmed to measure the fiber loss of three approximately equal length sections. These three sections spanned the entire fiber length except for the very ends which were obscured by the end echoes. A sample of at least 24 fibers was measured in each cable before plowing. During plowing four of these fibers were continuously monitored. Immediately after plowing, all originally tested fibers were retested. The use of the computer allowed automatic retesting (real-time monitoring) of the fiber paths. The field test measurements were automatically stored, compared to initial data, and the differences printed out giving immediate feedback on the effects of plowing.

Results

In the five plowed cables, 212 fibers were tested, resulting in 636 loss readings. A histogram of the changes in these losses from before to after plowing is shown in Figure 4. In comparison, the inset in Figure 4 shows typical measurement repeatability which was determined by retesting 65 fibers. The two distributions are essentially identical. We conclude that plowing caused no detectable fiber loss variations.

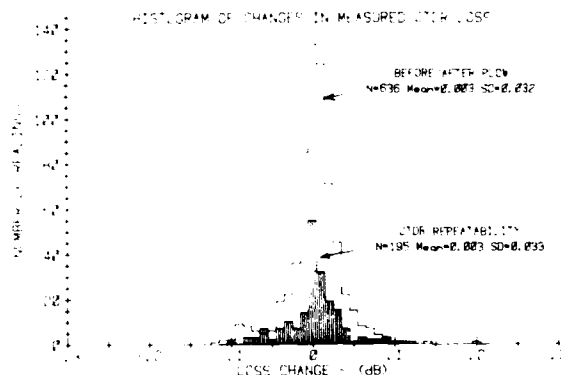


FIGURE 4

References

1. S. D. Personick, "Photon Probe - An Optical-fiber Time Domain Reflectometer," B.S.T.J., 56 (March 1977), p. 355.
2. P. F. Gagen and M. R. Santana, "Design and Performance of a Crossply Lightguide Cable Sheath," Proc. 28th IWCS, (Cherry Hill, NJ, November 1975), p. 391.
3. C. M. Miller, "Fiber Optic Array Splicing With Etched Silicon Chips," B.S.T.J., 57, (January 1978), p. 75.



Mr. Judy has been a Member of Technical Staff at Bell Laboratories for 15 years. He has worked on the measurement and theory of coaxial, paired and lightguide cables and on the design and development of test equipment. He received a B.S.E.E. from the University of Maryland in 1967 and a M.S.E.E. from the University of Michigan in 1968.



Mr. Swiderski joined Bell Laboratories in 1967 after which he received his A.A. in Electronics Technology in 1968. His work included development of memory devices, coaxial cable and components, paired cable, sheath and protection design, high voltage testing, and lightning measurement. He is a Member of Technical Staff (SP) in the Lightguide Applications and Field Testing Group.



Mr. Fangmann is a Member of Technical Staff in the Cable and Wire Department at Bell Laboratories in Norcross, Ga. He is currently working on Lightguide Systems and Applications Engineering. His previous assignments have included coaxial cable design and development, outside plant engineering and splicing operations studies. Mr. Fangmann received the B.S. degree in Engineering-Physics from Loyola College, Baltimore and the M.S. degree in Engineering-Mechanics from the University of Arizona.

AD P000596

PRACTICAL INSTRUMENTATION FOR FIBER OPTIC EVALUATION

PAUL WENDLAND, Ph.D.

PHOTODYNE INC.

As fiber optic technology develops and applications increase, greater attention is centered on instrumentation to monitor characteristics and performance of the individual components and of the system. In this paper on fiber optic instrumentation, special emphasis is given to the needs for instrumentation to be used under typical "field" conditions.

5. Low weight
6. No electromagnetic interference
7. Small crosstalk and high security
8. Natural abundance of glass materials, especially those containing a high concentration of silica
9. High resistance to chemical attack and temperature variations

OUTLINE

- I. OPTICAL FIBER COMMUNICATION SYSTEMS
- II. OPTICAL POWER MEASUREMENTS
- III. FIBER ATTENUATION (LOSS) MEASUREMENTS
- IV. FAULT LOCATION
- V. OPTICAL PULSE DISPERSION
- VI. SYSTEM MODELING

I. OPTICAL FIBER COMMUNICATION SYSTEMS

Optical fibers have a number of excellent transmission characteristics:

1. Large bandwidth (1 and 100 GHz, respectively, for multimode and single-mode fibers over 1km)
2. Low loss over a wide range of wavelengths (less than 1dB/km, corresponding to a 25% loss per km)
3. Flexibility
4. Small size (a clad glass fiber has a diameter of about 100 μ m and a total diameter, inclusive of the plastic coatings, of 1-2mm)

In these fiber optic transmission systems, conversions between electrical and optical signals are accomplished by light-source devices, such as semiconductor LDs (laser diodes) and LEDs (light-emitting diodes), and by photodetectors, such as APDs (avalanche photodiodes) and Pin-PDs (Pin photodiodes). The intensity-modulated signals are transmitted via optical fibers.

Optical fibers can be classified as silica glass, multi-component glass, plastic, and other optical fibers. Silica fibers are predominant in long-haul, large-capacity transmission, utilizing their low-loss characteristics to the absolute maximum. Plastic optical fibers are used for very short-haul transmission because of their low cost and ease of handling.

As shown in Figure 1, an optical fiber communications system consists of terminal equipment, terminal repeaters (electrical/optical transducers), and optical fibers. The terminal equipment has exactly the same measured parameters as conventional coaxial cables. Therefore, the electrical/optical transducers and optical fibers are the items to be measured by optical communications measuring instruments.

Optical Fiber

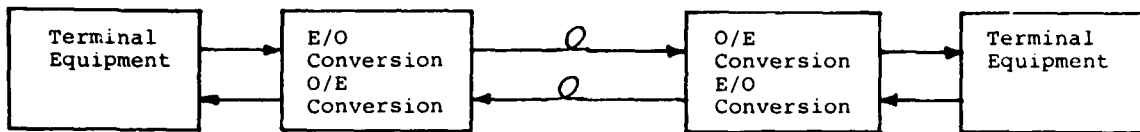


Figure 1. Optical Fiber Communications System Diagram.

II. OPTICAL POWER MEASUREMENTS

The information transmitted through a fiber optic (FO) system is carried by a beam of light. This beam of light can be described as a group of photons carrying power from one point to another. Optical power measurements are thus basic to fiber optics. The following measurements are typical of FO systems:

- . Absolute radiant power output of the source, which is as important to fiber optics as absolute current and voltage are to electronics. If an optical source delivers significantly less than its rated output, lowering the total dB-loss of a system's passive components will not always compensate for the weak input.

- . Fiber power loss, which depends on the fiber length and on the angle of launch; measurement of fiber loss can be difficult.

- . Connector and splice losses, which involve specifications of both the light coupled into a fiber's core and the light coupled into its cladding; fiber specs are usually for light coupled into the core only. The surest resolution to this inconsistency is to measure the optical power into and out of the connector or splice.

- . Receiver sensitivity. Whether or not the system photodetectors provide gain, they convert incident light into electrical current. Measuring the efficiency of the conversion--or responsivity--requires an optical-power meter and an ammeter.

It is most convenient to measure all these variables directly in decibels (dB)--the standard communications unit. When expressed in dB, system gains and losses can be easily perceived and quickly evaluated.

Decibel units are the logarithmic transformations of the basic optical power unit, watts, and submultiples of watts. Decibel units are useful in

compressing power measurement data that has a wide dynamic range. These units are commonly used in fiber optic measurement. Table 1 gives the definitions of decibel units and gives a conversion table between dBm and mW.

TABLE 1 CLARIFICATION OF OPTICAL dB UNITS

Measurements of optical radiation power are expressed in watts. Decibel (dB) power is:

$$\text{dB} = 10 \log \left[\frac{P_{\text{sig}}}{P_{\text{ref}}} \right]$$

where P_{sig} is the power to be measured and P_{ref} is the reference power.

For 1-mW reference power:

$$\text{dBm} = 10 \log \left[\frac{P_{\text{sig}}}{1 \text{ mW}} \right]$$

For 1-μW reference power:

$$\text{dBμ} = 10 \log \left[\frac{P_{\text{sig}}}{1 \text{ μW}} \right]$$

With both P_{sig} and P_{ref} variable, the dB-power formula expresses the log ratio of the two unknowns in dB.

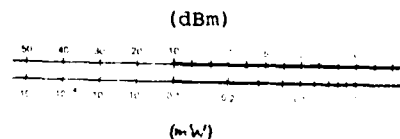
Light-power loss of an optical data-link element is:

$$L (\text{dB}) = 10 \log \left[\frac{P_o}{P_{\text{in}}} \right]$$

The input power (P_{in}) and output power (P_o) of a component can be measured in dBm units, dBμ units, or dB units without a known reference. The loss, L , expressed in decibels, is the same:

$$\begin{aligned} L (\text{dB}) &= \text{dBm} (P_o) - \text{dBm} (P_{\text{in}}) \\ &= \text{dBμ} (P_o) - \text{dBμ} (P_{\text{in}}) \end{aligned}$$

mW to dBm conversion



Silicon photodiodes are most often used as the basic sensor for optical power measurements as wavelengths ranging from 400nm to 1000nm. A one square centimeter silicon photodiode has a typical dynamic range from one picowatt to one milliwatt. Today's silicon detectors appear to perform near the natural dynamic limits that their basic band structure allows.

Many junction structures are possible and have been tested, but three are almost exclusively used in fiber optic instrumentation. These are PIN, PN and APD (avalanche photodiode). The APD version costs more than the other two types, and is employed most often for high-speed applications. The APD is not intrinsically faster than the PIN type, since electron-hole pairs in silicon reach a limiting electric field induced velocity long before they reach avalanche, but the gain produced in the avalanche process makes the signal much easier to extract.

Germanium photodiodes have been widely used for optical power measurements from 1000nm to 1800nm. It seems that commercially available devices have not yet reached the natural low light level detection limits established by electron-hole pair thermal excitation across the band gap.

InGaAs photodiodes are now being marketed for the 1000nm to 1800nm band which exhibit lower dark leakage currents than germanium types. They cost much more than germanium types, and are only available with small active area (typically 0.5mm).

Figure 2 shows a typical measurement geometry for fiber optics. Large area photodiodes allow easy coupling with high mechanical dimensional tolerances. The large collecting numerical aperture of this configuration prevents loss of light during the measurement process. Beware, however, of power density limits of the detector.

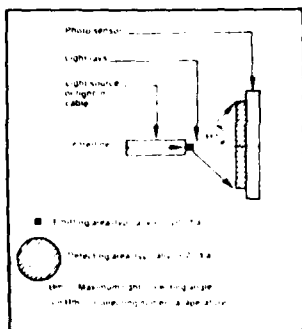


Figure 2. Large Area photodiode sensors yield collecting numerical apertures above .5.

Figure 3 shows the light spot formed on the detector surface from a fiber output end. The relationship between total power out of the fiber and power density on the detector surface is:

$$(1) P_d = P / \pi t^2 (NA)^2$$

where: P_d = power density on detector (mW/mm²)

P = output power from fiber (mW)

t = separation of fiber end and detector (mm)

NA = fiber numerical aperture

For instance, a fiber with a NA of 0.2, located 1 mm from a detector surface, and emitting 100 microwatts (0.1mW), would produce a power density on the detector surface of 0.8 mW/mm². Consult the manufacturer's specifications for power density limits. Specifications are often exceeded before the power limit is reached for a fully illuminated detector.

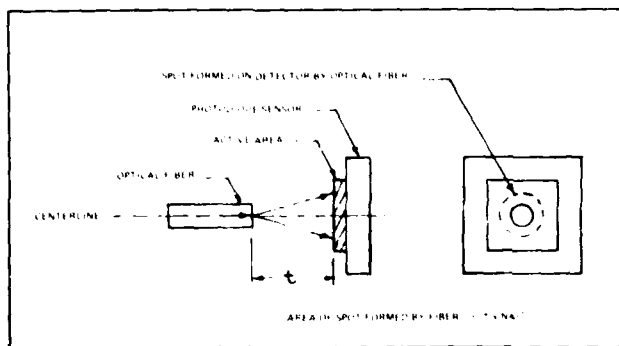


Figure 3. Beware power density limits of optical power sensors.

Figure 4 is a photograph of a typical optical power meter for use in field or lab. The 11XE employs a silicon sensor head, covers a dynamic range from -80dBm to +2dBm, and a spectral range from 600nm to 1000nm. The 12XE employs a germanium sensor head, covers a dynamic range from -60dBm to +2dBm, and a spectral range from -60dBm to +20dBm. These pocket size instruments are autoranging and autozeroing, and have only one switch for off/on power.

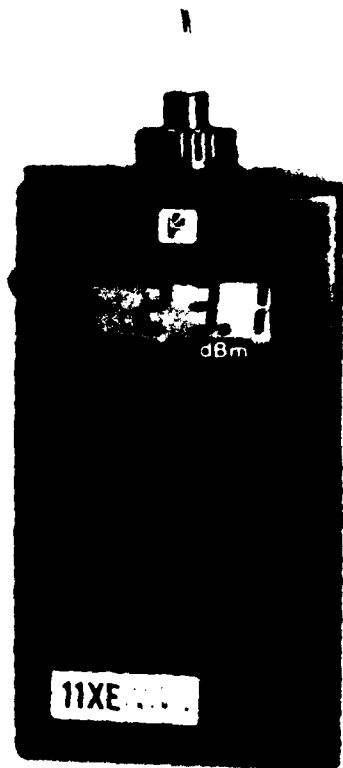


Figure 4. Photograph of a typical portable fiber optic power meter.

III. FIBER ATTENUATION (LOSS) MEASUREMENTS

Fiber attenuation refers to the loss in optical power when the light beam travels from one point to another point in the FO system. Attenuation is typically defined as ten times the log of the ratio of output power to input power, and symbolized as dB. Since attenuation in dB is a power ratio, absolute units, such as dBm or dBu, are not applicable. The relationship between power loss in dB and percent power loss is shown in Figure 5.

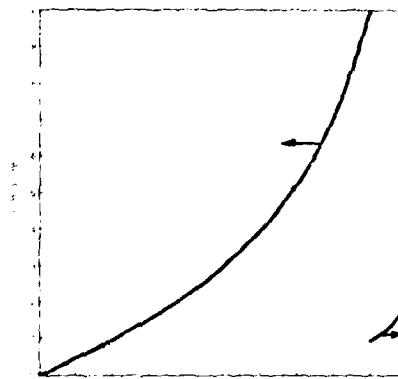


Figure 5. Conversion between % loss and dB loss.

Attenuation per unit length of an optical fiber can conveniently be represented by the cable-loss factor (CLF) in dB/km/:

$$CLF = \frac{P_i - P_o}{L}, \quad (1)$$

where

P_i = input power in dB

P_o = output power in dB

L = cable length in km

The power output of the source is quite different than the effective input power to the fiber. Loss mechanisms extract a heavy toll on light sent to the fiber's core; for example, not all of the source light falls on the core and the launch angle may direct some of the light into the fiber cladding.

The cable-substitution method can be used to find the CLF even when the launched power is unknown. The substitution method involves comparing the power outputs of two unequal lengths of otherwise identical cables. For both cables, the power sources, the source-to-cable coupling and the unknown amounts of power actually launched into the core must be identical. Hence, the following equation gives the CLF:

$$CLF = \frac{P_1 - P_2}{L}, \quad (2)$$

where

P_1 = power out of cable 1 in dB

P_2 = power out of cable 2 in dB

L = difference in cable lengths in km

The cables should be long enough so that light initially coupled into the cladding will die out, ensuring that the output powers measured come solely from the cores. Alternatively, light propagating in the cladding can be "stripped out" by submersing the cable, for a short distance near the launching end, in a fluid or gel with a refractive index that matches the cladding's refractive index.

Loss measurements can be made on one cable alone if the cable can be cut. The output power level is measured before and after a piece is cut from the cable. The two measurements are substituted for the P_1 and P_2 values in Eq. 2, to determine the dB loss. The advantage of this scheme is that it does not require two separate but identical cables and launching conditions.

The difference between the optical power input and the optical power output of a connector or splice equals either the connector loss or the splice loss. Making measurements directly in dB simplifies the required calculations. If the connector in question is attached to a long cable, the CLF must be subtracted from the total loss measured for the connector.

Different modes (paths) propagating in the fiber show different loss characteristics. Multimode optical fibers support hundreds of these waveguide modes. A question arises as to what possible modes should actually be excited in a fiber attenuation measurement. An equilibrium mode distribution (EMD) in a fiber is one the fiber naturally produces by differential mode attenuation, mixing and redistribution.

Redistribution occurs after some significant length that is greater than a mode coupling length. It is typically greater than 100 meters. An equilibrium mode distribution (or, at least, a reproducible mode distribution) is the desired result for fiber attenuation measurement setups. Without such a distribution, it would be impossible to obtain an attenuation value, in dB/km, that was independent of fiber length.

Three different techniques have been used to achieve reproducible mode distributions: (1) beam optics, (2) mode filters, and (3) long-length fiber. Figure 6 illustrates these three approaches.

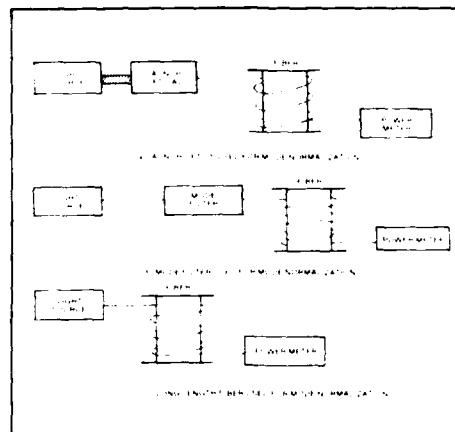


Figure 6. Three different mode control schemes for fiber attenuation measurements.

In the beam optics approach, launch conditions are carefully controlled and high loss modes (paths) are restricted from ever being excited. This requires precise control of launch spot diameter and launch NA. The Electronic Industries Association (EIA) recommends a 70/70 launch. Only 70 ± 5 percent of the center of the fiber core diameter should be filled and only 70 ± 5 percent of the fiber NA should be filled by the launch light beam.

In the mode filter approach, all modes are initially excited by overfilling the core in both spot size and NA. A "mode filter" is then used to simulate the mode distribution at the end of a long length of fiber. A typical mode filter, first used by the Bell Telephone System, is created by loosely wrapping five turns of the fiber being tested around a smooth steel mandrel of 0.5 inch diameter. The mode filter strips off the power and propagates in the unwanted high-loss modes.

In the long-length fiber approach, unwanted (high-loss) modes are eliminated from the measurement simply because they do not propagate over the full fiber length in either the reference fiber or measured fiber. Attenuation is measured in all of these three "mode reproducing" setups using the previously described two-point, or cutback, techniques.

The advantage of the beam optics approach is precision mode control. The disadvantage is that not every electrical engineer will want to try to place a 35 μm diameter light spot dead on the center of 50 μm diameter fiber core. The advantage of the mode filter is that short fiber lengths can be used. The disadvantage is less precision in selecting mode launching. The advantage of the long-length fiber approach is simplicity. The disadvantage is that an EMD may only be reached after many kilometers with some of the new low-loss, high quality fibers.

Figure 7 is a photograph of an optical multimeter, comprising one optical source, and two matched receivers. CLF can be directly measured with this unit.

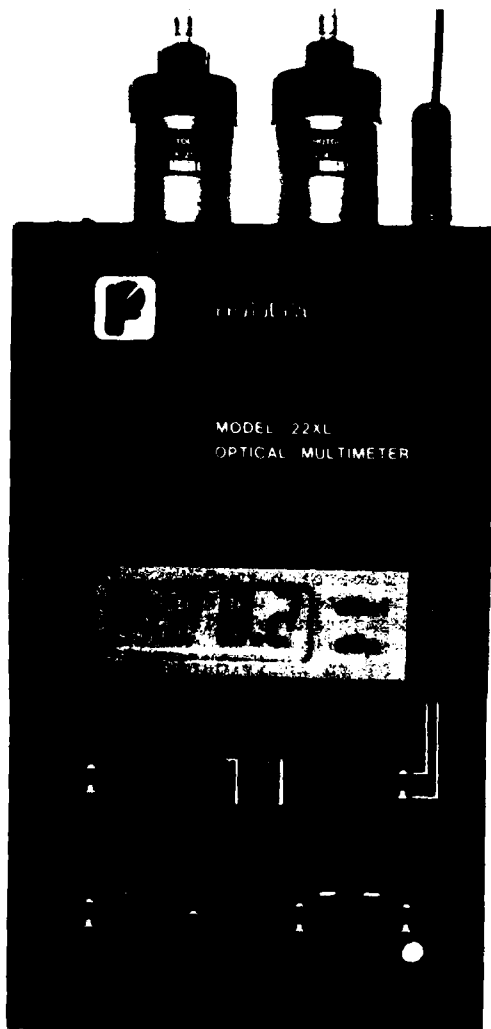


Figure 7. An Optic Multimeter for numerous fiber optic measurements.

IV. FAULT LOCATION

The location of faults and breaks within an optical fiber cable is accomplished with an Optical Time Domain Reflectometer. An OTDR can be thought of as a one-dimensional, closed circuit optical radar. It has the advantage of requiring only one end of the optical fiber to be available for measurements. A high intensity, short duration light pulse from the source is launched into the fiber, but the directional optical coupler stops the initial laser light from reaching the photodetector. This photodetector only records return signals (backscattered light). This backscattered light arises from two principal sources: (1) Fresnel reflections at fiber ends, breaks, and connectors; and (2) Rayleigh scattering from fiber inhomogeneity. A representational signal from an OTDR is shown in Figure 8. This backscattered signal has the form of an exponential decay. The Rayleigh backscattered signal levels are typically 30 to 40dB below the Fresnel back reflection levels from a perfect break. A perfect break (cleave) produces a four percent back reflection.

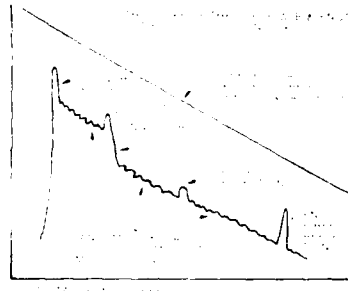


Figure 8. A representational signal from an OTDR.

Figure 9 shows the block diagram of a microcomputer controlled OTDR system which accomplishes an active search and display of fiber discontinuities. Fiber faults show up as short time period discontinuities in the return signal. The differentiated return signal goes to a comparator. The reference level at which the comparator passes the signal to the counter is set by the microcomputer. The microcomputer begins the counter sequence at the same instant that the laser pulse is initiated. The count is stopped when the return signal flows through the comparator. The microcomputer then has two pieces of data: (1) the comparator signal level, corresponding to the return signal height; and (2) the total count from the counter, corresponding to distance from fiber end to defect. The microcomputer can find and display a

variety of defects, as long as they are separated by a slight magnitude difference, corresponding to different comparator reference level settings.

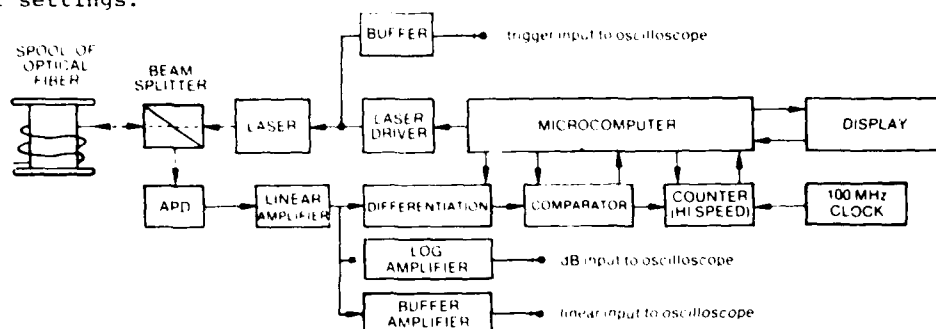


Figure 9. A block diagram of a microcomputer controlled OTDR.

Figure 10 is a photograph of a field portable OTDR. This unit automatically finds and displays the distance in feet or meters to defects, connectors, breaks, and end of cable. The relative sizes of each of the return reflected signals from discontinuities in the optical fiber are also displayed. The 16-character LCD display scrolls through the results of the automatic measurement process. When used with an external scope, the log output provides a measure of optical fiber attenuation or connector attenuation directly in dB. This unit has a range of 20 k and 25dB (one way).

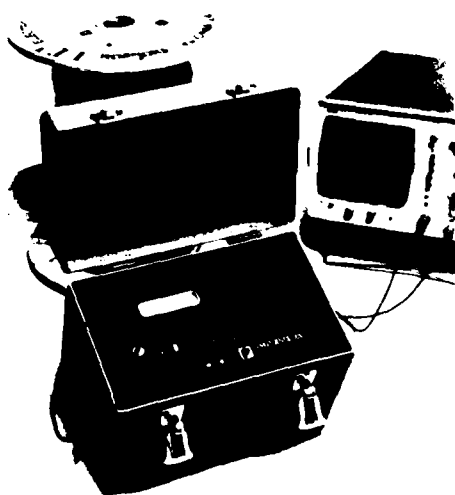


Figure 10. Photograph of a field portable OTDR.

V. OPTICAL PULSE DISPERSION

Some optical modes (paths) take longer than others to traverse a fiber. Modes simultaneously launched by a pulse source will not all arrive at the opposite end of the fiber at the same time. Pulse broadening will be observed. This pulse broadening depends on differential mode delay. The effect is called modal dispersion. Since the observed modal delay depends on the specific modes present throughout the length of the fiber, the observed delay will depend on a variety of conditions: (1) the actual modes launched by the source, (2) mode attenuation, (3) mode mixing. Thus, it is difficult to extrapolate modal delay from one length of fiber to another, or from one set of launch conditions to another.

In addition to modal dispersion, chromatic dispersion is present. Chromatic dispersion results both from material dispersion (different wavelengths propagating at different effective velocities), and waveguide dispersion of an individual mode. Modal dispersion (rather than chromatic dispersion) is usually the dominant effect for multimode fibers.

Figure 11 is a diagram for an experimental setup to measure dispersion. The measurement is simply a direct comparison of the fiber's output pulse to its input pulse. The input pulse must be short (typically 200 ps) in order to resolve minimum pulse broadening effects.² Since the source should have a very narrow spectral emission bandwidth, a laser operating in the stimulated

emission regime (1-2nm linewidth) is required.

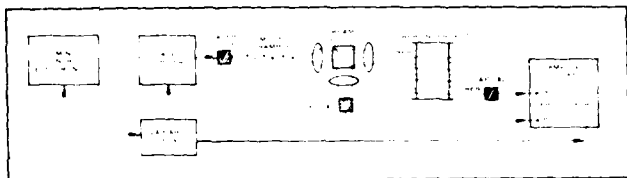


Figure 11. Test setup to measure optical pulse dispersion.

The detector must be capable of faithfully reproducing both source pulse and received pulse. This requires an APD with rise and decay time of 200 ps or less. There is still no consensus on what launching conditions facilitate the best prediction of bandwidth. EIA proposals suggest overfilling the core and N.A. of the fiber being tested. Short pulse laser diode radiation pattern outputs are difficult to reliably characterize. Mode scramblers located between the laser source and the fiber being tested overfill the core and N.A. One such mode scrambler² consists of 7 nylon posts 1 cm in diameter, placed on 1.3 cm centers.

VI. SYSTEM MODELING

In designing a fiber optic transmission system, it is recognized that there is a relationship between the intelligibility of the received signal and the power level of that signal. Also, there is a relationship between the original signal and the actual power received. Thus, with a given power source and detector, one can optimize the bit-rate times length product for a given transmission medium. As the bit-rate increases, the relationship of fiber bandwidth to length becomes apparent. Increased power may be required to maintain the bit-error rate (BER) at an acceptable level at the receiver. Given these relationships, one may roughly calculate the performance at a few carefully chosen experimental points in the overall system model and consider the trade-offs.

A variable optical attenuator can be placed somewhere in a fiber optic link. This instrument can alter the power level received by the detector. When applied to analog fiber optic systems the noise equivalent input power can be determined by using the attenuator to turn down the input signal to the receiver until this signal equals the noise background. When applied to digital systems, the attenuator can again be used to vary the power

received and the bit-error rate.

Figure 12 shows a photograph of a typical optical attenuator. This unit uses two independently rotating dials to vary attenuation in 1dB digital increments from 1dB to 89dB.

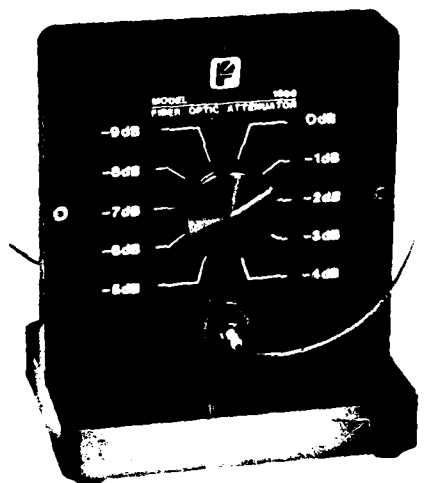


Figure 12. A typical fiber optic attenuator for system modeling.

REFERENCES

1. Franzen, D.L., Day, G.W., and Gallaway, R.I. Laser Focus, August (1981).
2. National Bureau of Standards Technical Note 1019, D. L. Franzen, G.W. Day, February (1980).

Author Index

Abadia, V.	109	Kimmich, K.	390
Aloisio, C. J.	350	Knoch, R. H.	337
Asano, Y.	153	Kobayashi, T.	45
Atin Balbás, J.	89	Koehler, P. G.	1
Berchem, W.	401	Kojima, T.	51
Board, B. L.	300	Korbelak, K.	358
Bohannon, W. D., Jr.	31	Kume, S.	77
Boscher, D.	178	Kurokawa, M.	77
Burley, R. A.	10	Lane, D.	265
Butler, C. M.	283	Leahy, T. P.	1
Byzio, E.	70	Le Nir, V. L.	38
Campbell, B. D.	149	Levy, A. C.	313
Cascarano, W. A.	38	Lichliter, T. P.	1
Chattler, L. M.	221	Lovern, T. N., II.	283
Chazelas, E.	178	Maezawa, T.	198
Checklund, J.	293	Mariñosa, J. L.	109
Claassens, A. M. J. M.	320	Matsumoto, M.	169
Crews, E. W.	16	Mayer, H. A.	401
Dageförde, H. G.	401	McBride, L. E.	193
Davidson, G. M.	377	Metz, S.	390
Delagi, R. G.	193	Meyerstein, M.	271
Delebecque, R.	178	Miyauchi, M.	169
Delme Jones, D.	371	Morales, A. A.	163
Díaz Cortijo, J.	89	Nabeshima, H.	45
Dillow, H. M.	350	Nakae, H.	437
Dufour, I. G.	122	Ney, E. L.	337
Eastwood, H. K.	70	Nuro, Y.	466
Eichenbaum, B. R.	396	Nishi, O.	63
Ejiri, Y.	466	Nishimura, M.	63, 437
Ernbo, A.	137	Nogueira, A. T.	98
Fangmann, R. E.	473	Nunokawa, M.	466
Fetterolf, J.	277	Obara, Y.	77
Frost, G. W.	256	Okazato, A.	45
Fujimura, S.	437	Olszewski, J. A.	131
Furusawa, K.	466	Petrin, J.	70
Fuse, K.	77	Pettersson, G. A.	137
Gerdes, R. J.	131	Pokorny, R. J.	256
Golt, J. S., Jr.	104	Przybyla, L. J.	411
Grooten, A. T. M.	320	Rahman, M. M.	377
Haibara, T.	169	Ramsay, M. M.	371
Hale, P. G.	371	Refi, J. J.	237
Haraguchi, M.	153	Riley, E. W.	444
Hau, K. K.	70	Rondan, B. F.	163
Hayashi, D. G.	10	Rost, H.	337
Hirashima, T.	452	Rozendaal, J.	320
Holte, N.	207	Ruddell, H. J.	300
Horima, H.	63	Russell, J. N.	371
Ichikawa, O.	381	Sabia, R.	313, 396
Inada, K.	45	Saitoh, Y.	381
Ishi, K.	417	Sakamoto, K.	381
Iwakabe, E.	198	Sanada, K.	459
Iwazaki, M.	63	Santana, M. R.	396
Judy, A. F.	473	Sato, N.	417
Kalomiris, V. E.	185	Satou, A.	437
Katahira, T.	417	Schmidt, W.	390
Kaufman, S.	411	Schreiber, H. P.	293
Keith, R. H.	245	Seike, T.	153
Kimata, L.	77	Shannon, M. A.	38

Shibuya, K.....	51	Triplett, J. T.....	149
Shintani, T.....	452	Tsujimoto, K.....	45
Shirasaka, Y.....	77	Tylor, R. E.....	149
Simon, P. M.....	149	Venkatesan, P. S.....	358
Smith, E. E.....	411	Warren, P. C.....	345
Suematsu, T.....	459	Watanabe, O.....	45
Sugiyama, N.....	51	Wendland, P.....	476
Suzuki, H.....	417	West, D. E.....	31
Suzuki, S.....	63	Whiteley, R. H.....	427
Swiderski, M. J.....	473	Williams, J. L.....	411
Tanaka, H.....	452	Yagi, K.....	51
Tarbox, J. W.....	23	Yamamoto, S.....	437
Tate, L. D.....	396	Yokota, H.....	63
Taylor, C. R.....	350	Yoshida, H.....	459
Tencer, C.....	98	Yoshinaga, A.....	51
Titchmarsh, J. G.....	371	Yoshizawa, A.....	198
Tokumaru, Y.....	153	Yoshizawa, M.....	77
Townsend, R. C.....	371	Young, B.....	265
Trenkler, Y.....	193		



IWCS

International Wire & Cable Symposium

**SPONSORED BY U.S. ARMY COMMUNICATIONS—ELECTRONICS COMMAND
(CECOM), FORT MONMOUTH, NEW JERSEY
15, 16, and 17 November 1983**

Hyatt Cherry Hill, Cherry Hill, N.J.

Please provide in the space below a 100-500 word abstract (20 copies) of proposed technical paper on such subjects as design, application, materials, and manufacturing of Communications and Electronics Wire & Cable of interest to the commercial and military electronics industries. Such offers should be submitted no later than 15 Apr 1983 to the Commanding General, U.S. Army Communications - Electronics Command, ATTN: DRSEL-COMRM, (W.Conti) Fort Monmouth, NJ 07703.

Title: _____

Authors: _____

Company: _____

Address: _____